

# Basics of Foundation Design

*Electronic Edition, January 2025*

**Bengt H. Fellenius**

**Dr. Tech., P.Eng.**

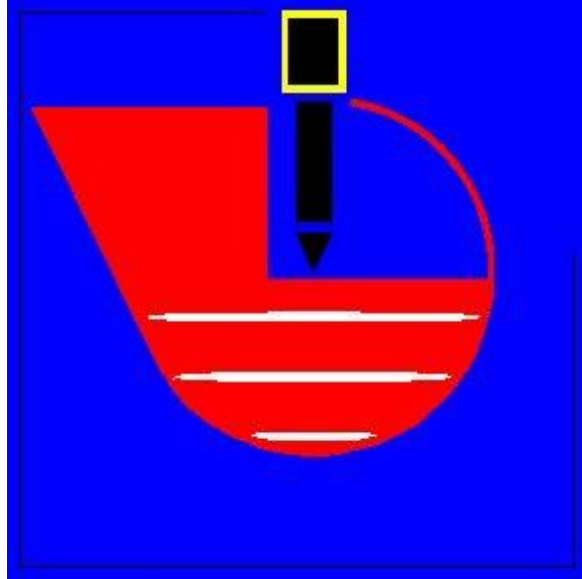
2375 Rothesay Avenue  
Sidney, British Columbia  
Canada, V8L 2B9

E-address: <[Bengt@Fellenius.net](mailto:Bengt@Fellenius.net)>  
Web site: [www.Fellenius.net](http://www.Fellenius.net)



**Reference:**

Fellenius, B.H., 2025. Basics of foundation design.  
Electronic Edition, [www.Fellenius.net](http://www.Fellenius.net), 570 p.



# Basics of Foundation Design

*Electronic Edition, January 2025*

**Bengt H. Fellenius**

**Dr. Tech., P.Eng.**

2375 Rothesay Avenue  
Sidney, British Columbia  
Canada, V8L 2B9

E-address: <[Bengt@Fellenius.net](mailto:Bengt@Fellenius.net)>  
Web site: [www.Fellenius.net](http://www.Fellenius.net)

---



## P R E F A C E

The “Red Book” presents a background to conventional foundation analysis and design. The text started as a compendium of the contents of courses in foundation design I gave during my years as Professor at the University of Ottawa, Department of Civil Engineering. Later on, it became a background document to the software developed by my former student and good friend, Pierre Goudreault and marketed by UniSoft GS Ltd ([www/unisoftGS.com](http://www.unisoftGS.com)).

The text is not intended to replace the more comprehensive ‘standard’ textbooks, but rather to support and augment these in a few important areas, supplying methods applicable to practical cases handled daily by practicing engineers and providing the basic soil mechanics background to those methods.

It concentrates on the static design of foundations. Although the topic is far from exhaustively treated, it does intend to present most of the basic material needed for a practicing engineer involved in routine geotechnical design, as well as provide the tools for an engineering student to approach and solve common geotechnical design problems. Indeed, I make the somewhat brazen claim that the text actually goes a good deal beyond what the average geotechnical engineers usually deals with in the course of an ordinary design practice. However, the "Red Book" is not intended to replace conventional text books, but to supplement them. Therefore, many already well-covered areas in conventional text books are not addressed in the "Red Book".

The text emphasizes two main aspects of geotechnical analysis, the use of effective stress analysis and the understanding that the distribution of pore pressures in the field is fundamental to the relevance of any foundation design. Indeed, foundation design requires a solid understanding of the, in principle simple, but in reality very complex, interaction of solid particles with the water and gas present in the pores, that is an in-depth recognition of the most basic tenet in soil mechanics, the *principlium* of effective stress.

To avoid the easily introduced errors of using buoyant unit weight, I strongly advise to use the straight-forward method of calculating the effective stress from determining separately the total stress and pore pressure distributions, finding the effective stress distribution quite simply as a subtraction between the two. The method is useful for the student and the practicing engineer alike.

The text starts with a brief summary of phase system calculations and how to determine the vertical distribution of stress underneath a loaded area applying the methods of 2:1, Boussinesq, and Westergaard.

I have long held that the piezocone (CPTU) is invaluable for the engineer charged with determining a soil profile and estimating a range of key routine soil parameters at a site. Accordingly, the second chapter gives a background to the soil profiling from CPTU data and determining soil compressibility from CPTU results.

The third chapter comprises a summary of methods of routine settlement analysis based on change of effective stress. More in-depth aspects, such as lateral flow are very only cursorily introduced or not at all, allowing the text to expand on the influence on the distribution of vertical stress due to adjacent loads, excavations, and groundwater table changes being present or acting simultaneously with the foundation analyzed.

Consolidation analysis is treated sparingly in the book, but for the use and design of acceleration of consolidation by means of vertical drains (Chapter 4), which is a very constructive tool for the geotechnical engineers that could be put to much more use in the current state-of-the-practice. Some new emphasis is placed on the analysis and calculation of secondary compression.

Chapter 5 deals with earth stress—‘earth pressure’—with emphasis on the Coulomb formulas and the effect of sloping retaining walls and sloping ground surface with surcharge and/or limited area surface or line loads per the requirements in current design manuals and codes. Chapter 6 addresses conventional methods of analyzing bearing capacity of shallow foundations is introduced and the importance of combining the bearing capacity design analysis with earth stress and horizontal and inclined loading is emphasized. The Limit States Design, or Load and Resistance Factor Design, for retaining walls and footings is also addressed in this context.

Chapter 7 addresses analysis and design of piles and pile groups, which topic is only very parsimoniously treated in most textbooks, and its treatment there is then often misleading. In this book, therefore, I have spent a good deal of effort on presenting the static design of piles considering "capacity", negative skin friction, and settlement, emphasizing the interaction of load-transfer and settlement (downdrag), which process I have termed "the Unified Piled Foundation Design" or just "the Unified Method" now accepted in up-to-date codes and standards. The settlement analysis of piles and pile groups combines load-transfer movement and settlement due to increase of effective stress in the soil due to the load applied to the piles and to the other effects in the immediate area of the pile group. The use of basic principles for design analysis of wide piled foundations is detailed as based on the necessity of strain-compatibility and the Fellenius-Franke method.

Chapter 8 deals with performance, analysis, and modeling of static loading tests, including the bidirectional test. In my opinion, no analysis of piles is completed until the results of the test are presented in terms of load distributions correlated to an effective stress analysis referencing the observed and/or expected foundation movement and settlement. I have emphasized pile load-movement response as expressed in t-z and q-z curves.

Chapter 9 contains basics of dynamic analysis and monitoring of pile driving. The treatment is not directed toward serving the expert, but is intended as background information for the general practicing engineer. The chapter includes aspects of vibratory driving and how vibrations from pile driving can affect neighboring areas and buildings.

Chapter 10 presents a summary of vibratory compaction including a couple of case histories. The chapter is intended to serve as a guide to planning and execution of compaction for reduction of settlement and for liquefaction remediation.

A brief chapter, Chapter 11, on slope stability analysis is also included intended as a brief background to a basic undergraduate course.

I have some critique on the use of working stress and limits states (factor of safety and load and resistance factors) in regard to use of "capacity" and "ultimate resistance". Chapter 12 presents a background and principles of this use.

Frequently, many of the difficulties experienced by the student in learning to use the analytical tools and methods of geotechnical engineering, as well as by the practicing engineer in applying the 'standard' knowledge and procedures, lie with a less than perfect feel for the terminology and concepts involved. To assist in this area, I have included a brief chapter (Chapter 13) on preferred terminology and an explanation to common foundation terms.

Everyone surely recognizes that the success of a design to a large extent rests on an equally successful construction of the designed project. However, many engineers appear oblivious to the key prerequisite for success of the construction: a dispute-free interaction between the engineers and the contractors during the construction, as judged from the many acutely inept specs texts common in the field. I have added a strongly felt commentary on the subject of terminology and style (Chapter 14).

A limited set of solved examples and problems for individual practice are presented in Chapters 15 and 16, respectively. The problems are of different degree of complexity, but even when very simple, they intend to be realistic and have some relevance to the practice of engineering design.

Finally, most facts, principles, and recommendations put forward in this book are those of others. Although several pertinent references are included in the book (Chapter 17), these are more to indicate to the reader where additional information can be obtained on a particular topic, rather than to give professional credit. However, I am well aware of my considerable indebtedness to others in the profession from mentors, colleagues, friends, and collaborators throughout my career, too many to mention. The opinions and sometimes strong statements are my own, however, and I am equally aware that time might suggest I should change them, often, but not always, toward the mellow side.

The "Red Book" is available for free downloading from my web site, [[www.Fellenius.net](http://www.Fellenius.net)] and dissemination of copies is encouraged. I have appreciated receiving comments and questions triggered by the earlier versions of the book and hope that this revised and expanded text will bring additional e-messages with questions and suggestions from students and colleagues (<Bengt@Fellenius.net>). Not least welcome are those pointing out typos and mistakes in the text in need of correction.

Note that the downloading link on my web site includes copies of several technical articles that provide a wider treatment of the subject matters.

The 2025 edition is updated from previous edition by correction of a few typos, some reformatting and rephrasing, expansion of a few issues, and improvement of phrasings. I have added some points in regard to addressing the consolidation in Chapter 3, design of wide piled rafts in Chapter 7, and static testing in Chapter 8. Examples 15.6.3 and 15.7 in Chapter 15 have been edited.

I am indebted to Dr. Mauricio Ochoa, PE, for his pertinent and much appreciated suggestions for clarifications and add-ons through several editions of the Red Book, as well as to Mr. Dmitry Olshansky, P.Eng., for alerting me to several typos and unclear expressions in the text, now revised.

Sidney January 2025  
Bengt H. Fellenius

# BASICS OF FOUNDATION DESIGN

## TABLE OF CONTENTS

- 1. Classification, Effective Stress, and Stress Distribution (18 pages)**
  - 1.1 Introduction
  - 1.2 Phase Parameters
  - 1.3 Soil Classification by Grain Size
  - 1.4 Effective Stress
  - 1.5 Stress Distribution
  - 1.6 Boussinesq Distribution
  - 1.7 Newmark Influence Chart
  - 1.8 Westergaard Distribution
  - 1.9 Characteristic Point
  
- 2. Cone Penetration Testing (44 pages)**
  - 2.1 Introduction
  - 2.2. Brief Survey of Soil Profiling Methods
    - 2.21 Begeman (1965)
    - 2.22 Sanglerat et al., (1974)
    - 2.23 Schmertmann (1978)
    - 2.24 Douglas and Olsen (1981)
    - 2.25 Vos (1982)
    - 2.26 Robertson et al., (1986) and Campanella and Robertson (1988)
    - 2.27 Robertson (1990)
  - 2.3 The Eslami-Fellenius CPTU Profiling and Classification
  - 2.4 The Eslami-Fellenius and Robertson (1990) Methods
  - 2.5 Comparisons
  - 2.6 Profiling Case Example
  - 2.7 Dissipation Time Measurement
  - 2.8 Inclination Measurement
  - 2.9 Shear-wave Measurement
  - 2.10 CPT Depth and Stress Adjustment
  - 2.11 Determining the Janbu Modulus Number,  $m$ , from CPT
  - 2.12 Determining Soil Parameters from CPTU Measurements
    - 2.12.1 Undrained Shear Strength
    - 2.12.2 Overconsolidation Ratio, OCR
    - 2.12.3 Earth Stress Coefficient,  $K_0$
    - 2.12.4 Friction Angle
    - 2.12.5 Density Index,  $I_D$
    - 2.12.6 Conversion to SPT N-index
    - 2.12.7 Determining the E-Modulus from CPT Cone-stress
    - 2.12.8 Assessing Liquefaction Susceptibility
      - 2.12.8.1 Cyclic Stress Ratio, CSR, and Cyclic Resistance Ratio, CRR
      - 2.12.8.2 Factor of Safety,  $F_S$ , against Liquefaction
      - 2.12.8.3 Comparison to Liquefaction Susceptibility Determined from SPT N-indices

- 3. Settlement (30 pages)**
  - 3.1 Introduction
  - 3.2 Movement, Settlement, and Creep
  - 3.3 Linear Elastic Deformation
  - 3.4 Non-Linear Elastic Deformation
  - 3.5 The Janbu Tangent Modulus Approach
    - 3.5.1 General
    - 3.5.2 Typical values of Modulus Number,  $m$
    - 3.5.3 Dense Coarse-Grained Soil,  $j = 1$
    - 3.5.4 Sandy or Silty Soil,  $j = 0.5$
    - 3.5.5 Cohesive Soil,  $j = 0$
    - 3.5.6 Application to Compacted Soils and Proctor Tests
  - 3.6 Evaluating oedometer tests by the  $e$ - $\lg p$  and the strain-stress methods
  - 3.7 The Janbu Method Compared to Conventional Methods
  - 3.8 Relative Degree of Compressibility
  - 3.9 Time Dependent Settlement
  - 3.10 Secondary Compression
  - 3.11 Example
  - 3.12 Magnitude of Acceptable Settlement
  - 3.13 Calculation of Settlement
  - 3.14 Special Approach — Block Analysis
  - 3.15 Horizontal Movement Caused By Embankment Load
  - 3.16 Settlement of footings
  - 3.17 Long-term Settlement of fill
  
- 4. Vertical drains to accelerate settlement (20 pages)**
  - 4.1 Introduction
  - 4.2 Conventional Approach to Dissipation and Consolidation
  - 4.3 Combined Vertical and Horizontal Flow
  - 4.4 Practical Aspects Influencing the Design of a Vertical Drain Project
    - 4.4.1 Drainage Blanket on the Ground Surface
    - 4.4.2 Effect of Winter Conditions
    - 4.4.3 Depth of Installation
    - 4.4.4 Width of Installation
    - 4.4.5 Effect of Pervious Horizontal Zones, Lenses, and Layers
    - 4.4.6 Surcharging
    - 4.4.7 Stage Construction
    - 4.4.8 Loading by Means of Vacuum
    - 4.4.9 Pore Pressure Gradient and Artesian Flow
    - 4.4.10 Secondary Compression
    - 4.4.11 Monitoring and Instrumentation
  - 4.5. Sand Drains
  - 4.6. Wick Drains
    - 4.6.1 Definition
    - 4.6.2 Permeability of the Filter Jacket
    - 4.6.3 Discharge Capacity
    - 4.6.4 Microfolding and Crimping
    - 4.6.5 Handling on Site
    - 4.6.6 Axial Tensile Strength of the Drain Core
    - 4.6.7 Smear Zone
    - 4.6.8 Site Investigation
    - 4.6.9 Spacing of Wick Drains
  - 4.7 Closing remarks



- 5. Earth Stress (14 pages)**
  - 5.1 Introduction
  - 5.2 The earth Stress Coefficient
  - 5.3 Active and Passive Earth Stress
  - 5.4 Surcharge, Line, and Strip Loads
  - 5.5 Factor of Safety and Resistance Factors
  - 5.6 Aspects of Structural Design
  - 5.7 Anchored Sheet-Pile Wall Example
  - 5.8 Retaining Wall on Footing Example
  - 5.9 Retaining with multiple horizontal supports
  - 5.10 Collapse of shored trench
  
- 6. Shallow Foundations (14 pages)**
  - 6.1 Introduction
  - 6.2 The Bearing Capacity Formula
  - 6.3 Inclined and Eccentric Loads
  - 6.4 Inclination and Shape factors
  - 6.5 Overturning
  - 6.6 Sliding
  - 6.7 Combined Calculation of a Wall and Footing
  - 6.8 Numerical Example
  - 6.9 Presumptive Stress
  - 6.10 Words of Caution
  
- 7. Static Analysis of Pile Load Transfer (102 pages)**
  - 7.1 Introduction
  - 7.2 Static Analysis
    - 7.2.1 Shaft Resistance
    - 7.2.2 Toe Resistance
    - 7.2.3 Ultimate Resistance
    - 7.2.4 Service Conditions
  - 7.3 Load-movement and load transfer
  - 7.4 Critical Depth
  - 7.5 Effect of Installation
  - 7.6 Residual Force
  - 7.7 Analysis of Tapered, Non-cylindrical, and Helical Piles
  - 7.8 Standard Penetration Test, SPT
  - 7.9 Cone Penetrometer Test, CPTU
    - 7.9.1 Schmertmann and Nottingham
    - 7.9.2 deRuiter and Beringen (Dutch)
    - 7.9.3 LCPC (French)
    - 7.9.4 Meyerhof
    - 7.9.5 Tumay and Fakhroo
    - 7.9.6 The ICP
    - 7.9.7 Eslami and Fellenius
    - 7.9.8 Comments on the Methods
  - 7.10 The Pressuremeter and Dilatometer Methods
    - 7.10.1 The Pressuremeter Method
    - 7.10.2 The Dilatometer Method
  - 7.11 Comments on Axial "Pile Capacity"
  - 7.12 Installation Phase
  - 7.13 Structural Strength

- 7.14 Negative Skin Friction, Equilibrium Plane, and Drag Force
  - 7.14.1 A pioneering case history
  - 7.14.2 Length of the Transition Zone
- 7.15 The Unified Design Method for Drag Force, Settlement, and Downdrag
  - 7.15.1 Steps of calculation
  - 7.15.2 Drag Force
  - 7.15.3 A case History of Applying the Unified Design Method
- 7.16 Piles in Swelling Soil
- 7.17 Settlement of Single Piles and Narrow Piled Foundations
  - 7.17.1 Load-transfer movement of single piles and narrow piled foundations
  - 7.17.2 Settlement below the pile toe level
  - 7.17.3 Downdrag
- 7.18 Wide Piled Foundations
  - 7.18.1 Case References
  - 7.18.2 Settlement due to compression of pile and soil body
  - 7.18.3 Settlement due to pile compression and load transfer movement
  - 7.18.4 Settlement due to compression of the soil below the pile toe level
  - 7.18.5 Contact stress
  - 7.18.6 Load distribution across the raft and between piles
  - 7.18.7 Design and long-term conditions
  - 7.18.7 Conventional analysis of a wide piled raft
  - 7.18.8 Settlement across the wide piled foundations
- 7.19 Piled Raft and Piled Pad Foundations
- 7.20. A Few Related Comments
  - 7.20.1 Pile Spacing
  - 7.20.2 Pile Size
  - 7.20.3 Design of Piles for Horizontal Loading
  - 7.20.4 Seismic Design of Lateral Pile Behavior
  - 7.20.5 Pile Testing
  - 7.20.6 Pile Jetting
  - 7.20.7 Bitumen Coating
  - 7.20.8 Pile Buckling
  - 7.20.9 Plugging of Open-Toe Pipe Piles and in-between Flanges of H-piles
  - 7.20.10 Sweeping and Bending of Piles
  - 7.20.11 Influence on Adjacent Foundations
  - 7.20.12 Reducing differential load or settlement by shortening or lengthening perimeter piles
- 7.21 Capacity as a function of time
- 7.22 Scour
- 7.23 Conclusions

## **8. Analysis of Results from the Static Loading Test (86 pages)**

- 8.1 Introduction
- 8.2 Common Definitions of "Capacity"
  - 8.2.1 Davisson Offset Limit
  - 8.2.2 Hansen 80-% criterion
  - 8.2.3 Hansen 90-% criterion
  - 8.2.4 Chin-Kondner Extrapolation
  - 8.2.5 Decourt Extrapolation
  - 8.2.6 De Beer Intersection or Yield Load
  - 8.2.7 The Creep Method
  - 8.2.8 Load at Maximum Curvature
- 8.3 Factor of Safety

- 8.4 Choice of Criterion
- 8.5 Force-movement Response and t-z/q-z Functions
  - 8.5.1 The Gwizdala function
  - 8.5.2 The Hyperbolic function
  - 8.5.3 The vander Veen function
  - 8.5.4 The 80-% function
  - 8.5.5 The Zhang function
  - 8.5.6 The Vijayvergiya function
  - 8.5.7 The Rahman function
  - 8.5.8 The Eight function curves compiled
- 8.6 Instrumented Tests
  - 8.6.1 Telltale Instrumentation
  - 8.6.2 Determining Load Distribution from Telltale Measurements
  - 8.6.3 Brief Notes on Strain-gage Instrumentation
- 8.7 The Bidirectional Test
  - 8.7.1 Equivalent Head-down Load-distribution
  - 8.7.2 Equivalent Head-down Loading Test
- 8.8 Residual Force
  - 8.8.1 Principles of Development of Residual Force
  - 8.8.2 Residual Force in an Instrumented pile
  - 8.8.3 False" and "True" Load Distributions and Determining Distribution of Residual Force
  - 8.8.4 Case history of residual force and other influences
  - 8.8.5 Case history on calculation true load distribution
- 8.9 Modulus of 'Elasticity' and Axial Stiffness of the Instrumented pile
  - 8.9.1 Aspects to consider
  - 8.9.2 Converting strain to load using the pile secant stiffness
  - 8.9.3 The tangent method
  - 8.9.4 Limitation of the tangent method
  - 8.9.5 Adverse effect of unloading/reloading cycles
  - 8.9.6 Concluding remarks on modulus and EA-parameter
  - 8.9.7 Procedure for fitting a simulated test curve to a measured using t-z and q-z functions
- 8.10 Example of Evaluation of Records from a Head-down Test
  - 8.10.1 Introduction
  - 8.10.2 Test results
  - 8.10.3 Analysis of the test results
  - 8.10.4 Closing remarks
- 8.11 Example of use of results from a routine test

## **9. Pile Dynamics (54 pages)**

- 9.1 Introduction
- 9.2. Principles of Hammer Function and Performance
- 9.3. Hammer Types
  - 9.3.1 Drop hammers
  - 9.3.2 Air/Steam hammers
  - 9.3.3 Diesel hammers
  - 9.3.4 Direct-drive hammers
  - 9.3.5 Vibratory hammers
- 9.4 Basic Concepts
- 9.5 Wave Equation Analysis of Pile Driving
- 9.6 Hammer selection by means of wave equation analysis
- 9.7 Aspects to consider in reviewing results of wave equation analysis

- 9.8 High-strain dynamic testing with the Pile Driving Analyzer
  - 9.8.1 Wave traces
  - 9.8.2 Transferred energy
  - 9.8.3 Movement
- 9.9 Pile Integrity
  - 9.9.1 Integrity determined from high-strain testing
  - 9.9.2 Integrity determined from low-strain testing
- 9.10 Case Method Estimate of Capacity
- 9.11 CAPWAP determined pile capacity
- 9.12 Results of a PDA Test
- 9.13 Comments on current state of practice of dynamic monitoring
- 9.14 Long duration impulse testing method—The Statnamic and Fundex Methods
- 9.15 Vibratory pile driving
  - 9.15.1 Pile shaft resistance
  - 9.15.2 Pile toe resistance
  - 9.15.3 Vibrator performance parameters
  - 9.15.4 Vibratory driving planned from penetration tests
- 9.16 Vibration caused by pile driving
- 9.17 Settlement, compaction, and densification caused by pile driving vibrations

## **10. Vibratory Compaction (42 pages)**

- 10.1 Introduction
- 10.2 Vibrator Characteristics
- 10.3 Overview of Compaction Methods
  - 10.3.1 Dynamic compaction
  - 10.3.2 Impact roller
  - 10.3.3 Vibratory compaction plate
  - 10.3.4 Displacement column method
  - 10.3.5 Vibro-probe compaction method
  - 10.3.6 Vibroflotation
  - 10.3.7 Compaction by explosives
- 10.4 Resonance Compaction System
- 10.5 Vibratory Compaction Process
  - 10.5.1 Compaction point spacing
  - 10.5.2 Compaction process
  - 10.5.3 Vibration frequency
  - 10.5.4 Liquefaction during vibratory compaction
  - 10.5.5 Horizontal ground vibrations
  - 10.5.6 Horizontal stress increase
  - 10.5.7 Preloading effect of vibratory compaction
  - 10.5.8 Increase of soil strength and stiffness with time
  - 10.5.8 Compactability
  - 10.5.9 Compactability
- 10.6 Analysis of Results of Deep Compaction
  - 10.6.1 Determining compressibility of the compacted soil
  - 10.6.2 Determining susceptibility to liquefaction
  - 10.6.1 Drivability assessment
- 10.7. Case Histories
  - 10.7.1 Liquefaction risk and achieving compaction/densification
  - 10.7.2 Underwater resonance compaction of sand fill inside a cofferdam
  - 10.7.3 Vibratory compaction at Annacis Channel, BC
  - 10.7.4 Compaction from pile driving

- 11. Slope Stability (10 pages)**
  - 11.1 Introduction
  - 11.2 Example of slip circle analysis
  - 11.3 Friction circle
  - 11.4 Logarithmic spiral
  - 11.5 Analysis for  $c'$ - $\phi'$  conditions
  - 11.6 Software
  
- 12. Working Stress and Load and Resistance Factor Design (16 pages)**
  - 12.1 Introduction
  - 12.2 The Factor of Safety
  - 12.3 Limit States and Load and Resistance Factor Design
  - 12.4 Factor of safety and resistance factors for piled foundations
  - 12.5 The Eurocode and the AASHTO Specs
    - 12.5.1 The Eurocode
    - 12.5.2 The AASHTO Specs
  - 12.6 Serviceability Limit States
  - 12.7 Concluding Remarks
  
- 13. Specifications and Dispute Avoidance (8 pages)**
  - 13.1 Introduction and examples
  - 13.2 A few special pointers
  
- 14. Terminology and Style (18 pages)**
  - 14.1 Introduction and basic definitions
  - 14.2 Brief compilation of some definitions and terms
  - 14.3 Units
  - 14.4 Spelling rules and special aspects on style
  - 14.5 References and bibliography
  - 14.6 Re-use of figures and data
  - 14.7 Some useful unit conversions
  
- 15. Examples (47 pages)**
  - 15.1 Introduction
  - 15.2 Stress calculations
  - 15.3 Settlement calculations
  - 15.4 Earth stress and bearing capacity of retaining walls
  - 15.5 Pile capacity and load-transfer
  - 15.6 Analysis of pile loading tests
  - 15.7 Design of piled foundations for settlement
  
- 16. Problems (10 pages)**
  - 16.1 Introduction
  - 16.2 Stress distribution
  - 16.3 Settlement analysis
  - 16.4 Earth stress and bearing capacity of shallow foundations
  - 16.5 Deep foundations
  
- 17. References (22 pages)**
  
- 18. Index (4 pages)**



# CHAPTER 1

## CLASSIFICATION, EFFECTIVE STRESS, and STRESS DISTRIBUTION

### 1.1 Introduction

Before a foundation design can be embarked on, the associated soil profile must be well established. The soil profile is compiled from three cornerstones of information:

- assessment of the overall site geology
- in-situ testing results, particularly continuous tests, such as the CPTU
- pore pressure (piezometer) observations
- laboratory classification and testing of recovered soil samples
- particulars on the type and condition of the foundations of adjacent structures

The soil description must also include a summary of the overall geology of the site. N.B., projects where construction difficulties, disputes, and litigations arise often have one thing in common: borehole logs and soundings were thought sufficient when determining the soil profile—they were not—and linear interpolation between boreholes was applied disregarding information on geology, scant as it was.

The essential part of the foundation design is to devise a foundation type and size that will result in acceptable values of deformation (settlement) and an adequate margin of safety to excessive deformation, the latter is frequently thought to mean margin of safety to "failure", i.e., defined as full mobilization of the soil strength. Deformation is *due to change* of effective stress and soil shear resistance is *proportional* to effective stress. Therefore, all foundation designs must start with determining the effective stress distribution of the soil around and below the foundation unit. That initial distribution then serves as basis for the design analysis. The current condition may well be quite different in the future—the long-term condition lying years ahead in time.

Effective stress is the total stress minus the pore pressure (the water pressure in the voids). Determining the effective stress requires that the basic parameters of the soil are known. The basic parameters are the pore pressure distribution and the Phase Parameters, such as water content<sup>1)</sup> and total density. Unfortunately, far too many soil reports on site conditions lack adequate information on both pore pressure distribution and phase parameters.

### 1.2 Phase Parameters

Soil is an "interparticulate medium". A soil mass consists of a heterogeneous collection of solid particles with voids in between. The solids are made up of grains of minerals or organic material. The voids contain water and gas. The water can be clean (pure) or include dissolved salts and gas. The gas is similar

---

<sup>1)</sup> The term "moisture content" is sometimes used in the same sense as "water content". Most people, even geotechnical engineers, will consider that calling a soil "moist", "damp", or "wet" signifies three different conditions of the soils (though undefined numerically). It follows that laymen—read lawyers and judges—will believe and expect that "moisture content" is something different to "water content", perhaps thinking that the former indicates a less than saturated soil. However, there is no difference. Saying "moisture" instead of "water" implies, or intends to imply, that the speaker possesses a greater degree of sophistication than conveyed by simply saying "water content" and, because the term is not immediately understood by the layman, it intends to send the message that the Speaker is in the "know", a specialist of some stature. Don't fall into that trap. Use "water content". Remember, we should strive to use simple terms that laymen can understand. (Abbreviated quote from Chapter 14).

to ordinary air, sometimes mixed with gas generated from decaying organic matter. The *solids*, the *water*, and the *gas* are termed the three **phases** of the soil.

To aid a rational analysis of a soil mass, the three phases are “disconnected”. Soil analysis makes use of basic definitions and relations of volume, mass, density, water content, saturation, void ratio, etc., as indicated in Figure 1.1. The definitions are related and knowledge of a few will let the geotechnical engineer derive all the others.

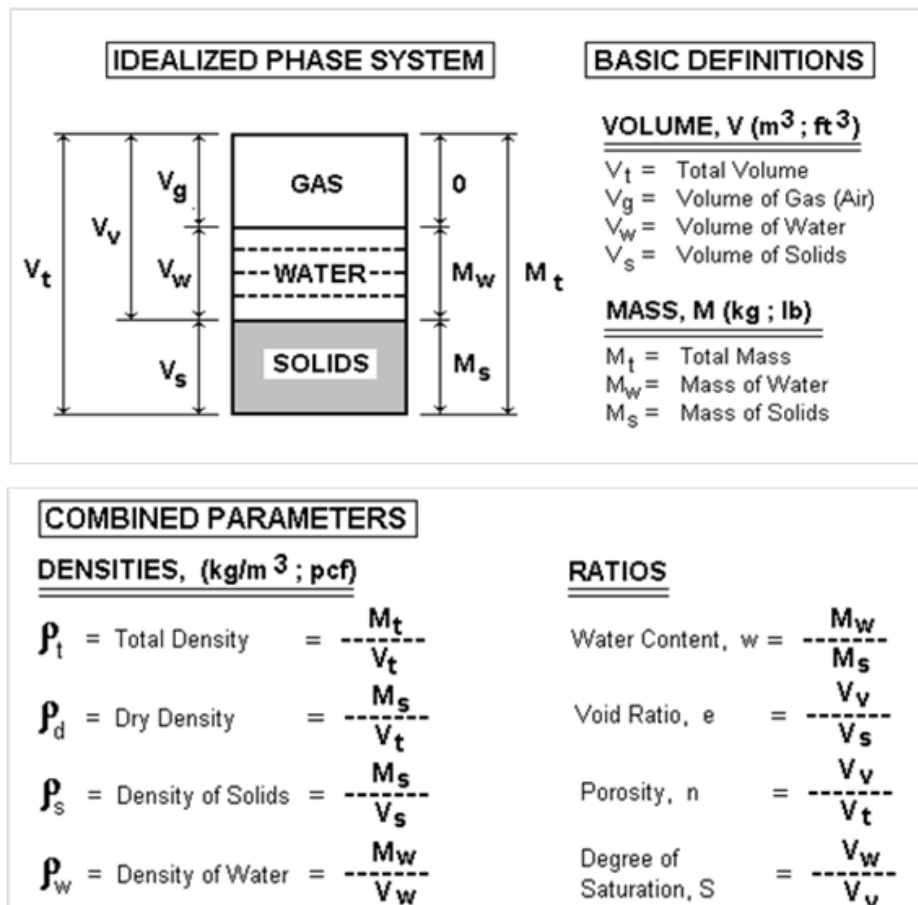


Fig. 1.1 The Phase System definitions

The need for phase systems calculation arises, for example, when the engineer wants to establish the effective stress profile at a site and does not know the total density of the soil, only the water content. Or, when determining the dry density and degree of saturation from the initial water content and total density in a Proctor test. Or, when calculating the final void ratio from the measured final water content in an oedometer test. While the water content is usually a measured quantity and, as such, a reliable number, many of the other parameters reported by a laboratory are based on an assumed value of solid density, usually taken as 2,670 kg/m<sup>3</sup> plus the assumption that the tested sample is saturated. The latter assumption is often very wrong and the error can result in significantly incorrect soil parameters.

Starting from the definitions shown in Figure 1.1, a series of useful formulae can be derived, as follows:

$$(1.1) \quad S = \frac{w}{\rho_w} \times \frac{\rho_s \rho_d}{\rho_s - \rho_d} = \frac{w}{e} \times \frac{\rho_s}{\rho_w}$$



$$(1.2) \quad w = S \rho_w \times \frac{\rho_s - \rho_d}{\rho_s \rho_d} = \frac{\rho_t}{\rho_d} - 1$$

$$(1.3) \quad \rho_{SAT} = \frac{M_w + \rho_w V_g + M_s}{V_t} = \rho_d + \rho_w \left(1 - \frac{\rho_d}{\rho_s}\right) = \frac{\rho_d}{\rho_s} (\rho_s + e \rho_w) = \rho_s \frac{1+w}{1+e}$$

$$(1.4) \quad \rho_d = \frac{\rho_s}{1+e} = \frac{\rho_t}{1+w} = \frac{\rho_w S}{w + \frac{\rho_w}{\rho_s} S}$$

$$(1.5) \quad \rho_t = \frac{\rho_s(1+w)}{1+e} = \rho_d(1+w)$$

$$(1.6) \quad e = \frac{n}{1-n} = \frac{\rho_s}{\rho_d} - 1 = \frac{w}{S} \times \frac{\rho_s}{\rho_w}$$

$$(1.7) \quad n = \frac{e}{1+e} = 1 - \frac{\rho_d}{\rho_s}$$

When performing phase calculations, the engineer normally knows or assumes the value of the density of the soil solids,  $\rho_s$ . Sometimes, the soil can be assumed to be fully saturated (however, presence of gas in fine-grained soils may often result in their not being fully saturated even well below the groundwater table; organic soils are rarely saturated and fills are almost never saturated). Knowing the density of the solids and one more parameter, such as the water content, all other relations can be calculated using the above formulae (they can also be found in many elementary textbooks, or easily be derived from the basic definitions and relations). I have included a few of the equations in an Excel "365 Cribsheet", which can be downloaded from my web site: [www.Fellenius.net](http://www.Fellenius.net).

The density of water is usually  $1,000 \text{ kg/m}^3$ . However, temperature and, especially, salt content can change this value by more than a few percentage points. For example, places in Syracuse, NY, have groundwater that has a salt content of up to 16 % by weight. Such large salt content cannot be disregarded when determining distribution of pore pressure and effective stress.

While most silica-based clays can be assumed to be made up of particles with a solid density of  $2,670 \text{ kg/m}^3$  (165 pcf), the solid density of other clay types may be quite different. For example, particles of calcareous clays can have a solid density of  $2,800 \text{ kg/m}^3$  (175 pcf). However, at the same time, calcareous soils, in particular coral sands, can have such a large portion of voids that the solid density is quite low compared to that of silica soils (note, "solid density" is often called "bulk density"). Volcanic sands (pumiceous material) can also have a low bulk density.

Soils composed of different minerals can have a very different mechanical response to load. For example, just a few percent of mica, a clay mineral, in a sand will make the sand both weaker and more compressible, all other aspects equal (Gilboy 1928).

Organic materials usually have a dry density that is much smaller than inorganic material. Therefore, when soils contain organics, their in-place average solid density of the particles is usually smaller than for inorganic materials. If the organic content is 3 % (of dry weight) or larger, the soil should be called "slightly organic" and at 5 % organic content, the soil should be called "organic" (as adjective). Organic soils will have smaller shear strength and larger compressibility as opposed to inorganic soils. For example, an organic clay will exhibit much increased secondary compression (Section 3.9).

Soil grains are composed of minerals and the solid density varies between different minerals. [Table 1.1](#) below lists some values of solid density for minerals that are common in rocks and, therefore, common in soils. The need for listing the density parameters with units could have been avoided by using the ratio of the densities of the solids to the density of water, which ratio was termed "specific gravity" in old terminology, now abandoned. In modern international terminology, the ratio is sometimes called "relative density" (see the note below the table). However, presenting the density parameter with units, as opposed to relating it to the density of water, avoids the conflict of which term to use; either the correct term, "solid density" with mass units, which many, but not all, would misunderstand, or the incorrect term, which all understand, but the use of which would suggest ignorance of current terminology convention. (Shifting to a home-made term, such as "specific density", which sometimes pops up in the literature, does not make the ignorance smaller).

**Table 1.1 Solid Density for Minerals**

Mineral Type	Solid Density	
	kg/m <sup>3</sup>	pcf
Amphibole	≅3,000+	190
Calcite	2,800	180
Quartz	2,670	165
Mica	2,800	175
Pyrite	5,000	310
Illite	2,700	170

The term "relative density", designated, " $D_r$ ", is used when describing a state of "compactness" or "compactness condition". The defined states are very loose, loose, compact, dense, and very dense. Relative density is not expressed in mass/volume, but is correlated to the N-index of the Standard Penetration test, SPT (for the correlation, see the Excel "365 Cribsheet", which can be downloaded from my web site: [www.Fellenius.net](http://www.Fellenius.net)).

The total density of soil depends not only on the mineral of the grains, but very much also on the soil void ratio and degree of saturation. Therefore, the total density of soils can vary within wide boundaries. [Tables 1.2 and 1.3](#) list some representative values.

A frequently applied expression is the "density index",  $I_D$ . The definition of the density index,  $I_D$ , is based on the assumption that the void ratio of the soil can be reliably determined for standardized procedures to create "maximum" and "minimum" density of a natural soil [ $I_D = (e_{max} - e)/(e_{max} - e_{min})$ ]. Over the years, the density index has been used as a parameter to describe geotechnical parameters of sand deposits and correlations have been developed to estimate the angle of internal friction, liquefaction potential, and soil modulus. However, as has been shown by many, e.g., Tavenas and LaRochelle (1972), the density index is a highly imprecise and non-reproducible parameter as explained below.

**Table 1.2 Total saturated density for some typical soils**

Soil Type	<u>Saturated Total Density</u>	
	Metric (SI) units kg/m <sup>3</sup>	English units pcf
Sands; gravels	1,900 - 2,300	118 - 144
Sandy Silts	1,700 - 2,200	105 - 138
Clayey Silts and Silts	1,500 - 1,900	95 - 120
Soft clays	1,300 - 1,800	80 - 112
Firm clays	1,600 - 2,100	100 - 130
Glacial till	2,100 - 2,400	130 - 150
Peat	1,000 - 1,200	62 - 75
Organic silt	1,200 - 1,900	75 - 118
Granular fill	1,900 - 2,200	118 - 140

**Table 1.3 Total saturated density for uniform silica sand**

“Relative” Density	Total Saturated Density (kg/m <sup>3</sup> )	Water Content (%)	Void Ratio (approximate) (- - -)
Very dense	2,200	15	0.4
Dense	2,100	19	0.5
Compact	2,050	22	0.6
Loose	2,000	26	0.7
Very loose	1,900	30	0.8

Values are based on the solid density being 2,670 kg/m<sup>3</sup>

A void ratio value determined on a soil sample, usually coarse-grained, is usually provided with two-decimal precision. However, the void ratio value is rarely more precise than by about  $0.05 \pm$ . For loose to compact sand, the in-situ void ratio typically ranges from about 0.40 through 0.60, depending on grain size gradation. Therefore, for a given sample, say, with an in-situ void ratio of 0.40, where typically, the maximum and minimum void ratios lie between 0.30 and 0.70, the  $I_D$  is 75 %. However, considering that the error, very likely, would be 0.05 up or down for each of the three values, the error in a particular  $I_D$  could be almost 20 %. (A 0.05 change in void ratio corresponds to a less than 2 % change in water content for a sand with  $e = 0.40$ , assuming that the degree of saturation,  $S$ , is 100 %, which is difficult to ensure for a sand sample). Tavenas and LaRoche (1972) presented an extensive and detailed study of the Density Index and indicated that the average error is 18 % and concluded that the index “*cannot be used as a base parameter of any calculation*”. Indeed, any formula or numerical expression applying the  $I_D$  should be considered suspect and only applied with great caution, if at all.

### 1.3 Soil Classification by Grain Size

All languages have terms for "clay", "sand", "gravel", etc. that are primarily based on grain size assessment. In the very beginning of the 20th century, Atterberg, a Swedish scientist and agriculturalist, proposed a classification system based on specific grain sizes. With minor modifications, the Atterberg system is still used and are the basis of the International Geotechnical Standard listed in Table 1.4.

Soil is made up of grains with a wide range of sizes and is named according to the portion of the specific grain sizes. Several classification systems are in use, e.g., ASTM, AASHTO, and International Geotechnical Society. Table 1.5 indicates the latter, which is also the Canadian standard (CFEM 1992).

The International (and Canadian) naming convention differs in some aspects from the AASHTO and ASTM systems which are dominant in US practice. For example, the boundary between silt and sand in the international standard is at 0.060 mm, whereas the AASHTO and ASTM standards place that boundary at Sieve #200 which has an opening of 0.075 mm. Table 1.5 follows the International standard. For details and examples of classification systems, see Holtz and Kovacs (1981) and Holtz et al. (2011).

**Table 1.4 Classification of Grain Size Boundaries (mm)**

<b>Clay</b>	<0.002		
<b>Silt</b>			
Fine silt	0.002	—	0.006
Medium silt	0.006	—	0.02
Coarse silt	0.02	—	0.06
<b>Sand</b>			
Fine sand	0.06	—	0.2
Medium sand	0.2	—	0.6
Coarse sand	0.6	—	2.0
<b>Gravel</b>			
Fine gravel	2	—	6
Medium gravel	6	—	20
Coarse gravel	20	—	60
<b>Cobbles</b>	60	—	200
<b>Boulders</b>			>200

**Table 1.5 Classification of Grain Size Combinations (mm)**

"Noun" (Clay, Silt, Sand, Gravel)	35	< 100 %
"and" plus "noun"	20 %	< 35 %
"adjective" (clayey, silty, sandy)	10%	< 20%
"trace" (clay, silt, sand, gravel)	1 %	< 10 %

The grain size distribution for a soil is determined using a standard set of sieves. Conventionally, the results of the sieve analysis are plotted in diagram drawn with the abscissa in logarithmic scale as shown in Figure 1.2. The three grain size curves, A, B, and C, shown are classified according to Table 1.5 as A: "*Sand trace gravel trace silt*". B: "*Sandy clay some silt*", and C: would be named *clayey sandy silt some gravel*. Samples A and B are alluvial soils and are suitably named. However, Sample C, having 21 %, 44 %, 23 %, and 12 % of clay, silt, sand, and gravel size grains, is from a glacial till, for which soil, all grain size portions are conventionally named as adjective to the noun "till", i.e., Sample C is a "*clayey sandy silty glacial till*".

The grain-size fractions are fundamental parameters for a foundation design. The above classification follows the Canadian standard (and the international). Several other systems are in use. In the US, the Unified Soil Classification System (USCS) is the dominant system (e.g., Holtz and Kovacs 1981 and Holtz et al. 2011). Therefore, in addition to the soil description, every borehole log in a geotechnical engineering report should include the results of grain size analyses (with numericals) to allow the users to apply their preferred system.

Note that soils are also classified by grain angularity, constituent minerals, organic content, etc.

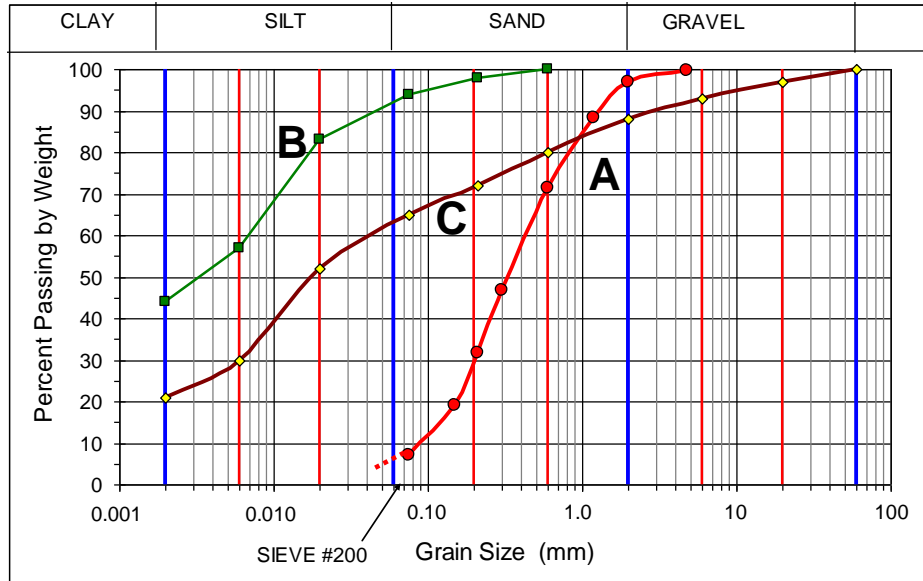


Fig. 1.2 Grain size diagram

Sometimes, grain-size analysis results are plotted in a three-axes diagram called "ternary diagram" as illustrated in Figure 1.3, which allows for a description according to grain size portions Clay+Silt+Sand to be obtained at a glance.

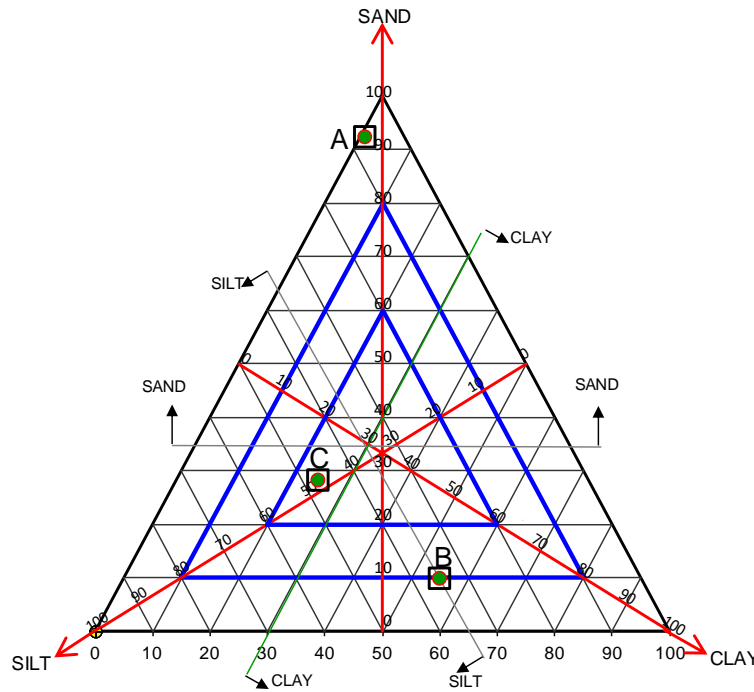


Fig. 1.3 Example of a ternary diagram

#### 1.4. Effective Stress

As mentioned, effective stress is the total stress minus the pore pressure (the water pressure in the voids). Total stress at a certain depth below a level ground surface is the easiest of all values to determine as it is the summation of the total unit weight (total density times gravity constant) and depth. Where the pore pressure is hydrostatically distributed below the groundwater table, which is defined as the uppermost level of zero pore pressure (equal to atmospheric pressure), the pore pressure at a certain depth is equal to the density of water times the distance from that depth up to the groundwater table. (Notice, the soil can be partially saturated also above the groundwater table. Then, because of capillary action, pore pressures in the partially saturated zone above the groundwater table may be negative. In routine calculations, however, pore pressures are usually assumed to be zero in the zone above the groundwater table).

Notice that the pore pressure distribution is not always hydrostatic, far from always, actually. Hydrostatic pore water pressure has a vertical pressure gradient that is equal to unity (no vertical flow). However, the pore pressure at a site may have a downward gradient from a perched groundwater table, or an upward gradient from an **aquifer** down below (an aquifer is a soil layer containing free-flowing water, or a layer sandwiched between soil layers that are less "free-flowing", i.e., less pervious than the boundary layers). Moreover, in areas below or close to the seashore and in areas close to bedrock containing salt (NaCl), the pore water may include dissolved salt and its density may be correspondingly larger than 1,000 kg/m<sup>3</sup>.

Frequently, the common method of determining the effective stress,  $\Delta\sigma'$ , contributed by a specific soil layer is to multiply the buoyant unit weight,  $\gamma'$ , of the soil with the layer thickness,  $\Delta h$ , as indicated in Eq. 1.8a.

$$(1.8a) \quad \Delta\sigma' = \gamma' \Delta h$$

The effective stress at a depth,  $\sigma'_z$  is the sum of the contributions from the soil layers, as follows.

$$(1.8b) \quad \sigma'_z = \sum(\gamma' \Delta h)$$

The buoyant unit weight,  $\gamma'$ , is often thought to be equal to the total unit weight ( $\gamma_t$ ) of the soil minus the unit weight of water ( $\gamma_w$ ) which presupposes that there is no vertical gradient or water flow in the soil,  $i = 0$ , defined below. However, this is only a special case. Because most sites display either an upward flow (maybe even artesian; the head at a point is greater than the depth to the point) or a downward flow, calculations of effective stress must consider the effect of the gradient—the buoyant unit weight is a function of the gradient in the soil as follows (Eq. 1.8c). N.B., the term "flow" implies a movement at some velocity of the water. However, it is here assumed that the flow is extremely slow and occurs without imparting any dynamic effect.

$$(1.8c) \quad \gamma' = \gamma_t - \gamma_w(1-i)$$

where  $\sigma'$  = effective overburden stress

$\Delta h$  = layer thickness

$\gamma'$  = buoyant unit weight

$\gamma_t$  = total (bulk) unit weight

$\gamma_w$  = unit weight of water

$i$  = gradient; the difference of head at two points (difference in water elevation) divided by the distance the water has to flow between these two points (equal head means no flow,  $i = 0$ ). Upward flow direction is defined as negative direction, i.e.,  $i < 0$ .

A vertical flow is a non-hydrostatic condition. If the flow is upward, the gradient is negative; if downward, the gradient is positive. The flow can be minimal and have no obvious velocity. For artesian conditions, which is a non-hydrostatic condition, the then upward gradient results in the buoyant weight of the soil is smaller than for a hydrostatic condition from the ground surface downward. Therefore, the effective stress is smaller too and the soil strength is smaller than for the hydrostatic condition. For example, a "quick sand" condition occurs when the upward gradient is so large, ( $i$  approaches unity) that the effective stress (and buoyant unit weight,  $\gamma'$ ), approaches zero. Note that "quick sand" is not a particularly "quick" type of sand, but a soil, usually a silty fine sand, subjected to an upward pore pressure gradient. (You cannot sink in quick sand. You will actually float because your unit weight is half that of the quick sand. So, theoretically, you cannot drown. In practice, of course, it depends on which half of you that is submerged).

The gradient in a non-hydrostatic condition is often awkward to determine. However, the difficulty can be avoided, because the effective stress is most easily found by calculating the total stress and the pore water pressure separately. The effective stress is then obtained by subtracting the latter from the former.

Note, the difference in terminology—effective *stress* and pore *pressure*—which reflects the fundamental difference between forces in soil as opposed to in water. Stress is directional, that is, stress changes depend on the orientation of the plane of action in the soil. In contrast, pressure is omni-directional, that is, independent of the orientation; equal in all directions. Don't use the term "*soil pressure*", it is a misnomer. The term "pressure" should only be applied to gas and water.

The soil stresses, total and effective, and the water pressures are determined, as follows: The **total vertical stress** (symbol  $\sigma_z$ ) at a point in the soil profile (also called "total overburden stress") is calculated as the stress exerted by a soil column determined by multiplying the soil total (or bulk) unit weight with the height of the column (or the sum of separate weights when the soil profile is made up of a series of separate soil layers having different unit weights). The symbol for the total unit weight is  $\gamma_t$  (the subscript "t" stands for "total").

$$(1.9) \quad \sigma_z = \gamma_t z \quad \text{or:} \quad \sigma_z = \sum \Delta \sigma_z = \sum (\gamma_t \Delta h)$$

Similarly, the **pore pressure** (symbol  $u$ ), as measured in a stand-pipe, is equal to the unit weight of water,  $\gamma_w$ , times the height of the water column,  $h$ , in the stand-pipe. (If the pore pressure is measured directly, the head of water (height of the water column) is equal to the pressure divided by the unit weight of the water,  $\gamma_w$ ). For an informative detailed discussion on pore pressure see Lu and Likos 2023.

$$(1.10) \quad u = \gamma_w h$$

The height of the column of water (the head) representing the water pressure is usually not the distance to the ground surface nor, even, to the groundwater table. For this reason, the height is usually referred to as the "phreatic height" or the "piezometric height" to separate it from the depth below the groundwater table or depth below the ground surface.

The pore pressure distribution is determined by applying the fact that (in stationary situations) the pore pressure distribution can be assumed linear in each individual, or separate, soil layer, and, in pervious soil layers "sandwiched" between less pervious layers, the pore pressure is hydrostatic (that is, the vertical gradient within the sandwiched layer is unity. Note, if the pore pressure distribution within a specific soil layer is not linear, then, the soil layer is undergoing consolidation, which is not a stationary condition).

The **effective overburden stress** (symbol  $\sigma'_z$ ), also called "effective vertical stress", is then obtained as the difference between total stress ( $\sigma_z$ ) and pore pressure ( $u$ ).

$$(1.11) \quad \sigma'_z = \sigma_z - u_z = \gamma_t z - \gamma_w h$$

Usually, the geotechnical engineer provides a unit density,  $\rho$ , instead of the unit weight,  $\gamma$ . The unit density is mass per volume and unit weight is force per volume. Because in the customary English system of units, both types of units are given as lb/volume, the difference is not clear (that one is pound-mass and the other is pound-force is not normally indicated, though pound-force is the most common variant). In the SI-system, unit density is given in  $\text{kg/m}^3$  and unit weight is given in  $\text{N/m}^3$ . Unit weight is unit density times the gravitational constant,  $g$ . (For most foundation engineering purposes, the gravitational constant can be taken to be  $10 \text{ m/s}^2$  rather than the overly exact value of  $9.81 \text{ m/s}^2$ ; besides, the second decimal varies across the Earth). Beware of asinine terms such as “weight density”.

$$(1.12) \quad \gamma = \rho g$$

Many soil reports do not indicate the bulk or total soil density,  $\rho_t$ , and provide only the water content,  $w$ , and the dry density,  $\rho_d$ . Knowing the dry density and water content, the total density of a saturated soil can be calculated as:

$$(1.13) \quad \rho_t = \rho_d (1 + w)$$

### 1.5 Stress Distribution

Load applied to the surface of a body distributes into the body over a successively wider area. The simplest way to calculate the stress distribution is by means of the 2(V):1(H) method. This method assumes that the load is distributed over an area that increases in width in proportion to the depth below the loaded area, as is illustrated in Figure 1.4. Since the vertical load,  $Q$ , acts over the increasingly larger area, the stress (load per surface area) diminishes with depth. The mathematical relation is as follows.

$$(1.14) \quad q_z = q_0 \times \frac{B \times L}{(B + z) \times (L + z)}$$

where  $q_z$  = stress at Depth  $z$   
 $z$  = depth where  $q_z$  is considered  
 $B$  = width (breadth) of loaded area  
 $L$  = length of loaded area  
 $q_0$  = applied stress =  $Q/B \times L$ .

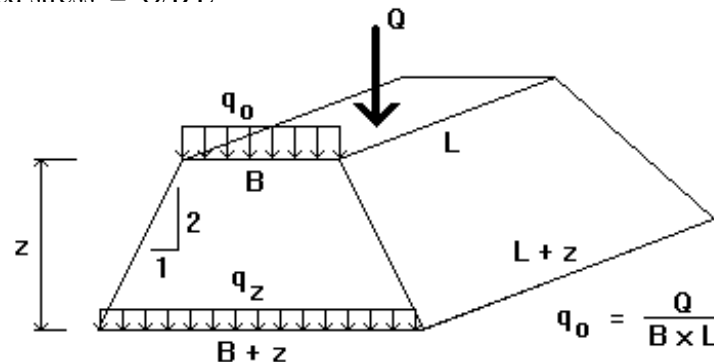


Fig. 1.4 The 2:1 method

Note, the 2:1 distribution is only valid inside (below) the footprint of the loaded area and must never be used to calculate stress outside the footprint.



**Example 1.1** The principles of calculating effective stress and stress distribution are illustrated by the calculations involved in the following soil profile: An upper 4 m thick layer of normally consolidated sandy silt lies on 17 m of soft, compressible, slightly overconsolidated clay, followed by 6 m of medium dense silty sand, below which follows a thick deposit of medium dense to very dense sandy ablation glacial till to end of borehole at 33 m depth. The densities of the four soil layers and the earth fill are:  $2,000 \text{ kg/m}^3$ ,  $1,700 \text{ kg/m}^3$ ,  $2,100 \text{ kg/m}^3$ ,  $2,200 \text{ kg/m}^3$ , and  $2,000 \text{ kg/m}^3$ , respectively. The groundwater table lies at a depth of 1.0 m. For “original conditions” (or initial condition), the pore pressure is hydrostatically distributed from the groundwater table throughout the soil profile. For “final conditions”, the pore pressure in the sand has increased to a phreatic height above ground of 5 m; the fact that the phreatic height reaches above ground makes the pressure condition “artesian”. It is still hydrostatically distributed in the sand (as is the case when a more pervious soil layer is sandwiched between less pervious soils—a key fact to consider when calculating the distribution of pore pressure and effective stress; a non-linear distribution within a soil layer is a sign of ongoing consolidation). Moreover, the pore pressure in the clay has become non-hydrostatic. Note, however, that it is linear, assuming that the “final” condition is long-term, i.e., the pore pressure has stabilized. The pore pressure in the glacial till is assumed to remain hydrostatically distributed. Finally, for those “final conditions”, a 1.5 m thick earth fill has been placed over a square area with a 36 m side.

Calculate the distribution of total and effective stresses, and pore pressure underneath the center of the earth fill before and after placing the earth fill. Distribute the earth fill, by means of the 2:1-method, that is, distribute the load from the fill area evenly over an area that increases in width and length by an amount equal to the depth below the base of fill area (Eq. 1.14).

Table 1.6 presents the results of the stress calculation for the Example 1.1 conditions. The calculation results are presented in the format of a spread sheet, a “hand calculation” format, to ease verifying the computer calculations. Notice that performing the calculations at every metre depth is normally not necessary. The table includes a comparison between the non-hydrostatic pore pressure values and the hydrostatic, as well as the effect of the earth fill, which can be seen from the difference in the values of total stress for “original” and “final” conditions.

The stress distribution below the center of the loaded area shown in Table 1.6 was calculated by means of the 2:1-method. However, the 2:1-method is rather approximate and limited in use. Compare, for example, the vertical stress below a loaded footing that is either a square or a circle with a side or diameter of  $B$ . For the same contact stress,  $q_0$ , the 2:1-method, strictly applied to the side and diameter values, indicates that the vertical distributions of stress,  $[q_z = q_0/(B + z)^2]$  are equal for the square and the circular footings. Yet, the total applied load on the square footing is  $4/\pi = 1.27$  times larger than the total load on the circular footing. Therefore, if applying the 2:1-method to circles and other non-rectangular areas, they should be modeled as a rectangle of an equal size (‘equivalent’) area. Thus, a circle is modeled as an equivalent square with a side equal to the circle radius times  $\sqrt{\pi}$ .

Notice, the 2:1-method is inappropriate to use for determining the stress distribution below a point at any other location than well within the loaded area. For this reason, it cannot be used to combine stress from two or more loaded areas unless the footprints are similar and have the same center. To calculate the stresses induced from more than one loaded area and/or below an off-center location, more elaborate methods, such as the Boussinesq distribution (Section 1.6), are required.

**TABLE 1.6**  
**STRESS DISTRIBUTION (2:1 METHOD) BELOW CENTER OF EARTH FILL**  
 [Calculations by means of UniSettle]

ORIGINAL CONDITION (no earth fill)				FINAL CONDITION (with earth fill)		
Depth (m)	$\sigma_0$ (kPa)	$u_0$ (kPa)	$\sigma_0'$ (kPa)	$\sigma_1$ (kPa)	$u_1$ (kPa)	$\sigma_1'$ (kPa)
<b>Layer 1</b>	<b>Sandy silt</b>	$\rho = 2,000 \text{ kg/m}^3$				
0.00	0.0	0.0	0.0	30.0	0.0	30.0
1.00 (GWT)	20.0	0.0	20.0	48.4	0.0	48.4
2.00	40.0	10.0	30.0	66.9	10.0	56.9
3.00	60.0	20.0	40.0	85.6	20.0	65.6
4.00	80.0	30.0	50.0	104.3	30.0	74.3
<b>Layer 2</b>	<b>Soft Clay</b>	$\rho = 1,700 \text{ kg/m}^3$				
4.00	80.0	30.0	50.0	104.3	30.0	74.3
5.00	97.0	40.0	57.0	120.1	43.5	76.6
6.00	114.0	50.0	64.0	136.0	57.1	79.0
7.00	131.0	60.0	71.0	152.0	70.6	81.4
8.00	148.0	70.0	78.0	168.1	84.1	84.0
9.00	165.0	80.0	85.0	184.2	97.6	86.6
10.00	182.0	90.0	92.0	200.4	111.2	89.2
11.00	199.0	100.0	99.0	216.6	124.7	91.9
12.00	216.0	110.0	106.0	232.9	138.2	94.6
13.00	233.0	120.0	113.0	249.2	151.8	97.4
14.00	250.0	130.0	120.0	265.6	165.3	100.3
15.00	267.0	140.0	127.0	281.9	178.8	103.1
16.00	284.0	150.0	134.0	298.4	192.4	106.0
17.00	301.0	160.0	141.0	314.8	205.9	109.0
18.00	318.0	170.0	148.0	331.3	219.4	111.9
19.00	335.0	180.0	155.0	347.9	232.9	114.9
20.00	352.0	190.0	162.0	364.4	246.5	117.9
21.00	369.0	200.0	169.0	381.0	260.0	121.0
<b>Layer 3</b>	<b>Silty Sand</b>	$\rho = 2,100 \text{ kg/m}^3$				
21.00	369.0	200.0	169.0	381.0	260.0	121.0
22.00	390.0	210.0	180.0	401.6	270.0	131.6
23.00	411.0	220.0	191.0	422.2	280.0	142.2
24.00	432.0	230.0	202.0	442.8	290.0	152.8
25.00	453.0	240.0	213.0	463.4	300.0	163.4
26.00	474.0	250.0	224.0	484.1	310.0	174.1
27.00	495.0	260.0	235.0	504.8	320.0	184.8
<b>Layer 4</b>	<b>Ablation Till</b>	$\rho = 2,200 \text{ kg/m}^3$				
27.00	495.0	260.0	235.0	504.8	320.0	184.8
28.00	517.0	270.0	247.0	526.5	330.0	196.5
29.00	539.0	280.0	259.0	548.2	340.0	208.2
30.00	561.0	290.0	271.0	569.9	350.0	219.9
31.00	583.0	300.0	283.0	591.7	360.0	231.7
32.00	605.0	310.0	295.0	613.4	370.0	243.4
33.00	627.0	320.0	307.0	635.2	380.0	255.2

## 1.6 Boussinesq Distribution

The Boussinesq distribution (Boussinesq 1885, Holtz and Kovacs 1981, Holtz et al. 2011) assumes that the soil is a homogeneous, isotropic, linearly elastic half sphere (Poisson's ratio equal to 0.5). The following relation gives the vertical distribution of the stress resulting from the point load. The stress down the soil below the point load, vertically and radially, are given by the vertical and radial distances to the point of application (Figure 1.5) and calculated by Eqs. 1.15a and Eq. 1.15b.

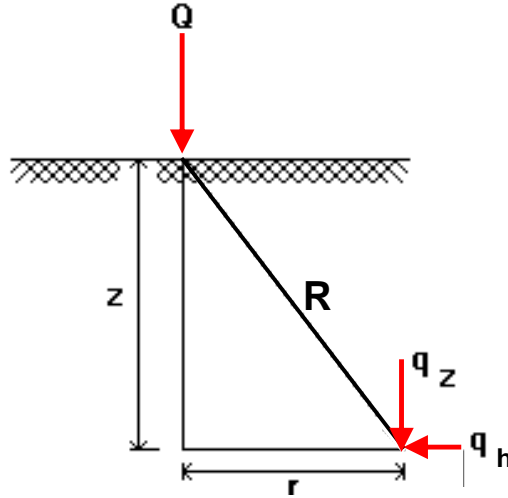


Fig. 1.5. Definition of terms used in Eq. 1.15.

$$(1.15a) \quad q_z = Q \frac{3z^3}{2\pi(r^2 + z^2)^{5/2}} \quad (1.15b) \quad q_h = Q \frac{3r^2z}{2\pi(r^2 + z^2)^{5/2}}$$

where

- Q = the point load (the total load, no stress)
- R = radial distance from point load to point of interest at Depth z.  $R = (r^2 + z^2)^{1/2}$
- r = projection of radial distance to the point of interest
- z = depth to point of interest
- $q_z$  = vertical stress at point of interest at Depth z
- $q_h$  = horizontal radial stress at point of interest at Depth z

By means of integrating the point load relation (Eq. 1.15) under a specific area, e.g., a footing or embankment, a relation for the stress imposed by the area at a point at any desired depth and horizontal location.

A footing is usually placed in an excavation and often a fill is placed next to the footing. When calculating the stress increase from a footing load, the changes in effective stress from the excavations and fills must be included, which, therefore, precludes the use of the 2:1-method (unless all such excavations and fills are concentric with the footing).

Similarly, by means of integrating the point-load relation (Eqs. 1.15a and 1.15b) along a line, a relation for the stress imposed by a line load, P (force/unit length), can be determined per Eqs. 1.16a and 1.16b. These relations can be used for a long (though, not too wide) embankment, for example. (See also Section 5.4 and Figure 5.3).

$$(1.16a) \quad q_z = P \frac{2z^3}{\pi(r^2 + z^2)^2} \quad (1.16b) \quad q_h = P \frac{2xz}{\pi(r^2 + z^2)^2}$$

where  $P$  = line load (force/unit length)  
 $q_z$  = stress at Depth  $z$   
 $z$  = depth where  $q_z$  is considered  
 $r$  = radial distance to the point of application

### 1.7 Newmark Influence Chart

The assumption of ideally elastic response produces an exaggerated radial stress distribution near the location of the point-load. Thus, immediately below the location of a single point and to a distance radially away from the location, the Boussinesq point-load formula does not provide realistic values, as illustrated in Figure 1.6. However, for a series of point-loads evenly spread out over an area and acting together, the sum (integration) of the errors of the point-loads will be compensated. Newmark (1935) integrated Eq. 1.15 over a finite area and obtained a relation, Eq. 1.17, for the stress,  $q_z$ , under the **corner of a uniformly loaded rectangular** area, for example, a footing.

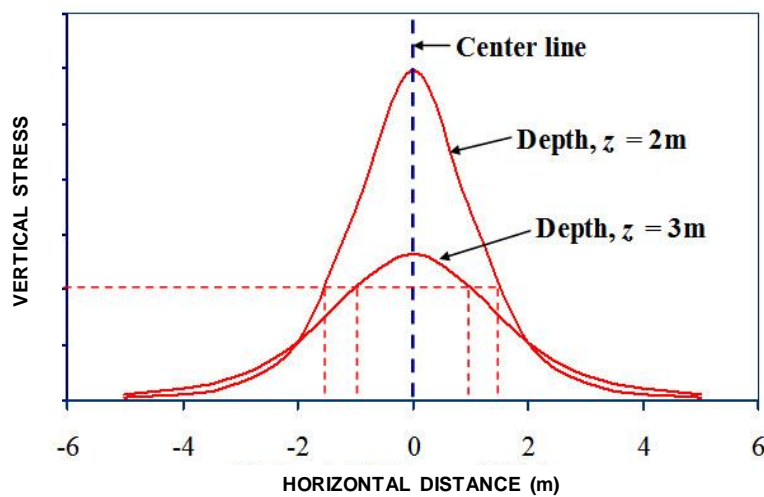


Fig. 1.6. Radial distribution of stress at 2 m and 3 m depth below a point load.

$$(1.17) \quad q_z = q_0 \times I \quad I = \frac{A \times B + C}{4\pi}$$

$$\text{where } A = \frac{2mn\sqrt{m^2+n^2+1}}{m^2+n^2+1+m^2n^2}, \quad B = \frac{m^2+n^2+2}{m^2+n^2+1}, \quad \text{and } C = \arctan \left[ \frac{2mn\sqrt{m^2+n^2+1}}{m^2+n^2+1-m^2n^2} \right]$$

and  $m = x/z$   
 $n = y/z$   
 $x$  = length of the loaded area  
 $y$  = width of the loaded area  
 $z$  = depth to the point under the corner  
 where the stress is calculated

Eq. 1.17 is valid when  $m^2 + n^2 + 1 \geq m^2n^2$ , which might not be true for a shallow depth. Then, for depths smaller than the width/ $\sqrt{2}$ , Eq. 1.17 becomes Eq. 1.17a (i.e., for where  $m^2 + n^2 + 1 \leq m^2n^2$ ).

$$\text{Eq. 17a } q_z = q_0 \times I = \frac{A \times B + \pi - C}{4\pi}$$

Newmark (1935) included the shallow depth adjustment according to Eq. 1.17a. However, this equation is not normally included in available textbooks describing the Newmark approach.

Notice that Eq. 1.17 provides the stress in only one point; for stresses at other points, for example when determining the vertical distribution at several depths below the corner point, the calculations have to be performed for each depth. To determine the stress below a point other than the corner point, the area has to be split in several parts, all with a corner at the point in question and the results of multiple calculations summed up to give the answer. Indeed, the relations are rather cumbersome to use. Also restricting the usefulness in engineering practice of the footing relation is that an irregularly shaped area has to be broken up in several smaller rectangular areas. Recognizing this, Newmark (1942) published diagrams called influence charts by which the time and effort necessary for the calculation of the stress below a point was considerably shortened even for an area with an irregularly shaped footprint.

Until the advent of the computer and spread-sheet programs, the influence chart was faster to use than Eq. 1.17, and the Newmark charts became an indispensable tool for all geotechnical engineers. Others developed charts using the Boussinesq basic equation to apply to non-rectangular areas and non-uniformly loaded areas, for example, a uniformly loaded circle or a the trapezoidal load from a sloping embankment. Holtz and Kovacs (1981) and Holtz et al. (2011) include several references to developments based on the Boussinesq basic relation.

Figure 1.7 shows two stress distributions calculated using Eq. 1.15 (Boussinesq) and Eq. 1.17 (Newmark), respectively. The point-load stress distributions were calculated as a point-load equal to the total load integrated from a 1.0-m diameter circle stressed by 100 kPa with one distribution below the point load and one 0.5 m off to the side (i.e., below the circle perimeter). The Newmark stress distribution was calculated for the corner of a 0.5-m square with a stress of 100 kPa and adding the four corner values (i.e., multiplying the corner value by 4) provided the stress distribution below the center of a 1.0-m square footing.

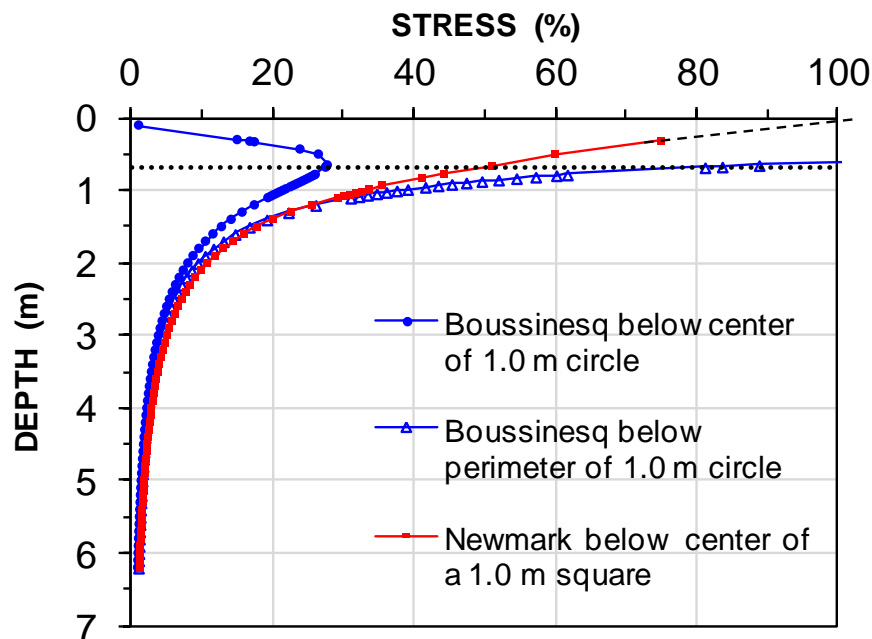


Fig. 1.7. Calculated stress distribution

## 1.8 Westergaard Distribution

Westergaard (1938) suggested that in soil with horizontal layers that restrict horizontal expansion, it would be appropriate to assume that the soil layers are rigid horizontally (Poisson's ratio equal to zero) allowing only vertical compression for an imposed stress. Westergaard's solution for the stress caused by a point load is given in Eq. 1.18.

$$(1.18) \quad q_z = \frac{Q}{\pi z^2} = \frac{Q}{\left[1 + 2(r/z)^2\right]^{3/2}}$$

where  $Q$  = total load applied  
 $q_z$  = stress at Depth  $z$   
 $z$  = depth where  $q_z$  is considered  
 $r$  = radial distance to the point of application

An integration of the Westergaard relation similar to the integration of the Boussinesq relation (Eq. 1.16) results in Eq. 1.19 (Taylor 1948). For the same reason of incompatibility of dimensions between Load and Stress, a “kink” appears also for the Westergaard solution.

$$(1.19) \quad q_z = q_0 \times I = q_0 \frac{1}{2\pi} \arctan \left[ \frac{1}{\sqrt{D+E+F}} \right]$$

$$\text{where} \quad D = \frac{1}{2m^2} \quad E = \frac{1}{2n^2} \quad F = \frac{1}{4m^2n^2}$$

where  $m = x/z$   
 $n = y/z$   
 $x$  = length of the loaded area  
 $y$  = width of the loaded area  
 $z$  = depth to the point under the corner  
 for where the stress is calculated

Influence charts similar to the Newmark charts for the Boussinesq relation have been developed also for the Westergaard relation. The difference between stresses calculated by one or the other method is small and considered less significant than the differences between reality and the idealistic assumptions behind either theory. The Westergaard method is often preferred over the Boussinesq method when calculating stress distribution in layered soils and below the center portion of a loaded wide flexible mat.

## 1.9 Characteristic Point

A small diameter footing, of about 1 metre width, can normally be assumed to distribute the contact stress evenly over the footing contact area. However, this cannot be assumed to be the case for wider footings. Both the Boussinesq and the Westergaard distributions assume ideally flexible footings (and ideally elastic soil), which is not the case for real footings, which are neither fully flexible nor absolutely rigid and soils are only approximately elastic in loading. Kany (1959) and Steinbrenner (1934; 1936) showed that below a so-called **characteristic point**, the vertical stress distribution is equal for flexible and rigid footings. In an ideally elastic soil, the characteristic point is located at a distance of  $0.13B$  and  $0.13L$  in from the side (edge) of a rectangular footing of width,  $B$ , and length,  $L$ , and at a distance of  $0.08R$  in from the perimeter of a circular footing of radius  $R$ . The distances from the center are  $0.37$  times  $B$  or  $L$ .

and 0.42 times the circle radius, respectively, i.e., about 0.4 times width, length, or diameter of either a footing or circle. Thus, when applying Boussinesq method of stress distribution to a regularly shaped, more or less rigid footing, the stress below the characteristic point is normally used rather than the stress below the center of the footing to arrive at a representative stress distribution for the settlement calculation. Indeed, with regard to vertical stress distribution, we can live with the fact that footings are not ideally flexible or rigid and natural soils are far from perfectly elastic.

The calculations by either of Boussinesq or Westergaard methods are time-consuming. The 2:1 method is faster to use and it is therefore the most commonly used method in engineering practice. Moreover, the 2:1 distribution lies close to the Boussinesq distribution for the characteristic point. However, for calculation of stress imposed by a loaded area outside its own footprint, the 2:1 method cannot be used. Unfortunately, the work involved in a "hand calculation" of stress distribution according the Boussinesq or Westergaard equations for anything but the simplest case involves a substantial effort. To reduce the effort, before-computer calculations were normally restricted to involve only a single or very few loaded areas. Stress history, e.g., the local preconsolidation effect of previously loaded areas at a site, was rarely included. Computer programs are now available which greatly simplify and speed up the calculation effort. In particular, the advent of the UniSettle program (Goudreault and Fellenius 2011, [www.unisoftGS.com](http://www.unisoftGS.com)) has drastically reduced the routine calculation effort even for the most complex conditions and vastly increased the usefulness of the Boussinesq and Westergaard methods.

**Example.** Figure 1.8 illustrates the difference between the three stress calculation methods for a square flexible footing with a side ("diameter") equal to "B" and loaded at its center, and, forestalling the presentation in Chapter 3, Figure 1.9 shows the distribution of settlement for the three stress distributions shown in Figure 1.8. The settlement values have been normalized to the settlement calculated for the distribution calculated according to the Boussinesq method.

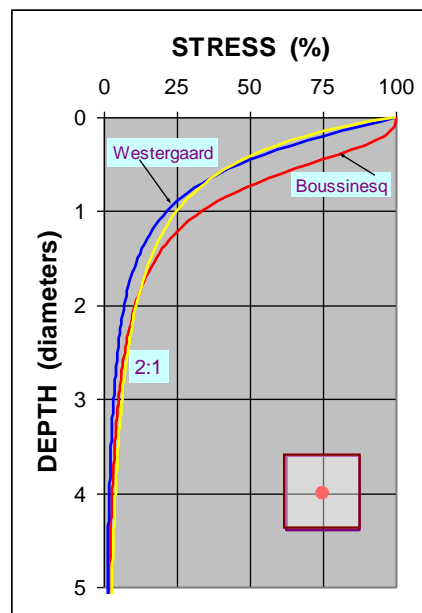


Fig. 1.8 Comparison between the methods

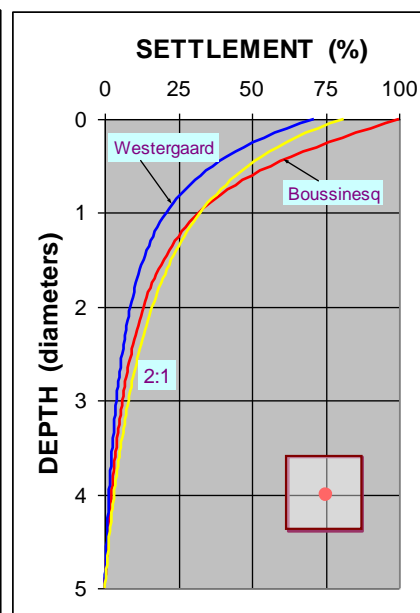


Fig. 1.9 Settlement distributions

Figure 1.10 shows the stress distributions and Figure 1.11 shows the settlement distributions (Boussinesq, Westergaard, and 2-1) for when the load is applied at the so-called characteristic point ( $x = y = 0.37B$  from the center of the footing), below which the stress distributions are the same for a flexible as for a rigid footing.

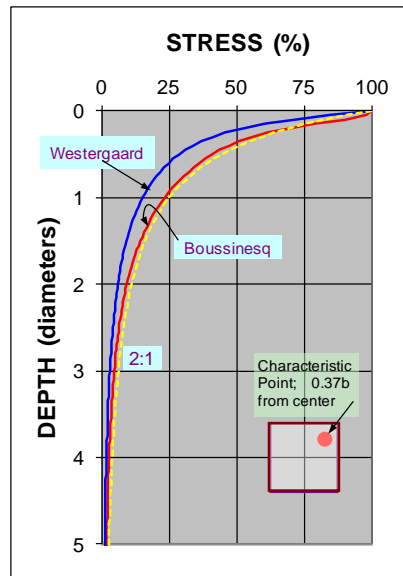


Fig. 1.10 Comparison between the methods

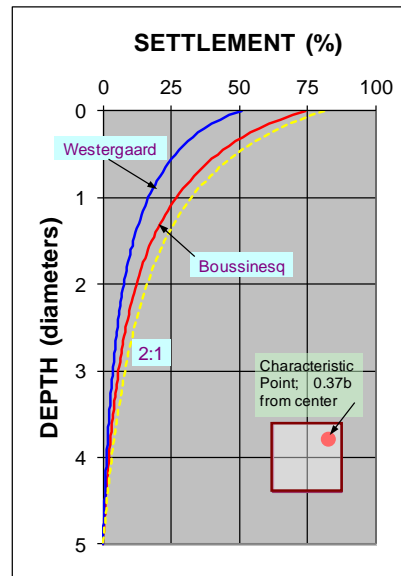


Fig. 1.11 Settlement distributions

**Example.** As illustrated in Figure 1.12, calculations using Boussinesq distribution can be used to determine how stress applied to the soil from one building may affect an adjacent existing building.

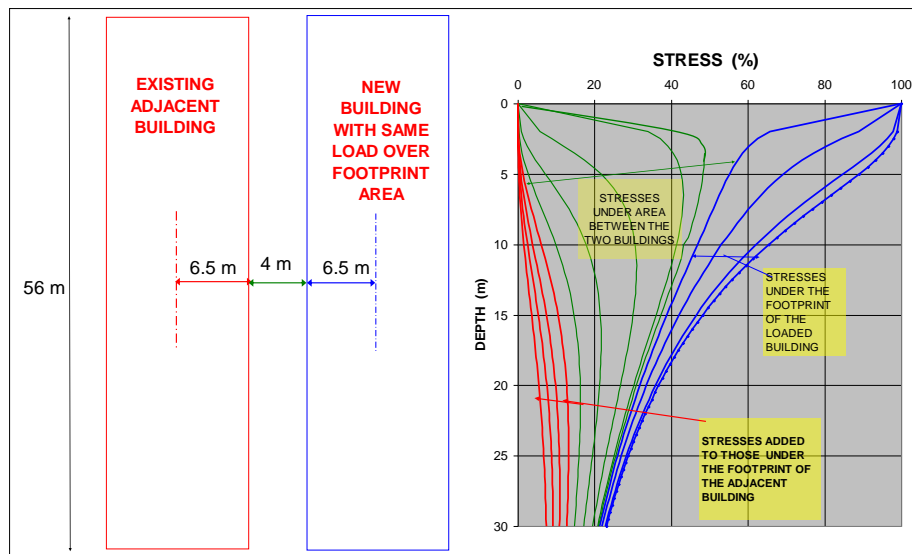


Fig. 1.12 Influence on stress from one building over to an adjacent building.

The stress exerted by the "existing building" under the new building is smaller than the preconsolidation margin of the soil (though quite close to it), which means that its induced settlement will be small. The "new building" (exerting the same stress on the soil) adds to the existing stress from the existing building to the soils below this building, resulting in additional settlement for the "existing building". The settlement due to the stress from the "existing building" acting under the footprint of the "new building" will have already occurred when the "new building" was constructed. The settlement of just one building is small and acceptable. Together the long-term settlement due to stresses becoming larger than the preconsolidation stress, might be unacceptable. The analysis of the second building settlement needs to consider that the first building reduced or eliminated the preconsolidation margin underneath the footprint of the new building. Simple stress calculations will make the problem and potential undesirable effect very clear. (For aspects on settlement analysis, see Chapter 3).



## CHAPTER 2

### SOIL PROFILING WITH THE CONE PENETROMETER

#### 2.1 Introduction

Design of foundations presupposes that the soil conditions (profile and parameters) at the site have been established by a geotechnical site investigation, employing soil boring, sampling, and in-situ sounding methods, such as the standard penetration test, SPT, the cone penetrometer test, CPT, or dynamic cone penetration test, DPT. Most in-situ methods consist of intermittent sampling, e.g., the standard penetration test with split-spoon sampling and probing for density—the N-index. Other intermittent methods are the vane, VST, dilatometer, DMT, and pressuremeter tests, PMT. Common continuous in-situ tests are the cone penetrometer tests, CPT and DPT.

In-situ sounding by standardized penetrometers came along early in the development of geotechnical engineering. For example, the Swedish weight-sounding device (Swedish State Railways Geotechnical Commission 1922), which is a continuous sounding method with a screw cone still is in use in Sweden and Finland. The cone resistance obtained by this device and other early penetrometers included the influence of soil friction along the rod surface. In the 1930s, a “mechanical cone penetrometer” was developed in the Netherlands where the rods to the cone point were placed inside an outer pipe (a sleeve), separating the cone rods from the soil (Begemann 1953). The mechanical penetrometer test was carried out by first pushing the entire system to obtain the combined resistance. Intermittently, every even metre or so, the cone point was advanced a small distance while the outer tubing was held immobile, thus obtaining the cone resistance separately at that intermittent depth. The difference was the total shaft resistance.

Begemann (1963) introduced a short section sleeve, immediately above the cone point. The sleeve arrangement enabled measuring the shaft resistance (“sleeve friction”) over a short distance near the cone. Sensors were placed in the cone and the sleeve to measure the cone and sleeve resistances directly and separately (Begemann 1963). This penetrometer became known as the “electrical cone penetrometer”. Records were eventually obtained by means of a pen writing on a rotating roll of paper.

In the early 1980s, piezometer elements were incorporated with the electrical cone penetrometer, leading to the modern cone version, “the piezocone”, which provides values of cone and sleeve resistances, and pore pressure at close distances, usually every 25 mm, but frequently every 10 mm—indeed, there is no reason for not recording at every 10 mm. The sleeve resistance is regarded as not being accurate (e.g., Lunne et al. 1986, Robertson 1990).

Figure 2.1 shows an example of a piezocone to a depth of 30 m at the site where the soil profile consists of three layers: an upper layer of soft to firm clay, a middle layer of compact silt, and a lower layer of dense sand. The groundwater table lies at a depth of 2.5 m. The CPT values shown in the diagram have been determined at every 50 mm rather than by the more desirable 10 mm distance.

While a CPT sounding is always aimed vertical, it might drift in the soil, which will cause the cone point to deviate from the vertical below the starting point. The sounding depth will then be shorter; the cone point “lifts”. For most cone soundings, deviation from the depth and exact location vertically below the “cone location” is inconsequential. However, for deep soundings, both deviations can be substantial. Modern CPT equipment measure the angle from the vertical in two directions, which allows the operator to calculate the deviation from the ideal. Curiously, the inclination measurements are often not included

with a final report. They should be. And, the values should be analyzed as to potential deviation from verticality resulting in horizontal drift and incorrect depth indication.

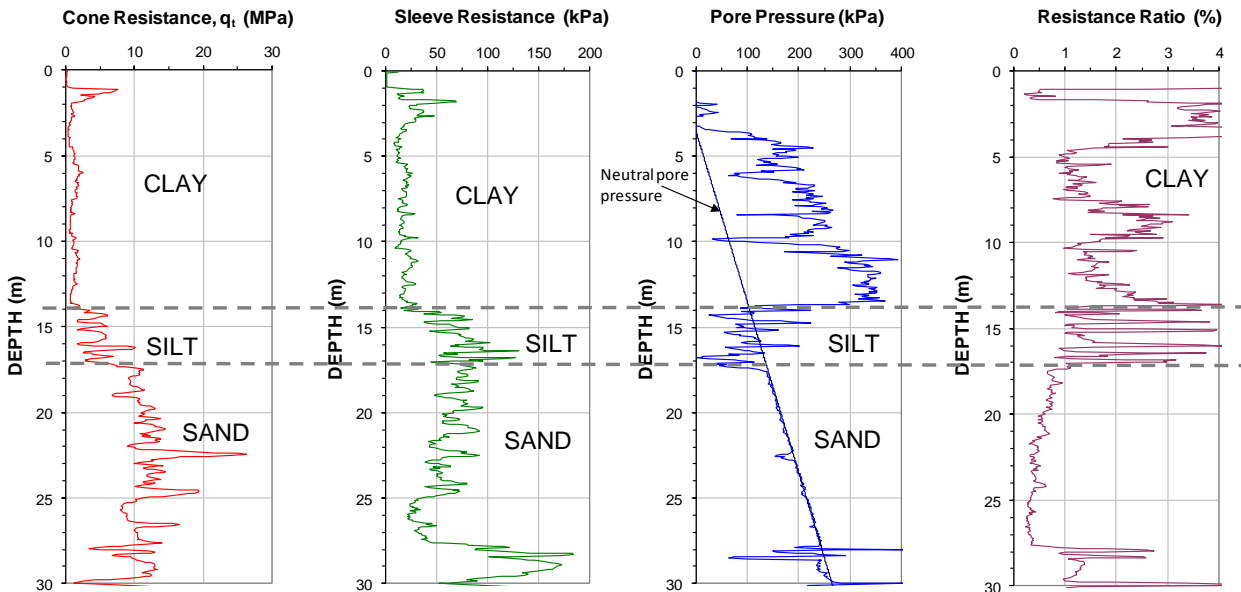


Fig. 2.1 Results from a piezocone to a depth of 30 m (site in Alberta; Fellenius 2004)

The cone penetrometer does not provide a measurement of static resistance, but records the resistance at a certain rate of penetration (now standardized to 20 mm/s). Therefore, pore water pressures develop (increase) in the soil at the location of the cone point and sleeve that add to the “neutral” pore water pressure. In dense fine sands, which are prone to dilation, the then reduced pore pressure can significantly reduce the "neutral" pressure. In pervious soils, such as sands, the pore pressure changes are small, while in less pervious soils, such as silts and clays, they can be quite large.

Measurements with the piezocone included adjusting the cone resistance for the pore pressure acting on the cone shoulder (Baligh et al. 1981; Campanella et al. 1982, Campanella and Robertson 1988). See Section 2.2.6 and Eq. 2.1 below.

The cone penetrometer test, is simple, fast to perform, economical, supplies continuous records with depth, and allows a variety of sensors to be incorporated with the penetrometer. The direct numerical values produced by the test have been used as input to geotechnical formulae, usually of empirical nature, to determine capacity and settlement, and for soil profiling.

Early cone penetrometers gave limited information that could be used for determining soil type and were limited to determining the location of soil type boundaries. The soil type had to be confirmed from the results of conventional borings. Empirical interpretations were possible but they were limited to the geological area where they had been developed. Begemann (1965) is credited with having presented the first rational soil profiling method based on CPT soundings. With the advent of the piezocone, the CPTU, the cone penetrometer was established as an accurate site investigation tool.

This chapter is a summary to indicate some of the uses of the cone penetrometer test. For a more thorough account, the reader is directed to the many reports and papers by Tom Lunne, Paul Mayne, and Peter Robertson and, specifically, Kulhawy and Mayne (1990), Lunne et al. (1986), Lunne et al. (1997), Mayne et al. (1990), Mayne et al. (2001), Mayne et al. (2002), Mayne (2007), Robertson and Campanella (1983), and Robertson (2007a; 2007b).

## 2.2 Brief Survey of Soil Profiling Methods

### 2.2.1 Begemann (1965)

Begemann (1965) pioneered soil profiling from the CPT, showing that, while coarse-grained soils generally demonstrate larger values of cone resistance,  $q_c$ , and sleeve resistance,  $f_s$ , as opposed to fine-grained soils, the soil type is not a strict function of either cone sleeve resistance, but of the combination of the these values.

Figure 2.2 presents the Begemann soil profiling chart, showing (linear scales)  $q_c$  as a function of  $f_s$ . Begemann showed that the soil type is a function of the ratio, the resistance ratio (“resistance ratio”),  $f_R$ , between the sleeve and cone resistances as indicated by the slope of the fanned-out lines. Table 2.1 shows the soil types for the Begemann data base correlated to resistance ratio. The Begemann chart and table were derived from tests in Dutch soils with the mechanical cone. That is, the chart is site-specific, i.e., directly applicable only to the specific geologic locality where it was developed. For example, the cone tests in sand show a resistance ratio smaller than 1 %. A distinction too frequently overlooked is that Begemann did not suggest that the resistance ratio alone governs the soil type. Aspects, such as overconsolidation, whether a recent or old sedimentary soil, or a residual soil, mineralogical content, etc. will influence the resistance ratio, and, therefore, the interpretation, as will a recent fill or excavation. It is a mistake to believe that the CPTU can duplicate the sieve analysis, or replace it in a soils investigation.

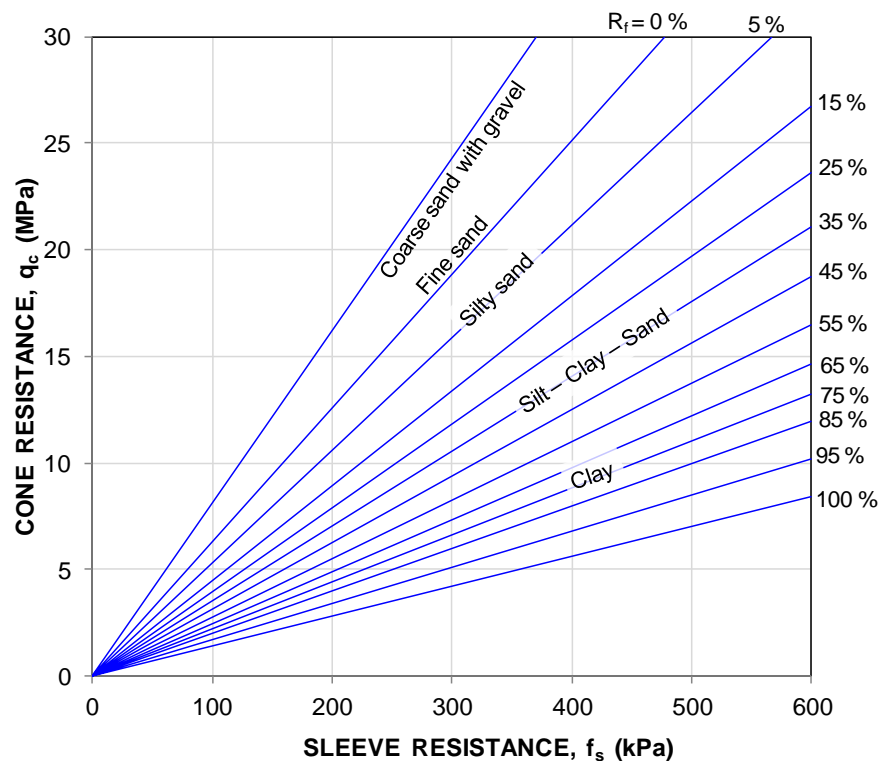


Figure 2.2 The Begemann original profiling chart. The %-values refer to percent fines (Begemann, 1965)

**Table 2.1 Soil Type as a Function of Resistance Ratio (Begemann, 1965)**

Coarse sand with gravel through fine sand	1.2 %	-	1.6 %
Silty sand	1.6 %	-	2.2 %
Silty sandy clayey soils	2.2 %	-	3.2 %
Clay and loam, and loam soils	3.2 %	-	4.1 %
Clay	4.1 %	-	7.0 %
Peat			>7 %

### 2.2.2 Sanglerat et al. (1974)

Sanglerat et al. (1974) proposed the chart shown in Figure 2.3A presenting cone resistance,  $q_c$ , (logarithmic scale) versus sleeve resistance from soundings using a 80 mm diameter research penetrometer. Figure 2.3B shows the same graph but with the cone resistance in linear scale. The green curves indicate the range of values ordinarily encountered. The change from Begemann’s type of plotting to plotting against the resistance ratio is unfortunate. This manner of plotting has the apparent advantage of combining the two important parameters, the cone resistance and the resistance ratio. However, plotting the cone resistance versus the resistance ratio implies, falsely, that the values are independent of each other; the resistance ratio would be the independent variable and the cone resistance the dependent variable. In reality, the resistance ratio is the inverse of the ordinate and the values are patently not independent—the cone resistance is plotted against its own inverse self, multiplied by a variable that ranges, normally, from a low of about 0.01 through a high of about 0.07.

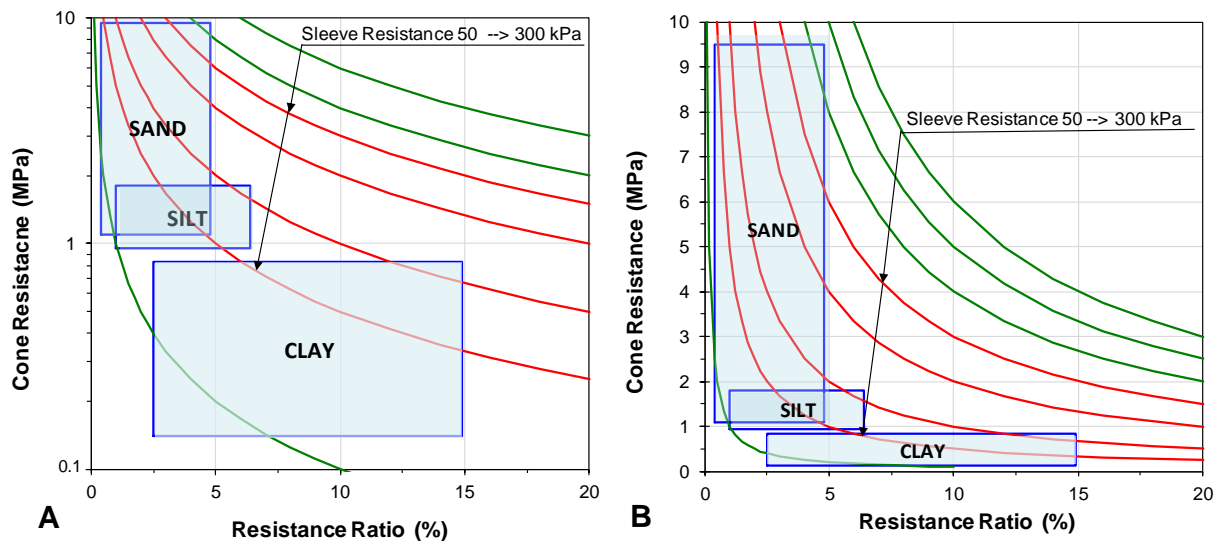


Fig. 2.3 Plot of data from research penetrometer with the cone resistance in log scale and linear scale. The resistance ratio is the ratio,  $R_f$ , between the sleeve resistance and the cone resistance(after Sanglerat et al. 1974)

As is very evident in Figure 2.3, regardless of the actual values, the plotting of data against own inverse values will predispose the plot to a hyperbolically shaped zone ranging from large ordinate values at small abscissa values through small ordinate values at large abscissa values. The resolution of data representing fine-grained soils is very much exaggerated as opposed to the resolution of the data representing coarse-grained soils. This is made obvious in the Figure 2.3B, which shows the data in linear scale. Simply, while both cone resistance and sleeve resistance are important soil profiling parameters, plotting one as a function of the other distorts the information. The figure also shows that plotting against the resistance ratio restricts the usable area of the graph, and, therefore, the potential resolution of the test data.

From this time on, the Begemann manner of plotting the cone resistance against the sleeve resistance was discarded in favor of Sanglerat's plotting cone resistance against the resistance ratio. However, this development—plotting the cone resistance against itself (its inverted self) modified by the sleeve resistance value—is unfortunate.

### 2.2.3 Schmertmann (1978)

Schmertmann (1978) proposed the soil profiling chart shown in Figure 2.4A. The chart is based on results from mechanical cone data in “North Central Florida” and Figure 2.4B shows the profiling according to the Begemann style of plotting CPT data. The chart indicates envelopes of zones of common soil type. It also presents boundaries for density of sands and consistency (undrained shear strength) of clays and silts, which are imposed by definition and not related to the soil profile interpreted from the CPT results.

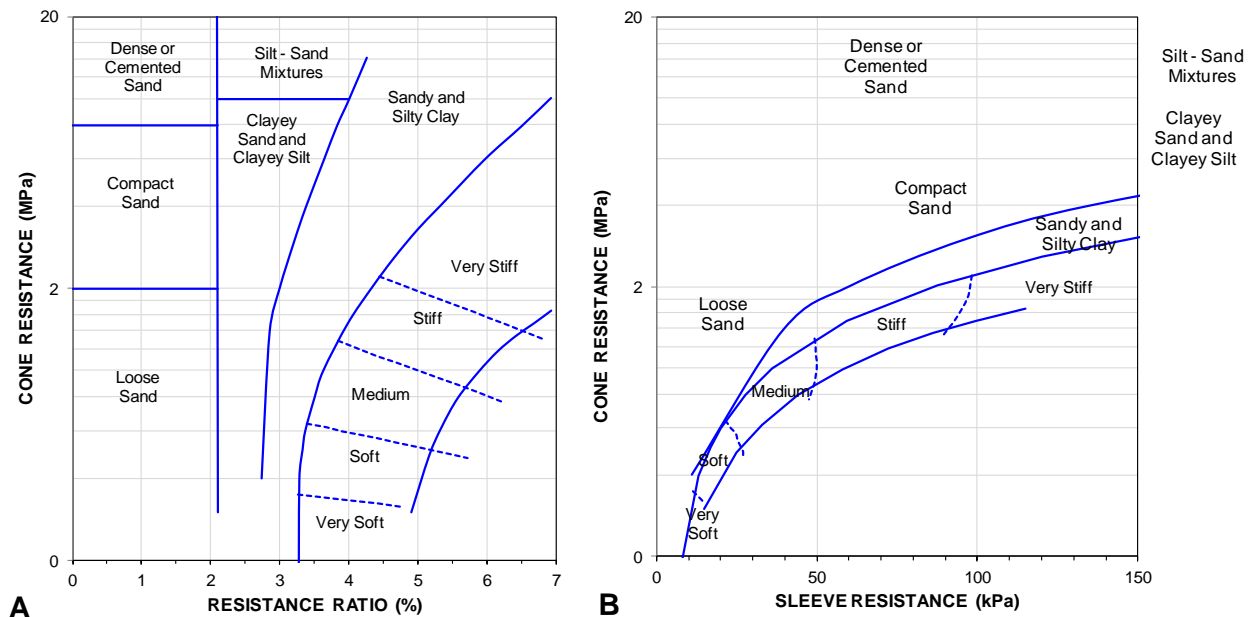


Fig. 2.4 The Schmertmann profiling chart (Schmertmann, 1978). (A) the original axes, (B) The Schmertmann profiling chart converted to a Begemann type profiling chart.

Notice, however, that the soil type is not just defined by the resistance ratio, but also by upper and lower limit of cone resistance in the Schmertmann graph. The boundary between compact and dense sand are slightly different to those applied today.

Also the Schmertmann chart plots the cone resistance against the resistance ratio, that is, the data are plotted against their inverse self. Figure 2.4B shows the Schmertmann chart converted to a Begemann type graph. When the plotting of the data against own inverse values is removed, a qualitative, visual effect comes forth that is quite different from that of Figure 2.4A. Note also that the consistency boundaries do not any longer appear to be very logical.

Schmertmann (1978) stated that the correlations shown in Figure 2.4A may be significantly different in areas of dissimilar geology. The chart is intended for typical reference and includes two warnings: “*Local correlations are preferred*” and “*Resistance ratio values decrease in accuracy with low values of  $q_c$* ”. Schmertmann also mentioned that soil sensitivity, resistance sleeve surface roughness, soil ductility, and pore pressure effects can influence the chart correlation. Notwithstanding the caveat, the Schmertmann chart is very commonly applied “as is” in North American practice.

### 2.2.4 Douglas and Olsen (1981)

Douglas and Olsen (1981) proposed a soil profiling chart based on tests with the electrical cone penetrometer. The chart, which is shown in Figure 2.5A, appends classification per the unified soil classification system to the soil type zones. The chart also indicates trends for liquidity index and earth stress coefficient, as well as sensitive soils and “metastable sands”. The Douglas and Olsen chart envelopes several zones using three upward curving lines representing increasing content of coarse-grained soil. The chart distinguishes where soils are sensitive or “metastable”.

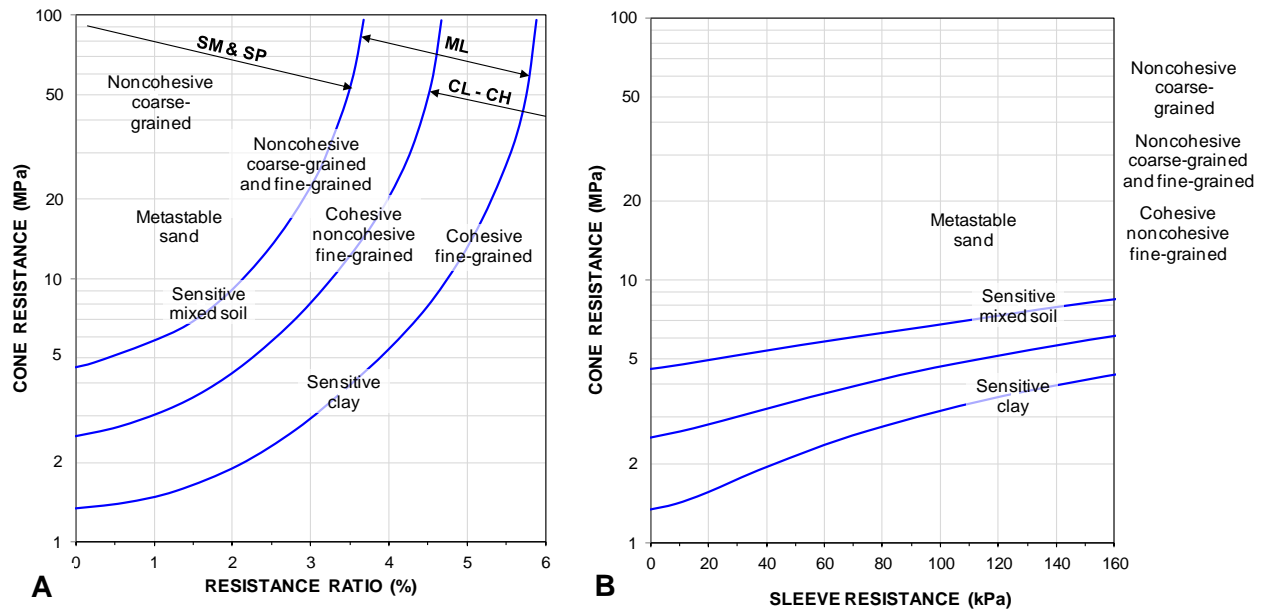


Fig. 2.5 The Douglas and Olsen profiling chart (Douglas and Olsen 1981). (A) the original axes, (B) The Douglas and Olsen profiling chart converted to a Begemann type profiling chart.

Comparing the Douglas and Olsen chart (Figure 2.5A) with the Schmertmann chart (Figure 2.4A), a difference emerges in implied soil type response: while in the Schmertmann chart, the soil type envelopes curve downward, in the Douglas and Olsen chart they curve upward. Zones for sand and for clay are approximately the same in the two charts, however.

A comparison between the Douglas and Olsen and Schmertmann charts is more relevant if the charts are prepared per the Begemann type of presentation. Thus, Figure 2.5B shows the Douglas and Olsen chart converted to a Begemann type graph. The figure includes the three curved envelopes. The sleeve resistance is limited to 160 kPa, which is a practical limit for actual conditions. Three of the labels in the original chart fall outside this limit (two were combined here to fit). Moreover, it is hard to accept that the areas indicated as metastable or sensitive are correctly identified in the original chart

Obviously, plotting the cone resistance versus the resistance ratio, i.e., against its inverse self will easily lead to distorted conclusions from the graph.

### 2.2.5 Vos (1982)

Vos (1982) suggested using the electrical cone penetrometer for Dutch soils to identify soil types from the resistance ratio, as shown in Table 2.2 (Vos, 1982). The percentage values are similar but not identical to those recommended by Begemann (1965).

**TABLE 2.2 Soil Behavior Categories as a Function of Resistance Ratio**

Coarse sand and gravel		<1.0%
Fine sand	1.0 %-	1.5 %
Silt	1.5 %-	3.0 %
Clay	3.0%-	7.0%
Peat	>7 %	

### 2.2.6 Robertson et al. (1986)

Robertson et al. (1986) and Campanella and Robertson (1988) presented a profiling chart (Figure 2.6), which was the first chart to be based on the piezocone, i.e., the first to include adjusting the cone resistance for pore pressure at the shoulder according to Eq. 2.1, as proposed by Torstensson (1975) and Wissia et al. (1975). See also Section 2.3 and Figure 2.10b.

$$(2.1) \quad q_t = q_c + u_2(1-a)$$

where  $q_t$  = cone resistance adjusted for pore water pressure on shoulder. N.B., the  $q_t$  is a total stress parameter (cf., Section 2.3).

$q_c$  = measured cone resistance

$u_2$  = pore pressure measured at cone shoulder

$a$  = ratio between cone base to shoulder area

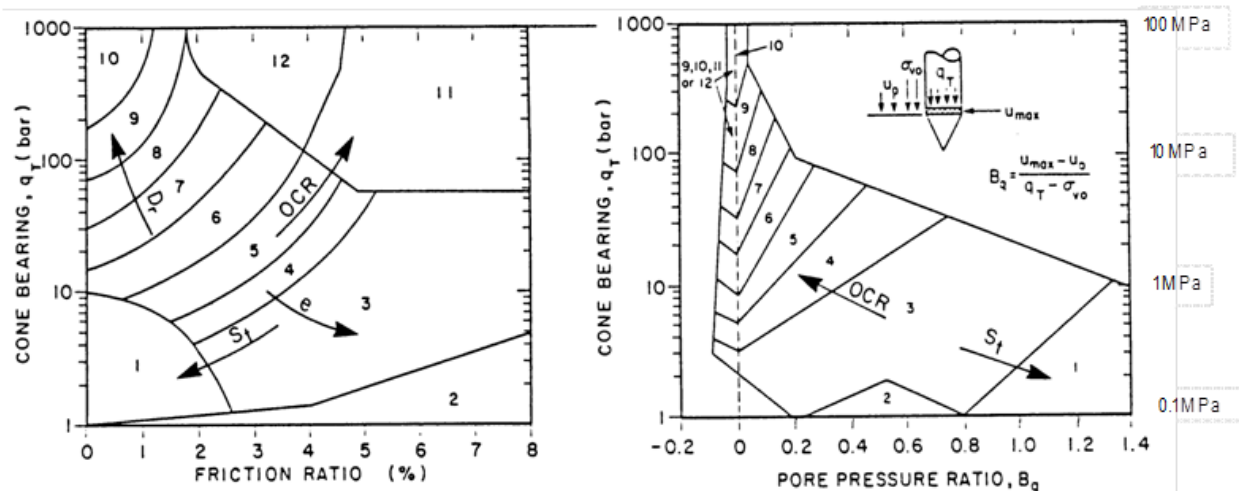


Fig. 2.6 Profiling chart per Robertson et al. (1986; used with permission)

The Robertson et al. (1986) profiling chart is presented in Figure 2.6 identifies numbered areas that separate the soil in categories in twelve grain-size defined zones, as follows.

- |                                |  |
|--------------------------------|--|
| 1. Sensitive fine-grained soil | 7. Silty sand to sandy silt                          |
| 2. Organic soil                | 8. Sand to silty sand                                |
| 3. Clay                        | 9. Sand  |
| 4. Silty clay to clay          | 10. Sand to gravelly sand                            |
| 5. Clayey silt to silty clay   | 11. Very stiff fine-grained soil                     |
| 6. Sandy silt to clayey silt   | 12. Overconsolidated or cemented sand to clayey sand |

A novel information in the profiling chart is the delineation of Zones 1, 11, and 12, representing somewhat extreme soil responses, enabling the CPTU to uncover more than just soil grain size. The rather detailed separation of the in-between zones, Zones 3 through 10 indicate a gradual transition from fine-grained to coarse-grained soil.

As mentioned above, plotting of cone resistance value against the resistance ratio is plotting the cone resistance against itself (its inverted self) modified by the sleeve resistance, distorting the results. Yet, as indicated in Figure 2.7, the measured values of cone resistance and sleeve resistance can just as easily be plotted separately. The resistance ratio is a valuable parameter and it is included as an array of lines ranging from a ratio of 0.1 % through 25 %.

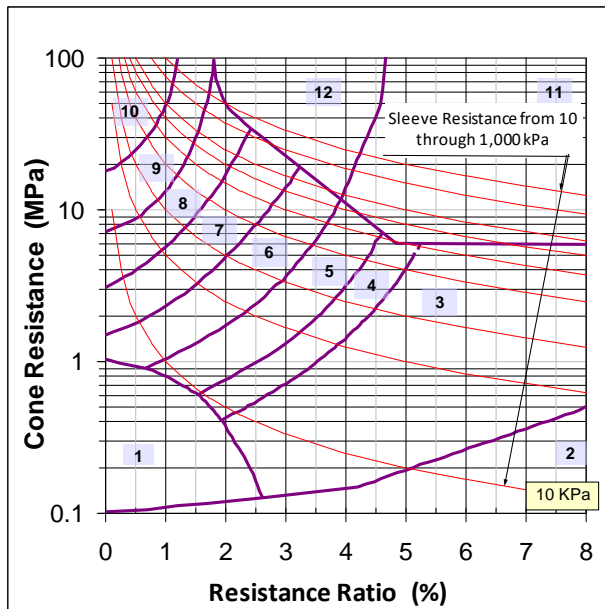


Fig. 2.7A The profiling chart shown in Fig. 2.6A

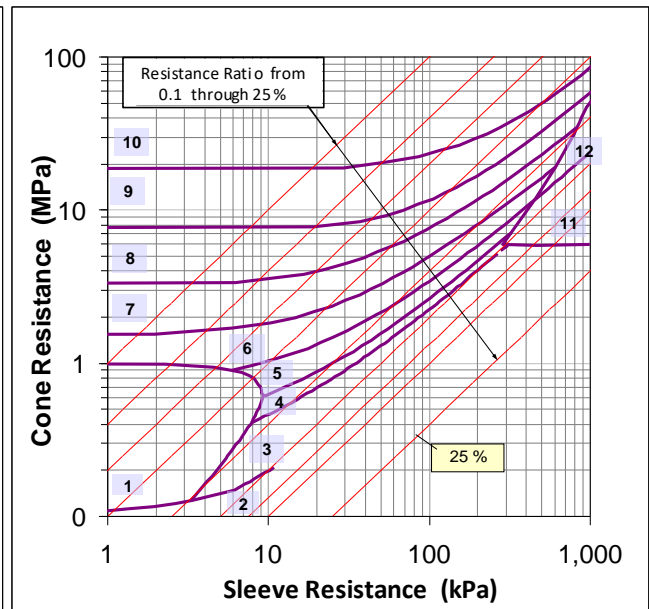


Fig. 2.7B The profiling chart plotted as Cone Resistance vs. Sleeve Resistance

The Robertson et al. (1986) profiling chart (Figure 2.6) introduced a pore pressure ratio,  $B_q$ , defined by Eq. 2.2, as follows.

$$(2.2) \quad B_q = \frac{u_2 - u_0}{q_t - \sigma_v}$$



where  $B_q$  = pore pressure ratio  
 $U_2$  = pore pressure measured at cone shoulder  
 $u_0$  = in-situ pore pressure (often called "neutral pore pressure")  
 $q_t$  = cone resistance corrected for pore water pressure on shoulder  
 $\sigma_v$  = total overburden stress

Essentially, the  $B_q$ -value shows change of pore pressure divided by cone resistance,  $q_t$ . Directly, the  $B_q$ -chart (Figure 2.8) shows zones where the  $U_2$  pore pressures become smaller than the neutral pore pressures ( $u_0$ ) in the soil during the advancement of the penetrometer, resulting in negative  $B_q$ -values. Otherwise, the  $B_q$ -chart appears to be an alternative rather than an auxiliary chart; one can use one or the other depending on preference. However, near the upper envelopes, a CPTU datum plotting in a particular soil-type zone in the resistance ratio chart will not always appear in the same soil-type zone in the  $B_q$ -chart. Robertson et al. (1986) points out that "occasionally soils will fall within different zones on each chart" and recommends that the users study the pore pressure rate of dissipation (if measured) to decide which zone applies to questioned data.

The pore pressure ratio,  $B_q$ , is an inverse function of the cone resistance,  $q_t$ . Therefore, also the  $B_q$ -plot represents the data as a function of their own self values.

**Eslami and Fellenius (1996)** proposed a pore pressure ratio,  $B_E$ , defined, as follows.

$$(2.3) \quad B_E = \frac{u_2 - u_0}{u_0}$$

where  $B_E$  = pore pressure ratio  
 $u_0$  = neutral pore pressure  
 $U_2$  = pore pressure measured at the cone shoulder

The  $B_E$ -value shows the relative change of pore pressure introduced by pushing the cone.

There is little information obtained from the pore pressure ratios that is not available directly from the measured pore pressure ( $U_2$ ) and resistance ratio,  $f_R$ .

### 2.2.7 Robertson (1990)

Robertson (1990) proposed a development of the Robertson et al. (1986) profiling chart, shown in Figure 2.8, plotting a "normalized cone resistance",  $q_{cnrm}$ , against a "normalized resistance ratio",  $R_{fnrm}$ , in a cone resistance chart. The accompanying pore pressure ratio chart plots the "normalized cone resistance" against the pore pressure ratio,  $B_q$ , defined by Eq. 2.2 applying the same  $B_q$ -limits as the previous chart (Zone 2 is not included in Figure 2.8).

The normalized cone resistance is defined by Eq. 2.4.

$$(2.4) \quad q_{cnrm} = \frac{q_t - \sigma_v}{\sigma'_v}$$

where  $q_{cnrm}'$  = cone resistance normalized according to Robertson (1990)  
 $q_t$  = cone resistance corrected for pore water pressure on shoulder  
 $\sigma_v$  = total overburden stress  
 $\sigma_v'$  = effective overburden stress  
 $(q_t - \sigma_v)$  = net cone resistance

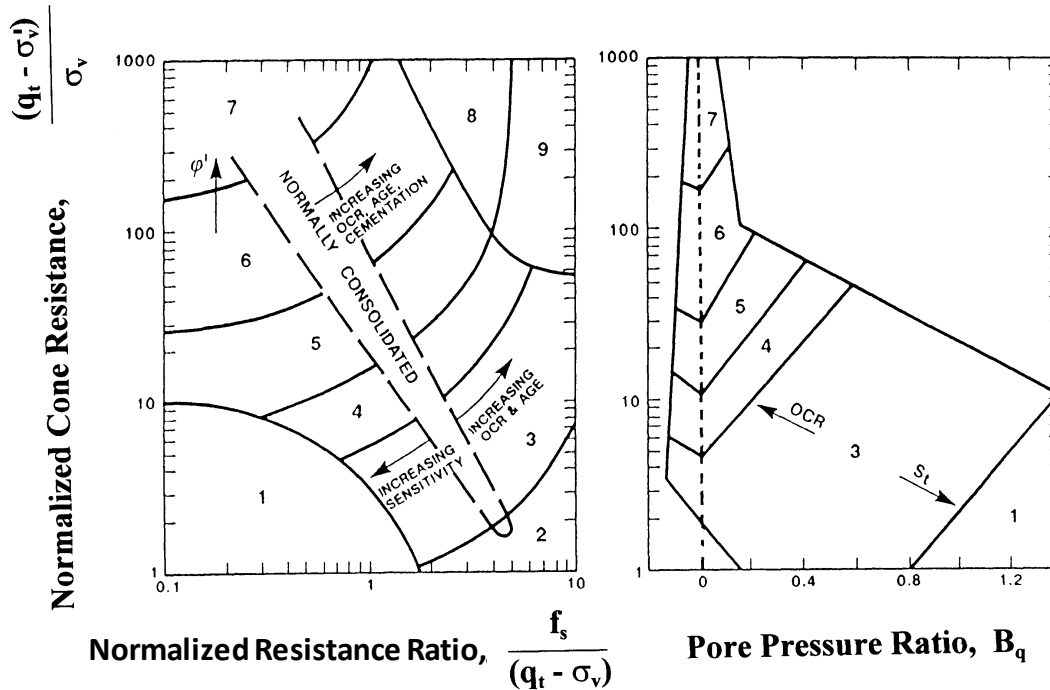


Fig. 2.8 Profiling chart per Robertson (1990; used with permission)

The numbered areas in the profiling chart separate the soil behavior categories in nine zones, as follows.

- |  |  |
|--|--|
| 1. Sensitive, fine-grained soils             | 6. Sand [silty sand to clean sand]                             |
| 2. Organic soils and peat                    | 7. Sand to gravelly sand                                       |
| 3. Clays [clay to silty clay]                | 8. Sand – clayey sand to “very stiff” sand                     |
| 4. Silt mixtures [silty clay to clayey silt] | 9. Very stiff, fine-grained, overconsolidated or cemented soil |
| 5. Sand mixtures [sandy silt to silty sand]  |  |

The normalized resistance ratio is defined as the sleeve resistance over the net cone resistance, as follows.

$$(2.5) \quad R_{fnm} = \frac{f_s}{q_t - \sigma_v}$$

where  $f_s$  = sleeve resistance  
 $q_t$  = cone resistance corrected for pore water pressure on shoulder  
 $\sigma_v$  = total overburden stress

The two first and two last soil types are the same as those used by Robertson et al. (1986) and Types 3 through 7 correspond to former Types 3 through 10. The Robertson (1990) normalized profiling chart has seen extensive use in engineering practice (as has the Robertson et al. 1986 chart).

The normalization is professedly to compensate for that the cone resistance is influenced by the overburden stress. Therefore, when analyzing deep CPTU soundings (i.e., deeper than about 30 m), a profiling chart developed for more shallow soundings does not apply well to the deeper sites. At very shallow depths, however, the proposed normalization will tend to lift the data in the chart and imply a coarser soil than necessarily the case. Moreover, where soil layers alternate (in the extreme, say, from soil bulk density ranging from  $1,400 \text{ kg/m}^3$  through  $2,100 \text{ kg/m}^3$ ) and/or where upward or downward pore pressure gradients exist, the normalization is unwieldy. For these reasons, it would appear that the normalization merely exchanges one difficulty for another.

More important, the chart still includes the plotting of data against the inverse of own self. This is not necessary. A chart with the same soil zones could just as well have been produced with normalized cone resistance against a normalized sleeve resistance.

Accepting the Robertson (1990) normalization, [Figures 2.9A and 2.9B](#) show the envelopes of the Robertson (1990) chart ([Figure 2.8](#)) converted to a Begemann type chart. The ordinate is the same and the abscissa is the multiplier of the normalized cone resistance and the normalized resistance factor of the original chart (the normalized sleeve resistance is the sleeve resistance divided by the effective overburden stress). Where needed, the envelopes have been extended with a thin line to the frame of the diagram.

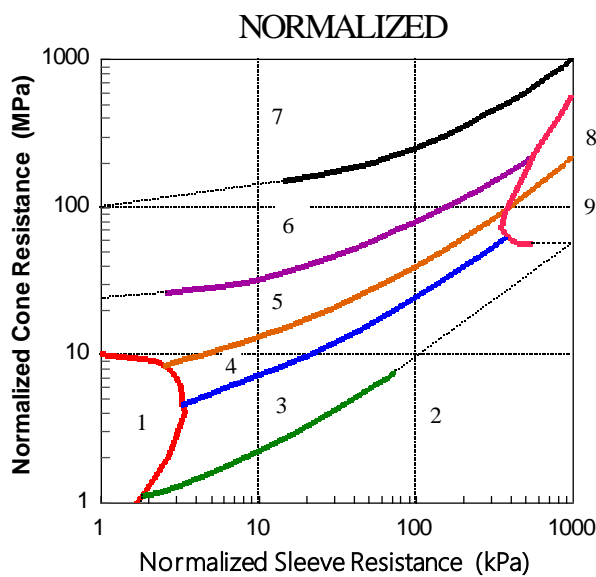


Fig. 2.9A Normalized corrected cone resistance vs. normalized sleeve resistance

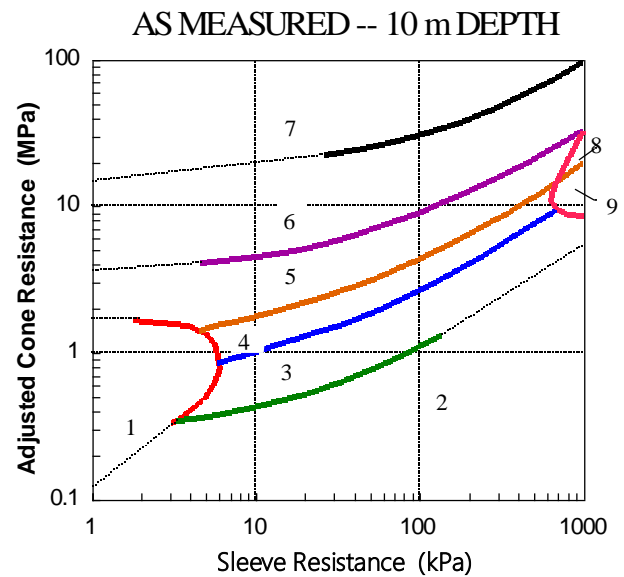


Fig. 2.9B Pore-pressure corrected cone resistance vs. sleeve resistance

[Figure 2.9b](#) presents the usual Begemann type profiling chart converted from [Figure 2.8](#) under the assumption that the data apply to a depth of about 10 m at a site where the groundwater table lies about 2 m below the ground surface. This chart is approximately representative for a depth range of about 5 m to 30 m. Comparing the “normalized” chart with the “as measured” chart does not indicate that normalization would be advantageous.

Other early profiling charts were proposed by Searle (1979), Jones and Rust (1982), Olsen and Farr (1986), Olsen and Malone (1988), Erwig (1988). CPTU charts similar to that of Robertson (1990) were proposed by Larsson and Mulabdic (1991), Jefferies and Davies (1991, 1993), and Olsen and Mitchell (1995). Robertson (2016) has further developed his CPTU classification approach to separate classification per grain size from the per soil response.

### 2.3 The Eslami-Fellenius CPTU Profiling and Soil Behavior Type Classification Method

To investigate the use of cone penetrometer data in pile design, Eslami and Fellenius (1997) compiled a database consisting of CPT and CPTU data linked with results of boring, sampling, laboratory testing, and routine soil characteristics. The cases are from 18 sources reporting data from 20 sites in 5 countries. About half of the cases are from piezocone tests, CPTU, and include pore pressure measurements ( $U_2$ ). Non-CPTU tests are from sand soils and were used with the assumption that the  $U_2$ -values are approximately equal to the neutral pore pressure ( $u_0$ ). The database values are separated on five main soil behavior categories as follows.

- |   |                              |
|---|------------------------------|
| 1. Very soft Clay or Sensitive and Collapsible Clay and/or Silt | 4a. Sandy Silt               |
| 2. Clay and/or Silt   | 4b. Silty Sand               |
| 3. Silty Clay and/or Clayey Silt                                | 5. Sand, and/or Sandy Gravel |

The boundaries were plotted in a Begemann type profiling chart and Figure 2.10 shows the envelopes for the five soil types. The chart shows with both logarithmic and linear abscissa scales. The database did not include cases with cemented soils or very stiff clays, and, for this reason, no envelopes for such soil types are included in the chart. Note, the soil descriptions are approximate and they can vary due to preload ("preconsolidation") level and other factors. The CPTU test is not equal to or a replacement for a grain-size analysis of soil samples.

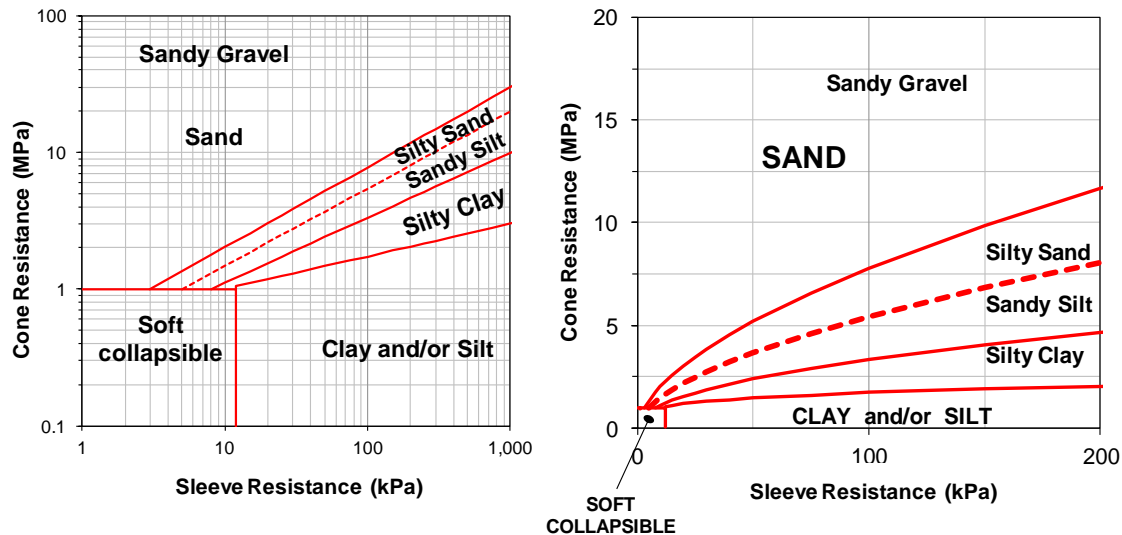


Fig. 2.10 The Eslami-Fellenius profiling chart (Eslami 1996; Eslami and Fellenius, 1997)

Plotting the effective cone resistance,  $q_E$ , (by subtracting the pore pressure,  $U_2$ , from the pore pressure adjusted cone resistance to obtain an "effective" resistance) was found to provide a more consistent delineation of envelopes than a plot of only the pore pressure adjusted resistance,  $q_t$ . Figure 2.11 shows the process of determining the pore-pressure adjusted cone resistance,  $q_t$ , and "effective" response resistance,  $q_E$  (obtained by subtracting the  $U_2$  pore pressure from  $q_t$ ).

Because the sleeve resistance is a rather approximate measurement, no similar benefit was found in producing an "effective" sleeve resistance. In dense, coarse-grained soils, the  $q_E$ -value differs only marginally from the  $q_t$ -value. In contrast, cone tests in fine-grained soils could generate substantial values of excess pore water pressure causing the  $q_E$ -value to be much smaller than the  $q_t$ -value, indeed, even negative, in which case the value should be taken as equal to zero.

The  $q_E$ -value was also found to be a consistent value for use in relation to soil responses, such as pile shaft and pile toe resistances (Eslami 1996, Eslami and Fellenius 1995; 1996; 1997). Notice, however, that, as mentioned by Robertson (1990), the measured pore water pressure is a function of where the pore pressure gage is located. The pore pressure acting against the cone surface is not necessarily the same as the pore pressure acting on the cone shoulder, which means that the  $q_t$  is not fully representative for the total stress acting on the cone. Neither, therefore, is using  $q_E$  instead of  $q_t$ . Using  $u_0$  instead of  $U_2$  may be preferable ( $q_E = q_t - u_0$ ). Note,  $q_E$  is not a generally accepted effective stress parameter. However, in a non-preloaded (prestressed) sand, it makes very little difference whether or not  $q_c$ ,  $q_t$ , or  $q_E$ , are used.

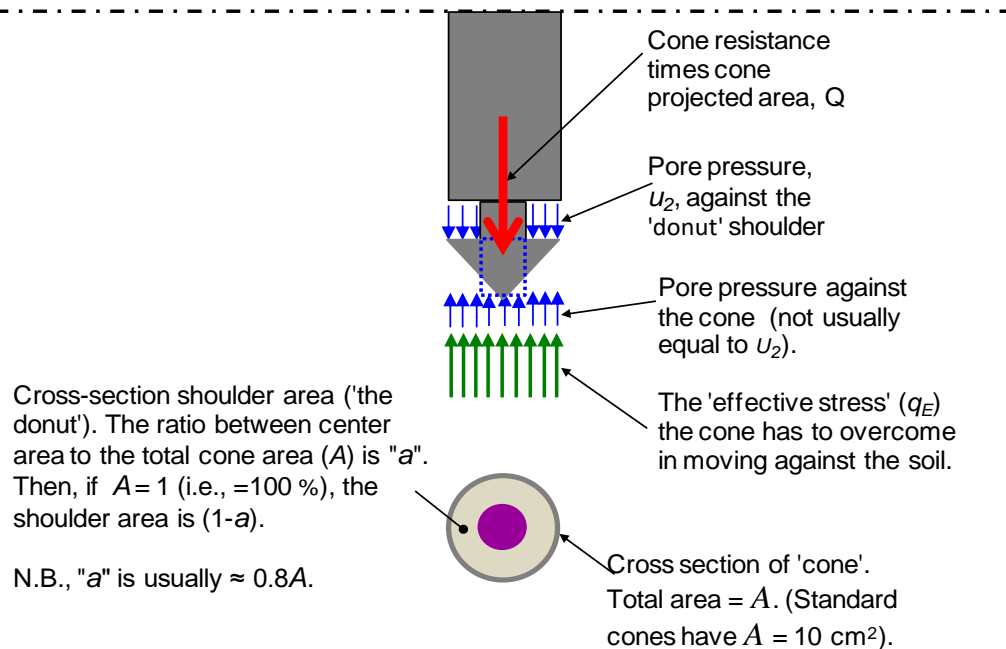


Fig. 2.11 Derivation of the "Eslami 'effective' cone resistance,  $q_E$ " (Eslami 1996)

The conventional CPTU approach includes balancing the difference in pore pressure due to the fact that, above the cone, pore pressure only acts against the cone shoulder, whereas below the cone, pore pressure acts against the total area of the cone (when measured, called  $U_1$ ). Moreover, the measured cone resistance,  $q_c$ , is aided by the pore pressure on the shoulder ( $U_2$ ) in acting against the effective stress plus the pore pressure, i.e., the total stress. Balancing downward and upward acting forces requires adding the pore pressure on the shoulder to the measured cone resistance. Thus, the measured cone resistance is, conventionally, adjusted by adding the pore pressure contribution,  $U_2(1-a)$  from the shoulder, as expressed in Eq. 2.1. N.B., the so-adjusted cone resistance represents a total stress condition.

In order to know the effective stress condition, the pore pressure at the cone depth has to be subtracted from the pore-pressure adjusted cone resistance,  $q_t$ . If that pore pressure is equal to  $U_2$ , Eq. 2.1 changes to Eq. 2.6. Other than in pervious sand, the  $U_2$ -pore pressure is not equal to the neutral pore pressure at the cone depth. However, in pervious soils, such as sand, it matters little whether or not the cone resistance is pore-pressure adjusted, while in soils with low permeability, such as clays, although the pore pressure in the soil volume affected by the cone penetration is not accurately known (not usually equal to  $U_2$ ), yet, using the pore pressure-adjusted cone resistance is more appropriate than using the Eslami cone resistance,  $q_E$ .

$$(2.6) \quad q_E = (q_t - u_2) = q_c - u_2 \quad a$$

where  $q_E$  = Eslami cone resistance  
 $q_t$  = cone resistance adjusted for pore water pressure on shoulder (Eq. 2.1)  
 $u_2$  = pore pressure measured at cone shoulder

The Eslami-Fellenius chart is primarily intended for soil type (profiling) analysis of CPTU data. With regard to the grain-size boundaries between the main soil fractions (clay, silt, sand, and gravel), international and North American practices agree. In contrast, differences exist with regard to how soil-type names are modified according to the contents of other than the main soil fraction. The chart applies the name convention summarized in Section 1.3, which is the one indicated in the Canadian Foundation Engineering Manual (1992; 2006).

The data from the CPT diagrams presented in Figure 2.1 are presented in the chart shown in Figure 2.12. The three layers are presented with different symbols and the chart is shown in both logarithmic and linear scale. Obviously, linear scales enable larger resolution for more detailed assessment.

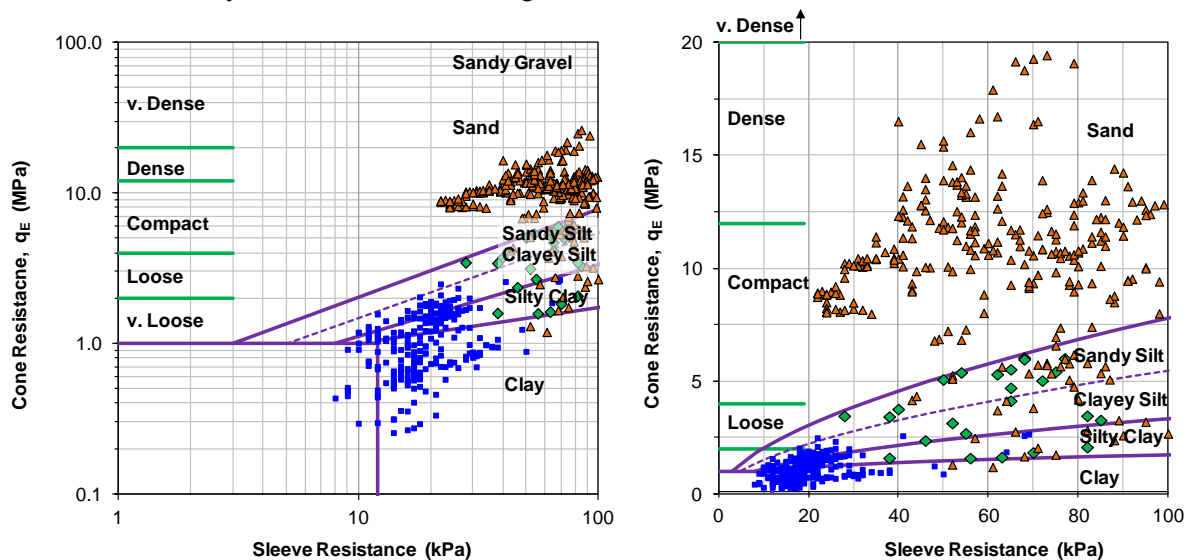


Fig. 2.12 The CPT sounding shown in Fig. 2.1 plotted in a Eslami-Fellenius profiling chart in both logarithmic and linear scales.

## 2.4 Comparison between the Eslami-Fellenius and Robertson (1990) Methods

To provide a direct comparison between the Robertson (1990) profiling chart and the Eslami-Fellenius chart, three short series of CPTU data were compiled from sites with very different geologic origin where the soil profiles had been established independently of the CPTU. The borehole information provides soil description and water content of recovered samples. For one of the cases, the grain size distribution is also available. The CPTU-diagrams and the soil classification charts from the site are shown in Figures 2.13 and Figure 2.14. The soil and CPTU information for the specific points are compiled in Table 2.3. The three sites are:

1. North Western University, **Evanston**, Illinois (Finno 1989). CPTU data were obtained in a soil profile consisting of 7 m of sand deposited on normally consolidated silty clay. The piezometer was attached to the cone face ( $U1$ ) and not behind the shoulder ( $U2$ ). The method of converting the pore pressure measurement to the  $U2$ -value presented by Finno (1989) has been accepted here, although the conversion is disputed. For comments, see Mayne et al. (1990).

2. Along the shore of Fraser River, **Vancouver**, British Columbia (personal communication, V. Sowa, 1998). A 20 m thick mixed soil profile of deltaic deposits of clay, silt, and sand. The first four data points are essentially variations of silty clay or clayey silt. The fifth is a silty sand.
3. University of Massachusetts, **Amherst**, Massachusetts (personal communication, P. Mayne, 1998). A soil profile (Lutenegger and Miller 1995) consisting of 5 m of a thick homogeneous overconsolidated clayey silt. This case includes also information on grain size distribution. The borehole records show the soil samples for data points Nos. 3 through 7 to be essentially identical. The  $U_2$ -measurements indicate substantial negative values, that is, the overconsolidated clay dilates as the cone is advanced.

**TABLE 2.3 Soil and CPTU information**

No.	Depth (m)	Description	Water Content (%)	Soil Fractions (%)	CPTU Data		
					$q_t$ (MPa)	$f_s$ (kPa)	$U_2$ (kPa)
<b>Evanston, IL (Groundwater table at 4.5 m)</b>							
1	1.5	SAND, Fine to medium, trace gravel	29		25.08	191.5	49.8
2	3.4	SAND, Medium, trace gravel	16		3.48	47.9	16.0
3	6.7	SAND, Fine, trace silt, organics	26		32.03	162.8	111.7
4	8.5	Silty CLAY, trace sand	28		0.51	21.13	6.4
5	9.5	Silty CLAY, little gravel	22		0.99	57.53	9.6
6	12.8	Silty CLAY, little gravel	23		0.69	19.23	83.0
7	16.5	Silty CLAY, little gravel	24		0.77	17.24	27.1
<b>Vancouver, BC (Groundwater table at 3.5 m)</b>							
1	3.7	CLAY to Clayey SILT	52		0.27	16.1	82.5
2	5.8	Clayey SILT to SILT	34		1.74	20.0	177.1
3	10.2	Silty CLAY	47		1.03	13.4	183.5
4	14.3	Silty CLAY	40		4.53	60.2	54.3
5	17.5	Silty SAND	25		10.22	77.8	118.5
<b>Amherst, MA (Groundwater table at 2.0 m)</b>							
				Clay Silt Sand			
1	0.6	SAND and SILT, trace clay	20	10 30 60	2.04	47.5	-9.4
2	1.5	Clayey SILT, trace sand	28	23 67 10	2.29	103.3	-47.3
3	2.0	Clayey SILT, trace sand	36	21 75 4	1.87	117.0	-69.5
4	2.5	Clayey SILT, trace sand	29	33 65 2	1.86	117.0	-70.3
5	3.0	Clayey SILT, trace sand	40	36 62 2	1.37	46.8	-66.3
6	3.5	Clayey SILT, trace sand	53	40 58 2	1.38	48.9	-50.7
7	4.0	Clayey SILT, trace sand	60	40 58	0.91	17.9	-46.9
8	4.5	Clayey SILT	30	42 57 1	0.55	12.9	-29.3

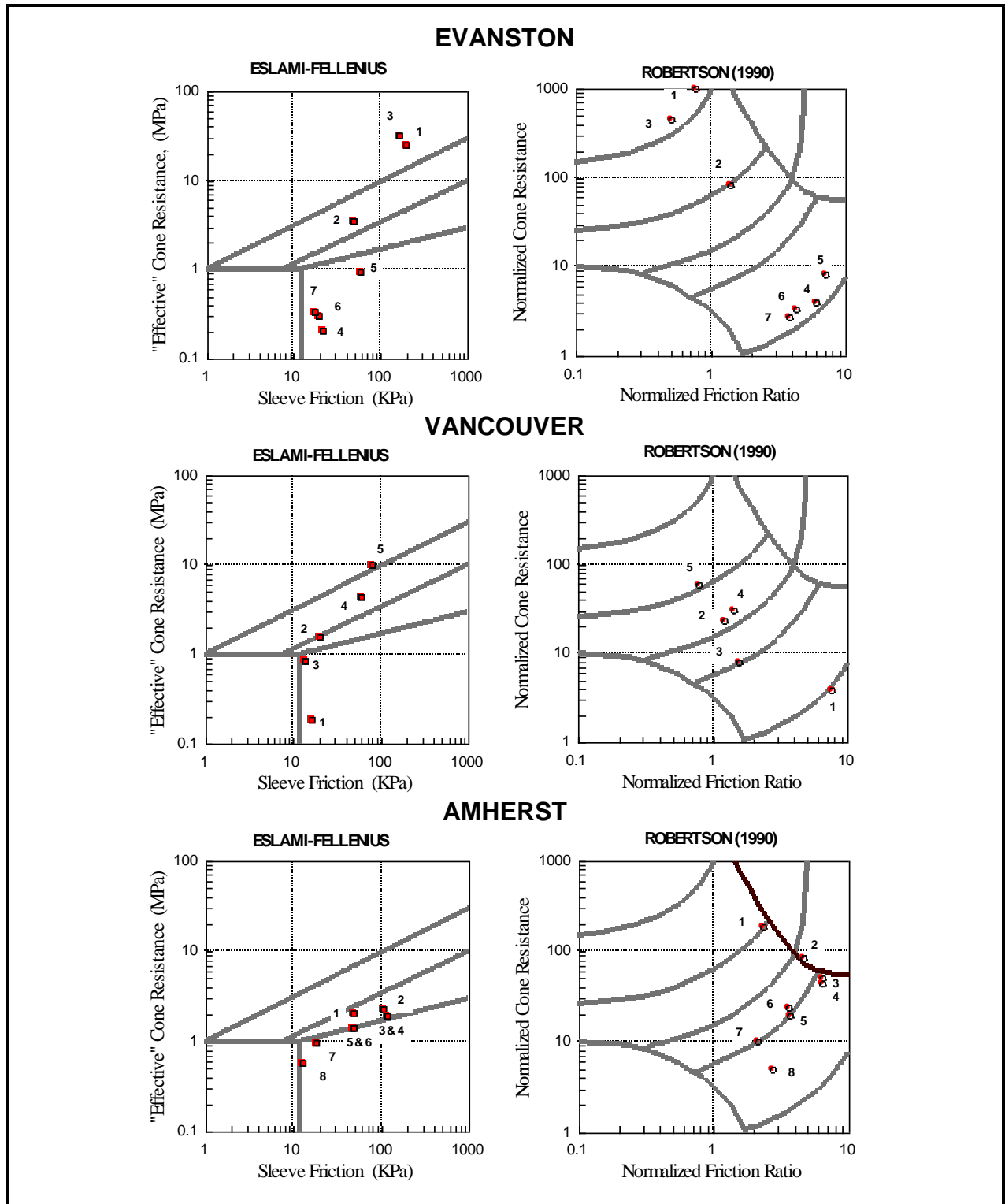


Fig. 2.13 Comparison between the Table 1 data plotted in Eslami-Fellenius and Robertson profiling charts. [Note that the boundary line between silty sand ("Area 4") and Sand (Area "5") in the former chart is drawn rising from sleeve resistance of 1 kPa, per an early definition from when the method was first developed].



For each case, the soil information in Table 1 is from depths where the CPTU data were consistent over a 0.5 m length. Then, the CPTU data from 150 mm above and below the middle of this depth range were averaged using geometric averaging, preferred over the arithmetic average as it is less subject to influence of unrepresentative spikes and troughs in the data (a redundant effort, however, as the records contain no such spikes and troughs). The CPTU data were analyzed by the Eslami-Fellenius (1996) and the Robertson (1990) profiling methods and the results are shown in [Figure 2.13](#).

**Evanston data:** The first three samples are from a sand soil and both methods identify the CPTU data accordingly. The remaining data points (Nos. 4 through 7) given as Silty Clay in the borehole records are identified as Clay/Silt by the Eslami-Fellenius and as Clay to Silty Clay by the Robertson method, that is, both methods agree with the independent soil classification.

**Vancouver data:** Both methods properly identify the first four data points to range from Clayey Silt to Silty Clay in agreement with the independent soil classification. The fifth sample (Silty Sand) is identified correctly by the Eslami-Fellenius method as a Sand close to the boundary to Silty Sand and Sandy Silt. The Robertson method identifies the soil as a Sandy Silt to Clayey Silt, which also is essentially correct.

**Amherst data:** Both methods identify the soils to be silt or clay or silt and clay mixtures. Moreover, both methods place Points 3 through 7 on the same soil type boundary line, that is, confirming the similarity between the soil samples. However, the spread of plotted points appear to be larger for the Robertson method; possibly due that its profiling does not consider the pore pressures developed by the advancing penetrometer (but for the pore pressure on the shoulder, of course), while the Eslami-Fellenius method does account for the substantial negative pore pressures that developed.

## 2.5 Comparisons

- I. The CPT methods (mechanical cones) do not correct for the pore pressure on the cone shoulder and the profiling developed based on CPT data may not be relevant outside the local area where they were developed. The error due to omitting the pore water pressure correction is large in fine-grained soils and small in coarse-grained soils.
- II. Except for the profiling chart by Begemann (1965) and Eslami-Fellenius (1997), all of the referenced soil profiling methods plot the cone resistance versus its own inverse value in one form or another. This generates data distortion and violates the rule that dependent and independent variables must be rigorously separated.
- III. Some profiling methods, e.g., Robertson (1990), include normalization which requires unwieldy manipulation of the CPT data. For example, in a layered soil, should a guesstimated “typical” density value be used in determining the overburden stress or a value that accurately reflects the density? Moreover, regardless of soil layering, determining the effective overburden stress (needed for normalization) requires knowledge of the pore pressure distribution, which is not always hydrostatic but can have an upward or downward gradient and this information is rarely available.
- IV. The normalization by division with the effective overburden stress does not seem relevant. For example, the normalized values of fine-grained soils obtained at shallow depth (where the overburden stress is small) will often plot in zones for coarse-grained soil.
- V. The Robertson (1990) and the Eslami-Fellenius (1997) CPTU methods of soil profiling were applied to data from three geographically apart sites having known soils of different types and geologic origins. Both methods identified the soil types accurately.

- VI. Eslami-Fellenius (1996) method has the advantage over the Robertson (1990) that it avoids the solecism of plotting data against their own inverted values and associated distortion of the data.
- VII. Eslami-Fellenius (1997) method has the additional advantage over other referenced piezocone methods in that it allows the user to directly assess a value without first having to determine distribution of total and effective stress to use in a subtraction and multiplication effort in calculating a “normalized” set of values.
- VIII. A soil profiling chart based on a Begemann type plot, such as the Eslami-Fellenius (1996) method can easily be expanded by adding delineation of strength and consistency of fine-grained soils and relative density and resistance angle of coarse-grained soils per the user preferred definitions or per applicable standards.
- IX. No doubt, CPTU sounding information from a specific area or site can be used to further detail a soil profiling chart and result in delineation of additional zones of interest. However, there is a danger in producing a very detailed chart inasmuch the resulting site dependency easily gets lost leading an inexperienced user to apply the detailed distinctions beyond their geologic validity.
- X. The CPTU is an excellent tool for the geotechnical engineer in developing a site profile. Naturally, it cannot serve as the exclusive site investigation tool and soil sampling is still required. However, when the CPTU is used govern the depths from where to recover soil samples for detailed laboratory study, fewer sample levels are needed, reducing the costs of a site investigation while simultaneously increasing the quality of the information because important layer information and layer boundaries are not overlooked.

## 2.6 Profiling case example

Figure 2.14 shows  $q_b$ ,  $f_s$ ,  $U_2$ ,  $u_0$ , and  $f_R$  diagrams from a CPTU sounding in a sand deposit (in the Fraser River delta outside Vancouver, BC). Borehole samples indicate the soil profile to consist of loose to medium to fine silty sand containing layers or zones of silt, silty clay, and clay. As indicated in the figure, the borehole records agree well with the layering established using the profiling methods of Eslami-Fellenius (1997). The reading spacing was 10 mm. The depth measurements are corrected for the CPT rod inclination (deviation was in the form of a gentle sweep): the depth indicated by the accumulated rod lengths was 94 m, whereas the inclination-corrected maximum depth was 90.5 m (see Section 2.8).

The overall soil profile can be separated on four main zones, as indicated below. The soil descriptions was confirmed from bore hole samples. The colored block diagrams to the right are obtained from soil profiling using the CPTU data.

0 m	-	2.6 m	Coarse SAND
2.6 m	-	6.0 m	CLAY, Silty CLAY
6.0 m	-	13.0 m	Medium to fine SAND and Silty SAND (Fine sand portion = 30 % to 80 %)
12.5 m	-	16.0 m	Fine SAND trace silt
16.0 m	-	34.0 m	Fine to medium SAND
34.0 m	-	38.0 m	Silty SAND
38.0 m	-	70.0 m	CLAY with numerous silt seams and sandy clay
70 m	====>		Silty CLAY with seams of silt and sandy silt

Established by the pore pressure dissipation measurements (see Section 2.7), the pore pressure distribution in the clay layer below 38 m depth is artesian; the pore pressure head above ground is about 7 m.

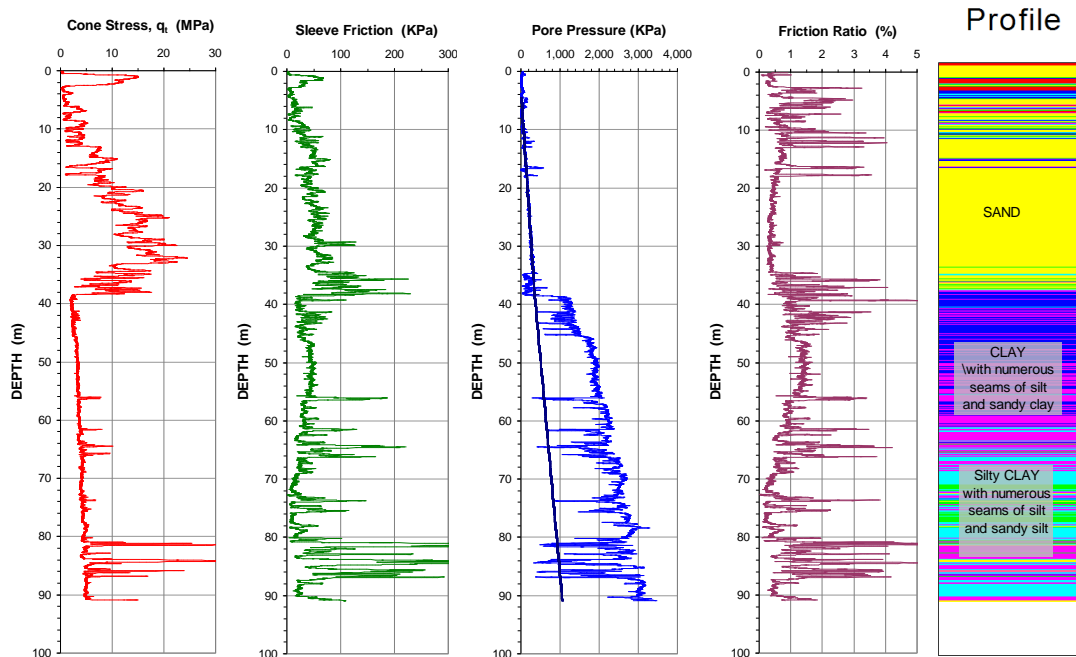


Fig. 2.14 CPTU sounding diagrams with profiling according to the Eslami-Fellenius(1997) method. Data from Amini et al. (2008).

The soil profile determined from CPTU data is usually in agreement with the soil profile determined from the conventional grain size distribution. In normally consolidated sedimentary soils, the CPTU-determined soil profile usually agrees well with grain-size description determined from soil samples. However, in overconsolidated or residual soils, the CPTU soil profile can often deviate from the soil sample description. Every site investigation employing CPTU sounding should include soil sampling. It is not necessary to obtain the soil samples in regular boreholes. Modern CPTU equipment includes the means to push down a plastic sampling tube inside a steel pipe of the same size as the cone rod. A continuous core of soil is recovered from where "disturbed" samples can be selected for detailed study. Figure 2.15 shows sections of four such cores recovered next to a CPTU sounding.



Fig. 2.15 Sections of soil cores , ranging from fill, sandy clay, clay, through sand with pieces of gravel. Sampling by means of CPTU device equipped with separate sampler.

**Figure 2.16** shows all cone data for the upper 20 m plotted in a Eslami-Fellenius profiling chart with **Figure 2.16A** showing the data plotted using axes in the usual logarithmic scales. However, the logarithmic plot only serves the purpose of compressing data so that all can be shown together. The log scale makes small relative changes of small values show up and yet includes similarly relative changes for larger values. However, when, as in the example case, the span between the small and the larger values is limited, the plot can preferably be made using linear scales, as shown in **Figure 2.16B**.

**Figure 2.17** (on Page 2-22) shows the data in profiling charts according to the Robertson 1986 method in logarithmic and linear scales. The linear plot indicates that the organic soil distinction (Layer 2) is probably not practical and that the separation between Layers 4 and 5 could well be considered as one layer. **Figure 2.18** (on Page 2-23) shows the same for Robertson 1990 method. It is clearly evident from **Figure 2.18B** that the method is not suitable for linear plotting even for a relatively small range of values of the example.

## 2.7 Dissipation Time Measurement

In fine-grained soils, the time for the dissipation of the generated pore pressure is of interest. Usually in conjunction with adding a rod to the rod assembly, the cone is kept unmoving and the pore pressures ( $u_2$ ) are recorded. The dissipation time to neutral pore pressure is considered a measure of the coefficient of consolidation,  $c_H$ . (Mayne et al. 1990; 2001). The pore pressure after full dissipation is a measure of the phreatic height at that depth and can be used as indication of pore pressure gradient in the soil (as was done in the case of the CPTU sounding shown in **Figure 2.13**).

## 2.8 Inclination Measurement

When a cone is pushed into the ground it is started vertically, but, understandably, the cone rod assembly will start to bend in the soil and the cone will deviate from the vertical line through the starting point on the ground. All CPT systems incorporate inclination measurements and the inclination is recorded for each measurements of cone resistance, sleeve resistance, and pore pressure. Sometimes, only a value of the maximum inclination is recorded. This will allow a calculation of the radial and vertical deviation of the cone, but not the direction. Other cones show the inclination in two perpendicular directions, which measurements then allow for a calculation of the maximum inclination and the location of the cone at each depth. Down to depths of about 30 m, the deviation is usually not significant. **Figure 2.19** shows deviation records that are unmistakably large; the cone moved 12 m laterally away from the starting point and the bending caused the depth measurement of 30 m to in reality have been slightly less than 28 m — "the cone is lifting its foot". Inclination measurements are not often reported. Obviously, they should be checked and the cone data corrected for depth deviation, when appropriate.

## 2.9 Shear -wave Measurement

The seismic CPTU, the SCPTU, incorporates a geophone for measuring the arrival time of a shear wave generated on the ground surface close to the cone rod. The shear-wave is generated by giving a horizontal impact to a steel plate placed on the ground surface and the time for generating the impact and arrival at the geophone are recorded. The test is normally performed when adding a cone rod to the rod length (that is, the cone is not moving). Impacts are given at intermittent depths and the results are evaluated as the difference in travel time between geophone from the previous test depth and the current depth, resulting in the shear wave velocity for the soil between the two depths. The shear wave velocity is then used directly in analysis or converted to low-strain dynamic shear modulus ( $G_{max}$ ). Or combined with vibration velocity when assessing the risk for vibration settlement due to pile driving (see Chapter 10).

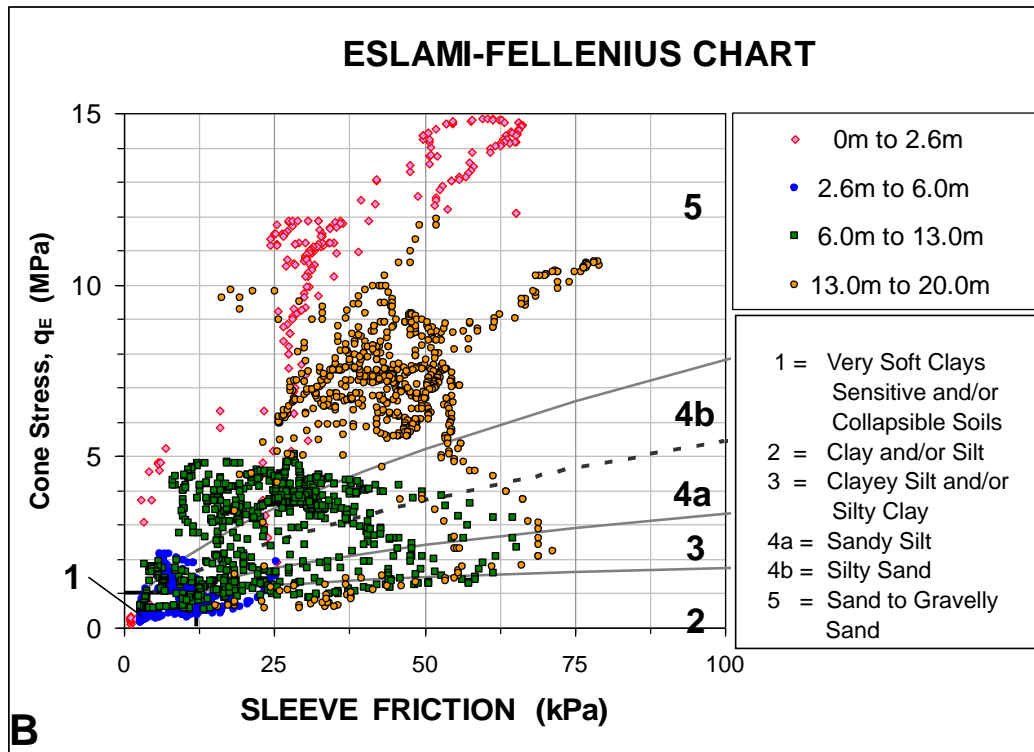
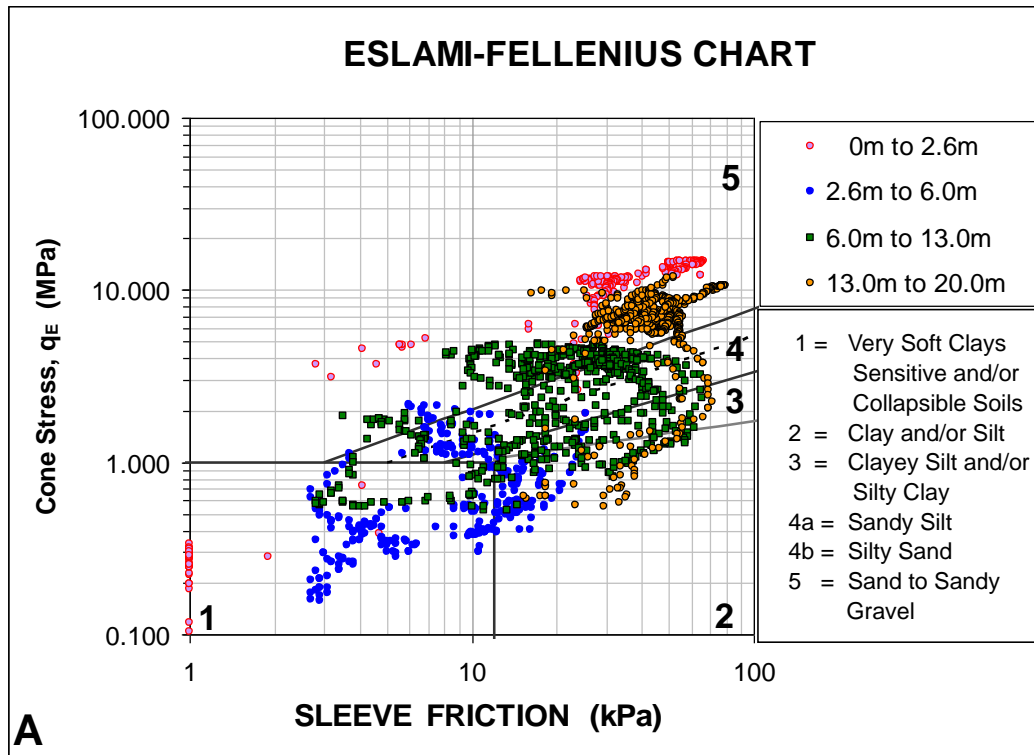


Fig. 2.16 A. Eslami-Fellenius profiling chart with axes in logarithmic scale  
 B. Eslami-Fellenius profiling chart with axes in linear scale

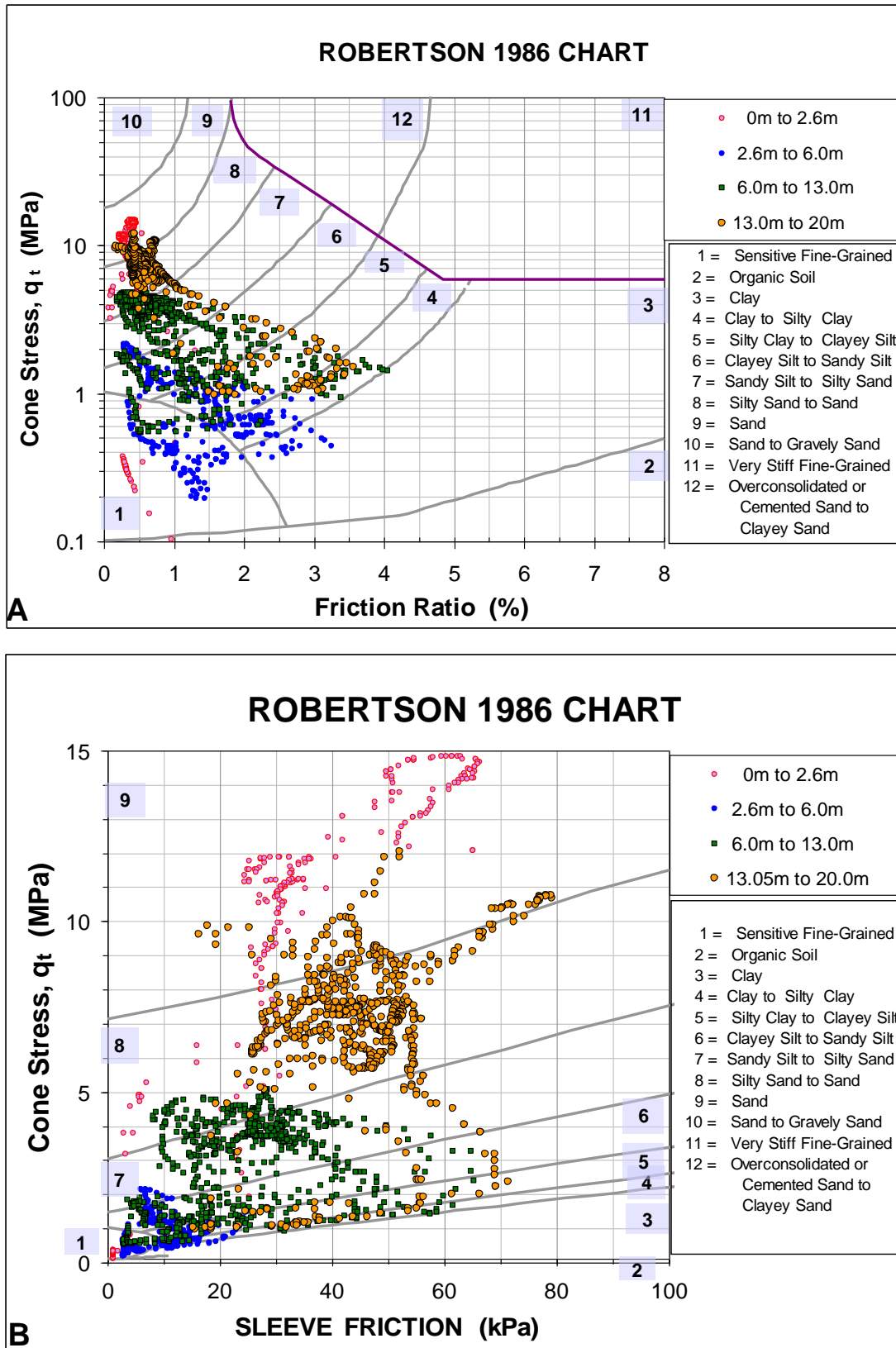


Fig. 2.17 A. Robertson 1986 profiling chart with axes in logarithmic scale  
 B. Robertson 1986 profiling chart with axes in linear scale

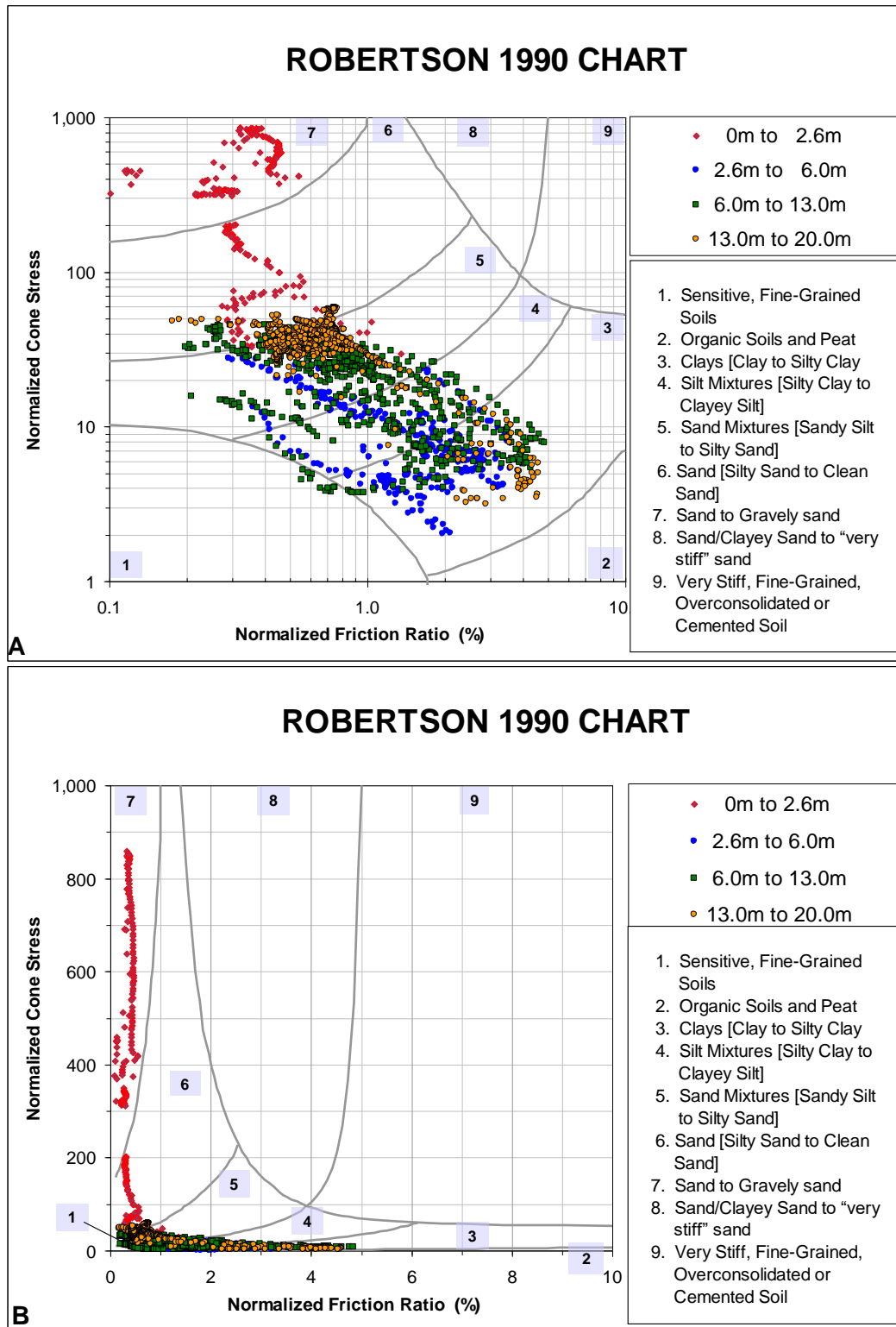


Fig. 2.18 A. Robertson 1990 profiling chart with axes in logarithmic scale  
 B. Robertson 1990 profiling chart with axes in linear scale

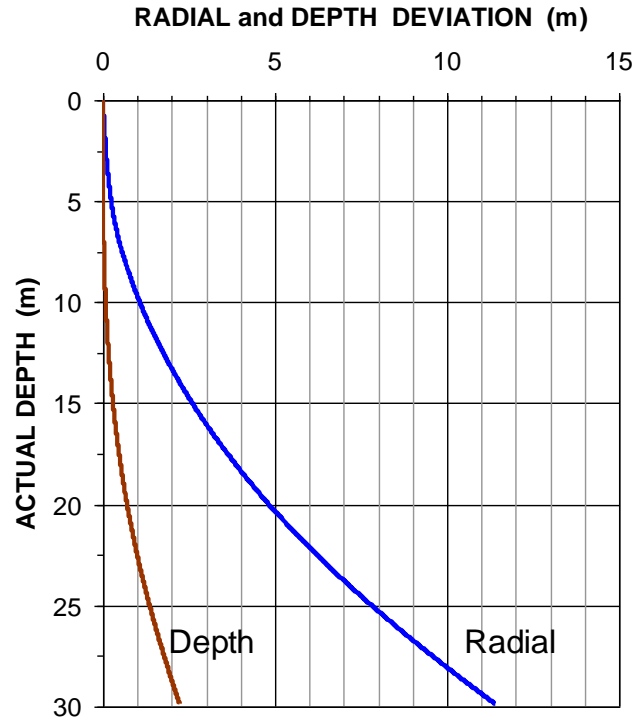


Fig. 2.19 Radial and depth deviation for a 30 m deep cone sounding in Squamish, BC

## 2.10 Depth and Stress Adjustment

The results of cone and sleeve resistance measurements as used for compressibility reference are affected by the effective overburden stress (Jamiołkowski et al. 1988). Therefore, it is necessary to consider this effect when interpreting CPT results used for settlement analysis. For the depth adjustment of the cone resistance, Massarsch (1994) proposed to apply a dimensionless adjustment factor,  $C_M$ , to the cone resistance according to Eq. 2.7, based on the mean effective stress,  $\sigma'_m$ .

$$(2.7) \quad C_M = \left( \frac{\sigma'_m}{\sigma_r} \right)^{0.5}$$

where  $C_M$  = stress adjustment factor  $\leq 2.5$   
 $\sigma'_m$  = mean effective stress (kPa), determined according to Eq. 2.8.  
 $\sigma_r$  = reference stress = 100 kPa

$$(2.8) \quad \sigma'_m = \frac{\sigma'_v (1 + 2K_0)}{3}$$

where  $\sigma'_m$  = mean effective stress  
 $\sigma'_v$  = vertical effective stress  
 $K_0$  = coefficient of horizontal earth stress at rest =  $\sigma'_h / \sigma'_v$  (effective stress condition)  
 $\sigma'_h$  = horizontal effective stress

The stress-adjusted (or depth-adjusted) cone penetration resistance,  $q_{tM}$ , is



$$(2.9) \quad q_{tM} = q_t C_M$$

where  $q_{tM}$  = stress-adjusted (depth-adjusted) cone resistance  
 $q_t$  = cone resistance  
 $C_M$  = stress adjustment factor  $\leq 2.5$

At shallow depth and toward the ground surface, values per Eq. 2.9 increase disproportionately and it is necessary to limit the adjustment factor to a value of 2.5.

Determining the mean stress (Eq. 2.8) requires knowledge of the coefficient of earth stress at rest,  $K_0$ . In normally consolidated soils, the magnitude of the horizontal earth stress is usually assumed to follow Eq. 2.10 (Jaky 1948). For notes on determining  $K_0$  from CPTU records, see Clause 2.12.3.

$$(2.10) \quad K_0 = 1 - \sin \phi'$$

where  $K_0$  = coefficient of horizontal earth stress (effective stress condition)  
 $\phi'$  = effective friction angle

The effective friction angle for normally consolidated sand and silt ranges between  $30^\circ$  and  $36^\circ$ , which range corresponds to the relatively narrow range of a  $K_0$  of about 0.4 through 0.6.

Compaction results in an increase of the earth stress coefficient at rest,  $K_0$ . However, in overconsolidated soils, that is, compacted soils, it is more difficult to estimate  $K_0$ . Several investigators have proposed empirical relationships between the earth stress coefficient of normally and overconsolidated sands and the overconsolidation ratio, OCR, as given in Eq. 2.11.

$$(2.11) \quad \frac{K_1}{K_0} = OCR^k \quad \text{which converts to: (2.11a) } OCR = \left(\frac{K_1}{K_0}\right)^{\frac{1}{k}} \quad \text{and 2.11b } K_0 = K_1/OCR^k$$

where  $K_0$  = coefficient of earth stress at rest for normally consolidated sand  
 $K_1$  = coefficient of earth stress at rest for overconsolidated sand  
 $\beta k$  = empirically determined exponent, usually assumed equal to about 0.5

The "normally consolidated sand" and the "overconsolidated sand" can be a hydraulic fill before and after compaction. The after-to-before ratio,  $K_1/K_0$ , of the earth stress coefficients can be considered equal to the after-to-before ratio,  $f_{s1}/f_{s0}$ , of between the sleeve resistance. Thus, assuming that the coefficient,  $k$ , is 0.5, Eq. 2.11 becomes Eq. 2.11c.

$$(2.11c) \quad OCR = (f_{s1}/f_{s0})^2.$$

### 2.11 Determining the Janbu Modulus Number, $m$ , from CPT

The most important aspect of a soils investigation and a geotechnical design of a foundation is to assess the settlement of the foundation. For cohesive soils the necessary soil parameters are determined from laboratory tests on 'undisturbed' samples. For coarse-grained soil layers, acceptably undisturbed samples are difficult to obtain and test. The CPTU tool allows a determination of the soil compressibility in terms of the Janbu modulus number,  $m$ , which is a parameter that, for cohesive soil, is equal to the conventional  $C_c e_0$  relation. It also is used for expressing compressibility of soils that can be assumed to respond linearly to a load change, conventionally expressed by an E-modulus. It is particularly useful when assessing potential settlement in intermediate soils, such as silty sand and sandy silt. The background and application of the Janbu modulus number is shown in detail in Section 3.5; for E-modulus in Section 3.3.

Massarsch (1994b) proposed a semi-empirical relationship shown in Eq. 2.12 between the modulus number and the cone resistance adjusted for depth according to Section 2.10.

$$(2.12) \quad m = a \left( \frac{q_{tM}}{\sigma_r} \right)^{0.5}$$

where  $m$  = modulus number (---)  
 $a$  = empirical modulus modifier, which depends on soil type (---)  
 $q_{tM}$  = stress-adjusted (depth-adjusted) cone resistance (Eq. 2.9) (kPa)  
 $\sigma_r$  = reference stress = 100 kPa

The modulus modifier,  $a$ , has been determined from the evaluation of extensive field and laboratory data (Massarsch 1994) and shown to vary within a relatively narrow range for each soil type. Massarsch et al. (1997) proposed the values for silt, sand, and gravel listed in Table 2.4 supplemented with a graph showing the ranges for "a" plotted in an Eslami-Fellenius soil-profiling chart with sleeve resistance in linear scale.

Eqs. 2.7 through 2.12 can be combined in a single equation, Eq. 2.13.

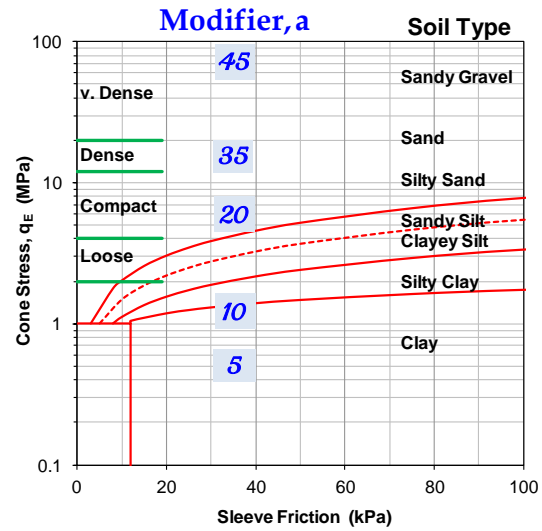
$$(2.13)$$

where  $m$  = modulus number (---)  
 $a$  = empirical modulus modifier, which depends on soil type (---)  
 $q_t$  = cone resistance (kPa)  
 $\sigma_r$  = reference stress = 100 kPa  
 $\sigma_v$  = effective overburden stress (kPa)  
 $K_0$  = coefficient of earth stress at rest for normally consolidated sand (---)

**TABLE 2.4** Modulus Modifier Factor,  $a$ , for different soil types (Massarsch et al. 1997)

Soil Type	Modulus Modifier, $a$
Soft clay	3*)
Firm clay	5*)
Silt, organic soft	7
Silt, loose	12
Silt, compact	15
Silt, dense	20
Sand, silty loose	20
Sand, loose	22
Sand, compact	28
Sand, dense	35
Gravel, loose	35
Gravel, compact	40
Gravel, dense	45

\* These values are based on limited calibration to tests in normally consolidated lacustrine and marine clays. Clays at other sites may differ considerably.



In sand, pore pressures are usually very small in relation to the cone resistance. Therefore, whether the cone resistance is applied as  $q_c^-$ ,  $q_t^-$ ,  $q_E^-$ , or  $q_{cM}$ -values matters little in comparison to the need for correlation (calibration) to actual conditions.

CPT readings are taken intermittently at closely spaced distances, normally every 20 mm, preferably every 10 mm. It is often beneficial to filter the cone resistance values,  $q_t$ , so that the peaks and troughs in the data are removed. The most useful filtering is obtained by a geometric average over a short length, say, about 0.5 m.

The values of the Modulus Modifier,  $a$ , given in Table 2.4 have been verified in compacted hydraulic fills. They have yet to be verified in naturally deposited soils. Therefore, use of the values should be coupled with cautionary judgment. At sites where oedometer testing of recovered ‘undisturbed’ samples can be performed, the CPT data from the corresponding layer can, and should be, calibrated to verify the Modulus Modifier for the site.

The effect of filtering and depth-adjusting the  $q_t$  values and calculation of the modulus number profile is illustrated in Figure 2.20 using the CPT soundings of Figure 2.1.

The CPTU sounding used as example in Figure 2.1 to show profiles of various soil parameters has also been used to calculate the compressibility (modulus number) for the profile (site in Alberta; Fellenius 2004).

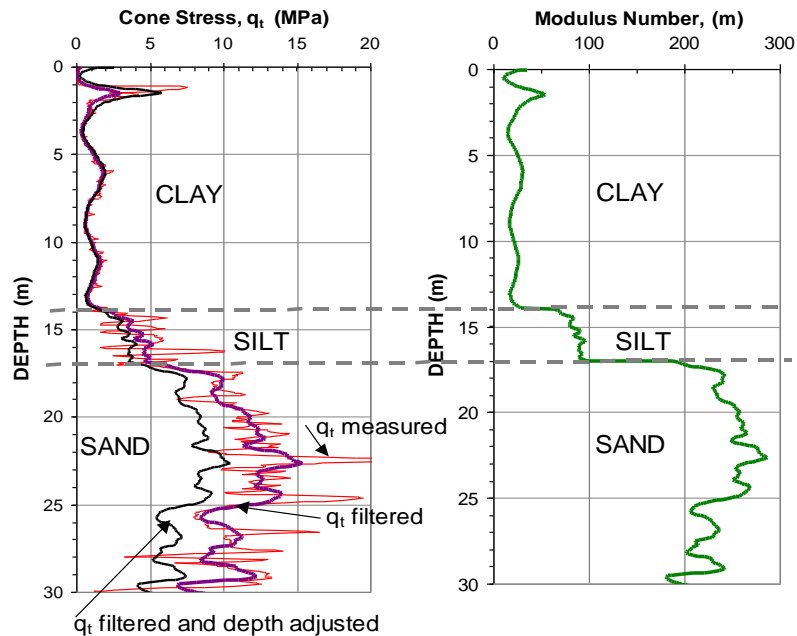


Fig. 2.20 Example of filtered and depth-adjusted  $q_t$  and profile of the resulting modulus number,  $m$

Figure 2.21 shows the unfiltered  $q_t$ -profile, the filtered  $q_t$ -profile, and the depth-adjusted values. The second of the three diagrams shows the calculated modulus number profile with the modulus numbers from oedometer tests as adjusted in the fit. The third shows a profile of the modifier,  $a$ , used in the fit.

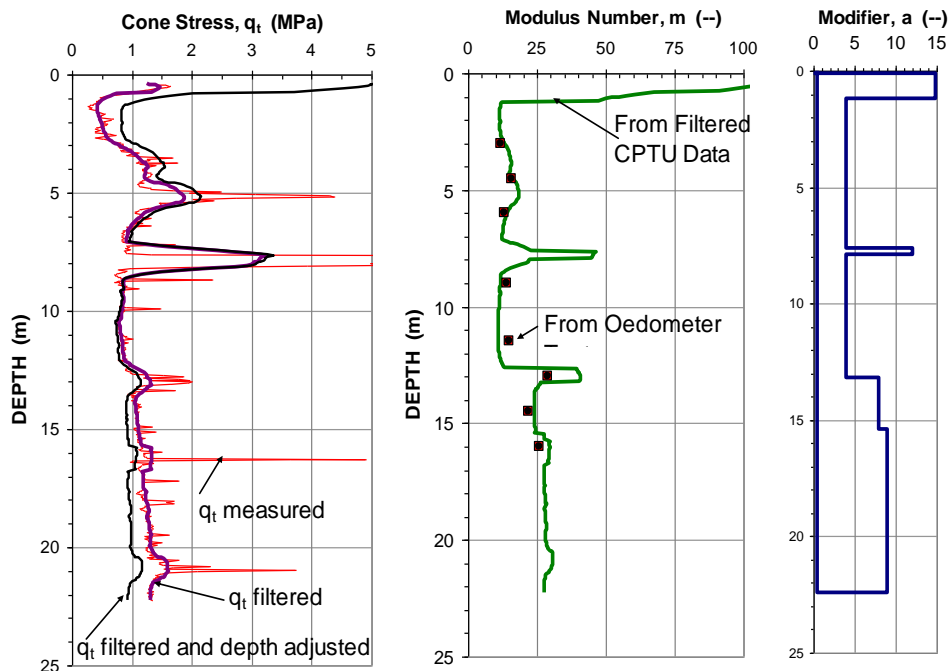


Fig. 2.21 Example of filtered and depth-adjusted  $q_t$  values and profile of the resulting modulus number,  $m$ , fitted by means of the modifier,  $a$ , to  $m$ -numbers determined in the oedometer tests.

## 2.12 Determining Soil Parameters from CPTU Measurements

Many geotechnical parameters are diffuse by themselves. Their reliability depends to a large extent on how they are applied, in what geology, for what design problem, and foremost, on what experience the user of the relation has in the application of the parameter. When a parameter is obtained through correlation to the cone penetrometer results, the user's direct experience becomes even more important. **No formula promoting a relation between a geotechnical parameter and the CPT results should be accepted without thorough correlation to independent test results at the site considered.** However, when such correlation, which by necessity is intermittent, has proven a consistent relation at a site, then, it can be used to establish a more detailed distribution of the parameters at a site from the CPTU profile.

### 2.12.1 Undrained Shear Strength

A popular application for CPT results is to estimate values of undrained shear strength and several correlations exist. The popularity exists despite that undrained shear strength can be determined by so many methods, such as in-situ vane, unconfined compression test, triaxial testing, direct shear, simple shear, etc. The method of determining the undrained shear strength often varies with the design problem to be addressed. Eq. 2.14 is typical of the relations which have been proposed for determining the undrained shear strength from CPTU data. (Kulhawy and Mayne 1990).

$$(2.14) \quad \tau_u = \frac{q_t - \sigma_v}{N_{kt}}$$

where

- $\tau_u$  = undrained shear strength
- $q_t$  = cone resistance corrected for pore water pressure on shoulder (Eq. 2.1)
- $\sigma_v$  = total overburden stress
- $N_{kt}$  = a coefficient;  $10 < N_{kt} < 20$

An example of undrained shear strength values calculated from Eq. 2.15 is presented in Figure 2.22A along with the main cone-stress profile. The sounding is from a site in Alberta 185 km north of Edmonton described by Fellenius (2008). The groundwater table lies at a depth of 1.5 m and the pore water pressure is hydrostatically distributed. The soil profile consists of 7.5 m of soft silty clay with a water content of about 35 % through 70 %, a Liquid Limit of about 60 % through 70 %, a Plastic Limit of about 15 through 40 , and a Plasticity Index of about 25. The Janbu modulus number ranges from about 12 through 20. The upper about 7 m of the clay is overconsolidated with an OCR of about 2 through 5. Triaxial consolidated and undrained tests and direct shear testing on the clay indicated a strain-softening soil having a friction angle ranging from 21° through 25° with a residual (post peak) value of about 21°. A small cohesion intercept was found in the range of 10 kPa through 25 kPa. The clay is a re worked, transported, and re deposited glacial till clay. The clay is interrupted at 5 m depth by an about 0.5 m thick layer of silty sand. At a depth of 7.5 m lies a second 0.5 m thick layer of silty sand. The sand is followed by soft silty sandy gravely ablation clay till that continues to the end of the borehole at a depth of about 25 m. The ranges of water content and indices of the clay till are about the same as those of the upper clay layer. Consolidation tests on samples from the clay till show the Janbu modulus number of the clay to range from 20 through 30. No recompression modulus is available, but the sandy clay till is clearly overconsolidated.

A second example of undrained shear strength values calculated from Eq. 2.7 is presented in Figure 2.23B. The sounding is from the Langley, BC. Below 5 m depth, the soils consist of lightly to over-consolidated stiff clay to large depth. Some thin sand layers exist between 33 m and 37 m depth.

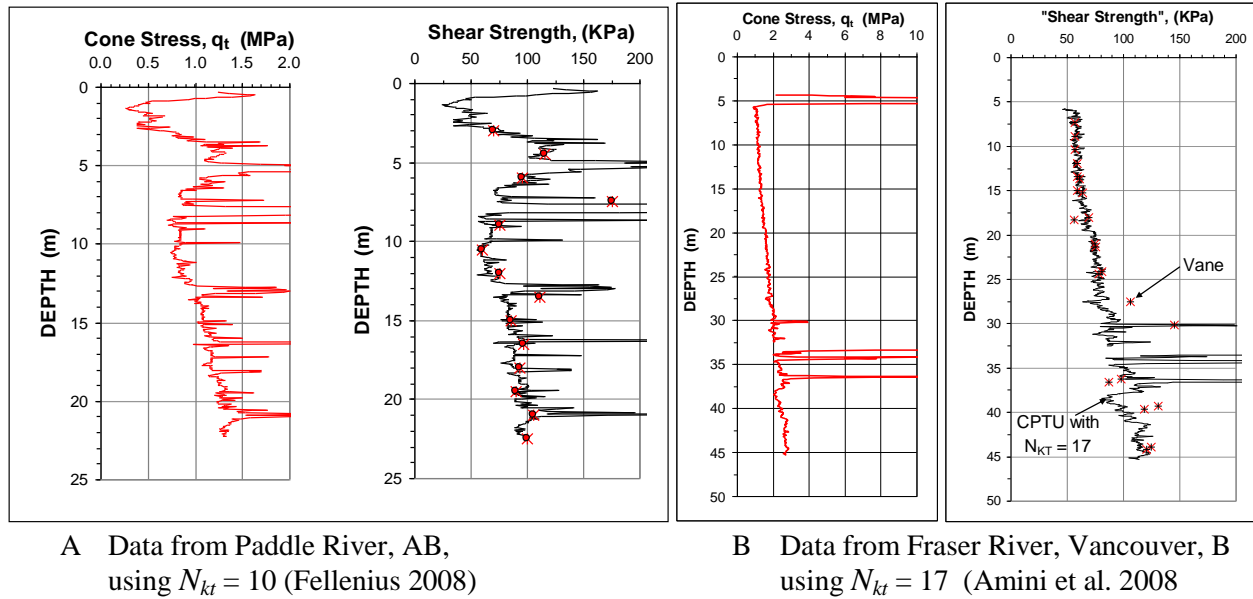


Fig. 2.22 Cone resistance ( $q_t$ ) and undrained shear strength profiles fitted to a vane shear profile from tests next to the CPTU sounding.

### 2.12.2 Overconsolidation Ratio, OCR

Correlations between the CPTU test data and the overconsolidation ratio, OCR, have also been proposed. As the stress condition in sand is not governed by consolidation, the better term is "prestress ratio", but the old term has been retained in this document. Eq. 2.15 presents one method (Kulhawy and Mayne 1990).

$$(2.15) \quad OCR = C_{OCR} \frac{q_t - \sigma_v}{\sigma'_v}$$

where  $OCR$  = overconsolidation ratio (prestress ratio)

$C_{OCR}$  = a coefficient;  $\cong 0.2 < C_{OCR} < \cong 0.3$

$q_t$  = cone resistance corrected for pore water pressure on shoulder (Eq. 2.1).

Note,  $q_t$  is a total stress parameter.

$\sigma_v$  = total overburden stress

$\sigma'_v$  = effective overburden stress

An OCR profile from the Alberta CPTU sounding is shown in [Figure 2.23](#) fitted to OCR values determined in eight oedometer tests on Shelby samples recovered in a bore hole next to the CPTU sounding. The fit was obtained with an OCR-coefficient,  $C_{OCR}$ , of 0.2.

### 2.12.3 Earth Stress Coefficient, $K_0$

Also the earth stress coefficient,  $K_0$ , the ratio between vertical and horizontal effective stress,  $\sigma'_v/\sigma'_h$ , can be correlated to CPTU test results. Eq. 2.16 illustrates one method commonly referenced (Kulhawy and Mayne 1990). The relation usually returns  $K_0$ -coefficients that are larger than unity and should only be considered a guide.

$$(2.16) \quad K_0 = C_K \frac{q_t - \sigma_v}{\sigma'_v}$$

where

- $K_0$  = earth stress coefficient
- $C_K$  = a coefficient;  $C_K \cong 0.1$
- $q_t$  = cone resistance corrected for pore water pressure on shoulder (Eq. 2.1)
- $\sigma_v$  = total overburden stress
- $\sigma'_v$  = effective overburden stress

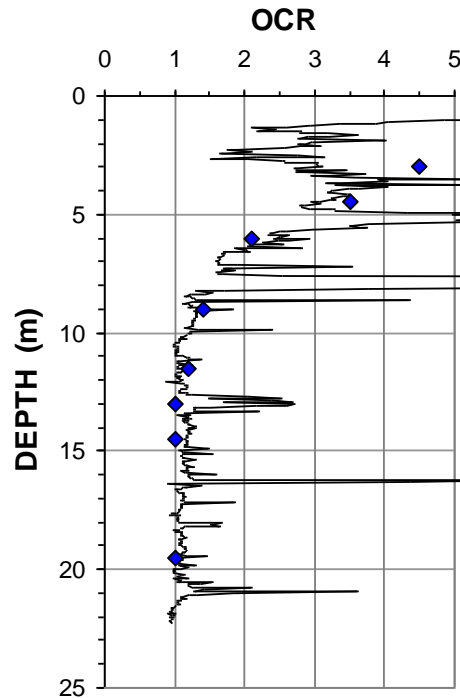


Fig. 2.23 OCR profile fitted to OCR values determined from oedometer tests on Shelby samples. Data from Paddle River site, Alberta (Fellenius 2008).

A  $K_0$ -profile from the Alberta CPTU sounding is shown in [Figure 2.24](#).

#### 2.12.4 Friction Angle

The CPTU results are frequently used to estimate a value for the effective friction angle of sand, typically, using the relation shown in Eq. 2.17 (Robertson and Campanella 1983).

$$(2.17) \quad \tan \phi' = C_\phi \lg \frac{q_t}{\sigma'_v} + K_\phi$$

where

- $\phi'$  = effective friction angle
- $C_\phi$  = a coefficient;  $C_\phi \cong 0.37$  ( $= 1/2.68$ )
- $K_\phi$  = a coefficient;  $K_\phi \cong 0.1$
- $q_t$  = cone resistance corrected for pore water pressure on shoulder (Eq. 2.1)
- $\sigma'_v$  = effective overburden stress

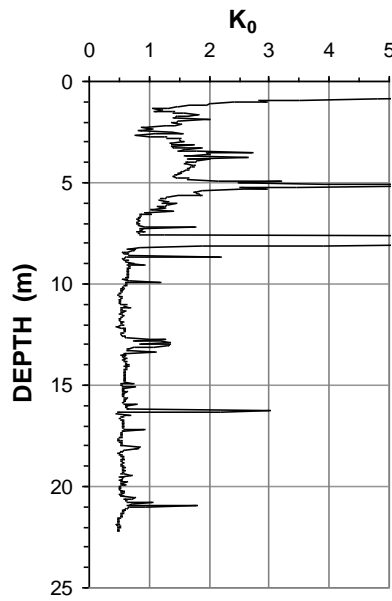


Fig. 2.24  $K_0$  profile determined from the CPTU sounding. Data from Paddle River site, Alberta (Fellenius 2006).

A  $\phi'$ -profile from the Alberta CPTU sounding is shown in Figure 2.25. The profile also includes three friction angle values determined in triaxial tests. The basic 0.37  $C_\phi$ - and 0.1  $K_\phi$  coefficients are used..

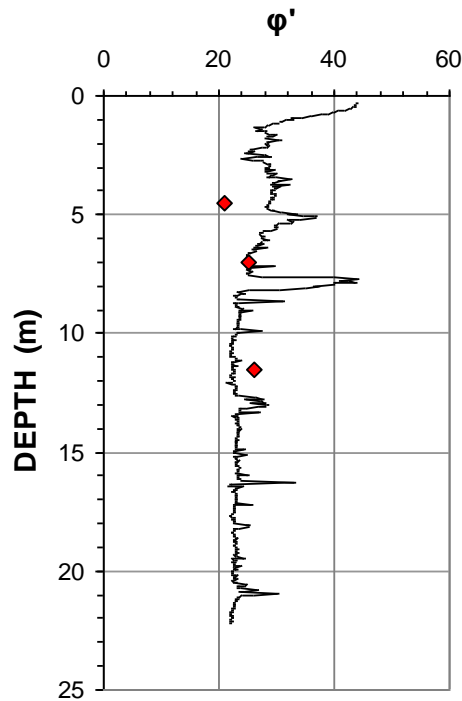


Fig. 2.25 Friction angle,  $\phi'$ , profile determined from the CPTU sounding with three values from triaxial tests. The basic 0.37  $C_\phi$  and  $K_\phi$  coefficients are used. Data from Paddle River site, Alberta (Fellenius 2006).



### 2.12.5 Density Index, $I_D$

Equation 2.18 shows an empirical relation for the Density Index (Kulhawy and Mayne 1990) determined from the cone resistance. Note, however, that any formula or numerical expression applying the  $I_D$  should be considered suspect and only applied with great caution. For details, see Chapter 1, Section 1.2.

$$(2.18) \quad I_D = \sqrt{\frac{q_d}{305F_{OCR}F_{AGE}}} = \sqrt{\frac{q_d}{300}}$$

where  $I_D$  = density index  
 $q_{cl}$  = normalized cone resistance ( $1/\sqrt{(\sigma'/\sigma_r)}$ , where  $\sigma_r = 100$  kPa)  
 $F_{OCR}$  = adjustment factor for overconsolidation ratio (OCR)  $\sim 1$   
 $F_{AGE}$  = adjustment factor for age  $\sim 1$

Baldi et al. (1986) presented an empirical relation for the Density Index shown in Eq. 2.19.

$$(2.19) \quad I_D = \left(\frac{1}{2.61}\right) \ln\left(\frac{q_c}{181\sigma_m^{0.55}}\right)$$

where  $I_D$  = density index  
 $q_c$  = cone resistance  
 $\sigma_m$  = mean effective overburden stress =  $\sigma'_v(1 + K_0)/3$   
 $\sigma'_v$  = effective overburden stress  
 $K_0$  = earth stress coefficient

The density index is primarily intended to be applied to sands. Figure 2.26 shows the results from a CPT sounding in a loose sand at Vilano Beach Florida (McVay et al. 1999).

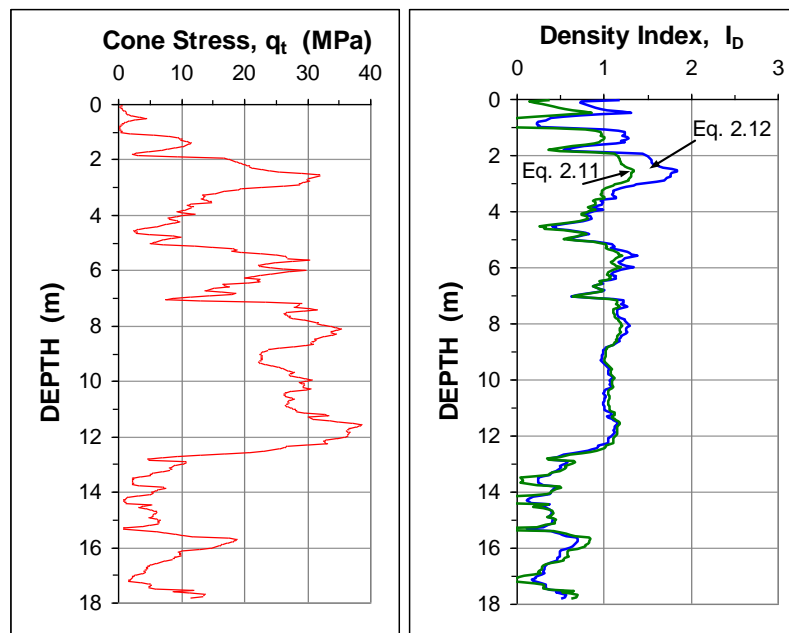


Fig. 2.26 Profiles of cone resistance and Density Index,  $I_D$ , determined from the CPTU sounding according to Eq. 2.11 and 2.12. No reference values are available from the site. (CPT data from McVay et al. 1999).

### 2.12.6 Conversion to SPT N-index

Robertson et al. (1983) presented correlations between CPT cone resistance values and N-indices from SPTs at 18 sites, as shown in Figure 2.27A. The conversion ratios are plotted to the mean grain size determined for the SPT samples. The log-scale on the abscissa overemphasizes the data in the fine-grained soils. The data are therefore shown also with the abscissa in linear scale, Figure 2.27B, which demonstrates that the scatter in the ratio values is rather large.

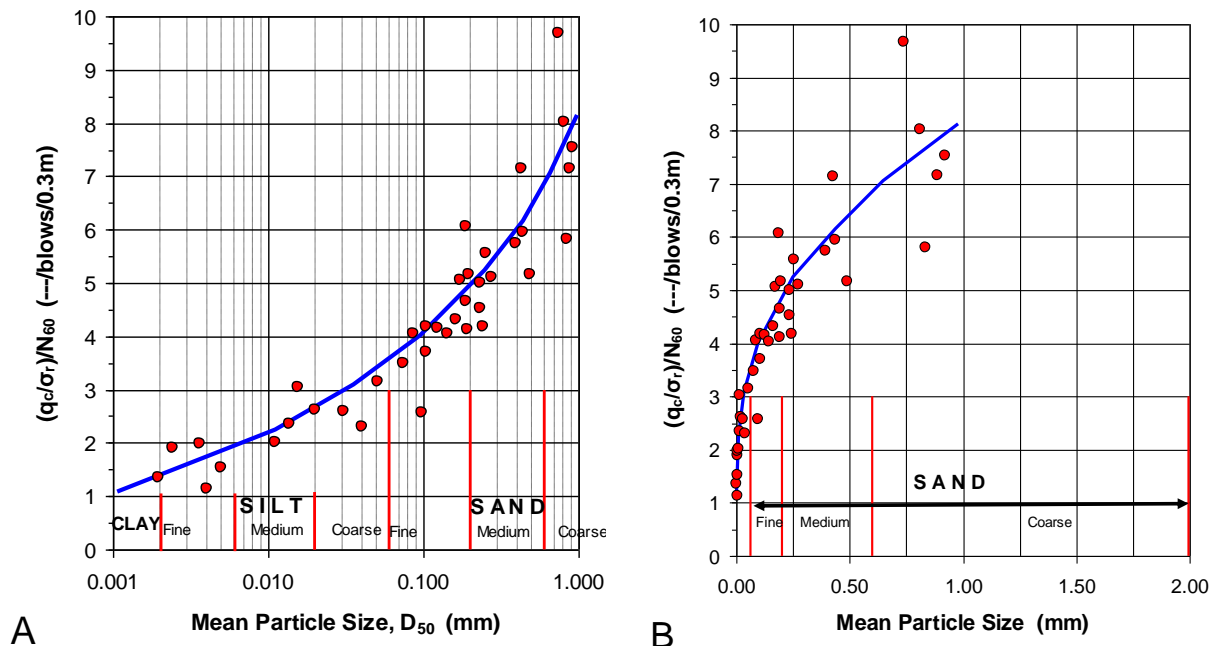


Fig. 2.27 Correlations between CPT cone resistance values,  $q_c$  (kPa) divided by  $\sigma_r$  (= 100 kPa) and SPT  $N_{60}$ -indices from 18 sites. Fig. 2.28A abscissa is in Log-scale and Fig. 2.28B abscissa is in linear scale. Data from Robertson et al. 1983.

The conversion curve shown by Robertson et al. (1983) has seen much use for determining N-indices from CPT soundings in order to apply the so-determined "N"-values to various calculations. Actually, these days, the cone resistance is the pore pressure corrected stress,  $q_t$ . The conversion results are rather questionable, however. The conversions do not just show a scatter, conversions at other sites are often very different to those shown in Figure 2.27. For example, Figure 2.28 shows a plot of the same data supplemented with conversions obtained from N-indices presented by McVay et al. (1999) for the Vilano Beach site, Florida. The mean grain diameter for the Florida site is not known and all data points are plotted at  $d = 0.65$  mm, which is a reasonably representative value for the sand at the site. However, even if the actual mid-range grain size had been known, the plot would still neither have shown any relation to the 1983 curve, nor to any other correlation.

In-situ classification of "relative density" of coarse-grained soils is usually referenced to the SPT-index value. However, the cone resistance of the CPTU provides a more consistent and reliable such reference. Thus, in very loose soils  $q_t$  is  $<2$  MPa, in loose soils,  $q_t$  ranges from 2 through 4, in compact from 4 through 12, in dense from 12 - 20, and in very dense soil,  $q_t$  is  $>20$  MPa.

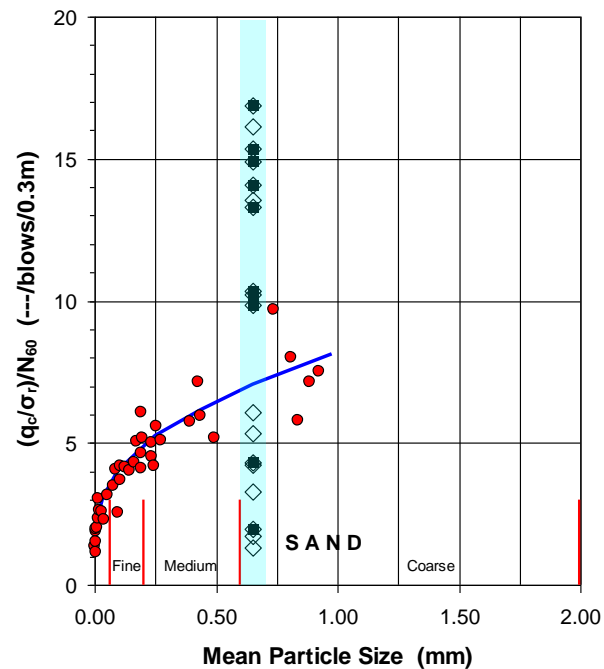


Fig. 2.28 The SPT-CPT correlations of Fig. 2.25 supplemented with correlations from Vilano Beach site, Florida. Data from McVay et al. 1999.

### 2.12.7 Determining the E-Modulus from CPT cone-stress

When calculating settlement, the E-modulus of interest is the modulus for an average applied stress limited to a value equal to about 25 % of the estimated ultimate bearing resistance. The modulus is called  $E_{25}$ , and it can be related to the average cone resistance according to the relationship given in Eq. 2.20.

$$(2.20) \quad E_{25} = \alpha q_t$$

where  $E_{25}$  = secant modulus for a stress equal to about 25 % of the ultimate stress  
 $\alpha$  = an empirical coefficient  
 $q_t$  = cone resistance

Test data indicate that the empirical coefficient,  $\alpha$ , varies considerably and depends on the soil type and stress conditions as well as on the applied load level. According to the Canadian Foundation Engineering Manual (1985, 1992), when correlated to plate load tests on sand,  $\alpha$  varies between 1.5 and 4. Based on a review of results of cone tests in normally consolidated, uncemented sand in calibration chambers, Robertson and Campanella (1986) proposed a range for  $\alpha$  between 1.3 and 3.0. This range agrees well with recommendation by Schmertmann (1970) for use of CPT data to analyze settlement of isolated footings on coarse-grained soils. Dahlberg (1975) performed tests in overconsolidated sand and found that  $\alpha$  ranged from 2.4 through 4, increasing with increasing value of  $q_t$ . The Canadian Foundation Engineering Manual (1992) states that  $\alpha$  is a function of soil type and compactness, as listed in Table 2.5. The values of  $\alpha$  shown in the table apply to a settlement analysis in soils that can be assumed to have a linear ("elastic") response to a load increase.

**TABLE 2.5**  $\alpha$  from Static Cone Penetration Tests (CFEM 1992)

Soil type	$\alpha$
Silt and sand	1.5
Compact sand	2.0
Dense sand	3.0
Sand and gravel	4.0

### 2.12.8 Assessing Liquefaction Susceptibility

When an earthquake hits, as the name implies, the soil will "quake in shear"; movements back and forth occur (or, more rarely, up and down). If the shear movements, as is most commonly the case, make smaller grains move into the voids between larger grains, the soil volume reduces—the soil contracts—and pore pressure increases and effective stress decreases. In a series of repeated shaking—cyclic shear—the pore pressure increases can accumulate, affect a large volume of soil, and cause a complete loss of effective stress, i.e., the soil liquefies. If so, the volume loss in the liquefied zone will cause the foundations placed on the ground above to settle by the amount of the volume decrease. Shear movements of magnitude associated with an earthquake in fine-grained and cohesive soils are considered less susceptible to liquefaction, as the soil grains in such soil cannot as easily be rearranged by the shaking. Moreover, dense coarse-grained soil will not liquefy, because when the grains in such soils are rearranged and move relative each other, they "climb over each other"<sup>1)</sup> and the soil elements affected will actually increase in volume—dilate, and the pore pressures will decrease rather than increase—the soil does not liquefy. However, loose coarse-grained soil are contractant and the looser the soil, the more prone to liquefaction it is. [Figure 2.29](#) illustrates the sometime drastic consequence of liquefaction.



Fig. 2.29 Effect of liquefaction from the 7.4 Magnitude Kocaeli Earthquake of August 17, 1999 in Turkey. Courtesy of Dr. N.J. Gardner, University of Ottawa.

<sup>1</sup> When subjected to a shear movement, initially, also a dense sand will contract, but when the movement gets larger, as in the case of an earthquake shaking, dense sand will dilate.

In the following, principles of the assessment of liquefaction susceptibility are presented. The material is not exhaustive and the reader is strongly recommended to review the references for additional information.

### 2.12.8.1 Cyclic Stress Ratio, CSR, and Cyclic Resistance Ratio, CRR

Data from CPTU soundings are often employed to assess susceptibility due to earthquake induced liquefaction. The following summarizes the procedures of Robertson and Wride (1998) and Youd et al. (2001). The analysis starts by determining the driving effect, called **Cyclic Stress Ratio, CSR**, calculated from Eqs. 2.21 through 2.23 (Seed and Idriss 1971).

$$(2.21) \quad CSR = 0.65(MWF) \frac{a_{max}}{g} \frac{\sigma_v}{\sigma'_v} r_d$$

$$(2.22) \quad MWF = \left( \frac{M}{7.5} \right)^{2.56}$$

$$(2.23) \quad r_d = 1 - 0.015z$$

where

- $CSR$  = **Cyclic Stress Ratio**
- $MWF$  = Earthquake Magnitude Weighting Factor, dimensionless; increases with increasing earthquake magnitude,  $M$
- $M$  = earthquake magnitude per Richter scale, dimensionless
- $a_{max}$  = maximum horizontal acceleration at ground surface ( $m/s^2$ )
- $g$  = gravity constant ( $m/s^2$ ), dimensionless
- $r_d$  = stress reduction coefficient for depth, dimensionless
- $z$  = depth below ground surface (m)

Usually the term  $a_{max}/g$  is given as a ratio to the gravity constant, "g", e.g., 0.12g. When  $M$  is equal to a magnitude of 7.5,  $MWF$  becomes equal to unity. (Thus, for, say, magnitudes ranging from 6.0 through 8.0,  $MWF$  ranges from 0.57 through 1.19).  $MWF$  is the inverse of the Magnitude Scaling Factor,  $MSF$ , also commonly used for weighting or scaling earthquake magnitudes. For recommendations regarding choice of  $MWF$  or  $MSF$ , see Youd et al. (2001). Note that while the energy per the Richter scale,  $M$ , is the energy at source, the maximum horizontal acceleration pertains to the site considered. The two are somewhat proportional, in that a large earthquake (large "M") will normally cause a large "a", although the CSR depends exponentially on the "M" input, whereas the influence of "a" is linear.

The depth factor or stress reduction coefficient,  $r_d$ , serves to respond to the observation that the incidence of liquefaction reduces with depth. Different authors have proposed slightly larger values for the constant applied to the depth,  $z$ , in Eq. 2.15, as summarized by Youd et al. (2001) and Moss et al. (2006).

The ability of the soil to resist liquefaction is calculated using a **Cyclic Resistance Ratio, CRR**, applied to CPTU results as determined according to an approach proposed by Robertson and Campanella (1985) further developed by Robertson and Wride (1998), who correlated information for a large number of earthquakes. [Figure 2.30](#) shows the CSR-values as calculated from Eqs. 2.21 through 2.23 and plotted against values of Normalized Cone resistance,  $q_{c1}$ , as defined by Eq. 2.24. The plotted data points are from where liquefaction occurred and where it did not occur, and the boundary between the two scenarios is termed the CRR-curve. It is considered applicable to clean sand defined as sand with a fines content smaller than 5 %, which is also the upper boundary for free-draining sand.

$$(2.24) \quad q_{cl} = q_t \sqrt{\frac{\sigma_r}{\sigma_v}}$$

where  $q_{cl}$  = cone resistance normalized for liquefaction calculation ( $q_{cl} \leq 1.7q_t$ )  
 $q_t$  = cone resistance. In sand, whether the cone resistance is uncorrected  $q_c$ , or corrected,  $q_r$ , for the pore pressure,  $u_2$ , on the cone shoulder makes very little difference to the normalized cone resistance value  
 $\sigma_r$  = reference stress = 100 kPa (= atmospheric pressure)

The boundary line is the Cyclic Resistance Ratio Curve, CRR, which is also shown as a linear regression curve (Eq. 2.17) for the boundary values ( $M=7.5$ ). The two dashed curves show the boundary curves for sand with fines contents of 15 % and 35 %, respectively (copied from Stark and Olsen 1995). The original diagram divided the cone resistance,  $q_c$ , by atmospheric pressure to make the number non-dimensional.

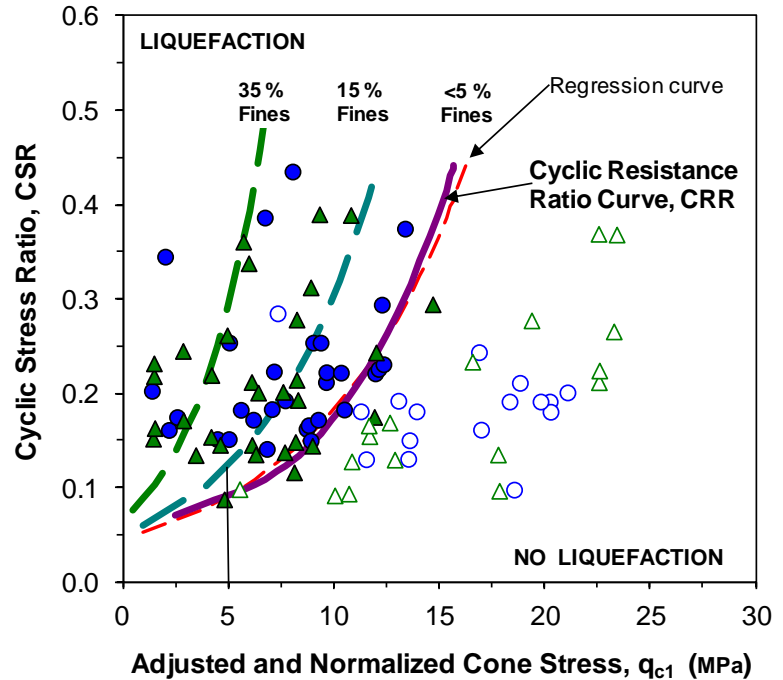


Fig. 2.30 Correlations between CRR-values calculated from actual earthquakes versus  $q_{cl}$ -values for cases of liquefaction (solid symbols) and no liquefaction (open symbols), and boundary curve (solid line) according to Robertson and Wride (1998) and Youd et al. (2001).

According to the sources of Figure 2.30, sand containing fines will be less liquefiable, that is, the boundary line moves to the left for increasing fines contents. Stark and Olsen (1995) presented a graph similar to that shown, which included boundary lines for fines contents of 15 % and 35 %. These curves have been added to the graph. However, recent findings have questioned that fines content would reduce seismic susceptibility (Bray and Sancio 2006; 2007, Boulanger and Idriss 2006; 2007, Boardman 2007).

The boundary curve for the Cyclic Resistance Ratio Curve, CRR, applicable to clean sand is determined according to Eqs. 2.25a and 2.25b. The curve can be approximated by means of regression analysis, which gives Eq. 2.25c.

$$(2.25a) \quad CRR = 0.833 \left( \frac{q_{cl}}{100} \right) + 0.05 \quad \text{for } q_{cl} < 50 \text{ MPa}$$

$$(2.25b) \quad CRR = 93 \left( \frac{q_{c1}}{100} \right)^3 + 0.08 \quad \text{for } 50 < q_{c1} < 160 \text{ MPa}$$

$$(2.25c) \quad CRR = 0.045 (e^{0.14q_{c1}})$$

where  $CRR$  = Cyclic Resistance Ratio  
 $q_{c1}$  = cone resistance normalized for liquefaction calculation; (MPa) (Eq. 2.24)  
 $e$  = base of the natural logarithm = 2.718

N.B., the constants "0.833" are as quoted; there's no typo; notice the exponent:  $(q_{c1}/100)^3$  in Eq. 2.25.

The two curves for fines contents of 15 % and 35 % correspond to Eqs. 2.26a and 2.26b, respectively.

$$(2.26a) \quad CRR = 0.045 (e^{0.20q_{c1}})$$

$$(2.26b) \quad CRR = 0.065 (e^{0.30q_{c1}})$$

Juang and Jiang (2000) presented the graph shown in [Figure 2.31](#), similar to that in [Figure 2.30](#), showing boundary curves for probability of liquefaction,  $P_L$ , ranging from 0.1 through 0.9. Mathematical expressions for the curves are given by Eqs. 2.27a through 2.27f. The curve (Eq. 2.27d) for a probability of 0.5 is almost identical to the boundary curve (Eq. 2.25) of [Figure 2.30](#).

$$(2.27a) \quad CRR_{P_L=0.1} = 0.025 (e^{0.14q_{c1}})$$

$$(2.27b) \quad CRR_{P_L=0.2} = 0.033 (e^{0.14q_{c1}})$$

$$(2.27c) \quad CRR_{P_L=0.3} = 0.038 (e^{0.14q_{c1}})$$

$$(2.27d) \quad CRR_{P_L=0.5} = 0.046 (e^{0.14q_{c1}})$$

$$(2.27e) \quad CRR_{P_L=0.7} = 0.057 (e^{0.14q_{c1}})$$

$$(2.27f) \quad CRR_{P_L=0.9} = 0.085 (e^{0.14q_{c1}})$$

where  $CRR$  = Cyclic Resistance Ratio from the CPTU data  
 $P_L$  = probability of liquefaction  
 $e$  = base of the natural logarithm = 2.718  
 $q_c$  = cone resistance (kPa)

Moss et al. (2006) presented methodologies for deterministic and probabilistic assessment of seismic soil liquefaction triggering potential based on the cone penetration test. The data base includes observations at 18 earthquake events and studies of the response of sand layers at 182 localities affected by the earthquake. Of these, liquefaction was observed at 138 cases and the sand did not liquefy in 44 cases. Two of the case histories (Kocaeli, Turkey, and Chi-Chi, Taiwan, involving 32 observations) were from quakes occurring after 1998. The Moss et al. (2006) assessment makes use of probabilistic and statistics as well as information in addition to the cone sounding information. For deterministic assessment, the approach is similar to the approach by Robertson and Wride (1998) as illustrated in [Figure 2.32](#).

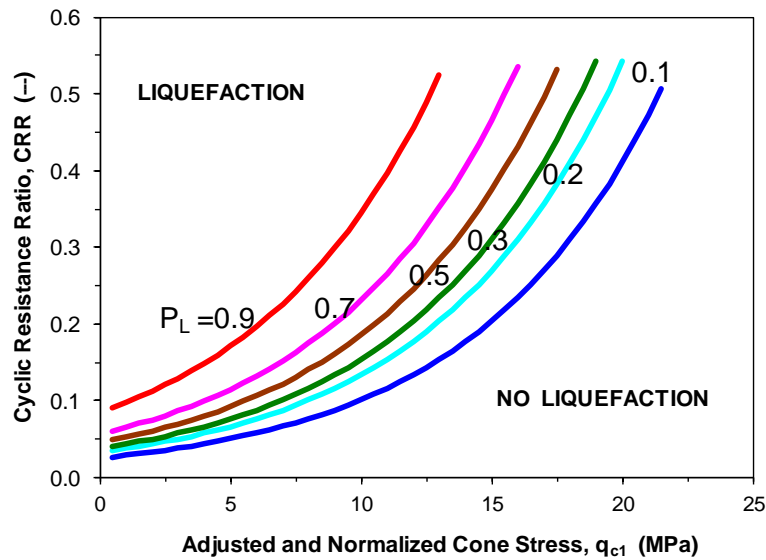


Fig. 2.31 Correlations between CRR-values and  $q_{c1}$ -values for different probabilities of liquefaction,  $P_L$ . Data from Juang and Jiang (2000).

Figure 2.32 shows cases of liquefaction (solid symbols) and no liquefaction (open symbols), according to Moss et al. (2006) and boundary curve (solid line) according to Robertson and Wride (1998) and Youd et al. (2001). The boundary line is the Cyclic Resistance Ratio Curve, CRR. The two dashed curves show the boundary curves for sand with fines contents of 15 % and 35 %, respectively (copied from Stark and Olsen 1995, Eqs. 2.19a and 2.19b).

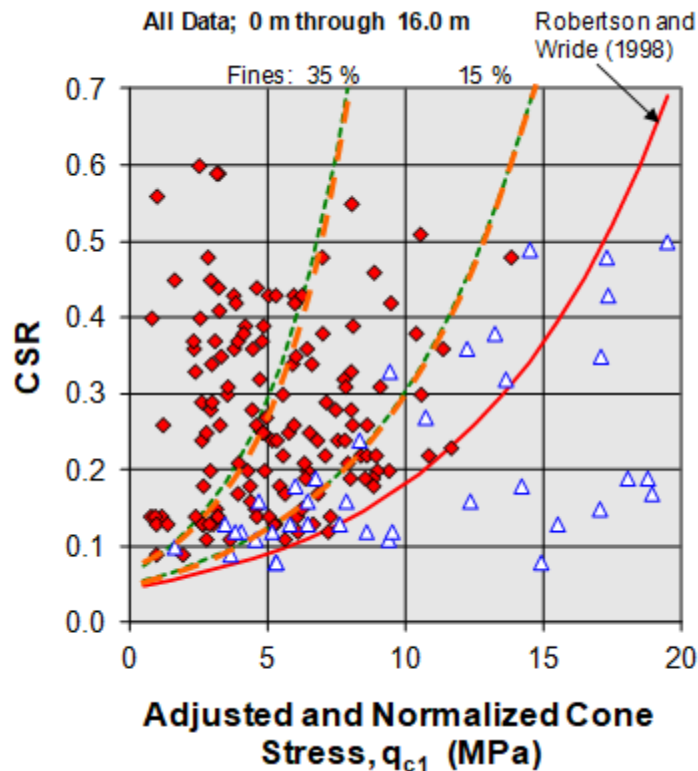


Fig. 2.32 Correlations between CRR-values calculated from actual earthquakes versus  $q_{c1}$ -values



Figures 2.33A and 2.33B present the Moss et al. (2006) data plotted as earthquake acceleration ( $q_{\max}/g$ ) versus not-normalized cone resistance (the as-measured cone resistance). In an actual case, this is the format of the first information available and the figures are useful as aid toward whether or not a detailed liquefaction study is necessary. Figure 33A shows only the data from ground surface to depth of 6.0 m. Figure 33B shows all data in the data base. The dashed curve is the Robertson and Wride CRR curve plotted against the  $q_c$ -values as if they were  $q_{c1}$ -values. The curve is only included in the figures to serve as reference to Figure 2.32. Figure 33A demonstrates that for shallow depth (<6 m), and a moderate magnitude earthquake (<0.25g), liquefaction was not observed for as-measured cone resistance larger than 5 MPa.

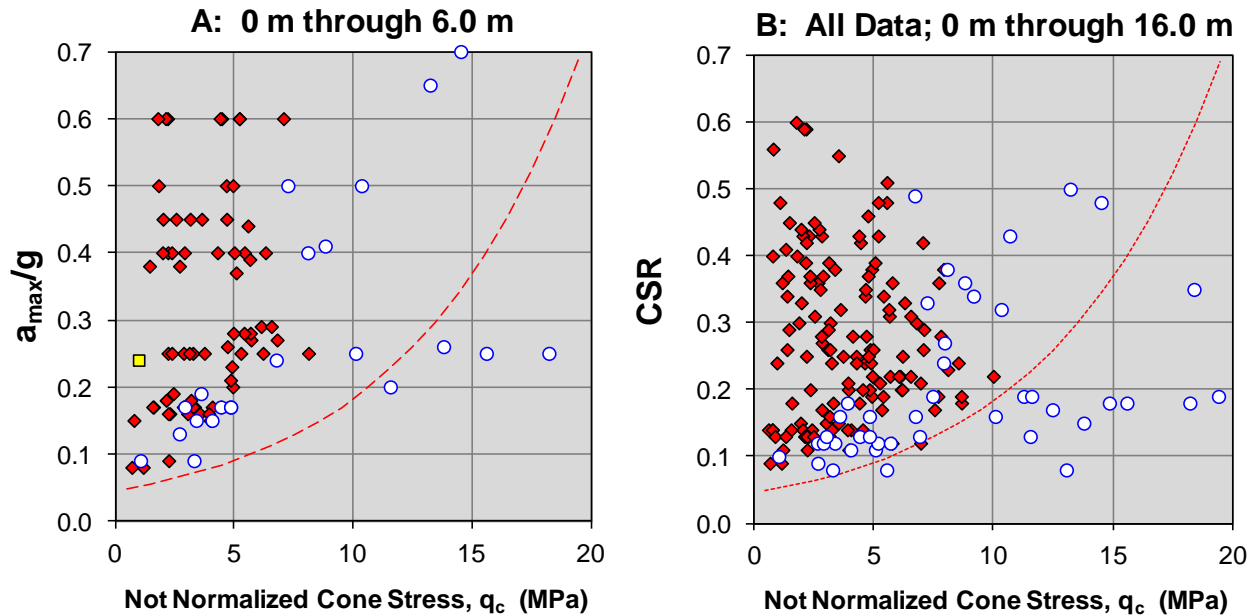


Fig. 2.33 The data points presented as earthquake acceleration ( $q_{\max}/g$ ) versus not-normalized cone resistance (the as-measured cone resistance).

### 2.12.8.2 Factor of Safety, $F_s$ , against Liquefaction

The factor of safety ( $F_s$ ) against liquefaction is the ratio between the resisting condition represented by the CRR-value and the earthquake condition represented by the CSR-value, according to Eq. 2.28.

$$(2.28) \quad F_s = \frac{CRR}{CSR} MWF$$

where

- $F_s$  = factor of safety against liquefaction
- $CRR$  = Cyclic Resistance Ratio from the CPTU data
- $CSR$  = Cyclic Stress Ratio from the seismic conditions
- $MWF$  = Magnitude Weighting Factor

A  $F_s$  smaller than unity does not necessarily mean that liquefaction will occur for the considered earthquake magnitude. However, it does indicate the need for a closer look at the risk and susceptibility and a detailed study of the current main references, e.g., Youd et al. (2001) and Moss et al. (2006).

### 2.12.8.3 Comparison to Liquefaction Susceptibility Determined from SPT N-indices

Evaluation of liquefaction resistance was formerly—and still is in many places—based on the SPT Index. It is generally considered necessary to adjust the N-index to depth, i.e., overburden stress, by means of a coefficient called "normalization factor",  $C_N$ , proposed by Seed 1976 for earthquake applications specifically. The N-index is also adjusted to a value for standard condition of energy. The latter is obtained by using transducers for measuring impact stress and acceleration (see Chapter 9) to determine the energy transferred to the SPT rods. As "standard" transferred energy is 60 % of the nominal energy, the measured N-index is proportioned to the actually transferred energy. (Note deviation of the actual transferred energy from 60 % of nominal by more than 25% up or down is not acceptable). The so-adjusted index is expressed in Eqs. 2.29 and 2.30.

$$(2.29) \quad (N_1)_{60} = C_N N_{60}$$

where  $N_I$  = stress-adjusted (depth-adjusted) N-index  
 $C_N$  = normalization factor expressed  
 $N_{60}$  = SPT N-index energy corrected

$$(2.30) \quad C_N = 1 - 1.25 \log \left( \frac{\sigma'_v}{\sigma_r} \right)$$

where  $\sigma'_v$  = effective overburden stress  
 $\sigma_r$  = reference stress = 100 kPa

The normalization factors, Eqs. 2.16 and 2.23, are very similar as indicated in Figure 2.34, where they are plotted together. The assumptions are a soil with a density of 2,000 kg/m<sup>3</sup> and a groundwater table at the ground surface. Below a depth of about 3 m, the factors are almost identical. At a depth of about 10 m, both normalization factors are about equal to unity (effective overburden stress is about equal to the reference stress).

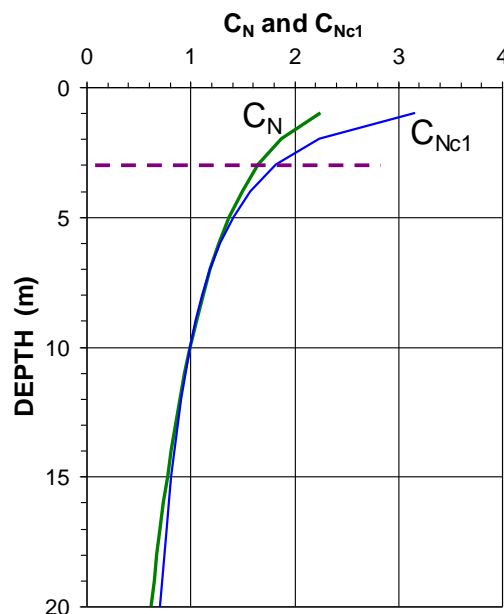


Fig. 2.34 Comparison between the normalization factors for SPT-index and CPT cone resistance,  $q_c$ .

Figure 2.35 shows calculated  $CSR$ -values versus corresponding  $(N_1)_{60}$ -values from sites where liquefaction effects did or did not occur for earthquakes with magnitudes of approximately 7.5. The  $CRR$  curve on this graph was conservatively positioned to separate data points from sites where liquefaction occurred from data points from sites with no liquefaction. Curves were developed for granular soils with fines contents of 5% or less, 15%, and 35% as shown on the plot. The  $CRR$  curve for fines contents smaller than 5% is the basic penetration criterion for the simplified procedure and is called the "SPT clean sand base curve". The curves are valid only for magnitude 7.5 earthquake, but the values can be adjusted by means of the  $MWF$  according to Eq. 2.13 (for other suggested relations see Moss et al. 2006).

The boundary  $CRR$  curve in the original graph is plotted per Eq. 2.31 (Figure 2.36). The dashed curve next to the boundary curve is a regression curve fitting the boundary curve per Eq. 2.32a. Similarly, the two dotted curves showing the boundary curves for fines contents are approximately fitted to Eqs. 2.32b and 2.32c.

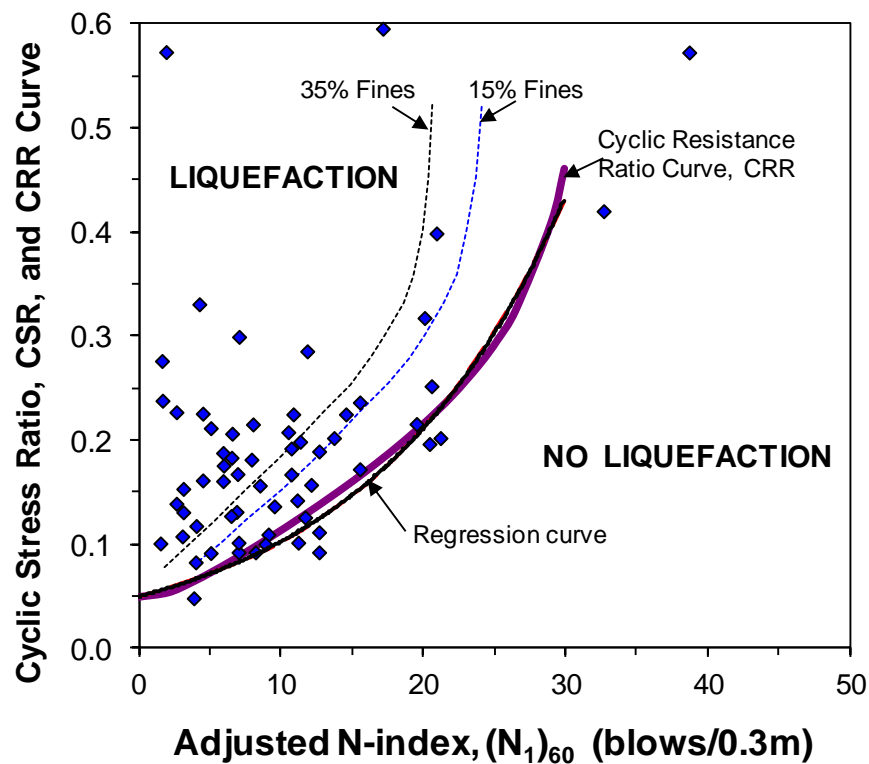


Fig. 2.35 Correlations between  $CRR$ -values and Adjusted  $N$ -indices. Data from Youd et al. (2001) as modified from Seed et al. (1985).

$$(2.31) \quad CRR = \frac{1}{34 - N} + \frac{N}{135} + \frac{50}{(10N + 45)^2} - \frac{1}{200}$$

$$(2.32a) \quad CRR_{FC < 5\%} = 0.050 \alpha e^{0.072N_{60}}$$

$$(2.32b) \quad CRR_{FC = 0.1\%} = 0.060 \alpha e^{0.084N_{60}}$$

$$(2.32c) \quad CRR_{FC = 0.3\%} = 0.070 \alpha e^{0.092N_{60}}$$

The adjusted SPT-N indices,  $(N_1)_{60}$ , can be correlated to the adjusted and normalized cone resistance,  $q_{c1}$ , over the respective values of cyclic stress resistance,  $CSR$ . For equal  $CSR$ -values, the relation between the two is approximately linear—the ratio is 0.18, that is,  $(N_1)_{60} = 1.8q_{c1}$  (the linear regression coefficient is 0.99). As mentioned, at a depth of 10 m, the normalization factor  $C_N$  is approximately equal to unity, i.e., the  $(N_1)_{60}$ -values is equal to  $N_{60}$ , (Eqs. 2.22 and 2.23). Similarly, the factor  $\sqrt{(\sigma_r/\sigma'_v)}$  in Eq. 2.15 is equal to unity at this depth. Therefore, the normalized cone resistance,  $q_{c1}$ , is equal to  $q_c$ . So, the ratio at 10 m depth between  $q_c$  and  $(N)_{60}$  becomes about 2. This means, for example, that at about 10 m depth, a loose sand, as indicated by a cone resistance of, say, 3 MPa, correlates to an  $N$ -index of 6 blows/0.3 m, which does correspond to a loose relative density when judged from the  $N$ -index.

As the normalization factors are very similar, the mentioned about-2 ratio is independent of depth (once below 3 m depth). Referring to Section 2.12.6, the  $q_c/\sigma_r$ -ratio between a  $q_c$  equal to 3 MPa and an  $N_{60}$  equal to 6 bl./0.3m is 5. To lie on the curve of Figure 2.27, this value would apply to a "fine sand". The agreement is hardly coincidental, however. Much of the experience behind Figure 2.30 and its curves was transferred from the data behind Figure 2.35. It is obvious from the discussion in Section 2.12.8.1 that correlation between the SPT index and the cone resistance is highly variable. It is questionable how relevant and useful a conversion from an SPT Index value to a cone resistance would be for an actual site. One would be better served pushing a cone in the first place.

## CHAPTER 3

### SETTLEMENT

#### 3.1 Introduction

A foundation is a constructed unit that transfers the load from a superstructure to the ground. With regard to vertical loads, most foundations receive a more or less concentrated load from the superstructure and transfer this load to the soil underneath the foundation, distributing the load as a stress over the “footprint” of the foundation. The foremost requirement for a proper foundation is that the change of stress due to the soil-structure interaction must not give rise to a deformation of the soil that results in a settlement of the superstructure in excess of what the superstructure can tolerate.

Deformation is expressed by the terms movement, displacement, and settlement. The terms are not synonyms—they are related, but not equal. It is important not to confuse them.

Settlement analysis must combine the classical, well-established consolidation theory with immediate and secondary compression. Calculating settlement as a part of a design, which is in fact a prediction, is relatively easy. The problem is knowing what input parameters to apply. The knowledge is gained by back-calculating records of actual measurements. There are quite a few available.

#### 3.2 Movement and Settlement: Immediate, Consolidation, and Secondary Compression

**Movement** occurs as a response when a stress is applied to a soil, resulting in a transfer of stress to the soil, when the involved, or influenced, soil volume successively increases as the stress increases. For example, movement results when load increments are added to a pile or to a plate in a static loading test (where, erroneously, the term "settlement" is often used instead of "movement"). "Movement" is the term to use when the involved, or affected, soil volume increases as the load (stress) gets larger.

**Settlement** is volume reduction of specific soil volume as a consequence of an *increase in effective stress*. Settlement consists of either one or the sum of immediate compression, consolidation settlement, and secondary compression (secondary compression is included here because it is initiated by a change of effective stress although it occurs without change of effective stress, see below). As a term, "settlement" is used when the total stress is constant and the outer boundaries of the involved, or influenced, soil zone stay the same during the increase of the effective stress.

**Immediate compression** (also often called immediate settlement) is the result of compression of the soil grains (soil skeleton) and, N.B., of volume reduction of any free gas present in the voids. It is usually assumed to be linearly proportional to the change of stress. The immediate compression is therefore often called 'elastic' compression. It occurs quickly and is normally small (it is not associated with reduction of voids volume, i.e., expulsion of water; consolidation).

**Consolidation** (also called primary consolidation, but the adjective "primary" is unnecessary) is settlement as effective stress increases due to dissipation of pore pressures (expelling water from the soil body). In the process, the imposed stress, initially carried by the pore water, is transferred to the soil structure. Consolidation occurs slowly in fine-grained soils and faster in more pervious soils.

**Secondary Compression** is a term for compression (of the soil skeleton) occurring without an increase of effective stress, but it is triggered by the change of effective stress. Of course, there is an expulsion of

water in the process, but secondary compression is a slow long-term process, occurring without appreciable increase or change of stress or pore pressure. Sometimes, the term "creep" is used to mean secondary compression, but "creep" is also used to indicate ongoing movements for no increase of shear force (i.e., plastic response). So, to avoid confusion, the term "secondary compression" should be used to refer to settlement occurring after end of consolidation without increase of effective stress, i.e., without reduction of pore pressure (dissipation of excess pore pressure). The term "secondary" is a vestige of the original use of "secondary" to indicate that it followed consolidation, then termed "primary", to indicate that it occurred first. It is practical to keep "secondary" in order not to confuse the process with the fact that settlement is the accumulated compression due to all actions.

The magnitude of the settlement depends on the *relative increase of effective stress*: Other than for a truly 'elastic' response, the larger the existing effective stress before a specific additional stress is applied, the smaller the induced settlement. Indeed, most soil materials do not show a linear relation between stress and strain. Cohesive soils, in particular, have a distinct stress-strain non-linearity.

The amount of deformation for a given applied stress depends on the distribution of that stress change (relative existing stress) in the affected soil mass and the compressibility of the soil layer. The change of effective stress is the difference between the initial (original) effective stress and the final effective stress. (See Chapter 1 and Table 1.6 for an example of how to calculate the distribution of the effective stresses at a site).

### 3.3 Linear Deformation ("Elastic")

Linear stress-strain behavior follows Hooke's law ("elastic modulus method") according to Eq. 3.1.

$$(3.1) \quad \varepsilon = \frac{\Delta\sigma'}{E}$$

where  $\varepsilon$  = induced strain in a soil layer  
 $\Delta\sigma'$  = imposed change of effective stress in the soil layer  
 $E$  = elastic modulus of the soil layer

The "elastic modulus" is often called Young's modulus. Strictly speaking, however, Young's modulus is the modulus when lateral expansion is allowed. When lateral expansion is prevented, the modulus is called "constrained modulus",  $D$  (or  $M$ ), and it is larger than the Young modulus,  $E$ . The constrained modulus is also called the "oedometer" modulus. For ideally elastic material, the ratio between  $D$  and  $E$  is shown in Eq. 3.2.

$$(3.2) \quad \frac{D}{E} = \frac{(1-\nu)}{(1+\nu)(1-2\nu)}$$

where  $D$  = constrained modulus  
 $E$  = Young's modulus  
 $\nu$  = Poisson's ratio

Poisson's ratio expresses how a compression in the direction of loading is counteracted by lateral expansion in the perpendicular direction. Incompressible materials have a Poisson's ratio of 0.5. Such materials may compress in the direction of loading, but the volume is unchanged. For a soil material with a Poisson's ratio of 0.3, a common value, the constrained modulus is 35 % larger than the Young's modulus. (As an illustration, unrelated to settlement of soils, but not to foundation engineering: the

concrete inside a concrete-filled thick-wall pipe pile is partially constrained by the pipe as opposed to the concrete in a concrete pile. Therefore, when analyzing strain gages records from a loading test on a concreted pipe pile, it can be expected that its axial stiffness is larger than that for a bored pile with the casing removed after casting.

The deformation of a soil layer,  $s$ , is the strain,  $\varepsilon$ , times the thickness,  $h$ , of the layer. The settlement,  $S$ , of the foundation is the sum of the deformations of the soil layers below the foundation (Eq. 3.3).

$$(3.3) \quad S = \sum s = \sum (\varepsilon h)$$

### 3.4 Non-Linear Deformation

Stress-strain behavior is non-linear for most soils. The non-linearity cannot be disregarded when analyzing compressible soils, such as silts and clays, that is, the linear elastic modulus approach is not appropriate for these soils. Non-linear stress-strain behavior of compressible soils is conventionally modeled by Eq. 3.4.

$$(3.4) \quad \varepsilon = \frac{C_c}{1+e_0} \lg \frac{\sigma'_1}{\sigma'_0} = CR \lg \frac{\sigma'_1}{\sigma'_0}$$

where  $\varepsilon$  = strain induced by increase of effective stress from  $\sigma'_0$  to  $\sigma'_1$  (--), often =  $e_{CONS}$   
 $C_c$  = compression index (--)  
 $e_0$  = initial void ratio (--)  
 $\sigma'_0$  = original (or initial) effective stress (Pa)  
 $\sigma'_1$  = final effective stress (Pa)  
 $CR$  = compression ratio =  $C_c/(1 + e_0)$  (--)

The compression index and the void ratio parameters,  $C_c$  and  $e_0$ , are established by means of oedometer (consolidometer; compressometer) tests in the laboratory or, sometimes, by empirical correlations based on index properties and experience of the geology of the site. Note, the oedometer test compresses the soil in constrained mode.

If the soil is overconsolidated, that is, consolidated to a stress (preconsolidation stress),  $\sigma'_p$ , larger than the existing effective stress, Eq. 3.4 changes to Eq. 3.5.

$$(3.5) \quad \varepsilon = \frac{1}{1+e_0} \left( C_{cr} \lg \frac{\sigma'_p}{\sigma'_0} + C_c \lg \frac{\sigma'_1}{\sigma'_p} \right) \quad \text{and} \quad \varepsilon = \frac{1}{1+e_0} C_{cr} \lg \frac{\sigma'_1}{\sigma'_0} \quad \text{when } \sigma'_1 < \sigma'_p$$

where  $\sigma'_p$  = preconsolidation stress =  $\sigma'_0 + \Delta\sigma'_c$  (Pa)  
 $\sigma'_0$  = current effective stress (Pa).  $\sigma'_p - \sigma'_0$  = preconsolidation (precompression) margin  
 $C_{cr}$  = re-compression index (--)  
 $C_c$  = compression index (--)

Thus, in conventional engineering practice of settlement design for normally consolidated soils, two compression parameters need to be established; the  $C_c$  and the  $e_0$ . Actually, on surprisingly many occasions, geotechnical engineers only report the  $C_c$ , neglecting to include the  $e_0$ . Worse, when they do report both parameters, they often report the  $C_c$  from the oedometer test and the  $e_0$  from a different soil specimen than that used for determining the compression index! This is not acceptable, of course. The inconvenient challenge of ascertaining what  $C_c$ -value goes with what  $e_0$ -value is removed by using the

Janbu tangent modulus approach instead of the  $C_c$  and  $e_0$  approach, applying the Janbu modulus number,  $m$ , instead, as determined directly from the oedometer test (c.f., Section 5). Or by using the MIT approach, where the compressibility of the soil is characterized by the ratios  $C_c/(1 + e_0)$  and  $C_{cr}/(1 + e_0)$  as single parameters (usually called Compression Ratio,  $CR$ , and Recompression Ratio,  $RR$ , respectively). See Eqs. 4 and 5 and Section 7.

As an aside, Swedish and Finnish practices apply a strain value, called  $\varepsilon_2$ , equal to the strain for a doubling of the applied stress. For the latter, Eq. 3.5 becomes:

$$(3.6) \quad \varepsilon = \frac{\varepsilon_{2r}}{1g2} \lg \frac{\sigma'_p}{\sigma'_0} + \frac{\varepsilon_2}{1g2} \lg \frac{\sigma'_1}{\sigma'_p}$$

where  $\varepsilon_{2r}$  = " $\varepsilon_2$ -compressibility" for reloading  
 $\varepsilon_2$  = " $\varepsilon_2$ -compressibility" for virgin loading

### 3.5 The Janbu Approach

#### 3.5.1 General

The Janbu approach, proposed by Nilmar Janbu in the early 1960s (Janbu 1963; 1965; 1967), combines the basic principles of linear and non-linear stress-strain behavior. The method applies to all soils, clays as well as sand. By the Janbu method, the relation between stress and strain is simply a function of two non-dimensional parameters that are unique for any soil: a stress exponent,  $j$ , and a modulus number,  $m$ . (Strictly, the modulus is for constrained ("oedometer") condition). Professor Janbu has presented a comprehensive summary of his method (Janbu 1998).

The Janbu approach is based on the definition of the conventional tangent modulus,  $M_t = \partial\sigma/\partial\varepsilon$ , by the following expression (Eq. 3.7).

$$(3.7) \quad M_t = \frac{\partial\sigma}{\partial\varepsilon} = m\sigma_r \left(\frac{\sigma'}{\sigma_r}\right)^{1-j}$$

where  $M_t$  = tangent modulus (dimensionless)  
 $\varepsilon$  = strain induced by increase of effective stress (dimensionless)  
 $\sigma'$  = effective stress (kPa)  
 $j$  = a stress exponent (dimensionless)  
 $m$  = a modulus number (dimensionless)  
 $\sigma'_r$  = a reference stress, a constant, which for all practical purposes is equal to 100 kPa ( $\approx 1$  tsf  $\approx 2$  ksf  $\approx 1$  kg/cm<sup>2</sup>  $\approx 1$  at), i.e., atmospheric pressure

Integrating Eq. 3.7 delivers Eq. 3.8, expressing strain as a function of modulus number and stress exponent.

$$(3.8) \quad \varepsilon = \frac{1}{mj} \left[ \left(\frac{\sigma'_1}{\sigma'_r}\right)^j - \left(\frac{\sigma'_0}{\sigma'_r}\right)^j \right]$$



where  $\varepsilon$  = strain induced by increase of effective stress. When the strain is developed due to consolidation (pore pressure dissipation,  $\varepsilon$  is written  $\varepsilon_{\text{CONS}}$ )

$\sigma'_0$  = original effective stress

$\sigma'_1$  = final effective stress

$j$  = stress exponent

$m$  = modulus number, determined from laboratory test and/or from back-calculation of results from field tests

$\sigma'_r$  = reference stress, a constant, equal to 100 kPa ( $\approx 1$  tsf  $\approx 2$  ksf  $\approx 1$  kg/cm<sup>2</sup>  $\approx 1$  at)

Mathematically, any stress exponent value can be used in Eq. 3.8 other than exactly 0. A value smaller than unity agrees with the observation that, for each increment of stress, the deformation increment becomes progressively smaller. A negative exponent will overstate that trend. An exponent equal to unity indicates a linear stress-deformation response to load. A value larger than unity implies a soil where the deformation increment increases with increasing stress. It has no practical application.

As Eq. 3.8 cannot handle  $j = 0$ , the relation for  $j = 0$  needs to be developed from Eq. 3.7 and it then results in Eq. 3.9. Calculations using Eqs. 3.7 and 3.8 for very small values of  $j$ , say, 0.01, give essentially the same result.

$$(3.9) \quad \varepsilon = \frac{1}{m} \ln \frac{\sigma'_1}{\sigma'_0}$$

Figure 3.1 shows an array of strain calculated for multiples of increasing stress change for  $j$ -exponents of zero, 0.25, 0.5, and 1.0.

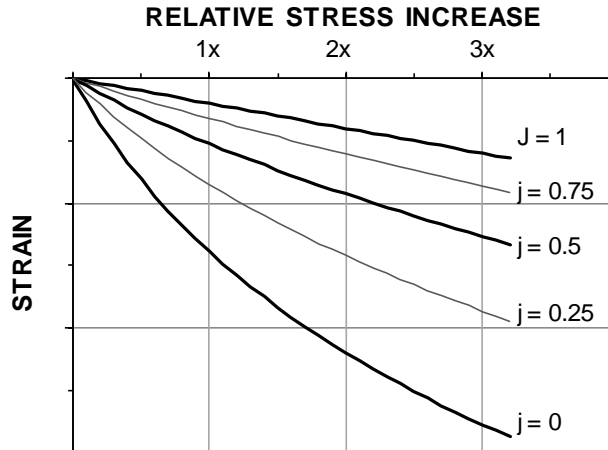


Fig. 3.1 Comparison between strain calculated by Eq. 3.8 for four different stress exponents

A series of tests on sand, silt, and clay is plotted Figure 3.2, showing two diagrams: stress exponent and modulus number, respectively, plotted versus the porosity of the soil material (Janbu 1963). As indicated, the finer the soil, the smaller the stress exponent and modulus numbers. Note that the modulus numbers are in logarithmic scale and, the range is really quite wide; clays show a range from below a value of  $m = 10$  indicating very compressible clay, to 10 - 20 indicating compressible clay, and to 50 and beyond indicating a normal to low compressibility. Silt and sand would overlap, though a dense silt would normally be expected to have a larger modulus number than a stiff clay. I added the density scale to Janbu's porosity scale in order to assist myself and other porosity-challenged fellows. The density is saturated density calculated for a solid density equal to 2,600 kg/m.

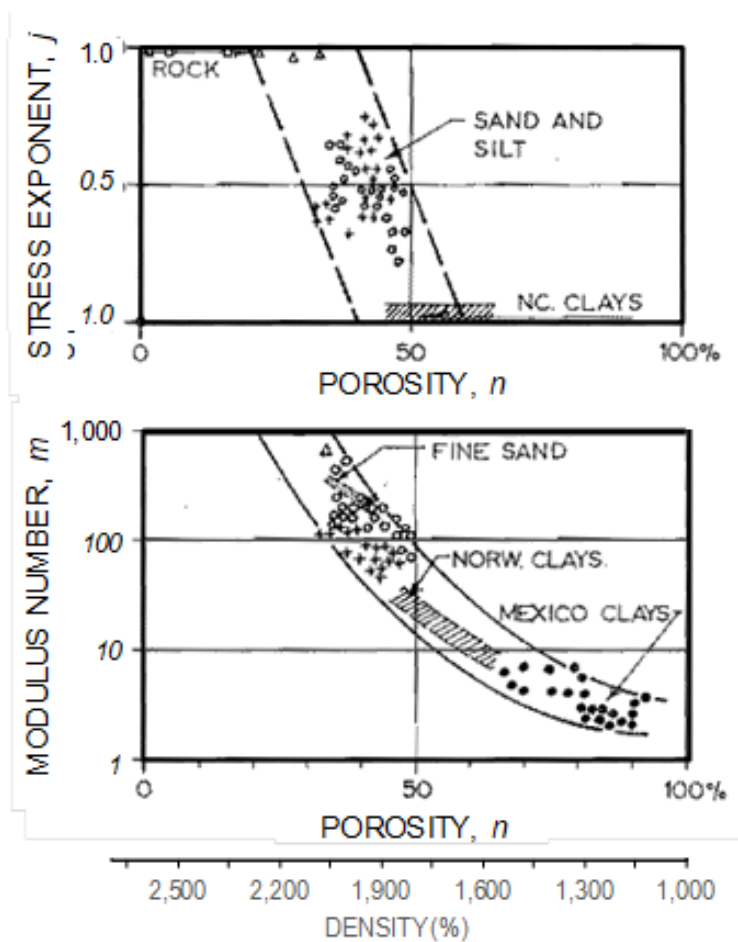


Fig. 3.2 Variation of stress exponent and modulus numbers with porosity (Janbu 1963).

### 3.5.2 Typical Values of Modulus Number, $m$

With knowledge of the original effective stress, the increase of stress, and the type of soil involved (without which knowledge, no reliable settlement analysis can ever be made), the only soil parameter required is the modulus number. The modulus numbers to use in a particular case can be determined from conventional laboratory testing, as well as in-situ tests. As a reference, Table 3.1, which is based on data by Janbu (1963; 1967), shows a range of normally conservative modulus numbers,  $m$ , which are typical of various soil types. Re-compression modulus numbers,  $m_r$ , can often be expected to range from 8 to 12 times the number for normally consolidated conditions. A smaller ratio is often an indication of sample disturbance.

The table also shows a range of stress exponents with  $j = 0$  for clays, a range from 0.25 through 0.75 for intermediate soils, and values of 1 for very dense sand to very dense till. The values are indicated as a guide only and in an actual design case, it is advisable to verify them to actual observations and experience.

Note also that strictly speaking, the modulus number (and  $C_c-e_0$ ) obtained from an oedometer test should be reduced before being applied to a practical case due to the fact that the oedometer value is from constrained condition whereas the practical case is under unconstrained conditions. In view of all the uncertainties involved in the analysis, such reduction is usually not implemented.

**TABLE 3.1 Typical and Normally Conservative Modulus Numbers**

SOIL TYPE	MODULUS NUMBER, m	STRESS EXP., j
Till, very dense to dense	1,000 — 300	1
Gravel	400 — 40	1
Sand very dense	400 — 250	1
Sand dense	400 — 250	0.75
compact	250 — 150	0.75
loose	150 — 100	0.5
Silt dense	200 — 80	0.5
compact	80 — 60	0.5
loose	60 — 40	0.25
Clayey silt, soft	10 — 5	0.25
<b>Clays</b>		
Silty clay hard, stiff	60 — 20	0
Silty clay stiff, firm	20 — 10	0
Soft marine clays and organic clays	20 — 5	0
Peat	5 — 1	0

Depending on mineral composition and age, actual soil layers may show different combination of m and j.

The modulus numbers in the table are approximate and mixed soils will be different. For example, a silty sand will be more compressible than a clean sand of the same density (Huang et al. 1999). Similarly, a sand containing even a small amount of mica, a few percent is enough, will be substantially more compressible than a sand with no mica (Gilboy 1928).

Designing for settlement of a foundation is a prediction exercise. The quality of the prediction, that is, the agreement between the calculated and the actual settlement value, depends on how accurately the soil profile and stress distributions applied to the analysis represent the site conditions, and how closely the loads, fills, and excavations at the site resemble those actually occurring. The quality depends also on the quality of the soil parameters used as input to the analysis. Soil parameters for cohesive soils depend on the quality of the sampling and laboratory testing. Clay samples tested in the laboratory should be from carefully obtained 'undisturbed' samples. When testing overconsolidated clays, paradoxically, the more disturbed the sample is, the less compressible the clay appears to be. The error which this could cause is to a degree 'compensated for' by the simultaneous apparent reduction in the preconsolidation stress determined from the test curve. Furthermore, high quality sampling and oedometer tests are costly, which limits the amounts of information procured for a routine project. The designer usually runs the tests on the 'worst' samples and arrives at a 'conservative' prediction. This may be acceptable, but never so when the word 'conservative' is nothing but a disguise for the then more appropriate terms 'erroneous' and 'unrepresentative'. Then, the end results may perhaps not even be on the 'safe side'.

Non-cohesive soils cannot easily be sampled and tested (however, as indicated in Section 3.13, CPT sounding can be used to estimate a compressibility profile for a site). Therefore, settlement analysis of foundations in such soils must rely on empirical relations derived from in-situ tests and experience values. Usually, non-cohesive soils are less compressible than cohesive soils and have a pronounced pre-loading ("overconsolidation") condition. Therefore, testing of compressibility and analysis of settlement is often considered less important for non-cohesive soils. However, considering the current trend toward larger loads and foundation stresses, cautious foundation design must address also the settlement expected in non-cohesive soils.

Regardless of which methods that are used for calculating—predicting—the settlement, it is necessary to refer the analysis results back to basics. That is, if the settlement values used for the assessment of the foundation design are not determined from a so backed-up analysis, the foundation should be evaluated to indicate what range of compressibility parameters (Janbu modulus numbers) the settlement values represent for the actual soil profile and conditions of effective stress and load. For example, if the design of the superstructure indicates that a settlement of 35 mm is the acceptable limit, the foundation design engineer should calculate—back-calculate—the modulus numbers that correspond to the limit under the given conditions of soil profile and effective stress and compare the results to the parameters obtained from the soils investigation. This back-calculation provides a comparison between the values of compressibility (modulus numbers) applied to the design and the values that would be 'right on' and is often more revealing than a comparison between the settlements calculated using soil-investigation values to the permissible values (size of margin). The effort also provides a worthwhile check on the reasonableness of the results.

### 3.5.3 Dense Coarse-Grained Soil — $j = 1$

The stress-strain behavior (settlement) in dense coarse-grained soils, such as glacial till, can be assumed to be 'elastic', which means that the stress exponent is equal to unity ( $j = 1$ ) and the compression is 'linearly elastic'. It is normally assumed that **immediate compression** is linearly elastic, i.e.,  $M_i$  and  $m_i$  are constant and the stress exponent,  $j$ , is equal to unity. By inserting  $j = 1$  and considering that the reference stress,  $\sigma_r$ , is equal to 100 kPa, Eq. 3.7 becomes Eq. 3.9.

$$(3.10) \quad \varepsilon = \frac{1}{100m} (\sigma'_1 - \sigma'_0) = \frac{1}{100m} \Delta \sigma'$$

Notice, because the reference stress is inserted with a value in the SI-system of units, Eq. 3.9 presupposes that  $M$  is given in the same system of units, i.e., in Pa. If the units for  $M$  are in tsf or ksf, Eq. 3.9 changes to Eqs. 3.9a or 3.9b, respectively.

$$(3.10a) \quad \varepsilon = \frac{1}{m} (\sigma'_1 - \sigma'_0) = \frac{1}{m} \Delta \sigma' \quad (3.10b) \quad \varepsilon = \frac{1}{2m} (\sigma'_1 - \sigma'_0) = \frac{1}{2m} \Delta \sigma'$$

Comparing Eqs. 3.1 and 3.10 for soils with a stress exponent of unity and considering that the reference stress,  $\sigma_r$ , as expressed in Eq. 10, is equal to 100 kPa, for modulus in units of **kPa**, **tsf**, and **ksf**, the respective relations between the modulus number and the modulus are expressed in Eqs. 3.11

$$(3.11) \quad \begin{array}{lll} m = M/100 & (3.11a) \quad m = M & (3.11b) \quad m = M/2 \\ \text{units in kPa} & \text{units in tsf} & \text{units in ksf} \end{array}$$

### 3.5.4 Sandy or Silty Soil — $j = 0.5$

Janbu's original concept considered a gradual increase of the stress exponent,  $j$ , from zero to unity when going from clay to dense gravel, though applying a gradual change is considered unnecessary in practice. Values of " $j$ " other than  $j = 0$  or  $j = 1$ , are only used for **sandy or silty** soils, where the stress exponent is often taken as ranging from 0.5 to 0.75. By inserting  $j = 0.5$  and considering that the reference stress is 100 kPa, Eq. 3.8 simplifies to Eq. 3.12. For a soil, which is expected to have a non-linear response ( $j = 0.5$ ), where an average modulus is known for a range of stress, combining Eqs. 3.9 and 3.12 can enable a modulus number to be calibrated from (i.e., fitted to) a known modulus and stress range.

The Janbu modulus number can also be estimated from results of a CPTU sounding, as described in Section 2.11. This is an advantage of the Janbu approach because determining compressibility of coarse-grained soils in the laboratory is difficult.

$$(3.12) \quad \varepsilon = \frac{1}{5m} (\sqrt{\sigma'_1} - \sqrt{\sigma'_0}) \quad \text{units in kPa}$$

Notice, Eq. 3.12 is not independent of the choice of units and the stress values must be inserted in kPa. That is, a value of 5 MPa is to be inserted as "5,000" and a value of 300 Pa as "0.3".

In English units and with stress in units of tsf or, alternatively, in ksf, Eq. 3.12 becomes

$$(3.12a) \quad \varepsilon = \frac{2}{m} (\sqrt{\sigma'_1} - \sqrt{\sigma'_0}) \quad \text{units in tsf} \quad (3.12b) \quad \varepsilon = \frac{\sqrt{2}}{m} (\sqrt{\sigma'_1} - \sqrt{\sigma'_0}) \quad \text{units in ksf}$$

Take care, the equations are not independent of units—to repeat, the stress units must be inserted in units of tsf and ksf, respectively.

If the soil is **overconsolidated** or preloaded and the final stress exceeds the preconsolidation or preloading stress, Eqs. 3.12, 3.12a and 3.12b change to:

$$(3.12) \quad \varepsilon = \frac{1}{5m_r} (\sqrt{\sigma'_p} - \sqrt{\sigma'_0}) + \frac{1}{5m} (\sqrt{\sigma'_1} - \sqrt{\sigma'_p}) \quad \text{units in kPa}$$

$$(3.12a) \quad \varepsilon = \frac{2}{m_r} (\sqrt{\sigma'_p} - \sqrt{\sigma'_0}) + \frac{2}{m} (\sqrt{\sigma'_1} - \sqrt{\sigma'_p}) \quad \text{units in tsf}$$

$$(3.12b) \quad \varepsilon = \frac{\sqrt{2}}{m_r} (\sqrt{\sigma'_p} - \sqrt{\sigma'_0}) + \frac{\sqrt{2}}{m} (\sqrt{\sigma'_1} - \sqrt{\sigma'_p}) \quad \text{units in ksf}$$

where  $\sigma'_0$  = original effective stress (kPa, tsf, and ksf, respectively)  
 $\sigma'_p$  = preconsolidation stress (kPa, tsf, and ksf, respectively)  
 $\sigma'_1$  = final effective stress;  $\sigma'_1 > \sigma'_p$  (kPa, tsf, and ksf, respectively)  
 $m$  = modulus number (dimensionless)  
 $m_r$  = recompression modulus number (dimensionless)

If the soil is overconsolidated and the imposed stress does not result in a new (final) stress that exceeds the preconsolidation stress, Eqs. 3.12, 3.12a, and 3.12b become:

$$(3.13) \quad \varepsilon = \frac{1}{5m_r} (\sqrt{\sigma'_1} - \sqrt{\sigma'_0}) \quad \text{units in kPa}$$

$$(3.13a) \quad \varepsilon = \frac{2}{m_r} (\sqrt{\sigma'_1} - \sqrt{\sigma'_0}) \quad \text{units in tsf}$$

$$(3.13b) \quad \varepsilon = \frac{\sqrt{2}}{m_r} (\sqrt{\sigma'_1} - \sqrt{\sigma'_0}) \quad \text{units in ksf}$$

### 3.5.5 Cohesive Soil — $j = 0$

In cohesive soil, the stress exponent is zero,  $j = 0$ . For **normally consolidated** cohesive soils, the integration of Eq. 3.7 then results in Eq. 3.14, the same as Eq. 3.4, and independent of the stress units).

$$(3.14) \quad \varepsilon = \frac{1}{m} \ln \frac{\sigma'_1}{\sigma'_0}$$

Most natural soils other than very young or organic clays are **overconsolidated**. Thus, in an overconsolidated, cohesive soil, Eq. 3.15 applies:

$$(3.15) \quad \varepsilon = \frac{1}{m_r} \ln \frac{\sigma'_p}{\sigma'_0} + \frac{1}{m} \ln \frac{\sigma'_1}{\sigma'_p}$$

Notice, the ratio  $(\sigma'_p/\sigma'_0)$  is equal to the **Overconsolidation Ratio**, OCR. However, the measure of overconsolidation is better expressed as a stress difference, or "**Preconsolidation Margin**" ("**Prestress Margin**" in a sand):  $\sigma'_p - \sigma'_0$ . An oedometer test determines the preconsolidation margin for a sample obtained from a specific depth, not the OCR for the profile. An OCR should therefore never be stated without being coupled to the depth to which it applies. Better then to use the preconsolidation margin ("pre-load margin"),  $\Delta\sigma'_c$ , as the main parameter. For example, an area that has had 2 m of soil removed now would exhibit a preconsolidation margin,  $\Delta\sigma'_c$ , of about 40 kPa throughout the soil body. However, at a depth of 1 m below the new ground surface (also the groundwater table), the OCR would be about 5, reducing to only about 1.1 at 10 m depth.

By the way, soils can be normally consolidated or overconsolidated, but never "underconsolidated". The latter is just a misnomer for soils that are "undergoing consolidation". In soils undergoing consolidation, the actual effective overburden stress is equal to the actual preconsolidation stress. If piezometer measurements at a site indicates that the effective overburden stress is larger than the preconsolidation stress determined in consolidation testing, then, either, or both, of the results of the consolidation test or of the determination of effective overburden stress are wrong. "Undergoing consolidation" means that pore pressure dissipation is occurring at the site and that the pore-pressure distribution in a soil layer is non-linear. N.B., so is the distribution of effective stress.

If the applied foundation stress does not result in a new stress that exceeds the preconsolidation stress, Eq. 3.15 becomes Eq. 3.16.

$$(3.16) \quad \varepsilon = \frac{1}{m_r} \ln \frac{\sigma'_1}{\sigma'_0}$$

### 3.5.6 Application to Compacted Soils and Proctor Tests

Compacted fills usually consist of coarse-grained soil, e.g., sand and gravel, which are brought to a certain at-least density by various means of compaction. Often, a standard laboratory compaction test, such as the Proctor test (Holtz and Kovacs 1981, Holtz et al. 2011), is used to provide a reference density, i.e., “optimum dry density”. Then, satisfactory field compaction requires that the dry density of the fill is shown to be at least a certain percentage of the Proctor optimum value. Note, the reference is dry density. Because of the ease of determining water content as opposed to determining density (density requires a known volume of the soil sample before the sampling), frequently, the acceptance criterion in the field is the water content relative to the “water content at optimum density”. However, because the degree of saturation varies in the fill, using a water-content criterion is a poor substitute for reference to the actual dry density.

Proctor density tests are performed on unsaturated soil specimens, which means that compression is fast as it does not require squeezing out any water and therefore, strictly, means that consolidation is not involved. The common conception is that consolidation is settlement—well, it is part of it—leads many to think “no-consolidation, so no-settlement” for a load placed on the fill. This could be an explanation for why nobody ever indicates the compressibility of the densified soil as a reference in addition to the Proctor density value. This, apart from the fact that if a soil is compacted on the dry side of the optimum dry density, it might compress if it later on becomes saturated. Indeed, compacted soils have compressibility and will compress when loaded, albeit to a smaller extent than uncompacted. For further information see Lin and Lovell (1981).

It is usually assumed that a fill compacted to 95 % of Proctor optimum dry density will neither settle under its own weight nor when loaded by a footing, and this with some justification, too. However, fills are sometimes subjected to very large loads and sometimes the compaction was to a low Proctor value, say 90%. Then, noticeable settlement will occur. Therefore, in addition to the Proctor optimum dry density, information on the compressibility (deformation modulus), or better still, the modulus number,  $m$ , (with the stress exponent,  $j$ , equal to unity) are important for the design decisions, as are the preconsolidation or preloading stress,  $\sigma'_c$ , and the preconsolidation or preloading margin,  $\Delta\sigma'_c$ . Note, compacted soils are invariably preloaded (“precompressed”).

Requiring a specific compaction result, i.e., density, means that a certain at-least compressibility (modulus or modulus number,  $m$ ) is *de-facto* required. It is desirable (indeed, so desirable that it should be mandatory) that every compaction specification in addition to listing the percentage of the Proctor dry density value (be it Standard Proctor or Modified Proctor) also declares what compressibility that this represents and provides the maximum settlement this represents for the load applied in the project. As mentioned, if the maximum settlement and the maximum stress are known, if only from a judgment call, then, a back-calculation will produce the equivalent compressibility for the case.

Because of sample disturbance and other influences, the fact that most soils are preconsolidated or preloaded is often overlooked. Some even believe that preconsolidation only applies to clays. Actually, coarse-grained soils, indeed, sand, are almost always preloaded (or “prestressed” or “precompressed”), and significantly so (hydraulic fill being an exception). However, the values of OCR or preload margin are difficult to determine by conventional soil investigation methods.

The compressibility values employed in an analysis are often empirical values obtained from relatively low stress levels applicable to the preconsolidation condition. When a foundation exerting larger stress is considered, the stress level might exceed the prestress level. The settlement is then governed by the virgin compressibility of the soil. If so, the settlements will be larger, much larger, than those based on low-stress level experience values.

### 3.6 Evaluating oedometer tests by the $e$ -log $p$ and the strain-stress methods

To repeat, with regard to the options of linearly elastic response to an applied load, the Janbu method with the stress exponent set equal to unity is mathematically the same as using a linear modulus. Similarly, the Janbu method with the stress exponent equal to zero, is mathematically the same as using the  $C_c/e_0$  method. The Janbu method adds a third option, that of  $j = 0.5$ , which is applicable to silty sand and sandy silt, which method is not covered by the conventional-habitual- $C_c/e_0$  method. Sometimes,  $j = 0.75$  is chosen for analysis of sand response (Massarsch 2021, personal communication).

The Janbu modulus numbers are easy to use. For clays, it provides a single unified parameter, the modulus number. With only one parameter, it is easy for the geotechnical engineer to establish a reference data base of values.

Figure 3.3 presents the results of an oedometer test (consolidation test) plotted both in the conventional (North American) manner (Figure 3.3A) as void ratio ( $e$ ) versus  $\lg p'$  and as strain ( $\epsilon$ ) versus  $\lg p'$  (Figure 3.3B). The same test data are used for both diagrams. The compression index,  $C_c$ , is determined to 0.38 in the first diagram as the void ratio distance for one log cycle. The modulus number,  $m$ , is determined to 12 from the second diagram as the inverse of the strain obtained for a stress change from  $\sigma'_0 = p$  to  $\sigma'_1 = 2.718p$  (Eq. 3.14).

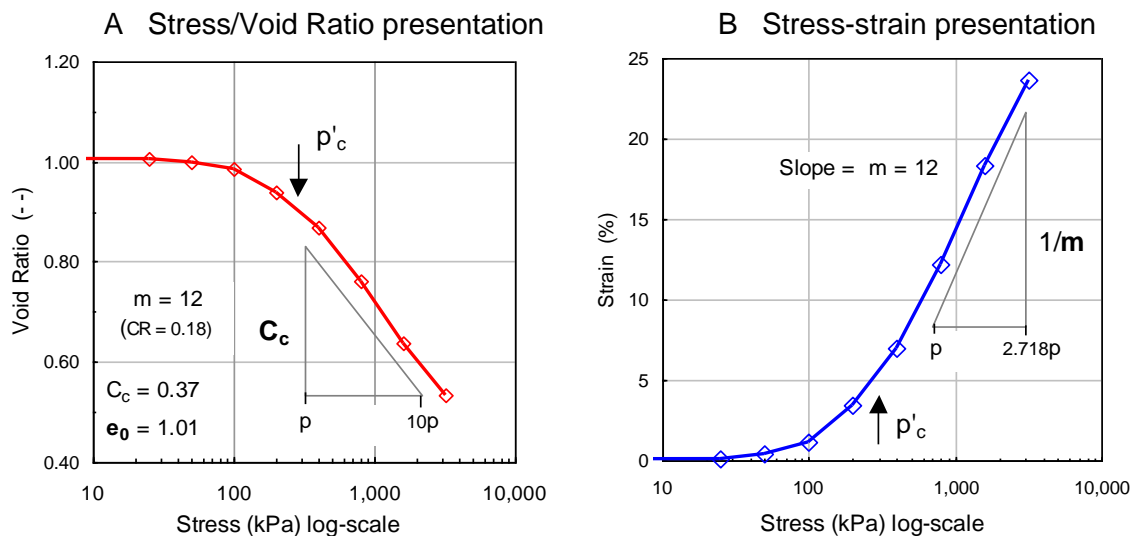


Fig. 3.3 Results from a consolidometer test (data from Bowles, 1988). (The preconsolidation stress is taken directly from the source, where it was indicated to have been determined "by eye-balling" to 280 kPa).

The recompression index and recompression modulus number are determined in similar manner. Most geotechnical textbooks include details on how to analyze the results of an oedometer test, for example Holtz and Kovacs (1981) and Holtz et al. (2011), which also include advice about correction for sample disturbance.

Preconsolidation stress is often difficult to determine even from oedometer test on high quality undisturbed samples. Janbu (1998) recommended determining it from a plot of the slope of the tangent modulus line, as shown in Figure 3.4. The preconsolidation stress is clearly noticeable at the applied stress of 200 kPa. Most textbooks include several conventional methods of determining the consolidation stress. Grozic et al. (2003) described details of the methods and offered an interesting discussion on the processes. See also Tanaka et al. (2001), Umar and Sadrekarimi (2017) and references therein.



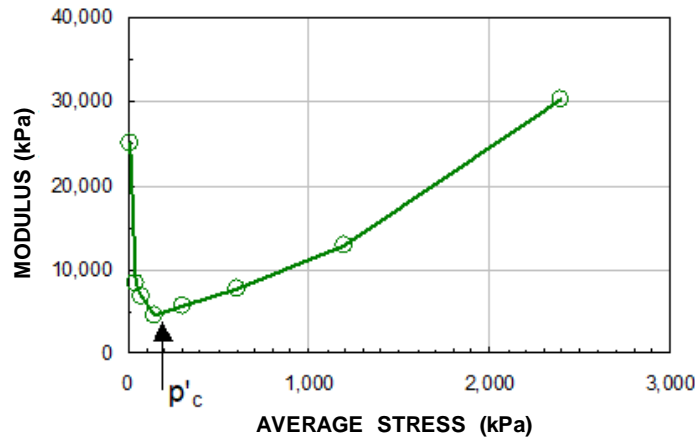


Fig. 3.4 The tangent modulus plot to determine preconsolidation stress according to Janbu (1998)

### 3.7 The Janbu Method Compared to Conventional Methods

The Janbu tangent modulus method is not different to—does not contrast or conflict with—the 'conventional' methods. The Janbu method for calculation of settlements and the conventional elastic modulus approach give identical results, as do the Janbu method and the conventional  $C_c e_0$ -method (Eqs. 3.4 and 3.5, and Eqs. 3.13 and 3.14). There are simple direct conversions between the modulus numbers and the  $E$ -modulus (or " $M$ -" or " $D$ -modulus") and the  $C_c e_0$  values. The relation for a linearly elastic soil (" $E$ -modulus soils") is given in Eq. 3.10 (the equation is repeated below).

$$(3.17) \quad m = E/100 \quad \mathbf{E \text{ in units of kPa}} \quad \text{or} \quad (3.17a) \quad m = E \cdot 10^{-5} \quad \mathbf{E \text{ in units of Pa}}$$

$$(3.17b) \quad m = E \quad \mathbf{E \text{ in units of tsf}} \quad (3.17c) \quad m = E/2 \quad \mathbf{E \text{ in units of ksf}}$$

The conversion relation between the conventional  $C_c e_0$  method and the Janbu modulus method is given in Eq. 3.18.

$$(3.18) \quad m = \ln 10 \frac{1+e_0}{C_c} = 2.3 \frac{1+e_0}{C_c} = 2.3/CR$$

Where  $CR = \text{compression ratio} = C_c/(1 + e_0)$

Although mathematically equal, the MIT approach (Section 3.4) has a disadvantage over the Janbu method in that its compressibility values ( $CR$ ) are smaller than unity, requiring expressing values with decimals, while the Janbu modulus numbers are larger than unity and whole numbers. For example, for modulus numbers of 5, 10, 50, to 100, which span most of the compressibility range of cohesive soil, become  $CR$ -values of 0.46, 0.23, 0.046, and 0.023. Moreover, apart from the unwieldy three-decimal format required for the later numbers in the series, the MIT  $CR$ -values have no apparent correlation for expressing the compressibility of non-cohesive soils, which correlation the Janbu method provides.

Similarly, a strict mathematical relation can be determined for the Swedish-Finnish  $\varepsilon_2$ -approach (Eq. 3.6), as given in Eq. 3.19. The  $\varepsilon_2$  is the compression ratio for a doubling of the stress and is usually reported in %-units.

$$(3.19) \quad m = \ln 10 \frac{\lg 2}{\varepsilon_2} = 2.3 \frac{\lg 2}{\varepsilon_2} = \frac{0.69}{\varepsilon_2}$$

The Janbu method of treating the intermediate soils (sandy silt, silty sand, and sand) is “extra” to the  $C_c e_0$  method and the elastic method (Eqs. 3.12 and 3.13).

The following couple of examples will demonstrate the advantage of the Janbu modulus number approach as opposed to the conventional  $C_c e_0$  approach.

Figure 3.5 shows results from oedometer tests on an overconsolidated Texas Gulf Clay (Beaumont clay), with void ratios ranging from about 0.4 through 1.2 (Endley et al. 1996). Figure 3.5A presents a range of  $C_c$ -values, which imply that the compressibility expressed as increased  $C_c$ -value, would be increasing with depth (the associated values of voids ratio,  $e$ , are not shown. However, Figure 3.3B, which shows the  $C_c e_0$ -values converted to Janbu modulus numbers, demonstrates that there is no such trend with depth. The modulus numbers range—from about 10 through almost 40—is quite wide, going from high through low compressibility.

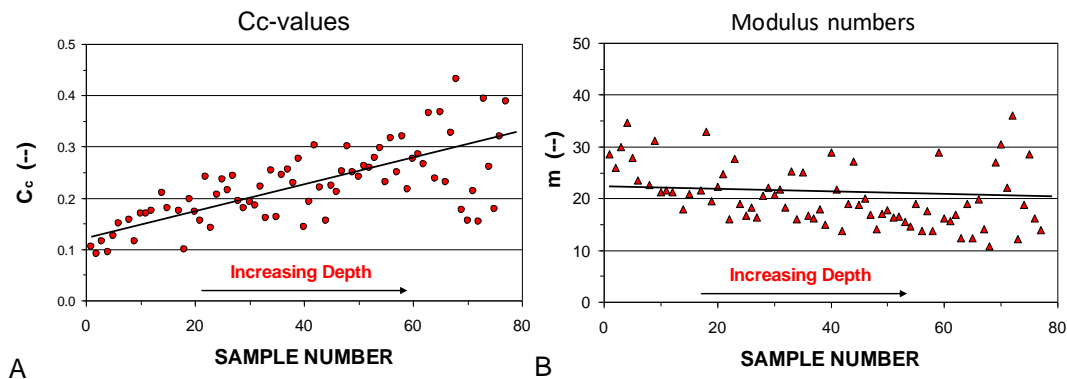


Fig. 3.5  $C_c$ -values and modulus numbers from Beaumont clay. Data from Endley et al. 1996.

Figure 3.6 presents results from oedometer tests on a normally consolidated to slightly overconsolidated silty clay outside Vancouver, BC with void ratios ranging from about 0.8 through 1.4. The relative range between the smallest and largest  $C_c$ -value (a factor of 2) suggests a somewhat wider range of compressibility than the actual, represented by the modulus number where the relative range between the smallest and largest value is a factor of 1.3. The average modulus number is approximately 10, which is the upper boundary of a very compressible soil.

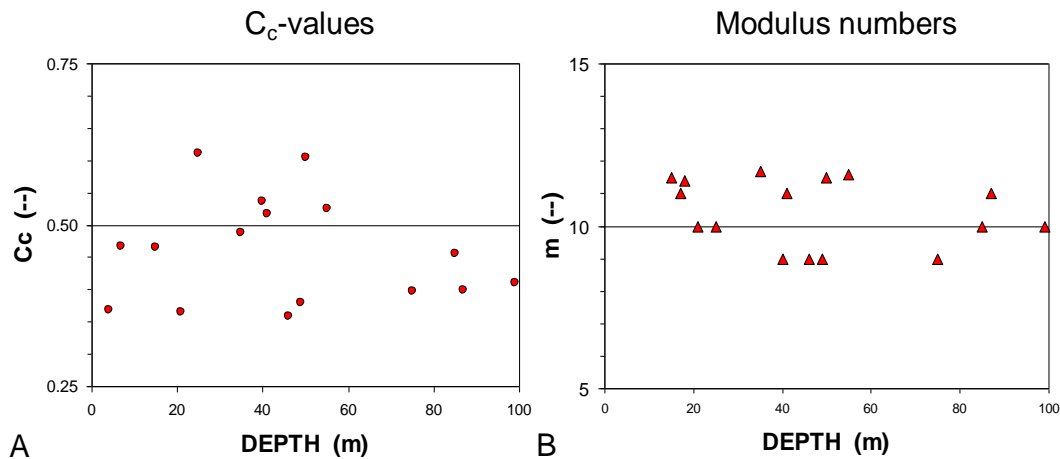


Fig. 3.6  $C_c$ -values and modulus numbers from Fraser River clay, BC.

The Janbu method is widely used internationally and by several North American engineering companies and engineers. However, many others are yet reluctant to use the Janbu approach, despite its obvious advantages over the conventional  $C_c e_0$ -method. The approach has been available for more than twenty years in the second and third editions of the broadly used Canadian Foundation Engineering Manual, CFEM (1985; 1992). (Regrettably, by accident or other, the committee revising the CFEM for the fourth Edition (published in 2006) omitted to keep the Janbu approach in the Manual). Even more so, considering that the Janbu modulus number has important application for assessing liquefaction risk and soil densification as described in Clauses 2.12.8 and 10.6.1.

Those not fully convinced by the previous examples, should reflect on the results shown in Figure 3.7 and 3.8. The right graph in Figure 3.7A shows a fairly typical array of  $C_c$ -values ranging from about 0.3 through 0.9, implying a randomly varying compressibility. However, when coupled with the associated  $e_0$ -values, as shown in the left graph in Figure 3.7B, a different picture evolves: the compressibility is constant for the  $C_c$ -values. N.B., the values plotted in Fig A were selected because they do show a constant modulus number. Similarly, Figure 3.8A shows a set of constant  $C_c$ -values, that is, they imply a constant compressibility, selected because when coupled with their associated  $e_0$ -values, again, as shown in Figure 3.8B, the picture shows the compressibility to be highly varying. (Data from Endley et al. 1996).

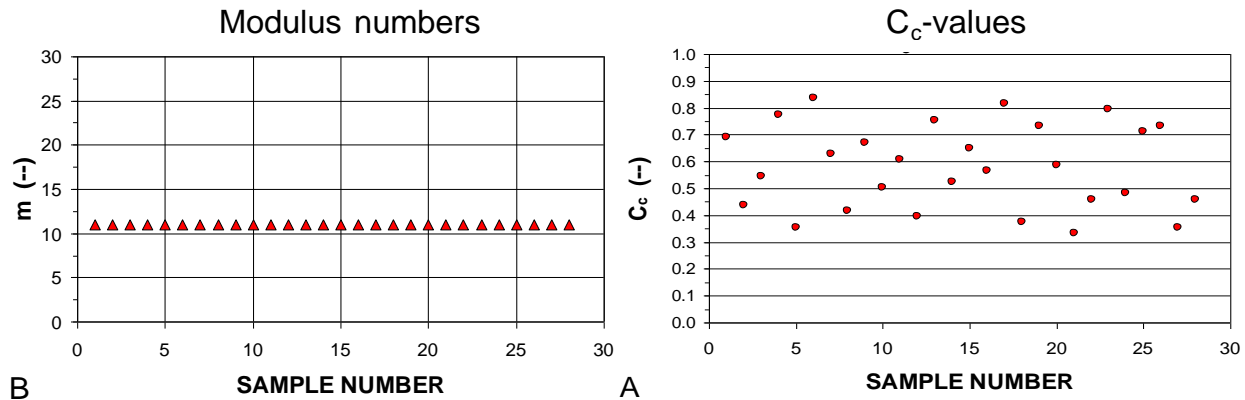


Fig. 3.7  $C_c$ -indices (A), converted to "m"-numbers via associated void ratios,  $e_0$  (B).

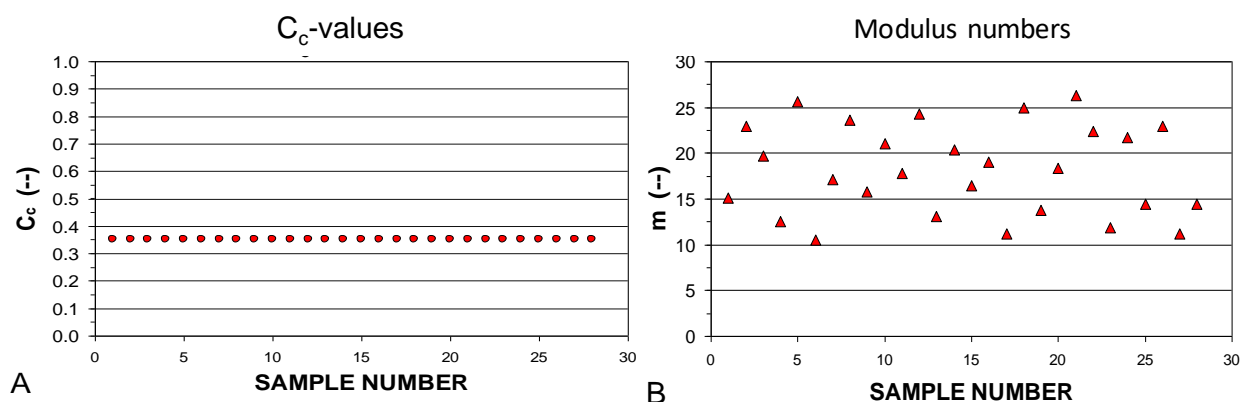


Fig. 3.8 "Selected" constant  $C_c$ -indices, and converted via associated "selected" void ratios,  $e_0$ , to "m"-numbers.

Engineers working in a for them well-known area, where the soils, therefore, have a familiar range of water contents and void ratios, can work well only classifying compressibility from  $C_c$ -values. However, when encountering foundation problems in different geologies, a good advice is to start using the modulus number as the measure of and reference to soil compressibility.

Moreover, all parameters determined from laboratory tests include errors or imprecisions. The compressibility expressed by a modulus number is expressed in applied stress and relative deformation. The conventional  $C_c e_0$ -compressibility is expressed in void ratio and stress with void ratio calculated from compression (strain) with input of weight, water content, and assumed (sometimes measured) soil solid density. Every measurements has an error or imprecision. Thus, the compressibility expressed by the modulus number is affected by imprecision of two measurements, while the compressibility expressed by  $C_c e_0$  is affected by imprecision of three measurements combined with an assumed constant. Obviously, the effect of potential imprecision and error of the data of the former is much less than that of the latter.

### 3.8 Relative Degree of Compressibility

Some will express the degree of compressibility using the compression index,  $C_c$ . However, this is not practical because a specific  $C_c$  alone cannot be referred to as representing a degree of compressibility, etc., without also coupling it with the  $e_0$ -value and few can correlate to two variable numbers simultaneously. In contrast, as the Janbu modulus number is a single number, it lends itself well to indicate a relative degree of compressibility of the soil. There is no standard established for ranged of compressibility per the Janbu modulus number. I like to use the ranges listed in [Table 3.2](#).

**TABLE 3.2 Ranges of Compressibility**

Very compressible	$m < 10$
Compressible	$m 10 - 20$
Medium Compressibility	$m 20 - 30$
Moderate compressibility	$m 30 - 50$
Low Compressibility	$m > 50$

[Figure 3.9](#) shows the relation between so-defined ranges of compressibility and values of  $C_c$  and  $e_0$ .

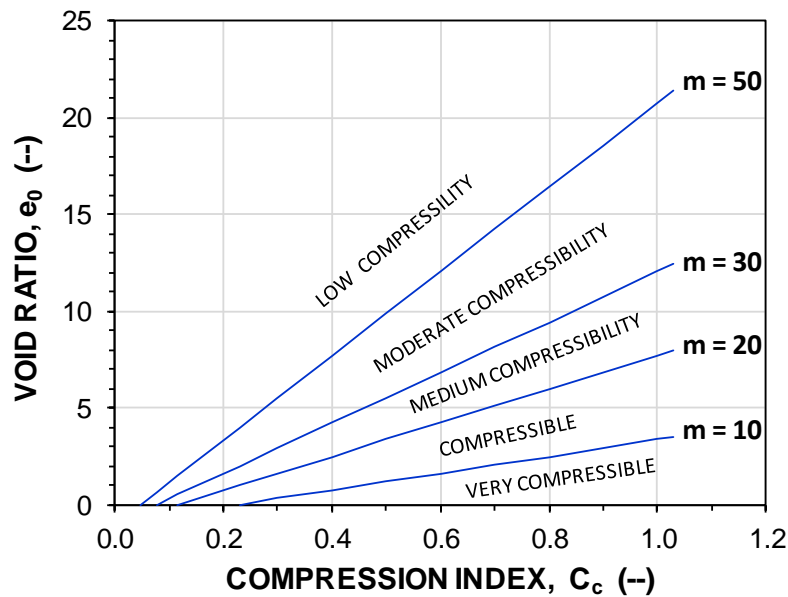


Fig. 3.9 Compressibility based on  $C_c$  and void ratio correlated to ranges per Janbu modulus number

On increasing stress, the grain structure will show an immediate reduction in volume ("immediate compression"). However, no change of pore volume will occur before the water occupying the pores is expelled ("squeezed out") by the stress increase, which process is rapid in coarse-grained soils and slow in fine-grained soils. The process is called consolidation, and it usually occurs with an increase of both undrained and drained soil shear strength. In very fine clays, the consolidation can even take a longer time than the life expectancy of the building, or of the designing engineer, at least. By analogy with heat dissipation in solid materials, the Terzaghi consolidation theory indicates simple relations for the time required for the consolidation. The most commonly applied theory builds on the assumption that water is leaving the soil at one surface boundary (upper or lower) and not at all at the opposite boundary (nor horizontally). The consolidation is rapid in the beginning, when the driving (forcing) pore pressures are greater and slows down with time as the pressures reduce. The analysis makes use of the relative amount of consolidation obtained at a certain time, called average degree of consolidation, which is defined in Eq. 3.20.

$$(3.20) \quad U_{v,AVG} = \frac{S_t}{S_f} = 1 - \frac{u_t}{u_0}$$

where  $U_{v,AVG}$  = average degree of consolidation for vertical drainage  
 $S_t$  = settlement at Time  $t$   
 $S_f$  = final settlement at full consolidation  
 $u_t$  = average pore pressure at Time  $t$   
 $u_0$  = initial average pore pressure (on application of the load at Time  $t = 0$ )

Notice that the pore pressure varies throughout the soil layer and that Eq. 3.21 assumes an average value through the soil profile. In contrast, the settlement values are not the average, but the accumulated values.

The definition of degree of consolidation presumes that it is same whether determined by settlement or pore pressure dissipation. If you believe in the classical theory, and why not, the 100-% consolidation is the same as the difference between final and initial effective stress and the dissipated pore pressure is the degree of consolidation times that effective stress change. Of course, a measured settlement is an average for an appreciable body of soil, whereas a pore pressure is a pressure in a point. (Note, the pore pressure in a specific point can vary due to a number of seemingly unrelated effects. For a brief account, see Li and Likos 1923). There is always the question whether or not that pore pressure is representative for the soil body. Moreover, the degree determined from measured settlement cannot be determined until all the settlement has occurred, whereas the degree determined from pore pressure is known from the start and at any time, so questionable or not, that degree is the one we can determine when the settlement is ongoing. Further confusing the matter is that the two ways of determining the degree of consolidation are not quite equal at any one time. And, what is 100 % consolidation? It only occurs at infinite time. In practice, the settlement calculated for a degree of consolidation of 90 or 95 % is what most consider be the "100-% value".

The time for achieving certain degree consolidation is, as follows (Eq. 3.21).

$$(3.21) \quad t = T_v \frac{H^2}{c_v}$$

where  $t$  = time to obtain a certain degree of consolidation (s)  
 $T_v$  = a dimensionless time coefficient  
 $c_v$  = coefficient of consolidation expressed as area/time ( $m^2/s$ )  
 $H$  = length of the longest drainage path (m)

The time coefficient,  $T_v$ , is a function of the type of pore pressure distribution. Of course, the shape of the distribution affects the average pore pressure values and a parabolic shape is usually assumed.

The interrelations for  $T_v$  and  $U_{v,AVG}$  are given in Eqs. 3.23a through 3.23c (Holtz and Kovacs 1981, Holtz et al. (2011)). Eqs. 3.22a and 3.22b are valid for  $U_{v,AVG} > 60\%$ . For  $U_{v,AVG} < 60\%$ , Eqs. 3.22c and 3.22d apply.

$$(3.22a) \quad U_{v,AVG} = 1 - \frac{8}{\pi^2} \exp\left(-\frac{\pi^2}{4} T_v\right) \quad \text{if } U_{v,AVG} > 60\%$$

where  $U_{v,AVG} =$  **average** degree of consolidation for vertical drainage (%)

$$(3.22b) \quad T_v = 1.781 - 0.931 \lg(100 - U_{v,AVG}) \quad \text{if } U_{v,AVG} > 0.60$$

$$(3.22c) \quad U_{v,AVG} = \sqrt{\frac{4T_v}{\pi}} \quad \text{if } U_{v,AVG} < 60\%$$

$$(3.22d) \quad T_v = \frac{\pi}{4} U_{v,AVG}^2 \quad \text{if } U_{v,AVG} < 60\%$$

Approximate values of  $T_v$  for different average values of the average degree of consolidation,  $U_{AVG}$ , are given in Table 3.3. For more exact values and values to use when the pore pressure distribution is different, see, for example, Holtz and Kovacs (1981), Holtz et al. (2011).

**TABLE 3.3** Approximate values of  $T_v$  for different average values of the degree of consolidation,  $U_{AVG}$  (%)

$U_{AVG}$	25	0.50	0.70	0.80	0.90	“1.00”
$T_v$	0.05	0.20	0.40	0.57	0.85	$\approx 1.00$

Note  $U_{AVG}$  is usually given in percent. However, here it is a ratio, a number between 0 and unity.

The SI base units for the parameters of Eq. 3.23 are s (time in seconds),  $m^2/s$  (coefficient of consolidation,  $c_v$ ), and m (length in metre). Often, practitioners desire to obtain the time directly in everyday units, such as days, months, or years with different persons preferring different units, which means that a Babylonian confusion can easily develop with numbers produced in an assortment of units, such as  $m^2/year$ ,  $cm^2/year$ , and  $cm^2/month$ , even  $ft^2/month$  and  $ft^2/year$ , instead of the more appropriate base SI-unit,  $m^2/s$ . (Take care to avoid confusion and risk of mistakes by ensuring that equations are always designed for input of values in base SI-units). This said, it can be argued that an exception from the requirement of using base SI-units is justified in order to avoid the  $10^{-8}$  number or decimals and, therefore, apply the units  $m^2/year$  to calculations per the SI-system and  $ft^2/year$  to those per the English system of units. (To convert from  $m^2/year$  to  $ft^2/year$ , multiply by 10.76). Table 3.4 shows multipliers for converting the SI base-unit,  $m^2/s$ , (and other units) to  $m^2/year$  or  $ft^2/year$ . (A  $c_v = 8 \cdot 10^{-8} m^2/s$  converts to  $8 \cdot 0.315 = 2.52 m^2/yr$ ).

**TABLE 3.4** Multipliers for conversion from miscellaneous units of coefficient of consolidation,  $C_v$ , to  $\text{m}^2/\text{year}$  and  $\text{ft}^2/\text{year}$ .

Unit	$1 \cdot 10^{-8} \text{ m}^2/\text{s}$	$1 \cdot 10^{-4} \text{ cm}^2/\text{s}$	$1 \text{ m}^2/\text{day}$	$1 \text{ m}^2/\text{year}$	$1 \text{ ft}^2/\text{year}$	$\text{ft}^2/\text{month}$	$1 \text{ ft}^2/\text{day}$
to $\text{m}^2/\text{year}$	0.315	0.315	365	1	0.093	1.12	33.9
to $\text{ft}^2/\text{year}$	3.39	3.39	3,930	10.76	1	12	365

Roy E. Olson (Olson 1998) suggested that in order to honor Terzaghi, the base units for the  $c_v$ -coefficient should be given the symbol “T”. Thus, a value of  $1 \text{ m}^2/\text{s} \times 10^{-8}$  ( $= 0.32 \text{ m}^2/\text{year}$ ) would become  $10 \text{ nT}$ , where “n” stands for “nano” and is equal to  $10^{-9}$ . It is a pity that the suggestion did not catch on.

Holtz and Kovacs (1981), Holtz et al. (2011) reported common  $c_v$ -values ranging from a low of  $0.5 \cdot 10^{-8} \text{ m}^2/\text{s}$  in Swedish sensitive clays, about  $3 \cdot 10^{-8} \text{ m}^2/\text{s}$  in San Francisco Bay Mud, and about  $40 \cdot 10^{-8} \text{ m}^2/\text{s}$  in Boston Blue Clay (0.16, 0.95, and  $12.6 \text{ m}^2/\text{year}$ , respectively).

The coefficient of consolidation is determined in the laboratory oedometer test (some in-situ tests can also provide  $c_v$ -values) and it can rarely be obtained more accurately than within a ratio ranging from 2 to 3.

The longest drainage path,  $H$ , for a soil layer that drains at both surface boundaries is half the layer thickness. If drainage only occurs at one boundary,  $H$  is equal to the full layer thickness. Naturally, in layered soils, what value of  $H$  to use is difficult to ascertain, as each layer drains into its adjacent layers, as addressed below.

In saturated soils, water has to be expelled from the soil before the pore volume can reduce. In soils containing gas and in partially saturated soils, however, initially the process appears to be rapid, because gas (air) will readily compress when subjected to an increase of pressure, allowing the pore volume to decrease rapidly. Settlement due to the latter change is often mistaken for the immediate compression of the soil. Well, it is immediate, but it is not due to compression of the soil skeleton. The compression of the soil skeleton is permanent, whereas the compression of the gas bubbles is temporary.

Inorganic soils below the groundwater table are usually saturated and contain no gas. In contrast, organic soils will invariably contain gas in the form of small bubbles (as well as gas dissolved in the water, which gas becomes free gas—bubbles— on release of confining pressure when sampling the soil) and these soils will appear to have a large immediate compression when load is applied. During the consolidation process, as the pore pressure gradually reduces, the bubbles return to their original size and the consolidation process will appear to be slower than the actual rate, indeed, measurements of the development will appear to suggest that the consolidation is completed. The remaining settlement will be believed to be caused by secondary compression, (Section 3.10). Such 'secondary compression' will appear to be unusually large.

Generally, the determination—prediction—of the time for a settlement to develop is filled with uncertainty and it is difficult to reliably estimate the amount of settlement occurring within a specific time after the load application. The prediction is not any easier when one has to consider the development during the build-up of the load. For details on the subject, see Ladd (1991).

Loading a soil by placing a certain thickness of fill over a certain area takes time. Most case analyses assume that all fill is placed simultaneously so all monitoring has a common start date (time). However, as placing the fill invariably occurs over time, therefore, a back-analysis needs to input the fill as a number of loaded areas placed at the actual times—if now that information is available in the back-analyzed case record.

Of old, the consolidation theory recognizes two cases: either a double-drained or a single-drained layer. The problem with reality, though, is that soils are made up of more than one layer and, therefore, they drain into each other. A few very complex computer models can tackle a case having a profile made up of couple of such layers by assuming special numerical relations for each soil layer that slow down the classical relations as based on numerous more or less sophisticated conditions. The trouble is that the input to the software built into the models has no acceptable field data to verify the veracity of the assumed functions involved. There are only a few full-scale case histories where the consolidation process was monitored individually in "sandwiched" soil layers in a multi-layered clay profile. However, the results of most of these cases are muddled up by varying loading times, disturbance effects, and ratio between horizontal and vertical dissipation directions. The main difficulty, though, is that full-scale case studies have to be carried over many years.

I have found that practicing engineers with long experience are quite good at estimating the time for consolidation of a compressible layer by applying judgment. There is usually a main soil layer, an "alpha", that dominates the settlement response to load. So, for design (or back-calculation), the time for full consolidation in that  $\alpha$ -layer is first estimated. The consolidation times for all other layers are then considered in relation to the  $\alpha$ -layer allowing for a longer or shorter time as deemed appropriate (the process also includes re-assessing the time for the  $\alpha$ -layer). The process includes assessing the input of layer thickness, densities, compressibilities, preconsolidation margin, etc., as guided by the site investigation information. (First, input the time for full consolidation of the " $\alpha$ -layer". Second, go to the other layers and input the consolidation time for these—now, a shorter or longer time value, as you judge applicable in reference to your " $\alpha$ -layer". Note that once the time for full consolidation is chosen, the coefficient of consolidation,  $c_v$ , is decided by the geometry, and you need to convince yourself that the values are reasonable for each layer. Anyway, chances are that you will obtain an acceptable distribution of the time-dependent settlement of each layer and, therefore, of the ground surface or the foundation.

An additional, and sometimes not so marginal, factor is that the settlement means that a portion of the soil at a position immediately above the groundwater table has lowered to immediately below the table, which creates a gradual buoyancy effect (reduction of the effective stress throughout the soil profile). When it needs to be considered, simply input of a corresponding time-spaced series of appropriate negative loads.

The rather long consolidation time in clay soils can be shortened considerably by means of vertical drains (see Chapter 4). Vertical drains installed at a spacing ranging from about 1.0 m through 3.0 m have been very successful in accelerating consolidation to develop in weeks or months as opposed to requiring years. In the past, vertical drains consisted of sand drains and installation disturbance in some soils often made the drains cause more problems than they solved (Casagrande and Poulos 1969). However, the sand drain is now replaced by premanufactured vertical drains, pvd, (or band-shaped drains or "wick drains"), most which do not share the difficulties and adverse behavior of sand drains (some do, however, and quality and performance of wick drains vary from type to type, usually in inverse to the cost of material).

Theoretically, when vertical drains have been installed, the drainage is in the horizontal direction. Therefore, the design formulae are developed based on radial drainage. However, vertical drains connect horizontal layers of greater permeability, which frequently are interspersed in natural soils (See Section 5.3.5). This must be addressed in the design. The way to determine the existence and frequency of such horizontal permeable layers, is by careful scrutiny of continuous Shelby-tube sampling or by CPT in-situ sounding. If the extruded Shelby-tube samples are left to dry in room temperature, then, after a few days or so, pervious layers or bands of silt and sand will show up as light-colored partitions in the sample. After full drying, the layers will no longer be visible. The CPT in-situ sounding needs to be performed with readings taken every 10 mm to establish presence of thin free-draining bands (this does not infer any extra costs and, anyway, should be the norm for all CPT soundings).



Where settlement at a certain time after start of loading needs to be calculated and the degree of consolidation in the various soil layers is known (or has been calculated) for that time, a short-cut value of consolidation settlement can be obtained by dividing the modulus number with the value of the degree of consolidation and using the so-adjusted modulus number for the calculation.

Consolidation, or time-dependent settlement, is not an exclusive domain of cohesive soils. Settlement of coarse-grained soils, indeed sand, can sometimes display a time-dependent response, which can be modeled by consolidation theory as expressed in Eq. 3.21.

### 3.10 Secondary Compression

The progress of settlement due to an imposed stress increase continues after the end of the consolidation because the soil skeleton continues to compress beyond the dissipation of the excess pore pressures, albeit slowly and at a smaller rate (flatter slope in the linear settlement vs. log-time plot), which process is called "secondary compression" (note, secondary compression must not be called "secondary consolidation", as there is no consolidation, i.e., dissipation of pore pressures, involved). This progression of immediate compression and consolidation into secondary compression is complex.

Secondary compression occurs under constant effective stress. Some have argued that secondary compression also develops during and in parallel to consolidation. However, secondary compression is compression occurring at no pore pressure change, so, by definition, it would not exist together with a pore pressure change, i.e., change of effective stress, notwithstanding that it, ostensibly, is triggered when a change of effective stress is imposed. The logic is here somewhat unsatisfactory.

Terzaghi and Peck (1948) wrote: *The secondary time effect is probably a consequence of the fact that the compression of a layer of clay is [also] associated with slippage between grains. Since the bond between grains consists of layers of absorbed water with very high viscosity, the resistance of these layers to deformation by shear will delay the compression even if the time lag resulting from the low permeability of the clay were negligible.* I have not seen a better explanation to the phenomenon.

The secondary compression strain, denoted  $\epsilon_{2nd}$ , is a function of a "coefficient of secondary compression,  $C_\alpha$ ", a non-dimensional number, as indicated in Eq. 3.23 (See Holtz and Kovacs 1981, Holtz et al. 2011). The equation shows a relation for the amount of compression developing over time after the consolidation is completed, i.e., after  $t_{CONS}$ . Notice that secondary compression is not a function of the applied load (stress increase) itself, but of the time relative to the time for the consolidation. For a consolidation test that shows a straight line in the void ratio vs. log-time ( $e$  vs.  $\lg t$ ),  $C_\alpha$  is equal to  $\Delta e$  for a full log cycle of time.

$$(3.23) \quad \epsilon_{2nd} = \frac{C_\alpha}{1+e_0} \lg \frac{t_\alpha}{t_{CONS}}$$

where

- $\epsilon_{2nd}$  = secondary compression strain (thus,  $\epsilon_{2nd} = \epsilon_{CONS} C_\alpha / C_c$ )
- $C_\alpha$  = coefficient of secondary compression
- $e_0$  = initial void ratio
- $t_\alpha$  = time (s) elapsed since start of consolidation ( $t_\alpha > t_{CONS}$ ).
- $t_{CONS}$  = time for completing the consolidation process, which is time between start of the consolidation process (placing the load) and, usually, the time for reaching 90 % degree of consolidation per Eq. 3.21.

The practical question is what value to use for,  $t_{CONS}$ , because, theoretically, the time for 100 % consolidation is infinite. The usual engineering approach is to use the time for reaching 90% degree of consolidation,  $U$ , which, according to Table 3.3, corresponds to a  $T_v$ -factor of 0.85 for use in Eqs. 3.21 and 3.22. N.B., there is absolutely no theoretical reason for tying the start of the secondary compression to the 90% of  $U$ . It is just a handy definition that fits observations.

Note, in determining the amount of secondary compression that will occur (or has occurred) at a certain time, the length of time to input in the equation, the  $t_\alpha$ , is counted from the start of the consolidation. Thus, the ratio between the starting time,  $t_\alpha$ , and duration of consolidation,  $t_{CONS}$ , is always  $\geq 1$ .

The value of  $C_\alpha$  is usually expressed in relation to the compression index,  $C_c$ , i.e., as  $C_\alpha/C_c$ -ratio, ranging from 0.04 through 0.01 (Holtz and Kovacs 1981, Holtz et al. 2011). For example, the  $C_\alpha/C_c$ -ratio of a soft clay having  $C_c$  of about 0.3 and void ratio of about unity ( i.e., a modulus number of 15), would infer a  $C_\alpha$  ranging from 0.012 through 0.003 (Holtz and Kovacs 1981, Holtz et al. 2011).

Often, the  $C_\alpha$  is not known directly, but its ratio to the compression index,  $C_\alpha/C_c$ , may be available as a typical number. Then, when calculating settlement using the Janbu modulus number and combining Eqs. 3.23 and 3.18, the secondary compression can be determined from Eq. 3.24, which equation is also useful when the modulus number, has been evaluated from a strain vs. log-stress diagram.

$$(3.24) \quad \epsilon_{2nd} = \frac{C_\alpha}{C_c} \frac{\ln 10}{m} \lg \frac{t_\alpha}{t_{CONS}} \quad [\ln 10 = 2.3]$$

where

- $\epsilon_{2nd}$  = secondary compression strain (thus,  $\epsilon_{2nd} = \epsilon_{CONS} C_\alpha/C_c$ )
- $C_\alpha$  = coefficient of secondary compression
- $C_c$  = consolidation index
- $t_\alpha$  = length of time (s) considered from time of start of consolidation ( $t_\alpha > t_{CONS}$ ).
- $t_{CONS}$  = time for completing the consolidation process

Even after about a decade or two past the end of consolidation, secondary compression has rarely become larger than the immediate compression and commonly not larger than  $\approx 10$  % of the consolidation settlement. (Nevertheless, it could be substantial in organic soils, e.g., Chang 1981). Note, as mentioned in Sections 3.2 and 3.9), when the soil contains gas, the settlement observed over time might easily be interpreted to indicate larger than true immediate and larger than true secondary compressions.

Secondary compression is defined as the settlement that starts to develop when the consolidation is over, (i.e., at 90 % degree of consolidation). Most projects involve several load areas influencing the stresses and the time for start of consolidation below and near each other , and those areas and start times govern the start and the development with time of the secondary compression for each other. Therefore, it is difficult to decide when the consolidation starts and when it is completed in regard to a specific foundation. Invariably, in a actual case, a judgment call is required in deciding what input to use for the calculation. Moreover, for the secondary compression to start requires a start of consolidation, and, because applying a load smaller than the preconsolidation stress results in a minimal pore pressure increase and a short "consolidation" time, practice is to assume much smaller coefficient of secondary compression for layers where the applied load has not exceeded the preconsolidation margin. Some contend that secondary compression does not occur unless consolidation has been triggered by an applied stress being larger than the preconsolidation stress.

Eqs. 3.23 and 3.24 mean that secondary compression would increase if the consolidation time would decrease, e.g., by shortening the drainage path. This does not make sense, of course. It is a consequence of the fact that secondary compression is an empirical concept without proper theoretical basis that tries to rationalize the factual observation that settlement continues (at a diminishing rate) for a long time after the induced pore pressures have dissipated. It should therefore be calculated for consolidation not being accelerated by the presence of vertical drains.

As illustrated in Figure 3.10A, a part of the problem lies in the fact that the end of consolidation occurs first close to the boundaries and last in the center of the consolidating soil layer. Therefore, calculating the secondary compression to start when the average pore pressure,  $U_{AVG}$ , has reduced to 90 % of the initial means that for a secondary compression developing according to Eq. 3.23, part of the compression would occur before  $t_{CONS}$  and part later, as suggested in Figure 3.10B.

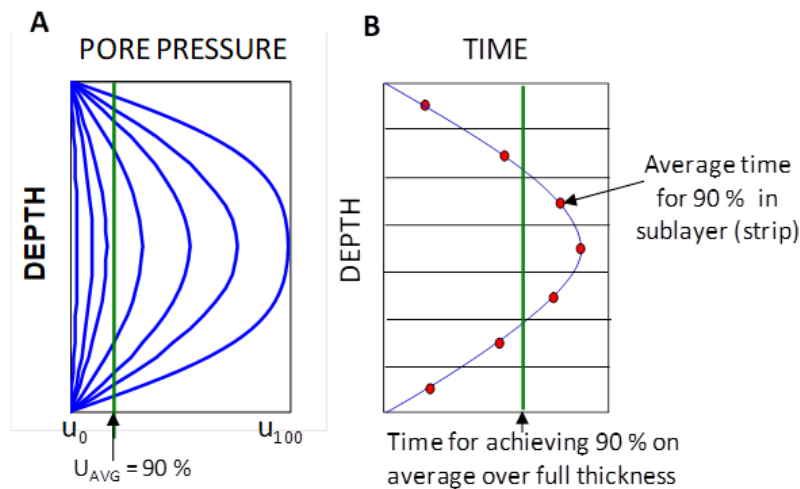


Fig. 3.10 A. Pore pressure distribution at different consolidation times within a soil layer  
B. Average time for achieving 90 % consolidation in layer and sublayers

The distribution curves shown in Figure 3.10A are calculated using UniSettle (Goudreault and Fellenius 2023), applying Eq. 3.25 cited from Holtz and Kovacs (1981) and Holtz et al. (2011), Eq. B.2.13.

$$\text{Eq. 3.25} \quad u = (\sigma'_2 - \sigma'_1) \sum_{n=0}^{\infty} \frac{4}{(2n+1)\pi} \sin\left(\frac{2n+1}{2} \pi \frac{z}{H}\right) \times \exp - \left[ \frac{(2n+1)^2}{4} \pi^2 \frac{k(1+e_1)}{\underbrace{a_v \rho_w g}_{c_v}} \frac{t}{H^2} \right]$$

where  $\sigma'$  = effective stress  
 $H$  = drainage length (half layer thickness)  
 $z$  = depth  
 $k$  = permeability  
 $e$  = void ratio  
 $c_v$  = coefficient of consolidation

The quandary is compounded for a soil profile comprising more than one consolidating layer where the pore pressure in the layers drains into the next layer (c.f., Section 3.9).

The simple fact is that a soil structure once affected by an increase of load continues to compress for the longest time albeit overshadowed by, first, immediate compression, and, second, by the slow consolidation reduction of pore volume continuing unrestrained into the length of time ever at a decaying rate. Therefore, there is some disturbing logic in assuming that secondary compression, being triggered by the start of a consolidation, would only start to develop at some specific value after some time, but still in the early years of the many years of consolidation.

Moreover, adding the secondary compression to the settlement vs. time curve due to immediate compression and consolidation, introduces a kink to the curve not seen in reality, as demonstrated in Figure 3.11, calculated from the parameters using the software UniSettle4 (Goudreault and Fellenius 2011). To remove the kink effect, some apply the secondary compression, calculated according to Eq. 3.23, to start with the onset of consolidation. This removes the problem that the end of consolidation does not occur simultaneously across the soil layer, but it increases the calculated total settlement.

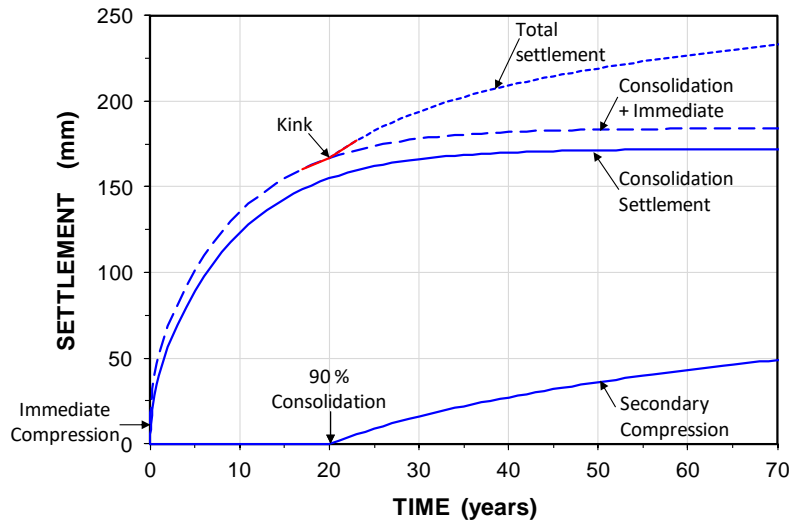


Fig. 3.11 Settlement vs. time for Immediate, Consolidation, and Secondary processes

The mechanics of secondary compression may seem quite well established. However, the conventional model is just a description that fits observations. The lack of a sound theory was questioned by Schmertmann (1983) and his questions are still unanswered.

### 3.11 Example

The following example involves a 12 m thick clay layer above a free-draining sand layer. The groundwater table is located at the ground surface and the pore pressure distribution is hydrostatic. The soil parameters necessary for the calculation of settlement and time development are contained in Table 3.4. The parameters are made up but are reasonably realistic.

**TABLE 3.4 Soil Parameters**

Parameter	Unit	Value	Parameter	Unit	Value	Parameter	Unit	Value
$w_n$	(%)	<b>25</b>	$U_{AVG}$	(%)	<b>90</b>	$j$	(---)	<b>0</b>
$e$	(---)	0.660	$\Delta\sigma'$	(kPa)	10	$m$	(---)	<b>20</b>
$\rho_t$	kg/m <sup>3</sup>	2,000	$C_c$	(---)	0.19	$m_r$	(---)	<b>200</b>
$\rho_s$	(kg/m <sup>3</sup> )	<b>2,670</b>	$C_{cr}$	(---)	0.019	$E_{ic}$	(MPa)	<b>20</b>
$T_v$	(---)	<b>0.85</b>	$t_{CONS}$	(year)	12	$C_v$	(m <sup>2</sup> /year)	2.5
$C\alpha$	(---)	<b>0.005</b>						

$U_{AVG}$  is the degree of consolidation (90 %) assigned to at the start of secondary compression. Parameter values not in bold are inferred from the bolded parameters.

An 1.5 m thick fill with a total density of  $2,000 \text{ kg/m}^3$  is placed on the ground surface exerting a 15-kPa stress. Figure 3.12 shows the results of calculations of immediate compression, consolidation, secondary compression, and total settlement. The solid lines show the result for the conventional calculation using  $U_{AVG}$  and the dashed curves show the results considering average pore pressure as varying from top to bottom per in a soil layer as indicated in Figure 3.10B. The adjustment to compute the start of the 90-% consolidation considering the distance to the boundaries removes the "kink". It also indicates that the secondary compression occurs somewhat earlier in time.

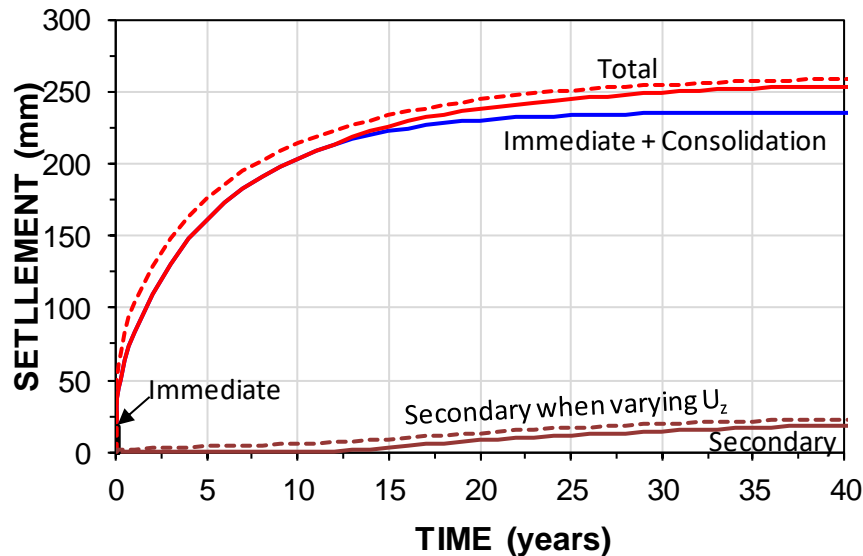


Fig. 3.12 Settlements with time for  $U_{AVG}$  and  $U_z$

### 3.12 Magnitude of Acceptable Settlement

Settlement analysis is often limited to ascertaining that the expected settlement would not exceed one inch. (Realizing that 25 mm is too precise a value when transferring this limit to the SI-system, some have argued whether “the metric inch” should be 20 mm or 30 mm!). However, in evaluating settlement in a design, the calculations need to provide more than just an upper boundary. The actual settlement value and both total and differential settlements must be evaluated. The Canadian Foundation Engineering Manual (1992) listed acceptable displacement criteria in terms of maximum deflection between point supports, maximum slope of continuous structures, and rotation limits for structures. The multitude of limits demonstrate clearly that the acceptable settlement varies with the type and size of structure considered. Moreover, modern structures often have small tolerance for settlement and, therefore, require that the design engages a more thorough settlement analysis than was required in the past. The advent of the computer and development of sophisticated yet simple to use design software has enabled the structural engineers to be very precise in the analysis of deformation of a structure and the effect of deformations on the stress and strain in various parts of a structure. As a not-so-surprising consequence, requests for “settlement-free” foundations have increased. This means that the geotechnical analysis must determine also the magnitude of small values of settlement.

When the geotechnical engineer is vague on the predicted settlement, the structural designer “plays it safe” and increases the size of footings or changes the foundation type, which may increase the costs of the structure. These days, in fact, the geotechnical engineer can no longer just offer an estimated “less than one inch” value, but must provide a more accurate value by performing a thorough analysis

considering soil compressibility, soil layering, and load variations. Moreover, the analysis must be put into the full context of the structure, which necessitates a continuous communication between the geotechnical and structural engineers during the design effort. Building codes have started to recognize the complexity of the problem and mandate that the designers collaborate continuously during the design phases as well as during the construction. See, for example, the Canadian Highway Bridge Design Code, CAN/CSA-S6 2006 (Canadian Standards Council 2006).

### 3.13 Calculation of Settlement

Calculation of settlement should be performed in the following steps. The steps apply in equal measure to immediate settlement, consolidation settlement, and secondary compression.

1. Establish the soil profile (i.e., the soil layering and pore pressure distribution; Chapter 2) at the initial state for the site and foundation unit(s) so that the initial effective stress ( $\sigma'_0$ ) distribution is adequately established (Chapter 1).
2. Determine and compile the soil compressibility parameters, i.e., the modulus number and stress exponents (or the “conventional” parameters), and consider both virgin and reloading conditions, as well as preconsolidation margin.
3. Determine the stress distribution (e.g., Boussinesq) imposed by the foundation units(s) and any changes to the initial site conditions (excavations, fills, groundwater table lowering, etc.) and calculate the new (the final) distribution of effective stress,  $\sigma'_1$ .
4. Divide each soil layer in a suitable number of sub layers and calculate the initial and final effective stress representative for each sub layer using the suitable equations given in this chapter. (Perform the calculations in either the middle of each sub layer, or at both top and bottom of each and take an average of these two; if the sub layers are reasonably thin, the two approaches will give equal result).
5. Calculate for each sub layer the strain caused by the change of effective stress from  $\sigma'_0$  to  $\sigma'_1$  (Section 3.5 contains the formulae to use).
6. Multiply each calculated strain value with its appropriate layer thickness to determine the settlement for each sub layer and add up to find the accumulated settlement value (Eq. 3.3).

Software, such as UniSettle (Goudreault and Fellenius 2006; 2011; 2024) greatly simplify the calculation process. In particular, where Step 3 includes several components and when loads are applied at different times so that consolidation starts and finishes at different times.

A settlement analysis must incorporate all relevant facts. Because the person performing the analysis does not know all details of a project, important facts may get overlooked, such as that the site information does not include that the ground has either been or will be excavated or backfilled prior to construction, or that stress from an adjacent structure or embankment will have affect the existing stresses underneath the foundation that is being analyzed. Often, even though all the relevant facts from the local site are applied, regional conditions must also be included in the analysis. For example, in the Texas Gulf Coast Region, notably in Greater Houston area, past lowering of the groundwater table due water mining in deep wells (starting in the 1920s) have resulted in a regional subsidence—in places as much or larger than 2 m—and a large downward water gradient. Downward gradients larger than 0.25 ('negative head' larger than 100 m) have been measured at depths of 400 m. The groundwater table is now rising (since ceasing to pump in the mid-1970s). [Figure 3.13](#) presents observations in three deep wells from 1930 onward.

The clay soils in the Greater Houston area are desiccated and overconsolidated from ancient desiccation and from the recent lowering of the pore pressures. The overconsolidation degree is getting larger as the water pressures now are returning to pre-1920 levels. Old and new foundations need to take the changing pore pressure gradient into account. Figure 3.14 shows settlement observations for the San Jacinto Monument (Briaud et al. 2007) and that, after completed construction in 1936, the initial moderate groundwater mining did not affect the consolidation settlement of the monument. However, as also shown, the increased and accelerated lowering of the groundwater from 1940 onward did appreciably affect the settlement development. The heavy blue line with solid dots shows the measured settlement of the Monument. The dashed line marked "Monument only" is the assumed settlement of the monument had there been no groundwater lowering. Note that the ordinate scales for settlement and depth to water table (in well), respectively, are different.

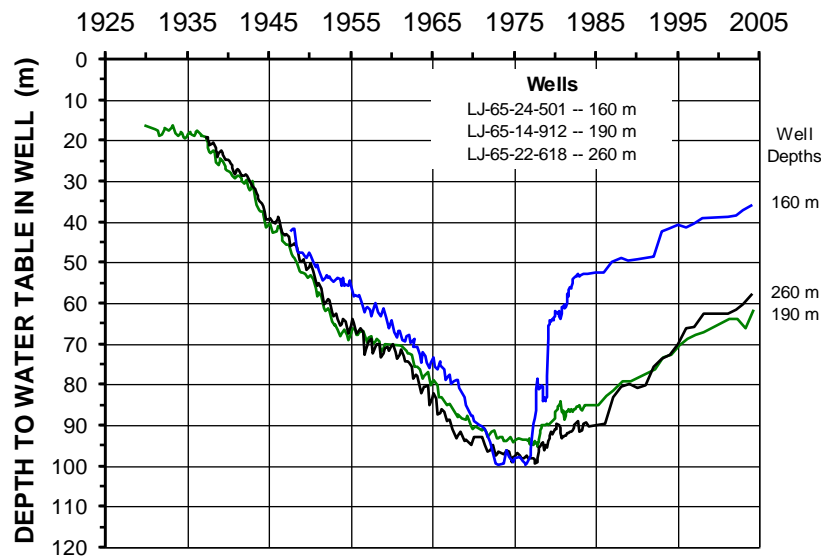


Fig. 3.13 Example of measured depth to water level in 160 m through 350 m deep wells near the San Jacinto Monument. (Data from Barbie et al. 2005 and Fellenius and Ochoa 2009).

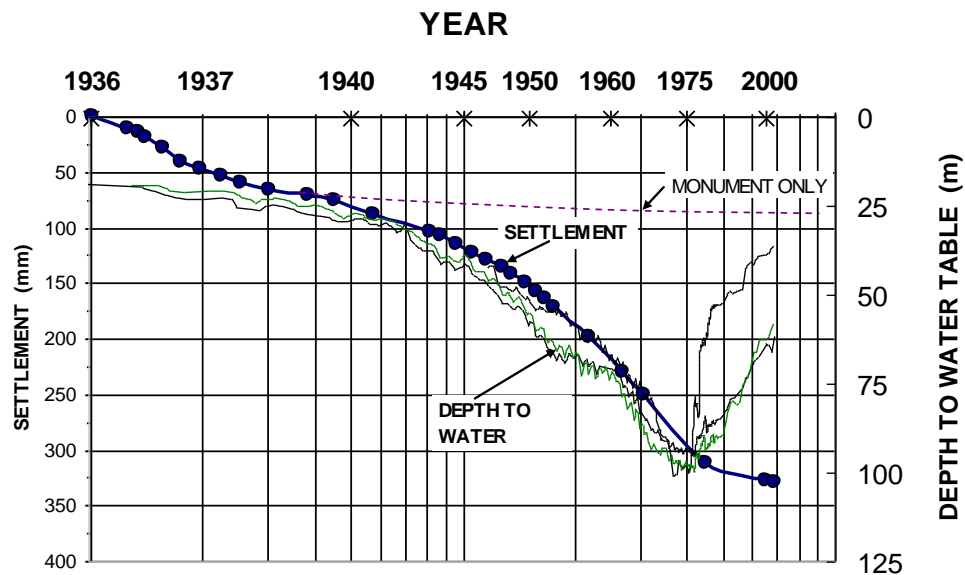


Fig. 3.14 Observed settlement of the San Jacinto Monument plotted together with the observed depths to water in wells near the Monument. (Data from Fellenius and Ochoa 2009).

For either back analysis (for future reference) or for design calculations of expected settlement, the local regional pore pressure conditions must be carefully established and, therefore, all site investigations must include installing piezometers geared to establish the pore pressure distribution.

### 3.14 Special Approach -- Block Analysis

When a foundation design analysis indicates a likelihood that ordinary foundations (footings, rafts, or mats) would experience excessive settlement, site improvement techniques are frequently employed. For example, deep vibratory compaction, dynamic consolidation, stone-columns, or lime-cement columns. Common for these techniques is that the compressibility of an upper soil zone (the depth of the treatment) at the site is improved. The result of the treatment is rarely uniform. It usually consists of treating vertical zones (columns) leaving untreated soil in between, e.g., installing piles, which is in a sense applying a soil improvement method. Provided the overall treated area is equal or larger than the footprint of the foundation, the settlement analysis consists of determining the average (proportional) modulus number of the treated zone as indicated in Eq. 3.25. This average is then applied to calculations for the treated zone replacing the original soil modulus.

$$(3.25) \quad m_{AVG} = \frac{m_{UNTR} \times A_{UNTR} + m_{TR} \times A_{TR}}{A_{UNTR} + A_{TR}}$$

where  $m_{AVG}$  = average modulus number for the treated zone

$m_{UNTR}$  = modulus number for untreated soil

$m_{TR}$  = modulus number for treated soil

$A_{UNTR}$  = area of untreated soil

$A_{TR}$  = area of treated soil

When the size of the footprint is at least about equal to the treated area, the imposed stress is assumed to be transferred undiminished through the treated zone (taken as a block of soil), i.e., *no stress distribution within the treated zone (or out from its side)*. The block will compress for the load and the compression (settlement contribution) is determined using the average modulus and applying elastic stress-strain (stress exponent = unity). At the bottom of the block, the imposed stress is now distributed down into the soil and the resulting strains and settlements are calculated as before.

### 3.15 Horizontal Movement Caused By Embankment Load

As shown in [Figure 3.15](#), placing an embankment or a raft on the ground will not only cause settlement (vertical deformation), also horizontal deformation will result. Depending on stress level, width of the foundation, and, of course, the soil properties, the horizontal movement, typically at a 2 to 4 m depth, will be about 10 % plus-minus about 5 % of vertical. See also [Figure 4.7](#). The ratio is larger for narrow foundations.

### 3.16 Settlement of footings

Single footings and strip footings are usually narrow element (small width) that are affected by stress concentration at the edges and horizontal soil movements occurring together with the compression due to consolidation. The theoretical compression of the soil according to the analysis principles described in this chapter suggest that the settlement (movement) for a series of applied equal stress increment to a footing would show a diminishing rate of movement. However, actual observations indicate the opposite for narrow-width footings. The scenario is illustrated in [Figure 3.16](#).



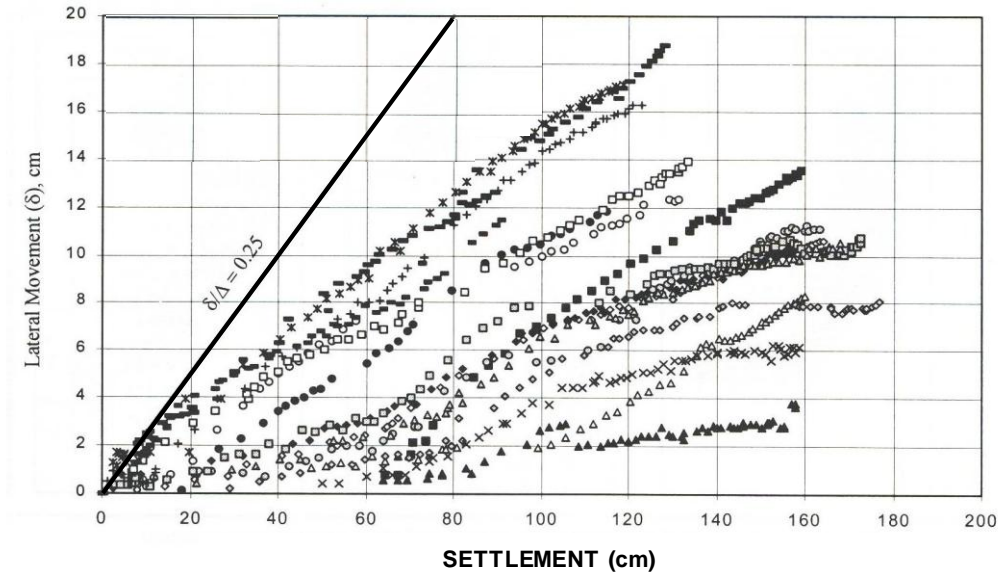


Fig. 3.15 Horizontal movement below the embankment edge. From Moh and Lin (2006)

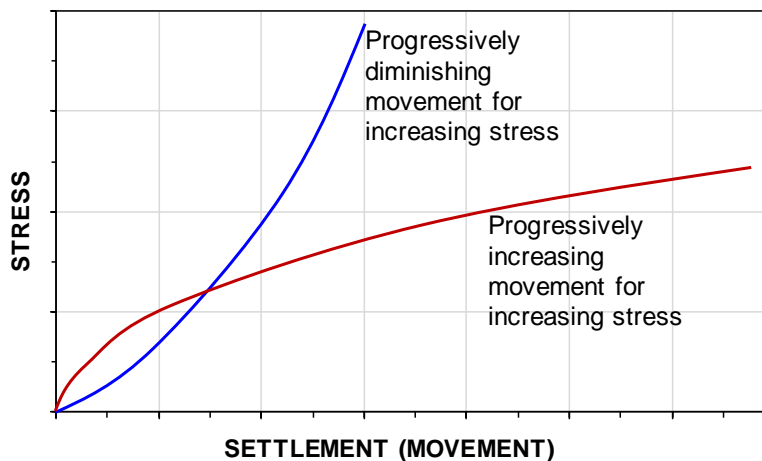


Fig. 3.16 Settlement for a series of equal stress increments per theoretical settlement analysis compared to for actual response of narrow footings

The main reason for the fact that the settlement of a footing due to an applied load (stress) will be larger than that calculated theoretically using conventional settlement theory is the development of horizontal movement near the sides of the footing. This effect reduces in significance with increasing footing width.

An increased settlement as opposed to decreased when increasing the applied stress can be explained as a consequence of horizontal movement releasing stress (resistance reduces) near the sides of the footing, which causes the stress underneath the center to increase.

Figure 3.17 (same data as in Figure 6.7) presents the results of loading tests in sand on three square footings of 1.0 m, 1.5 m, and 2.5 m, and two footings of 3.0 m diameter. Figure 3.17A shows the load-movement for the individual footings and Figure 3.16B shows the results as stress versus movement divided with the footing width. The latter figure is important because it shows that the stress vs. normalized movement is independent is essentially equal for different size footings (or pile toes).

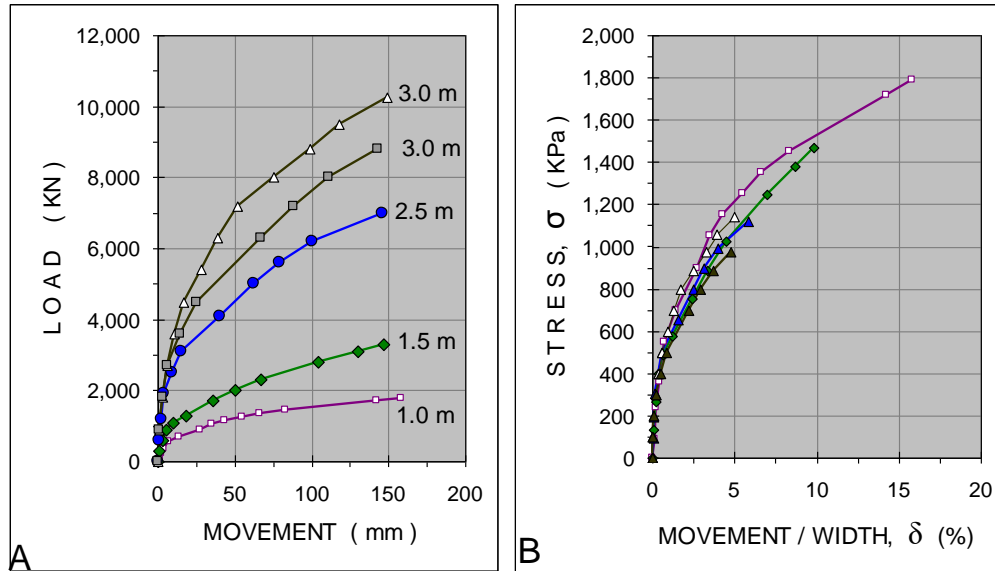


Fig. 3.17 Observed load-movement (A) and stress-normalized movement (B) of five footings tested at Texas A&M University (data from Briaud and Gibbens 1994, 1999).

The observed settlement of a footing is therefore best analyzed using a load-movement relations, a  $q$ - $z$  function, such as the Gwizdala  $q$ - $z$  function (see Section 8.11). As for everything else, without reference to observations (i.e., experience), the prediction becomes difficult.

### 3.17 Long-term Settlement of fill

Uncompacted fill composed of coarse-grained soil, e.g., rock fill behind quay walls will, of course, just like other coarse-grained fill layer, show immediate compression and a consolidation portion. The latter cannot be distinguished from the immediate compression because the associated forcing out of the water occurs quickly. However, unlike natural and compacted fill deposits, the rockfill will also undergo long-term compression—ostensibly, due to "self-weight". The term is used because of the absence of a any increase of force or load and for lack of a better term. The long-term compression is caused by rearrangement of rockfill skeleton (deformation at contact points) and effect of soil crushing. The rate of compression (settlement) over time reduces progressively ('logarithmically') much similar to the development of secondary compression of a clay soil. The actual amount of compression due to self weight over, say, a 30 to 50 year period depends on several factors, for example, size and gradation, angularity, mineral composition (hardness), method of placement, placed above or below water level, etc., and can range from less than 1 % of height to as much as 5 %, depending on the array of these factors. Sharp (1996) has presented several case histories on this issue.

## CHAPTER 4

### VERTICAL DRAINS TO ACCELERATE SETTLEMENT

#### 4.1 Introduction

All materials will undergo volume change when subjected to stress change and soils are no exception. Unlike steel or concrete and other solids, soils are made up of granular materials: grains. Moreover, the pores between the grains are usually filled with water, often a water and air mix (gas). This fact makes the response of soil to an increase of stress more complex as opposed to other building materials. The shear strength of soil is more important for foundation design than the compressive strength, for example. An increase of stress results in an more or less immediate ‘initial’ small, so-called ‘elastic’, compression of the soil skeleton. The central aspect, however, is that in order for a volume change to take place due to an increase of stress, the space between the grains, the pores, must be able to reduce in volume. In a saturated soil, this requires that the water first leaves the pore volume—is squeezed out of the soil pores.

If the soil is non-saturated due to presence of gas, an additional immediate volume change is caused by a portion of the free gas (‘bubbles’) converts to liquid state when pressure is increased. The corresponding volume change (settlement) cannot be distinguished from the immediate compression of the soil grains (see Section 3.8). However, further reduction of pore volume cannot take place without the water in the pores leaving the pores. The driving force in the latter process is the initial increase of pore pressure, which at first is about equal to the average of the imposed stress increase. As the water leaves the soil, the pressure reduces, “dissipates”, until, finally, all the imposed stress is carried as contact stress between the grains. The process is called “consolidation” and it is presented in Section 3.8. In the process, the bubbles return to their original size and pressure and the consolidation process will appear to be slower than the actual rate(see Section 3.9).

The consolidation time is governed by how easy or difficult is for the water to flow through the soil along with the drainage path, the latter is the length the water has to flow to leave the zone of increased stress. The measure of the "difficulty" of the water to flow is the soil hydraulic conductivity (“permeability”) and the time is more or less a linear function of the “permeability” (related to the “coefficient of consolidation”), but it is an exponential function (square) of the drainage path. Therefore, if the drainage path can be shortened, the time for the consolidation settlement, which is the largest part of the three components of the settlement, can be shortened, “accelerated”, substantially. This is achieved by inserting drains into the soil, providing the water with the easy means of travel—“escape”—from the zone of stress increase. The spacing between the drains controls the length of the drainage path. For example, drains installed at a spacing that is a tenth of the thickness of a soil layer that is drained on both sides could, theoretically, shorten the consolidation time to a percentage point or two of the case without drains. An additional benefit is that because the water flows horizontally toward the drains (flows radially, rather), the flow is faster due to the fact that the horizontal hydraulic conductivity of the soil normally is much larger than that in the vertical direction.

The potential benefit of using vertical drains became obvious very soon after Terzaghi in 1926 published his theory of consolidation. Thus, vertical drains have been used in engineering practice for almost 100 years. At first, vertical drains were made of columns of free-draining sand (sand drains) installed by various means (Barron 1947). In about 1945, premanufactured bandshaped drains, termed “wick drains” (see Section 4.6), were invented (Kjellman 1947) and, since about 1970, the technical and

economical advantages of the wick drain have all but excluded the use of sand drains. Holtz et al. (1991) have presented a comprehensive account of the history of vertical drains. Lately, the preferred name is "Premanufactured Vertical Drains", PVD. However, I have retained the "wick drain" term in this chapter.

#### 4.2 Conventional Approach to Pore Pressure Dissipation and Consolidation of a Drain Project

The basic principles of the behavior of consolidation in the presence of vertical drains is illustrated in Figure 4.1. The dissipation of the excess pore pressures in the soil body is governed by the water flowing horizontally toward the drain and then up to the groundwater table. (Vertical flow toward draining layers above and below the soil body is usually disregarded). The pore water pressure distribution inside the drain is assumed to be hydrostatic at all times.

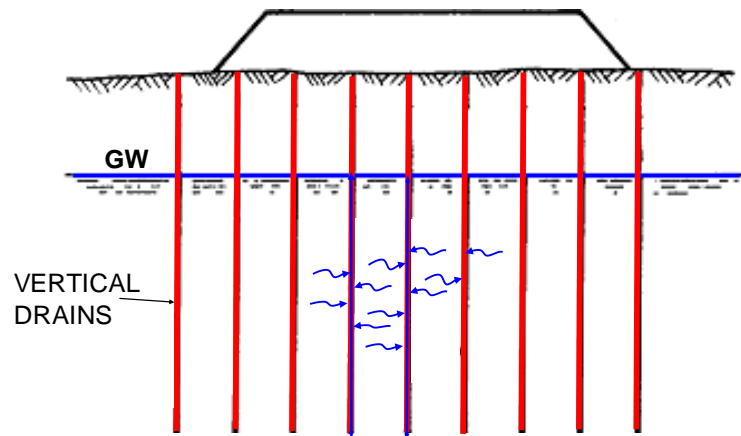


Fig. 4.1 Basic principles of consolidation process in the presence of vertical drains

For the analysis of acceleration of pore pressure dissipation in fine-grained soils (consolidation) for a vertical drain project and subsequent settlement, Barron (1948) and Kjellman (1948a; 1948b) developed a theory based on radial flow toward a circular drain in the center of a cylinder of homogeneous soil with an impervious outer boundary surface (Hansbo 1960; 1979; 1981; 1994). Vertical flow (drainage) was assumed not to occur in the soil. The theory is summarized in the Kjellman-Barron formula, Eq. 4.1. The Kjellman-Barron formula is based on the assumption of presence of horizontal (radial) flow only and a homogeneous soil.

$$(4.1) \quad t = \frac{D^2}{8c_h} \left[ \ln \frac{D}{d} - 0.75 \right] \ln \frac{1}{1-U_h}$$

where

- $t$  = time from start of consolidation (s)
- $D$  = zone of influence of a drain (m)
- $d$  = equivalent diameter of a drain (m)
- $U_h$  = average degree of consolidation for radial (horizontal) flow (–)
- $c_h$  = coefficient of horizontal consolidation (m<sup>2</sup>/s)  
[1 m<sup>2</sup>/s = 3.2 x 10<sup>7</sup> m<sup>2</sup>/year; Section 3.8; Table 3.4]

Eq. 4.1 can be rearranged to give the relation for the average degree of consolidation,  $U_h$ .

$$(4.1a) \quad U_h = 1 - \exp \left[ \frac{-8 c_h t}{D^2 \left( \ln \frac{D}{d} - 0.75 \right)} \right]$$

Figure 4.2 shows two simplified sketches of the principle for consolidation of a soil layer without and with vertical drains, respectively. Figure 4.2A shows a soil layer sandwiched between free-draining boundaries: the ground surface and a free-draining soil layer below the consolidating layer. The parabolic shape curve indicates the pore pressure distribution at a particular time. The time required for a certain degree of consolidation (in addition to the soil parameters of the case) is primarily a function of the longest drainage path, that is, half the thickness of the clay layer and assuming vertical flow. Figure 4.2B shows the corresponding picture where vertical drains have been installed. Here, the consolidation time is primarily a function of the spacing of the drains and horizontal flow.

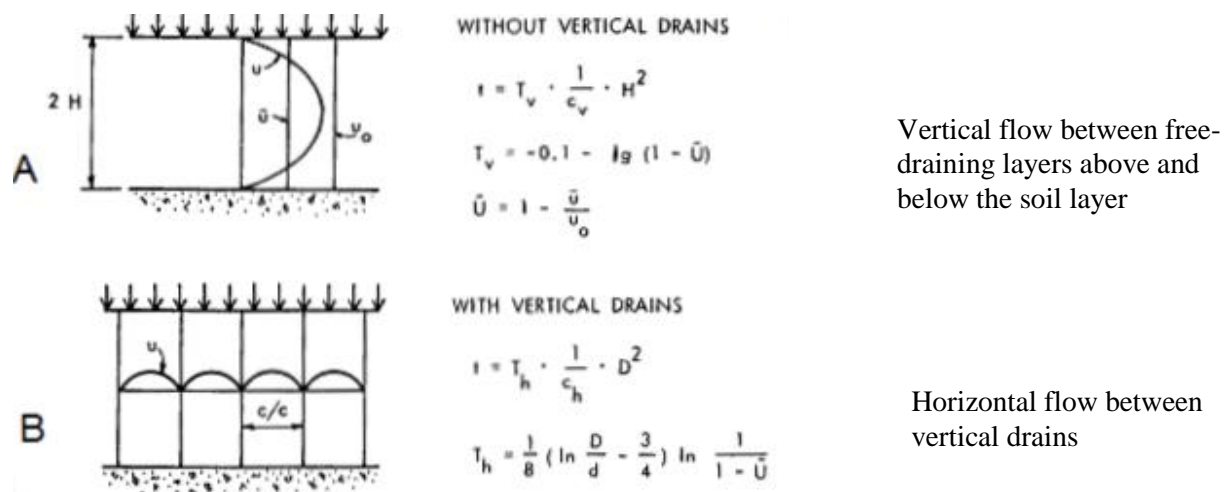


Fig. 4.2 Principles and formulae for consolidation of a soil layer

Note that the pore pressure in the drain is essentially hydrostatic. That is, the flow through the drain to the boundaries (ground surface and drain bottom) is a low-gradient flow. Indeed, the theoretical analysis assumes no gradient inside the drain. Therefore, testing the flow characteristics (conductivity; "ease of flow") of wick drains should be at very low gradients. Test under as large a gradient as unity is common, but it is unrealistic and could show unrepresentative drain response (see Section 4.5.3).

Relations for average degree of consolidation combining horizontal and vertical flows have been developed for vertical drains. However, the contribution of vertical drainage to the rate of consolidation is very small as opposed to the contribution by the horizontal drainage—the drainage toward the drains. In a typical case, vertical drainage alone could require 20 years, while installing drains to take advantage of horizontal drainage along the so-shortened distance could reduce the time significantly, indeed, to just a few months. Obviously, the contribution of the vertical drainage is minimal.

The zone of influence of a drain is defined as the diameter of a cylinder having the same cross section area as the area influenced by the drain. That is, if in a given large area of Size  $A$  there are  $n$  drains placed at some equal spacing and in some grid pattern, each drain influences the area  $A/n$ . Thus, for drains with a center-to-center spacing,  $c/c$ , in a square or triangular pattern, the zone of influence,  $D$ , is  $1.13 c/c$  or  $1.05 c/c$ , respectively, as illustrated in Figure 4.3.

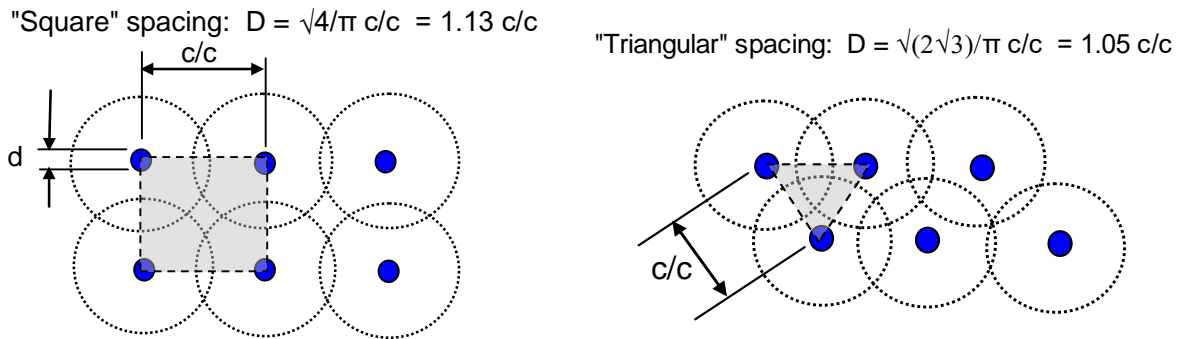


Fig. 4.3 Width of the Zone of influence for square and triangular spacings,  $c/c$ , between drains.

In the case of sand drains, the equivalent diameter,  $d$ , is often taken as equal to the nominal diameter of the sand drain. In the case of wick drains (Section 4.5), no agreement exists on what to use as the equivalent diameter of the drain. One approach used is simply to equalize the outside surface area of the wick drain with a circular drain of the same surface and assign the equivalent diameter of the wick drain to be the nominal diameter of that circular drain. However, this approach does not recognize the difference between the usually open surface of the premanufactured drain and the rather closed surface of the sand drain, nor the differences between various makes of wick drains. Strictly speaking, the equivalent diameter of a wick drain should be termed "the equivalent cylinder diameter" to separate it from 'the equivalent sand drain diameter'. Fellenius (1977) suggested that the equivalent cylinder diameter of a sand drain is the nominal diameter of the sand drain multiplied by the porosity of the sand in the drain. The porosity of loose, free-draining sand is normally about 0.4 to 0.5. Thus, the equivalent cylinder diameter of a sand drain is about half of the nominal diameter and, alternatively, the equivalent cylinder diameter of the wick drain becomes about twice that determined its total outside area.

However, the question of what value of equivalent diameter to use is not of importance in practice because the consolidation time is not very sensitive to the variations of the value of the equivalent cylinder diameter. (In contrast, the consolidation time is very sensitive to the spacing of the drains). For wick drains of, commonly, 100-mm width, values proposed as the equivalent cylinder diameter have ranged between 30 mm and 80 mm, and full-scale studies have indicated that the performance of such drains have equaled the performance of sand drains of 200 mm to 300 mm in nominal diameter (Hansbo 1960; 1979; 1981; 1994).

The average degree of consolidation at a certain time,  $\bar{U}$ , is defined as the ratio between the average increase of effective stress,  $\Delta\sigma'$ , in the soil over the applied stress causing the consolidation process, i.e.,  $\Delta\sigma'/q$ . In practice, average degree of consolidation is determined from measurements of either pore pressure increase or settlement and defined as 1 minus the ratio between the average pore pressure increase in the soil over the total pore-pressure increase resulting from the applied stress,  $\bar{U} = 1 - u/u_0$ , or,  $\bar{U} = \Delta S/S_f$ , the amount of settlement obtained over the final amount of settlement at completed consolidation. Because pore pressures can be determined at the start of a project, whereas the value of the final settlement is not obtained until after the project is completed, the degree of consolidation is usually based on pore pressure measurements. However, pore pressures and pore-pressure dissipation vary with the distance to the draining layer and, in particular, with the distance to the drains. Seasonal variation is also a factor. Therefore, and in particular because pore-pressure measurements are usually made in only a few points, pore pressure values are very imprecise references to the average degree of consolidation.

The rate of consolidation may differ at different depths and locations due not least to variations of layer thickness. Therefore, also the average degree of consolidation based on settlement observations is also a rather ambiguous value, unless related to measurements of the compression of each specific layer (difference between settlement at top and bottom of the layer) and as the average of several such layers.

In a homogeneous soil layer, the horizontal coefficient of consolidation,  $c_h$ , is usually several times larger than the vertical coefficient,  $c_v$ . Moreover, dissipation time calculated according to the Kjellman-Barron formula (Eq. 4.1), is inversely proportional to the  $c_h$ -value. Note, however, that the drain installation will disturb the soil and break down the horizontal pathways nearest the drain (create a "smear zone") and, therefore, the benefit of the undisturbed horizontal coefficient may not be available. For sand drains, in particular displacement-type sand drains, a  $c_h$ -value greater than the  $c_v$ -value can rarely be mobilized.

For a detailed theoretical calculation, to consider the effect of a smear zone would seem necessary. However, in practice, other practical aspects (See Section 4.3) are far more influential for the process of accelerating settlement and theoretical refinements are rarely justified (see also Section 4.6.7). Considering smear zone effect in an actual wick-drain project distracts the attention from the important aspects of choosing representative parameters and assessing the site conditions correctly.

The coefficient of consolidation,  $c_v$ , varies widely in natural soils (see Section 3.8). In **normally consolidated** clays, it usually ranges from  $1 \times 10^{-8} \text{ m}^2/\text{s}$  to  $30 \times 10^{-8} \text{ m}^2/\text{s}$  (3 to 100  $\text{m}^2/\text{year}$ ). In silty clays and clayey silts, it can range from  $5 \times 10^{-8} \text{ m}^2/\text{s}$  to  $50 \times 10^{-8} \text{ m}^2/\text{s}$  (16 to 160  $\text{m}^2/\text{year}$ ).

The coefficient of consolidation,  $c_v$ , is normally determined from laboratory testing of undisturbed soil samples or, preferably, in-situ by determining the pore-pressure dissipation time in a piezocone (CPTU; see Chapter 2). The actual  $c_h$ -coefficient to use requires considerable judgment in its selection, and it can, at best, not be determined more closely than within a relative range of three to five times. This means that engineering design of a project requires supporting data for selection of the  $c_h$ -coefficient in order to avoid the necessity of employing an excessively conservative approach.

The duration of the primary consolidation,  $t_{\text{CONS}}$ , without the presence of vertical drains can take many years. When drains have been installed, the duration is typically shortened to a few months. Moreover, a vertical drain project will include estimating the magnitude and rate of the secondary compression (Chapter 3, Section 3.9), which involves calculations with input of coefficient of secondary compression,  $C_\alpha$ , and duration of the primary consolidation  $t_{\text{CONS}}$ . First, the  $C_\alpha$  is considered to be a soil parameter that is independent of whether the consolidation is achieved by vertical or horizontal drainage. A paradox is then that if using the, typically, 50 to 100 times shorter time for  $t_{\text{CONS}}$  for horizontal drainage (wick drains case), as opposed to that for vertical drainage, will result in that the calculated settlement due to secondary compression will come out as an order of magnitude larger for a project where the consolidation process is having accelerated by means of vertical drains, as opposed to the magnitude for where no vertical drains are used. However, secondary compression is not governed by the direction of water flow nor can it reasonably be a function of the length of the drainage path. Therefore, the paradoxical discrepancy is not true. It is the result of the fact mentioned in Section 3.9 that the secondary compression concept is an empirical approach to fit observations to some reasonable way of calculating and predicting the process. To resolve the discrepancy, when estimating the magnitude of secondary compression developing after the end of consolidation for a vertical drain project, the duration required for the consolidation had there been no drains should be estimated and used in calculating the settlement due to secondary compression.

### 4.3 Combined vertical and horizontal flow

Carillo (1942 and Asaoka (1978) developed Eq. 4.2 to express the average degree of consolidation for the case of combined horizontal and vertical consolidation.

$$(4.2) \quad U_{comb} = 1 - (1 - U_h)(1 - U_v)$$

where  $U_{comb}$  = Combined average degree of consolidation  
 $U_h$  = Average degree of horizontal (radial) consolidation  
 $U_v$  = Average degree of vertical consolidation

Note that (1) the distance between the drains (the drain spacing) is small, (2) the horizontal coefficient of consolidation,  $c_h$ , is larger than the vertical coefficient,  $c_v$ , and (3) that the thickness of the clay layer is normally much larger than the drain spacing. The equation suggests that  $U_{comb}$  average degree is always smaller, but it should not be taken to mean that the vertical flow has a reducing effect on the rate of consolidation. The equation indicates simply that the effect of vertical consolidation is not significant.

### 4.4 Practical Aspects Influencing the Design of a Vertical Drain Project

In addition to the theoretical aspects, a design of a vertical drain project is affected by several practical matters, as outlined in this section. (The simplifications of the Kjellman-Barron formula is addressed in Section 4.7.1 inasmuch they affect the outcome of a design calculation).

#### 4.4.1 Drainage Blanket on the Ground Surface and Back Pressure

Unless the drains are taken into a free-draining soil layer below the fine-grained layer to be drained, the ground surface must be equipped with a drainage blanket and/or trenches to receive and lead away the water discharged from the drains. Sometimes, the natural ground at a site may provide sufficient drainage to serve as the drainage blanket. However, most projects will need to include a drainage blanket on the ground surface. Absence of a suitable drainage blanket may result in water ponding in the bowl-shaped depression that develops as the soil settles, creating a back pressure in the drains that impairs the consolidation process. This is illustrated in Figure 4.4.

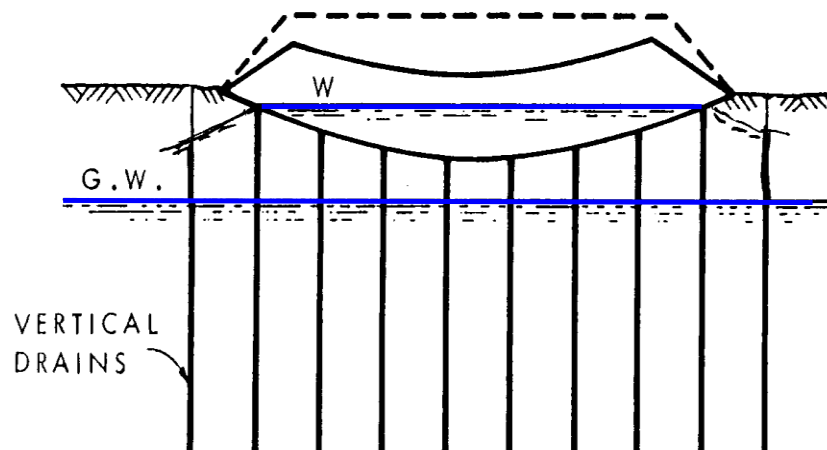


Fig. 4.4 Effect of water ponding below the embankment in the absence of a surface drainage blanket



Ponding due to insufficient horizontal drainage on the ground surface is not acceptable, of course. In a design of a vertical drain project, the expected dishing of the ground must be calculated and a surface drainage scheme designed that ensures a discharge of any accumulated water away from the treated area at all times to eliminate the risk for back pressure in the drains.

The build-up of back pressure due to ponding will halt or slow down the time development of the consolidation settlement, which, if the process is monitored, is discernible as a flattening out of the time-settlement curve—a slow-down. If the flattening is indeed a temporary slow-down, there will be an increased settlement rate at the end of the slow-down and the curve will show a "hump". The onset of the "hump" may lead to the false conclusion that the primary settlement has been obtained. However, eventually, the back pressure will disappear, and the settlement, delayed due to the back pressure, will recur.

Where the groundwater level lies close to the original ground surface, the embankment fill might settle below the groundwater table. Then, the total vertical stress imposed to the original ground surface over and above the existing vertical stress reduces accordingly, which the modeling needs to take into consideration.

#### **4.4.2 Effect of Winter Conditions**

In areas where Winter conditions prevail, consideration must be given to the risk of the ground frost reducing or preventing the drain discharge at the groundwater table or into the drainage blanket at the ground surface building up a back pressure. The result is similar to that of ponding: a slow-down of the settlement, which can be mistaken for the project having reached the end of the primary consolidation. After the Spring thaw, the settlement will recur.

#### **4.4.3 Depth of Installation**

The installation depth is governed by several considerations. One is that drains will not accelerate consolidation unless the imposed stress triggering the consolidation brings the effective stress in the soil to a value that is larger than the preconsolidation stress. i.e., the imposed stress is larger than the preconsolidation margin. The imposed stress decreases with depth (as, for example, determined by Boussinesq formulae; Chapter 3). From this consideration, the optimum depth of the drains is where the imposed stress is equal to the preconsolidation margin. However, other considerations may show that a deeper installation is desirable, e.g., to assure water discharge into a deeper located pervious soil layer.

#### **4.4.4 Width of Installation**

Drains installed underneath an embankment to accelerate consolidation must be distributed across the entire footprint of the embankment and a small horizontal distance beyond. A rule-of-thumb is to place the outermost row of the drains at a distance out from the foot of the embankment of about a third to half the height of the embankment. If the drains are installed over a smaller width, not only will differential settlement (bowing or dishing) increase during the consolidation period, the consolidation time will become longer.

#### **4.4.5 Effect of Pervious Horizontal Zones, Lenses, Bands, and Layers**

The assumption of only homogeneous soil, whether with only radial flow or radial flow combined with vertical flow, used in the derivation of the formulae is not realistic. In fact, most fine-grained clay soils contain horizontal zones of pervious soil consisting of thin lenses, bands, or even layers of coarse-grained soil, such as silty sand or sand. These layers have no influence on the consolidation process where and when no drains are used. However, where vertical drains have been installed, the drainage is to a large

extent controlled by the vertical communication between these zones as facilitated by the drains. As illustrated in Figure 4.5, the consolidation is then by way of slow vertical flow in the fine-grained soil to the lenses, followed by rapid horizontal flow in the lens to the vertical drain, and, then, in the drain to the surface blanket. In effect, the lenses take on the important function of drainage boundaries of the less pervious layers of the soil body sandwiched between the lenses. That is, the mechanism is still very much that of a vertical drainage, much accelerated.

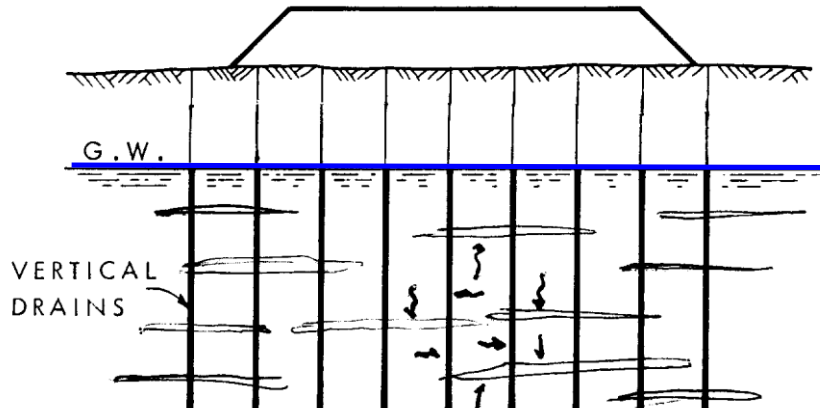


Fig. 4.5 Actual flow in a soil containing pervious lenses, bands, or layers

It is vital for a design of vertical drain project to establish the presence of such lenses, bands, or layers of coarse-grained soil and their vertical spacing. Conventional boreholes and laboratory analysis of recovered samples are rarely fully suitable for this purpose and, usually, once it becomes clear that vertical drains are considered for a project, additional field investigation involving both undisturbed sampling, CPTU tests, and special laboratory testing may become necessary.

#### 4.4.6 Surcharging

The rate of consolidation always slows down significantly toward the end of the consolidation period. The time between about 80 % and 95 % of primary consolidation can require as long time as that from start to 80 %, and the time from 95 % to, say, 98 % can take a very long time. It is not practical to design for a target completion level greater than an average degree of consolidation of 80 %. To reach even that level within a reasonable time requires a surcharge ("overload") to be placed along with embankment. The surcharge is an extra embankment load (extra height) that is removed when the average degree of consolidation has reached the target level, usually about 80 % of the average degree of consolidation for the embankment plus surcharge. The magnitude of the surcharge load should be designed so that after removal, the consolidation of the remaining embankment is completed, resulting in more than a "100 % consolidation" for the embankment without the surcharge. The timing of the removal of the surcharge normally coincides with preparing the embankment for paving of the road bed.

The results of a vertical drain project must always be monitored. This means that the programme must include a carefully designed schedule of ground surface measurements of settlement as well as a good number of depth-anchors or similar gages to monitor the distribution of settlement. Piezometers to measure pore pressures are also required (the analysis of pore pressure records must be made with due respect to fact that the distance between a piezometer tip and a drain cannot be known with good accuracy). The time to remove the surcharge must depend on the measurement data. It is helpful to plot the settlement values a settlement versus log-time as the project proceeds. Such lin-log plots will show the settlement plot to appear in an approximately straight line on reaching 80+ % consolidation. Such plots should represent the development in individual soil layers, not just be from ground surface values.

A monitoring programme should include several stations measuring pore pressure distribution and settlement distribution with depth (not just settlement of the ground surface) and monitoring should commence very early in the project; immediately on preparing the ground and before placing the first lift of the fill.

It is absolutely necessary to realize that the purpose of the monitoring programme is not just to confirm that the project performed satisfactorily, that is, performed as intended and expected. The monitoring programme must be designed to respond to the key purpose of providing records for early discovery and analysis in case the project would not perform satisfactorily and, also, to provide data that will be sufficient for a comprehensive study of the conditions so that a remedial programme can be designed if needed (see also Section 4.4.10). To the same end, it is very worthwhile to include in the monitoring arrangement a station away from the drain area to monitor the performance for conditions of no drains but otherwise identical to those of the project. For a case history reporting an unsatisfactory performance of a wick drain project, see Fellenius and Nguyen (2013; 2017).

Figure 4.6 shows settlements measured in one point below a test embankment, where wick-drains were installed. The dotted lines indicate the reducing fill height due to the ongoing settlement. On removal of the surcharge (to half height), settlement essentially ceased (a small heave is expected to occur, provided full consolidation has had time to develop for the remaining embankment height).

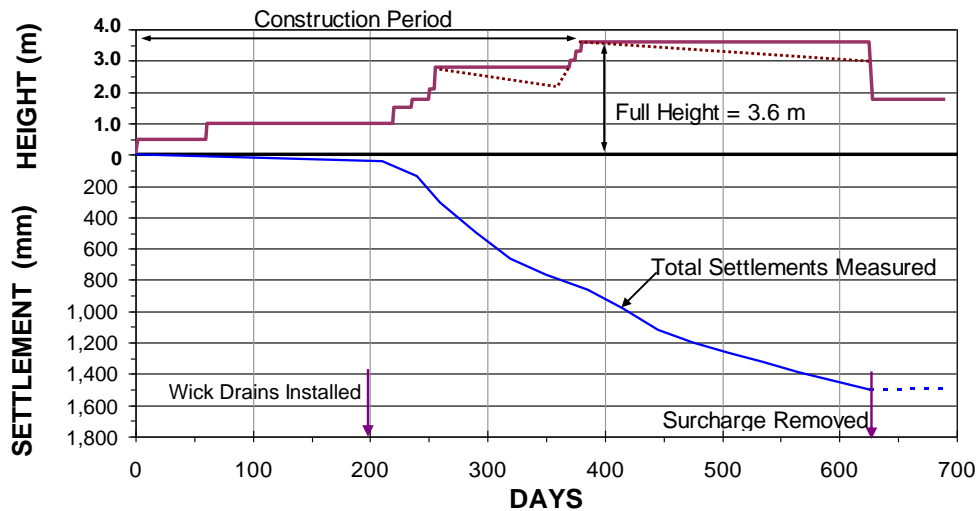


Fig. 4.6 Settlement measured for a stage-constructed test embankment. Data from Moh and Lin (2006), used with permission.

On completion of the consolidation, the soil supporting the embankment is normally-consolidated. This means that future settlement may occur due to small additional loading of the soil from, for example, a moderate raising of the elevation of the road bed or widening the embankment during future maintenance work (e.g., re-paving), or, indeed, even from a load increase due to seasonal variation of the groundwater table (a lowering of the groundwater table will increase the effective stress and initiate—renew—the consolidation). For this reason, it is advisable that the project be designed so as to leave the soil underneath the final structure at a suitable level of preconsolidation stress. This means that the design of a vertical drain project should always incorporate a surcharge (i.e., an "overload"; an extra embankment load to be removed on completion of the consolidation). At a wide site, the placing of surcharge can be staggered to limit the amount of material necessary to eventually be removed from the site. NB, after careful monitoring and evaluation (engineering review).

### 4.4.7 Stage Construction

Constructing an embankment to full height in one stage may give rise to concern for the stability of the embankment. Lateral soil spreading will be of concern and not just slope failure. Usually, the instability occurs in the beginning of construction and the risk subsides as the pore pressures reduce due to the consolidation. The stability of the embankment can be ensured during the construction by building in stages—stage construction—and with careful monitoring and evaluation of the consolidation progress. The construction time can be very long, however, unless accelerated by means of vertical drains.

Vertical drains are very effective means to minimize lateral spreading and improve embankment stability. The drains accelerate the consolidation process so that the construction rate is not at all, or only moderately, affected by the stability concern, whereas constructing the embankment without drains would have necessitated stage construction and generally prolonged the construction time and/or necessitated incorporating relief embankments or other resource-demanding methods to offset the concern for stability and lateral movements.

Figure 4.7 shows observed settlements and movements for a stage-constructed 3.6 m high test embankment during the construction of the new Bangkok International Airport, Thailand. Settlement was monitored in center and at embankment edges and horizontal movement was monitored near the sides of embankment. Time from start to end of surcharge placement was nine months. Observation time after end of surcharge placement was eleven months. Compare the maximum lateral movements at the embankment edges, about 180 mm, to the settlements, 1,400 mm. The lateral movements were large. However, without the drains they could easily have twice as large. Note also that the lateral movement was the reason for the fact that the edges of the embankment settled more than the center in this case. See also Figure 3.11.

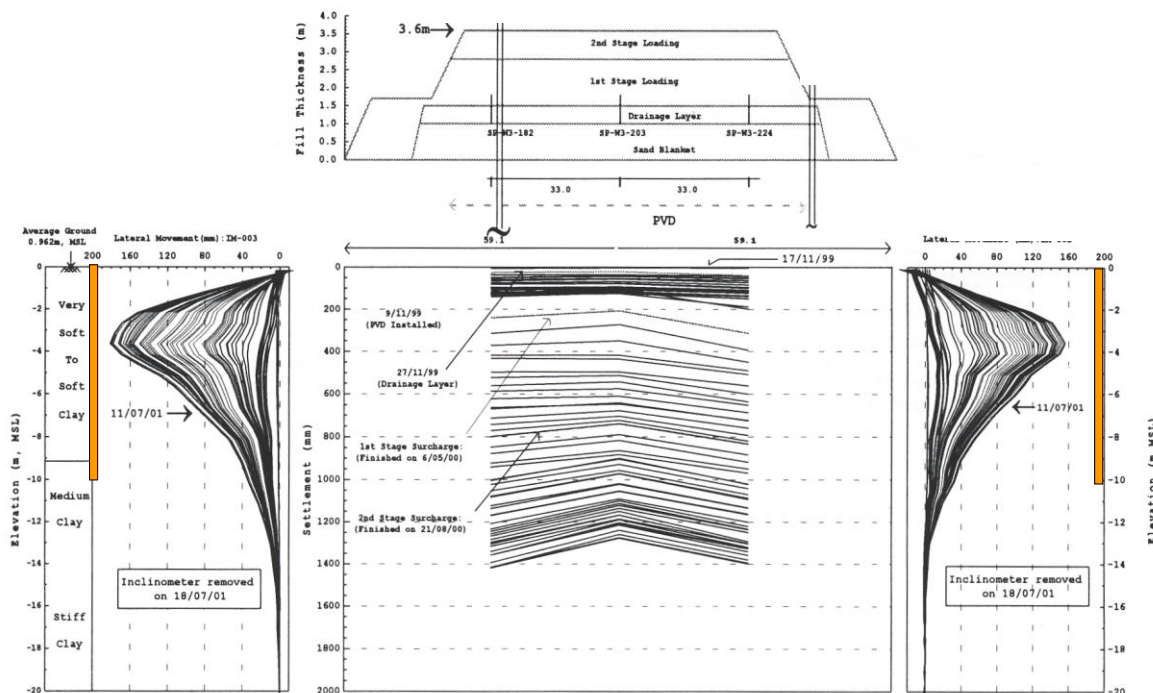


Fig. 4.7 Settlement and lateral movement for a stage-constructed 3.6 m high test embankment. From Moh and Lin (2006); used with permission.

#### 4.4.8 Loading by Means of Pumping to Achieve Vacuum Effect

Instead of, or in conjunction with, an embankment load, the stress increase driving the consolidation process can be by means of suction, that is, applying a vacuum on the ground surface with vertical drains installed in the ground (Holtz and Wager 1975). Usually, the vacuum method involves placing an impervious membrane (a tarp) on the ground and pumping out the air underneath it (Chai et al. 2005; 2006). The tarp is sensitive to escape of air, however, and it is therefore difficult to maintain the vacuum underneath the tarp. The vacuum method involves many practical issues not mentioned here. One alternative application of the method includes connecting each drain to a suction pipe (Cortlever et al. 2006).

The theoretical maximum vacuum is equal to the atmospheric pressure (100 kPa), which corresponds to an about 5 m high embankment. However, the actual vacuum possible is no more than about half the theoretical maximum. A difference between applying a stress using the vacuum method is that the stress does not cause outward lateral movement, but inward, albeit small. Also, even in very soft soils, no slope stability concerns exist. Combining the vacuum method with an embankment loading may eliminate the need for stage-construction.

Pumping in wells drilled to pervious sand lenses or layers in or below the layer to consolidate will also accelerate the consolidation. The primary effect of the pumping is to reduce the pore pressure in the drains at the location of the pervious layers and, thus, lower the pore pressures in the full length of the vertical drains, which will increase the horizontal gradient toward the drains. Some effect will be achieved from the lowering of the pore pressures in the drainage zone below the consolidating layer, which improves also the vertical drainage of the layer; shortens the consolidation time.

#### 4.4.9 Pore Pressure Gradient and Artesian Flow

Bridges and associated embankments are usually placed near rivers, in valleys, or other low-lying areas. Most of these areas are characterized by a clay layer underlain by pervious soils that function as an aquifer separated from the surficial water table. Commonly, the pore pressure distribution in the lower layers at the site has an upward gradient, it may even be artesian. Drains installed at these sites will not change the pore pressure in the lower soils. However, the drains may change the pore pressure gradient to hydrostatic. This change will offset some of the increase of effective stress due to the embankment and have the beneficial effect of reducing the magnitude of the embankment-induced settlement. However, the change of the pore pressure distribution from upward gradient to hydrostatic distribution will act as a back pressure and slow down the consolidation rate. To adjust for this, an extra surcharge may be required. Moreover, arranging for a proper surface drainage of the site will be important as water may be transported up to the ground surface from the lower soil layers for a very long time.

#### 4.4.10 Monitoring and Instrumentation

It is imperative to verify that the consolidation proceeds as postulated in the design. Therefore, a vertical drain project must always be combined with an instrumentation programme to monitor the progress of the consolidation in terms of **settlement and pore pressure** development during the entire consolidation period, and often include also lateral movement during the construction. Pore pressures must be monitored also outside the area affected by either the embankment or the drains to serve as independent reference to the measurements.

Instrumentation installed at a construction site has a poor survival rate. It is very difficult to protect the instrumentation from inadvertent damage. Sometimes, to avoid disturbing the construction work, the monitoring may have to be postponed. Often, a scheduled reading may have to be omitted as it may be too risky for a technician to approach the gage readout unit. Therefore, the monitoring programme should include buried gages and readings by remote sensing. As it is normally not possible for the monitoring programme to control the construction and to ensure that records are taken at important construction milestones, the programme should include automatic data logging set to take readings at frequent intervals. Still, the possibility of damage to the gages cannot be discounted. Therefore, a certain level of redundancy in the layout of instrumentation is necessary.

The monitoring programme must include frequent correlations between the monitoring results and the design to catch any anomalies that can adversely affect the project. To this end, the design should include calculations of expected response at the locations of planned instrumentation. However, a design can never anticipate every event that will arise at a construction project. Therefore, the design should preauthorize provisions for performing analysis of the effect of unexpected events, such as extreme rainfall or drought during the monitoring period, unanticipated construction events involving fill, excavation, or pumping of groundwater, delays of completion of the construction, etc., so that necessary calculations are not delayed because time otherwise required for authorizing the subsequent analyses and adding supplemental instrumentation. Instrumentation design (type, placement depths and locations etc.) is a task for a specialist—the inexperienced must solicit assistance.

#### **4.5 Sand Drains**

The sand drain was the first type of vertical drain to be used for accelerating the pore pressure dissipation (during the mid-1930s). The following aspects are specific to the use of sand drains.

Sand drains are usually made by driving, augering, or vibrating a pipe into the ground, filling it with sand and withdrawing it. As indicated by Casagrande and Poulos (1969), the installation of full-displacement sand drains (driven drains) in soils that are sensitive to disturbance and displacement may decrease hydraulic conductivity and increase compressibility. As a consequence, the settlement could actually increase due to the construction of the drains.

The sand used in a sand drain must be free draining (not just "clean"), which means that the portion of fine-grained soil in the sand—in the completed sand drain—must not exceed 5 % by weight and preferably be less than 3 %. Constructing sand drains by pouring sand down a jetted water-filled hole will have the effect that silt and clay under suspension in the water will mix with the sand and cause the fines contents to increase to the point that the sand is no longer free-draining. In theory, this can be avoided by washing the hole with water until the water is clear. However, in the process, the hole will widen and the site will become very muddy and, potentially, the mud will render useless the drainage blanket on the ground. Simply put, a free-standing hole that can be washed clear of fines is made in a soil that does not need drains. If the hole is created by washing out the soil, then, before the sand is placed, a pipe must be inserted into which the sand is poured. The pipe is withdrawn after the pipe has been filled with sand. It is advisable to withdraw the pipe using vibratory equipment to make sure that the sand does not arch inside the pipe.

Sand drains are apt to neck and become disrupted during the installation work, or as a consequence of horizontal movements in the soil. The function of a necked or disrupted drain is severely reduced.

Sand drains have been constructed in the form of sand-filled long bags, hoses, called "sand wicks", which are inserted into a drilled hole

The stated disadvantages notwithstanding, sand drains can be useful where large flows of water are expected, in soils less sensitive to disturbance by the installation, and where the ratio of length to the nominal diameter of the drain is not greater than 50, and the ratio of spacing to nominal diameter is larger than 10.

Since the advent of the prefabricated bandshaped drain, the wick drain, sand drains are rarely used as vertical drains to accelerate consolidation in fine-grained soils.

## 4.6 Wick Drains

### 4.6.1 Definition

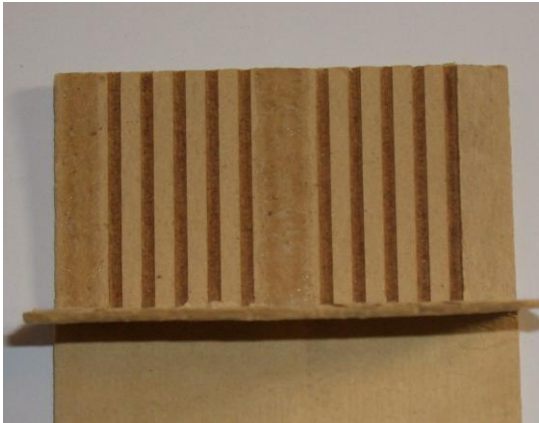
A wick drain is a prefabricated band-shaped about 100 mm wide and 5 mm to 10 mm thick unit consisting in principle of a channeled (grooved or studded) core wrapped with a filter jacket (Figures 4.8 -4.10). Installation is usually by means of a mandrel pushed into the ground (Figure 4.11). The filter jacket serves the purpose of letting water into the drain core while preventing fine soil particles from entering. The channels lead the water up to a drainage layer on the ground surface, or to the groundwater table, or down to a draining layer below the consolidating soil layer. For details see Holtz et al. (2011).

### 4.6.2 Permeability of the Filter Jacket

There are statements in the literature (e.g., Hansbo 1979) that the drain filter would not need to be any more pervious to water than the soil is, that is, have a hydraulic conductivity of about  $1 \times 10^{-8}$  m/s. This value is representative to that of a practically impervious membrane and the statement is fundamentally wrong. The filter must be able to accept an inflow of water not only from clay soil, but also from coarser soils, such as silty, fine sand typically found in lenses, or layers in most fine-grained soils—plentiful in most clays. In such soils, the portion reaching the drain through the clay is practically negligible. Moreover, the *outflow*, i.e., the discharge, of water must also be considered: **what enters the drain must exit the drain** (c.f., Figure 4.10). While the drain receives water over its full length, typically, 5 m through over 20 m, it must be capable of discharging this water through a very short distance of its length (discharge through the end—either end— of the drain is a rather special case). Therefore, the hydraulic conductivity of the filter must not be so small as to impede the outflow of water. Generally, the filter must have a hydraulic conductivity (permeability coefficient) no smaller than that of coarse silt or fine sand, approximately  $1 \times 10^{-6}$  m/s.

If the permeability of the drain filter is such that a head above the groundwater table appears inside the drain, the so developed back pressure (Figure 4.12) will slow down the consolidation process and impair the function of the drain. Examples exist where, due to a too low hydraulic conductivity of the filter jacket, the water has risen more than two metre inside the drain above the groundwater table before a balance was achieved between inflow in the soil below and outflow in the soil above the groundwater table (Fellenius 1981). The effect was that about one metre of surcharge was wasted to compensate for the two metre rise of the water. It is the rare occasion that the cut-off end of the drain is placed at the groundwater table (removing the need for the water to leave the drain through the filter jacket).

The Kjellman Cardboard Wick, 1942



The Geodrain, 1976



The Alidrain or Burcan Drain, 1978



The Mebra Drain; 1984 (Castle board Drain, 1979)



Fig. 4.8 Photos of four types of wick drains



Fig. 4.9 View over a site after completed wick drain installation





Fig. 4.10 Water discharging from a drain immediately outside the embankment



Fig. 4.11 Installation of wick drains type Alidrain (courtesy of J.C. Brodeur, Burcan Industries Ltd.)

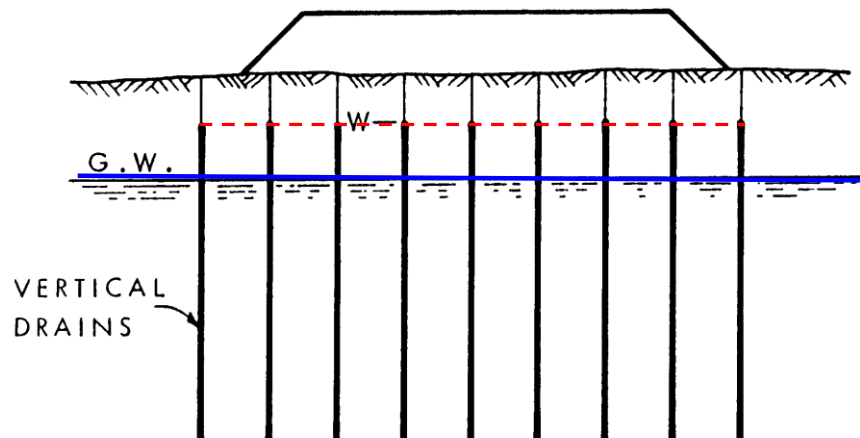


Fig. 4.12 Back pressure in wick drains with filter jacket inadequate for discharge of water

### 4.6.3 Discharge Capacity

An aspect of importance to a wick drain is the discharge capacity (well resistance) of the drain. Holtz et al. (1991) define the discharge capacity of a drain as the longitudinal flow under a gradient of unity (1.00). However, when this definition is coupled with the, by others, oft-repeated statement that the discharge capacity of most drain wicks is greater than  $100 \text{ m}^3/\text{year}$ , i.e.,  $20 \text{ cm}^3/\text{minute}$  (the volume in a small-size glass of water), the inevitable conclusion is that the discharge capacity is not important. The face value of this conclusion is correct, discharge capacity at a gradient of unity is not important. However, discharge capacity at low gradient is very important! The flow in a drain occurs under a very small gradient, about 0.01, not 1.00. Note that the basic premise of the Kjellman-Barron relation that the pore pressure distribution inside the drain is hydrostatic is not quite true—a gradient of zero means no flow! As to the actual discharge, in the extreme, consolidation settlement accelerated by means of drains can amount to about 0.1 m to 0.5 m, for the first month. A drain typically discharges water from a plan area, "footprint", of about  $2 \text{ m}^2$ . Therefore, the corresponding discharge per drain is approximately  $0.2 \text{ m}^3$  to  $1 \text{ m}^3$  per month, or  $0.005$  to  $0.02 \text{ cm}^3/\text{minute}$ . To achieve this flow of water under the more realistic small gradient, adequate discharge capacity and well resistance to outflow are important factors to consider.

Nevertheless, laboratory tests suggest that most modern prefabricated drains have adequate discharge capacity and acceptably small well resistance. That is, water having entered through the filter is not appreciably impeded from flowing up toward the groundwater table through the drain (or down into pervious non-consolidating layers, if the drains have been installed to reach into such layers). ***Nota Bene***, this is conditional on that one can assume that the drains stay straight and have no kinks or folds (microfolds) crimping the drain core. However, this one cannot assume, because, as the soil consolidates, the drains shorten and develop a multitude of kinks and folds, as explained in the following.

Not all drain are alike. Some drains are less suitable for use to large depth. A drain that has a soft compressible core will compress due to the large soil stress at depth and the water flow through the drain will be impeded. The drain core must be strong enough to resist large, lateral (confining) soil stresses without collapsing as this could close off the longitudinal drainage path. For example, at a depth of 20 m in a clay soil underneath a 10-m high embankment, the effective soil stress can exceed 400 kPa, and it is important that the drain can resist this stress without the function of the drain becoming impaired. Fellenius and Nguyen (2013; 2017) report a case of a project failure due to the fact that the wick drains did not function below about 20 m depth because the drain core compressed.

#### 4.6.4 Microfolding and Crimping

Settlement is the accumulation of relative compression of the soil which for most cases ranges from about 5 % through 20 % and beyond. A drain cannot buckle out into the soil, nor can it compress elastically, but must accommodate the soil compression in shortening through developing series of folds—microfolds, also termed "crimping". Microfolds will reduce the discharge capacity if the grooves or channels impede or close off the flow of the water when folded over. Some drain types are more susceptible to the crimping effect of microfolding than others. Most of the time, though, the filter jacket will channel the water so as to circumvent a blocked location. Drains where the filter jacket is kept away from the central core by a series of studs, which maintain the open flow area inside the drain, as opposed to longitudinal grooves or channels, can accommodate microfolding without impeding the flow of water. It is important to verify that a wick drain considered for use at a site, will be able to resist the significant soil forces and movements without becoming compressed or folded to the point of ceasing to function.

#### 4.6.5 Handling on Site

The wick drain is often manhandled on the construction site: it is dragged on a truck floor and on the ground, it is left in the sun and in the rain, it gets soaked and is then allowed to freeze, it is stepped on, etc. This puts great demands on strength, in particular wet strength, on the filter and the glue, or weld, used to hold the longitudinal filter seam together. Clay or mud can easily enter and block off the flow in the drain core through a rip or tear in the filter. One such spot in a drain may be enough to considerably impair its function. The filter must have an adequate strength, dry or wet.

#### 4.6.6 Axial Tensile Strength of the Drain Core

A factor also affecting the proper function of a drain and its discharge ability is the tensile strength of the drain core. Wick drains are installed from a roll placed near the ground from where they are pulled up to the top of the installation rig, where they pass over a pulley and go down into an installation mandrel that is forced into the ground. Ever so often, the mandrel tip meets resistance in an interbedded dense layer. This resistance is often overcome very suddenly resulting in an abrupt increase of mandrel installation velocity with the consequence that the drain is yanked down. The filter jacket is usually loose and able to accommodate the sudden pull, but many types of wick drains have thin and weak cores that can easily be torn apart. A drain with a partial or full-width tear of the core will not function well and, as the damage is inside, it cannot be seen by the field inspection. Obviously, adequate tensile strength of the drain core is an important condition to consider in the selection of a drain.

#### 4.6.7 Smear Zone

When moving the installation mandrel down and up in a clay, a zone nearest the mandrel is remolded. This zone is called the smear zone. The Kjellman-Barron solution can be refined by incorporating a smear zone into the formula apparatus. It is questionable how important a role smear plays, however. A wick drain has typically a cross sectional area of  $5 \text{ cm}^2$ . It is sometimes installed using a flattened mandrel having a cross section of about  $100 \text{ cm}^2$ , or, more commonly, using a circular mandrel having a cross section of  $200 \text{ cm}^2$ . The installation, therefore, leaves a considerable void in the ground, which, on withdrawing the mandrel, is partially, and more or less immediately, closed up. In the process, fissures open out from the drain and into the soil. The fissuring and "closing of the void" may be affected by the installation of the next drain, placing of fill on the ground, and/or by the passing of time. The net effect will vary with depth and from locality to locality. However, the creation of a void and its closing up, and creation of fissures is far more important than what thickness and parameters to assign to a smear zone. To incorporate smear in the Kjellman-Barron radial flow formula mostly serves as a fudge concept to fit the formula to data in a back-calculation. Therefore, incorporating smear zone effects in a design of a wick-drain project is not meaningful.

#### 4.6.8 Site Investigation

A properly designed and executed subsurface investigation is vital to any geotechnical design. Unfortunately, it is the rare project where the designer has the luxury of knowing the soil in sufficient detail. On many occasions, the paucity of information forces the designer to base the design on “playing it safe”. The design of a wick drain project will be very much assisted by having CPTU soundings and continuous tube sampling, as both will aid in determining the presence and extent of lenses, bands, and seams in the soil. It is always a good idea to extract the tube sample and check for presence of silt lenses. They are not visible on extraction, but will appear after a couple of days of air drying. Figure 4.13 shows a photo of an extracted length of a Shelby tube sample of clay. The "after 1 hour" photo does not imply anything other than a homogenous condition. However, after three days of air drying, silt layers interspersed in the clay show up as light streaks. The gap in the "After 3 days" photo is where a silty sand layer was. Those more pervious seams greatly accelerate the horizontal flow in the soil, because the pore water in the clay can move the short distance to the seam and take the faster route to the vertical drain. After complete drying, the streaks are no longer visible.



Fig. 4.13 Photos of extracted Shelby tube clay sample let to air dry

#### 4.6.9 Spacing of Wick Drains

The design of the spacing to use for a wick drain project can be calculated by means of the Kjellman-Barron formula (Eq. 4.1) with input of the coefficient of consolidation and the desired time for the desired degree of consolidation to be achieved with due consideration of the amount of surcharge to use, etc. More sophisticated analysis methods are available. However, the accuracy of the input is frequently such that the spacing can only be determined within a fairly wide range, be the calculation based on the simple or the sophisticated methods. It is often more to the point to consider that a suitable spacing of drains in a homogeneous clay is usually between 1.0 m and 1.2 m, in a silty clay between 1.2 m to 1.6 m, and in a coarser soil between 1.5 m to 2.0 m. The low-range values apply when presence of appreciable seams or lenses have not been found and the upper-range values apply to sites and soils where distinct seams or lenses of silt or sand have been established to exist. It is often meaningful to include an initial test area with a narrow spacing (which will provide a rapid response) and monitor the pore pressures and settlement for a month or so until most of the consolidation has developed. The observations can then be used to calibrate the site. The design of the rest of the site can then, potentially, be completed with a wider spacing saving costs and time.

#### 4.7 Closing remarks

Acceleration of settlement by means of vertical wick drains an approach with many spin-off benefits. The drains will accelerate the settlement, maybe to the point that, for example in case of a highway, when the road is about to be paved, most of the consolidation settlement has occurred, which minimizes future maintenance costs. If a structure, be it a bridge or a building is to be placed on piles and downdrag (i.e., settlement) is a concern for the piles, a quite common situation, accelerating the settlement with drains so that the settlement occurs before the structure is completed, may alleviate the downdrag problem. If lateral spreading (horizontal movements in the soil) due to fills or embankments imposes lateral movements in the soil that cause the piles to bend, wick drains will reduce the maximum pore pressures and reduce the lateral spreading (Harris et al. 2003).

All projects for acceleration of settlement should include a surcharge fill that is removed on the monitoring gages showing that the soil has reached a certain degree of consolidation, say, 80 % of total. Then, when removing the surcharge down to the as-designed ground level, the soil is actually preconsolidated, i.e., has a preconsolidation margin ensuring that future settlement is minimal and ensuring that new fill due to maintenance, etc. can be accommodated without subsequent settlement, allowing for the . This also removes the uncertainty of the magnitude of settlement imposed by the fill. Moreover, other than for very small area sites, if selecting a first portion of the site for installing the drains with minimal spacing, when the results are back-analyzed, the precise spacing and surcharge height to use for following portions of the project for optimizing costs and time. Larger sites can be designed to allow sequential ("rolling") placement of the surcharge so as to minimize the costs of the removal of the surplus amount at the end of the project drain-phase.

An high quality study of the effect of a wick drain improved site should include measurements for the development of settlement and pore pressure also for an area without drains in order for full reference material to be obtained.

The analysis of the site conditions aided by the more careful site investigation will have the beneficial effect that the designers will become more aware of what the site entails and be able to improve on the overall geotechnical design for the site and the structures involved. In this regard, note the comments in Section 4.4.10 on monitoring a wick drain project.



## CHAPTER 5

### EARTH STRESS — EARTH PRESSURE

#### 5.1 Introduction

“Earth stress” is the term for soil stress exerted against the side of a foundation structure—a “wall”. Many use the term “earth pressure” instead, which is incorrect in principle because “pressure” denotes an omni-directional situation, such as pressure in water, whereas the stress in soil is directional—a vector or a tensor. The misnomer is solidly anchored in the profession and to try to correct it is probably futile. Nevertheless, this chapter applies the term “earth stress”.

Earth stress is stress against a wall from a retained soil body. Loads supported on or in the soil body near the wall will add to the earth stress. The magnitude of the stress against a wall is determined by the physical parameters of the soil, the physical interaction between the soil and the wall, the flexibility of the wall, and the direction and magnitude as well as manner of movement (tilting and/or translation) of the wall. The latter aspect is particularly important. When the wall moves outward, that is, away from the soil—by the soil pushing onto the wall, moving out it or tilting it away, an ‘active’ condition is at hand and the earth stress is said to be “active”. If instead the wall moves toward the soil—by outside forces pushing the wall into the soil—the earth stress is said to be “passive”. In terms of magnitude, the active stress against the wall is much smaller than the passive stress; the relative magnitude can be a factor of ten, and, in terms of amount of movement required for full development of stress, the active stress requires a smaller movement than that required for developing the passive stress. The displacement necessary for full active condition is about 1 % of the wall height; less in dense sand, more in soft clay, and that necessary for full passive condition is about 5 % of the wall height; less in dense sand, more in soft clay. Many text books and manuals include diagrams illustrating the relative displacement necessary to fully develop the active stress (reduce the intensity) and ditto for the passive stress (increase the intensity) for a range of conditions.

Conventionally, the unit stress at a point on the wall is proportional to the overburden stress in the soil immediately outside the wall. The proportionality factor is called “earth stress coefficient” and given the symbol “K” (the word “coefficient” is spelled “Koefficient” in German, Terzaghi’s first language). The earth stress acting against the wall at a point is a product of the K-coefficient and the overburden stress. In a soil deposited by regular geologic process in horizontal planes, the horizontal stress is about half of the stress in vertical direction, that is, the earth stress coefficient is about 0.5 (notice, the value can vary significantly; see also Section 3.13.3). It is called the “coefficient of earth stress at rest” (“coefficient of earth pressure at rest”) and denoted  $K_0$  (pronounced “K-naught”). Once a movement or an unbalanced force is imposed, the ratio changes. If the wall is let to move and the soil follows suit, the earth stress coefficient reduces to a minimum value called “coefficient of active earth stress” and denoted  $K_a$ . Conversely, if the wall forced toward the soil, the earth stress coefficient increases to a maximum value called “coefficient of passive earth stress” and denoted  $K_p$ .

The earth stress coefficient is a function of many physical parameters, such as the soil strength expressed by the friction angle, the roughness of the wall surface in contact with the soil, the inclination of the wall, and the effective overburden stress. The effective overburden stress is governed by the weight of the soil, the depth of the point below the ground surface, and the pore pressure acting at the point. Despite this complexity, the earth stress coefficient is determined from simple formulae.

## 5.2 The Earth Stress Coefficient

Figure 5.1 shows an inclined, rough-surface gravity retaining wall subjected to earth stress from a non-cohesive soil body with an inclined ground surface. The unit active earth stress against the wall acts at an angle of  $\delta$  formed by a counter-clockwise rotation to a line normal to the wall surface. The unit active earth stress is calculated as  $K_a$  times the effective overburden stress and the coefficient,  $K_a$ , is given in Eq. 5.1a.

$$(5.1a) \quad K_a = \frac{\sin(\beta - \phi')}{\sin\beta [\sqrt{\sin(\beta + \delta) + \sqrt{\sin(\delta + \phi') \sin(\phi' - \alpha) / \sin(\beta - \alpha)}}]}$$

where

- $\alpha$  = slope of the ground surface measured counter clock-wise from the horizontal
- $\beta$  = inclination of the wall surface measured counter clock-wise from the base
- $\phi'$  = effective internal friction angle of the soil
- $\delta$  = effective wall friction angle and the rotation of the earth stress measured counter clock-wise from the normal to the wall surface

Figure 5.1 shows that for active earth stress, the earth stress has a counter clock-wise rotation,  $\delta$ , relative the normal to the wall surface and the passive earth stress coefficient,  $K_a$ , is given in Eq. 5.1a.

The horizontal component of the active earth stress,  $K_{ah}$ , is given in Eq. 5.1b

$$(5.1b) \quad K_{ah} = K_a \sin(\beta + \delta)$$

If the wall is vertical and smooth, that is,  $\beta = 90^\circ$  and  $\delta = 0^\circ$ , then, Eqs. 5.1a and 5.1b both reduce to Eq. 5.1c.

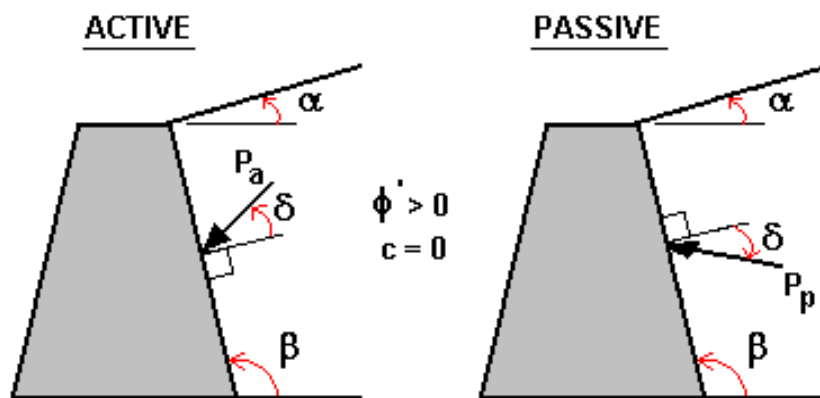


Fig. 5.1 Earth stress against the face of a rough surface gravity wall from a soil body with an inclined ground surface.

$$(5.1c) \quad K_{ah} = K_a = \frac{1 - \sin \phi'}{1 + \sin \phi'} = \tan^2(45^\circ - \phi'/2)$$



Figure 5.1 shows that for passive earth stress, the earth stress has a clock-wise rotation,  $\delta$ , relative the normal to the wall surface and the passive earth stress coefficient,  $K_p$ , is given in Eq. 5.2a.

$$(5.2a) \quad K_p = \frac{\sin(\beta + \phi')}{\sin\beta [\sqrt{\sin(\beta - \delta) + \sqrt{\sin(\delta + \phi') \sin(\phi' + \alpha) / \sin(\beta - \alpha)}}]}$$

where parameters and symbols are the same as in Figure 5.1a

The horizontal component of the passive earth stress,  $K_{ph}$ , is given in Eq. 5.2b

$$(5.2b) \quad K_{ph} = K_p \sin(\beta - \delta)$$

If the wall is vertical and smooth, that is,  $\beta = 90^\circ$  and  $\delta = 0^\circ$ , Eqs. 5.2a and 5.2b both reduce to Eq. 5.2c

$$(5.2c) \quad K_{ph} = K_p = \frac{1 + \sin \phi'}{1 - \sin \phi'} = \tan^2(45^\circ + \phi/2)$$

Notice that in Figure 5.1 the wall friction angle (the rotation of the normal force against the wall surface) occurs in different directions for the active and passive cases. The directions indicate the situation for the soil wedge movement relative to the wall—downward in the active case and upward in the passive case. That is, in the active case, the wall moves outward and down; in the passive case, the wall is forced inward and up. For special cases, an outside force may move (slide) the wall in a direction that is opposite to the usual direction (for example, a wall simultaneously retaining soil and supporting a vertical load). The corresponding effect on the earth stress coefficient can be determined by inserting the wall friction angle,  $\delta$ , with a negative sign in Eqs. 5.1a and 5.2a.

### 5.3 Active and Passive Earth Stress

The unit active earth stress,  $p_a$ , in a soil exhibiting both cohesion and friction is given by Eq. 5.3

$$(5.3) \quad p_a = K_a \sigma'_z - 2c' \sqrt{K_a}$$

where  $\sigma'_z$  = effective overburden stress  
 $c'$  = effective cohesion intercept

The unit passive earth stress,  $p_p$ , in a soil exhibiting both cohesion and friction is given by Eq. 5.4

$$(5.4) \quad p_p = K_p \sigma'_z + 2c' \sqrt{K_p}$$

Usually, if pore water pressure exists in the soil next to a retaining wall, it can be assumed to be hydrostatic and the effective overburden stress be calculated using a buoyant unit weight. However, when this is not the case, the pore pressure gradient must be considered in the determination of the effective stress distribution, as indicated in Section 1.4, Eq. 1.8c.

The pressure of the water must be added to the earth stress. Below the water table, therefore, active and passive earth stress are given by Eqs. 5.5 and 5.6, respectively.

$$(5.5) \quad p_a = K_a \sigma'_z - 2c' \sqrt{K_a} + u$$

$$(5.6) \quad p_p = K_p \sigma'_z + 2c' \sqrt{K_p} + u$$

where  $u$  = the pore water pressure

In total stress analysis, which may be applicable to cohesive soils with  $\phi = 0$ , Eqs. 5.1a and 5.2a reduce to Eq. 5.7a; Eqs. 5.1b and 5.2b reduce to Eq. 5.7b.

$$(5.7a) \quad K_a = K_p = \frac{1}{\sin \beta} \quad \text{and} \quad (5.7b) \quad K_{ah} = K_{ap} = 1$$

where  $\beta$  = inclination of the wall from Eq. 5.1a

Where  $\phi = 0$ , and where the undrained shear strength,  $\tau_u$ , of the soil is used in lieu of effective cohesion, Eqs. 5.5 and 5.6 reduce to Eqs. 5.8a and 5.8b.

$$(5.8a) \quad p_a = \sigma_z - 2\tau_u$$

$$(5.8b) \quad p_p = \sigma_z + 2\tau_u$$

where  $\sigma_z$  = the total overburden stress

Notice, however, that if a crack develops near the wall that can be filled with water, the force against the wall will increase. Therefore, the earth stress calculated by Eqs. 5.8a and 5.8b should always be assumed to be at least equal to the water pressure,  $u$ , acting against the wall from the water-filled crack (even if the soil away from the wall could be assumed to stay “dry”).

Figure 5.2 illustrates an inclined, rough-surface wall having on the side to the right (“active side” or “inboard side”) a soil (a backfill, say) with a sloping ground surface. A smaller height soil exists on the other side (the “passive side” or the “outboard side”). The inboard soil is saturated and a water table exists at about mid-height of the wall. The inboard soil is retained by the wall and the soil is therefore in an active state. The soil layer on the outboard side aids the wall in retaining the active side soil and water. It is therefore in a passive state.

The figure includes the angles  $\alpha$ ,  $\beta$ , and  $\delta$ , which are parameters used in Eqs. 5.1a and 5.2a. They denote the slope of the ground surface, the slope of the wall surface, and the wall friction angle and rotation of the earth stress acting on the wall surface. (The equations also include the angle  $\phi'$ , but this angle cannot be shown, because the soil internal friction angle is not a geometric feature).

The two diagrams illustrate the horizontal passive and active earth stress ( $p_{ph}$  and  $p_{ah}$ ) acting against the wall (proportional to the vertical effective stress within the soil layers). The distribution of water pressure,  $u$ , against the passive and active side of the wall is also shown.

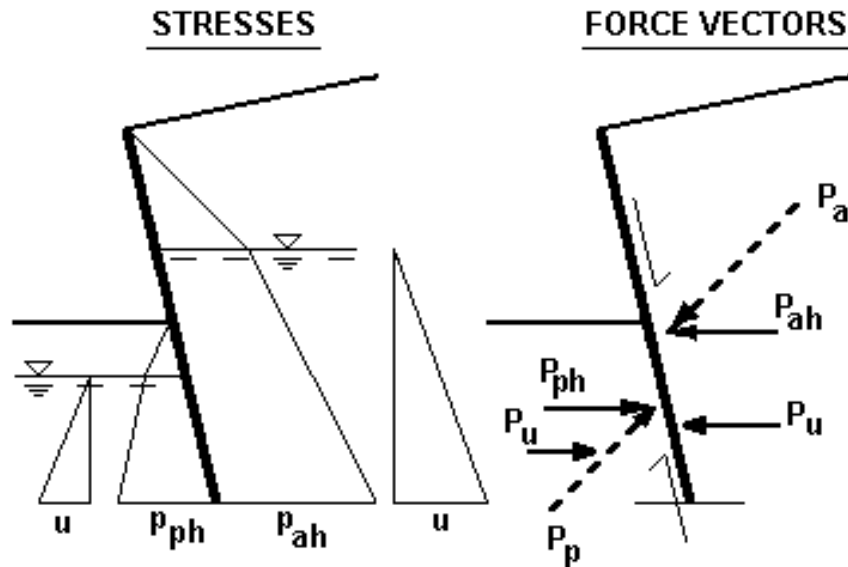


Fig. 5.2 Stresses and force vectors against an inclined wall

The force vectors ( $P_{ph}$  and  $P_{ah}$ ) are the sum of all the horizontal earth stresses and act in the centroids of the stress diagrams. Notice, because of the wall friction, the total earth stress force vectors ( $P_p$  and  $P_a$ , the dashed vectors) are not normal to the wall surface. Notice also that the wall friction vectors acting along the wall surface on the active and passive side point in opposing directions. (The weight of the wall and the forces at the base of the wall are not shown, and neither is the net bending moment).

In developing the forces, movements will have occurred that mobilize the active and passive states (and, also, the contact stresses and sliding resistance at the base of the wall). However, the wall as shown is in equilibrium, that is, the movements have ceased. The movements may well have been sufficiently large to develop active stress (and, probably, also the full sliding resistance, depending on the type of soil present under the base of the wall). However, no more passive resistance has developed than that necessary to halt the movement of the wall. (Remember, the movement necessary for full passive resistance is larger than for full active resistance).

When cohesion dominates in the retained soil, Eq. 5.3 may result in a negative active earth stress near the ground surface. Negative earth stress implies a tension stress onto the wall, which cannot occur. Therefore, when calculating earth stress, the negative values should be disregarded.

#### 5.4 Surcharge, Line, and Strip Loads

A surcharge over the ground surface increases the earth stress on the wall. A uniform surcharge load can be considered quite simply by including its effect when calculating the effective overburden stress. However, other forces on the ground surface, such as strip loads, line loads, and point loads also cause earth stress. Strip loads, which are loads on areas of limited extent (limited size footprint), and line and point loads produce non-uniform contribution to the effective overburden stress and, therefore, their contribution to the earth stress is difficult to determine. Terzaghi (1954) applied Boussinesq stress distribution to calculate the earth stress from line loads and strip loads. This approach has been widely accepted in current codes and manuals (e.g., Canadian Foundation Engineering Manual 1992; 2006, NAVFAC DM7 1982).

Figure 5.3 illustrates the principles of the stress acting on a wall due to surface loads calculated according to Boussinesq distribution. The so calculated stress is independent of the earth stress coefficient, the soil strength parameters, and, indeed, whether an active or a passive state exists in the soil. The figure shows the Boussinesq distributions for the horizontal stress at a depth,  $z$ , below the ground surface from a line load, a uniformly loaded strip load, and a strip load with a linearly varying stress on the ground surface applied at and along a horizontal distance,  $x$ , from the wall. The equations are given by Eqs. 5.9a through 5.9.c. For symbols, see Figure 5.4. Notice, the angles  $\alpha$  and  $\beta$  are not the same as those used in Eq. 5.1,  $\alpha$  is the angle between the vector to the edge of the strip load, and  $\beta$  is the angle between the wall and the left vector to the strip.

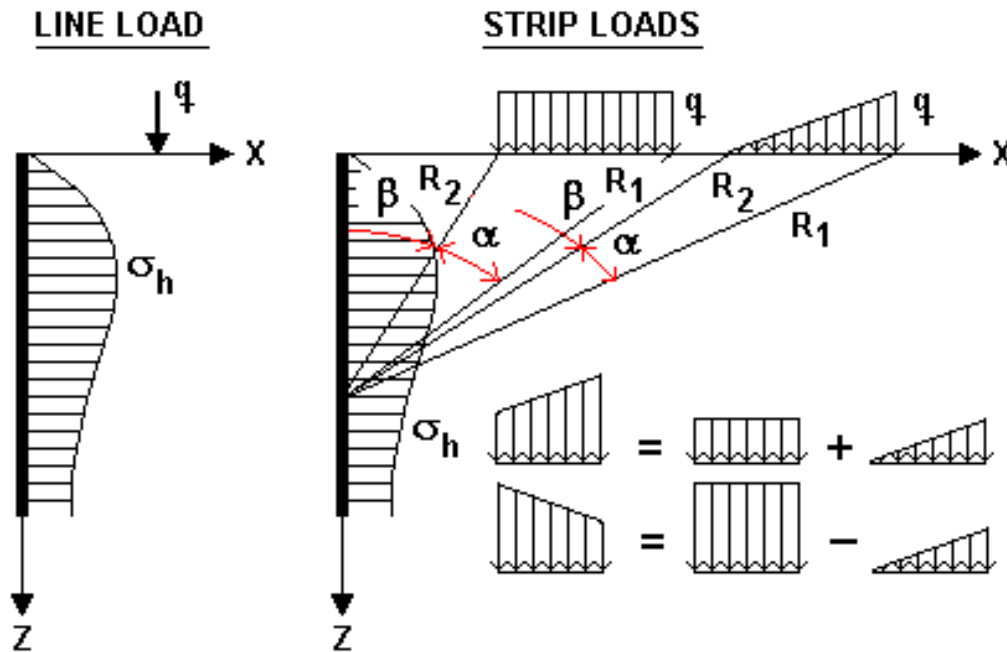


Fig. 5.3 Earth stress on a wall from line and strip loads on the ground surface as determined by integration from Boussinesq distribution (Fellenius and Goudreault 1995)

Stress from an applied line load,  $q$  (force/unit length; compare Eq. 1.16 b):

$$(5.9a) \quad \sigma_h = \frac{2q}{\pi} \frac{x^2 z}{(x^2 + z^2)^2}$$

where  $z$  = depth  
 $x$  = distance from the wall to the applied stress,  $q$

Stress from uniform strip load,  $q$  (force/unit area):

$$(5.9b) \quad \sigma_h = \frac{q}{\pi} [\alpha - \sin \alpha \cos(\alpha + 2\beta)]$$

where  $\alpha$  and  $\beta$  are defined in Figure 5.3

Stress from a uniform strip with a stress (force/unit area) that ranges linearly from zero at one side to  $q$  at the other side:

$$(5.9c) \quad \sigma_h = \frac{q}{\pi} \left[ \frac{x\alpha}{\beta} - \frac{z}{\beta} \ln\left(\frac{R_1^2}{R_2^2}\right) + \frac{\sin 2\beta}{2} \right]$$

Integration of the equations gives the expression for the horizontal earth stress acting against a wall resulting from the line and strip loads. As mentioned above, the integrated value is doubled to provide the earth stress acting on the wall. A linearly increasing or decreasing strip load can be determined by combining Eqs. 5.9b and 5.9c.

Terzaghi (1953) presented nomograms for finding the point of application of the resultant of the unit earth stress acting against a vertical wall. By means of applying numerical computer methods, the location of the earth stress resultant and its magnitude can be directly located and, moreover, also the solution for inclined walls be determined.

According to Terzaghi (1954), the earth stress calculated according to Eq. 5.9a is not valid for a line load acting closer to the wall than a distance of 40 % of the wall height. For such line loads, the earth stress should be assumed equal to the earth stress from a line load at a distance of 40 % of the height. The resulting force on the wall is 55 % of the line load and its point of application lies about 60 % of the wall height above the wall base.

For a cantilever wall having a base or a footing, a surface load will, of course, also act against the horizontal surface of the base, as indicated in [Figure 5.4](#). The vertical stress on the base can be determined from Eqs. 5.10a through 5.10c applying the symbols used in [Figure 5.3](#) and Eqs. 5.9a through 5.9c.

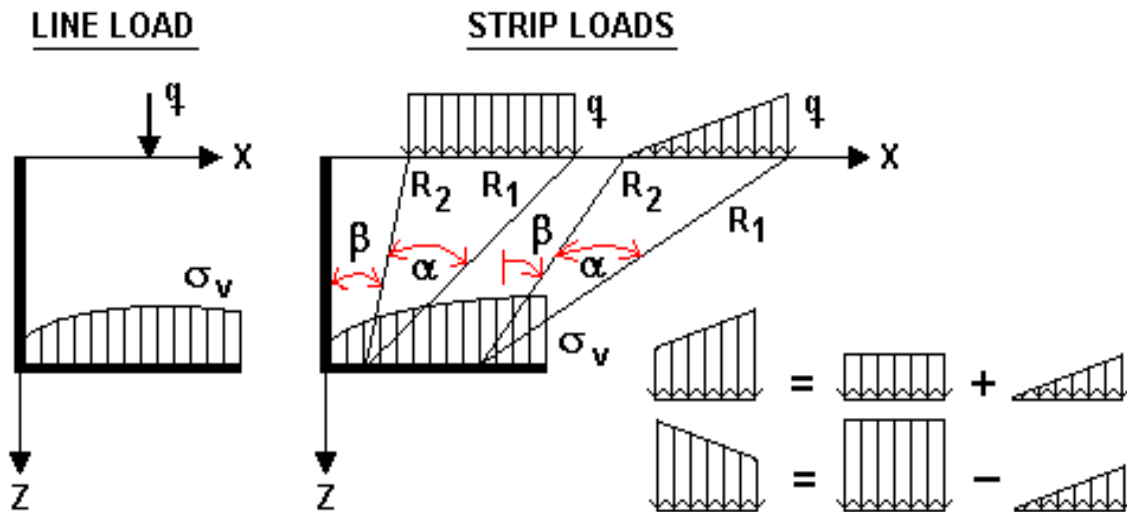


Fig. 5.4 Vertical earth stress on the base of a cantilever wall from line and strip strip loads on the ground surface as determined by Boussinesq distribution (Fellenius and Goudreault 1995)

Vertical stress from a line load,  $q$ :

$$(5.10a) \quad \sigma_v = \frac{2q}{\pi} \frac{z^3}{(x^2 + z^2)^2}$$

Vertical stress from a uniform strip load,  $q$ :

$$(5.10b) \quad \sigma_v = \frac{q}{\pi} [\alpha + \sin \alpha \cos(\alpha + 2\beta)]$$

Vertical stress from uniform strip load that ranges linearly from zero at one side to  $q$  at the other side:

$$(5.10c) \quad \sigma_v = \frac{q}{\pi} \left[ \frac{x\alpha}{\beta} - \frac{\sin 2\beta}{2} \right]$$

Integration of the equations gives the resulting vertical earth stress acting against the base and, also, its location. A linearly increasing or decreasing strip load can be determined by combining Eqs. 5.10b and 5.10c. Notice, the stress according to Eqs. 5.10a through 5.10c acting on the base can have a stabilizing influence on a footing foundation.

## 5.5 Factors of Safety and Resistance Factors

In a design for earth stress forces, the factors of safety (resistance factors in LRFD) appropriate to the structures and types of loads involved should be applied. Note, however, that "safety" against overturning and location of the resultant, should be applied without any factor of safety or resistance factor on the loads and earth forces, but the stability be ensured per the location of the resultant. See also Section 6.6.

## 5.6 Aspects of Structural Design

Once the geometry of the structure and the geotechnical aspects of the design (such as the bearing resistance, settlement, and sliding resistance) are acceptable, the structural engineer has to ensure that the retaining structure itself is able to sustain the forces acting on each of its parts, such as the stem, the toe, and the heel. The stem is the vertical portion of the structure supporting the horizontal components of all loads. The toe is the portion of the footing located on the "outboard side" of the retaining structure and the heel is the portion of the footing located on the "inboard side" of the retaining structure.

While the overall geometry of the footing supporting a wall structure is often dictated by the external stability of the retaining wall (active stress), the structural design (member thickness, reinforcing steel, etc.) is based entirely on the internal stability (backfill stress).

### 5.6.1 Stem Design

The stem must be designed for shear, compression, and, most important, bending stresses. The shear forces acting on the stem are the summation of all horizontal forces acting above the top of the footing toe. In addition to shear forces, the stem must be capable of resisting compression forces. These forces can include the weight of the stem, the vertical components of the soil forces acting along the face of the stem (inclined stem and/or wall friction exist), and other vertical forces acting directly on the stem.

Bending forces acting on the stem are obtained by multiplying all shear and compression forces by their respective distances to the base of the stem. The design of the stem must consider both the loads applied during the construction stage as well as loads during service conditions. Often in the design of the stem, the effect of the passive forces will be excluded while loads are added that are induced by the compaction of the backfill on the active side of the stem.

For concrete walls, the thickness of the stem and the amount and spacing of reinforcing steel should be sized based on the interaction of the shear, compression, and bending forces.

### 5.6.2 Toe Design

The footing toe area is designed to resist the upward stresses created by the bearing layer at equilibrium condition. The design assumes that there is no deformation of the footing or the stem following installation of the backfill. It is also assumed that sliding or bearing failure will not occur. According to the Ontario Highway Bridge Design Code (OHBDC 1991), the design of the toe should consider both a uniform and a linear contact stress distribution. The design must include shear and bending forces. For concrete structures, these forces will usually dictate the amount and spacing of the bottom reinforcing steel in the footing.

### 5.6.3 Heel Design

The footing heel area is designed to resist the downward stresses caused by the fill and forces on the inboard side. The design assumes that the structure will rotate around a point located at the toe of the footing. All loads from the active side, included in the external stability design, must be included also in the bending and shear design of the heel. For concrete structures, the heel design will usually dictate the amount and spacing of upper surface reinforcing steel in the footing.

### 5.6.4 Drainage

Apart from design cases involving footings and walls designed in water, such as a sea wall, both footing and wall should be provided with drainage (pinholes, french drains, etc.) to ensure that no water can collect under the footing or behind the wall. This is particularly important in areas where freezing conditions can occur or where swelling soils exist under the footing or behind the wall. The commonly occurring tilting and cracking condition of walls along driveways etc. is not due to earth stress from the weight of the retained soil, but to a neglect of frost and/or swelling conditions.

## 5.7 Anchored Sheet-Pile Wall Example

An anchored sheet-pile wall will be constructed in a 5 m deep lake to retain a reclaimed area, as indicated in [Figure 5.5](#). The original soil consists of medium sand. The backfill will be medium to coarse sand and the fill height is 7 m. A tie-back anchor will be installed at a 1.5-m depth. Calculate the sheet-pile installation depth and the force in the anchor assuming the sheet pile is a free-end case. Cohesion,  $c'$ , can be assumed to be 0 and all shear forces along the sheet-pile wall can be disregarded. For now, do not include any safety margin for the input or any factors of safety. The example is taken from Taylor (1948) with some adjustment of numbers. It also appears, with similar number changes, in many, if not most, modern textbooks.

Proceed by first determining the sheet-pile length on the condition of equal rotating moment around the anchor level (i.e., net moment = 0) and then the anchor tension on the condition that the sum of all horizontal forces must be zero. The procedure is easily performed in an Excel spreadsheet.

[Table 5.1](#) compiles the calculations, as performed in Excel and [Figure 5.6](#) shows a plot of the distributions of earth stress against the wall

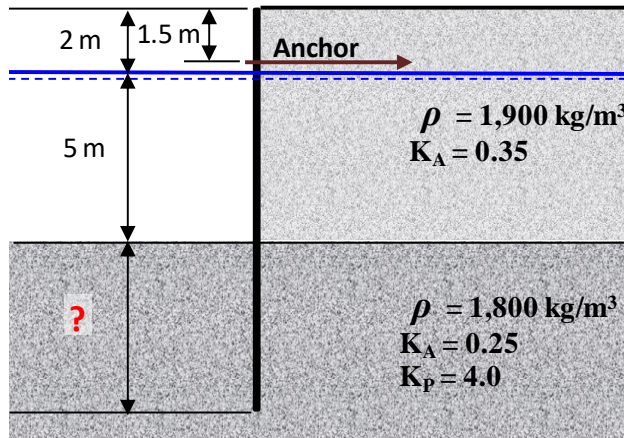


Fig. 5.5 Vertical view of sheet-pile wall

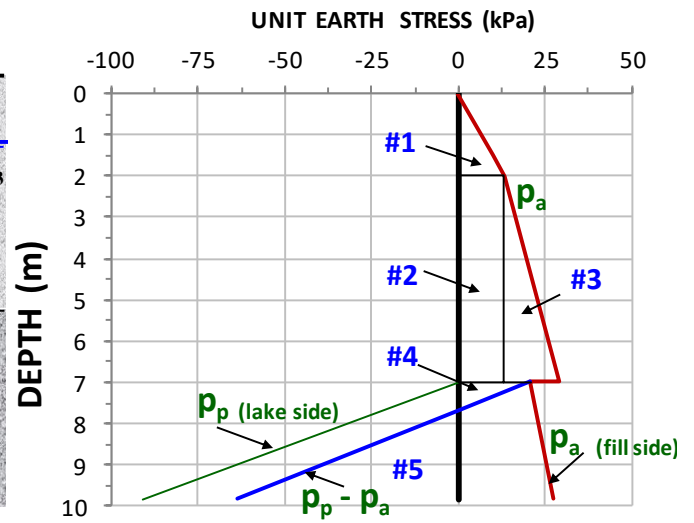


Fig. 5.6 Distribution of active and passive earth stress

**Table 5.1 Calculation Results**

Active side					Passive side				
DEPTH	$\sigma$	$u$	$\sigma'$	$p_a$	$\sigma$	$u$	$\sigma'$	$p_p$	$ p_p - p_a $
0.0	0.0	0.0	0.0	0.0					
1.5	28.5	0.0	28.5	10.0					
2.0	38.0	0.0	38.0	13.3					
7.0	133.0	50.0	83.0	29.1					
7.0	133.0	50.0	83.0	20.8	50.0	50.0	0.0	0.0	20.8
7.7	145.6	57.0	88.6	22.2	62.6	57.0	5.6	-22.4	≈0 (7.7 m by interpolation)
9.579	182.6	75.8	103.3	25.9	96.4	75.8	20.6	-82.5	56.6 (9.579 m is by trial and error' for M = 0)
		Σ121.6			Σ102.3				

	Area	Arm	M	ΣM
#1	13.3	0.2	2.3	2.3
#2	66.5	3.0	199.5	201.8
#3	39.4	3.8	150.8	352.6
#4	7.3	6.0	43.3	395.9
#5	53.1	-7.5	-395.9	≈0

Anchor 73.3 kN (the balance between lake-side and fill-side forces)

The shown solution procedure disregards axial stiffness and bending of the sheet piles, which come into play when assuming that the sheet-pile end condition is fixed. The axial stiffness and bending of the sheet-pile wall will have a large influence on the embedment depth and the anchor force. The 'ultimate sheet-pile' with a fixed end is a cantilever pile, i.e., a sheet-pile wall with no tie back anchor. The penetration (embedment depth) necessary is then a function also of the pile bending stiffness.



### 5.8 Retaining Wall on Footing Example

A retaining wall with dimensions as shown in Figure 5.7 has been constructed on an existing ground. The area behind and in front of the wall was then backfilled with a coarse-grained soil having a total density,  $\rho_t$ , of  $1,750 \text{ kg/m}^3$  and an internal friction angle,  $\phi'$ , of  $32^\circ$ . Cohesion,  $c'$ , can be assumed to be 0. There is no water table and the backfill is free-draining. Calculate the active and passive earth stresses acting on the wall and where the resultant to all forces cuts the base of the footing. (Assume that the thickness of the wall and its footing is small).

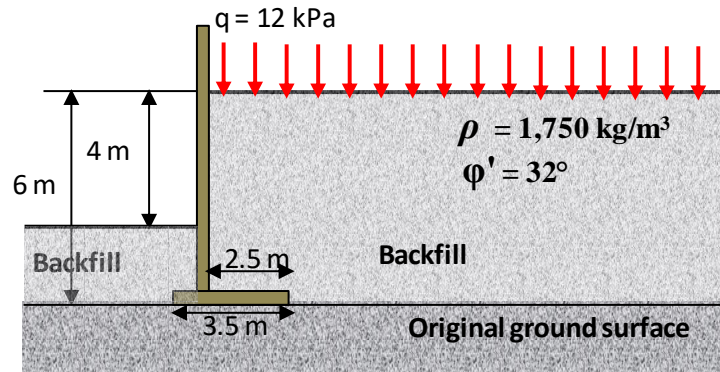


Fig. 5.7 Vertical view of retaining wall

Eqs. 5.1c and 5.2c give  $K_a = 0.31$  and  $K_p = 3.25$ .

Seven gravity forces, loads, and earth stresses affect the wall as indicated in Figure 5.8. They can be combined to show a single force, the resultant. Calculation results are shown in Table 5.2.

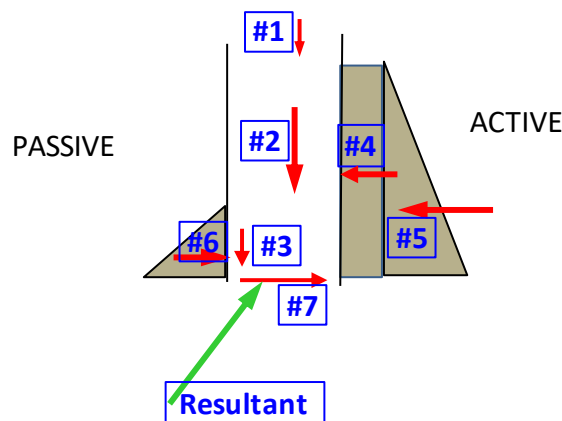


Fig. 5.8 Forces and stresses affecting the wall

The governing condition is the location of the resultant. To determine this, calculate the rotational moment around the footing toe (left edge of the footing in Figure 5.7).

**Table 5.2 Forces and rotational moment**

	Force (kN)	Arm to toe (m)	M (kNm)
#1 = 12 x 2.5	= 30	2.25	67.5
#2 = 17.5 x 2.5 x 6	= 262.5	2.25	590.6
#3 = 17.5 x 1 x 2	= 35	0.5	18.0
#4 = 0.31(12 x 6)	= 22.3	3.0	66.9
#5 = 0.31(17.5 x 6 x 6/2)	= 97.7	2.0	195.4
#6 = 3.25(17.5 x 2 x 2/2)	= 114	0.7	-76.4
#7 = (30+262+35) x tan 32	= 204	0	0

Moments around the footing toe

Vertical:  $Q=(30+262+35) = 327$ ;  $M=(67.5+590.6+18) = 676 \implies v_{\text{off toe}} = 676/327 = 2.1 \text{ m}$

Horizontal:  $Q=(22+98-114) = 6$ ;  $M=(67+195-76) = 186 \implies h_{\text{above}} = 186/6 = 31.0 \text{ m}$

Figure 5.9 indicates how to determine the location of the resultant.

$X/31 = 6/327 \implies X = 0.6 \text{ m}$   
well within the middle third.

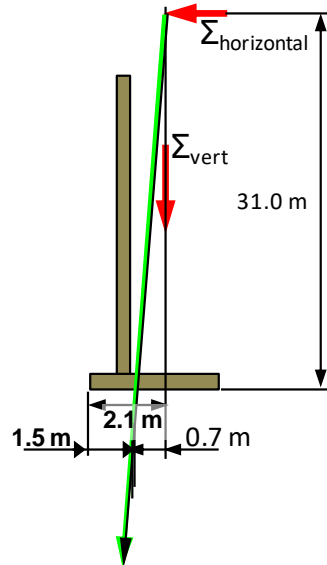


Fig. 5.9 Forces and stresses affecting the wall

**5.9 Retaining with multiple horizontal supports**

In case of a wall retaining a backfill, it is common to assume that the anchor forces increase proportionally to the increase of earth stress (triangularly distributed) acting on the wall, as the height of the retained soil increases. However, the conventional method to construct a shoring, a retaining wall, involves step-by-step excavation and installation horizontal supports (struts, anchors, tie-backs, raker supports, etc.) designed to hold back the earth stress acting on the wall. The wall can consist of a series of soldier piles with the distance between them covered by "wood lagging", a slurry trench with the slurry replaced by concrete, pile-in-pile walls (secant walls), and others. The earth stress against a wall retaining soil during a gradually deepening excavation, will be larger than that imposed by a backfill. Moreover, the force in the uppermost anchor row will be larger than that in the uppermost row of the backfill-supporting wall. Terzaghi and Peck (1948) recommended that the total earth stress be increased by a factor of 1.3 and the anchor forces be set equal as shown in Figure 5.10, thus redistributing the earth stress.

A similar redistribution is recommended for walls retaining cohesive soil, soft to firm and stiff to hard, respectively.

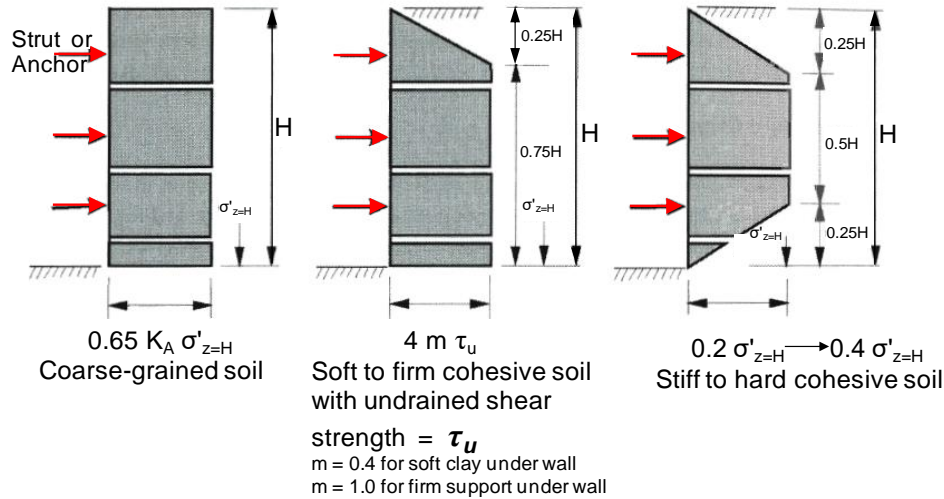


Fig. 5.10 Redistribution of earth stress for effect of progressive excavation and strut placement

Figure 5.11 shows an anchored sheet-pile wall constructed to shore up a 6 m deep excavation in a medium to coarse sand with three tie-back anchors at depths of 1.5, 3.0, and 5.0 m. A fill is placed on the ground surface.

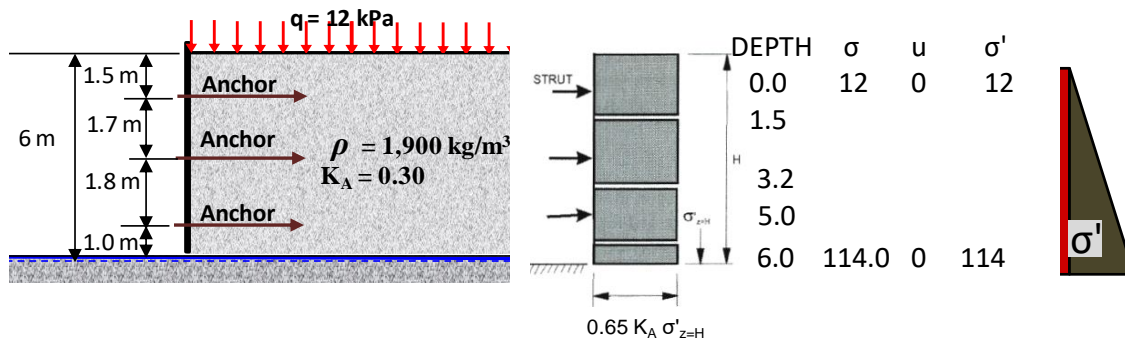


Fig. 5.11 Example

The total earth stress per metre of wall is:

$$\text{Total Earth Stress} = K_A h (\sigma'_{\text{ground}} + \sigma'_{\text{bottom}}) = 0.3 \times 6.0 \times (12 + 114)/2 = 113 \text{ KN}$$

$$\text{The force in each anchor} = 0.65 \times 113/3 = 25 \text{ KN}$$

As each row of anchors is installed as the excavation proceeds, it makes sense to prestress them to at least 1.5 times the expected force, i.e., to about 40 kN and, also, to have anchors that can take an overstress to about twice the expected force without breaking.

### 5.10 Collapse of shored trench

It is not always recognized that the shear force along the inside of the wall assists in reducing the strut force. Figure 5.12 shows an about 1.8 m deep trench excavated between two sheet pile walls shored up by one strut. The force vector diagram indicates the strut force. N.B., the force at the bottom of the trench is disregarded and the diagram is not to scale.

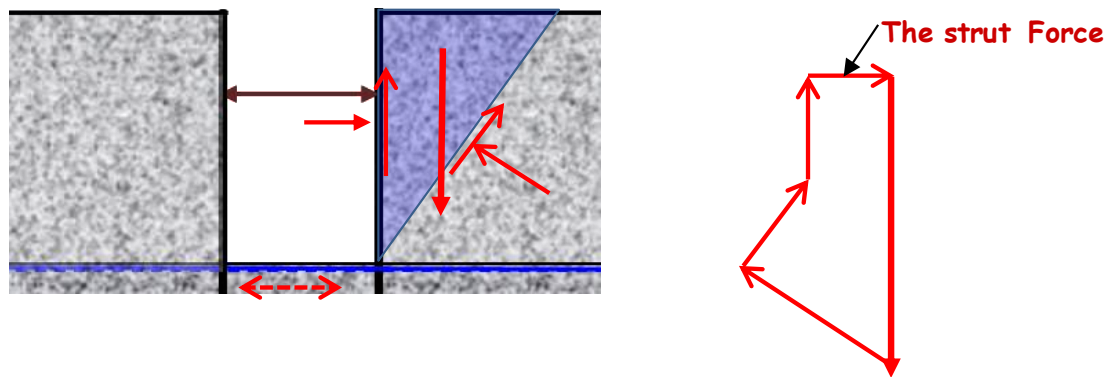


Fig. 5.11 A trench shored up with one strut and showing a force vector diagram of the forces

As indeed happened in a real case, assume that the excavator starts traveling with one track on the top of the sheet pile wall. In the real case, it was observed that this caused a small downward movement of the wall. Coincidentally, a couple of struts broke and the trench collapsed. Was the collapse really coincidental? Figure 5.12 shows a similar force vector diagram for the condition of the sheet piles moving downward.

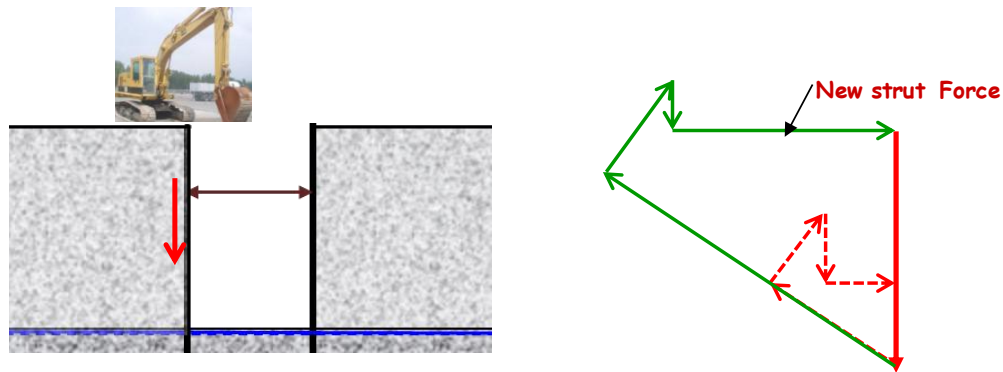


Fig. 5.12 The force vector diagram for when travels on top of the sheet pile wall

As suggested by the force vector diagram, when the shear force along the inside of the sheet pile wall reverted direction, the strut force increased significantly. In the illustrated case, the increase was sufficient to buckle the strut. The single twist of fate of the case is the unfortunate fact that the collapse took the life of one person who was in the trench at the location of the collapse.

## CHAPTER 6

### SHALLOW FOUNDATIONS

#### 6.1 Introduction

When Society started building structures imposing large concentrated loads onto the soil, occasionally, catastrophic failures occurred. Initially, the understanding of foundation behavior merely progressed from the lessons of one failure to the next. Later, much later, laboratory tests were run of model footings on different soils and the test results were extrapolated to the behavior of full-scale foundations by means of theoretical analysis. For example, loading tests on **model size footings** gave load-movement curves with a distinct peak value—a "bearing capacity failure"—agreeing with a theoretical analysis that the capacity (not the settlement) controlled the response of a footing to load. Such tests further suggested that the "bearing capacity" in terms of stress of a model footing in clay is independent of the footing size, while, in contrast, tests on model footings in sand resulted in "capacities" in terms of stress that increased with the footing size (see Section 6.10).

However, tests on **full-size footings** have shown that bearing capacity in terms of a specific ultimate resistance at which failure occurs, does not exist. It has been shown conclusively that the theoretical treatment of bearing capacity provides an incorrect picture of actual response of footings to load. The practicing design engineer is strongly advised against actually applying the formulas and relations presented. The details behind this recommendation are presented in Section 6.10. Sections 6.3 through 6.9 are only provided to present the historical or conventional approach—and in geotechnical engineering, as in other areas of Life, we have to recognize the lessons as learnt throughout history. I do not suggest that all formulas and relations would be correct.

#### 6.2 Inclined and Eccentric Loads

[Figure 6.1](#) shows a cross sections of two strip footings of equal width,  $B$ , subjected to vertical, concentric load,  $Q_v$ . The load on the left footing is just vertical. The load on the right footing has a horizontal component,  $Q_h$ . The applied contact stress,  $q$ , is stress per unit length ( $q = Q_v/B$ ) and it mobilizes a soil resistance,  $r$ .

However, loads on footings are normally inclined, as shown for the footing to the right; often also eccentric. Loading a footing eccentrically will reduce the stability of the footing. An off-center load will increase the stress (edge stress) on one side and decrease it on the opposing side. A large edge stress can be the starting point of a bearing failure. The edge stress is taken into account by replacing the full footing width ( $B$ ) with an effective footing width ( $B'$ ) in the bearing capacity formula (Eq. 6.1a; which assumes a uniform load). Failure occurs when edge stress exceeds the soil strength.

The effective footing width is the width of a smaller footing having the resultant load in its center. That is, the calculated stress decreases because of the reduced width ( $\gamma$ -component in Eq. 6.1) and the applied stress is increased because it is calculated over the effective area as  $q = Q/(B' L)$ . The approach is approximate and its use is limited to the requirement that the contact stress must not be reduced beyond a zero value at the opposite edge ("no tension at the heel"). This means that the resultant must fall within the middle third of the footing, that is, the eccentricity must not be greater than  $B/6$  (= 16.7 % of the footing width). [Figure 6.2](#) illustrates the difference in contact stress between a footing loaded within its middle third area as opposed to outside that area.

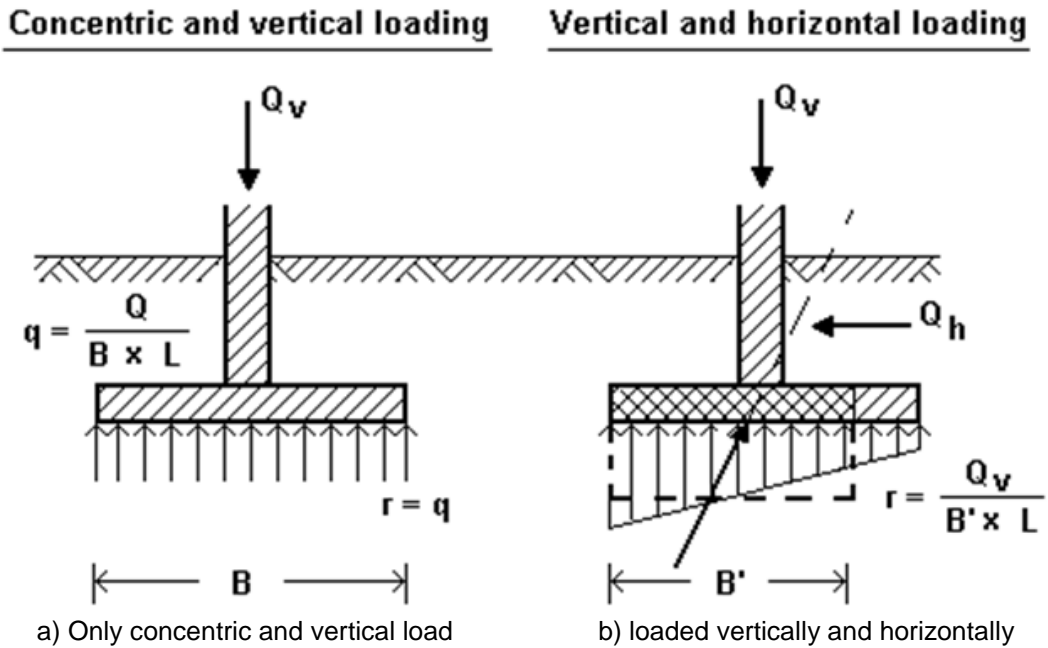


Fig. 6.1 A strip footing

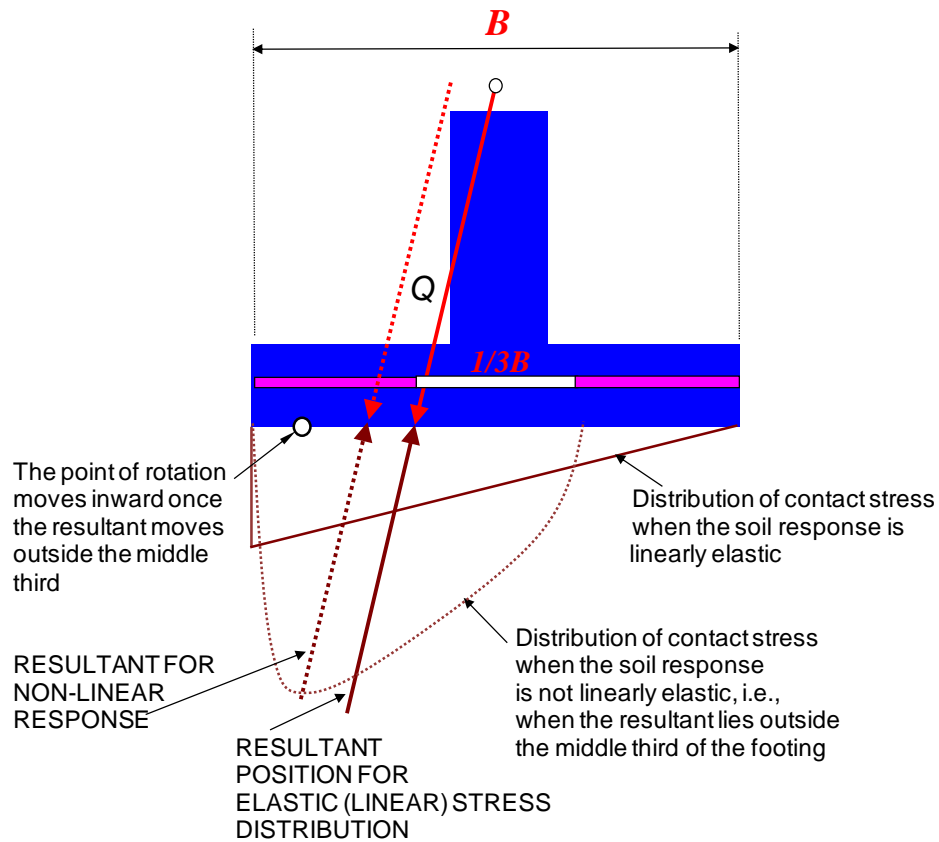


Fig. 6.2 Contact stress distributions when the resultant lies within the middle third and outside.

## 6.2 The Bearing Capacity Formula

Buisman (1935; 1940) and Terzaghi (1943) developed the “bearing capacity formula” given in Eq. 6.1 with details in Eqs. 6.2a through 6.2d. The premise of the formula is that the footing foundation has infinite length (“continuous”) and the load is vertical and concentric with the footing center line, the soil is homogeneous, and the ground surface is horizontal.

$$(6.1) \quad r_u = c' N_c + q' N_q + 0.5 B \gamma' N_\gamma$$

where

$r_u$	=	ultimate unit resistance of the footing
$c'$	=	effective cohesion intercept
$B$	=	footing width
$q'$	=	overburden effective stress at the foundation level
$\gamma'$	=	average effective unit weight of the soil below the foundation
$N_c, N_q, N_\gamma$	=	non-dimensional bearing capacity factors

When the groundwater table lies above or at the base of a footing, the effective unit weight,  $\gamma'$ , is the buoyant unit weight of the soil. When it lies below the base and at a distance equal to the width,  $B$ ,  $\gamma'$  is equal to the total unit weight. When the groundwater table lies within a distance of  $B$ , the value of  $\gamma'$  in Eq. 6.1a is equal to the average buoyant value. The formula as based on the model shown in Figure 6.3.

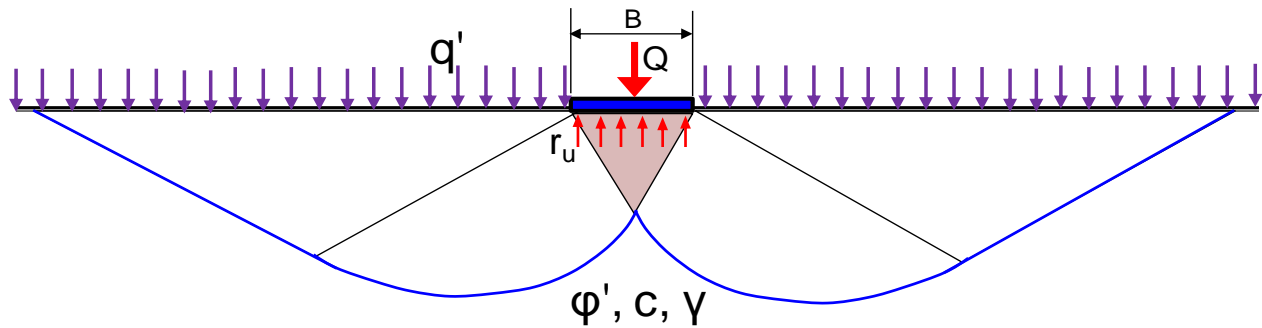


Fig. 6.3 The model for the Triple- $N$  Formula

The bearing capacity factors are a function of the effective friction angle of the soil. Notice, for friction angles larger than about  $37^\circ$ , the bearing capacity factors increase rapidly. The factors were originated by Buisman (1935; 1940) and Terzaghi (1943), later modified by Meyerhof (1951; 1963), Hansen (1961), and others. According to the Canadian Foundation Engineering Manual (1992), the bearing capacity factors, which are somewhat interdependent, are as follows.

$$(6.2a) \quad N_q = e^{\pi \tan \phi'} \left( \frac{1 + \sin \phi'}{1 - \sin \phi'} \right) \quad \phi' \rightarrow 0 \quad N_q \rightarrow 1$$

$$(6.2b) \quad N_c = (N_q - 1)(\cot \phi') \quad \phi' \rightarrow 0 \quad N_c \rightarrow \pi + 2 = 5.14$$

$$(6.2c) \quad N_\gamma = 1.5(N_q - 1)(\tan \phi') \quad \phi' \rightarrow 0 \quad N_\gamma \rightarrow 0$$

where  $\phi'$  = the effective internal friction angle of the soil

Terzaghi and many others refined the original coefficients of the "triple  $N$  formula", relying mainly on results of test on model footings. The range of published values for the  $N_q$ -coefficient is about 50 through about 600. (This wide range of the key parameter should have alerted the profession to that the pertinence of the formula is questionable. Indeed, it is amazing that the arbitrary nature of the  $N$ -coefficients has not long ago sent the formula to the place where it belongs—the museum of old paradigms whose time has passed).

Equation 6.2c is not the only one used for determining the  $N_\gamma$  bearing capacity coefficient. Eq. 6.2d, for example, is a commonly applied relation that was developed by Vesic (1973; 1975) by means of fitting a curve to a set of values from values in a table produced by Caquot and Kerisel (1953):

$$(6.2d) \quad N_\gamma = 2(N_q + 1)(\tan\phi) \quad \phi \rightarrow 0 \quad N_\gamma \rightarrow 0$$

Vesic (1975) presented a table listing the factors according to Eq. 6.1e ranging from  $0^\circ$  through  $50^\circ$ , which table is reproduced in the AASHTO Specifications (1992).

There are many other expressions in use for the  $N_\gamma$  bearing capacity factor. For example, the German code DIN 4017 uses  $N_\gamma = 2(N_q - 1)(\tan\phi)$  in its expression, that is, a “-” sign instead of a “+” sign (Hansbo 1994). For details, see Tomlinson (1980), Bowles (1988), and (Hansbo 1994).

#### 6.4 Inclination and Shape Factors

Combining a vertical load with a horizontal load, that is, inclining the resultant load, will also reduce the bearing capacity of a footing. The effect of the inclination is expressed by means of reduction factors called Inclination Factors,  $i$ . An inclination may have an indirect additional effect due to that the resultant to the load on most occasions acts off center, reducing the effective area of the footing.

Also the shape of the footing influences the capacity, which is expressed by means of reduction factors called Shape Factors,  $s$ . The bearing capacity formula is derived under the assumption of an infinitely long strip footing. A footing with finite length,  $L$ , will have a contribution of soil resistance from the footing ends. This contribution is what the shape factors adjust for, making the formula with its bearing capacity factors applicable also to rectangular shaped footings. Notice, Eq. 6.3 does not include Depth Factors. However, many will consider the depth of the footing by including the overburden stress,  $q'$ .

Thus, to represent the general case of a footing subjected to both inclined and eccentric load, Eq. 6.1a changes to Eq. 6.2.

$$(6.3) \quad r_u = s_c i_c c' N_c + s_q i_q q' N_q + s_\gamma i_\gamma 0.5B \gamma' N_\gamma$$

where factors not defined earlier are

$$\begin{aligned} s_c, s_q, s_\gamma &= \text{non-dimensional shape factors} \\ i_c, i_q, i_\gamma &= \text{non-dimensional inclination factors} \\ B' &= \text{equivalent or effective footing width} \end{aligned}$$

When the load is offset from the center of the footing toward the long side, the L-side, rather than toward the short side, the B-side, the bearing stress is assumed to act over a footing area of  $B$  times  $L'$ . When the



resultant is eccentric in the directions of both the short and long sides of the footing, the effective area according to the Ontario Highway Bridge Design Code (1991) takes the shape of a triangle with the resultant in its centroid. In contrast, the AASHTO Specifications (1992) defines the effective area as a rectangle with sides  $B'$  and  $L'$ .

As long as the resultant falls within the middle third of the footing width, it can acceptably be assumed that the stress distribution below the footing is approximately linear. However, when the resultant moves beyond the third point, that is, closer to the edge of the footing, not only does the edge stress increase rapidly, the assumption of linearity is no longer valid. The requirement of having the resultant in the middle third is, therefore, very important in the design. In fact, if the resultant lies outside the middle third, the adequacy of the design becomes highly questionable. See also Section 6.6.

The shape factors are given in Eqs. 6.4a through 6.3k.

$$(6.4a) \quad s_c = s_q = 1 + \frac{B'}{L'} \frac{N_q}{N_c}$$

$$(6.4b) \quad s_\gamma = 1 - 0.4 \frac{B'}{L'}$$

where  $B'$  = equivalent or effective footing width

$L'$  = equivalent or effective footing length

According to the Canadian Foundation Engineering Manual (1992) and the OHBDC (1991), the inclination factors are:

$$(6.4c) \quad i_c = i_q = \left(1 - \frac{\alpha}{90^\circ}\right)^2$$

$$(6.4d) \quad i_\gamma = \left(1 - \frac{\alpha}{\phi'}\right)^2$$

where  $\alpha$  = the inclination of the resultant (angle to the vertical)

$\phi'$  = the effective internal friction angle of the soil

As for the case of the bearing capacity factor  $N_\gamma$ , different expressions for the inclination factor  $i_\gamma$  are in use. Hansen (1961) proposed to use

$$(6.4e) \quad i_\gamma = \left(1 - \frac{P}{Q + B' L' c' \cot \phi'}\right)^2$$

where  $P$  = the horizontal resultant to the forces  
 $Q$  = the vertical resultant to the forces  
 $c'$  = effective cohesion intercept  
 $\phi'$  = effective friction angle  
 $B'$  = equivalent or effective footing width  
 $L'$  = equivalent or effective footing length

Vesic (1975) proposed to use an expression similar to Eq. 6.4e, but with an exponent “m” instead of the exponent of “2”, where m is determined as follows:

$$(6.4f) \quad m = \frac{2 + \frac{L}{B}}{1 + \frac{L}{B}}$$

The AASHTO Specifications (AASHTO 1992) includes a somewhat different definition of the inclination factors, as follows:

$$(6.4g) \quad i_c = i_q - \frac{1 - i_q}{N_c \tan \phi'} \quad \text{for } \phi' > 0$$

$$(6.4h) \quad i_c = 1 - \frac{nP}{B' L' c' N_c} \quad \text{for } \phi' = 0$$

$$(6.4i) \quad i_q = 1 - \frac{nP}{\theta + B' L' c' \cot \phi'}$$

$$(6.4j) \quad i_\gamma = 1 - \frac{(n+1)P}{\theta + B' L' c' \cot \phi'}$$

The factor “n” is determined as follows:

$$(6.4k) \quad n = \frac{2 + L'/B'}{1 + L'/B'} \cos^2 \theta + \frac{2 + B'/L'}{2 + B'/L'} \sin^2 \theta$$

where  $\theta$  = angle of load eccentricity (angle of the force resultant with the long side of the footing)  
 $B'$  = equivalent or effective footing width  
 $L'$  = equivalent or effective footing length

Notice, all the above inclination factors as quoted from the various sources can result in values that are larger than unity. Such a calculation result is an indication of that the particular expression used is not valid.

Many textbooks present a basic formulae multiplied with influence factors for shape and inclination of the resultant. These influence factors are calculated from formulae similar to the ones listed above and are often to be determined from nomograms as opposed to from formulae. They may also include considerations of stress distribution for different shapes (or with separate influence factors added). Such influence factors are from before the advent of the computer, when calculations were time-consuming.

### 6.5 Overturning

Frequently, one finds in text books and codes that the stability of a footing is expressed as an overturning ratio: “Factor-of-Safety against overturning”. This is the ratio between rotating moment around the toe of the footing taken as the quotient between the forces that try to topple (overturn) the footing and the forces that counteract the overturning. Commonly, the recommended “factor-of-safety against overturning” is 1.5. However, while the ratio between the calculated moments may be 1.5, the Factor of Safety,  $F_s$ , is not 1.5. For the factor of safety concept to be valid, a value of  $F_s$  close to unity must be possible, which is not the case when the resultant moves beyond the third point. For such a situation, the combination of increasing edge stress and progressively developing non-linearity causes the point of rotation to move inward (see Figure 6.3). At an overturning ratio of about 1.2, failure becomes imminent. Ballerinas dance on toe, real footings do not, and the overturning ratio must not be thought of as being the same as a factor of safety. **Safety against overturning cannot be by a factor of safety. It is best guarded against by keeping the resultant inside the middle third of the footing.**

Indeed, many failures ostensibly claimed to be confirming a collapse per the bearing capacity triple-N formula, are instead due to the force resultant moving past the third point due to one side of the footing settling more than the other sides; the foundation start to tilt. Tall structures on raft foundations are particularly prone to this.

### 6.6 Sliding

The calculation of a footing stability must include a check that the safety against horizontal sliding is sufficient. The calculation is simple and consists of determining the ratio between the sum of the horizontal resistance and the sum of all horizontal loads,  $\Sigma R_h / \Sigma Q_h$  at the interface between the footing underside and the soil. This ratio is taken as the factor of safety against sliding. Usually, the safety against sliding is considered satisfactory if the factor of safety lies in the range of 1.5 through 1.8. The horizontal resistance is made up of friction ( $\Sigma Q_v \tan \phi'$ ) and cohesion components ( $c'BL$ ).

### 6.7 Combined Calculation of a Retaining Wall and Footing

Figure 6.4 illustrates the general case of earth stress acting on a ‘stubby’ cantilever wall. The bearing capacity of the footing has to consider loads from sources not shown in the figure, such as the weight of the wall itself and the outside forces acting on the wall and the soil. The earth stress governing the structural design of the wall (P1) is determined from the product of the active earth stress coefficient ( $K_a$ ) and the effective overburden stress. The calculations must consider the soil internal friction angle ( $\phi$ ), inclination of the wall ( $\beta$ ), wall friction ( $\tan \delta$ ), as well as sloping of the ground surface ( $\alpha$ ). When the heel of the footing and/or the ground surface are sloping, the average height (H1) is used in the calculation of the effective overburden stress used for P1, as shown in the figure. Notice, many codes postulates that the backfill soil nearest the wall stem may not relax into full active condition. These codes therefore require a larger earth stress coefficient (closer to  $K_0$ ) in the calculation of the earth stress acting directly on the stem. The vertical component of the earth stress is often disregarded because including it would necessitate the corresponding reduction of the weight of the soil resting on the base.

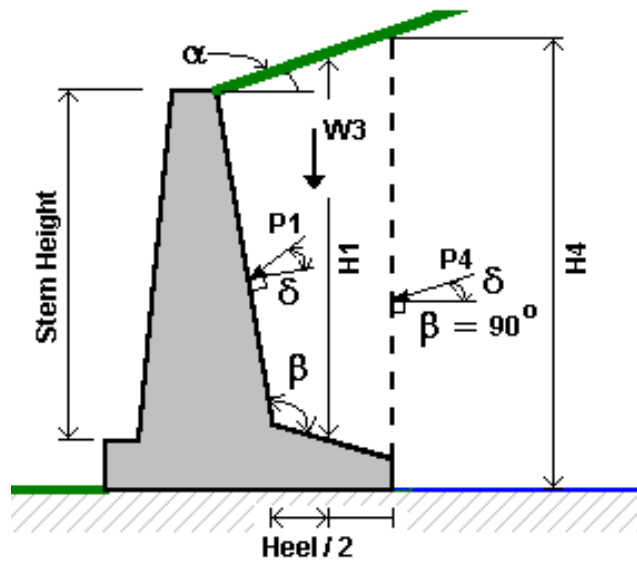


Fig. 6.4 Example of forces acting on a cantilever wall

The geotechnical design for bearing capacity and overturning requires the calculation of the resultant of all loads acting on a free body comprised by the wall and footing and the soil resting on the heel. The earth stress (P4) to include in the calculation of the force resultant acts against the boundary of the free body, which is a normal rising from the heel, that is, its earth stress coefficient is determined from a  $\beta$  equal to  $90^\circ$ . Notice also that the height of the normal (H4) is used in determining the overburden stress applied in calculating P4.

In contrast to the case for the earth stress against the stem, the earth stress acting on the normal from the heel should be calculated disregarding wall friction in the soil (Tschebotarioff 1978).

In summary, the design for capacity of a footing consists of ensuring that the factors of safety on bearing capacity of a uniformly loaded equivalent footing and on sliding are adequate, and verifying that the edge stress is not excessive.

## 6.8 Numerical Examples

### 6.8.1 Example 1

Calculate the factor of safety against bearing capacity failure for a 5-ft square spread footing placed at a depth of 2 ft below ground well above the groundwater table and loaded by 76 kips. The soil consists of sand with a 121 pcf total density,  $\rho_t$ . Cohesion,  $c'$ , is zero.

The working stress is 4.75 ksf, the effective stress,  $q'$ , at the foundation depth is 242 psf, and the bearing capacity factors,  $N_q$ , and  $N_\gamma$  are 21 and 19, respectively. Because the footing is square, shape factors apply:  $s_{q, square} = 1.6$  and  $s_{\gamma, square} = 0.6$ . The calculated  $r_u$  is 15.45 ksf and the factor of safety,  $F_s$ , is  $(15.45 - q')/4.75 = 3.2$ . The more logical approach would be to add the  $q'$  to the applied stress. However, this would only make a decimal change to  $F_s$  for the example, as for most cases.

A factor of safety of 3 or larger would for most imply a design with a solid safety against an undesirable outcome. However, the question of safe or not safe does not rest with the issue of capacity, but with the deformation—settlement—of the footing. If the sand in the example has a Janbu modulus number of, say, 100 and is essentially elastic in response ( $E = 200$  ksf), then the settlement of the footing for the load will be about 0.9 inch, which probably would be an acceptable value. However, if the sand deposit is not 5 ft thick below the footing but 30 ft, then the calculated settlement (Boussinesq distribution) would increase by about 30 % and perhaps approach the limit of acceptance. The calculated bearing capacity would not change however.

### 6.8.2 Example 2

The bearing capacity calculations are illustrated in a numerical example summarized in Figure 6.5. The example involves a 10.0 m long and 8.0 m high, vertically and horizontally loaded retaining wall (bridge abutment). The wall is assumed to be infinitely thin so that its weight can be neglected in the calculations. It is placed on the surface of a ‘natural’ coarse-grained soil and a coarse material (backfill) is placed behind the wall and over the toe area. A 1.0 m thick fill is placed in front of the wall and over the toe area. The groundwater table lies close the ground surface at the base of the wall and the ground surface is horizontal.

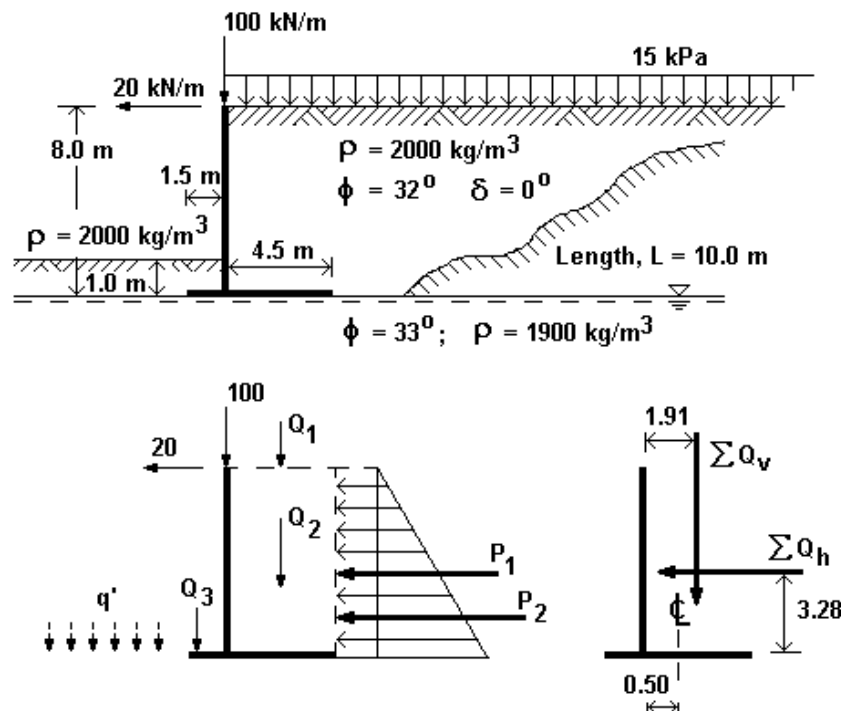


Fig. 6.5 Cantilever wall example (Fellenius 1995)

In any analysis of a foundation case, a free-body diagram is necessary to ensure that all forces are accounted for in the analysis, such as shown in Figure 6.5. Although the length of the wall is finite, it is normally advantageous to calculate the forces per unit length of the wall (the length,  $L$ , then only enters into the calculations when determining the shape factors).

The vertical forces denoted  $Q_1$  and  $Q_2$  are loads on the base (heel portion).  $Q_1$  is from the surcharge on the ground surface calculated over a width equal to the length of the heel.  $Q_2$  is the weight of the soil on the heel. The two horizontal forces denoted  $P_1$  and  $P_2$  are the active earth stress forces acting on a fictitious wall rising from the heel, which wall is the boundary of the free body. Because this fictitious wall is soil, it is commonly assumed that wall friction does not occur (Tschebotarioff, 1978).

Because of compaction of the backfill and the inherent stiffness of the stem, the earth stress coefficient to use for earth stress against the stem is larger than that for active stress. This earth stress is of importance for the structural design of the stem and it is quite different from the earth stress to consider in the stability analysis of the wall.

Figure 6.5 does not include any passive earth stress in front of the wall, because this front wall earth stress is normally neglected in practice. The design assumes that movements are large enough to develop active earth stress behind the wall, but not large enough to develop fully the passive earth stress against the front of the wall. Not just because the passive earth stress is small, but also because in many projects a more or less narrow trench for burying pipes and other conduits is often dug in front of the wall. This, of course, eliminates the passive earth stress, albeit temporarily.

Calculations by applying the above quoted equations from the Canadian Foundation Engineering Manual (CFEM 1985) result in the following.

$$\begin{aligned}
 \phi' &= 32^\circ \implies I = 0.307 & K_p &\text{ is assumed to be zero} \\
 \phi' &= 33^\circ \implies N_q = 26.09 & N_c &= 38.64 \quad N_\gamma = 25.44 \\
 i_q &= i_c = 0.69 & i_\gamma &= 0.28 & s_q = s_c = 1.34 & s_\gamma = 0.80 \\
 e &= 0.50 \text{ m} & B' &= 5.0 \text{ m} & r_u &= 603 \text{ kPa} & q &= 183 \text{ kPa} \\
 F_s\text{-bearing} &= 3.29 & F_s\text{-sliding} &= 2.35 & \text{Overturning ratio} &= 3.76
 \end{aligned}$$

The design calculations show that the factors of safety (see Chapter 10) against bearing failure and against sliding are 3.29 and 2.35, respectively. The resultant acts at a point on the base of the footing at a distance of 0.50 m from the center, which is smaller than the limit of 1.00 m. Thus, it appears as if the footing is safe and stable and the edge stress acceptable. However, a calculation result must always be reviewed in a “*what if*” situation. That is, what if for some reason the backfill in front of the wall were to be removed? Well, this seemingly minor change results in a reduction of the calculated factor of safety to 0.90. The possibility that this fill is removed at some time during the life of the structure is real. Therefore, despite that under the given conditions for the design problem, the factor of safety for the footing is adequate, the wall structure may not be safe.

### 6.8.3 Example 3

A very long footing will be constructed in a normally consolidated sand (dimensions and soil parameters are shown in Figure 6.6). The resultants to all vertical and horizontal forces are denoted V and H, respectively and act along lines as shown. The counteracting resultant to all activating forces is denoted R. The sand deposit is 9 m thick and followed by bedrock.

- A. Is the resultant within the middle third?
- B. Calculate the factor of safety,  $F_{s, bearing}$ , according to the Bearing Capacity Formula
- C. Calculate the factor of safety,  $F_{s, sliding}$
- D. Calculate the settlement of the footing. Assume that the modulus number indicated in the figure covers both immediate and long-term settlement. Use stress distribution per the 2V:1H-method.

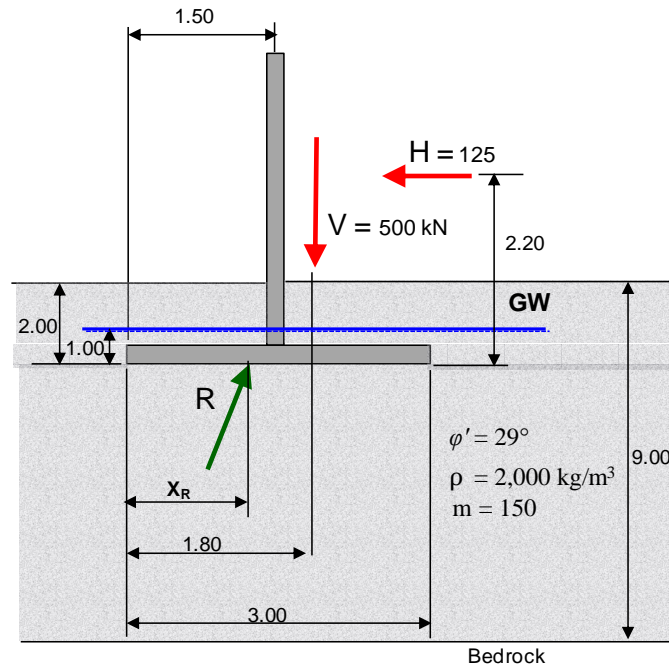


Fig. 6.6 Continuous footing in sand (calculations per metre length)

Determine first the location of the resultant, i.e., its distance,  $x_R$ , from the left side of the footing, by taking static moment over the footing side.

$$1.80V - 2.20H = x_R V \implies 1.80 \cdot 500 - 2.20 \cdot 125 = x_R \cdot 500 \implies x_R = 1.25 \text{ m from the toe (side)}$$

A. The middle third limit is 1.00 m from the footing side, so the resultant lies within the middle third.

B. The Bearing Capacity Formula:  $r_u = q' N_q + 0.5 B' \gamma' N_\gamma$

$$q' = \sigma'_{z=2.00} = 2.0 \cdot 20 - 1.0 \cdot 10 = 30 \text{ kPa}$$

$$N_q = 16 \quad N_\gamma = 13 \quad \gamma' = 20 - 10 \quad B' = 2x \quad x_R = 2.50 \text{ m}$$

$$r_u = 30 \cdot 6 + 0.5 \cdot 2.5 \cdot 10 \cdot 13 = 643 \text{ kPa}$$

$$q_{\text{applied}} = V/B' = 500/2.5 = 200 \text{ kPa}$$

$$F_{s, \text{bearing}} = 643/200 = 3.21$$

C. The sliding force is  $H = 125 \text{ kN}$

The shear resistance is  $V \tan \phi' = 500 \cdot 0.50 = 250$

$$F_{s, \text{sliding}} = 250/125 = 2.0$$

D. Determine the effective stress at initial condition,  $\sigma'_0$ , and add the 2(V):1(H) or Boussinesq distribution from the 500-kN stress over the  $B'$  area ( $= 200 \text{ kPa}$ ) to obtain  $\sigma'_1$ . Use the basic relations in Chapter 3 for strain and settlement ( $s = \Sigma (\epsilon \Delta H)$ ) to find the total settlement for the footing. Table 6.1 shows the calculations as carried out using UniSettle software (immediate and secondary compressions are excluded)

**TABLE 6.1 Calculations of stress and settlement distributions**

Depth (m)	Initial Condition			2:1			Boussinesq		
	Total Stress (kPa)	Pore Pressure (kPa)	Initial Eff. Stress (kPa)	Footing Stress (kPa)	Final Eff. Stress (kPa)	Total, S Sttlmnt (mm)	Footing Stress (kPa)	Final Eff. Stress (kPa)	Total, S Sttlmnt (mm)
0.0	0	0	0	0	0	44.5	0.0	0.0	45.6
1 (GW)	20	0	20	0	20	44.5	0.0	20.0	45.6
2.0	40	10	30	200	230	44.5	200.0	230.0	45.6
3.0	60	20	40	142.8	182.8	32.6	176.2	216.2	33.3
4.0	80	30	50	111.1	161.1	23.7	128.4	178.4	23.4
5.0	100	40	60	90.9	150.9	16.8	95.5	155.5	16.0
6.0	120	50	70	76.9	146.9	11.2	74.8	144.8	10.4
7.0	140	60	80	66.6	146.6	6.8	61.2	141.2	6.1
8.0	160	70	90	58.8	148.8	3.1	51.6	141.6	2.7
9.0	180	80	100	52.6	152.6	0.0	44.6	144.6	0.0

The settlement calculations could also be for the stress distributed over the full 3.0 m width, B, applying, either an average uniformly distributed stress (167.7 kPa), or considering the fact that the stress along one side is larger than along the other because of the horizontal load. Either way, the stress distribution should then have to be with the Boussinesq method, which would result in about 26 mm of calculated average settlement, as opposed to the 46 mm for the B'-width shown in table 6.1 (regarding the characteristic point; see Section 1.9). Obviously for simple cases, such as of the example case, the accuracy offered by a sophisticated calculation is often not true. (Table 6.1 and this paragraph are amended).

### 6.9 Presumptive Stress

Frequently, footing designs based on a so-called presumptive-stress approach that applies certain, intentionally conservative working stress values governed by assessment of the soil profile and the local geology at the site according to the local practice of the geology. Table 6.2 present a typical such an array of values.

**TABLE 6.2 Presumed Stress**

Soil Type	Condition	Presumed Stress	
Clay	Stiff to hard	300 to 600	kPa
	Stiff	150 to 300	kPa
	Firm	75 to 150	kPa
	Soft	<75	kPa
Sand	Dense	>300	kPa
	Compact	100 to 300	kPa
	Loose	<100	kPa
Sand + Gravel	Dense	>600	kPa
	Compact	200 to 600	kPa
	Loose	<200	kPa
Shale, sound sedimentary rock	Medium strength	3	MPa
	Weak to medium	1 to 3	MPa
	Very weak	0.5	MPa



## 6.10 Words of Caution

Some words of caution: Footing design must emphasize settlement analysis. The bearing capacity formula approach is, mildly put, very approximate and should never be taken as anything beyond a simple estimate for purpose of comparing a footing design to previous designs. Most current codes and standards put an unrealistic reliance on the formula, which is made worse by the modern trend toward LFRD or ULS applying partial factors of safety (or resistance factors) to the various parameters.

The bearing capacity formula applies best to the behavior of small model footings in dense sand. When used to simulate applying load to actual, real-life footings, the formula's relevance is very much in question. Full-scale tests show that no clear ultimate value can be obtained even at very large deformations (unless the loading rate is such that excess pore pressure cannot dissipate in time but accumulate). When critical state soil mechanics came about (Roscoe et al. 1958, advancing the concept proposed by Casagrande 1935), the reason for the model tests reaching an ultimate value became clear: Model tests affect only the soil to shallow depth, where even the loosest soil behaves as an overconsolidated soil. That is, in loading, after some initial volume change, the soil first dilates and then contracts resulting in a stress-deformation curve that implies an ultimate resistance (e.g., Been and Jefferies 1991, Altaee and Fellenius 1994).

Figure 6.7 presents results from loading tests performed by Ismael (1985) on square footings with sides of 0.25 m, 0.50 m, 0.75 m, and 1.00 m at a site where the soils consisted of fine sand 2.8 m above the groundwater table. The sand was compact, as indicated by a N-index equal to 20 blows/0.3 m. The footings were placed at a depth of 1.0 m. The measured stress-movement behavior of the footing is shown in the left diagram. The middle diagram, stress versus movement, shows that, at equal stress, the larger the footing the larger the movement. The diagram to the right shows the data plotted as stress versus relative movement, i.e., the measured movement divided by the footing side. Notice that the curves are gently curving having no break or other indication of failure despite relative movements as large as 10 % to 15 % of the footing side.

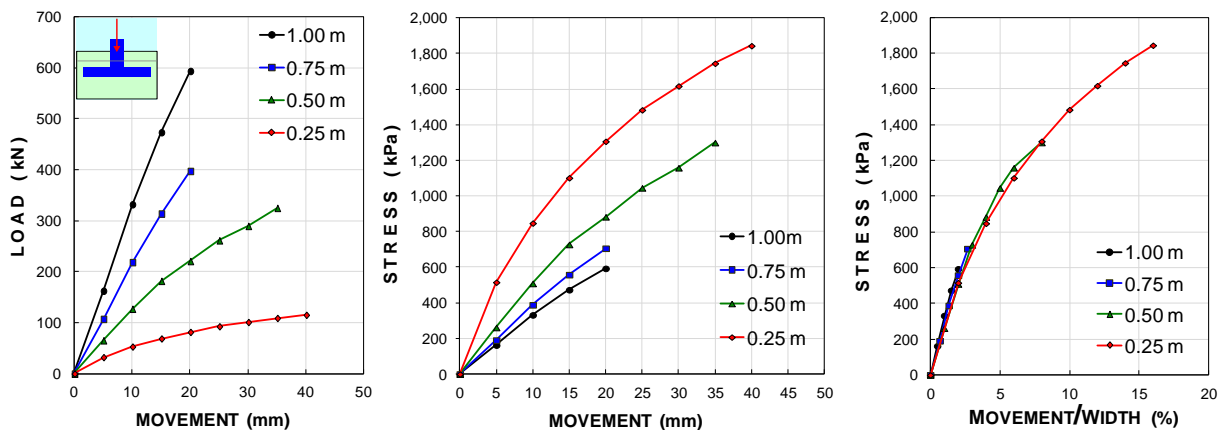


Fig. 6.7 Results of static loading tests on square footings in well graded sand (Data from Ismael, 1985)

Loading a footing in cohesive soil will generate pore pressures and a subsequent consolidation process during the dissipation. The soil layers below a footing conditions are rarely absolutely uniform in compressibility and layer thickness, which means that the consolidation settlement will vary across the footings and the structure will tilt toward the side where the settlement is the largest. The tilting will move the resultant toward that site, which in turn will increase the settlement and tilt and might increase to pore pressures until the footing fails, ostensibly as a bearing capacity failure, but in reality a result of excessive and settlement and gradually increasing stress applied to the foundation side.

Similar static loading tests on square footings placed at a depth of 0.8 m in sand were performed by Briaud and Gibbens (1994) and Briaud et al. (1999) in a slightly preconsolidated, silty fine sand well above the groundwater table (also presented in Section 3.14.1). The natural void ratio of the sand was 0.8. The footing sides were 1.0 m, 1.5 m, 2.0 m, and 3.0 m. Two footings were of the size 3.0 m. The results of the test are presented in Figure 6.8, which, again, shows no indication of failure despite the large relative movements. (The normalized curves fit a q-z function coefficient of 0.4 for both case records, see Chapter 8).

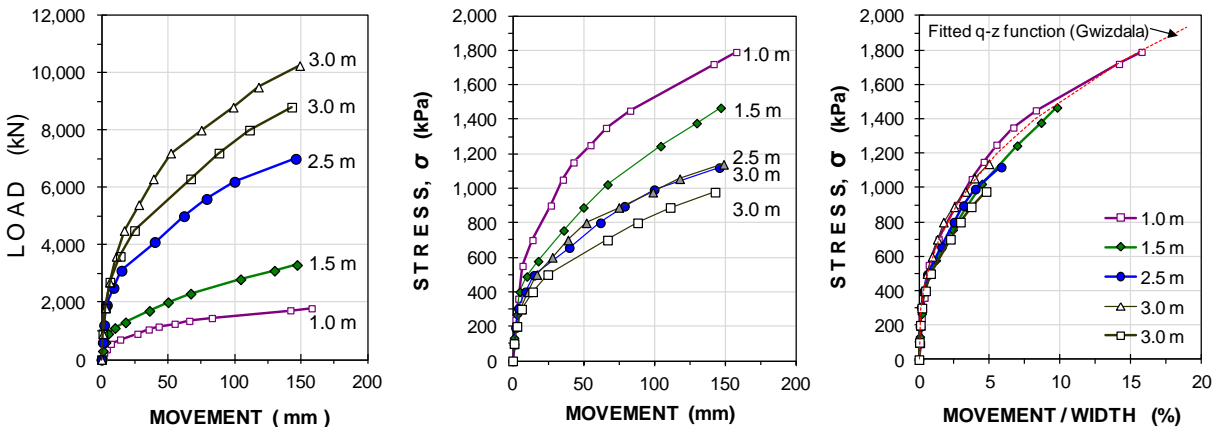


Fig. 6.8 Results of static loading tests on square footings in well graded sand  
(Data from Briaud and Gibbens 1994)

The indisputable fact is that bearing capacity of a real-size footing does not really exist. The concept of capacity is a condition associated with shear failure. However, in contrast to a body sliding against a soil (the case of a footing sliding along its base or of shaft resistance when a pile slides against the soil), the movement of soil body affected by the applied load is governed by deformation characteristics of the soil and the fact that the affected soil body increases for each load applied. That is, the volume of soil involved changes all through the loading. When the basic concept for a response is wrong, simply, any interpretation of the results based on that concept is also wrong!

The foregoing two tests and several others available in the literature, e.g., Fellenius (2009; 2011) show conclusively that bearing failure, i.e., capacity or ultimate resistance, does not exist for a normal loading case. (Fellenius 2016). As mentioned, the exception is in clays when the imposed loading is rapid enough to generate pore pressures and uneven settlement, and when the soil is preconsolidated so the loading generates negative pore pressures and failure occurs when the pore pressures return to normal values.

The fallacies of the bearing capacity formula notwithstanding, the formula is frequently applied to current foundation designs and most building codes, handbooks, and guidelines recommend its use. Therefore, applying the bearing capacity formula to routine designs is still considered within the accepted standard of care. Moreover, there is a fundamental difference between the movements recorded in a loading test and the settlement of a footing for a long-term unchanging load. This should be recognized and a footing design, therefore, should be based on deformation analysis, not on capacity.

Finally, the design must consider the construction of the footing. The footing base must be prepared so it is "undisturbed": free of remolded and loosened soils and not affected by running water or freezing. If the foundation level is raised, the backfill must be engineered, that is, be compacted to a satisfactory density.

## CHAPTER 7

### STATIC ANALYSIS OF PILE LOAD-TRANSFER

#### 7.1 Introduction

Where placing a structure on a shallow foundation would mean unacceptable settlement, or where scour and other environmental hazards exist that could impair the structure in the future, a deep foundation needs to be used. Deep foundations are usually piled foundations, that is, foundations supported on piles installed by driving, pushing ("jacked-in" or "pressed-in"), or constructed in-situ (bored piles, cast-in-situ piles, drilled-shafts, caissons, augercasts, buried, etc.—it's a sweet child that has many names), to competent soils through soft, compressible soil layers. Piles can be made of wood, concrete, or steel, or of composite materials, such as concrete-filled steel pipes or an upper concrete section connected to a lower wood, steel, or helical section, or open or closed cross sections such as pipe pile, H-piles, or helical piles. They can be round, square, hexagonal, octagonal, rectangular (e.g., "barrettes"), even triangular, and straight-shafted, step-tapered, or conical. They can be short or long, or slender or stubby. In order to arrive at a reliable design, all the particulars of the pile must be considered together with the soil data, including also whether it primarily is shaft bearing or toe bearing, whether it is a single pile or one in a group of piles and, then, whether it is an interior or perimeter pile, its method of construction, etc.

Analysis using undrained shear strength (so-called  $\alpha$ -method), is a stress-independent method that has limited application, because it does not recognize that the load transfer between a pile and the soil is governed by effective stress behavior (i.e., the pile resistance is proportional to the effective overburden stress). Piles socketed into rock would be an exception. Therefore, an effective stress analysis (also called  $\beta$ -method) is the preferred method. Sometimes, the  $\beta$ -method includes an adhesion (effective cohesion intercept) component. The adhesion component is normally not applicable to driven piles, but may sometimes be useful for bored piles. The " $\alpha$ - and  $\beta$ -methods", usually refer to shaft resistance, specifically. The stress-independent method is often termed "total stress method" which is a misnomer; originating in coupling the name to the alternative analysis method, the effective-stress method, mistakenly leading to using the term "total stress" as a counter to the term "effective stress".

Design of a piled foundation for axial load starts with an analysis of how the load is transferred to the soil, too often thought limited to determining only a pile "capacity", sometimes separating the "capacity" on ultimate components of shaft and toe resistances. (The "capacity" is a very imprecise concept, which is why I here write the term inside quotation marks). The load-transfer analysis is often called static analysis or, quite inappropriately, "capacity" analysis. The load-transfer analysis is a necessary part of a settlement analysis, because settlement analysis of a piled foundation cannot be separated from how the load from the structure is, or is to be, transferred to the soil.

All foundation design methods are primarily based on empirical correlations, of course, whether by use of  $\alpha$ -or  $\beta$ -methods. Any case analyzed by the  $\alpha$ -method can also be analyzed by the  $\beta$ -method. However, I have seen cases where an effective stress method analysis ( $\beta$ -coefficients), matched to the results of a static loading test, also matched the reduced resistance of a same toe-depth pile tested after the site had been excavated resulting in reduced effective stress. In contrast, an analysis by the  $\alpha$ -method matched to the results of the first static loading test would not match the softer response of the second test.

In bedrock, which is a cohesive material, the  $\alpha$ -method is usually employed, as the shaft shear is mostly a function of the bond between the pile shaft and the rock surface, which in sound bedrock is not proportional to overburden stress. However, in weathered (decomposed) bedrock consisting of a conglomerate of rock pieces in a matrix of soil, the shaft resistance is indeed proportional to the surrounding effective stress, usually, in-turn, proportional to the overburden stress.

Whether shaft resistance is analyzed in terms of  $\alpha$ -method or  $\beta$ -method, design analysis usually centers around ultimate resistance. This is not a useful approach, however, the analysis by either method should refer to resistance for a specific movement, not an ultimate condition. Specifically so when no clear definition the ultimate condition is included.

This chapter addresses theoretical analysis. However, the principles of the analyses are correlated to results of actual field tests, i.e., to reality—analysis of load transfer for piles cannot be removed from reference to good experience, direct or indirect.

## 7.2 Static Analysis

Static analysis of axial pile response involves considering the load—sustained (dead) and transient (live)—applied to the head of a pile and transferred to the soil by means of shaft and toe resistance as indicated in Figure 7.1.

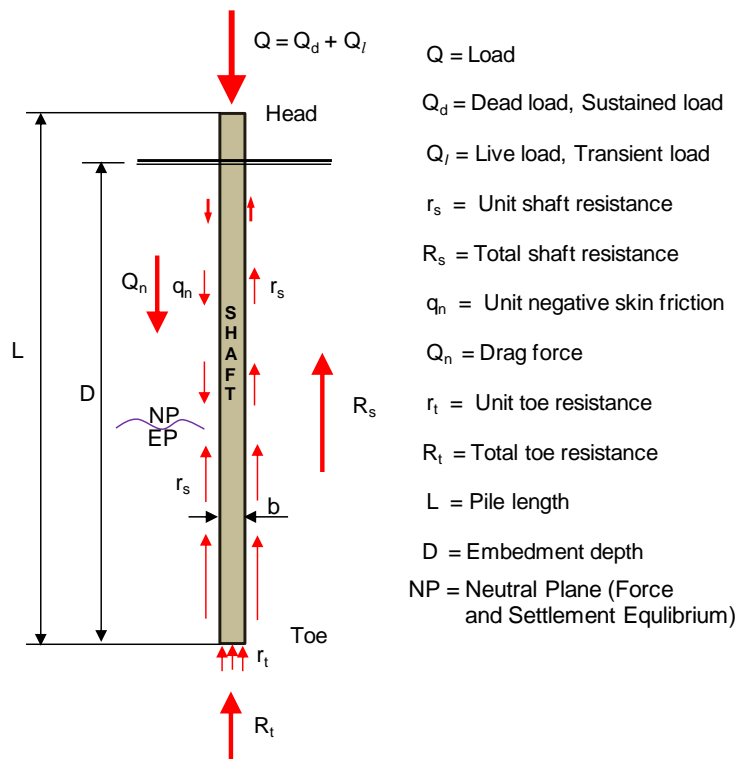


Fig. 7.1 Transfer of load to a pile and from the pile to the soil

Not shown in the figure, but intimately associated with the resistance indicated by the arrows, is the movement associated with the load-transfer. This will be addressed in Chapter 8.

### 7.2.1 Shaft resistance

**The Beta Method.** The general numerical relation for the unit shaft resistance,  $r_s$ , of a short pile element is

$$(7.1a) \quad r_s = \beta \sigma'_z$$

where  $\beta$  = Bjerrum-Burland coefficient (or "effective-stress proportionality-coefficient").  
 Note, as applicable to the specific movement considered  
 $\sigma'_z$  = effective overburden stress

Eq. 7.1a expresses that unit shaft resistance is directly proportional to the effective overburden stress (for the specific relative movement). This proportionality is qualitatively correct, though it is a simplified approach and disregards rotation of principal stresses, shear angle, break-up of cementation, creep, and many other aspects.

The input of unit shaft resistance is usually thought of being that for ultimate resistance. But, the relation is true for any induced movement between the surface of the pile element and the soil and there's no need to consider it only applicable to ultimate conditions. Indeed, Eq. 7.1a presumes a specific relative movement between the pile. Therefore, the shear resistance must always refer to the particular relative movement between a pile element and the adjacent soil. Again, the principles here presented are valid also for condition other than defined as representing the "ultimate".

When the Eq. 7.1a-relation refers to ultimate resistance, the resistance is often presumed to be plastic for movements beyond a maximum or peak value. However, in most soils, the shaft resistance does change also with movement beyond that at for an ultimate resistance (as defined by some definition or other; c.f., Section 8.2). It usually increases, but, sometimes, it also decreases (strain-hardening and strain-softening response, respectively; c.f., Section 8.11).

Figure 7.2 shows back-calculated unit shaft-shear vs. movement for two pile elements along a pile (i.e., measured at gage levels at two separate depths in an instrumented pile subjected to a static loading test). For "plastic response", the resistance became constant after a small initial movement. It can obviously be considered to represent an ultimate value independent of movement and it is what most persons assume for analysis of assuming ultimate conditions. However, actual resistance response is mostly represented the strain-hardening response shown in the graph to the right or by strain-softening response, c.f., Section 8.5 and Figure 8.9. In regard to toe resistance, the strain-hardening governs. Only in special circumstances will a toe response show a plastic response. The resistance-movement curves are called  $t$ - $z$  (for shaft resistance) and  $q$ - $z$  (for toe resistance).

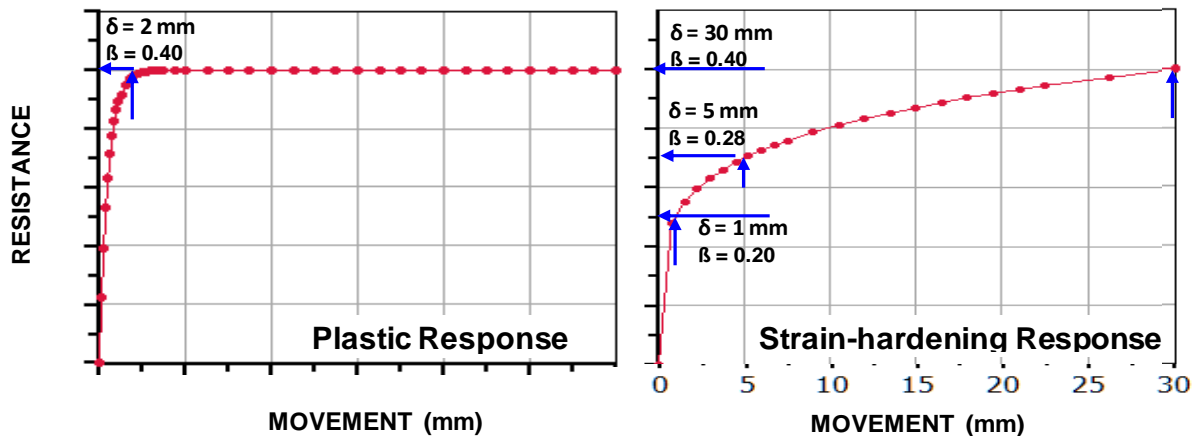


Fig. 7.2 Resistance of a pile element vs. relative movement between pile and soil

The interaction between the pile surface and the soil occurs in a zone or band around the pile, not as a localized slip. Thus, nearest the pile, shear forces develop along with compression and the "movement" is the relative movement between the boundaries of the affected zone, one close to the pile surface, but not necessarily right at the surface, and the other away from the pile. Measurements on piles near a loaded piles (as in a static loading test) have shown that loading the test pile imposed "passive" vertical movements on piles located several pile diameters away (e.g., Caputo and Viggiani 1984, Lee and Xiao 2001). Fellenius et al. (2004) when performing a static loading test on a 400-mm steel pile in clay, found that measured pore pressure increased 1.2 m (3 pile diameters) away from the pile surface at 13.7, 16.7, and 29.3 m depths as additional load increments were placed on the pile head.

The direction of the movement has no effect on the load-movement for the shaft resistance. That is, push or pull, positive or negative direction, the shear stress response is the same. Contrary to common belief, the movement necessary for the mobilization of unit resistance, shaft or toe, is independent of the diameter of the pile.

The accumulated shaft resistance from Depth 0 through Depth  $z$  is

$$(7.1b) \quad R_s = \int A_s r_s dz = \int A_s (c' + \beta \sigma'_z) dz$$

where

- $R_s$  = shaft resistance accumulated along the pile
- $A_s$  = circumferential area of the pile at Depth  $z$  (i.e., surface area over a unit length of the pile, e.g., a pile element)
- $r_s$  = unit shaft resistance along a pile element
- $c'$  = cohesion intercept (normally disregarded)

The beta-coefficient varies with soil gradation, mineralogical composition, density, depositional history (genesis), grain angularity, pile construction method, etc. [Table 7.1](#) shows what approximate range of  $\beta$ -coefficients expressing an **ultimate resistance** to expect from basic soil types, which I once compiled from different case histories (CFEM 1985). The values were derived from pile tests in mechanically weathered, inorganic, alluvially transported and deposited, and glacial soils. Other soils, in particular, highly overconsolidated soils (see O'Neill and Reese 1999), or soils with organics (e.g., “muck”), residual soils, calcareous soils, micaceous soils, and many others may—nay, will—exhibit different ranges of  $\beta$ -coefficients.

**TABLE 7.1**  
**Approximate Published Ranges of Beta-coefficients**

SOIL	Phi	Beta
Clay	25 - 30	0.15 - 0.35
Silt	28 - 34	0.25 - 0.50
Sand	32 - 40	0.30 - 0.90
Gravel	35 - 45	0.35 - 0.80

The actual beta-coefficients back-calculated from results of static loading tests can deviate significantly from the values shown in the table. For example, Rollins et al. (2005) compiled back-calculated average beta-coefficients for presumed ultimate resistances from a large number of case histories reporting results of uplift tests for different types (material) of piles in sand as shown in [Figure 7.3](#) (the dashed trend line is mine). [Figure 7.4](#) shows average beta-coefficients (again, for presumed ultimate resistances) back-calculated from case histories involving uplift tests on open- and closed-toe pipe piles and precast concrete piles, as reported by Clausen et al. (2005).

The cited results do not support the frequently expressed view that shaft resistance is smaller for steel piles as opposed to rougher-surface piles, such as concrete piles.

Available analysis results from measurements of distribution of shaft resistance, indicate unquestionably that the unit shaft resistance at any specific movement between the pile element and the soil increases more or less linearly with depth. This is best modeled by means of a proportionality coefficient (i.e., the beta-coefficient,  $\beta$ ) applied to the effective stress. As mentioned, the actual  $\beta$ -coefficient, can obviously vary within rather large ranges and depends on not just grain size distribution, but also on mineral composition, overconsolidation ratio, whether sedimentary or weathered residual soil, what definition of "ultimate resistance" was used, etc., not to forget the magnitude of the relative movement between the pile surface and the soil.

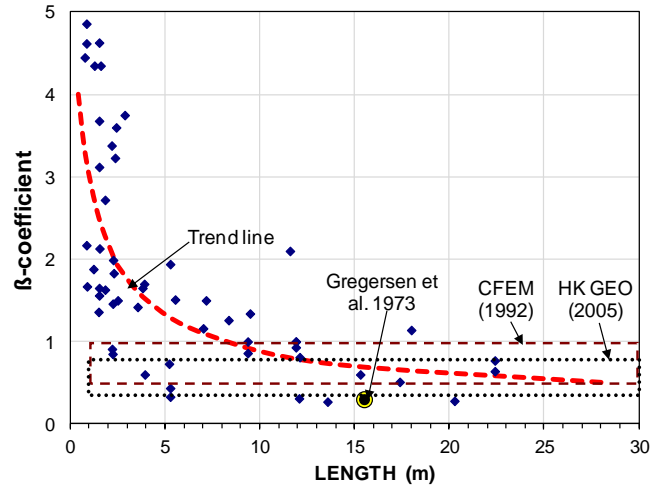


Fig. 7.3 Beta-coefficient for piles in sand versus embedment length. (Data from Rollins et al. 2005 with ranges suggested by CFEM 1992, Gregersen et al. 1973, and Hong Kong Geo 2006).

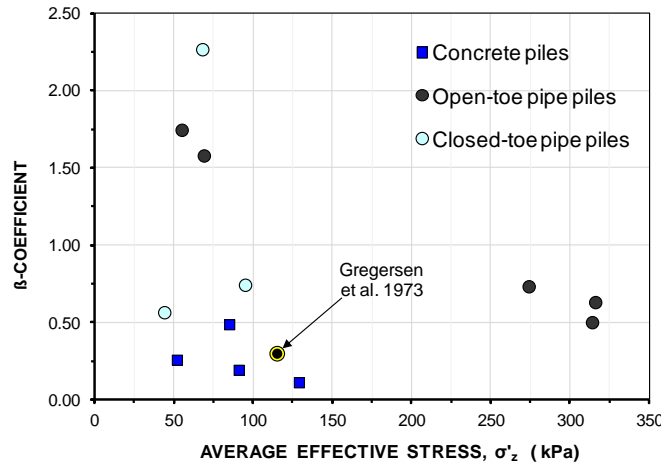


Fig. 7.4 Beta-coefficient in sand versus average effective stress. (Data from Clausen et al. 2005)

The  $\beta$  to apply must always be considered together with the geologic formation of the site and past back-calculated values. For example, I have cases with beta-coefficient in granular soil equal to about 0.1 and at other geologies with similar grain size and soil density, but with differences in mineralogical contents, grain angularity, depositional history, age, etc., the back-calculated beta-coefficients are about 2! A value must always be established with reference to observed values. Not to what is stated in a text book. And, a value does not have meaning until associated with the particular movement that generated it.

Clausen et al. (2005) also compiled cases from piles in clay: beta-coefficients versus plasticity index at ultimate resistance movement, as shown in Figure 7.5. For additional comments on  $\beta$  in clay, see O'Neill (2001).

Soils that exhibit an ultimate shear resistance (plastic shear response after some movement between the pile and the soil) are typically soft clay and non-dilating sand. Most accounts of shaft resistance response in the literature report almost elastic-plastic shapes. Indeed, many case histories report a post-peak reduction of shaft resistance. However, other than in soft clays, the shaft resistance response is usually more in the shape of a gently rising curve showing no sudden peak or change that could be taken as an indication of ultimate resistance.

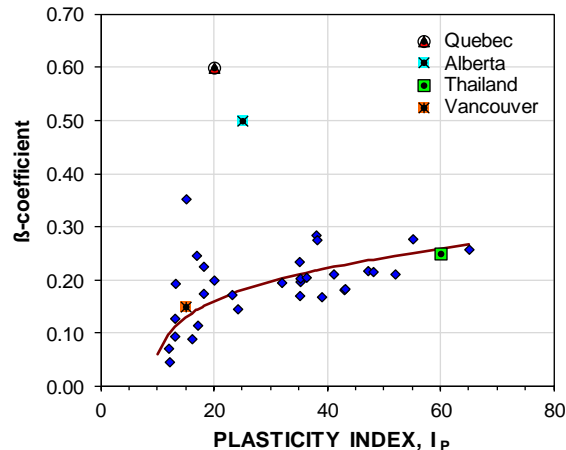


Fig. 7.5 Beta-coefficient for piles in clay versus plasticity index,  $I_p$ . (Data from Clausen et al. 2005 with results from four cases added; Fellenius 2006).

Figure 7.6 presents unit shaft resistance measured along a bored 1,800 mm diameter test pile constructed in HoChiMinh City in the Mekong delta, Vietnam, for the Sunrise City Towers at depths of 73, 75, 77, and 83 m. Only about 3 mm movement was required to develop a peak resistance, and at less than a millimetre further movement, sudden plunging developed; no records were obtained between about 5 mm and 35 mm (Fellenius and Nguyen 2013).

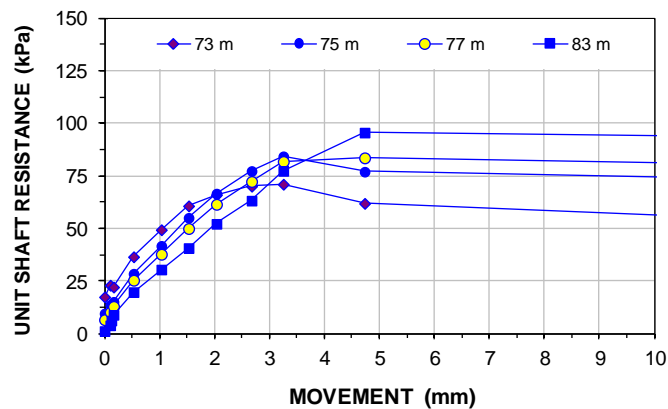


Fig. 7.6 Unit shaft resistance measured in a 1.8 m diameter bored pile constructed in silty sandy clay and clayey sand. (Fellenius and Nguyen 2013).

A few publications indicate that the unit shaft resistance would be a function also of the pile diameter. However, notwithstanding that the pile construction may have affected the shaft response differently for narrow as opposed to wide piles, as already mentioned, shaft resistance is not a function of pile diameter. As to it being a function of a diameter (and radius, i.e., curvature), think of the answer to a question of what is the unit shaft resistance for a barrette (a rectangular pile with a width sometimes not much smaller than its length), as compared to that of a round or square pile cross section? And, would the unit resistance differ between the short and long sides of the barrette?

**The Alpha Method.** The original alpha-method, as mentioned, set the unit shaft resistance equal to the undrained shear strength,  $s_u$ , times a coefficient,  $\alpha$ . Tomlinson (1957) suggested that  $\alpha$  be 1.0 up to a strength value of 1.0 ksf (50 kPa), reducing from there with increasing shear strength beyond 1.0 ksf. Randolph (1985) and others have suggested that  $\alpha$  be adjusted to depth according to Eq. 7.2a, which approach can be characterized as a hybrid effective-stress method ( $\beta$ -method). Many other  $s_u$ - $\alpha$  relations have been proposed.



$$(7.2a) \quad r_s = (s_u/\sigma'_z)^{\text{exp}} s_u$$

where

- $r_s$  = unit shaft resistance
- $s_u$  = undrained shear strength
- exp = exponent = 0.5 for  $(s_u/\sigma'_z) \leq 1$  and = 0.25 for  $(s_u/\sigma'_z) > 1$
- $\sigma'_z$  = overburden effective stress

**The Lambda Method.** Vijayvergia and Focht (1972) compiled a large number of results from static loading tests on essentially shaft bearing piles in reasonably uniform soil and found that the mean unit shaft resistance (ultimate, no less) for these test results was a function of depth and could be correlated to the sum of the mean overburden effective stress plus twice the mean undrained shear strength within the embedment depth, as shown in Eq. 7.2b.

$$(7.2b) \quad r_m = \lambda(\sigma'_m + 2c_m)$$

where

- $r_m$  = mean ultimate shaft resistance along the pile
- $\lambda$  = the 'lambda' correlation coefficient
- $\sigma'_m$  = mean overburden effective stress
- $c_m$  = mean undrained shear strength

The correlation factor is called "lambda" and it is a function of pile embedment depth, reducing with increasing depth, as shown in [Table 7.2](#).

**TABLE 7.2**  
**Approximate Values of  $\lambda$**

Embedment		$\lambda$
(Feet)	(m)	(-)
0	0	0.50
10	3	0.36
25	7	0.27
50	15	0.22
75	23	0.17
100	30	0.15
200	60	0.12

The lambda method is almost exclusively applied to the Gulf of Mexico soils to determine the shaft resistance for heavily loaded pipe piles for offshore structures in relatively uniform soils. Again, if used, the method should be correlated back to an effective stress calculation and the corresponding beta-ratios and unit toe resistances be determined from the calculation for future reference.

### 7.2.2 Toe resistance

For reasons of conformity, I suppose, also unit toe resistance is often presumed proportional to the effective stress, i.e., the effective stress at the pile toe. Based on this premise, the unit toe resistance is:

$$(7.3) \quad r_t = N_t \sigma'_{z=D}$$

where  $r_t$  = unit toe resistance (total toe force,  $R_t$ , is  $r_t$  times toe area,  $A_t$ )  
 $N_t$  = toe bearing "capacity" coefficient  
 $D$  = embedment depth  
 $\sigma'_{z=D}$  = effective overburden stress at the pile toe

Conventionally, it is assumed that also the pile toe response will display an ultimate resistance.. However, in contrast to the shaft response, which is governed by shear movement, the toe response is governed by compression and displacement of soil. Therefore, a supposedly ultimate toe resistance, expressed in a toe-coefficient,  $N_t$ , varies widely. Table 7.3 (Fellenius et al. 1989) shows a proposed approximate range of values for the four basic soil types. Some, e.g., CEFM 1992, have expounded on the values of the toe proportionality coefficient,  $N_t$ , suggesting correlation to not just soil type, but also to construction methods, such as bored or driven piles. Generally, the  $N_t$ -values are thought typical of those determined in i.e., interpreted from) a static loading test to "failure" (see Chapter 8, Sections 8.2 - 8.8). Notice that the maximum pile toe movement induced in a static loading test is normally only about 5 mm to 12 mm from the start of the test; a larger test-imposed toe movement is rare and, if so, the toe resistance and its  $N_t$ -correlation to effective stress would increase accordingly.

**TABLE 7.3 Approximate Range of  $N_t$**

SOIL	Phi	$N_t$
Clay	25 - 30	3 - 30
Silt	28 - 34	20 - 40
Sand	32 - 40	30 - 150
Gravel	35 - 45	60 - 300

The toe proportionality coefficient,  $N_t$ , is sometimes stated to be of some relation to the conventional bearing "capacity" coefficient,  $N_q$ , but the validity of any such relation is not real. The truth is that neither the  $N_q$ -coefficient for a footing (See Chapter 6) nor the  $N_t$ -coefficient correctly represent the response to an imposed load unless coupled with a specific movement as opposed to an ultimate value.

The  $N_t$ - implied correlation to overburden stress very approximate. Although a function of depth (indicated by Eq. 7.3), in contrast to the shaft resistance, the toe resistance is not linearly proportional to depth (effective stress). Within reasonable depth range in a uniform soil, the unit toe resistance can be assumed constant (independent of depth) and it is more practical to work with a specific value of toe stress when estimating the toe force (of course, always as a function of the specific toe penetration (movement)).

The common premise of ultimate toe resistance is false. While, shaft resistance is indeed a function of shear force development along the surface of the pile, in contrast, toe resistance is less a function of shear forces in the soil and more a function of deformation due to compression (settlement) of the soil below the pile toe and to a small displacement of the soil, i.e., penetration of the pile toe into the soil at the pile toe level, countered by the overburden stress. This is an additional reason for it being more constructive to estimate a specific value of unit toe resistance,  $r_t$ , (again, as a function of imposed toe penetration).

As discussed by Fellenius (1999; 2011), the concept of bearing "capacity" does not apply to a pile toe. Instead, the pile toe load-movement is a function of the load-transfer response of the soil at and below the pile toe in a relation called q-z curve (See Section 8.12). The toe resistance does not exhibit an ultimate value, but continues to increase with increasing toe movement. The  $r_t$ -resistance (or  $N_t$ -coefficient) is therefore best determined by back-calculation of tests having imposed a known toe movement. Unfortunately, however, the toe resistance is frequently just assumed or based on textbook presumptions.

Figure 7.7 shows unit toe resistances measured in two bored test piles of 1,500 mm and 1,800 mm diameter constructed with the pile toe in silty sandy clay and clayey sand (same piles as those of the example shown in Figure 7.5). Figure 7.8 shows unit toe resistances measured in two bored test piles of 1,500 mm and 2,000 mm diameter constructed at an adjacent site, both to 75-m depth, with the pile toe in compact silty sand. The absence of indication of approaching "failure" despite the large movements is typical for a pile toe response (as well as for a footing response; compare Section 6.10). Note also that the average unit toe resistance versus movement shows no influence that would be due to pile diameter as the diameters are quite similar. Although not apparent in the Figure 7.8, normalizing the unit toe stress to pile diameter does normally indicate a softer toe response for a larger diameter.

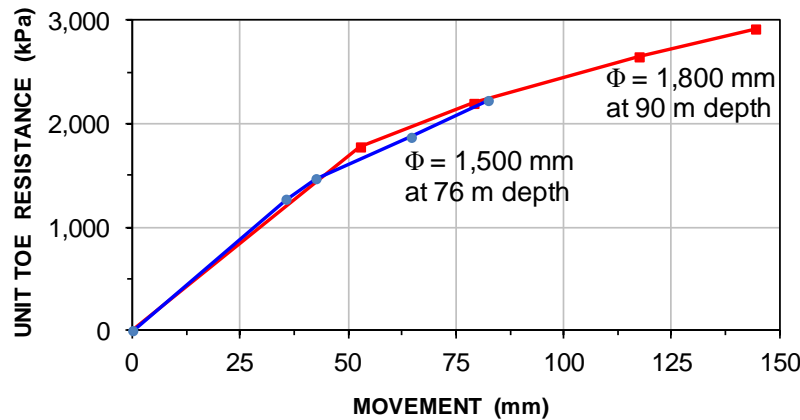


Fig. 7.7 Unit toe resistance measured in two bored piles with different diameters constructed to different depths at the same site with slightly different diameter (Data from Fellenius and Nguyen 2013).

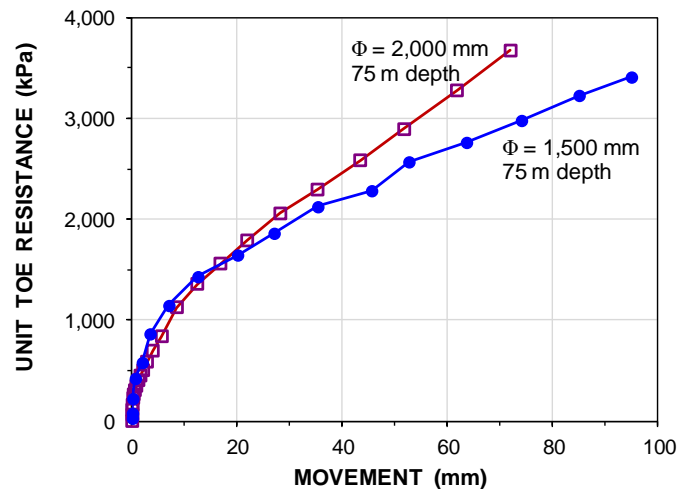


Fig. 7.8 Unit toe resistance measured in two bored piles with different diameter (1,500 and 2,000 mm) constructed to the same 75-m depth (Data from Fellenius and Nguyen 2014).

### 7.2.3 Ultimate resistance ("capacity")

The Target load,  $Q_{trg}$ , as the sum of the shaft and toe resistances,  $R_s$  and  $R_t$  (Eq. 7.4), is often taken to express the "capacity" of the pile,  $Q_{ult}$ , (alternatively written  $R_{ult}$  or  $R_{t,rg}$ ). The shaft resistance may at times be an "ultimate", representing a plastic shaft shear response, but as shown in Figures 7.7 and 7.8, assuming an ultimate toe resistance is unrealistic.

$$(7.4) \quad Q_{trg} = R_s + R_t$$

where

- $Q_{trg}$  = target resistance (often taken as the ultimate resistance or "capacity",  $Q_{ult}$ , Note, there is no "ultimate" for the pile toe; ultimate resistance is a highly imprecise concept)
- $R_s$  = total shaft resistance for the target load, alternatively written  $R_{s,trg}$
- $R_t$  = total toe resistance for the target load, alternatively written  $R_{t,trg}$

N.B., the commonly used term "ultimate capacity" is a misnomer, a tautology. The term is a mix of the alternative terms "ultimate resistance" and "capacity". Although one cannot be mistaken of the meaning of "ultimate capacity", the adjective should not be used, because it makes the use of other adjectives seem proper, such as "load capacity", "allowable capacity", "design capacity", "working capacity", "carrying capacity", which are at best awkward and at worst misleading. Sometimes, even the person modifying "capacity" with these adjectives is unsure of the meaning. The only modifiers to use with the term "capacity" for piles are "long-term capacity", "short-term capacity", and "bearing capacity". The term "geotechnical capacity" may be used to contrast to "structural strength" (calling the latter "structural capacity" is awkward and should be avoided).

Moreover, "capacity" and "ultimate resistance" are very diffuse terms that are meaningless until they are defined by a specific movement, a shape of a load-movement curve, or other, as indicated in Section 7.3 and Chapter 8.

Eq. 7.5 shows the relation for the load in pile,  $Q_z$ , at Depth  $z$  for a certain load at the pile head,  $Q_{trg}$ , when the shaft resistance is assumed fully mobilized.

$$(7.5) \quad Q_z = Q_{trg} - \int A_s \beta_{trg} \sigma'_z dz = Q_{trg} - (R_s)_z$$

where

- $Q_z$  = axial force at depth  $z$  for target condition
- $Q_{trg}$  = target resistance (often assumed to be the ultimate resistance or "capacity")
- $A_s$  = Circumferential area of pile
- $\beta_{trg}$  = beta target coefficient
- $\sigma'_z$  = effective overburden stress
- $(R_s)_z$  = total target shaft resistance to Depth  $z$

Both shaft and toe resistances develop due to movement. The movement can either be in response to a load applied to the pile or be due to downdrag (soil settling more than the pile, "dragging it down"). In the ideal elastic-plastic load-movement case, the magnitude of the movement beyond the small values necessary before the plastic state is reached is not important. However, in most cases of shaft resistance and in every case of toe resistance, a stand-alone ultimate resistance value does not exist; the resistance is always a function of the movement. It follows that **pile capacity is a fudge concept**. A design based on applying a factor or safety (or resistance facto) to a "capacity", defined one way or another, is a blurred and oversimplified approach—it is also quite inadequate and often very wrong). The current overreliance in the design of piled foundations (as well as footings) on factors of safety (or resistance factors) applied to a "capacity", defined or not, is neither logical nor safe. As will be outlined below, design should be based on deformation and settlement analysis.

#### 7.2.4 Service conditions

During service conditions, loads from the structure ("working loads") will be applied to the pile head via a pile cap (for pile groups, the term "raft" is often used instead of "cap". Sometimes, the terms "slab" or "mat" are used, then, mostly indicating an on-grade arrangement as opposed to a pile-supported foundation structure). The working loads are normally separated on permanent (or 'dead' or 'sustained') loads,  $Q_{dead}$ , and transient (or 'live') loads,  $Q_{live}$ . (See definitions of 'dead' and 'live' in Chapter 14). Not generally recognized is that, even if soil settlements are small, even when too small to be readily

noticeable, in the long-term, the soil will in the majority of cases, move down in relation to the pile and in the process add axial force to the pile by accumulation of negative skin friction. (An exception is a pile in swelling soils and the exception is limited to the length of pile in the swelling zone, where then 'positive skin friction' develops. For analysis swelling response, see Section 7.16). Over the long-term, small relative movements always occur between a pile shaft and the soil that are sufficient to develop significant negative skin friction as well as a corresponding shaft resistance (the term "negative" and "positive" refer to the direction of shear acting along the pile surface and the separation of the terms "friction" and "resistance" signifies whether the shear is introduced by the soil or by a response to outside forces). Therefore, every pile develops eventually an equilibrium of forces between, on the one side, the sum of the sustained (dead) load applied to the pile head,  $Q_{\text{dead}}$ , and a drag force,  $Q_n$ , induced by negative skin friction along the upper part of the pile, and positive shaft resistance and toe resistance in the lower part of the pile.

The point of "**force equilibrium**", is the depth where the shear stress along the pile changes over from negative skin friction into positive shaft resistance. Similarly, where there is no relative displacement between the pile and the soil, a "**settlement equilibrium**" will develop. When the two are at the same depth, the equilibrium relations are at a depth that I in the past called "neutral plane", a term with many other uses in engineering analysis. Therefore, I now prefer to use the term "**equilibrium plane**", **EP**. The transition zone develops where the unit shaft resistance changes from negative to positive direction. The transition is not sudden, but occurs along a certain zone length or height. Note, where the soil settlements are small, the length of the transition zone will be large. Note also that the larger the toe resistance, the deeper lies the equilibrium plane. And, the larger the sustained (dead) load, the shallower the depth.

The key aspect of the foregoing is that the development of an equilibrium plane and drag force due to negative skin friction is an always occurring phenomenon in piles and not limited to where large soil settlement occurs around the piles. Numerous well-documented case histories testify to the veracity of the underlined statement (Fellenius 2004).

For piles designed with a normal margin against failure (e.g., designed with a factor-of-safety on the "capacity"), the equilibrium plane lies below the mid-point of a pile. The extreme case is for a pile bearing on bedrock, where the location of the EP is at the pile toe, i.e., at the bedrock. For a lightly loaded, dominantly shaft-bearing pile 'floating' in a homogeneous soil with linearly increasing shear resistance, the EP typically lies at a depth which is about equal to the lower third point of the pile embedment length. This is the origin of the "Terzaghi-Peck" rule of calculating the settlement of a pile group consisting of shaft bearing piles ("floating piles") in uniform soil as the settlement for an equivalent flexible raft placed at the lower third point of the pile. See also comments on "Piled Raft and Pile Pad Foundations" in Section 7.19.

**Table 7.4** presents an example of a conventional analysis: A 305-mm square, precast, prestressed concrete pile is assumed driven to 27 m depth at a site where the soil profile consists of a 4 m thick upper layer of silt deposited on 17 m of clay, followed by 4 m of dense silty sand on a thick deposit of dense glacial till. The soil density values are 2,000, 1,700, 2,100, and 2,200 kg/m<sup>3</sup>, respectively. The groundwater table is located at 1.0 m depth below grade and the pore pressure distribution is hydrostatic. Concurrent with the construction, a 1.5 m thick earth fill is placed over a large area at the site imposing a 30-kPa ground stress and resulting in consolidation of the clay. The pile will be subjected to dead and live loads (N.B., unfactored) of 800 kN and 200 kN, respectively.

I first developed this simple example back in the 1960s and have used it to illustrate effective stress calculation in courses and in the Red Book, Edition 1 and onward. The input values were derived from experience of precast concrete piles driven into the glacial soil geology of Scandinavia and Eastern Canada, representing, as was the approach back then, ultimate resistance values and this even for the toe response. Unlike back then, today, we know that the calculation input cannot be separated from the movement imposed by the applied load and the long-term subsidence at the site.

The soil parameter input, assumed to represent ultimate resistance condition, was applied to an effective stress analysis to determine the force distribution for the applied load. The input values of  $\beta_{trg}$  were, 0.40, 0.30, 0.50, and 0.55, in the silt, soft clay, silty sand, and glacial till, respectively, and the input unit toe resistance,  $r_{t,trg}$ , in the glacial till, was 12 MPa. The fact that the pile is driven 2 m into the glacial till demonstrates that the till is hardly a base till. It would not likely have been possible to drive the pile a distance of 2 m into a base till. The analysis results in a spread-sheet calculated "capacity" of 2,980 kN.

**TABLE 7.4 CALCULATION OF FORCE DISTRIBUTION**

Size, $\Phi = 305$ mm	Live Load, $Q_l = 200$ kN	Shaft Resistance, $R_s = 1,864$ kN
Area, $A_s = 1.220$ m <sup>2</sup> /m	Dead Load, $Q_d = 800$ kN	Toe Resistance, $R_t = 1,116$ kN
Area, $A_t = 0.093$ m <sup>2</sup>	Total Load = 1,000 kN	Total Resistance, $R_{trg} = 2,980$ kN
$F_s = 3.0$	Depth to EP = 20.9 m	Force at N.P., $Q_{max} = 1,783$ kN

-DEPTH (m)	TOTAL STRESS (kPa)	PORE PRES. (kPa)	EFFECTIVE STRESS (kPa)	$r_s$ (kPa)	$Q_d+Q_n$ (kN)	$R_u-R_s$ (kN)
<b>LAYER 1 Sandy Silt</b> $\rho = 2,000$ kg/m <sup>3</sup> $\beta_{trg} = 0.40$						
0	30	0	30	12.0	800	2,980
1 (GWT)	50	0	50	20.0	820	2,961
4	110	30	80	32.0	915	2,866
<b>LAYER 2 Soft Clay</b> $\rho = 1,700$ kg/m <sup>3</sup> $\beta_{trg} = 0.30$						
4	110	30	80	24.0	915	2,866
20.9 (EP)	388	190	198	59.4	1,783	2,008
21	399	200	199	59.7	1,782	1,998
<b>LAYER 3 Silty sand</b> $\rho = 2,100$ kg/m <sup>3</sup> $\beta_{trg} = 0.50$						
21	399	200	199	99.5	1,782	1,998
25	483	240	243	121.5	1,459	1,459
<b>LAYER 4 Glacial Till</b> $\rho = 2,200$ kg/m <sup>3</sup> $\beta_{trg} = 0.55$						
25	483	240	243	133.7	1,459	1,459
27	527	260	267	146.9	1,116	1,116

The example does not include a settlement analysis. Had that been considered as a part of the analysis, additional input would have been needed, such as compressibilities (such as for immediate compression, consolidation, and secondary compression conditions), consolidation coefficient (See Chapter 3) of the soil. The pile has reached well into the competent sand layer, which will not compress much for the increase of effective stress due to the pile loads and the earth fill. Therefore, the settlement of the pile group will be minimal and consist mostly of pile compression due to the sustained load and drag force due to consolidation of the soft clay. Settlement analysis will be discussed in Sections 7.17 and 7.18.

The table shows the calculated load and resistance distributions for the example pile (the two rightmost columns) employing the indicated beta-coefficients and toe resistance under, to repeat, the assumption that they represent ultimate values.

A factor-of-safety of 3.0 is usually applied to an analysis of "capacity" of a single pile not referenced to direct test records of pile response:  $2,991/3.0 \approx 1,000 = 800 + 200$  kN. The calculations show that to achieve a 3,000-kN "capacity" ("capacity" that, of course, must agree with some definition of "capacity" based on pile movement), when applying the assumed values of  $\beta$  and  $r_t$ , the piles have to be installed to a 2-m penetration into the sandy till layer, i.e., depth of 27 m.

The calculations results are plotted in Figure 7.9A in the form of two curves: one determined per Eq. 7.5, starting at the unfactored 800-kN sustained target load,  $Q_{dead}$ , increasing with depth due to the shaft resistance, negative skin friction. The value plotted at the pile toe is the calculated toe resistance determined per Eq. 7.6 and the second curve starts from this force by increasing with shaft resistance until it reaches the pile head. the intersection of the two curves is the "force equilibrium". The curves are assumed to represent the long-term distribution at a site.

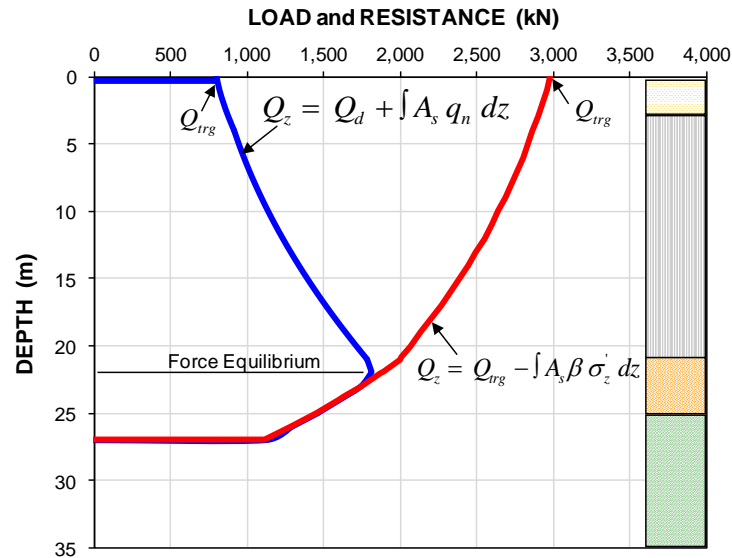


Fig. 7.9A Typical load-transfer and resistance curves, and force-equilibrium

The force distribution curve assumes that the movement of the pile toe into the soil is about equal to that found in a static loading test to “failure”. The 12,000-kPa toe resistance is unlikely to be true, however, unless that pile toe had moved at least 15 to 30 mm, as in a static loading test.

$$(7.6) \quad Q_z = Q_d + \int A_s q_n dz = Q_d + Q_n$$

where

- $Q_z$  = axial force in the pile for long-term condition
- $Q_d$  = dead load applied to the pile (always unfactored)
- $Q_n$  = drag force at the equilibrium plane
- $A_s$  = circumferential pile area
- $q_n$  = unit negative skin friction =  $\beta \sigma'_z$
- $\beta$  = beta coefficient
- $\sigma'_z$  = effective overburden stress

The transition between the resistance curve (Eq. 7.5) and the force-transfer curve (Eq. 7.6) is in reality not the sudden kink the equations suggest, but a gradual curve changing from increasing to decreasing trend over a **transition zone** with a certain length (here about 1 m) along the pile. The length of the transition zone varies with the type of soil and the rate or gradient of the relative movement between the pile and the soil at the equilibrium plane. Its length can be estimated to be the length over which the relative movement between the pile and the soil is smaller than about 5 mm. Thus, if the transition zone would be disregarded, then, the theoretically calculated value of the axial force in the pile at the indicated equilibrium plane, EP, the maximum force, is higher than the real value and it is easy to overestimate the magnitude of the drag force and, therefore, the maximum axial force in the pile. Notice, also, that the calculations are interactive inasmuch that a change of the value of the sustained (dead) load applied to a pile will change the location of the EP and the magnitude of the maximum axial force in the pile (which occurs at the EP).

The length of the transition zone is a function of the relative movement between the pile and the soil and inversely proportional to the movement. To estimate the length, after having applied the unified-method analysis (force-settlement analysis) to determine the equilibrium plane, look at the settlement equilibrium and the pile and soil settlement curves and estimate where—above and below the equilibrium plane—the relative movement between the pile and the soil exceeds a few millimetre. The length of the transition zone is the distance between the two so-distanced points. At sites with downdrag concerns, the length is usually short, only about a metre because the soil settlement at the EP is then usually large.

The maximum axial force in the example pile is 1,809 kN, when including the about 1,000 kN drag force—which is of no consequence to the design, unless the design is governed by an outmoded code. As mentioned, the maximum axial force is not relevant for assessing the geotechnical response of a pile, it is only of concern for the pile structural strength, and a 1,800 maximum force is of no concern for a pile such as the example pile.

Since the example was first introduced, technology and understanding has advanced. Today, an estimate of the response of a pile to applied load needs to start with the response of the individual pile elements as expressed in  $t$ - $z$  and  $q$ - $z$  functions (c.f., Section 8.11). Figure 7.9B shows a set of functions aimed to produce a reasonably fitting simulation of a static loading test that would have resulted in the ultimate resistance parameters indicated in Table 7.4. The  $q$ - $z$  function represents the toe response and its initial part had to be rather steep to suit the stated ultimate total and toe resistances. This implies a presence of residual toe force (c.f., Section 8.12), which is entirely commensurable with a pile driven into till. A simulation of a static loading test would be easier (more practical) if the functions would be based on smaller movement as opposed to the movements for the presumed ultimate resistance. However, either set would produce the simulated load-movement curves of a static loading test shown in Figure 7.9C.

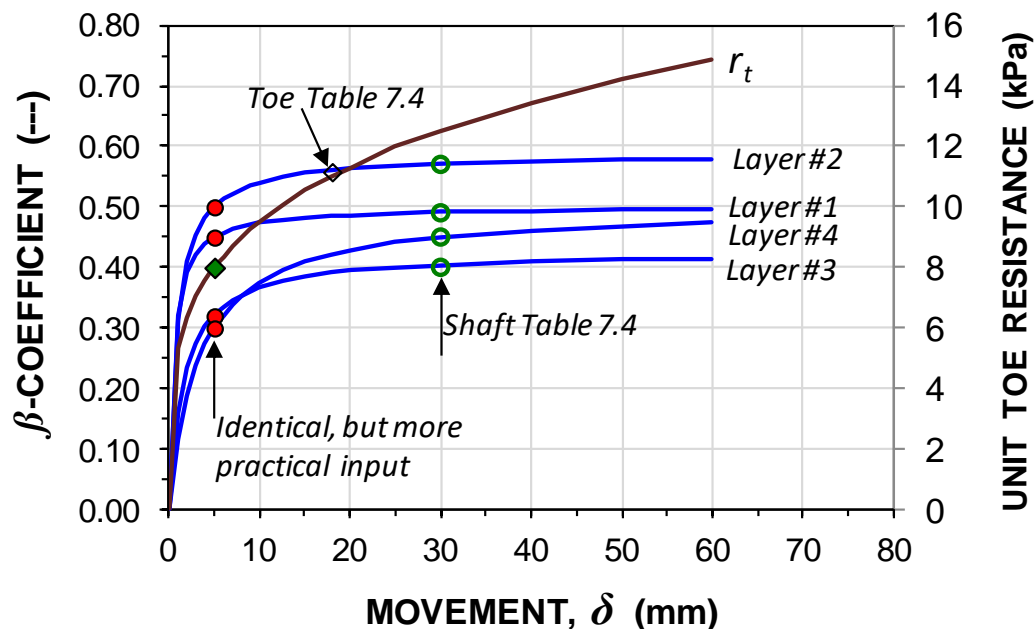


Fig. 7.9B Assumed  $t$ - $z$  and  $q$ - $z$  functions suiting the example



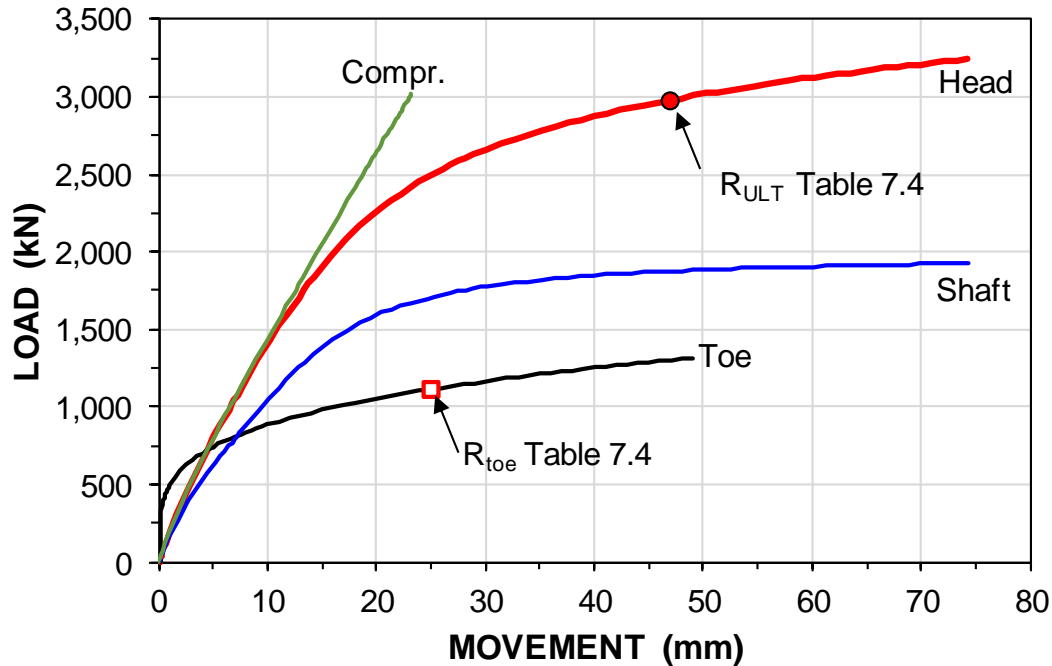


Fig. 7.9C Simulated static loading test

The ultimate values of [Table 7.4](#) are indicated in the figure. The simulation aimed to show the "ultimate toe force" of 1,116 kN ( $r_{toe}$ ) and the toe movement for this force to occur for the 2,980 kN applied load ( $R_{ULT}$ ) and pile-head movement. (Which is why it was necessary to assume presence of residual force). Most certainly, a somewhat different load-movement curves would have been obtained were the t-z and q-z functions to be tweaked. More important, there would for each be no agreement amongst practitioners about the actual interpretation of the "capacity" to be estimated from the pile-head load-movement curve (Section 8.4 and Figure 8.8).

Design calculation of the long-term response of a piled foundation must include calculating the settlement of the soil layers within the affected soil body. To complete the example, the compressibility of the four layers has been estimated in order to provide a potential settlement distribution due to the fill and sustained pile load. The calculation follows the unified method as addressed in Sections 7.14 - 7.15.

[Figure 7.9D Graph i](#) shows the force distribution similar to [Figure 7.9A](#), but the distributions are calculated applying the actual movements between the pile elements and the soil, as calculated and indicated in [Figures 7.9D Graph ii](#) and [7.9D Graph iii](#). The latter graph illustrates how the shear force reduces above and below the Equilibrium Plane (i.e., within the transfer zone). Of course, in case of a plastic soil, the shear force outside the transfer zone is the mobilized ultimate shaft resistance. However, in a strain-hardening soil, the shear resistance would be smaller than the ultimate (or maximum—there may not be an ultimate discernible for the t-z curve), or be significantly smaller than the peak shear force in a strain-softening soil. The key aspect of the analysis is to apply the resistance versus s movement for the pile element, the t-z/q-z relations to determine the long-term settlement of the pile, as indicated in the [7.9Dii](#) graph, the long-term settlement being the important part of a design as opposed to the rather trivial "capacity".

The calculations to produce the graphs in [Figure 7.9D](#) were performed using UniPile6 (2024).

A main advancement of the unified analysis method is that it allows for analysis of pile groups, cf., Sections 7.17 - 7.19.

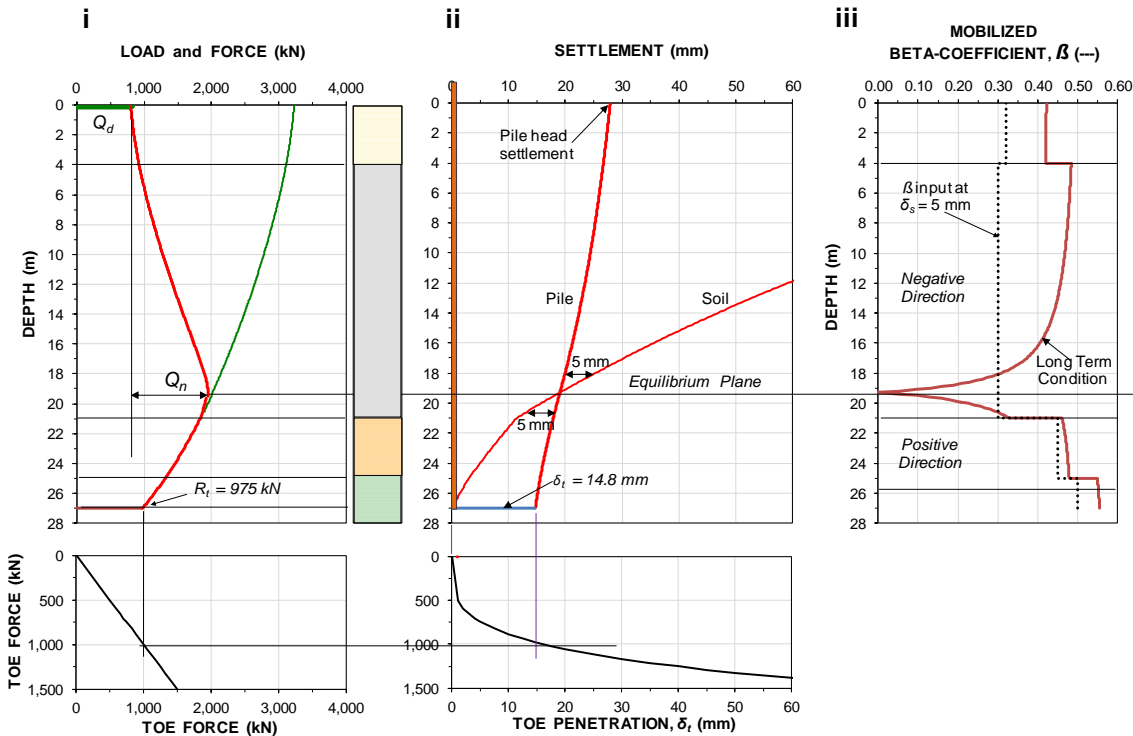


Fig. 7.9.D Results of the unified method analysis

### 7.3 Load-movement and Load Transfer

The foregoing presents the conventional bearing-"capacity" ultimate-resistance approach, based on a pile having a specific resistance value called "capacity" (subject to definition; c.f., Chapter 8) amounting to the sum of ultimate resistances—usually presumed plastic—of all the elements making up the pile. As also shown, the reality is very different, even for the case of a well-defined ultimate resistance. We can assume a typical case of a pile is in a strain-softening soil, where the resistance of each pile element builds up to a peak at a small initial shear movement, whereafter it reduces—softens. For reasons of simplicity, assume that all pile elements making up the pile have the same  $t$ - $z$  strain-softening shaft-resistance relation. The pile toe response follows a  $q$ - $z$  relation (for  $t$ - $z$  and  $q$ - $z$  functions, c.f., Chapter 8), which means that the pile-toe load-movement response never reaches an ultimate condition, but will be a continuous, gently rising curve.

The pile load-movement curves (head, shaft, and toe) for the assumed pile are shown in the upper left graph in Figure 7.10 and combines all the responses of the various pile elements and the  $EA$ -parameter (c.f., Chapter 8). The  $t$ - $z$  curves used to simulate the response and the  $q$ - $z$  response of the pile toe element are also shown in the figure. Most would probably take the red dot at the peak of the pile-head load-movement curve to represent the pile "capacity". The figure shows that, at that stage in the test, however, only one or a few of the pile elements would be at a stage representing the element peak resistance. The elements in the upper part of the pile will be at a post-peak state and the elements closer to the pile toe will be at pre-peak state. The pile toe has hardly begun to move and the mobilized toe resistance is small.

See Chapter 8 for pile-head load-movement curves and strain-hardening  $t$ - $z$  responses, where no "capacity" is obvious. Special definitions would be needed in order to obtain one from the test results. Those cases share with the case shown in the preceding figure the condition that whatever definition of pile "capacity" that would be applied to the pile-head curve, it will not harmonize with or correlate to the ultimate resistance defined or chosen for the individual pile elements, for example, by calculations from undrained shear strength or similar feature.

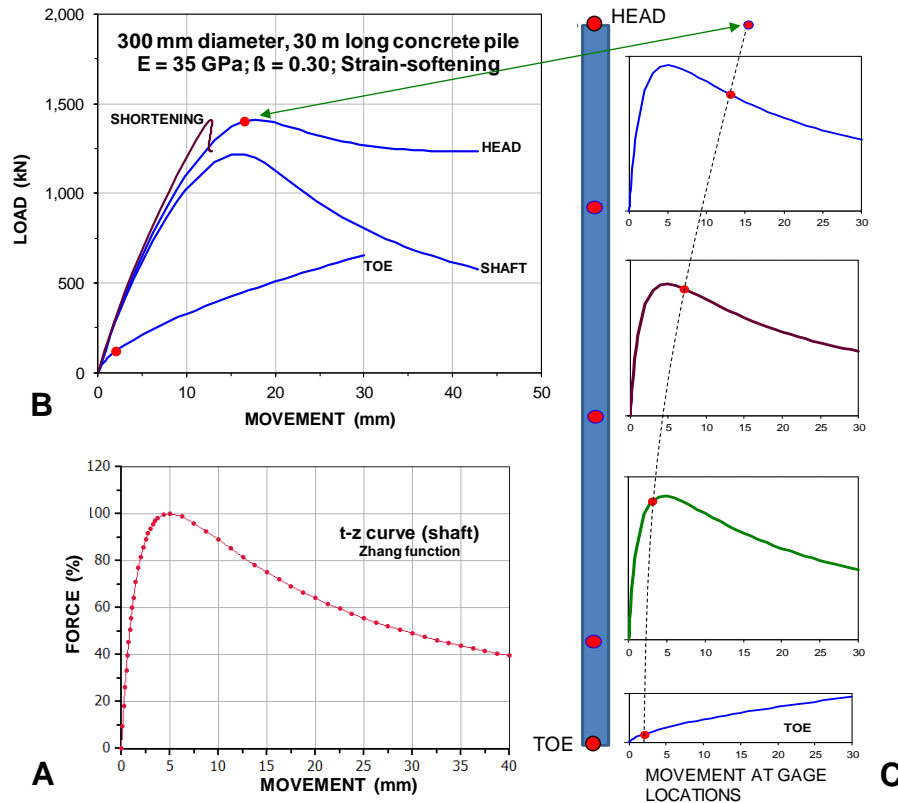


Fig. 7.10 Load-movement curves and t-z curves

Some pile loading tests may show a "strain-softening response" at the pile head without the soil response actually being strain-softening at the pile elements, but, say, approximately elastic-plastic, N.B., for constant effective stress. This is because the load increment, applied after the peak load has been reached, causes increased pile movement with regard to both magnitude and rate (i.e., added movement per applied load increment). Continued loading beyond the peak increases pore pressure, which reduces the effective stress and it is reflected by reduced shaft resistance. The interrelations are complex. A very slow loading using very small increments of load would not increase the pore pressure—would, therefore, not show reduced shaft shear—but such tests would be rather impractical.

Movement of a pile (of the pile head) due to load-transfer is necessary for mobilizing the soil resistance along the shaft and at the pile toe. If all shaft resistance has become mobilized, the movement is composed of the compression of the pile, which is determined by the pile stiffness and the axial force as it reduces with depth due to shaft resistance, and the pile toe movement. It follows that the pile toe response governs the load-transfer movement of a pile.

#### 7.4 Critical Depth

Many texts suggest the existence of a so-called 'critical depth' below which the shaft and toe resistances would be constant and independent of the increasing effective stress. This concept is a fallacy and based on incorrect interpretation of test data and should not be applied. Fellenius and Altae (1994; 1996) discussed the "Critical Depth" and the reasons for how such an erroneous concept could come about. (N.B., some authors have applied the term "critical depth" to the phenomenon of reduction of the unit shaft resistance along very long offshore piles, where the resistance at depth in a homogeneous soil can start to decrease, but that is not the generally understood meaning of the term as applied "on-shore").

## 7.5 Effect of Installation

Whether a pile is installed by driving, drilling, or other means, the installation affects—disturbs—the soil. Before the disturbance from the pile installation has subsided, it is difficult to determine the magnitude of what shaft and toe resistances to expect. For instance, presence of dissipating excess pore pressures causes uncertainty in the magnitude of the effective stress in the soil and the strength gain (set-up) due to reconsolidation is hard to estimate. Such installation effects can take long time to disappear, especially in clays. They can be estimated in an effective stress analysis using suitable assumptions as to the distribution of pore pressure along the pile at any particular time. Usually, to calculate the installation effect, a good estimate can be obtained by assuming presence of excess pore pressures in the fine-grained soil layers—the finer the soil, the larger the induced pore pressures—taking care that the pore pressure employed in the analysis must not exceed the total overburden stress. The reconsolidation process returns the pore pressures to the original conditions and when all the induced excess pore pressures have dissipated, the long-term response is established. For a case-history example, see Fellenius (2008). Notice, in some soils, even sands, the increase of resistance, the set-up, can continue also well after the pore pressures induced during the driving have dissipated, which is called the "aging effect" (Bullock et al. 2005, Fellenius 2014b).

## 7.6 Residual Force

The dissipation of induced excess pore pressures (called “reconsolidation”) imposes force (axial) in the pile by negative skin friction in the upper part of the pile, which is resisted by positive shaft resistance in the lower part of the pile and some toe resistance. In driven piles, residual force also results from strain built in or locked-in during the driving. Residual force, as well as "capacity", may continue to increase also after the excess pore pressures have dissipated.

The quantitative consequence of not recognizing the residual force in the evaluation of results from a static loading test, is that erroneous conclusions will be drawn from the test: the shaft resistance appears larger than the true value, while the toe resistance appears correspondingly smaller. Typically, when presence of residual force is not recognized (meaning: when it is present and not adjusted for), the distribution of axial load in the pile evaluated from the test records will be with an increasing slope with depth, indicating a unit shaft resistance that gets smaller with depth, as opposed to the more realistic shape (in a homogeneous soil) of decreasing slope, indicating a progressively increasing shaft resistance. This is illustrated in Chapter 8, Figures 8.36 through 8.37 and 8.46.

The existence of residual force in piles has been known for a long time. To my knowledge, Nordlund (1963) was the first to point out its importance for evaluating force distribution from the results of an instrumented static pile loading test. However, it is not easy to demonstrate that test data are influenced by residual force. To quantify the effect is even more difficult. Practice is, regrettably, to consider the residual force to be small and not significant to the analysis and to proceed with an evaluation based on “zeroing” all gages immediately before the start of the test. That is, the problem is 'solved' by declaring it not to exist. This is why the soil mechanics literature includes theories applying “critical depth” and statements that unit shaft resistance would stay constant or even reduce as a function of depth in a homogeneous soil. For more details on this effect and how to analyze the test data to account for residual force, see Hunter and Davisson (1969), Bozozuk et al. (1978), O'Neill et al. (1982), Altae et al. (1992; 1993), Fellenius and Altae (1994; 1996), and Fellenius (2002b).

Again, "capacity" as a term means ultimate resistance, and, in contrast to ultimate shaft resistance, ultimate toe resistance does not exist. As used in the practice, the "capacity" of a pile determined from a static loading test is the load for which the load movement of the pile head appears to show continued movement for a small increase of applied load, failure occurs, the pile "plunges". This 'failure' value is a combination of strain-softening shaft resistance and toe resistance as indicated in [Figure 7.11](#), which illustrates a softening (post-peak) response of the pile-head despite an increasing toe resistance. The pile-

toe load-movement curve also includes a suggested effect of a residual (locked-in) toe force. If this residual force is disregarded, the toe-load vs. toe-movement could mistakenly be thought to imply an ultimate toe resistance, i.e., toe "capacity". For additional discussion on this topic see Chapter 8.

### 7.7 Analysis of Tapered, Non cylindrical, and Helical Piles

Many piles are not cylindrical or otherwise uniform in shape throughout the length. The most common example is the wood pile, which has a conical shape with the diameter tapering off with depth. Step-tapered piles are also common, consisting of two or more concrete-filled steel tubes (pipes) of different diameters connected to each other, normally, the larger above the smaller. Sometimes, a pile can consist of a steel pipe with a lower conical section, for example, the Monotube pile, and the Steel-Taper-Tube pile, which typically have a 25 feet (7.6 m) long conical toe section, tapering the diameter down from 14 inches (355 mm) to 8 inches (203 mm). Composite piles can have an upper concrete section joined to a smaller diameter H-pile extension.

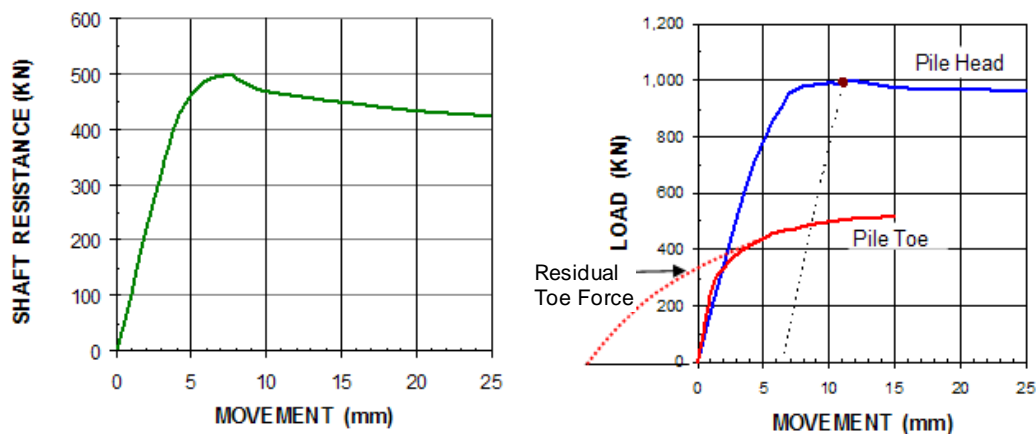


Fig. 7.11 Load-Movement curves for shaft resistance and for total ("Pile Head") and toe resistances.

For the step-tapered piles, each 'step' provides an extra resistance point, which needs to be considered in an analysis. (The GRLWEAP wave equation program, for example, can model a pile with a diameter change as having a second pile toe at the location of the 'step'). In a static analysis, each such step can be considered as an extra pile toe with a donut-shaped area,  $A_t$ , and assigned a corresponding toe resistance per Eq. 7.3b, or unit toe resistance value,  $r_t$ , times the donut area. Each such extra toe-resistance donut-value is then added to the shaft resistance calculated using the actual pile diameter.

The analysis of how a helical pile—single helix or multiple helices—is best analyzed as each helix serving as an extra pile toe with its representative "toe" resistance. Naturally, no such analysis can be meaningful without correlation to the movement generating the resistances with due recognition that the resistance vs. movement relations are different for shaft ( $t$ - $z$  functions) and toe ( $q$ - $z$  function) responses. Closely spaced helices can result in the pile responding as a straight-shaft pile with a diameter equal to the helix diameter. Moreover, the "donut" toe resistance does not necessarily appear the same as a pile-toe resistance would at that same depth, but require its own  $q$ - $z$  function in an analysis.

Piles with a continuous taper (conical piles, such as wood piles) are less easy to analyze. Nordlund (1963) suggested a taper adjustment factor to use to increase the unit shaft resistance in sand for conical piles. The analysis was based on the fact that, due to the taper, the loading and associated movement introduces passive resistance increase of the effective stress against the pile surface. The adjustment factor is a function of the taper angle and the soil friction angle. A taper angle of  $1^\circ$  (0.25-inch/foot) in a sand with a  $35^\circ$  friction angle would give an adjustment factor of about 4. At a 0.5-taper angle, the Nordlund factor

would be about 2. As an alternative, the analysis could divide the soil into sub-layers of some thickness and, at the bottom of each such sub-layer, project the diameter change between the upper and lower sub-layer boundaries. Each such donut-shaped area is then treated as an extra toe similar to the analysis of the step-taper pile. The shaft resistance is calculated using the mean diameter of the pile over the same “stepped” length. The shaft resistance over each such particular "element" length consists of the sum of the shear resistance over the shaft area and the toe resistance of the “donut” area. This method requires that a unit toe resistance value,  $r_t$ , and  $q$ - $z$  function be assigned to each “stepped” length. Of course, the “donut” method applies to piles in all types of soil.

The donut-effect does not come into play for negative direction of the shaft shear for a tapered pile. This means that, when determining the response of a pile to tension loading, or to downdrag and drag force, i.e., negative direction shear forces, the effect of the taper (the "donut effect") should be excluded. In addition, the analysis must consider that the shear response along the tapered length is considerably smaller in "pull" as opposed to in "push" (in contrast to straight-shaft pile for which the shaft resistance in pull" and "push" are the same). Similarly, when assessing negative skin friction, the "donut effect" of the taper must be disregarded. Below the equilibrium plane, however, the effect should be included. Note, including it will influence the location of the equilibrium plane (because the “donut effect” of the taper increases the resistance below the equilibrium plane, thus lowering the depth of the force equilibrium). This approach enables accepting that shaft resistance is equal in negative and positive direction, but the added resistance below the E.P. for a tapered pile due to the positive response of the taper, can be included in the calculation.

## 7.8 Standard Penetration Test, SPT, Method for Determining Axial Pile "Capacity"

For the purpose of offering a historical background, this section quotes recommendations of the past on the use of the N-index in estimating the "capacity" of a pile. For many years, the N-index of standard penetration test has been used to calculate "capacity" of piles. However, the standard penetration test (SPT) is a subjective and highly variable test. The Canadian Foundation Engineering Manual (1992) lists the numerous irrational factors influencing the N-index. The person doing the analysis using the N-index must consider the split-spoon sample of the soil obtained in the test and relate the analysis to the site and to area-specific experience of the SPT-test. These days, N-indices are usually adjusted to the  $N_{60}$ -value, which is the value after correction to an impact energy equal to 60 % of the nominal positional energy of the 63.5 kg-weight falling from 760-mm height. Several additional adjustments have also been proposed. Meyerhof (1976) compiled and rationalized some of the experience then available and recommended that the "capacity" be a function of the N-index (Eq. 7.7). N.B., Meyerhof "calibrated" N-indices to tests on primarily Franki-piles in Eastern Canada—in glacial till and coarse-grained soils.

$$(7.7) \quad R = R_t + R_s = mN_t A_t + n\bar{N}_s A_s D$$

where

- $m$  = a toe coefficient
- $n$  = a shaft coefficient
- $N_t$  = N-index at the pile toe (taken as a pure number)
- $\bar{N}_s$  = N-index average along the pile shaft (taken as a pure number)
- $A_t$  = pile toe area
- $A_s$  = unit shaft area; circumferential area
- $D$  = embedment depth

For values inserted into Eq. 7.7 using base SI-units, that is,  $\mathbf{R}$  in newton,  $\mathbf{D}$  in metre, and  $\mathbf{A}$  in  $\text{m}^2/\text{m}$ , the toe and shaft coefficients,  $\mathbf{m}$  and  $\mathbf{n}$ , become:

$$\begin{aligned} \mathbf{m} &= 400 \cdot 10^3 \text{ for driven piles and } 120 \cdot 10^3 \text{ for bored piles (N/m}^2\text{)} \\ \mathbf{n} &= 2 \cdot 10^3 \text{ for driven piles and } 1 \cdot 10^3 \text{ for bored piles (N/m}^2\text{)} \end{aligned}$$

For values inserted into Eq. 7.7 using English units with **R** in kips, **D** in feet, and **A** in ft<sup>2</sup>/ft, the toe and shaft coefficients, **m** and **n**, become:

$$\begin{aligned} m &= 8 \text{ for driven piles and } 2.4 \text{ for bored piles (ksf)} \\ n &= 0.04 \text{ for driven piles and } 0.02 \text{ for bored piles (ksf)} \end{aligned}$$

Decourt (1989; 1995) suggested that the pile "capacity" should be calculated according to Eq. 7.8. The equation presumes that values are input in base SI-units, that is, **R<sub>t</sub>** and **R<sub>s</sub>** in newton, **D** in metre, **A<sub>t</sub>** in m<sup>2</sup> and **A<sub>s</sub>** in m<sup>2</sup>/m.

$$(7.8) \quad R = R_t + R_s = K N_t A_t + \alpha(2.8N_s + 10) A_s D$$

where

- R<sub>t</sub>** = total toe resistance
- R<sub>s</sub>** = total shaft resistance
- K** = a toe coefficient per soil type and construction method as listed in Table 7.5
- α** = a shaft coefficient per soil type and construction method as listed in Table 7.6
- N<sub>t</sub>** = N-index at the pile toe (taken as a pure number)
- N<sub>s</sub>** = N-index average along the pile shaft (taken as a pure number)
- A<sub>t</sub>** = pile toe area
- A<sub>s</sub>** = unit shaft area; circumferential area
- D** = embedment depth

**TABLE 7.5 Toe Coefficient K** (Decourt 1989; 1995)

Soil Type	Displacement Piles	Non-Displacement Piles
Sand	325 · 10 <sup>3</sup>	165 · 10 <sup>3</sup>
Sandy Silt	205 · 10 <sup>3</sup>	115 · 10 <sup>3</sup>
Clayey Silt	165 · 10 <sup>3</sup>	100 · 10 <sup>3</sup>
Clay	100 · 10 <sup>3</sup>	80 · 10 <sup>3</sup>

**TABLE 7.6 Shaft Coefficient α** (Decourt 1989; 1995)

Soil Type	Displacement Piles	Non-Displacement Piles
Sand	1 · 10 <sup>3</sup>	0.6 · 10 <sup>3</sup>
Sandy Silt	1 · 10 <sup>3</sup>	0.5 · 10 <sup>3</sup>
Clayey Silt	1 · 10 <sup>3</sup>	1 · 10 <sup>3</sup>
Clay	1 · 10 <sup>3</sup>	1 · 10 <sup>3</sup>

O'Neill and Reese (1999) and Brown (2018) suggested calculating the **toe resistance, r<sub>t</sub>**, of a drilled shaft in cohesionless soil as given in Eq. 7.9. For piles with a toe diameter larger than 1,270 mm (50 inches), the toe resistance calculated according to Eq. 7.9 should be reduced by multiplication with a factor, **f<sub>t</sub>**, according to Eqs. 7.10a and 10b with units per the system used—SI or US customary.

$$(7.9) \quad r_t = 0.59 \left( N_{60} \frac{\sigma_{ref}}{\sigma'_z} \right)^{0.8} \sigma'_z$$

$$(7.10a) \quad f_t = 1.3/b \quad \text{with } b \text{ in units of metre}$$

$$(7.10b) \quad f_t = 50/b \quad \text{with } b \text{ in units of inches}$$

where  $r_t$  = toe resistance in units of MPa and ksf, respectively  
 $N_{60}$  = N-index (blows/0.3 m) energy-corrected taken as a pure number  
 $\sigma'_{ref}$  = a reference stress, a constant, which for all practical purposes is equal to 100 kPa (originally, it was set to 1 atmosphere pressure, 1 kg/cm<sup>2</sup>)  
 $\sigma'_z$  = overburden stress at the depth of the pile toe  
 $b$  = diameter of the pile toe (mm or inch)  
 $f_t$  = toe resistance correction factor (non-dimensional)

With regard to **shaft resistance**, O'Neill and Reese (1999) suggested applying effective stress approach, calculating the beta-coefficient (Section 7.2) for drilled shafts in cohesionless soil directly, as given in Eqs. 7.11 and 7.12. The calculated unit shaft resistance,  $r_s = \beta\sigma'_z$ , must not exceed 200 kPa (was originally 4 ksf). Note that for  $N_{60} > 15$ , the O'Neill-Reese beta-coefficient only depends on the depth,  $z$ , and does not apply at depths greater than about 40 m (37.48 m). The equations are included in AASHTO (2010). However, for unstated reason, AASHTO changed the factor "0.245" to "0.135".

$$(7.11) \quad \beta = \frac{N_{60}}{15} (1.5 - 0.245\sqrt{z}) \quad \text{for } N_{60} \leq 15$$

$$(7.12) \quad \beta = 1.5 - 0.245\sqrt{z} \quad \text{for } N_{60} > 15$$

where  $\beta$  = the beta-coefficient (the effective stress proportionality coefficient)  
 $z$  = the SPT sampling depth  
 $N_{60}$  = N-index (blows/0.3 m) energy-corrected

The test and the N-index have substantial qualitative value for the experienced geotechnical engineer, but should be used only very cautiously for quantitative analysis. Indeed, I believe that using the N-index numerically in formulae, such as Eqs. 7.7 through 7.12, is unsafe and imprudent unless used with correlation to prior experience from not just the same geology but also the same site. As I stated in Chapter 6, it is amazing that the arbitrary nature of the calculated N-factors has not long ago sent the SPT-formulae to the place where they belong—the museum of old paradigms whose time has passed.

## 7.9 Cone Penetration Test, CPTU, Method for Determining Axial Pile "Capacity"

The static cone penetrometer appears to resemble a pile. There is shaft resistance in the form of the sleeve resistance measured immediately above the cone, and there is toe resistance in the form of the directly applied and measured cone resistance. Despite the resemblance, there is little scientific reason for why cone and sleeve resistances measured for the small diameter cone pushed at a constant rate into the soil would have any correlation to the long-term static response of the pile, ostensibly, the ultimate resistance, to boot! That is, other than the fact that site-specific correlations can be and have been found. Without site-specific reference to such correlations—"calibrations"—relying on the analysis of "capacity" using results from the static cone makes for a very uncertain design. The following account of the various methods are offered primarily for reasons of including historical content in this textbook.

Two main approaches for application of cone data to pile design has evolved: indirect and direct methods.

**Indirect CPT methods** employ soil parameters, such as friction angle and undrained shear strength estimated from the cone data as based on bearing "capacity" and/or cavity expansion theories. The approach involves significant uncertainties. The indirect methods disregard horizontal stress, apply strip-footing bearing "capacity" theory, and neglect soil compressibility and strain softening. These methods are not particularly suitable for use in engineering practice and are here not further referenced.



**Direct CPT methods** more or less equal the cone resistance with the pile ultimate unit resistance. Some methods may use the cone sleeve resistance in determining unit shaft resistance. Several methods modify the resistance values to consider the difference in diameter between the pile and the cone, a “scaling” effect. A common thought is that the influence of mean effective stress, soil compressibility, and stiffness affect the pile and the cone in equal measure, which eliminates the need to supplement the field data with laboratory testing and to calculate intermediate values, such as  $K_s$  and  $N_q$ .

Correlation of CPT-determined pile "capacity" is rather poor and essentially absent for individual pile elements. In view of the fact that the definition of "capacity" varies so much in the practice, as evidenced by Figure 8.8, basing a "capacity" on results of analysis of a CPT-test or other in-situ test, by any of published numerical methods, is mostly an exercise in futility (Fellenius 2017).

Nevertheless, the cone penetrometer test, CPT, has been and is used for numerical or quantitative determination of pile "capacity". Seven methods are presented in the following. The first six are based on the mechanical or the electric cones and do not correct for the pore pressures acting on the cone shoulder. The seventh method is the Eslami-Fellenius method, which is based on the piezocone, CPTU. Of course, the Eslami-Fellenius method can also be applied to CPT results, subject to suitable assumptions made on the distribution of the pore pressure, usually applying the neutral pore pressure,  $u_0$ . None of the methods is better or worse than the other.

1. Schmertmann and Nottingham
2. deRuiter and Beringen (commonly called the "Dutch Method" or the “European Method”)
3. Bustamante and Gianselli (commonly called the "LCPC Method" or the “French Method”)
4. Meyerhof (method for sand)
5. Tumay and Fakhroo (method limited to piles in soft clay)
6. ICP method
7. University of Western Australia method
8. Eslami and Fellenius

Often, CPT and CPTU data include a small amount of randomly distributed extreme values, "peaks and troughs", that may be representative for the response of the cone to the soil characteristics, but not for a pile having a much larger diameter. Keeping the extreme values will have a minor influence on the pile shaft resistance, but it will have a major influence on the pile toe resistance. Therefore, when calculating pile toe "capacity", it is common practice to manually filter and smooth the data by either applying a "minimum path" rule or, more subjectively, by reducing the influence of the peaks and troughs from the records. To establish a representative value of the cone resistance to the pile unit toe resistance, the methods average the CPT data over an "influence zone to filter the toe resistance. The first six methods employ arithmetic average, whereas the eighth method (Eslami-Fellenius method) employs geometric mean.

### 7.9.1 Schmertmann and Nottingham

#### Toe resistance

The **Schmertmann and Nottingham** method is based on a summary of the work on model and full-scale piles presented by Nottingham (1975) and Schmertmann (1978). The unit toe resistance,  $r_t$ , is a "minimum path" average obtained from the cone resistance in an influence zone extending from  $8b$  above the pile toe ( $b$  is the pile diameter) and  $0.7b$  or  $4b$ , as indicated in [Figure 7.12](#).

The procedure consists of five steps of filtering the  $q_c$  data to “minimum path” values. Step 1 is determining two averages of cone resistance within the zone below the pile toe, one for a zone depth of  $0.7b$  and one for  $4b$  along the path "a" through "b". The smaller of the two is retained. (The zone height  $0.7b$  applies to where the cone resistance increases with depth below the pile toe). Step 2 is determining the smallest cone resistance within the zone used for the Step 1. Step 3 consists of

determining the average of the two values per Steps 1 and 2. Step 4 is determining the average cone resistance in the zone above the pile toe according to the minimum path. (Usually, just the average of the cone resistance within the zone is good enough). Step 5, finally, is determining the average of the Step 3 and Step 4 values. This value is denoted  $q_{ca}$ .

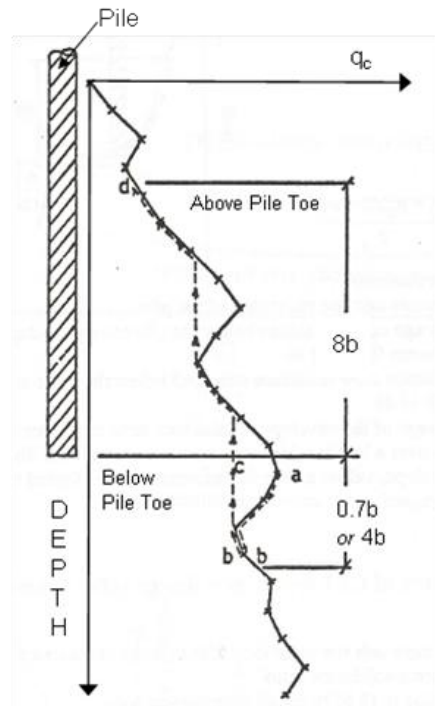


Fig. 7.12 Determining the influence zone for toe resistance (Schmertmann, 1978)

The pile toe resistance is then determined according to Eq. 7.13.

$$(7.13) \quad r_t = C q_{ca}$$

where

- $r_t$  = pile unit toe resistance; an upper limit of 15 MPa is imposed
- $C$  = correlation coefficient governed by the overconsolidation ratio, OCR
- $q_{ca}$  = the cone resistance filtered in the influence zone per the above procedure

The correlation coefficient,  $C$ , ranges from 0.5 through 1.0 depending on overconsolidation ratio, OCR, according to one of the “1” through “3” slopes between the toe resistance,  $r_t$ , and the minimum-path average of the cone resistance (“filtered in the influence zone”), as indicated in Figure 7.13. The relations are usually also applied to a pile toe located in clay.

### Unit shaft resistance

The unit shaft resistance,  $r_s$ , may be determined from the sleeve resistance as expressed by Eq. 7.14.

$$(7.14) \quad r_s = K_f f_s$$

where

- $r_s$  = pile unit shaft resistance; an upper limit of 120 kPa is imposed
- $K_f$  = a dimensionless coefficient
- $f_s$  = sleeve resistance

Figure 7.14 shows that, in clay,  $K_f$  is a function of the sleeve resistance and ranges from 0.2 through 1.25.

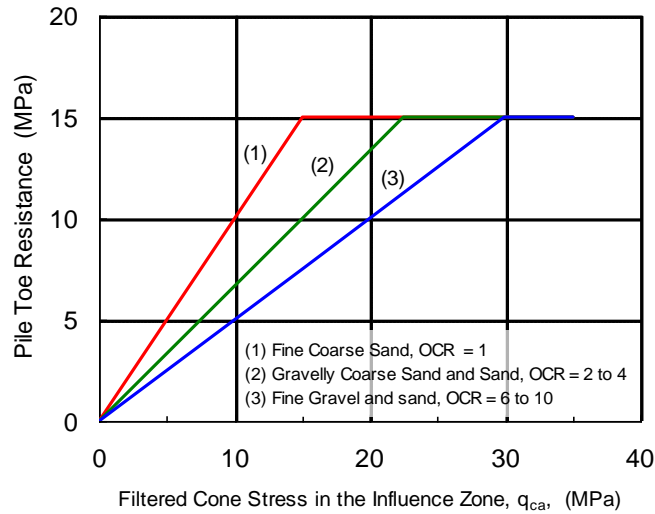


Fig. 7.13 Adjustment of unit toe resistance to OCR (after Nottingham 1975)

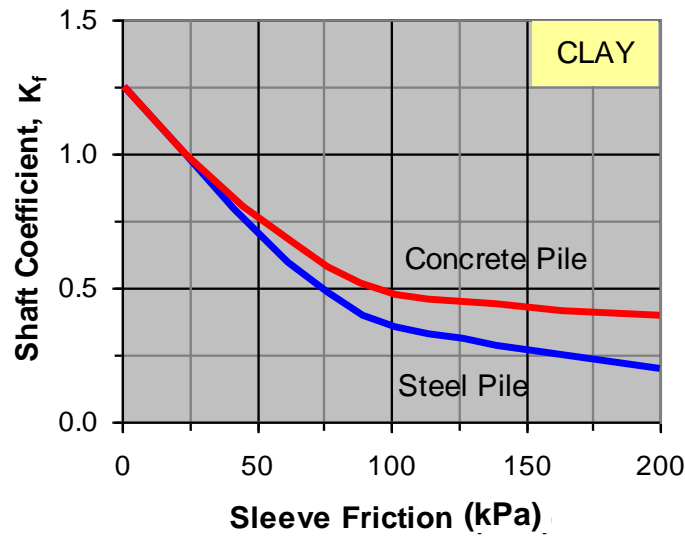


Fig. 7.14 Shaft coefficients for use in Eq. 7.14 (after Nottingham 1975)

In sand,  $K_f$  is assumed to be a function of the pile embedment ratio,  $D/b$ . Within a depth of the first eight pile diameters below the ground surface ( $D/b = 8$ ), the  $K_f$ -coefficient is linearly interpolated from zero at the ground surface to 2.5. Hereunder, the value reduces from 2.5 to 0.891 at an embedment of 20  $D/b$ .

Simply applying  $K_f = 0.9$  straight out is usually satisfactory. Alternatively, in sand, but not in clay, the shaft resistance may be determined from the cone resistance,  $q_c$ , according to Eq. 7.15.

$$(7.15) \quad r_s = K_c q_c$$

where

$r_s$	=	unit shaft resistance; an upper limit of 120 kPa is imposed
$K_c$	=	a dimensionless coefficient; a function of the pile type.
		for open toe, steel piles $K_c = 0.008$
		for closed-toe pipe piles $K_c = 0.018$
		for concrete piles $K_c = 0.012$
$q_c$	=	cone resistance

### 7.9.2 deRuiter and Beringen

#### Toe resistance

The “Dutch” method was presented by deRuiter and Beringen (1979). For unit toe resistance of a pile in sand, the method is the same as the Schmertmann and Nottingham method. In clay, the unit toe resistance is determined from shear strength analysis according to conventional bearing "capacity" theory as indicated in Eqs. 7.16 and 7.17.

$$(7.16) \quad r_t = 5 S_u$$

$$(7.17) \quad S_u = \frac{q_c}{N_k}$$

where

$r_t$	=	pile unit toe resistance; an upper limit of 15 MPa is imposed
$S_u$	=	undrained shear strength
$N_k$	=	a dimensionless coefficient, ranging from 15 through 20, usually = 20

#### Shaft resistance

In **sand**, the unit shaft resistance is the smallest of the sleeve resistance,  $f_s$ , and  $q_c/300$ .

In **clay**, the unit shaft resistance may also be determined from the undrained shear strength,  $S_u$ , as given in Eq. 7.18.

$$(7.18) \quad r_s = \alpha S_u = \alpha \frac{q_c}{N_k}$$

where

$r_s$	=	pile unit shaft resistance
$\alpha$	=	adhesion factor equal to 1.0 for normally consolidated clay and 0.5 for overconsolidated clay
$S_u$	=	undrained shear strength according to Eq. 7.17

An upper limit of 120 kPa is imposed on the unit shaft resistance.

### 7.9.3 LCPC

**LCPC 1982.** The LCPC method, also called the “French” or “Bustamante” method (LCPC = Laboratoire Central des Ponts et Chaussees) method is based on experimental work of Bustamante and Gianceselli (1982) for the French Highway Department. For details, see CFEM 1992. The method does not include either of sleeve resistance,  $f_s$ , and correction of the cone resistance for the pore pressure,  $U_2$ , acting on the cone shoulder.

### Toe resistance

The unit toe resistance,  $r_t$ , is determined from the cone resistance within an influence zone of  $1.5b$  above and  $1.5b$  below the pile toe, as illustrated in Figure 7.15 (“ $b$ ” is the pile diameter). First, the cone resistance within the influence zone is averaged to  $q_{ca}$ . Next, an average,  $q_{caa}$ , is calculated of the average of the  $q_{ca}$ -values that are within a range of  $0.7$  through  $1.3$  of  $q_{ca}$ . Finally, the toe resistance is obtained from multiplying the equivalent value with a correlation coefficient,  $C_{LCPC}$ , according to Eq. 7.19.

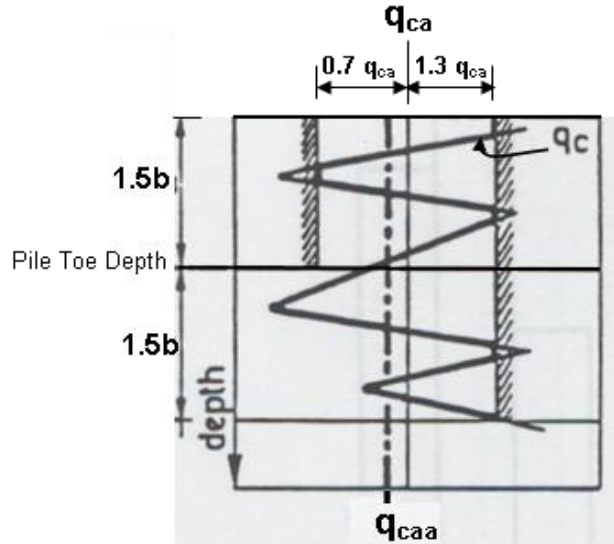


Fig. 7.15 Averaging the cone resistance according to the LCPC method. The “ $b$ ” stands for pile toe diameter. (Bustamante and Gianselli, 1982).

$$(7.19) \quad r_t = C_{LCPC} q_{caa}$$

where

- $r_t$  = pile unit toe resistance; an upper limit of 15 MPa is imposed
- $C_{LCPC}$  = correlation coefficient (Table 7.7A)
- $q_{caa}$  = average cone resistance in the influence zone

As indicated in Table 7.7A, for driven steel piles and driven precast piles, the correlation coefficient,  $C_{LCPC}$ , ranges from 0.45 through 0.55 in clay and from 0.40 through 0.50 in sand. For bored piles, the values are about 20 % smaller.

**TABLE 7.7A Coefficients of Unit Toe Resistance in the LCPC Method**  
(Bustamante and Gianselli 1982)

Soil Type	Cone Resistance (MPa)	Bored Piles	Driven Piles
		$C_{LCPC}$ (---)	$C_{LCPC}$ (---)
CLAY	– $q_c < 1$	0.40	0.50
	$1 < q_c < 5$	0.35	0.45
	$5 < q_c$ –	0.45	0.55
SAND	– $q_c < 12$	0.40	0.50
	$12 < q_c < -$	0.30	0.40

**Shaft resistance**

The unit shaft resistance,  $r_s$ , is determined from Eq. 7.20 with the  $K_{LCPC}$ -coefficient ranging from 0.5 % through 3.0 %, as governed by magnitude of the cone resistance, type of soil, and type of pile. Table 7.7B shows upper limits of the unit shaft resistance, ranging from 15 kPa through 120 kPa depending on soil type, pile type, and pile installation method.

$$(7.20) \quad r_s = K_{LCPC} q_c \leq J \quad (\text{see Table 7.7B})$$

- where
- $r_s$  = unit shaft resistance; for imposed limits
  - $K_{LCPC}$  = a dimensionless coefficient; a function of the pile type and cone resistance
  - $J$  = upper limit value of unit shaft resistance
  - $q_c$  = cone resistance (note, not corrected for pore pressure on cone shoulder)

The limits shown in Table 7.7B are developed in its own practice and geologic setting, and it is questionable if they have any general validity. It is common for users to either remove the limits or to adjust them to new values. Many also apply other values, personally preferred, of the K and J coefficients, as well as the C-coefficient for toe resistance. Therefore, where the LCPC method or a "modified LCPC method" is claimed to be used, the method is often not the actual method by Bustamante and Gianselli (1982), but simply a method whereby the CPT cone resistance by some correlation is used to calculate pile shaft and toe resistances. Such adjustments do not remove the rather capricious nature of the limits.

The correlation between unit shaft resistance and cone resistance,  $q_c$ , is represented graphically in Figure 7.16 showing the values in "CLAY" and Figure 7.17 showing the values in "SAND". Note, the LCPC method does not correct the cone resistance for the pore pressure on the cone shoulder.

**TABLE 7.7B Coefficients and Limits of Unit Shaft Resistance in the LCPC Method Quoted from the CFEM (1992)**

Soil Type	Cone resistance (MPa)	Concrete Piles & Bored Piles	Steel Piles	Maximum $r_s$
		$K_{LCPC}$ (—)	$K_{LCPC}$ (—)	J (kPa)
CLAY	– $q_c < 1$	0.011 (1/90)	0.033 (1/30)	15
	1 < $q_c < 5$	0.025 (1/40)	0.011 (1/80)	35
	5 < $q_c$ –	0.017 (1/60)	0.008 (1/120)	35
	(for $q_c > 5$ , the unit shaft resistance, $r_s$ , is always larger than 35 kPa)			
SAND	– $q_c < 5$	0.017 (1/60)	0.008 (1/120)	35
	5 < $q_c < 12$	0.010 (1/100)	0.005 (1/200)	80
	12 < $q_c$ –	0.007 (1/150)	0.005 (1/200)	120

The values in parenthesis are the inverse of the  $K_{LCPC}$  -coefficient (the format of the original presentation).

An updated LCPC method, LCPC 2012, was published in 2012 (AFNOR (2012), NF P 94-262. *Justification des ouvrages géotechniques, Normes d'application nationale de l'Eurocode 7, Afnor, Paris, July 2012*) as summarized below. The summary does not include all details and before trusting a site-specific application, a user should consult the original document.

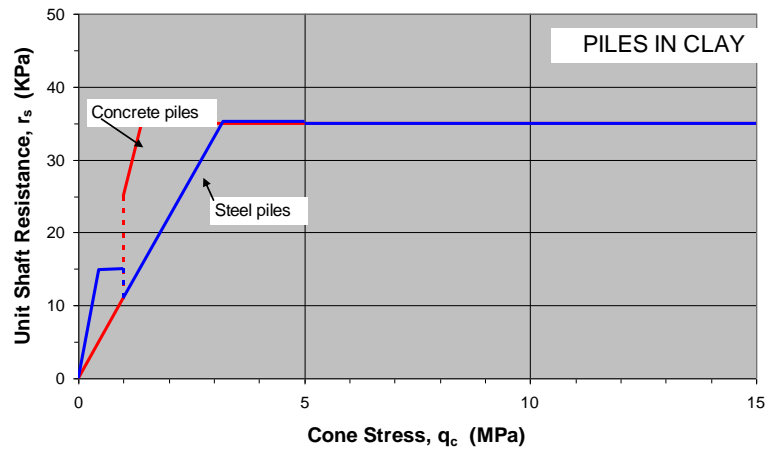


Fig. 7.16 Unit shaft resistance versus cone resistance,  $q_c$ , for piles in clay according to the LCPC 2012

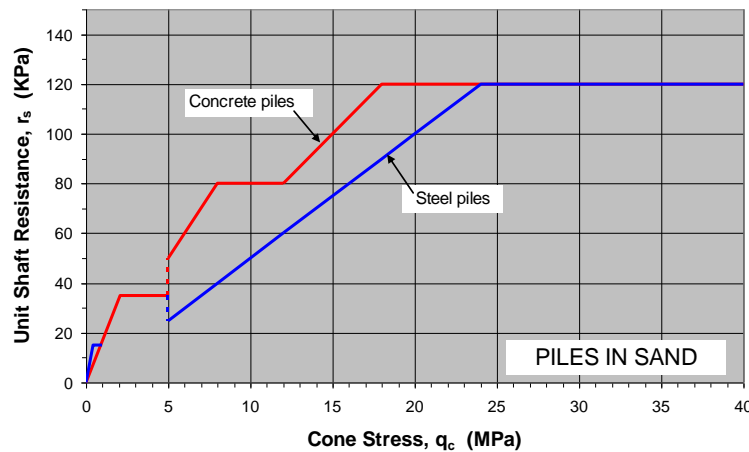


Figure 7.17 Unit shaft resistance versus cone resistance,  $q_c$ , for piles in sand according to the LCPC 2012

Similarly to CPT1982, CPT2012 does not adjust the cone resistance for pore pressure, does not include aspects of sleeve resistance, and the soil profile is assessed by methods other than the CPT results

The 2012 version **unit toe resistance** is obtained according to Eq. 7.21 with some adjustment according to embedment depth.

$$(7.21) \quad r_t = k_c q_{ce}$$

where

- $r_t$  = toe resistance
- $k_c$  = CPT-factor per Table 7.8
- $q_{ce}$  = average cone resistance within a zone of height of  $b + 3a$  below and above the pile toe depth
- $b$  = pile toe diameter
- $a$  =  $b/2$ ;  $\leq 500$  mm

The CPT-factor is determined according soil type and pile class (a Eurocode classification) to values ranging from 0.15 through 0.50 (Table 7.8).

**Table 7.8** CPT factor  $k_c$  for a relative embedment  $D_{\text{depth}}/b > 5$

Soil Type Pile Class <sup>(c)</sup>	Clay % CaCO <sub>3</sub> < 30 % Silt	Intermediate soil	Sand Gravel	Chalk	Marl and limestone	Layered or fragmented rock <sup>(a)</sup>
1	0.40 <sup>(b)</sup>	0.30 <sup>(b)</sup>	0.20 <sup>(b)</sup>	0.30 <sup>(b)</sup>	0.30 <sup>(b)</sup>	0.30 <sup>(b)</sup>
2	0.45	0.30	0.25	0.30	0.30	0.30
3	0.50	0.50	0.50	0.40	0.35	0.35
4	0.45	0.40	0.40	0.40	0.40	0.40
5 #	0.35	0.30	0.25	0.15	0.15	0.15
6 #	0.40	0.40	0.40	0.35	0.20	0.20
7 #	0.35	0.25	0.15	0.15	0.15	0.15
8	0.45 <sup>(b)</sup>	0.30 <sup>(b)</sup>	0.20 <sup>(b)</sup>	0.30 <sup>(b)</sup>	0.30 <sup>(b)</sup>	0.25 <sup>(b)</sup>

For piles installed by vibratory driving a reduction of 50% should be made on the  $k_c$ -factor.

(a) The value of  $k_c$  for weathered and fragmented rock should be taken equal to that of a loose formation in the table to which the material concerned resembles most closely. In the case of sound rock, it is necessary to assess whether an adjustment based on obvious pessimism is sufficient, or whether it is appropriate to have recourse to a specific methods of rock mechanics.

(b) For micropiles, peak resistance is normally not taken into account.

(c) Reference should be made to the choice of perimeters and areas of the piles to be considered in the calculations.

The LCPC2012 version **unit shaft resistance** is obtained according to Eq. 7.22, but , if used for design, the calculated unit shaft resistances must not exceed those defined in Table 7.11.

$$(7.22) \quad r_s = \alpha_{\text{pile-soil}} f_{\text{soil}} q_c$$

where  $r_s$  = unit shaft resistance  
 $\alpha_{\text{pile-soil}}$  = CPT-factor per Table 7.9  
 $f_{\text{soil}}$  = modifier to type of soil, cone resistance, and parameters  $a$ ,  $b$ , and  $c$  per Eq. 7.23 and Table 7.10  
 $q_c$  = cone resistance

$$(7.23) \quad f_{\text{soil}} = (aq_c + b)(1 - e^{-cq_c})$$

where  $f_{\text{soil}}$  = modifier to type of soil, cone resistance, and parameters  $a$ ,  $b$ , and  $c$  per Eq. 7.23 and Table 7.10  
 $a$ ,  $b$ ,  $c$  = parameters of Table 7.10  
 $q_c$  = cone resistance



**Table 7.9** CPT factor  $\alpha_{\text{pile-soil}}$ 

Pile Class	Construction method	Clay % CaCO <sub>3</sub> < 30 % Silt	Intermediate soil	Sand Grave	Chalk	Marl and limestone	Layered or fragmented rock
1	Bored (piles and barrettes)	0.55	0.65	0.70	0.80	1.40	1.50
2	Drilled with mud	0.65	0.80	1.00	0.80	1.40	1.50
3	Drilled, casing permanent	0.35	0.40	0.40	0.25	0.85	—
4	Drilled, casing recovered	0.65	0.80	1.00	0.75	0.13	—
5	Single or mud drilled with grooves	0.70	0.85	—	—	—	—
6	Drilled or continuous auger	0.75	0.90	1.25	0.95	1.50	1.50
7	Screw pile, cast	0.95	1.15	1.45	0.75	1.60	—
8	Screw pile, pipe	0.30	0.35	0.40	0.45	0.65	—
9	Driven precast or prestressed	0.55	0.65	1.00	0.45	0.85	—
10	Driven coated concrete	1.00	1.20	1.45	0.85	1.50	—
11	Driven, grouted	0.60	0.70	1.00	0.95	0.95	—
12	Driven steel, closed toe	0.40	0.50	0.85	0.20	0.85	—
13	Driven steel, open toe	0.60	0.70	0.50	0.25	0.95	0.95
14	Driven H-pile	0.55	0.65	0.70	0.20	0.95	0.85
15	HP driven injected	1.35	1.60	2.00	1.10	2.25	2.25
16	Driven sheet pile	0.45	0.55	0.55	0.20	1.25	1.15
17	Micropile Type I	—	—	—	—	—	—
18	Micropile Type II	—	—	—	—	—	—
19	Pile or micropile injected (Type III)	1.35	1.60	2.00	1.10	2.25	2.25
20	Pile or micropile injected (Type IV)	1.70	2.05	2.65	1.40	2.90	2.90

For piles, installed by vibratory driving a reduction of 30% should be made on the values.

For micropiles, the proposed values presume strict and careful execution of the corresponding injection.

For Pile Class 17 and 18, the unit shaft resistance of the technically closest pile or micropile techniques should be considered.

The values mentioned for Pile Class 6 are given for piles made with continuous recording of drilling and concreting parameters. The values mentioned for Pile Class 7 installed by concreting directly to the concrete pump apply to continuous recording of the process. Otherwise, discontinuities and deterioration of the pile may occur during construction.

**Table 7.10** Parameters  $a$ ,  $b$ , and  $c$  of modifier  $f_{\text{soil}}$ 

Soil type	Clay	Intermediate soil	Sand	Chalk	Marl and limestone	Layered or fragmented rock
a	0.0018	0.0015	0.0012	0.0015	0.0015	0.0015
b	0.1	0.1	0.1	0.1	0.1	0.1
c	0.4	0.25	0.15	0.25	0.25	0.25

**Table 7.11** Maximum unit shaft resistance (kPa)

Class No.	Construction Method	Clay	Silt	Sand	Chalk	Marl Limestone	Fragmnt. Rock
1	Bored (piles and barrettes)	90	90	90	200	170	200
2	Drilled with mud	90	90	90	200	170	200
3	Drilled, casing permanent	50	50	50	50	90	—
4	Drilled, casing recovered	90	90	90	170	170	—
5	Single or mud drilled with grooves	90	90	—	—	—	—
6	Drilled single- or double-rotation continuous auger	90	90	170	200	200	200
7	Screw pile, cast	130	130	200	170	170	—
8	Screw pile, pipe	50	50	90	90	90	—
9	Driven precast or prestressed	130	130	130	90	90	—
10	Driven coated concrete	170	170	260	200	200	—
11	Driven grouted	90	90	130	260	200	—
12	Driven steel, closed toe	90	90	90	50	90	—
13	Driven steel, open toe	90	90	50	50	90	90
14	Driven H-pile	90	90	130	50	90	90
15	H-pile injected	200	200	380	320	320	320
16	Driven sheet pile	90	90	50	50	90	90
17	Micropile Type I	—	—	—	—	—	—
18	Micropile Type II	—	—	—	—	—	—
19	Pile or micropile injected (Type III)	200	200	380	320	320	320
20	Pile or micropile injected (Type IV)	200	200	440	440	440	500

The LCPC2012 method enables a user to choose parameters that always will show a right-on capacity 'prediction' once a post-test judicious adjustment is made to the parameter choices offered in the tables.

#### 7.9.4 Meyerhof

##### Toe resistance

The **Meyerhof** method (Meyerhof 1951; 1963; 1976) is intended for calculating the "capacity" of piles in sand. For unit toe resistance, the influence of scale effect of piles and shallow penetration in dense sand strata is considered by applying two modification factors,  $C_1$  and  $C_2$ , to the  $q_c$  average. The unit toe resistance for driven piles is given by Eq. 7.24.

$$(7.24) \quad r_t = q_{ca} C_1 C_2$$

- where
- $r_t$  = unit toe resistance; for bored piles, reduce  $r_t$  to 70 % of Eq. 7.24
  - $q_{ca}$  = arithmetic average of cone resistance,  $q_c$ , in a zone ranging from "1b" below through "4b" above pile toe
  - $C_1$  =  $[(b + 0.5)/2b]^n$ ; modification factor for scale effect  
when  $b > 0.5$  m, otherwise  $C_1 = 1$
  - $C_2$  =  $D/10b$ ; modification for penetration into dense strata

- $n$  = when  $D < 10b$ , otherwise  $C_2 = 1$   
 an exponent equal to  
 1 for loose sand ( $q_c < 5$  MPa)  
 2 for medium dense sand ( $5 < q_c < 12$  MPa)  
 3 for dense sand ( $q_c > 12$  MPa)  
 $b$  = pile diameter  
 $D$  = embedment of pile in a dense sand layer

### Shaft resistance

For driven piles, the ultimate unit shaft resistance is either taken as equal to the sleeve resistance,  $f_s$ , or 50 % of the cone resistance,  $q_c$ , as indicated in Eqs. 7.25 and 7.26. For bored piles, reduction factors of 70 % and 50 %, respectively, are applied to these calculated values of shaft resistance.

$$(7.25) \quad r_s = K_f f_s \quad K_f = 1.0$$

$$(7.26) \quad r_s = K_c q_c \quad K_c = 0.5$$

- where
- $r_s$  = unit shaft resistance
  - $K_f$  = sleeve resistance modification coefficient
  - $K_c$  = cone resistance modification coefficient
  - $f_s$  = unit sleeve resistance, **kPa**
  - $q_c$  = unit cone resistance, **kPa**

### 7.9.5 Tumay and Fakhroo

#### Toe resistance

The **Tumay and Fakhroo** method is based on an experimental study in clay soils in Louisiana (Tumay and Fakhroo 1981). The **unit toe resistance** is determined in the same way as in the Schmertmann and Nottingham method, Eq. 7.13.

#### Shaft resistance

The ultimate unit shaft resistance is determined according to Eq. 7.27 with the  $K_f$ -coefficient determined according to Eq. 7.28 (note that the  $K$ -coefficient is not dimensionless in this equation).

$$(7.27) \quad r_s = K_f f_s$$

- where
- $r_s$  = pile unit shaft resistance, kPa
  - $K_f$  = a coefficient
  - $f_s$  = unit sleeve resistance, **kPa**

$$(7.28) \quad K_f = 0.5 + 9.5e^{-90f_s}$$

- where
- $e$  = base of natural logarithm = 2.718
  - $f_s$  = unit sleeve resistance, **MPa**

### 7.9.6 ICP Method

Jardine et al. (2005) present the Imperial College method of using CPT results to determine pile "capacity" in sand and clay. As in the other CPT methods, the sleeve resistance is not considered and the

cone resistance is not corrected for the effect of the pore pressure acting on the cone shoulder. The following description is limited to the method for sand, as it is a bit simpler than the method for clay.

### Toe resistance in sand

The ICP method applies the cone resistance with adjustment to the relative difference between the cone diameter and the pile toe diameter as indicated in Eq. 7.29.

$$(7.29) \quad r_t = q_{ca} \left[ 1 - 0.5 \lg \left( \frac{b_{pile}}{b_{cone}} \right) \right]$$

where

- $r_t$  = pile unit toe resistance
- $q_{ca}$  = unit cone resistance filtered according to the LCPC method
- $b_{pile}$  = pile toe diameter
- $b_{cone}$  = cone diameter; 36 mm for a cone with 10 cm<sup>2</sup> base area

For pile diameters larger than 900 mm, a lower limit of  $r_t = 0.3q_c$  applies. Moreover, for piles driven open-toe, a different set of equations apply, which depends on whether or not the pile is plugged.

### Shaft resistance in sand

According to the ICP method, the unit shaft resistance of closed-toe piles driven in sand is determined according to Eqs. 7.30 and 7.31, which I offer without comments, leaving the reader to judge the engineering relevance of the equations.

$$(7.30) \quad r_s = K_J q_c$$

where  $K_J$  is determined according to Eq. 7.28.

$$(7.31) \quad K_J = \left\{ 0.0145 \frac{\sigma'_z}{\sigma_r} \left( \frac{\sigma'_z}{\sigma_r} \right)^{0.13} \left( \frac{b}{h_f} \right)^{0.38} + [2q_c (0.0203 + 0.00125 \frac{q_c}{\sigma'_z \sigma_r})^{-0.5} - 1.216 \times 10^{-6} \left( \frac{q_c^2}{\sigma'_z \sigma_r} \right)^{-1} \frac{0.01}{b}] \right\} \tan \delta$$

where

- $\sigma'_z$  = effective overburden stress
- $\sigma'_r$  = effective radial stress
- $b$  = pile diameter
- $h_f$  = depth below considered point to pile toe; limited to 8b
- $\delta$  = interface angle of resistance

To quote: Eq. 7.31 employs principles of "Coulomb failure criterion", "free-field vertical effective stress ( $\sigma'_z$ ) normalized by absolute atmospheric pressure", "local radial effective stress ( $\sigma'_r$ ) with dilatant increase", and "interface angle of friction at constant volume test" (or estimate from graph), is "uncorrected for overconsolidation" and applies to compression loading. The method has been developed by fitting to results from all of six field tests listed by Jardine et al. (2005).

### 7.9.7 Eslami and Fellenius

The Eslami-Fellenius method makes use of the piezocone, CPTU, which is a cone penetrometer equipped with a gage measuring the pore pressure at the cone (usually immediately behind the cone; at the cone shoulder, the so-called U2-position), which is a considerable advancement on the static cone. By means of the piezocone, the cone information can be related more dependably to soil parameters and a more detailed analysis be performed.

**Toe resistance** In the Eslami and Fellenius CPTU method (Eslami 1996; Eslami and Fellenius 1995; 1996; 1997; Fellenius and Eslami 2000), the cone resistance is transferred to an apparent “effective” cone resistance,  $q_E$ , by subtracting the measured pore pressure,  $U_2$ , from the measured cone resistance (after correcting it for the pore pressure acting against the shoulder). See Section 2.3, Figure 2.11. The pile **unit toe resistance** is the geometric average of the “effective” cone resistance over an influence zone that depends on the soil layering, which reduces—removes—potentially disproportionate influences of odd “peaks and troughs”, which the simple arithmetic average used by the CPT methods does not do. When a pile is installed through a weak soil into a dense soil, the average is determined over an **influence zone** extending from  $4b$  below the pile toe through a height of  $8b$  above the pile toe. When a pile is installed through a dense soil into a weak soil, the average above the pile toe is determined over an influence zone height of  $2b$  above the pile toe as opposed to  $8b$ . The relation is given in Eq. 7.32.

$$(7.32) \quad r_t = C_t q_{Eg}$$

where  $r_t$  = pile unit toe resistance  
 $C_t$  = toe correlation coefficient (toe adjustment factor)  
 $q_{Eg}$  = geometric average of the  $q_E$  one stress over the influence zone ( $q_t$  after correction for pore pressure on shoulder and adjustment to “effective” stress)

The toe correlation coefficient,  $C_t$ , also called toe adjustment factor, is a function of the pile size (toe diameter). The larger the pile diameter, the larger the movement required to mobilize the toe resistance. Therefore, the “usable” pile toe resistance diminishes with increasing pile toe diameter. The adjustment factor should be determined by the relation given in Eq. 7.33.

$$(7.33) \quad C_t = \frac{1}{3b} \quad C_t = \frac{12}{b} \quad C_t = \frac{1}{b}$$

(['b' in metre]                      ['b' in inches]                      ['b' in feet])

where  $b$  = pile diameter in units of either metre (or inches or feet)

**Shaft resistance** Also the ultimate unit shaft resistance is correlated to the average “effective” cone resistance with a modification according to soil type per the approach detailed below. The  $C_s$  correlation coefficient is determined from the soil profiling chart (Chapter 2, Figure 2.10), which uses both cone resistance and sleeve resistance. However, because the sleeve resistance is a more variable measurement than the cone resistance, the sleeve resistance value is not applied directly, but follows Eq. 7.34. Where  $U_2$  is large, it is sometimes more realistic to use  $u_0$ .

$$(7.34) \quad r_s = C_s q_E$$

where  $r_s$  = pile unit shaft resistance  
 $C_s$  = shaft correlation coefficient, which is a function of soil type determined from the Eslami-Fellenius soil profiling and Table 7.12  
 $q_E$  = cone resistance after correction for pore pressure on the cone shoulder and adjustment to apparent “effective” stress;  $q_E = q_t - U_2$ . Again, where  $U_2$  is large, it is sometimes more realistic to use  $u_0$ .

Figure 7.18 shows the unit shaft resistances for piles in sand according to the Eslami-Fellenius method, which separates the sand (Types 4a, 4b, and 5 in Table 7.8), overlain that of the LCPC method, which does not differentiate between different types of sand. The difference between  $q_c$  and  $q_t$  is disregarded in the figure. The comparison shows the difference in principle between the methods in that the resistance determined by the LCPC method only pertains to the two types of soil for all values of  $q_c$  making no

difference between types of sand, while the E-F method indicates a range of values as a function of the sand gradation (as determined from the CPTU soil classification—behavior type).

**TABLE 7.12 Shaft Correlation Coefficient,  $C_s$**

Soil Type	$C_s$
1. Soft sensitive soils	0.08
2. Clay	0.05
3. Silty clay, stiff clay and clayey silt	0.025
4a. Sandy silt and silt	0.015
4b. Fine sand or silty sand	0.010
5. Sand to sandy gravel	0.004

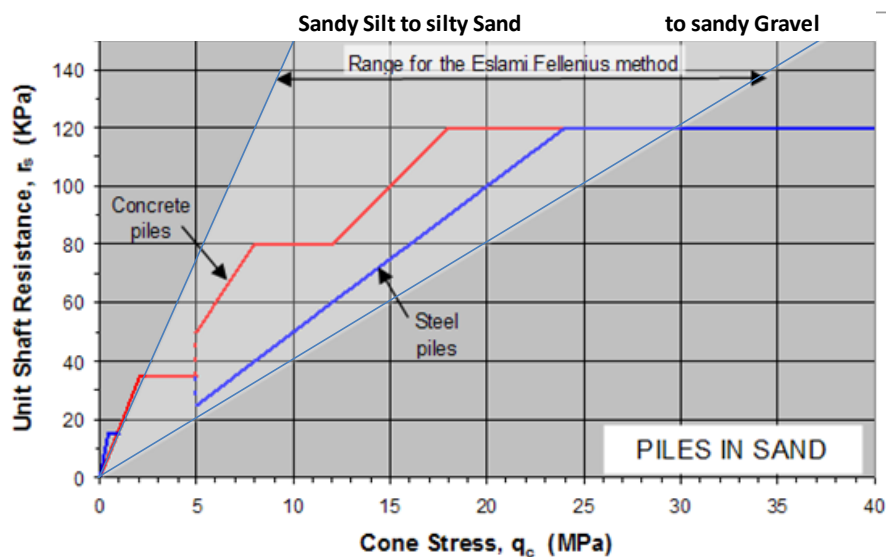


Fig. 7.18 Comparing unit shaft resistance versus cone resistance,  $q_c$ , for piles in sand according to the LCPC method (the red and blue lines) that of the Eslami-Fellenius method

Notice, all analysis of pile "capacity", whether from laboratory data, SPT-data, CPT-data, or other methods should be correlated back to an effective stress calculation and the corresponding beta- and  $N_f$ -coefficients be determined from the calculation for future reference.

Soil is variable, and digestive judgment of the various analysis results can and must be exercised to filter the data for computation of pile "capacity", and site-specific experience is almost always absolutely necessary. The more representative the information is, the less likely the designer is to jump to false conclusions, but one must always reckon with an uncertainty in the prediction.

While the soil types indicate a much larger differentiation than the "clay/sand" division of the CPT-methods, the shaft correlation coefficients values shown in Table 7.8 still present sudden changes when the  $q_t$  and  $f_s$  values change from plotting above and below a line in the soil classification chart. It is advisable to always plot the data in the soil classification chart and apply the same shaft correlation coefficient to soil layers that show data points that are grouped together even if they straddle a boundary line. If results from measured shaft distribution is available, the correlation coefficient should be determined by fitting to the measured shaft resistance. As mentioned, large U2 pore pressures can result in unrealistically small calculated resistances. It is then better to use  $q_t$ -values than  $q_E$ -values. When only having a CPT sounding,  $q_E$  can be calculated using  $q_c$ :  $q_E = q_c - U2$  or  $q_E = q_c - u_0$ .

### 7.9.8 Comments on the CPT and CPTU methods

The primary weakness of all CPT methods is that they are calibrated to a single point on the load-movement curve, the "capacity", disregarding all aspects of shape of the load-movement response and, indeed, that the "capacity" is defined according to several different ways (Section 8.2). Moreover, difficulties arise in applying some of the recommendations of the methods. For example:

1. Although the recommendations are specified to soil type (clay and sand; very cursorily characterized), but for the Eslami-Fellenius CPTU-method, the CPT pile-response estimates are not used for identifying the actual soil type. Instead, the soil profile governing the coefficients relies on information from conventional boring and sampling, and laboratory testing, which may not be fully relevant to the CPT data.
2. All the CPT methods include random smoothing and filtering of the CPT data to eliminate extreme values. This results in considerable operator-subjective influence of the results.
3. The CPT methods were developed before the advent of the piezocone and, therefore, disregard the pore pressure acting on the cone shoulder (Campanella and Robertson, 1988). The difference in unadjusted and adjusted cone resistance is smaller in sand, larger in clay.
4. All of the CPT methods are developed in a specific geographic area with more or less unique geological conditions, that is, each method is based on limited types of piles and soils and may not be relevant outside its related local area.
5. The upper limit of 15 MPa, which is imposed on the unit toe resistance in the Schmertmann and Nottingham, and European methods, is not reasonable in very dense sands where values of pile unit toe resistance higher than 15 MPa may occur. All CPT methods impose an upper limit also to the unit shaft resistance. For example, the upper limits (15 kPa, 35 kPa, 80 kPa, and 120 kPa) imposed in the French (LCPC) method quoted in Table 7.7B. Values of pile unit shaft resistance higher than the recommended limits occur frequently. Obviously, the limits are arbitrary and their general relevance is questionable.
6. All CPT methods involve a judgment in selecting the coefficient to apply to the average cone resistance used in determining the unit toe resistance.
7. In the Schmertmann and Nottingham and the European methods, the overconsolidation ratio, OCR is used to relate  $q_c$  to  $r_t$ . However, while the OCR is normally known in clay, it is rarely known for sand.
8. In the European (Dutch) method, considerable uncertainty results when converting cone data to undrained shear strength,  $S_u$ , and, then, in using  $S_u$  to estimate the pile toe "capacity".  $S_u$  is not a unique parameter and depends significantly on the type of test used, strain rate, and the orientation of the failure plane. Furthermore, drained soil characteristics govern long-term pile "capacity" also in cohesive soils. The use of undrained strength characteristics for long-term "capacity" is therefore not justified. (Nor is it really a direct CPT method).
9. In the LCPC1982 method, the length of the influence zone is very limited, perhaps, too limited. (The influence zone is the zone above and below the pile toe in which the cone resistance is averaged). Particularly if the soil strength decreases below the pile toe, the soil average must include the conditions over a depth larger than 1.5b distance below the pile toe.
10. The LCPC and the ICP methods make no use of sleeve resistance, which disregards an important aspect of the CPT results and soil characterization.

11. The correlations between CPT or CPTU values to pile shaft and toe resistances are totally empirical and each depends on the data-base used for its development. In fact, there is no scientifically defensible reason that the stress recorded by a cone pushed slowly into the soil would correlate to the long-term ultimate resistance of a pile of often 50 to 100 times wider size—other than the fact that, on many occasions, a relation can be and has been established.
12. While some CPT/CPTU methods may have more appeal to a designer than others, the fact is that which method works at a site varies with site geology, pile type, and many other conditions specific to a site. No one method is at all times better than the others. It is necessary to always establish for the site involved which method to use by direct tests or careful correlation to other non-CPT/CPTU methods.
13. All estimates of "capacity" based on cone sounding results by any method are uncertain and should not be accepted without reference to observations—calibrations—proving their suitability for the particular geology and site.
14. All CPT/CPTU methods are statistical correlations to a data base of test records and pile capacities estimated from the test by a variety of methods that can result in capacity values differing more than by a factor of 2 from each other, include errors due to presence of residual force, involve incorrect separation of shaft resistance from toe resistance components, and disregard all correlations between cone resistance and pile-soil movement. No pile response derived from an in-situ method should be accepted unless the method has shown to agree with actual pile response established at the particular site or at a site acceptably representative for the actual site conditions, construction, and geology.
15. The CPTU-sounding in-situ method is an invaluable tool for geotechnical engineering. It is understandable that it is continually coupled with outmoded approaches, such as numerical capacity assessment, but this regrettable causes practice to disregard its main use that for soil profile definition and aid to the all important qualitative assessment of the soil response.
16. There are numerous additional methods for calculating "capacity" of a pile from results of a CPT or CPTU sounding. For example the University of Western Australia method (Doan and Lehane 2021, Lehane et al 2022). Comprehensive compilations of methods are presented by Doan and Lehane 2020; 2021; 2022) and Eslami et al. 2020.

## 7.10 The Pressuremeter and Dilatometer Methods

Over the past couple of decades, additional in-situ methods have been developed, such as the pressuremeter and the dilatometer. Both measure the horizontal movement due to an expanding membrane.

### 7.10.1 The Pressuremeter Method, PMT

The pressuremeter test (PMT) consists of expanding a 75 mm wide cylinder into the borehole side and measuring pressure and volume change. According to French standard of applying pressuremeter (PMT) records to analysis of pile response, (Abchir et al. 2016 and AFNOR 2012), the unit shaft resistance,  $r_s$ , along a pile element and the unit toe resistance,  $r_t$ , are proportional to the net limit pressure,  $p_l^*$ , determined in the PMT. The proportionality coefficients are denoted  $\alpha_{pile-soil}$  and  $k_p$ , respectively, and coefficients are calibrated to "capacity" determined in static loading tests defined as the pile head that moved the pile head a distance equal to 10 % of the pile diameter (with no reference to pile length and pile-toe movement). The coefficients range from 1.1 through 1.7 and 0.05 through 0.15, respectively, and depend on a multitude of factors, such as soil type, method of pile construction, and pile type. The net



limit pressure,  $p_l^*$ , is the large strain pressuremeter pressure,  $p_L$ , subtracted by the pressure at the beginning of the test,  $p_{oh}$ , and depends on soil type and soil strength. For example, Briaud (2013) indicates that  $p_l^*$  can range from 200 through 800 kPa in firm and stiff clays ( $\tau_u = 12$  to 25 kPa and 25 to 50 kPa, respectively).

### 7.10.2 The Dilatometer Method, DMT

The dilatometer test consists of pushing a 230 mm long, 95 mm wide, flat blade into the soil to a desired depth. The test consists of expanding a 60 mm wide, circular membrane into the soil a 1.1 mm distance. Two pressures,  $p_0$ , and  $p_1$ , are recorded: the pressure acting on the blade at start of the test and the pressure required for the 1.1-mm expansion. The difference,  $p_1 - p_0$ , is denoted  $p_\Delta$ . The method determines three moduli: The  $I_D$ -material index (which is related to soil type: clay  $0.1 < I_D < 0.6$ , silt  $0.6 < I_D < 1.8$ , and sand  $1.8 < I_D < 10$ ), the  $K_D$  = horizontal stress index (which is obtained by dividing the  $p_\Delta$  by the effective stress at the test depth), and the  $E_D$  = dilatometer modulus (which is  $p_\Delta$  multiplied by 34.7). The undrained shear strength,  $\tau_u$ , is  $= 0.22 \sigma'_v (0.5K_D)^{1.25}$ , or approximately  $= 0.1$  January 2024. (Lechowicz et al. 2017). The pile shaft resistance,  $r_s$ , is then equal to  $\alpha\tau_u$ —thus, it is calculated using the  $\alpha$ -method. Others have proposed slightly different and, also more complex, relations for the undrained shear strength from the dilatometer records.

### 7.11 Comments on Axial Pile "Capacity"

The static "capacity" of a pile is most reliable when determined in a full-scale static-loading test on an instrumented pile or in bidirectional tests (see Chapter 8). However, the test determines the "capacity" of the specific test pile(s), only. The load response of other piles at the site must still be determined by analysis, albeit one that now can be calibrated by the response determined for the particular test pile. Note, the "capacity" is often according to some unstated definition. As emphasized several times in the foregoing, all resistances and parameters should be referenced to a static analysis using effective stress parameters correlated to movement. Thus, when taken from test results, they must be assessed against the relative movement between the pile elements and the soil at which they were determined. Moreover, despite the numerous static loading tests that have been carried out and the many papers that have reported on such tests and their analyses, the understanding of static pile testing in current engineering practice leaves much to be desired. The reason is that engineers have concerned themselves with mainly the question of "capacity", finding little of practical value in analyzing the pile-soil interaction and the load-transfer, i.e., determining the distribution of resistance along the pile and the load-movement behavior of the pile, which aspects are of major importance for safe and economical foundation design.

The field test can also be in the form of a dynamic test (Chapter 9), that is, during the driving or restriking of the pile, measurements are taken and later analyzed to determine the static resistance of the pile mobilized during a blow from the pile driving hammer. The uncertainty involved in transferring the dynamic data to static behavior is offset by the ease of having results from more than one test pile. Of course, also the "capacity" and force distribution found in the dynamic test should be referenced to a static analysis, not just taken as a definite value. Note, the reference must be to an effective stress analysis with due inclusion of the pore pressure distribution along the pile at the time of the dynamic test.

### 7.12 Installation Phase

Most design analyses pertain to the service condition of the pile and are not quite representative for the installation (construction) phase. However, as implied above (Section 7.6), it is equally important that the design includes an analysis of the conditions during the installation (the construction, the drilling, the driving, etc.) of the piles. For example, when driving a pile, the stress conditions in the soil are different from those during the service condition, and during the pile driving, large excess pore pressures are induced in a soft clay layer and, probably, also in a silty sand, which further reduces the effective stress.

The design must include the selection of the pile driving hammer, which requires the use of software for wave equation analysis, called WEAP analysis (Goble et al. 1980; GRL 2002; Hannigan 1990). This analysis requires input of soil resistance in the form as result of static load-transfer analysis. For the installation (initial driving) conditions, the input is calculated considering the induced pore pressures. For restriking conditions, the analysis should consider the effect of soil set-up.

By means of wave equation analysis, pile penetration resistance (blow-count) at end-of-initial-driving (EOID) and restriking (RSTR) can be estimated. However, the analysis also provides information on what driving stresses to expect, indeed, even the length of time and the number of blows necessary to drive the pile. The most commonly used result is the bearing graph, that is, a curve showing the ultimate resistance ("capacity") versus the penetration resistance (blow count). As in the case of the static analysis, the parameters to input to a wave equation analysis can vary within upper and lower limits, which results in not one curve, but a band of curves within envelopes as shown in Figure 7.19.

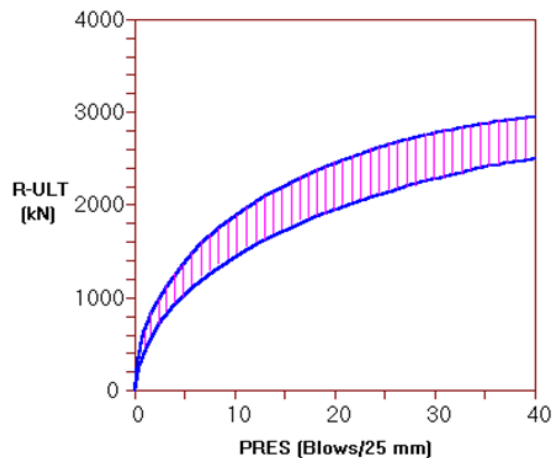


Fig. 7.19 Bearing graph from WEAP analysis

The input parameters consist of the distribution of static resistance, which requires a prior static analysis. Additional input consists of the particular hammer to use with its expected efficiency, etc., the dynamic parameters for the soil, such as damping and quake values, and many other parameters. It should be obvious that no one should expect a single answer to the analysis. The figure shows that at an EOID penetration resistance (PRES) of 10 blows/ 25mm the mobilized "capacity" will range from about 1,400 kN through about 1,900 kN. Similarly, a 2,000 kN capacity may be found at a PRES of 12 blows/25 mm through about 21 blows/25 mm.

Notice that the wave equation analysis postulates observation of the actual penetration resistance when driving the piles, as well as a preceding static analysis. Then, common practice is to combine the analysis with a factor of safety on "capacity" ranging from 2.5 (never smaller) through 3.0.

The bearing graph of the particular case demonstrates that the hammer selected for the driving cannot drive the pile against a "capacity" of about 3,000 kN "capacity" expected after full set-up. That is, restriking cannot then prove out the "capacity". Bringing in a larger hammer, may be a costly proposition. It may also be quite unnecessary. If the soil profile is well known, the static analysis correlated to the soil profile and to careful observation during the entire installation driving for a few piles, sufficient information is usually obtained to support a satisfactory analysis of the pile "capacity" and load-transfer. That is, the "capacity" after set-up is inferred and sufficient for the required factor of safety.

When conditions are less consistent, when savings may result, and when safety otherwise suggests it to be good practice, the pile "capacity" is tested directly. Conventionally, this is made by means of a static loading test. Since about 1975, also dynamic tests are often performed (Chapter 9). Static tests are costly

and time-consuming, and are, therefore, usually limited to one or a few piles. In contrast, dynamic tests can be obtained quickly and economically, and be performed on several piles, thus providing assurance in numbers. For larger projects, both static and dynamic tests are often used.

### 7.13 Structural Strength

Design for structural strength includes consideration of the conditions at the pile head and at the force equilibrium plane. N.B., for long-term conditions in a "unified method" of analysis (Section 7.15). At the pile head, the axial loads consist of dead and live load (combined with bending at the pile head), but no drag force. At the force equilibrium plane, the loads consist of dead load and drag force, but no live load. (Live load and drag force cannot occur at the same time and must, therefore, not be combined in the analysis).

Most limitations of allowable axial load or factored resistance for piles originate in considerations of the conditions at the pile head, or pile cap, rather, and driving conditions. At the pile cap, the axial load is combined with bending and shear forces. In the driving of a pile, the achievable "capacity" is not determined by the axial strength of the pile but by the combination of the hammer ability and the pile impedance,  $EA/c$ . It does not make sense to apply the same limits of structural strength at the equilibrium plane as at the pile cap. Moreover, it should be recognized that, for axial structural strength of the pile, the design considers the pile material, a material that is significantly better known and which strength varies less than the soil strength. Therefore, the restrictions on the axial force (the safety factor) should be smaller than those applied to soil strength.

Very long piles installed in soils where the settlement, general subsidence, occurs over most of the length of the piles can be subjected to drag force that raises concerns that the structural strength of the piles is being approached. This is rarely the case before the depth to the equilibrium plane is about 80 to 100 pile diameters. Not grouted thin-walled pipes being an obvious exception.

For composite piles, such as concrete-filled pipe piles and axially reinforced concrete piles, one cannot calculate the allowable stress by adding the "safe" values for each of the various materials, but must design according to strain compatibility in recognition of that all parts of the pile cross section deforms at the same strain (Clause 7.18.5). Thus, a poor-strength (low modulus) concrete cannot be compensated by using a high-yield steel and, conversely, a high-strength, large modulus concrete with a ordinary yield steel will only marginally boost the combined stiffness. Whether the calculation of the reinforced pile is for ultimate strength or allowable load, it is the strain-compatibility that governs; the strain is equal for the cross section. Therefore, the stress in the concrete and stress in the steel is governed by the imposed strain and the respective areas of concrete and steel ( $A_c$  and  $A_s$ ) and the respective E-moduli of concrete and steel ( $E_c$  and  $E_s$ ). The axial force is determined by the strain times the  $E_{\text{average}}$  times  $A_{\text{total}}$ , the EA-parameter.

If an axial strength is determined for a pile, the allowable maximum stress at the equilibrium plane can be set to 70 % of the strength. A better approach is to limit the unfactored axial load at the equilibrium plane to a value that induces a 1-millistrain (1 mm/1 m) maximum compression strain into the pile with neither concrete nor steel becoming stressed beyond 70 % of its structural strength or yield value. See Section 7.14 for a discussion on the location of the equilibrium plane and the magnitude of the drag force.

## 7.14 Negative Skin Friction, Equilibrium Plane, and Drag Force

### 7.14.1 A pioneering case history

The rules for the static analysis presented in this chapter pertain to single piles and include the basics of the topic. They are derived from many well-documented case histories from around the world. Some of these are summarized by Fellenius (1998; 2006). A major reference is the remarkable case history presented by Endo et al. (1969), from whose work Figure 7.20 is quoted, and the case history by Okabe (1977); see Section 7.18.1C. The figure shows two diagrams that clearly demonstrate the interdependence of the long-term load-transfer and settlement of a single pile and soil.

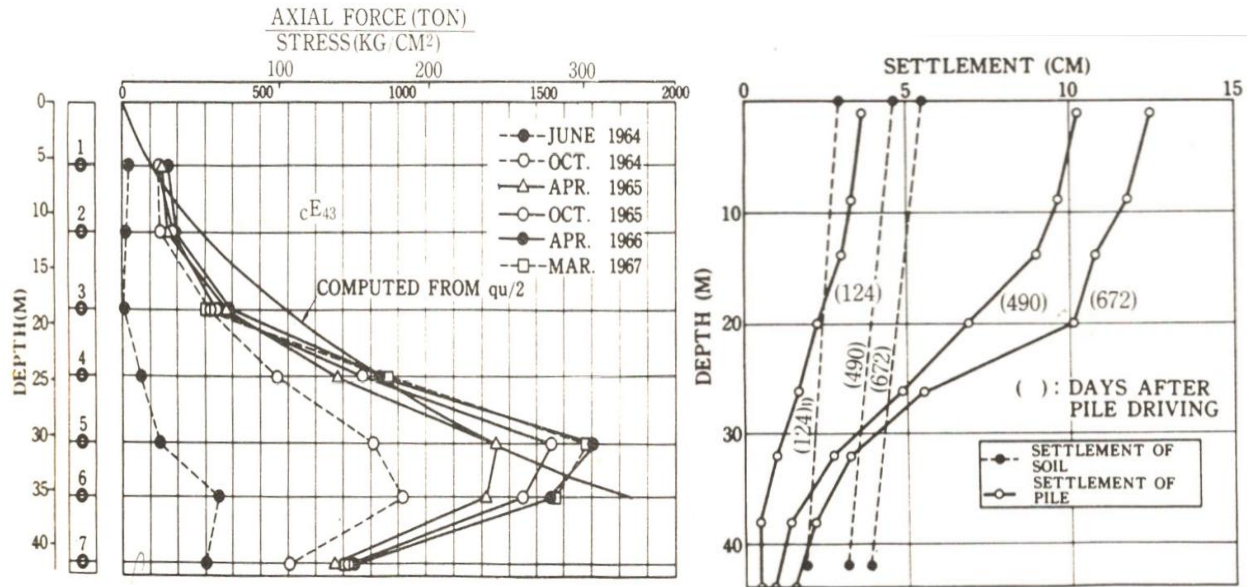


Fig. 7.20 Combination of two diagrams quoted from Endo et al. (1969)

The left diagram shows the force distribution measured during almost three years after the installation of a telltale-instrumented steel pile. The force in the pile increase due to negative skin friction to a force equilibrium—maximum drag force value at force equilibrium—and reduces from there due to positive shaft resistance.

The diagram to the right shows the measured settlement of the soil and the pile over the same time period. Note that the distributions of settlement for the pile and the soil intersect defining the settlement equilibrium. The Endo et al. (1969) paper is the first to indicate the correlation between the force and settlement equilibriums, the correlation being that they occur at the same depth—at the Equilibrium Plane or Equilibrium Point, EP (which are better terms than Neutral Plane or Neutral Point).

Note that the shear forces increased with depth and that, during the last three years of monitoring, the negative skin friction in the upper portion of the pile did not appreciably increase despite the ongoing soil settlement. The paper also presents measurements of pore pressure development (not cited here) showing that, in the upper portion of the soil, the pore pressures did not change much during the last few years of observation. This means that the effective stress did not change appreciably during that time in that zone. At depth, however, the pore pressures dissipated with time, and, consequently, the effective stress increased, and, the negative skin friction and positive shaft resistance increased accordingly. Clearly, the shear forces are proportional to the effective overburden stress. The depth to the EP increased with time and, from about Day 490, it stabilized at about 30 m depth.

The data in Figure 7.20 are combined in Figures 7.21A and 7.21B to show the increase of toe force with time after the monitoring start and the toe force versus toe penetration. Figure A shows that the downdrag caused toe penetration reached a maximum after about a year and Figure B shows that the force-movement of the pile toe increased with increasing toe penetration. The force-penetration development correlates to a Gwizdala q-z function (See Chapter 8, Clause 11.1) with a coefficient equal to 0.55.

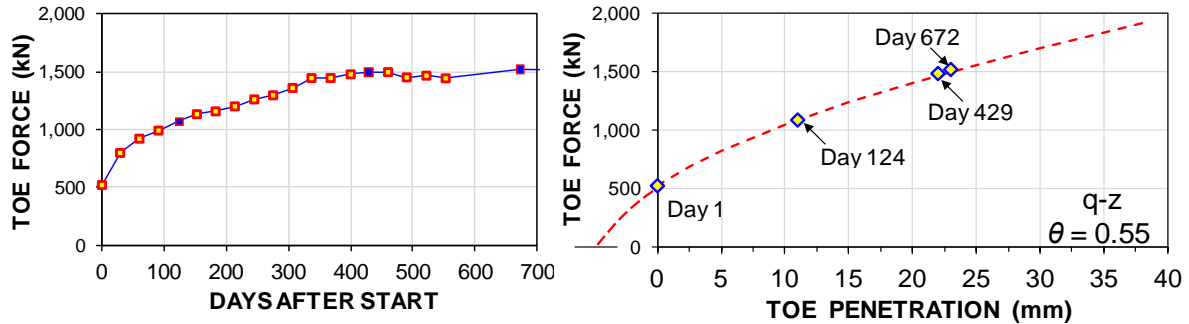


Fig. 7.21A Toe force vs. days after start

Fig. 7.21B Toe force vs. toe penetration

### 7.14.2 Length of the Transition Zone

The main principle of determining the interaction between load-transfer and settlement, as well as the associated magnitude of the drag force is shown in Figure 7.22 for two cases, Cases 1 and 2. I have assumed that the two would show the same load-movement diagram in a static loading test and that they are identical with regard to the distributions of resistance. The left diagram in the figure shows force distribution starting from the sustained (dead) load applied to the pile. No live load is shown because live load has no influence on a long-term force distributions. The right diagram shows the distribution with depth of soil and pile settlement and the pile toe movements for two different distributions of soil settlement. The "Target resistance" of the analysis is the pile-head load for Case 2. The vertical double arrows indicate the length of the transition zone for each of the two cases. For details, see Section 7.15.

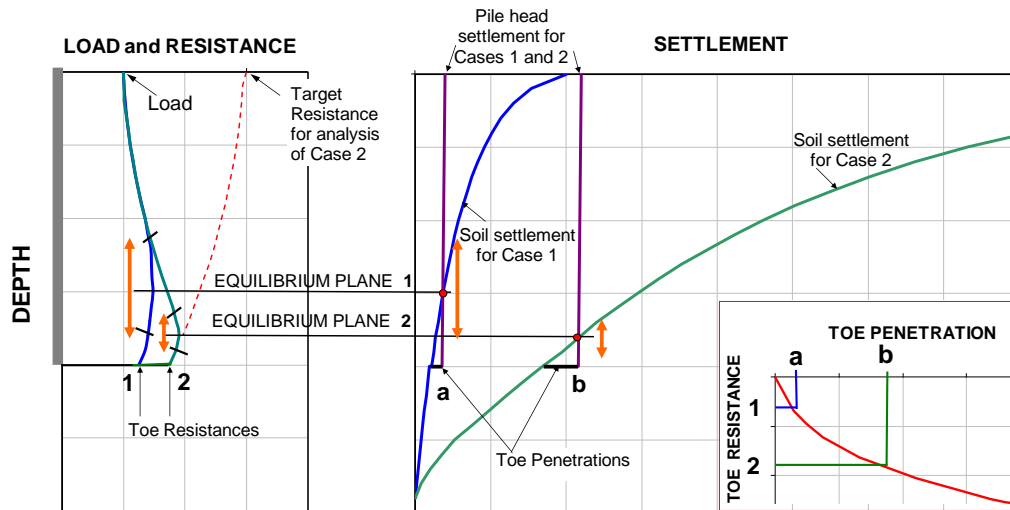


Fig. 7.22 Load-and-resistance diagram combined with settlement and toe load-movement diagrams.

Case 1 is associated with small settlement (small general subsidence) of the surrounding soil, while the soil settlement for Case 2 is much larger, as indicated by the settlement diagram. The relative movement between the soil and the pile develops negative skin friction along the upper portion of the pile and positive shaft resistance in the lower portion, but for an in-between transition zone. The length of the transition zone is governed by the distance for which the relative movement between the pile and the soil

is very small, smaller than the few millimetre necessary to fully mobilize the shear forces (Section 7.2). At a site where the soil settlement is small, this minimal relative movement does not materialize nearest the equilibrium plane and the length of the transition zone can, then, be significant. The main point of the two cases is that while the load-movement in a static test may be the same for the piles, it is the long-term soil settlement and the downdrag that determines the long-term settlement—and suitability—of the piled foundation.

The figure demonstrates a second important principle. The toe resistance is a function of the pile toe movement imposed by the downdrag, as is illustrated as the “Toe Penetrations” in the settlement diagram.

Case 2 presents a case where the soil settlement is no longer small. The effect of the larger settlement is that the toe movement is larger. As a result, the mobilized toe resistance is larger and the equilibrium plane, has moved down. Moreover, the transition zone is shorter. The maximum load, that is, the sum of the dead load and the drag force, is therefore larger. If the settlement were to become even larger, the toe penetration would increase, the equilibrium plane would move further down, transition zone would become even shorter, and the drag force would become larger.

For a given resistance distribution, the figure illustrates that the magnitude of the relative movement between the pile and the soil is one of the factors governing the magnitude of the drag force and the location of the equilibrium plane—and the pile settlement.

Many use the terms “drag force” and “downdrag” as interchangeable terms. Even in combination: “downdrag force”! However, although related, the terms are not synonyms. “Drag force” is the integration of the negative skin friction along the pile. Its maximum value occurs at the equilibrium plane. Its action on a pile is similar to that of the prestressing force in a prestressed concrete pile. (N.B., the latter is never called “prestressing load”). “Downdrag” refers to pile settlement when the soil ‘hangs’ on the pile dragging it down. The two terms can be said to be the inverse of each other. Where drag force is at its maximum, e.g., for a pile supported on bedrock, the downdrag is minimal. On the other hand, when the downdrag is large, e.g., for a ‘floating’ pile, the drag force is small, but downdrag could be considerable. Provided that the pile axial strength is not exceeded by the sum of the dead load and the drag force, presence of drag force is beneficial as it prestresses the pile, minimizing the ‘elastic’ compression of the pile due to live loads, etc. N.B., it is therefore necessary to do the analysis with unfactored dead load and drag force. In assessing the effect, a margin is considered by, for example, applying a factor of safety or load/resistance factors to the end result. In contrast to the drag force, downdrag is usually undesirable. At a site where the soils are expected to settle due to general subsidence or effect of fills, groundwater lowering, adjacent structures, etc., the problem to address is the downdrag, not the drag force.

The heading indicates that the text will deal with “Equilibrium Plane and the Magnitude of the Drag Force”. The foregoing couple of paragraphs demonstrate the fact that the two aspects cannot be separated from aspects of settlement and soil movement.

## **7.15 Unified Design Method for Drag Force, Settlement, and Downdrag.**

### **7.15.1 Steps of calculation**

The design of load and settlement of piled foundations supported on single piles or narrow pile groups is called the Unified Method (Fellenius 1984, 1988, 2004) and consists of the three calculation steps listed below. (For wide piled foundations, see Section 7.18). The design approach must include assessing whether or not the design should include performing and analyzing a static loading test before the design is finalized and/or a static test at the end of construction to validate the work. The need for a static loading test can usually be anticipated and should be considered early in the design. It must not appear as an ‘uninvited and unwelcome guest to the party’.

1. Compile all soil data and perform a static analysis of the load-transfer as detailed in Sections 7.1 through 7.14.
2. Calculate the expected **settlement** profile including all aspects that can result in a change of effective stress at, below, or near the pile(s). Note, settlement directly due to the pile-supported loads (dead load) is mostly determined by load-transfer movements and further settlement due to the pile-supported load increasing the stress in the soil below the pile toe level. This settlement is usually insignificant for narrow pile groups (groups comprising no more than 4 rows). Additional settlement can be caused by downdrag (please note that drag force does not cause settlement, it is the result of settlement). Verify that the settlement does not exceed the maximum value permitted by the structural design of the supported structure with due consideration of permissible differential settlement.
3. Note that the location of the equilibrium plane (EP) must be determined using unfactored parameters and forces. The analysis requires the use of known (or test determined, or estimated by 'informed' assumptions) distributions of force and of force-movements, i.e.,  $t$ - $z$  and  $q$ - $z$  functions (Section 8.11). Then, the location of the EP can be determined from the pile toe load-movement response ( $q$ - $z$  function) and a fit be established between pile toe load and pile toe penetration into the soil. The process is iterative and comprises searching for the balance between pile toe penetration, pile toe force, and depth to the EP. Of course, as it is a settlement analysis, the relevant forces must be unfactored.
4. Run an initial set of analyses calculating the various force distributions relating them to the settlement distributions and determine the potentially possible toe resistance for each force distribution. This result in a range of possible depth to the equilibrium plane from a 'no-higher-than' depth and a 'no-deeper-than' depth. The settlement of the piled foundation will be the settlement at the equilibrium plane plus the compression of the pile fore the sustained load and drag force.
5. Verify that the maximum load in the pile, which is the sum of the dead load and the drag force at the lowest depth of the equilibrium plane is adequately smaller than the **structural strength** of the pile, say, by an appropriate factor of safety (usually 1.5), or that the strain resulting from the maximum load is not larger than 1 millistrain (do not include the live load in this calculation). Note, the maximum load is a function of the location of the equilibrium plane, the degree of mobilization of the toe resistance, and the length of the transition zone (the zone of transfer from fully mobilized negative skin friction to fully mobilized positive shaft resistance above and below the equilibrium plane, respectively).

The Unified Method is accepted in several standards and codes. Since 2024 also by the US (Coffman et al. 2024). The method, is simple to perform in an interactive spreadsheet procedure, but this is quite time-consuming. The UniPile6 software ([www.unisoftGS.com](http://www.unisoftGS.com)) will perform both settlement and resistance analysis to deliver simulated loading test load-movement response, settlement of the soil and the pile, as well as the drag force and depth to the EP and enable fast what-if alternatives and back-calculations to fit actual measurements.

Regrettably, a conventional piled foundation design is usually limited to determining "capacity" and applying a safety factor to the working load (or, in design per LRFD, a resistance factor to the "capacity" and a load factor to the working load). A correctly performed settlement analysis verifying that the settlement will have a suitable margin to the maximum settlement (particularly the differential settlement) that the structure can accept will make the "capacity" analysis redundant. However, the conventional approach is still required in most codes and standards and it will, therefore, have to be included in a foundation design. Also, it is not a good idea to abandon a 'proven' method for a new before obtaining good experience with the new, albeit more reliable and safe method. Therefore, a designer should maintain the conventional method as a parallel approach for quite some time after having adopted settlement as the deciding criterion for a foundation design. The following steps need to be considered.

1. For driven piles, perform wave equation analysis to select the appropriate pile driving hammer and to decide on the driving and termination criteria (for driven piles). Document the observations (that is, keep complete and carefully prepared logs!).
2. Verify that the supported loads (dead and live) satisfy the code-required factor of safety, or load and resistance factors, when correlated to the ultimate pile resistance ("capacity") per a stated definition (the drag force must not be included in this calculation). This is a factor-of-safety or ultimate-limit state-design approach and the ultimate resistance is best defined as a "factored-up" load that induces a pile movement that could cause the foundation to collapse.
3. A design applying a factor of safety to "capacity" in determining the allowable load, the smallest factor of safety to apply to a theoretical analysis is 3.0. If the "capacity" is determined from assessing the results of a static loading test (note, **the "capacity" definition must always be declared**), the factor of safety can be reduced, but rarely to a value smaller than 2.0. A factor of safety lower than 3.0 must not be applied to a "capacity" expected to be established in a future static loading test, i.e., a test yet to be performed. The "capacity" expected to be demonstrated in that future test must be treated as a theoretical value and, therefore, be used with  $F_s = 3.0$ . See also Chapter 12, Section 12.4 and Fig.12.3.
4. When the desired working loads imply a factor of safety of 2.5 or smaller, it is necessary to verify the pile "capacity" by means of static or dynamic testing. N.B., with due consideration of the respective movements pertinent to the shaft and toe resistance responses for the pile.
5. Observe carefully the pile construction and verify that the work proceeds as anticipated.

Figure 7.23 illustrates the analysis of the load-transfer curve for the shaft and toe resistances mobilized for a specific set of conditions, that is, as always, the shaft and toe resistances are correlated to a specific movement. The diagrams assume that the soil is subsiding along the full length of the pile and recognizes that the unit negative skin friction,  $q_n$ , and unit positive shaft resistance,  $r_s$ , are equal. Notice, a key factor in the analysis is the estimate of the interaction of pile toe resistance and pile toe penetration. The figure further assumes that the soil movement relative to the pile near the equilibrium plane is large enough to ensure that the height of the transition zone is small, as shown in the figure. If, on the other hand, the soil-pile movement would be small, the transition zone will be longer and the pile toe movement smaller, i.e., the toe resistance will be smaller and the equilibrium plane will lie higher c.f., Section 7.2.4). Of course, this will not necessarily affect the allowable load if it is determined based on pile "capacity"—but, it should. The curve labeled " $Q_d + \Sigma|q_n|$ " is the long-term force distribution starting from the applied dead load and the curve labeled " $R_{ltr} - \Sigma R_s$ " is the long-term resistance distribution starting at the pile toe,  $R_t$ , and rising by accumulating the target shaft resistance,  $R_s$  to a specific "Target Resistance,  $R_{trg}$ " at the pile head (which can be, but does not have to be, the "ultimate resistance", determined one way or another). The intersection of the two curves is the location of the force equilibrium.

Reducing the dead load on the pile has little effect on the maximum load in the pile; the depth to the force equilibrium would increase and the drag force would increase to make up for the reduction in the dead load. Obviously, if presence of drag force, as opposed to the magnitude of drag force, would be of concern, increasing the dead load would reduce the drag force! Clearly, the drag force is an environmental effect that should not be mistaken for something akin with the load from the supported structure, as is so mistakenly expressed in many codes and standards.



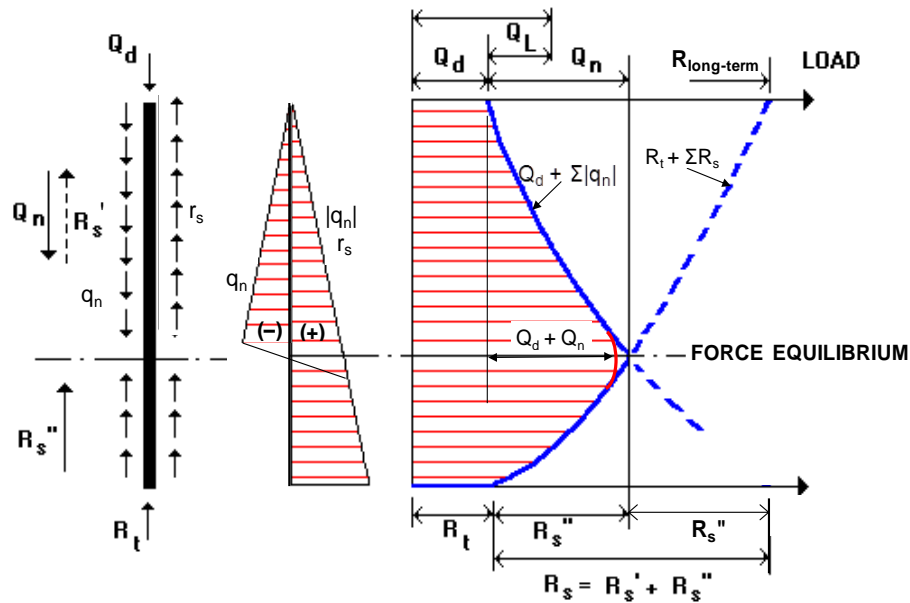


Fig. 7.23 Construing the Force Equilibrium

### 7.15.2 Drag force

That negative skin friction develops where the soil settles around the pile is obvious. So is the fact that the negative skin friction accumulates to an axial force in the pile. Less obvious, but well-established in the many full-scale tests reported (Fellenius 2006 has compiled several case histories) is that the drag force develops primarily due to the fact that the pile and the soil are materials that have to function together despite their being of very different material (different E-modulus) and, therefore, the pile reacts to the small movement always occurring in a soil body. Already a movement no larger than a millimetre will cause shear forces to develop along the interface between the pile and the soil. This will result in an equilibrium force between downward and upward acting accumulated shear. The force at the equilibrium depth is called "drag force". Many use the term "drag load", but this is a misnomer because it leads to the false idea that it somehow is similar to the load applied to the pile from the structure. Moreover, the drag force is not an independent entity, but an environmental force which development and magnitude depend on the pile toe response and the sustained (dead) load from the structure supported by the pile. To repeat, the drag force must not be included when considering the allowable load (or the factored load) on the pile. It is only important with regard to the axial strength of the pile. And, a transient (live) load cannot combine with the drag force, because there cannot be negative direction of shear at the same time as a positive direction. This obvious fact is not understood in many codes and standards, e.g., the EuroCode (2022).

### 7.15.3 A case history of applying the unified design method

Fellenius and Ochoa (2009) presented the results of testing and analysis of a 25 m long, strain-gage instrumented auger-cast pile constructed in sand and silty clay to bearing in a glacial till and designed according to the Unified Design Method. The spacing between the piles was large enough for the piles to act as single foundation-supporting piles. Figure 7.24 shows the distributions of load and settlement for a typical pile, a test pile, at the site. For reference, an ultimate resistance ("capacity",  $R_{ult}$ ) of 4,500 kN is indicated in the figure. In the long-term, effective stress will increase due to a fill placed over the site, which will increase the shaft resistance along the pile. In addition, the fill will cause soil settlement, which will cause negative skin friction to develop. Consequently, the long-term force distribution will increase downward from the applied dead load to a maximum at the location where there is no relative movement between the pile and the soil—the force equilibrium.

The site was subject to ongoing general subsidence along the full length of the pile. However, the pile toe was located in a competent not-subsiding soil. The settlement and the pile compression established the depth to the settlement equilibrium.

The enforced toe movement generates a pile toe force that together with the applied sustained load and the shaft resistance gives a force-equilibrium depth equal to the settlement-equilibrium. The diagrams demonstrate that the applied load is increased or reduced, or, similarly, if the settlement is increased or reduced, the location of the equilibrium plane and, therefore, the penetration of the pile toe, will change, and, therefore, also the pile-toe force, which in turn will change the location of the force equilibrium, etc. Forces, settlement, and movements are interrelated and the design cannot simply be based on a factor of safety approach, but must also consider movement and settlement aspects.

The example section (Section 10.4) includes an additional numerical analysis of an example taken from the Commentary on the Eurocode (Frank et al. 2004).

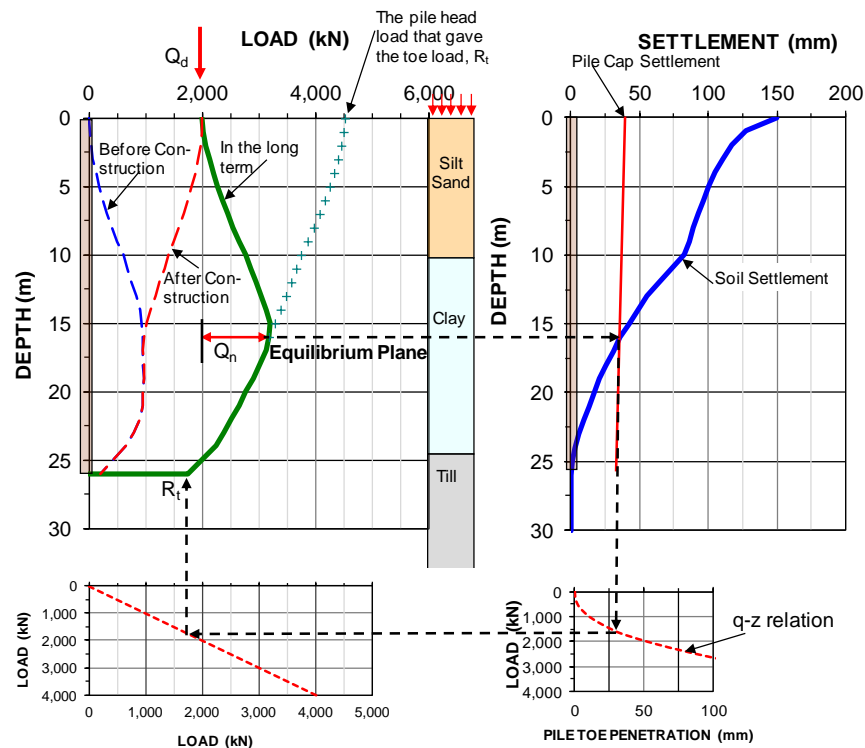


Fig. 7.24 Example of the Unified Design Method and correlation between toe penetration and toe load (Fellenius and Ochoa 2009)

### 7.16 Piles in Swelling Soil

Soil movement due to swelling soil does not induce negative skin friction, but positive skin friction. The analysis of the distributions of shaft shear and load in the pile installed in swelling soil follows the same principles as for piles in settling soil, only the directions and signs are reversed. Figure 7.25A shows the distribution of load for a pile in either a swelling soil along its full length (left side) or in a subsiding soil (right side). The curves are mirror images of each other. For both, a force equilibrium develops; a tension force in the swelling soil and compression force (drag force) in the subsiding soil. When adding a sustained (dead) load to the pile head, as shown in Figure 7.25B, the axial force reduces. However, the depth to the force equilibrium changes. The figures demonstrate that the effect of passive soil movement (swelling or subsidence) can be analyzed using the same principles of force transfer as for settling soil

### 7.17 Settlement of Single piles and Narrow Piled Foundations

The primary aspect in the design of a piled foundation is determining—predicting—its settlement (Chapter 3). Settlement of a single pile or narrow piled foundation is caused by three factors. First, by the load-transfer movement, developing when the supported load is placed on the pile; second, by the increase of stress below the pile from the load supported by the piled foundation, and, third, by downdrag (if present) due to changes of soil effective stress due to other aspects than the pile load, e.g., fill, other loaded areas, groundwater lowering, etc.

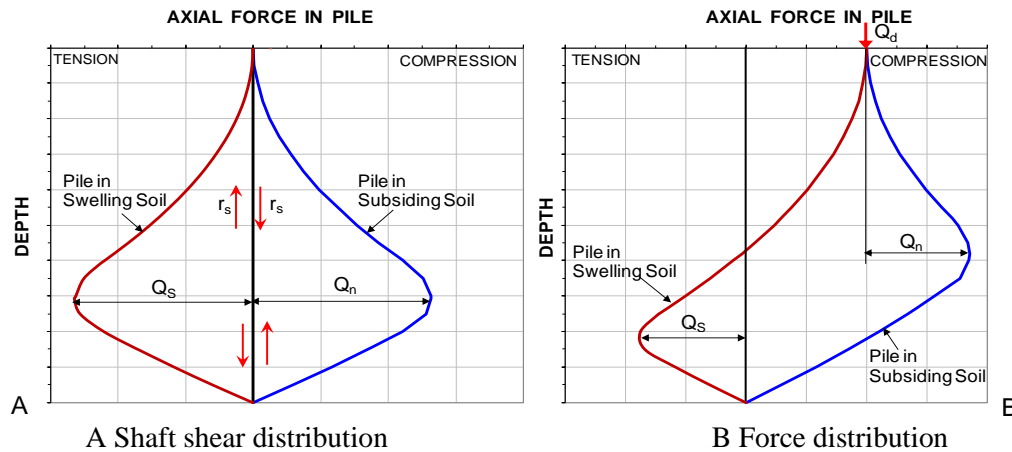


Fig. 7.25 A pile in swelling soil underlain by a non-swelling soil

#### 7.17.1 Load-transfer movement of single piles and narrow piled foundations

Mobilizing the shaft resistance requires only a small movement, frequently no more than a few millimetre. When the load from a supported structure is first applied to a pile (single pile or a narrow pile group), only a very small portion, if any, will reach the pile toe. The pile head movement is determined by the axial compression due to the load plus the portion, if any, of the applied load that reached the pile toe and the subsequent pile toe movement.

The analysis procedure is as follows: Calculate and plot the distribution of the shaft resistance and determine (make an assumption for) the magnitude of toe resistance and toe movement that result from applying the dead load to the pile—the load-transfer movement for the load from the structure. This requires estimating pile compression for the force distribution, and applying a  $t$ - $z$  relation to all pile element from pile head to pile toe and a  $q$ - $z$  relation for the pile toe. (The  $t$ - $z$  and  $q$ - $z$  relations, see Section 8.11, can either be theoretical or be obtained by back-calculation of the results from a static loading test. Few head-down tests measure pile-toe load-movement, but most bidirectional tests do; see Section 8.15).

The possibility that a portion of the force distribution might have developed before the load was placed on the pile needs to be taken into account. The load-transfer movement is the sum of the pile shortening and the pile toe movement due to the pile toe load and includes the shaft movement necessary to mobilize the shaft resistance for the element immediately above the pile toe, which also is equal to the beginning (initial) pile toe movement. The additional pile toe movement is caused by load beyond the shaft resistance reaching the pile toe.

The load-transfer movement for interior piles in a wide pile group is different to that of single piles and narrow pile groups and is addressed in Section 7.18.

### 7.17.2 Settlement below the pile toe level

For wide pile groups—five or more rows—the settlement of the pile group below the pile toe level due to the applied load can be substantial). For single piles and narrow pile groups—no more than four rows—the settlement beyond or in addition to the load-transfer movement (the t-z and q-z relations) is usually small because the stress increase in the soil layers below the pile toe level affects a limited volume (depth) of soil, whether the soil compressibility below the pile toe level is small or not.

The geotechnical literature includes many reports on tests involving groups of piles, mostly groups of no more than four to nine piles, total. Of course, depending on the pile spacing, a pile in such narrow groups respond similarly to single piles—more or less. However, the observations on such small groups, even if in full-scale, have little relevance to the response of wide pile groups.

It must be recognized that the narrow group made up of a few individual piles in a common cap may have different embedment lengths and toe resistance mobilized to different extent. The piles have two things in common, however. They are connected to the same pile cap. If the cap can be presumed rigid, which is the normal condition for most narrow groups, all pile heads move equally, and the piles must have developed a common equilibrium plane at about the same depth somewhere down in the soil (long-term condition, of course). For the equilibrium plane to be the same (be common) for the piles in the group, with the mentioned variation of length, etc., the axial force at the pile head due to the dead load applied to the cap must differ between the piles, and where the conditions at the pile toe level vary for the piles, the mobilized pile toe resistance will also differ between the piles. Conversely, a pile with a softer toe resistance than the other piles in the narrow group will carry a smaller portion of the dead load. If a pile is damaged at the toe, it is possible that the pile exerts a negative force at the cap and, thus, actually increases the total load on the other piles (or the pile pulls out from the cap).

The settlement of a pile group, narrow or wide, is the combination of the pile compression for the axial force, the toe movement, and the settlement below an assumed "equivalent raft" at the pile toe loaded with the dead load applied to the piled foundation. The equivalent raft approach addresses the overlap effect of the loads between the piles in the group. The settlement of the equivalent raft occurs with time as the result of the stress change imposed by the applied load combined with other changes of the effective stress from, for example, fills, change of groundwater table and pore pressure distribution, unloading due to excavations, loads placed on adjacent foundations, etc.

For a group of shaft-bearing piles in clay supporting a piled foundation, Terzaghi and Peck (1948) proposed that the settlement of the piled foundation could be calculated as that of an equivalent raft, having the same footprint as that of the piled foundation, located at the lower third point of the pile length, and loaded by the same load as the piled foundation. For the particular example they used, the lower third point happened to be close to the depth of the equilibrium plane (Section 7.2). Terzaghi and Peck (1948) also suggested distributing the raft stress according the 2:1-method. Bjerrum et al. (1957) compared applying the equivalent raft method to two alternative placements of the raft: at the lower third point and at the pile toe depth, and distributed the stress underneath the center of the equivalent raft using the nomograms of Newmark (1942), i.e., the Boussinesq method. Fellenius (1984) proposed (for narrow pile groups) that the equivalent raft should be placed at the equilibrium plane regardless of the depth to the lower third point and applied the settlement analysis of the so-placed equivalent raft to narrow pile groups in all types of soils, which became the start of the Unified Design Method of pile groups (Fellenius 1984; 1988; 2004; 2011; 2016a). See also Section 7.17.3.

The settlement calculation of the equivalent raft and the piled foundation can be performed according to conventional calculations for change of effective stress, as well as more sophisticated methods. Were the Unified Design Method applied to determine the settlement of the equivalent raft at the equilibrium plane, the soil compressibility must include the stiffening effect of the "pile-reinforced" soil. The "reinforcement effect due to the piles" results in the deformation between the equilibrium plane and the pile toe level (for

interior piles in a narrow group will be small. Therefore, the equivalent raft can just as well be placed at the pile toe and the pile shortening and load-transfer movement be added to the settlement of the equivalent raft. Note, though, that when calculating the settlement of the ground or a footing located outside the footprint of the piled foundation, no such soil stiffening effect due to the presence of the piles should be included.

The settlement caused by the change of effective stress due to the total load applied to the piles can simply be assumed as that caused by the change of effective stress due to load on an equivalent raft with a footprint located at the depth of the equilibrium plane equal to that of the pile group footprint,  $B$  and  $L$ . From here and to the pile toe depth, the stress is then transferred to the soil as a truncated cone to a projected equivalent raft with an accordingly larger width and length. (For a wide pile group, the method for determining the size of the equivalent raft projected to the pile toe level is not applicable as the projected shaft resistance is only implemented by the perimeter piles, which have little or no shaft resistance to spread out into the surrounding soil). For a narrow-width pile group, however, the width and length of the equivalent raft to project to the pile toe from the pile group footprint at the equilibrium plane is important.

Because the foundation footprint stress at the equilibrium plane is not distributed out into the soil immediately below the equilibrium plane, but gradually along the length of pile between the equilibrium plane and the pile toe, a conventional Boussinesq (or a  $2(V):1(H)$  distribution) from the equilibrium plane results in too large a projected equivalent raft at the pile toe. A distribution using  $5(V):1(H)$  provides more realistic stress distribution at the pile toe level. Therefore, I later modified the Unified Design Method for narrow pile groups by calculating the settlement as that from an equivalent raft placed at the pile toe level with a widened width determined by spreading the load due to positive shaft resistance between the equilibrium plane and the pile toe (the distance, " $d$ ", below the equilibrium plane). The raft size to be calculated as with a width of  $B + 2d/5$  and length  $L + 2d/5$ , as indicated in Figure 7.26 (only one pile is shown). Below the projected equivalent raft at the pile toe, the stress distribution is calculated using Boussinesq distribution or by  $2(V):1(H)$  for an average value. The Boussinesq method can consider differential settlement across the raft; the equivalent raft is typically a flexible raft.

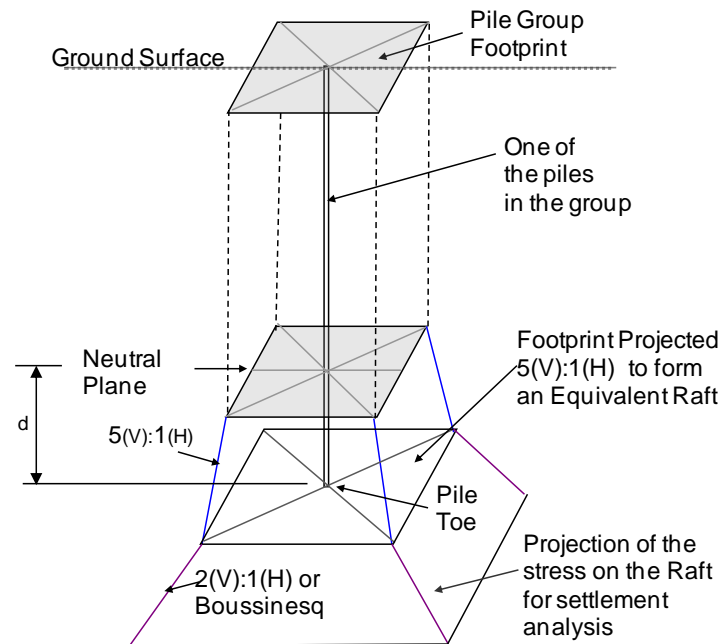


Fig. 7.26 Widening of the equivalent raft for a narrow group of piles.

The portion of the soil between the equilibrium plane and the pile toe depth is ‘reinforced’ with the piles, i.e., they are stiffened up and, therefore, not very compressible. As mentioned, when calculating the soil settlement outside the piled foundation footprint, the reinforcing effect of the piles is disregarded, however. Thus, the difference in settlement calculated for a point right at the edge of the pile cap and one a small distance away will indicate the “hang-up” effect for the pile group—the difference of settlement between the piled foundation and the area around it.

Be the piled foundation flexible or rigid, the average settlement below the equivalent raft is best calculated for the characteristic point defined in Chapter 1, Sections 1.9 and 1.10. The “characteristic point” calculation of stress according to the Boussinesq method produces a settlement value quite close to that produced by the 2:1-method. For differential settlement within a piled foundation placed on a flexible raft (cap) with influence of adjacent footings or fills—usually the case—the calculations need to employ the Boussinesq method.

### 7.17.3 Downdrag

Frequently, a site will be subjected to general subsidence, which can be due to many causes, e.g., fill placed locally (a road embankment) or over the entire site, groundwater lowering, adjacent foundation load, etc., or secondary compression. The resulting downward movement (settlement) of the soil surrounding the pile (single pile, narrow pile group, or perimeter piles of a wide pile group) changes the positive direction shaft resistance to negative direction, “negative skin friction”. This results in additional pile compression and a pile toe movement according to the pertinent toe stiffness response (q-z relation). As the soil settles around the pile, a force equilibrium develops between the dead load applied to the pile head and the drag force (the accumulated negative skin friction) versus the positive shaft resistance and toe resistance. The process will cause an increased pile toe resistance, which magnitude can be estimated in an iterative procedure matching toe resistance and toe movement according to the q-z relation applied. The calculation will result in additional pile shortening and also establish the settlement equilibrium, which is additional to the load transfer movement.

The magnitude of the drag force depends on the assumed height (or length) of the transition zone. (See Clause 7.14.2 and [Figure 7.21](#), above). The height has no influence on the location of the equilibrium plane, however, nor on the magnitude of the pile toe movement. The main thing that matters for the location of the equilibrium plane is the interaction between the pile and the soil at the pile toe.

An obvious result of the development of the equilibrium plane is that, in service condition for a single pile or a narrow group of piles, no portion of the dead load is transferred to the soil independently from the pile cap—the sharing of the supported load between contact stress and load on the piles is a function of strain compatibility between the soil and the piles. Moreover, live loads do not cause settlement and neither does a drag force. (Large number of repeated transient loads—cyclic loading—being an exception).

In a routine case, it is usually sufficient to just make sure that the equilibrium plane lies below a level which indicates a settlement that can be accepted—“*equilibrium plane lies in non-compressive soil*”. However, when analyzing not just single piles or a few piles clustered together, but wide pile groups, matters can become more complicated, because the compression of the soil below the pile toe level must then be calculated as indicated above and in Section 7.18.

The Unified Design Method considers actually occurring loads, deformations, and movements, whereas the conventional “capacity-design” means considering forces only and, to boot, forces for an ultimate condition that supposedly will never develop. The main principles of the unified method was proposed 40 years ago (Fellenius 1984a; 1988). However, many have still difficulty in taking the step from the conventional “capacity-reasoning” to the more rational “deformation-reasoning” of the Unified Design Method. Now that the method has been accepted by the US Federal Highway Administration (Coffman et

al. 2024), most people will find the "step" easier. The following notes aim to explain the basics of the method as applied to single piles and narrow pile groups. It is also pertinent to the perimeter piles of a wide pile group.

Consider a hypothetical case of a single 300 mm diameter, round, concrete pile installed through 25 m of clay and 5 m into an underlying sand. Figure 7.27 shows typical load-movement curves determined from a hypothetical static loading test on the pile calculated using the UniPile software (www.unisoftGS.com). The test is assumed to have been carried out in equal load increments (125 kN) until significant pile toe movements were recorded. The pile head load-movement curve shows the load (1,180 kN) that corresponds to the Offset Limit (Section 8.2). The load applied to the pile head that resulted in a movement equal to 10% of the pile-head diameter (30 mm) is also shown. The 10% value is frequently used as a definition of capacity (Section 8.1). This definition originates in a misconception of a recommendation by Terzaghi (Likins et al. 2012).

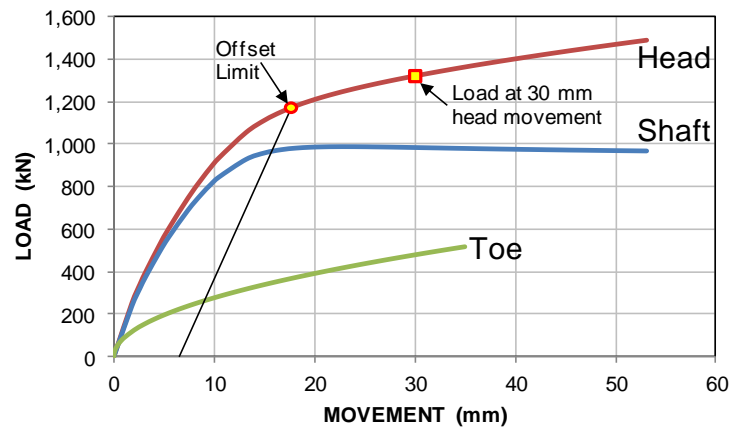


Fig. 7.27 Hypothetical case of results of a static loading test.

The hypothetical pile is assumed to have been instrumented for measuring the distribution of axial force down the pile during the static loading test. The hypothetically measured force distributions for the applied loads are shown in Figure 7.28 also calculated using UniPile for assumed  $t$ - $z$  functions (c.f., Section 8.11) for the shaft (clay and sand) and  $q$ - $z$  function for the pile toe as indicated along the middle of the graph. The distributions can be determined from actual tests on well-instrumented piles or, theoretically, by employing either  $\alpha$ - or  $\beta$ -methods of analysis, as long as they are firmly anchored in reality. The figure also shows the hypothetical distribution of settlement (soil subsidence) at the site assumed to be caused by a small lowering of the groundwater table or by an equivalent change of effective stress triggering a consolidation process. Notice that the soil below the pile toe level was assumed sufficiently dense or stiff not to experience any appreciable settlement due to the groundwater table lowering or to the equivalent increase of stress to the soil. It is important to realize that the soil along the entire length of the pile is subsiding (though the amount is minimal near the pile toe).

The shaft resistance  $t$ - $z$  curves represent the shear-movement response of the soil along the pile. Depending on piles and soil, the response in any given case will differ from that of another case. Responses may exhibit large and small movement before a peak shear resistance, before continuing in a strain-hardening, strain-softening, or plastic mode. Normally, the shear is not associated with volume change, although, it is conceivable that, on occasions, the soil nearest the pile surface can contract or dilate due to the shear movement, with corresponding slight effect on the single-pile  $t$ - $z$  curve.

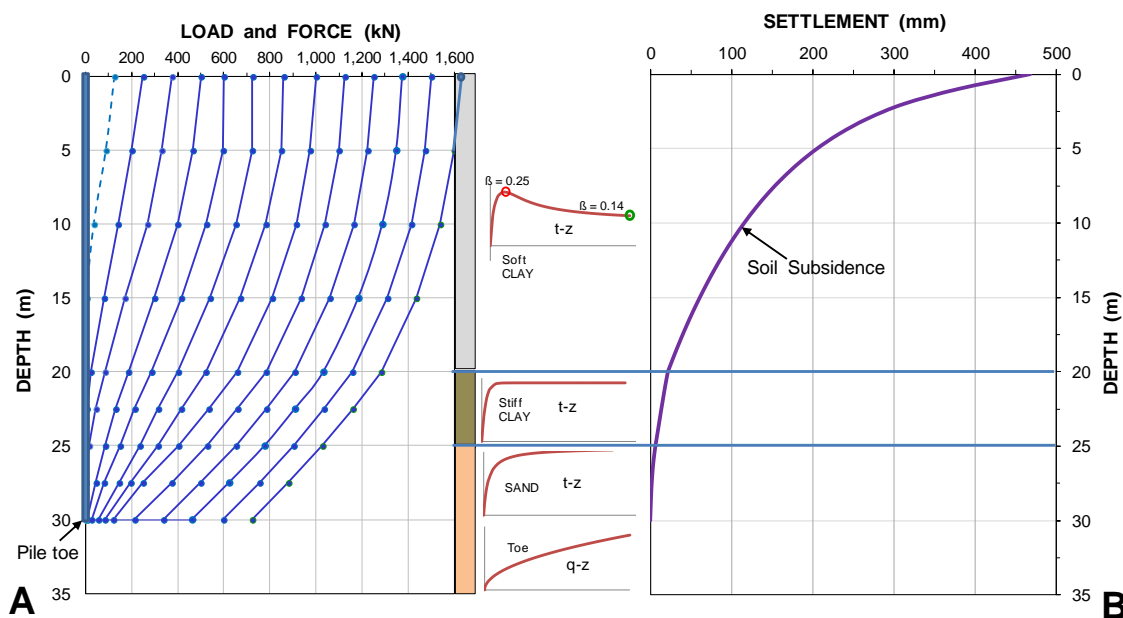


Fig. 7.28 Distributions of axial force in the pile and settlement of the soil around the pile.

At the pile toe, however, the downward movement of the pile (per  $q$ - $z$  function), compresses and displaces the soil both below the pile toe level, to the side, and—marginally, and to a limited height—also up along the side of the pile. The  $q$ - $z$  function incorporates both effects and combines the effects of soil being displaced and the soil volume being changed due to the shear forces that develop around the toe of the single pile, where both compression and dilation can occur. However, it does not incorporate the combined influence of compression due to piles in a group.

The conventional approach is to determine a "safe" working load by applying some definition of "capacity" to the pile head load-movement curve. (The definitions actually used in the engineering practice for what constitutes "capacity" differ widely—and bewilderingly so; Section 8.8 presents examples). The working load is then determined by dividing the "capacity" with a factor of safety, a number larger than unity or, in LRFD, multiplying it with a resistance factor smaller than unity to find the "factored resistance". It is often assumed, mistakenly, that the serviceability (settlement aspect) of the piled foundation is ensured by this approach.

When there is no general subsidence at the site, the approach usually results in a piled foundation that does not experience adverse deformations for the applied working load. On the other hand, when the soil, as in this example, settles around the pile, drag force and downdrag will develop. Some codes and standards, e.g., the Eurocode, add the calculated drag force to the working load, which is an incorrect approach. Even considering the fact that the magnitude of the drag force is often underestimated, this approach often results in that the pile, as originally designed, will seem to be unable to carry the desired working load and, therefore, the design is changed to employ larger, longer piles, and/or adding piles. More enlightened codes and standards, e.g., the Canadian Foundation Engineering Manual, the Canadian Bridge Design Code, the Australian Building Code, US Corps of Engineers, etc., recognize that this approach is not just ignorant, but costly, and, that it yet does not ensure a safe foundation (Fellenius 2014c; 2016a). Since 2024 also the US FHWA is in agreement (Coffman et al. 2024). The drag force is not the issue, the downdrag is, and the action of the settling soil has to be assessed in a settlement analysis.



The unified design method—the "force and settlement equilibriums design"—considers the pile and soil deformation (settlement) and recognizes the fundamental reality that forces and movements are related and cannot be considered separately from each other. Thus, design of piled foundations according to the unified method involves matching the force and settlement interaction. A force equilibrium is determined as the location where the downward acting axial forces (dead load and drag force) are equal to the upward acting forces (positive shaft resistance below the equilibrium depth and toe resistance). The settlement equilibrium is determined as the location where the pile and the soil settle equally (the direction of shear forces along the pile changes from negative to positive at this location). When the shaft shear response is correctly identified, the two equilibriums occur at the same depth, called "equilibrium plane".

For the hypothetical case considered, as the supported structure is constructed, it will impose a sustained (dead) unfactored working load, say, 600 kN. The unfactored transient (live) load for the case is assumed to be about 100 kN. The loading test indicates that the load transfer movement due to the 600-kN load will be smaller than 10 mm. The purpose of the settlement analysis per the unified method is to determine the magnitude of the additional settlement that will develop in the long-term.

Figure 7.29 repeats Figure 7.28 and adds a dashed curve to the set of force distribution curves labeled "Increase of load due to negative skin friction", which mirrors the distribution of shaft resistance. The curve starts at the pile head at a load equal to the 600-kN unfactored sustained working load for the pile.

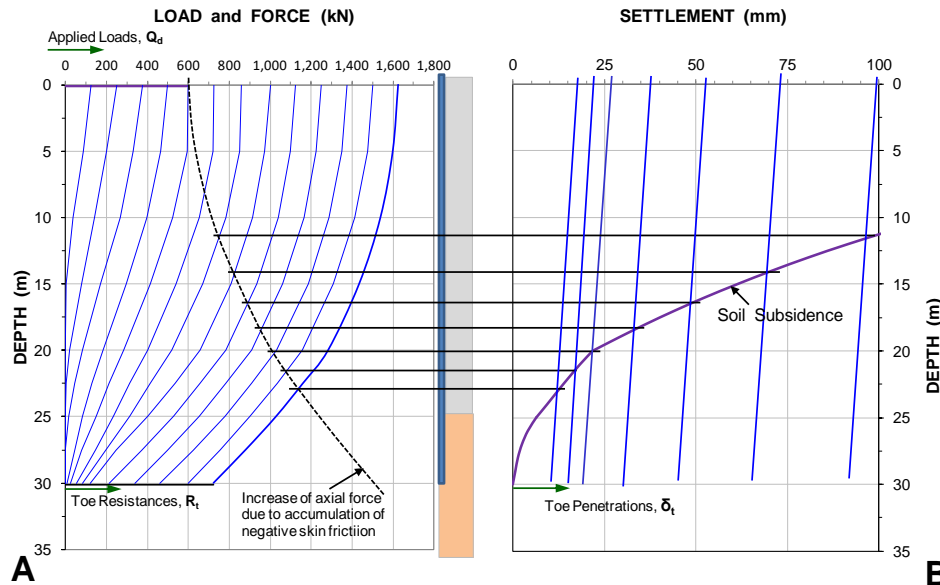


Fig. 7.29 Potential force and settlement equilibrium lines added to Figure 7.28 (Fellenius 2017; 2019).

Each of the many intersections between the curve labeled "Increase of axial force load due to accumulation of negative skin friction" and the force distributions curves is a force-equilibrium and a potential equilibrium plane for the load applied to the pile head. (You may want to review Figures 7.20, 7.22, and 7.24 in addition to Figures 7.28 and 7.29).

In the figure, a series of horizontal lines that intersect with the settlement curve has been added, extending from each force-equilibrium intersection with the dashed curve to intersect with the settlement distribution. Each intersection is a potential settlement-equilibrium and potential equilibrium plane (note, the settlement scale is changed). At each settlement-equilibrium, a slightly sloping line is drawn representing the pile shortening for the axial force in the pile. At the pile toe, the distance between this line and the soil settlement at the pile toe level represents the pile toe penetration for the particular location of the settlement-equilibrium plane. Each intersection of the slanting lines with the line at the pile cap level indicates the settlement of the foundation.

The task is to determine which of the potential equilibrium planes that represents the long-term settlement of the supported foundation. N.B., shaft shear requires a relative movement between the pile and the soil. If the force at the pile toe is not large enough to move the toe, the shaft resistance nearest above the pile toe will not be appreciably mobilized. However, settlement of the pile head would then not be much of an issue as such soil would not show subsidence below the pile toe level.

The figure shows several potential locations of force- and settlement-equilibriums. However, there is only one location (depth) that is true, that is, only one location for which the pile toe force determines a location of the force-equilibrium that is at the same location (depth) for which a settlement-equilibrium combines with a pile toe penetration that, according to the pile toe load-movement curve, corresponds to the pile toe force in the force distribution diagram.

The true equilibrium plane location can be determined by trial-and-error as illustrated in Figure 7.30. Assume a first-attempt toe-force (mobilized toe-resistance), and extend the force distribution (the green dashed line) from this force upward to intersect with the drag force curve from the sustained load ( $Q_d$ ). Then, draw a horizontal line from there to intersect with the settlement distribution curve. If this intersection is the settlement-equilibrium depth, then, the end of the sloping pile line will determine the pile toe penetration. The corresponding pile toe resistance is determined by correlation with the pile toe load-movement curve. As shown in the figure, this first-attempt resistance does not match the originally assumed toe force, the starting toe resistance. A new starting toe resistance is therefore selected and the process is repeated. After two or three attempts, a match, the closed (red) loop, is obtained as shown in Figure 7.31.

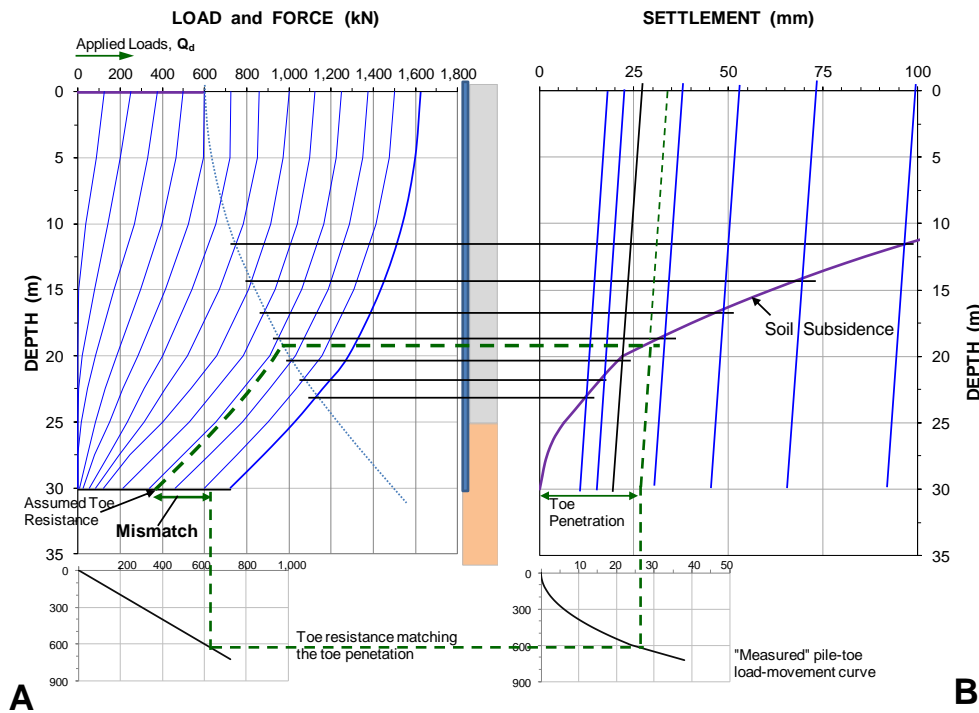


Fig. 7.30 First attempt to find the true equilibrium plane resulting in "mismatch".

The purpose of matching the force- and settlement-equilibriums to the pile toe movement and the pile toe force (never choose one without the other) is to determine—predict—the settlement of the single pile or small pile group—by analysis. There is a misconception around that the movement measured for a specific applied load in a static loading test directly represents the settlement of a pile for the load. It does so only for a single pile—approximately—with no influence of other piles or general subsidence.

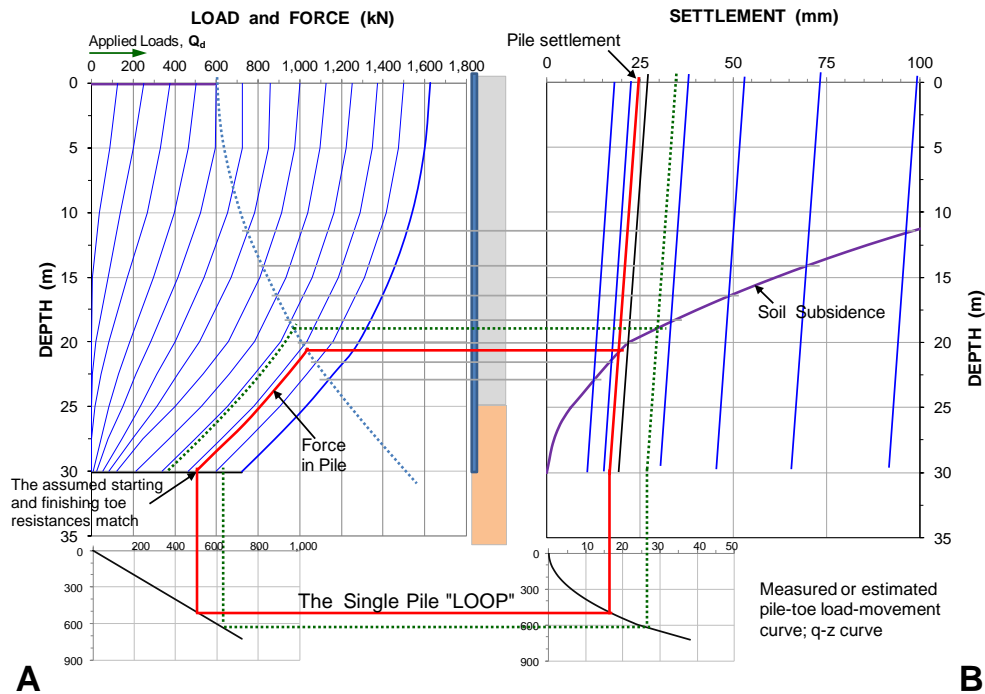


Fig. 7.31 Final match between starting and finished toe resistance and determining the pile settlement.

Note, however, that the static loading test does not measure settlement, but movement, and the movement is often just the accumulated axial compression of the pile for the applied test load. Nevertheless, knowing the movement response of a single pile for an applied load, in particular the pile-toe force-movement, is a vital part of determining the settlement for that pile, as illustrated in the foregoing.

The analysis shown produced a calculated pile head long-term settlement of about 25 mm, which is satisfactory for most piled foundations. Depending on the height of the transition zone (transition from negative to positive shaft shear directions), the drag force for the example case will amount to about 350 through 400 kN. It will prestress the pile and its effect will essentially be beneficial. The maximum axial force at the equilibrium plane will be about 1,000 kN, which is well within the pile structural strength. When, as in this case, the loads from the supported structure also include transient (live) loads (here 100 kN), these will just replace a similar magnitude of drag force. There will be a small pile shortening, but it is recovered when the live load is gone. Live loads do not add to the long-term settlement.

Above the equilibrium plane, the soil moves down relative to the pile and, below the equilibrium plane, the pile moves down relative to the soil. The process and the steps in determining the long-term response is illustrated in Figures 7.27 through 7.30. At the equilibrium plane, the relative movement between the pile and the soil is zero. In other words, whatever the magnitude of soil settlement occurring at the equilibrium plane, that settlement is equal to the settlement of the pile (or of the narrow pile group or of the perimeter piles of wide pile group; Section 7.18) at that depth. It is called **downdrag**. Between the pile head and the equilibrium plane, usually rather small additional settlement of the piled foundation occurs due to axial shortening of the pile as caused by the supported loads and the drag force. The settlement at the equilibrium plane plus shortening of the pile add to the load transfer movement and settlement due to the load supported by the piled foundation and to other causes in the soil below the pile toe level.

Note that the location of the equilibrium plane (as **force equilibrium**) must be in balance with the pile toe force and the pile toe movement (i.e., its penetration into the soil). That penetration is equal to the difference in settlement between the equilibrium plane and the pile toe adjusted for the pile shortening for the average axial load between the equilibrium plane and the pile toe. The foregoing graphical procedure can easily be performed numerically, say in UniPile ([www.unisoftGS.com](http://www.unisoftGS.com)), with input of appropriate parameters and functions simulating the distributions of force, toe movement, pile compression, and soil settlement.

The magnitude of the downdrag is determined by the stress changes and compressibility of the soil below the pile toe level and, to some extent, also the downdrag-enforced penetration of the pile toe into the soil when it is "dragged down" by the interactive process of soil settlement and pile toe penetration.

Note that most of the various software and methods purporting to calculate pile settlement only calculate the load-transfer movement of the pile for an applied load, such as that measured in a short-term static loading test, which rarely reflects the long-term settlement of the piled foundation and usually correlates poorly to pile group settlement.

Moreover, in order to explain the principles and to illustrate the procedure, I used graphs. However, this procedure is time-consuming. For design of an actual piled foundation, the calculation is quickly performed by means of the UniPile Version 6 software. The UniPile enables back-analysis of a static loading test, applying t-z and q-z functions, applying the unified design method, calculating long-term settlement, and determining the response of single piles as well as narrow and wide pile groups, including what-if estimates of load distribution across a raft.

## 7.18 Wide Piled Foundations

The response of a wide piled foundation, a piled raft, is different to that of a single pile or a narrow piled foundation. ("Wide" refers to pile groups with five or more piles along the shortest side; sometimes as few as four). Unfortunately, case histories on response of wide pile groups to load are rare. Clause 7.18.1 provides details of a few of the cases.

The settlement due to the load placed on a piled raft is a function of three main phenomena: (1) compression of the body of piles and soil due to the load, (2) pile-toe load-transfer movement, and (3) compression of the soil below the pile toe level, as detailed in Clauses 7.18.2 through 7.18.5. The contact stress and spatial distribution of the applied load differ across the raft and this is addressed in Clauses 7.18.5 and 7.18.6.

### 7.18.1 Case References

**7.18.1A.** Hansbo (1984) reported a case history comprising long-term response of two adjacent four-storey buildings in Göteborg, Sweden, supported on square 300-mm precast concrete piles driven in a thick deposit of soft clay with a water content of 60 to 80 % and a Liquid Limit of about 60 %. The clay was very compressible ; the Janbu modulus number was about 5. Building 1 was constructed on a grillage of concrete beams (contact area was not reported) and Building 2 on a 400 mm thick raft. Both foundations were placed on engineered fill. The footprint areas of the buildings were about 700 and 900 m<sup>2</sup>, respectively. The foundation piles comprised an upper 8 m length of square 300 mm precast concrete pile extended by a wood pile to 26 m depth. Building 1 was supported on 211 piles under the grillage beams and Building 2 on 104 piles evenly distributed at about 3.0 m spacing. The Building 2 pile group had a width of five rows, which places the pile group at the border line of narrow to wide pile group. The footprint ratios, FR, were 2.3 and 0.8 %, respectively (c.f., Clause 7.18.2 and Eq. 7.35).

The nominal total average load over each building footprint corresponded to 66 and 60 kPa, respectively—quite similar values. The estimated average sustained loads for the two designs were 220

and 520 kN/pile, respectively—quite different values. The conservatively estimated pile "capacity" was stated to be 330 kN/pile. At the end of construction, the average measured pile loads were about 150 and 280 kN/pile for the two buildings, respectively. The differences, 70 kN and 240 kN/pile, respectively, between measured load at the pile head and calculated nominal sustained load can be assumed to represent contact load, likely quite variable for Building 1.

For Building 2, the 240 kN difference in contact load correlates to 28 kPa average contact stress, reasonably close to the average measured contact stress at Building 2 of about 40 kPa. The 280 kN axial force at the pile head combined with a 30-GPa E-modulus correlates to an axial strain of about 100  $\mu\epsilon$ . That strain combined with a 40 kPa contact stress correlates to a  $E_{\text{soil}}$ -modulus of 400 MPa; perhaps OK for the engineered fill, but not at all commensurate with the E-modulus of the soft clay below, which means that, in the clay layer, a good deal of the "contact load" would have been transferred to the pile.

Figure 7.32 shows that the buildings settled on average about the same amount, about 40 mm, over a 13-year period. The equivalent-pier shortening was smaller for Building 1, reflecting its smaller average pile load, toe penetration, and, larger pier EA-parameter, but because of its larger average stress over the footprint, this difference was compensated by the settlement below the pile toe level being larger.

The case history indicates very clearly that, for a wide piled foundation, the bearing of a single pile is irrelevant to the foundation response to the supported load.

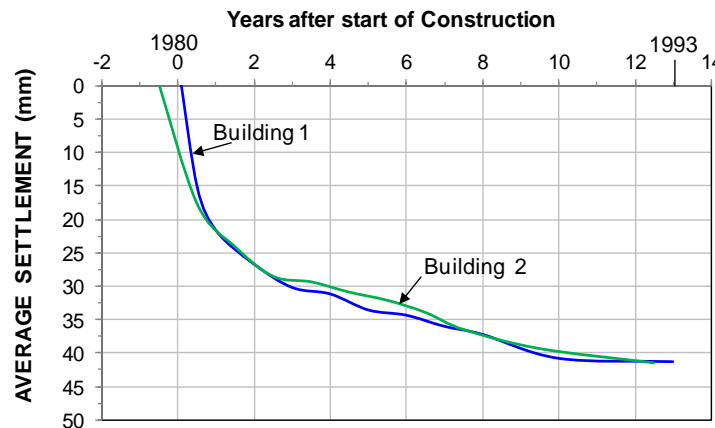


Fig. 7.32 Settlement measured for the two buildings over 13 years

**7.18.1B.** Russo and Viggiani (1995) presented a case history of a wide piled foundation supporting the main pier of a cable-stayed bridge over the Garigliano River in Southern Italy. The raft was 3 m thick. The scour-protecting pile wall was not connected to the pier raft. The pile group comprised 144 steel pipe piles with a 406 mm diameter installed to 40 m depth at a spacing,  $c/c$ , of 1.2 m. The footprint ratio, FR, was 9.2 %.

The loads were measured as the rigid pier was constructed and some time afterward. Figure 7.33 shows that, as the pier was constructed, the load on the perimeter piles (corner and side piles) was larger than the load on the interior piles. This is due to the fact that the response of interior piles is softer than that of perimeter piles because a rigid raft cannot adjust to the bowl-shaped deformations resulting from the fact that piles in the center settle more than piles at the periphery of a loaded raft. The site was affected by general subsidence, which affects the perimeter piles, but not the interior piles: the subsidence imposed drag force and downdrag on the perimeter piles. To maintain the balance of force and settlement (including axial compression), the raft load on the perimeter piles (side and corner) decreased after the end of construction and the reduced amount of load was transferred to the interior piles. As the figure shows, the interactive effect was prominent for the corner and interior piles. The total load on the pier did not change.

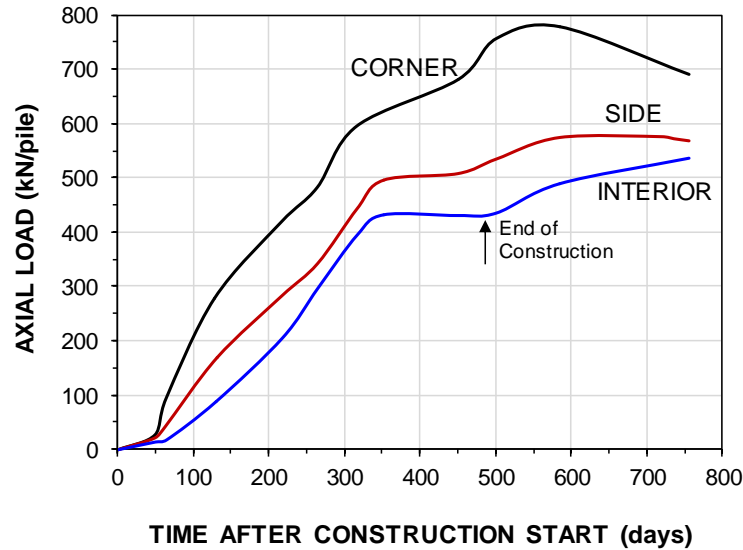


Fig. 7.33 Axial pile loads measured during and after construction (Russo and Viggiani 1995).

After construction, the general subsidence imposed drag force and downdrag on the perimeter piles, softening their response. It is likely that the development of downdrag was lessened by the presence of the enveloping pile wall. With time after end of construction, the needed balance of force and settlement (including axial compression) resulted in a decreased load on the perimeter piles (side and corner) and a corresponding increase of load on the interior piles. As the figure shows, the post-construction interactive effect was prominent for the corner and interior piles. The total load on the pier did not change.

**7.18.1C.** Figure 7.34 illustrates a remarkable case history by Okabe (1977) from a bridge pier on 38 pipe piles, 700 mm in diameter, 40 m long, driven through compressible silt and clay, and seated in a sand below 38 m depth. The pile spacing, c/c, was 1.5 m and the Footprint Ratio, FR, was 14 % (c.f., Eq. 7.35). The raft, thickness was not stated, was placed at about 2 m depth. Three interior piles, one perimeter pile, and one single pile away from the group were instrumented to measure force. The figure shows the monitoring records obtained after 1,040 days.

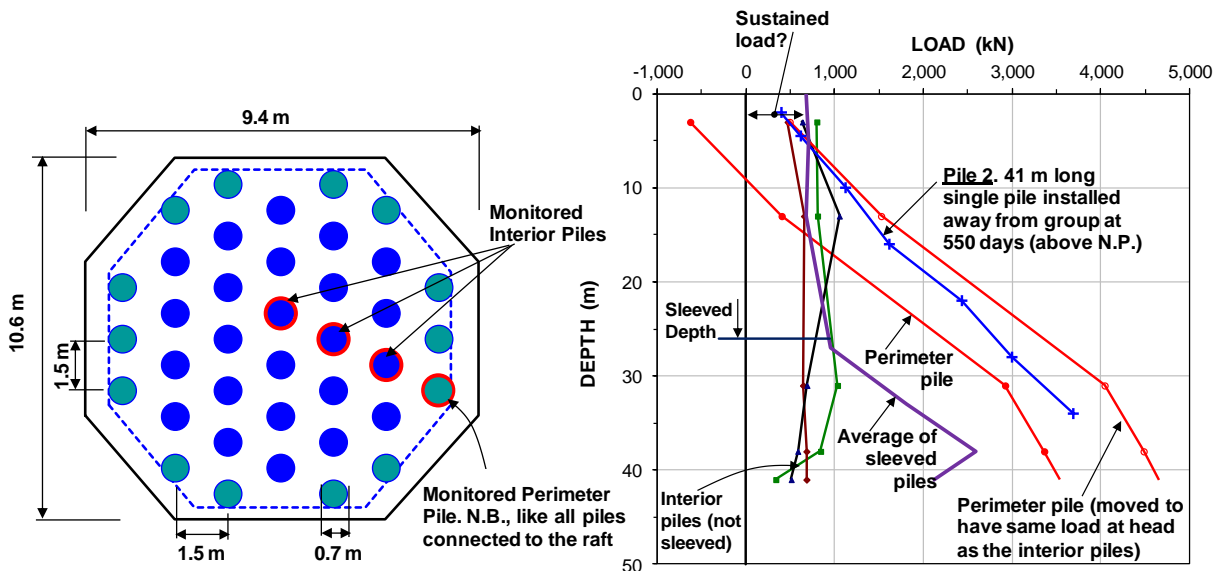


Fig. 7.34 Axial pile forces in interior and perimeter piles measured 1,040 days after construction (after Okabe 1977)

The site was subjected to general subsidence due to water mining in the sand. Monitoring a single pile; the records are included in the graph, showed it to develop negative skin friction and significant drag force. The perimeter pile of the group of piles developed a drag force about equal to that for the single pile. However, the interior piles were neither affected by negative skin friction nor positive shaft resistance and the sustained load resulted in minimal toe penetration and shaft resistance immediately above the pile toe for the interior piles. The measured negative load on the interior piles is likely the result of the pull force due to the downdrag and drag force on the perimeter piles transferred to the interior piles.

**7.18.1D. Fellenius et al. 2019** reported a static loading test a pile group comprising thirteen 300 mm diameter, 9.5 m long pressure-grouted bored piles installed in silty sand and connected to a rigid pile raft. **Figure 7.35** shows the pile-group load-movement measured in the test and the schematic distribution of force from the pile head down to the pile toe. Note the increase of axial force in the natural soil as opposed to in the engineered fill below the pile raft and that the pile shaft was engaged from the pile toe upward.

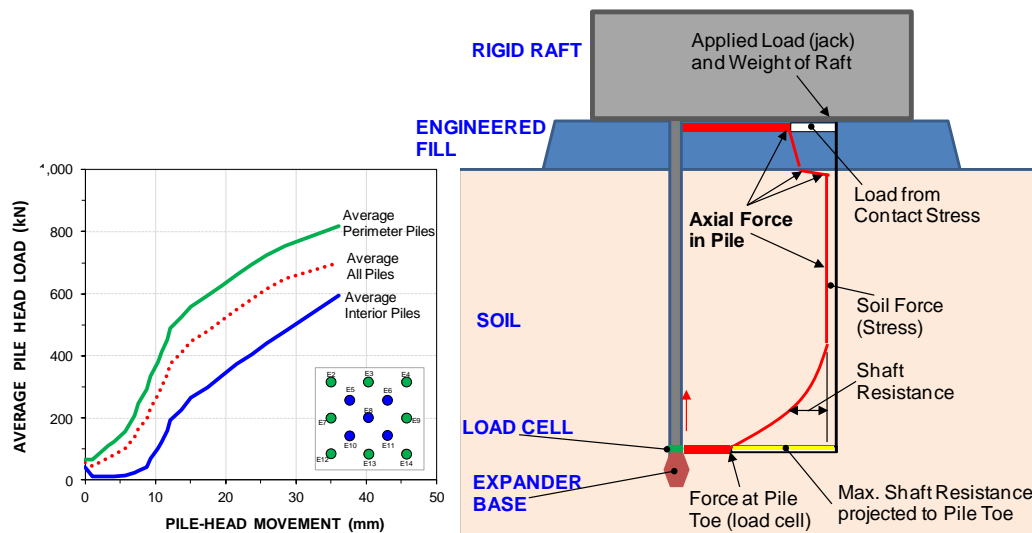


Fig. 7.35 Pile-head load-movement curves and interior pile distribution of axial force

**7.18.1E.** Fellenius (2019) summarized several case histories: Auxilla et al. (2009) presented measurements of raft-soil interface (contact stress) for three 70 m tall cement silos. Yamashita et al. (2011a; 2011b, 2013) reported observations of load and contact stress for a 54 m tall building on a continuous piled raft during construction and during one year afterward. Yamashita et al. (2012) presented a case history on a 12-storey building on a wide pile group and a soil-improvement grid of walls. Kakurai et al. (1987) reported 420 days of measurements of load and contact stress on 24 m embedment driven pipe piles under piled raft supporting a silo building. Liew et al. (2002) reported measurements on a 17.5 m wide tank raft supported on shaft bearing piles in soft compressible clay. Broms (1976) compared settlement measured for two square embankments on a 15 m thick deposit of compressible soft clay, where one of the two embankments was supported on a grid of 500-mm diameter, 6 m deep cement-mix columns.

Yamashita et al. (2011a) also reported a case history of measuring foundation stress under two buildings in Tokyo, 7 and 12 storeys, respectively, supported on a grid of soil-cement walls and piles. The soil at the foundation levels was soft silt and loose sand, respectively. About four years after construction, the contact stress on the grid walls for the two buildings ranged from about 100 through 300 Pa, respectively, and the contact stress for foundations on intact soil ranged from about 15 through 50 kPa, respectively, i.e., the ratio was about 6. This is about the same ratio to be expected from the comparing the E-moduli of the soil-cement mix and the sand.

Yamashita et al. (2013) reported measurements on a similar 12-storey building in Tokyo of found about the same ratio of stress for grid-wall and natural soil. At the end of construction, the measured contact stresses were 114 kPa at the cement-soil wall and 28 kPa at the intact soil, corresponding to a ratio of 4.

The primary results of the mentioned case histories is that when back-calculating the axial pile load and the soil stress to the E-modulus of the pile and soil, respectively, interior piles and soil have the same strain. That is, strain compatibility governs the response of the interior piles. The analogy to a reinforced concrete column is obvious. When load is applied to a column head, the resulting stress in the rebars and in the concrete develops in proportion to the moduli of the materials (steel and concrete) and their respective areas of the column cross section (c.f., Section 7.13). If down the column, a crack exists cleanly across the section, then, all load will be in the rebars. Further down, when again the column is sound, the distribution of loads, stresses, and strains between the rebar and concrete is back in relation to the relative E-moduli of rebar to concrete.

It would have been interesting to know the strain in the piles, but it was not measured by Yamashita et al. (2011a; 2013). However, the axial strain in a pile resulting from an applied load can easily be 100  $\mu\epsilon$  and more. With typical E-moduli of 200 GPa (steel), 30 GPa (reinforced concrete), or 5 GPa (wood), a 100  $\mu\epsilon$  strain represents significant axial pile stress. Strain compatibility requires that the strain in the soil is the same as the strain in the pile. For soil, the E-modulus is about three orders of magnitude smaller than that of a pile and the unit soil stress is, therefore, not large. There is little difference in this regard between conventional piled foundations with closely spaced piles, about 2.5 to 4 pile diameters, and "pile-enhanced footings", which term is often used for piled rafts with piles spaced 6 to 10 pile diameters apart (c.f., Clause 7.18.5). However, widely spaced piles leave a large raft area between the piles and, thus, the contact stress over the contact area integrates to a large contact load, particularly, if the contact is in engineered soil compacted to large density and modulus.

It is important to realize that the term "contact stress" refers to the soil stress immediately under the foundation raft. Where contact stress was reported in the mentioned case histories, it was usually measured in engineered backfill placed on the natural ground, which is much stiffer than the natural soil below. Strain compatibility means that the soil stress is smaller in the softer or less stiff soil below (c.f., [Figure 7.35](#)), and, conversely, the stress in the pile is correspondingly greater. Further down, say, in more competent soil layers, the distribution difference is reversed. The average stress across the footprint with depth is unchanged, however (for a wide group, perimeter piles have considerable shaft resistance, but the interior piles have much less and only along a length immediately above the pile toe; c.f., Clause 7.18.3). Moreover, a piled foundation with the raft some distance above the ground will obviously not have any contact stress, but the requirement of strain compatibility is still valid for the soil layers along the pile down in the soil and the stress in the piles and soil will there be distributed according to the relative proportion of stiffness. It is very important, though, to realize that in a zone above the pile-toe level, i.e., near the boundary between the pile-reinforced soil and the soil without piles (i.e., the soil layer below the pile-toe), the picture changes as addressed in Clause 7.18.2.

It is obvious that the contact stress is linked to the E-modulus of the soil where the stress measurement is made. Therefore, the "pile-enhanced footing" concept is a fallacy. The strain compatibility governs and the modulus of the soil and pile together with ratios of footprint areas will determine the portion of load that is directed to the piles and the portion directed to the soil. Moreover, the rigidity of the pile raft will determine the distribution of strain across the raft.

### **7.18.2 Settlement due to compression of pile-soil body**

The load-transfer movement due to compression of the pile-soil body can be determined as the compression of an equivalent pier with an E-modulus equal to that of the pile and soil combined, as expressed in Eq. 7.35.



$$(7.35) \quad E_{pile+soil} = FR \times E_{pile} + (1-FR)E_{soil} \approx FR \times E_{pile}$$

where

$$FR = \text{Footprint Ratio} = A_{piles} / (A_{piles} + A_{soil})$$

$$E_{pile} = \text{E-modulus of the pile}$$

$$E_{soil} = \text{E-modulus of the soil}$$

The Footprint Ratio (FR) is the ratio between the total area of all piles over the total footprint area of the pile group defined by the envelop around the piles. (N.B., the shape of the pile raft is irrelevant). The FR depends mainly on the spacing and marginally on the pile shape being circular or square and the piles placed in equilateral or square grid. A group of circular piles placed symmetrically at a spacing of 3 pile diameters in a wide foundation at equilateral (triangular) configuration) has FR of 10.1 %, whereas the FR is 8.7 % for the piles placed at a 3 diameter spacing in a square grid. (On an aside, my experience is that when the Footprint Ratio exceeds 15 %, difficulties with the pile construction usually occur at the site. Best is to aim for a FR no larger than about 10 %. See also Section 7.19).

The contribution to the foundation settlement from compression of the pier comprising soil and piles is then expressed in Eq. 7.36 as the shortening of a pier with height, H, when loaded by a total load, Q, and as a function of the Footprint Ratio. In a layered soil (different E-modulus) either calculated layer-for-layer or use the average E-modulus for the soil layers and piles.

$$(7.36) \quad \Delta L = \frac{QH}{E_{Pile+Soil} A_{Raft}}$$

where

$$\Delta L = \text{compression of the equivalent pier with length } L$$

$$Q = \text{load applied to the foundation raft}$$

$$H = \text{height of equivalent pier (i.e., length of piles)}$$

$$A_{Raft} = \text{footprint area of the raft}$$

$$E_{Pile+Soil} = \text{combined E-modulus (Eq. 7.35), as representative for the average across the raft}$$

### 7.18.3 Settlement due to pile compression and load transfer movement

In regard to load-transfer movement, a perimeter pile (side pile or corner pile, the outermost row and, sometimes, also the next row in), respond similar to a single pile or a pile in a narrow group. However, the interior piles respond quite differently.

Franke (1991) stated that "*When load is applied to a group of piles, the shaft resistance is not mobilized the way it is in a single pile, from the head to the toe, but from the toe to the head*"<sup>1</sup>. This applies to interior pile in a group and means that for an interior pile, in contrast to a perimeter pile, the load applied to the raft is unaffected by shaft resistance due to the applied load, but for a length nearest the pile toe. For a uniformly distributed load, therefore, both the compression and pile toe penetration will be larger for an interior pile than for a perimeter pile. Moreover, because perimeter piles are affected by shaft resistance starting at the ground surface, their response is stiffer than that of the interior piles. Therefore, in case of a rigid raft, the perimeter piles will receive a larger portion of the sustained load as opposed to the interior piles. The following analysis illustrates the concept, which is independent of the rigidity of the raft, i.e., it applies to flexible and rigid rafts. The Okabe (1977) case records confirm the principle.

<sup>1</sup> Franke (1991) actually wrote: "... from top to tip and from tip to top" making his phrasing of the statement the single context I know where using the terms "top" and "tip" does sound good and well.

Going back to the analogy to the concrete column (c.f., 7.18.1E): If the column rests on a base (a floor) of some soft material and the rebars protrude a small distance, then, on loading the column, all load is in the rebars. That is, so it is at first. Then, more or less immediately, the rebars start to penetrate into the floor and will do so until the penetration is equal to the rebar protrusion, which is when the concrete starts to experience stress against the floor which unloads the rebars and further penetration of the rebars might cease because the floor takes the stress. If concrete—the matrix—would not be concrete but some soft material, then, the bars could still be pushed into the base, into the floor as it were, provided that the matrix around the rebars would be compressed as much as the rebars are pushed into the base. The reinforced concrete column is a model of a pile-soil body with the rebars as piles.

The pile toe resistance depends on the pile toe soil stiffness (load-penetration relations, i.e., the particular  $q$ - $z$  function, c.f., Section 8.11). Self-evidently, the toe penetration can also be stated to be the distance the soil moves upward around the piles. The toe resistance is equal to the applied axial load after the shaft resistance engaged by the soil in moving up along the pile has been subtracted from the applied load. The toe penetration is the load-transfer movement of the pile for the applied load. The key factor is that the distance the soil compresses (moves) up along the pile is equal to the distance the pile toe moves into the soil, no more, no less—a truth so obvious that once realized, it may appear trivial. This is the "Fellenius-Franke principle": the response of an **interior pile** follows the requirement that the penetration of a toe force resulting from an applied load is coupled to an equally large movement of the soil immediately above the pile toe between the pile and the soil. The latter diminishes with the distance above the pile toe and the corresponding shaft resistance along this length of pile. N.B., above this length, or zone, there is no more shaft resistance along the interior pile.

The piles inside a pile group, the interior piles, will interact and there will be strain compatibility for the pile and the soil, much like the interaction and interplay of stress between the reinforcement and the concrete in a reinforced concrete element. Any axial load that is shed to the soil is transferred from the soil to a neighboring pile that, in turn sends some of its own load to the first pile or to other piles. For example, Caputo and Viggiani (1984), when performing a static loading test on a pile measured movements of an adjacent pile, and a not so adjacent pile, demonstrated that the soil-shaft interaction is not restricted to a thin zone nearest the pile, but can extend a considerable distance out. Obviously, piles in a group do interact.

**Illustrative example.** The principles are illustrated in the following, using the test results presented in Section 8.10 of a test pile, a part of a wide piled-raft foundation supported on 400-mm diameter, round concrete piles at a three-diameter spacing in a square grid and constructed to 42 m depth in a soil profile comprising 5 m of soft clay, 11 m of compact sand, 24 m of silt and clay on a sand deposit. A 1.5 m thick fill assumed to add 30 kPa stress placed across the area outside the foundation footprint and lowering the a groundwater table from 3 to 5 m depth will result in about 25 mm long-term general subsidence at the site. The applied unfactored sustained load was 1,000 kN/pile. The live load was 200 kN/pile. An additional and similar example is presented in Chapter 15 (Example 15.6.3).

The results of the back-analysis of the results of the static loading test illustrate the procedure for determining when the toe movement for the toe force and the upward movement (compression) of the soil in-between the piles are equal. According to the Fellenius-Franke principle, the so-determined shaft resistance is equal to the difference between the toe force and the sustained load. [Figure 7.36A](#) shows the pile toe resistance versus toe movement, the  $q$ - $z$  curve, as determined in the test (or as it could have been obtained in an 'informed' assessment of project conditions). The green curve is the sustained load subtracted by the shaft resistance engaged upward from the pile toe plotted vs. the pile toe movement. It actually also shows the pile-toe force-movement. The intersection point between the curves determines the only true toe resistance for the conditions. Both curves were obtained in a simulated bidirectional static loading test, as shown in the [Figure 7.36B](#). The bidirectional cell was assumed placed right at the pile toe. (In a real test, the cell would be placed some small distance above the toe and the toe response would have to be back-calculated).

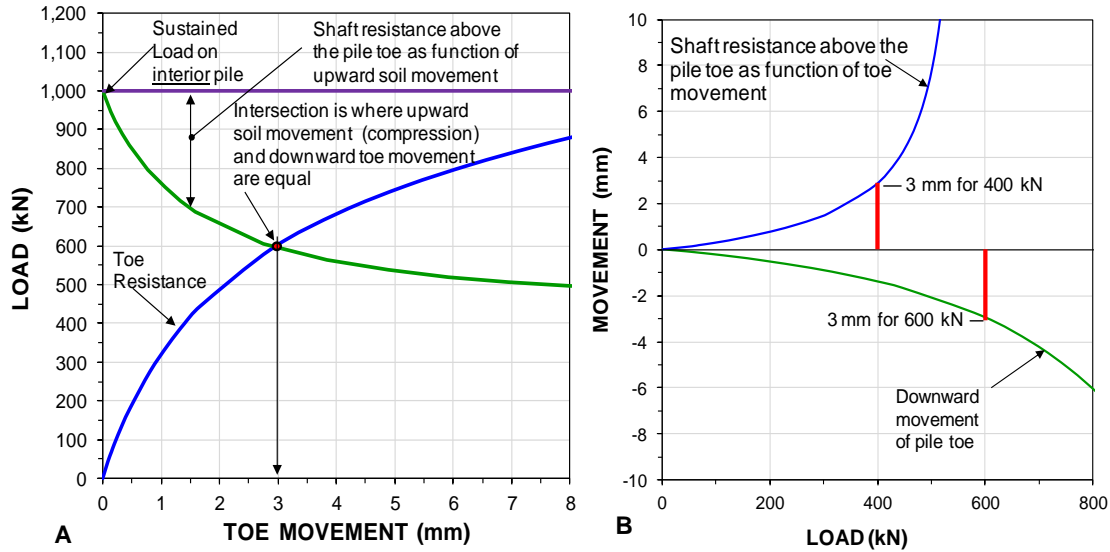


Fig. 7.36. The process for determining the load-transfer toe-movement for interior piles.

Figure 7.37A shows an alternative display of the upward and downward load-movements at the pile toe in the simulated bidirectional test and the movement for when the combined upward and downward loads, equals the 1,000-kN sustained load.

Figure 7.37B compares the force distributions for perimeter and single piles for equal applied load and indicates that the interior pile will engage shaft resistance along an about 5-m length above the pile toe level. For the perimeter piles, affected by the same 1,000 kN applied load, the pile starts to engage the soil at the pile head, mobilizing shaft resistance along just about the full pile length). Thus, the pile-head movement for the perimeter pile of the example consists of pile compression (about 6 mm) and the toe movement is minimal. In contrast, the interior pile will experience a much larger pile compression and larger pile toe penetration, here, about 3-mm.

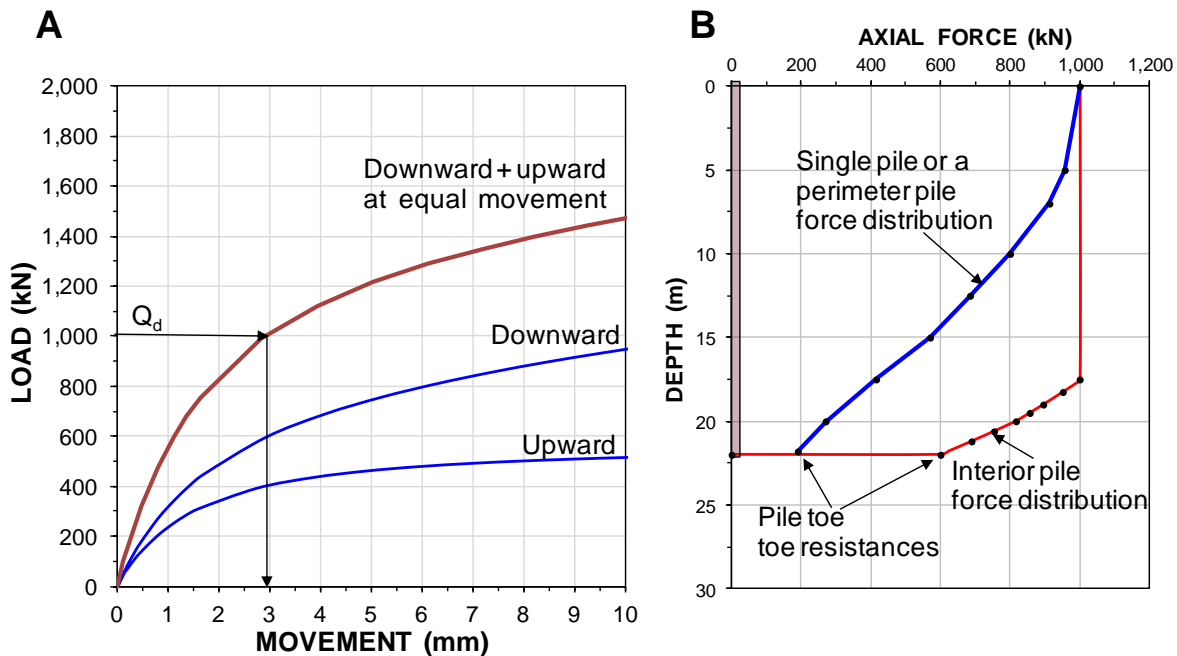


Fig. 7.37. Force distribution for perimeter and interior piles under a flexible raft (same load per pile).

The construction of intersection point movement is only valid for a specific applied load. Each such applied load and construction will establish the pile toe load-movement for the particular load. The pile head movement is then this curve plus the pile compression for the applied load.

The analysis assumes that the shaft shear between the interior pile and the soil immediately above the pile toe level, moving upward as it were, follows the same t-z function as when a single pile is moved upward relative to the soil. The veracity of the assumption is unknown; no measurements have ever been published on a study of the scenario.

The footprint ratio of the pile group is 8.7 % and the 1,000-kN load correlates to a uniform stress of 555 kPa over the raft. The response of the perimeter (side and corner) piles are assumed similar to that of a single pile at the site. The E-modulus of the pile is 30 GPa. Thus, the E-modulus ( $E_{pile+soil}$ ) of the pile and soil together (the "pier") is 2,600 MPa, as calculated by Eq. 7.35. Accordingly, the pier compression of the wide group encompassing 22 m long piles is 8 mm.

The [Figure 7.34](#) case record (Okabe 1977) shows that perimeter piles at a site with subsiding soil will be affected by drag force increasing the compression of perimeter piles and adding settlement due to downdrag, reducing the settlement difference between the perimeter and interior pile, indeed, even reverse it (see Clause 7.20.12). Therefore, if the "slight" subsidence at the site instead would be significant, the subsequent downdrag would increase the settlement of the perimeter piles and it might become larger than the interior piles—the raft would hog. The analysis could then again be used to estimate how much longer the perimeter piles would need to be to eliminate the hogging and ensure a uniform settlement distribution.

The foregoing presumes that the raft is flexible, that is, all piles have the same load from the uniformly distributed stress applied to the raft. In case of a more rigid raft, the settlement difference will be smaller for either of the two, but, in the absence of general subsidence, the raft will transfer load from the interior piles to the perimeter piles. And, in the presence of general subsidence, from the perimeter piles to the interior piles. Either case will impact the bending stress in the raft.

A raft can be either rigid or flexible. As was indicated in [Figure 7.38](#), if the raft is rigid, the pile head movements are equal for all piles. Then, because the shaft resistance for a perimeter pile develops from the raft level, the response of the perimeter pile is stiffer than that of the interior piles and, therefore, the load at the head of the perimeter pile will be larger than that of the interior pile. If the raft is flexible, the loads will be equal, and, because of the response of the perimeter pile is stiffer, its movement will be smaller than that of the interior pile. (The movements shown in the graph do neither include the effect of the settlement below the pile toe level nor influence of general subsidence). As a raft is never totally rigid or totally flexible, the actual load of any case will be somewhere in-between the extremes, as the red circles indicate in the figure. The procedure is helpful for determining the difference in load and/or movement for interior and perimeter piles once the average load is known together with the measured or estimated load-movement curves.

#### **7.18.4 Settlement due to compression of the soil below the pile toe level**

Settlement due compression of the soils below the pile toe level can be determined as that of an equivalent flexible raft at the pile toe level loaded with the total load, uniformly distributed, applied to the pile raft at the foundation level (c.f., Clause 7.17.2) as addressed in [Figure 7.39](#). Note that all contributions to the effective stress below the equivalent raft needs to be included in the calculation. The settlement of a flexible raft will vary across the raft diameter; be largest in the center and smallest along the sides (e.g., calculated by means of the Boussinesq stress distribution). The equivalent raft is always flexible even when the actual raft is rigid, and will, therefore, "dish", if the stress distribution is uniform. Perhaps, less so than a fully flexible raft, but still significant.

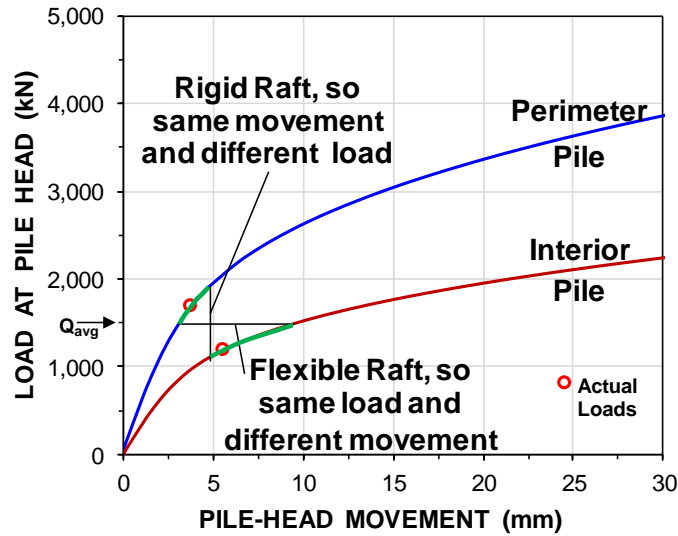


Fig. 7.38 Comparison of load distribution for a perimeter pile and an interior pile in a wide pile group.

Kany (1959) and Steinbrenner (1934; 1936) showed that the stress distribution below the characteristic point (See Section 1.9) is independent of the raft degree of flexibility and are, therefore, equal for the rafts—flexible or rigid. Conventionally, the settlement of the rigid raft is that calculated at the characteristic point for an applied stress equal to the average stress across the raft. It is usually assumed that the average settlement for the flexible raft is equal to the settlement at the characteristic point. Note, that the compressibility (stiffness) of the pile-soil pier needs to be proportioned between the pile and soil E-moduli and respective areas to an  $(AE)_{combined}$ , as indicated in Eq. 7.35.

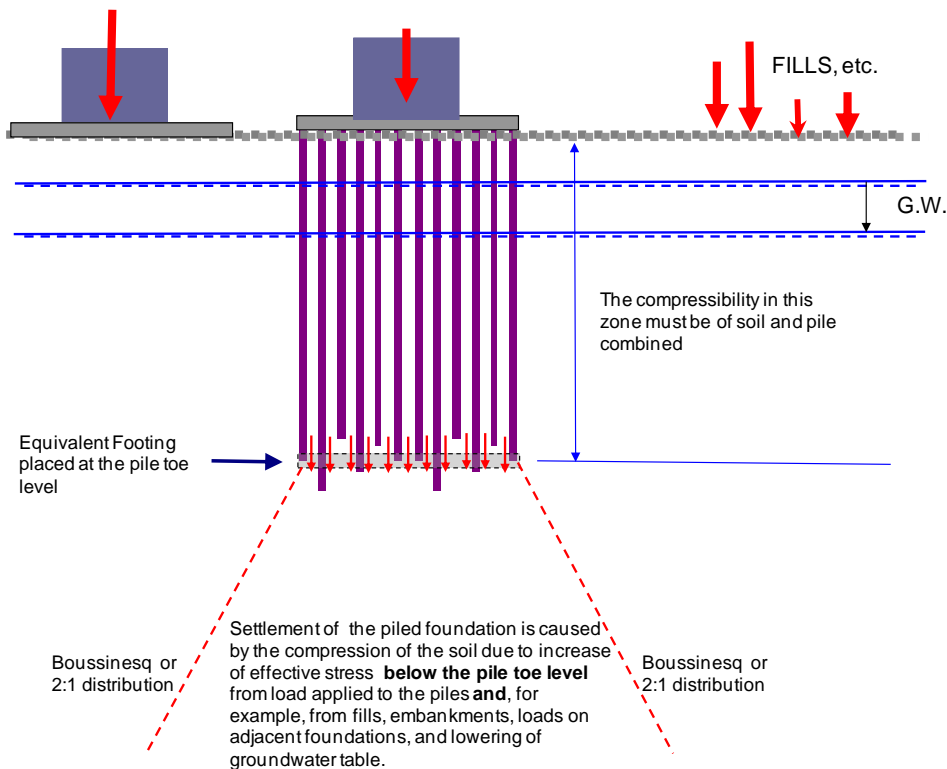


Fig. 7.39. The equivalent raft for calculation of settlement below the pile toe level.

The settlement of a piled raft depends on the sustained pile load, the pile compression for the load, the load-transfer movement and the toe penetration, the location of the pile in the group, and the settlement below the pile toe level. Table 7.13 compiles the settlement values for the perimeter and interior piles in the wide group for an applied load equal to 1,000 kN/pile and indicates that for the presented case, the interior pile will settle more than the perimeter piles—the pile raft will sag ("dish"; become bowl-shaped)—very slightly for this case, but at another site and with other piles of other length, the settlement differences might be larger. The analysis would be the same, however. Indeed, it could be used to estimate how much shorter the perimeter piles should be to eliminate the sagging and ensure a uniform settlement across the raft.

**Table 7.13** Settlement summary

Pile (location)	Compression (mm)	Toe Penetration (mm)	Soil below pile toe level (mm)	Total (mm)
Corner pile	6	0	8 to 10	14 to 16
Mid-side pile	6	0	12 to 15	18 to 21
Interior pile	8	3	15 to 20	26 to 31

#### 7.18.5 Contact stress

Just like the rebars and the concrete in the reinforced concrete column, the distribution of the raft load to the piles and to contact stress develops according to the respective E-moduli of the piles and soil, and to the respective areas of pile and soil. Ordinarily, the strain introduced in the pile is in the range of 100 to 200 microstrain, which, for a 400 mm diameter square concrete pile correlates to about 400 to 800 kN load range. Most natural soils surrounding a pile would have a modulus that is at least two, maybe more than three, orders of magnitude smaller than the modulus of the pile material. A 200 microstrain soil-strain combined with, say, a soil E-modulus of 50 MPa, will amount to 10 kPa contact stress. At, say, a 5-m<sup>2</sup>, footprint area per pile, this correlates to a 50 kN load—"contact raft load"—from the raft to the soil over each pile's footprint area from the raft. Coincidentally, the contact stress is often about equal to the "wet load" of the concrete raft. (But this correlation, as it were, is no causation). If, instead, the soil immediately below the raft placed on the natural soil is a well-compacted coarse-grained backfill with an E-modulus of 200 MPa, the portion carried by the soil would become 200 kN, seemingly relieving the piles of considerable load. However, down in the natural soil below the backfill, the natural soil having a small E-modulus, much of the load would go back into the piles.

Strain compatibility requires, for example, that, if deeper down, the soil matrix is very compressible (say, the pile goes through a layer of soft clay), some of the load is transferred to the piles increasing the strain in the pile and reducing the load in the soil until its new compatibility value. (The soil strain will also increase as it must stay the same as that in the pile). Then, in the, say, stiff soils further down, the reverse happens: load is transferred from the pile to the soil until a new equilibrium is established. These changes occur with minimum of relative movement between the pile and the soil. In other words, assuming that the piled raft can be enhanced by some of the load being independently carried by the soil as contact stress is a delusion. It is simply not possible to assign a working load for the piles, whether a "safe" load or one close to the pile "capacity" and expecting the pile load to be the actual load and that contact stress will make up additional resistance margin to a satisfactory total factor of safety. Within a short distance below the ground surface, whether or not the underside of the raft is touching the soil surface has no effect. The "enhanced raft" concept is a fallacy.

### 7.18.6 Load distribution across the raft and between piles

As a piled raft is neither ideally flexible nor rigid, reality lies somewhere in-between, depending on pile spacing and on thickness and width of raft. To repeat, for a uniformly loaded, ideally fully flexible piled raft, all piles have the same load, but will settle differently; the center piles will settle more than the perimeter piles. In contrast, each pile supporting a uniformly loaded, fully rigid raft will settle the same as the other piles, but the loads for the perimeter piles will be larger, sometimes much larger, than for the interior piles (c.f., Figure 7.37). The exception is for pile groups in subsiding soil, where the perimeter piles will compress also due to accumulated negative skin friction. It might actually move more than the interior piles and have less load from the structure).

Horikoshi and Randolph (1997) defined raft to soil stiffness ratio,  $K_f$ , as function of properties of raft and soil and raft breadth and width. For square rafts and equal Poisson Ratio of pile and soil, the stiffness ratio is expressed in Eq. 7.37.

$$(7.37) \quad K_r = (6/FR)(t/L)^3$$

where  $K_f$  = stiffness ratio  
 $FR$  = Footprint Ratio (Clause 7.18.2)  
 $t$  = raft thickness  
 $L$  = raft length (= raft width)

For a center-to-center spacing,  $c/c$ , ranging from  $5b$  through  $3b$ ,  $F_R$  ranges from about 4 % through about 10% and  $K_r$  ranges from  $0.09L$  through  $0.12L$ , i.e.  $\approx 0.1L$ . Basile (2019) expressed the relative degree of rigidity as ranging from fully flexible through fully rigid as raft thickness,  $t$ , to raft relative circular width,  $D_{equ}$ , as a function of the stiffness ratio, as presented in Figure 7.40.

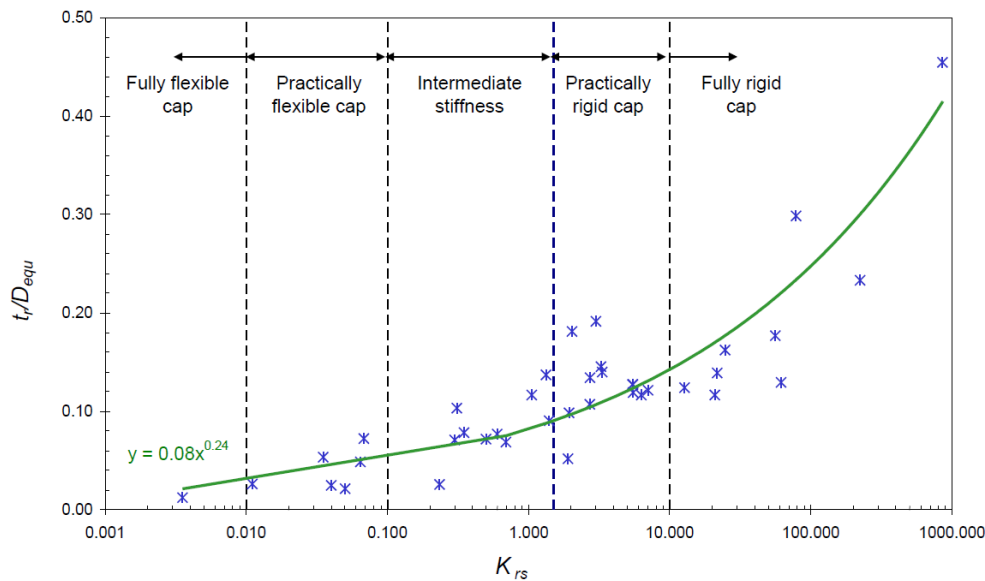


Fig. 7.40. Relative rigidity of a raft as function of stiffness ratio,  $K_f$  (Basile 2019)

Perimeter piles will develop shaft resistance and, therefore, shed axial force, which will result in smaller axial compression as opposed to an interior pile subjected to equal load. The smaller load reaching the pile toe will result in a smaller toe penetration as opposed to the interior pile. Therefore, depending on specific conditions, such as length of piles, spacing of piles, rigidity of the raft, compressibility of the soil below the pile toe level, whether the conditions are for short-term or long-term, etc., the load distribution between the piles across a piled raft, and differential settlement, and dishing and bending of the raft, will vary. Note also that presence of walls on the raft will affect the rigidity of the raft.

For short-term conditions and at sites not subjected to general subsidence or stress increase from fill, adjacent foundations, etc., in case of a reasonably rigid raft, the load received by perimeter piles will usually be larger than that received by the interior piles. To minimize dishing, stress differences, and bending in the raft, the perimeter piles can then be constructed shorter than the interior piles.

However, where conditions do involve subsidence and stress increase from external sources, the subsequent development of negative skin friction and downdrag will unload the perimeter piles (c.f. Okabe 1977 and Figure 7.34). If so, in order to ensure even stress distribution and reduce dishing, the perimeter piles should instead be longer than the interior piles (See Clause 7.20.12).

As mentioned, the distribution of the soil settlement at the pile toe level follows a dishing shape. The foundation raft has a more rigid response, but some dishing will occur with the perimeter piles settling less than the interior piles. In the case of a rigid raft, because the raft settlement at the perimeter would be about the same as in the center (the settlement of the perimeter piles would be about the same as that of the interior piles), the perimeter piles (installed at equal lengths) would have to compress more than interior piles and the pile toe move more, which requires a larger pile head load.

Because of the reduction of load for the interior piles and increase for the perimeter piles, the dishing of the equivalent raft of the rigid piled raft will be less pronounced than for the flexible piled raft. However, be the raft rigid or flexible, the conditions of the soil layers below the pile toe level will still have to be considered in determining the raft settlement.

The ideally rigid raft will not experience dishing and the settlement will be smaller and about equal to the settlement at the characteristic point, as suggested by Steinbrenner (1934; 1936) and Kany (1959). This settlement is in addition to pile compression and load transfer movement.

### 7.18.7 Design and long-term conditions

Returning to the Section 8.10 example, as mentioned, after construction of the supported structure, an 1.5 m thick engineered fill was placed over the general site and the groundwater was lowered. As shown in Figure 7.41, one effect of this is a stiffer pile response—some would say the capacity has increased—because the increased effective stress due to the fill and lowering of the groundwater table. This is illustrated by the rise of the Target Point (for an effective stress analysis of a single pile employing the same  $\beta$ -coefficients and unit toe stress as input for the test conditions). An additional effect, potentially unfavorable, is caused by the fact that the increase of effective stress will start a consolidation process that will develop downdrag on single piles and narrow pile groups at the site. Also the interior piles will be subjected this, a small part, due to the groundwater table lowering. The subsequent downdrag could be the main issue of importance for the piled foundation design, as addressed in the following.

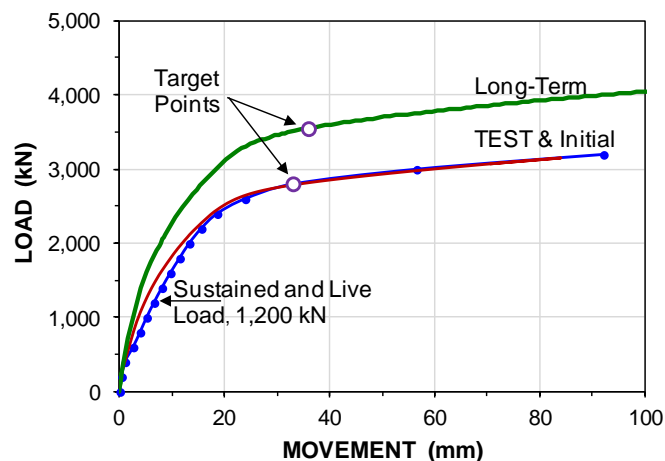


Fig. 7.41 Pile-head load-movements at the test (initial) and long-term conditions



The load-movement analysis of the static loading test shows that on applying the mentioned 1,200-kN sustained plus transient loads, single piles and small or narrow pile groups will experience a load-transfer settlement consisting of about 5 mm of 'elastic' shortening (compression) of the pile. The pile toe will receive no load and will therefore not move—the load will be carried in full by shaft resistance.

In the long-term, the lowering of the groundwater table and the placing of the general fill will increase the effective stress. Therefore, in time, with due consideration of time for the water table to go down and for consolidation of the clay to develop, the site will subside. A simple calculation will show that, at the pile-toe level, the soil will settle about 15 mm, which amount will show up as foundation settlement for the single piles or small groups in addition to the 'elastic' shortening for the applied load.

However, the more important analysis is combining the depth of the force equilibrium to the depth of the intersection of the pile and soil settlement, the settlement equilibrium to find the Equilibrium Plane per the unified method described in Sections 7.15 and 7.17. The analysis comprises finding, for the single pile, the long-term load at the pile toe (in a load-distribution diagram) that agrees with the long-term pile toe movement in a settlement distribution diagram. [Figure 7.42](#) shows the calculated long-term distribution of load and settlement performed applying the Unified Method and UniPile software to a single pile at the subject project, which is also the response of a pile in a narrow group or a perimeter pile in a wide group. See also the similar example is presented in Chapter 15 (Example 15.7.1).

However, the designers were not interested in the settlement issue, but were shocked by the back-analysis, which indicated a 1,300-kN drag force, actually larger than the applied sustained load on the pile. They therefore decided to increase the pile diameter to 600 mm to increase the pile capacity—at a substantial increase also of the foundation costs for the unwitting Owner to cover—and, of course, also a proportional increase of the drag force.

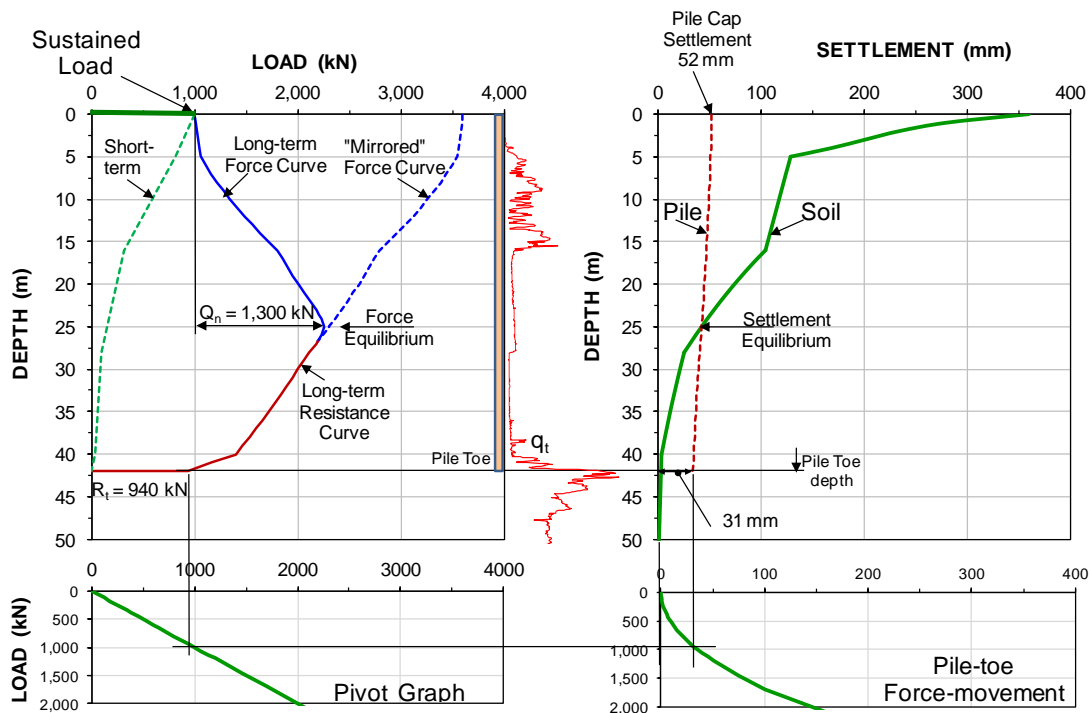


Fig. 7.42 Load and settlement distributions for the long-term conditions of a 400-mm single pile

Figure 7.43 shows the calculated long-term load-movement results for a 600-mm pile with no other change made. As expected, the 600-mm pile is stiffer than the 400-mm pile and, by any definition, the capacity will have increased.

No further testing was carried out and the foundation design was changed to the 600-mm pile constructed to the same 42-m depth as for the original 400-mm pile. The question is now, will the settlement issue have been improved by the shift to the larger pile? It is easy to check the answer in an analysis. Figure 7.44 shows the distributions of load and settlement of the single 600-mm pile performed by a similar unified analysis as for the long-term conditions of the single 400-mm pile. And, yes, the analysis shows that the equilibrium plane has been lowered and the calculated settlement reduced to the, perhaps more manageable, smaller value of 40 mm. However, the drag force has actually increased and is now about twice the sustained load. The designers were not interested to hear about this, however. They continued their work with the design changed to comprise 600-mm piles, in happy ignorance of the actual design issue of their project.

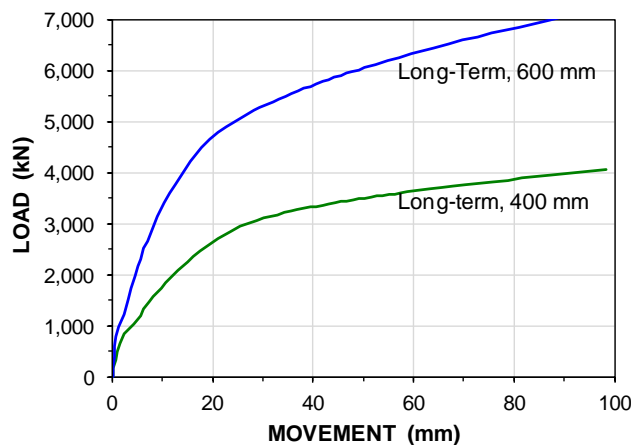


Fig. 7.43. Pile-head load-movements for long-term conditions of the 400-mm and 600-mm piles.

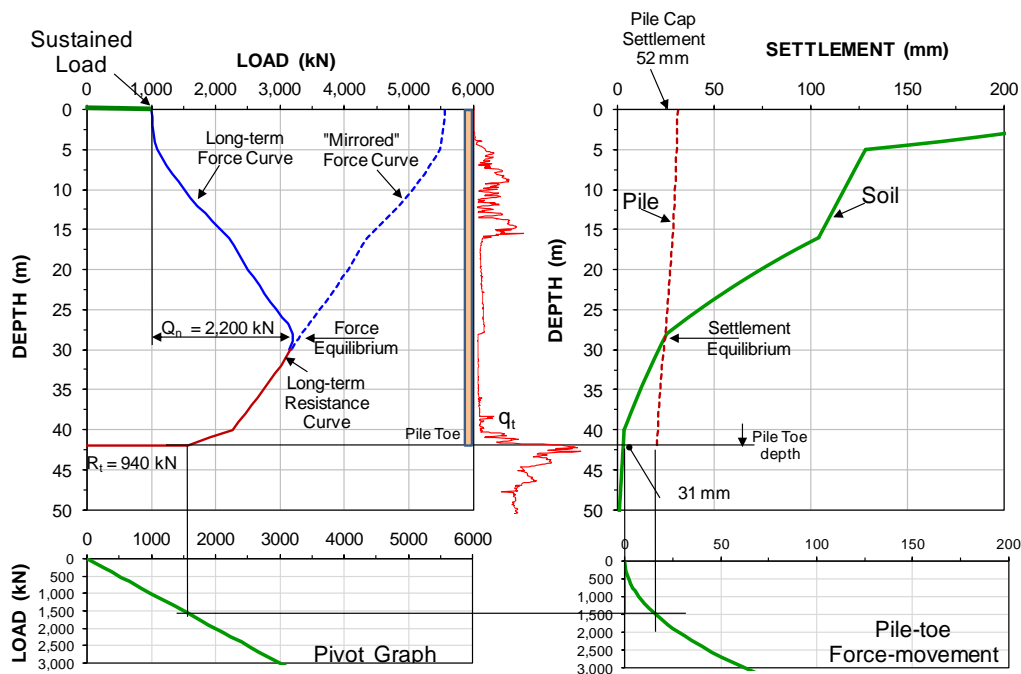


Fig. 7.44 Load and settlement distributions for the long-term conditions of the single 600-mm pile

### 7.18.8 Conventional analysis of a wide piled raft

It is common to see that the response of a pile in a group of piles is assumed to be similar to that of a single pile and that each pile in the group, regardless of position, is assumed to engage the soil from the ground downward. If the pile cap is on the ground, there is a contact stress. The contact stress is assumed to contribute to the bearing of the piles and to be independent of the portion of the load carried by the piles. The effect of relative movement between the pile and the soil is normally not recognized. Sometimes, a reduction coefficient is applied to the pile "capacity" to account for "group effect". Conventionally, if the piled foundation is located where there is general subsidence, all piles are considered to be subjected to drag force and downdrag (whether or not this analysis then considers the effect of the drag force and downdrag properly, I leave aside here). A such common or "conventional" analysis is illustrated in the left sketch in Figure 7.45. The sketch to the right shows the response according to the unified method addressed in the foregoing and illustrates that the interior piles have no shaft resistance above the zone above the pile toe level.

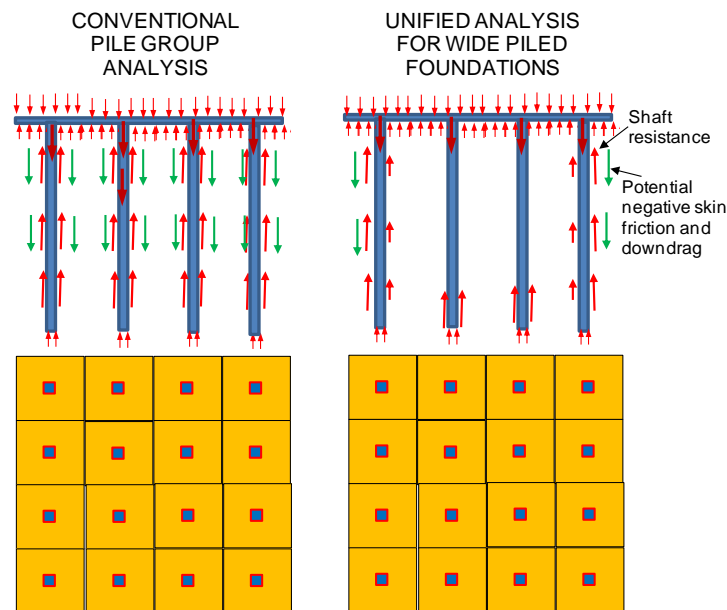


Fig. 7.45 Comparison between conventional and unified method of analysis of a wide pile group.

The sketch in the figure to the right illustrating the unified design method implies that negative skin friction does not affect an interior pile in a wide pile group. This is definitely true for subsidence caused by stress from surrounding loads, such as adjacent footings and fill. However, long-term consolidation due to fill or due to general lowering of the groundwater table will make also the soil in-between the piles compress over time and transfer drag force to the piles. N.B., the drag force is then small, because it cannot be larger than the buoyant weight of the soil in-between the piles. Moreover, the relative movement between the pile surface and the soil will be small and the strain in soil and pile will still be more or less equal. That the contact stress has reduced or disappeared has no effect further down the soil.

The contact stress determined in the conventional approach usually involves calculation by a bearing capacity formula and reducing the ultimate stress by a factor of safety, or just by applying a presumed stress. It is obviously not correct.

The conventional method relies on that shaft resistance develops for the interior piles. However, presence of shaft resistance would mean that the pile has moved down relative the soil and developed positive shaft resistance, which, in turn, would mean that the raft (bearing on the piles) has moved down, which would mean that when the raft moved down, the soil moved down relative to the pile, which would infer

negative skin friction—this is a loop that cannot physically occur. The more logical condition, the unified method of analysis, is illustrated to the right in the figure. The response of the perimeter piles is similar for the two analyses. However, the interior piles of a wide group will not transfer load to the soil via shaft resistance until near the pile toe level (c.f., Section 18.3). And, though not specifically shown, strain compatibility requires that the soil is subjected to the same strain as that experienced by the piles and vice versa. Moreover, this mutual condition extends throughout the soil profile down to the boundary zone where the pile and soil are influenced by the soil above the pile toe level is compressed, "pushed up", between the piles.

To emphasize the difference between the two methods of analysis, Figure 7.46 shows the details of the response of an interior pile. The conventional analysis relies on a "capacity" approach. It usually applies a pile "capacity" adjusted with prescribed factored resistances and adds the contact stress. The unified method considers compression of the pile for the actually applied load and adds the load-transfer movement to find the settlement of the foundation for that load. N.B., the analysis applies unfactored parameters.

Conventionally, design of a pile group with small pile spacing, say, about 3 pile diameters, is assumed to not include a contribution due to contact stress. However, at wider spacing, this contribution is included and the piled foundation is termed "pile-enhanced footing", "piled raft", or similar. Such spacing distinction is irrelevant to the unified method of analysis because the unified method addresses settlement and not "capacity" and the spacing and contact stress are implicitly included in the design analysis.

The figure again demonstrates that the load-transfer movement of the interior pile is larger than that of the perimeter piles. A rigid cap attempts to have all pile heads move equally, which means that load is transferred from interior piles to perimeter piles in order to even out the differences in movement, as discussed in Section 7.18.3 and illustrated in Figure 7.38.

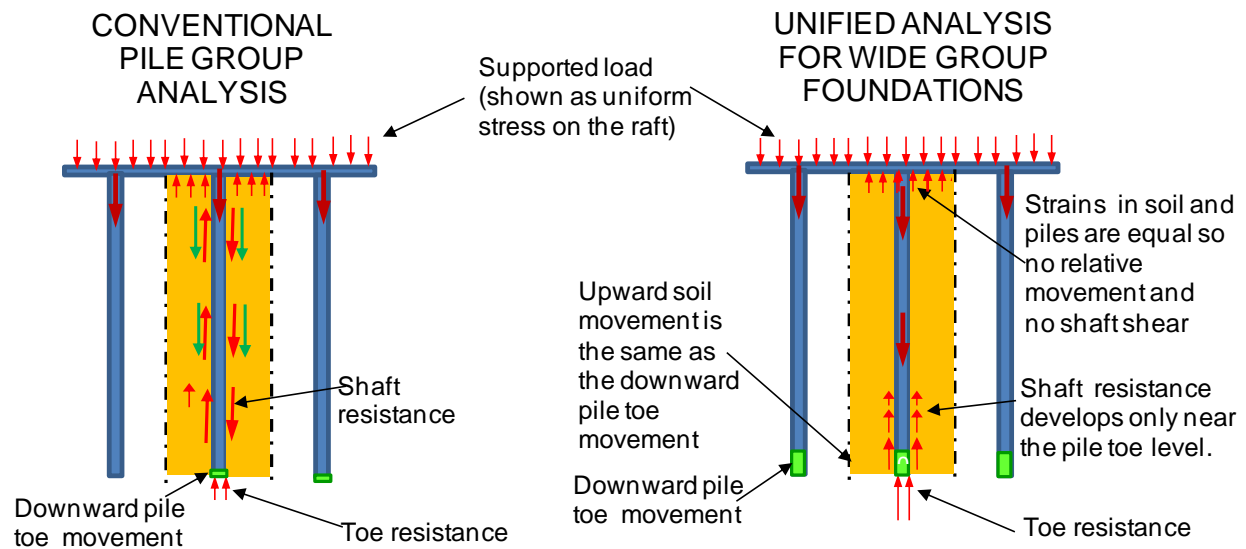


Fig. 7.46 Comparison between conventional and unified methods of analysis of interior piles

### 7.19 Piled Raft and Piled Pad Foundations

The oldest form of piled foundations were not rafts, but a group of piles with soil compacted around and above the pile heads to form a pad on which the structure was placed. Structurally, there are advantages in having a structural raft stressed uniformly over the footprint. The old technique has therefore been revived

in the modern "piled pad foundation", which is similar to a piled raft foundation<sup>2)</sup>, but with piles that are not connected to the raft, these days commonly called "inclusive piles". The foundation is analyzed as a conventional footing cast on the compacted fill above the pile-reinforced soil with the footing stress distributed out into the soil from the pile toe level, not from the footing base.

In Scandinavian countries, piles have since long been used to support road embankments without being connected to any structural element. A recent modern application of a piled pad foundation is the foundations for the Rion-Antirion bridge piers (Pecker 2004, Dobry et al. 2007, Paniagua et al. 2007). Another is the foundations of the piers supporting the Golden Ears Bridge in Vancouver, BC, illustrated in Figure 7.47 (Sampaco et al. 2008), which piles consist of 350 mm diameter (square), 36 m long prestressed concrete piles reinforcing the silty clay at the site to reduce settlement. To provide lateral resistance in a seismic event, the foundation was supplied with 900 mm diameter, 5 m long bored piles connected to the footing and pile cap. The latter piles will not add any bearing to the foundation. Instead, they actually add a small load due to transfer of the drag force that will be developing along their full length.

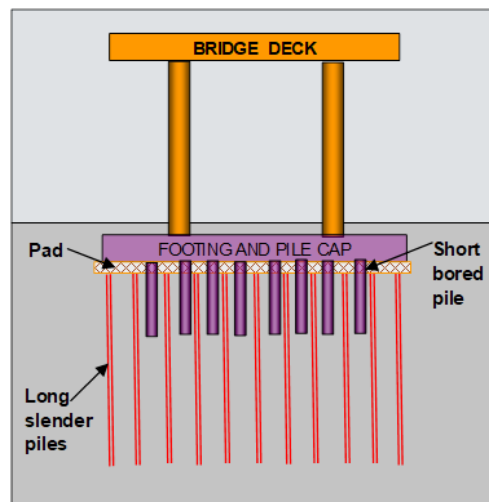


Fig. 7.47 Piled pad foundations for the Golden Ears Bridge piers. The short bored piles carry lateral forces, the long slender piles carry the structure (after Sampaco et al. 2008)

With regard to the soil response to vertical loads of the foundation, the difference between a piled raft and a piled pad is small (though the structural design of the concrete raft and the footing will be different). The main difference between the raft and the pad approaches lies with regard to the response of the foundations to horizontal loading, seismic events, and lateral spreading (soil and piles) and absence of stress concentrations for the raft. Cases of actual earthquake impacting pile-pad foundations show that the pile pad foundation provides the structure with a beneficial cushioning effect during a seismic event (Yamashita et al. 2011 and Yamashita et al. 2013).

The piles for a conventional piled raft foundation are laterally connected by the raft, which minimizes the effect of any lateral spreading. In contrast, a piled pad provides essentially only sliding resistance to horizontal loading. Therefore, lateral spreading needs to be restricted by other means. The potential of lateral soil-spreading under the foundation can be offset by having the pile group area larger than the area (footprint) of the footing on the pad, incorporating horizontal soil reinforcement in the pad, minimizing the lateral spreading by incorporating vertical drains (wick drains, see Chapter 4) to suitable depths, etc.

<sup>2)</sup> The pile pad foundation is sometimes fancily called "column-supported embankment foundation", "inclusion piled foundation", or "disconnected footing concept"; none of which is a good term.

Perhaps the largest difference between the piled raft with widely spaced piles (so-called "enhanced footing") and piled pad foundation, as opposed to a conventional piled foundation lies in that the former are soil improvement methods to be analyzed from the view of deformation (vertical and horizontal), whereas the conventional foundation also needs, or so some codes state, to be analyzed from a bearing "capacity" view with due application of factor-of-safety to the pile "capacity". N.B., if the latter indicates "safe" condition, this does not mean that the foundation is adequate. In contrast, if the settlement analysis shows satisfactory conditions, the foundation is satisfactory.

**7.20. A Few Related Comments**

**7.20.1 Pile Spacing**

Determining the size of the pile cap (piled raft) is a part of the design. The size is decided by the pile spacing and the number of piles in the pile group. The decisive parameter is the center-to-center, *c/c*, distance between the piles, which is expressed in pile diameter (the face-to-face distance of non-circular piles). Pile caps are not cheap, therefore, piles are often placed at *c/c* spacings of only 2.5 to 3 pile diameters. A *c/c* of 2.5 diameters can be considered OK for short toe-bearing piles, but it is too close for long shaft-bearing piles. The longer the pile, the larger the risk for physical interference between the piles during the installation, be the piles driven or bored. Therefore, the criterion for minimum pile spacing must be a function of the pile length. A suggestion is given in Eq. 7.38.

$$(7.38) \quad c/c = 2.5b + 0.02D$$

where  $c/c$  = minimum center-to-center pile spacing  
 $b$  = pile diameter (face to face distance for non circular pile section)  
 $D$  = pile embedment length

The pile spacing for a group of long piles can become large and result in expensive pile caps. For example, Eq. 7.38 requires a spacing of 2.25 m (4.5 diameters) for a group of 0.5 m diameter, 50 m long piles. If a group of three rows, the spacing at the pile head can be appreciably reduced, if the outer row(s) of piles are inclined outward by a small amount, say, 1(V):10(H) or even 1(V):20(H).

Still, the spacing is not an absolute. Piles can be placed very close to each other, indeed, even touching. For example, when used to serve as a retaining wall around a basement, as well as a support of a future wall. An interesting recent development is replacing a large diameter bored pile with several smaller diameter piles essentially covering the same footprint. Figure 7.48A illustrates four about 1.2-m diameter CFA piles having replaced a 2.5-m diameter bored pile for a tall building Florida, USA (Baquerizo 2015).

The sketch to the right in Figure 7.48A shows the approximately clover leaf shape of the final "new" pile. The not grouted center is not shown. Figure 7.48B shows an about 3.6 m long and 1.2 m wide barrette replaced by twelve 0.6-m diameter CFA piles. Static loading tests on special test piles proved out the approach.

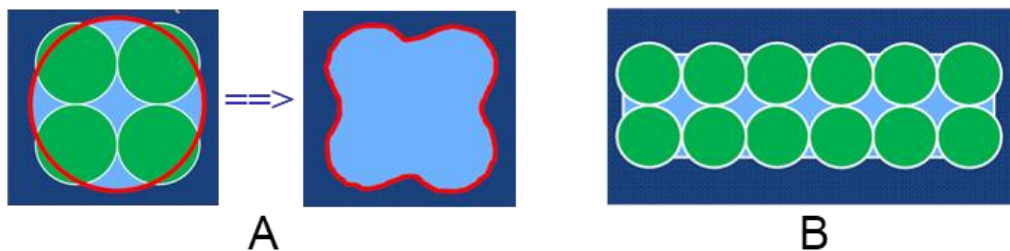


Fig. 7.48 Four piles replacing a single pile and twelve piles replacing a barrette

### 7.20.2 Pile size

The equipment available to the foundation industry in the past limited the size of the piles that could be constructed. However, during the past decade or two, means to construct very large diameter piles have been developed and piles several metre in diameter can be constructed, indeed, even piles with rectangular cross section, called "barrettes", that can be several metre in side length; i.e., so large that it could be a matter of preferred definition whether the pile is a pile or a wall. This development has gone hand in hand with the development of even taller buildings and larger loads concentrated to a small area. The result is that large loads do not any more need to be supported on wide pile groups made up of many piles in a common cap, but can be supported on just a few piles or a single large diameter pile; in effect, a heavy loaded column can continue as a large diameter pile, which could save money otherwise spent on a pile cap. However, wide pile groups of large diameter piles with large loads are frequently used that comprise several rows and columns, notwithstanding that smaller diameter piles within about the same size pile cap (about same footprint ratio) might support the same total load, require less thick pile raft, and be less costly to construct. Not to mention that the bidding for the foundation contract will be of interest also to smaller contractors that would not bid on the large-pile-diameter project due to their not having the capital allowing them to obtain the large equipment. (Smaller diameter piles are usually cheaper and require thinner and cheaper pile caps). The construction is faster, verifying pile "capacity" and integrity is less costly, and distributing the loads on a larger number of points (piles) reduces risk. Note, however, in the selection of a pile size, constructability issues/limitations should always be considered.

### 7.20.3 Design of piles for horizontal loading

Because foundation loads act in many different directions, depending on the load combination, piles are rarely loaded in true axial direction only. Therefore, a more or less significant lateral component of the total pile load always acts in combination with an axial load, be it in compression or tension. The imposed lateral component is resisted by the bending stiffness of the pile, the degree of pile fixity, and the shear resistance and passive resistance mobilized in the soil surrounding the upper length of the pile.

An imposed horizontal load can also be carried by means of inclined piles, if the horizontal component of the axial pile load is at least equal to and acting in the opposite direction to the imposed horizontal load. Obviously, this approach has its limits as the inclination cannot be impractically large. It should, preferably, not be greater than 4(vertical) to 1(horizontal). Also, only one load combination can provide the optimal lateral component.

In general, it is not correct to resist lateral loads by means of combining the soil resistance for the piles (inclined as well as vertical) with the lateral component of the vertical load applied to the inclined piles. The reason is that resisting an imposed lateral load requires the pile to move somewhat against the soil. The pile will rotate due to such movement and an inclined pile will then either push up against or pull down from the pile cap, which will substantially change the axial force in the pile.

Buried pile caps and foundation walls can often contribute considerably to the lateral resistance (Mokwa and Duncan 2001). The compaction and stiffness response of the backfill and natural soil then becomes an important issue.

In design of vertical piles installed in a homogeneous soil and subjected to horizontal loads, an approximate and usually conservative approach is to assume that each pile can sustain a horizontal load equal to the passive earth stress acting on an equivalent wall with depth of  $6b$  and width  $3b$ , where  $b$  is the pile diameter, or face-to-face distance.

Similarly, CFEM 1985 suggested that the lateral resistance of a pile group be approximated by the soil resistance on the group calculated as the passive earth stress over an equivalent wall with depth equal to  $6b$  and width equal to as indicated in Eq. 7.39.

$$(7.39) \quad L_e = L + 2B$$

where  $L_e$  = width of the equivalent wall  
 $L$  = width of the pile group in the plan perpendicular  
to the direction of the imposed loads  
 $B$  = width of the pile group in a plane parallel  
to the direction of the imposed loads

The lateral resistance calculated according to Eq. 7.36 must not exceed the sum of the lateral resistance of the individual piles in the group. That is, for a group of  $n$  piles, the equivalent width of the group,  $L_e$ , must be smaller than  $n$  times the equivalent width of the individual pile, i.e.,  $n$  times  $3b$ . For an imposed load not parallel to a side of the group, calculate for the two cases comprising the components of the imposed load parallel to the sides.

The very simplified approach expressed above does not give any indication of movement. Neither does it differentiate between piles with fixed heads and those with heads free to rotate, nor consider influence of pile bending stiffness, non-uniform soil, pile type, and type of loading. Because the governing design aspect with regard to lateral response of piles is lateral displacement, and the lateral "capacity" or ultimate resistance is of secondary importance, the usefulness of the simplified approach is very limited in engineering practice.

The analysis of lateral behavior of piles must consider two main aspects: First, the pile response: the bending stiffness of the pile, how the head is connected (free head, or fully or partially restrained pile-head rotation) and, second, the soil response: the input in the analysis must include the soil resistance as a function of the magnitude of lateral movement. Whether the loading is static or cyclic is an important aspect to consider. The depth affected may exceed 6 pile diameters in very soft soil, but then the movement is so large that the pile lateral resistance is irrelevant.

The first aspect is modeled by treating the pile as a beam on an "elastic" foundation, which is done by solving a fourth-degree differential equation with input of axial load on the pile, material properties of the pile, and the soil resistance as a nonlinear function of the pile displacement.

The derivation of lateral stress may make use of a simple concept called "coefficient of subgrade reaction" having the dimension of force per volume (Terzaghi 1955). The coefficient is a function of the soil density or strength, the depth below the ground surface, and the diameter (side-to-side) of the pile. In cohesionless soils, the Eq. 7.40 relation is used.

$$(7.40) \quad k_s = n_h \frac{z}{b}$$

where  $k_s$  = coefficient of horizontal subgrade reaction ( $N/m^3$ )  
 $n_h$  = coefficient related to soil density ( $N/m^3$ )  
 $z$  = depth (m)  
 $b$  = pile diameter (m)

The intensity of the lateral stress,  $p_z$  (in units of  $N/m$ ), a soil reaction mobilized on the pile at Depth  $z$  follows a "p-y" concept (Eq. 7.41).

$$(7.41) \quad p_z = k_s y_z b$$

where  $p_z$  = lateral stress ( $N/m$ )  
 $y_z$  = the horizontal displacement of the pile at Depth  $z$  (m)  
 $b$  = pile diameter (m)



Combining Eqs. 7.40 and 7.41:

$$(7.42) \quad p_z = n_h y_z z$$

The fourth-order relation governing the behavior of a laterally loaded pile is then as follows:

$$(7.43) \quad Q_h = EI \frac{d^4 y}{dx^4} + Q_v \frac{d^2 y}{dx^2} - p_z$$

where

- $Q_h$  = lateral load on the pile
- $EI$  = bending stiffness (flexural rigidity) (Note, for concrete piles, the bending stiffness reduces with bending moment)
- $Q_v$  = axial load on the pile

Design charts have been developed that, for an input of imposed load, basic pile data, and soil coefficients, provide values of displacement and bending moment. See, for instance, the Canadian Foundation Engineering Manual (CFEM 1985; 1992). The software LPILE and GROUP by Ensoft Inc. is a useful program for analysis lateral response of single piles and its manual provides a solid background to the topic. Duncan et al. (1992) provides in-depth discussion and recommendations.

The CFEM design charts cannot consider all the many variations possible in an actual case. For instance, the p-y curve can be a smooth rising curve, can have an ideal elastic-plastic shape, or can be decaying after a peak value, much like a t-z curve. As an analysis without simplifying shortcuts is very tedious and time-consuming, resorting to charts was necessary in the past. However, with the advent of the personal computer, special software has been developed, which makes the calculations easy and fast. In fact, as in the case of pile driving analysis and wave equation programs, engineering design today has no need for computational simplifications. Exact solutions can be obtained as easily as approximate ones. Several proprietary and public-domain programs are available for analysis of laterally loaded piles.

One must not be led to believe that, because an analysis is theoretically correct, the results also describe the true behavior of the pile or pile group. The results must be correlated to pertinent experience, and, lacking this, to a full-scale test at the site. If the experience is limited and funds are lacking for a full-scale correlation test, then, a prudent choice of input data is necessary, as well as using wide movement margins and large margins of safety.

Designing and analyzing a lateral test is much more complex than for the case of axial response of piles. In service, a laterally loaded pile in a group of piles almost always has the pile heads in a partially fixed-head (rotation-restrained) condition. However, a fixed-head test is more difficult and costly to perform as opposed to a free-head test. A lateral test without inclusion of measurement of lateral deflection down the pile (bending) is of limited value. While an axial test should not include unloading cycles, a lateral test should be a cyclic test and include a large number of cycles at different load levels. The lateral interaction between piles in a group is a complex phenomenon and much more sensitivity to the influence of neighboring piles than is the axially tested pile (Brown et al. 1987; 1988, Ochoa and O'Neill 1988; 1989, and Rollins et al. 1998).

#### 7.20.4 Seismic design of lateral pile behavior

A seismic wave appears to a piled foundation as a soil movement forcing the piles to move with the soil in the direction of the wave. Thus, a horizontal force develops in the foundation slowing down the movement. The movement is resisted by the pile cap (depending on the structure supported); bending and shear are induced in the piles. A half period later, the soil swings back, but the pile cap is still moving in the first direction, so the forces increase. This situation is not the same as one originated by a static force.

Seismic lateral pile design consists of determining the probable amplitude and frequency of the seismic wave as well as the natural frequency of the foundation and structure supported by the piles. The first requirement is, as in all seismic design, that the natural frequency of the foundation and structure must not be the same as that of the seismic wave (a phenomenon called "resonance"), which would greatly increase movements. Then, the probable maximum displacement, bending, and shear induced at the pile cap are estimated. Finally, the pile connection and the pile cap are designed to resist the induced forces.

In the past, seismic design consisted of assigning a horizontal force equal to a pseudo-static load as a percentage of the gravity load from the supported structure, e.g., 10 %, proceeding to do a static design. Often, this approach resulted in installing some of the piles as inclined piles to resist the load by the horizontal component of the axial force in the inclined piles. This is not just very arbitrary, it is also wrong. The earthquake does not produce a load, but a movement, a horizontal displacement (and axial force). The horizontal force is simply the result of that movement and its magnitude is a function of the flexural stiffness (rigidity) of the pile and its connection to the pile cap. The larger the rigidity, the larger the horizontal load for equal movement. Moreover, when seismic wave moves a vertical pile in the group sideways, the force is mainly a shear force at the connection of the piles to the pile cap. In contrast, an inclined pile moved parallel to the inclination plane will try to rise. As the pile cap prevents the rise, the pile will have to compress, causing the axial force to increase. The increased load could actually be large enough to push the pile down and result in a permanent deformation—the pile is pulled away from the foundation when the direction of forces is reversed. In contrast, where the movement occurs in the direction of the inclination, the pile may experience a pull and will have to become longer to stay in the pile cap. Thus, its load will reduce—the pile could be pulled up or, in the extreme, be torn apart. Then, when the seismic action swings back, the roles of the two inclined piles will reverse. After a few cycles of seismic action, the inclined piles will have punched through the pile cap, developed cracks, become disconnected from the pile cap, lost bearing "capacity"—essentially, the foundation could be left with only the vertical piles to carry the structure, which might be too much for them. If this worst scenario would not occur, at least the foundation will be impaired and the structure suffer differential movements. Inclined piles are not suitable for resisting seismic forces. If a piled foundation is expected to have to resist seismic horizontal forces, it is normally better to do this by means other than inclined piles.

In case of a seismic event, the solution is not to socket the piles or stiffen them by other means, but soften the effect on the superstructure by changing to a pile-pad design, that is placing the raft on a soil-improved ground and combining the piles with a soil stiffening system, e.g., rammed aggregate piers ("Geopiers") or grid-form deep-mixing walls. See for example Yamashita et al. 2013.

An analysis of seismic horizontal loads on vertical piles can be made by pseudo-static analysis. However, one should realize that the so-determined horizontal force on the pile and its connection to the pile cap is not a force causing a movement, but one resulting from an induced movement—the seismic displacement.

### **7.20.5 Pile testing**

A pile design should consider the need and/or value of a pile test. A "routine static loading test", one involving only loading the pile head in eight steps to twice the allowable load and recording the pile head movement, is essentially only justified if performed for proof-testing reasons. The only information attainable from such a test is that the pile "capacity" was not reached, providing no information on the load-transfer and portion of shaft and toe resistances. A test involving only the load applied to the pile head and the movement of the pile head is, therefore, rarely worth the money and effort, especially if the loading procedure comprises load increments of different duration and/or an unloading/reloading sequence or two.

First of all, a static loading test should be performed by building up the applied load by a good number of equal load increments with constant load-holding duration, no unloading/reloading, to a maximum load of at least twice the desired unfactored service load. Second, an instrumented test pile (where the instrumentation is designed to determine the load-transfer) will be very advantageous for most projects. If performed during the design phase, the results can provide significant technical and savings benefits to a project. For example, the design of a piling project a properly designed and executed pile test will save money and time as well as improve safety. Replacing the conventional head-down test with a bidirectional-cell test will be advantageous because the results of a bidirectional test, properly planned, are superior to those of the head-down test (see Section 8.7). Adding dynamic tests with proper analysis (PDA with CAPWAP) might also provide valuable information on load-transfer (see Chapter 9). In particular for driven piles, where information on pile, hammer, soil response is obtained. A main benefit of the dynamic test is the opportunity to test more than one pile.

### 7.20.6 Pile jetting

Where dense soil or limitations of the pile driving hammer hamper the installation of a pile, or if the intent is just to speed up the driving, the construction often resorts to water jetting. The water jet serves to cut the soil ahead of the pile toe. For hollow piles, pipe piles and cylinder piles, the spoils are left to flow up inside the pile. When the flow is along the outside of the pile, the effect is a reduction of the shaft resistance, sometimes to the point of the pile sinking into the void created by the jetting. The objective of the jetting may range from the cutting of the dense soil ahead of the pile toe or just to obtain the lubricating flow along the pile shaft. When the objective is to cut the soil, a large water pressure combined with small diameter jet nozzle is needed to obtain a large velocity water jet. When the objective is to obtain a "lubricating" flow, the jet nozzle must be large enough to provide for the needed flow of water. It is necessary to watch the flow so the water flowing up along the pile does not become so large that the soil near the surface erodes causing a crater that would make the pile lose lateral support. It is also necessary to ensure that the jet cutting ahead is symmetrical so that the pile will not drift to the side. To limit the risk of sideways shifting ("pile walking"), outside placement of jetting pipes is risky as opposed to inside placement, say, in a center hole cast in a concrete pile.

Water pumps for jetting are large-volume, large-pressure pumps able of providing small flow at large pressure and large flow at small pressure. The pumps are usually rated for a flow of 200 gal/min to 400 gal/min, i.e., 0.01 m<sup>3</sup>/s to 0.02 m<sup>3</sup>/s to account for the significant energy loss occurring in the pipes and nozzle during jetting. The flow is simply measured by a flow meter. The flow rate at the pump and out through the jet nozzle and at any point in the system is the same, of course.

The governing jetting pressure is the pressure at the jet nozzle. The pressure at the jet nozzle is significantly smaller than that at the pump due to energy losses. However, while the pump pressure can be measured, measuring it at the nozzle is practically impossible. The pressure at the nozzle can be estimated from simple relations represented by Eqs. 7.44 and 7.45 (Torricelli and Bernoulli relations) combined into Eq. 7.45a. However, the relations are used to design the jet nozzle as appropriate for the requirements of volume (flow) and jetting pressure in the specific case.

$$(7.44) \quad Q = \mu A v$$

where

$Q$	=	flow rate (m <sup>3</sup> /s)
$\mu$	=	jetting coefficient $\approx 0.8$
$A$	=	cross sectional area of nozzle
$v$	=	velocity (m/s)

$$(7.45) \quad \frac{v^2}{2g} = \frac{p}{\gamma} \quad \text{which converts to: Eq. 7.45a} \quad v^2 = \frac{2p}{\rho}$$

where

- $v$  = velocity (m/s)
- $g$  = gravity constant (m/s<sup>2</sup>)
- $p$  = pressure difference between inside jet pipe at nozzle and in soil outside
- $\gamma$  = unit weight of water (kN/m<sup>3</sup>)
- $\rho$  = unit density of water (kg/m<sup>3</sup>)

$$(7.46) \quad A = \frac{Q\sqrt{\rho}}{\mu\sqrt{2p}}$$

where

- $A$  = cross sectional area of nozzle
- $Q$  = flow rate (m<sup>3</sup>/s)
- $\mu$  = jetting coefficient  $\approx 0.8$
- $\rho$  = unit density of water (kg/m<sup>3</sup>);  $\approx 1,000 \text{ kg/m}^3$
- $p$  = pressure; difference between inside jet pipe at nozzle and in soil outside

Inserting the values (0.8 and 1,000) for  $\mu$  and  $\rho$  into Eq. 7.45, produces Eq. 7.47.

$$(7.47) \quad A = 28 \frac{Q}{\sqrt{p}}$$

For example, to obtain a cutting jet with a flow of 1 L/s (0.001 m<sup>3</sup>/s; 16 us gallons/minute) combined with a jet pressure of 1.4 kPa (~200 psi), the cross sectional area of the jet nozzle need to be 7 cm<sup>2</sup>. That is, the diameter of the nozzle needs to be 30 mm (1.2 inch). Specification for jetting cannot just indicate the volume and pressure (at the pump), also the diameter of the jet nozzle(s) needs to be stated. The design needs also consider the frictional loss in the length of flow from pump to nozzle.

During jetting and after completion of jetting, a pile will have very small toe resistance. Therefore it is recommended practice to drive (re-drive) the pile at least one metre beyond the depth where the jetting was terminated. This driving must proceed with caution to make sure that damaging tensile reflections do not occur in the pile.

The shaft resistance in the jetted zone is not just reduced during the jetting, the shaft resistance is often smaller after the jetting as opposed to the conditions without jetting. Driving the pile, "re-driving", after finished jetting will not restore the original shaft resistance.

### 7.20.7 Bitumen coating

When the drag force (plus dead load) is expected to be larger than the pile structural strength can accept, or the soil settlement at the equilibrium plane (settlement equilibrium) is larger than the structure can tolerate, the drag force (the negative skin friction) can be reduced and/or the equilibrium plane be lowered by means of applying a coat of bitumen (asphalt) to the pile surface. Resorting to such reduction of shaft shear is messy, costly, and time-consuming. In most cases, it is also not necessary, which a proper analysis of the long-term conditions for the piles and the piled foundation would show. Moreover, other solutions may show to be more efficient and useful. However, bitumen coating is efficient in reducing negative skin friction and the drag force, as well as in lowering the equilibrium plane. Note, a bitumen coat will equally well reduce the positive shaft resistance and, hence, lower the pile "capacity"—i.e., soften the pile response to load.

A bitumen coat can be quite thin, a layer of 1 mm to 2 mm will reduce the negative skin friction to values of about 10 % of the value for the uncoated pile, depending on the thickness of the bitumen coat. Full-scale tests have shown shear resistance—negative skin friction—of an about one millimetre thick coat to be about 10 kPa. The primary concern lies with making sure that the bitumen is not scraped off or spalls off in driving the pile. The bitumen is usually heated and brushed on to the pile. In a cold climate, the coat can spall off, i.e., loosen and fall off in sheets "sailing" down from the piles like sheets of glass. The potential injury to people and damage to property down below is considerable. In a hot climate, the coat may flow off the pile before the pile is driven. A dusty pile surface—be the pile a concrete pile or a steel pile—may have to be primed by "painting" the surface with very thin layer of heated, hard bitumen before applying the shear layer. Figure 7.49 illustrates brushing the shear layer onto a primed surface of a concrete pile. Figure 7.50 shows a coated pile being driven through a protective casing. Note that the bitumen has flowed and formed a belly under the pile after the coating was applied.



Fig. 7.49 View of applying a bitumen coat to a concrete pile



Fig. 7.50 View of a bitumen-coated pile driven through a protective casing  
The left side of the pile was the pile underside in storage

A functional bitumen coat on a pile to reduce shaft resistance can be obtained from a regular bitumen supplier. The same bitumen as used for road payment can be used. Be careful about roofing bitumen as often some fibers have been added to make it flow less. Note also, that driving through coarse soil will scrape off the bitumen coat—even a "thick one"—and preboring, or driving through a pre-installed casing, or another means to protect the bitumen, may be necessary. Moreover, in hot weather, it may be necessary to employ a two-layer bitumen coat to ensure that the bitumen will not flow off between coating the pile and driving it. The inner coat is the about 1 mm to 2 mm "slip coat" and an outer coat of about the same thickness of very stiff bitumen is then applied to cover the inner coat to keep it in place.

The range of bitumen to use depends on the climate of the site location. Beyond a depth of a few metre, the ground temperature is about equal to the average annual temperature of the site. Therefore, a harder bitumen is recommended for use in tropical climate than in a cold climate. For most sites, a bitumen of penetration 80/100 (ASTM D946) is suitable (Fellenius 1975a; 1979).

### 7.20.8 Pile buckling

Buckling of piles is often thought to be a design condition, and, indeed, in air, buckling could be an issue. However, even the softest inorganic soil is able to confine a pile and prevent buckling, which is a parallel to the fact that the soil support is always sufficient to prevent a pile from moving toward or into it. This means that when the soils moves, the pile has no option other than to move right along. Therefore, piles in slopes and near excavations, where the soil moves, will move with the soil. [Figure 7.51](#) is a 1979 photo from Port of Seattle, WA, and shows how 24-inch diameter, prestressed concrete piles supporting a dock broke when a hydraulic fill of very soft silt flowed against the piles.

Of course, buckling can be an issue for dog-legged or severely bent piles, see Clause 7.20.10.



Fig. 7.51 View of the consequence of a hydraulic fill of fine silt flowing against 24-inch piles.

### 7.20.9 Plugging of open-toe pipe piles and in-between flanges of H-piles

Plugging of the inside of a pipe pile driven open-toe is a common occurrence. If a definite plug has formed that moves down with the pile, the pile acts as a closed-toe pile. The soil mass inside the pile will be of importance for the driving, but not for the static shaft resistance under service conditions. For design, it is a matter of whether to trust that the resistance of the plug will act as toe resistance available in the long-term. In case of an open-toe pipe driven through soft or loose soil and into a competent dense soil therein forming a base, the so-obtained toe resistance can be trusted in most conditions. In contrast, when driving a pipe pile with an inside column—a "core"—, the pipe slides over the column and, in the driving, shaft resistance is mobilized both outside and inside the pipe. That is, inside shaft resistance will occur along the entire length of the soil column. However, when the pile is loaded statically, the core will combine with the pipe and only its lowest length will be affected. The "static resistance" determined by

dynamic measurements (Chapter 9) will therefore be larger than the static resistance determined in a subsequent static loading test. Figure 7.52 taken from Fellenius (2015a), illustrates that static condition. The figure exaggerates the length ("height") of the core portion engaged by shaft shear and compression movement.

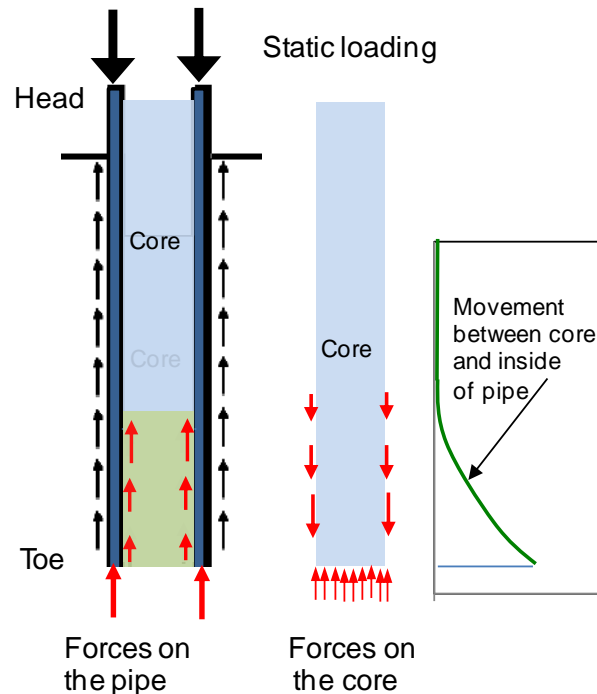


Fig. 7.52 Force vectors in static loading of an open-toe pipe pile with inside soil column, a "core".

Paik et al. (2003) and Ko and Jeong (2015) performed static loading tests on double-walled pipe piles separating outside and inside shaft shear, showing that the inside soil column was only affected a distance up from the pile toe corresponding to the compression of the core for the load acting at the pile toe.

The response of the pipe and the core is similar to that of interior piles in a pile group and the soil in-between the piles. Moreover, the core can be modeled (thought of) as a pile turned upside down and tested from below with the pipe as the "soil". The key point to realize is that a such core-pile is axially very soft in relation to a real pile. Its axial deformation modulus,  $E$ , is about equal to that of soil, albeit compressed under confined condition. The stiffness of the core is, therefore, about 3 to 4 order-of-magnitudes smaller than that of a real pile of the same diameter. Moreover, as indicated by O'Neill and Raines (1991), the effective stress in the core is constant (uniform material is assumed). Therefore, the ultimate unit shear resistance between the core and the inside of the pipe is more or less constant and modeling the shear force distribution along the core should be by means of average shear force; by the  $\alpha$ -method analysis so to speak. (In contrast, the shaft resistance along the outer pipe, of course, must be modeled using effective stress principles).

In modeling the core as a soft pile pushed upward a distance equal to that of the pile toe movement in a static loading test, with the toe force compressing the core, we can appreciate that the imposed movement can never result in a large force at the bottom of the soft core and that the force on the core base will have been "spent" within a short distance up from the core bottom. The force-movement response of the core—unit shear resistance along the inside of the pipe—is more or less an elastic-plastic response, combined with the gradual mobilization of the core length, the response is similar to a pile toe response, i.e., an almost linear or relatively gently curving, force-movement of a pile toe. The difference is the magnitude of toe force and the stiffness, i.e., the slope of the curve.

Fellenius (2015a) presented simulations shown in Figure 7.53 of simulations of the response to static loading of two 11 m long pipe piles, one open-toe and one closed-toe, with OD 711 mm and 7 mm wall thickness driven into a sand similar to the test piles employed by Paik et al. (2003). The simulation was made using an average beta-coefficient of 0.40 along the outside of the pipe and a toe resistance acting on the wall area for the open-toe pipe and the full toe area for the closed-toe pipe. The t-z function was assumed to be a hyperbolic function with the 0.40 beta-coefficient mobilized at a relative movement of 5 mm between the shaft and the soil and a function coefficient,  $C_1$ , of 0.0080 (c.f., Chapter 8). The toe resistance is simulated by a Gwizdala (ratio) function with a function coefficient,  $\theta$ , of 0.600 (exponent) and toe-resistance of 0.7 and 2.0 MPa mobilized at 5 and 30-mm toe movements, respectively. The inside shaft response along the short length (2.5 m) above the pile toe at 5-mm movement can be disregarded. For sake of theoretical completeness, however, it is added to the total and shaft resistance curves.

The simulated load-movement curves for the pile driven open-toe (left diagram) assumes that a soil core exists inside the full length of the pipe after the driving. The outer shaft resistance is the same as that for the closed-toe case. Moreover, it is assumed that the shear force between the core and the pipe has been activated along a 2.5 m length at the 30-mm toe movement.

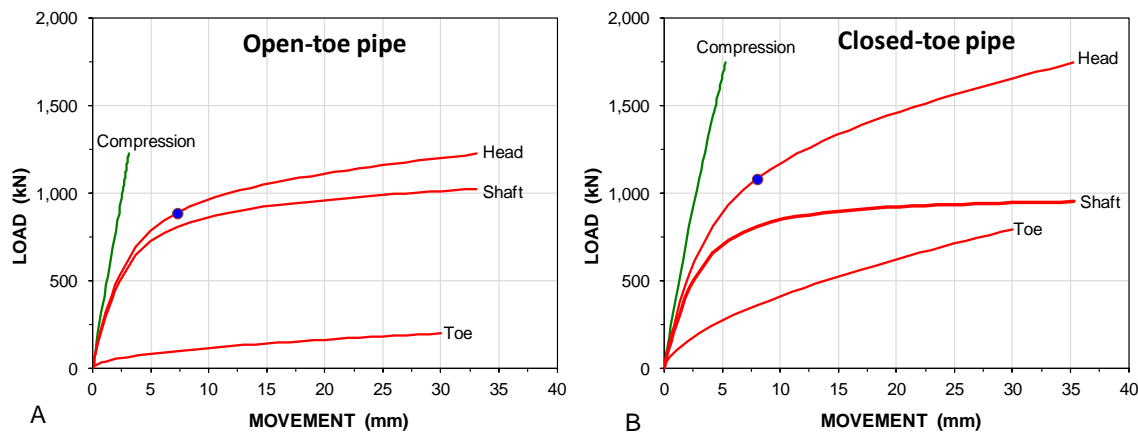


Fig. 7.53 Load-movement curves for a static loading test on (A) open-toe and (B) closed-toe piles

One can here either add the "core" effect to the inside shaft resistance to the outside shaft resistance of the pile, as done for the shaft resistance curve in the figure, or add a toe resistance from the soil stress on the core in pushing up the core calculated as a "soil pile" to the toe resistance acting on the wall of the pile.

The circular dot in each of Figs. 7.49A and 7.49B indicates the pile head load for a 5 mm toe movement of the simulated pile, which is usually a safe value of "allowable load". The difference in toe resistance at the end-of-test 30-mm toe movement between the response of the open- and closed-toe pipe piles is about 600 kN. At the more moderate 5 mm toe movement, the difference is only about 200 kN.

In back-calculating the results of an actual static loading test on an open-toe pipe pile with a soil core and modeling the forces measured in various locations along the pile, the core effect cannot be treated as an ultimate toe resistance, but needs to be considered as an add-on movement-dependent resistance along a lower length of the core. This add-on shaft shear can be obtained by modeling the core effect separately, simulating its response as if were tested upward in a bidirectional test. While the core base (pile toe) movement is easily measured, the unit shaft shear along the core and the core stiffness will have to be assumed or determined in special tests.



When driving an open-toe pipe pile, the question is if the pile will develop a rigid plug and, therefore, start responding like a closed-toe pile, and, as an inside soil core then develops, what will the soil resistance response to the driving be? Then, for the design of service conditions, the follow-up question is will the long-term static response be that of the rigid plug or the soil column? Answer to the latter, service condition question, will come from reference to results of static loading tests on full-scale pipe piles of different diameters and length with measured core response and back-analysis of the static load-movement measurements of the pile and the core as suggested above.

Plugging can also occur in-between the flanges of an H-pile. Whether plugged or not, for static response, the shaft resistance up along the pile should be calculated on the "square" because the shear resistance will act on the smallest circumferential area. The shear surface will only be the "H" if the shear force for soil to steel contact is much smaller than that at soil to soil. If "plugged" at the toe, the effect of the soil "core" inside the flanges can be analyzed in the same manner as for the inside core of the pipe pile, i.e., by adding the "pile-head response" of a soft, "upside-down" pile at the H-pile toe to the toe resistance of the "H" steel section. It would have a marginal effect, only, on the pile toe load-movement response.

Analyzing an H-pile is harder than analyzing the open-toe pipe pile, because the plug/column can occur along different length of the pile. Indeed, also at different times during the interval of the driving impact.

#### 7.20.10 Sweeping and bending of piles

**Inclinometer Measurements.** Practically all piles, particularly driven piles, are more or less out of design alignment, and a perfectly straight pile is a theoretical concept, seldom achieved in practice. It should be recognized that the deviation from alignment of a deep foundation unit has little influence on its response to load either with regard to settlement or to "capacity". Its inclination deviation may be important for the structure supported on the pile, however. Therefore, assigning a specific tolerance value of deviation from specified inclination only applies to the pile at the pile cap or cut-off location (as does a specific deviation of location).

When long piles are driven into any type of soil, or shorter piles are driven through soils containing obstructions, the piles can bend, dogleg, and even break, without this being recognized by usual inspection means after the driving. Pipe piles, and cylinder concrete piles, that are closed at the toe provide the possibility of inspection of the curvature and integrity down the pipe. A pipe-pile driven open-toe that got filled with soil during the driving can be cleaned out to provide access to the inside of the pile. It is normally not possible to inspect a precast concrete pile or an H-pile for bending. However, by casting a center tube in the precast concrete pile and attaching a small diameter inclinometer tube to the flanges of the H-pile before it is driven, access is provided for inspection down the pile after driving.

The location of a pile and its curvature can be determined from lowering an inclinometer down the pile, if access is provided by the open pipe or through a center pipe (Fellenius 1972a). [Figure 7.54](#) shows an actual example of deviations between the pile head and pile toe locations for a group of 60 m (200 ft) long, vertically driven prestressed concrete piles in soft soil (Keehi Interchange, Hawaii, 1977). The piles were made from two segments spliced with a mechanical splice. The main cause of the deviations was found to be that the piles were cast with the pile segment ends not being square with the pile. When this was corrected, the piles drove with only small deviations.

Bending of piles can be in gradually changing inclination—sweep—or in the form of a sudden change of direction, so-called "dogleg". A significant sweep may cause the bending stress (fiber stress) in the pile to become excessive and initiate a slow structural failure. A dog-leg is by definition a structurally failed pile. As bending of piles is only rarely investigated, only few published records of excessively bent pile exist.

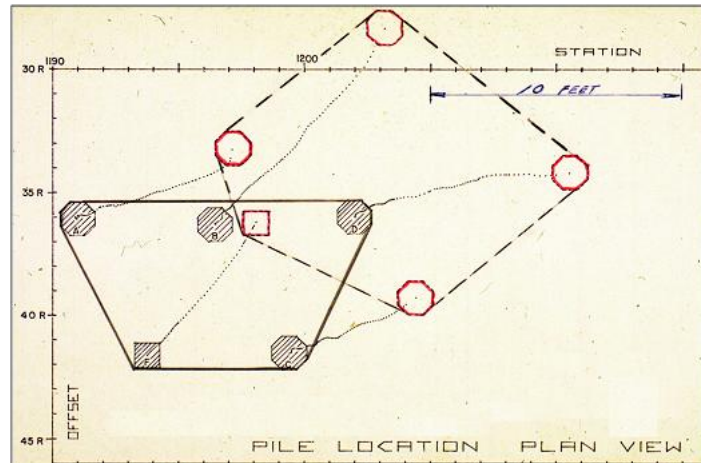


Fig. 7.54 Example of deviations determined by inclinometer measurements in 60 m long prestressed piles.

A key aspect of the pre-installation is to verify that the pile segments ends are square, in particular the end of the first segments that will constitute the pile toe. An out-of-square pile toe will act like a rudder and cause drifting and bending of the pile. The out-of-squareness limit measured across a pile diameter is 1:100, as measured, say, by using a carpenter's square.

The limits for sweep are expressed in terms of change of inclination in the inclination plane in degrees per 1.0 metre. The pile splices are assessed in terms of inclination change over a 0.5 to 1.0 m length above and below the splice. The sweeping of a pile segment (the curvature) is assessed over a ten metre length of pile in terms of bending radius (Eq. 7.48).

$$(7.48) \quad R = \Delta L / \Delta \alpha$$

where  $R$  = bending radius  
 $\Delta L$  = length of pile considered  
 $\Delta \alpha$  = change of angle (radians) in the inclination plane

The rules for assessing pile bending are that, before installation, all segments intended for inclinometer measurements should be checked for initial bending by measuring the pitch (height of arc; horizontally) along a line from segment beginning to segment end along the segment side (Eq. 7.48) in two perpendicular planes (measure the second plane after turning the segment 90 degrees).

$$(Eq.7.48) \quad R = L^2 / 8h$$

where  $R$  = bending radius  
 $L$  = segment length  
 $h$  = pitch

The limit for change of inclination across a splice, 1.0 m above and 1.0m below, is 0.8 degrees/metre for piles with a diameter ranging from about 300 mm through about 400 mm, with less strict values for slender piles and stricter for wider piles (Fellenius 1972a). This corresponds to a 150 m bending radius.

The inclination change that defines an unacceptable deviation, a dogleg, in the pile is 1.0° measured over 1.0 m length. This is a very strict requirement that should be assessed in the light of variations from a straight line measured before the driving of the pile.

The acceptance limit for inclination change over a ten metre length of pile (the difference between a pile considered straight as opposed to crooked or doglegged) is a bending radius larger than 300 to 400 m when assessed along a 10 m length of the pile. The larger (i.e., stricter) limit radius applies to the upper about 30 m length of pile if in soft soil. The bending radius along a ten metre length is best determined as a running average (geometric mean) of the radius values per 1.0 m. For example, Bjerrum (1954) reported that Norwegian authorities applied an acceptance limit of 350 m bending radius.

**Curvature Probe.** For a pipe pile, inspection down the open pile is often only carried out by lowering a flashlight into the pipe, or center tube, to check that the pile is sound, which it is considered to be if the flash light can reach the bottom of the pile while still being seen from above. However, dust and water can obstruct the light, and if the light disappears because the pile is bent, there is no possibility to determine from this fact whether the pile is just gently sweeping, which is of little concern, or whether the pile is severely bent, or doglegged. In such a case, a specially designed, but simple, curvature probe can be used to vindicate undamaged piles, and to provide data for aid in judging and evaluating a suspect pile.

The curvature probe consists of a stiff, straight pipe of dimensions so chosen that it, theoretically, will 'jam' inside the pipe, or center tube, at a predetermined limiting bending radius expressed in Eq. 7.49 (Fellenius 1972a). The principle of the use of the curvature probe is illustrated in Figure 7.55.

$$(7.49) \quad R = \frac{L^2}{8t} = \frac{L^2}{8(D_1 - D_2)}$$

Where

- R = Bending radius (m)
- L = Probe length (m)
- t = Annulus  $D_1 - D_2$  (mm)
- $D_1$  = Inside diameter of the pile or center tube (mm)
- $D_2$  = Outside diameter of the curvature probe (mm)

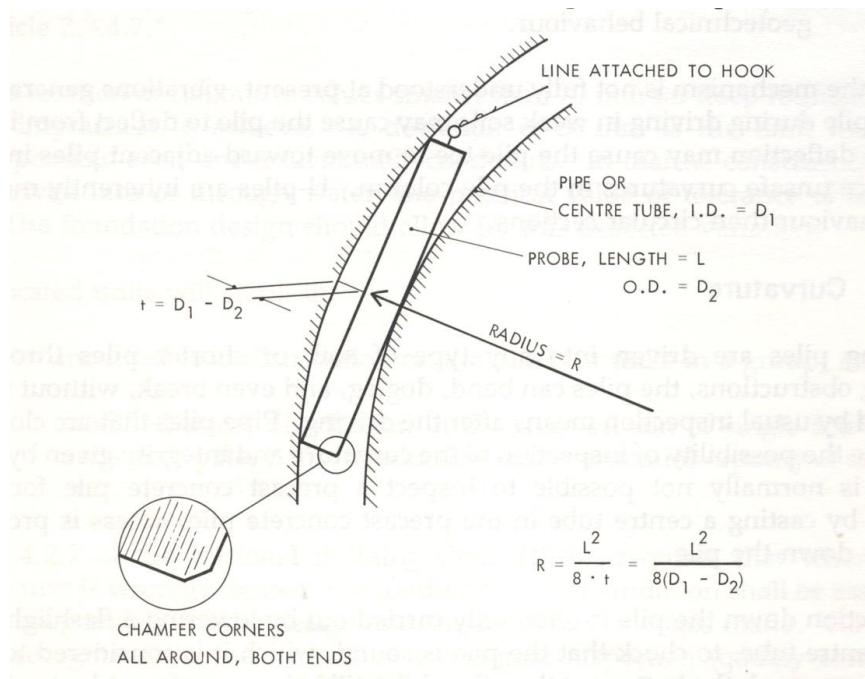


Fig. 7.55 Principle of the curvature probe

Keeping costs down, both the probe and the center tube should be made from standard pipe sizes. The probe must be stiff, that is, be a heavy-wall pipe. The length of a probe for use in steel pipe piles can be determined from selecting a probe with diameter (outside) that is about 80 % of the inside diameter of the pipe.

The passage of the curvature probe down the pile is affected by numerous imprecisions, such as ovality of the shape of the pipe, diameter tolerances of pipe, unavoidable 'snaking' of the center tube cast in a concrete pile, offsets when splicing pile, etc. However, the curvature probe is not intended to be an exact instrument for determining bending. (If exact measurement is desired, lower an inclinometer down the pile). Instead, the curvature probe is a refinement of the slow, crude, and imprecise inspection by eye and flashlight. Its main purpose is to vindicate piles, which otherwise may have to be rejected. Consequently, in deciding the limiting bending radius, one should not base the design on calculations of the bending moment ( $M$ ) and fiber stress (the radius determined from the relation:  $M = EI/R$ ). Such calculations imply a non-existent exact relation and will suggest that the limiting bending radius be larger than about 400 m. Probes designed according to such strict values are impractical and cause more difficulties than they solve. Practice has shown that the most suitable probes are those designed for limiting radii of 200 m and 100 m, the 100-m probe being used only if the 200-m probe 'jams'. Any 'jamming' (inability of the probe to reach the bottom of the pile) would then be evaluated, considering location of the 'stop', pile driving records, results from probing neighboring piles, intended use of the pile, etc.

The passage of the curvature probe down the pile is affected by numerous imprecisions, such as ovality of the shape of the pipe, diameter tolerances of pipe, unavoidable 'snaking' of the center tube cast in a concrete pile, offsets when splicing pile, etc. However, the curvature probe is not intended to be an exact instrument for determining bending. (If exact measurement is desired, lower an inclinometer down the pile). Instead, the curvature probe is a refinement of the slow, crude, and imprecise inspection by eye and flashlight. Its main purpose is to vindicate piles, which otherwise may have to be rejected. Consequently, in deciding the limiting bending radius, one should not base the design on calculations of the bending moment ( $M$ ) and fiber stress (the radius determined from the relation:  $M = EI/R$ ). Such calculations imply a non-existent exact relation and would suggest that a limiting bending radius for a probe test could be set larger than about 400 m. Probes designed according to such strict values are impractical and cause more difficulties than they solve. Practice has shown that the most suitable probes are those designed for limiting radii of 200 m and 100 m, the 100-m probe being used only if the 200-m probe 'jams'. Any 'jamming' (inability of the probe to reach the bottom of the pile) would then be evaluated, considering location of the 'stop', pile driving records, results from probing neighboring piles, intended use of the pile, need for confirming inclinometer measurements, etc.

A center pipe for placement in a precast concrete pile usually consists of small diameter, 1.5-inch (40 mm) steel tubing cast concentrically in the pile. Sometimes, for purpose of special testing, such as telltale instrumentation in combination with inclinometer measurements, larger diameter center pipes are used. Up to 6 inches (150 mm) pipes have been used in practice in 16-inch (400 mm) piles. For cost reasons, the larger center pipes often consist of PVC-pipes. (When center pipes larger than 6 inches are used, the pile is more to be considered a hollow pile or a hollow-core cylinder pile—a spun-pile—with a certain wall thickness).

A suitable size of center tube in precast concrete piles is 1.5 inch schedule 40 (inside diameter 40.9 mm), with a corresponding size of pipe for the curvature probe of 1.0 inch schedule 80 (33.4 mm outside diameter).

It is important that the splicing of the center pipe in the casting form is made without lips or burrs on the inside, obstructing the pipe. The splicing of the tubes must be made square and with outside couplings to ensure that no inside lips or edges are obstructing the passage of the probe. Center tubes made of PVC are cheaper than made from steel, but they are more apt to snake laterally, to float in the fresh concrete, and

to be dislocated by the vibrator. Steel center tubes are preferred, as they are stiffer and heavier. When using PVC-pipes, it must be considered that the PVC exhibits an appreciable thermal expansion and contraction from the heat generated during the hydration of the concrete. Conical connections (splicing) must therefore not be used. Naturally, all PVC-couplings must be almost water tight to prevent the cement solution from entering the tubes.

In mechanically spliced piles, the center pipe is taken through the splices by means of a special standard arrangement, which supports the center pipe through the splicing plates and ensures that it is truly perpendicular to the plates. The splicing plates must be equipped with o-ring seals. Otherwise, due to the very large pore pressures generated and the remolding of the soil nearest the pile surface during the pile driving, soil would enter the center pipe and costly cleaning work would be required after the driving. That the seal is properly designed and arranged is essential. For instance, I have observed that the center pipe in 200 ft (60 m) long spliced pile filled completely with clay due to a faulty O-ring in one of the splices.

To ensure a straight center tube, it must be supported in the casting form and tied to the longitudinal reinforcement. A center tube is considered straight in the casting form before pouring the concrete, if the maximum deviation of the tube, as measured over a distance of 4 metre is 5 mm. This deviation tolerance corresponds to a calculated bending radius of 400 m. The limit is quite liberal. Practice has shown that there is no difficulty in having the tubes cast within this tolerance.

Piles with center tubes are usually also equipped with pile shoes. Where that is the case, it is necessary to supply the base plate of the shoes with a receiving pipe to center the tube in the pile, and to ensure positively that the tube at the toe of the pile (the zone of particular importance in the inspection) is straight (i.e., square with the pile).

If splices are used in the pile, a similar centering of the tube is necessary to enable the probe to pass through the splices without encountering difficulties due to offset of centers, 'knees', etc.

It is advisable to check that the tubes are straight and unobstructed after casting by pushing the probe into and through the center tube, while the pile lies on the ground in the casting yard (the probe has to be attached to the end of a standard pipe of small diameter, or pulled through by a line blown ahead through the tube). [Figure 7.56](#) shows such a test in progress on an about 30 m (100 ft) long prestressed concrete pile segment. Bending was induced in the pile segment to verify the practicality of the bending radius assigned to the curvature probe.

Adding a center pipe to precast concrete piles increases in-place cost per unit length of the pile by about 10 percent. However, properly handled, the total costs are reduced because the tremendous assurance gained by adding center pipes to the pile and carrying out a qualified inspection through these, will in almost every case justify an increase of the design load and reduction in the number of piles for the project. I have experienced projects, where, if the center pipes in the piles had not been used, a reduction of the recommended safe allowable load would have been necessary, whereas having the center pipes resulted in a recommendation to use increased allowable loads.

Center pipes have additional advantageous uses. For instance, providing a center pipe in a pile selected for a static loading test lends itself very obviously, and very cheaply, to accommodate a guide-pipe encased telltale rod to the bottom of the pipe. This rod is then used to record the pile toe movements during the loading test.

Center pipes provide the possibility of jetting a pile through dense soil layers in order to reduce driving time, increase penetration, and/or reduce bending.



Fig. 7.56 Verifying the practicality of the curvature probe

Standard arrangements are available for pile shoes and driving plates, which will allow the jetting through the soil, when required. The practical advantage is that standard pile segments are used. Therefore, if jetting is found to be advisable at a site, this can be resorted to without much cost increase or delay, provided the piles are already equipped with center pipes.

Again, with a slight change of pile shoe design, the center pipe can be used to insert a drill rod through the pile and to drill beyond the pile toe for grouting a soil or rock anchor into the ground, when in need of an increased tensile "capacity". Or in the case of a pile driven to sloping bedrock, when the pile-toe support even when using rock shoes is doubtful, a steel rod can be dropped through the center pipe and beyond the pile toe into a drilled hole and grouted to provide the desired fixity of the pile toe.

The simplest way to determine if piles are excessively bent is to measure the pile curvature after driving by means of an inclinometer. The inclinometer determines the inclination of the pile in two planes. These records are simple to use in calculating the location of the pile in the ground and the horizontal (drift) and vertical (lift) deviations of the pile from the intended direction. The pile is assessed not by the drift, but by its curvature in terms of bending radius.

#### 7.20.11 Influence on Adjacent Foundations

Driving a pile group produces heave and lateral movements, as well as pore pressures, which displace the soil upward and outward and increase pore pressures within and around the footprint of the pile group. When driving in soft clay near already existing foundation—shallow or deep—the movements and pore pressures can adversely affect the existing foundations. Bozozuk et al. (1978) found that the effect of driving a group of piles at a spacing of 3 to 4 pile diameters was that the piles created a heave within the pile group corresponding to about 50 % of the total pile volume and the remaining volume could be represented by a line from the heave at the edge of the group to intersection with a line rising at 2(V):(1H) from the pile toe level to the ground surface as illustrated in Figure 7.57. Moreover, inclinometer and settlement measurements showed an extent of horizontal displacement and heave outside the group as illustrated by the shaded area. Undesirable settlement can also result from driving piles in sand (Chapter 9, Section 9.15).

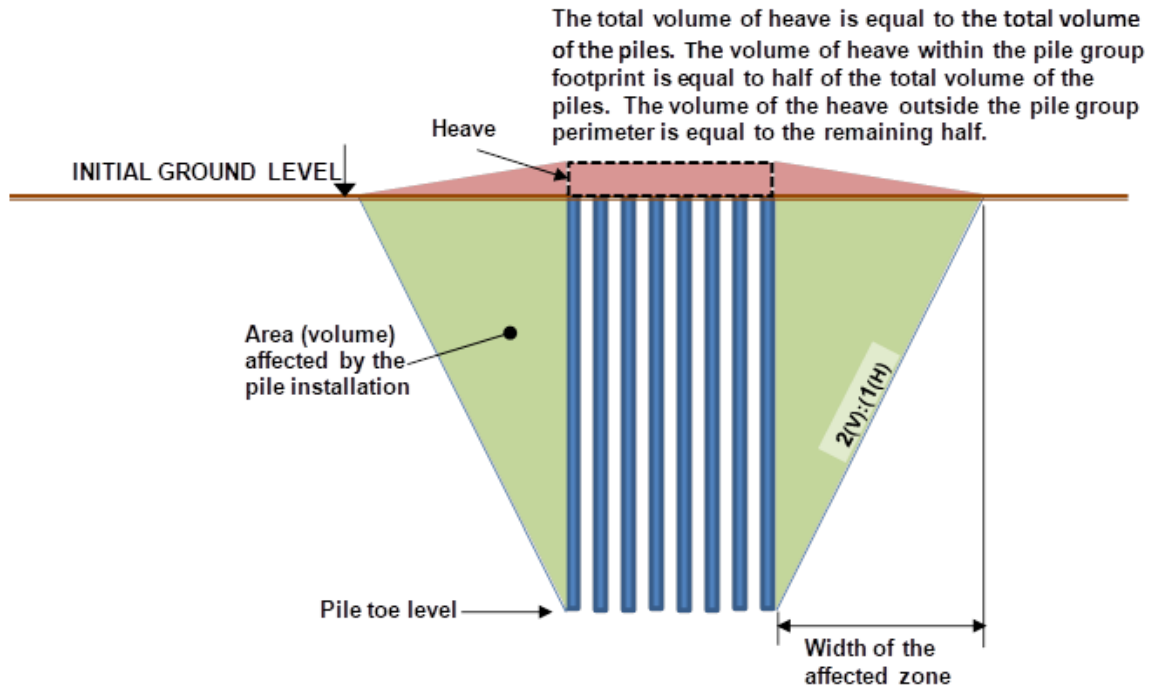


Fig. 7.57 Amount of heave and zone affected by driving a group of piles into soft clay

#### 7.20.12 Reducing differential settlement by shortening perimeter piles

The distribution of load between piles in the center of a raft as compared to piles along the perimeter is to a large degree a function of the rigidity of the raft itself and how the distribution of load from the supported structure is affected by its rigidity and that of the raft. As mentioned in Clause 7.18.6, even if the load applied to the raft is uniform, in case of a fully rigid raft, the perimeter piles will carry larger load than the interior piles, but the raft settlement will be the same across the raft. On the other hand, for piles supporting a fully flexible raft, the loads will be equal, but the settlement under the center will be much larger than under the perimeter. Compounding the difference between the perimeter and interior piles, because the perimeter piles have significantly more shaft resistance than interior piles, they appear stiffer and, thus, they will take on larger loads than the softer-response interior piles.

The effect of differential settlement across the raft and/or different load for perimeter as opposed to interior piles, can be alleviated by making the perimeter piles shorter, thus, appearing softer than the full-length piles and, therefore, reducing the trend to transfer load from the center area to the perimeter, as shown in Figure 7.58. This has been applied in Germany by Katzenbach et al. (2012).

However, for wide piled foundations in subsiding areas, the perimeter piles will be subjected to downdrag, which will have the effect of softening the response of the perimeter piles. This will reduce the load transferred from the perimeter to the center of the pile group, indeed reversing the transfer direction, possibly even resulting in tension load for the perimeter piles, as was measured by Okabe (1977). For such conditions, it would instead be more rational to lengthen the perimeter piles, as illustrated in Figure 7.59. The necessity of such lengthening is not a decision based on pile "capacity", but on long-term differential settlement considering the differing response of perimeter and interior piles as well as the settlement below the pile toe level.

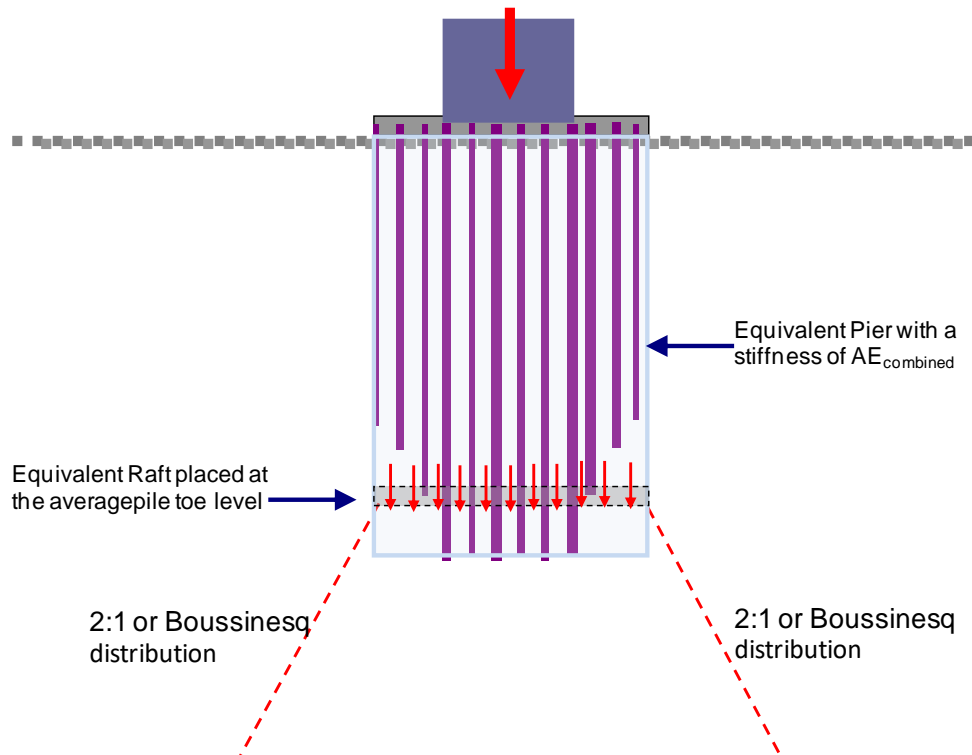
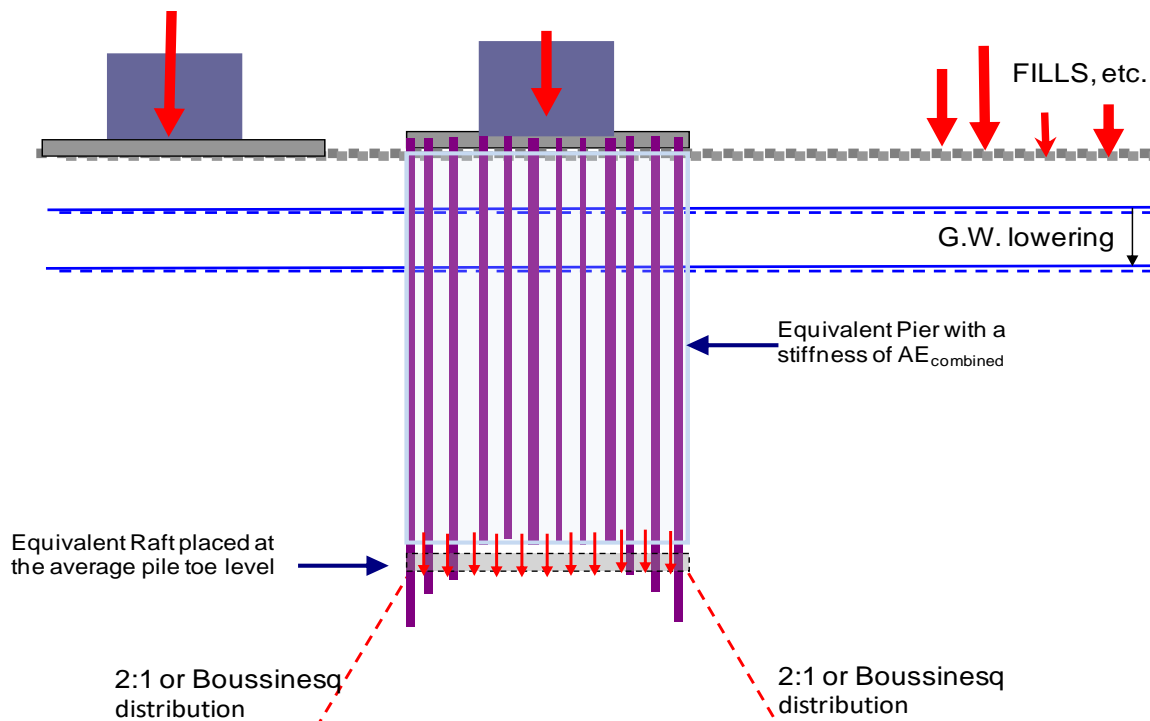


Fig. 7.58 Shortened perimeter piles to reduce differential settlement and load differences.



Settlement of the piled foundation is caused by the compression of the soil from external load applied to the piles **and** downdrag due to increase of effective stress **below the neutral plane** (from fills, embankments, loads on adjacent foundations, lowering of groundwater table, etc.).

Fig. 7.59 Lengthening of perimeter to minimize downdrag.



### 7.21 "Capacity" as a Function of Time

"Capacity" is thought of as being a given quantity. Once determined, that's it, right! Of course, we all accept that a capacity determined in a theoretical analysis may not agree fully with the capacity found in a static loading test and we may have to adjust our parameters once we have test data. However, while our analysis of the test results does not usually consider the effect of time, Nature always considers time. It is not irrelevant whether or not we test a pile two weeks, a month, half a year, or longer after it was driven or constructed. "Capacity" will change with time—usually increase and so will stiffness response. ("Capacity" decreasing with time is a phenomenon associated with resistance due to temporary pore pressure decrease and a subsequent return of pore pressure and it usually occurs within the first hour or so after construction).

"Capacity" increase with time is not something limited to small diameter piles, it is a reality for all sizes and lengths of pile. Figure 7.60 shows the full-length pile shaft resistance determined in static loading tests on two "companion" strain-gage instrumented piles, one tested 42 days after construction and one tested 31 days later, 72 days after construction (Teparaska 2015). Both piles were 1.2 m times 3.0 m barrettes constructed under bentonite slurry in a Bangkok, Thailand, with 67 m embedment into about 22 m of soft clay deposited on about 28 m of medium dense to dense silt and sand followed at 50 m depth by layers hard clay and very dense sand. The data indicate that, at this site, a significant increase of soil shear stiffness developed also after the initial 43-day wait between construction and testing. Movement data for the case are estimates from the pile head movement and the larger movement required to reach the peak value for test Pile TP-2 may be an exaggeration. For Pile TP-1, a 60 kPa average ultimate shaft resistance could be defined to have been reached at an average pile-head movement of about 5 mm. Defining the ultimate average shaft resistance for Pile TP-2 at the resistance reached at the same movement indicates 75 kPa, whereas the peak resistance appears to have required an about 15-mm movement (pile compression was small).

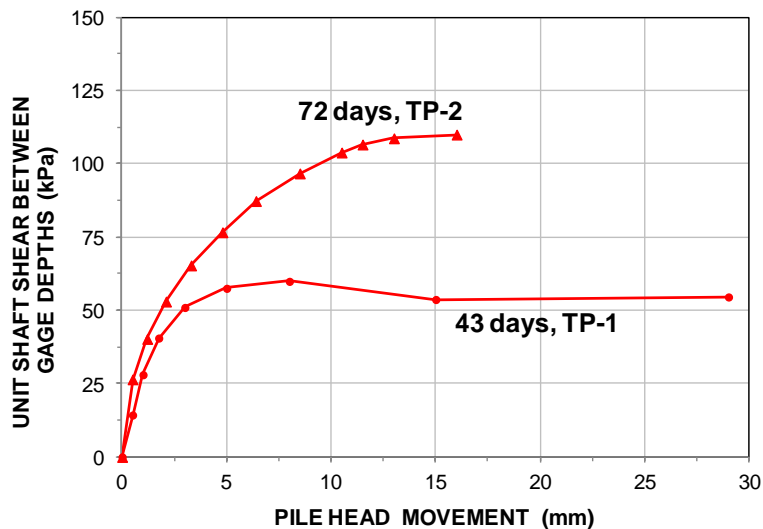


Fig. 7.60 Shaft resistance vs. average gage movement on two occasions after construction (Data from Teparaska 2015)

Pile "capacity" usually presumes also a pile toe "capacity". However, pile toe "capacity" does not exist in reality other than as a "declared" value. Of course, in many instances, the stiffness of a pile toe response does increase with time. However, the mechanisms involved at the toe are not the same as those involved along the shaft. Nevertheless, overlooking the variations due to difference definition of pile "capacity" as based on the pile-head load-movement curve, a large number of tests on different pile in different geologies do show increasing values with time. Figure 7.61 shows the "capacities" determined at three

sites plotted versus days in logarithmic scale. The "Sandpoint" case is from a test on a 400-mm diameter, 45 m long concrete-filled steel tube driven in soft clay (Fellenius et. al. 2004) with a dynamic test performed 1 hour, a static loading test 48 days later, and a dynamic test 8 years after the end of driving. The "Paddle River" case is from static loading tests on two 324-mm diameter, steel pipe piles driven in stiff till clay near Edmonton, Alberta, one 16 m long and one 20 m (Fellenius 2008). The "Konrad-Roy" case (Konrad and Roy 1981) is from static loading tests on a 200-mm diameter, 7.6 m long steel pipe pile driven in soft clay (the "capacity" values are scaled up by a factor of 10).

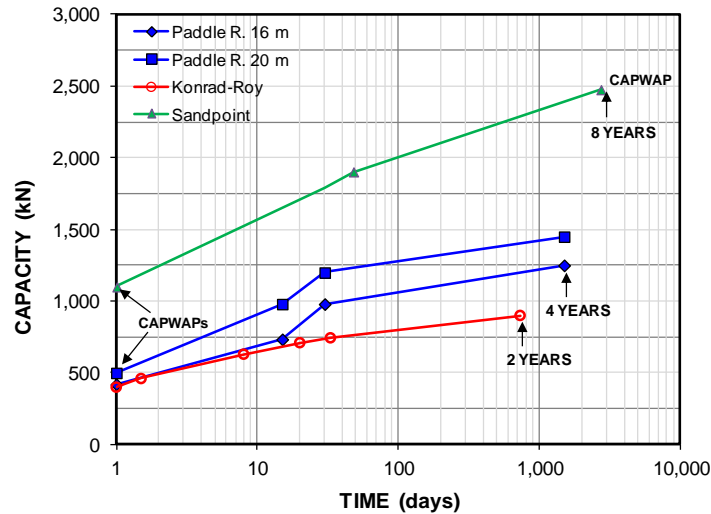


Fig. 7.61 "Capacity" determined at days after driving

The "capacity" increase is a function of increase of effective stress due to dissipation of the excess pore pressures created during the construction and, also, of aging. When studying the increase over a short time after the construction, the trend appears to be linear in a logarithmic time scale. However, beyond about 100 days, when most of the excess pore pressures can be assumed to have dissipated, the trend is different and the "capacity" growth rate to reduce. Figure 7.62 shows two linear trends (the same data plotted normalized to "capacity" of 100 % or that at 100 days). One for the days during the pore pressure dissipation time and one for the small growth after the pore pressure dissipation. Another word for pore pressure dissipation is consolidation. There is a tempting analogy with the settlement theory for clays consisting of a "primary" process during the dissipation (consolidation) and a "secondary" process thereafter (as in secondary compression).

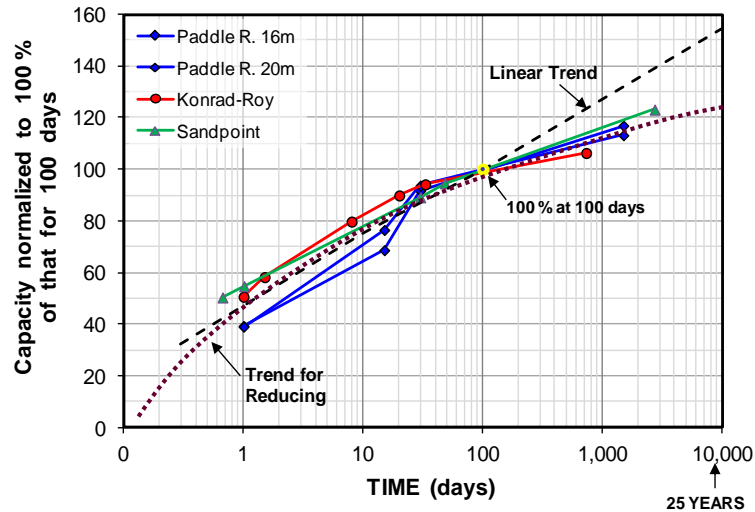


Fig. 7.62 "Capacities" normalized to 100 % of 100-day values

The lesser rate of "capacity" increase during the "secondary" process makes a lot of sense. In a way, it is a parallel to the lesser rate of increase of settlement due to secondary compression after the end of the consolidation period.

Indeed, "capacity" is a very subjective value already before we take the time-development into account. So, why is it that it is the main value, sometimes the only value, that our Codes and Standards have us base our piled foundation design on?

## 7.22 Scour

Scour is the term for "Nature's excavation" resulting from rapid water action, e.g., the Hurricane Sandy ravaging the US East coast in 2013 causing collapse of several bridge foundations—piled foundations. The effect of wave and flowing water is not just to remove the bottom sediment over a wide area around the foundations (general scour), but also to create a hole around the foundations (local scour). The latter removes the contact between the piles and the soil to some depth. More important, the over a wide area general scour and the local scour remove overburden, which reduces the effective stress around the length of pile still in contact with the soil, i.e., the shaft resistance is reduced also for the length of pile below the bottom of the scoured hole.

The FHWA manual (Hanningan et al. 2006) recommended that potential scour around piled foundations be estimated by two components. First, the depth of the general scour and then a local scour determined as an inverted cone to a certain depth,  $Z_s$ , determined from scour depth analysis and/or observations of past events (Figure 7.63). The slope of the scour sides are estimated to be 2(H): 1(V). That is, the cone diameter at the new sea or river bed to be 4 times the depth.

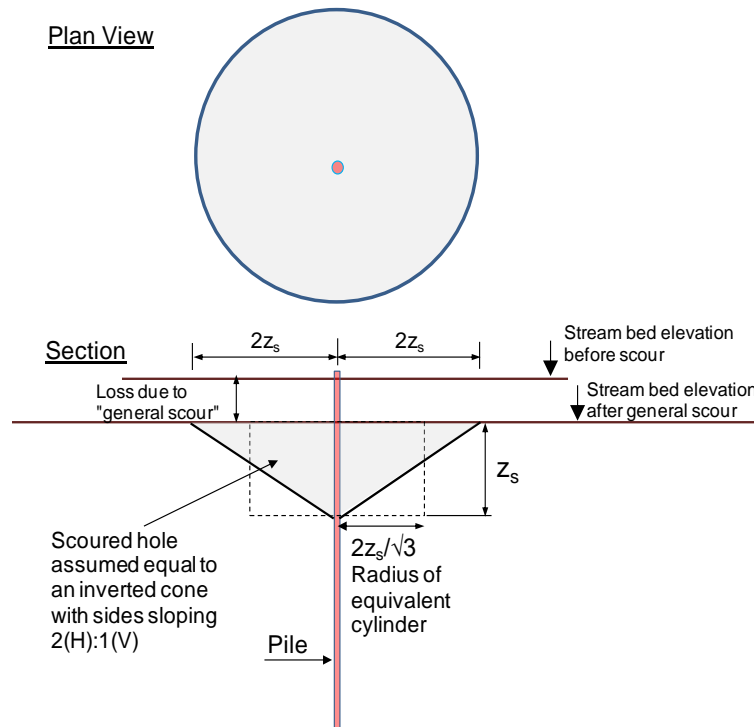


Fig. 7.63 Scour configuration according to the FHWA Manual

The FHWA manual recommends the obvious that shaft resistance (and lateral resistance) only be considered for the length of pile below the scour hole bottom. However, the additional recommendation that the effect of the unloading of the soil due to the general and local scour below the scoured hole be disregarded is incorrect on the unsafe side. The unloading will have a significant effect on the effective overburden stress and the shaft resistance along the remaining embedment length. Indeed, it also has a small reducing effect on the toe resistance (stiffness, rather). For that matter, it is not particularly onerous to include the unloading in an effective stress analysis of the "after-scour" conditions.

Figure 7.64 shows the force distributions for before and during a scour event (per calculations performed using customary US units) for a driven 36-inch square, 80 ft long concrete pile. The general scour depth is 15 ft and the local scour depth is 18 ft. The before- and after-scour conditions are determined in an effective stress analysis using the beta-coefficients as listed in to the right of the figure. The toe resistance is simply assigned a value of 1,000 kips and assumed to not change due to the unloading by the scour. In order to simplify the calculations, the unloading effect of the local scour hole is calculated as the reduced stress due to a cylinder with a radius equal to  $2/\sqrt{3}$  times  $Z_s$  (equal mass).

The force distribution before scour is determined from effective stress analysis of test results. The scoured-out hole is assumed to be an inverted cone with a circular base approximated to a cylinder. To avoid cluttering up the graph, the toe resistance is assumed unchanged. In reality, the toe resistance will reduce somewhat due to the loss of overburden stress.

The pile bearing "capacity" and force distribution (the beta-coefficients) are assumed to have been determined in testing (static loading tests or dynamic with PDA/CAPWAP) during the construction of the piled foundations calibrating the response to load. The figure presumes that the desired working load is 700 kips and the required factor of safety during a scour event is 2.0, i.e., the desired "capacity" is 1,400 kips. The calibration of the conditions, the assigned scour conditions indicated the design results: the piles needed to be driven to 80 ft depth and to a "capacity" of close to 2,000 kips to account for potential general and local scour.

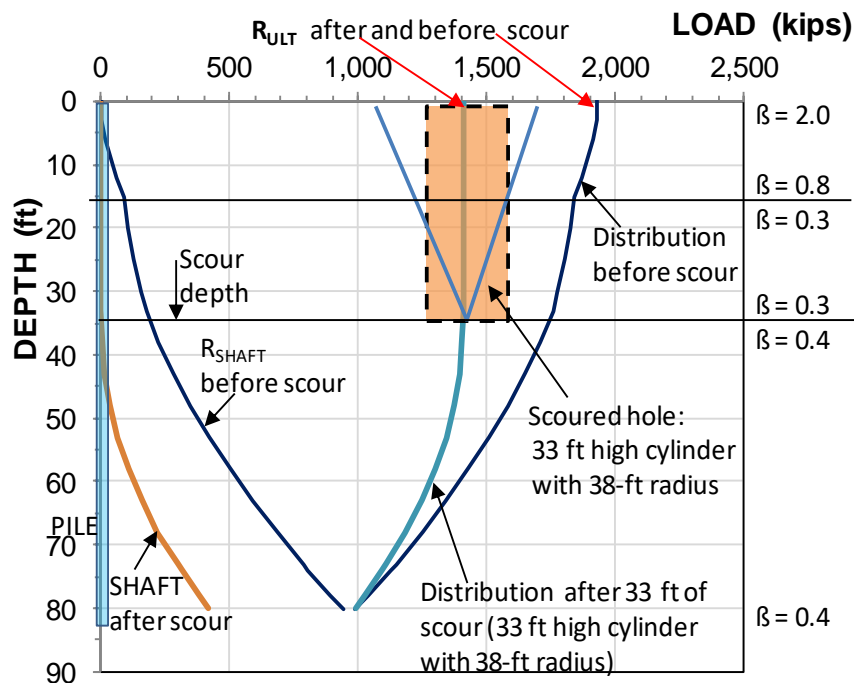


Fig. 7.64 Force distributions at "capacity" before and after-scour

## 7.23 Conclusions

The current state-of-the-practice of design of a piled foundation, is to determine the "capacity" of a pile representative for the project and apply a factor of safety (WSD approach) or resistance factor (ULS or LRFD approach) to a representative project pile to establish whether the intended working load can be accepted. It is an apparent anomaly that the various codes and standards will indicate the factors with two decimals, but do not indicate what "capacity" to assign to the pile other than by method for its determination, such as lab or in-situ tests, static loading test, or dynamic test. Some argue that, to bring more order into the process, a distinct method for determining "capacity" must be established, at least for results from a static loading test. I disagree. The process involves so many variables, e.g., testing methods, construction procedures, short- and long-term effects, not to mention, sensitivity of the structure and variation of actual load, that the process is really a large set of engineering judgment calls. In my opinion, the geotechnical engineer on records has to be the person to assess all the variables, "capacity" and its definition being just one of them, to arrive at the safe working load considering all aspects of the case. Naturally, in close dialogue with the structural engineer for the project. That process cannot be brought down to a single definite factor to fit all cases.

As to compression and tension loading, while the unit shaft resistance (t-z response) is independent of the direction of shear, the consequence of being wrong is more severe for a tension condition. Therefore, it makes sense to have a larger factor of safety for tension as opposed to compression condition. Note, for tension loading, the "settlement" analysis is by means of t-z analysis and it is the deciding approach.

For design of a pile group, some consider "capacity" of the group as the sum of the single piles times a reduction factor, a "group efficiency factor". However, the response of a group, such as the example case in the foregoing, is by load-movement and settlement. Estimating "capacity" by applying a group efficiency coefficient is not meaningful. Indeed, "superstitious" (Kezdi 1965).

A foundation design should always be directed toward determining settlement letting "capacity" reasoning take second place. The unified method satisfies the requirement by employing interaction of forces and movements to determine the short- and long-term settlements for a single pile or a narrow pile group.

I cannot emphasize enough that pile design is design for settlement. Design of piles to sound competent bedrock is easy, the structural strength of the pile governs. Design of single piles bearing in competent, low-compressibility soil is similarly easy—the load-movement response at the pile toe will govern (along with pile structural strength; the equilibrium plane will be at the pile toe or slightly above). For single piles and narrow groups, where the soils at the pile toe are less competent, the equilibrium plane will be higher up in the soil, and the settlement at the equilibrium plane will govern as it will be the cause of additional pile -toe movement. For a wide group with less competent soil below the pile toe level, the design is governed by the load-transfer movement and the settlement at the pile toe elevation, i.e., the sum of the compression below the pile toe level. The simplest analysis of the latter is to calculate the settlement for an equivalent raft placed at the pile toe elevation.

Note, pile design requires that the site investigation is geared to determine the compressibility characteristic in the deeper soil layers, so a settlement analysis can be made. A design based on "*the capacity is with a factor of safety of two or better, so we will have no settlement*" is an inadequate approach as many have learnt to their peril. Note, the settlement is only partially caused by the load on the piles. Unless the pile group is very large, the bothersome settlement is that caused by other factors than the pile loads, such as, fills, groundwater table lowering, neighboring structures, regional subsidence, etc. So, again, a statement that "*once capacity is shown to be OK, settlement will be OK, too*" is not valid. However, the inverse statement "*once settlement is shown to be OK, capacity will be OK, too*" is valid.

Design for "capacity" and settlement is a "belt and braces" approach. "Capacity" is the belt, and however fancy it is and how strong it seems to be, its success in preventing the pants from sliding down depends not just on the strength, many other aspects may control: e.g., the size of a proverbial beer belly in relation to the hip, so-to-speak. Settlement is the braces. If strong enough, then, be they ugly or silly, be the belly wide or not, the braces will prevent excessive downward movement. A piled foundation may fail, and many have (as shown by their developing excessive movement) despite the factor of safety of the individual piles shown to have been larger than 2 and 3. No piled foundation responding adequately regarding pile movement and foundation settlement has ever 'failed'.

The adequacy of the design calculations is not a function of the sophistication of the model or the computer program employed, but of (1) the adequacy of the soil information and (2) the quality and representativeness of the parameters used as input to the analyses. Both are somewhat lacking in the foundation design state-of-practice.

Moreover, when a theory involves more than one or two parameters, before it can be stated that it truly represents actual response so as to be useful to predict a response, i.e., be used in the design of a foundation, the calibration of the method applied to the model per measured response must also include measurements of the relevant input parameters of the model.

Calling a calculation "a prediction" does not make it a reliable forecast. If the analysis model depends on pile-soil interaction, it is not sufficient to just measure axial force distribution in the piles. The soil forces and soil deformations must also be recorded and the model verifies against the observations.

To improve the reliability of the design of piled foundations, research building up case histories must include instrumentation and monitoring of response to load applied to a pile group and single piles, including recording not just the settlement of the pile cap, but also:

- the movements between the pile and the soil at depths, in particular at the pile toe level
- the distribution of strain and movement in the soil with depth
- the axial force distribution—both in perimeter and interior piles
- the pile toe penetration into the soil and this compared to that of a single pile
- the settlement below the pile toe level
- the earth stress against the piles
- the subsidence of the area outside the pile group

It is not financially possible to carry out a stand-alone research project on a wide piled foundation, but detailed instrumentation for force and movement that are monitored over time for actual, well-defined projects with symmetrical pile groups (e.g., wide storage tanks, bridge pier foundations, etc.) are not costly, but surely needed. Public agencies have a duty to arrange for such studies in order for the profession to gain knowledge and enable savings on future projects. Alas, short-sighted budgeting and lack of understanding—indeed, ignorance—of the need make such approaches rare.

For single piles and narrow pile groups, the fundamental (pun intended) unknown to address in a design is the load-movement response and the load-distribution for a working load applied to the pile(s) and the conditions for the long term—the life of the supported structure. If an engineer has good local experience and confidence using the  $\alpha$  method (the stress independent method) for shaft resistance and the associated deformation, by all means, use it. It meets the need for employing local practice and the past approach in the design, which is a very important part of a design. However, the "good local experience" is difficult to export to other sites. Experience correlated to the  $\beta$ -method has a wider applicability because it includes reference to the overburden stress and pore pressure distribution, which the  $\alpha$ -method does not address.

Some see a conflict between a stress-independent analysis (alpha-method) and an effective stress analysis (beta-method), c.f., Clause 7.2.1). Personally, I have no problem with either approach (provided that the movement is considered along with the unit shaft resistance value for each pile element). While I hold that the "beta-method" is superior to the "alpha-method", if faced with a for me unknown geology, I would put more weight on the " $\alpha$ "-approach applied by persons with the proper local experience. That is, I would accept the " $r_{s\alpha}$ " if the persons rely on their experience in telling me that it would be suitable. I would, then, transfer the " $r_{s\alpha}$ " to what movement would be required for the unit shaft resistance to develop and see what force-movement relation that could be reasonable to put it into context of a general shear-movement response. Next, I would find out the experience of the persons in regard to what depths and soil layers their advice to me relates to. Having digested the information, I would use our combined assessment toward deciding on the design recommendations. It does not matter here if we stay with the " $\alpha$ " or shift to " $\beta$ ". The vital condition is the ensuring reference to experience and back-analyzed data from projects representative for the site. Nevertheless, I would still convert the final assessment to an effective stress analysis because this is the best way for transferring the experience and lessons learnt to future projects.

As discussed in Clauses 7.18.6 and 7.20.12, the most common distribution for a wide group with a raft rigidity somewhere in-between practically flexible and practically rigid is that the interior (center) piles will both settle more and take on smaller loads than the perimeter piles. Moreover, the interior piles will have no or only little shaft resistance and have it in a zone immediately above the pile toe level, but the perimeter piles will have shaft shear starting from the pile-head level and respond similar to single piles. However, in case of significant general subsidence around the foundation generating downdrag on the perimeter piles, the reverse load and settlement situation may be the case.

Generally, to come up with a design for a piled foundation, the engineer applies the information on the project structure and the soil, selects the appropriate design parameters, and performs the analysis of the response of the foundation to the structure, applying the theoretical approach fitting the case combined with the relevant experience from similar projects in the similar geology that enables confidence in the analysis results. The key aspect is that the design must rely on correlation of representative experience comprising suitability of soil parameters through relevance of theoretical analyses. When that is not assured, performing static loading test is advisable. Moreover, a design supported by static testing (properly scheduled and performed) will often involve savings of costs and time.





## CHAPTER 8

### ANALYSIS OF RESULTS FROM THE STATIC AXIAL LOADING TEST

#### 8.1 Introduction

For piled foundation design, it is necessary to 'unearth' the response of the piles to the loads from the supported structure or confirm that the response agrees with the assumptions made. The most common such effort is by means of a static loading test and, conventionally, determining capacity is thought to be the primary purpose of the test. (As this chapter defines capacity, I will refrain from placing the term inside quotation marks, otherwise pertinent for this very diffuse concept). The capacity is understood to be the load—the ultimate load, the load applied to the pile when the movement measured at the pile head occurs under a sustained load or for only a slight increase of the applied load—the pile plunges. This definition is inadequate, however, because large movements are required for a pile to plunge, if ever, and the maximum load in the test is often governed less by the capacity of the pile-soil system and more by that of the man-pump system. On most occasions, a distinct plunging load is not obtained in the test and, therefore, if still desired, the ultimate load reached in the test must be determined by a specific definition based on the load-movement records of the test.

Originating in a misinterpretation of a statement by Terzaghi (1942), an odd definition of pile capacity is stated to be the load for which the pile head movement is 10 % of the diameter of the pile. However, Terzaghi stated that determining the capacity of a pile from analysis of records of a static loading test should not be undertaken unless the pile (a 12-inch diameter pile was the subject of the discussion) had moved at least 10 % of the pile toe diameter, which in more ways than one is quite a different matter; his statement was not to claim that capacity would be a function of pile diameter—he knew better—but to make clear that to derive a capacity from a test requires that the pile, notably the pile toe, has moved a reasonable length against the soil (Likins et al. 2012). It is regrettable that the misconception of the 10-% statement has crept into several standards and codes, e.g., the Eurocode and the API Standard . Setting the limit to 5 % for large diameter piles does not improve the approach.

If we consider unit resistance rather than total, a capacity—whether for shaft resistance or toe resistance—is irrelevant of pile diameter or curvature of the pile shaft. Just think of how the unit resistance along the side of a barrette could be governed by the width of the barrette. In regard to a pile toe, the observations of the footing tests reported in Section 6.10, for example, show that an ultimate toe resistance, i.e., bearing capacity, does not exist.

Of old, Canadian practice was to define capacity as the test load that resulted in a 1.5-inch pile head movement, which definition applies to movement allowed by the pile-supported superstructure rather than to the pile response to load. If applied to the pile response, notably, load-movement, it does not consider the elastic shortening of the pile, which can be substantial for long piles. The magnitude of the pile-head movement does not have anything to do with a specific ultimate resistance of a pile element in a static loading test. But, of course, the pile-head movement is the most important criterion of all, a movement limit is a key part of a pile design, but it does not define capacity in the 'ultimate' sense of the word.

Sometimes, the pile capacity is defined as the load at the intersection of two pseudo-straight lines, approximating an initial pseudo-elastic portion of the load-movement curve and a final pseudo-plastic portion, as eye-balled from the graph. This definition results in interpreted capacity values that depend greatly on judgment and, above all, on the scale of the graph. Change the scales and the perceived capacity value changes also. The interpretation of a loading test is influenced by many occurrences, but the draughting manner should not be one of them.

Without a proper definition, interpretation of capacity becomes a meaningless venture. To be useful, a definition of pile capacity from the load-movement curve must be based on some mathematical rule and generate a repeatable value that is independent of scale relations, a judgment call, or the eye-balling ability of the individual interpreter. Furthermore, it has to consider shape of the load-movement curve, or, if not, it must consider the length of the pile (which the shape of the curve indirectly does).

As detailed below (Section 8.2), Fellenius (1975b; 1980) presented definitions of pile capacity evaluated from load-movement records of a static loading test. Of these particular interest are those that can be applied to the response of a pile element: Davisson Offset Limit, Hansen 90-% criterion, Chin-Kondner and Decourt Extrapolations (hyperbolic shape), Gwizdala function (exponential shape), vander Veen exponential function, and Vijayvergiya and Rahman functions. The Davisson Offset Limit is very commonly applied to tests on driven piles. An additional limit could be the Maximum Curvature Point, although it is overly dependent on the accuracy of measurements and, therefore impractical. All are detailed in the Sections 8.2 - 8.8. The algorithms of the Gwizdala function and the Chin-Kondner extrapolation methods are useful for load-transfer analysis (Section 8.11). Note, the capacity obtained from summation of ultimate shear force (shear strength) along the pile elements is not the same as the capacity deduced from the pile-head load-movement (see Section 7.3 and Figure 7.10).

There is more to a static loading test than definition of capacity. As a minimum requirement, the test should be performed and reported in accordance with the ASTM guidelines (D1143 and D3689) for axial loading (compression and tension, respectively), keeping in mind that the ASTM guidelines refer to routine testing. Tests for special purposes may well need stricter performance rules.

Two of the most common errors in performing a static loading test are to include unloading/reloading cycles and to let the load-holding duration vary between load increments. For an instrumented test, stages of unloading/reloading and differing load-holding durations will make it next to impossible to get reliable evaluation from the strain-gage data (see Clause 8.10.5). If unloading/reloading cycles are thought needed, say, because it being required by a less than knowledgeable representative of the owner, complete the primary test first and then carry out cyclic testing by a series of load cycles between selected values of load. Moreover, don't confuse a single or a couple of unload/reload events with cyclic testing. In cyclic testing, a large number of cycles are applied between two load values, usually at least 20, sometimes up to 100 (for information and comments on cyclic testing methods, see Fellenius 1975b).

Believing that holding a load at a certain magnitude constant for a longer time (24 hours is a common length of such long load-holding time), or at several such load magnitudes, would provide direct information for predicting settlement of a piled foundation, is a very much misconceived belief. Such interspersed load-holding events have little relevance to analysis or prediction of settlement. However, they do mess up the means for a reliable analysis and interpretation of the results of the test, including using the test results for a settlement analysis. A proper and useful static loading test should consist of load increments that are equal in magnitude, applied at equal intervals of time, and held constant for equal length of time. The number of increments to the maximum load (as estimated to be close to a capacity) should be about 20. If the maximum test load is smaller than perceived "ultimate capacity", the number of increments should be reduced. The load-holding duration can be short, some maintain that 5 minutes are more than enough, some maintain that at least a 60-minute load-holding is required. The common point is that the durations must be equal. Appreciating the value of redundancy of readings, I usually choose a load-holding time of 15 minutes, sometimes more, rarely less. A test requiring 20 increments applied every 15 minutes will be over in five hours.

The two errors mentioned—unloading/reloading and differing load-holding duration—originate in old practice from before we had the concept of ultimate resistance and factor of safety, and before we had the means to test and the understanding of what we do when we test. Piles were simply tested by assessing movements at load levels of working load and multiples of working load. Assessment was by the net and

gross movements as well as slope of load-movement between the unload/reload points. All utterly meaningless and long since discarded from good practice.

Unloading and reloading steps are vestigial items that must be purged from any modern practice that aims to follow sound, up-to-date, and knowledgeable engineering principles. The old approach of unloading/reloading and holding the load "still" for unequal durations is akin to trying to wag a tail presumed extending from one's tailbone.

A head-down test on an uninstrumented pile is usually a waste of money. If a test is considered necessary, the pile must be instrumented so that the force distribution can be determined (see Section 8.13). The minimum instrumentation is telltales (or similar) to measure pile toe movement. However, a reasonably short pile, say, no more than about 15 m in a one or two-layer soil profile tested by means of a bidirectional test arrangement (Section 8.15) does not normally need any other instrumentation down the pile other than to measure the imposed movements at the location of the cell assembly (using, say, telltales).

Most static loading tests are terminated too early. To enable a reliable interpretation, a test should continue at least to a 30-mm toe movement, preferably well beyond.

## **8.2. Common Definitions of "Capacity"**

Few concepts are more diffuse and addressed with more uncertainty than the capacity of a single pile be it determined by analysis or a static loading test. It is considered a to be an ultimate condition resulting in large increase of movement for next to no increase of load. Easy to declare to be the case when calculating it using soil strength parameters. As to determined from the load-movement curve of a static loading test, the same end-condition is assumed, but often found not appearing. While a value can be produced by eyeballing the curve, most would realize that a mathematically strict definition is required that is independent of judgment call and plotting scales. As shown in the following, practice has developed several such definitions or methods. However, there is no consensus as to which method to use. Many do not have a clear choice or reason for a choice (see [Figure 8.8](#) below).

### **8.2.1 Davisson Offset Limit**

The Davisson limit load, "the Offset Limit", is defined as the load corresponding to the movement which exceeds the elastic compression of the pile by an offset of 0.15 inch (4 mm) plus a factor equal to the diameter of the pile divided by 120 (Eqs. 8.1a and 8.1b). The Offset Limit Method, proposed by Davisson (1972), primarily for driven piles, is presented in [Figure 8.1](#), showing the load-movement results of a static loading test performed on a 112 ft (34 m) long, 12-inch (300 mm) precast concrete pile. For the 12-inch diameter example pile, the offset is 0.25 inch (6 mm) and the intersection with the load-movement curve is the offset-limit load; 375 kips (1,670 kN), occurring at a 0.8 inch (20 mm) pile-head movement.

Notice that the Offset Limit Load is not necessarily a capacity or ultimate resistance. The method is based on the assumption that a perceived capacity is reached at a certain small toe movement and tries to estimate that movement by adjusting it to the stiffness of the pile which is a function of pile material, length, and diameter. M.T. Davisson developed it by correlating subjectively-estimated pile-capacities for a large number of pile loading tests to one common criterion. It is primarily intended for test results from small diameter driven piles tested according to "quick" methods and it has gained a widespread use in phase with the increasing popularity of wave equation analysis of driven piles and dynamic measurements.

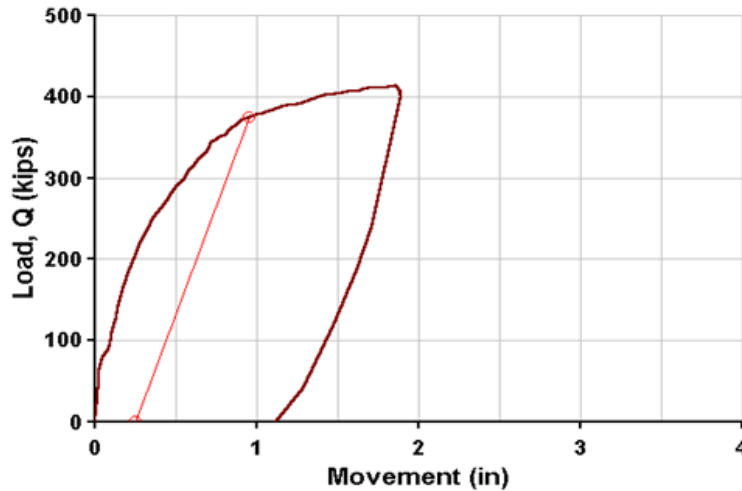


Fig. 8.1 The Offset Limit Method

(Eq. 8.1a)      OFFSET (inches)            =    0.15 + b/120

(Eq. 8.1b)      OFFSET (SI-units—mm)=    4 + b/120

where            b    =    pile diameter (face-to-face; inch or mm, respectively)

The offset distance is by some thought to be the pile toe movement produced by the load applied to the pile head load equal to the offset limit. This is incorrect.

**8.2.2 Hansen 80-% Criterion**

Hansen (1963) applied a "strain-softening" function with a peak value,  $Q_u$ , at a movement,  $\delta_u$ , ( $Q_u/\delta_u$ ) in proposing a definition for pile capacity as the load,  $Q_u$ , for which the measured pile-head load-movement curve starts to be four times the movement obtained for 80 % of that load, that is, a point on the curve with coordinates  $0.80Q_u/0.25\delta_u$ .

The method applies to tests on piles in a strain-softening soil and determines the peak resistance in the test from which the resistance then reduces due to soil strain-softening. The ‘80%-criterion’ can be estimated directly from the load-movement curve, but it is more accurately determined in a plot of the square root of each movement value divided by its load value and plotted against the movement. Figure 8.2 shows the plot of  $\sqrt{(Q/\delta)}$  square root of movement over load versus pile head movement for the same example as used for the Davisson construction (with the load and movement values of the example converted to SI-units). The 80-% pile-head load-movement curve constructed per Equation 8.2 has been added for reference as measured and as constructed from the assumption of the curve satisfying the 80-% criterion for every measured movement (along with the 90-% curve, see Clause 8.3.2). The dashed curve shown in the figure for the 80-% load-movement curve can also be manually constructed by taking a pile-head-load,  $Q_n$  (say, the maximum load applied) and its movement,  $\delta_n$ , and plotting the immediately preceding load-movement pair,  $Q_{n-1}/\delta_{n-1}$ , as  $Q_{n-1} = 0.80Q_n$  and  $\delta_{n-1} = 0.25\delta_n$ , etc., until the movement becomes insignificant.

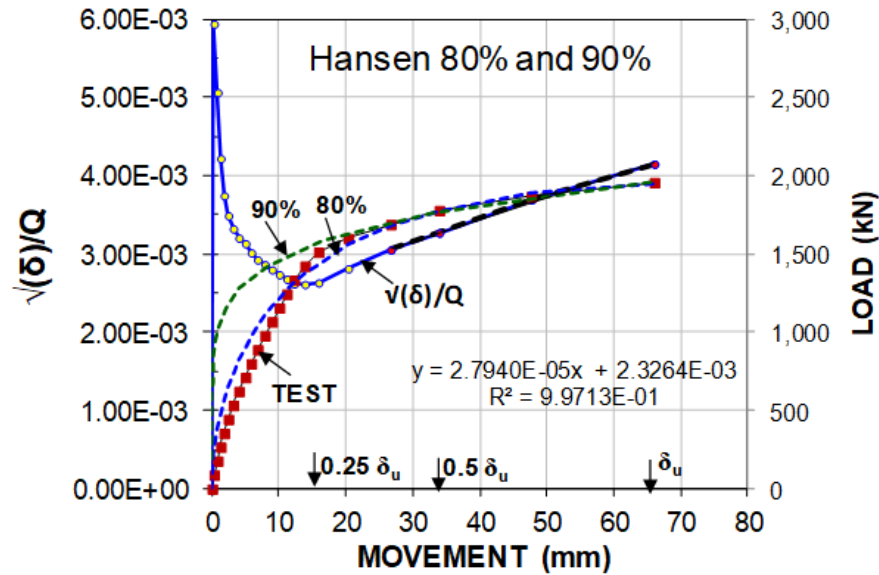


Fig. 8.2 Hansen's Plot for the 80 and 90 percent criteria

Normally, the 80%-criterion agrees well with the intuitively perceived “plunging failure” of the pile. The following simple relations (Eqs. 8.2 through 8.4) are derived for use in computing the capacity or ultimate resistance,  $Q_u$ , according to the Hansen 80%-criterion:

$$(Eq. 8.2) \quad Q = \frac{\sqrt{\delta}}{C_1\delta + C_2}$$

$$(Eq. 8.3) \quad Q_u = \frac{1}{2\sqrt{C_1C_2}}$$

$$(Eq. 8.4) \quad \delta_u = \frac{C_2}{C_1}$$

Where

- $Q$  = any applied load
- $\delta$  = the movement associated with Load  $Q$
- $Q_u$  = peak load or ultimate load
- $\delta_u$  = movement at the peak load
- $C_1$  = slope of the straight line in the  $\sqrt{\delta}/Q$  versus movement diagram
- $C_2$  = y-intercept of the straight line in the  $\sqrt{\delta}/Q$  versus movement diagram

The 80-% criterion determines the load-movement curve for which the Hansen plot becomes a straight line. Eq. 8.2, above, is the equation for the straight portion, which slope,  $C_1$ , and Y-intercept,  $C_2$ , can be determined by linear regression of the straight portion of the Hansen plotted line. Eq. 8.2 is the relation for the ‘ideal’ curve, shown as a dashed line, in Figure 8.2. Eq. 8.3 expresses the ultimate resistance,  $Q_u$ , as a function of  $C_1$  and  $C_2$ . Eq. 8.4 expresses the movement,  $\delta_u$ , for the peak resistance,  $Q_u$ .

For the example shown in Fig. 8.2, Eq. 8.2 indicates, coincidentally, that the Hansen Ultimate Load is equal to the 1,960-kN maximum (peak) test load applied to the pile head. Eq. 8.4 indicates that the peak was reached at  $\delta_u = 83$  mm. The figure does not show that beyond the 83-mm movement, the resistance reduces (strain-softens).

When using the Hansen 80%-criterion in evaluating a test, it is important to check that the point  $0.80 Q_u/0.25 \delta_u$  indeed lies on or near the measured load-movement curve. The relevance of evaluation can be reviewed by superimposing the load-movement curve according to Eq. 8.2 on the observed load-movement curve. The two curves should be more or less overlapping from the load equal to about 80 % of the ultimate load,  $Q_u$ , per the Hansen 80-% criterion at  $0.25 \delta_u$ .

### 8.2.3 Hansen 90-% Criterion

Hansen (1963) also proposed a 90-% criterion, which defines pile capacity as the load,  $Q_u$ , for which the measured load-movement curve starts to be twice the movement of the pile head as obtained for 90 % of that load, the  $0.90 Q_u/0.5 \delta_u$  point on the curve. This definition of capacity was adopted by the Swedish Pile Commission (1970) and has had some acceptance in the Scandinavian countries. The dashed curve shown in the figure (c.f., Fig. 8.2) is the load-movement curve determined by manual construction from the capacity taken as the maximum load applied to the pile in the test,  $Q_n$ , and its movement,  $\delta_n$ , where the immediate preceding load-movement pair,  $Q_{n-1}/\delta_{n-1}$ , is determined as  $Q_{n-1} = 0.9Q_n$  and  $\delta_{n-1} = 0.5\delta_n$ , etc. until the movement becomes insignificant.

A curve that mathematically satisfies the 90-% criterion at every point is a power function expressed in Eq. 8.5. However, it is faster and simpler to check for  $Q_u$  directly on the load-movement curve.

$$(Eq. 8.5) \quad Q = Q_u \left( \frac{\delta}{\delta_u} \right)^{0.152}$$

Where

$Q$	=	any applied load
$\delta$	=	movement associated with Load $Q$
$Q_u$	=	ultimate load; actually any other load
$\delta_u$	=	movement at $Q_u$

The principle behind the Hansen 90%-criterion is that the point  $0.90 Q_u/0.5 \delta_u$  indeed lies on the measured load-movement curve. The relevance of this for a tests is obtained by superimposing a calculated load-movement curve according to Eq. 8.5 (or a manually constructed curve) on the observed load-movement curve. The two curves should be more or less overlapping from the load equal to about 80 % of the Hansen-80% ultimate load at  $0.25 \delta_u$  to the load,  $Q_u$ , considered as the ultimate load or "the capacity".

A load movement curve constructed as an extrapolation of the Hansen 90-% criterion will show increasing load with increasing movement *ad infinitum*. That is, neither the 80-% nor the 90-% relations have a true  $Q_u$ -value. They are nothing but special Gwizdala functions (Gwizdala 1996; see Clause 8.11.1) with exponent,  $\theta$ , equal to 0.152 and 0.161, respectively.

### 8.2.4 Chin-Kondner Extrapolation

Figure 8.3 gives a method proposed by Chin (1970; 1971) for piles (in applying the general work by Kondner 1963). To apply the Chin-Kondner method, divide each movement with its corresponding load and plot the resulting value against the movement. As shown in the figure, after some initial variation, the plotted values fall on a straight line. The inverse slope of this line is the Chin-Kondner Extrapolation to the ultimate load (Eq. 8.5). The method essentially comprises fitting the test data to a hyperbolic curve and extending it. The load reached asymptotically at infinitely large movement is the capacity. It is, therefore, always an extrapolation of the test. However, a primary principle and requirement of a capacity evaluated from a static loading test and combined with a factor of safety or resistance factor, is that it must not be larger than the maximum load applied in the test. Therefore, the value of the Chin-Kondner method as a definition of capacity is limited.

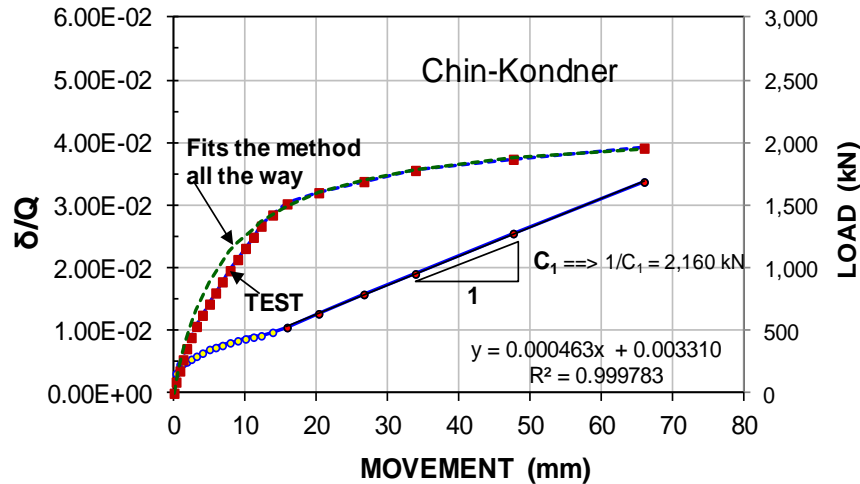


Fig. 8.3 Chin-Kondner Extrapolation method

$$(Eq. 8.5) \quad Q_u = \frac{1}{C_1}$$

Where  $Q_u$  = capacity or ultimate load (i.e., load at infinite movement;  $\delta \rightarrow \infty$ )  
 $C_1$  = slope of the straight line in the  $\delta/Q$  versus movement diagram

The inverse slope of the straight line for the example indicates a Chin-Kondner Extrapolation Limit of 2,160 kN, a value exceeding the 1,960-kN maximum test load applied to the pile head. As mentioned, although some indeed use the Chin-Kondner Extrapolation Limit as the pile capacity established in the test (with an appropriately large factor of safety), this approach is not advisable.

The criterion determines the load-movement curve for which the Chin-Kondner plot,  $Q/\delta$  vs.  $\delta$ , is a straight line throughout. Eq. 8.6 gives the relation for the curve, the 'ideal' curve, which is shown as a dashed line in figure. If larger than measured values are input, the continued plot becomes the "hyperbolic extrapolation" of the test data. Eq. 8.7 rephrases the equation to express the movement for a certain applied load,  $Q$ .

$$(Eq. 8.6) \quad Q = \frac{\delta}{C_1\delta + C_2}$$

$$(Eq. 8.7) \quad \delta = \frac{QC_2}{1 - QC_1}$$

Where  $Q$  = applied load  
 $\delta$  = movement associated with Load  $Q$   
 $C_1$  = slope of the straight line in the  $\delta/Q$  versus movement diagram  
 $C_2$  = y-intercept of the straight line in the  $\delta/Q$  versus movement diagram

Chin (1978) proposed to use the Chin-Kondner method to check the consistency of a pile response to a test process. Thus, if during the progress of a static loading test, a weakness in the pile would develop in the pile, the Chin-Kondner line would show a kink. Therefore, there is considerable merit in plotting the readings per the Chin-Kondner method as the test progresses. Moreover, the Chin-Kondner limit load is of interest when judging the results of a static loading test, particularly in conjunction with the values determined according to the other capacity definitions.

Generally speaking, two points will determine a line and third point on the same line confirms the line. However, it is very easy to arrive at a false Chin-Kondner value if applied too early in the test. Normally, the correct straight line does not start to materialize until the test load has passed the Davisson Offset Limit. As an approximate rule, the Chin-Kondner Extrapolation load is about 20 % to 40 % greater than the Offset limit. When this is not a case, it is advisable to take a closer look at all the test data.

The Chin-Kondner method is applicable to both quick and slow tests, provided constant time intervals between load increments are used. Procedures that include unloading/reloading cycles and/or unequal load increments are therefore not applicable.

### 8.2.5 Decourt Extrapolation

Decourt (1999; 2008) proposed a method, which construction is similar to those used in Chin-Kondner and Hansen methods. To apply the method, divide each load with its corresponding movement and plot the resulting value against the applied load. The results are shown in the left of the two diagrams of Figure 8.4, a curve that tends to a line for which the extrapolation intersects with the abscissa (units are customary US-units). A linear regression over the apparent line (last five points in the example case) determines the line. The Decourt extrapolation load limit is the value of load at the intersection, 474 kips (2,110 kN) in this case. As shown in the right diagram of the figure, similarly to the Chin-Kondner and Hansen methods, an ‘ideal’ curve can be calculated and compared to the actual load-movement curve of the test.

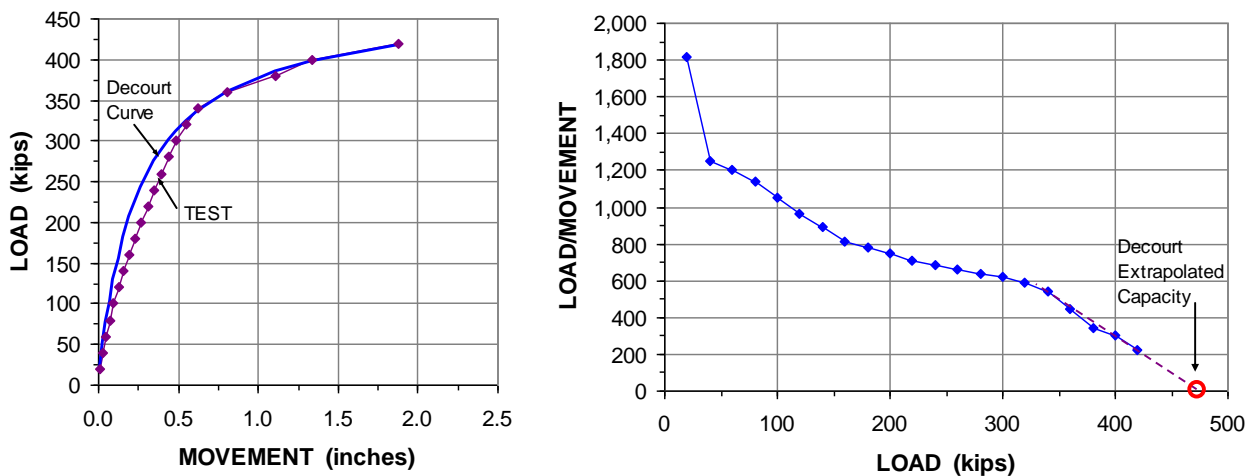


Fig. 8.4 Decourt Extrapolation method

The Decourt extrapolation load is equal to the ratio between the y-intercept and the slope of the line as given in Eq. 8.8. The equation of the ‘ideal’ curve is given in Eq. 8.9.

$$(Eq. 8.8) \quad Q_u = \frac{C_2}{C_1}$$

$$(Eq. 8.9) \quad Q = \frac{C_2 \delta}{1 - C_1 \delta}$$



Where

- $Q$  = applied load
- $Q_u$  = capacity or ultimate load
- $\delta$  = movement for  $Q$
- $C_1$  = slope of the straight line in the  $Q/\delta$  versus movement diagram
- $C_2$  = y-intercept of the straight line in the  $Q/\delta$  versus movement diagram

Results from using the Decourt method are very similar to those of the Chin-Kondner method because both methods assume the load-movement to be hyperbolic. The Decourt method has the advantage that a plot prepared while the static loading test is in progress will allow the User to ‘eyeball’ the projected (extrapolated) "Decourt ultimate resistance"—once a straight line plot starts to develop. The limitations of the Decourt method are the same as those for the Chin-Kondner method.

### 8.2.6 DeBeer Intersection Yield Load

If a trend is difficult to discern when analyzing data, a well-known trick is to plot the data to logarithmic scale rather than to linear scale. Then, provided the data spread is an order of magnitude or two, all relations become linear, i.e., they show a "clear trend". (Determining the slope and axis intercept of the line and using this for some "mathematical truths" is not advisable; such "truths" rarely serve other purpose than that of fooling oneself).

DeBeer (1968) and DeBeer and Walays (1972) made use of the logarithmic linearity. Not by creating a “mathematical truth”, but by letting the linearity demonstrate where a change had occurred in the test. They therefore plotted the load-movement data in a double-logarithmic diagram. If the load-movement log-log plot shows (with some approximation) two different trend lines connecting the data before and after a certain point, respectively, this "point of intersection" is the ultimate load (provided the number of points allow the linear trends to develop). DeBeer called the load at the intersection the "yield load". Figure 8.5 shows that the intersection occurs at a load of 360 kips (1,600 kN) for the example test.

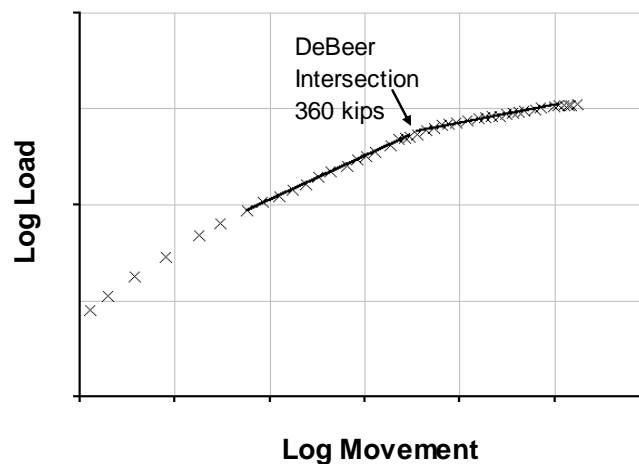


Fig. 8.5 DeBeer’s double-logarithmic plot of load-movement data

### 8.2.7 The Creep Method

For loading tests applying equal increments of load applied at equal intervals of time, Housel (1956) proposed that the movement of the pile head during the later part of each load duration be plotted against the applied total load. These “creep” movements would plot along two straight lines, which intersection is termed the “creep load”. For examples of the Creep Method, see Stoll (1961). The example used in the foregoing, being taken from a constant-rate-of-penetration, CRP, test, is not applicable to the Creep

Method. Figure 8.6 illustrates the creep method with data taken from a test where the quick maintained-load method was used with increments applied every ten minutes. The graph plots the “creep” values measured between the six-minute and ten-minute readings. The intersection between the two trends indicates a Creep Limit of 550 kips. For reference to the test, the small diagram beside the figure shows the load-movement diagram of the test and the Offset Limit Load.

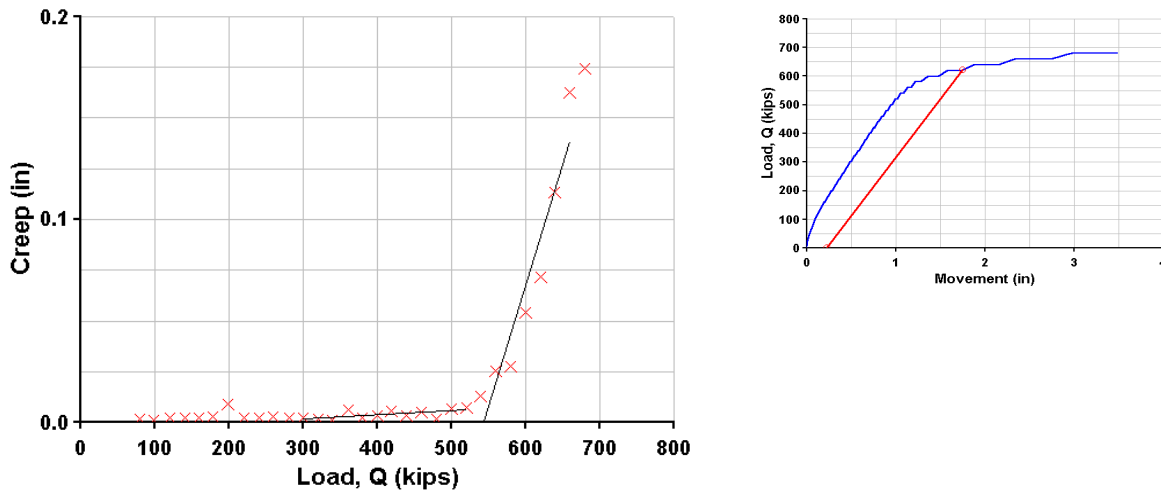


Fig. 8.6 Plot for determining the creep limit

If the "creep load" is to be considered in a test evaluation, it is important that the test was free of any unloading/reloading cycle and/or that all load holding durations were equal. Then when a kink appears, similar to that shown in the above figure, it is usually a sign of not a "creep load", but that the shaft resistance has become fully mobilized and the pile toe, therefore has started to receive load and move; such information is better obtained by means of a toe telltale and other instrumentation.

### 8.2.8 Load at Maximum Curvature, Shen-Niu

When applying increments of load to the pile head, the movement increases progressively with the increasing load until the ultimate resistance is reached, say, as a state of continued movement for no increase of load—i.e., plastic deformation. Of course, plastic deformation develops progressively down the pile. Eventually, the plastic deformation becomes the dominate feature of the curve. At loads smaller than that load, the curvature of the load-movement curve increases progressively. Beyond the load, the curve becomes more of a straight line. This response occurs at the point of maximum curvature of the load-movement curve. Provided that the increments are reasonably small so that the load-movement curve is built from a number of closely spaced points, the location of maximum curvature can usually be “eye-balled” to determine the limit load.

Shen and Niu (1991) proposed to determine the curvature by its mathematical definition and to plot the curvature of the load-movement curve against the applied load, as shown in Figure 8.7. Their mathematical treatment is quoted below. (Shen and Niu state that the third derivative is the curvature, which is not quite correct. Moreover, there is no merit in studying the third derivative instead of the curvature of the load-movement curve). Initially, this plot shows a constant value or a small gradual increase until a peak is obtained followed by troughs and peaks. The first peak is defined as the yield load. Shen and Niu defined the first peak to occur as the Yield Limit Load and claimed that the second peak occurs at the ultimate load.

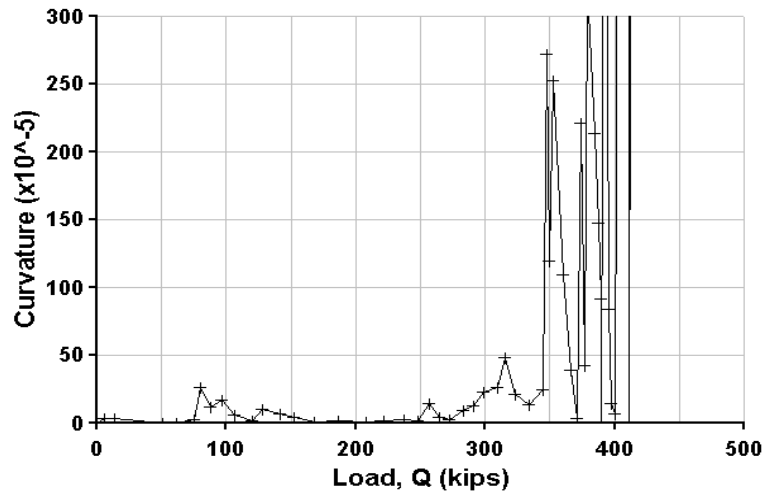


Fig. 8.7 Plot for determining the load-movement curve maximum curvature

First, the slope,  $K$ , of the load-movement curve is determined:

$$(Eq. 8.10) \quad K = \frac{\Delta\delta}{\Delta Q} = \frac{\delta_i - \delta_{i-1}}{Q_i - Q_{i-1}}$$

Eq. 8.11 then shows the change of slope for a change of load

$$(Eq. 8.11) \quad \Delta K = \frac{\Delta K}{\Delta Q} = \frac{K_{i+1} - K_i}{Q_{i+1} - Q_i}$$

The second and third derivatives are:

$$(Eq. 8.12) \quad \Delta^2 K = \frac{\Delta^2 K}{\Delta Q^2} = \frac{\Delta K_{i+1} - \Delta K_i}{\Delta Q_{i+1} - \Delta Q_i}$$

$$(Eq. 8.13) \quad \Delta^3 K = \frac{\Delta^3 K}{\Delta Q^3} = \frac{\Delta^2 K_{i+1} - \Delta^2 K_i}{\Delta Q_{i+1}^2 - \Delta Q_i^2}$$

Strictly, the curvature,  $\rho$ , is

$$(Eq. 8.14) \quad \rho = \frac{\Delta^2 K}{(1 + K^2)^{3/2}}$$

The primary condition for the Shen-Niu yield-load method to be useful is that all load increments are equal and accurately determined. Even a small variation in magnitude of the load increments or irregular movement values will result in a hodgepodge of peaks to appear in the curvature graph, or, even, in a false yield load. It is then more practical to eyeball the point of maximum curvature from the load-movement curve.

### 8.3 Factor of Safety

To determine the allowable load on a pile, pile capacity evaluated from the load-movement curve of a static loading test is normally divided by a factor of safety (or multiplied by a resistance factor in ULS design or LRFD for factored resistance). The factor of safety is not a singular value applicable at all times. The value to use depends on the desired avoidance of unacceptable consequence of a failure, as well as on the level of knowledge and control of the aspects influencing the variation of capacity at the site. Not least important are, one, the method used to determine or define the ultimate load from the test results and, two, how representative the test is for the site. For piled foundations, practice has developed toward using a range of factors. See also the discussion on Factor-of-Safety presented in Chapter 11.

In a testing programme performed early in the design work and testing piles that are not necessarily the same type, size, or length as those which will be used for the final project, it is common to apply a safety factor of at least 2.5 to the capacity evaluated from the test results—often applied without too much thought placed on what definition of capacity that was employed. In the case of testing during a final design phase, when the loading test occurs under conditions well representative for the project, the safety factor is usually 2.0 or 2.2, again, applied to a rather ambiguously determined capacity. When a test is performed for purpose of verifying the final design, testing a pile that is installed by the actual piling contractor and intended for the actual project, the factor commonly applied is 2.0. Well into the project, when testing is carried out for purpose of proof testing and conditions are favorable, the factor may be further reduced and become 1.8. A reduced safety factor may also be warranted when limited variability is confirmed by means of combining the design with detailed site investigation and control procedures of high quality. One must also consider the number of tests performed and the scatter of results between tests. Not to forget the assurance gained by means of incorporating dynamic methods for controlling hammer performance and capacity assessment alongside the static methods of testing and analysis.

However, the value of the factor of safety to apply depends, as mentioned, on the method used to determine the capacity. A conservative method, such as the Davisson Offset Limit Load, warrants the use of a smaller factor as opposed to when applying a method such as the Hansen 80%-criterion. It is good practice to apply more than one method for defining the capacity and to apply to each method its own factor of safety letting the smallest allowable load govern the design. That is, the different analysis methods define lower and upper boundaries of the ultimate resistance. Moreover, the lower boundary does not have to be the Offset Limit. It can be defined as the load on the pile when the load-moment curve starts to fit (becomes close to) the “ideal” Hansen, Chin-Kondner, or Decourt load-movement curves. All criteria should be coupled with an assessment of the movements associated with an assigned working load and an analysis of the long-term settlement of the foundation supported by the pile(s).

In **factored design** (LRFD—Load and Resistance Factor Design or ULS design—Ultimate Limit State Design), a “resistance factor” is applied to the capacity and a “load factor” is applied to the load. Considering both the fact that factored design must always be coupled with a serviceability limit state design (SLS—Serviceability Limit State Design, or unfactored design), it has been proposed that the pile capacity should be determined by a method closer to the plunging limit load, that is, the Hansen 80 %-criterion would preferred over the Offset Limit Load. Note, that the serviceability limit state addresses settlement. Therefore, the load-transfer distribution determined in a back-calculation of an instrumented—or simulated—static loading test is valuable, indeed necessary, when assessing settlement of a piled foundation. Moreover, it should be remembered that, while there are many piled foundations that have failed to support a structure adequately despite a customary factor of safety applied to a capacity value, there are no such unacceptable foundations where the design correctly assessed the settlement aspects.

## 8.4 Choice of criterion

It is difficult to make a rational choice of the best capacity criterion to use, because the preferred criterion depends heavily on one's past experience and conception of what constitutes the ultimate resistance of a pile. One of the main reasons for having a strict criterion is, after all, to enable compatible reference cases to be established.

The Davisson Offset Limit is very sensitive to errors in the measurements of load and movement and requires well maintained equipment and accurate measurements. No static loading test should rely on the jack pressure for determining the applied load. A load-cell must be used at all times (Fellenius 1984b). In a sense, the Offset Limit is a modification of the 1.5 inch movement, the "gross movement", criterion of the past. Moreover, the Offset-Limit method is an empirical method that does not really consider the shape of the load-movement curve and the actual transfer of the applied load to the soil. However, it is easy to apply and has gained a wide acceptance, because it has the merit of allowing the engineer, when proof-testing a pile for a certain allowable load, to determine in advance the maximum allowable movement for this load with consideration of the length and size of the pile. Thus, as proposed by Fellenius (1975b), contract specifications can be drawn up including an acceptance criterion for piles proof tested according to quick testing methods. The specifications can simply call for a test to at least twice the design load, as usual, and declare that at a test load equal to a factor,  $F$ , times the design load, the movement shall be smaller than the elastic column compression of the pile, plus 0.15 inch (4 mm), plus a value equal to the diameter divided by 120. The factor  $F$  is a safety factor and should be chosen according to circumstances in each case. The usual range is 1.8 through 2.0.

The Hansen 80%-criterion is often close to what one subjectively accepts as the "true" ultimate resistance determined from the load-movement curve of the static loading test. This may occur even if the soil is not truly strain-softening or the peak resistance has not been reached. The value is then smaller than the Chin-Kondner or Decourt extrapolated values. Note, however, that the Hansen 80-% method is more sensitive to inaccuracies of the test data than are the Chin-Kondner and Decourt methods.

In contrast to the Hansen 80-% criterion, the Hansen 90-% criterion is not useful and could give misleading results. It is only mentioned here because it is in use in some places, so a reference is needed. If required for curve fitting, the ratio function (Gwizdala 1996) is more suitable for the fitting procedure, as it will establish the actual best-fit function coefficient ( $\theta$ ) and independent of the Hansen  $\theta$ -values (0.152 and 0.161).

The Chin-Kondner Extrapolation method and the Decourt Extrapolation method, allow continuous check on the test, if a plot is made as the test proceeds, and an extrapolating prediction of the maximum load that will be applied during the test. Sudden kinks or slope changes in the Chin-Kondner line indicate that something is amiss with either the pile or with the test arrangement (Chin 1978).

The Hansen's 80%, and the Chin-Kondner and Decourt methods allow the later part of the load-movement curve to be plotted according to a mathematical relation, and, which is often very tempting, they make possible an "exact" extrapolation of the curve. That is, it is easy to fool oneself and believe that the extrapolated part of the curve is as true as the measured. As mentioned earlier, whatever one's preferred mathematical criterion, the pile capacity value intended for use in design of a pile foundation must not be higher than the maximum load applied to the pile in the test.

The shape of the pile-head load-movement curve is influenced by the length of the pile (i.e., by the amount of pile shortening) and whether or not the pile is affected by residual force. Moreover, piles are used in order to control and limit the amount of settlement of the supported foundation. What settlement to consider acceptable is a function of the response of the structure, not of the piles directly. Always, after applying an appropriately conservative factor of safety (working stress) or resistance factor (ULS design

or LRFD) to the capacity, the primary issue becomes whether or not the settlement of the foundation for the sustained portion of working load (unfactored) is acceptable, i.e., if it is smaller than the limit, with a margin, of what is acceptable for the structure. In many cases, the assigned working load will have to be reduced or the pile be installed deeper in order to ensure that the settlement is smaller than the assigned limit. In other cases, the settlement analysis can show that the load can be increased or the piles be installed to a more shallow depth.

Be the choice of capacity definition difficult or not, most current standards and code presuppose, if not outright require, that a capacity be determined from a pile loading test. Indeed, most of the time, the foremost reason for at all carrying out a loading test is to determine the capacity of the test pile. I have since long been interested in seeing how this is reflected in the practice. On occasion, I have, therefore, disseminated pile-head load-movement curves to individuals active in design of piled foundations and asked them to send me back what capacity the curves would represent in their opinion and by their preferred method, e.g., Fellenius (2013; 2017). Figure 8.8 shows the results from one such event, the capacity values determined by 94 individual participants in analyzing a static loading test pile-head load-movement curve on a 450-mm diameter, 10 m long bored (CFA) pile in silty sand. N.B. the capacities are not predictions. They are assessed and determined from the actual load-movement curve. The demonstrated scatter of interpreted capacity values is not unique, but found in several similar studies.

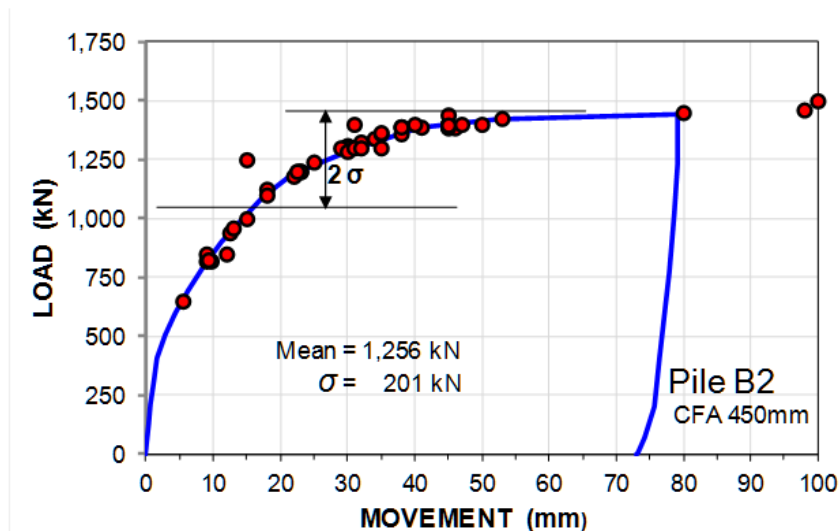


Fig. 8.8 54 capacities determined from an actual pile-head load-movement curve as assessed by 94 participants (Fellenius 2017).

It is obvious that the profession does not have a common approach to determining a pile capacity from a static loading test. I have on other occasions pursued similar studies asking participants to tell me what factor of safety and resistance factor they would apply to their capacity values: the factors of safety received have ranged from a low of 1.8 through a high of 2.5 and the resistance factors have ranged between 0.65 through 0.7, a much closer span, which is because most codes encompassing the limit states design, or LRFD, do indicate the factor to apply to the capacity of a static loading test. However, the same codes do not indicate how to determine the capacity itself! The EuroCode is an exception, but it prescribes capacity as the load that produced a pile-head movement equal to 10% of the pile diameter!

By any appreciation of the state-of-the-practice, the situation demonstrated by the spread of values actually applied shown in Figure 8.8 is scary. Some comfort is by the fact that, as indicated in Sections 7.17 and 7.18, settlement is the primary aspect for a piled foundation design. Capacity is rather irrelevant and the practice would be better off not using it.

### 8.5 Force-Movement Response and t-z/q-z functions

The resistance of a pile to the load applied in a static loading test is governed by the relative movement between the pile and the soil, or, rather, the sum of the resistance of each pile element and the movement at the pile elements for that applied load and pile head movement. A resistance is always coupled to a movement. Theoretically, when performing a static loading test, instead of applying a series of increments of load, one can just as well (theoretically, that is) impose a series of predetermined increments of movement and record the resulting levels of load. For example, this is actually how the constant-rate-of-penetration test is performed (small equal movements applied at equal short time intervals). However, it is far more practical to perform a test by adding predetermined increments of load to the pile head and recording the subsequent so-imposed movements.

In a head-down static loading test, the resistance in the upper regions of the soil profile is engaged (mobilized) first. That is, the shaft resistance is engaged progressively from the pile head and down the pile. The first increment of load only engages a short upper portion of the pile. The actual length is determined by the length necessary to reach an equilibrium between the applied load and the shaft resistance (mobilized as the pile head is moved down). The movement is the ‘elastic’ shortening (compression) of the length of pile active in the transfer of the load from the pile to the soil. The pile toe does not receive any load until all the soil along the pile shaft has become engaged. Up till that time, the movement of the pile head is the accumulated ‘elastic’ shortenings of the pile. Note that the movement necessary for mobilizing shaft resistance is very much smaller than the movement necessary for mobilizing any significant toe resistance. If the soil along the pile shaft has a strain-softening response, the shaft resistance may be reducing along some of the upper length even before the pile toe is engaged (See Section 7.3 and Figure 7.10). Figure 8.9 shows a few typical shapes of resistance versus movement curves for a pile element.

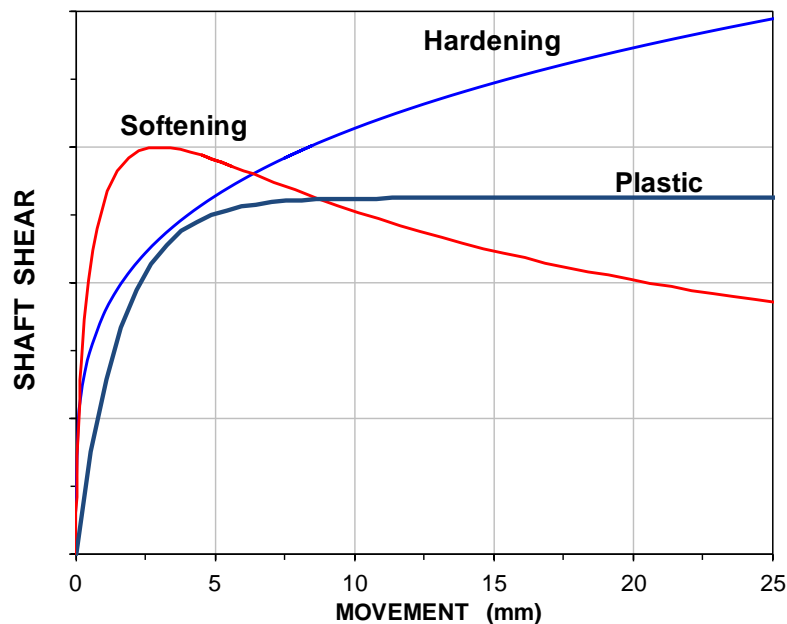


Fig. 8.9 Typical shapes of shear resistance versus movement between a pile element and soil

Resistance versus movement curves (load-movement curves) for shaft and toe resistances are called t-z function for shaft resistance and q-z function for toe resistance. The t-z function applies to the response of a short element and represents the shaft resistance response of the element along the pile, i.e., unit shaft resistance vs. movement. The process has little meaning if applied to a longer length of a pile, indeed the full pile length.

When t-z/q-z functions are addressed in available codes or standards, they are mostly indicated as elastic-plastic curves, or, for shaft response, as an initial more or less straight line to a peak followed by one or two steps indicating a softening after the peak. Most, if not all, imply an ultimate toe resistance. For example, the American Petroleum Institute, API, standard recommends using a q-z curve in sand and in clay that appears to reach a horizontal line, an ultimate resistance, at a movement equal to 10 % of the diameter<sup>1</sup>. The API figure is unchanged from the API version of 40 years ago and over this time, it has not been realized that the numbers behind the plot—they are included with the figure—do not correspond to the plotted curve. The numbers actually correlate precisely to a Gwizdala function (c.f., 8.5.1) with a coefficient,  $\theta$ , of 0.33. If the numbers would be measured in a loading-test, the coefficient would represent a q-z response of a pile subjected to residual toe force, a rather special case and not a "shoe that fits all".

Section 8.5.1 presents t-z/q-z functions governed by known (chosen) target value of unit resistance,  $r_{trg}$ , combined with an assumed (or measured) movement for that resistance,  $\delta_{trg}$ , plus a coefficient specific to the t-z/q-z function considered. When a value of  $r_{trg}$  has been determined in a calculation of a simulated response of the pile to applied load or from measurements, and a movement,  $\delta_{trg}$ , for that value has also been either assumed or measured, then, each of the functions will only depend on that additional coefficient. In using the t-z/q-z functions, it is convenient to normalize the value to 100 % of the target resistance and to set all other measured resistances to a ratio (%) of that target resistance,  $r_{trg}$ .

I have compiled the various t-z and q-z functions in an Excel template "cribsheet" (Fellenius 2016) available as #365 at my web site that can be used to back-calculate load-movement records for a pile element and fitting a suitable t-z/q-z function to test records as based on a single "function coefficient".

### 8.5.1 The Gwizdala Function

A t-z or q-z curve can be defined by Eq. 8.15 as the ratio of two resistances equal to the ratio of the respective movements raised to an exponent, a function coefficient (Gwizdala 1996, Fellenius 1999). The function is also called the Ratio function or Power function.

$$(Eq. 8.15) \quad \frac{r_1}{r_2} = \left( \frac{\delta_1}{\delta_2} \right)^\theta$$

where

- $r_1$  = Resistance 1
- $r_2$  = Resistance 2
- $\delta_1$  = movement mobilized at  $r_1$
- $\delta_2$  = movement mobilized at  $r_2$
- $\theta$  = function coefficient;  $0 \leq \theta \leq 1$

Although the stress at infinite movement,  $\delta_{inf}$ , is infinitely large, an ultimate, or target, value can be defined as the load occurring at any definite or specific movement. When a target resistance and target movement are known or assumed, the shape or the t-z/q-z curve is governed by the  $\theta$ -coefficient ("**Exp**"), as illustrated in Figure 8.10, showing the resistance and the movement in percent of target resistance and target movement. Notice, a custom t-z/q-z curve can be computed for resistance and movement larger than the target value.

<sup>1</sup> The second and third paragraphs of the Introduction present facts and comments on that definition of ultimate toe resistance.



The Gwizdala Function t-z curve for shaft resistance and the q-z curves for toe resistance usually take different  $\Theta$ -coefficients. A Gwizdala curve with a coefficient ranging from 0.05 through 0.30 is typical for a shaft resistance, while toe resistance response is closer to curves with exponents between 0.4 and 1.0. A resistance curve, shaft or toe, conforming to a coefficient larger than 1.0 would be extraordinary. For toe resistance, it could be used to model a pile with a gap, or some softened zone, below the pile toe that has to be closed or densified before the soil resistance can be fully engaged. Gwizdala (1996) has suggested several relations for the  $\Theta$ -coefficient as a function of soil and pile type.

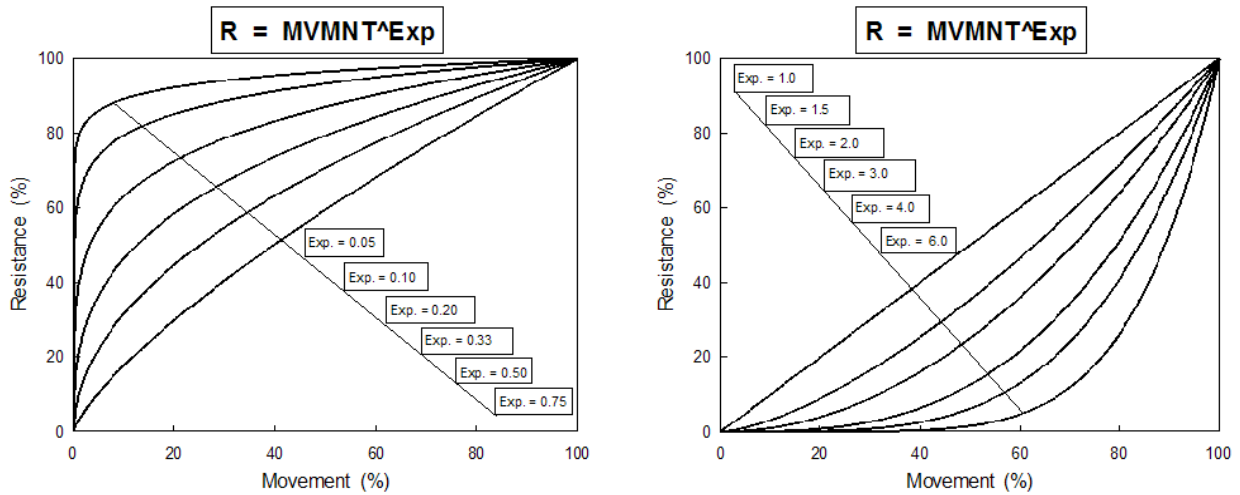


Fig. 8.10 Shape of t-z and q-z curves for a range of exponents

The symbols in Eq. 8.15 can be modified, as follows: the pair  $r_1/\delta_1$  can be set to a variable pair,  $r/\delta$ , and  $r_2/\delta_2$  be set to a "target pair",  $r_{trg}/\delta_{trg}$ . Eq. 8.15 then becomes Eq. 8.16 and shows the equation for unit resistance—shaft or toe—at a certain movement according to the Gwizdala Function in relation to the target resistance and target movement.

$$(Eq. 8.16) \quad r = r_{trg} \left( \frac{\delta}{\delta_{trg}} \right)^\theta$$

where  $r$  = force variable (shaft resistance or toe stress)  
 $r_{trg}$  = target resistance  
 $\delta$  = movement variable  
 $\delta_{trg}$  = movement at  $r_{trg}$   
 $\Theta$  = function coefficient;  $0 \leq \Theta \leq 1$

(Note,  $r_{trg}$  and  $\delta_{trg}$  can be from any point on the curve, as long as they are from the same pair).

The concept of a "target", i.e., a specific value of stress and movement, is useful when matching a contiguous stress-movement response to a t-z function. Figure 8.11 shows t-z curves plotted from Eq. 8.16 assuming a Gwizdala Exponent,  $\Theta$ , ranging from 0.15 through 1.00 and that the curve must have a load or stress,  $r_{trg}$ , equal to 100 % of the stress that results in a movement,  $\delta_{trg}$ , set equal to 100 % of some specific movement. The two make for a  $r_{trg}/\delta_{trg}$  load/movement pair. That is, the variable is the function coefficient. Different coefficients will result in different shapes of the t-z curve, but they will all go through the target point,  $r_{trg}/\delta_{trg}$  load/movement. A coefficient of 1.0 makes the curve appear as a straight line through the target point.

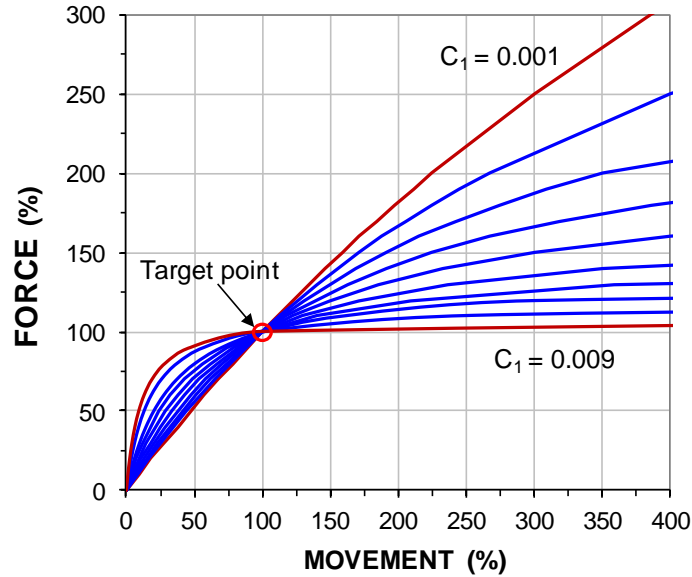


Fig. 8.11 Gwizdala Function for t-z shaft shear force vs. movement

### 8.5.2 The Hyperbolic Function

It is very common to find that actual test records of shaft resistance fit a Chin-Kondner hyperbolic function (see Section 8.4) as expressed by Eqs. 8.17a through 8.17c.

$$\text{(Eq. 8.17a)} \quad r = \frac{\delta}{C_1 \delta + C_2} \quad \text{(Eq. 8.17b)} \quad C_1 = \frac{1}{r_{\text{inf}}} \quad \text{(Eq. 8.17c)} \quad C_2 = \delta \left( \frac{1}{r} - \frac{1}{r_{\text{inf}}} \right)$$

where

- $r$  = shaft shear force variable (or toe stress) associated with  $\delta$
- $\delta$  = movement variable associated with  $r$
- $C_1$  = the slope of the line in a  $r/\delta$  vs.  $\delta$  diagram; the Chin-Kondner plot
- $C_2$  = ordinate intercept the  $r/\delta$  vs.  $\delta$  diagram
- $r_1/\delta_1$  = any stress/movement pair, usually a "target" pair,  $r_{\text{trg}}/\delta_{\text{trg}}$
- $r_{\text{inf}}$  = ultimate resistance, occurring at infinite movement, which then is the  $1/C_1$ -value.

When the extrapolation to  $r_{\text{inf}}$  is less than obvious, both the  $C_1$  and  $C_2$  are best determined by plotting, from the measured data, the  $\delta/r$  values versus the measured movements,  $\delta$ , and then select an appropriate part of the plot for a linear regression calculation, which directly provides  $C_1$  and  $C_2$ , as the respective values of the slope and intercept of the regressed line. Note that  $C_2$  can be expressed as a function of  $C_1$  and the target pair,  $r_1/\delta_1$ . In effect, once  $C_1$  is chosen,  $C_2$  is determined (Eq. 8.17c).

Figure 8.12 shows hyperbolic t-z curves for a  $r_{\text{trg}} = 100\%$  occurring for a movement of 100% ( $\delta_{\text{trg}}$ ) for  $C_1$ -coefficients ranging from 0.001 through 0.009 for resistances at infinite movement ( $\delta_{\text{inf}}$ ) of ten and 1.11 times that at the target resistance, respectively. That is, the input of  $C_1$  is the Chin-Kondner function coefficient and it decides the shape of the curve for the chosen 100-% target resistance and 100-% target movement.

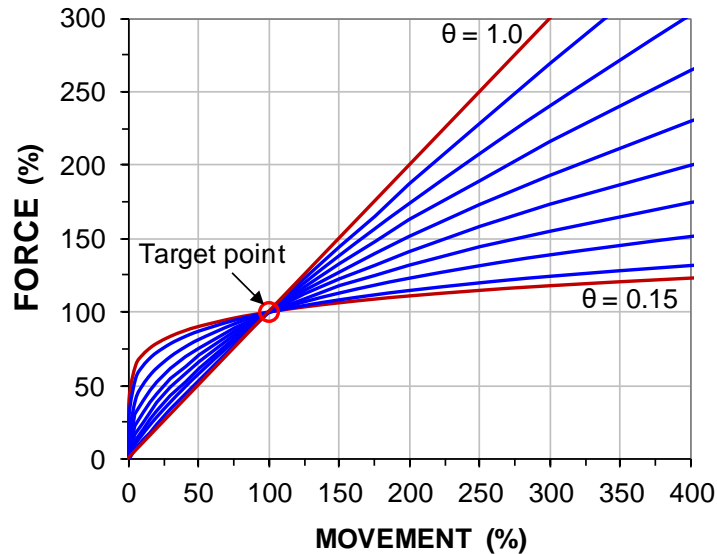


Fig. 8.12 The hyperbolic (Chin-Kondner) for t-z shaft shear force vs. movement

### 8.5.3 The vander Veen (Exponential) Function

When fitting measured stress-movement values to an elastic-plastic t-z response, sometimes the kink occurring at the change from the initial straight, sloping line (the ‘elastic’ line) and the final horizontal straight line (the ‘plastic’ line) can be disturbing. Then, the fit obtained by the vander Veen function can show to be more suitable, as it provides a smoother transition between the initial rising line to the final horizontal plastic shape.

Figure 8.13 shows a t-z stress-movement curve plotted as given by Eq. 8.18 (vander Veen 1953) with coefficient,  $b$ , ranging from 0.01 through 0.20. Set equal to 0.54, the curve reaches a 100-% target stress or load,  $r_{trg}$ , at a target movement,  $\delta_{trg}$ , of 100 %.

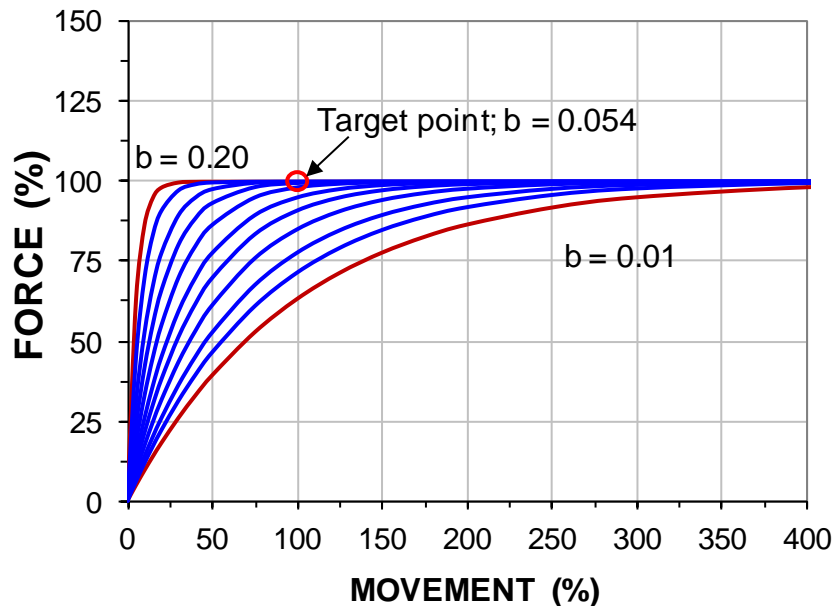


Fig. 8.13 vander Veen exponential function for t-z shaft shear force vs. movement

$$(Eq. 8.18) \quad r = r_{inf}(1 - e^{-b\delta})$$

where

$r$	=	shaft shear force variable (or toe stress)
$r_{inf}$	=	shaft shear force (or toe stress) at infinite movement
$\delta$	=	movement variable
$b$	=	function coefficient
$e$	=	base of the natural logarithm = 2.718

If an infinite target resistance,  $r_{trg}$ , of 100 % is desired at and beyond a specific target movement,  $\delta_{trg}$ , then, a fit to this pair is achieved by varying the function coefficient ( $b$ ) until the curve just about reaches this target pair,  $r_{trg}/\delta_{trg}$ .

### 8.5.4 The Hansen 80-% Function

Shaft resistance often shows a strain-softening post-peak response, that is, after reaching a peak value,  $r_{peak}$ , which is then the “ultimate” resistance, the resistance reduces with further movement. The Gwizdala (Ratio), Chin-Kondner (Hyperbolic), and vander Veen (Exponential) functions are less suitable for simulating the response to the applied load for piles exhibiting strain-softening. However, the Hansen 80-% function (See Section 8.3) enables a strain-softening response to be modeled. The Hansen 80-% function is expressed in Eqs. 8.19a through 8.19e.

Figure 8.14 shows a stress-movement curve plotted from Eq. 8.19a on the assumption that  $r_{peak} = 100$  % is the peak stress and occurs at movement set to 100 %. ( $\delta_{trg} = \delta_{peak}$ ). This result was achieved for a  $C_1$ -coefficient equal to 0.0005 (the  $C_2$ -intercept is a function of  $C_1$  as given by Eq. 8.19c).

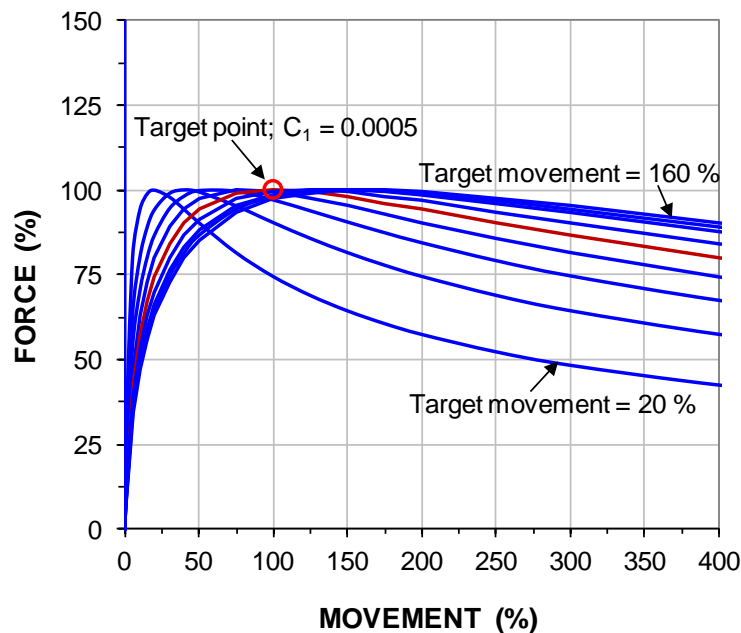


Fig. 8.14 Hansen 80-% function for t-z shaft shear force vs. movement

An input of  $r_{peak} = r_{trg} = 100$  % and an associated movement determines the Hansen 80-% Function, that is, any target pair input fixes the shape of the curve. Therefore, the Hansen 80-% Function has a limited use with regard to fitting measured load-movement unless the target movement,  $\delta_{trg}$ , is equal to the movement for the measured peak and results in a simulated shape that is similar to that of the shape of the measured load-movement, in particular for the strain-softening part (movement beyond the target movement).

$$(Eq. 8.19a) \quad r = \frac{\sqrt{\delta}}{C_1\delta + C_2} \quad (Eq. 8.19c) \quad C_1 = \frac{1}{2r_{peak}\sqrt{\delta_{peak}}} \quad (Eq. 8.19d) \quad C_2 = \frac{\sqrt{\delta_{peak}}}{2r_{peak}}$$

$$(Eq. 8.19d) \quad r_{peak} = \frac{1}{2\sqrt{C_1C_2}} \quad (Eq. 8.19e) \quad \delta_{peak} = \frac{C_2}{C_1}$$

where  $r$  = shaft shear force variable (or toe stress)  
 $\delta$  = movement variable  
 $C_1$  = the slope of the straight line in the  $\sqrt{\delta}/r$  versus movement ( $\delta$ ) diagram  
 $C_2$  = ordinate intercept of the straight line in the  $\sqrt{\delta}/r$  versus movement ( $\delta$ ) diagram  
 $r_{peak}$  = peak resistance, often taken as the target resistance  
 $\delta_{peak}$  = movement at the peak resistance, often taken as the target movement

### 8.5.5 The Zhang Function

Zhang and Zhang (2012) presented an additional strain-softening function, a function leading up to a peak and reducing thereafter with increased movement, as expressed in Eqs. 8.20a through 8.20f. The  $a$ -,  $b$ - and  $c$ -coefficients are interrelated and Eqs. 8.20e and 8.20f express ' $b$ ' and ' $c$ ' as functions of ' $a$ '.

$$(Eq. 8.20a) \quad r = \frac{\delta(a+c\delta)}{(a+b\delta)^2} \quad (Eq. 8.20b) \quad r_u = \frac{1}{4(b-c)}$$

$$(Eq. 8.20c) \quad \delta_u = \frac{a}{b-2c} \quad (Eq. 8.20d) \quad r_{inf} = \frac{c}{r_u b^2}$$

$$(Eq. 8.20e) \quad b = \frac{1}{2r_{peak}} - \frac{a}{\delta_{peak}} \quad (Eq. 8.20f) \quad c = \frac{1}{4r_{peak}} - \frac{a}{\delta_{peak}}$$

where  $r$  = shaft shear force variable (or toe stress)  
 $\delta$  = movement variable  
 $r_u = r_{peak}$  = peak resistance  
 $\delta_u = \delta_{peak}$  = movement at peak resistance  
 $a, b,$  and  $c$  = coefficients (" $b$ " and " $c$ " are functions of " $a$ ")  
 $r_{inf}$  = resistance at infinitely large movement (must always be  $\geq 0$ )

A fit to a measured force-movement curve can be found by defining the target pair as the values of peak resistance and movement at the ultimate resistance, and fine-tuning for the ' $a$ '-coefficient, letting the ' $b$ '- and ' $c$ '-coefficients be determined by the ' $a$ '-coefficient and the target  $r_{peak}$  and  $\delta_{peak}$  values until a fit to the measured curve is achieved. In contrast to the Hansen 80-% strain-softening conditions, any target pair can be input as long as the resistance at infinite movement is larger than zero ( $r_{inf} \geq 0$ ).

Figure 8.15 shows a load-movement curve plotted from Eqs. 8.17a through 8.17f on the assumption that  $r_{peak}$  is equal to 100 % load and occurs at a movement set to 100 %. The ' $a$ '-coefficient can range from 0 through 0.100. The curve with ' $a$ ' = 0 is an unrealistic case, as it would indicate a totally plastic soil response. An ' $a$ '-coefficient of 0.01 represents softening to zero resistance at infinite movement. A softening to 50 % of the peak resistance ( $r_{peak}$ ) at infinite movement would be obtained using an ' $a$ '-coefficient of 0.009 and its shape would then be similar to the Hansen 80%-curve.

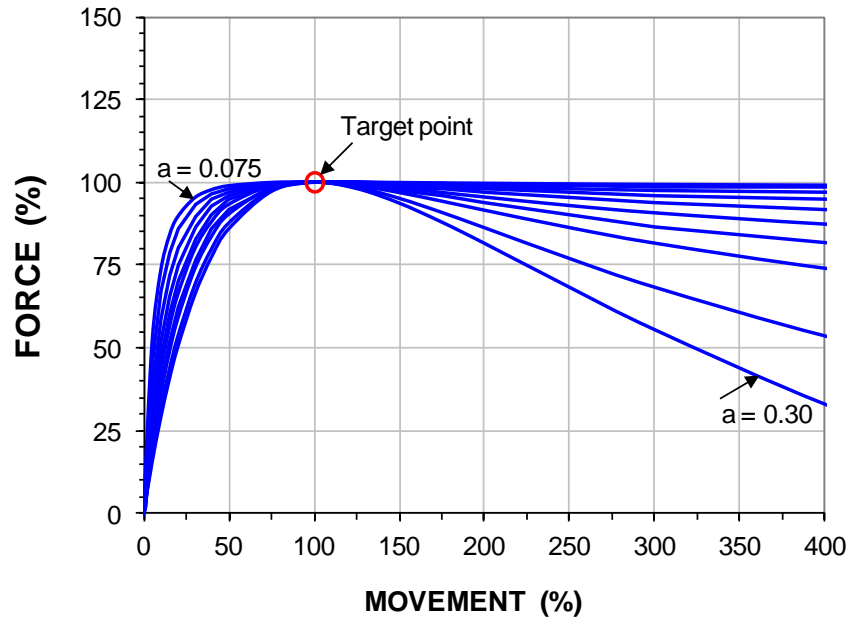


Fig. 8.15 Zhang function for t-z shaft shear force vs. movement

The shape of the Zhang Function is controlled by input of the 'a'-coefficient. The larger the 'a', the more pronounced the strain-softening after the peak. However, the  $r_{inf}$  cannot become smaller than zero, which determines the largest acceptable input of 'a' for different target movements,  $\delta_{trg}$ . Thus, for a range of target movements ranging from 1 mm through 80 mm, the 'a'-coefficient must be smaller than the values listed in Table 8.1. A value smaller than that listed for the particular target movement,  $\delta_{trg}$ , would infer a negative  $r_{inf}$ .

**TABLE 8.1 The upper limit of the 'a'-coefficient as a function of the target movement,  $\delta_{trg}$** 

$\delta_{trg}$ (mm)	1	2	3	4	5	6	7	8	9	10
a	0.0025	0.0050	0.0075	0.0100	0.0125	0.0150	0.0175	0.0200	0.0225	0.0250
$\delta_{trg}$ (mm)	12	15	20	25	30	40	50	60	70	80
a	0.0300	0.0375	0.0500	0.0625	0.0750	0.1000	0.1250	0.1500	0.1750	0.2000

### 8.5.6 The Vijayvergiya Function

Vijayvergiya (1977) presented the function expressed in Eq. 8.21, which also represents a strain-softening curve. Figure 8.16 shows a series of curves per the Vijayvergiya function. When the curve is set to go through a target point, a V-coefficient is equal to 2 will make the peak force equal to the target force at the target movement. The use in practice of the Vijayvergiya function is to assume a peak stress or load equal to a perceived ultimate resistance and to assign a constant V-coefficient of 2. Assuming the coefficient to be constant disregards the fact that the function implies a strain-softening after the peak stress as opposed to a plastic (ultimate) value. Moreover, assuming it to be constant fixes the shape and in effect claims that "one size fits all".

$$(Eq. 8.21) \quad r = r_{trg} \left( V \sqrt{\frac{\delta}{\delta_{trg}}} - (V-1) \frac{\delta}{\delta_{trg}} \right)$$

where

- $r$  = shaft shear force variable (or toe stress)
- $\delta$  = movement variable
- $r_{trg}$  = target resistance
- $\delta_{trg}$  = movement at target resistance
- $V$  = coefficient

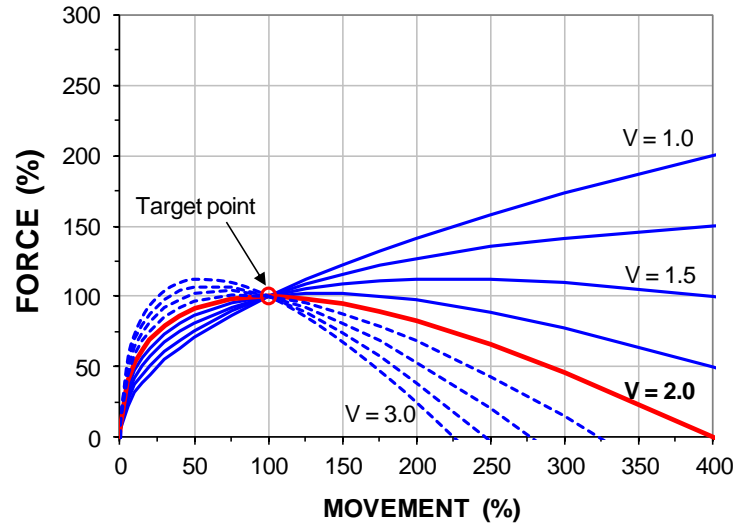


Fig. 8.16 Vijayvergiya function for t-z shaft shear force vs. movement

### 8.5.7 The Rahman Function

M.M. Rahman (personal communication 2018) developed a strain-softening function based on a parabolic relation according to Eq. 8.22. The function equation includes two function coefficients: one denoted "M" and one denoted "F". Usually, in fitting to an actual load-movement curve, M and F range from about 1.0 through 3.0 and 1.5 through 2.0, respectively.

$$\text{Eq. 8.22} \quad Q_n = Q_{trg} \left( \frac{\delta_{trg} \delta^{F-1} + \delta_{trg}^{F-1} \delta_n}{\delta_{trg}^F + \delta_n^F} \right)^{\frac{1}{M}}$$

Where

- $Q_n$  = applied load
- $\delta_n$  = movement paired with  $Q_n$
- $Q_{trg}$  = target load or resistance
- $\delta_{trg}$  = target movement (paired with  $Q_{trg}$ )
- $M$  = function coefficient;  $> 0$
- $F$  = function coefficient;  $> 1.0$

Figure 8.17 shows the Rahman strain-softening function curves. The curves are shown for, to the left, a fixed function coefficient,  $M = 1.00$ , and a range of function coefficients,  $F$ , and, to the right, a fixed function coefficient,  $F = 2.00$  and a range of function coefficients,  $M$ . In fitting to actual test records, it is most practical to start with  $F = 2$  and, then, when having obtained a reasonably good fit by varying "M" in a trial-and-error procedure, fine-tune the fit by means of varying "F", while keeping the "M" unchanged. The Rahman function enables fitting for strain-softening response where the stress-movement conditions change after a peak value. For example, fitting (back-calculating) to a response that is affected by residual force.

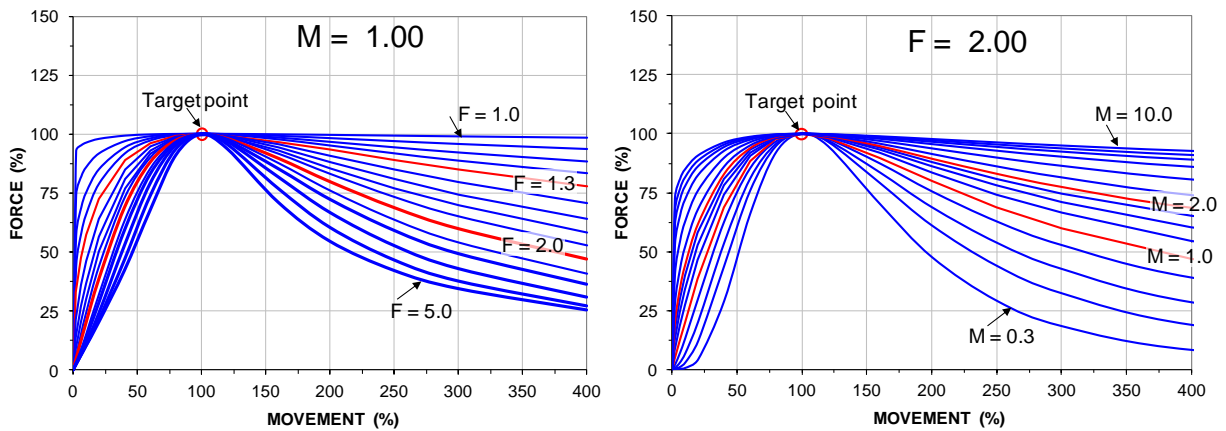


Fig. 8.17 Rahman function for t-z shaft shear force vs. movement.

### 8.5.8 The eight function curves compiled

Figure 8.18 shows a compilation of the eight function curves fitted to a measured pile-element load-movement curve (blue diamonds). The test curve indicates a slight strain-hardening response. All curves are calculated using a target pair that resulted in the closest fit to the measured test data. The initial part of all eight shows a reasonably good fit to the test data. The best fit for the test results was obtained by the Hyperbolic (Chin-Kondner) and the vander Veen Functions, even the Zhang function, although its last point lies below the curve, as the Zhang function models strain-softening.

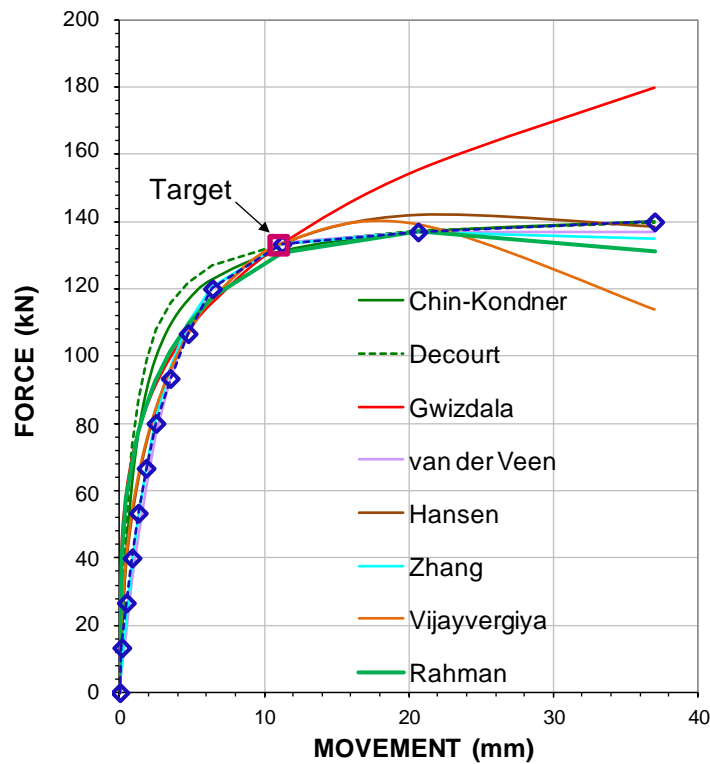


Fig. 8.18 Example of eight t-z functions fitted to a load-movement curve measured for a pile element (gage location).



The Gwizdala Function has the built-in assumption that the resistance continues to increase with movement beyond the value perceived as the ultimate resistance, and the Chin-Kondner (Hyperbolic Function implies a finite ultimate resistance, but one that occurs at an infinitely large movement). The Hyperbolic Function and the Hansen 80-% Function are particularly well suited to simulate shaft resistance response. As a pile toe resistance does not show any tendency to ultimate resistance, to model its load-movement response, I have found the Gwizdala Ratio Function most 'fitting'. Note that the fitting to a pile head-movement is rarely the same as that fitted to the individual pile elements (See Section 7.3, Figure 7.10). Indeed, there is little sense in using load-transfer functions to back-calculate the pile-head load-movement response, as opposed to addressing the individual pile-soil elements—the toe response being fundamentally different to the shaft shear response.

Figure 8.19 shows back-calculated t-z functions fitted to the shaft response of an 800-mm diameter bored pile in a fine-grained soil measured at two separate pile elements in the pile (Bohn et al. 2017). Both examples indicate strain-softening shaft resistance response. The "Element 1" graph shows a peak resistance at a movement of no more than 5 mm, while the test on "Element 2" shows that the peak did not appear before the movement relative the pile and the soil was 20 mm. The best-fit back-calculations for each of the eight t-z functions to the measured curves show a reasonable to excellent fit for the curve portion before the peak resistance for all but the Hansen and Vijayvergiya functions. Of course, neither of the three strain-hardening functions, Chin-Kondner, Decourt, and Gwizdala, can show agreement to the post-peak resistance, which is the obvious case also for the vander Veen function with its plastic post-peak response. Neither was it possible to obtain a good post-peak fit of the Hansen and Vijayvergiya strain-softening functions. However, for both examples, the Zhang and Rahman functions gave a good fit to the measured load-movement throughout. Indeed, the Rahman fit is excellent.

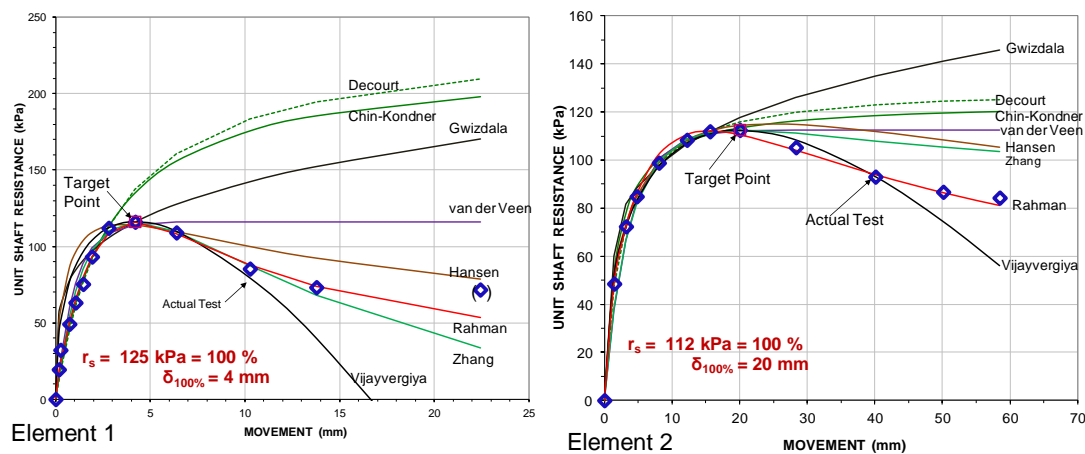


Fig. 8.19 Comparison of best-fit functions to two actual records of unit strain-softening shaft resistance (kPa) vs. movement (mm). Data from Bohn et al. 2017.

Shaft resistance (the t-z curve) is a shear-dependent concept. Therefore, other than due to the fact that different construction procedures may have made the soil response different for small diameter piles as opposed to large diameter piles, the shaft resistance, the t-z curve is qualitatively independent of the pile diameter, that is, the unit shaft resistance,  $r_s$ , and the movement,  $\delta$ , are independent of the pile diameter. In contrast, for toe resistance, the q-z response is a deformation concept and the movement,  $\delta$ , is proportional to the pile diameter (increases with the pile diameter) for the same unit stress (see Sections 6.2 and 7.2). However, its normalized value is independent of the diameter. Estimating pile toe movement by calculating it as a case of settlement of a footing in a soil of appropriate compressibility can be helpful in finding what function and function coefficient to use.

## 8.6 Instrumented Tests

Our profession is gradually realizing that a conventional static "head-down" loading test on a pile provides limited information. While the load-movement measured at the pile head may establish the capacity of the pile (per one definition or other), it gives no quantitative information on the load-transfer mechanism (magnitude of the toe resistance and the distribution of shaft resistance). Yet, this information is what the designer often needs in order to complete or verify a safe and economical design. Therefore, the conventional test arrangement is frequently expanded to include instrumentation to obtain the required information. Instrumentation can consist of telltales and strain-gages.

### 8.6.1 Telltale instrumentation

The oldest form of instrumenting a test pile is to place one or several telltales to measure the pile toe movement and compression (shortening) during the test. N.B., recording the pile toe movement as an addition to a static loading test greatly enhances the value of the test. Telltales are usually small diameter rods installed inside guide pipes. Installing such telltales properly is not a simple task. There must be no friction along the length because the friction will cause random shortening (compression) of the telltale adversely affecting the measurements. This means that the telltale rod and guide pipe must both be straight. Friction can be reduced by having the annulus between the telltale rod and guide pipe filled with oil. The telltale rods must not be assembled on the ground and then hoisted above the pile for insertion, as this will invariably cause kinks in the telltale rod and cause it during the test to push against the guide pipe with undesirable friction adversely affecting the records. Therefore, a telltale should be installed by one rod at a time spliced onto the rod string as the telltale is lowered. Or, using a crane to lift the string as one rod after another is added to the bottom of the string, then, lower the string (the full length, now straight, telltale) into the pile.

Telltales should always be installed to measure pile shortening directly. This is because extraneous small movements of the reference beam always occur and they result in large errors of the shortening values. If you do not measure shortening directly, forget about using the telltale data other than for movement. Moreover, determining compression over a short distance as the difference between two telltale records brings in differentiation error and the results have low reliability.

A modern type of telltale system is to use an anchor at the pile toe connected with tensioned wires which elongation or shortening is recorded using a vibrating-wire sensor (c.f., Clause 8.7.2). Of course, neither the rod telltale nor the anchor extensometer is restricted to being the only such gage in a test pile.

It is futile to try to expect that telltale measurements can be accurately converted to force in the pile. However, they can serve as back-up records.

### 8.6.2 Determining load distribution from telltale measurements

The telltale-measured compression (shortening of the pile over the telltale length) can be used for determining the approximate force distribution mobilized by an applied test load. The measured compression is converted to average strain by division with the telltale length,  $L$ , and, then, to average load by multiplication with the pile axial stiffness,  $EA/L$  (just "EA" is not the stiffness and it is therefore called "EA-parameter"). The so-determined force is considered to represent—to define—the average over the telltale length. An alternative definition "average load",  $Q_{ing}$ , is the arithmetic mean of the applied load and the load at the pile toe (telltale foot). The two "averages" are not necessarily equal. For the simple case of a constant unit shaft resistance, however, both averages do give the same value and both lie on the straight-line load distribution exactly at the pile mid-depth (half the telltale length below the pile head), as indicated in [Figure 8.20](#). The line marked " $r_s$ " represents, qualitatively, the distribution of unit shaft resistance. Usually, the average load calculated from the compression (converted to strain) is plotted at the mid-point of the telltale length.

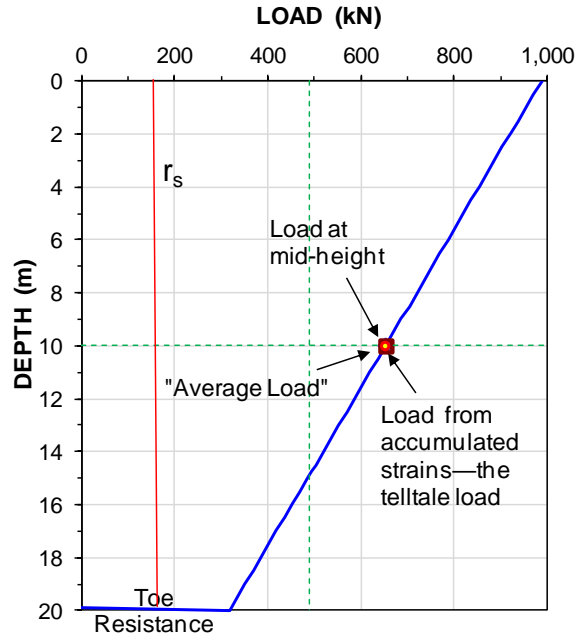


Fig. 8.20 Force distribution for constant unit shaft resistance.

Figure 8.21 presents the results of a static loading test performed on a 20 m long pile instrumented with a telltale to the pile toe for measuring the pile toe movement. The pile toe load was not measured. The figure includes the pile compression (“COMPR.”). The load-movement diagram for the pile head shows that the pile clearly has reached an ultimate resistance. In fact, the pile “plunged”. Judging by the curve showing the applied load versus the pile toe movement, it would appear that also the pile toe reached an ultimate resistance—in other words, the toe bearing capacity was reached. However, this was not the case.

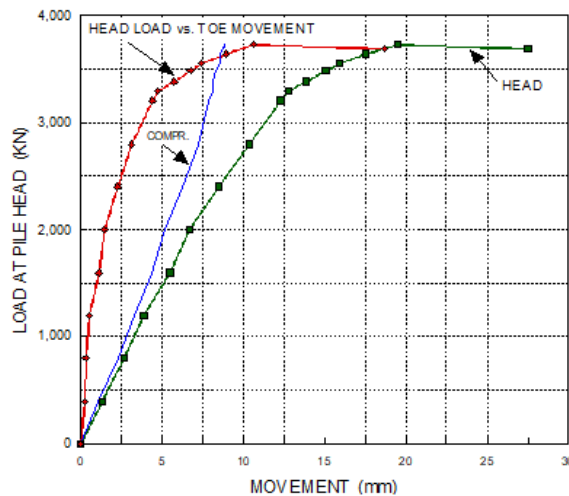


Fig. 8.21 Load-movement diagram of a static loading test on a 20 m long, 450 mm diameter closed-toe pipe pile in compact sand with telltale measurements of toe movement (Fellenius 1999)

Most of the shaft resistance was probably mobilized at or before a toe movement of about 2 mm to 3 mm, that is, at an applied load of about 2,500 kN. At an applied load beyond about 3,300 kN, where the movements start to increase progressively, the shaft resistance might even have started to reduce (if the shaft resistance would be strain softening). Thus, approximately between pile toe movements of about 3 mm to about 10 mm, the shaft resistance can be assumed to be fully mobilized and,

conservatively assumed, be approximately constant. An adjacent uplift test indicated that the ultimate shaft resistance of the pile was about 2,000 kN. When subtracting the 2,000 kN from the total load over this range of the measured toe movement, the toe load can be estimated. This is shown in Figure 8.22, which also shows an extrapolation of the toe load-movement curve beyond the 10-mm movement, implying a slight strain softening pile shaft resistance. Extrapolating the toe curve toward the ordinate indicates the existence of a residual toe force in the pile, i.e., a force in the pile prior to the start of the static loading test.

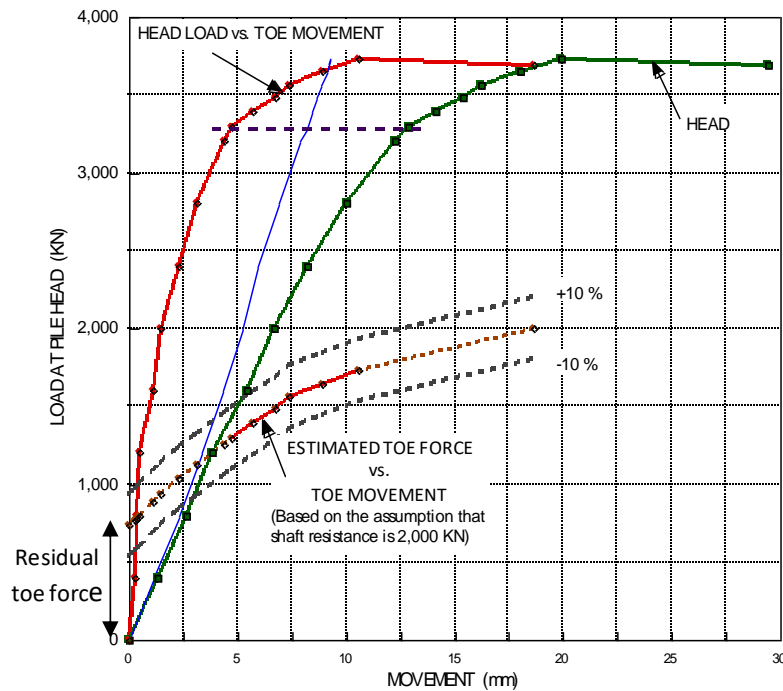


Fig. 8.22 The same test data as shown in Fig. 8.21 with the results of analysis of the load-movement of the pile toe. The results from a static loading test on an adjacent pile instrumented with strain-gages indicated that the shaft resistance would be about 2,000 kN (Fellenius 1999).

If a test is instrumented with two (or more) telltales (different lengths), the difference in shortening between the two telltales represents the shortening of the length between the shorter telltale foot and the longer telltale foot. Note, however, that a telltale measurement always includes a measurement error, or uncertainty. The error in the calculated load is normally small in relation to the measured shortening. However, as also the difference of shortening between values from two telltales can sometimes be small, the error that was negligible for each single value can then become large for the combined value.

When planning a new test, use vibrating wire strain gages or extensometers rather than telltales rods for determining load. A telltale rod to the pile toe to measure the total compression of the pile (and pile-toe movement) is always good to include, however.

As mentioned, these days, telltales consist of extensometers attached to anchors rather than telltale rods. Such gages provide better accuracy and enable more reliable values. Records from two or more extensometer anchors can be combined, as used in the Glostrex system (Figure 8.23, which combines several anchors in a string so that the shortening (and, therefore, both strain and load) are measured between anchor points at short distances distributed down the pile (Hanifah and Lee 2006).



Fig. 8.23 A Glostrex anchor placed down in a cylinder pile (Hanifah and Lee 2006),

### 8.6.3 Brief notes on strain-gage instrumentation

Most instrumentation in a test pile comprises a system consisting of vibrating-wire strain-gages or electrical resistance gages. Attaching single-level gages to a rod that is connected to a reinforcing cage placed in the pile before concrete is placed or a rod pushed into the concrete immediately after it is poured makes for an inadequate instrumentation; one not suitable for detailed analysis. That is, not unless it can be assured that each gage is placed exactly in the center of the pile, e.g., by means of a Glostrex anchor system in pipe pile or a cylinder pile, or in a center pipe carefully cast into a prestressed concrete pile. A gage level must have a pair of gages placed diametrically opposed at equal radial distance from the center in order to compensate for axial bending of the pile—unavoidable and with significant effect even when small. The average stress over the pile cross section is then the mean of the two gage values. If one of the two gages making up a pair is damaged, then, the records of the surviving gage are not useful and must be discarded.

Having three well functioning gages instead of two at a gage level would seem to improve accuracy of measurements. Yes, it does. However, the improvement is only marginal. Moreover, the mean of three gage values is not the average stress over the pile cross section unless the gages are placed very precisely at the corner of an equilateral triangle, something very difficult to achieve. The latter would need to be calculated from the three values using an elaborate algorithm. Then, if one of the three gages would "die", the other two cannot be trusted and their measurements must be discarded. Thus, adding a third gage has reduced the redundancy. If redundancy is desired, then, use two pairs at each gage level, not three single gages. If then one of the four gages "dies", discard the data of its "partner" and use the data from the surviving pair.

Figure 8.24 illustrates how bending can affect strain-gage measurements during a static loading test and shows the importance of always discarding the "surviving" gage of a pair where one of the pair has "died". The records are shown as applied load plotted versus measured strain as taken from a gage level comprising two gage pairs, Pair A and C and Pair B and D. The gages of each pair were placed diametrically opposed in a bored test pile. Both pairs functioned well in the test. As indicated, the average of Pairs A&C and B&D, as well as of all four gages gave essentially the same average load-curve. However, if we assume that Gage B "died", then the average of the "surviving" gages, A&C and D, is quite off the true curve, about  $100 \mu\epsilon$  at the maximum load, as would the records showing the average of Gages A&C and B had Gage D been the gage that died, instead, but 'the other way'. And, had the average been taken by combining one "surviving" gage in each pair, the resulting error would have been even larger. The magnitude of the about  $100 \mu\epsilon$  error for the illustrated case should be considered in the light of the fact that the average strain for the maximum load was about  $400 \mu\epsilon$ .

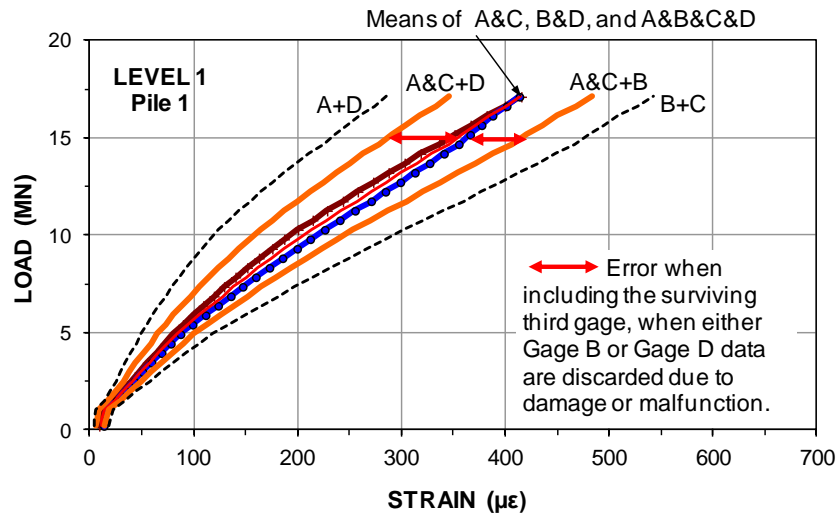


Fig. 8.24 Strains measured in four strain-gages—two pairs—with averages of the pairs and of all four gages (from Fellenius and Tan 2012).

Vibrating wire strain-gages are designed with a wire tensioned between two supports attached to a common base. When the base elongates due to an outside force, the wire stretches and its frequency changes. A magnet is placed close to the wire and it can be excited to "pluck" the string and then to pick up the frequency of the vibrations. The vibration frequency is calibrated to the strain between the supports and, thus, the frequency reading indicates the strain. To ensure maximum precision, the last step in the manufacture is annealing the gage to remove potential internal stress. The reading precision is about  $1 \mu\epsilon$  and a  $5\text{-}\mu\epsilon$  change between two readings can be considered to represent the reading accuracy.

Ideally, the metal of the wire and the gage-base should have the same thermal coefficient so the gage would be insensitive to temperature change (as long as the new temperature is the same over the entire gage). In practice, however, while the body is made of high quality steel with a thermal coefficient of  $13.2 \mu\epsilon/^\circ\text{C}$ , the body is usually made from mild steel with a coefficient of  $12 \mu\epsilon/^\circ\text{C}$ . Thus, a reduction of temperature results in an increase of wire frequency for a VW-gage, which corresponds to about  $0.3 \mu\epsilon/^\circ\text{C}$ , theoretically, implying a strain increase, i.e., reduction of stress or increase of the zero reading (zero reference for a 'free' gage), but one of little effect in practice.

Low temperature sensitivity is important for gages placed in a pile, as the temperature above ground is usually quite different to that down in the ground. Moreover, for concrete piles, the hydration of the concrete causes the temperature to rise during the first about 16 to 20 hours to a peak usually about 60 to 80 °C, but the temperature could even reach the boiling point. The subsequent cooling can take many weeks and may not have been concluded at the start of the static loading test. Because concrete and steel have dissimilar thermal coefficients, the cooling will introduce strain in the gages that has no relation to a shear between the pile and the soil.

The thermal coefficient of concrete depends mainly on the ballast mineral and, for minerals typically used as ballast, it can range from values as low as 5 to as high as  $14 \mu\epsilon/^\circ\text{C}$ . It decreases with increase in the water-cement ratio, increases with age, is smaller below than above the freezing point, and is smaller for saturated concrete than for dried out concrete. Although the thermal coefficient of concrete can actually range between 7 and  $12 \mu\epsilon/^\circ\text{C}$ , it is normally considered to be about  $10 \mu\epsilon/^\circ\text{C}$ , that is, a  $2 \mu\epsilon/^\circ\text{C}$  difference between wire and body. Thus, a reduction of temperature results in a decrease of the zero reference for a VW-gage.

The two effects are independent and superpositional. Thus, the cooling of a bored pile during set-up period due to temperature sensitivity of the gage and to the difference in thermal sensitivity between concrete and reinforcement a gage will see a reduction of the zero reference amounting to about  $2 \mu\epsilon/^\circ\text{C}$  developing between the day after casting and day of the loading test.

The contraction due to cooling for bored piles socketed in rock or very dense soil, where a strong bond to the soil as developed before the main part of the pile has cooled, can on occasions be resisted by the bonding, causing local zones of tension along the pile that can be so large that micro-cracking of the concrete develops (Sinnreich 2012). A static loading test with strain gages located in micro cracked zone will then show confusing gage records. First, the initial loading steps will close these micro-cracks. This will cause large strain to be recorded for the initial load increments, which may appear as large portion of the applied load reaching the gage level. When the micro-cracks have closed, the force strain returns to true relationship. Such micro cracking will make interpretation of strain gage data difficult and could cause misinterpretation of the force distribution in the test pile.

For modern systems, the process of "plucking" the wire and reading the frequency is almost immediate and even the readings of a large number of gages can be assumed to be simultaneously obtained. However, a few "old" equipments are still around where seconds are spent waiting for a steady vibration. Then, the readings are not simultaneous, which is unacceptable. Proper systems for recording gages for a static loading test must be set up with gages and data acquisition that can read (scan) a large number of gages more or less simultaneously, i.e., recording all gages within a maximum 20-s time—or faster. There is little sense in having strain-gage instrumentation without means of more or less simultaneous reading of the gages.

The reading precision of a vibration wire gage is  $1 \mu\epsilon$ , which means that any error of load calculated from strain measurements depend on other factors than the gage performance, such as unknown pile modulus and pile area as well as error in the value of the applied external load. Note also that strain-gage measurements, although not the gage itself, are affected by presence of residual force (Section 8.14).

The vibrating wire is commonly supplied as a "sister bar" which is the name used for a gage (factory-attached) to a small diameter, about 1 m long rebar that can be affixed to a reinforcement cage to ensure that the gage will not tilt during the construction. Field-attaching the actual vibrating wire gage, an about 50 to 100 mm long piece, directly to the reinforcing cage provides much less assurance of avoiding tilting of the gage. If a tilt occurs, it will result in the gage records being significantly off and the evaluation of the records will become misleading.

Strain can also be measured using fibre-optic gage lines, which can provide records of almost continuous strain distribution with accuracy almost that of the VW system, but they are also more sensitive to temperature change than the VW-system. Moreover, the read-out and data collector is rather expensive. N.B., also the fibre optic lines must be installed in diametrically opposed pairs. Just one line in the center of the pile is not good enough—the nominal geometric center is rarely the center of the forces or bending plane.

## 8.7 The Bidirectional Test

It is difficult to determine the what portion of the applied test load that reaches the pile toe. Even when a strain-gage pair is placed at the pile toe and a telltale is used to measure the pile toe movement, interpretation of the data from a conventional "head-down" test is complex. While the portion of the applied load reaching the pile toe ostensibly can be determined from the strain-gage measurement, the actual load is often not known due to a residual force present at the pile toe already before the start of the static loading test. Then, the pile cross section and the E-modulus of the pile at the gage location may not be known correctly, which will throw off the load evaluation.

The difficulty associated with wanting to know the pile-toe load-movement response, but only knowing the pile-head load-movement response, is overcome in the bidirectional test, BD-test, which incorporates one or more sacrificial hydraulic jack-like device(s) placed at or near the toe (base) of the pile to be tested (be it a driven pile, augercast pile, drilled-shaft pile, precast pile, pipe pile, full-displacement pile, H-pile, or a barrette). Figure 8.25 shows a schematic picture of the bidirectional test.

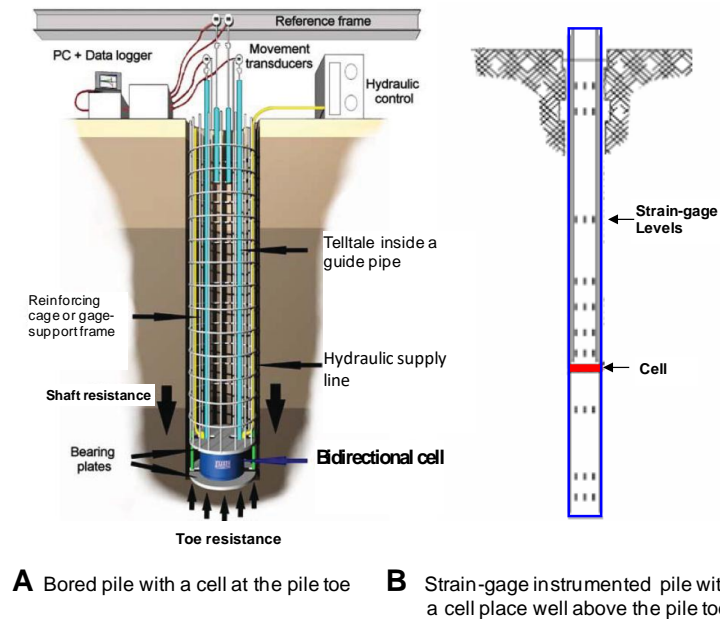


Fig. 8.25 Pile with bidirectional cell (from Loadtest Inc. flier with permission).

Early bidirectional testing was performed by Gibson and Devenny (1973), Amir (1983), and Horvath et al. (1983). About the same time, an independent development took place in Brazil (Elisio 1983; 1986), which led to an industrial production of bidirectional tests offered commercially by Arcos Engenharia Ltda., Brazil, to the piling industry. Independently, in the late 1980s, Dr. Jorj Osterberg saw the need for and use of a test employing a hydraulic jack arrangement placed at or near the pile toe (Osterberg 1998) and established a US corporation called Loadtest Inc. to pursue the bidirectional technique. When Dr. Osterberg in 1989 learnt about the existence and availability of the Brazilian device, the US and Brazilian companies collaborated. Outside Brazil, somewhat unmerited, the bidirectional test is now called the “Osterberg Cell test” or the “O-cell test”. During the now about 30+ years of commercial application, Loadtest Inc. advanced the practice of strain-gage instrumentation in conjunction with the bidirectional test, which has vastly contributed to the knowledge and state-of-the-art of how to measure pile response to load much beyond bidirectional tests.

The system uses water for the hydraulic fluid. When hydraulic pressure is applied to the cell—the hydraulic jack—it expands, pushing the upper length upward and the lower length downward. In addition to the cell pressure, which is calibrated to applied load, the test incorporates movement measurements: telltales extending from the cell upper plate to the ground surface to measure the shortening of the pile above the cell, and, when adjusted to the upward movement of the pile head, the measurements provide the upward movement of the cell upper plate in relation to the soil. The expansion of the cell (separation of the upper and bottom cell plates) is measured by displacement transducers (at least two) placed between the plates. The downward movement of the cell base plate is obtained as the difference between the upward movement of the upper plate and the cell plate separation. Finally, an additional set of telltales measures the pile toe movement. Sometimes, in case of a cell assembly close to the pile toe, the latter telltales are omitted.



The test procedure consists of applying load increments to the pile by means of incrementally increasing pressure in the cell and recording the resulting plate separation, toe movement, and pile head movement. The upward and downward load-movements do not represent equal response to the applied load. The upward load-movement is governed by the shear resistance characteristics of the soil along the shaft, whereas the downward load-movement is governed by the compressibility of the soil below the pile toe (for a cell placed near the pile toe). The fact that in a conventional “head-down” test, the shaft moves downward, while in the bidirectional test it moves upward, is of no consequence for the determination of the shaft resistance. Unit shaft resistances in the upward or the downward directions (positive and negative) are equal.

At the start of the test, the pressure in the cell is zero and the axial load (“pre-existing” load) in the pile at the cell level consists of the buoyant weight of the pile plus any residual force in the pile at the cell level. This load is carried structurally by the cell assembly and the pile structure. The first pressure increments transfer the “pre-existing” axial force to pressure in the cell hydraulic fluid. The completed transfer of this force to the cell is when the cell upper and bottom plates start to separate, opening the cell.

The cell assembly is built with an internal bond between the plates, the cell cover is welded to the bottom plate, construction feature that enables the cell assembly to be attached to the reinforcing cage and lowered with it into the pile. Before the test start, pressure is applied to the cell to break the bond and, also, to create a horizontal fracture zone that separates the pile into an upper and lower length, which, respectively, are pushed upward and downward by the cell pressure applied in the test. Carefully executed, the bond-breaking pressure (load) is usually small, only affecting the pile and soil nearest the bidirectional cell level. Small or not, it is important to record the force and movements during loading toward the bond breaking and in unloading (if now the jack pressure is released after the breaking of the bond, as opposed to proceeding directly to the first load increment of the test schedule; the latter is preferable). The bond-breaking records are useful for the evaluation of the test and the pile response to load. Unfortunately, the engineering practice often omits reporting them.

The cell system is saturated by supplying water to the cell-pressure pipe (water is normally the hydraulic fluid used for the test). The water in the cell-pressure pipe results in a hydrostatic pressure at the footprint area of the cell portion of the cross section. A separate water-filled pipe from the ground surface to the cell level ensures that the hydrostatic pressure (pore pressure) acts on the cross section of the pile outside the cell area as soon as the two plates have separated by a minute distance. The phreatic height of the pore water in the soil at the cell level the hydraulic pressure gage (at the ground surface, usually) is usually not significantly different to the distance to the groundwater table and, therefore, before the start of the test, the hydrostatic pressure of the water column between the pressure gage and the BD cell is about the same as the pore pressure (if hydrostatically distributed) in the ground at the cell level. That is, after breaking the bond, a zero (i.e., 0) BD reading of the hydraulic pressure gage indicates that there is no force in the cell. However, pressure of the water column is there.

Before the cell pressure can impose a change of axial force in the pile, the weight of the pile must be transferred to the BD cell. This weight is the pile buoyant weight because after breaking the bond and obtaining the minute first separation of the cell plate, the pile is subjected to a hydraulic force, equal to the pore pressure at the cell location and equal in the upward and downward direction. For the upward directed force, the hydraulic force reduces the pile weight carried by the cell to the buoyant pile weight, which is the force now recorded by the cell pressure (the minute upward movement of the upper cell plate and the pile is assumed to have mobilized no shaft resistance). To know the force in the cell that moves the upper length of the pile upward engaging the pile shaft resistance, the pile buoyant weight must be subtracted from the cell force. The upward hydraulic force is the pore pressure at the cell level times the full cross section of the pile (when considering the water pressure inside the BD cell). Practice is to subtract that buoyant weight from the upward-directed load-movement records.

For the downward directed action, the water force is compensated by the about as large upward directed force at the pile toe and the total force. Moreover, the total cell force represent a condition similar to the of a head-down pile from the equivalent depth of the bidirectional cell. Therefore, the buoyant weight is not subtracted from the downward-directed load-movement records. It would be like subtracting it twice as the pore pressure is acting on the level of the cell assembly and excluded from the BD measured value.

Theoretically, the cell load minus the pile buoyant weight versus the upward movement of the upper cell plate is the load-movement response of the pile shaft. The total load in the bidirectional cell versus the downward movement is the load-movement response of the cell bottom plate, that is of the pile toe, if the bidirectional cell would be located at or near the pile toe (strictly, it is the load-movement of the shaft length below the cell level and the pile toe in combination). This advantage of measuring load-movement response of the pile shaft separately from that of the pile toe is not available for a conventional, head-down, static loading test.

Moreover, the measured cell load includes the residual force (if any is present), which is a very important advantage of the bidirectional test over a conventional head-down test. In contrast, when the pile is instrumented with strain gages, the gage values do not register the residual forces; they only show the forces imposed in the pile over and above those already there at the start of the test (See Fig. 8.46 below). When evaluating gage records, therefore, the potential presence of residual force needs to be taken into account in order to establish the true distribution of load in the pile from the gages. (The method of adjusting records for presence of residual force is addressed in Section 8.14). If residual force is present in the pile, it affects the initial shape of the upward and downward load-movement curves, but it does not affect the peak force of the curve, if any.

When the full “pre-existing” load in the pile has been transferred to pressure in the cell, a further increase of pressure expands the cell, that is, the upper plate moves upward and the bottom plate moves downward. The separation of the cell plates result in an opening of a space (a void) in the soil, which introduces tension in the soil near the cell level. Usually, for an cell-assembly located near the pile toe, this has only marginal effect on the response. However, for a cell-assembly located up in the pile, it could affect the shaft shear forces within a small zone above and below the cell and, thus, distort the records of a strain-gage level within that zone because the cell load will not be evenly distributed in the pile immediately above and below the cell location. Therefore, for the strain-gage measurements to accurately represent the average stress distribution, they should be placed no closer than about two pile diameters above and/or below the cell. (N.B., for the same reason, strain gages should not be placed closer to the pile head than about two pile diameters).

[Figure 8.26](#) presents typical results of a bidirectional cell test on a 520-mm diameter, 13 m long, bored pile in silty sand (performed in Brazil as early as 1981). The diagram shows the downward and upward movements of the pile as measured at the location of the bidirectional cell placed 2.0 m above the pile toe.

An additional example of results from a bidirectional cell test is shown in [Figure 8.27](#). The test was carried out on a strain-gage instrumented, 1,200 mm diameter, 40 m long bored pile (Loadtest 2002) for a bridge foundation. The soil profile consisted of about 10 m of clayey silt, on about 15 m of sandy silt deposited at about 25 m depth on dense to very dense sand with gravel. The depth to the groundwater table was 4.0 m. A 540-mm diameter bidirectional cell was placed at 35 m depth, 5 m above the pile toe. The test was terminated at a maximum cell load of about 8,000 kN, when the upward response of the shaft was in an ultimate resistance mode. The maximum upward and downward movements were 100 mm and 60 mm, respectively. The test procedure was a quick test in fourteen increments, each held for 10 minutes. No unloading/reloading cycles that would have disturbed the test were included. The figure shows the measured upward and downward curves for the applied bidirectional-cell loads, including a simulation of the curves (as discussed below) produced by the UniPile software ([www.unisoftGS.com](http://www.unisoftGS.com)).

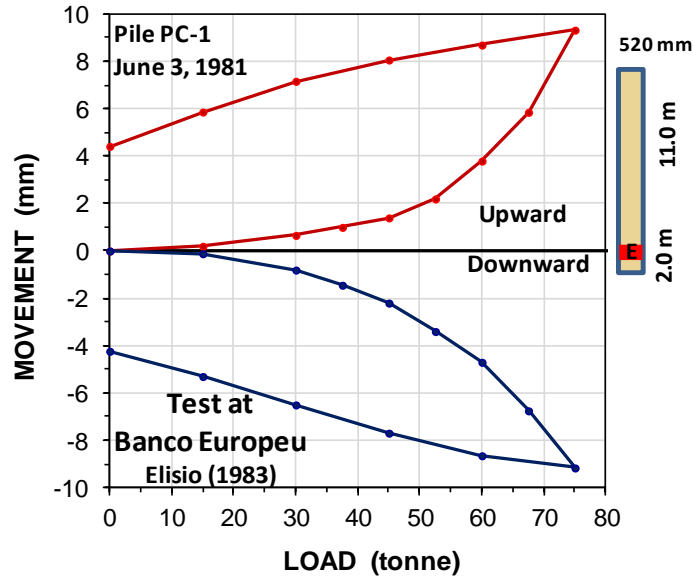


Fig. 8.26 Main results of a bidirectional cell test: Upward and downward load-movements measured in a test on a 520-mm diameter, 13 m long pile (data from Elisio 1983).

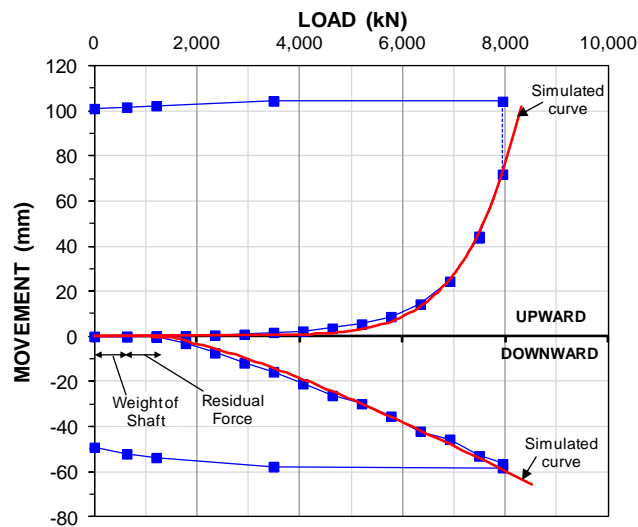


Fig. 8.27 Results of a bidirectional test on a 1,200 mm diameter, 40 m long bored pile.

### 8.7.1 The Equivalent Head-down Load-distribution

The load distributions determined from measured BD loads and the axial forces at the strain-gage levels are plotted in Figure 8.28. The strain-gage instrumentation was at four levels: 9 m, 17 m, 23 m, and 29 m depths. The strain records were used to determine the pile EA-parameter and the load distribution in the pile at the gage levels. The curve to the right starting at 16,000 kN is the **equivalent head-down load-distribution** for the final load applied as obtained by “flipping over”—mirroring—the distribution of the maximum cell load as evaluated from the strain-gage records, thus providing the distribution of an equivalent head-down test encountering the same maximum shaft shear and toe responses as the cell test. The cell loads and the head-down distribution are adjusted for the pile buoyant weight. An effective stress back-calculation of the load distribution at the maximum load was fitted to the equivalent head-down distribution and the fit to a target load chosen as equal to the maximum applied load indicated the beta-coefficients shown to the right. (An effective-stress back-analysis should always be carried out on the results of a static loading test—be it a bidirectional or a conventional head-down test).

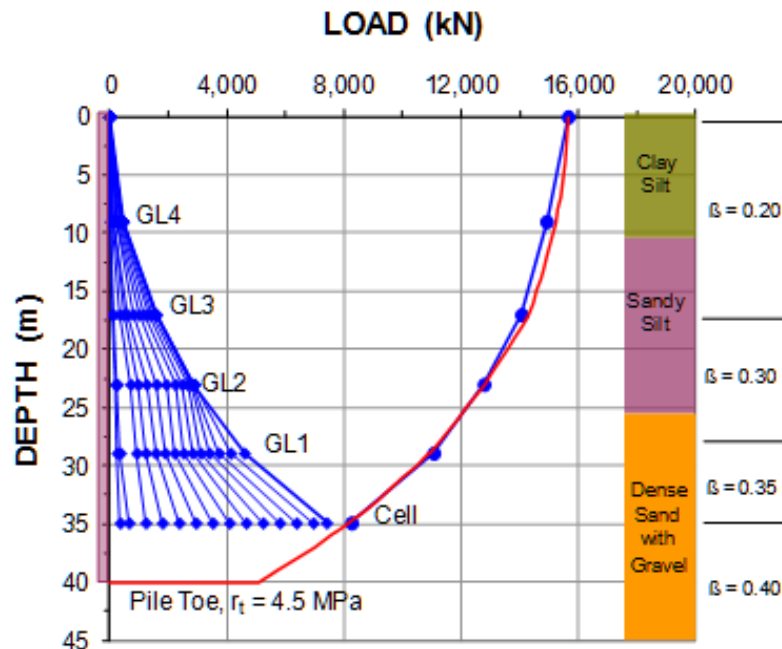


Fig. 8.28 Measured load distribution and the equivalent head-down load-distribution for the last maximum cell load ( $r_t$  = toe resistance).

### 8.7.2 The Equivalent Head-down Loading Test

The results from a bidirectional cell test can also be used to produce an **equivalent head-down load-movement** curve, which can be constructed by adding the upward and downward loads measured for equal movements with adjustment to the larger pile compression obtained in a head-down test, reflecting the fact that, in a head-down test, the pile axial 'elastic' shortening is larger than that measured in a bidirectional cell test. In a head-down test, the loads at the pile toe, below the BD cell assembly, rather, are conveyed through the shaft, compressing it. This method does not consider the fact that the upward load-movement in the bidirectional test “starts” by operating against the larger resistance at depth and engages the smaller resistance at shallow depth toward the end of the test. Therefore, the so-produced equivalent head-down load-movement curve will usually show a stiffer beginning and a softer ending as opposed to the conventional head-down test curves.

Once a fit to the measured upward and downward records is established (c.f., Figure 8.27), the UniPile software can determine the equivalent head-down curves using the so-calibrated soil response. Figure 8.29 shows equivalent pile-head load-movement curve along with the simulated equivalent shaft and toe resistances curves. The equivalent pile-head curve manually produced from the test data is also included. The slight difference between the directly calculated curve and the simulation is due to the fact that the manual method used for constructing the equivalent head-down curve from the test records does not include the effect of the head-down test engaging the upper soil layers before the lower, thus producing a slightly stiffer curve.

Be the test a conventional head-down test or a bidirectional cell test, the conventional capacity evaluation is of little relevance to the pile assessment. However, in contrast to a routine head-down test, the bidirectional test is not limited to just a capacity analysis, but it also supports the far more important analysis of the settlement of the piled foundation. This is because the bidirectional test provides the distribution of resistance along the pile, which is central to determining the settlement of the pile or, rather, that of the structure founded on the piled foundation.

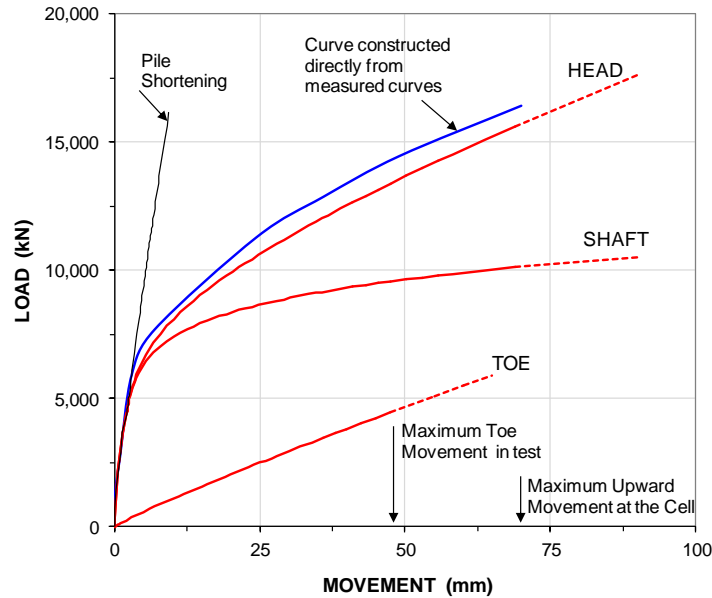


Fig. 8.29 The equivalent pile-head load-movement curves of the bidirectional test.

When, as often is the case, a project involves settlement concerns, the load-distribution curve from a bidirectional test and the pile-toe load-movement relation allow a detailed analysis of the movement response of the pile for the applied load from the supported structure coupled with the effect of the settlement in the surrounding soil.

## 8.8 Residual Force

The load-movement of a pile head consists of three components: the load-movement of the shaft resistance, the compression of the pile, and the load-movement of the pile toe. The combined load-movement components reflect the relative magnitude of the three. Only the shaft resistance may exhibit an ultimate resistance. In contrast, the compression of the soil below the pile toe is a more or less linear response to the applied load and does not have an ultimate value (disregarding a structural failure in case the load would reach the strength of the pile material). The load-movement of the pile toe is also a more or less linear response to the load and has no failure value. Therefore, the concept of an ultimate toe resistance, a toe failure load, or capacity, is really a fallacy; a design based on the ultimate load is a quasi concept of uncertain relevance for the assessment of the suitability of a piled foundation design.

Residual force is an additional factor that can affect an interpretation of pile response based on the shape of the pile head load-movement curve. Figure 8.30 presents the results from a test on a 15 m long, 600 mm diameter, press-in (jacked-in) concrete pile (Fellenius 2014a). The test included measuring the total shaft and the toe resistances versus the movement in a head-down static loading test (all axial force in the pile was assumed zero at the start of the test). The test reached a peak load (6,500 kN) at an about 20-mm movement of the pile head whereafter the continued test response was a plunging mode. The maximum toe movement was 60 mm. Because the pile was installed by jacking ("press-in pile"), a considerable residual force was present in the pile at the start of the static test. At the peak load, the shaft resistance response (as assumed induced in the test) and the load at the pile toe were 5,300 kN and 1,200 kN, respectively. Figure 8.31 shows the load-movement curve that would have been measured had the pile not had any residual force. The Davisson Offset Limit and pile head movement for a 30-mm toe movement are indicated in both figures. Both simulation alternatives are obtained using the UniPile software.

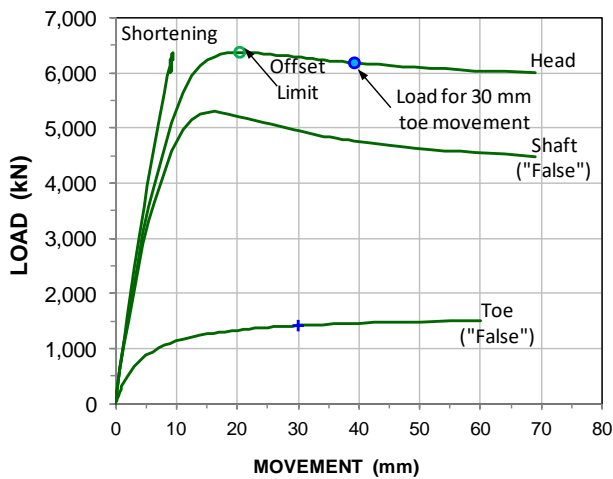


Fig. 8.30. Jacked-in pile with residual force.

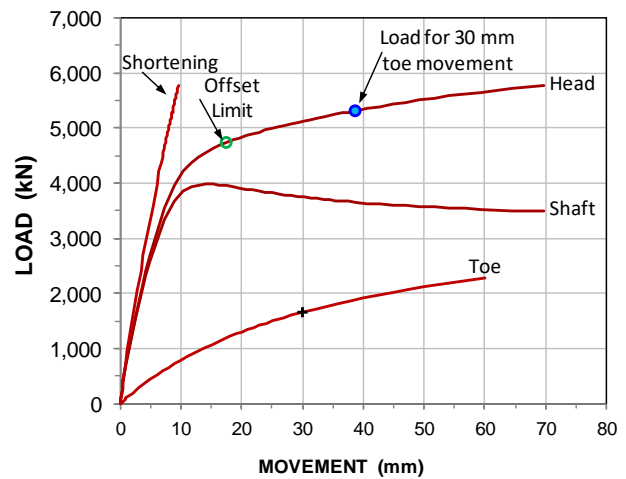


Fig. 8.31. Same pile without residual force.

The larger shaft resistance shown in the left graph is just apparent—indeed "false". The toe resistance measurements do not include the residual toe force, which means that the measured pile toe load-movement is too small and also "false". As mentioned, the graph to the right shows the "true" shaft and toe resistance curves for the pile; "true" meaning "without residual force". Comparing the load-movement curves by any definition of capacity, the residual force has had the effect of producing a load-movement curve that indicates a larger capacity than that found if the residual force had not been present. Obviously, the press-in method of installation produces a stiffer pile than does a pile installed without building in residual force, which is a beneficial effect. However, it may also result in a misleading value of "ultimate" resistance.

Generally, presence of residual force will result in an overestimation of pile capacity, overestimation of shaft resistance, and a corresponding underestimation of the toe resistance. Indeed, the residual force can even cause the records to indicate—falsely so—a tendency for ultimate toe resistance! It is prudent always to consider the possibility that residual force may have affected the test results and, if so, how.

The presence of residual force in a test pile is a quite common situation. Unfortunately, it is often disregarded in test analyses. The literature contains many cases with partial to full loss of shaft resistance in the last about one third to one quarter of the pile embedment similar to the two examples shown in [Figures 8.32 and 8.33](#). Judging from the CPT-diagram in the latter figure, the true shaft resistance would have been expected to instead increase with depth. Many more similar examples exist and I have discussed a few in Fellenius (2002).

[Figure 8.34](#) shows distributions presented in a classic paper (Gregersen et al. 1973), where the axial force present in a driven pile was measured before the start of the test. The graph also shows the "true distribution" and the forces imposed by the test ("false distribution").

It is of course desirable to measure the distribution of axial force present at the start of a test. Unfortunately, this is rarely possible for many reasons, mainly due to lack of understanding of the necessity. However, "the true distribution" can be estimated from the measured "false distribution". The next clause will present the principles of development and consequence of residual force along with comments on how to go from the "false" to the "true".

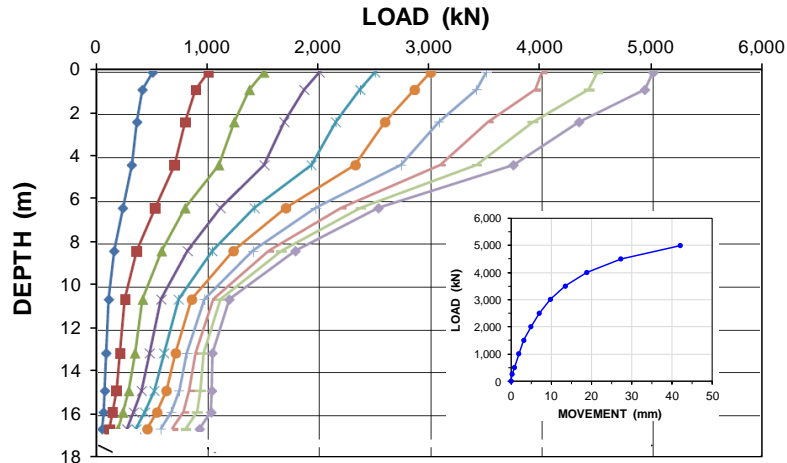


Fig. 8.32. Load distribution for a 620 mm diameter, 16.6 m long screw pile (Burlon 2016).

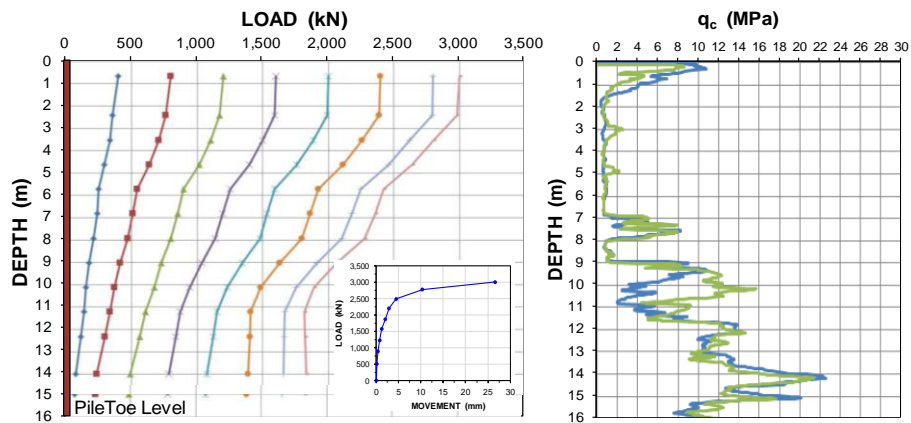


Fig. 8.33. Load distribution for a 510 mm diameter, 16 m driven cast-in-place pile with toe enlarged to 600 mm width (Verstraelen et al. 2016).

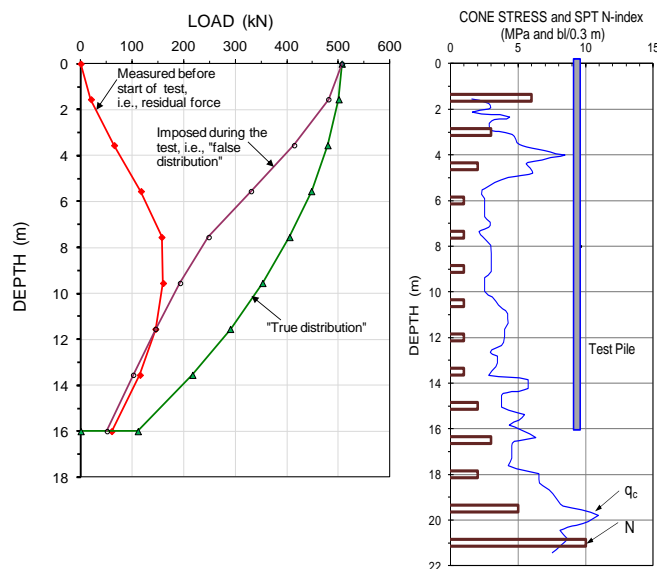


Fig. 8.34. Load distribution for a precast concrete pile driven into sand (Gregersen et al. 1973) with the residual force actually measured.

### 8.8.1 Principles of Development of Residual Force

Residual force develops in principle by the same mechanism as that for a drag force. The term "residual force" is used when the force has developed before the static loading test. The term "drag force" is used when the force develops after construction of the structure supported by piled foundation.

**Above the Equilibrium Plane (E.P.).** Figure 8.35 shows the development of residual force in a test pile due to subsiding soil above the E.P., determined in the analysis of hypothetical test records. The dashed curve shows a true virgin force movement condition for a pile element in the form of a t-z function starting at Point *O* going to Point *A*. In a static loading test, carried out after residual force has developed along Path *OB*, the shear along a pile element will follow Path *BB'A*. An interpreter of the test records (strain-gage data), not realizing the presence of the residual force, will consider the path to be Path *OA'* and arrive at values of shaft resistance much larger than the true value, possibly even twice as large.

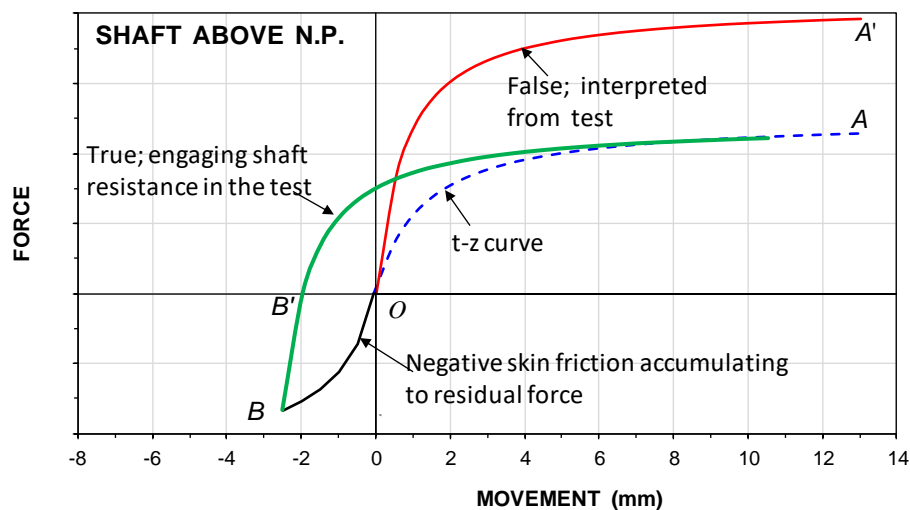


Fig. 8.35. The effect of "false" resistance from downdrag developing before start of a static test.

**Below the Equilibrium Plane (E.P.)** Note, in loading the pile, the residual force is gradually reduced. Before all residual force is overcome (Point *B'*), the strain-gage records will indicate increasing strain—and load—in the pile, while yet some residual force remains in the pile. As shown in Figure 8.36, below the N.P., the residual force has built up along Path *OB*. The loading test introduces a continued loading of the pile along Path *BA*. However, an innocent interpreter would believe the path is along *OA'*, greatly underestimating the resistance—along shaft and at toe.

Figure 8.37 shows the principles for residual force remaining in a pile upon unloading of a driving force that mobilized a toe resistance. The loading impact force causes the pile to move via Path *OC* and, as the pile toe springs back along Path *CB*, it leaves a residual force at Point *B* ("N.P. = E.P."). During the subsequent static loading test (or driving test; CAPWAP), the pile toe is engaged along Path *BCA*. The interpreter will believe that the measured toe response starts at Point *A* and follows Path *OA'* (maybe also notice that the toe force is rather small). The residual toe force is countered by a negative direction shear force along the pile elements above the pile toe and the effect on the static loading test records is then similar to that shown in Figure 8.36, above. *The same conditions apply to the force remaining in a pile after implementing unloading as a part of an unloading-reloading schedule.*



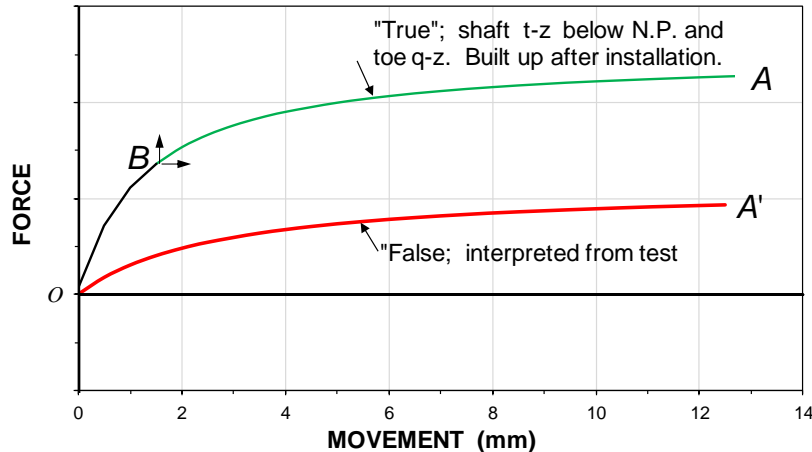


Fig. 8.36. Pre-loading by residual force along the lower length of the pile and pre-loading of the pile toe.

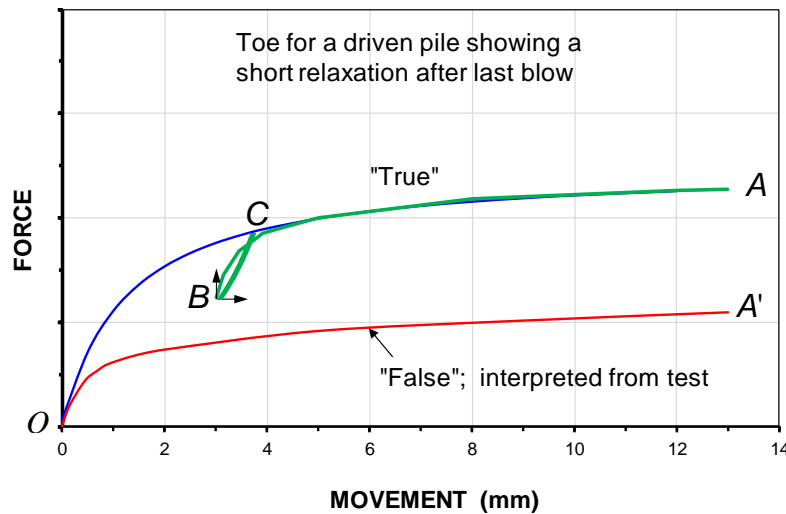


Fig. 8.37. Residual force at the pile toe in case of a driven pile.

### 8.8.2 Residual Force in an Instrumented Pile

Before a static loading test is started on an instrumented pile, the no-load gage reading may change with time and there will be axial force present in the pile in addition to the own weight of the pile. For example, the concrete in a concreted pipe pile or a precast pile is affected by aging and time-dependent changes. In case of a prestressed pile, some change of the zero strain introduced by the release of the strands continues for days after their release. For a bored pile, the value of “zero strain” is not that clearly defined in the first place—is the “zero” before concreting or immediately after, or, perhaps, at a specific time later? In fact, the “zero reading” of a gage is not one value but several, and all need to be included in the engineering report of the test (and considered in the evaluation of the test results). Then, soil reconsolidating after the disturbance caused by the construction can imposed axial force, called residual force. Frequently, on-going general subsidence will have imposed drag force in a pile between construction and testing that will affect the strain in the pile and possibly not be noted in the gage records. (the forces due to swelling of concrete causing strain might be compensated by compression due to drag force, for example). To enable an assessment of potential residual force affecting the evaluated load distribution, gage records should be taken immediately before (and after) every event of the piling work and not just during the actual loading test.

The evaluation of the gage records is greatly assisted if the test on the instrumented pile is a bidirectional cell test, as this test method provides the load-response independently of residual force. In contrast, a conventional "head-down" static loading tests does not measure—account for—the residual force. Be the test bidirectional or head-down instrumented, the change of strain measured at the gage locations does not provide information on residual force—not directly, that is.

For a strain-gage instrumented **bored** pile, there are three series of key readings to obtain and document in the test report in addition to the readings during the actual test. The first series is the reading of all gages before and immediately after placing the gages in the test pile (reinforcing cage). The second series comprises the readings taken before and after placing concrete in the test pile and during the hydration process and spread out during the set-up wait period. The third series, which includes telltale readings, is that taken immediately before starting the test (adding any pressure to the cell) usually termed the "zero" reading.

For a **driven prestressed concrete pile**, the first reading is the reading taken immediately before placing the gages in the casting forms. Second is the reading after the release of the strands and removal of the piles from the form. Third is the reading before placing the pile in the leads to start driving. Fourth is the reading immediately after completion of driving. Fifth is the "zero"-reading immediately before starting the test.

### 8.8.3 "False" and "True" Load Distributions and Determining Distribution of Residual Force

The "true" force distribution response to an applied load is difficult to find and it cannot be determined exactly from the test records. However, if the "false" distribution is well ascertained by measurements, the back-and-forth trial-and error approach illustrated in Figure 8.38 will produce a fair representation of the true distribution. N.B., for the particular force distribution addressed. Each force distribution will engage a slightly different portion of the residual force.

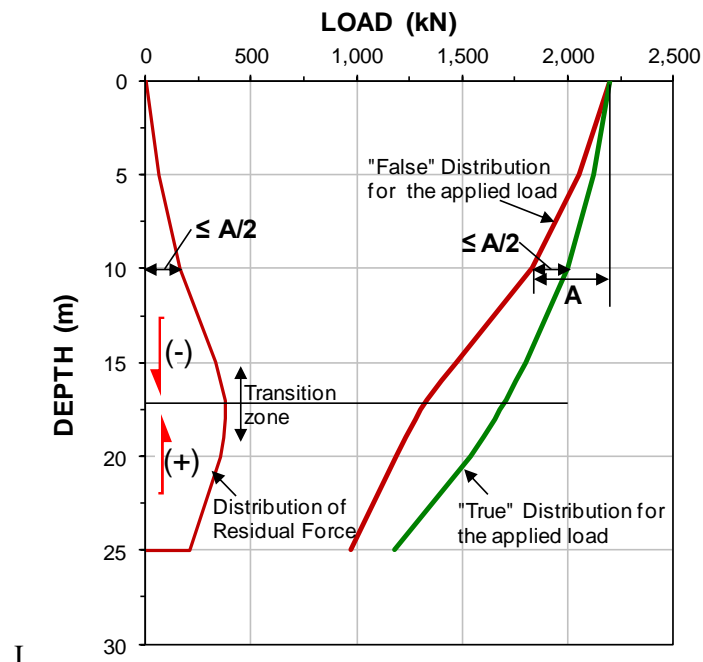


Fig. 8.38. Procedure for estimating distribution of residual force and "true" resistance.

If residual force is present and for what length of pile is not known, of course. If suspected, the assumption is made that the shaft resistance ( $A$ ) at one point along the upper length of the pile is "false" and it includes the effect of "true" shaft resistance plus residual force. The residual force (also plotted

separately near the ordinate) can be as large as half the "true" shaft resistance—if fully mobilized resistance—smaller if not fully mobilized (it can never be larger). However if the so-determined distribution is extended down the soil, it will be soon be obvious that the negative skin friction that accumulates to the residual force must start to diminish and, at some depth, change to positive shaft resistance. This requires the "true" distribution curve to be adjusted accordingly, while recognizing that the interacting curves must not show kinks or sudden or reversed changes. Near the pile toe, the slope of the residual force distribution cannot be less steep (be flatter) than the "true" distribution and it cannot show less than zero force. The slopes are equal if the residual force in this zone is due to fully mobilized shaft resistance. In the latter case, the "false" distribution curve becomes vertical (c.f., Figures 8.32 and 8.32). The procedure includes judgment and two persons are not likely to arrive at identical solutions.

Figure 8.39 shows an example of analysis results from a static loading test on a 457-mm diameter continuous flight auger pile, CFA-pile, drilled in one continuous operation to 22.7 m embedment (Jacobs and Fellenius 2022) at a site with an ongoing general subsidence. The  $q_c$ -diagram shows that the measured force distributions must be "false" when compared to the  $q_c$ - and N-index distribution also shown in the figure. The "true" distribution, on the other hand, agrees well with the latter. The rules for the analysis, mentioned above, leave little room for an other than shown realistic "true" distribution. For example, while a zero toe residual force would abide by the rules, it would be illogical to have a residual shaft resistance, but no residual toe resistance. Similarly, it would be unlikely that the residual force would be equal to the fully mobilized shaft resistance all along the pile. A transition zone starting somewhere below SG-5 is more likely.

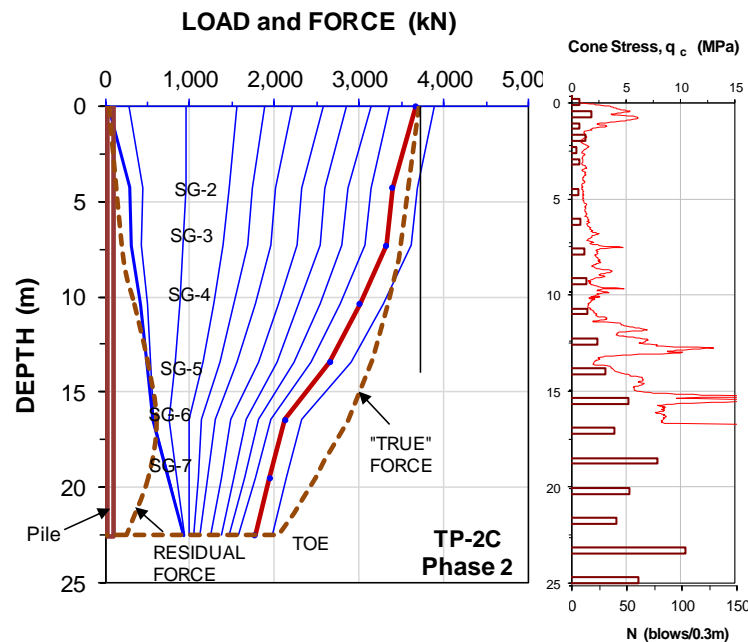


Fig. 8.39 "False" and "true" force distributions for an instrumented CFA pile.

### 8.8.3 Case history of Residual Force and Other Influences

Strains may develop that have no connection to the average axial strain in a pile caused by applying load to the pile. An example of this is the elongation of the reinforcing bars (with strain gage attached) due to the temperature rise at the outset of the grouting of a pile shown in Figure 8.40: measurements of temperature and strain during the 5 first days after the driving and grouting. The records are from a strain-gage instrumented 600 mm diameter, 35 m long spun-pile driven through clay and silt into sand at Myeonji site near Busan, Korea. The about 300 mm annulus was grouted after the driving (Fellenius et al. 2009).

Over the initial about 12 h of increasing temperature from the hydration, the peak temperature reached almost boiling point. The thermal elongation of the bars was partially prevented by the grout, resulting in an imposing significant of stress (negative strain) in the bars. When the pile started to cool after having reached the peak temperature, the records indicated a reversal of the strain to tension, as also caused by the grout partially preventing the shortening of the gage bar. After about three days of cooling, the further strain change was small because further change of temperature was small. The gages now indicated a net tension which does not correspond to any development of shear forces along the pile. (The vibrating wire gages are practically insensitive the temperature change). The evaluation of the gage records included correction for difference in thermal coefficient between the grout/concrete and the steel by applying the known difference in thermal coefficient. However, before the grout/concrete fully interacted with the steel, the two materials were partially able to elongate/shorten independently, which effect was not reversed in the following cooling phase because the bars and the concrete now interacted through the bond steel to concrete.

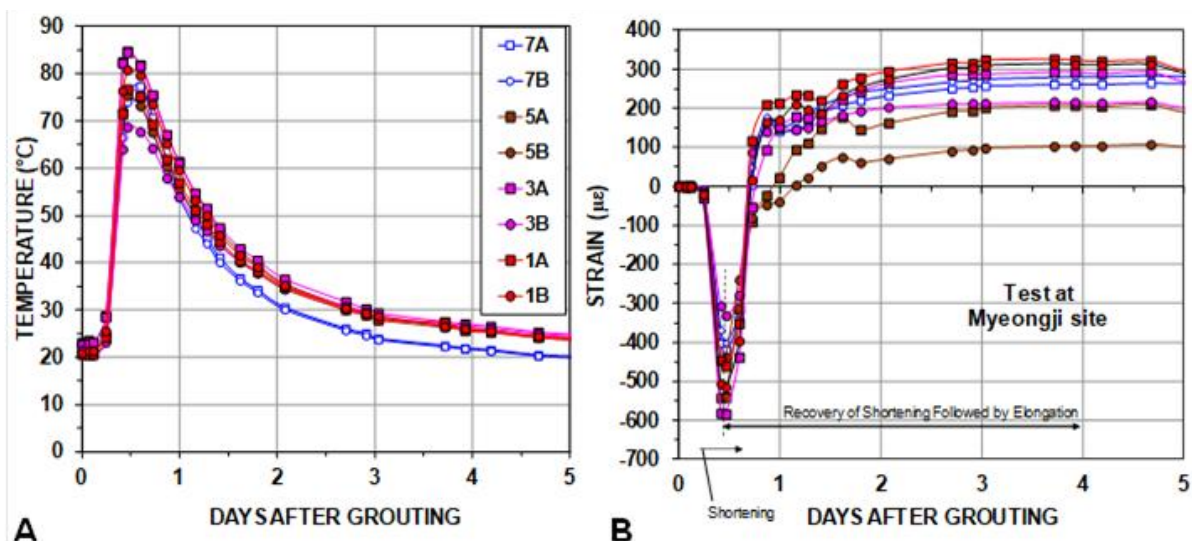


Fig. 8.40 Development of temperature and strain in a 35 m long spun-pile pile during first 5 days after grouting (reducing strain indicates compression/shortening) (Fellenius et al. 2009).

Figure 8.41 shows that after about 5 to 10 days, the temperature of the gages, but for the gage pair nearest the ground surface (SG7A and 7B) had reached a near constant value, the soil temperature (which is the average annual temperature of the ground at a site). However, but for the SG7 gage pair, the strain in the pile continued to decrease over the next about 40 days. As discussed by Fellenius et al. (2009) and Kim et al. (2011), the pile is affected by build-up of residual force creating compression in the pile and swelling due to absorption of water from the ground creating tension strain. Near the ground surface, the build-up is small and the strain change is almost entirely caused by swelling.

#### 8.8.4 Case history on calculation true load distribution

The following is an example for determining the distribution of residual force. The pile was a 235 mm side square precast concrete pile driven 19 m into a sand deposit (Axelsson 2000). The distribution is from a CAPWAP analysis of dynamic test results (See Chapter 9).

Figure 8.42A shows a cone stress,  $q_t$ , diagram from a CPTU sounding close to the test pile. The sand is loose to compact. Figure 8.42B shows the CAPWAP-determined load distribution for the first blow of restrike on the pile 216 days after initial driving. The load distribution graphs indicates that the unit shaft resistance reduces with depth, which does not agree with the increasing cone resistance and effective stress.

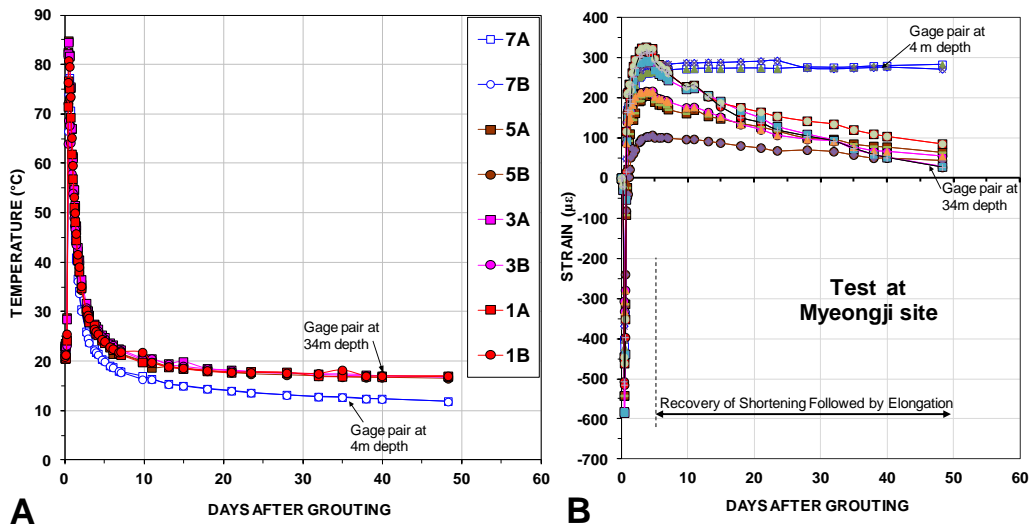


Fig. 8.41 Development of temperature and strain in a 35 m long spun-pile during 50 days after grouting the interior void (Fellenius et al. 2009).

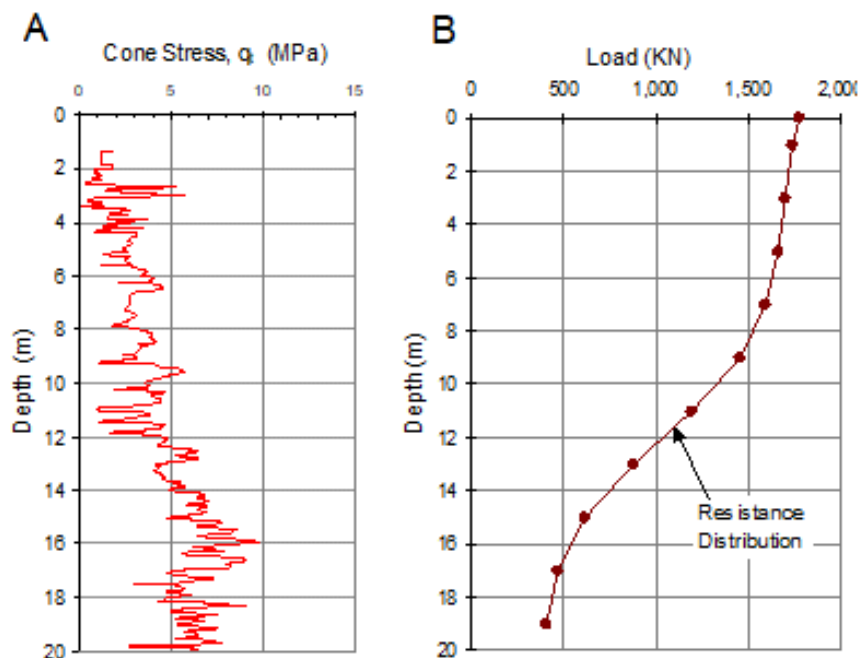


Fig. 8.42 A: CPT profile. B: CAPWAP determined load-distribution.

As described in Chapter 9, CAPWAP analysis makes use of strain and acceleration measured for an impact with a pile driving hammer. The analysis delivers amongst other results the static resistance mobilized by the impact. In the calculation, the pile is simulated as a series of many short elements and the results are presented element per element, as had measurements been made at many equally spaced gage levels along the pile. The CAPWAP program allows an adjustment of the wave-trace matching for locked-in load due to the immediately preceding impact, but it does not include the effect of the pile being subjected to residual force before driving. Therefore, the CAPWAP analysis results are equally distorted by presence of residual force as are the results of the strain-gage measurements in a static loading test on an instrumented pile.

Determining the distribution of residual force and adjusting the load distribution from “false” to “true” is an action simple in principle. Figures 8.43 and 8.44 indicate the procedure, which builds on the assumption that at and near the ground surface, the residual force is the result of fully mobilized negative skin friction that deeper down changes to partially mobilized and, then, at the neutral plane, switches over to partially mobilized positive shaft resistance and, perhaps, near the pile toe, to fully mobilized positive shaft resistance. If this sounds similar to the development of drag force and a neutral plane in a pile, it is because the two phenomena are essentially one-and-the-same. When the subject is the load locked-in in a pile just before the start of a static loading test, the term is “residual force”. When the subject is the long-term distribution after a structure has been built, the term is “drag force”.

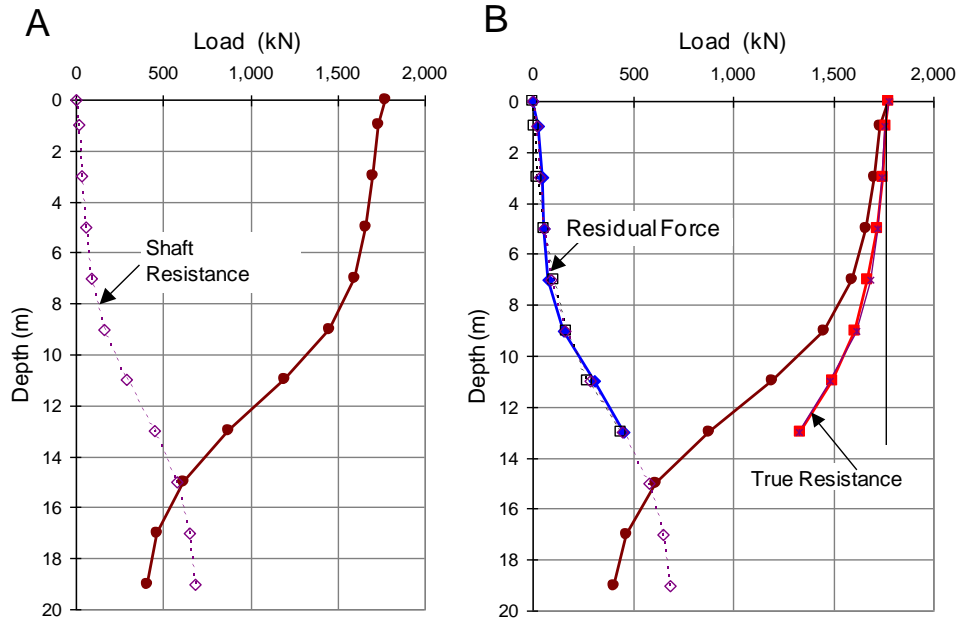


Fig. 8.43 Procedure for determining the distribution of residual force and “true” resistance.

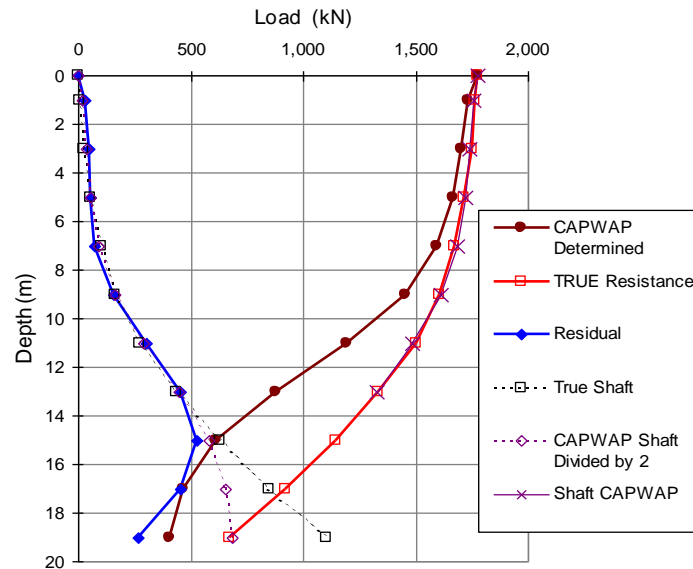


Fig. 8.44 Final results: Measured load, residual force, and true resistance.

The CAPWAP determined ultimate resistance is 1,770 kN. The total shaft resistance is 1,360 kN and the toe resistance is 410 kN. The CAPWAP distribution has an “S-shape indicating that the unit shaft resistance increases with depth to a depth of about 13 m. However, below this depth, the distribution curve indicates that the unit shaft resistance is progressively becoming smaller with depth. From a depth of about 15 m, the unit shaft resistance is very small. This distribution is not consistent with the soil profile established by the CPT sounding. Instead, the resistance distribution is consistent with a pile subjected to residual force. Because the soil is relatively homogeneous—an important condition—the data can be used to determine the distribution of residual force as well as the resistance distribution unaffected by the residual force, the “true” ultimate resistance.

The analysis procedure is based on the assumption that the negative skin friction is fully mobilized and equal to the positive shaft resistance mobilized by the impact (“applied test load”). Thus, where the residual force is built up from fully mobilized negative skin friction, the “true” shaft resistance (positive or negative direction of shear) is half of that determined directly from the test data. Fig. 8.44 demonstrates the procedure. A curve has been added that shows half the CAPWAP determined shaft resistance: Starting at the ground surface and to a depth of 13 m, the curvature increases progressively. To this depth, it represents the distribution of the residual force and, also, of the true shaft resistance. The progressive increase indicates proportionally to the effective overburden stress. A back-calculation of the shaft resistance shows that the beta-coefficient (the proportionality factor in the effective stress analysis) is about 0.6.

Below the 13-m depth, however, the “half-curve” bends off. The depth is where the transition from negative skin friction to positive toe resistance starts and the assumption of fully mobilized negative skin friction is no longer valid. To extend the residual-force distribution curve beyond the 13 m depth, one has to resort to the assumption that the beta-coefficient found in the upper soil layers applies also to the soil layers below 13 m depth and calculate the continuation of the true resistance distribution. The continuation of the distribution of the residual force is then obtained as the difference between the true resistance and the CAPWAP determined distribution. The results of this calculation show that the residual pile toe force was about 230 kN, which means that the test toe load of 410 kN in reality was 640 kN.

The objective of the analysis procedure is to obtain a more representative distribution of resistance for the test pile. The CAPWAP determined resistance distribution misrepresents the condition unless the distribution is corrected for residual force. The corrected shaft and toe resistances are about 1,100 kN and 640 kN as opposed the direct values of 1,360 kN and 410 kN. In the example, the long wait time between end-of-driving, EOD and beginning-of-restrike, BOR, is probably the reason for the obvious presence of residual force.

Figure 8.45 shows the distribution unit residual force in a fictional static loading test on an instrumented test pile. A residual force is assumed to be present and amount to 80 % of the fully mobilized shear force. The figure shows the consequence for the distribution of load in the pile. It is obvious that were the presence of residual force not recognized, the load distribution evaluated from the six strain-gage records and, notably, the toe resistance, would be quite erroneous.

Also the load records from an instrumented bidirectional test are affected by presence of residual force, as illustrated in Figure 8.46. If the residual force distribution has a transition from negative to positive shear force above the level of the bidirectional cell assembly and a strain-gage level is located in that zone, then, that force between it and the next gage level would only seemingly agree. Note, the load distribution indicated by the VW gages imply a considerable difference in shaft resistance between the lower VW gages, leading an interpreter to reject the VW data.

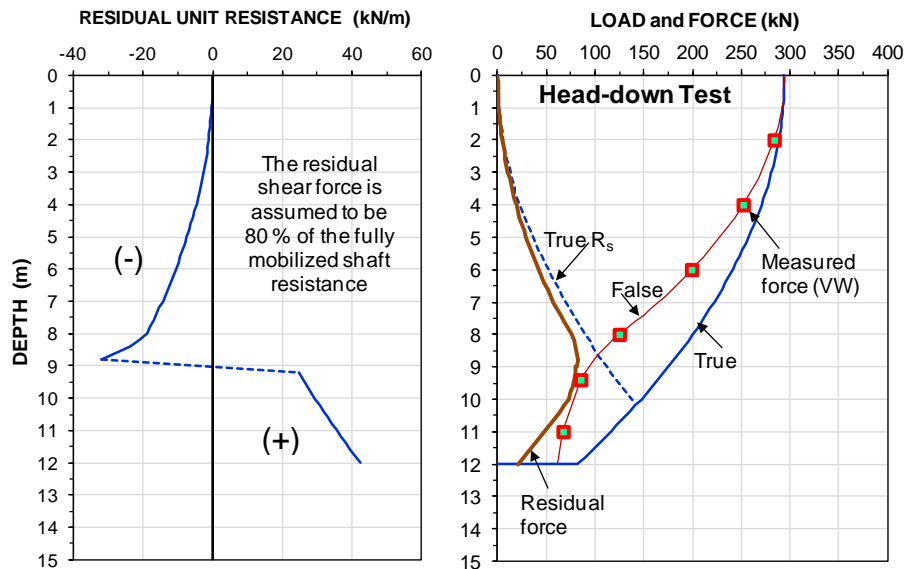


Fig. 8.45 Comparison of measured load values in a pile affected by residual force as opposed to true load-distributions for a conventional head-down test.

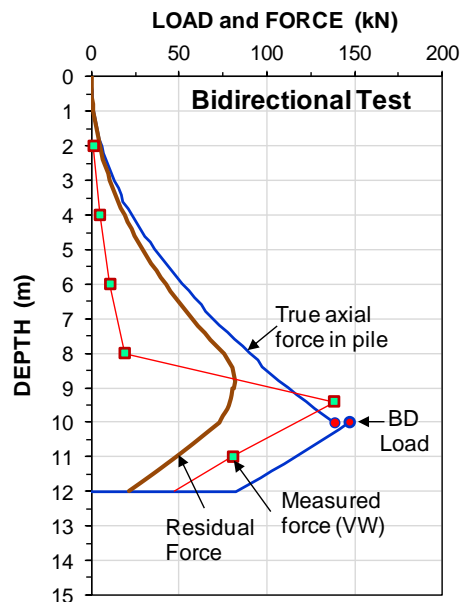


Fig. 8.46 Results of the same pile subjected to a simulated bidirectional test.

However, most piles will to a larger or smaller extent be affected by residual force, that is, most load distributions evaluated from a static loading test will show presence of residual force. If the pile is a bored pile tested relatively soon after its construction, the amount residual force is often found to be insignificant, even negligible. For driven piles, residual force is a common occurrence, however.

Presence of residual force may lead to misinterpretation of the strain records and load calculation, as well as inaccurate determination of the axial stiffness. It is important to note that the load applied by the bidirectional cell is independent of presence of residual force and its load takes precedence over any determination of load from the strain-gage records. The inescapable conclusion is that, if conditions are suitable for a bidirectional test, performing a bidirectional test is always preferable to the uncertainties of performing a conventional head-down test.



## 8.9 Modulus of ‘Elasticity’ and Axial Stiffness of the Instrumented Pile

### 8.9.1 Aspects to consider

In arranging for instrumentation of a pile, several aspects must be considered. The gages must be symmetrically placed pairs to eliminate influence of bending moment. If the gages are installed in a concrete pile, a key point is how to ensure that the gages survive the installation—a strain-gage often finds the visit from a vibrator a most traumatic experience, for example. We need the assistance of specialists for this work. The survival of gage cables during the installation of the pile is no less important. Therefore, the knowledge and interested participation and collaboration of the piling contractor, more precisely, the field crew, is vital.

Once the gages have survived the pile manufacture and installation—or most of the gages, a certain redundancy is advised—the test can proceed and all should be well. That is, provided the participation of a specialist is ensured, who has experience in arranging the data acquisition system for recording the measurement. However, the geotechnical engineer then often relaxes in the false security of having all these knowledgeable friends to rely on and fails to realize that the reason for why the friends do not interfere with the testing programme and testing method is not that they trust the geotechnical engineer’s superior knowledge, but because advising on the test programme and method is not their mandate.

I cannot emphasize enough that the information obtained from a static loading test on an instrumented pile is distorted by unloading events, uneven load-level durations, and/or uneven magnitude of load increments. Therefore, a static loading test for determining load transfer should be carried through in one continuous direction of movement and load without disruptions or unloading. Moreover, all load increments levels should be equal and all load levels should be kept an equal length of time—an occasional extended load holding will adversely affect the interpretation of the results while providing nothing useful in return.

So, once all the thoughts, know-how, planning, and hands-on have gone into the testing and the test data are secured, the rest is straightforward, is it not? No, this is where the fun starts. This step is where strain is converted to force, a detail that is surprisingly often treated rather cavalierly in the test data evaluation.

### 8.9.2 Converting strain to load using the pile stiffness

Pile instrumentation means placing strain gages at selected depths in a pile. As indicated by the term, the gages provide values of strain, not load or force, which difference many think is trivial. Force is just strain multiplied by the area and the elastic modulus of the pile material and the forces are linearly proportional to the measured strains by the elastic modulus, right? Thus, the measured strains are transferred to force by use of the modulus of the pile material and of the pile cross sectional area. For steel piles, this is normally no problem and, for bored piles, precast concrete piles, prestressed concrete piles, and concreted pipe piles, the modulus is a combined modulus of the steel and concrete, normally proportional to area and modulus, as shown in Eq. 8.23.

$$(Eq. 8.23) \quad E_{comb} = \frac{E_s A_s + E_c A_c}{A_s + A_c}$$

where

- $E_{comb}$  = combined modulus
- $E_s$  = modulus for steel
- $A_s$  = area of steel
- $E_c$  = modulus for concrete
- $A_c$  = area of concrete

The modulus of steel is known accurately as it is a constant value ( $29.5 \times 10^6$  ksi or 205 GPa). However, the E-modulus of H-piles and 'reject' pipes of Grades B and C are considered to have of 240 and 270 GPa, respectively. In contrast, not only does the concrete modulus range widely, the concrete modulus is also a function of the applied stress or strain. Common relations for its calculation, such as the relation between

the modulus and the cylinder strength or unit weight, e.g., as proposed by the American Concrete Institute ACI 318-14 Manual:  $E_{\text{concrete}} = 57,000\sqrt{f_c}$  (psi) or  $E_{\text{concrete}} = 4,700\sqrt{\sigma_{\text{strength}}}$  (MPa) are not particularly reliable and should not be used to indicate a numerical value for an E-modulus to use in converting the measured strain to stress. The formulas main usefulness is limited to indicate that E-modulus is about proportional to concrete strength.

A steel pile is only an all-steel pile in driving—during the test, it is often a concrete-filled steel pipe. The modulus to use in determining the load is the combined value of the steel and concrete modulus (Eq. 8.23). By the way, for the modulus to represent the concrete in a concrete-filled steel pipe, would you choose the modulus for unconfined or the confined condition (see Section 3.3 and Eq. 3.2)?

Were the records from loading a free-standing pile (like a column), the slope of a plot of applied load versus strain would indeed represent the stiffness of the column. In contrast to a column, however, in a pile, the axial force with depth is not constant, but diminishes due to the shaft resistance along the pile over the distance from the load application (at the pile head or at the bidirectional cell). Therefore, before the shaft resistance is fully mobilized, the slope of the load-versus-strain curve measured at a gage level is steeper than that of its equivalent column, i.e., the apparent stiffness is larger than the true stiffness of the pile. Once the shaft resistance is fully mobilized and, **if** then the continued response is plastic, the slope of the curve is equal to the true stiffness of the pile. However, if the continued shaft resistance would be strain-hardening, the slope would still show a slope that is steeper than true, and, if the continued shaft resistance would be strain-softening, the slope would indicate a slope that is smaller than the true, (i.e., larger and smaller stiffness, respectively).

Moreover, the elastic modulus of concrete is not a constant, but a function of the amount of imposed load, or better stated, of the imposed strain, reducing with increasing stress or strain. This means that when load is applied to a pile or a column, the load-movement follows a curve, not a straight line. Over the large stress range imposed during a static loading test, the difference between the initial and the final moduli for a concrete pile can be substantial. Approximating the load-strain curve to a straight line may introduce significant error in the load evaluation from the strain measurement. However, the stress-strain curve can with sufficient accuracy be assumed to follow a second-degree line:  $y = ax^2 + bx + c$ , where  $y$  is stress and  $x$  is strain (Fellenius 1989). The trick is to determine the integration constants "a" and "b" ("c" is zero)—and to find out whether or not the soil response is other than plastic.

The load can be calculated from the strain records by multiplying the measured strain with the pile material stiffness,  $EA/L$  ( $E$ -modulus, area  $A$ , and unit length  $L$  (usually taken as 1 metre). The pile stiffness or, rather, the  $EA$ -parameter, can be determined directly from the load-strain data, provided that the records are obtained at a calibration gage located near the pile head so they are unaffected by shaft resistance. As the calibration gage is unaffected by shaft resistance, the  $EA$ -parameter can be determined from linear regression of the load divided by the strain,  $Q/\epsilon$ , plotted versus vs. the strain (the "secant  $EA$ -parameter") or linear regression of the change of load divided by change of strain,  $\Delta Q/\Delta\epsilon$ , plotted versus vs. the strain (the "tangent  $EA$ -parameter"). The latter is a differentiation method and, as such, affected by small error or imprecision of the records. [Figures 8.47A and 8.47B](#) show secant and tangent  $EA$ -parameters from a static loading test on a 1.83 m diameter, open toe, strain-gage instrumented, driven, steel pipe pile with a 38 mm thick wall (Bradshaw et al. 2012). The pile was not concreted. The uppermost strain-gage level was 1.8 m (1.0 pile diameter) below the pile head and 1.2 m below the ground surface. It is important that the calibration gage is from a level essentially unaffected by shaft resistance. The static loading test was a quick test with 23 equal increments of 1,100 kN applied every 10 minutes to a maximum load of 25,500 kN, when bearing failure developed. The loads were measured with a separate load cell. As should be the case, the  $EA$ -parameter of the steel pile is constant. (The area of steel,  $A$ , was not precisely known, but it can, if desired, now be established by the linear-regression back-calculation).

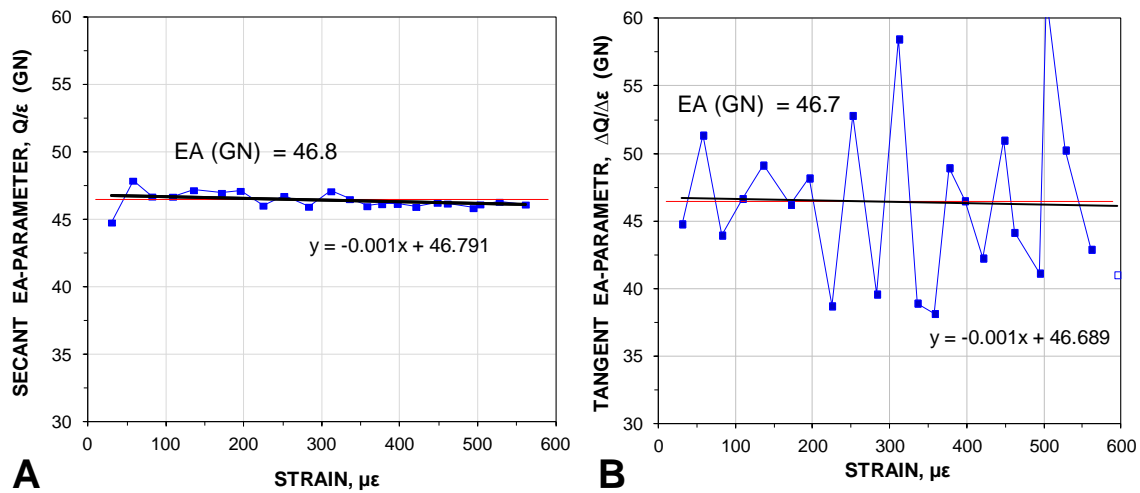


Fig. 8.47 Stiffness vs. measured strain for a not-concreted steel pipe pile (Fellenius 2012).

For a concreted pipe pile or for a concrete pile—driven or bored—the load-strain relation is normally linear, but, as mentioned, concrete is sometimes strain-dependent, as illustrated in Figure 8.48, showing the near-pile-head gage level records of a head-down test on a 600-mm diameter spun pile driven in Pusan, Korea (Kim et al. 2011). The load-strain line is not linear, but slightly curved, that is, the stiffness of the pile is strain-dependent and diminishes with increasing strain. The slope of the load-strain line from the origin to  $Q = 7,200$  kN represents the average secant stiffness of the pile, or EA-parameter.

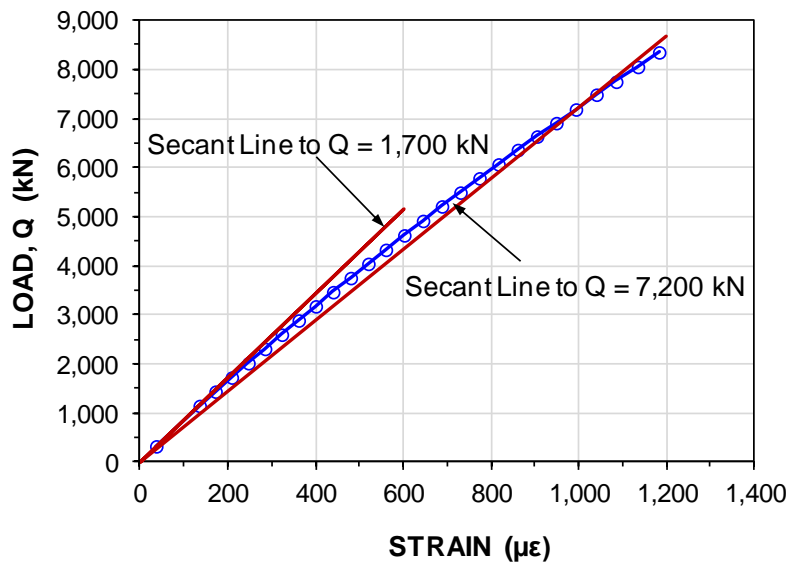


Fig. 8.48 Load vs. strain for gage records close to the pile head for the spun pile.

To better discern the actual EA-value at a specific load-strain point, Figure 8.49 shows the load divided by the measured strain,  $Q/\epsilon$  vs. strain. The EA-parameter is a secant function of strain,  $E_s A = a\epsilon + b$ , with "a" being the slope of the line and "b" the ordinate intercept. The relation shows that over a range of 1,000  $m\epsilon$ , the EA-value reduced by about 15 %.

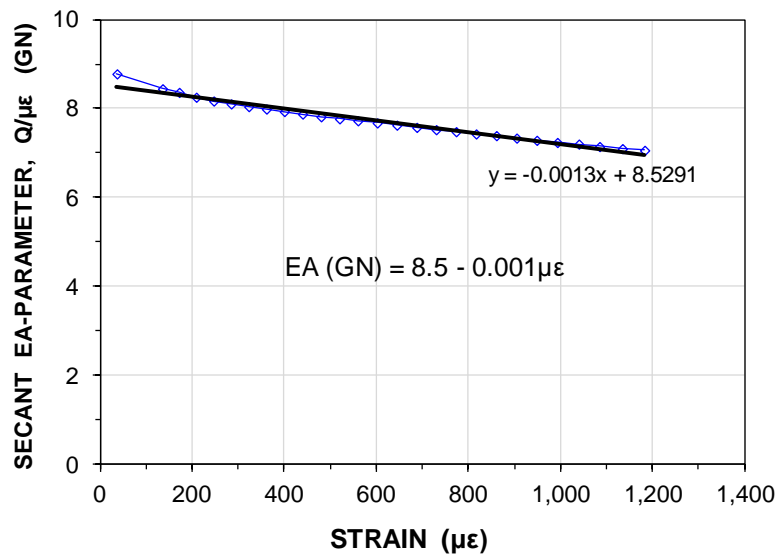


Fig. 8.49 Near pile-head gage level secant stiffness vs. measured strain for the spun-pile.

Note, important conditions for the direct secant method to be applicable is that the zero reference for load is correct, the pile has essentially no shaft resistance between the jack and the gage level, the pile has negligible locked-in (residual) strains from a previous loading/unloading, and the test is performed with equal size load increments, equal load-holding durations, without any unloading-reloading sequences. Unfortunately, not many tests are carried out with these conditions satisfied.

The straight-line response is not always immediately apparent because the "zero"-reference of the records (load and/or strain) may not have been accurately known. This is illustrated in [Figure 8.50](#), which is from a head-down static loading test on a 900-mm diameter bored pile installed in Jakarta, Indonesia. The gage level was from the gage level nearest the pile head, about 1.5 m below the ground surface. The secant stiffness trend was not fully established for the first couple of values. This is because in the beginning of a test, the zero reference for strain might be uncertain. An adjustment—"correction"—of a mere  $8 \mu\epsilon$  added to all strain records removed the initially curved portion of the secant line and established the secant line. Note that the adjustment of the stiffness is in regard to the zero condition stiffness reference and applies equally to all strain records. "Correcting" individual strain records for, say, residual strain for a gage level affected by shaft resistance, is akin to falsifying data.

### 8.9.3 The tangent method

An error in the initial (the "zero") reference of strain when applying the direct secant method can be overcome by instead determining the tangent EA-parameter (incremental parameter). The construction of the tangent value (change of load over change of strain vs. strain) is similar to that of the secant value (change of load over strain vs. strain). The tangent modulus of a pile, if a straight line, can be used to establish the expression for the secant elastic modulus line allowing for converting every measured strain value to stress and force via its corresponding strain-dependent secant modulus. For a pile taken as a free-standing column (case of no shaft resistance), the tangent value is a straight line, which, for a pile composed of a material with reducing E-modulus, slopes from an initial value toward smaller values with increasing strain. The tangent modulus can directly be converted to the secant modulus by the fact that the slope of the tangent modulus is twice that of the secant modulus. Thus, every measured strain value can be converted to stress via its corresponding strain-dependent, so-determined, secant stiffness.

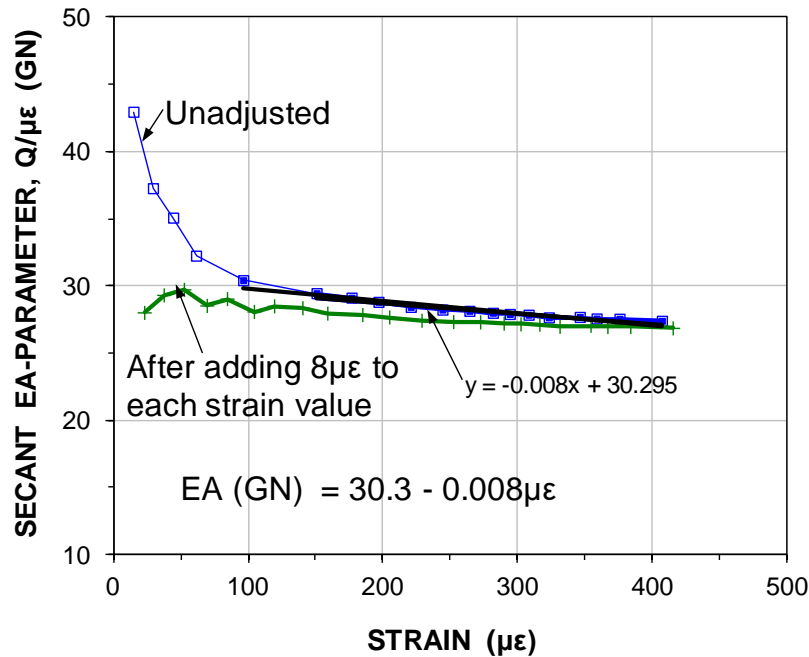


Fig. 8.50 Secant stiffness ( $Q/\mu\epsilon$ ) vs. measured strain for a 900-mm bored pile (data from GeoOptima 2011).

To numerically convert a tangent stiffness relation to a secant stiffness relation is simple. Eqs. 8.24 - 8.27 show the interrelations of  $E_t$  and  $E_s$ . (The following presents the mathematics without the pile cross section area,  $A$ ).

The equation for the tangent modulus,  $E_t$ :

$$(Eq. 8.24) \quad E_t = \left( \frac{d\sigma}{d\epsilon} \right) = a\epsilon + b$$

which can be integrated to provide a relation for stress as a function of the strain:

$$(Eq. 8.25) \quad \sigma = \left( \frac{a}{2} \right) \epsilon^2 + b\epsilon$$

Eq. 8.26 indicates stress as a function of secant modulus and strain

$$(Eq. 8.26) \quad \sigma = E_s \epsilon$$

Combining Eqs. 8.25 and 8.26:

$$(Eq. 8.27) \quad \sigma = E_s \epsilon = 0.5a\epsilon^2 + b\epsilon \implies E_s = 0.5a\epsilon + b$$

where

- $E_t$  = tangent modulus of composite pile material. [N.B., the proper term for this modulus is really "chord" rather than "tangent". However, if the two points are very close, the chord and tangent modulus can be considered equal. In actual tests, they are not, but I have kept using the term "tangent", because shifting to "chord" would be "over-academic"].
- $E_s$  = secant modulus of composite pile material
- $E_t$  = tangent modulus of composite pile material ( $E_t = a \varepsilon + b$ )
- $\sigma$  = stress (load divided by cross section area)
- $d\sigma$  =  $(\sigma_{n+1} - \sigma_n)$  = change of stress from one load increment to the next
- $a$  = slope of the tangent modulus line
- $\varepsilon$  = measured strain (always measured in units of microstrain,  $\mu\varepsilon$ ;  $\mu = 10^{-6}$ ).
- $d\varepsilon$  =  $(\varepsilon_{n+1} - \varepsilon_n)$  = change of strain from one load increment to the next
- $b$  = y-intercept of the tangent modulus line (i.e., initial tangent modulus)

For a gage located near the pile head (in particular, if above the ground surface, the tangent modulus calculated for each increment is unaffected by shaft resistance and it is the true modulus. For gage records from further down the pile, the first load increments reaching the gage levels are substantially reduced by shaft resistance along the pile above the gage location and the induced strain does not permit determining a modulus value. However, in contrast to the direct secant method, the tangent stiffness method is applicable also to the records affected by shaft resistance between the applied load (jack on the pile head or bidirectional cell). Initially, therefore, the tangent modulus values will be large, but as the shaft resistance is mobilized down the pile, the strain increments become larger and, therefore, the calculated modulus values become smaller. When all shaft resistance above a gage level is mobilized and if the shaft resistance response is plastic, (see Clause 8.9.4), the modulus values calculated for the subsequent increases in load at that gage location are the tangent modulus values of the pile cross section.

Figure 8.51 shows a tangent stiffness (incremental stiffness for an one-unit length pile element) plot of strain-gage records from the same head-down static loading test records (close-to the pile head, and, therefore, unaffected by shaft resistance) as used for the secant modulus plot (compare Figure 8.50). The linear regression of the values shown in the figure is  $E_t A = 29.2 - 0.012\mu\varepsilon$ , which, per Eqs. 8.24 - 8.27, is essentially the same  $EA_s$ -relation ( $EA_s = 30.3 - 0.008\mu\varepsilon$ ) as the direct secant method. However, one could quite well decide to disregard the change with increasing strain and use a constant E-A-parameter equal to the 27 GN average value of the central portion,  $\approx 200\mu\varepsilon$ , of the parameter range.

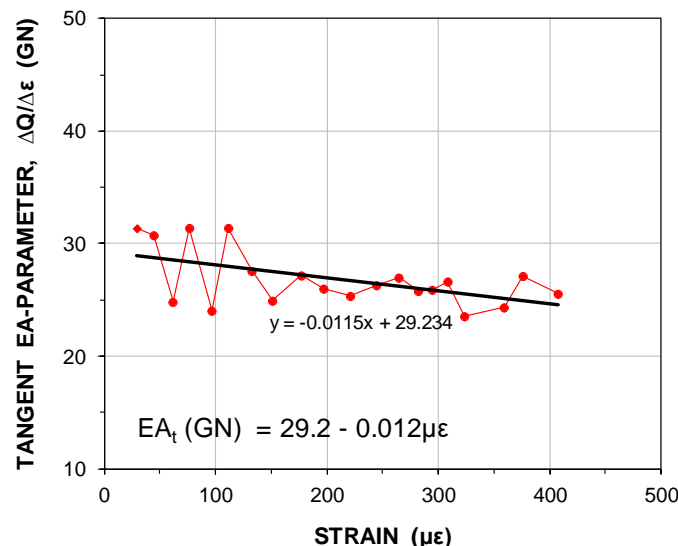


Fig. 8.51 Tangent stiffness determined from the strain records unaffected by shaft resistance.

The tangent stiffness plot eliminates the uncertainty of the "zero"-reading. However, because differentiation will exaggerate small variations in the data, a tangent plot will show more scatter than found in the secant method. The secant plot is less sensitive to such variations and produces a smoother curve, but requires a well-established zero-level. Moreover, the tangent method (also called the "incremental method") can be used also for gage readings that are influenced by shaft resistance, that is, for gage readings down the pile. However, as mentioned, only if the shaft resistance beyond full mobilization is plastic (Clause 8.9.4), which condition is not usually satisfied.

Note, the incremental stiffness method requires that the test data are from a properly performed test where all increments are equal and held for equal length of time, and where no unloading/reloading cycles have been included. If not, the gage evaluation will be adversely affected, possibly show to be useless without wishful guesswork.

Theoretically, the knowledge of the strain-dependent, composite, secant modulus relation, the measured strain values are converted to the stress in the pile at the gage location. The load at the gage is then obtained by multiplying the stress by the pile cross sectional area. However, other than for a premanufactured piles, such as a precast concrete pile or a steel pile, the pile size is not known accurately. But it does not have to be known, because, the evaluation of axial load in a pile does not require accurate knowledge of the pile cross section area,  $A$ , if, instead of thinking  $E$ -modulus, the calculation is best made from the  $EA$ -parameter, directly.

**Procedure.** When data reduction is completed, the evaluation of the test data starts by calculating and plotting the tangent  $EA$ -parameter for each gage level for each load increment (the values are change of measured load or stress divided by change of measured strain and they are plotted versus the measured strain). For a gage located near the pile head (in particular, if above the ground surface), determine also the secant  $EA$ -parameter

For gages located further down the pile, only the tangent stiffness methods applies. As mentioned, at first, the load increments reaching the gage level are substantially reduced by shaft resistance along the pile above the gage location and a linear relation will not develop until the shaft resistance is fully mobilized above the gage location. Initially, therefore, the tangent values calculated from the full load increment divided by the measured strain will be large. However, as the shaft resistance is being mobilized down the pile, the strain increments become larger and the calculated stiffness values become smaller. Provided that the shaft resistance is plastic, when all shaft resistance above a gage location is mobilized (head-down test), the thereafter calculated tangent values at that gage location represent the tangent  $EA$ -parameter of the pile cross section at the gage location.

**Tangent Stiffness Example.** To illustrate the tangent stiffness approach, [Figure 8.52](#) shows the results of a static loading test on a 20 m long Monotube pile. The pile is a thin-wall steel pipe pile, tapered over the lowest 8.6 m length. For complete information on the test, see Fellenius et al. (2000).

The soil consisted of compact sand assumed to exhibit a close to plastic shear-movement response. Vibrating wire strain gages were placed at seven levels, with Gage Level 1 at the ground surface. Gage Levels 2 through 5 were placed at depths of about 2, 4, 9, and 12 m, respectively, in the straight portion of the pile. Gage Level 6 was placed in the middle of the tapered portion of the pile, and Gage Level 7 was placed at the pile toe. Because the load-strain curves of Gage Levels 1, 2, and 3 have only small offsets and very similar slopes, it is obvious that not much shaft resistance developed above the Gage Level 3.

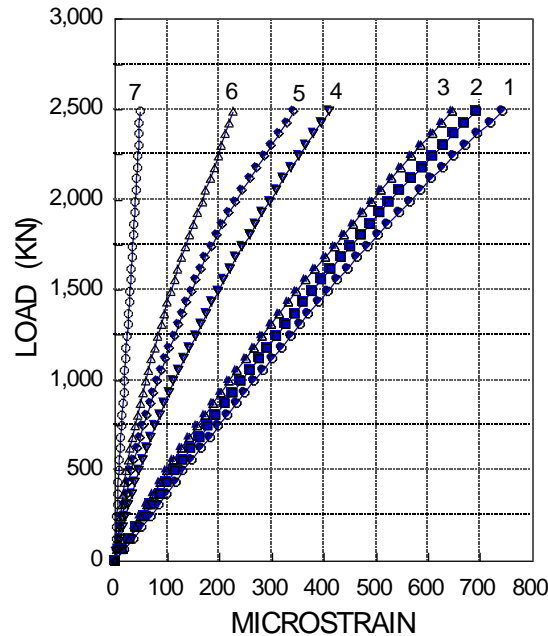


Fig. 8.52 Strain measured at Gage Levels 1 through 7 (Fellenius et al. 2000).

Figure 8.53 shows curves of applied load and measured strain for the Gages Levels 1 through 5, levels in the straight upper length of the pile. The similarity of the curve indicates that the shaft resistance response, once fully mobilized, is plastic. Therefore, the values of  $E_s A$  (the slope of the line) represent the actual pile stiffness.

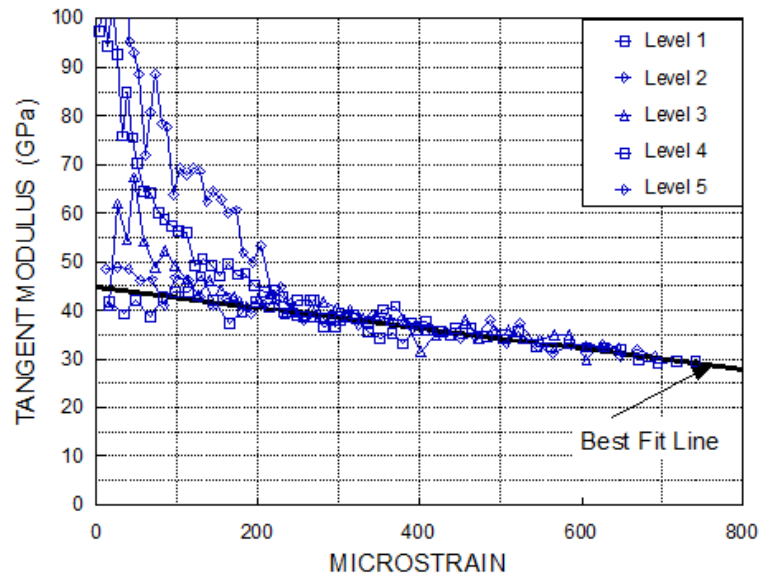


Fig. 8.53 Tangent modulus vs. strain (Fellenius et al. 2000).

Linear regression of the slope of the tangent-modulus line indicates that the initial tangent modulus is 44.8 GPa (the constant “b” in the equations). The slope of the line (coefficient “a” in the equations) is -0.02 GPa per microstrain ( $\mu\epsilon$ ). The coefficient for the secant modulus line is half this value. Figure 8.54 shows the both the tangent and secant relations for Level 1, the gage level nearest the pile head in the head-down test on the Monotube pile, a level unaffected by shaft resistance. Because the tangent relation is from differentiation, it shows a larger scatter than the direct secant relations. The linear



regression of the tangent modulus relation and conversion to secant relation agrees well with the secant relation obtained from the strain-gage records. The consistency of the linear regression line of the series of tangent modulus lines and the close agreement between the secant modulus line determined from the direct secant method and the secant modulus line determined from the tangent modulus method indicate that the relation can be used for determining the load distribution also for the records deeper down the pile. The  $E_t$ -modulus ranging from about 44 GPa at minimal strain through about 35 at  $700 \mu\epsilon$  is that of steel and concrete combined. The  $E_s$ -modulus ranged from 44 GPa through 37 GPa at  $700 \mu\epsilon$ .

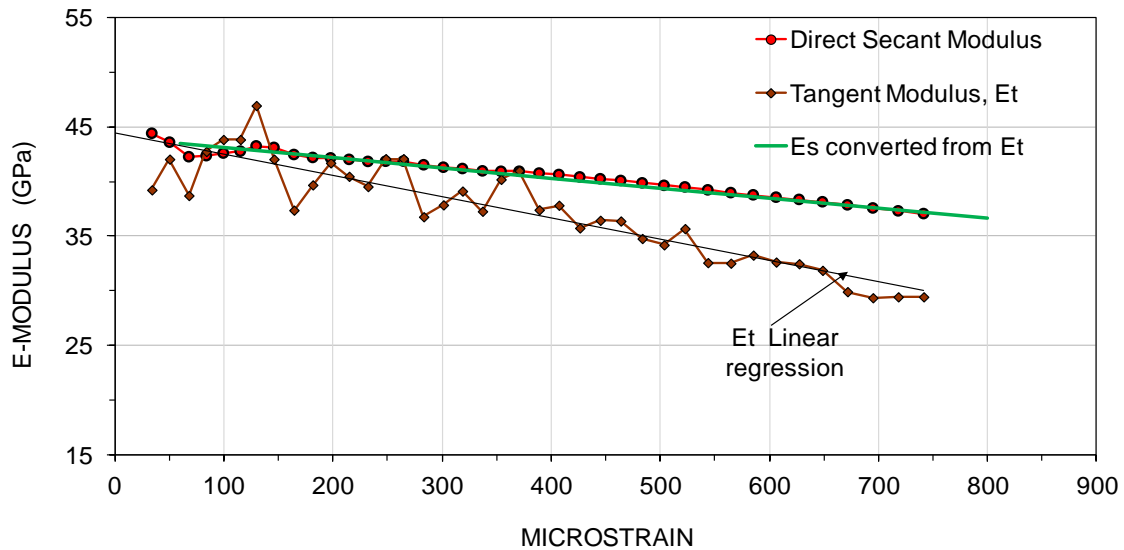


Fig. 8.54 Direct secant and tangent moduli for the uppermost gage level.

The pile cross sectional area as well as the proportion of concrete and steel change in the tapered length of the pile. The load-strain relation must be corrected for the changes in area before the loads can be calculated from the measured strains. This is simple to do when realizing that the modulus relation is composed of the area-weighted steel and concrete moduli. Conventional calculation using the known steel modulus gives the value of the concrete tangent modulus. The so-determined concrete modulus was then used as input to a calculation of the combined modulus for the composite cross sections at the locations of Gage Levels 6 and 7, respectively, in the tapered pile portion.

Figure 8.55 presents the strain gage readings converted to load, and plotted against depth to show the load distribution in the pile as evaluated from the measurements of strain (c.f., Eq. 8.27). The figure presents the distribution of the loads actually applied to the pile in the test. Note, however, that the strain values measured in the static loading test do not include the strain in the pile that existed before the start of the test due to residual force. Where residual force exists, the values of applied load must be adjusted for the residual force before the true load distribution can be established. The subject pile is clearly affected by residual force because the slope of the load distribution line for loads after the shaft resistance has been fully mobilized are steeper at depth than near the ground, implying larger unit shaft resistance at shallow depth as opposed to deeper down, which is not true in a relatively uniform soil such as at this site. Determining the measured values of load presented in the foregoing is only the starting point of the analysis. So, of course, next comes assessing whether or not the pile is subjected to residual force, and the magnitude of it, that is, establishing the "true" distribution. Figure 8.56 presents the final result for the Monotube pile after adjustment to residual force.

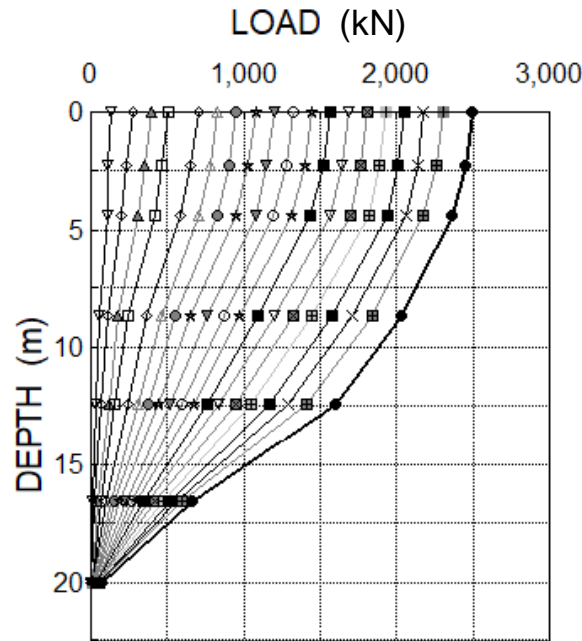


Fig. 8.55 Force distribution for each load applied to the pile head.

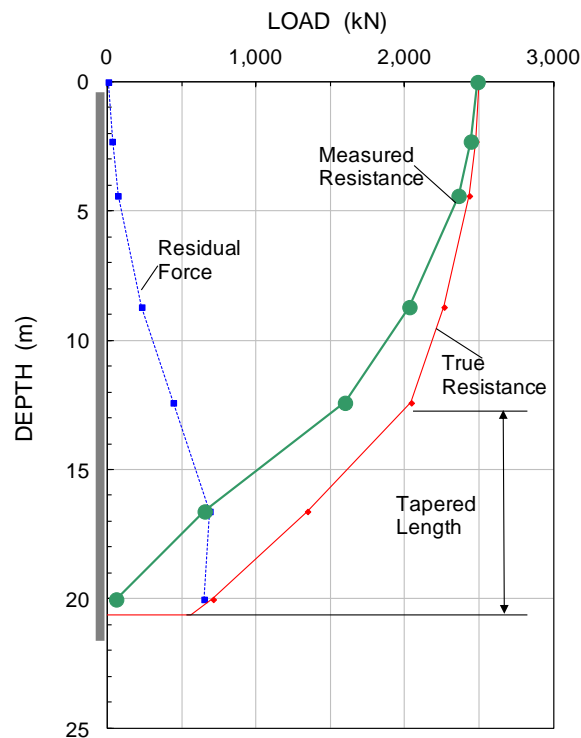


Fig. 8.56 The example case with measured load, residual force, and true resistance.

#### 8.9.4 Limitation of the tangent method

The tangent stiffness method presumes a plastic response to movement of the pile in relation to the soil. Back in the 1980s, the stiffness was thought to be only negligibly affected by soil exhibiting moderate strain-hardening or strain-softening. The fact is, however, that the evaluated of the pile can indeed be quite different from the actual EA-parameter. The following fictional example of results of a static

loading test on an instrumented pile illustrates the response in a non-plastic soil. The example pertains to a 650-mm diameter, 25 m long pile in a soil with a  $2,000\text{-kg/m}^3$  density and a pore pressure that is hydrostatically distributed from a groundwater table at 1.0-m depth. The beta-coefficient is 0.30 throughout the soil profile as mobilized at 5-mm movement for all pile elements. The unit pile toe stress is 5 MPa as mobilized at 5 mm movement. The pile material is reinforced concrete with a  $2,400\text{ kg/m}^3$  density and an E-modulus of 30 GPa which is assumed to be constant across the full strain or stress range of the test.

To calculate the results of the virtual static loading test on the pile based on the foregoing values, the only additional information needed is the soil load-movement response to applied load, i.e., t-z and q-z functions. Three alternative assumptions, illustrated in Figure 8.57, are now introduced. First t-z alternative is according to the vander Veen t-z function (Clause 8.5.3) with a function coefficient,  $b$ , of 1.00 modeling a soil response that initially is more or less linearly elastic becoming plastic at a 5-mm movement. Second alternative is a Chin-Kondner hyperbolic function (Clause 8.5.2) with a function coefficient,  $C_1$ , of 0.0093, modeling a strain-hardening soil for which the load-movement shape for the first 5 mm movement response is more or less equal to that of the first alternative, but, for movement continuing beyond 5-mm, the resistance increases, becoming 120 % of that at 5 mm at 40 mm movement. Third alternative is a Zhang function (Clause 8.5.5) with a function coefficient,  $a$ , of 0.0090 modeling a strain-softening soil that reaches a peak at 5 mm movement and softening beyond this to 80% of that at 5 mm at 40 mm movement. For all three alternatives, the toe response is set to a Gwizdala q-z function (Clause 8.5.1) with a function coefficient,  $\theta$ , of 0.50, and a 5-MPa unit toe resistance,  $r_t$ .

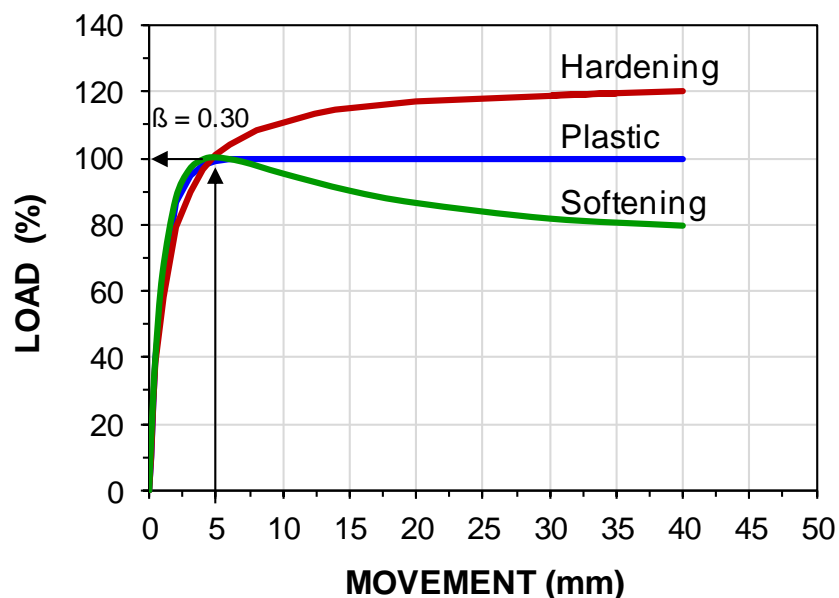


Fig. 8.57 Three alternative t-z functions.

The pile and soil information was input to UniPile to simulate a static loading test with four strain-gage levels at 4, 12, 18, and 23 m below the ground surface (and pile head). The simulation produced precise 'measurements' of load, strains, and movements at pile head, gage levels, and pile toe for each of the three alternative soil responses whose only difference is in regard to the t-z functions. As mentioned, the pile toe response (q-z) is the same for all three alternatives. Note, the input of a constant E-modulus (30 GPa), means that the axial stiffness,  $EA/L$ , is 10 GN/m, also constant. Thus, a 'measured' strain value,  $s$  ( $\mu\epsilon$ ), converts to a load,  $Q = 10s$  (kN).

Figure 8.58 shows for the three piles the applied load at the pile head and shaft resistance versus pile head movement and the pile toe load-movement. The applied test loads are only indicated for the test on the pile with plastic shaft response.

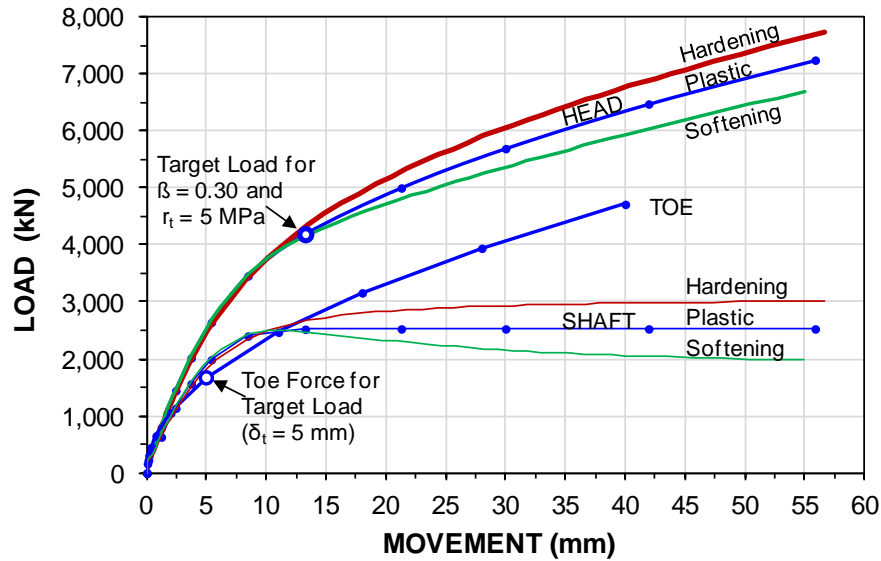


Fig. 8.58 The load-movement results of the three simulated tests.

Figure 8.59A shows the simulated distributions of load at the assumed gage levels for the pile subjected to plastic shaft response. The distribution for the chosen shaft resistance beta-coefficient at each pile element and the toe resistance for 5-mm movement, respectively—the Target Load—is indicated by the red curve. This distribution is set to be the same for all three alternatives. Figure 8.59B shows the distributions at a 6,000-kN applied load for all three assumed t-z functions: hardening, plastic, and softening.

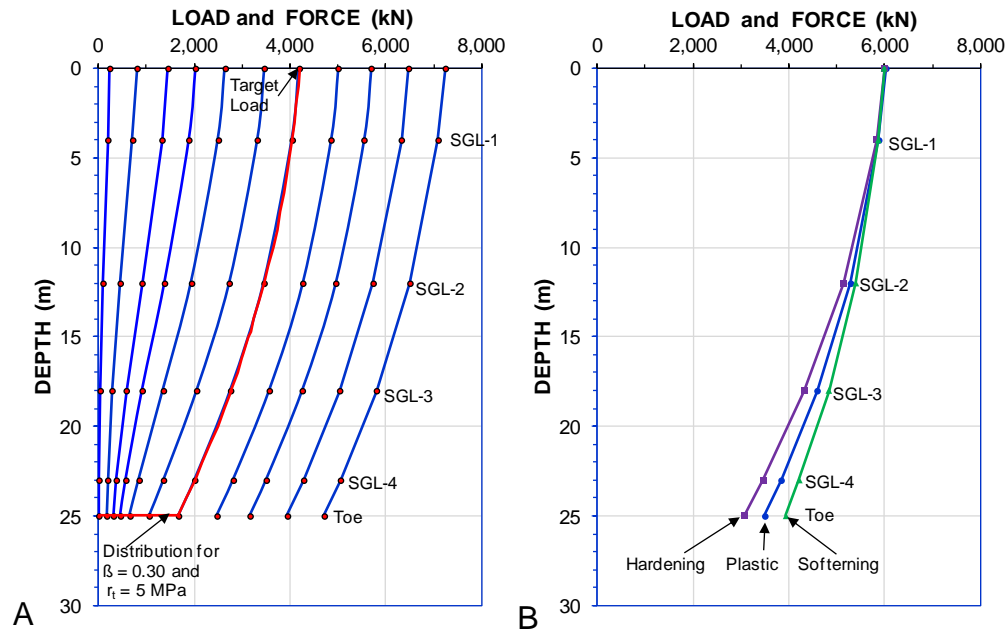


Fig. 8.59 A. The load distribution for the pile subjected to plastic t-z response.  
 B. Distributions at 6,000 kN for hardening, plastic, and softening t-z functions.

The three alternative load-movement results allow for a back-calculation of the "test results" as if they were from actual tests, in regard to determining the tangent modulus relations for the gage levels, which is the very purpose of simulating the static loading tests. Figure 8.60 shows the tangent EA-parameter for the alternative of **plastic** soil response at the four gage levels. As no surprise, beyond the loads affected by shaft resistance above the gage level, the stiffness is a constant value and the same 10 GN/m as that used for determining the loads in the simulation. Gage level SGL-4 is 4.0 m below the pile head and its records include the effect of shaft resistance between the pile head and the gage level. Therefore, the stiffness determined by the secant EA-parameter method applied to the SGL-4 records is to some small degree affected by shaft resistance between the pile head and the gage level. However, although not shown, by subtracting  $10 \mu\epsilon$  from each strain value, a straight-line relation can be obtained that indicates a 10.0-GN/m direct secant stiffness,  $E_s A$ . Thus, the back-calculation results for **plastic** response verify the pile stiffness—of course.

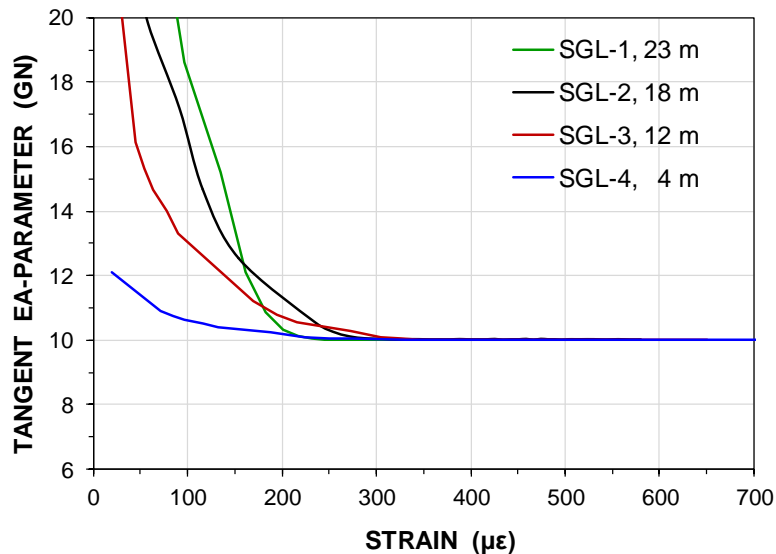


Fig. 8.60 Tangent stiffness for to plastic t-z response.

The tangent EA-parameter and the SGL-4 secant EA-parameter for the alternative of **hardening** t-z response are shown in Figure 8.61. The tangent stiffness evaluated from the uppermost gage level, SGL-4, (blue line) shows  $E_t A = 10$  GN/m, constant after the first about  $200 \mu\epsilon$  and close to the actual value. However, the EA-values of the gages further down (SGL-1 through SGL-3) do not imply a horizontal line anywhere close to the true 10-GN value. The response of SGL-3 at 12 m depth implies a stiffness relation, indicated by the dashed line, that would be interpreted to a tangent  $E_t A$ -parameter reducing with increasing strain from an about 12 GN/m initial value to less than 10 GN/m at large strain. The  $E_s A$  would change correspondingly with increasing strain. The plot of the two deeper gage levels show even larger stiffness reduction for increasing strain. It is obvious that the strain-hardening soil response falsely indicated a pile material stiffness that reduces with increasing strain. (Had the assumed pile material exhibited reduction of concrete stiffness with increasing strain, the stiffness reduction would have been larger. Examples of pile stiffness reduction with increasing strain are shown in Figures 8.50 and 8.53).

Figure 8.62 shows the stiffness for the alternative of **softening** t-z response. Again, the shallow gage level, SGL-4 indicated the correct pile stiffness. However, for the deeper gage levels, there was little agreement between the calculated tangent stiffness and actual stiffness until very large strain and large movement had developed (where the t-z curve shows little change with increasing movement, c.f. Fig. 8.51, and the response is essentially plastic).

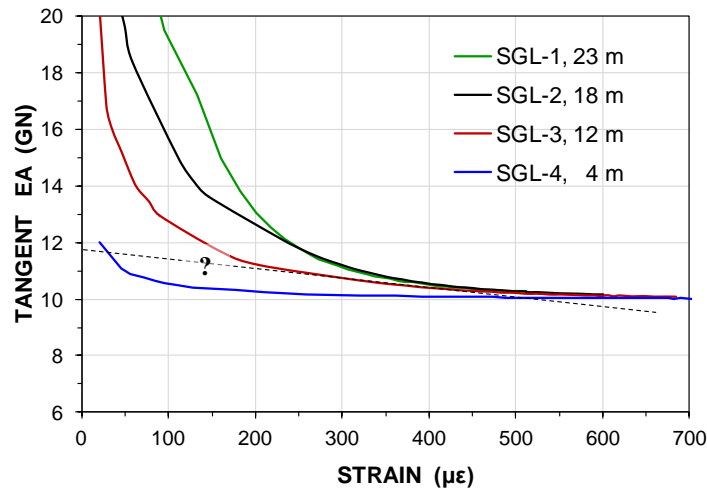


Fig. 8.61 Tangent EA-parameter for hardening t-z response.

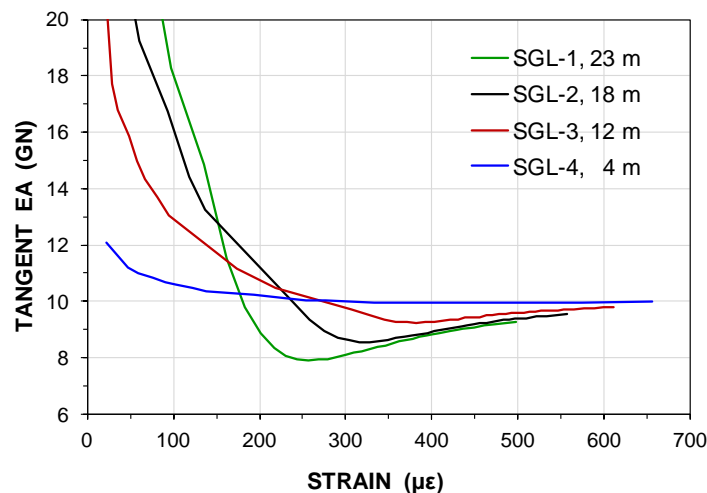


Fig. 8.62 Tangent EA-parameter for softening t-z response; element length.

Repeating the simulations for case with t-z functions of different movement before the 100 % resistance and/or different ratio between shaft resistance and toe resistance would result in quantitatively different  $E_s A$  relations for the hardening, and softening analyses. However, all show that for hardening and softening t-z response of the soil above a gage level, the hardening will tend to indicate an average that is larger than the true value. In case of a softening response, the tangent method will instead indicate a non-linear smaller than true stiffness relation that only at large strain approaches something close to the true value.

The foregoing indicates a limitation of the analysis of the strain records according to the tangent method in strain-hardening or strain-softening soil. This significantly affects the reliability and use of not just the method, but of strain-gage instrumentation. Therefore, unless the pile axial stiffness is determined from gage records more or less unaffected by the soil resistance, a non-constant axial stiffness determined from strain-gage evaluation must be considered vague and be treated as approximate. However, only few head-down tests include placing a gage pair near the pile head. In contrast, a strain-gage level is often located near a bidirectional cell and its recorded values can then be suitable for assessing the pile stiffness. Note, however, that those gage levels must be close enough to the cell level to only include a small influence of shaft resistance between the cell and gage level, but sufficiently away from the cell for the pile cross section to have developed a uniform (plane) stress across the pile.

Note that a bidirectional test provides a load at the cell assembly level, the applied load, that is independent of modulus uncertainty, residual force, and cross section variations. Therefore, the bidirectional test is significantly more suitable for assessing the load distribution of a pile than a strain-gage instrumented, head-down test.

### 8.9.5 The adverse effect on strain-gage records from unloading/reloading cycles

**Case 1. Driven pile.** Unloading and reloading cycles have a strong adverse effect on the interpretation of strain-gage records, as illustrated in the following. Figure 8.63 shows the results of a head-down static loading test on a strain-gage instrumented, 600-mm diameter, 56 m embedment depth, cylinder pile, a spun-pile, with the central void grouted after the driving (Kim et al. 2011). At an applied load of about 8,400 kN, a hydraulic leak developed that necessitated unloading the pile. After repairs, the test started anew and reached a load of about 9,000 kN at which the pile started plunging. The labels "1L" and "2L" indicate the pile-head load-movement curves for the virgin and re-loading phases of the loading test. (The accidental unloading occurred very near the maximum load, so, fortuitously, the test results were still suitable for the particular project).

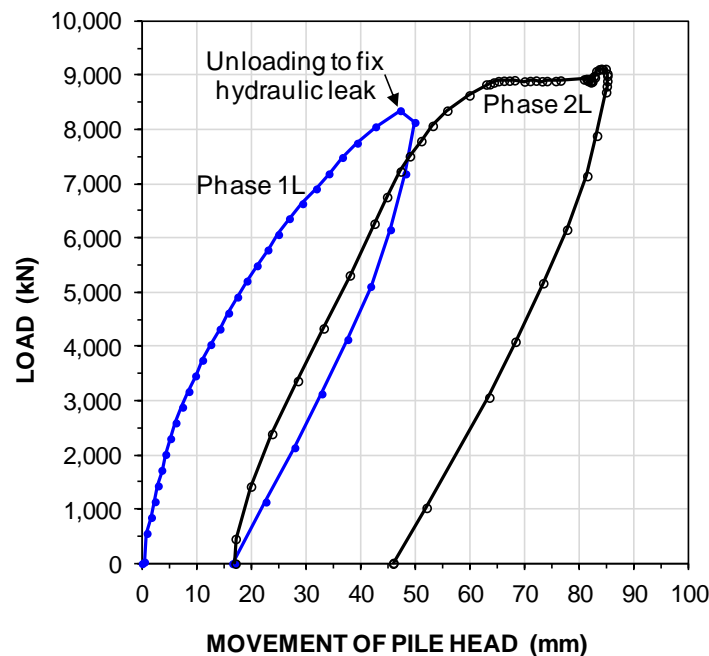


Fig. 8.63 Pile-head load-movement for the 600-mm cylinder pile with unloading-reloading event.

Often the best way to evaluate the pile EA-parameter from a plot of applied load versus strain is that shown in Figure 8.64 for the uppermost gage level, SGL-12 located 1.0 m below the ground surface. The red line is sloping at the stiffness equal to 7.0 GN, which appears to be suitable for both the virgin loading and re-loading events. For a simple plot of distribution of load versus depth calculated from the strains measured at various strain-gage pairs down the pile, this could often be sufficient for the calculations. However, not so for a precise analysis or further detailing of the test results.

The axial stiffness of a concrete pile is a function of the imposed strain, and for a gage level close to the pile head (i.e., a gage located where the pile is not influenced by soil resistance), plotting the "secant EA" (load/strain vs. strain) will show the secant stiffness, if the pile has essentially zero prior strain, that is, if the loading is for virgin conditions (Cycle 1L). Figure 8.65 shows for the 600-mm cylinder pile case how the secant EA-parameter is obtained from a linear regression of the 1L-secant line. For comparison, the figure also includes the tangent EA for the SGL-12 records. As the gage level is unaffected by shaft

resistance between the jack on the pile head and the gage level, the two methods agree well. The initial (very low strain) stiffness was 8.3 GN/m, which correlates to an E-modulus equal to 29 GPa. The secant stiffness reduced with increasing strain and is about 7.0 GN/m at 6,000  $\mu\epsilon$ , correlating to an E-modulus of 24 GPa. The spun pile was a prestressed, high-strength concrete pile that usually has a larger E-modulus. However, the concrete in the central void, which was about half the pile cross sectional area, was essentially a grout with a smaller E-modulus and the figures shows the combined, proportionally reduced E-modulus.

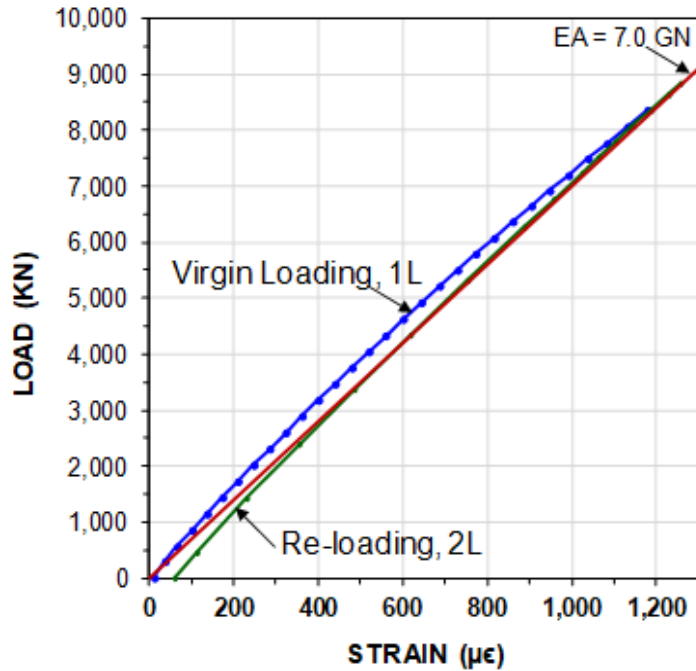


Fig. 8.64 Load-strain plot for virgin loading and re-loading with approximate stiffness line ( $EA/L = 7.0 \text{ GN/m}$ ).

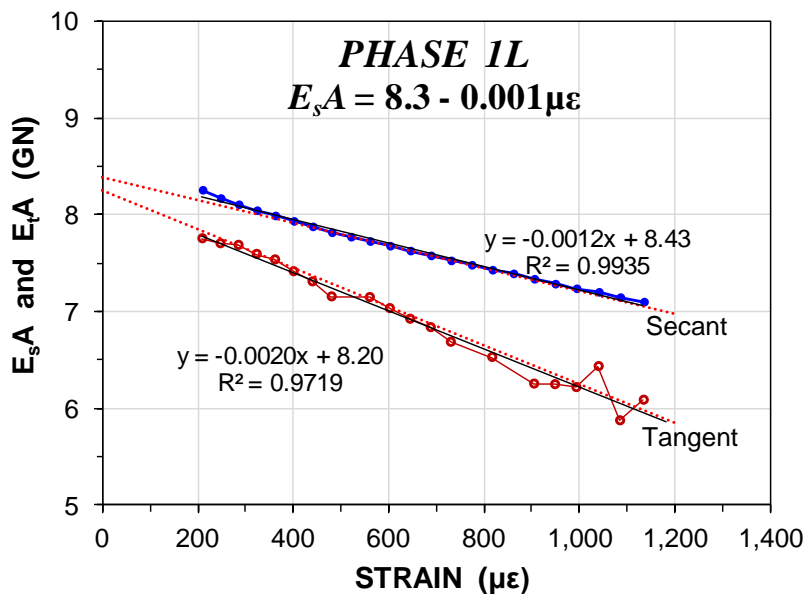


Fig. 8.65 Secant and tangent EA plots from SGL-12 close to the pile-head.



Figure 8.66 replots the secant EA-parameter from the virgin phase together with the secant plot from the re-loading phase demonstrating that the strain records from the reloading phase were very much affected by the strains imposed by the preceding phase. Subtracting  $59 \mu\epsilon$  from all strain values moved the results closer to the virgin stiffness, but not to an acceptable accuracy.

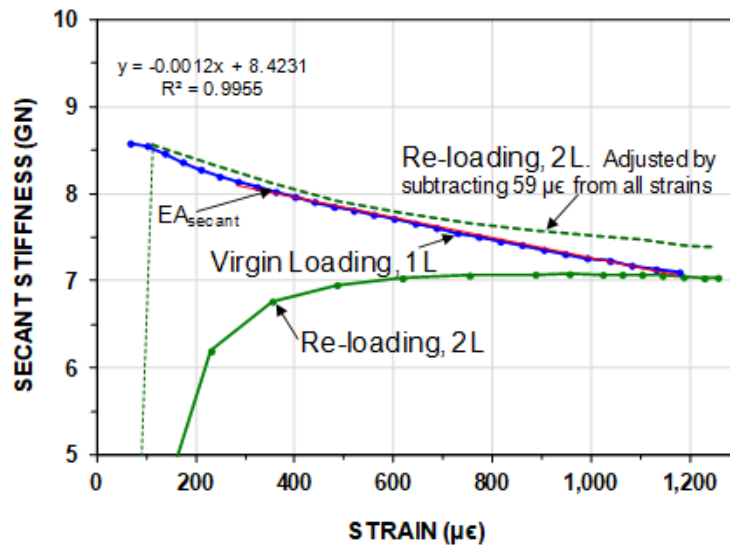


Fig. 8.66 Secant EA plot of the from the near-the pile-head gage records.

Figure 8.67 shows the tangent method applied to the same gage records. Note, the gage records are from a gage level close to the pile head and, therefore, not affected by shaft resistance or non-plastic t-z response. The only difference is the re-loading.

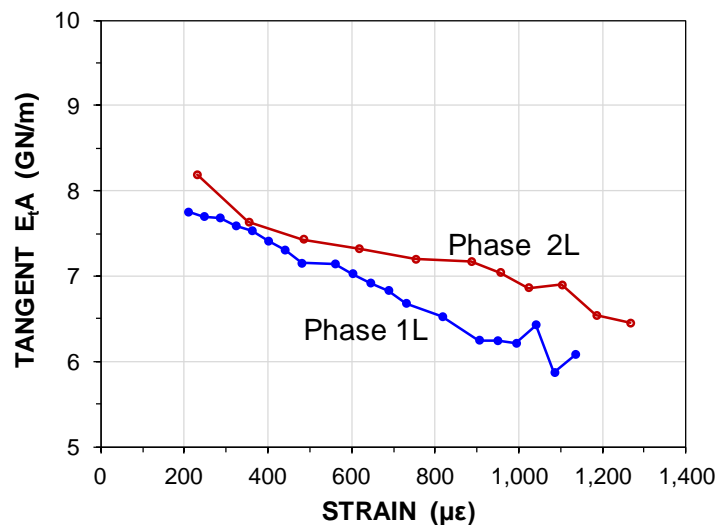


Fig. 8.67 Incremental stiffness ("tangent stiffness") for virgin loading and re-loading.

**Case 2. Bored Pile.** Figure 8.68 shows an example of a bidirectional test on a 1.85 m diameter, 65 m long bored pile, for which, again, an accidental hydraulic leak necessitated an unloading and reloading cycle (Thurber Engineering Inc., Edmonton; personal communication 2016). The pile constructed with a 8.7-m length in clay shale and siltstone below the bidirectional cell level. The figure shows the downward load-movement cell records.

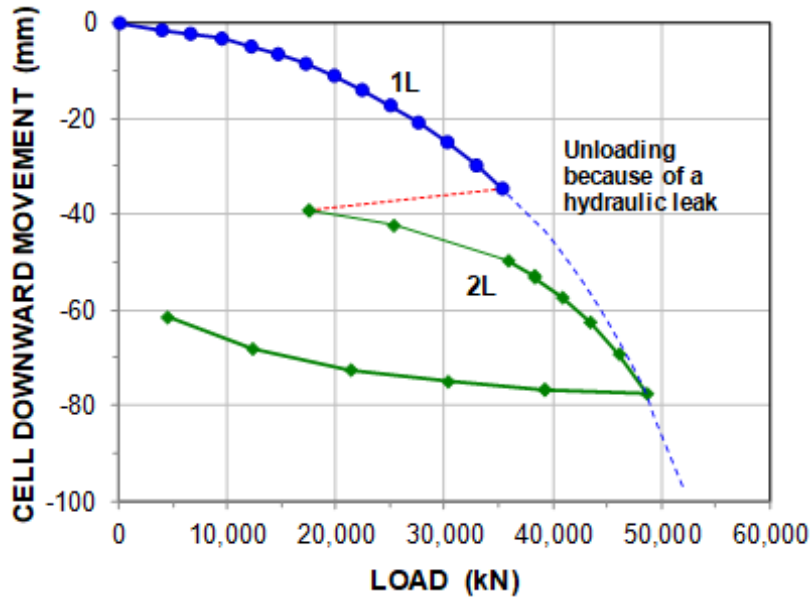


Fig. 8.68 Cell load versus downward movement for the 1,850-mm diameter bored pile.

Figure 8.69 shows the load-strain records of the two loading events for the gage level 3.0 m (1.6 b) below the bidirectional cell (where the records are only moderately affected by shaft resistance). It would appear that the unloading-reloading has not particularly affected the load-strain response.

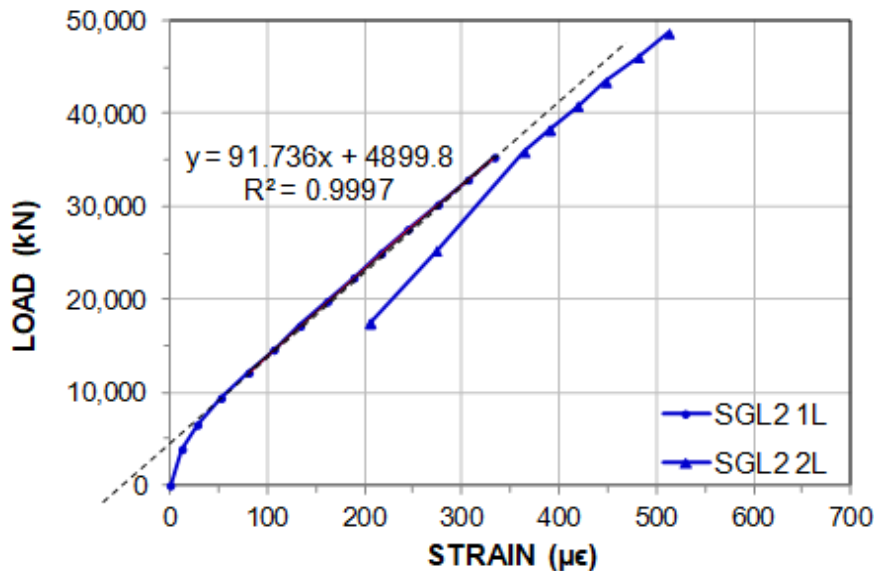


Fig. 8.69 Load-strain records of the virgin and re-loading events for SGL-3.

However, Figure 8.70 shows that, when plotting the data in a stiffness diagram using either direct secant and tangent methods, the effect of the unloading/reloading has eliminated the suitability of using the re-loading records for detailed analysis of the strain-gage records of Cycle 2L. (The secant method can be applied to gage records close to the bidirectional cell, similar to a head-down test, for where the shaft resistance between the cell and the gage levels is small). Because the incremental stiffness method relies on differentiation, a "correction" similar to that attempted for the secant method is not possible and the reloading has adversely, and irreparably, affected the strain-gage evaluation possibilities.

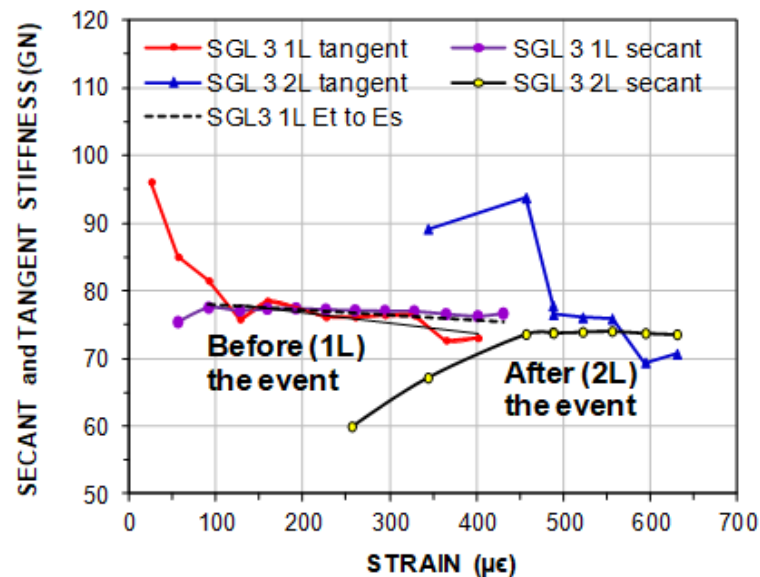


Fig. 8.70 Incremental stiffness ("tangent stiffness") for virgin loading and re-loading; L = 1.0 m.

Similar to the test on the cylinder pile, the records before the accidental unloading were sufficient for the test records to meet the design objectives of the test for the particular project.

The two case histories are from unintentional unloading/reloading events. However, they make it clear that to intentionally include such events in a test programme is undesirable, inadvisable, and regrettable.

### 8.9.7 Procedure for fitting a simulated test curve to a measured using t-z and q-z functions

There is much more to analyzing results of a static loading test than determining a capacity. A pile can be perceived as a string of short elements, each located in a soil for which the interaction of shear forces mobilized by movement follows one of the t-z functions described in Section 8.5 and, for the pile-toe element, also a q-z function. Using these elements and their soil interaction allows for a simulation of the pile response to load—from a structure or in a static loading test. For a routine head-down test, usually only the pile-head load-movement is available for a simulation fit (i.e., back-calculation. Some well-planned tests include a toe-telltale pair that measures the toe movement (albeit no pile toe force). In case of a strain-gage instrumented pile, each strain gage location (i.e., a pile element) will provide a load, but no directly measured movement (unless the instrumentation is by Glostrex system, see Section 8.6 and Figure 8.23). The most useful test method for detailed analysis is the bidirectional test (Section 8.13), because it separates the shaft resistance along the upper length of the pile (above the cell assembly) from the combined shaft and toe resistances of the lower length of the pile (below the cell assembly).

Static loading tests on long test piles normally include strain-gage and telltale instrumentation. Whether just from a routine head-down test or all the way to a bidirectional test on an instrumented pile, the measured load-movement response (or responses) at the gage levels is the primary reference to matching simulated to measured curves in the analysis.

The analysis can be produced in a regular spreadsheet template prepared with pertinent t-z and q-z functions. However, this effort can be quite time-consuming. I have the advantage of using UniPile, a commercially available software ([www.unisoftGS.com](http://www.unisoftGS.com)), and the following pertains to the use of this software for back-analysis of force-movement gage-records measured in an instrumented test pile.

(1) Start the analysis by building a case file with the appropriate pile details, the soil profile (soil layer thickness and densities), groundwater table (include the pore pressure distribution, if it is non-hydrostatic), and other factors, such as loads and excavations, which influence the effective overburden stress distribution near the test pile.

(2) Select a target load on the pie-head load-movement curve for a load that appears to have induced some toe movement, say 5 mm, then, determine in an effective stress analysis what beta-coefficient(s) that will fit (return) that target load. The analysis results in a force distribution, i.e., axial force versus depth for the chosen target load. The relevance of the various preliminary beta-coefficients or unit stress values that gave the back-calculated fit to the target load depends on the complexity of the soil profile and the relevance of the input parameters. The procedure applies also to stress-independent analysis ( $\alpha$ -method), although stress-independent shaft shear resistance does not consider important aspects, such as effect of excavated or filled areas and pore pressure distribution; plainly stated, it is less realistic and, therefore, not that useful.

(3) For a head-down test, select the lowest gage level force-movement record (curve), which would be the gage level and pile element that incorporates the toe response. For the chosen target movement, the 5-mm value is often the most suitable. Select toe stress and beta-coefficient that results in the force determined for the gage strain at that movement. (As the toe stress and the beta-coefficient are interrelated, some judgment is necessary here and the analysis may have to come back later to the this lowest gage level in the continued processing of the gage records to re-adjust the first choice). When the calculated force is equal to the measured target force, pursue a trial-and error set of analyses employing various t-z and q-z relations to make a calculated force-movement curve fit the measured, pivoting it as is were around the target value.

(4) Proceed to the next gage level above and repeat the procedure. When the calculated and measured force-movement curves for this gage level agree, proceed to the next level up, etc. The pile head load-movement will be the last gage fitting as it were. Each "next level calculation" incorporates the results of the calculations for the records of the below gage level. The fitting will therefore incorporate and offset any imprecision in that preceding calculation, minimizing the data imprecisions.

Once a calculated force-movement has been produced for all gage levels and the pile-head, the full pile-soil response comprising load-movement and force distribution have been established. The so-calibrated (back-calculated) soil-pile data can be used for analyzing the response of a longer or shorter pile, a pile with a larger or smaller diameter, or a pile where the soil layers are slightly thicker or thinner. That is, the results can be used to represent other piles at the site and beyond. Moreover, the test pile is a single pile and its response is similar to that of a perimeter pile. The results of the fitting analysis can, therefore, be used to analyze the response of interior piles in a wide group of piles, by modifying the analysis to that of a hypothetical bidirectional test on a pile with the BD assembly placed at the pile toe, as detailed in Section 7.18.3.

An alternative process would be to calculate the force difference between two gage levels and fit that difference to an analysis for one or the other of the force moments curves of the gage level, or their average, perhaps. And, then repeat for the next between-gages pile portions. However, this is a differential approach and it is unlikely to result in a set of soil-pile parameters that will fit the final simulation, that of the full length conditions, the main pile-head load-movement curve. Therefore, this approach is not "fitting".

### 8.9.7 Concluding remarks on Modulus and Stiffness

Be the test a simple proof test or an elaborate instrumented test, a careful analysis of the recorded data is necessary. Perform the test to an at least 10 mm toe movement, preferably well beyond this value; more for large diameter piles as then the analysis results will become more valid for transfer of the test result to other piles for the same project as well as for gaining insight of general validity. Notice, forgetting that piles are subjected to residual force throws the most elaborate instrumentation and analysis scheme to the wind.

As indicated in the foregoing, the concept of ultimate resistance (capacity) does not apply to the pile toe. This means that the pile toe does not develop an ultimate resistance. Nevertheless, a load-movement curve of a pile toe subjected to residual force may show an initial steep portion transiting to a flatter shape, which may imply approaching an ultimate resistance. This false impression is because the presence of a residual toe force results in the initial movements being small, but, progressively, larger once the residual force is surpassed, will imply approaching a kind of ultimate response.

For most piles used in current practice, the failure load inferred from the pile head load-movement curve occurs at a pile toe movement (small if additional to any introduced by residual force) in the range of 5 mm through 15 mm, about 10 mm on average. In a test performed for reasons beyond simple proof testing, as a minimum requirement, a toe telltale should be included in the test and the analysis of the test results include establishing the q-z curve for the pile toe. The data and analysis will then enable estimating the long-term pile toe movement and pile toe force, which information is necessary for locating the neutral plane, determining the maximum force in the pile, and verifying the long-term settlement.

It is often more advantageous to perform a bidirectional cell test instead of a head-down test, because the bidirectional test will enable the analysis to separate the shaft and toe resistances, establish the pile-toe load-movement behavior, and disclose presence of any residual force in the pile (at the location of the cell). Moreover, for moderate length piles, about 15 m or less, performing a bidirectional test avoids the uncertainty of force distribution assessed from strain-gage records and, also, allows saving of costs because instrumenting a bidirectional test for determining the force distribution is not necessary for moderate length piles.

A small or moderate size project can normally only afford one static loading test. For driven piles, the pile driving can become a part of a dynamic test by means of the Pile Driving Analyzer and the analysis of measured strain and acceleration in the Analyzer and by means of CAPWAP and WEAP analysis (See Chapter 9). Dynamic testing is often useful also for bored piles. The dynamic test has the advantage of low cost and the possibility of testing several piles at the site to identify variations and ranges of results. It determines the adequacy of the pile driving equipment and enables the engineers to put capacity into context with the installation procedures. A CAPWAP analysis also produces the distribution of shaft resistance along the pile and determines the pile toe resistance. N.B., high-strain testing and CAPWAP analysis do not replace performing a static loading test on an instrumented test pile and, if the test pile would be affected by residual force, the results of both would exaggerate the shaft resistance and underestimate the toe resistance correspondingly. However, by also performing a dynamic test and CAPWAP analysis of the records from initial driving and from restrike after some time (letting set-up develop along with increased residual force), as well as testing a slightly shorter pile not driven to full toe resistance, the dynamic test will assist the analyses of the static loading test at moderate extra costs.

When applying the results of a static loading test on a single pile to the design of a foundation supported by a group of piles, it quickly becomes obvious that the capacity of the single pile and the associated factor of safety are not always appropriate for the design of the piled foundation. Do not let the effort

toward evaluating the pile capacity and factor of safety overshadow the fact that, in the end, it is the settlement of the piled foundation that governs. The serviceability is the key aspect of a design.

To assess the settlement issue, the analysis of the loading test should produce information on the force distribution, the location of the neutral plane, and the anticipated settlement of the soils around the piles. When the results of even a routine test performed with no instrumentation are combined with a well-established soil profile and a static analysis (Chapter 7), reasonably representative load and resistance distributions can sometimes be derived even when the test is limited to just the pile-head load-movement records. The more important the project, the more information needs to be made available. The more detailed and representative the analysis of the pile behavior—for which a static loading test is only a part of the overall design effort—the more representative the settlement analysis will become.

It is important to realize that the analysis of the results of a static loading test is never better than the test allows. The so-called “standard test procedure” of loading up the pile in eight increments waiting for “zero movement” to occur at each load level and then keeping the maximum load on the pile for 24 hours is not a good level test. Of course, if the pile capacity, however defined, is larger than twice the working load (the usual maximum load applied in a routine pile loading test), the results of the “standard” method test are able to show a presumption of a worthwhile test. However, a test by this method gives no information on what the margin to a not worthwhile condition might be and gives no information on any potential savings of efforts, such as relaxing of pile depths, and pile construction method, etc. On the other hand, if the pile capacity is inadequate so that the pile fails before the maximum load, the “standard test procedure” provides very little information to use for assessing the pile response in relation to a reduced working load. Nothing is so bad, however, that it cannot be made worse. Some “engineers”, some codes, even, incorporate, at one or two load levels, stages of unloading and reloading of the pile and/or extra load-holding period, and “seating” the system by a load increments or two before the “real” tests start, ensuring that the test results are practically useless for informed engineering decisions.

Frankly, the “standard 8-increment, 24- to 72-hour duration, test procedure” is only good for when the pile is good and not when it isn’t. To ensure best resolution of data, the number of load increments should be reduced if the maximum scheduled test load is estimated to be significantly smaller than a perceived ultimate resistance.

The method that provides the best data for analysis of capacity and load-transfer is a test performed by means of several small increments applied at constant short time intervals. For example, the test should aim for applying a series of 15 increments to an estimated load approximately close to a perceived ultimate resistance or to at least twice the working load, each increment applied after a specific load-holding duration, usually at every 15 minutes. When the applied load has reached the specified maximum load and, if then the reaction system allows applying larger load, adding one or a few additional increments of the same size and load-holding time as the previous will enhance the value of the test at minimal cost. After the last (the “maximum”) load has been on the pile for the chosen increment duration (load-holding time), the pile should be unloaded in about six or eight steps with each held constant for a short time, usually a hold-time of 2 minutes for the decrements is sufficient.

Notice, once a test is started with a certain increment magnitude and duration, do not change this at any time during the test. It is a common mistake to reduce the load increment size when the movement of the pile starts to increase. So, don’t. Start out with sufficiently small increments, instead. And, notice, the response of the pile in the early part of the test is quite important for the analysis of the overall test results. As are a records of load and movement, “zero” records, taken before starting the test, which should include records during at least an hour with no load applied to the pile. In an instrumented pile, if at all possible, all gages should be monitored at least over a few days before they are installed in the pile and a few days before the day of the static test.

For some special cases, cyclic testing may provide useful information. However, the cyclic loading should not be combined with a conventional test for load-transfer, but must be performed separately. If conventional and cyclic tests are carried out on the same test pile, the cyclic loading test should take place after completion of the conventional test. Note, stages of simple unloading and reloading makes no cyclic test. A useful cyclic test requires many cycles, usually 20 to 50, and the sequence should be designed to fit the actual conditions of interest.

The absolutely best static loading test for obtaining an optimum of information to use in the design of a piled foundation is to perform a bidirectional cell test. The test should be designed to move both the shaft above the cell and the length below the cell with emphasis on moving the pile toe a sufficient amount. The Case I bidirectional test reported in Section 8.14, Figs. 8.31 and 8.32 was balanced, that is, the tests established both the shaft and toe resistance responses. Should a test not engage the shaft resistance to a satisfactory movement, it is easy to carry out a head-down test with the cell open so that all pile toe resistance is eliminated from the test—assuming that, in planning and setting up the test, the option of a light-load head-down test had had been included. Note that the bidirectional upward test will have resulted in considerable residual force in the length above the cell level, which will compromise the strain-records of the head-down test. The toe resistance will in such a case have been determined from the bidirectional test and the shaft resistance in the head-down test. Moreover, if it, instead, was the shaft that moved too much before a desired toe movement has been achieved, an arrangement can be made to provide necessary reaction to add to the shaft resistance so a repeat bidirectional cell test can move the pile toe.

It is important to recognize, however, that a head-down test following a bidirectional test will be a test on a pile with residual forces built in from the preceding bidirectional test, which fact and effect will have to be incorporated in the analysis of the test data.

Note, if the pile is a bored pile with some bulges along its length above the bidirectional cell level, this will have introduced resistance points affecting a subsequent head-down test. The head-down reverses the direction of movement and these resistance points will not engage the soil appreciably until the "reverse direction" movement becomes about the same as that of the first. The difference will imply a less stiff initial response to the applied loads for the second test. Moreover, the strain records of the repeated loading will be affected by locked-in strains and not be fully suitable for detailed analysis of the load distribution.

A head-down static loading test must be performed using a jack pump able to provide automatic pressure-holding and mechanical increase of pressure to generate the next load. Manual activation of the pump to hold the load and manual pumping to raise the load to the next level is a thing of the past and has no place in today's world, where high quality of the engineering work is required and expected. Moreover, the load actually applied to the pile in a head-down test must be monitored by a separate load cell, not determined from jack pressure values. A common mistake in recording the test measurements is to let the records show the load that was intended to be applied to the pile head instead of keeping records that show the load that was actually applied. By all means, let the jack pressure guide you to the load to apply, but let the data logger (data collector) record the load by means of a separate load cell (and log also the jack pressure).

The days of manually reading the gages and noting down the values are long since gone. A static loading test must have all readings obtained by a data logger (data collector; data acquisition system). Moreover, the data logger must be able to record all records with reference to a common date-time stamp. Do not try to save costs by having two separate data loggers and believe that the records can be reliable "married" via the time-stamp for each set of records. My experience is that ever so often a line shift is made and a "divorce" occurs before the marriage is, well, completed.

If someone balks at the quality requirements, rather arguing about the cost of the purchase of the equipment, point out that omitting the use of the data logger and load cell is rather dim-witted in light of, first, the fact that the costs are minimal compared to the costs of the tests and, second, not including proper equipment might jeopardize much of the value of the test. The argument that "*we have never needed this before*" is hardly worth a comment; someone from the stone age cannot comprehend much of the comments anyway. But, ignorance and learning aversion is no excuse.

Often overlooked is the desirability to measure the movement of the support of the beam that is used for reference to the pile head movement, the upward movement of the anchor piles and/or the loaded platform, and the movement of the ground surface radially out from the test pile. Such records must be a standard component of a quality static loading test.

After the test is concluded, the records must be reviewed and analyzed. There is not much one can do with a conventional routine test involving only the pile-head load-movement records. Instrumented tests need some work, of course. In instrumenting a test pile than an H-pile or a not grouted pipe pile, a strain-gage pair must be placed at the pile head, but not closer than about two pile diameters below. The analysis should always include the test data the zero-strain from the factory calibration, the readings after having attached the gages (sister bars) to the reinforcing cage (or similar), the readings immediately after lowering the instrumented reinforcing cage in the pile, the readings immediate before and after concreting (grouting) the pile, and frequently during the wait time before the start of the static loading test (more frequently during the first 48 hours). Strain-gages are equipped with a temperature sensor, so record and report also the temperature.

Compile the test records in a spread sheet table. Then, proceed with the following:

- 1) Verify the relevance of all records by plotting and reviewing for all gages the applied load versus the individually measured strains and the average of each gage, as well as telltale records.
- 2) Plot the secant EA-parameter (applied load divided by strain,  $Q/\mu\epsilon$ ) versus the average strain for the gage pair closest to the pile head or to the bidirectional cell. It should appear as a straight line, possibly with some slope. An initial curved portion of the  $E_sA$  plot is often a sign of less accurate zero-value. Try shifting (correcting) the zero value by a few strains to see if this would straighten out the plot.
- 3) Plot for all gage pairs, the tangent EA-parameter (increment of applied load divided by increments of measured strain,  $\Delta Q/\Delta\mu\epsilon$ ) versus the average strain. This will aid the judgment call for deciding what EA-parameter to use. The same for all gage records or different values to different gage levels. A plotted line that is not horizontal is more a consequence of non-plastic shaft resistance than an E-modulus varying with stress (See Section 8.9).
- 4) Use the values of secant parameter,  $E_sA$ , to calculate (multiply EA and measured values of average strain) and plot the results as force-distributions for the applied loads and a series of force-movement curves.

## **8.10 Example of Evaluation and Use of Records From a Head-down Test**

### **8.10.1 Introduction**

A static loading test was performed on a 400-mm diameter, 42 m long, pile drilled under slurry in clay and sand. An about 3 m long temporary casing was placed at the ground surface during the drilling (the diameter was not reported). The soil profile comprised 5 m of soft clay, 11 m of compact sand, 24 m of silt and clay on a sand deposit. [Figure 8.71](#) shows a CPTU sounding diagram from near the test pile.



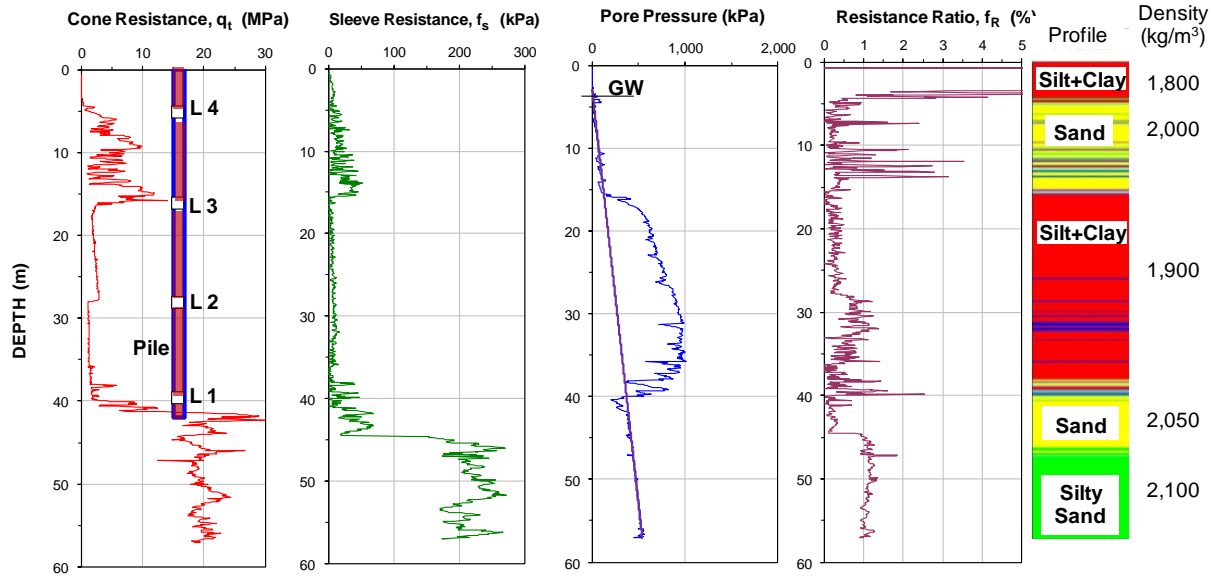


Fig. 8.71 CPTU sounding diagram

Figure 8.72 shows the virgin condition compressibility in terms of Janbu modulus number,  $m$  (see Section 3.5), as estimated from the CPTU sounding applying the method described in Section 2.11 and UniPile6 ([www.unisoftGS.com](http://www.unisoftGS.com)). The values of preconsolidation margin,  $\Delta\sigma'$ , were assumed.

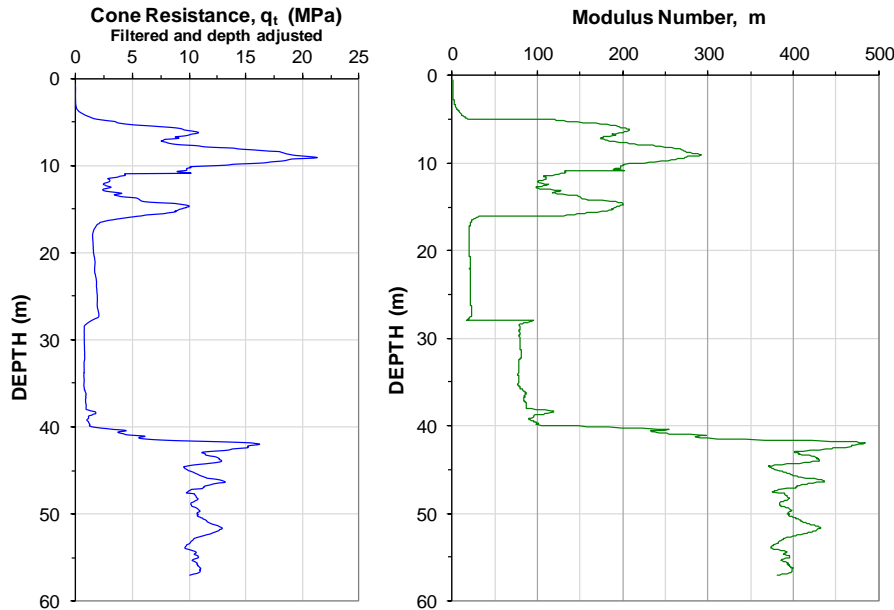


Fig. 8.72 Virgin modulus numbers estimated from the CPTU sounding (Massarsch 1994)

The pile head was level with the ground surface and the pile embedment length was 42 m. The test pile was equipped with four levels (L1 to L4) of single pairs of vibrating wire gages (VW). A single telltale (TTL) was installed to each gage level measuring the movement of each gage level along with the pile head movement. Subtraction of the telltale values from the pile head movement provided the compression over the length of pile above the gage level. (This arrangement means that the compression data then combined precision errors of two gages—differentiation. However, this critique does not apply to the example the compressions were not used to determine strain).

The static loading test comprised sixteen 200-kN load increments. Load readings were by load cell. Load-holding was 15 minutes. For each set of readings, the next load increment was only applied after the last VW-reading had been secured. Table 8.2 lists the 15-minute measurements of each increment level. Intermediate readings and jack readings were not reported. Only the average of each gage pair was reported. No information was reported on length of time between cleaning of slurry and concreting.

The loading test was performed before the construction of the foundation production piles. The intended unfactored sustained (dead) load and transient (live) loads from the structure were 1,000 kN and 200 kN, respectively.

After completion of the supported structure, an about 1.5 m thick engineered fill was placed over the general site (the fill is assumed to exert a 30-kPa stress to the ground) and the groundwater table will be lowered from the 3.0 m depth at the time of the static test to 5 m depth, hydrostatic distribution, for the long-term condition. Thus, the piles will be subjected to downdrag due to the subsequent consolidation of the silt and clay layers, i.e., general subsidence. The project comprised foundations supported on single piles and narrow pile groups as well as wide pile groups.

### 8.10.2 Test results

The measurements of the static loading test are compiled in Table 8.2.

**Table 8.2. Results of Static Loading Test (Instrumented 400-mm diameter, 42 m bored pile)**

Load (#)	Pile Head Data			Level 1--40m		Level 2--28m		Level 3--16m		Level 4--5m	
	Time (min)	LOAD (kN)	Head (mm)	TTL Mvmnt (mm)	VW Strain ( $\mu\epsilon$ )	TTL Mvmnt (mm)	VW Strain ( $\mu\epsilon$ )	TTL Mvmnt (mm)	VW Strain ( $\mu\epsilon$ )	TTL Mvmnt (mm)	VW Strain ( $\mu\epsilon$ )
L1-0	0	0	0.00	0.00	0	0.00	0	0.00	0	0.00	0
L1-1	15	200	0.35	0.00	0	0.01	7	0.05	27	0.34	65
L1-2	30	400	0.99	0.00	1	0.02	10	0.19	54	0.95	99
L1-3	45	600	2.55	0.00	1	0.05	17	0.28	68	2.12	160
L1-4	60	800	3.86	0.01	5	0.19	24	0.85	85	3.23	221
L1-5	75	1,000	5.12	0.02	8	0.31	38	1.29	122	4.51	272
L1-6	90	1,200	6.52	0.04	19	0.59	69	1.91	170	5.58	325
L1-7	105	1,400	8.02	0.08	31	0.89	101	2.58	221	6.83	377
L1-8	120	1,600	9.63	0.13	46	1.14	136	3.24	273	8.22	430
L1-9	135	1,800	11.39	0.19	61	1.37	177	4.25	324	9.84	482
L1-10	150	2,000	13.22	0.33	86	1.90	225	5.74	379	11.21	536
L1-11	165	2,200	15.51	0.66	104	2.81	277	8.04	433	12.94	590
L1-12	180	2,400	18.52	1.21	124	4.07	331	9.84	487	15.02	642
L1-13	195	2,600	23.84	4.98	158	8.66	385	14.00	544	20.96	696
L1-14	210	2,800	33.00	11.79	208	16.24	439	21.97	594	29.31	753
L1-15	225	3,000	56.44	32.21	259	36.81	493	42.96	647	52.30	809
L1-16	240	3,200	92.00	66.25	309	71.28	544	78.00	697	87.69	863

Figure 8.73 shows the load-movement of pile head and of Telltale TTL1 at Gage Level L1, 2.0 m above the pile toe (per the load applied to the pile head). Figure 8.74 shows the strains measured at all four gage levels. Figure 8.75 shows the pile head movement and the telltale-measured movements at the gage levels. The dashed line indicates the 2,800-kN applied load—the chosen "Target Point" or "Target Load" (addressed below).

Strain could have been estimated from the telltale shortening, too, but with much less precision. Had the pile compression, pile-head to gage-level, been arranged to measure the compression directly, the precision would have been much better, because calculating the compression by combining movement measurements from two sources greatly increases the error of the compression values. This is moot, in this case, because the purpose of the telltales was to measure movement, not to obtain compression for determining strain.

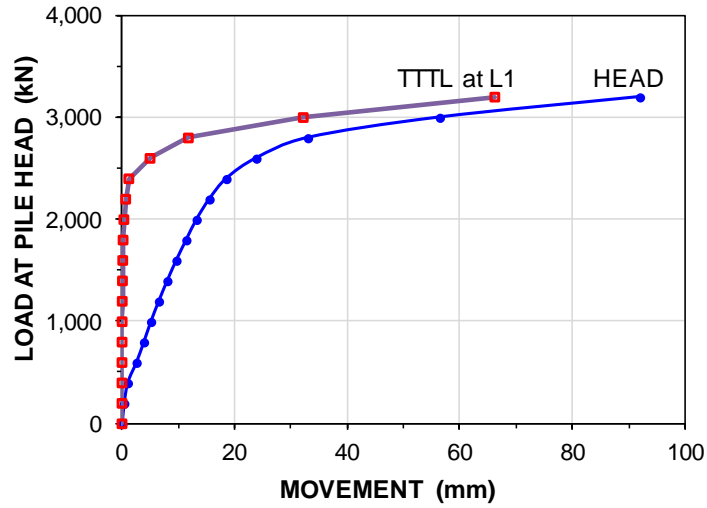


Fig. 8.73 Load-movements for the pile head and TTL1 at L1 (approximately that for the pile "toe")

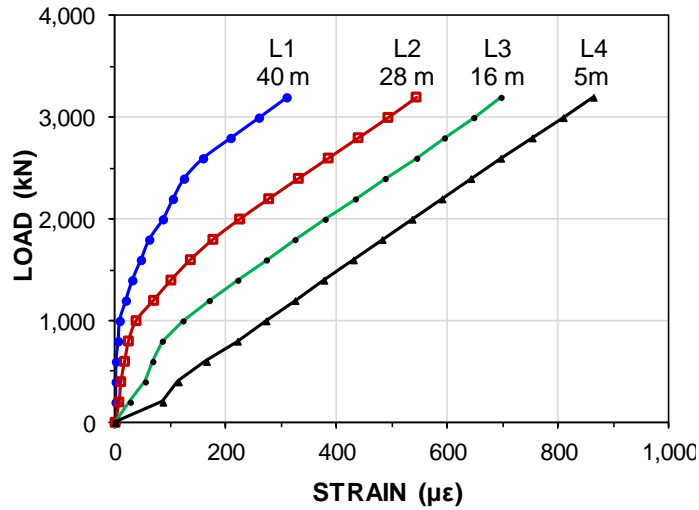


Fig. 8.74 Strain measured at Gage Levels L1 through L4 for the applied loads

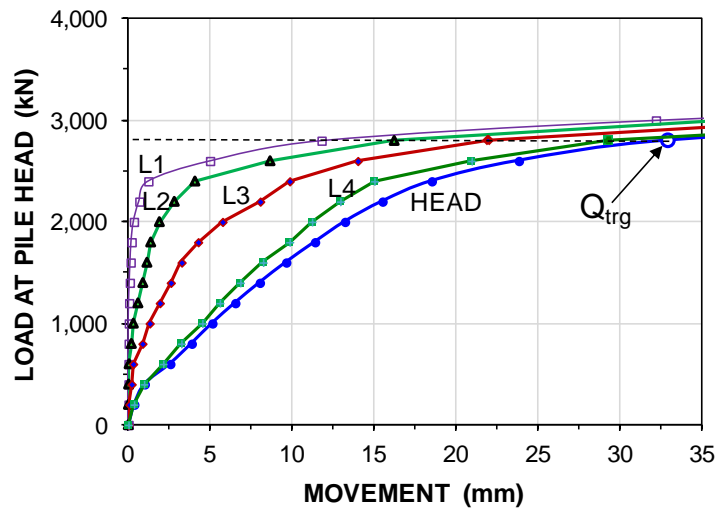


Fig. 8.75 Applied load versus movements measured at pile head and gage levels ( $Q_{trg}$  = Target Load)

Figure 8.76 shows the pile-head load-movement, pile compression, and the applied load vs. the pile toe movement. The 2,800-kN Target Point (load and movement) from Figure 8.75 is indicated. A Target Load is not intended to represent an ultimate resistance. It is subjectively chosen amongst the loads that caused a definite, but one not too large, toe movement. If movement development is acute for small initial loads, then, the Target should be at small movements. If the development is gradual, the target can be at a load that resulted in larger movements. Another of the applied loads could equally well have been chosen. The movement of TTL1, "the toe movement", was 11.8 mm for the Target Load. At the intended unfactored working load (1,200 kN, sustained plus live), the load-transfer movement was about 8 mm and consisted of pile compression only. The axial force distribution for the Target Load was fitted to an effective stress analysis.

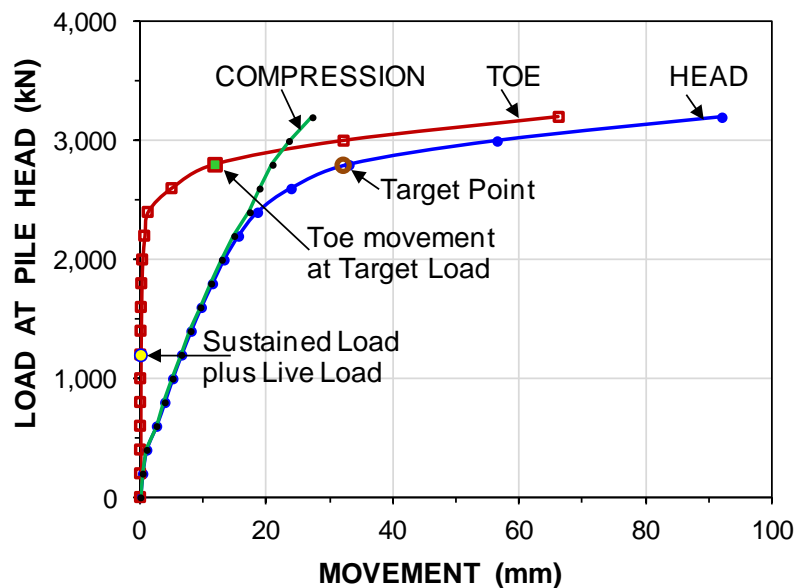


Fig. 8.76 Load-movements for the pile head and pile "toe" with the pile compression and Target Point (Pile-head load-movement)

### 8.10.3 Analysis of the test results

The strain-gage records were used to determine the pile EA-parameter from gage level L4 is located 2 m below the upper 3-m temporary casing 5.0 m below the pile head. The soil between the pile head and the uppermost gage level, L4, at (and is very soft according to the CPTU sounding) only providing a minimal shaft resistance. Therefore, the direct secant method (slope of the applied load versus strain curve) is considered applicable to the L4 gage records. Figure 8.77 shows a plot of the calculated secant EA vs. strain for the gage level closest to the pile head and Figure 8.78 shows the tangent EA values for all four gage levels. Both plots show stiffness being essentially constant for increasing strain or stress (beyond the initial records) implying that the shaft shear could be plastic, i.e., neither strain-hardening nor strain-softening. The calculations indicate that the pile axial stiffness was 3.7 GN/m, which for the nominal pile cross section area of 0.1257 m<sup>2</sup> correlates to an E-modulus of 29.44 GPa, i.e., about 30 GPa, which is a realistic value.

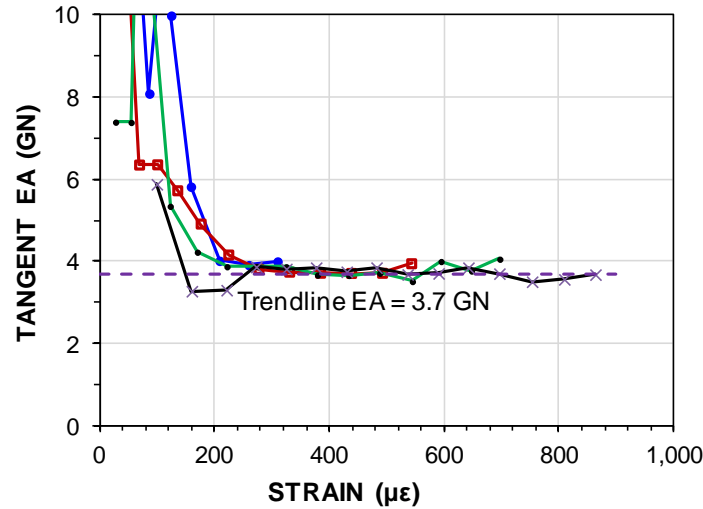


Fig. 8.77 Secant EA at L4

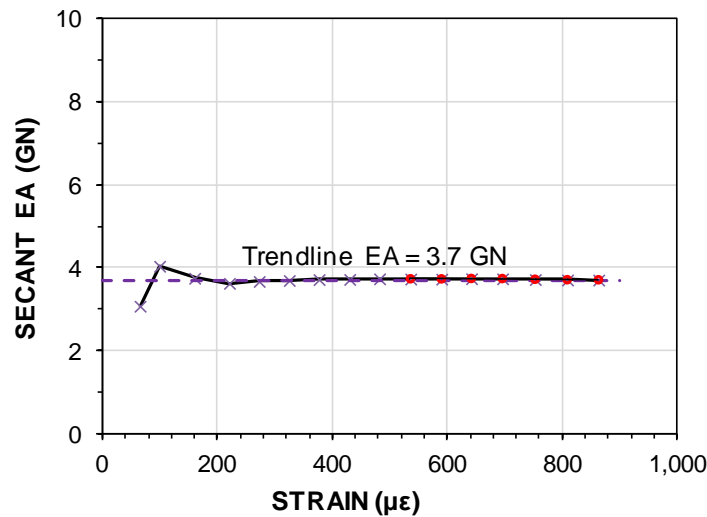


Fig. 8.78 Tangent EA

The so-determined EA-parameter was used to calculate the axial force for each strain-value. [Figure 8.79](#) shows the VW-force distributions at the depth of each gage level plotted for each applied load. To illustrate the use of telltale compression for estimating force, forces calculated from the telltale compression at the applied 2,800-kN load, chosen as Target Load, have been added at mid-point of the telltale lengths. The latter were determined from the telltale-determined compressions divided by the telltale length to obtain average strain, which was then divided by the pile EA-parameter (3.7 GN) to get the average load over the telltale length, e.g., "TTL 2 to 3"). As the shaft resistance is not constant over the telltale lengths, the so-determined average should be plotted somewhat below the mid-point of the telltale. However, as this "somewhat" depth cannot be determined with confidence (see Clause 8.7.2), the averages have simply been plotted at the respective mid-points. The TTL-determined load distributions differ from the VW-determined. This is because, as mentioned in the foregoing, telltale records are not accurate means for either determining magnitude or location of the average loads, although, if compression had been the primary measurement, as opposed to movement, a better agreement with the strain-gage evaluated loads would probably have been found. The pile-toe Target force (lowest dashed extension) is included to ensure that the values plotted at the lowest VG-gage depth are not mistaken for the toe forces.

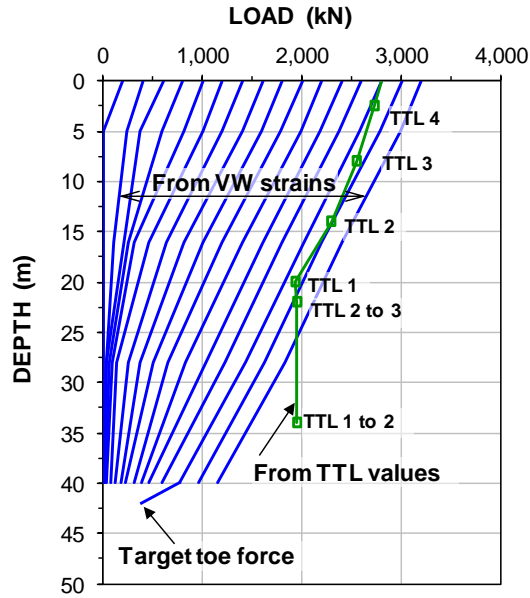


Fig. 8.79 Force distributions at VW-gages and from telltales at the 2,800-kN Target Load

The CPTU sounding was input to UniPile and the load distribution was calculated applying the Schmertmann, Eslami-Fellenius (E-F), LCPC, UWA, and Dutch methods (see Section 7.9). The results (Figure 8.80) show a scatter of distributions (note, always is the case because the methods are different) with the LCPC-distribution quite close to the distribution obtained by the VW-gages for the 2,800-kN Target-Load. Note, the CPT load-distributions are ostensibly the distribution for an ultimate resistance as per "the eye of the beholder". However, the Target load chosen has no other significance than being a load that produced a noticeable movement at, primarily, the pile toe. Therefore, agreement or non-agreement with the Target-Load distribution is just a coincidence. While the distributions of the CPT/CPTU-methods are ostensibly the distribution for capacity—note, only the E-F method states the capacity definition (Davisson's offset limit) that was used in their development—the Target Load was just the load that resulted in a movement deemed suitable as reference for the analysis.

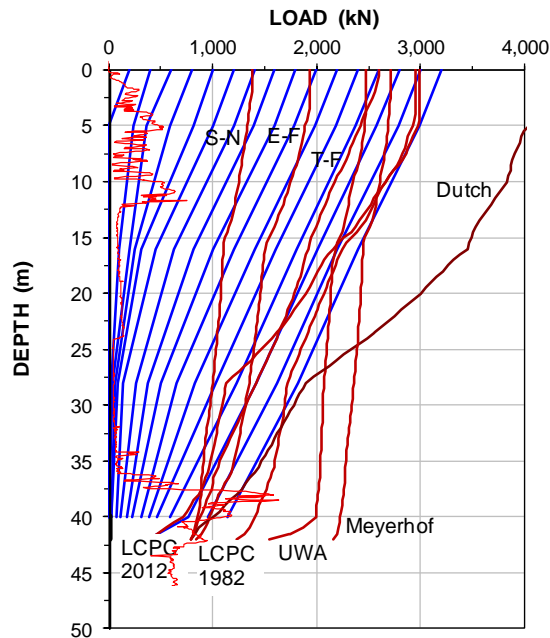


Fig. 8.80 Load distributions from VW records compared to distributions per CPT/CPTU methods

The soil densities and groundwater level were input to the UniPile program and the distribution of effective stress was calculated. The effective stress times a beta-coefficient is equal to unit shaft resistance. A force distribution was started from the applied 2,800-kN Target diminishing with depth by the shaft resistance and the calculated force was fitted to the measured at each gage level, L1 through L4, thus, back-calculating beta-coefficients along the pile. Figure 8.81 shows the so-calculated distribution (green shade) with the so-determined beta-coefficients shown to the left in the graph. For the 2.0 m length between the pile toe and L1, the beta-coefficient and the toe resistance can be considered interdependent.

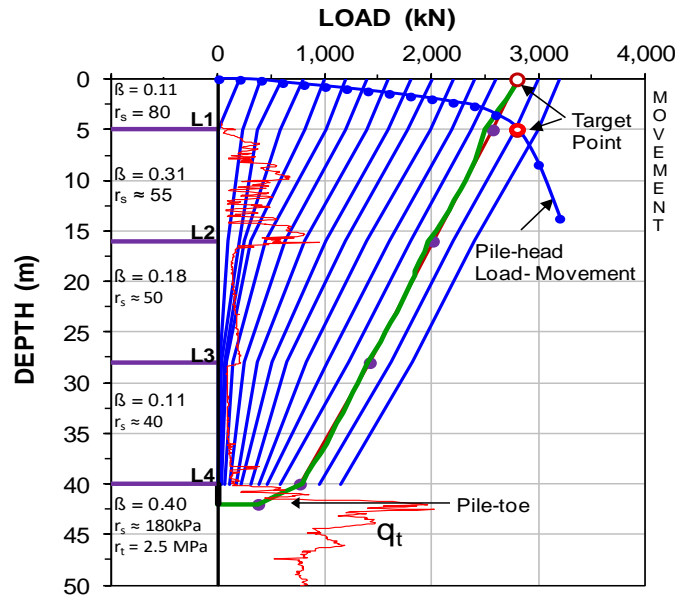


Fig. 8.81. Load distributions from VW-gages and UniPile effective stress analysis

Also provided with each beta-coefficient label are the corresponding average unit shaft resistance,  $r_s$ , as determined from the difference of VW-calculated load between two gage levels, Dividing that difference with the mean effective stress in the layer and dividing it the pile circumference, it would be in the format of a beta-coefficient. However, the value would differ from those shown, which is because the would-be calculation is a differentiation method and, therefore, imprecise.

The linear shape of force distributions and their lack of correlation to the CPT  $q_c$  distribution could be a sign of residual force in the pile. However the appearance may be caused by the larger shaft resistance in the 5-16 m layer as opposed to the soil below 16 m depth—suggested by the CPT sounding  $q_c$  resistance.

Next action was fitting calculated load-movement curves to the actual load-movement curves from the strain-gage determined loads versus the telltale-measured gage-level movements. The process was performed in UniPile by assigning the loads at each gage level for the 2,800-kN Target Load at the pile head to correspond to the  $\beta$ -coefficients to be at their 100 % and selecting a t-z curve (t-z function; c.f., Section 8.11) that resulted in a fit between the load distribution curve calculated by UniPile to the one measured.

The fitting to the force-movement curves started with the lowest gage level, L1. When a fit was obtained, the procedure was repeated for the next level, L2, and so on. When the fit for the last level, L4, was completed, the pile-head load movement curve was calculated. As mentioned, in calculating the load, UniPile applies the Beta (and/or  $r_s$ ) at the 100-% input value. The load-movement calculation used the fitted beta-coefficients and the measured movement induced by the Target Load (c.f., Figure 8.74 and Table 8.3). The fitting procedure then established the function coefficient deciding the shape of the t-z (or q-z) curve.

Figure 8.82 shows the actual input for the 5.0 m thick, upper soft clay layer and all four t-z function curves are compiled in Figure 8.83 together with the q-z function (pile toe). The data quality allowed a very precise assessment of the softening to plastic shaft-resistance response beyond what is normally possible. Table 8.3 shows the input that gave the fit for the test records. Finally, Figure 8.84 compiles the measured and calculated (fitted) curves. Solid lines are measured curves and dashed lines are curves calculated by UniPile in the fitting procedure. A line connects the gage-level movements for the Target Load. Note, the calculated curves are obtained by combining the t-z/q-z functions with the respective beta-coefficients for the Target load and movement.

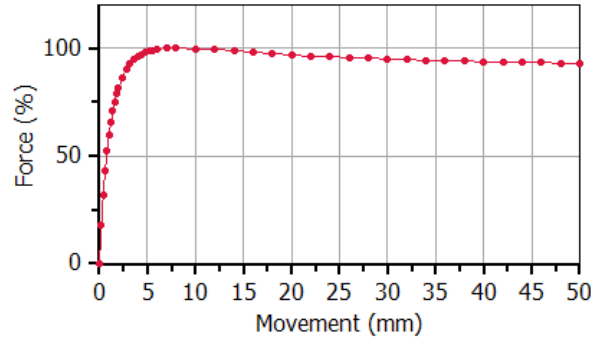


Fig. 8.82 The Zhang strain-softening t-z curve used as input for the 5.0 m thick upper soft clay layer

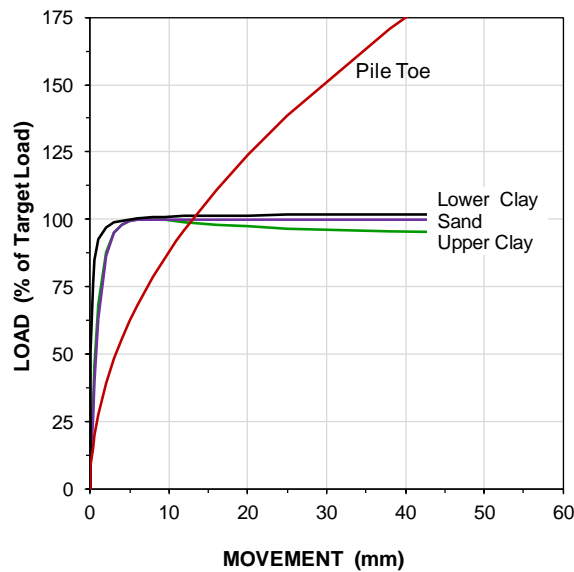


Fig. 8.83 Compilation of all four t-z curves used as input for the load-movement measurements

**Table 8.3.** The t-z and q-z input to UniPile

Depth (m) (m)	Soil Type	Density (kg/m <sup>3</sup> ) (kg/m <sup>3</sup> )	t-z/q-z Method	Movement <sup>*)</sup> at Target (mm)	Function Coefficient (--)	Beta (β) Coefficient (--)	r <sub>t</sub> (MPa)
0 - 5	Clay	1,800	Zhang	7	0.010	1.10	
5 - 16	Sand	2,000	vander Veen	4+	1.000	0.31	
16 - 28	Clay	2,000	Chin-Kondner	18	0.010	0.18	
28 - 42	Sand	1,900	vander Veen	5+	1.000	0.11	
Toe	Sand	2.05	Gwizdala	13	0.300	0.40	2.5

\*) For the t-z functions, the input of "Movement at Target" was to direct the shape of the t-z curve. For the q-z curve, it was the movement for the actual pile toe movement, the TTL1-value, at the Target Load.



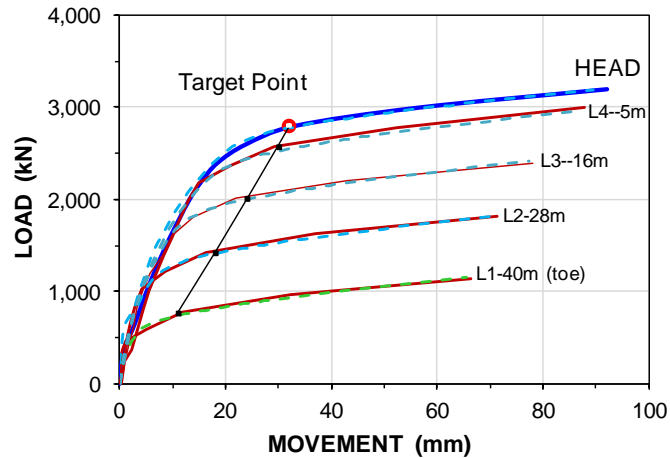


Fig. 8.84 Measured and fitted load-movement curves of pile head and gage levels

The parameters determined in the back-analysis of the test data can be used to analyze what response to expect for a pile similar to the test pile to a range of applied loads (sustained loads from a supported structure), as well as the analyzing what a change of pile size, embedment depth, etc. would entail for the supported structure.

As a note on the side, when assessing the pile response by reference to CPT-soundings, the distribution of ultimate resistance calculated by the various CPT methods can be of interest. Figure 8.85 shows the load-movement based on the  $t$ - $z$  and  $q$ - $z$  functions derived from the fitting to the loading-test and the ultimate resistance calculated at each CPT-record by using the respective ultimate resistances of the CPT-method of each record as the target value in producing the load-movement curves the same way as it was using the target resistance calculated with the beta-coefficients. Each CPT-method total ultimate resistance is indicated with a diamond symbol in the figure. The circle symbols indicate the measured load-movement points of the static loading test. See also Figure 8.80. The two figures must not be taken as indicating a rating of agreement between a CPT-method and the result of a static loading test. A different site, different test pile, different CPT-sounding, a similar set of curves would likely be produced, but one implying different rating results for a comparison of CPT-method results to the test. It is often stated, however, that comparing the results of CPT-analyses to the results of a static loading test at a site, one analysis method can be found that is "calibrated" to the conditions, and, therefore useful for extending the results of the CPT analysis to other piles at a site. Nevertheless, the primary purpose of a CPT sounding is to address—classify—the soil layering, not to use numerically to determine pile static resistance.

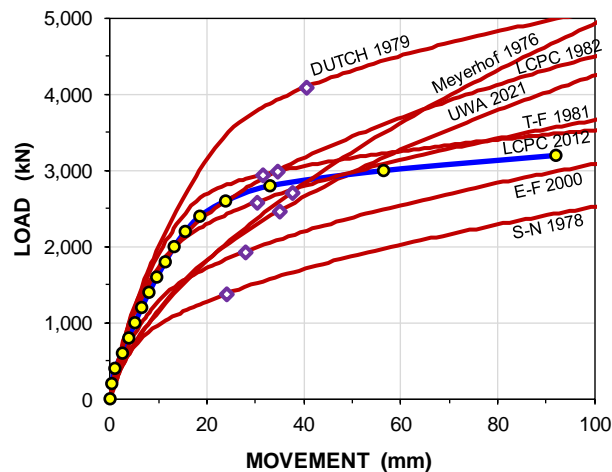


Fig. 8.85 Load-movement curves from CPT calculations with the actual test curve

### 8.10.4 Closing remarks

The test results make for an instructive analysis case. However, I find the test records a little bit too neat for me to fully trust the records beyond use as an illustration for analysis. For example, the 200-kN load increments, originally delivered with decimals, are unusually exact for being the loads actually applied, and I have rarely seen secant and tangent modulus plots with such close agreement and absence of erratic values. Moreover, I would have expected a filter cake to have been developed along the pile during the wait time between completed drilling and cleaning of the slurry and tremie-concreting the pile. Thus, the back-calculated beta-coefficients (Table 8.3) are probably more representative of pile-filter-cake resistance than of pile-soil resistance. I also believe that a good deal of debris must have accumulated at the bottom of the hole and the evaluated pile toe response, therefore, was softer than it would have been had the bottom of the hole been properly cleaned.

That is to say, that no reference should be made to the evaluated values as fully true, only to the process of evaluating of test records, which is my purpose of here presenting the case. The analysis approach can be additionally reviewed in the similar static loading test example in Chapter 15, Example 15.6.3.

### 8.11 Example of use of results from a routine test

To reiterate the futility of applying the concept of capacity, Figure 8.86 shows load-movement results of a head-down static loading test on a 300-mm diameter, round, 20 m long, prestressed concrete pile driven in a loose to compact clayey, silty sand. The test was instrumented to enable determining the toe load-movement response. The desired working load (sustained, no live) was 600 kN. Two different designers, Persons A and B, used the pile-head load-movement curve measured in the test to determine pile capacity and concluded that the pile capacity was 1,000 kN and 1,500 kN, respectively, obviously applying different definitions. The span between the values is typical for what of what I frequently encounter in projects. Coincidentally, it is very close to the two standard deviations span of the assessments established in the capacity survey summarized in Figure 8.8 (Section 8.4). Both A and B wanted to apply a factor of safety of 2.0. Then, B arrived at the decision that the pile is good for the desired working load, while A wanted to reject or, at least, downgrade the pile.

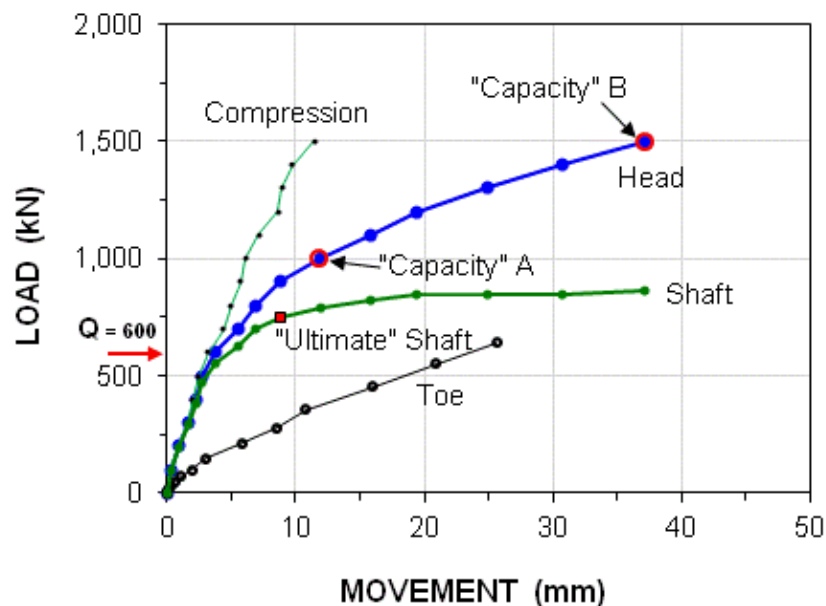


Fig. 8.86. Pile load-movement curves with capacity assessments by Persons A and B

Both A and B calculated the capacity employing effective stress analysis and both applied a beta-coefficient of 0.25 for determining "ultimate" shaft resistance,  $R_{ULT,s}$ , arriving at the same 750 kN-value. the red square plotted on the shaft curve. However, they diverged in regard to what to call the "ultimate toe resistance",  $R_{ULT,t}$ , applying 250 and 650 kN, respectively, as "ultimate toe resistance". Person B's 650-kN toe resistance was simply the toe force measured in the test at the test load Person B had assigned as "capacity".

Who of the two persons, A and B, is right and who is wrong? Should the pile be accepted or rejected? Actually, neither is right because neither A nor B realized that  $\beta$ -coefficient and toe response are meaningless unless coupled to movements and that assessing the suitability of the pile for a working load, be the pile single or a one of a group of piles, must include settlement analysis and be correlated to the response to settlement of the supported structure.

Back-calculation of the results of the static loading test provided the necessary information for assessing the suitability of the piles. The assessment must not be per the artificial concept of capacity, but by fitting a load-movement response to the pile response. Figure 8.87. shows the t-z and q-z functions that gave the fit. The load-movement analysis can then be used to determine the axial force distribution and, combined with the site conditions, be applied to a settlement analysis. The t-z function is related to the  $\beta$ -coefficient for the various movements (constant effective stress) as opposed to the usual percentage of a specific shear stress-movement value. The t-z function is a hyperbolic (Chin-Kondner) with a function coefficient of 0.0082 (asymptotic resistance,  $1/C_1$ , of 122 %) and a 3-mm target movement for 100% target resistance at a beta-coefficient of 0.30. The q-z function of the fit was a Gwizdala function with a  $\theta = 0.70$  function-coefficient and a target toe-force of 140-kN at a 3-mm target movement (and 630 kN at 26 mm movement). The groundwater table was assumed to be at the ground surface.

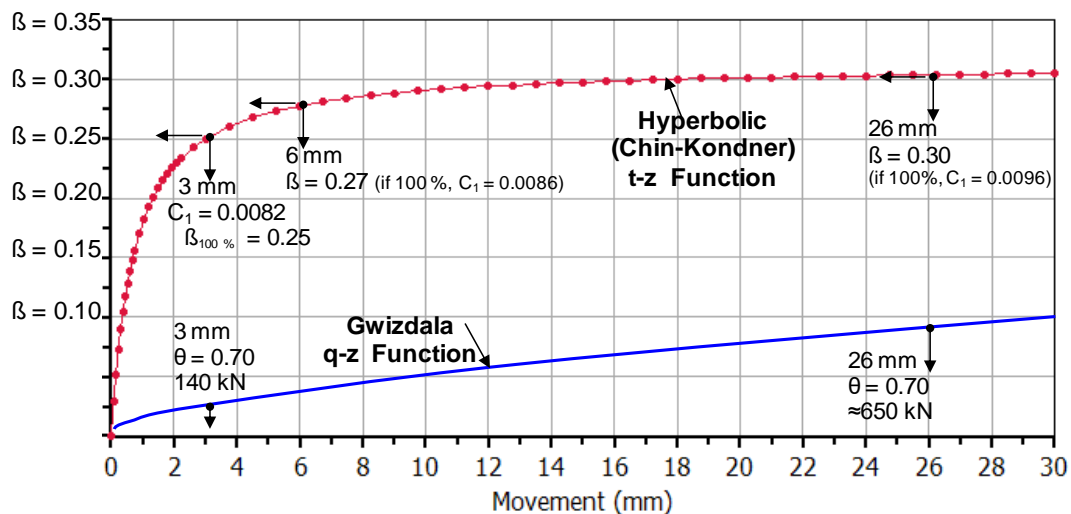


Fig. 8.87. The t-z and q-z response of the test pile

These results can be used to produce the force distributions for different loads applied to the pile head and, more important, the long-term force distribution for the 600-kN sustained load, which, coupled with the distribution of soil settlement, will enable determining the long-term settlement of the piled foundation. For example, as affected by a potential general subsidence at the site (see Section 7.17).

What matters for the design of the piled foundation is not what and how to define and determine a capacity. If the site will not experience any settlement due to general subsidence and only single piles and narrow pile groups are contemplated, then, a pile with a 600-kN sustained load will result in an about 5 mm total long-term settlement due to compression and toe movement, which will in most cases will be well below permissible values. If, on the other hand, the site will be affected by general

subsidence, a neutral plane will then develop and the settlement of the soil at the neutral plane will be the settlement of the piled foundation (plus pile compression). Thus, to accept or not to accept the piles for the 600-kN sustained load will be governed by the particular settlement conditions at the site—definitely not by a subjectively established capacity divided by some factor of safety.

Figure 8.88 shows the load distributions for the two values of capacity as deduced by Persons A and B from the loading test.

Whether or not the design decision of Persons A and B as to the sustained load are correct depends entirely on the actual distribution of the settlement to expect at the site. Figure 8.89 shows the Load and Resistance graph together with the Settlement graph according to the unified method. Two alternative settlement scenarios are shown. If the force and resistance equilibriums of Person A (blue curves) are correct, then, the pile foundation will only settle about 'half-an-inch' and the margin toward excessive settlement would appear to be good. It would then seem that the rejection of the 600-kN load by Person A is not reasonable. On the other hand, if the alternative of general subsidence (larger settlement) at the site is true, then, the force distribution will be different and the settlement of the piled foundation will be larger and might become excessive. So, if the force and resistance equilibriums of Person B (red curves) are correct, then, the piled foundation will settle slightly more than an 'inch', which structural designers may find excessive for a piled foundation. A more detailed study of the conditions might then be advisable before finalizing the design.

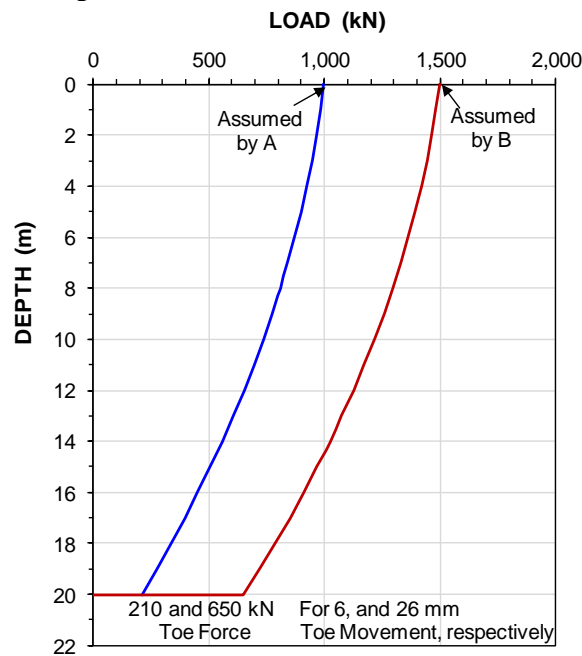


Fig. 8.88 Force distributions as deduced by Persons A and B

Indeed, the acceptance of the 600-kN sustained load depends of the settlement assessment with due consideration of the t-z and q-z responses. The initial assessment of "capacity" is irrelevant to the design.

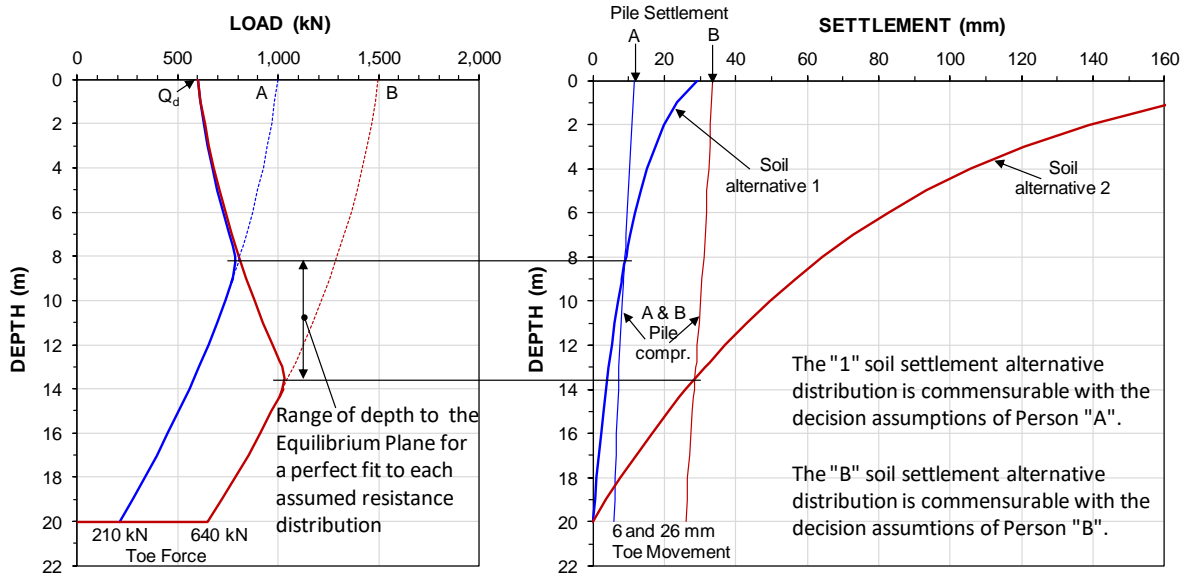


Fig. 8.89 Unified method correlations per the Persons A and B cases



*In spite of their obvious deficiencies and unreliability, pile driving formulas still enjoy great popularity among practicing engineers, because the use of these formulas reduces the design of pile foundations to a very simple procedure. The price one pays for this artificial simplification is very high.* Karl Terzaghi (1942); Repeated by Terzaghi in Theoretical Soil Mechanics. John Wiley & Sons, New York (Terzaghi 1943).

## CHAPTER 9

### PILE DYNAMICS

#### 9.1 Introduction

The development of the wave equation analysis from the pre-computer era of the fifties (Smith 1960) through the advent of a computer version in the mid-seventies was a quantum leap in foundation engineering. For the first time, a design could consider the entire pile driving system, such as wave propagation characteristics, particle-velocity dependent aspects (damping), soil deformation characteristics, soil resistance (total as well as its distribution of resistance along the pile shaft and between the pile shaft and the pile toe), hammer behavior, and hammer cushion and pile cushion parameters.

The full power of the wave equation analysis is first realized when it was combined with dynamic monitoring of the pile during driving. The dynamic monitoring consists in principle of recording and analyzing the strain and acceleration induced in the pile by the hammer impact. It was developed in the USA by Drs. G.G. Goble and F. Rausche, and co-workers at Case Western University in the late 1960s and early 1970s. It has since evolved further and, as of the early 1980s, it was accepted all over the world as a viable tool in geotechnical engineering practice.

Pile driving consists of forcing a pile to penetrate into the ground by means of a series of short duration impacts. The impact force has to be greater than the static soil resistance, because a portion of the force is needed to overcome the dynamic resistance to the pile penetration (the dynamic resistance is a function of the particle velocity of the pile). Mass of the ram (hammer), ram impact velocity, specifics of the pile helmet and of cushioning element such as hammer and pile cushions, as well as cross section of the ram, and cross section and length of the pile are all important factors to consider in an analysis of a specific pile driving situation. Of course, also the soil parameters, such as strength, shaft resistance including its distribution along the pile, toe resistance, and dynamic soil parameters, must be included in the analysis. It is obvious that for an analysis to be relevant requires that information used as input to the analysis correctly represents the conditions at the site. It a complex undertaking. Just because a computer program allows input of many parameters does not mean that the analysis results are true to the situation analyzed.

The soil resistance acting against a driven pile is based on the same mechanics as the resistance developed from a static load on the pile. That is, the resistance is governed by the principle of effective stress. Therefore, to estimate in the design stage how a pile will behave during driving at a specific site requires reliable information on the soil conditions including the location of the groundwater table and the pore pressure distribution. For method and details of the static analysis procedures, refer to Chapter 7.

The design of piles for support of a structure is directed toward the site conditions prevailing during the life of the structure. However, the conditions during the pile installation can differ substantially from those of the service situation—invariably and considerably. The installation may be represented by the initial driving conditions, while the service situation may be represented by the restrike conditions.

Questions of importance at the outset of the pile driving are the site conditions, including soil profile and details such as the following: will the piles be driven in an excavation or from the existing ground surface, is there a fill on the ground near the piles, and where is the groundwater table and what is the pore pressure distribution? Additional important questions are: will the soils be remolded by the driving and develop excess pore pressures? Is there a risk for the opposite, that is, dilating conditions, which may impart a false resistance? Could the soils become densified during the continued pile installation and cause the conditions to change as the pile driving progresses? To properly analyze the pile driving conditions and select the pile driving hammer requires the answers to questions such as these.

In restriking, the pore pressure distribution, and, therefore, the resistance distribution is very different to that developing during the initial driving. For this reason, a pile construction project normally involves restriking of piles for verification of "capacity". Usually, the restrike observation indicates that a set-up has occurred. (Notice, it is not possible to quantify the amount of soil set-up unless the hammer is able to move the pile). On occasions, the restrike will show that relaxation, i.e., diminishing "capacity", the opposite to soil set-up, may have occurred, instead.

As is the case for so much in engineering design and analysis, the last few decades have produced immense gains in the understanding of "how things are and how they behave". Thus, the complexity of pile driving in combination with the complexity of the transfer of the loads from the structure to a pile can now be addressed by rational analysis. In the past, analysis of pile driving was simply a matter of applying a so-called pile driving formula to combine "blow count" and "capacity". Several hundred such formulae exist. They are all fundamentally flawed and lack proper empirical support. Their continued use is strongly discouraged.<sup>1)</sup>

## 9.2. Principles of Hammer Function and Performance

Rather simplistically expressed, a pile can be installed by means of a static force, i.e. a load, which forces the pile into the soil until it will not advance further. Such installation techniques exist and the piles are called "jacked-in piles", see for example Yang et al. (2006) and Fellenius (2015). The jacked load is then about equal to the static "capacity" of the pile. However, for most piles and conditions, the magnitude of the static load needs to be so large as to make it impractical to use a static load to install a pile other than under special conditions.

---

<sup>1</sup> In the past, when an engineer applied a "proven" formula — "proven" by the engineer through years of well-thought-through experience from the actual pile type and geology of the experience — the use of a dynamic formula could be defended. It did not matter what formula the engineer preferred to use, the engineer's ability was the decisive aspect. That solid experience is vital is of course true also when applying modern methods. The engineers of today, however, can lessen the learning pain and save much trouble and costs by relating their experience to the modern methods. Sadly, despite all the advances, dynamic formulae are still in use. For example, some Transportation Authorities and their engineers even include nomograms of the Hiley formula in the contract specifications, refusing to take notice of the advances in technology and practice! Well, each generation has its share of die-hards. A couple of centuries or so ago, they, or their counterpart of the days, claimed that the Earth was flat, that ships made of iron could not float, that the future could be predicted by looking at the color of the innards of a freshly killed chicken, etc., rejecting all evidence to the contrary. Let's make it absolutely clear, basing a pile design today on a dynamic formula shows unacceptable ignorance and demonstrates incompetence. Note, however, that the use of the most sophisticated computer program does not provide any better results unless coupled with experience and good judgment.



In driving a pile, one is faced with the question of what portion of the applied dynamic force is effective in overcoming the "capacity" (that is, the "useful" static soil resistance) and what portion is used-up to overcome the resistance to the pile movement, or, rather, its velocity of penetration. This velocity dependent resistance is called damping. In principle, a pile is driven by placing a small weight some distance over the pile head and releasing it to fall. In falling, the weight picks up velocity, and, on impacting the pile head, it slows down before bouncing off the pile head. The weight's change of velocity, that is, this deceleration, creates a force between the hammer and the pile during the short duration of the contact. Even a relatively light weight impacting at a certain significant velocity can give rise to a considerable force in the pile, which then causes the pile to penetrate a short distance into the soil, overcoming static resistance, inertia of the masses involved, as well as overcoming resistance due to the velocity of penetration. Accumulation of impacts and consequential individual penetrations installs the pile.

The impact duration is so short, typically 0.05 seconds, that although the peak penetration velocity lies in the range of several metre/second, the net penetration for a blow is often no more than about a millimetre or two. (Considering 'elastic' response of pile and soil, the gross penetration per blow can be about 20 times larger). In contrast to forcing the pile down using a static force, when driving a pile, the damping force is often considerable. For this reason, the driving force must be much larger than the desired pile "capacity".<sup>2</sup>

The ratio between the mass of the impacting weight and the mass of the pile (or, rather, its cross section and total mass) and its velocity on impact will govern the magnitude of the impact force (impact stress) and the duration of the impact event. A light weight impacting at high velocity can create a large local stress, but the duration may be very short. A low-velocity impact from a heavy weight may have a long duration, but the force may not be enough to overcome the soil resistance. The impact velocity of a ram and the duration of a blow are, in a sense, measures of force and energy, respectively.

The force generated during the impact is not constant. It first builds up very rapidly to a peak and, then, decays at a lesser rate. The peak force can be very large, but be of such short duration that it results in no pile penetration. Yet, it could be larger than the strength of the pile material, which, of course, would result in damage to the pile head. By inserting a cushioning pad between the pile head and the impacting weight (the hammer or ram), this peak force is reduced and the impact duration is lengthened, thus both keeping the maximum force below damaging values and making it work longer, i.e., increasing the penetration per blow.

The effect of a hammer impact is a complex combination of factors, such as the velocity at impact of the hammer, the weight of the hammer (impacting mass) and the weight of the pile, the cross section of the hammer and the cross section of the pile, the various cushions in the system between the hammer and the pile, and the condition of the impact surfaces (for example, a damage to the pile head would have a subsequent cushioning effect on the impact, undesirable as it reduces the ability of the hammer to drive the pile), the weight of the supporting system involved (for example, the weight of the pile driving helmet), and last, but not least, the soil resistance, how much of the resistance is toe resistance and how much is shaft resistance, as well as the distribution of the shaft resistance. All these must be considered when selecting a hammer for a specific situation to achieve the desired results, that is, a pile installed the pile to a certain depth and/or "capacity", quickly and without damage.

---

<sup>2</sup> This seemingly obvious statement is far from always true. The allowable load relates to the pile "capacity" after the disturbance from the pile driving has dissipated. In the process, the pile will often gain "capacity" due to set-up (see Chapter 7).

Old rules-of-thumb, e.g., that the pile weight to ram weight ratio should be ‘at least 2 for an air/steam hammer’ and ‘at least 4 for a diesel hammer’ are still frequently quoted. These rules, however, only address one of the multitudes of influencing aspects. They are also very inaccurate and have no general validity.

The hammer energy, or rather, the hammer “**rated energy**” is frequently used to indicate the size of a hammer and its suitability for driving a certain pile. The rated energy is the weight of the ram times its travel length and it is, thus, the same as the “positional” energy of the hammer. The rated or positional energy is a rather diffuse term to use, because it has little reference to the energy actually delivered to the pile and, therefore, it says very little about the hammer performance. By an old rule-of-thumb, for example, for steel piles, the rated energy of a hammer was referenced to the cross section of the pile as  $6 \text{ MJ/m}^2$ . This rule has little merit and leads often to an incorrect choice of hammer. (In English units, the rule was 3 ft-kips per square inch of steel).

A more useful reference for pile driving energy is the “**transferred energy**”, which is energy actually transferred to a pile and, therefore, useful for the driving. It can be determined from measurements of acceleration and strain near the pile head during actual pile driving obtained by means of the Pile Driving Analyzer (see Section 9.7). The transferred energy value is determined after losses of energy have occurred (such as losses before the ram impacts the pile, impact losses, losses in the helmet, and between helmet and pile head).

Although, no single definition for hammer selection includes all aspects of the pile driving, energy is one of the more important aspects. Energy is addressed in more than one term, as explained in the following.

The term “**energy ratio**” is also commonly used to characterize a hammer function. The energy ratio is the ratio between the transferred energy and the rated energy. This value is highly variable as evidenced in the frequency charts shown in Figures 9.1 and 9.2. The measurements shown in the diagram were from properly functioning hammer and the variations are representative for variation that can occur in the field.

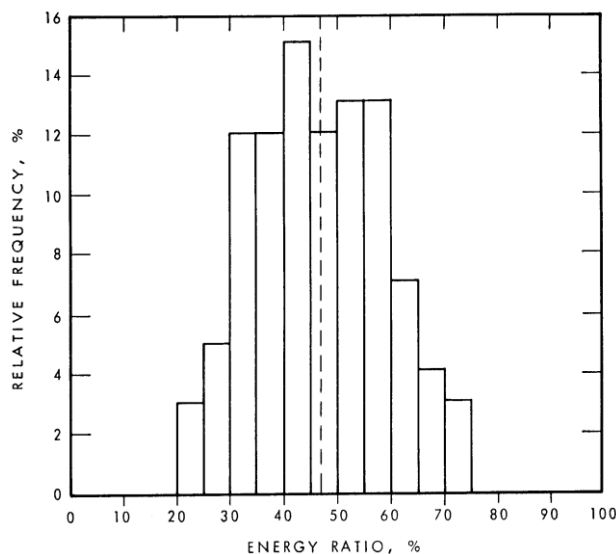


Fig. 9.1 Energy ratio

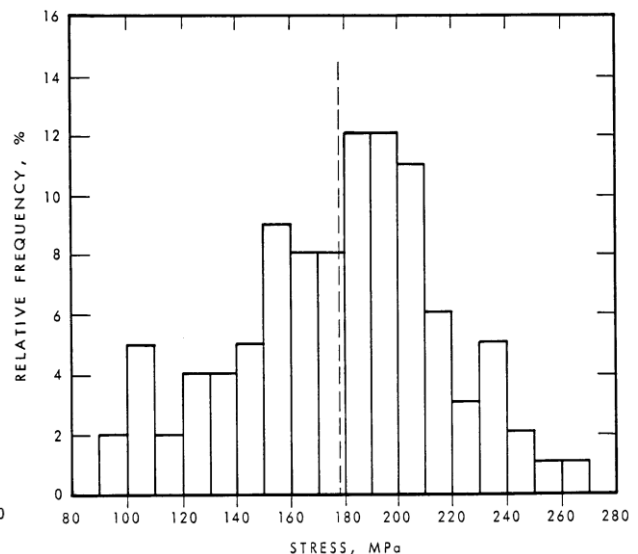


Fig. 9.2 Impact stress

From measurements on 226 steel piles (data from Fellenius et al. 1978)

For example, the term “**hammer efficiency**”. Hammer efficiency is defined as the ratio between the kinetic energy of the ram at impact to the ideal kinetic energy, which is a function of the ram velocity. A 100 % efficiency corresponds to ideal kinetic energy: the velocity the ram would be the same as the ram would have had in free fall in vacuum with no losses. Notice, the hammer efficiency does not consider the influence of cushioning and losses in the helmet, the helmet components, and the pile head.

Obviously, energy alone is not a sufficient measure of the characteristic of an impact. Knowledge of the magnitude of the impact force is also required and it is actually the more important parameter. However, as the frequency chart presented in Figure 9.2 demonstrates, field measurements indicate that also the impact stress varies considerably.

The reasons for the variations of energy and stress are only partly due to a variation of hammer size, hammer cushion characteristics, and hammer performance. The variations are also due to factors such as pile size (diameter and cross sectional area), pile length, and soil characteristics. As will be explained below, these factors can be taken into account in a wave equation analysis.

### 9.3. Hammer Types

The oldest pile driving hammer is the conventional “**drop hammer**”. Its essential function was described already by Caesar 2,000 years ago in an account of a Roman campaign against some Germanic tribe (building a bridge, no less). The drop hammer is still commonly used. As technology advanced, hammers that operate on steam power came into use around the turn of the century. Today, steam power is replaced by air power from compressors and the common term is now “**air/steam hammer**”. Hammers operating on diesel power, “**diesel hammers**”, were developed during the 1930s. An advancement of the air/steam hammer is the “**hydraulic hammer**”, which uses hydraulic pressure in lifting the ram as well as accelerating it downward to a large impact velocity after a small travel length. Electric power is used to operate “**vibratory hammers**”, which function on a principle very different to that of impact hammers. Commonly used hammers are described below.

#### 9.3.1 Drop Hammers

The conventional drop hammer consists chiefly of a weight that is hoisted to a distance above the pile head by means of a cable going up to a pulley on top of the leads and down to be wound up on a rotating drum in the pile driver machine. When released, the weight falls by gravity pulling the cable along and spinning the drum where the excess cable length is stored. The presence of the cable influences the efficiency of the hammer.<sup>3)</sup> The influence depends on total cable length (i.e., mass) as well as the length of cable on the drum, the length between the drum and the top of the leads, and the length of cable between the leads and the drop weight. This means, that the efficiency of the hammer operating near the top of the leads differs from when it operates near the ground. The amount of friction between the ram weight and the guides in the leads also influences the hammer operation and its efficiency. Whether the pile is vertical or inclined is another factor affecting the frictional losses during the “fall” and, therefore, the hammer efficiency. In addition, to minimize the bouncing and rattling of the weight, the operator usually tries to catch the hammer on the bounce, engaging the reversal of the drum before the impact. In the process, the cable is often tightened just before the impact, which results in a slowing down of the falling ram weight just before the impact, significantly reducing the efficiency of the impact.

---

<sup>3)</sup> Note, as indicated above, hammer efficiency is a defined ratio of kinetic energy and the term must not be used loosely to imply something unspecified but essentially good and desirable about the hammer.

### 9.3.2 Air/Steam Hammers

The air/steam hammer operates on compressed air from a compressor or steam from a boiler, which is fed to the hammer through a hose. Figure 9.3 illustrates the working principle of the single-acting air/steam hammer. (The figure is schematic and does not show assembly details such as slide bar, striker plate helmet items, etc.). At the start of the upstroke, a valve opens letting the air (or steam) into a cylinder and a piston, which hoists the ram. The air pressure and the volume of air getting into the cylinder controls the upward velocity of the ram. After a certain length of travel (the upward stroke), the ram passes an exhaust port and the exhaust valve opens (by a slide bar activating a cam), which vents the pressure in the cylinder and allows the ram to fall by gravity to impact the hammer cushion and helmet anvil. At the end of the downward stroke, another cam is activated which opens the inlet valve starting the cycle anew. The positional, nominal, or rated energy of the hammer is the stroke times the weight of the ram with its parts such as piston rod, keys, and slide bar.

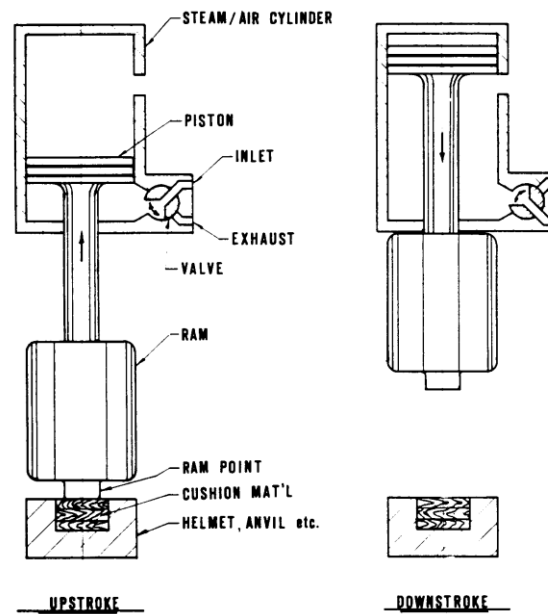


Fig. 9.3 The single-acting air/steam hammer (DFI 1979; used with permission)

As in the case of the drop hammer, the efficiency of the impact is reduced by friction acting against the downward moving ram. However, two very important aspects specific to the air/steam hammer can be of greater importance for the hammer efficiency. First, the inlet valve is always activated shortly before the impact, creating a small pre-admission of the air. If, however, the release cam is so placed that the valve opens too soon, the air that then is forced into the cylinder will slow the fall of the weight and reduce the hammer efficiency. The design of modern air/steam hammers is such as to trap some air in above the ram piston, which cushions the upward impact of the piston and gives the downward travel an initial “push”. The purpose of the “push” is also to compensate for the pre-admission at impact. For more details, see the hammer guidelines published by Deep Foundations Institute (DFI 1979).

When the air pressure of the compressor (or boiler) is high, it can accelerate the upward movement of the ram to a significant velocity at the opening of the exhaust port. If so, the inertia of the weight will make it overshoot and travel an additional distance before starting to fall (or increase the “push” pressure in the “trap”), which will add to the ram travel and seemingly increase the efficiency.

For the double-acting air/steam hammer, air (steam) is also introduced above the piston to accelerate the down stroke, as illustrated in Figure 9.4. The effect of this is to increase the impact rate, that is, the number of blows per minute. A single-acting hammer may perform at a rate of about 60 blows/minute, and a double acting may perform at twice this rate. The rated energy of the double-acting hammer is more difficult to determine. It is normally determined as the ram stroke times the sum of the weights and the area of the piston head multiplied by the downward acting air pressure. The actual efficiency is quite variable between hammers, even between hammers of the same model and type. Where the ram velocity at impact is measured, this determines the kinetic energy that then is used in lieu of rated energy.

A double-acting air/steam hammer is closed to its environment and can be operated submerged.

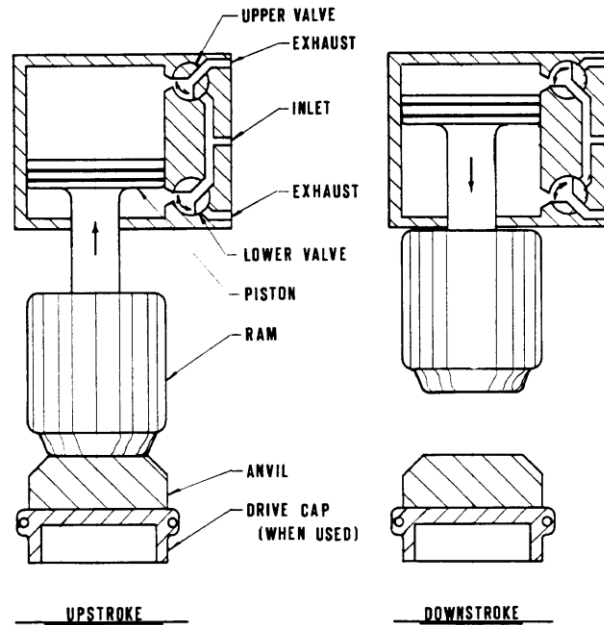


Fig. 9.4 The double-acting air/steam hammer (Deep Foundations Institute 1979)

### 9.3.3 Diesel Hammers

A diesel hammer consists in principle of a single cylinder engine. A diesel hammer is smaller and lighter than an air/steam hammer of similar capability. Figure 9.5 illustrates the working principle of a liquid injection **single-acting open-end diesel hammer**. The hammer is started by raising the ram with a lifting mechanism. At the upper end of its travel, the lifting mechanism releases the ram to descend under the action of gravity. When the lower end of the ram passes the exhaust ports, a certain volume of air is trapped, compressed, and, therefore, heated. Some time before impact, a certain amount of fuel is squirted into the cylinder onto the impact block. When the ram end impacts the impact block, the fuel splatters into the heated compressed air, and the combustion is initiated. There is a small combustion delay due to the time required for the fuel to mix with the hot air and to ignite. More volatile fuels have a shorter combustion delay as opposed to heavier fuels. This means, for example, that if winter fuel would be used in the summer, pre-ignition may result. Pre-ignition is combustion occurring before impact and can be caused by the wrong fuel type or an overheated hammer. Pre-ignition is usually undesirable.

The rebound of the pile and the combustion pressure push the ram upward. When the exhaust ports are cleared, some of the combustion products are exhausted leaving in the cylinder a volume of burned gases at ambient pressures. As the ram continues to travel upward, fresh air, drawn in through the exhaust ports, mixes with the remaining burned gases.

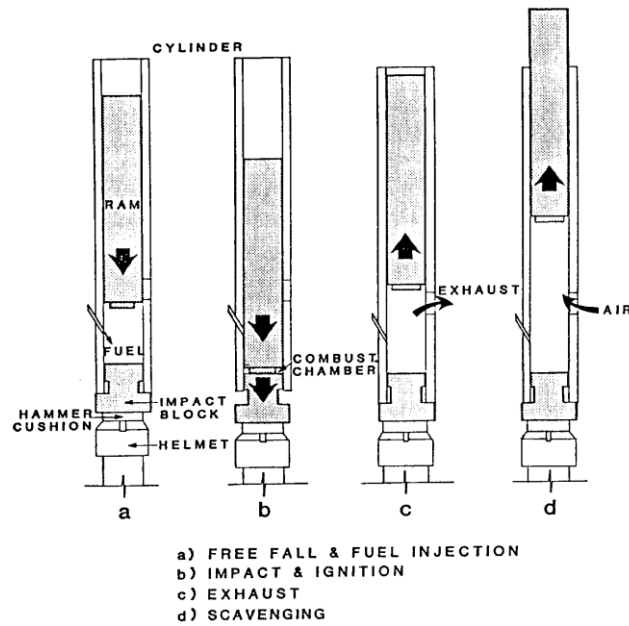


Fig. 9.5 Working principle of the liquid injection, open-end diesel hammer (GRL 2002)

The ram will rise to a height (stroke) that depends on the reaction of the pile and soil combination to the impact and to the energy provided by the combustion. It then descends under the action of gravity to start a new cycle. The nominal or rated energy of the hammer is the potential energy of the weight of the ram times its travel length. It has been claimed that the energy released in the combustion should be added to the potential energy. That approach, however, neglects the loss of energy due to the compression of the air in the combustion chamber.

The sequence of the combustion in the diesel hammer is illustrated in Figure 9.6 showing the pressure in the chamber from the time the exhaust port closes, during the precompression, at impact, and for the combustion duration, and until the exhaust port opens. The diagram illustrates how the pressure in the combustion chamber changes from the atmospheric pressure just before the exhaust port closes, during the compression of the air and the combustion process until the port again opens as triggered by the ram upstroke. During the sequence, the volume of the combustion chamber changes approximately in reverse proportion to the pressure. Different hammers follow different combustion paths and the effect on the pile of the combustion, therefore, differs between different hammers.

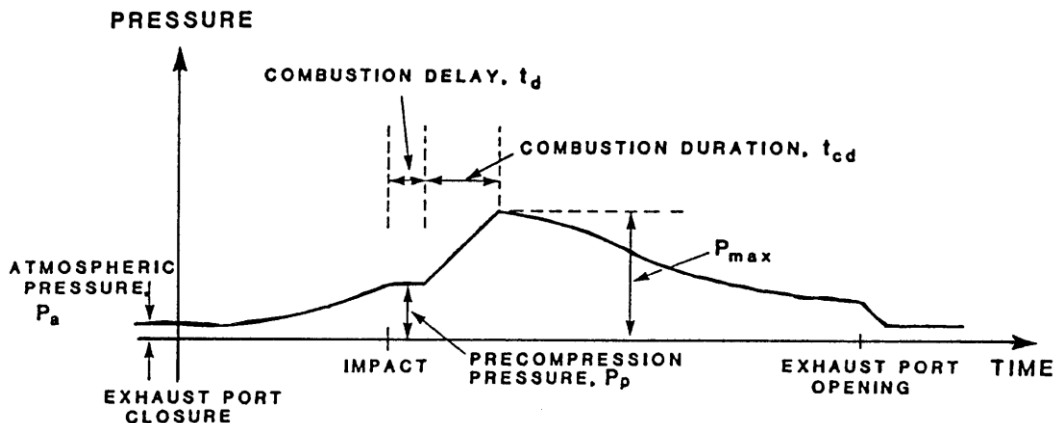


Fig. 9.6 Liquid injection diesel hammer: pressure in combustion chamber versus time (GRL 2002)

The pressure in the chamber can be reduced if the cylinder or impact block rings allow pressure to leak off resulting in poor compression and inadequate ram rise, that is, reduced efficiency. Other reasons for low ram rise is excessive friction between the ram and the cylinder wall, which may be due to inadequate lubrication or worn parts, or a poorly functioning fuel pump injecting too little fuel into the combustion chamber.

The reason for a low hammer rise lies usually not in a poorly functioning hammer. More common causes are “soft or spongy soils” or long flexible piles, which do not allow the combustion pressure to build up. The hammer rise (ram travel) of a single-acting diesel hammer is a function of the blow-rate, as shown in Eq. 9.1 (derived from the basic relations Acceleration =  $g$ ; Velocity =  $gt$ ; Distance =  $gt^2/2$  and recognizing that for each impact, the hammer travels the height-of-fall twice).

$$(9.1) \quad H = \frac{g}{8f^2}$$

where  $H$  = hammer stroke (m)  
 $g$  = gravity constant ( $m/s^2$ )  
 $f$  = frequency (blows/second)

In practice, however, the hammer blow rate is considered in blows per minute, BPM, and the expression for the hammer rise in metre is shown by Eq. 9.2 (English units—rise in feet—are given in Eq. 9.2a). The hammer rise (ft) as a function of the blow rate (blows/min) expressed by Eq. 9.2a is shown in [Figure 9.7](#).

$$(9.2) \quad H = \frac{4,400}{BPM^2}$$

$$(9.2a) \quad H = \frac{14,400}{BPM^2}$$

Eqs. 9.2 and 9.2a provide a simple means of determining the hammer rise in the field. The ram travel value so determined is more accurate than sighting against a bar to physically see the hammer rise against a marked stripe.

For some types of hammers, which are called **atomized injection hammers**, the fuel is injected at high pressure when the ram has descended to within a small distance of the impact block. The high pressure injection mixes the fuel with the hot compressed air, and combustion starts almost instantaneously. Injection then lasts until some time after impact, at which time the ram has traveled a certain distance up from the impact block. The times from the start of injection to impact and then to the end of combustion depend on the velocity of the ram. The higher the ram velocity, the shorter the time periods between ignition, impact, and end of combustion.

Similar to the drop hammer and air/steam hammer, on and during impact of a diesel hammer ram, the impact block, hammer cushion, and pile head move rapidly downward leaving cylinder with no support. Thus, it starts to descend by gravity and when it encounters the rebounding pile head, a secondary impact to the pile results called “**assembly drop**”.

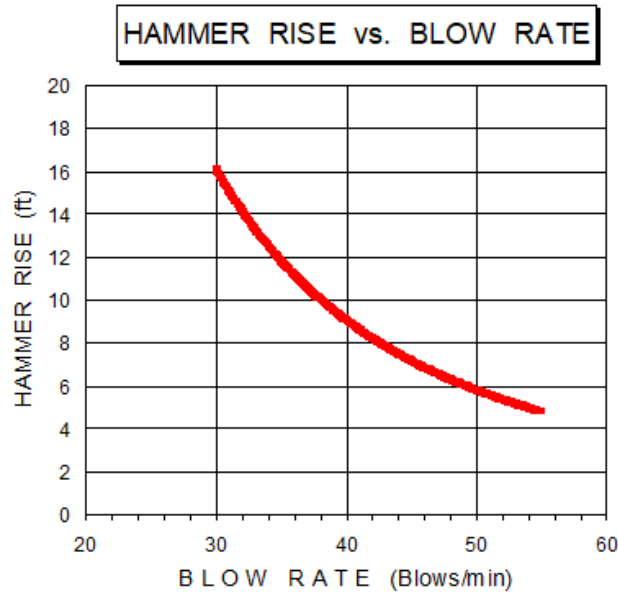


Fig. 9.7 Hammer rise (ft) as a function of blow-rate (BPM). Single-acting diesel hammer. Effect of friction in ram cylinder is not included)

**Closed-end diesel hammers** are very similar to open end diesel hammers, except for the addition of a bounce chamber at the top of the cylinder. The bounce chamber has ports which, when open, allow the pressure inside the chamber to equalize with atmospheric pressure. As the ram moves toward the cylinder top, it passes these ports and closes them. Once these ports are closed, the pressure in the bounce chamber increases rapidly, stops the ram, and prevents a metal to metal impact between ram and cylinder top. This pressure can increase only until it is in balance with the weight and inertial force of the cylinder itself. If the ram still has an upward velocity, uplift of the entire cylinder will result in noisy rattling and vibrations of the system, so-called “racking”. Racking of the hammer must not be tolerated as it can lead both to an unstable driving condition and to the destruction of the hammer. For this reason, the fuel amount, and hence maximum combustion chamber pressure, has to be reduced so that there is only a very slight “lift-off” or none at all.

#### 9.3.4 Direct-Drive Hammers

A recent modification of the atomized injection hammer is to replace the hammer cushion with a striker plate and to exchange the pile helmet for a lighter “direct drive housing”. This change, and other structural changes made necessary by the modification, improves the alignment between the hammer and the pile and reduces energy loss in the drive system. These modified hammers are called “direct drive hammers” and measurements have indicated the normally beneficial results that both impact force and transferred energy have increased due to the modification.

#### 9.3.5 Vibratory Hammers

The vibratory hammer is a mechanical sine-wave oscillator with weights rotating eccentrically in opposite directions so that their centripetal actions combine in the vertical direction (pile axis direction), but cancel out in the horizontal. The effect of the vibrations is an oscillating vertical force classified to frequency and amplitude.



Similarly to impact hammers, vibratory hammers introduce axial force to overcome shaft and toe resistance aided by the fact that the vibrations have reduced the resistance. It is important to realize that the reduction requires that the hammer vibration frequency is at least 50 % larger than the resonance frequency of the pile-soil-hammer system (See Section 9.14 and Chapter 10). The process works best in loose to compact silty sandy soils—compactable soils.

Two types of drivers exist: drivers working at high frequency, and drivers working with adjustable frequency that can operate in resonance with the natural frequency of the hammer-pile-soil system. For details, see Massarsch (2004; 2005) and Section 9.14.

Because the fundamental effect of the vibratory pile driving is to reduce or remove soil resistance, the "capacity" cannot be estimated from observations of pile penetration combined with hammer data, such as amplitude and frequency. This is because the static resistance ('capacity') of the pile during the driving is much smaller than the resistance (capacity) of the pile after the driving and only the resistance during the driving can be estimated from observations during the driving. The resistance removed by the vibrations is usually the larger portion and it is not known from any observation.

Several case histories have indicated that vibratory driven piles have smaller shaft resistance as opposed to impact driven piles. This is of importance for tension piles. Note, however, that the cases reported in the literature suffer from difficulties to separate shaft and toe resistance when interpreting the results of static loading tests as well as omission of the effect of residual force, which increases the value of the shaft resistance interpreted from a compression test and reduces it for the values interpreted from a tension test. The reality is more that the shaft resistance is more or less the same, whether a pile is impact or vibratory driven. However, the vibratory driving may result in a smaller toe stiffness.

#### 9.4 Basic Concepts

When a hammer impacts on a pile head, the force, or stress, transferred to the pile builds progressively to a peak value and then decays to zero. The entire event is over within a few hundreds of a second. During this time, the transfer initiates a compression strain wave that propagates down the pile at the speed of sound (which speed is a function of the pile material—steel, concrete, or wood). At the pile toe, the wave is reflected back toward to the pile head. If the pile toe is located in dense soil, the reflected wave is in compression. If the pile toe is located in soft soil, the reflection is in tension. Hard driving on concrete piles in soft soil can cause the tension forces to become so large that the pile may be torn apart, for example<sup>4)</sup>.

---

<sup>4)</sup> What driving tension to accept or permit in precast concrete piles is often mismanaged, be the piles ordinary reinforced or prestressed. Most standards and codes indicate the limit tension to be a percentage of the steel yield plus a portion of the concrete tension strength. For prestressed pile, the limit for the steel reinforcement (the strands) is often set to the net prestress value for the pile (leading some to believe that ordinary reinforced precast piles, having no net prestress, cannot accept driving tension!). However, the unacceptable level of driving tension will occur where the pile has developed a crack and where then only the reinforcement is left to resist the tension and hold the pile together. Therefore, no contribution can be counted on from the concrete tension strength—it may be a definite feature everywhere else in the pile, but not in that crack. The allowable driving tension is simply the steel yield divided by a factor of safety, usually about 1.5, which is applicable to ordinary reinforced as well as prestressed pile alike. Incidentally, the net prestress is usually about  $\approx 70\%$  of the strand yield point, that is about  $1/1.5$ , which makes the net prestress a good value for what tension value to accept, though the fact of the prestressing is not the relevant point in this context.

That pile driving must be analyzed by means of the theory of wave propagation in long rods has been known since the 1930s. The basics of the mathematical approach was presented by E.A. Smith in the late 1950s. When the computer came into common use in the early 1970s, wave equation analysis of pile driving was developed at the Texas A&M University, College Station, and at the Case Western Reserve University, Cleveland. Computer software for wave equation analysis has been available to the profession since 1976.

During the past two decades, a continuous development has taken place in the ease of use and, more important, the accuracy and representativeness of the wave equation analysis. Several generations of programs are in use as developed by different groups. The most versatile and generally accepted program is the GRLWEAP (2002).

Axial wave propagation occurs in a uniform, homogeneous rod—a pile—is governed by Eq. 9.3.

$$(9.3) \quad \sigma = \frac{E}{c} v \quad \text{derived from the "Wave Equation":} \quad \rho \frac{\partial^2 u}{\partial t^2} = E \frac{\partial^2 u}{\partial x^2}$$

where

$\sigma$	=	stress	
$E$	=	Young's modulus	
$c$	=	wave propagation speed	$c = \sqrt{\frac{E}{\rho}}$
$v$	=	particle velocity	

The wave equation analysis starts the pile driving simulation by letting the hammer ram impact the pile at a certain velocity, which is imparted to the pile head over a large number of small time increments. The analysis calculates the response of the pile and the soil. The hammer and the pile are simulated as a series of short infinitely stiff elements connected by weightless elastic springs. Below the ground surface, each pile element is affected by the soil resistance defined as having elastic and plastic response to movement and a damping (viscous) response to velocity. Thus, a 20 metre long pile driven at an embedment depth of 15 metre may be simulated as consisting of 20 pile elements and 15 soil elements. The time increments for the computation are set approximately equal to the time for the strain wave to travel the length of half a pile element. Considering that the speed of travel in a pile is in the range of about 3,000 m/s through 5,000+ m/s, each time increment is a fraction of a millisecond and the analysis of the full event involves more than a thousand calculations. During the first few increments, the momentum and kinetic energy of the ram is imparted to the pile accelerating the helmet, cushions, and pile head. As the calculation progresses, more and more pile elements become engaged. The computer keeps track of the development and can output how the pile elements move relative to each other and to the original position, as well as the velocities of each element and the forces and stresses developing in the pile.

The **damping** or viscous response of the soil is a linear function of the velocity of the pile element penetration (considering both downward and upward direction of pile movement). The damping response to the velocity of the pile is a crucial aspect of the wave equation simulation, because only by knowing the damping can the static resistance be separated from the total resistance to the driving. Parametric studies have indicated that in most cases, a linear function of velocity will result in acceptable agreement with actual behavior. Sometimes, an additional damping called radial damping is considered, which is dissipation of energy radially away from the pile as the strain wave travels down the pile.

The material constant, **impedance, Z**, is very important for the wave propagation. It is a function of pile modulus, cross section, and wave propagation speed in the pile as given in Eq. 9.4.

$$(9.4) \quad Z_p = \frac{E_p A_p}{c_p}$$

where  $Z_p$  = pile impedance  
 $E_p$  = Young's modulus of the pile material  
 $A_p$  = pile cross section area  
 $c_p$  = wave propagation speed (= speed of sound in the pile)

Combining Eqs. 9.3 and 9.4 yields Eq. 9.5 and shows that the force is equal to impedance times pile velocity. Or, in other words, force and wave speed in a pile are proportional to impedance. This fact is a key aspect of the study of force and velocity measurements obtained by means of the Pile Driving Analyzer (see Section 9.7).

$$(9.5) \quad \sigma A = F = Z_p v_p$$

where  $\sigma$  = axial stress in the pile  
 $A$  = pile cross section area  
 $F$  = force in the pile  
 $Z_p$  = pile impedance  
 $v_p$  = pile particle velocity

Eqs. 9.4 and 9.5 can be used to calculate the axial impact force in a pile during driving, as based on measurement of the pile particle velocity (also called "physical velocity"). Immediately before impact, the particle velocity of the hammer is  $v_0$ , while the particle velocity of the pile head is zero. When the hammer strikes the pile, a compression wave will be generated simultaneously in the pile and in the hammer. The hammer starts to slow down, by a velocity change denoted  $v_H$ , while the pile head starts to accelerate, gaining a velocity of  $v_p$ . (The pile head velocity before impact is zero, the velocity change at the pile head is the pile head velocity). Since the force between the hammer and the pile must be equal, applying Eq. 9.3 yields the relationship expressed in Eq. 9.6.

$$(9.6) \quad Z_H v_H = Z_p v_p$$

where  $Z_H$  = impedance of impact hammer  
 $Z_p$  = impedance of pile  
 $v_H$  = particle velocity of wave reflected up the hammer  
 $v_p$  = particle velocity of pile

At the contact surface, the velocity of the hammer — decreasing — and the velocity of the pile head — increasing — are equal, as expressed in Eq. 9.7. Note, the change of hammer particle velocity is directed upward, while the velocity direction of the pile head is downward (gravity hammer is assumed).

$$(9.7) \quad V_0 - v_H = v_p$$

where  $v_0$  = particle velocity of the hammer immediately before impact  
 $v_H$  = particle velocity of wave reflected up the hammer  
 $v_p$  = particle velocity of pile

Combining Eqs. 9.6 and 9.7 and rearranging the terms, yields Eq. 9.8.

$$(9.8) \quad v_p = \frac{v_0}{1 + \frac{Z_p}{Z_H}}$$

where

- $v_p$  = particle velocity of pile
- $v_0$  = particle velocity of the hammer immediately before impact
- $Z_H$  = impedance of hammer
- $Z_p$  = impedance of pile

Inserting  $Z_H = Z_p$ , into Eq. 9.8 yields Eq. 9.9, which shows that when the impedances of the hammer and the piles are equal, the particle velocity of the pile,  $v_p$ , in the pile behind the wave front will be half the hammer impact velocity,  $v_0$  (the velocity immediately before touching the pile head).

$$(9.9) \quad v_p = 0.5 v_0$$

where

- $v_p$  = particle velocity of pile
- $v_0$  = particle velocity of the hammer immediately before impact

Combining Eqs. 9.3, 9.5, and 9.9, yields Eq. 9.10 which expresses the magnitude of the impact force,  $F_i$ , at the pile head for equal impedance of hammer and pile.

$$(9.10) \quad F_i = 0.5 v_0 Z_p$$

where

- $F_i$  = force in pile
- $Z_p$  = impedance of pile
- $v_0$  = particle velocity of the hammer immediately before impact

The **duration of the impact**,  $t_0$ , that is, the time for when the pile and the hammer are in contact, is the time it takes for the strain wave to travel the length of the hammer,  $L_H$ , twice, i.e., from the top of the hammer to the bottom and back up to the top as expressed in Eq. 9.11a. Then, if the impedances of the hammer and the pile are equal, during the same time interval, the wave travels the length,  $L_W$ , as expressed in Eq. 9.11b. — Note, equal impedances do not mean that the wave velocities in hammer and pile are equal — Combining Eqs. 9.11a and 9.11b provides the **length of the stress wave** (or strain wave) in the pile as expressed by Eq. 9.11c.

$$(9.11a) \quad t_0 = \frac{2L_H}{c_H} \quad (9.11b) \quad t_0 = \frac{2L_W}{c_P} \quad (9.11c) \quad L_W = 2L_H \frac{c_P}{c_H}$$

where

- $t_0$  = duration of impact (i.e., duration of contact between hammer and pile head)
- $L_H$  = length of hammer
- $L_W$  = length of the compression wave in pile
- $c_H$  = velocity compression wave in hammer
- $c_P$  = velocity of compression wave in pile

When a hammer impacts a pile, the force generated in the pile slows down the motion of the hammer and a stress wave ("particle velocity wave") is generated that propagates down the pile. After quickly reaching a peak velocity (and force) — immediately if the pile head is infinitely rigid — the pile head starts moving slower, i.e., the generated particle velocity becomes smaller, and the impact force decays exponentially according to Eq. 9.12a, which expresses the **pile head force**. Combining Eqs. 9.3, 9.5, and 9.12a yields to show that, together with the impact velocity, the ratio between the ram impedance and the pile impedance governs the force a hammer develops in a pile. (For hammer and pile of same material, e.g., steel, the ratio is equal to the ratio of the cross sectional areas). A ram must always have an impedance larger than that of the pile or the hammer will do little else than bounce on the pile head.

$$(9.12a) \quad F = F_i e^{-\frac{Z_P}{M_H} t} \qquad (9.12b) \quad F = F_i e^{-\frac{M_P L_E}{M_H c_P}}$$

where

$F$	=	force at pile head	and	$F_i$	=	force at impact
$M_H$	=	mass of hammer element	and	$M_P$	=	mass of pile element
$e$	=	base of the natural logarithm (= 2.718)				
$Z_P$	=	impedance of the pile cross section				
$L_E$	=	length of pile element				
$t$	=	time				

If the pile is of non-uniform cross section, every change of impedance change will result in reflections. If the impedance of the upper pile portion is smaller than that of the lower, the pile will not drive well. When the reverse is the case, that is, the impedance of the upper pile portion is larger than that of the lower, a tension wave will reflect from the cross section change. For example, in marine projects, sometimes a concrete pile is extended by an H-pile, a "stinger". The impedances of the concrete segment and the steel H-pile segment should, ideally, be equal. However, the H-pile size (weight) is usually such that the impedance of the H-pile is smaller than that of the concrete pile. Therefore, a tensile wave will reflect from the cross section change (for a discussion, see Section 8, below). If the impedance change is too large, the reflected tension can damage the concrete portion of the pile, and if the change is substantial, such as in the case of an impedance ratio close to 2 or greater, the tension may exceed the tensile strength of the concrete pile. (A case history of the use of stinger piles is described in Section 9.11, Case 4).

As an important practical rule, the impedance of the lower section must never be smaller than half of the upper section. That it at all can work, is due to that the concrete pile end (i.e., where the two segments are joined) is not normally a free end, but is in contact with soil, which reduces the suddenness of the impedance change. However, this problem is compounded by that the purpose of the stinger is usually to achieve a better seating into dense competent soil. As the stinger is in contact with this soil, a strong compression wave may be reflected from the stinger toe and result in an increasing incident wave, which will result in that the tensile reflection from where the section are joined—where the impedance change occurred. If the concrete end is located in soft soil, damage may result.

When a pile has to be driven below the ground surface or below a water surface, a **follower** is often used. The same impedance aspects that governed the driving response of a pile governs also that of a follower. Ideally, a follower should have the same impedance as the pile. Usually, though, it designed for a somewhat larger impedance, because it must never ever have a smaller impedance than the pile, or the achievable "capacity" of the pile may reduce considerably as compared to the pile driven without a follower. Indeed, a too small follower may be doing little more than chipping away on the pile head.

A parameter of substantial importance for the drivability of the pile is the so-called **quake**, which is the movement between the pile and the soil required to mobilize full plastic resistance (see Figure 9.8). In other words, the quake is the zone of pile movement relative to the soil where elastic resistance governs the load transfer.

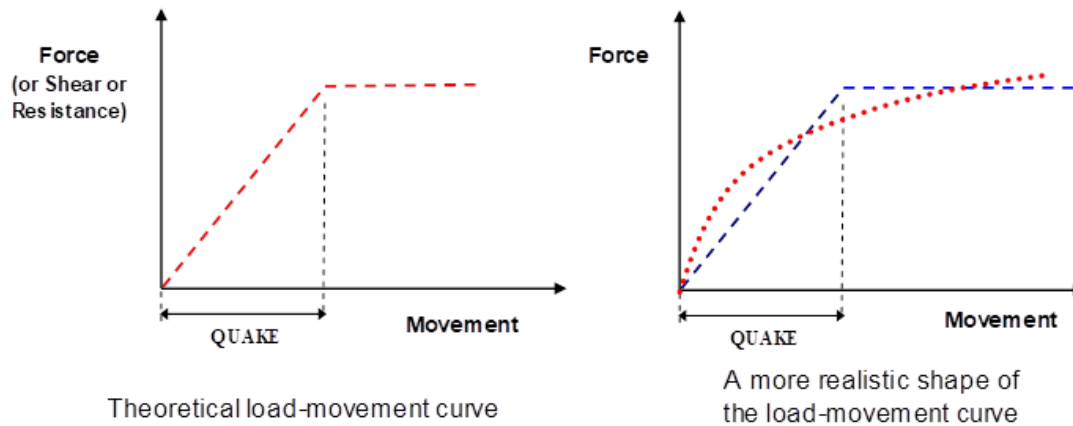


Fig. 9.8 Development of soil resistance to pile movement (q-z curves).

Along the pile shaft, the quake is usually small, about 2 mm to 3 mm or less. The value depends on the soil type and is independent of the size of the pile (diameter). In contrast, at the pile toe, the quake is a function of the pile diameter and, usually, about 1 % of the diameter. However, the range of values can be large; values of about 10 % of the diameter have been observed. The larger the quake, the more energy is required to move the pile and the less is available for overcoming the soil static resistance. For example, measurements and analyses have indicated that a hammer driving a pile into a soil where the quake was about 3 mm (0.1 inch) could achieve a final "capacity" of 3,000 kN (600 kips), but if the quake is 10 mm (0.4 inch), it could not even drive the pile beyond a "capacity" of 1,500 kN (300 kips) (Authier and Fellenius 1980). N.B., the quake implies a "capacity", which for a pile toe does not exist. It should be understood as a CAPWAP parameter and not as a representation of a true toe "capacity".

Aspects which sometimes can be important to include in an analysis are the effect of a soil adhering to the pile, particularly as a **plug** inside an open-end pipe pile or between the flanges of an H-pile. The plug will impart a toe resistance (Fellenius 2002). Similarly, the resistance from a soil column inside a pipe pile that has not plugged will add to the shaft resistance along the outside of the pile.

The **stiffness, k**, of the pile is an additional important parameter to consider in the analysis. The stiffness of an element is defined in Eq. 9.13. The stiffness of the pile is usually well known. The stiffness of details such as the hammer and pile cushions is often more difficult to determine. Cushion stiffness is particularly important for evaluating driving stresses. For example, a new pile cushion intended for driving a concrete pile can start out at a thickness of 150 mm of wood with a modulus of 300 MPa. Typically, after some hundred blows, the thickness has reduced to half and the modulus has increased five times. Consequently, the cushion stiffness has increased ten times.

$$(9.13) \quad k = \frac{EA}{L}$$

where

- $k$  = stiffness
- $E$  = Young's modulus of the pile material
- $A$  = pile cross sectional area
- $L$  = element length

A parameter related to the stiffness is the **coefficient of restitution**,  $e$ , which indicates the difference expressed in Eq. 9.14 between stiffness in loading (increasing stress) as opposed to in unloading (decreasing stress). A coefficient of restitution equal to unity only applies to ideal materials, although steel and concrete are normally assigned a value of unity. Cushion material have coefficients ranging from 0.5 through 0.8. For information on how to determine the coefficient of restitution see GRL (2002).

$$(9.14) \quad e = \sqrt{\frac{k_1}{k_2}}$$

where

- $e$  = coefficient of restitution
- $k_1$  = stiffness for increasing stress
- $k_2$  = stiffness for decreasing stress

When the initial compression wave with the force  $F_i(t)$  reaches the pile toe, the toe starts to move. The **pile toe force** is expressed by Eq. 9.15.

$$(9.15) \quad F_p(t) = F_i(t) + F_r(t)$$

where

- $F_p(t)$  = force in pile at toe at Time  $t$
- $F_i(t)$  = force of initial wave at pile toe
- $F_r(t)$  = force of reflected wave at pile toe

If the material below the pile is infinitely rigid,  $F_r = F_i$ , and Eq. 9.15 shows that  $F_p = 2F_i$ . If so, the strain wave will be reflected undiminished back up the pile and the stress at the pile toe will theoretically double. When the soil at the pile toe is less than infinitely rigid, the reflected wave at the pile toe,  $F_r(t)$ , is smaller, of course. The magnitude is governed by the stiffness of the soil. If the force in the pile represented by the downward propagating compression wave rises more slowly than the soil resistance increases due to the imposed toe movement, the reflected wave is in compression indicating a toe resistance. If the force in the compression wave rises faster than the soil resistance increases due to the imposed toe movement, the reflected wave is in tension. However, the force sent down and out into the soil from the pile toe will be a compression wave for both cases.

In this context and to illustrate the limitation of the dynamic formulae, the driving of two piles will be considered. Both piles are driven with the same potential ("positional") energy. First, assume that the on pile is driven with a hammer having a mass of 4,000 kg and is used at a height-of-fall of 1 m, representing a positional energy of 40 KJ. The impact velocity,  $v_0$ , is independent of the mass of the hammer and a function of gravity and height-of-fall, ( $v = \sqrt{2gh}$ ). Thus, the free-fall impact velocity is 4.3 m/s. If instead a 2,000 kg hammer is used at a height-of-fall of 2 m, the positional energy is the same, but the free-fall impact velocity is 6.3 m/s and the force generated in the pile overcoming the soil resistance will be larger. The stress in the pile at impact can be calculated from Eq. 9.16, as derived from Eqs. 9.3 - 9.5.

$$(9.16) \quad \sigma_p = \frac{E_p}{c_p} v_p$$

where  $\sigma_p$  = stress in the pile  
 $E_p$  = pile elastic modulus  
 $c_p$  = propagation speed of compression wave in the pile  
 $v_p$  = particle velocity in the pile

The impact stress in piles composed of steel, concrete, or wood can be calculated from the material parameters given in Table 9.1. In the case of a concrete pile and assuming equal potential energy, but at heights-of-fall of 1 m and 2 m, the calculated stresses in the pile are 44 MPa and 63 MPa, respectively. In case of a pile cross section of, say, 300 mm and area about 0.09 m<sup>2</sup>, the values correspond to theoretical impact forces are 4,000 kN and 5,600 kN. Allowing for losses down the pile due to reflections and damping, the maximum soil forces the impact wave could be expected to mobilize are about a third or a half of the theoretical impact force, i.e., about 2,000 to 3,000 kN for the "heavy" and "light" hammers, respectively. Moreover, because the lighter hammer generates a shorter stress-wave, its large stress may decay faster than the smaller stress generated by the heavier hammer and, therefore, the lighter hammer may be unable to drive a long a pile as the heavier hammer can. Where in the soil a resistance occur is also a factor. For example, a pile essentially subjected to toe resistance will benefit from a high stress level, as generated by the higher impact, whereas a pile driven against shaft resistance drives better when the stress-wave is longer and less apt to dampen out along the pile. A number of influencing factor are left out, but the comparison is an illustration of why the dynamic formulae, which are based on positional energy relations, are inadvisable for use in calculating pile bearing "capacity".

**Table 9.1 Typical Values**

Material	Density, $\rho$ (kg/m <sup>3</sup> )	Modulus, E (GPa)	Wave speed, c (m/s)
Steel	7,850	210	5,120
Concrete	2,450	40	4,000
Wood fresh or wet	1,000	16	3,300

The **maximum stress** in a pile that can be accepted and propagated is related to the maximum dynamic force that can be mobilized in the pile. The peak stress developed in an impact is expressed in Eq. 9.17, as developed from Eq. 9.16.

$$(9.17) \quad \sigma_p = \frac{E_p}{c_p} \sqrt{2gh}$$

where  $\sigma_p$  = stress in the pile  
 $E_p$  = pile elastic modulus  
 $c_p$  = propagation speed of the stress wave in pile; wave speed  
 $g$  = gravity constant  
 $h$  = critical height-of-fall

Transforming Eq. 9.17 into Eq. 9.18 yields an expression for a height that causes a stress equal to the strength of the pile material.



$$(9.18) \quad h_{cr} = \frac{\sigma_{P,max}^2}{2g\rho E_P}$$

where

$h_{cr}$	=	critical height-of-fall
$\sigma_{P,max}$	=	maximum stress in the pile $\leq$ strength of the pile material
$E_P$	=	pile elastic modulus
$g$	=	gravity constant
$\rho$	=	density of pile material

For a concrete pile with cylinder strength ranging between 30 MPa and 60 MPa and the material parameters listed in Table 9.1, the critical height-of-fall ranges between 0.5 m and 2.0 m (disregarding losses, usually assumed to amount to an approximately 20 % reduction of impact velocity). In the case of a steel pile with a material yield strength of 300 MPa, the critical height-of-fall becomes 2.8 m. (Note, no factor of safety is included and it is not recommended to specify the calculated limits of height-of-fall for a specific pile driving project).

The above brief discussion demonstrates that stress wave propagation during pile driving is affected by several factors, such as hammer weight, hammer impact velocity, and pile impedance. It is therefore not surprising that a single parameter, driving energy, cannot describe the pile driving operation correctly.

The total soil resistance  $R_{tot}$  during pile driving is composed of a movement-dependent (static) component,  $R_{stat}$ , and a velocity-dependent (dynamic) component,  $R_{dyn}$ , as expressed in Eq. 9.19.

$$(9.19) \quad R_{tot} = R_{stat} + R_{dyn}$$

where

$R_{tot}$	=	total pile resistance
$R_{stat}$	=	static pile resistance
$R_{dyn}$	=	dynamic pile resistance

The soil resistances can be modeled as a spring with a certain stiffness and a slider representing the static resistance plus a dashpot representing dynamic resistance—damping—as illustrated in Figure 9.9. (Note that the figure illustrates also when the direction of pile movement has reversed). For small movements, the static resistance is essentially a linear function of the movement of the pile relative the soil. The damping is a function of the velocity of the pile. Smith (1960) assumed that the damping force is proportional to the static soil resistance times pile velocity by a damping factor,  $J_s$ , with the dimension of inverse velocity. Goble et al. (1980) assumed that the damping force is proportional to the pile impedance times pile velocity by a dimensionless damping factor,  $J_c$ , called viscous damping factor, as expressed in Eq. 9.20.

$$(9.20) \quad R_{dyn} = J_c Z_P v_P$$

where

$R_{dyn}$	=	dynamic pile resistance
$J_c$	=	a viscous damping factor
$Z_P$	=	impedance of pile
$v_P$	=	particle velocity of pile

Typical and usually representative ranges of viscous damping factors are given in Table 9.2.

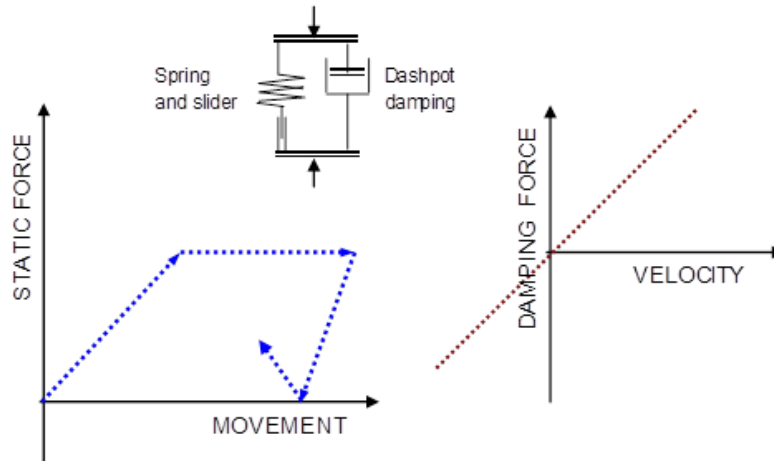


Fig. 9.9 Model and principles of soil resistance — elastic and plastic and damping

**Table 9.2.** Damping factors for different soils (Rausche et al. 1985).

Soil Type	$J_c$
Clay	0.60 – 1.10
Silty clay and clayey silt	0.40 – 0.70
Silt	0.20 – 0.45
Silty sand and sandy silt	0.15 – 0.30
Sand	0.05 – 0.20

It is generally assumed that  $J_c$  depends only on the dynamic soil properties. However, as shown by Massarsch and Fellenius (2008) and Fellenius and Massarsch (2008), in practice, measurements on different size and different material piles in the same soil do show different values of  $J_c$ . Iwanowski and Bodare (1988) derived the damping factor analytically, employing the model of a vibrating circular plate in an infinite elastic body to show that the damping factor depends not just on the soil type but also on the ratio between the impedance of the soil at the pile toe and the impedance of the pile. They arrived at the relationship expressed in Eq. 9.21, which is applicable to the conditions at the pile toe.

$$(9.21) \quad J_c = 2 \frac{\rho_t c_s A_t}{\rho_p c_p A_c} = 2 \frac{Z_s A_t}{Z_p A_c}$$

where

- $J_c$  = dimensionless damping factor
- $\rho_t$  = soil total (bulk) density of the soil
- $\rho_p$  = density of the pile material
- $c_s$  = shear wave speed in the soil
- $c_p$  = speed of the compression wave in the pile
- $A_t$  = pile area at pile toe in contact with soil
- $A_c$  = pile cross-sectional area
- $Z_s$  = impedance of the soil (determined from P-wave velocity)
- $Z_p$  = impedance of the pile at the pile toe

The equation shows that the damping factor,  $J_c$  depends on the ratio of the soil impedance to the pile impedance and of the ration of pile cross section area and pile toe area. The latter aspect is particularly important in the case of closed-toe or "plugged" pipe piles. Table 9.3 compiles  $J_c$  damping values calculated according to Eq. 9.21 for pile with an average soil density of  $\rho_t = 1,800 \text{ kg/m}^3$  and material parameters taken from Table 9.1. For the steel piles, a ratio between the pile toe area and the pile cross sectional area of 10 was assumed. Table 9.3 shows the results for soil compression wave velocities ranging from 250 m/s to 1,500 m/s. Where the actual soil compression wave speed can be determined, for example, from cross-hole tests, or seismic CPT soundings, Eq. 9.21 indicates a means for employing the wave speed (soil compression) to estimate  $J_c$  -factors for the piles of different sizes, geometries, and materials to be driven at a site.

**Table 9.3.** Values of viscous damping factor,  $J_c$ , for different pile materials and wave speeds

Material	Compression wave speed at pile toe, $c_p$ (m/s)					
	250	500	750	1,000	1,250	1,500
Steel	0.02	0.04	0.07	0.09	0.11	0.13
Concrete	0.09	0.18	0.28	<u>0.37</u>	0.46	0.55
Wood	0.27	0.55	0.82	1.09	1.36	1.64

## 9.5 Wave Equation Analysis of Pile Driving

The GRLWEAP program includes files that contain all basic information on hammers available in the industry. To perform an analysis of a pile driven with a specific hammer, the hammer is selected by its file number. Of course, when the analysis is for piles driven with drop hammers, or with special hammers that are not included in the software files, the particular data must be entered separately.

The GRLWEAP can perform a drivability analysis with output consisting of estimated penetration resistance (driving log), maximum compression and tension stresses induced during the driving, and many other factors of importance when selecting a pile driving hammer. The program also contains numerous other non-routine useful options. For additional information, see Hannigan (1990).

The most common routine output from a wave equation analysis consists of a bearing graph (ultimate resistance curve plotted versus the penetration resistance—often simply called "blow-count"<sup>5</sup>) and diagrams showing impact stress and transferred energy as a function of penetration resistance. Figure 9.10 presents a Bearing Graph showing the relation between the static soil resistance (pile "capacity"; R-ULT) versus the pile penetration resistance (PRES) at initial driving as the number of blows required for 25 mm penetration of the pile into the soil. The relation is shown as a band rather than as one curve, because natural variations in the soil, hammer performance, cushion characteristics, etc. make it impossible to expect a specific combination of hammer, pile, and soil at a specific site to give the response represented by a single curve. The WEAP analysis results should therefore normally be shown in a band with upper and lower boundaries of expected behavior. The band shown may appear narrow, but as is illustrated in the following, the band may not be narrow enough.

<sup>5</sup> Penetration resistance is number of blows per a unit of penetration, e. g., 25 mm, 0.3 m, or 1.0 m. Blow count is the actual number of blows counted for a specific penetration, or the inverse of this: a penetration for a specific number of blows. For example, on termination of the driving, an 11 mm penetration may be determined for 8 blows. That is, the blow count is 8 blows/11 mm, but the penetration resistance is 18 blows/25 mm. Sometimes the distinction is made clear by using the term "equivalent penetration resistance". Note, the "pile **driving** resistance" refers to force. But it is an ambiguous term that is best not used.

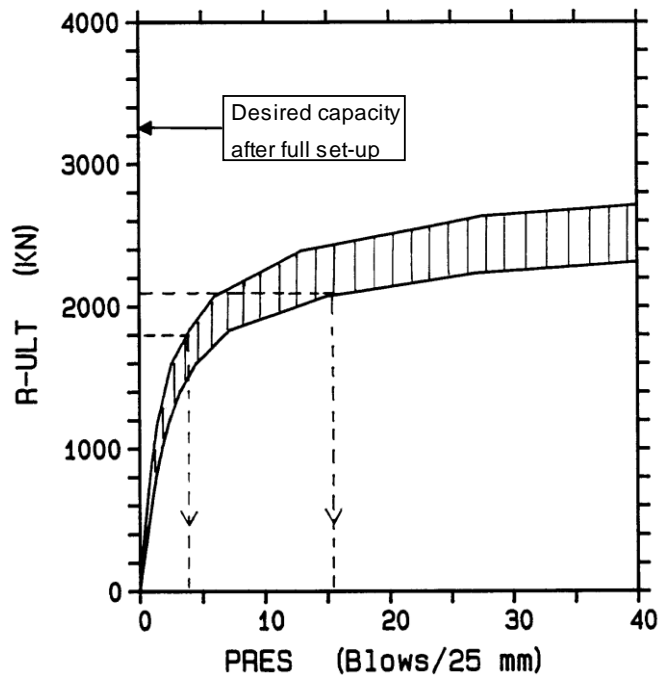


Fig. 9.10 WEAP Bearing Graph (Fellenius 1984)

With time after the initial driving, the soil gains strength and the pile "capacity" increases due to soil set-up. Of course, if the designer considers and takes advantage of the set-up, the hammer does not have to drive the pile to the desired final "capacity" at the end-of-initial-driving, only to a "capacity" that, becomes equal to the desired final value when set-up is added.

For the case illustrated, the set-up was expected to range from about 1,000 kN through 1,200 kN. Thus, considering the desired long-term "capacity" of 3,150 kN, the desired  $R_{ULT}$  at End-of-Initial-Driving, EOID, ranged from 1,950 kN through 2,150 kN. The pile response in terms of "capacity" ( $R_{ULT}$ ) versus Penetration Resistance (PRES) lies within a zone bounded by upper and lower estimates. The Bearing Graph indicates that the expected PRES values for this case would range from 4 blows/25 mm through 16 blows/25 mm. Obviously, the WEAP analysis *alone* is not a very exact tool to use for determining the EOID PRES. It must be coupled with a good deal of experience and judgment, and field observations.

The Bearing Graph is produced from assumed pile "capacity" values. For this reason, the WEAP analysis alone cannot be used for determining the "capacity" of a pile without being coupled to observed penetration resistance (and reliable static analysis). WEAP analysis is a design tool for predicting expected pile driving behavior (and for judging suitability of a hammer, etc.), not for determining "capacity". For the case illustrated in Figure 9.10,

Moreover, if initial driving is to a "capacity" near the upper limit of the ability of the hammer, the magnitude of the set-up cannot be proven by restriking the pile with the same hammer. For the case illustrated, the hammer is too light to mobilize the expected at least "capacity" of 3,150 kN, and the restriking would be meaningless and only show a small penetration per blow, i.e., a high PRES value.

## 9.6 Hammer Selection by Means of Wave Equation Analysis

The procedure of hammer selection for a given pile starts with a compilation of available experience from previous similar projects in the vicinity of the site and a list of hammers available amongst contractors who can be assumed interested in the project. This effort can be more or less elaborate, depending on the project at hand. Next comes performing a wave equation analysis of the pile driving at the site, as suggested below. Notice, there are many potential error sources. It is important to verify that assumed and actual field conditions are in agreement.

### Before start of construction

- Compile the information on the soils at the project site and the pile data. The soil data consist of thickness and horizontal extent of the soil layers and information on the location of the groundwater table and the pore pressure distribution. The pile data consist of the pile geometry and material parameters, supplemented with the estimated pile embedment depth and desired final "capacity".
- Calculate the static "capacity" of the pile at final conditions as well as during initial driving. For conditions during the initial driving, establish the extent of remolding and development of excess pore pressure along the pile. Establish also the "capacity" and resistance distribution at restrike conditions after the soil has reconsolidated and "set-up", and all excess pore pressures have dissipated.
- Establish a short list of hammers to be considered for the project. Sometimes, the hammer choice is obvious, sometimes, a range of hammers needs to be considered.
- For each hammer considered, perform a wave equation analysis to obtain a Bearing Graph for the end-of-initial-driving and restrike conditions with input of the static soil resistances and pile data as established earlier. For input of hammer data and soil damping and quake data, use the default values available in the program. This analysis is to serve a reference to the upper boundary conditions—the program default values are optimistic. Many soils exhibit damping and quake values that are higher than the default values. Furthermore, the hammer efficiency used as default in the program is for a well-functioning hammer and the actual hammer to be used for the project may be worn, in need of maintenance service, etc. Hence, its efficiency value is usually smaller than the default value. Repeat, therefore, the analysis with best estimate of actual hammer efficiency and dynamic soil parameters. This analysis will establish the more representative Bearing Graph for the case.
- A third Bearing Graph analysis with a pessimistic, or conservative, input of values is always advisable. It will establish the low boundary conditions at the site and together with the previous two analyses form a band that indicates the expected behavior.
- When a suitable hammer has been identified, perform a Drivability Analysis to verify that the pile can be driven to the depth and "capacity" desired. Also this analysis should be made with a range of input values to establish the upper and lower boundaries of the piling conditions at the site.
- Determine from the results of the analysis what hammer model and size and hammer performance to specify for the project. Hammers should not be specified as to rated energy, but to the what they will develop in the pile under the conditions prevailing at the site. That is, the specifications need to give required values of impact stress and transferred energy for the hammer, pile, and soil system. Suggested phrasings are given in Chapter 11.

### **During construction**

- For most projects, at the start of the pile driving, dynamic monitoring with the Pile Driving Analyzer (PDA; Section 9.8 should be performed. The PDA measurements combined with CAPWAP analyses (Section 9.11) will serve to show whether or not the hammer is performing as per the specifications. The measurements will also serve to confirm the relevance of the theoretical calculations (static and dynamic analyses) and, when appropriate, indicate the need for amendments. Although the primary purpose is to verify the pile "capacity", other PDA deliverables are hammer performance, transferred energy, pile stresses, soil set-up, etc.
- It is important that the conditions assumed in the analyses are related to the actual conditions. Check actual pile size, length, and material and verify that cushions and helmets as to size, material type, and condition. Then, ascertain that the hammer runs according to the manufacturer's specifications as to blow rate (blows/minute) and that the correct fuel is used. Request records from recent hammer maintenance.
- Depending on size of project, degree of difficulty, and other factors, additional PDA monitoring and analysis may be necessary during the construction work. If questions or difficulties arise during the continued work, new measurements and analysis will provide answers when correlated to the initial measurement results.

### **9.7 Aspects to Consider When Reviewing Results of Wave Equation Analysis**

- Check the pile stresses to verify that a safe pile installation is possible.
- If the desired "capacity" requires excessive penetration resistance (PRES values greater than 800 blows/metre—200 blows/foot), re-analyze with a more powerful hammer (pertinent to piles bearing in dense soil; piles driven to bedrock can be considered for larger PRES values if these can be expected to be met after a limited number of blows).
- If the penetration resistance is acceptable but compressive stresses are unacceptably high, re-analyze with either a reduced stroke (if hammer is adjustable) or an increased cushion thickness.
- If (for concrete piles) the penetration resistance is low but tension stresses are too high, either increase the cushion thickness or decrease the stroke or, possibly, use a hammer with a heavier ram, and then re-analyze.
- If both penetration resistance and compressive stresses are excessive, consider the use of not just a different hammer, but also a different pile.

### **9.8 High-Strain Dynamic Testing of Piles Using the Pile Driving Analyzer, PDA**

Dynamic monitoring consists in principle of attaching gages to the pile shortly below the pile head, measuring force and acceleration induced in the pile by the hammer impact (see [Figure 9.11](#)). The dynamic measurements are collected by a data acquisition unit called the Pile Driving Analyzer, PDA. A detailed guide for the performance of the PDA testing is given in ASTM Designation D4945-89.

### 9.8.1 Wave Traces

The PDA data are usually presented in the form of PDA "wave traces", which show the measured force and wave speed developments drawn against time as illustrated in Figure 9.12. The time indicated as  $0 L/c$ , is when the peak impact force occurs, and Time  $2 L/c$  is when the peak force has traveled down to the pile toe, been reflected there, and again appears at the gages at the pile head. The wave has traveled a distance of  $2 L$  at a wave speed of  $c$  (ranges from about 3,500 m/s in concrete through about 5,100 m/s in steel—12,500 ft/s and 16,700 ft/s, respectively). Peak force divided by the pile cross sectional area at the gage location is the impact stress. The acceleration integrated to pile physical velocity is simply called "velocity".

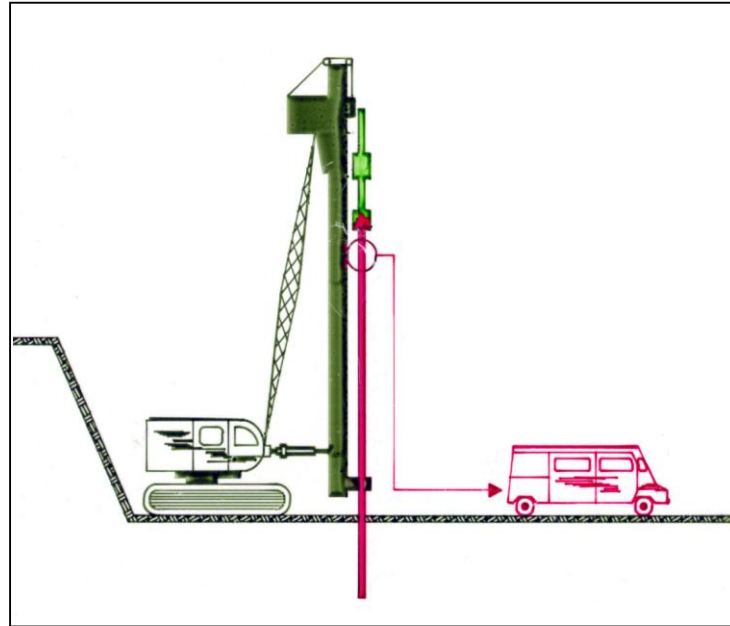


Fig. 9.11 Typical arrangement of dynamic monitoring with the Pile Driving Analyzer (PDA). The two pairs of PDA gages, the accelerometer and the strain-gage, are usually attached shortly below the pile head.

Notice that Figure 9.12 shows the force and velocity traces as initially overlapping. This is no coincidence. Force and velocity introduced by an impact are proportional by the impedance,  $Z = EA/c$ . ("c" is wave propagation speed; see Eq. 9.4, above). The most fundamental aspect of the wave traces lies in how they react to reflections from the soil, when the traces no longer overlap. When the stress wave on its way down the pile encounters a soil resistance, say at a distance "A" below the gage location, a reflected wave is sent back up the pile. This wave reaches the gages at Time  $2A/c$ . At that time, force is still being transferred from the hammer to the pile and the gages are still recording the force and physical velocity. The reflected stress-wave superimposes the downward wave and the gages now measure the combination of the waves. The reflected force will be a compression wave and this compression will add to the measured force, that is, the force wave will rise. At the same time, the resistance in the soil slows down the pile, that is, the measured velocity wave gets smaller—the trace dips. The consequence is a separation of the traces. The larger this separation, the greater the soil resistance. Soil resistance encountered by the pile toe has usually the most pronounced effect. It is evidenced by a sharp increase of the force wave and a decrease of the velocity wave, usually even a negative velocity—the pile rebounds.

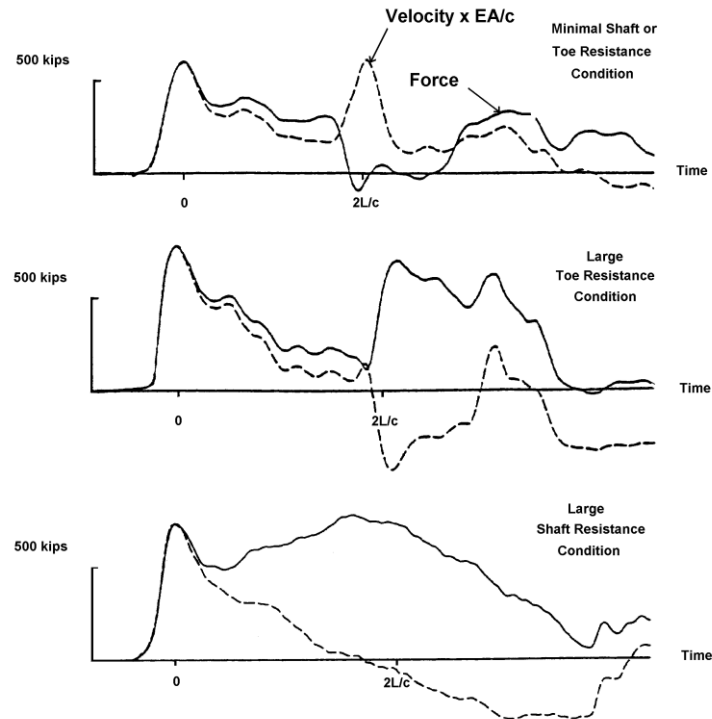


Fig. 9.12 Force and Velocity Wave Traces recorded during initial driving and restriking (Hannigan 1990; used with permission)

When dynamic measurements first started to be made in the 1950s, force could be measured by either an accelerometer or a strain gage. At the time, strain gages were prone to malfunction due to moisture and were more laborious to attach, as opposed to accelerometers. The latter were also more accurate, and could be (should be) attached at a single point. However, they were more prone to damage. Depending on preference, either gage type was used. It was not until Dr. Goble and co-workers attached both gage types to the test pile at the same time that the tremendous benefit became apparent of comparing the force determined from measured strain to the force determined from measured and integrated acceleration. The purpose of attaching both gages was that it was hypothesized that the pile "capacity" would be equal to the force (from the strain gage) when the pile velocity (from the integrated acceleration) was zero and no damping would exist. However, when the velocity at the pile head is zero, the velocity down the pile will not be zero, so the approach did not work and it was abandoned. The practice of using both gage types was retained, of course.

For a pile of length "L" below the gages, reflection from the pile toe will arrive to the gage location at Time  $2L/c$ . This is why the wave traces are always presented in the "L/c scale". The full length of the pile 'in time' is  $2L/c$  and the time of the arrival of a reflection in relation to the  $2L/c$  length is also a direct indication of where in the pile the resistance was encountered.

A resistance along the pile shaft will, as indicated, reflect a compression wave. So will a definite toe resistance as illustrated in the middle wave traces diagram of Figure 9.12, where the compression trace increases and the velocity trace decreases. Again, the larger the toe resistance, the larger the separation of the two traces. Indeed, the compression stress in the pile at the pile head at Time  $2L/c$  may turn out to be larger than the impacting wave at Time  $0L/c$ . This is because the toe reflection overlaps the incident wave which is still being transferred to the pile head from the hammer. In those cases, the maximum compression stress occurs at the pile toe not at the pile head.



A drop hammer does not bounce off the pile head on its impacting the pile head, only when the compression wave originating at the pile toe reaches the ram (if the pile toe is in contact with dense and competent soil). In case of a diesel hammer, its ram lifts off the anvil as a result of the combustion. However, a strong compression wave reflected from the pile toe will increase the upward velocity of the ram and it will reach higher than before. For the next blow, the fall be longer and, therefore, the impact velocity will be higher resulting in a stronger impact wave, which will generate a stronger reflected compression wave, which will send the ram even higher, and ... . If the operator is not quick in reducing the fuel setting, either the diesel hammer or the pile or both can become damaged.

If the soil at the pile toe is soft and unable to offer much resistance to the pile, the reflected wave will be a tensile wave. When the tensile wave reaches the gage location, the gages will record a reduction in the compression wave and an increase in the tensile wave. If the tensile wave is large (very little or no resistance at the pile toe, the pile head may lose contact with the pile driving helmet (temporarily, of course) which will be evidenced by the force trace dropping to the zero line and the velocity trace showing a pronounced peak. The magnitude of the tensile force is directly proportional to the impact wave. A large increase in the velocity trace at Time  $2L/c$  is a visual warning for excessive tension in the pile. This is of particular importance for concrete piles, which piles have limited tension strength.

Whether a tension or a compression wave will be reflected from the pile toe is not just a function of the strength of the soil at the pile toe. Strength is the ultimate resistance after imposing a movement. In brief, if the force in the pile at the pile toe rises faster than the increase of resistance due to the pile toe penetration, a tension wave is reflected. If, instead, the soil resistance increases at the faster rate, then, a compression wave results. Ordinarily, the quake is small, about 1 % of the pile diameter or 2 mm to 4 mm, and the acceleration of the pile toe is such that the pile toe resistance is mobilized faster than the rise of the force in the pile. However, some soils, for example some silty glacial tills and highly organic soils, demonstrate large quake values, e. g., 20 mm to 50 mm. Yet, these soils may have considerable strength once the pile toe has moved the distance of the quake. When driving piles in such soils, the pile toe will at first experience little resistance. When the pile toe movement is larger than the quake, the pile toe works against the full soil resistance. Dynamic measurements from piles driven in such soils, will show a tensile reflection at  $2L/c$  followed by a compression reflection. The sharper the rise of the impact wave, the clearer the picture. If the conditions are such that the peak of the impact wave has reached the pile toe before the pile toe has moved the distance of the quake, the full toe resistance will not be mobilized and the penetration resistance becomes large without this being ‘reflected’ by a corresponding pile "capacity". Simply expressed, a large quake will zap the efficacy of the driving (Fellenius and Authier 1980).

The visual message contained in the force and velocity records will provide the experienced PDA operator with much qualitative information on where in the soil the resistance originates—shaft bearing versus toe bearing, or combination of both—consistency in the response of the soil as well as in the behavior of the hammer, and many other aspects useful the assessment of a pile foundation. For example, it may be difficult to tell whether an earlier-than-expected-stopping-up of a pile is due to a malfunctioning hammer producing too small force or little energy, or if it is due to fuel pre-ignition. The PDA measurements of hammer transferred energy and impact force will serve as indisputable fact to determine whether or not a hammer is functioning as expected.

Included with routine display of PDA traces are Wave-Down and Wave-Up traces. The Wave-Down trace is produced by displaying the average of the velocity and force traces, thus eliminating the influence of the reflected wave and, as the name implies, obtaining a trace showing what the hammer is sending down into the pile. Similarly, half the difference between the two traces displays the reflected wave called Wave-Up, which is the soil response to the impact. [Figure 9.13](#) shows an example of a routine display of the wave traces (see below for explanation of the Movement and Energy traces).

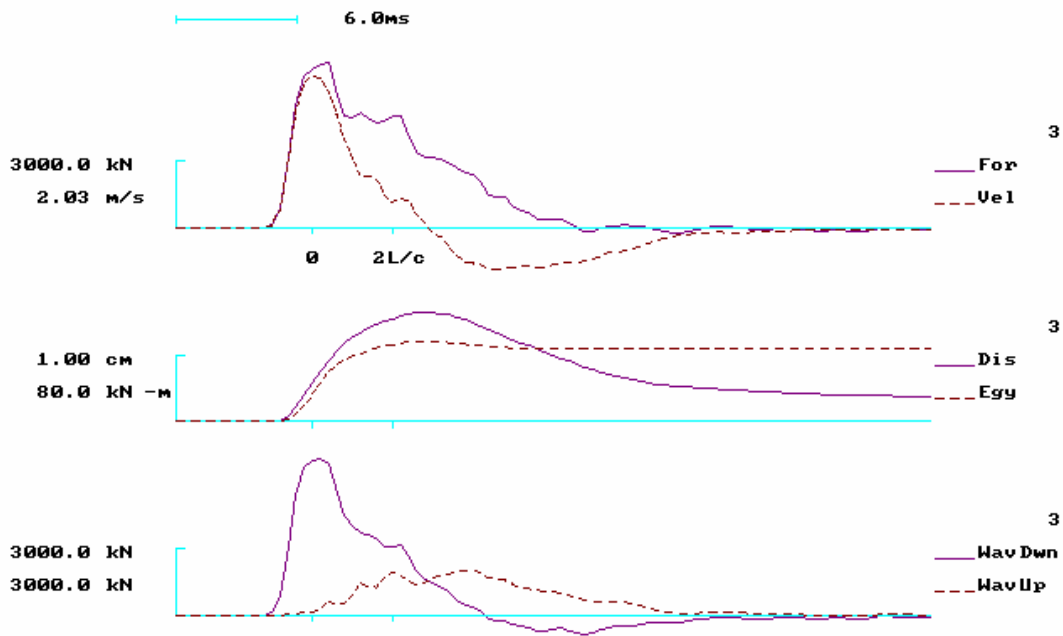


Fig. 9.13 Routine Display of PDA Wave Traces  
Force and Velocity, Movement ("Dis.") and Transferred Energy ("Egy."), and Wave Down and Wave Up

Comparing wave traces from different blows will often provided important information. For example, the discussion above referring to the strong compression wave reflecting from the pile toe is illustrated in [Figure 9.14](#) by two blows recorded from the initial driving of a steel pile through soft and loose silty soil to contact with a very dense glacial till. The pile toe was brought to contact with the glacial till between Blow 55 and Blow 65. The increased toe resistance resulted in a small increase of the impact force (from a stress of about 150 MPa to 170 MPa), which values are well within acceptable levels. However, for Blow 65 at Time  $2L/c$ , which is when the toe reflection reaches the pile head, a stress of 280 MPa was measured. This stress is very close to the steel yield for the pile material (reported to be 300 MPa). No surprise then that several of the pile were subsequently found to have considerable toe damage). Compounding the problem is the very small shaft resistance and a larger than usual toe quake. This is also obvious from the wave traces by the small separation of the traces and the “blip” immediately before Time  $2L/c$ .

### 9.8.2 Transferred Energy

The energy transferred from the hammer to the pile can be determined from PDA data as the integral of force times velocity times impedance. Its maximum value, called EMX, is usually referred to as the Transferred Energy. In assessing a hammer based on the transferred energy, it should be recognized that the values should be obtained during moderate penetration resistance and from when the maximum value does not occur much earlier than Time  $2L/c$ . Neither should a hammer be assessed by energy values determined from very easy driving. The consistency of the values of transferred energy is sometimes more important than the actual number.

### 9.8.3 Movement

A double integration of the acceleration produces a pile movement (displacement) trace, displaying the maximum and net penetration of the pile. An example is shown in the middle graph of [Figure 9.13](#), above.

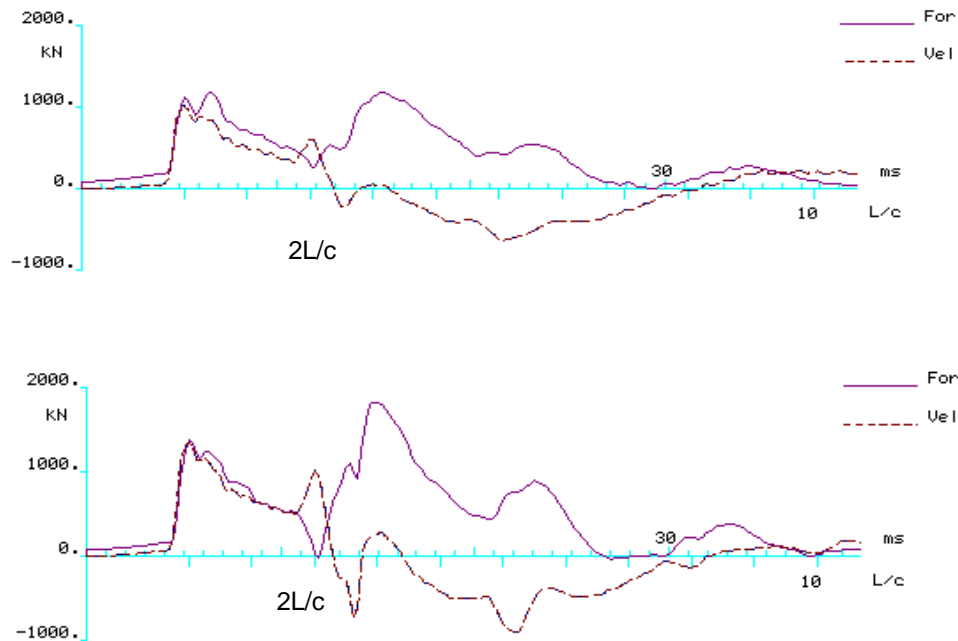


Fig. 9.14 Two Force and Velocity Wave Traces compared

## 9.9. Pile Integrity

### 9.9.1 Integrity Determined from High-strain Testing

In a free-standing, uniform rod, no reflections will appear before Time  $2L/c$ . For a pile, no sudden changes of shaft resistance normally occur along the pile. Therefore, the separation of the force and velocity traces caused by the shaft resistance is normally relatively gradual before Time  $2L/c$ . However, a sudden impedance reduction, for example, the intentional change of an H-Pile stinger at the end of a concrete section, will result in an increase of the velocity trace and a decrease of the force wave, a “blip” in the records. The magnitude of the “blip” is a sign of the magnitude of the impedance change. A partially broken length of a concrete pile is also an impedance change and will show up as a blip. The location along the time scale will indicate the location of the crack. A crack may be harder to distinguish, unless it is across a substantial part of the cross section. Rausche and Goble (1979) developed how the “blip” can be analyzed to produce a quantified value, called “beta” for the extent of the damage in the pile. The beta value corresponds approximately to the ratio of the reduced cross sectional area to the original undamaged cross sectional area. Beta values close to unity do not necessarily indicate a damage pile. However, a beta value smaller than 0.7 would in most cases indicate a damaged pile. Beta-values between 0.7 and 0.9 may indicate a change in the pile integrity, or impedance, but do not necessarily indicate damage. It must be recognized that an anomaly in the records does not necessarily indicate a defect in the pile. See also Salem et al. (1995) and Bullock (2012). [Figure 9.15](#) shows an example.

### 9.9.2 Integrity Determined from Low-strain Testing

The purpose of performing low-strain testing is to assess the structural integrity of driven or cast-in-place concrete piles, drilled-shafts, and wood piles, and to determine the length of different types piles including sheet piles where length records are missing or in doubt. A detailed guide for the performance of low-strain integrity testing is given in ASTM Designation D 5882-96.

The work consists of field measurements followed by data processing and interpretation. The measurements consists of hitting the pile with a hand-held hammer and recording the resulting signal with a sensitive accelerometer connected to a special field data collector (PIT Collector). The collector can display the signal (a velocity trace integrated from the measured acceleration) , process the data, and send the trace to a printer or transfer all the data to a computer. Special computer programs are used for data processing and analysis.

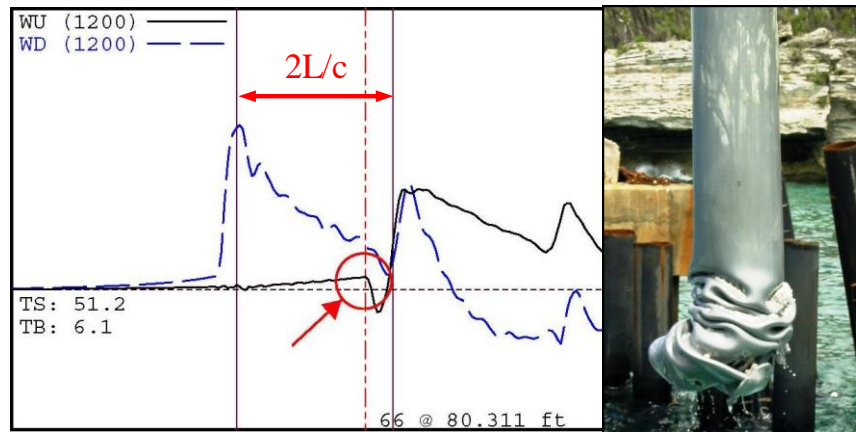


Fig. 9.15 Wave traces revealing damage to the pipe pile (later extracted).  
From Bullock (2012) used with permission.

Figure 9.16 shows schematically the principle of low-strain testing—collecting the pulse echo of signals generated by impacting the pile head with a hand-held hammer. The “motion sensor” transmits signals to a unit called the PIT Collector. The PIT Collector is equipped with a processor, and display and storage units. The stored processed data will be transferred to a PC for further processing and interpretation.

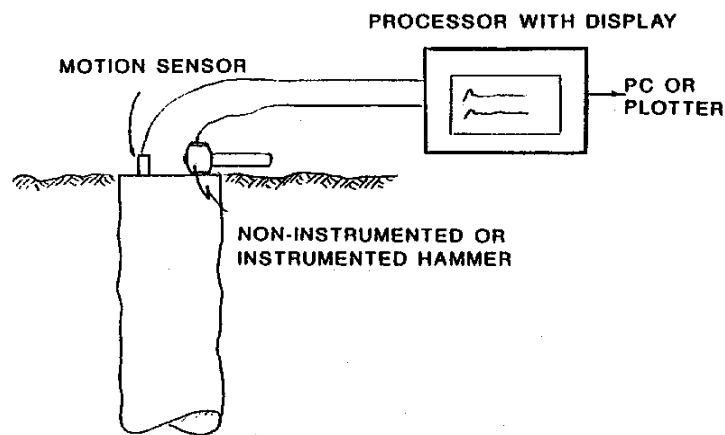


Fig. 9.16 Schematics of low-strain testing arrangement

The measurements are evaluated on site for preliminary assessment of the pile integrity. Questionable piles, if any, are identified and subjected to detailed analysis. The detailed analysis assists in identifying magnitude and location of structural concerns along the pile.

### 9.10 Case Method Estimate of "Capacity"

The data recorded by the PDA are displayed in real time (blow by blow) in the form of wave traces. Routinely, they are also treated analytically and values of stress, energy, etc., are displayed to the operator. The values include an estimate of pile "capacity" called the Case Method Estimate, CMES. The CMES method uses force and velocity measured at Times  $0 L/c$  and  $2 L/c$  to calculate the total (static and dynamic) resistance, RTL, as shown in Eq. 9.22.

$$(9.22) \quad RTL = \frac{F_{(t1)} + F_{(t1+2L/c)}}{2} + \frac{M c}{2L} (V_{(t1)} + V_{(t1+2L/c)})$$

where:

- $RTL$  = Total resistance
- $F_{(t1)}$  = Force measured at the time of maximum pile head velocity
- $F_{(t1+2L/c)}$  = Force measured at the return of the stress wave from the pile toe
- $M$  = Pile mass
- $c$  = Wave speed in the pile
- $L$  = Length of pile below gage location
- $V_{(t1)}$  = Pile velocity measured at the time of maximum pile head velocity
- $V_{(t1+2L/c)}$  = Pile velocity measured at the return of the stress wave from the pile toe

The total resistance is greater than the static bearing "capacity" and the difference is the damping force. Damping force is proportional to pile toe velocity and calculated as indicated in Eq. 9.23. (When velocity is zero just at the time when the pile starts to rebound ("unloads"), the total resistance (RTL) is a function of static resistance only. Initially in the development of the method of analysis of dynamic measurements, it was thought that the pile static "capacity" could be determined from this concept. However, the pile velocity is not zero all along the pile, so the approach was shown to be inapplicable (Goble et al. 1980). It was revived for the "long duration impulse testing method as indicated in Section 9.13).

$$(9.23) \quad R_d = J \frac{M c}{L} V_{(toe)} = J (F_{(t1)} + \frac{M c}{L} V_{(t1)} - RTL)$$

where

- $R_d$  = Damping force
- $J$  = Case damping factor
- $M$  = Pile mass
- $V_{toe}$  = Pile toe velocity
- $c$  = Wave speed in the pile
- $L$  = Length of pile below gage location
- $F_{(t1)}$  = Force measured at the time of maximum pile head velocity
- $V_{(t1)}$  = Pile velocity measured at the time of maximum pile head velocity
- $RTL$  = Total resistance

The PDA includes several CMES methods, some of which are damping-dependent and some are damping-independent. The damping-dependent methods evaluate the CMES value by subtracting the damping force,  $R_d$ , from the CMES value of total dynamic "capacity" (RTL). As shown in Eq. 9.23, the damping force is proportional to the measured pile physical velocity,  $V_{toe}$ .

The Case Damping factor ranges from zero to unity with the smaller values usually considered to represent damping in coarse-grained soil and the higher in fine-grained soils. The factor is only supposedly a soil parameter, however. Different piles driven at the same site may have different J-factors and a change of hammer may require a reassessment of the J-factor to apply (Fellenius et al. 1989). Therefore, what J-factor to apply to a certain combination of hammer, pile, and soil pile is far from a simple task, but one that requires calibration to actual static "capacity" and experience. A factor determined for EOID conditions may show to be off considerably for the restrrike (RSTR) condition, for example. It is always advisable to calibrate the CMES method "capacity" to the results of a CAPWAP analysis (Section 9.10).

The most common damping-dependent CMES methods are called RSP, RMX, and RSU. There is also a damping-independent method called RAU.

The **RSP** value is the CMES RTL value calculated from the force and velocity measurements recorded at Times 0 L/c and 2 L/c and applying a Case Damping factor, J, ranging from zero to unity. Typically, a CMES value indicated as RS6 is determined for a J = 0.6.

The **RMX** value is the maximum RSP value occurring in a 30 ms interval after Time 0 L/c, while keeping the 2 L/c distance constant. In case of hard driven piles, the RMX value is often more consistent than the RSP value. For details, see Hannigan (1990). Typically, a CMES value indicated as RX6 is determined for a J = 0.6. The RMX method is the most commonly applied method. Routinely, the output of RMX values will list the capacities for a range of J-factors, implying an upper and lower boundary of "capacity".

The **RSU** value may be applied to long shaft bearing piles where most of the movement is in the form of elastic response of the pile to the imposed forces. Often, for such piles, the velocity trace has a tendency to become negative (pile is rebounding) well before Time 2 L/c. This is associated with the length of the stress wave. As the wave progresses down the long pile and the peak of the wave passes, the force in the pile reduces. In response to the reduced force, the pile elongates. The soil resistance, which initially acts in the positive direction, becomes negative along the upper rebounding portion of the pile, working in the opposite direction to the static resistance mobilized along the lower portion of the pile (which still is moving downward). In the RSU method, the shaft resistance along the unloading length of the pile is determined, and then, half this value is added to the RSP value computed for the blow. For long shaft bearing piles, the RSU value, may provide the more representative "capacity" value. However, the RSU is very sensitive to the Case damping factor and should be used with caution.

The damping-independent **RAU** method consists of the RSP method applied to the results at the time when the toe velocity is zero (the Case J-factor is irrelevant for the results). The RAU method is intended for toe-bearing piles and, for such piles, it may sometimes show more consistent results than the RMX method. It also should be applied with considerable caution.

Although the CMES "capacity" is derived from wave theory, the values depend very much on choosing the proper J-factor and method, and, indeed, the representative blow record, that their use requires a good deal of experience and engineering judgment. This is not meant as a denigration of the CMES method, of course. There is much experience available and the methods have the advantage of being produced in real time blow for blow. When considered together with the measurements of impact force and transferred energy with due consideration to the soil conditions, and with calibration of a representative record to a signal-matching analysis (CAPWAP; see below), an experienced engineer can usually produce reliable estimates of "capacity" for every pile tested.

The estimate of "capacity" makes use of the wave reflected from the soil. It is often overlooked that the soil can never send back up to the gages any more than the hammer has sent down in the first place. Simply, the analysis of the record postulates that the full soil resistance is indeed mobilized. If the hammer is not able to move the pile, the full resistance of the pile is not mobilized. The PDA will then not be able to accurately determine the pile "capacity", but will deliver a "lower-bound" value. When the "capacity" is not fully mobilized, the "capacity" value is more subjected to operator judgment and, on occasions, the operator may actually overestimate the "capacity" and produce analysis results of dubious relevance.

Moreover, the "capacity" determined is the "capacity" at the time of the testing. If the pile is tested before set-up has developed, the "capacity" will be smaller than the one determined in a static loading test some time later. A test at RSTR (if the pile moves for the blow) is more representative for the long-term performance of a pile under load than is the test at EOID. (Provided now that the pile has been let to rest during the period between the initial driving and the restrike: no intermediate restriking and no other pile driven in the immediate vicinity).

A restrike will sometimes break down the bond between the pile and the soil and although in time the bond will be recovered this process is often slower than the rate of recovery (set-up) starting from the EOID condition. This is because a restrike does not introduce the any lateral displacement of the soil, while the initial driving introduces a considerable lateral displacement of the soil even in the case of so-called low-displacement piles such as H-piles.

Restriking is usually performed by giving the pile a certain small number of blows or the number necessary to for achieving a certain penetration. The pile "capacity" reduces with the number of blows given, because the restrike driving disturbs the bond between the pile and the soil and increases pore pressure around the pile. Therefore, the analysis for "capacity" is normally performed on one of the very first restrike blows, as analysis for one of the later blows would produce a smaller "capacity". Normally, the disturbance effect disappears within a few hours or days. However, a static test immediately following the completion of the restrike event may show a smaller "capacity" value than that determined in the analysis of the PDA data from an early restrike blow. Moreover, a static test is less traumatic for a pile than a dynamic restrike test. For this reason, when comparing dynamic and static test results on a pile, it is preferable to perform the static loading test first.

Performing the static test first is not a trivial recommendation, because when restriking the pile after a set-up period, it would normally have an adequate stick-up to accommodate the monitoring gages. Because a static test is normally performed with a minimum stick-up above ground (the pile is cut off before the test), attaching the gages after a static test may not be straight-forward and require hand excavation around the pile to provide access for placing the gages.

### **9.11. CAPWAP Determined Pile "Capacity"**

The two traces, force and velocity, are mutually independent records. By taking one trace, say the velocity, as an input to a wave equation computer program called CAPWAP, a force-trace can be calculated (Rausche et al. 1985). The shape of this calculated force trace depends on the actual hammer input given to the pile as represented by the measured velocity trace and on the distribution of static resistance and dynamic soil parameters used as input in the analysis. Because the latter are assumed values, at first the calculated force-trace will appear very different from the measured force-trace. However, by adjusting the latter data, the calculated and measured force traces can be made to agree better and the match quality is improved. Ultimately, after a few iteration runs on the computer, the

calculated force-trace is made to agree well with the measured trace. An agreement, ‘a good signal match’, means that the soil data (such as quake, damping, and ultimate shaft and toe resistance values) are close to those of the soil into which the pile was driven. In other words, the CAPWAP signal match has determined the static "capacity" of the pile and its distribution along the pile (as the sum of the resistances assigned to the analysis). Figure 9.17 presents an example of the results of a CAPWAP signal matching along with the wave traces and PDA data and is an example of a routine report sheet summarizing the data from one blow. When several piles have been tested, it is of value to compile all the PDA and CAPWAP results in a table, separating the basic measured values from the analyzed (computed) values.

**PDA Data Table**

EMAX (kJ)	Energy ratio (%)	Impact force (kN)	Max. force (kN)	Impact stress (MPa)	CSX (MPa)	CSB (MPa)	PRES (bl/25mm)	CASE Method Estimate (kN)			
								RX4	RX5	RX6	RA2
17.4	30.5	2,830	2,830	169	169	122	12	2,060	1,816	1,571	721

Emax: Maximum transferred energy CSX: Maximum compressive stress CSB: Maximum compressive stress, toe  
 RMJ: Case Method Estimate with a J-factor=J RA2: Case Method Estimate, damping independent PRES: Penetration resistance  
 Energy Ratio: Ratio between transferred and rated energy (57 kJ)

**CAPWAP Table**

Mobilized Static Resistance (kN)		Max. Stress (MPa)		Smith Damping (s/m)		Quake (mm)		
Total	Shaft	Toe	Compression	Tension	Shaft	Toe	Shaft	Toe
<b>1,724</b>	1,686	38	168	10	0.244	-	2.000	1.700

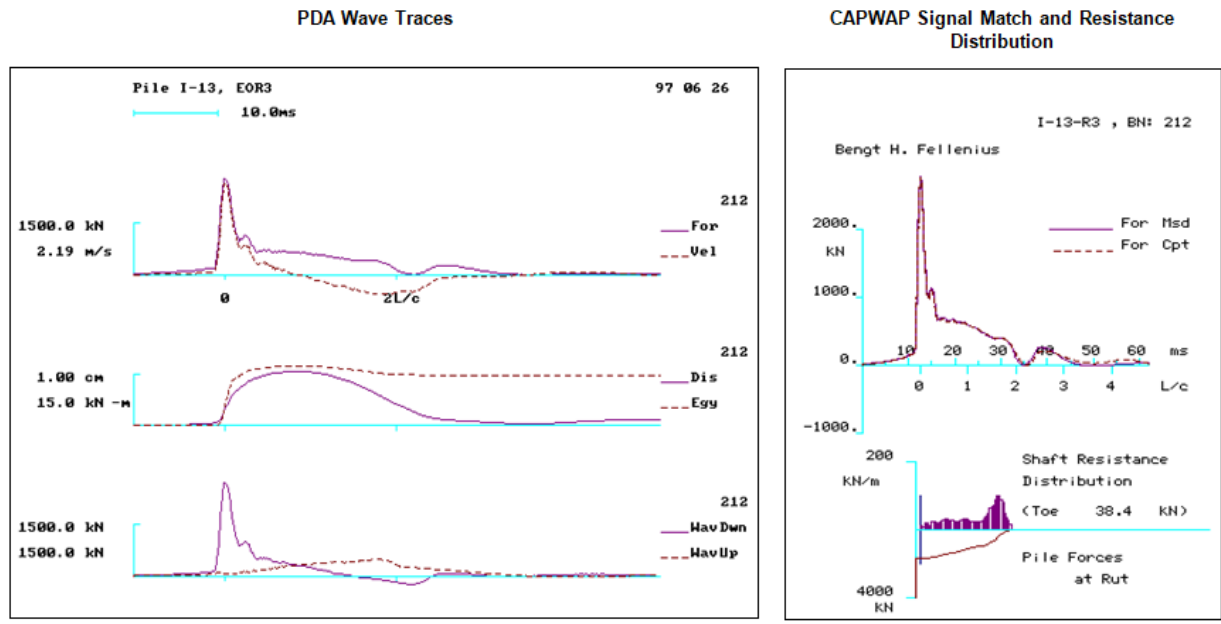


Fig. 9.17 Example of a routine PDA and CAPWAP summary sheet: Table and graph

The CAPWAP determined "capacity" is usually close to the "capacity" determined in a static loading test. This does not mean that it is identical to the value obtained from a static test. After all, the "capacity" of a test pile as evaluated from a static loading test can vary by 20 percent with the definition of failure load applied. Also, only very few static loading tests can be performed with an accuracy of 5 percent on load values. Moreover, the error in the load measurement in the static loading test is usually about 10 percent of the value, sometimes even greater.



A CAPWAP analysis performed on measurements taken when a pile penetrates at about 5 blows to 12 blows per inch will provide values of "capacity", which are reliable and representative for the static behavior of the pile at the time of the driving. Provided that the static test is equally well performed (not always the case), the two values of static "capacity" are normally within about 15 percent of each other. For all practical engineering purposes, this can be taken as complete agreement between the results considering that two different methods of testing are used.

In practice, engineers employing dynamic testing and CAPWAP analysis limit the analysis to the last impact given to the test pile at initial driving and the first (if possible) of the impacts given in restriking the test pile. They treat the dynamic tests as so much of a lesser cost static test. However, this is losing the full benefit of the dynamic test. Often at the end of initial driving, the full resistance is not mobilized (the pile is being driven at the maximum ability of the hammer to advanced the pile) and the CAPWAP-determined distribution may not be determined at the optimum use of the method. Therefore, also records of a blow from before the end of initial driving, say, from a foot above termination, should be subjected to a CAPWAP analysis and the results compared and discussed. Similarly, at restrike, also a record from the end of restrike, say the fifth or tenth blow should be analyzed. The latter analysis will often show a larger toe resistance than the analysis for very first restrike record (because the restriking has reduced the set-up and the shaft resistance being smaller allows more force and energy to reach the pile toe. Of course, an extra couple of CAPWAP analyses cost money—but so what, it is cheap money for the value obtained.

A CAPWAP analysis uses as input the speed of wave propagation,  $c$ , in the pile. Eqs. 9.11 through 9.17 show the importance and interdependence of the material density, impedance, and elastic modulus. The proper selection of the input parameters will govern the correct location of the soil and pile response (reflections) and of particular importance is the use of a correct wave speed for determining the elastic modulus. For a concrete pile, minute cracks—hairline fissures—can develop and together they could have the effect of slowing down the wave and require a smaller modulus to be input for the correct analysis results. The elastic modulus is usually determined from the time for the wave to reach the pile toe and be reflected up to the gage location at the pile head, Time  $2L/c$ . Also the evaluation of the impact force makes use of the elastic modulus. However, where hair line fissures have slowed down the wave speed and indicated a reduced modulus, no such reduction occurs at the gage location. In such cases, using the E-modulus input from the " $2L/c$ " time is not correct and a unreduced modulus applies.

It is import at that the blow selected for CAPWAP analysis is from where the maximum pile movement is larger than the quake resulting from the analysis. However, the pile movement should not be too much larger than the quake. The shape of the simulated load-movement curve, particularly for the pile toe, becomes less representative beyond the quake movement. When using the PDA/CAPWAP for reasons similar to performing a routine static loading test, or as a replacement for such, as a part of a field verification process where many piles are tested, the main purpose of the test and analysis is to establish a reliable level of at-least "capacity". However, when issues of load distribution, set-up also are a part of the study, then using a blow with a "perfect" record becomes vital. Often, running a CAPWAP on a couple of contiguous blows assists the final assessment. Doing an additional analysis on a blows recorded when the pile was a foot higher up is a prudent measure that may resolve many questions. Indeed, relying on the results from a single blow frequently insufficient and, because the blow record already exists, doing a second blow judiciously chosen is a reassurances obtained at a very low cost.

Aoki (2000) proposed a Dynamic Increasing Energy test, DIET, consisting of a succession of blows using a free-falling drop hammer and increasing the hammer rise from blow to blow, while monitoring the induced acceleration and strain with the Pile Driving Analyzer, and analyzing each blow by means of the CAPWAP program. The DIET test assumes that CAPWAP-determined static load-movement curves represent a series of loading-unloading, and reloading of the pile as in a static loading test to a

progressively larger maximum applied load. The curve from the first blow represents virgin condition and the following blows represent reloading condition. Fellenius (2014) presented a case history from Sao Paulo, Brazil (as reported Oliveira et al. 2008), where DIET tests were performed with four blows on a 700-mm diameter, 12 m long, CFA pile 66 days after constructing the pile. The results were compared to the load-movement curve measured in a static loading test 31 days after the dynamic test. Figure 9.18 shows the DIET load-movement curves for the pile head, shaft, and toe, and for the static loading test, all plotted in sequence of event. The dashed curves are back-calculated curves applying UniPile and t-z and q-z functions.

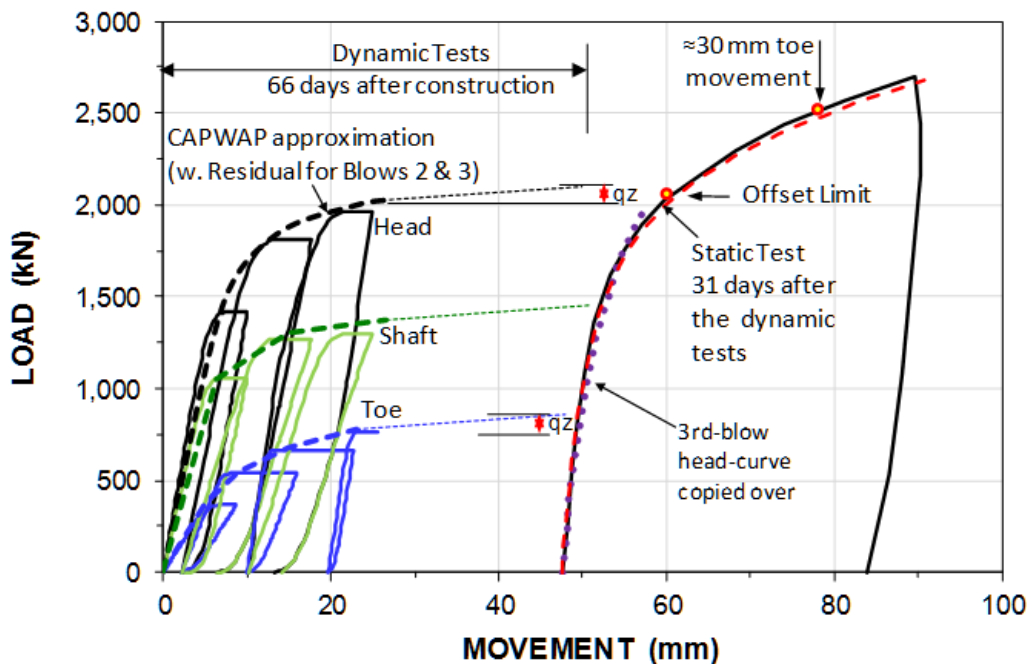


Figure 9.18 Load-movement curves for CAPWAP analyses and the static loading test (Fellenius 2014)

The results show that the CAPWAP-determined pile "capacity" agreed very well with the "capacity" of the static loading test, when defined by the offset limit (Section 8). The results also show that the dynamic tests stiffened up the pile giving an increase of the "capacity" determined from the load-movement of the static loading test. The increase was about 200 kN or 10 %. Indeed, The DIET method (dynamic testing and combining a series of blows with increasing force and CAPWAP analysis) provides results that more closely resemble those of a static loading test than does a single CAPWAP.

### 9.12. Results of a PDA Test

The cost of one conventional static test equals the costs of ten to twenty dynamic tests and analyses, sometimes more. Therefore, the savings realized by the use of dynamic testing can be considerable, even when several dynamic tests are performed to replace one static loading test. Moreover, pile "capacity" can vary considerably from one pile to the next and the single pile chosen for a static loading test may not be fully representative for the other piles at the site. The low cost of the dynamic test means that for relatively little money, when using dynamic testing, the "capacity" of several piles can be determined. Establishing the "capacity" of several piles gives a greater confidence in the adequacy of the pile foundation, as opposed to determining it for only one pile. Therefore, the PDA/CAPWAP applied to a driven pile project ensures a greater assurance for the job.

The CAPWAP results include a set of parameters to use as input to a wave equation analysis, which allows the wave equation can be used with confidence to simulate the continued pile driving at the site, even when changes are made to pile lengths, hammer, and pile size, etc.

The limitations mentioned above for when the full resistance is not mobilized apply also to the CAPWAP analysis, although the risk for overestimation of the "capacity" is smaller.

The distribution of the "capacity" on shaft and the toe resistances is determined with less accuracy as opposed to the total "capacity". The reason lies in that a pile is always to a smaller or larger degree subjected to residual force and the residual force cannot be fully considered in the CAPWAP analysis. The effect of residual force present in a test pile is an overestimation of the resistance along the upper length of the pile (shaft resistance) and an underestimation along the lower length (toe resistance). It has no effect on the total "capacity", of course. (It is not always appreciated that the sensitivity of the analysis results to residual force is equally great for the results of a static loading test).

A pile test will unavoidably change—disturb—the pile response to load. A dynamic test more so than a static test. It is not irrelevant, therefore, when comparing static and dynamic tests, for the best compatibility, the static loading test should "go first", as indicated in Fellenius (2008). This is not a trivial recommendation, because a dynamic test requires a stick-up of the pile head above ground, whereas a static loading test is preferably performed with a minimum stick-up.

Some preliminary results of the PDA testing will be available immediately after the test, indeed, even as the pile is being driven. For example, the transferred energy, the impact and maximum stresses in the pile, and a preliminary estimate of "capacity" according to the CMES method. The following is reported following processing in the office.

- Selected representative blow records including a graphic display of traces showing Force and Velocity, Transferred Energy and Pile Head Movement, and Wave Up and Wave Down.
- Blow data processed presented in tables showing a series of measured data for assessment of the pile driving hammer and pile.
- CAPWAP results showing for each analyzed blow the results in a CAPWAP diagram and the quantified results in tables.
- Complete pile driving diagram encompassing all dynamic data (Fig 9.17)

Figures 9.19 and 9.20 show examples of the measurements presented in a PDA diagram. The PDA diagram can be used to study how transferred energy, forces and stresses, hammer stroke, and penetration resistance vary with depth. When the PDA monitoring is performed not just for to serve as a simple routine test but to finalize a design, establish criteria for contract specifications, etc., then, a PDA diagram is of great value and assistance to the engineer's assessment of the piling.

The foregoing should make it quite clear that relying on a dynamic formula, that is, on essentially only the "blow-count" to determine "capacity" is a dangerous approach. Salem et al. 2008, present a case history where the blow count was considerably misleading, as was established in dynamic testing and CAPWAP analysis.

Lately, it has been stated that measurements on long, 10 to 20 feet (3 to 6 m) diameter, offshore piles have shown that the wave speed in these piles is faster than in other steel piles. These piles may have a 3/4 inch (20 mm) and more wall thickness, which would seem to be a thick wall. However, scaling down the diameter to that of a pile 12 to 24-inch pile diameter (0.3 to 0.6 m), the proportional wall thickness

becomes about 2 mm, which would make for a very flimsy pile. When such a pile is long, that is, longer than about 30 pile diameters, then, the toe of the thin-wall pile vibrates laterally like the end of a tuning fork, and if the toe is in a soft easily disturbed soil, liquefaction of the soil and loss of all shaft resistance near the pile toe will entail. On encountering that zone, the stress wave sends a tension reflection that can be interpreted as an indication of pile toe damage and/or loss of pile length, if the wave interpretation applies the conventional steel modulus. Field measurements have shown the indication to be false. Inputting a larger wave speed moves the origin of the reflection to below the pile toe, which removes the damage indication and lets the tension reflection be interpreted as a large-quake soil. When the pile toe reaches deeper located, more competent soil layers, the "damage" reflection may disappear, but, then, the wave speed is already established. It has been suggested that the large diameter piles are fabricated from different steel to that in smaller diameter piles (because similarly large wave speeds have not been reported from the smaller diameter piles) and that may be true. However, because the result of the calculation using the larger wave speed is a larger CAPWAP-determined "capacity". I suggest that whether the damage indication is true or false should first be ascertained by other means than modifying the elastic modulus of the steel.

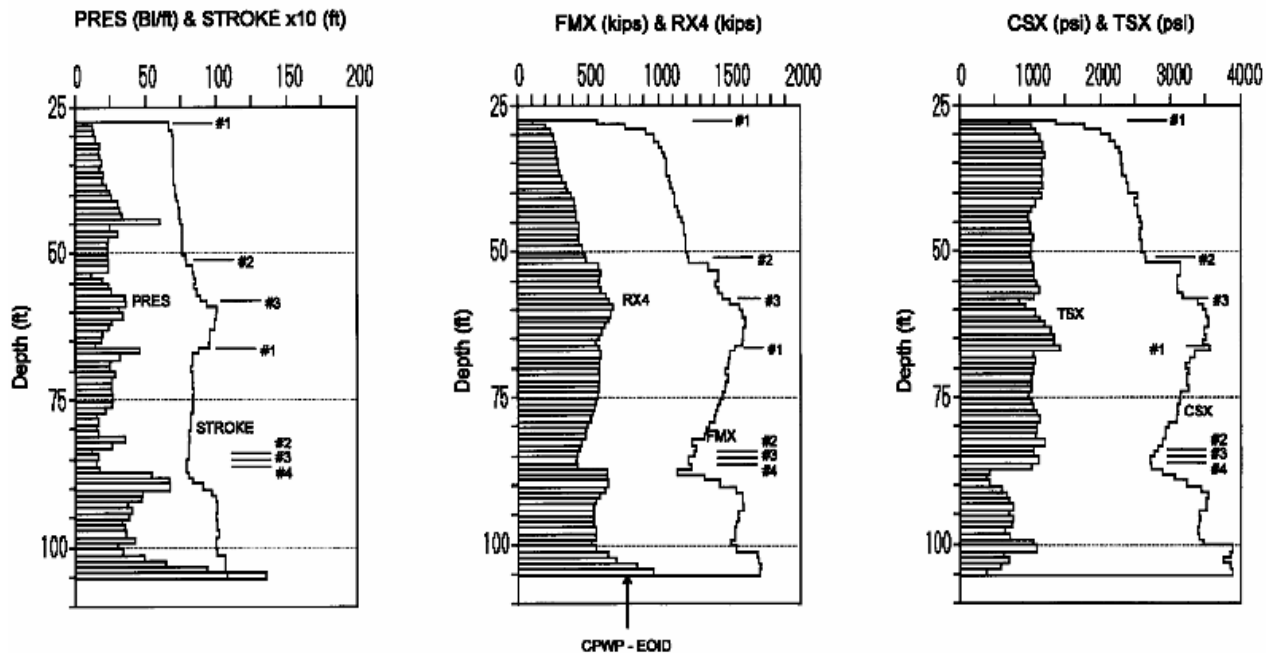


Fig. 9.19 Example of PDA Diagrams from the driving of a concrete pile (Labels #1 through #4 indicate hammer fuel setting)

### 9.13. Comments on Current State of Practice of Dynamic Monitoring

The release of the WEAP (wave equation analysis of pile driving) in the 1970s by George Goble and Frank Rausche marked the beginning of their great contributions to the geotechnical engineering practice—"the quantum leap." This chapter is based on my starting in 1977 experience with the WEAP and dynamic monitoring and introduces the basic principles of dynamic monitoring and analysis state of the practice. In early years, the WEAP was run at the company mainframe computer and input was by means of punch cards. The field testing using the PDA was by lugging the analyzer, a bulky tape recorder, an oscilloscope, and power-cable and gage-chord bundles to the site. If travel was by air, the PDA sat on the seat next to the engineer. For assessing the pile in the field, the measurements were printed out on a paper roll. In the mid-1980s, a screen was added to the PDA, it became digital, and data

were stored and accessible electronically also in the field. No more tape recorder and oscilloscope. At about the same time, the PC arrived and the WEAP became available for running on the office machine. Process was slow, while the PC ran a WEAP, it was time for a cigarette and a cup of coffee. To think through the input to the analysis, therefore, became an important time-saving effort. Soon thereafter also the CAPWAP became available for use on a PC.

The first International Stress Wave Conference in Stockholm in 1980 (it continued every fourth year, thereafter) started the international acceptance of the WEAP and high-strain dynamic monitoring. At the third conference, in Ottawa in 1988, the number of individuals outside of GRL performing CAPWAP analysis amounted to 17, with 14 from outside the U.S. Today, the high-strain dynamic monitoring is routine wherever piles are driven, and its use has been extended to testing non-driven piles.

The wave equation and high-strain dynamic method, then and now, is for assessing pile-soil response in terms of pile capacity and hammer performance. Over the years since, it has been extended to low-strain integrity testing and current advancement of technology has been incorporated. For example, the connection between pile gages is now wireless and the PDA is a tablet. The pile monitoring data can be sent to the “cloud” and enable remote testing. The process is so fast that an automatic signal matching (CAPWAP) can be made in real time on every blow. At some sites, every pile is tested, thus, the method is used for continuous quality control of the hammer-pile-soil system. However, the basic principles are pretty much the same.

#### **9.14. Long Duration Impulse Testing Method—The Statnamic and Fundex Methods**

In the conventional dynamic test, the imparted stress-wave has a steep rise and an intensity that changes along the pile length. That is, when the impact peak reaches the pile toe and the entire pile is engaged by the blow, force from the pile hammer transmitted to the pile varies and is superimposed by numerous reflections. The force in the pile varies considerable between the pile head and the pile toe. The steep rise of the stress-wave and the reflections are indeed the condition for the analysis. When the impact is “soft” and the rise, therefore, is less steep, it becomes difficult to determine in the analysis just from where the reflections originate and how large they are. However, in the 1990s, an alternative dynamic method of testing was developed, called Statnamic, here denoted “*long duration impulse method*” consisting of giving the pile just this soft-rising, almost constant force. The method is usually called “rapid loading test” and consists of impacting the pile in a way where the rise of force is much softer than in the pile driving impact, and the impulse (a better word than “impact”) was of a much longer duration. The long duration impulse usually makes the pile move as a rigid body, that is, the pile velocity at the pile head is the same as the velocity at the pile toe. This aspect made possible an analysis method, called the “*unloading point method*” for determining the pile “capacity” (Middendorp et al. 1992).

The long duration impulse method is a dynamic method. However, the transfer of the force to the piles, the impulse, can take 100 to 200 milliseconds, i.e., five to twenty times longer time than the time for a pile driving impact. The stress-wave velocity in the pile is the same, however. This means that the sharp changes of force experienced in the pile driving are absent and that the pile moves more or less as a rigid body. Although the ram travel is long, the peak force is reduced by that the impact velocity has been reduced. As a large ram mass is used, a large energy is still transferred to the pile. The key to the long duration impulse method lies in this slowing down of the transfer of the force from the impacting hammer to the pile. In method employed by a Dutch company, Fundex, this is achieved by letting the ram impact a series of plate springs which compression requires the hammer to move much more than required in case of the ordinary hammer and pile cushions, and thus reduce the kinetic energy in the transfer to the pile. The Statnamic method, developed by Berminghammer in Canada, achieves the effect in the pile in a radically different way, using a propellant to send a weight up in the air above the pile, in the process creating a downward force on the pile according to Newton's third law.

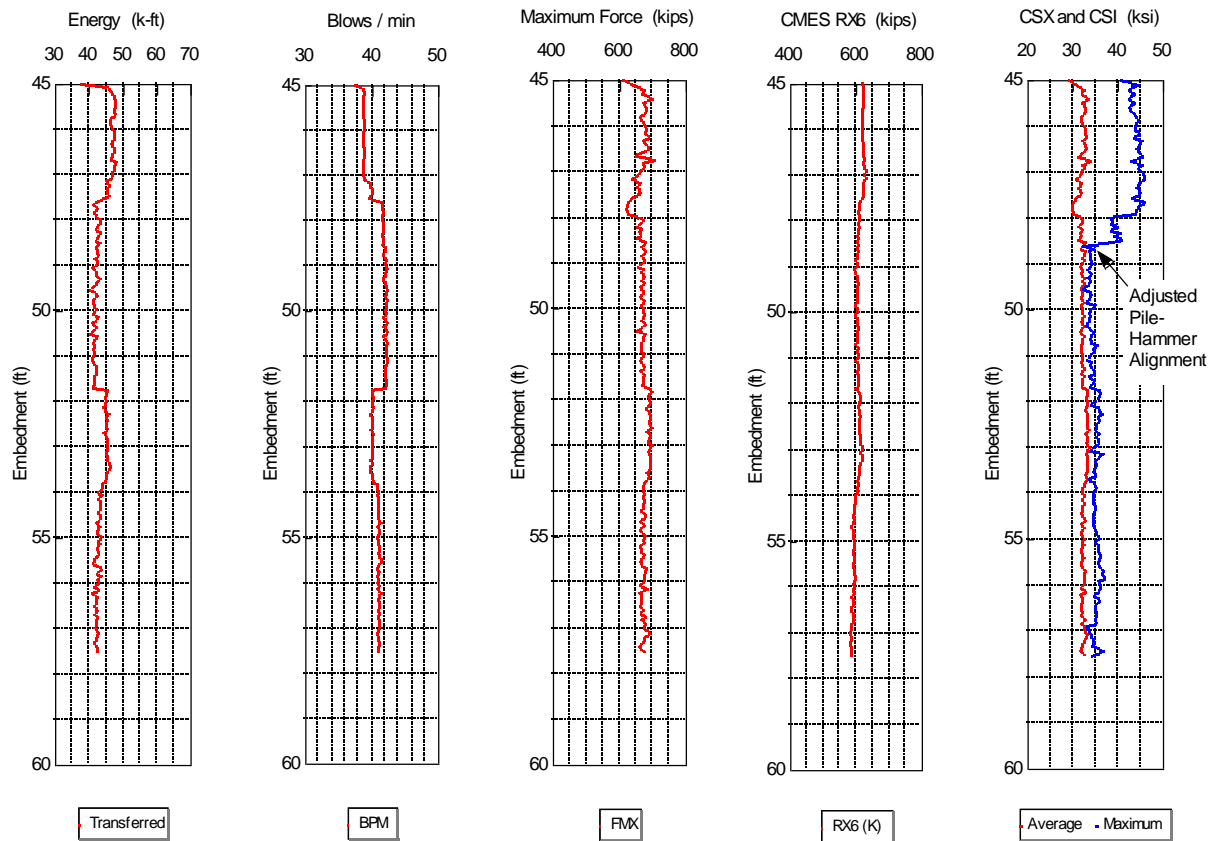


Fig. 9.20 Example of PDA Diagrams from the driving of a steel pile

The measurements consist of force, movement, acceleration, and time. The most important display of the results consists of a load-movement curve, as illustrated in Figure 9.21.

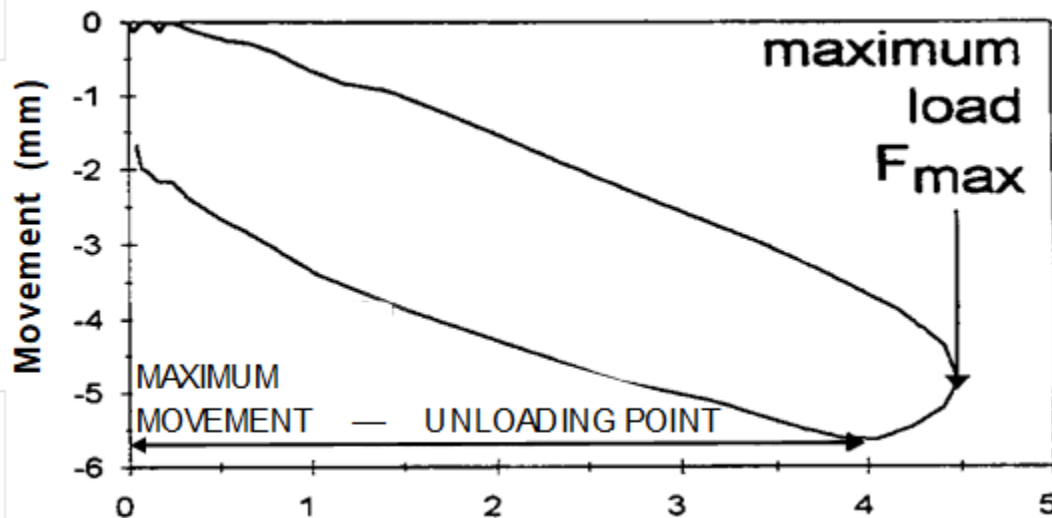


Fig. 9.21 Load-movement curve from Statnamic test (Bermingham et al. 1993)

Load, movement, velocity, and acceleration versus time are important records of the test. An example of these records are presented in Figure 9.22 (same test as in Figure 9.21). The maximum movement (about 4 mm in the example case) is where the pile direction changes from downward to upward, i.e., the pile rebounds, is called the "Unloading Point", "P-point" for short. The maximum load applied to the pile by the ram impulse (about 4.5 kN in the example case) occurs a short while (about 3 ms in the example case) before the pile reaches the maximum movement. Most important to realize is that the pile velocity is zero at the unloading point, while the acceleration (upward) is at its maximum. Shortly before and after the maximum force imposed, the velocity of the pile head and the pile toe are considered to be essentially equal, that is, no wave action occurs in the pile. This is assumed true beyond the point of maximum movement of the pile.

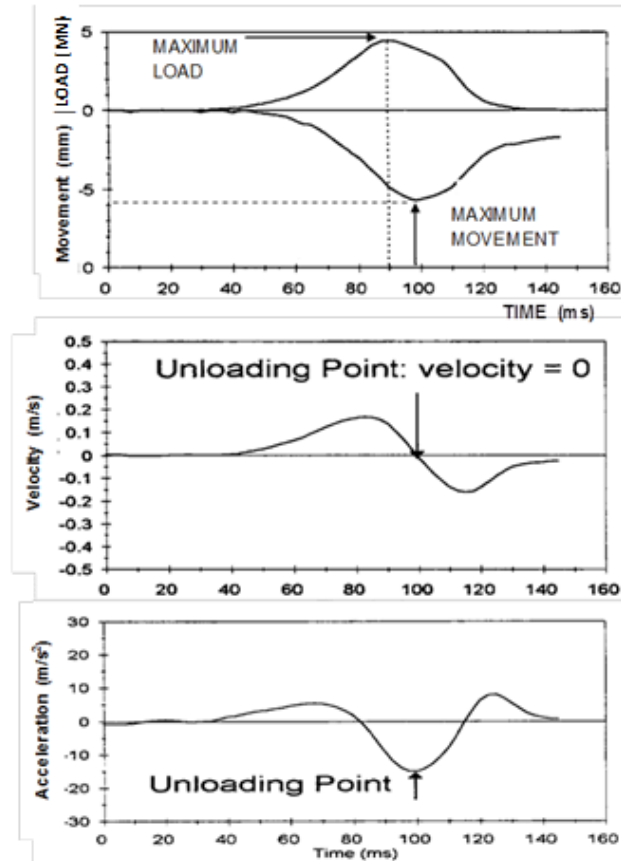


Fig. 9.22 Load, movement, velocity, and acceleration versus time from a Statnamic test (Bermingham et al. 1993; used with permission)

In the pile-driving dynamic test, the methods of analysis of the force and velocity measured in a dynamic test includes a separation of the damping portion (the velocity dependent portion) of the dynamic resistance. Inertia forces are considered negligible. In contrast, in the long duration impulse method, the velocity of the pile is zero at the unloading point, which means that damping is not present. However, the acceleration is large at this point and, therefore, inertia is a significant portion of the measured force.

The equilibrium between the measured force and the other forces acting on the pile at any time is described by Eq. 9.24 (Middendorp et al. 1992).

$$(9.24) \quad F = ma + cv + ku$$

where

$F$	=	measured force (downward)
$m$	=	mass of pile
$a$	=	acceleration (upward)
$c$	=	damping factor
$v$	=	velocity
$k$	=	modulus
$u$	=	movement

The two unknowns in Eq. 9.24 are the damping factor,  $c$ , and the modulus,  $k$ . The other values are either known or measured. As mentioned, at the unloading point, the velocity is zero along the full length of the pile. This becomes less true as the pile length increases, but for piles shorter than about 40 m, observations and research have shown the statement to be valid (Middendorp et al. 1998; Nishimura et al. 1998).

At the time of zero velocity, the damping component of Eq. 9.24 is zero, because the velocity is zero. This determines the static resistance at the unloading point, because the force and acceleration are measured quantities and the mass is known. Thus, the static resistance acting on the pile at the unloading point is obtained according to Eq. 9.25 as the value of measured force plus the inertia (note acceleration is upward—negative).

$$(9.25) \quad R_p = (F_p - ma_p)$$

where

$R_p$	=	static resistance at the UPM-point
$F_p$	=	force measured force at the UPM-point
$m$	=	mass of pile
$a_p$	=	acceleration measured at the UPM-Point

In the range between the maximum measured force and the unloading point, the load decreases (the pile decelerates; acceleration is negative) while the movement is still increasing, and the pile has a velocity (downward and reducing toward zero at the unloading point, which means that damping is present). These quantities are measured. Moreover, it is assumed that at the maximum force, the pile has mobilized the ultimate shaft resistance and the continued soil response is plastic until the unloading point is reached. That is, the static resistance is known and equal to the value determined by Eq. 9.25. This is the primary assumption of the Unloading Point Method for determining the pile "capacity" (Middendorp et al. 1992).

Eq. 9.24 can be rearranged to Eq. 9.26 indicating the solution for the damping factor.

$$(9.26) \quad c = \frac{F - ma - R_p}{v}$$

where

$c$	=	damping factor
$F$	=	measured force (downward)
$m$	=	mass of pile
$a$	=	acceleration (upward)
$R_p$	=	static resistance at the UPM-point
$v$	=	velocity



The value of the damping factor,  $c$ , in Eq. 9.26 is calculated for each instant in time between the maximum measured force and the unloading point. For the Statnamic test, the number of data points depends on the magnitude of movement of the pile after the maximum Statnamic force is reached. Typically, the number of data points collected in this range is 50 to 200. The  $c$  values are averaged and taken to represent the damping factor acting on the pile throughout the test. The measured force and acceleration plus the pile mass then determine the static load-movement curve according to Eq. 9.27.

$$(9.27) \quad R_P = F - ma - c_{avg} v$$

where

- $R_P$  = static resistance at the UPM-point
- $F$  = measured force (downward)
- $m$  = mass of pile
- $a$  = acceleration (upward)
- $c_{avg}$  = average damping factor between the maximum force and the P-point
- $v$  = velocity

Figure 9.23 illustrates the results of the analysis for a 9 m long, 910 mm diameter bored pile in clay (Justason and Fellenius 2001).

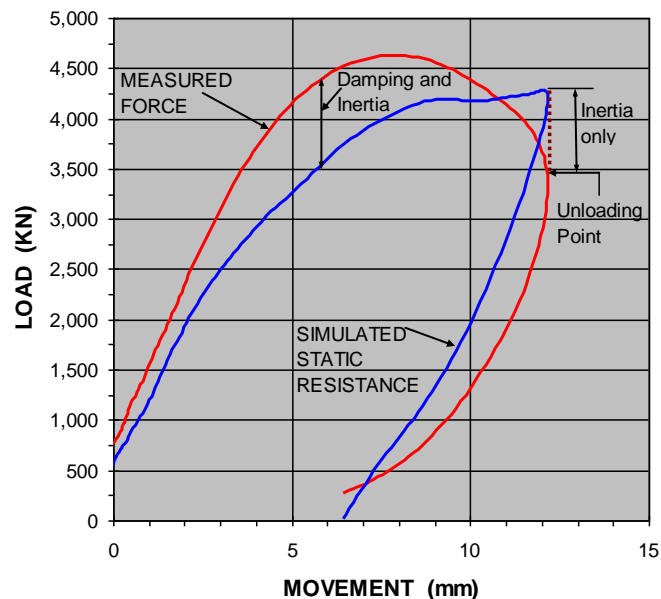


Fig. 9.23 Example of measured force-movement curve and simulated static load-movement curve Data from Justason and Fellenius (2001)

Lately, several papers have been published reporting case histories on "capacity" determined in a Statnamic test according to the Unloading Point Method, UPM, (e.g., Middendorp et al. 2008; Brown and Hyde 2008). The papers show that the method considerably overestimates the "capacity" determined on the same pile in a static loading test. In clay, the overestimation has been as large as close to a factor of two. The referenced papers hypothesize that the "capacity" overestimation is a result of the velocity of the pile and associated dynamic effects, notwithstanding that the UPM "capacity" is determined at zero velocity—non-dynamic condition—and recommend that a correction factor be applied to the UPM-determined "capacity". Such correction factors can never be general factors associated with the method, and it appears necessary to calibrate the Long Duration Impulse Testing Methods to a static loading test before relying on a UPM-determined response for a specific site and project.

### 9.15. Vibratory Pile Driving

The information in this section draws primarily from research and results presented by K.R. Massarsch (Massarsch 2000, 2002, 2004).

Vibratory driving is a common method for installing or extracting sheet piles and piles. Vibratory pile driving causes oscillating horizontal ground vibrations in coarse-grained soils. It can be shown that these horizontal vibrations reduce the shaft resistance during driving. The process results in the permanent increase of horizontal effective stress which causes arching around the vibrated pile. The most important parameters are vibration frequency, vibration amplitude, and eccentric moment. These parameters govern vibratory driving and, in particular, the soil resistance at the toe and along the shaft of a pile. The resonance frequency of the vibrator-pile-soil system, significantly affects pile penetration and emission of ground vibrations. At resonance of the vibrator-pile-soil system, the vertical vibration velocity in the soil reaches a maximum and pile penetration becomes very slow, whereas, beyond resonance, the vibration velocity decreases and the pile penetration is fast. (Resonance cannot occur in a direction perpendicular to the pile, i.e., the horizontal direction). Field monitoring of the vibratory driving process can be used to optimize vibratory pile driving.

Vibratory excitation affects a pile in a different way than does impact driving. In the case of vibratory driving, the pile is rigidly connected to the vibrator, resulting in minimal energy loss in transfer from the vibrator to the pile. The vibration frequency is relatively low, typically below 40 Hz (2,400 rpm), but larger than the resonance frequency of the pile-soil-hammer system. The wave length propagating down the pile is much longer than in the case of impact driving. It is generally recognized that vibratory driving is most effective in coarse-grained (frictional) soil and less efficient in fine-grained (cohesive) soil.

Modern vibrators are hydraulically driven, which allows continuous variation of the vibrator frequency during operation. The vertical oscillation of the vibrator is generated by counter-rotating eccentric masses. The peak value of the centrifugal force acting in the vertical direction depends on the eccentric moment and the circular frequency of the rotating eccentric masses, as expressed in Eq. 9.28.

$$(9.28) \quad F_v = M_t \omega^2$$

where  $F_v$  = centrifugal force  
 $M_c$  = eccentric moment  
 $\omega$  = circular frequency ( $\omega = 2\pi f$ ;) )

Eq. 9.28 shows that the displacement amplitude,  $s$ , is independent of the vibration frequency,  $f$ . In order to obtain the largest displacement amplitude, the total dynamic mass,  $m_t$ , should be kept as small as possible.

Many modern vibrators with variable eccentric moment and frequency enable the centrifugal force to be adjusted continuously during operation. The driving ability of the vibrator is determined by the vertical displacement amplitude (single amplitude) as a function of the eccentric moment and the total dynamic mass as expressed in Eq. 9.29. The total dynamic mass is the sum of all masses accelerated by the vibrator. This includes the rotating eccentric units, the pile, and the vibrator clamp. Note that most equipment manufacturers express the displacement amplitude as peak-to-peak ("double") amplitude.

$$(9.29) \quad s = \frac{M_e}{m_t}$$

where  $s$  = displacement amplitude (single)  
 $M_c$  = eccentric moment  
 $m_t$  = total dynamic mass

One important parameter that affects the penetration resistance during pile driving and during vibratory compaction is the operating frequency of the vibrator. Resonance vibration of the vibrator-pile-soil system is a function of several parameters with the shear wave speed (and therefore the shear modulus) being one of the most important. For most practical applications, the shear wave speed of undisturbed medium dense sand ranges between 150 and 250 m/s. However, in the presence of uninterrupted strong ground vibrations, the shear wave speed may reduce due to strain-softening effects. For most cases, the resonance frequency is in the range of 15 to 25 Hz and decreases with increasing pile length (and ratio of vibrator to pile mass). Note that the eccentric moment does not influence the resonance frequency.

An important such aspect of vibratory pile (or sheet pile) driving (or extraction) is that at-or close to-resonance, the penetration speed of the pile slows down dramatically, as the soil and pile (sheet pile) vibrate in phase. Vertical ground vibrations reach a peak at the resonance frequency of the vibrator-pile-soil system and the vertical vibration velocity is about 5 to 10 times larger than at the maximum vibration frequency. At resonance, shaft resistance builds up along the pile-soil interface, which enhances the transfer of vibration energy to the soil. This effect reduces penetration speed and can cause vibration problems during the operation. With increasing vibration frequency, the relative displacement between the pile and the soil increases, resulting in a reduction of shaft friction. Therefore, piles should be vibrated at a frequency of at least 1.5 times the resonance frequency in order to achieve efficient pile penetration and to minimize vibration emission.

Horizontal ground vibrations are significantly lower than the vertical. At frequencies below resonance, the relative movement between the pile and the soil is small, resulting in an almost static pile-soil interaction.

Vibrators with variable eccentric moment allow the machine operator to start up and shut down the vibrator at zero vibration amplitude, thereby reducing the risk of vibration amplification due to resonance.

The resistance of the soil along the pile consists of two components, pile shaft resistance and pile toe resistance as addressed in the next two clauses.

### 9.15.1 Pile Shaft Resistance

In the case of impact driving, the inertia of the pile and the static resistance along the pile-soil interface must be overcome in order to achieve a net pile penetration. At the end of each impact, the pile penetration slows down and static conditions return along the pile. In contrast, in the case of vibratory driving, the pile is kept axially (usually vertically) oscillating during the entire driving phase and the shaft resistance developing in vibratory driving is considerably smaller than that encountered in impact driving. Liquefaction is mentioned in the geotechnical literature as a possible cause of reduced shaft friction (permanent and/or temporary). However, liquefaction only develops in saturated soil and, yet, vibratory driving works well also in dry soil. Other causes mentioned are “rolling friction” and “material degradation”. However, these terms are mainly descriptive and, therefore, difficult to quantify.

A more rational explanation can be based on the cyclic forces generated during vibratory driving. Field measurements of ground vibrations during vibratory driving have shown that the vertically oscillating force creates—due to shaft resistance—also a horizontally oscillating force with a frequency that is twice the vertical vibration frequency. The horizontally oscillating wave field builds up pulsating horizontal stresses which reach a maximum at the end of each downward and upward end of the vibration cycle and

the shaft resistance of a pile is temporarily reduced. The soil is compressed horizontally, building up high horizontal effective stresses and, indeed, preconsolidates the soil adjacent to the pile. To optimize the shaft resistance for a vibratory driven pile, it is advantageous to toward the end of driving adjust the hammer to make the system operate at resonance frequency. Note, however, that for reasons of not impairing toe stiffness, the driving should terminate at high frequency.

In fine-grained (cohesive) soils, shaft resistance decreases due to strain and the number of vibration cycles (remolding) occurring when the relative displacement between the pile and the soil exceeds about 5 to 10 mm. The magnitude of the eccentric moment of the vibrator is therefore important for vibratory driving of piles in cohesive soils, as it determines the relative displacement between the pile and the soil (Eq. 9.28).

### **9.15.2 Pile Toe Resistance**

During a vibration cycle, when the pile has completed a downward motion and starts the upward rebound movement of the cycle, the soil below the pile toe will first follow the upward movement in an elastic response as the toe stress reduces. Soon, however, during the continued upward movement, the pile toe stress is reduced to zero and there is a separation of the pile toe from the underlying soil that increases if the upward movement continues. This causes causing a suction ("cavitation") between the pile toe and the soil below the toe, which is important because the suction can result in a remolding and/or loosening of the soil below the pile toe—even result in a net separation of the pile toe from the underlying soil and leave a gap below the pile toe. The toe resistance during the following cycle depends on the loosening and potential gap due to the preceding vibration cycle. The larger the amplitude, the larger the potentially adverse effect on toe stiffness. For this reason, it is advantageous to terminate the driving at large frequency and to reduce the vibration (displacement) amplitude gradually over a minute or two at the end of driving of toe-bearing piles, as opposed to a sudden vibration turn-off an end of driving.

### **9.15.3 Vibrator Performance Parameters**

During the last two decades, vibrators have experienced a rapid development in terms of power, range of operating parameters (eccentric moment and frequency) and monitoring of the driving and extraction process. (Initially, before 1990, most hydraulic vibrators had fixed eccentric moment, with a typical operating frequency of 22 to 30 Hz. These vibrators were mostly used for driving and extracting sheet piles).

The introduction of vibrators with variable frequency and amplitude allowed the resonance-free starting and shut-down of vibratory driving. Such vibrators allow the operating frequency and eccentric moment (and thus amplitude) to be varied according to driving requirements and soil conditions. The vibrator operation is computer-controlled and programmable.

The vibration amplitude given by vibrator manufacturers is usually in terms of double-amplitude and refer to a freely suspended vibrator (without clamp and pile/sheet pile). However, the vibration amplitude is an important parameter and must take into account the mass of also the clamping device and the pile. Note as indicated by Eq. 9.34, the displacement amplitude is not affected by the vibrator operating frequency.

An additional parameter to consider is the amplitude of the relative displacement between the pile and the soil, as it is important in regard to overcoming the toe resistance in coarse-grained soil and for the shaft resistance in cohesive soils. The larger the relative displacement between the pile and the soil, the more effective the driving process will be. The displacement amplitude depends on the total dynamic mass which must be accelerated by the vibrator and the eccentric moment. Therefore, if a pile is to be driven into clayey soil, a large eccentric moment will result in better driving performance.

With modern computerized equipment it is possible to acquire, display, and record information from a range of sensors, which can be mounted on the pile, the vibrator, the power pack, and the ground. Monitoring the vibratory driving process and the response of the ground and/or of adjacent structures is an important aspect of modern vibratory works. For instance, in the case of vibratory driving in the vicinity of vibration-sensitive buildings or equipment, the maximum vibration intensity needs to be controlled in order to ensure that specified limiting values are not exceeded. The monitoring usually consists of recording the following parameters:

- Position of pile
- Recording intervals (at least one reading per second) and time
- Depth of sheet pile during penetration or extraction (penetration speed)
- Operating frequency of vibrator
- Acceleration of vibrator
- Static force applied to the pile (pushing or lifting force affecting the vibrator weight)
- Hydraulic pressure of vibrator/power pack
- Vibration velocity on ground (geophones or accelerometers)
- Eccentric moment
- Centrifugal force
- Displacement amplitude (prior to and during the driving)

When piles or sheet piles are to be installed with vibratory driving equipment, the selection of the equipment and the installation process must be based on sound information obtained from geotechnical investigations. Having to replace an unsuitable vibrator will not only result in project delays and incur additional costs, the use of an unsuitable vibrator can, under unfavorable conditions, also produce damaging ground vibrations. The required vibrator "capacity" can be estimated based on soils information which includes records of CPT soundings, and results of field trials. With this proposed concept, it is possible to develop a correlation between penetration resistance and pile penetration speed for different vibrator types and pile sizes.

#### **9.15.4 Vibratory Driving Planned from Penetration Tests**

Rational design of a vibratory driving project requires site information that includes a well-established soil profile with soil description. The most reliable geotechnical information can be obtained from a continuous record of soil layering and density, such as provided by a CPTU sounding.

Unless past experience is available from vibratory driving in similar geology and comparable equipment, field trials are the best way of estimating the vibratory driving resistance of piles or sheet piles. During the driving test, it is important that the vibrator rests on the pile and is not held back by the machine operator, which would affect the penetration speed.

Vibratory driving of piles and sheet piles can be carried out with minimum environmental adverse effects, such as ground vibrations, noise, and soil disturbance. As the operating frequency of the vibrator has a strong influence on vibrations emitted from the vibrating pile, the highest risk of ground vibrations occurs when the vibrator is operated at the resonance frequency of the vibrator-pile-soil system. It is also when the pile penetration progress is the smallest.

#### **9.16. Vibration Caused by Pile Driving**

The information in this section draws primarily from research and results presented by K.R. Massarsch (Massarsch 1992; 2000; 2004; and Massarsch and Fellenius 2008; 2021).

During driving, energy is transmitted from the pile hammer to the pile, and, as the pile penetrates into the soil, both static and velocity-dependent (dynamic) dynamic resistances are generated. The dynamic soil resistance gives rise to ground vibrations which are transmitted through the soil, potentially, causing settlement in some soils, or adversely affecting nearby installations or structures on or in the ground. In this context, the process is more complex than realized by many, but the theoretical format is quite simple, as will be shown below. Based on work by Massarsch 2002; 2004, Massarsch and Fellenius (2008; 2014) discussed the interactive nature of the pile impedance and the soil impedance which can be used to assess the vibration effect of pile driving. The fact that the damping factor is a function of the ratio between the pile impedance and the soil impedance for P-waves is verified by a reanalysis of vibration measurements reported by Heckman and Hagerty (1978), who measured the intensity of ground vibrations at different distances away from piles being driven. The piles were of different type, size, and material. Heckman and Hagerty (1978) determined a 'k'-factor, expressed in Eq. 9.30, which governs the ground vibration intensity. The vibration velocity, also called peak particle velocity, PPV, is the standard measure of vibration intensity and reference to risk for vibration settlement due to pile driving.

$$(9.30) \quad v = k \frac{\sqrt{W}}{r}$$

where

$v$	=	vibration velocity, PPV, (m/s)
$W$	=	energy input at source (J)
$k$	=	an empirical vibration factor ( $\text{m}^2/\text{s}\sqrt{\text{J}}$ )
$r$	=	distance from pile (m)

The vibration velocity in Eq. 9.30 is not defined in terms of direction of measurement (vertical, horizontal, or resultant of components). Moreover, the empirical factor,  $k$ , is not dimensionless, which has caused some confusion in the literature. [Figure 9.24](#) presents the  $k$ -factor values of Heckman and Hagerty (1978) as a function of pile impedance and measurements of pile impedance.

The measurements were taken at different horizontal distances away from piles of different types and sizes driven with hammers of different rated energies. Unfortunately, the paper by Heckman and Hagerty (1978) is somewhat short on details regarding the driving method, ground conditions, and vibration measurements and, therefore, the data also include effects of ground vibration attenuation and, possibly, also effects of vibration amplification in soil layers. Yet, as shown in [Figure 9.25](#), a strong correlation exists between the pile impedance and the  $k$ -factor, as the ground vibrations increased markedly when the impedance of the pile decreased. In fact, ground vibrations can be ten times larger in the case of a pile with low impedance, as opposed to vibrations generated at the same distance from the driving of a pile with high impedance (Massarsch 1992; Massarsch and Fellenius 2008; Fellenius and Massarsch 2008).

The correlation shown in [Figures 9.23 and 9.24](#) is surprisingly good, considering that the measurements were taken in different soil conditions. The data provided by Heckman and Hagerty (1978) indicate that ground vibrations in the reported cases mainly originated from the pile toe. Indeed, the data confirm that the energy transmission efficacy correctly reflects the vibration emission from the pile to the surrounding soil layers.

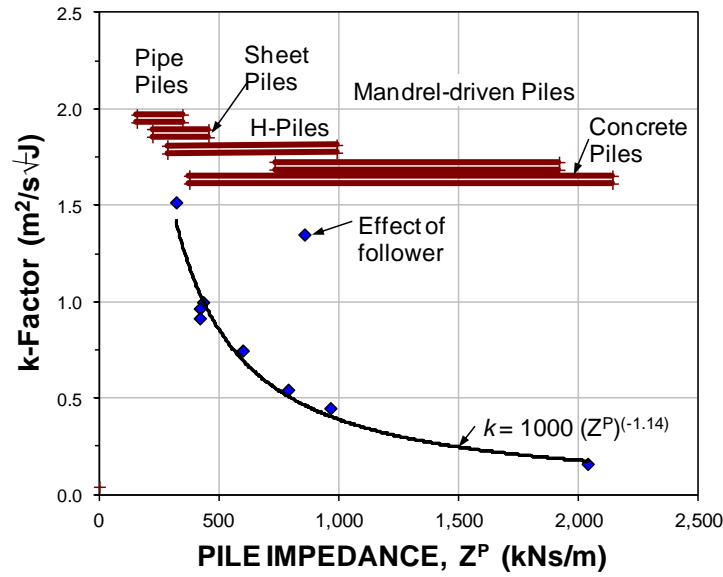


Fig. 9.24 Influence of pile impedance on the vibration factor, k (Eq. 9.30). (Data from Heckman and Hagerty 1978).

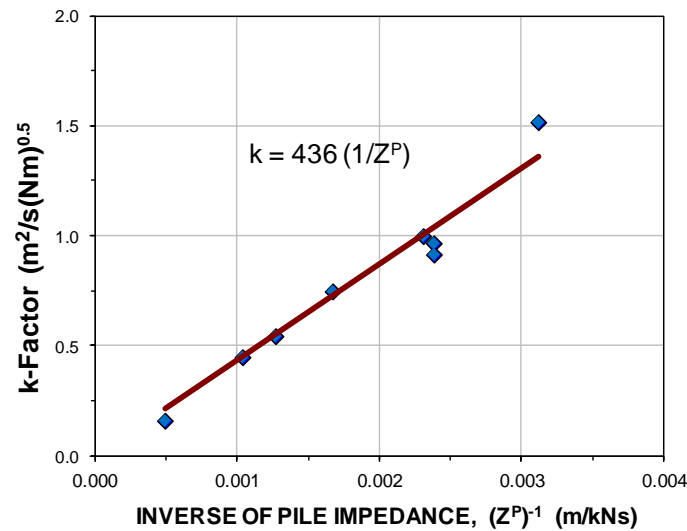


Fig. 9.25 Relationship between k-factor and inverse of pile impedance. Data from Figure 9.24 replotted.

Combining Eqs. (9.4) and (9.30) results in Eq. (9.31), which can be used for estimation of ground vibration from pile driving (Massarsch and Fellenius 2014).

$$(9.31) \quad v = \frac{436 \sqrt{F^H W_0}}{Z^P r}$$

where

- $v$  = vibration velocity (a physical velocity), PPV
- $Z_p$  = pile impedance
- $F^H$  = pile driving efficacy factor
- $W_0$  = nominal energy
- $F^H W_0$  = transferred energy obtained from dynamic measurements

Nilsson (1989) reported vibration velocity measurements from the driving of 270-mm diameter concrete piles through fill and overburden soils to dense glacial till at 25 m depth. Massarsch and Fellenius (2008; 2014) reanalyzed data using the relation expressed in Eq. 9.31, as shown in Figure 9.26.

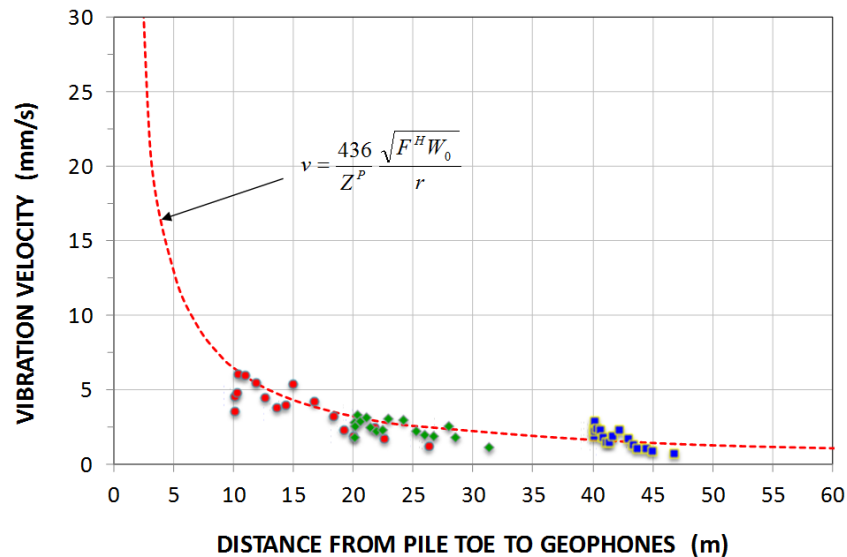


Fig. 9.26 Vibration velocity per Eq. 9.30 plotted with measurements of vibration velocity. (Data from Nilsson 1989, as presented by Massarsch and Fellenius 2014).

The transferred energy can be estimated or, better, be measured using dynamic measurements near the pile head (PDA measurements).

Under unfavorable conditions, the installation of piles or sheet piles can cause damage to buildings or other structures on the ground. Frequently, such damage is attributed to vibrations of the structure itself.

In the case of impact pile driving, the frequency content of ground vibrations cannot be controlled by changing the pile driving process. In contrast, during vibratory driving, the pile or sheet pile is rigidly attached to the vibrator, which oscillates vertically at a frequency, which can be chosen and modified by the operator. The operating frequency and amplitude of modern vibrators can be adjusted in order to achieve optimal driving while minimizing environmental impact. However, if a vibrator is operated at or near the resonance frequency of buildings or building elements, strong vibrations can be generated. This effect can be used to increase the efficiency of deep vibratory compaction systems, such as “resonance compaction” (Massarsch and Fellenius 2005).

When a pile penetrates easily into the ground, the intensity of transmitted vibrations will be low. However, vibrations increase when denser soil layers are encountered and pile penetration speed decreases. Ground vibrations depend thus on the geotechnical conditions which need to be considered in the risk assessment. During the initial phase of pile penetration, the source of vibrations will be located close to the ground surface. However, when the pile penetrates deeper into the ground, the source of vibrations becomes more complex. Vibrations can be emitted from the toe of the pile, but also along the



pile shaft. Therefore, geotechnical conditions are of great importance when trying to predict the intensity of ground vibrations and. It is important that the location is known of stiff soil layers, through which the pile shall be driven and which can give rise to strong ground vibrations. Massarsch and Fellenius (2008) present an in-depth discussion of factors influencing ground vibrations due to pile driving.

Building damage due to pile driving vibrations can be caused by settlement in the ground below an adjacent building foundation. The risk of settlement due to ground vibrations exists primarily in loose sand and silt. In other soils, such as soft clays, vibrations can contribute to, but are rarely the main source of settlement.

It is possible to determine critical vibration levels, which are based on the shear strain level generated by ground vibrations. When vibrations pass through material, strain is induced, which can be calculated, if the particle velocity and the wave speed of the pile are known. Soil strain caused by propagation of a compression wave (P-wave) can be determined from Eq. 9.32.

$$(9.32) \quad \varepsilon = \frac{V_p}{c_p}$$

where  $\varepsilon$  = induced strain  
 $v_p$  = particle velocity, PPV, measured in the direction parallel to the wave propagation  
 $c_p$  = wave speed in the direction parallel to the wave propagation

Similarly, as shown in Eq. 9.33, the shear strain,  $\gamma$ , can be calculated by dividing the particle velocity measured perpendicularly to the direction of wave propagation with the shear wave speed.

$$(9.33) \quad \gamma = \frac{V_s}{c_s}$$

where  $\gamma$  = shear strain  
 $v_s$  = particle velocity, PPV, measured in the direction perpendicular to the wave propagation  
 $c_s$  = shear-wave speed the direction parallel to the wave propagation

Determining shear wave speed is routine part of a CPTU sounding (Chapter 2, Section 2.9). Shear strain is an important parameter when assessing the risk of settlement in granular soils due to compaction (densification) or disturbance of cohesive soils. A threshold strain level,  $\gamma_t$ , exists below which it is unlikely that any rearrangement of soil particles can occur and, therefore, the vibrations will not generate an increase of pore water pressure in water-saturated sands. At a shear strain smaller than  $\gamma_t \approx 0.001\%$  ( $10 \mu\varepsilon$ ), the risk for settlement is low. When this level is exceeded, the risk of particle rearrangement and, therefore, settlement increases. At a shear strain level of  $\approx 0.010\%$  ( $100 \mu\varepsilon$ ), vibrations can start to cause settlement. Significant risk of settlements exists when the shear strain level exceeds  $\approx 0.100\%$  ( $1,000 \mu\varepsilon$ ).

It is important to note that shear modulus and shear wave speed are affected by shear strain. Massarsch (2004) showed that the shear wave speed decreases with increasing shear strain and that this reduction depends on the fines content (and plasticity index) of the soil. The reduction of shear wave speed is more pronounced in gravel and sand than in silt and is even smaller in clay. The effect must be appraised when determining the shear wave speed at a given strain level. Based on Eq. 9.32, and taking into account the reduction in shear wave speed with shear strain level, Massarsch (2002; 2008) proposed a simple chart

(Figure 9.27) showing the relationship between vibration velocity (particle velocity) and shear wave speed due to ground vibrations for three different levels of shear strain in relation to the risk for settlement in sand.

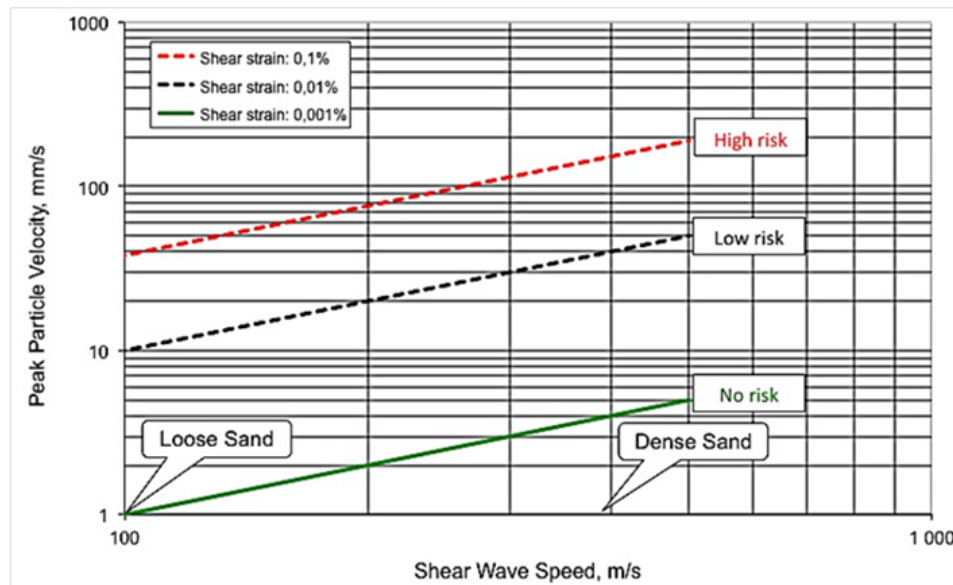


Fig. 9.27 Assessment of settlement risk in sand as function of amplitudes of shear-wave speed, shear strain, and vibration velocity (Massarsch 2004)

### 9.17. Settlement, Compaction, and Densification Caused by Pile Driving Vibrations

The information in this section draws primarily from research and results presented by K.R. Massarsch (Massarsch 2000, Massarsch and Fellenius 2014, and Massarsch et al. 2021).

The magnitude of settlement due to pile driving vibrations depends on several factors, such as soil type and stratification, groundwater conditions (degree of saturation), pile type, and method of pile installation (driving energy). For estimating settlements in a homogeneous sand deposit adjacent to a single pile, Massarsch (2004) proposed the basic procedure, illustrated in Figure 9.28, which shows that the most significant densification due to pile driving occurs within a zone corresponding to three pile diameters around the pile being driven. The volume reduction resulting from ground vibrations will cause significant settlements in a cone with an inclination 2(V):1(H), with its apex at a depth of 6 pile diameters below the pile toe. Thus, the settlement trough will extend a distance of  $3D + L/2$  from the centre of the pile, with maximum settlement at the centre of the pile. Maximum and average settlements, can be estimated using the Eq. 9.34 relationship, for an appropriate value of the soil compression factor,  $\alpha$ .

$$(9.34) \quad s_{\max} = \alpha(D + b); \quad s_{\text{avg}} = \frac{\alpha(D + 6b)}{3}$$

where

- $s_{\max}$  = maximum settlement
- $\alpha$  = soil compression factor
- $D$  = pile embedment
- $b$  = pile diameter

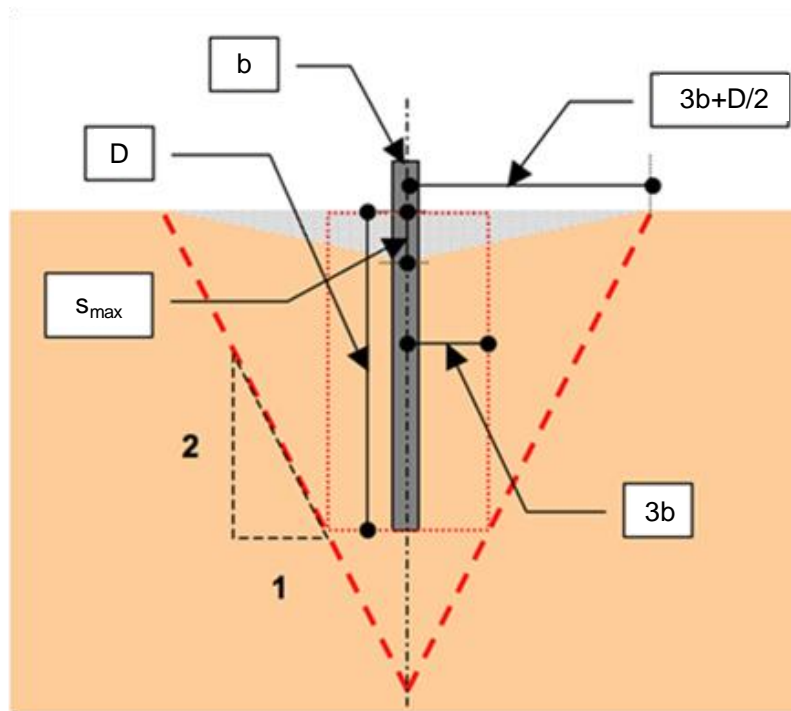


Fig. 9.28 Basic method of estimating settlements adjacent to a single pile in homogeneous sand (after Massarsch 2004)

Table 9.4 shows compression factors applicable to driving in very loose to very dense sand at driving energy ranging from low to high.

**TABLE 9.4** Compression factor,  $\alpha$ , for sand based on soil density and level of driving energy (Massarsch 2004)

Energy: <====>	Low	Average	High
Soil Compactness	----- Compression factor		
	$\alpha$		
Very loose	0.02	0.03	0.04
Loose	0.01	0.02	0.03
Medium	0.005	0.01	0.02
Dense	0.00	0.005	0.01
Very dense	0.00	0.00	0.005

Assume that a concrete pile with diameter  $b = 300$  mm and an embedment length  $D = 10$  m is installed in a deposit of medium dense sand. The pile is driven using an impact hammer and pile penetration is normal (stiff layers requiring high driving energy are assumed not to be present). The compression value,  $\alpha$ , for medium dense sand and average driving energy according to Table 9.4 is  $\alpha = 0.010$ . According to Eq. 9.34, the maximum settlement adjacent to the pile and the average surface settlement of the cone base are 118 mm and 39 mm, respectively. The radius of the settlement cone of the ground surface footprint is 5.9 m, resulting in an average surface slope of 1:50 (0.118/5.90).

Vibrations from construction activities, such as pile driving, are normally not likely to cause damage to buildings or building elements. Only in the case of very sensitive buildings with poor foundation conditions may settlements be initiated or existing cracking aggravated, e.g., foundations on loose to very loose sand. This aspect is not included in most vibration standards, which were primarily developed for blasting applications.

The Hong Kong Buildings Department has issued a Practice Note, APP-137 “Ground-borne Vibrations and Ground Settlements Arising from Pile Driving and Similar Operations” which provides guidelines on the control of ground-borne vibrations and ground settlements generated from pile driving or similar operations with a view to minimizing possible damage to adjacent properties and streets. This standard is the only one which suggests limiting values with regard to ground settlement and ground distortion. The Hong Kong acceptance limits for settlement is referenced to the vibration velocity as shown in [Table 9.5](#) (quoted from Massarsch and Fellenius 2014).

Table 9.5. Empirical guidelines according to HK Practice

Instrument	Criterion	Alert	Alarm	Action
Ground settlement	Total settlement	12 mm	18 mm	25 mm
Service settlement	Total settlement or angular distortion	12 mm or 1:600	18 mm or 1:450	25 mm or 1:300
Building tilting	Angular distortion	1:1000	1:750	1:500

Ground settlements should be considered on a case-by-case basis with respect to the integrity, stability, and functionality of the affected ground and structures.

Damage to building due to pile driving vibration (in shaking the building structure) is a separate issue outside the purpose of this chapter. For more information, see Massarsch 2002; 2004, 2008.

## CHAPTER 10

### VIBRATORY COMPACTION

#### 10.1 Introduction

In spite of the growing number of land reclamation projects built up from sand fill and remediation of liquefaction susceptible soils, little practical guidance can be found in the geotechnical literature regarding the planning, design, execution, and monitoring of compaction. This chapter aims to fill this void to some degree. It relies primarily on research by Dr. K.R. Massarsch (see Massarsch 1991a; 1991b; 1992; 1994a; 1994b; 1999a; 1999b; 2000; 2002; 2004a; 2004b; 2004c; 2005, 2023 and Massarsch and Fellenius 2001; 2005; 2014a; 214b; 2015; 2017a; 2017b; 2019).

Vibratory compaction of granular soils can be a technically and economically competitive to other soil improvement solutions, such as deep foundations. Vibratory compaction is most frequently used on large-scale projects to reduce settlement or to mitigate liquefaction. One reason for the limited application of vibratory compaction is a lack of understanding by geotechnical engineers how to estimate settlement in sand—prior to as well as after compaction (Chapter 3). This chapter focuses on design aspects and practical application of deep vibratory compaction.

An important application of vibratory compaction is the treatment of man-made soil, e.g., hydraulic fill for land reclamation projects. The range of densities achievable by the compacting of sand is typically at the boundary between the values giving acceptable performance and those resulting in unacceptable performance. Therefore, it is, at an early stage of a project, important to assess whether compaction is needed and, if so, to what degree. The density of sand placed under water (subaqueous fill) is generally lower than of sand placed above groundwater (subaerial fill). Lee (2001) found that the placement technique is the single most important factor controlling the geotechnical response of a given type of sand, when placed as a subaqueous or hydraulic fill. For example, the weakest zone of the latter type is generally located just beneath the groundwater level.

In most cases, compaction of a sand fill is required to reduce total and differential settlement. In addition, the effect of cyclic loading due to seismic or other dynamic forces (wave loading, blasting, construction activities or heavy traffic) may need to be considered.

A dynamically varying stress change (cyclic loading) imposed in a loose sand, i.e., dynamic action—stress changes occurring or imposed at some frequency—with the final stress being the same as the initial, results in a volume decrease. In geotechnical context, such increase of density is called "compaction". Densifying soil by compaction is an important part of the construction process to improve supporting conditions for foundations, roads, and earth retaining structures.

Generally, compaction by dynamic methods requires coarse-grained ("free-draining") soil. The particular soil type—that is, grain-size distributions, shape of the soil grains, amount and type of clay minerals—has a major influence on the "compatibility" and selection of methods for and process of compaction. Some methods are generally suitable, while others are limited to a particular soil type or condition. Methods that impose cyclic shear stresses along with compressive stresses are most effective.

Improvement by compaction must be performed for all engineered fill placed on the ground to serve as base of foundations. The fill is placed in layers, "lifts", that range in thickness from about a foot or less to a metre or more depending on conditions. Compaction is then carried out, lift by lift, by surface methods employing vibratory plates or rollers—small or large—or falling weights ("dynamic consolidation").

Where the foundation soils requiring improvement by compaction are thick, e.g., natural loose soil deposits or hydraulic fill, deep vibratory compaction is needed—carried out in a grid pattern, in one or several passes.

Compaction will be less efficient if the entire compaction process is carried out at a single frequency. Deep compaction is accomplished using different types of vertically oscillating probes that are excited by an impact hammer, a heavy vibrator mounted on the top of the probe, or by horizontally vibrating depth-vibrators (Vibroflotation system). The process involves the application of repeated cycles of dynamic force, which induce strain and small movement to the soil structure, resulting in a reconfiguration of soil particles to a denser state. In most soil compaction methods, vertically or horizontally oscillating vibrators are used. A brief summary of the characteristics of vibratory driving are presented in the following section.

## 10.2 Vibrator Characteristics

The static moment is an important parameter for vibrator applications. It is the product of the mass of the eccentric weights and the distance of their center of gravity to the rotation axis as indicated in Eq. 10.1.

$$(10.1) \quad M = G r$$

where  $M$  = Static moment (also called “eccentric moment”)  
 $G$  = Mass of eccentric weight(s)  
 $r$  = Distance of center of gravity to rotation axis of weight(s)

As Eq. 10.1 shows, the static moment is not affected by the vibration frequency,  $f$ .

The peak centrifugal force acts in the vertical direction and depends on the static moment and the circular frequency of the rotating eccentric mass (Eq. 10.2).

$$(10.2) \quad F_v = M \omega^2$$

where  $F_v$  = Peak centrifugal force  
 $M$  = Static moment  
 $\omega$  = Circular frequency of the eccentric mass

An additional important factor for soil compaction is the displacement amplitude of the probe, which should be at least 4 to 6 mm before the start of penetration (Massarsch 2023, Massarsch and Fellenius 2014a; 2014b). Before insertion of the probe in the ground, the vertical displacement amplitude of a free-hanging vibrator unit (comprising vibrator mass, clamp, and compaction probe), can be determined from static moment divided by the total dynamic mass excited by the dynamic vibratory action according to Eq. 10.3.

$$(10.3) \quad S_0 = S_G - S_P = 2S = 2 \frac{M}{G_D}$$

where  $S_0$  = Displacement amplitude defined as difference between ground ( $S_G$ ) and probe vibration amplitudes ( $S_P$ )  
 $G_D$  = Total dynamic mass (vibrator, clamp, and probe)  
 $M$  = Static moment

Modern vibrators can generate a centrifugal force of up to 4,000 kN or higher and the maximum displacement amplitude of the probe can exceed 30 mm. These enhancements in vibrator performance have opened new applications to the vibratory driving technique. Recently, hydraulically driven vibrators with variable frequency and variable eccentric moment (displacement amplitude) have been introduced. Figures 10.1 and 10.2 show the operating principles of a vibrator with eccentric masses, arranged at four separate rotation levels. During any stage of vibrator operation, the position of the lower row of masses can be changed relative to that of the upper row, thereby allowing the eccentric moment and the displacement amplitude, as well as frequency to be seamlessly and continuously adjusted during the compaction operation.

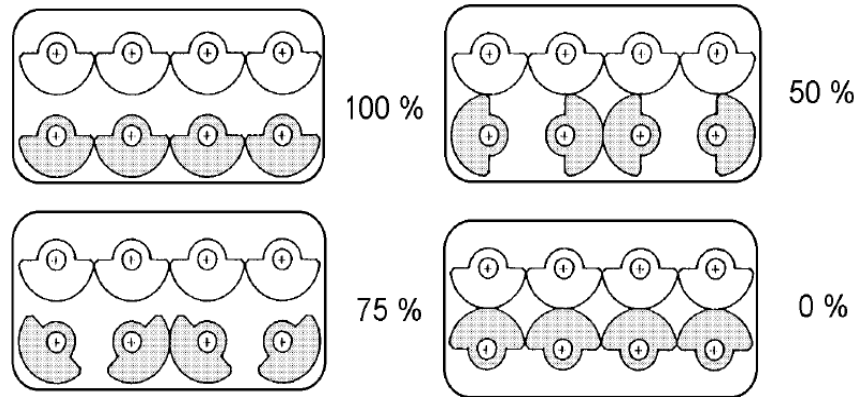
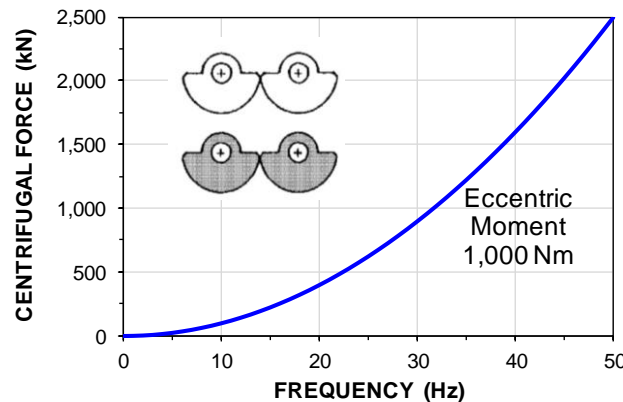


Fig. 10.1 Vibrator with dual rows of eccentric masses allowing variation of the static moment. Lower row (shaded) position indicates position in relation to upper row (not shaded).



b) Variation of centrifugal force during variation of vibration frequency

Fig. 10.2. Operating principle of hydraulic vibrator with variable frequency and displacement amplitude.

### 10.3 Overview of Compaction Methods

Deep vibratory equipment and applications are described extensively in the geotechnical literature; for example, see Massarsch (1991; 1999a; 1999b), Mitchell (1982), and Schlosser (1999). Each of the below discussed compaction methods has its optimal applications and limitations. The selection of one or a combination of several suitable methods is governed by a variety of factors, such as soil conditions, required degree of compaction, type of structure, maximum depth of compaction, and site-specific considerations, such as sensitivity of adjacent structures or installations, available time for completion of project, competence of contractor, access to equipment and material, etc.

It is common practice to award a soil compaction project to the lowest bidder. However, at the end of completion of a project, this may not always turn out to have been the optimal solution. The required compaction result may show to be less than required, or the assigned duration of work may have been significantly exceeded. Therefore, it is paramount for all types of soil compaction projects that a high degree of quality control and site supervision is implemented.

Soil compaction is a repetitive process and much can be gained from properly planned and executed compaction trials. The most important factors, which should be established and verified at the start of the project, are:

- required energy (intensity of vibration) imparted at each compaction point
- depth of required treatment
- spacing between compaction points
- duration of compaction in each point
- ground settlements due to compaction (at compaction point and overall)
- time interval between compaction passes (time for reconsolidation of soil after treatment)
- verification of the achieved compaction effect by field monitoring and in-situ tests
- potential increase of compaction effect with time after compaction
- ground vibrations in the vicinity (effects on adjacent structures and installations)
- effect on stability of nearby slopes or excavations
- monitoring of equipment performance and review of safety aspects.

Soil compaction methods can be classified according to the categories listed in Table 10.1. The compaction energy can be applied to the soil at the ground surface either by impact (falling weight) or by vibratory action (Figure 10.3). The compaction effect will be highest close to the ground surface (with the exception of a shallow, superficial layer) and decrease with depth. The effective depth of compaction is difficult to assess. It is influenced by a variety of factors, such as the geotechnical conditions, the type and quality of equipment, compaction procedure etc. There is also a risk of overcompaction in the soil layer close to the ground surface, adding costs due to protracted compaction work.

**Table 10.1. Classification of compaction methods.**

<b>Energy transfer from ground surface</b>	
<b>Impact</b>	Dynamic Compaction Impact roller
<b>Vibration</b>	Vibratory plate
<b>Energy transfer below ground surface</b>	
<b>Impact</b>	Driven tube/probe Driven piles Driven stone columns Explosives
<b>Vibration</b>	Vibroflotation Vibratory probes Resonance compaction

Compaction energy can be applied below the ground surface by different methods, using either impact or vibratory energy, as listed in the table. However, the most efficient way to densify deep deposits of granular material is to introduce the compaction energy at depth.



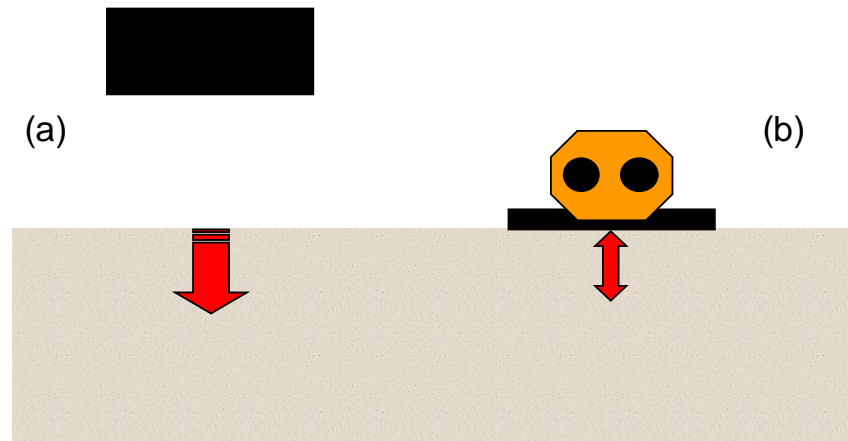


Fig. 10.3. Deep compaction methods applying energy at the ground surface.  
 a) Dynamic compaction      b) Vibratory plate compaction

### 10.3.1 Dynamic compaction

Soil densification by dynamic compaction (DC), also called “heavy tamping” is a well-known compaction method. The method was “rediscovered” by Menard, who transformed the tamping method into a rational compaction procedure. Soil is compacted by repeated, systematic application of high energy using a heavy weight (pounder). The imparted energy is transmitted from the ground surface to the deeper soil layers by propagating shear and compression waves, which force the soil particles into a denser state. In order to assure effective transfer of the applied energy, a 1 to 2 m thick coarse soil layer usually placed over the ground surface. Pounders can be square or circular in shape and made of steel or concrete and weights normally ranging from 5 to 25 tonne used with drop heights of up to 25 m. Heavier weights and larger drop heights have been used for compaction of deep soil deposits, but are not very common.

Dynamic compaction is carried out in several passes. During each pass, the weight is dropped repeatedly in a predetermined grid pattern. In the subsequent passes, compaction is carried out in-between the previously compacted points. The final pass, also called “ironing pass”, usually performed with low compaction energy, using a larger plate size and a reduced drop height. The objective of the ironing pass is to densify the superficial soil layers without remolding the already densified deeper layers. Mayne (1984) presented a detailed description of the dynamic compaction method.

Although the dynamic compaction method appears to be very simple, it requires careful design of the compaction process. The densification effect is strongly influenced by the dynamic response characteristics of the soil to be compacted, but also by the underlying soil layers. Usually, extensive compaction trials are needed to optimize the compaction process with respect to the required energy for achieving specified densification criteria. A major limitation of dynamic compaction is the lack of monitoring and quality control during the production phase. However, for research purposes, the pounder can be equipped with sensors to monitor the applied energy and to record the dynamic response of the soil layer. An example of the application of dynamic compaction in connection with a land reclamation project in Singapore is shown in [Figure 10.4](#) (Krogh and Lindgren 1997).



a) Compaction with 25 tonne mass and 25 m drop      b) Vibration monitoring on ground

Fig. 10.4 Dynamic compaction carried out in the trial area of Changi East Reclamation Project, Phase 1B. (Krogh and Lindgren 1997).

The maximum depth which can be achieved by dynamic compaction depends on several factors, such as the geotechnical properties of the soil layer to be compacted, the dynamic soil properties in and below the layer to be compacted (e.g., a soft clay layer below the layer to be densified can significantly reduce the compaction effect), the groundwater level, the compaction grid, the number of compaction passes, and the time interval between passes. Eq. 10.4 expresses a general rule for estimating the maximum effective depth,  $d_{max}$ , of compaction of a soil deposit.

$$(10.4) \quad d_{max} = \alpha \sqrt{H \cdot M}$$

where  $d_{max}$  = maximum effective depth  
 $\alpha$  = empirical factor  $< 1$   
 $H$  = average drop height  
 $M$  = pounder mass

The empirical factor,  $\alpha$ , usually ranges from 0.3 to 0.5, but should be determined for each site. The typical effective treatment depth for 15 m drop height and 15 tonne pounder mass is 7 to 8 m.

### 10.3.2 Impact roller

A simple, but in some cases surprisingly effective surface compaction method is the impact roller (Figure 10.5). A conventional tractor pulls a heavy prism- or triangular shaped mass, consisting of steel or concrete. The impact generated by the rotation of the heavy mass (up to 50 tonne) transfers sufficient energy to achieve medium compaction to a depth of several metre. The compaction process is usually based on site-specific correlation and little documented evidence about actually achieved compaction effects is available. The impact roller can be used on granular soils including crushed stone and rock fill. However, the surface to be treated must be carefully prepared (be evened) and have sufficient stiffness to allow rotation of the pulled heavy mass.



Fig. 10.5. Impact roller for deep compaction.

### 10.3.3 Vibratory compaction plate

Deep soil compaction can be carried out using a heavy steel plate, which is excited by strong vertical vibration. This compaction method has been made possible by the development of powerful hydraulic vibrators. The first vibrators were developed some 60 years ago in Russia and have since been used extensively on foundation projects world-wide. During the past decade, very powerful vibrators have been developed for soil compaction as well as for applications such as pile and sheet pile driving (addressed in Section 9.14). These vibrators are hydraulically driven, which allows continuous variation of the vibrator frequency during operation. Figure 10.6 shows two examples of vibrators mounted on compaction plates.



Fig. 10.6. Two types of vibratory compaction plate vibrators (operating at variable frequency).

The maximum depth of compaction depends primarily on the size (geometry) of the plate and on the applied energy (force and number of compaction cycles). Extensive investigations have been performed in connection with sub-marine soil compaction projects. Nelissen (1983) found that the compaction effect depended on the vibration frequency and the dynamic interaction of the plate-soil system.

Based on field trials on land and on the seabed, the optimal compaction parameters could be established. The compaction depth is about close to the diagonal length of the plate (i.e., to length and width in combination), typically, in the range of 4 to 6 m. The compaction effect can be enhanced by varying the operating frequency to match the system frequency of the vibrator-plate-soil system. Vibratory plates have been used successfully for underwater compaction. However, in such applications, the plate must be provided with circular openings to reduce the effect of the water column becoming excited by the vertically oscillating plate.

### 10.3.4 Displacement column

Driving of wood or concrete piles into deposits of granular soil is probably the oldest deep compaction method. However, because of the high equipment cost and the limited efficiency in loose soils, this method is not used extensively on larger projects. Clause 10.6.4 shows a case history of comparison of compaction effect achieved by installing wood piles driven by drop hammer, good effect, and diesel hammer less good. The stone-column method (also called "compacto-pile") is based on the Franki pile concept, where the energy is transmitted at the bottom of an open-toe steel tube. Figure 10.7a shows the basic principle of the Franki system. A heavy impact hammer with a mass of up to 10 tonne is dropped on a compacted stone and gravel plug placed at the bottom of a thick-wall steel tube. The steel tube can be driven into the ground by an impact or vibratory hammer. As a result of the vertical force, the soil below the pile toe is displaced and at the same time compacted. After the maximum depth has been reached, gravel or dry-mix concrete is added and the soil plug is expelled by a series of impacts using raised hammer fall. The tube is then withdrawn in steps adding gravel at each step. The step-wise process adds a compaction effect in the surrounding soil up along the pile. However, the method is time-consuming and therefore costly. Figure 10.7b shows a photo of a machine for construction of a Franki stone column. (when concrete, whether compacted or not, instead of stone and gravel is added on withdrawal of the steel tube, the term is "Franki pile" or "expanded-base pile").

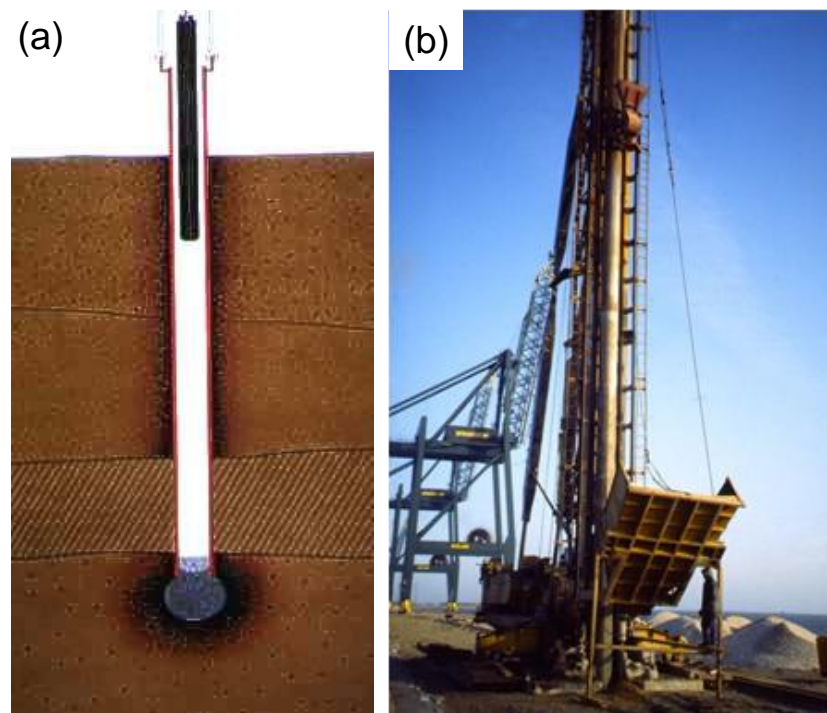


Fig. 10.7. Franki system compaction method. a) Principle. b) Franki stone column machine.

### 10.3.5 Vibro-probe compaction

Several deep compaction methods apply vibro-probe principles. The mass and shape of the compaction probe are important components of system. Different types of compaction probes have been developed, ranging from conventional pile (H-beam), steel tubes, or sheet pile profiles, to more sophisticated, purpose-built probes (terra probe, vibro-rod, and Y-probe). The probe is inserted, withdrawn, and reinserted in the ground with the aid of a heavy, vertically oscillating vibrator attached to its upper end. The compaction efficiency of a probe can be increased by introducing circular or rectangular openings

along the flanges of the probe. The efficiency is increased because reducing the weight and axial stiffness of the probe in relation to the vibrating mass increases the displacement amplitude and the transfer of energy to the surrounding soil during vibration, compared to a solid probe of the same size. A larger displacement amplitude of the oscillating probe increases the compaction efficiency, as does the increase of energy transfer.

Compaction probes can be provided with water-jetting equipment (See Clause 7.20.6) to facilitate penetration into stiff soil layers. Water jetting (c.f., Clause 7.20.6) also has a beneficial effect on the soil compaction efficacy, especially in unsaturated or partially water-saturated soil deposits. In some methods, water jetting is replaced by or combined with air jetting, especially when hard or stiff soil layers must be penetrated.

The vibro-rod method was initially developed in Japan and used a probe with short wings, attached to a vibratory hammer. A similar system, called Vibro-Wing, was developed in Sweden and uses an up to 15 m long steel rod, which is provided with 0.8 m long wings, spaced 0.5 m apart along the probe (Figure 10.8a). The TriStar probe (Figure 10.8b), comprises a three-bladed probe with horizontal steel plates attached to increase the probe-soil interaction.

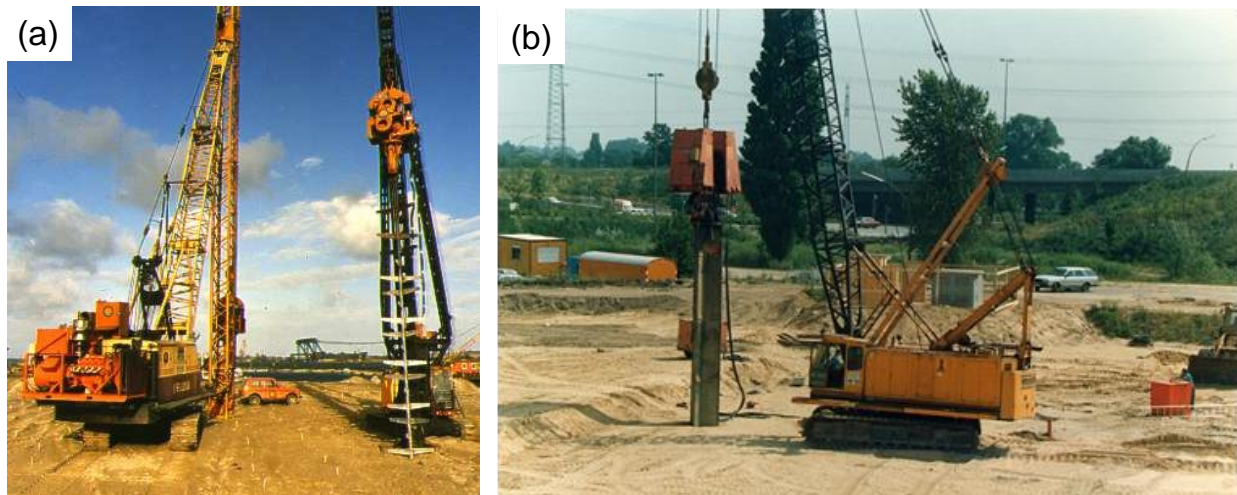


Fig. 10.8. Vibratory probe compaction. a) Vibro-Wing method. b) TriStar method.

### 10.3.6 Vibroflotation

The Vibroflotation method was invented in Germany almost 80 years ago, and its development has continued mainly there and in North America, where it was introduced in the 1940's. The equipment consists of three main parts: the vibrator, extension pipes, and a supporting crane (Figure 10.9). Vibroflotation is the most widely used deep compaction equipment and extensive experience has been accumulated over the past 30 years. The vibrator is incorporated in the lower end of a steel probe and rotates around the vertical axis in a pendulum action. Vibrator probe diameters range from 350 to 450 mm and the length is about 3 - 5 m, including a special flexible coupling, which connects the vibrator with the extension pipe. Units developing centrifugal forces up to 160 kN and variable vibration amplitudes up to 25 mm are available. Vibroflotation probes operate typically at frequencies between 30 and 50 Hz. The vibrator can either be driven by an electrical motor or a hydraulic system. The extension pipes have a slightly smaller diameter than the vibrator and a length dependent on the depth of required penetration.

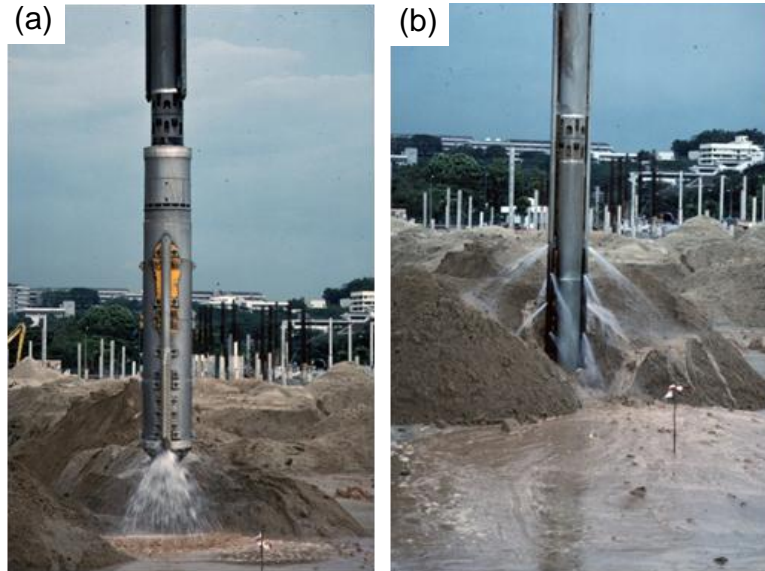


Fig. 10.9. Vibroflotation equipment with water jetting.  
 a) Water jetting at tip of probe b) Water jetting along the probe insertion tube

The vibroflotation probe is slowly lowered to the bottom of the soil layer and then gradually withdrawn in 0.5-1.0 m stages. The length of time spent at each compaction level depends on the soil type and the required degree of compaction. Generally, the finer the soil, the longer the time required achieving the same degree of compaction. In order to facilitate penetration of the equipment, water jetting is applied with a water pressure of up to 800 kPa and flow rates of up to 3,000 L/min. The water jetting transports the fine soil particles to the ground surface and replaces the fines with coarse material. The removal of fines results in well-compacted soil columns. However, fine particles can migrate into the more coarse-grained material and contaminate the stone columns. Thus, the composition of the stone column material must be chosen carefully in order to assure drainage along and within the stone column.

### 10.3.7 Compaction by explosives

Compaction using explosives (blast densification) has been used in Europe (particularly in Russia) and North America for a variety of projects. This technique is very attractive from an economic viewpoint, but is limited to large projects with deep deposits of water-saturated sands and gravels. The psychological effect of detonating explosive limits the application of this method to unpopulated areas.

Small explosive charges are installed in pre-bored holes at depth of approximately 2/3 of the depth of the zone to be densified. The shock of the explosive liquefies the soil.

### 10.4 Resonance Compaction System

An efficient system for deep vibratory soil compaction of granular soils is the resonance compaction system, also known as MRC (Massarsch 1991, 2023). The MRC concept is based on the vibration amplification at resonance and is described below. The resonance is achieved by varying the operating frequency during penetration, extraction and re-penetration. Another important part of the compaction system is the use of a flexible probe (Figure 10.10), which is designed to achieve optimal transfer of compaction energy from the vibrator to the soil. The probe profile has a double Y-shape (five blades), which increases the compaction influence area. To obtain maximum displacement amplitude of the probe—a key parameter for soil compaction—the dynamic mass should be kept as small as possible. This can, for example, be achieved by creating openings in the compaction probe, as mentioned. Note that the eccentric moment (c.f., Eq. 10.1) and the displacement amplitude are independent of vibration frequency.

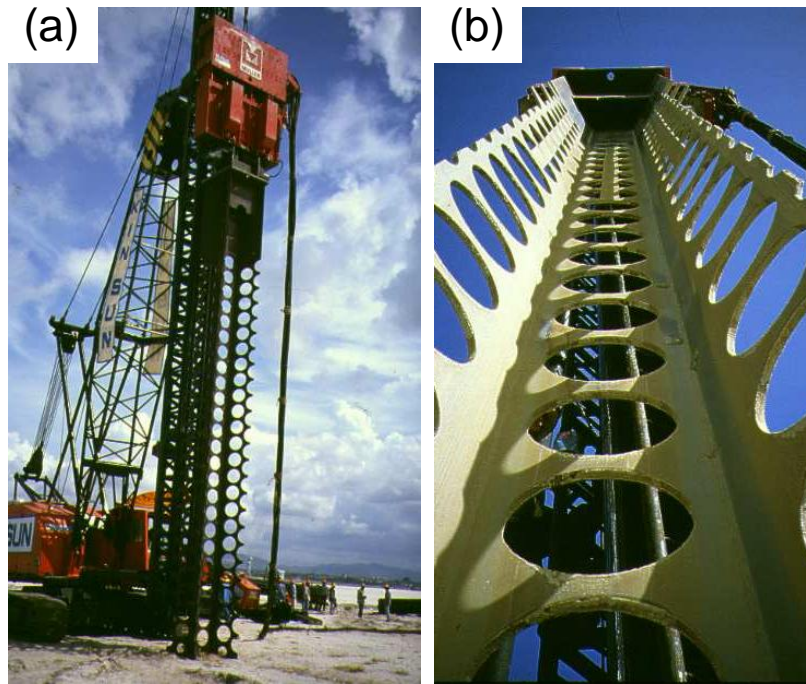


Fig. 10.10. Resonance compaction system, MRC, a system that uses a variable-frequency vibrator and a flexible (low axial stiffness) compaction probe.  
a) MRC compaction equipment. b) MRC compaction probe

When the vibrator frequency is gradually lowered after the probe has been inserted to the desired depth using high frequency, the probe penetration rate slows down and the intensity of the ground vibration increases. When the operating frequency of the vibrator approaches the resonance frequency of the vibrator–probe–soil system, the probe penetration is brought to a standstill, while, at the same time, the ground vibrations reach a maximum. At resonance stage, the vibrator energy is efficiently transmitted to the soil along the probe surface and vibration compaction is most effective. The compaction probe and the soil oscillate in phase, the relative displacement amplitude between the probe and the soil is small (yet friction is fully mobilized along the probe), resulting in efficient transfer of the vibrator energy from the probe to the surrounding soil.

The resonance frequency depends on several factors, such as the mass of the vibrator, the length and size of the compaction probe, and the shear-wave velocity of the soil. The resonance frequency will increase with increasing shear-wave velocity, reflecting a change of soil stiffness and soil strength (Massarsch and Westerberg 1995).

An important feature of the resonance compaction system is the electronic monitoring system, which continuously records all parameters of importance for the compaction process, such as vibrator frequency, probe penetration depth, power supply (hydraulic pressure) and ground vibration velocities (Figure 10.11).

The recorded information can be printed out on site, providing an accurate documentation of the actually performed compaction process. The documentation can be used for quality control as well as for optimization of the continuing compaction execution. The recorded information is also transmitted to an electronic control unit, mounted in the cabin of the compaction machine. It collects and evaluates important parameters and provides the machine operator with instructions on a display (Figure 10.12). Thus, the machine operator can continuously adapt the compaction work to achieve optimal densification throughout the whole compaction process.

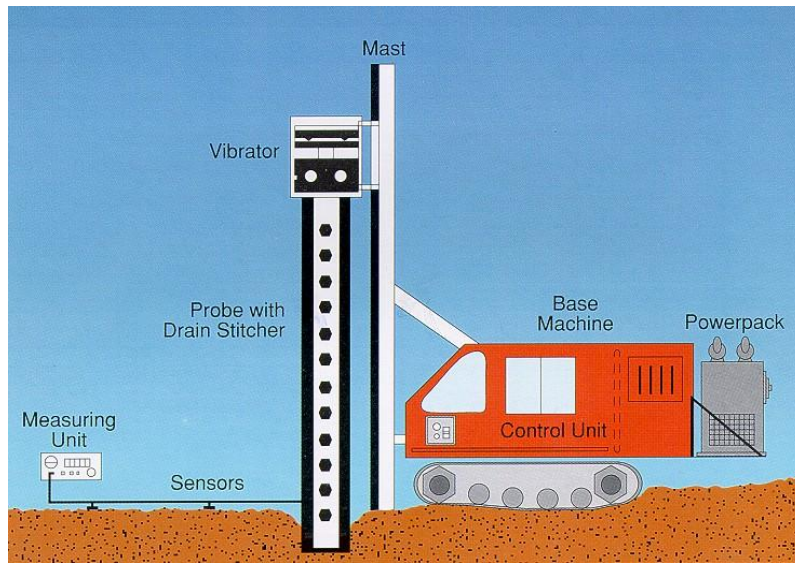


Fig. 10.11. MRC Resonance compaction system with electronic monitoring (Measuring Unit).

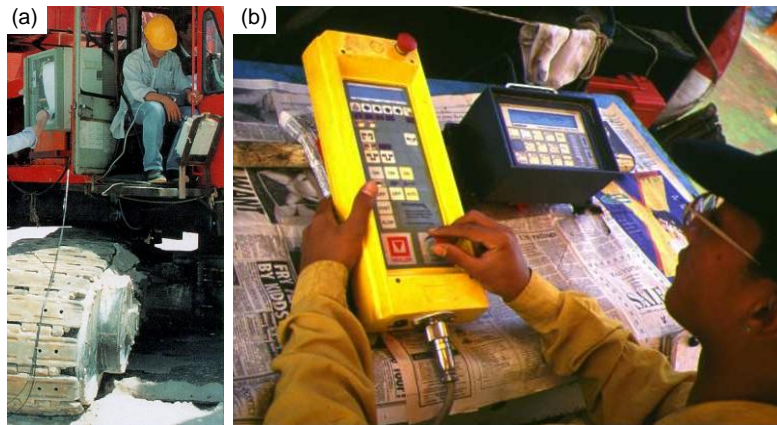


Fig. 10.12. MRC electronic control unit for adaptation of compaction process.  
 a) MRC field computer b) electronic process control system,

When using the resonance compaction unit, geophones measuring vibration velocity are installed on the ground surface, typically at a distance of about 4 m from the compaction point, as shown in [Figure 10.13](#). The geophone/ measurements are fed into a data acquisition system together with the other compaction parameters, such as probe penetration depth, vibrator acceleration, operating frequency, and the hydraulic pressure of the vibratory system (powerpack).

In loose to medium dense, water-saturated granular soil, vibrating at resonance can cause soil to liquefy around the probe. At onset of liquefaction, the pore pressure increases toward becoming equal to the total stress and the body of soil and water acts as a heavy liquid with little or no friction along the probe. With time, the excess pore water pressure dissipates, effective stress builds up, the friction between the probe surface and the surrounding soil is gradually mobilized, and the resonance frequency increases. The end result is a reduction of the soil volume (compaction), an increase in soil density (modulus), a permanent prestress effect, and elimination of the liquefaction susceptibility. In dense to very dense sand (such as after successful compaction), liquefaction does not occur at the resonance frequency.





Fig. 10.13. Ground vibrations measured adjacent to the compaction probe,

### 10.5 Vibratory Compaction Process

Deep vibratory compaction comprises the following three elements, which need to be adapted to the site conditions and densification requirements to achieve optimal performance

- Compaction equipment: compaction probe, vibrator and powerpack, and base machine
- Compaction process: compaction point grid and spacing, vibration frequency, and mode of probe insertion and extraction
- Process control and monitoring: production control and verification of densification effect.

The compaction process is an important element of deep vibratory compaction and addresses the following specifics:

- Compaction point spacing
- Vibration frequency
- Probe penetration and extraction
- Compaction energy
- Duration of compaction.

#### 10.5.1 Compaction point spacing

Compaction can be carried out in a triangular or rectangular grid. The spacing between compaction points needs to be chosen with respect to practical considerations, such as the overall geometry of the site, the reach of the compaction machine, and the number of compaction passes. Normally, during the first pass, a rectangular pattern of compaction points is chosen. During the subsequent passes, treatment points are located in the centroid of the primary grid, to optimize uniformity of treatment. The optimal compaction grid spacing should be determined—at least in the case of larger projects—by compaction trials. The spacing between compaction points typically ranges between 2.5 and 5 m.

It is generally advantageous to perform compaction in two passes, as this will result in more homogeneous soil densification. This aspect is of particular importance when impervious layers of silt or clay exist in the liquefiable soil deposit to be compacted, i.e., sandwiching it. Such soil deposits are usually prone to worsen liquefaction in the soil layer bounded by the impervious layers, as the bonding layers prevent or reduce the vertical flow of water and, thus, impede the dissipation of excess pore water pressure. However, if compaction is carried out in two passes, the probe will create drainage channels during the first pass, resulting in more efficient compaction during the second pass. An additional important consideration is that the first-pass compacted soil cylinders provide lateral resistance during the second pass, thereby making the treatment process more efficient.

During the first pass, the soil can be compacted according to a prescribed, regular compaction process (addressing duration of compaction and number of extraction cycles). For example, by assessing the compaction effect as to rate of probe penetration at start and end of compaction and/or by means of comparing the results of cone penetrometer tests before and after compaction. The compaction process can then be appropriately adjusted during the second pass to achieve the required degree of densification.

What spacing between compaction points to assign depends on several factors, such as the site conditions prior to compaction, the required degree of compaction, the size of the compaction probe (influence area), and the capacity of the vibrator. It is generally advantageous to use a smaller spacing with a shorter duration of compaction rather than a larger spacing with longer duration as the former will result in more homogeneous compaction of the soil deposit.

### 10.5.2 Compaction process

Deep vibratory compaction is a repetitive process, comprising three main phases: insertion of the compaction probe to the required depth, densification of the soil, and extraction of the compaction probe. The compaction process starts by inserting the probe into the ground with the vibrator operating at high frequency in order to reduce the soil resistance along the shaft and the toe and optimize the penetration rate. When the probe reaches the depth of the zone to be compacted, the frequency is adjusted to the resonance frequency of the soil layer, thereby amplifying the ground response. The process is monitored by the operator. The probe is held at this depth for a short while, letting the vibration energy be transmitted to the surrounding soil along the probe surface. N.B., if the probe is extracted at or close to the resonance frequency, the needed extraction force will be high and the compaction effect is reduced, even ruined due to soil loosening.

When the vibrator is operated at the system resonance frequency, the probe and the surrounding soil start to oscillate “in phase,” and the relative displacement between the probe and the soil becomes very small and an almost “static friction” develops along the probe shaft, and the probe penetration speed slows down. At the same time, the displacement amplitude of the probe increases markedly, resulting in strong ground vibrations and optimum soil compaction.

The most efficient compaction process is to insert the probe to the required depth(s) as rapidly as possible at a high vibration frequency, followed by compaction of the soil at or near the resonance frequency and, finally, to extract the probe at high vibration frequency. A typical compaction process is shown in [Figure 10.14](#).

For practical purposes, it can be assumed that the resistance at the toe of the probe is equivalent to the cone resistance. (2005). During vibratory driving at a high frequency, much of the vibration energy is consumed as heat along the shaft of the probe, and soil densification will be low. When the vibration frequency is gradually lowered, probe penetration speed decreases.

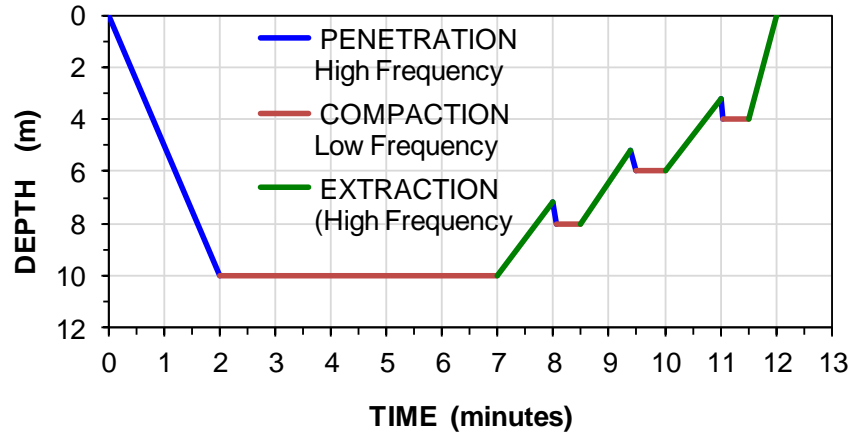


Figure 10.14 Compaction process and vibration frequencies at penetration, compaction, and extraction.

Compaction will be less efficient if the entire compaction process is carried out at a single frequency. Should a too high frequency be applied, most of the vibration energy will be converted into heat along the probe; and, should the vibration frequency be close to the system resonance frequency, probe penetration will be slow. At a high vibration frequency, the probe penetration resistance is mainly influenced by the soil resistance at the probe end. When the probe is operated at a frequency (approximately  $>35$  Hz) that is higher than the resonance frequency (typically 15 - 20 Hz) of the vibrator–probe–soil system, friction along the compaction probe is effectively reduced and the main resistance to penetration occurs at the toe of the compaction probe. Thus, in loose granular soil, where toe resistance is low, most of the vibration energy dissipates as heat along the probe surface, the ground vibrations are low, and the weight of the vibrator and probe causes the probe to sink into the ground at a significant rate of penetration. When the probe penetrates freely and is not held back, the probe penetration speed can be related to the cone resistance ( $q_c$ ) measured by the cone penetration test (CPT). The comparison between the rate of penetration and the CPT cone resistance,  $q_c$ , can be used on a site-specific basis to correlate the efficiency of the compaction effort in terms of probe penetration speed.

When carrying out deep vibratory compaction in two passes, during the second compaction pass, the probe is inserted in the diagonal points of the initial compaction grid, and the time required for the probe to penetrate the soil layer is recorded. If the penetration speed at the start of the second compaction pass is the same as during the first pass, the grid spacing was too large. If the penetration speed during the second pass is much lower than during the initial phase, the point spacing was chosen correctly or, possibly, closer than necessary. Thus, careful observations at the start of a compaction project or in a special preconstruction test phase can serve to decide on the optimum probe spacing to use.

To achieve optimal soil densification, it is important to use a compaction process where energy is transferred both along the shaft and at the bottom end of the penetrating probe. The most effective energy transfer occurs when the compaction probe is allowed to operate at the system resonance frequency with the vibrator resting on the probe (no tension in the leads supporting the vibrator and probe). If, instead, the probe is kept suspended and, thus, vibrated without the full weight of the vibrator and the probe applied to the soil, the compaction effect is reduced.

The duration of compaction in each point is an important parameter and depends on the soil properties prior to compaction, the required degree of densification, and the vibration energy transferred to the ground (intensity and duration). The optimal compaction grid spacing should be determined—at least in the case of larger projects—by compaction trials. As mentioned, in comparing the probe penetration speed during the first and the second compaction pass with penetration tests before and after compaction, the optimal compaction procedure can be established more reliably.

In many cases, the same duration of compaction is applied during the first and second pass. However, it may be advantageous to vary the duration of compaction during the second pass. During the first pass, a uniform compaction procedure should be applied across the entire site. During the second pass, the compaction time should be varied in each point depending on the observed probe penetration speed.

### 10.5.3 Vibration frequency

The vibration frequency is an important parameter of vibratory soil compaction and should be chosen with care. During insertion and extraction, it is desirable that the shaft resistance along the probe is as small as possible. This is achieved by using a high frequency—higher than about 30 Hz. Ground vibrations are then low and most of the vibration energy is converted into heat along the shaft of the probe and little energy reaches the soil body and shaft resistance is minimized. In contrast, during the compaction phase, the objective is to transfer the energy generated by the vibrator along the vertically oscillating compaction probe to the surrounding soil as efficiently as possible, which is achieved when the probe is vibrated in resonance with the soil—usually about 15–20 Hz. At resonance, probe penetration will become slow or stop completely.

Figure 10.15 shows the vertical vibration velocity on the ground surface, measured by a vibration sensor (geophone) at a distance of 4 m from the compaction probe.

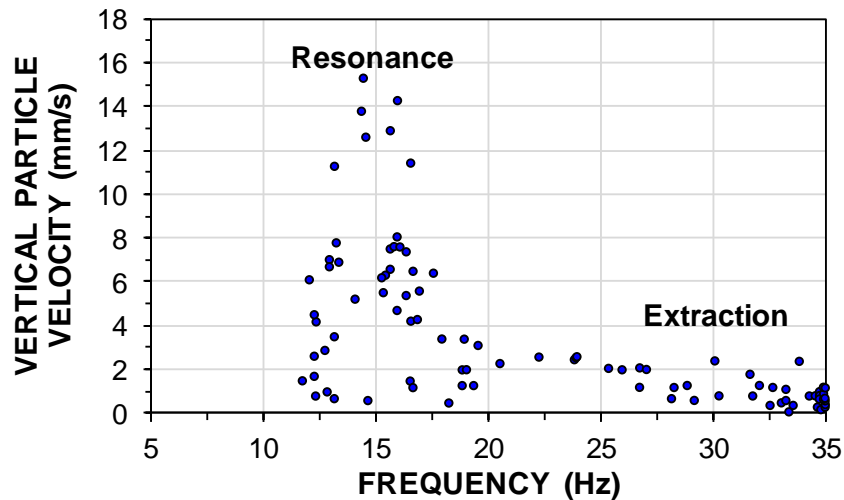


Figure 10.15 Ground vibration velocity during probe penetration, compaction, and extraction measured at 4 m distance from the compaction probe (Massarsch and Fellenius 2005).

As mentioned, it is advisable to carry out deep vibratory compaction in two passes. During the second compaction pass, the probe is inserted in the mid-points of the compaction grid, and the time required for the probe to penetrate the soil layer is again recorded. If the penetration speed at the start of the second compaction pass is the same as during the first pass, the grid spacing was too large. If the penetration speed during the second pass is much lower than during the initial phase, the point spacing was chosen correctly or, possibly, closer than necessary.

### 10.5.4 Liquefaction during vibratory compaction

When loose, water-saturated soils are treated by vibratory compaction, the soil nearest the compaction probe can liquefy and loose soil layers will densify, while the excess pore pressures dissipate. Once the soil has liquefied, compaction will be negligible until the excess pore water pressure has dissipated. If the permeability is not sufficiently high, excess pore water pressure generated in a zone surrounding the compaction probe will be slow to dissipate impairing the densification. Figure 10.16 shows evidence of liquefaction in the form of water collecting on the ground after a first compaction pass.



Fig. 10.16. Liquefaction of water-saturated sand during the initial phase of compaction. Note that water has collected on the ground surface. The original groundwater table was 4.5 m below the ground surface.

Indeed, deep vibratory compaction equipment can be used as a large-scale soil testing machine for assessing the liquefaction potential of a site, serving as a full-scale testing method to investigate the liquefaction hazard of layered soils, where liquefaction is controlled to a high degree by the drainage conditions of loose sand layers, sandwiched between layers of lower permeability. This can be accomplished by performing a resonance tests in the uncompacted soil and then comparing the vibration response of the soil after vibratory treatment. Such an approach would add valuable information to the less precise liquefaction analysis based on CPT data or, sometimes, on SPT records.

### 10.5.5 Horizontal ground vibrations

It is often assumed that in the case of a vertically oscillating compaction probe, only vertical ground vibrations are generated. However, the vertically oscillating probe causes strong horizontal stress pulses directed away from the probe during the downward movement of the probe. The horizontal stresses give rise to horizontal compression waves, resulting in permanent increase of horizontal stress in the soil.

Figure 10.17 shows the results of measurements of measurements of horizontal vibration velocity at the ground surface and at three depths below during vibratory compaction using the resonance compaction system (Krogh and Lindgren 1997). Horizontally oriented vibration sensors (geophones) were installed 2.9 m from the center of the compaction probe on the ground surface and at three depths. At the time of the vibration measurements, the compaction probe was at a depth of 5 m (at or just passed the lowest measuring point). The frequency of horizontal vibration generally ranged from 23 to 26 Hz; twice the vertical vibration frequency. The measurements showed that the horizontal velocity is about constant with depth.

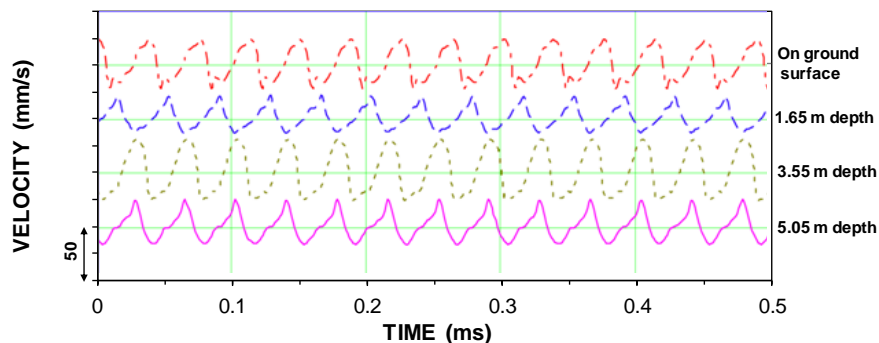


Fig. 10.17 Horizontal vibration amplitude measured during resonance compaction. (Negative and positive velocity indicate opposite direction of horizontal movement).

The vibration amplitude in the horizontal and vertical directions had approximately the same magnitude and the horizontal stress in the soil increased within the compacted depth—the earth stress coefficient,  $K_0$ , increased. That is, the vibratory compaction also resulted in a permanent increase in the horizontal effective stress, which effect is of considerable practical importance for sand fill, such as hydraulic fill, which is usually normally consolidated prior to compaction, but, as a result of vibratory compaction, the horizontal earth stress coefficient increases significantly (Massarsch and Fellenius 2002).

The increase of earth stress can be approximated from CPT sounding data. Eq. 10.5 shows the relation between sleeve friction and earth stress.

$$(10.5) \quad f_s = K_0 \tan \varphi'_a \sigma'_v$$

where

- $f_s$  = CPT sleeve friction
- $K_0$  = coefficient of earth stress at rest (before compaction)
- $\varphi'_a$  = the effective friction angle at the soil/CPT sleeve interface.
- $\sigma'_v$  = effective vertical stress

It can be assumed that the effective vertical stress,  $\sigma'_v$ , is unchanged by the compaction, thus, the ratio of the earth stress after to before compaction can be estimated as equal to the ratio of CPT sleeve resistance after and before compaction. This is expressed in Eq. 10.6.

$$(10.6) \quad K_{01}/K_{00} = f_{s1}/f_{s0}$$

where

- $K_{01}$  = coefficient of earth stress at rest after compaction
- $K_{00}$  = coefficient of earth stress at rest before compaction
- $f_{s1}$  = CPT sleeve resistance after compaction
- $f_{s0}$  = CPT sleeve resistance before compaction.

The horizontal stresses can vary significantly within the compacted soil. The highest horizontal stresses and stress increase will occur close to the compaction points and decrease with distance away. The initial stress anisotropy initiates a stress redistribution, which can to some extent explain observed change of soil strength and of soil stiffness with time after compaction.

### 10.5.6 Horizontal stress increase

For many geotechnical challenges, knowledge of the prestress condition ("overconsolidation ratio") is important. Empirical relationships have been proposed for the earth stress coefficient of normally and prestressed sands and for the overconsolidation ratio, OCR, as expressed in Eq. 10.7.

$$(10.7) \quad K_{01}/K_{00} = OCR^k, \text{ which converts to } K_{01} = K_{00} OCR^k$$

where

- $K_{01}$  = coefficient of earth stress at rest after compaction =  $K_{00} OCR^k$
- $K_{00}$  = Coefficient of earth stress at rest before compaction at OCR = 1.0
- $OCR^k$  = overconsolidation ratio after compaction
- $k$  = An empirically determined parameter.

Schmertmann (1985) recommended  $k = 0.42$ , based on compression chamber tests. Mayne and Kulhawy (1982) suggested  $k = 1 - \sin \varphi'$ . Jamiolkowski et al. (1988) found that the density expressed as Density Index,  $I_D$ , influences  $k$  and found it to range between 0.38 and 0.44 for medium dense sand ( $I_D = 0.5$ ). Figure 10.18 illustrates the relationship from Eq. 10.7, which shows that even a modest increase of the earth stress increases the overconsolidation ratio significantly.

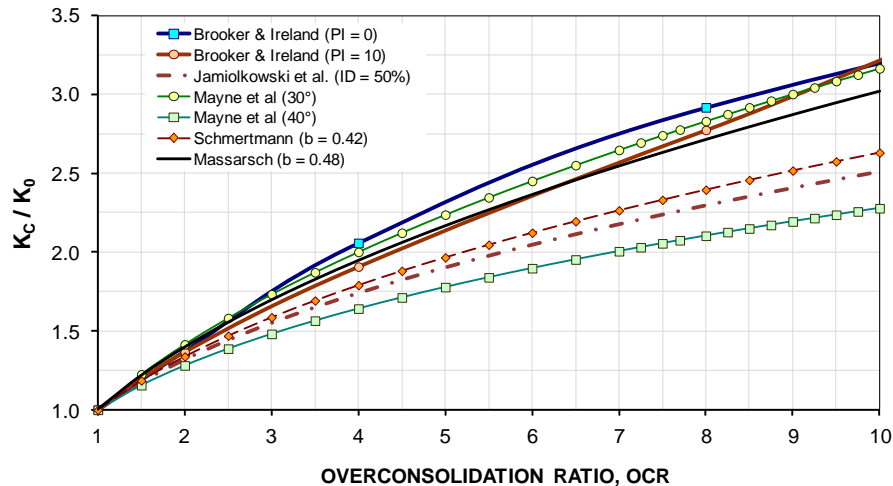


Fig. 10.18 Relationship between overconsolidation ratio and ratio of earth stress coefficients for overconsolidated and normally consolidated sand. (Massarsch and Fellenius 2001; 005).

Sleeve resistance measurements reported in the literature and the above shown field tests show that the ratio  $f_{s1}/f_{s0}$  ranges between 1.5 and 3.5. If it is assumed that the effective friction angle increases due to compaction from  $30^\circ$  to  $36^\circ$ ,  $K_{01}/K_{00}$  ranges according to Eq. 10.6 between 1.2 - 1.8. An average value of  $K_{01}/K_{00} = 1.6$  yields an overconsolidation ratio OCR according to Eq. 10.5 in the range of 2.5 - 4.0.

### 10.5.7 Preloading effect of vibratory compaction

The stress conditions in loose, water-saturated sand will undergo a complex change of stress conditions during vibratory compaction. Energy is transmitted from the compaction probe to the surrounding soil at the probe end as well as along the probe sides.

Prior to treatment, the stress conditions will be that of a normally consolidated soil. When the soil is subjected to repeated cycles of, high-amplitude vibration, the pore water pressure will gradually build up, reducing the effective stress. Indeed, during the initial phase of compaction, the soil in the vicinity of the compaction probe is likely to liquefy. Whether or not liquefaction will occur in a loose sand depends on the intensity and duration of vibrations and the rate of dissipation of the excess pore water pressure. Presence of soil layers with low permeability (e.g., silt and clay) will increase the liquefaction potential. At liquefaction of granular soils, the effective stress is zero as is the shear strength. Although the probe continues to vibrate, the soil will not respond as only little vibration energy can be transmitted to the soil. As the vibration continues, the excess pore water pressure will start to dissipate (by definition, the soil reconsolidates). The rate of reconsolidation will depend on the permeability of the soil (and presence of any interspersed layers).

Figure 10.19 illustrates the change of effective stresses in a dry granular soil that is subjected to repeated compaction cycles. The oscillating centrifugal forces generated during vibratory compaction temporarily increase and decrease the vertical and the horizontal effective stress along the compaction probe and at its tip. The initial stresses of the normally consolidated soil correspond to a stress level represented by Point A. During the first loading cycle, the stress path follows the  $K_{00}$ -line to stress level B. Unloading to stress level C occurs at zero lateral strain, that is, horizontal stresses remain locked in. Each reloading cycle increases the lateral earth stress, which can reach the passive earth stress. At the end of compaction, stress level D is reached. The vertical overburden stress is the same after as before compaction (stress level D; end of compaction), but the horizontal effective stresses have increased. The horizontal earth stress after compaction can reach the passive value,  $K_p$ .

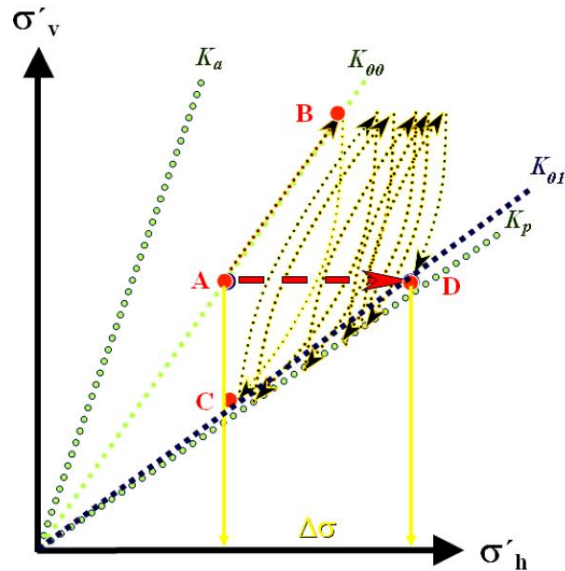


Fig. 10.19 Stress path of soil in the vicinity of a compaction probe during first compaction phase (stress level points A - B - C ... - D.

Also, other important aspects of vibratory compaction are shown in the figure. The change of the stress conditions from a normally consolidated state to an overconsolidated state is influenced by several factors, such as the compaction method, the state of stress state prior to compaction, and the strength and deformation properties of the soil. At resonance compaction, the vertically oscillating probe generates (as a result of friction between the probe and the soil) a high, horizontally oscillating force, which causes a permanent increase of horizontal soil stress after compaction.

### 10.5.8 Increase of soil strength and stiffness with time

Another important factor of soil compaction is the increase of soil strength and stiffness with time after compaction (e.g., Massarsch 1991, Schmertmann 1997, and Mitchell 1998). Post-densification CPTU results suggest that compacted natural and man-made deposits of clean sand may gain in strength with time after compaction even after the pore pressures induced during compaction have dissipated. The mechanism of this phenomenon is not yet fully understood. It is possible that the heterogeneous stress conditions (horizontal stress variation) in a soil deposit after compaction, might cause a rearrangement of soil particles with time in order to adjust to a more homogeneous stress field. This effect depends on several factors, such as geotechnical conditions, type and execution of compaction process, etc., and it is difficult to assess quantitatively without in-situ testing. Therefore, in the absence of a general theoretical concepts for estimating the change of soil strength or stiffness with time, it is recommended to perform CPTU tests at two time intervals after treatment; shortly (one day) after compaction as well as three weeks after compaction. Then, inspecting, and documenting the increase in regard to both cone resistance,  $q_c$ , and sleeve resistance,  $f_s$ .

### 10.5.9 Compactability

An important first question to be addressed by the geotechnical engineer is whether or not—and to what degree—a soil deposit can be improved by dynamic methods (vibratory or impact compaction). Mitchell (1982) identified suitable soil types according to grain size distribution and indicated that most coarse-grained soils with a "fines content" below 10 % (amount of particles smaller than 0.06 mm, Sieve #200; see Section 1.3) can be compacted by vibratory and impact methods. However, compaction assessment based on grain-size curves from sieve analysis has the disadvantage that, in order to obtain a realistic picture of the geotechnical conditions, a large number of soil samples and sieve analyses is required—larger than what is usually considered justifiable for a routine foundation project. Moreover, at the design



process, going back to a site in order to obtain additional samples is impractical due to time constraints. And, obtaining representative soil samples may prove to be difficult and costly because the soils at such sites are usually loose and water-saturated. Besides, soil lenses and layers of importance for the assessment may not be evident from the inspection of soil samples obtained intermittently. It is therefore preferable to base the assessment of compactability on results of CPT soundings, as the CPT presents continuous soil profiles reflecting variations in soil strength and compressibility, and, in the case of the piezocone (CPTU), also variations in hydraulic conductivity of the soil.

Massarsch (1991) proposed that the compactability of soils can be classified as “compactable”, “marginally compactable”, and “not compactable”. Figure 10.20 presents compactability boundaries in a conventional soil profiling chart based on a normalized CPT profiling chart (Robertson 1990).

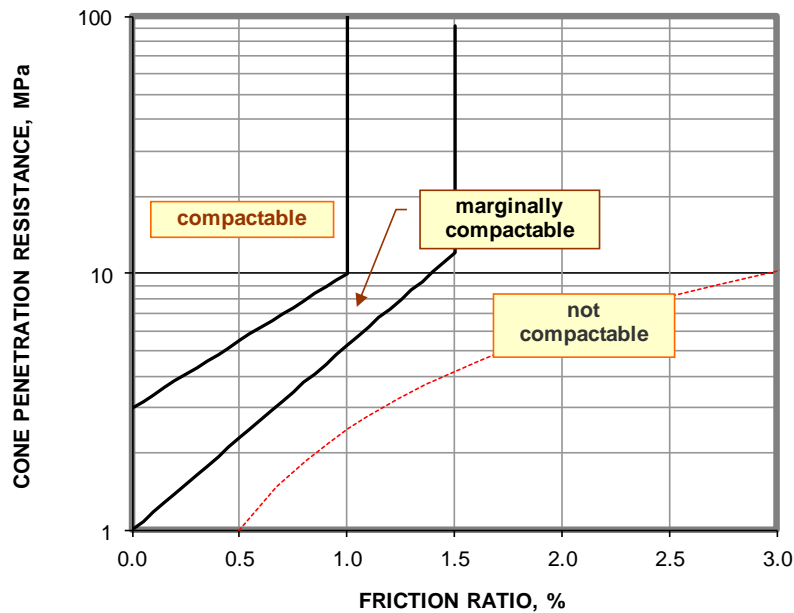


Fig. 10.20 Soil classification for deep compaction (after Massarsch 1991).

Figure 10.21 shows the same compactability boundaries where the cone stress is shown as a function of the sleeve friction rather than the friction ratio (Eslami and Fellenius, 1995; 1997; and Fellenius and Eslami, 2000; see Section 2.3). As the ranges of cone stress and sleeve friction applicable to compaction projects are relatively narrow, the usual logarithmic-scale compression of the axes can be dispensed with and, therefore, the graph resolution can be increased by showing the boundaries in linear scale axes (Figure 10.21b).

Compactable soils often show a pore pressure,  $U_2$ , that is larger than the neutral pore pressure,  $u_0$ .

Compaction criteria are frequently expressed in terms of cone stress. Note that project specifications need also to state the original ("natural") density (in units of  $\text{kg/m}^3$ ) of the soil or fill and indicate the required final density to be achieved by the compaction work. Similar to the depth adjustment employed for SPT data, it is preferable to express CPT compaction criteria in terms of a cone stress value adjusted with respect to the mean effective stress, i.e., adjusted for overburden stress (depth). This will better reflect uniformity of soil density, or lack of uniformity, as opposed to using the unadjusted cone stress. If the cone data are not adjusted according to the stress level (depth), applying a specific value of cone stress as a compaction criterion throughout a soil deposit may lead to the upper layers of the deposit becoming overcompacted while the deeper layers remain loose. When this aspect is not recognized, the result may be a soil deposit that is not uniformly compacted, as well as excessive compaction costs and undesirable loss of ground.

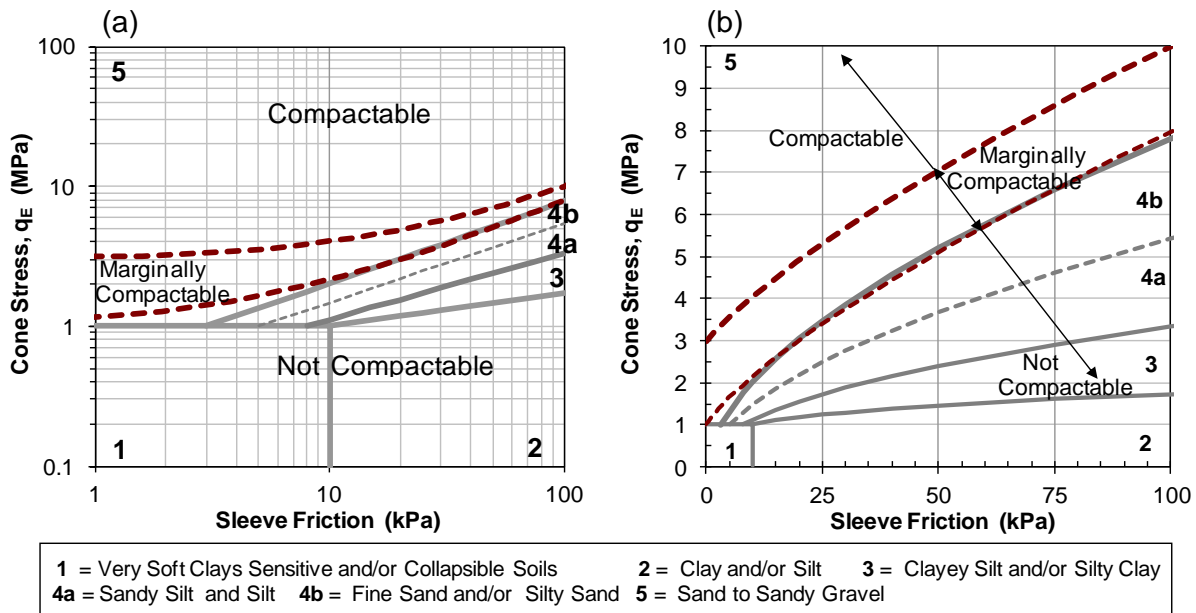


Fig. 10.21 Soil classification for deep compaction per profiling chart per Eslami-Fellenius (Eslami 1996).

## 10.6 Analysis of Results of Deep Compaction

Deep compaction of granular soils is carried out for two main reasons. First, to reduce soil compressibility and ensure no more than acceptable foundation settlement and, second, in areas entailing high seismic risk by remove liquefaction susceptibility in the event of an earthquake.

### 10.6.1 Determining compressibility of the compacted soil

A settlement analysis is fundamental to the design of all foundations and, in particular, for foundation on compacted soil. Chapter 3 presents the general background to settlement analysis. Usually, the adequacy of a compaction effort is based on results of SPT and CPT in-situ tests and, sometimes, on post-compaction density measurements with empirical reference and with minimal relation to the actual foundation loads and requirements. However, an in-situ test can provide soil compressibilities to enable an assessment of the suitability of the compaction work based on calculated settlement for the actual foundation loads. Compressibility is best expressed by the Janbu modulus numbers. Sections 2.10 - 2.12 describe determining the Janbu modulus numbers (which can be converted to E-modulus, if desired) using results of CPT soundings according to Massarsch (1994) and Massarsch and Fellenius (2018).

In summary, the method comprises determining for the CPT-profile the corresponding distribution of the depth-adjusted cone stress,  $q_{tM}$ , according to Eq. 10.8 (same as Eq. 2.9; Chapter 2), choosing the representative modulus modifier,  $a$ , from Table 2.4, and calculating the corresponding modulus numbers from Eq. 10.9 (same as Eq. 2.13 with  $K_0$  changed to  $K_{01}$ ).

$$(10.8) \quad q_{tM} = q_t C_M = q_t \left( \frac{\sigma_r}{\sigma'_m} \right)^{0.5}$$

where

- $q_{tM}$  = stress-adjusted (depth-adjusted) cone stress
- $q_t$  = cone stress
- $C_M$  = stress adjustment factor  $\leq 2.5$  (Eq.2.7)
- $\sigma_r$  = reference stress = 100 kPa
- $\sigma'_m$  = mean effective stress (Eq. 2.8)

$$(10.9) \quad m = a \left[ \left( \frac{q_t}{(\sigma'_r \sigma'_v)^{0.5}} \right) \left( \frac{3}{1+2K_{01}} \right)^{0.5} \right]^{0.5}$$

where

- $m$  = modulus number
- $a$  = empirical modulus modifier, which depends on soil type
- $q_t$  = cone stress
- $\sigma_r$  = reference stress = 100 kPa
- $\sigma_v$  = effective overburden stress
- $K_{01}$  = coefficient of earth stress at rest of the compacted soil determined from Eq. 10.6.

### 10.6.2 Determining susceptibility to liquefaction

The resonance compaction method can be used as an in-situ test for liquefaction susceptibility. If a vibrator is engaged to perform a couple of trial penetrations at a site combined with a couple of horizontally and vertically oriented vibration sensors (geophones) installed on the ground surface, the measurements will show if the sand is liquefiable and, if so, what effort would be required to mitigate the site. Similarly, during an ongoing site-improvement project employing deep compaction by any method, resonance compaction tests will show when the compaction results is satisfactory so as to prevent overcompaction.

The use of the vibratory resonance compaction supplements conventional tests using CPT sounding as a site-investigation tool and as post-compaction verification tool. See Chapter 2, Section 2.12.8.

### 10.6.3 Drivability assessment

The selection of the optimal vibrator capacity (eccentric moment and centrifugal force) for the installation of piles or sheet piles is an important part of project design. Equally important is to adjust the driving process (displacement amplitude and the vibration frequency). Also, the pile type (sheet pile, closed- or open-toe pipe pile, compaction probe), pile size (length and mass) will affect the drivability. Three alternatives are available to the project engineer when performing a drivability analysis: a) empirical methods; b) dynamic analyses, and c) back-analysis based on field trials.

A major difficulty with theoretical modeling of vibratory driving of piles is the selection of realistic geotechnical parameters, representing the dynamic pile-soil interaction. Unlike pile driving, where the limits of a pile driving hammer governs the pile "capacity" that can be achieved (for a certain, hammer, soil, and pile combination and reasonable termination criteria), a desired compaction can be achieved with an array of vibratory hammers. Choosing a hammer more powerful in terms of frequency range and eccentric moment will cost more to transport and operate, but it will achieve the desired compaction faster and at wider spacing. It might, therefore, be more economical for the project.

Due to the limitations of theoretical concepts to predict drivability, an alternative, and often best, approach is to use full-scale tests. Vibratory driving of a test pile can be used as a full-scale dynamic penetration test, provided that the vibration frequency is maintained constant throughout the driving.

In granular soil, the driving resistance of a pile is dominated by the toe resistance. The shaft resistance is significantly smaller than the static shaft resistance during driving at high frequency driving. However, when the pile is vibrated at the resonance frequency of the vibrator-pile-soil frequency (system frequency), the relative displacement between the shaft and the soil decreases and the unit shaft resistance can be closer to the static resistance.

There appears to exist an approximately linear relationship between the penetration speed and the in-situ penetration resistance obtained in CPT or SPT soundings. N.B., when the vibrator is operated at a maintained (constant) frequency. Thus, if distributions of penetration speed are established in a field trial for a specific vibration frequency, the data—vibration records and profile from an in-situ test—will be helpful in determining the penetration speed for the vibrator where the soil profile is different as indicated by the in-situ test records. That is, site-specific relationships can be developed for different types of penetration tests, pile sizes, and vibrator frequency and used to develop a knowledge base for different soil conditions, pile types, and vibrators. Such information would be more reliable than empirical charts or sophisticated theoretical models for use by a designer when charged by estimating the penetration speed (and thus the time required for driving) for varying soil conditions, based on conventional in-situ penetration tests. It should be noted, however, that many different methods exist for applying in-situ test records to determine the response of a pile to applied load and, currently, all are fraught with much uncertainty.

## 10.7. Case Histories

### 10.7.1 Liquefaction risk and achieving compaction/densification

As an example of calculations of factor of safety against liquefaction, results are presented of cone penetration soundings performed in a small trial area (12 m by 12 m) at Tung Chung, close to Hong Kong Chek Lap Kok Airport in a sand fill before and after seven days after vibratory densification (Massarsch and Fellenius 2002). The sand fill consisted partly of calcareous material (fragments of shells and clams), and contained about 15 % of fines and occasional layers of silt and silty sand. It was placed by bottom dumping, where the water depth exceeded 4 m, and by spraying, where the water depth was shallower. The final thickness of the sand fill prior to compaction was about 10 m. The water level was located about 1 m below the final fill surface. The sand fill was specified to contain less than 10 % of fines.

Figure 10.22 presents the results of a CPTU sounding through the as-placed fill before compaction, illustrating that the fill consists mainly of loose sand to a depth of about 4 m below which the sand contained frequent layers of silty sand and an occasional lens of silty clay and even clay.

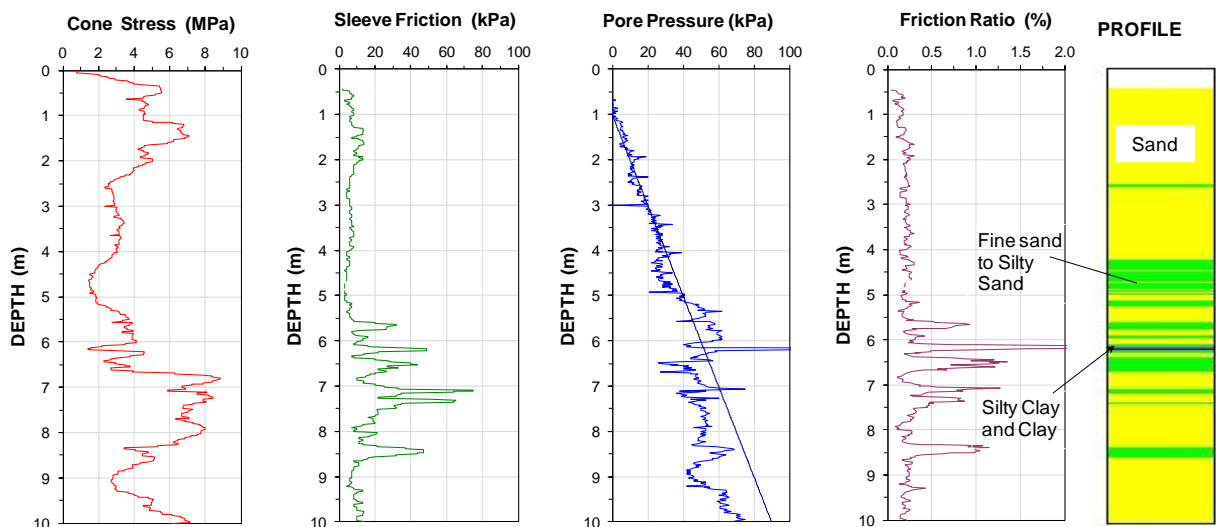


Fig. 10.22 Results of CPT in trial area prior to compaction. Note the lens of silty clay and clay.

The homogeneity of the fill is demonstrated in the profiling chart shown in Figure 10.23. The data points indicating silt, sandy silt, and silty sand are all from below 4 m depth. The silty clay and clay lens indicated in the figure at about 6 m depth is 40 to 60 mm thick as revealed by the three closely located values from 8.1 m depth. One value indicating clay and two values indicating silty clay.

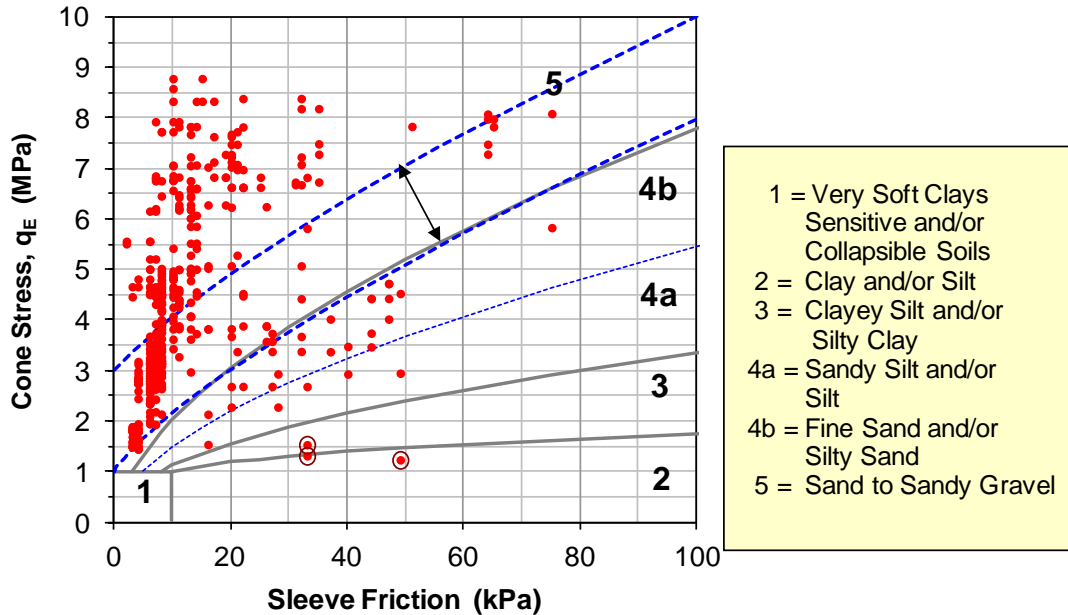


Fig. 10.23 CPT data from initial cone soundings plotted in an Eslami-Fellenius CPT profiling chart (Eslami and Fellenius 2000). (Data from Massarsch and Fellenius 2002).

The site was densified using the Müller Resonance Compaction (MRC) method (Massarsch and Westerberg 1995). The vibrator weighed 109 kN and was supported by a 100-tonne crawler crane. The vibrator could generate a maximum centrifugal force of 2,500 kN and a maximum eccentric moment of 1,000 J. The maximum pulling power of the vibrator was 600 kN. The vibrator frequency could be varied gradually at full power from 5 to 36 Hz. The maximum vibration amplitude of the vibrator without probe was 26 mm (double amplitude).

Generally, by changing the vibration frequency, the system makes use of the vibration amplification, which occurs when the soil deposit is excited at the resonance frequency. The vibration frequencies are adjusted during the compaction process in order to achieve optimal probe penetration and soil densification, as well as facilitate of probe extraction and, when extracting the vibrator probe, to avoid loosening (“uncompacting”) the compacted soil.

The results of three cone soundings performed seven days after the vibratory compaction are shown in Figure 10.24. Figure 10.25 compares the average of the seven-day curves to the average curves from before the compaction and shows that the compaction resulted in increased values of cone and sleeve resistances. The average curves are produced by means of a geometric average running over a distance of 500 mm, that is 25 values. The purpose of the averaging is to reduce the influence of thin layers of soft material that could cause a smaller than actual cone resistance and, therefore, indicate a larger than actual susceptibility to liquefaction.

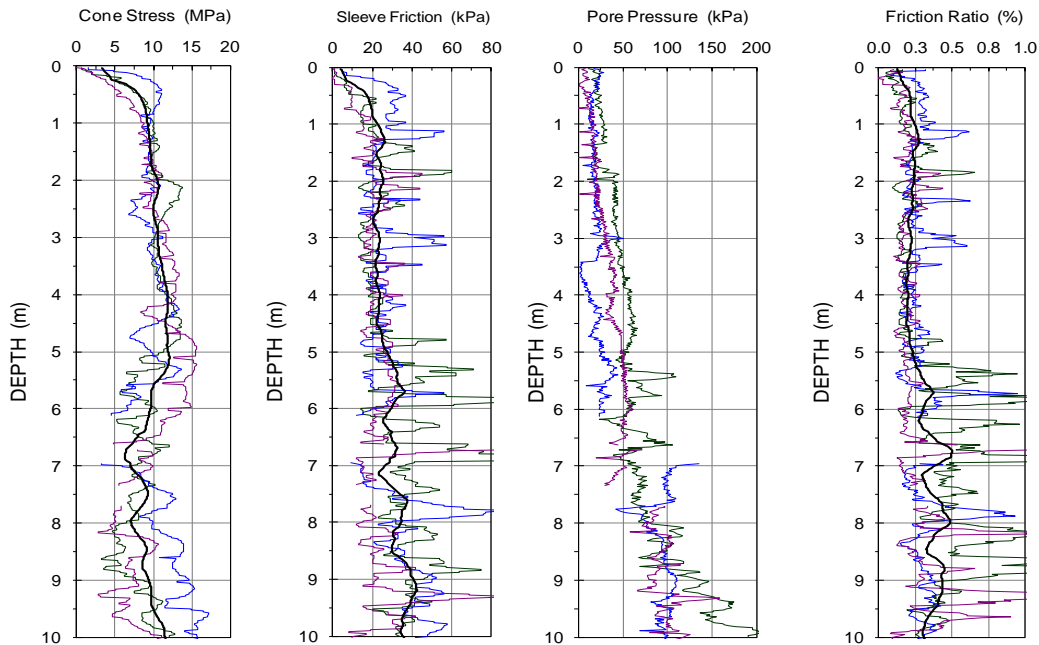


Fig. 10.24 Results of three CPTU soundings at Tung Chung, close to Chek Lap Kok Airport seven days after the compaction. The heavier lines show geometric average values.

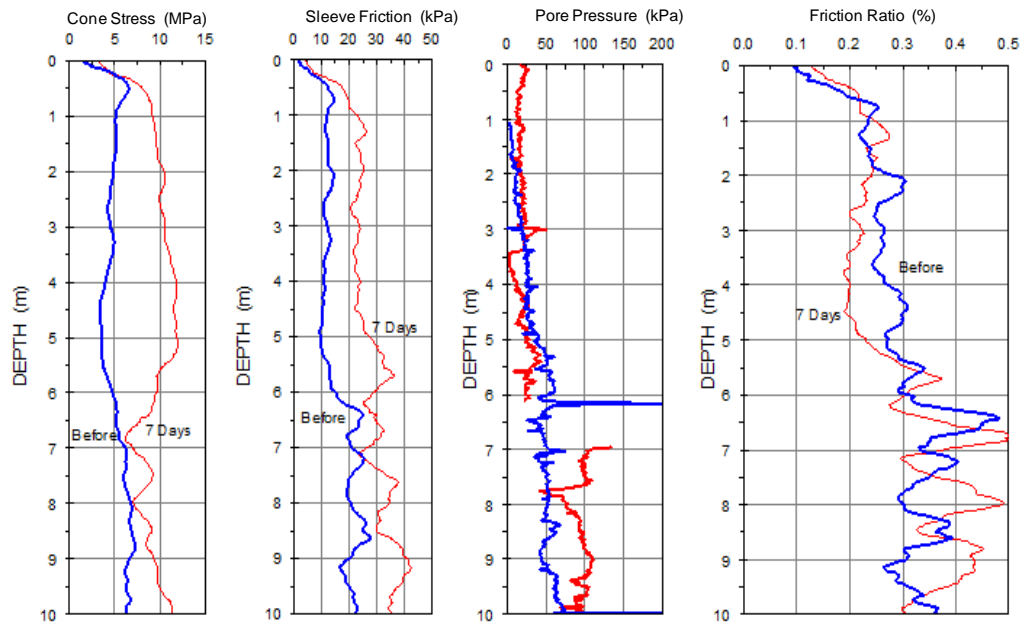


Fig. 10.25 Geometric average values of cone stress, sleeve friction, friction ratio, and measured pore pressure from CPTU soundings at Tung Chung close to Chek Lap Kok Airport before and seven days after the compaction.

Within the trial area, the groundwater table was about 2 m below the ground surface. The thickness of the sand fill was 14 m. During compaction, a large crater with a diameter corresponding to approximately twice the diameter of the compaction probe formed. In addition, a large settlement cone, extending up to 10 m from the compaction crater, could be observed. At each compaction point, the duration of

effective compaction was 5 and 10 min, respectively. During the initial phase of vibratory compaction, the sand fill liquefied and the groundwater rose to the surface in the compaction point. It is interesting to note that liquefaction did not occur during the second compaction pass; the soil was sufficiently densified in the first compaction phase to prevent liquefaction in the second.

Before compaction, the surface within the trial area had been leveled. The day after the first round of compaction, the surface was again leveled without an addition of sand fill, and its elevation was surveyed. The difference in elevation of before and after compaction gave a 640-mm average settlement of the surface within the trial area corresponding to 4.4% average compression (reduction of thickness).

No clear indication could be found that an increase in the duration of compaction would result in a significantly higher soil layer compression and, thus, improved compaction. It was decided to adopt a 5-minute compaction phase, resulting in an about 15 minute total duration of compaction at each compaction point.

During the second pass, the intermediate points at the centre of the initial grid were compacted. The distance between compaction points after completion of the second pass was 2.8 m. At seven of the points, the duration of compaction was 5 minutes and at duration at the remaining six points was 10 minutes. Figure 10.26 shows the depth vs. time at one compaction point. The probe was first inserted and let to penetrate rapidly to 11 m depth by high frequency (25 Hz) vibration. From 11 to 13 m, the probe was at resonance frequency (14 Hz) from which depth the probe was extracted in about 2 m steps at high frequency (25 Hz) and, then let to re-penetrate a distance of 1.0 to 1.5 m at resonance frequency (approximately). Probe extraction from 5 m depth was at high frequency.

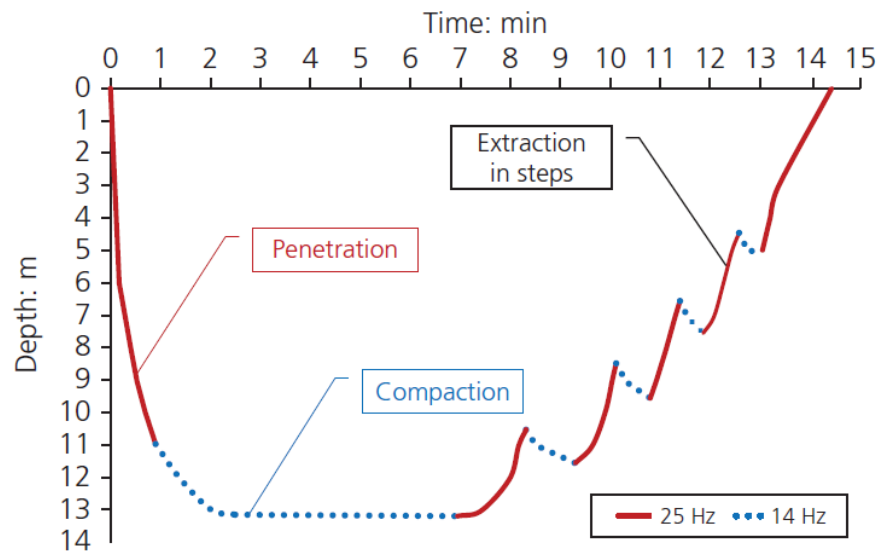


Fig. 10.26 Example of the resonance compaction process.

For purpose of demonstrating the seismic analysis described above, the susceptibility for liquefaction at the site is assumed to be affected by an earthquake of magnitude of 7.5 and a seismic acceleration of 30 % of gravity. This assumption determines the site-specific Cyclic Resistance Ratio,  $CRR$ , according to Chapter 2, Eqs. 2.13 through 2.15. The cone stress measurements determine the Cyclic Stress Ratio,  $CSR$ , from the "before" and "after" soundings, and the factor of safety against liquefaction is the  $CSR$  divided by the  $CRR$  as defined in Eq. 2.20. Figure 10.27 shows the calculated factors of safety for the before-and-after compaction and Figure 10.28 the-before-and-after compaction Janbu modulus numbers (see Section 10.7.1). The results demonstrate that the compaction was highly efficient above about 6 m depth and plain efficient in the finer soils below (fine sand and silt are not as suitable for compaction as sand).

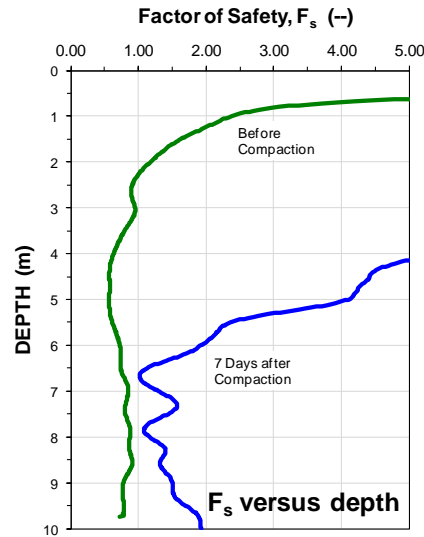


Fig. 10.27 Factor of safety against liquefaction before and after vibratory compaction.

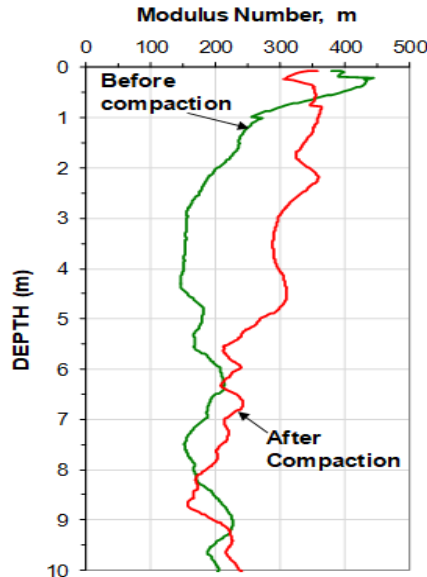


Fig. 10.28 Modulus number, m, before and after vibratory compaction.

### 10.7.2 Underwater resonance compaction of sand fill inside a cofferdam

A bridge constructed across the bay of Sundsvall employed a novel foundation solution to support bridge piers. Instead of conventional pile foundations, cofferdams consisting of steel sheet piles, filled with compacted sand to 14 m depth, were chosen. This solution has major advantages in the case of ship impact as the sand-filled steel caissons can absorb high horizontal forces. The bridge was built from 2011 to 2015 and is the longest (2,109 m) motorway bridge in Sweden (Massarsch et al. 2017).

Extensive geotechnical investigations, comprising cone penetration tests with pore water pressure measurements, heavy dynamic probing, field vane tests and Swedish weight sounding, were performed to investigate the complex geotechnical conditions. At the sea bed, very soft organic soil (gyttja) and soft silty clay were encountered. Below followed silt that progressively changed into sand at a maximum depth of about 14 m deposited on glacial till (moraine) of varying thickness resting on bedrock, which occurred at depths ranging from 5 m through 44 m below the sea bed, [Figure 10.29](#).



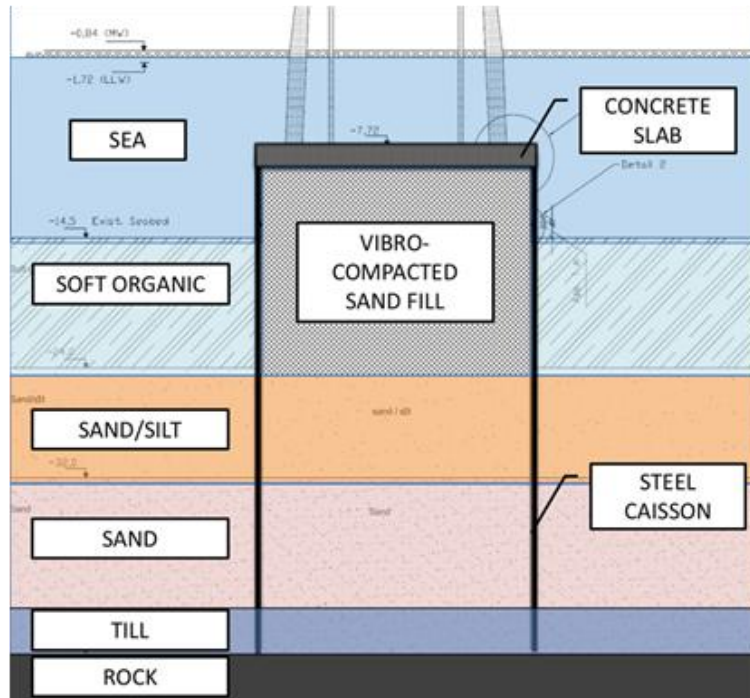


Fig. 10.29 Foundation conditions of bridge pier with vibratory-compacted sand inside steel caisson.

Soil compaction is most efficient during the resonance phase, see Figure 10.30, when the probe and the surrounding soil oscillate in phase. The total duration of compaction in each point was approximately 12 minutes. The figure shows amplitude (mm), depth (m), frequency (Hz), and penetration speed (cm/minute) as a function of time.

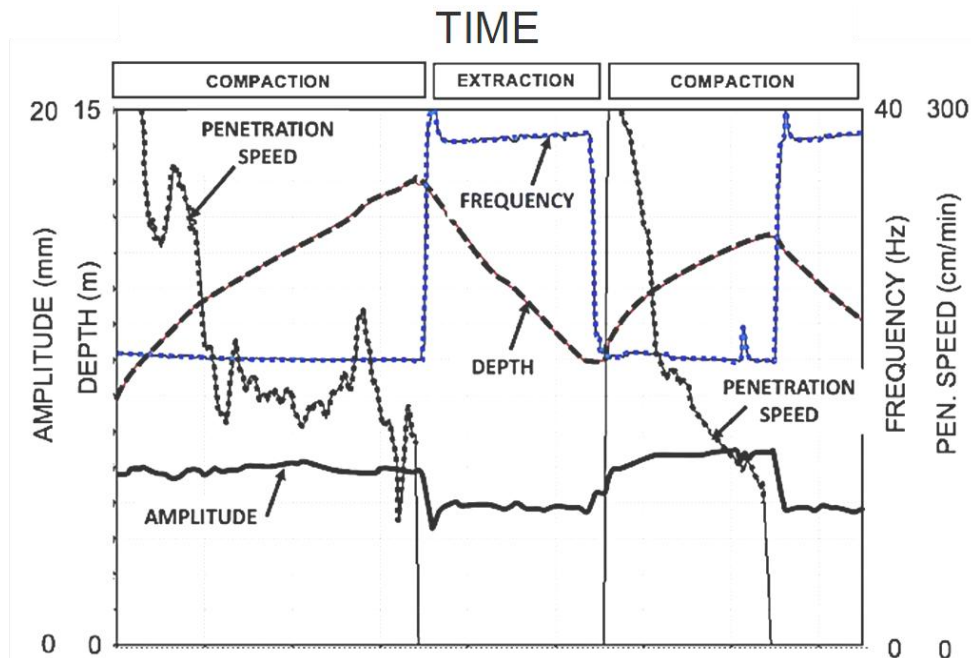


Fig. 10.30 Compaction with variation of different compaction parameters as a function of time. (Note, depth is shown in inverse scale).

Compaction was carried out in three phases. Figure 10.31 shows the results of CPT soundings pushed before compaction and after each of the three compaction phases. The required degree of compaction was specified in terms of cone stress. In the uncompacted fill, placed by dumping sand into the water-filled caisson, the cone stress was very low, typically 2 MPa at the surface increasing to 5 MPa at 7 m depth. Also, the sleeve friction was low, generally lower than 5 kPa. As a result of the first and second compaction pass, the cone stress increased to about 7 and 12 MPa, respectively. Sleeve friction increased following the first and second compaction pass, to about 10 and 20 kPa, respectively. After Phase 3, cone stress and sleeve friction increased significantly; the initial indication of loose state increased to dense after Phase 2 and became very dense after Phase 3 with values reaching 25 MPa. The sleeve friction values after Phase 3 exceeded 80 kPa. During the third compaction pass, the fill became so dense that the probe could penetrate only a few meters into the sand fill.

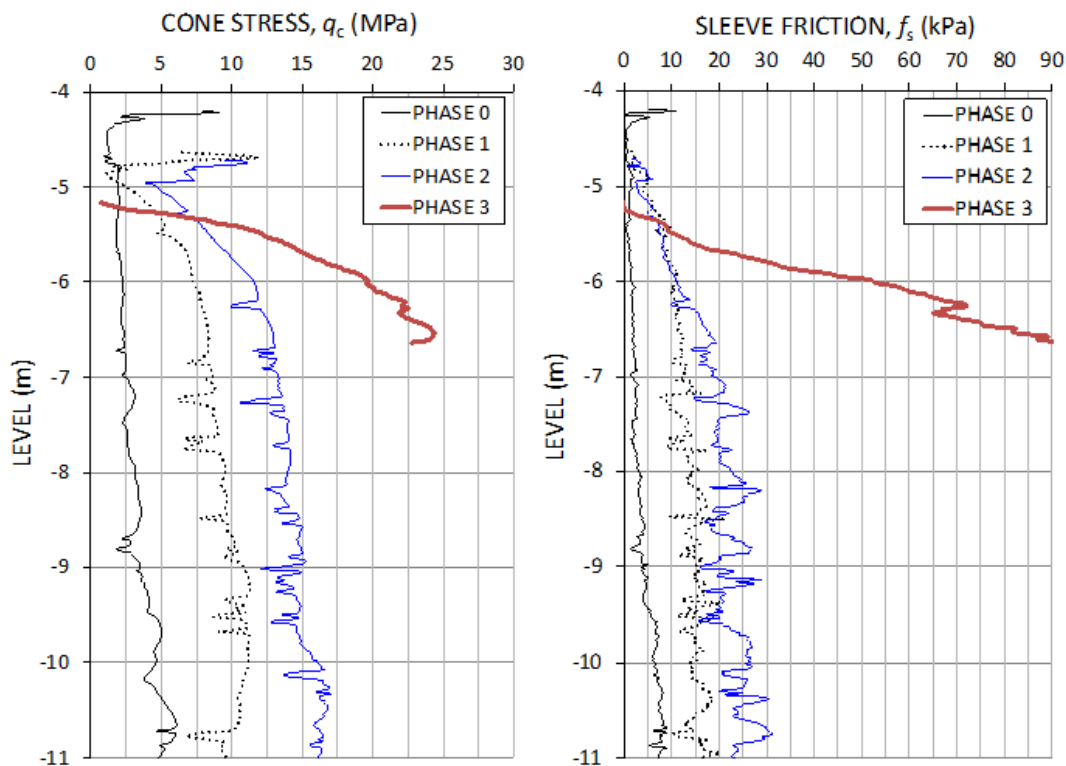


Fig. 10.31 Cone stress and sleeve friction from prior to compaction, and after each compaction phase.

The lateral displacements of the steel sheet piles were monitored using inclinometers. As a result of vibratory compaction, the sheet piles moved inward and toward the center of compaction, reflecting the volume decrease of the compacted sand fill. The surface of the compacted fill settled by almost 1 m. The settlements corresponded to about 8 % of the layer thickness, indicating a high degree of densification.

### 10.7.3 Vibratory compaction at Annacis Channel, BC

An interesting vibratory compaction project was carried out for an industrial development in the Fraser River delta adjacent to the Annacis Channel, Vancouver, BC. The soil deposit consisted of an about 2.5 m thick, loose sand fill, overlying an approximately 2 m of soft clayey silt (Massarsch and Fellenius 2017). Below, loose alluvial sand was encountered down to about 11 m depth, followed by stiff clay. The groundwater level varied but was on average located 2 m below the ground surface. The  $d_{50}$ -mean grain size was about 0.3 mm and the fines content was about 10%. Because of the liquefaction susceptibility at the site, the designer had decided to densify loose, granular soil layers along a 230 m long, 3.0 to 4.5 m wide area. Compaction was required to a depth of 10 to 11 m.

SPT N-indices in the alluvial sand ranged between 5 to 24 blows/0.3 m, with an average of  $N = 12$ , i.e., the relative density was loose to compact. Figure 10.32 shows the N-indices (SPT 2, SPT 3, and SPT 7) from three boreholes with SPT-sampling drilled before the start of compaction.

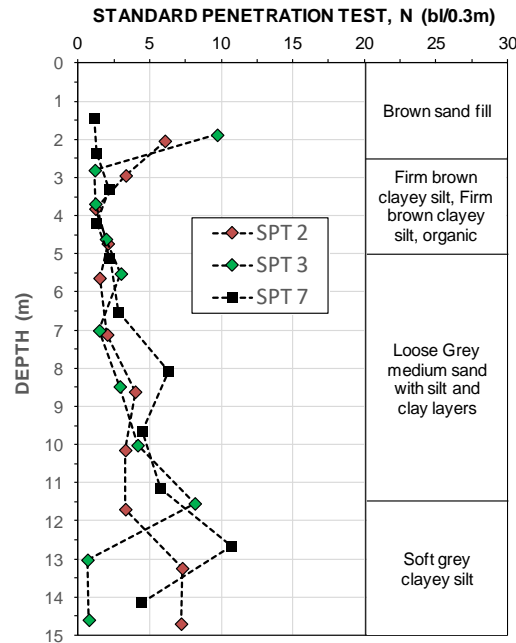


Fig. 10.32 Soil profile description and SPT indices in the project area prior to treatment.

The results from a CPTU sounding before compaction are shown in Figure 10.33. Down to 2.5 m, layers of dense sand exist with seams or bands of sandy silt. The cone stress,  $q_c$ , is larger than 5 MPa. Between 2.5 and 5 m, the soil consists of soft silt or loose silty sand with  $q_c$  ranging from 1.5 through 3 MPa. At about 4 to 5 m depth, the soil is sand with  $q_c$  of 4 to 7.5 MPa. The soil types differ locally at depths. Fine-grained layers, bands, or seams (silty and clayey) are interbedded in the sand deposit. Because these less permeable silt and clay layers impede vertical drainage, the liquefaction hazard could be amplified. Moreover, the sand deposit, sandwiched between these layers, would also be more difficult to compact.

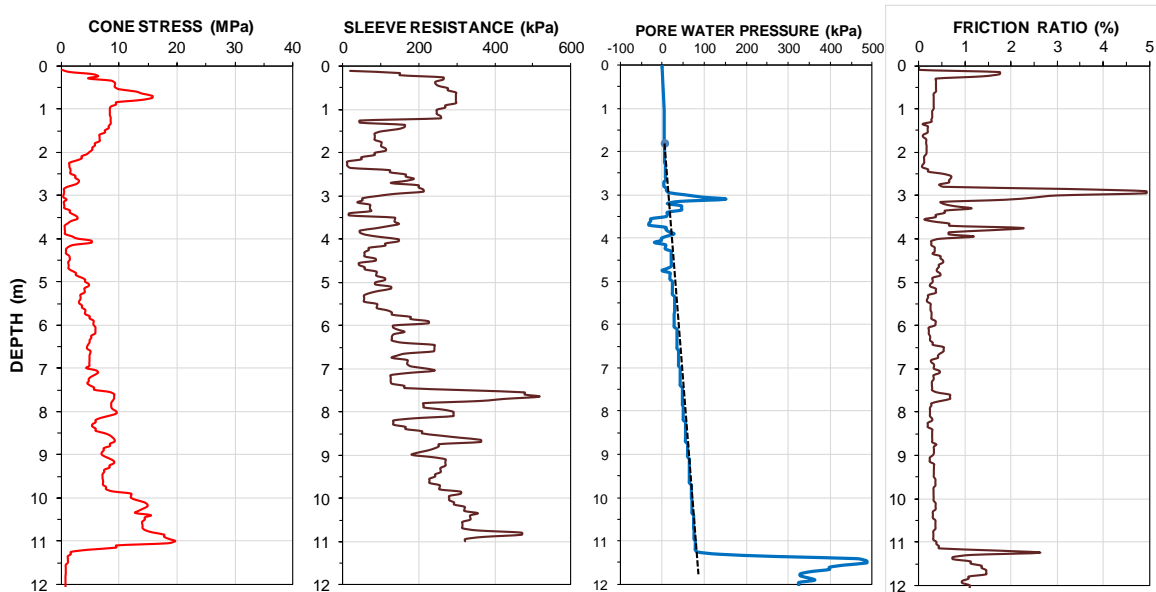


Fig. 10.33 Results of CPTU sounding executed before compaction.

Figure 10.34 shows the CPT cone stress and sleeve resistance measurements before, and 67 and 82 days after compaction, as measured between compaction points. The cone stress and the sleeve friction increased throughout the soil deposit, with the exception of the clayey silt layer between 3 and 4 m. It is interesting to note that the increase in cone stress and sleeve resistance continued even up to 82 days after compaction. The time effect, probably due to reconsolidation after dissipation of excess pore water pressure, is most pronounced in the soil layer between 6 and 10 m. Figure 10.35 shows the improvement in terms of ratio of cone stress and sleeve resistance prior to and 82 days after compaction.

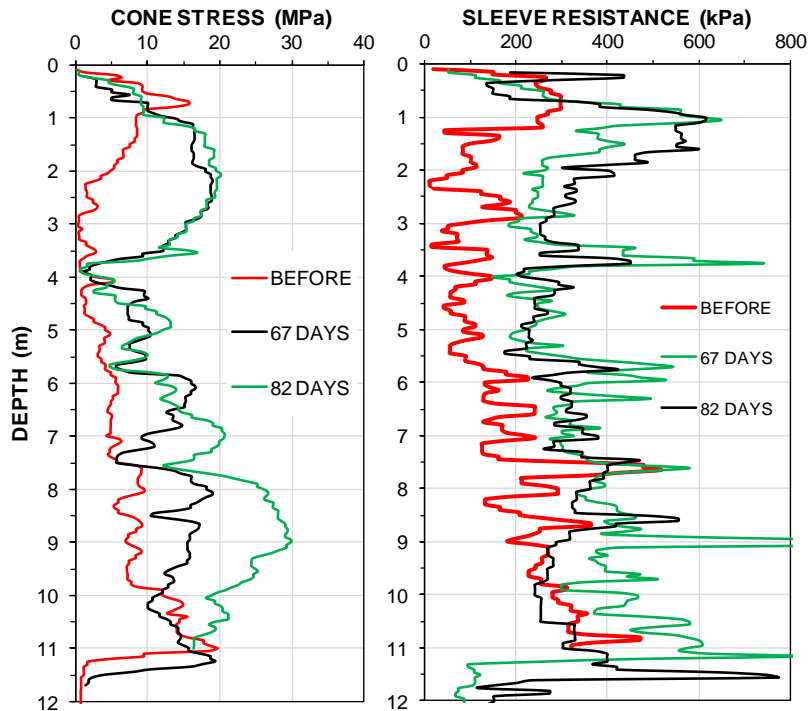


Fig. 10.34 Results of CPTU soundings executed before and at 67 and 82 days after compaction.

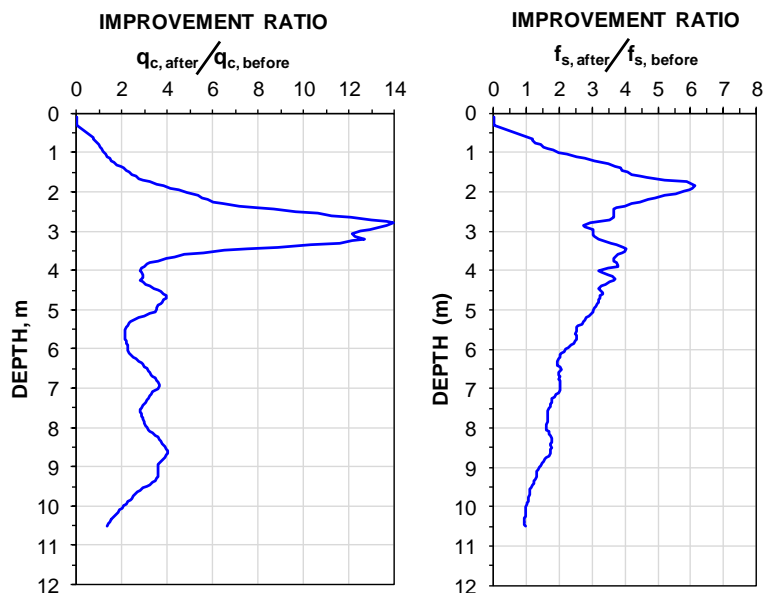


Fig. 10.35 Ratio of improvement of cone stress and sleeve resistance 82 days after compaction compared to values prior to compaction.

The compaction specifications required an increase of SPT N-indices to at least 14 blows/0.3 m at 4.5 m depth increasing to 17 at 9 m depth. These densification requirements were converted to equivalent cone stress values, using a cone to SPT ratio of  $q_c/N = 0.5$ , thus, requiring compaction in terms of CPT cone stress,  $q_c$ , ranging from 7 MPa at 4.5 m depth through 8.5 MPa at 9 m depth. The CPT soundings pushed after completion of the compaction showed the results to meet the requirements.

The compaction resulted in a significant increase of the compressibility as expressed by the Janbu modulus number. Figure 10.36 shows the distribution of the modulus number before and at 67 and 82 days after compaction as calculated using the relations in Clause 10.7.1. In the about 1 m thick (at the particular CPTs) soft silt layer between about 3.5 to 4.5 m depth, the compaction improvement in terms of compressibility was less successful as also at about 6 m depth.

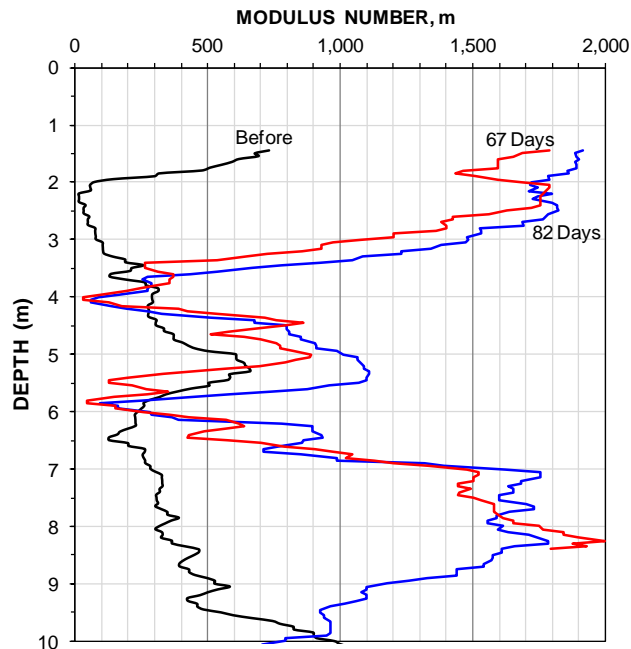


Fig. 10.36 Janbu modulus numbers before and after compaction.

The measured cone stress (CPT), sleeve resistance (CPT), horizontal stress (LSCPT), and horizontal stress index (DMT), as well as evaluated modulus numbers showed a significant increase as a result of compaction. It can be concluded that vibratory compaction causes preconsolidation, i.e., increases preconsolidation margin and OCR. This effect should be considered in geotechnical design, such as settlement analyses or liquefaction hazard assessment.

The project provided the opportunity to check the effect of the compaction by additional means, notably flat dilatometer tests (DMT), which were performed 111 days after treatment at several locations with slightly variable soil conditions.

The DMT was first introduced by Marchetti (Marchetti 1980). A DMT reference procedure was published by ISSMGE TC16 (Marchetti et al. 2001). The measured parameters are two pressure readings:  $p_0$ ,  $p_1$ , the initial reading and the reading at 1.1 mm expansion, respectively. The difference,  $p_1 - p_0$ , is denoted  $p_\Delta$ . The derived parameters are the material index  $I_D$  (which is related to soil type: clay  $0.1 < I_D < 0.6$ , silt  $0.6 < I_D < 1.8$ , and sand  $1.8 < I_D < 10$ .), the horizontal stress index  $K_D$ , (determined by dividing  $p_\Delta$  with the effective stress at the test depth), and the dilatometer modulus  $E_D$ . (which is  $p_\Delta$  multiplied by 34.7). Based on these three parameters, the constrained modulus,  $M$  (vertical loading), can be estimated from the relations in Eq. 10.9.

$$(10.9) \quad M = R_M E_D$$

$$\text{where } R_M = R_{M0} + (2.5 - R_{M0}) \lg K_D$$

$$R_{M0} = 0.14 + 0.15(I_D^5 - 0.6)$$

The time of testing was dictated by equipment availability and site access. Figure 10.37a shows the interpreted material index,  $I_D$ , and the DMT soil classification. The  $I_D$  ranges generally between 1 and 3, with the exception of lower values (0.1 to 1.0) in the several clay and silt layers, and the classification generally agrees with the soil type based on friction ratio from CPT.

Fig. 10.37b show the distribution of the constrained modulus,  $M$ , 111 days after compaction compared with the  $M$  from before compaction) is shown in. Again, due to the variability in the upper 6 m of soil, only the improvement in the lower part of the sand deposit (6 to 9 m) is of relevance. In this zone, the constrained modulus increased by a factor of 2 to 3.5.

An important consequence of vibratory compaction of sand is the change of horizontal stress. Figure 10.37c shows the distribution of the horizontal stress index,  $K_D$ , for three DMT soundings determined according to the procedure recommended by Marchetti et al (2001)—the compaction was terminated at 8.5 m depth for operational reasons. Neglecting the upper 6 m of variable soil layers, there is a noticeable increase of  $K_D$  in the compacted sand in the depth interval of 6 to 9 m. On average,  $K_D$  increased as a result of compaction by a factor of 1.5 to 2.5.

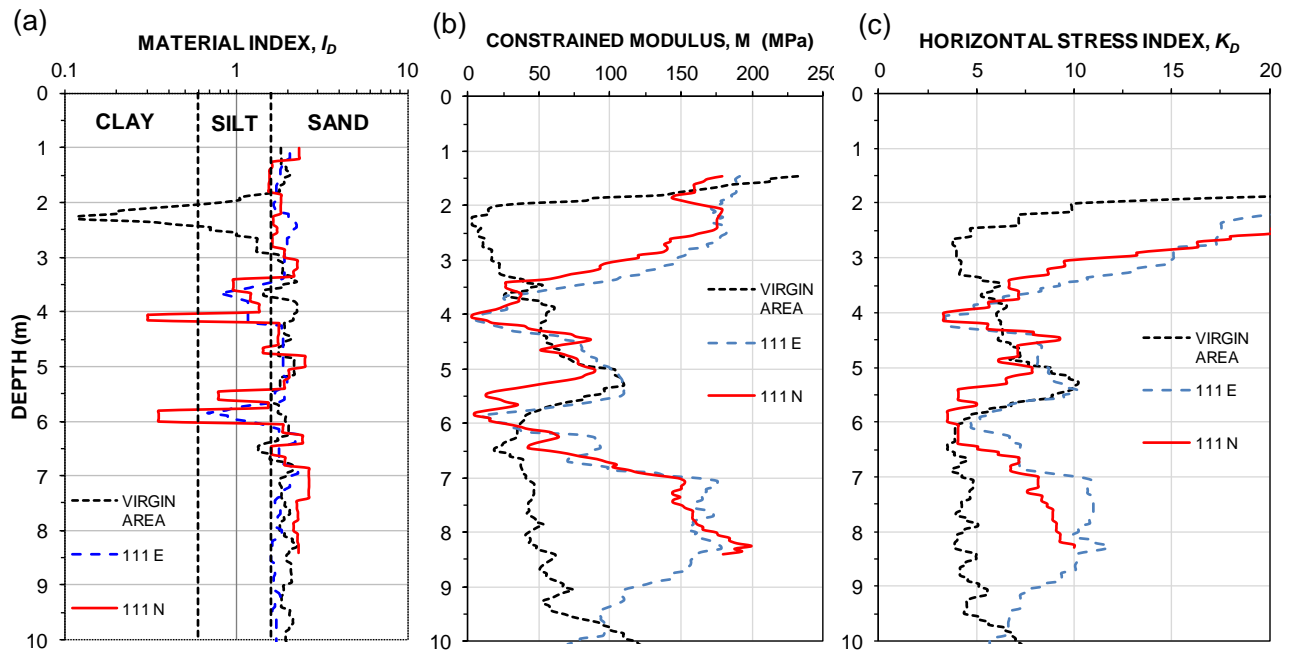


Fig. 10.37a Variation of DMT material index,  $I_D$  with depth. Material boundaries according to Marchetti et al. (2001) are indicated.

Fig. 10.37b Constrained modulus,  $M$ , determined from dilatometer modulus,  $E_D$ , before compaction and 111 days after compaction.

Fig. 10.37c Horizontal stress index,  $K_D$ , as function of depth before compaction and 111 days after compaction.

#### 10.7.4 Compaction from pile driving

Driving pile in loose sand frequently raises concern for the pile driving vibration causing settlement for adjacent foundations (discussed in Sections 9.14 and 9.15). Intentional compaction of loose soils is sometimes carried out by driving displacement piles, notably wood piles, in order to provide seismic remediation (densification) of a site exhibiting loose sand. A small densification effect results from the fact that the piles force the soil to occupy a smaller volume, sharing the original volume with the piles, as it were. However, this effect is marginal; about 50 % of the pile volume is diverted to heave and lateral displacement of the soil body. Unless the pile spacing is very small, the remaining pile volume does not make for any significant reduction (i.e., densification of the soil).

The main densification is achieved by the dynamics of the driving. The primary compaction effect is from the driving force, specifically the toe force (Massarsch and Fellenius 2008). The larger the dynamic force, the more pronounced the densification effect.

The pile driving hammer impact produces a dynamic force along a pile that is transmitted to the soil. The impact force is a function of the impact velocity of the drop weight or ram. However, for diesel hammers, the impact velocity of the ram is also a function of the soil response. This is because, when the pile toe is in loose soil, the reflected force wave is weaker and cannot send the ram back up as high as opposed to when the soil resistance is larger. When ram travel of the diesel hammer is thus shortened, the impact force is smaller and less efficient in compressing the fuel mix in the combustion chamber. Therefore, a smaller combustion force will develop as opposed to when the pile toe encounters stronger soil resistance (see Chapter 9). This was demonstrated at the Mission Bridge in B.C., Canada, where wood piles were driven in order to provide liquefaction remediation (D.W. Mitchell, Vancouver Pile Driving Ltd.; personal communication).

Because very loose sand will not generate much toe resistance and, moreover, only require only a few impacts for the piles to reach depth, compaction by means of pile driving is not efficient in loose soils and less so when driven by diesel hammers, as the latter require a good toe response to generate driving force.

Figure 10.38 contains the records of two CPTU soundings, "Area A" and "Area B", pushed before any piles were driven at the site (courtesy of W. Schwartz, Sky to Sea Drilling Ltd., Vancouver). The soundings show that the soil profile consists of about 9 m of mostly compact (Area A) and mostly very loose to loose (Area B) sand with silt, both followed by mostly compact sand with occasional loose layers. The sand became dense below about 20 m depth. The curve labeled "(B) $F_s$ " is the safety against liquefaction according to Chapter 2, Eq. 2.22 for the CPTU in Area B determined from input of an earthquake magnitude,  $M$ , of 7.5 (i.e.,  $MWF = 1.0$ ) and a ground surface peak horizontal acceleration,  $a_{max}$ , of 0.3 g (Vancouver, BC, lies in a high-risk earthquake zone). The  $F_s$  is larger than unity above 9 m depth for this CPTU sounding, but considering the small  $q_t$ -values, the upper 9 m of sand would probably liquefy if a large earthquake would strike the area (or rather, when it does). Figure 10.39 shows the CPTU soil classification chart (linear abscissa scale). Open and closed symbols are from Areas A and B, respectively.

The two soundings show that upper 9 m thick zones are different in the two areas. In Area A, it is coarser than in Area B and not loose, but compact. In contrast, below 9 m depth, there is little difference.

The toe diameter of the wood piles (the 'top of tree' is the pile toe) was about 10 to 13-inch and the butt diameter was about 13 to 15-inch. They were driven in 12 m lengths that were spliced at the site. Splicing was with joining the two lengths by a plate with a short dowel attached to the center of each side. The pile spacing was 1.25 m (about 3.5 pile diameters). The project specifications called for driving the piles with a diesel hammer or hydraulic hammer (at pile locations where the headroom was low). However, no sane person would want to do a splice with a heavy diesel hammer 15 m up in the air nor, then, attempt to carry out the light tapping needed for completing the splice with a diesel hammer. It was therefore

proposed to shift to using a gravity hammer (drop hammer). To meet the somewhat surprising argument that a drop hammer could not achieve the desired level of densification, a limited test was carried out in each of Areas A and B comprising one CPTU sounding pushed before and one pushed after piles had been driven. In Area A, the piles were driven with a Berminghammer B300 diesel hammer (1,700 kg ram). In Area B, the piles were driven with two hammers; an APE7.5, a hydraulic hammer with a 5,500 kg ram operated at a stroke limited to 0.6 m and a 2,500-kg drop hammer operated at a 1.5 through 2.5 m height of fall.

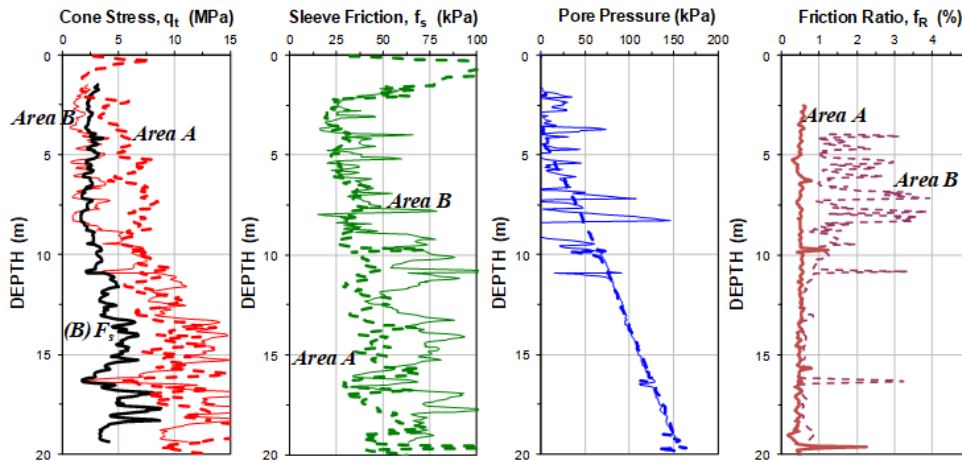


Fig. 10.38 Two CPTU soundings from before the pile driving

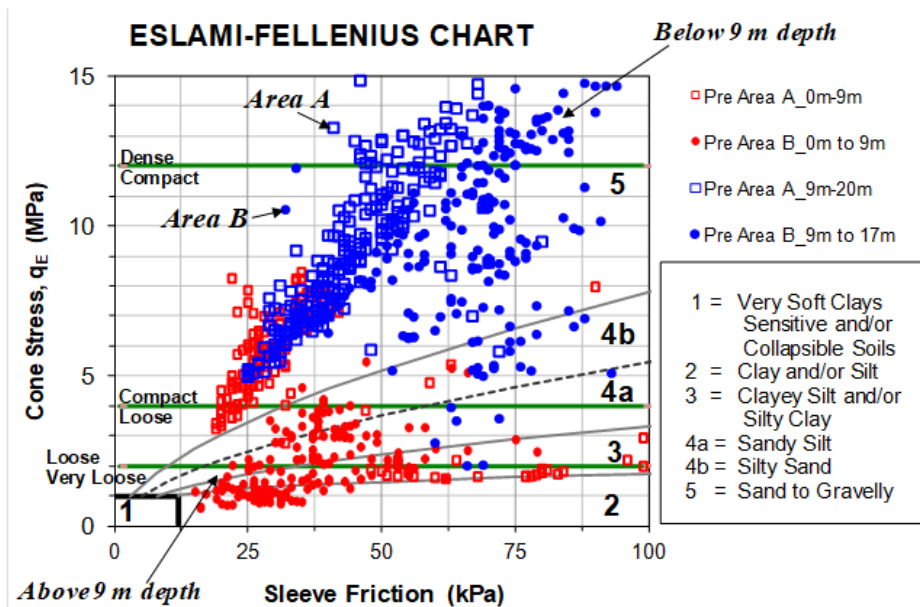


Fig. 10.39 Classification chart from the CPTU soundings shown in Fig. 10.38

The results of vibratory compaction are usually assessed by direct comparison between cone-stress distributions obtained from soundings pushed before and after compaction. However, the best comparison is by means of the modulus number calculated from the CPT results (see Section 2.11). Figures 10.40 through 10.42 show the cone stress and modulus number records from before and after the driving in Area A (Berminghammer B300) and Area B (hydraulic and drop hammers). No information is available on hammer settings and no dynamic or geophysical monitoring was undertaken in the test (see Chapter 9), which is regrettable, as such monitoring provides the best means for assessing the densification effect of the vibrations introduced by the compaction work.



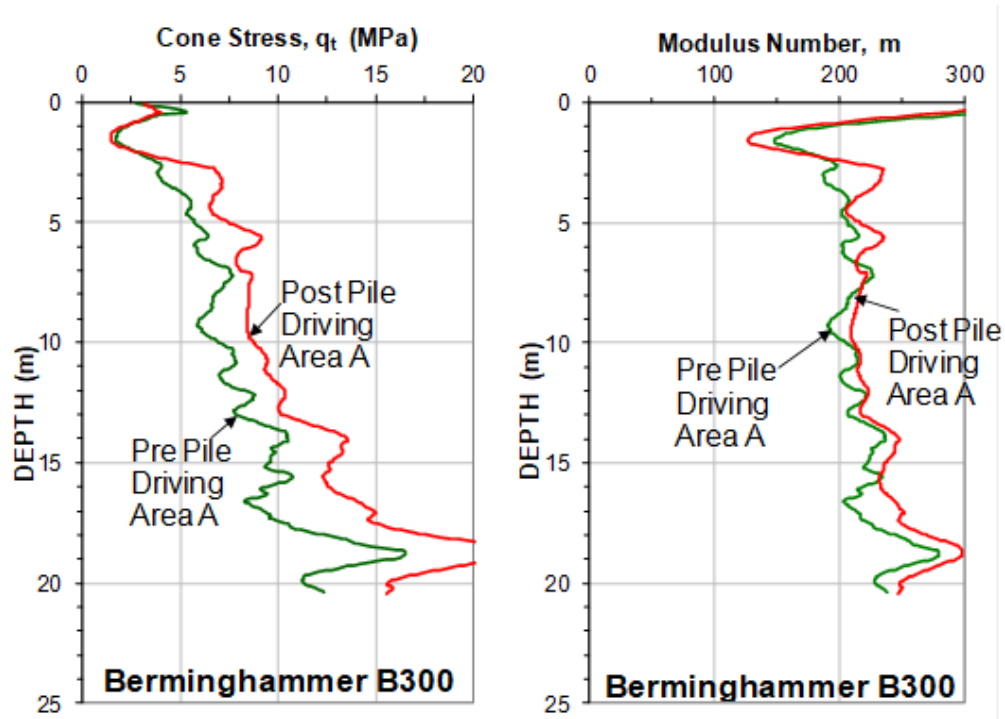


Fig. 10.40 Distribution of cone stress,  $q_t$ , and modulus number,  $m$ . Area A, zone of piles driven with Berminghammer 300 diesel hammer

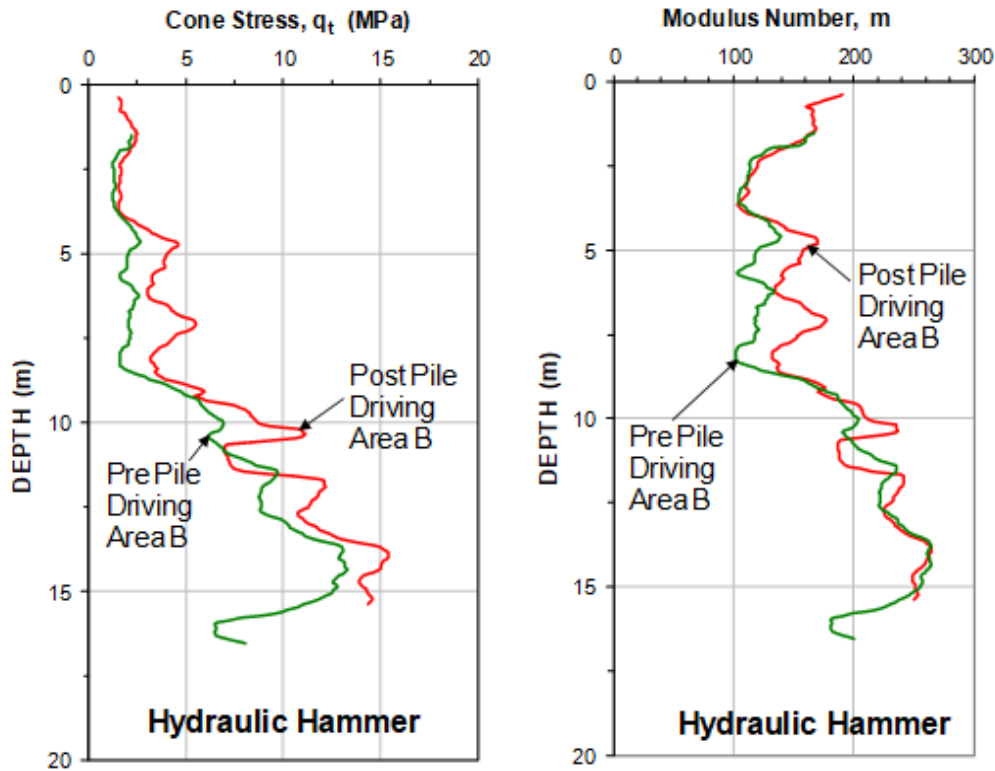


Fig. 10.41 Distribution of cone stress,  $q_t$ , and modulus number,  $m$ . Area B, zone of piles driven with APE 7.5a Hydraulic hammer

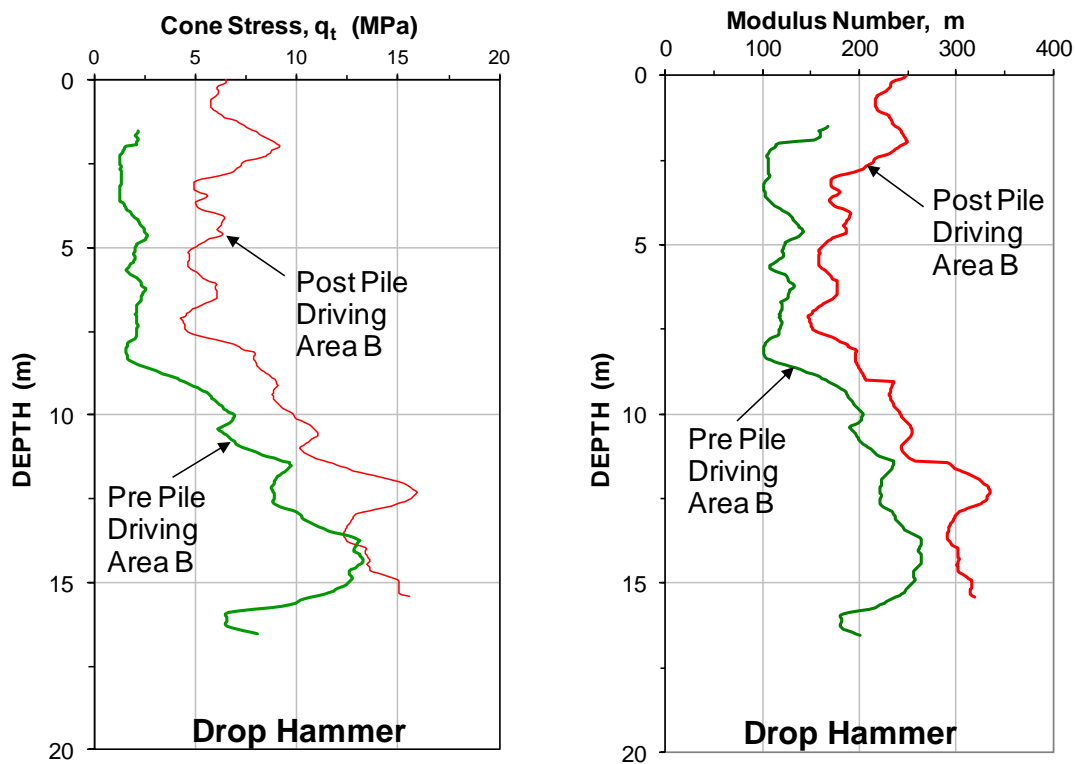


Fig. 10.42 Distribution of cone stress,  $q_t$ , and modulus number,  $m$ . Area B, zone of piles driven with the drop hammer.

The mechanical hammers, the Berminghammer B300 and the hydraulic hammer, appear to have achieved only moderate densification. In contrast, where the piles were driven with the drop hammer, the results show that the drop hammer achieved a pronounced densification, illustrating, as mentioned, that the dynamic force transmitted to the soil, which is maintained when using the drop hammer can be used to achieve a compaction.

Figure 10.43 shows a comparison between the pre- and post pile driving CPTU records with the drop hammer for the first pile segment and with the ASPE 7.5a after the splicing. The curves indicate a pronounced increase of cone stress and sleeve friction to about 9 m depth. Also below 9 m, an increase of cone stress due to the compaction effect is evident, but not so for the sleeve friction as would have been expected. It should be noted that the locations of the pre and post CPT-soundings are some 15 m apart.

The post-driving sleeve friction versus the pre-driving sleeve friction is shown in Figure 10.44. Above 8.8 m depth, the post-driving sleeve friction increased—within the depth where the drop hammer was used. However, below 8.8 m, where the diesel hammer was used, there was no significant increase and the ratio between post-driving and pre-driving records stayed at about unity.

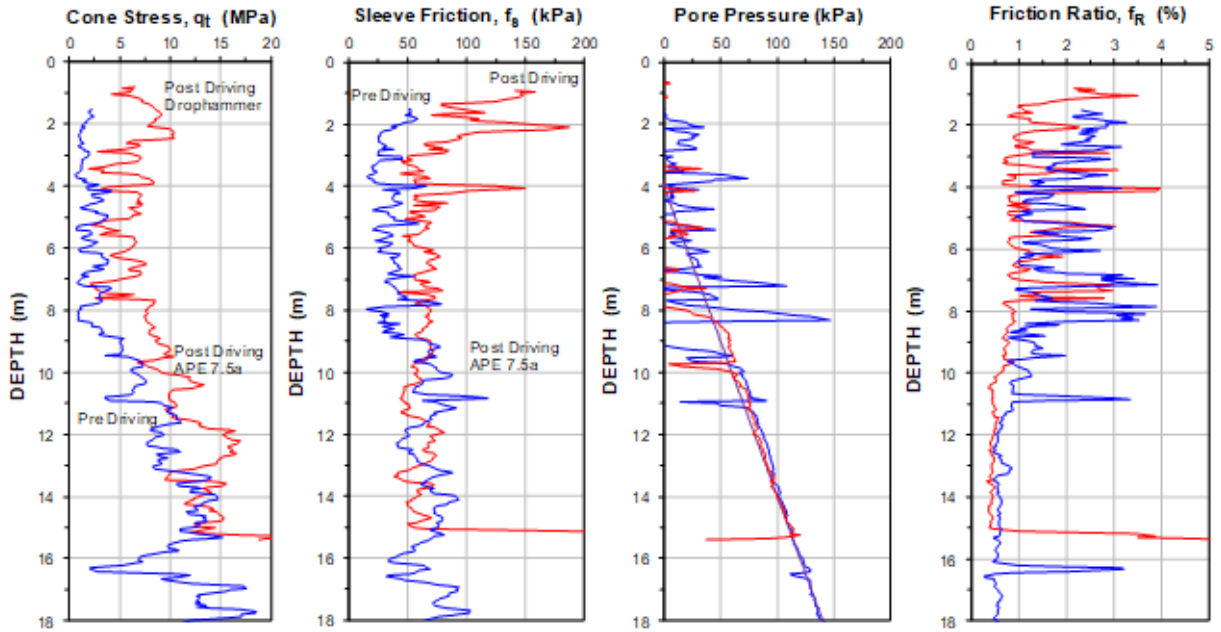


Fig. 10.43 Distribution of cone stress,  $q_t$ , sleeve friction,  $f_s$ , and pore pressure,  $u_2$ , before and after the pile driving

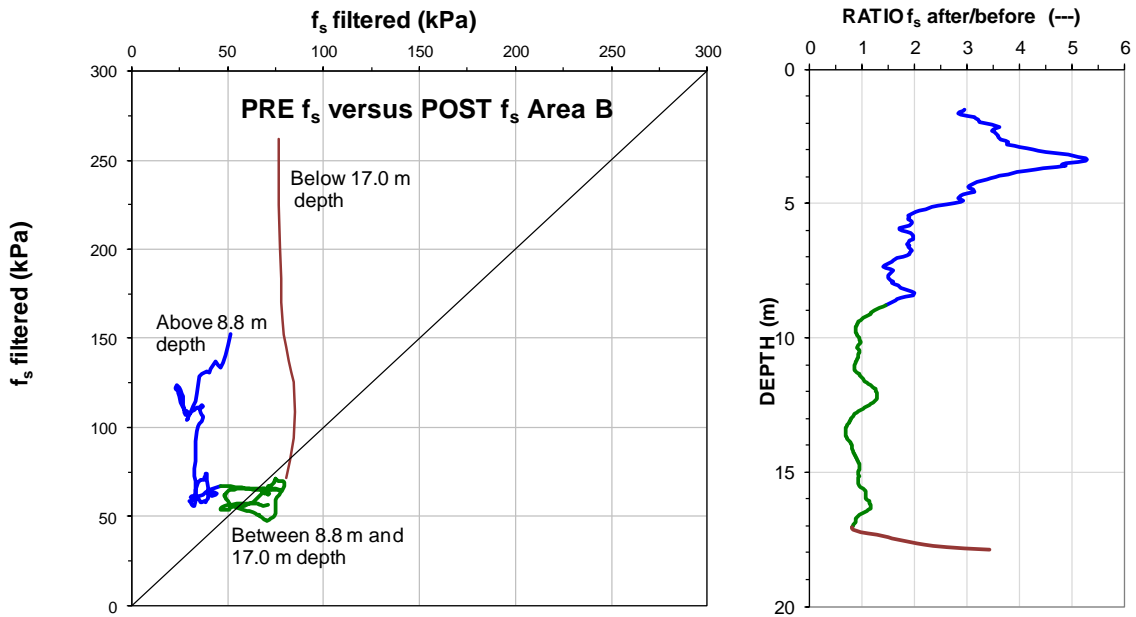


Fig. 10.44 Post- driving versus pre-driving sleeve friction,  $f_s$ , and distribution of the ratio between post- driving and pre-driving sleeve friction,  $f_s$ .

### 10.8 Concluding Remarks

Vibratory compaction aims to reduce the pore volume of granular soils, i.e., gravel and sand, which requires that the excess pore water can be discharged. In very dense soils, vibratory action can, however, cause loosening of the soil. This effect can be significant if the compaction probe is extracted at or close to the resonance frequency.

Presence of lenses or layer of low-permeability soil, i.e., clay and silt, may slow down or prevent full discharge of pore water, thus, reducing the desired level of compaction.

Vibratory compaction can be achieved by different methods, such as vibroflotation or vertically oscillating probes. Vibroflotation relies primarily on horizontal oscillations, while vertically oscillating probes generate primarily shear waves with a strong vertical vibration amplitude. Due to friction between the probe and the soil, additional horizontal vibrations are generated, which enhance compaction and increase of horizontal stress.

In loose, water-saturated soils, liquefaction can occur during the initial phase of compaction. In such a case, the interaction between the probe and the soil is lost temporarily but builds up gradually as the excess pore water pressure dissipates. Above a certain density, a soil deposit will dilate and, therefore, not liquefy even at strong vibrations.

Settlement ("ground loss") is a direct indicator of compaction. Further confirmation regarding the compaction effect can be obtained by noting the rate of probe penetration and frequency at resonance, and comparing the results of in-situ tests before and after compaction.

Compaction in granular soils (rearrangement of particles) is caused when the strain level (primarily shear strain) exceeds a critical value (about  $10^{-2}$  %—or  $100 \mu\epsilon$ ). Increased strain level makes for more efficient compaction.

The strain level during vibratory compaction depends on the ratio between the particle velocity and the wave propagation speed. Both can be measured and knowing the ratio makes it possible to determine the strain level in the vicinity of the probe.

Compaction is also affected by the number of vibration cycles. The larger the number of vibration cycles, the more effective is vibratory compaction. The dynamic stress generated by wave propagation is the product of particle velocity and soil impedance, similar to wave propagation in piles. Thus, compaction becomes most effective when the number of vibration cycles is increased.

The most effective compaction is achieved—independently of the method used—when large vibration velocity cycles are generated.

In order to enhance vertical vibratory compaction, the vibration velocity of the oscillating probe should be as large as possible. The vibration velocity of the probe depends on the mass (should be as low as possible) and the eccentric moment (should be as large as possible). The selection of the compaction system (size of vibrator and probe, respectively).

Probe openings reduce the mass (weight) of the probe and increase the interaction with the soil in transferring the vibration velocity of the probe to the surrounding soil.

The area of influence of the probe depends on its diameter (width of wings). Vibration velocity decreases with increasing distance from the probe. Thus, the wider the cross section of the probe (which interacts with the soil), the larger the area of influence. Therefore, a double Y-shaped probe optimizes the area affected by vibratory treatment.

At vertical resonance, the soil and the probe move in phase (almost simultaneously along the entire probe length). Resonance has two important advantages: resonance amplifies vibration transfer from the probe to the soil and, at resonance, the loss of vibration energy at the probe-soil interface is minimal (no heating at the probe surface).

Horizontal stress change is a supplementary consequence of vibratory compaction. The vertically oscillating probe generates waves in the horizontal direction that cause a permanent increase of horizontal stresses. The increase in horizontal effective stress results in preloading of the compacted soil. The preloading (overconsolidation effect) is an important beneficial effect of vibratory compaction.

Vibratory compaction can be carried out by different sizes of compaction systems. If smaller compaction equipment (less powerful vibrator and smaller probe size) is used, the compaction point spacing must be reduced. However, the dynamic force of the vibrator must be sufficiently to penetrate soil deposits to the required treatment depth and to extract the probe after compaction.

Another important parameter of vibratory compaction is the sequence of penetration and extraction of the probe. In soils which require more treatment, the number of extraction and re-penetration cycles must be increased.

The optimal compaction process (distance between compaction points, compaction sequence and variation of vibrator frequency) is best determined by field trials, supplemented by penetration tests.

The most effective vertical vibratory compaction method is characterized by:

- Vibrator with sufficiently high eccentric moment (which generates high vibration velocity)
- Increased probe diameter (double-Y shaped probe with wide wings)
- Light probe weight as this minimizes loss of probe vibration velocity
- Openings in the probe (which increase interaction between probe and soil)
- Compaction at resonance, which amplifies vibrations in the ground and increases the zone of influence.



## CHAPTER 11

### SLOPE STABILITY

#### 11.1 Introduction

Wherever the ground is sloping, shear forces are induced that tend to cause soil movements. The movements can be large and, in the extreme, sudden. We then talk about slope failure and slope instability. The effect of water in the process is very important, in particular, when the water pressure changes or seepage is introduced.

Early on, analysis of slope stability was made assuming interaction of soil bodies delineated by plane surface boundaries. For example, the sliding of a wedge of soil at a river bank sketched in [Figure 11.1](#), which can be analyzed—optimized—considering the force vectors involved for different wedge sizes. Or, similarly, the retained slope in [Figure 11.2](#), showing earth stress acting against a retaining wall, which alternatively is analyzed using Coulomb-Rankine principles of earth stress. The force vectors shown in the figures are generated by the downward movement of the wedges. Failure occurs for the river bank when the movement has mobilized a shear resistance,  $\tau$ , equal to the soil shear strength. For the wall, the shear force along the sloping shear plane governs the force,  $P$ , which can be of a magnitude that the retaining wall can accept without 'failure' (i.e., being pushed outward); the shear resistance,  $\tau$ , can then be smaller than or be at the strength limit.

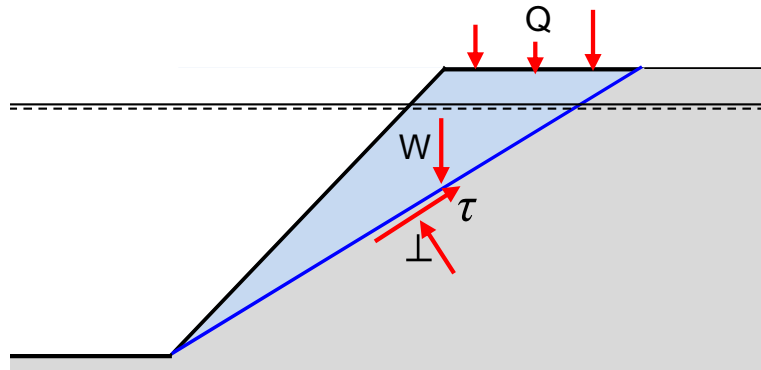


Fig. 11.1 A sliding soil wedge at a river bank held fast by shear resistance,  $\tau$ , along a failure plane

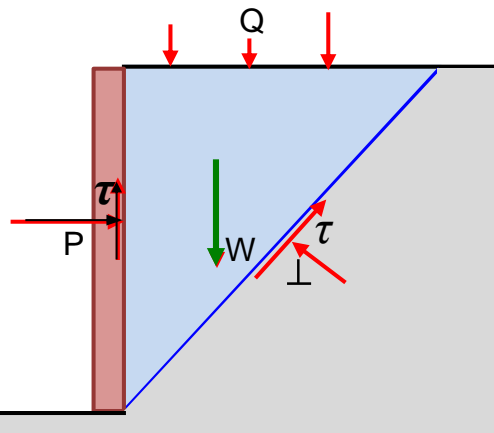


Fig. 11.2 Earth Stress; a sliding soil wedge retained by a wall

As the 1800s turned into the 1900s, industrial development and railway construction in Sweden necessitated extending the harbor of the Western Swedish city of Gothenburg (Göteborg). In 1905, the Harbor authorities established a design and construction department headed by W. Fellenius. In the years following, several large docks that could accommodate deep-draught ships were constructed. Amongst them, the Stigberg Quay (Stigbergskajen). In March 1916, this dock failed. The dock, a reinforced concrete structure on relatively short wood piles, a new approach at the time, had been constructed along the shoreline over a thick deposit of marine postglacial, soft clay. The design had been made applying slope stability analysis using friction along plane slip surfaces, which was the common method in these days. However, K. Petterson, an engineer and T. Hultin, chief engineer at the Harbor design and construction department, noticed that the failure surface was not plane but curved. Petterson and Hultin subsequently back-calculated the slide employing circular failure surfaces, still assuming the soil resistance to be friction,  $\tan \phi$ , and this method was used in the design of the replacement dock (Bjerrum and Flodin 1960).

W. Fellenius (1918; 1926; 1927; 1936) advanced the slip-circle method to include cohesion in combination with friction and developed analytical methods for the calculations—the Method of Slices—as well as nomograms and charts to simplify the rather elaborate and time-consuming effort necessary to establish the most dangerous slip circle—called "the probable"—in a back-analysis of an actual slope failure, representing a cross section through a soil cylinder body. He also initiated the definition of factor of safety as the ratio of resisting rotational moment of the forces to the forcing (overturning) rotational moment of forces, the "total factor of safety" for the design analysis of slopes.

The Swedish Geotechnical Commission (1922), chaired by W. Fellenius, established methods for determining the shear strength of cohesive soil, which made it possible for the profession to apply the slip-circle method in design employing shear strength values determined on soil samples in a  $\phi = 0^\circ$  approach. Fellenius (1929) also developed the slip-circle method for "bearing capacity" design of footings and vertical loads on horizontal ground, applying the mentioned definition of factor of safety, and applied the Friction Circle method for determining the earth stress on a retaining wall.

Figure 11.3 shows the basic principle of the method-of-slides. The sliding soil body is split up into vertical slices and the forces on each slice are determined from the soil input available to determine for each slice its increments of resisting and overturning rotational moments. Note, the angle  $\phi'$  is the angle of rotation of the tangentially and perpendicularly oriented forces acting against the surface of the arc at the bottom of the slice. That angle cannot be larger than the internal friction angle of the soil. The angle  $\alpha$  is the angle between the arc at the bottom of the slice to the horizontal. By leaving out the influence of horizontal slice forces, the analysis is statically determinate. The factor of safety,  $F_s$ , for the analyzed circle is the ratio of the sum of  $M_{RESISTING}$  to the sum of  $M_{OVERTURNING}$  as shown in Eq. 11.1.

$$(11.1) \quad F_s = \frac{M_{RESISTING}}{M_{OVERTURNING}}$$

Later research, e.g., Bishop (1955), developed slip-circle methods that included slice-forces interaction ("interslice forces") and showed that such analysis usually produced  $F_s$ -values that are a few percentage points smaller than the "Swedish slip-circle" analysis.



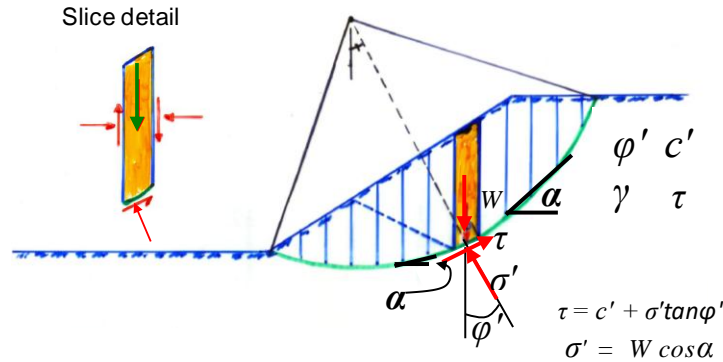


Fig. 11.3 The basic principle of the Method of Slices

Figure 11.4 shows the actual  $c'$ - $\phi'$  circle used by W. Fellenius (1926) in analyzing the Stigberg Quay failure. The text is in Swedish, the same figure was used with German text in 1927 (Fellenius 1927). The circle marked "FK" is stated to be "Most dangerous (i.e., critical) slip circle calculated applying cohesion and friction through Point D" (the land-side start of the failure zone)". The "friction circle" is explained in Section 11.3

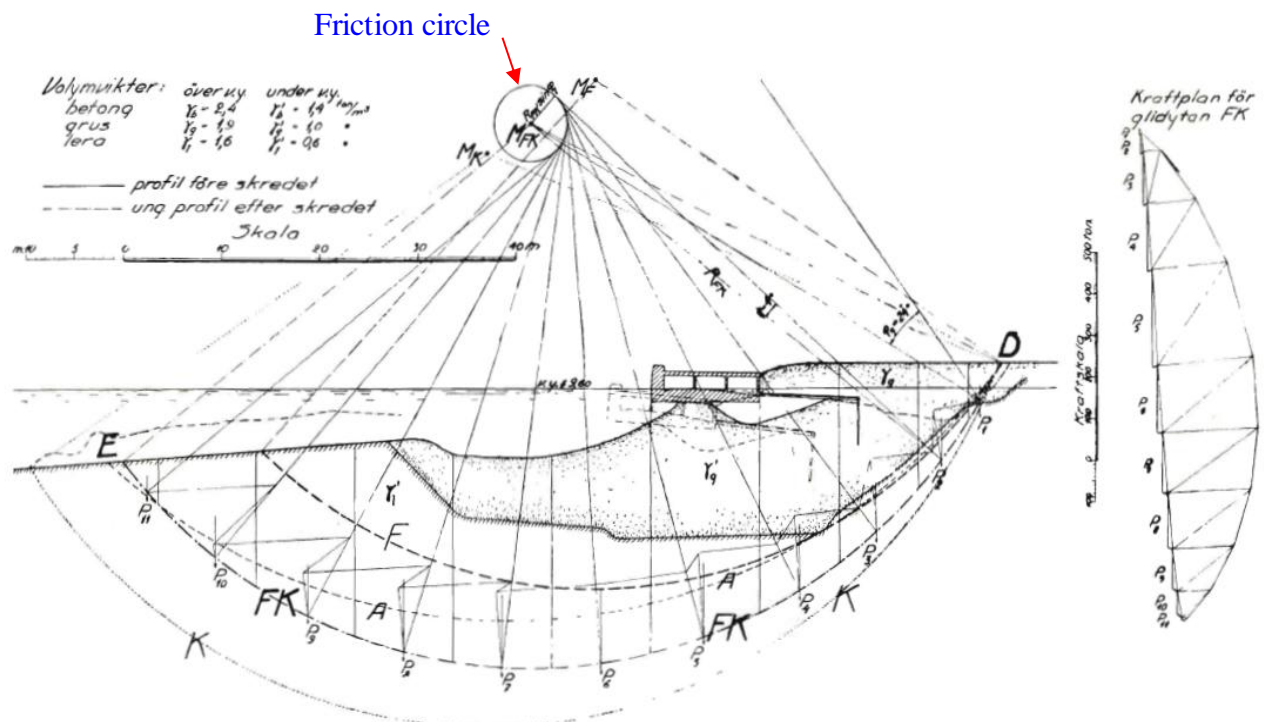


Bild 27. Skredet vid Stigbergskajen i Göteborg den 5:te mars 1916. A = farligaste friktionsglidyta genom skredets iakttagna inre ändpunkt, D, och sannolika yttre ändpunkt E; F = farligaste friktionsglidyta genom inre ändpunkten D; K = farligaste kohesionsglidyta genom inre ändpunkten D vid samverkande friktion och kohesion

Figure 11.4 Original slip circle for one section of the Stigberg Quay (W. Fellenius 1926; 1927)

W. Fellenius (1926; 1927) applied the slip circle analysis for determining earth stress as an alternative to the usual Coulomb method. Figure 11.5 is copied from the report and shows an example of earth stress (load/length of wall) calculation applying the friction circle for  $c'$ - $\phi'$  conditions in a graphic force-vector method. The "E" indicates the total earth-load against the wall (per metre length of wall).

To perform a slip circle analysis according to the methods of slices, the rotating cylinder is divided in a number of vertical slices. However, for simple geometries, uniform soil conditions, and when interslice forces can be disregarded, delineating the slope body into distinct parts, "slices", each providing forces and/or resistances, can be simplified, as illustrated in Figure 11.6. As mentioned, the disregard of the interslice forces usually results in a safety factor,  $F_s$ , that is slightly larger than that resulting from the calculation that includes these forces, i.e., disregarding the slice forces means "erring" on the safe side.

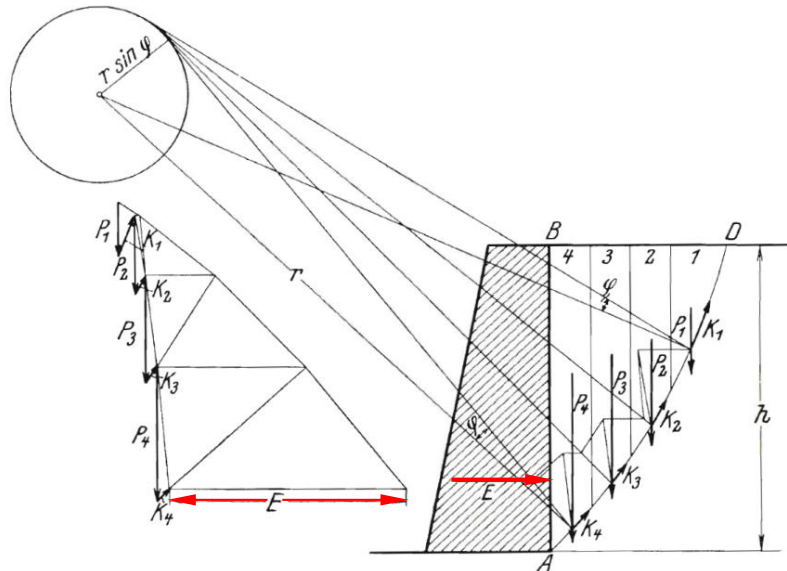


Figure 11.5 The method of slices applied to the calculation of earth stress against a wall (W. Fellenius 1926; 1927)

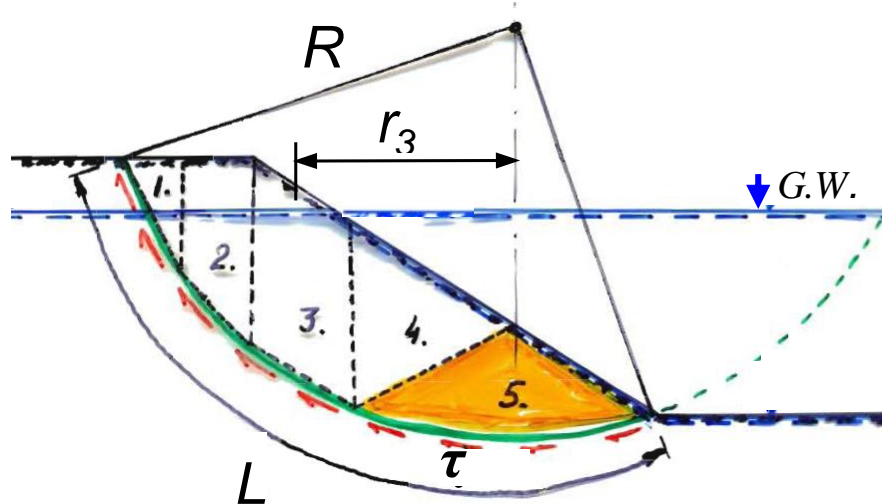


Figure 11.6 Simplified delineation of the "slices" for  $\phi=0$  and disregarding interslice forces

## 11.2 Example of Slip Circle Analysis

Figure 11.7 shows a cross section of a canal dug in a homogeneous clay layer having a total density of  $1,700 \text{ kg/m}^3$  and an undrained shear strength,  $\tau$ , of  $20 \text{ kPa}$ . The water level in the canal and the groundwater table in the clay is at Elev.  $+9.0 \text{ m}$ . The clay is fissured above Elev.  $+9.0 \text{ m}$  and a  $10\text{-kPa}$  uniform load acts on the horizontal ground surface along the canal. A potential slip circle is indicated, representing a cross section through a cylindrical soil body along the canal.

- A) Use total stress parameters to calculate the factor of safety of the canal slope for the indicated slip circle in a  $\phi = 0$  analysis.
- B) How would the factor of safety be affected if the water level in the canal is increased or lowered?
- C) The indicated toe circle is not the one with lowest factor of safety. Search out the most critical circle.

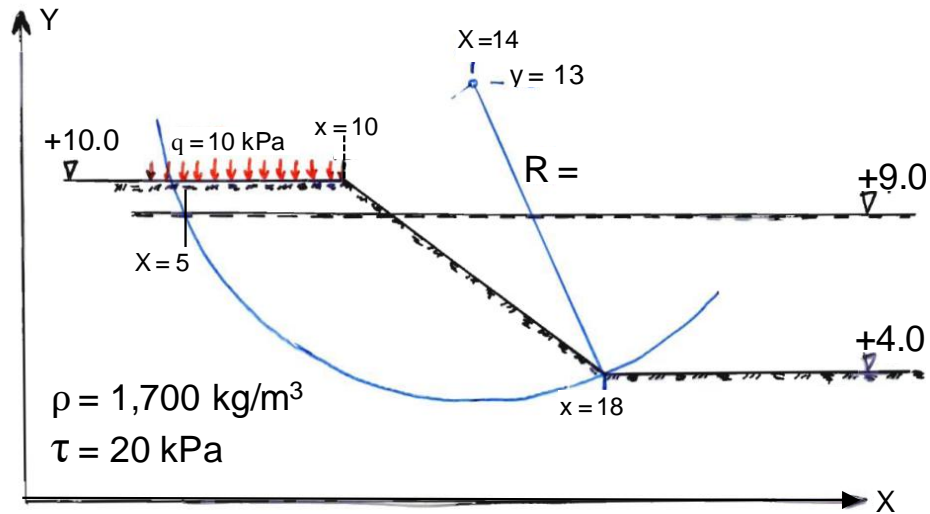


Figure 11.7 Example of  $\phi=0$  stability calculation for a canal dug in clay

Figure 11.8 shows a simple division into parts, Areas #1 through #6, active in the overturning moment. Area #7 has no lever arm for the rotation and Area #8 is too small to have any effect.

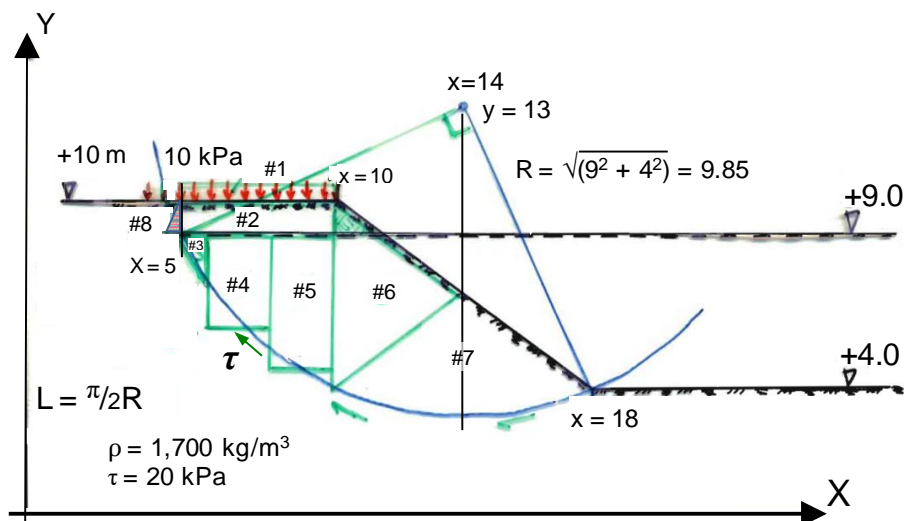


Figure 11.8 Division in Areas #1 through #8 (all distances are in metre)

The rotation moments are simply calculated as the areas times unit weight times lever arm, as follows.

**Water level at Elev.+9.0 m**

1.	$5.0 \times 10(5/2 + 4)$	=	325		
2.	$5.0 \times 1 \times 17(5/2 + 4)$	=	553		
3.	$0.5 \times 1 \times 1.5 \times 7(1/3 + 4 + 4)$	=	44	$\Sigma M_{\text{Forcing}}$	= 1,720 kNm/m
4.	$2 \times 3 \times 7(1 + 2 + 4)$	=	294	$M_{\text{Resisting}} = \tau L R = \tau (\pi/2) R^2$	= 3,047 kNm/m
5.	$2 \times 4 \times 7(1 + 4)$	=	280		
6.	$0.5 \times 4 \times 6 \times 7(2/3 \times 4)$	=	224	$F_s = 3,047/1,720$	= 1.77
7.	balances out	=	0		

What is the  $F_s$  for a sudden drop of GW to Elev. 4.0 m? First, the unit weight to use in the calculations would be  $17 \text{ kN/m}^3$ , throughout, which would result in  $M_{\text{Forcing}}$  increasing to 2,923 kNm/m, and  $F_s$  reducing to 1.04. The "sudden" lowering would also remove the balancing water pressure in the canal, but the water pressure in the soil along the slip surface (circle arc) would remain, however, which would add a horizontal force and create an overturning moment of about 1,000 kNm/m. (The lowering would constitute a condition called "rapid drawdown"). The canal slope would fail even before the water level had dropped to Elev.+4.0 m.

Because of the fissures in the uppermost 1.0 m thick layer, no benefit of shear resistance is considered in this zone. Instead, a vertical fissure in the crust can be assumed to exist rising up right at the spot where the circle cuts the 1.0-m depth. This defines the width of the fill and size of uppermost soil areas, Areas #1 and #2, active as forcing load (it also defines the "fortuitous" 90-degree angle of the slip circle). Area #2 lies above the groundwater table and its weight is calculated using the total unit weight of the clay. For Areas, #3 through #6, the buoyant unit weight is used. For Area #6, the fact that a small triangular part of Area 6 actually lies above the water table is neglected.

The fissure delineating Area #2 could be filled with water and the pore pressure would then result in a horizontal overturning force, as indicated by Area #8. Indeed, the fissure could even be closed, which would result in an extension of the slip circle through the upper 1.0-m layer and require adding the net effect of the shear resistance along the circle extension and the overturning force from the soil stress and the surcharge. For the example case, this has minimal effect and is simply disregarded in the analysis. However, disregarding the effect of a surficial layer, typically embankment fill, on a soft ground is often not advisable. For example, Figure 11.9 shows a case of an embankment on soft ground with a  $\phi=0$  circle through the soft ground and the slip surface continuing as a plane surface through the  $\phi>0$  embankment. The rotational moment from the embankment is simply calculated as active earth stress (plus water pressure when appropriate) acting against the vertical from the bottom of the embankment.

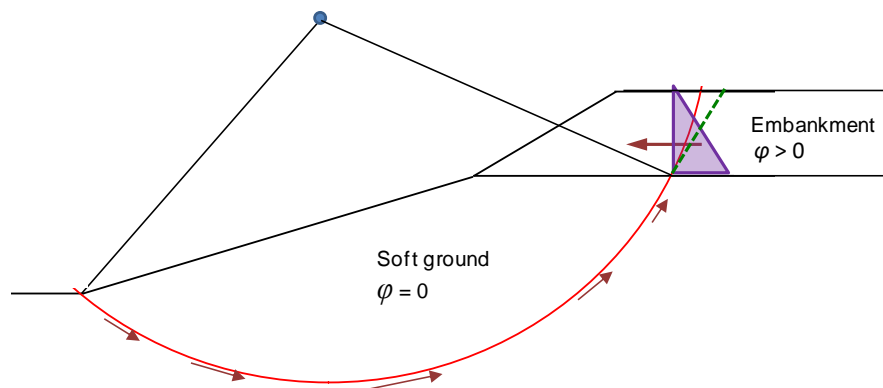


Figure 11.9 Combining a slip circle through  $\phi = 0$  soil with a plane surface through  $\phi > 0$  soil

### 11.3 The Friction Circle — $c = 0$ and $\phi > 0$ Analysis

When a soil body, e.g., a cylinder of soil, rotates and its surface slides against another soil body, the movement causes the perpendicular stress against the boundary surface to rotate around the contact point. The maximum angle of the latter rotation is equal to the soil friction angle,  $\phi$ . For a uniform soil and a constant friction angle, all stresses will be tangent to a circle concentric to the slip circle and with the radius equal to  $\sin \phi$  times the circle radius,  $R$  (W. Fellenius 1926; 1927, Taylor 1948). The resultant to all the stresses is vertical and lies at a distance from the slip circle center equal to  $KR \sin \phi$ , where "K" depends on the central angle of the circle and the distribution of the stresses against the circle arc. Taylor (1948) indicated that for most cases "K" is rather small, about 1.05. Figure 11.10 illustrates the principle of the Friction Circle.

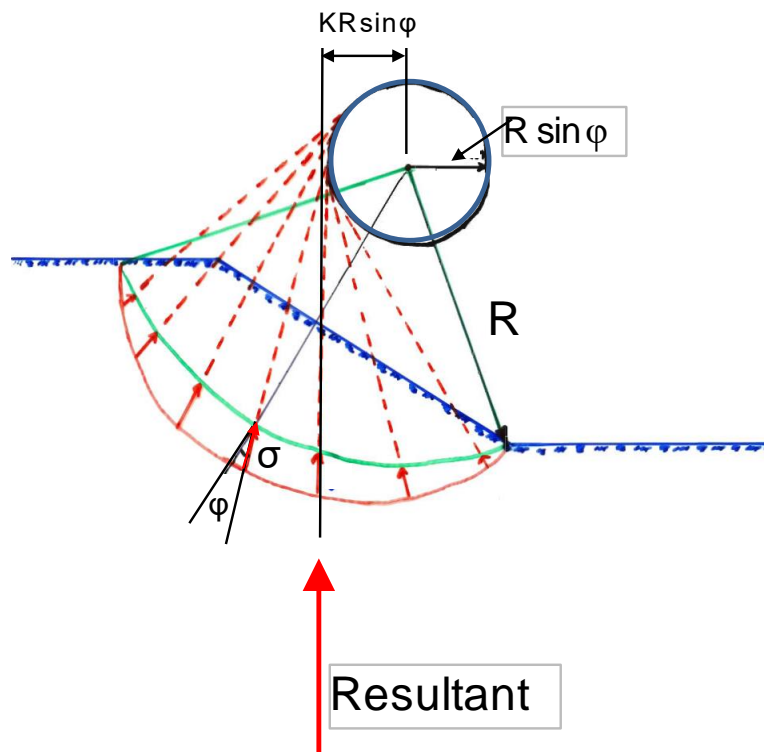


Figure 11.10 The Friction Circle

**Example** Figure 11.11 shows a slope in a coarse-grained formation with a strip footing placed at the crest of the slope. The footing stress is 100 kPa. The water table is located well below the lowest point of the circle. Determine the factor of safety of the slope and footing system.

Q:	$100 \times 4$	=	400	$M_Q =$	3,600 kNm/m
$W_1$ :	$20 \times \frac{1}{2} \times 8 \times 10$	=	800	$M_{W1} =$	6,100 kNm/m
$W_2$ :	$20 \times \frac{1}{2} \times 10 \times 10$	=	1,000	$M_{W2} =$	1,700 kNm/m
$W_3$ :	$20 \times 10 \times 1$	=	200	$M_{W3} =$	0 kNm/m
	$\Sigma$	=	2,400 kN/m	$\Sigma$	= 11,400 kNm/m



distances to the slope toe and one other point at the crest through which the spiral is thought to go. This will determine the  $r_0$ -distance (assumed to be horizontal line pointing to the left of the center as shown in Figure 11.12). Every and all input of  $\phi$ , will show a spiral going through the slope toe and chosen crest point. The spreadsheet can be written to calculate the weights to the left and the right of the spiral center and to determine the x-coordinate of the resultant. There will be one  $\phi$ -value for which this coordinate is close to the x-coordinate of the spiral center. Repeating the process for another spiral center location will give a new such  $\phi$ -value. In an iterative process, the location of the center that results in the lowest  $\phi$ -value represents the end result, the  $\phi_{\text{spiral}}$  for the case, and, as before,  $\tan \phi_{\text{spiral}} / \tan \phi_{\text{soil}}$  is the factor of safety.

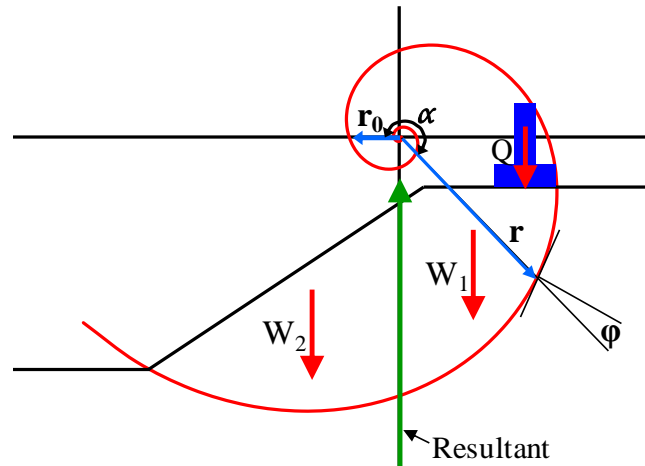


Figure 11.12 A logarithmic spiral fitted to a slope with a footing load on the crest level.

The length,  $s$ , of the arc of a spiral from  $r_0$  through  $r$  is given in Eq. 11.3, i.e., the length of the spiral for the angle of rotation,  $\alpha$ .

$$(11.3) \quad s = r_0 \frac{e^{\alpha \tan \phi} - 1}{\sin \phi}$$

where  $s$  = length of arc from  $r_0$  through  $r$   
 $\alpha$  = angle of rotation from  $r_0$  through  $r$   
 $\phi$  = angle between the normal and the radius at any point; a constant

The arc length,  $s_2 - s_1$ , between two points defined by  $r_2$  and  $\alpha_2$  and  $r_1$  and  $\alpha_1$ , respectively, is then easily obtained.

### 11.5 Analysis for $c'$ - $\phi'$ Conditions

Reanalyze the example in Section 11.2 in a  $c'$   $\phi'$  analysis with an effective cohesion,  $c'$ , of 8 kPa and an effective internal friction angle,  $\phi'_{\text{soil strength}}$ , of  $21^\circ$  at conditions with the water level at Elev.+9.0 m.

The resisting moment due to the cohesion,  $c' = 8$  kPa, is  $\tau L R = 8 (\pi/2) 97 = 1,219$  kNm/m

The sum of Areas #1 through #6 vertical forces is  $50 + 85 + 16 + 42 + 56 + 84 = 333$  kN/m. Area #7 must now be included, adding  $8 \times 3 \times \frac{1}{2} \times 7 = 84$  kN/m and making the total = 417 kN/m.

The total overturning moment,  $M_{\text{Forcing}}$  is still 1,720 kNm/m, which means that the net moment for the friction to resist is  $1,720 - 1,219 = 501$  kNm/m.

The lever arm is  $501/417 = 1.209$  m =  $KR \sin \varphi_{\text{mobilized}}$

$$\varphi_{\text{mobilized}} = \sin^{-1}(1.209/1.05 \times 9.85) = 6.7^\circ \text{ and } \tan \varphi_{\text{mobilized}} \ll \tan 21^\circ.$$

But, the foregoing includes the erroneous presupposition that the cohesion can be fully mobilized at the same time as the friction is only partially mobilized. To avoid this conflict, one can perform a series of repeat analyses with different degree of mobilization of the effective cohesion,  $c'$ , and iteratively search for what that degree of mobilization of the  $c'$  will result in the same value for the ratio between  $\tan \varphi_{\text{mobilized}}$  and  $\tan \varphi'_{\text{soil strength}}$ , which ratio then would represent the degree of mobilization of the friction. The inverse of that degree is then the factor of safety for the slope. However, the movement necessary to mobilize a certain portion of the cohesion is not usually that necessary to mobilize the same portion of the internal friction. A similar conundrum exists if using the logarithmic spiral for the calculation of the  $c'$ - $\varphi'$  condition.

Considering that some clays have distinct post-peak softening behavior and some soils, clay as well as sand, can be strain-hardening and the fact that soil profiles are built up of layers of different soils, once the case goes from the simple  $\varphi = 0$  or  $c = 0$  and uniform soil profile to  $c'$ - $\varphi'$  and variable soil profile, slope stability analysis becomes very complex.

## 11.6 Software

Before the computer became a universal tool for geotechnical engineers, stability analysis was performed by hand aided by the slide rule and graphic methods. As the calculation part of the analysis was time-consuming, thinking through the case to decide on the most probable location of the slip surface and the circle center was an investment in time well spent. In contrast, today's engineers have a host of slope stability software to choose between. Some are more sophisticated and complex than others, but every commercially available software will allow many more input options than engineers in the past would ever consider, or, rather, be able to consider. In fact, the analytical ability of the software goes much beyond the reliability of the input data. The ease of letting the computer do the work can lead to overlooking the dubiousity of the input, something that the engineers of old would not do as readily.

Commercially available software and some freeware range from simple limit equilibrium techniques through extensive numerical approaches. The engineer must fully understand the limitations of each method used by the software, as well as be able to appreciate if the method used correctly represents the probable failure mechanism. Most geotechnical general practitioners have limits in this regard and may need to seek the advice of the specialist. However, the project budget may have limits of funds to pay for the advice. A good help in resolving that predicament is to simplify the case to a level that can be analyzed using a "old-fashioned" hand calculation—a simple spreadsheet will often serve as a time saver, here. The analysis results may well show that the case is safe or can be made safe with little effort. NB, a large number of successful design were made before the advent of the computer program. If the hand calculation input shows a marginal stability and measures to alleviate this would be unacceptable for some reason, a well-understood and performed computer simulation must be undertaken. The computer solution may then show a satisfactory stability level. However, if the difference between the hand calculation and the computer simulation is large, it may be well advised to review the input and method used for the computer analysis. Indeed, having access to the results of a computer simulation does not remove the need for a thoughtful and thorough hand calculation using old and proven methods.



## CHAPTER 12

### WORKING STRESS AND LOAD AND RESISTANCE FACTOR DESIGN

#### 12.1 Introduction

Of old, people designed for expected settlement of footings and piles and there was no theoretical calculation of capacity. Full-scale tests were rare. When performed, a loading test usually aimed to reveal information on settlement response to load, rather than the ultimate resistance (capacity) of the tested foundation (Wendel 1900). The concept of capacity was introduced when, first, Stanton in 1859 and, then, by Wellington in 1893 (Chellis 1951). Wellington (1893) presented the Stanton and Engineering News formulas, which proposed a ratio between intended load and pile capacity (of driven piles), thus, introduced a factor of safety,  $F_S$ , (Likins et al. 2012).

In the 1910s, Wolmar Fellenius completed slope stability analysis to incorporate cohesive and friction strengths simultaneously and brought forward the  $F_S$ -concept as a ratio between induced rotating moment to the rotating moment that would occur in failure of the embankment (Massarsch and Fellenius 2012). Less known is that he also developed a calculation method for bearing capacity of footings based on the circular/cylindrical rotation analysis employing shear strength friction and cohesion and defining a factor of safety as the ratio between the calculated bearing capacity and the working load applied to the footing (Fellenius 1926). In 1943, Terzaghi presented his bearing capacity theory (the “triple N” formula, c.f., Eq. 6.1a) and adopted there the same definition of the safety factor. Since then, the use of the  $F_S$ -concept became a common approach. Indeed, settlement analysis is these days often not included—many assume that, if the factor of safety is good, settlement will not be of concern for the foundation. A mistaken assumption associated with many structural failures after excessive foundation movement and settlement.

Indeed, settlement is the governing aspect of a foundation design. Note, in contrast to the case of the old days, we do now know how to do a settlement analysis and do not need to continue relying on a perceived “capacity”. Besides, the bearing capacity theory for footings is totally wrong (Section 6.10). And, while we can determine—by some definition—the bearing capacity of a pile, again, it is the settlement of the pile, or pile group, that governs and that settlement is more a cause of what occurs around the pile than to the load applied to the pile (see Chapter 7).

With regard to piled foundations, while foundations supported on single piles, or on just a few piles, can be correlated to a  $F_S$ -criterion, this is not so for groups of piles. Piled foundations on wide group of piles need primarily, and definitely, to be designed for settlement. On occasions, the piles are not even connected to the foundation structure (Section 7.5) and, therefore, pile capacity and  $F_S$  is not an issue, but settlement always is. It is time to return to the design principles of the long past.

Of course, footings can experience a bearing capacity type failure. In particular, if small in width and placed at shallow depth. [Figure 12.1](#) shows a hypothetical case of a footing loaded to the point of a bearing capacity failure illustrated by a slip circle. If the footing is placed on clay and the load,  $Q$ , is brought on more or less suddenly, this is what well could happen. A practical case is loading a silo or a storage tank. However, if the load on a full size footing supporting sustained loads would be placed gradually (slowly) and concentrically (no tilting) and, if the load is larger than suitable for the conditions, although the foundation settlement will become so large that the structure supported on the footing will fail one way or another, no bearing capacity failure of the footing foundation will occur. The exception being if the soil is made up of a highly overconsolidated clay that, at first, reacts to the load by reduction

of the pore pressure, thus “fooling” the construction to believe that the footing can take more load than it actually can. In time, the pore pressures will return to the original level and the footing will fail. One may call this a case of a “delayed sudden failure”. However, no such case (nor any other) can be realistically analyzed with the “triple N” formula, Eq. 6.1a.

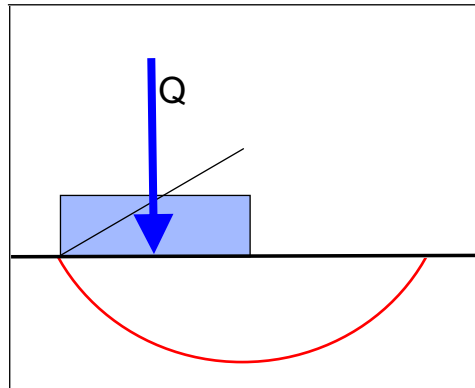


Fig. 12.1 Hypothetical case of bearing capacity failure analysis of a footing

If a footing is loaded by an off-center inclined load, the soil may become overstressed along one side and the settlement will be larger along that side than along the opposing side. The resulting tilt of the structure will move the resultant closer to the side and increase the stress along that side, which will increase the tilt yet again. Eventually, a progressive failure can occur in overturning as the resultant goes beyond the middle third and non-linear and non-constant static stress distribution response develops as the resultant keeps moving toward the edge (Section 6.6). Figure 12.2 shows a hypothetical such case. Assuming that the footing is reinforced concrete, or has other means to resist cracking in two, the stability benefits from the horizontal force,  $R_H$ , a tension force in the footing slab. However, **if the load is from an uneven fill instead**, there is no  $R_H$  helpful force. Instead, the fill will generate a force due to earth stress, as indicated by the light shaded triangle in the figure, that the sliding resistance may not be able to resist.

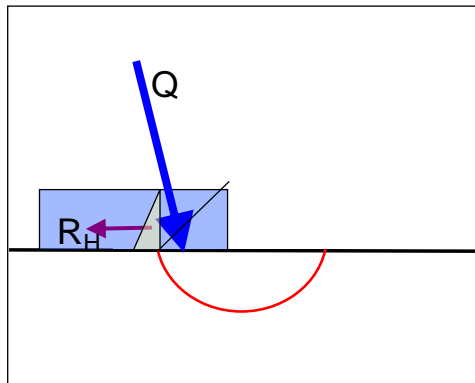


Fig. 12.2 Hypothetical case of bearing capacity failure of a footing with off-center and inclined load

In other words, bearing capacity may be of concern for footings, and a design will need to address and analyze this. However, not by the triple-N formula and not by looking at an off-center and inclined loading as a case that can be separated from a straightforward vertical load. In most cases, if a settlement analysis shows that the settlement will be within acceptable limits, “capacity” is more than adequate. If the analysis instead would show that the settlement instead is unacceptably large, would anyone care about what the calculated "capacity" value could be?

## 12.2 The Factor of Safety

All engineering designs must include a margin of safety against failure, as well as a margin against excessive deformation (settlement). The latter will be discussed in Section 12.3. With regard to the former, the margin is achieved by adopting a factor of safety defined as the available soil strength divided by the mobilized shear resistance. The available strength is either cohesion ( $c$ ) or friction ( $\tan \phi$ ), or both combined. (Notice that friction is not the friction angle,  $\phi$ , but its tangent,  $\tan \phi$ ). For bearing capacity of footings, the factor of safety is not defined as a ratio between strength and mobilized resistance, but as given by Eq. 12.1.

$$(12.1) \quad F_s = \frac{r_u - q'}{q_{allow}}$$

where

$F_s$	=	factor of safety
$r_u$	=	ultimate unit resistance (unit bearing capacity; stress applied at failure)
$q'$	=	overburden effective stress at the foundation level
$q_{allow}$	=	the allowable bearing stress (contact stress)

Geotechnical engineering practice is to use the bearing capacity formula and apply a factor of safety of 3.0 to the capacity is based on analysis, i.e., calculations using soil parameters. For footings, there is some confusion whether, in calculating the bearing capacity according to the "triple-N" formula (Eq. 6.1), the relation  $(N_q - 1)$  should be used in lieu of  $N_q$ . Moreover, whether or not to subtract the overburden stress,  $q'$ , from  $r_u$ , (as in Eq. 12.1) is also in some contention. The Canadian Foundation Engineering Manual (1992) omits the  $q'$  part. The difference has little practical importance, however. In coarse-grained soils, for example, the friction angle,  $\phi'$ , normally exceeds a value of  $33^\circ$  and the corresponding  $N_q$ -value exceeds 25, that is, when also considering the effect of  $N_\gamma$ , the "error" is no greater than a percentage point or two. In terms of the effect on the friction angle, the difference amounts to about  $0.2^\circ$ , which is too small to have any practical relevance.

More important, as mentioned, the definition of factor of safety given by Eq. 12.1 is very different from the definition when the factor of safety is applied to the shear strength value in the bearing capacity formula. This is because the ultimate resistance determined by the bearing capacity formula (Eq. 6.1) includes several aspects other than soil shear strength. Particularly so for foundations on soil having a substantial friction component. Depending on the particulars of each case, a value of 3 to 4 for the factor of safety defined by Eq. 12.1 corresponds, very approximately, to a factor of safety on shear strength in the range of 1.5 through 2.0 (Fellenius 1994).

In fact, the bearing capacity formula is wrought with much uncertainty and the factor of safety, be it 3 or 4, applied to a bearing capacity formula is really a "*factor of ignorance*" and does not always ensure an adequate footing foundation. Therefore, in the design of footings, be it in clays or sands, the settlement analysis should be given priority over the bearing capacity calculation.

The ultimate resistance according to the bearing capacity formula (Eq. 6.1), assumes a relatively incompressible subsoil. For footings placed on compressible soils, Vesic (1973; 1975) adjusted the formula by a 'rigidity factor', which considered soil compressibility resulting in a reduction of the calculated ultimate resistance,  $r_u$ . Where the soil is compressible enough to warrant such adjustment, settlement analysis, not bearing capacity analysis, should be let to govern the limiting (allowable) stress.

Notice, notwithstanding the settlement issue, it is equally important to consider stability against sliding and to limit load eccentricity. Either of the three may prove to govern a design.

### 12.3 Development of Limit States and Load and Resistance Factor Designs

The global factor to apply is an empirically determined function of the type of load—dead or live, common or exceptional. Initially, practice was to let those distinctions be taken care of by applying coefficients to the load values. From this basis, starting in Denmark some years ago, a "full partial factor of safety approach" grew, in which each component, load as well as resistance, be assigned its own uncertainty and importance. The design requirement is that the sum of factored resistances must be larger than the sum of factored loads.

The initial approach to geotechnical design, the working stress (WSD) consists of establishing the soil strength and determining the allowable shear by dividing the strength with a factor of safety—"global factor of safety approach". The particular value of the factor of safety to apply depends on the type of foundation problem as guided by experience and ranges from a low of about 1.3 applied to problems of slope stability of embankments to a high of 4 applied to bearing capacity equations for footings, while a factor of safety of about 2 is applied to pile "capacity" determined in a loading test and 3 to capacity determined by analysis. As mentioned, the capacity expressed by the bearing capacity equation does not just depend on soil strength values (cohesion and friction), other aspects are also included in the equation.

The partial factor of safety approach combines load factors, which increase the values of the various loads on a structure and its components, with resistance factors, which reduce the ultimate resistance or strength of the resisting components. This design approach is called Ultimate Limit States, ULS, or Load and Resistance Factor Design, LRFD.

Several countries and regions converted the foundation design approach from the working stress design, WSD, to a Limit States Design, LSD, or a Load and Resistance Factor Design, LRFD. New limit states codes have been enacted or proposed in Canada, USA, and Europe. Several Far Eastern countries are in a similar process. The Canadian efforts are contained in the Ontario Highway Bridge Design Code (OHBDC 1983; 1994) by the Ministry of Transportation and Communication, Ontario, MTO. A further development of this code to a Canadian National Code was published in 2006 by the Canadian Standards Association, CSA. The US development is led by the Federal Highway Administration, FHWA, and a report was published by Barker et al. (1991). The American Association of State Highway and Transportation Officials, AASHTO, has a Specification that applies LRFD rules to structural components as well as to the geotechnical design. The European Community, EC, has developed a limit states foundation code, Eurocode 7, which is being accepted as a National Code by all countries of the European Community.

Initially, Canadian geotechnical engineers were rather unwilling to consider changing to a ULS design approach as it applies to soils and foundations. However, in 1983, a committee formed by the Ontario Ministry of Transportation, MTO, produced a limit states design code for foundations of bridges and substructures. The 1983 Code very closely adopted the Danish system of partial factors of safety, where all factors are larger than or equal to unity (loads and other 'undesirable' effects are multiplied and resistances and other 'beneficial' effects, are divided by the respective factors). In contrast, in the Canadian version, all factors were multipliers larger than unity and the resistance factors were smaller than unity. Because the load factors were essentially already determined (the same values as applied to the superstructure were used), the code committee was left with determining what values to assign to the resistance factors. Notice the importance distinction that these resistance factors were applied to the soil strength.

Soil strength in classical soil mechanics is governed by cohesion,  $c$ , and friction,  $\tan \phi$ . After some comparison calculations between the final design according to the WSD and ULS (LFRD) approaches, a process known as ‘calibration’, the MTO committee adopted the reductions used in the Danish Code of applying resistance factors to cohesion and friction equal to 0.5 and 0.8, respectively. However, the calibration calculations showed considerable differences in the design end product between the ‘old’ and the ‘new’. A ‘fudge’ factor was therefore imposed called “resistance modification factor” to improve the calibration agreement. The idea was that once a calibration was established, the presumed benefits of the ULS approach as opposed to the WSD approach would let the profession advance the state-of-the-art. Such advancement was apparently not considered to be possible within the ‘old’ system. Details of the approach used in the MTO 1983 Code are presented in the 2nd edition of the Canadian Foundation Engineering Manual (CFEM 1985).

Very soon after implementation of the 1983 Code, the industry voiced considerable criticism against the new approach, claiming that designs according to the WSD and the ULS agreed poorly in many projects, in particular for more complicated design situations, such as certain high retaining walls and large pile groups. It is my impression that many in the industry, to overcome the difficulties, continued to design the frequent simple cases according to the WSD method and, thereafter—resorting to a one-to-one calibration—determined what the ULS values shear force parameters should be in the individual cases and reported these as the design values! Hardly a situation inspiring confidence in the new code. The root to the difficulty in establishing a transition from the WSD to the ULS was in the strict application of fixed values of the strength factors to fit all foundation cases, ignoring the existing practice of adjusting the factor-of-safety to the specific type of foundation problem and method of analysis. It soon became very obvious that the to-all-cases-applicable-one-value-resistance-modification-factor approach was not workable. For the same reason, neither is the partial-factor-of-safety approach (favored in the European code).

In 1988, the Ministry decided to revise the 1983 Code. A foundation code committee reviewed the experience thus far and came to the conclusion that the partial-factor-of-safety approach with fixed values on cohesion and friction should be abandoned. Of course, the Code could not be returned to the WSD approach, nor would this be desirable. Instead, it was decided to apply resistance factors to the ultimate resistance of a foundation rather than to the soil strength and to differentiate between types of foundations and methods of determining the capacity of the foundation. In 1992, it was decided that the MTO Ontario code should be further developed into a National Code on foundations under the auspices of the Canadian Standards Association, CSA, which work resulted in the 2006 National Standard of Canada, Canadian Highway Bridge Design Code, CAN/CSA-S6-06.

The 2006 Code specifies numerous loads and load factors, such as permanent (dead), transient (live), and exceptional loads; making differences between loads due to weight of building materials, earth stress, earth fill, wind, earthquake, collision, stream flow, etc., with consideration given to the effect of various load combinations, and providing minimum and maximum ranges for the load factors. The factors combine and it is not easy to come up with an estimated average factor; the average value for a typical design appears to hover around 1.25 on dead load and 1.40 on live load. The examples of unit weights of the soil backfill material, such as sandy soil, rock fill, and glacial till, are all given with values that assume that they are fully saturated. Because most backfills are drained, and therefore not fully saturated, this is an assumption supposedly on the safe side.

Independently of the MTO, a US Committee working on a contract from the US Federal Highway Administration, FHWA, developed a limit states design manual for bridge foundations (Barker et al. 1991) employing the same approach as that used by the MTO second committee. (Because the Eurocode has stayed with the partial factor-of-safety approach, there exists now a fundamental difference between the Eurocode and the Canadian and US approaches).

The Load and Resistance Factor Design as well as the Ultimate Limit states design for footings have one major thing in common with the Working Stress Design of old. All presume that bearing capacity is a reality and that it can be quantified and therefore be assigned a safety factor (partial factor or resistance factor, as the case may be). This is a fallacy, because, while bearing capacity exists as a concept, it does not exist in reality. What matters to a structure is the movement of its foundation and that this movement be no larger than the structure can accept<sup>1)</sup>.

Deformation of the structure and its components is determined in an unfactored analysis (all factors are equal to unity)<sup>2)</sup> and the resulting values are compared to what reasonably can be accepted without impairing the use of the structure, that is, its serviceability. This design approach is called Serviceability Limit States, SLS. e.g., the Canadian Highway Bridge Design Code, CAN/CSA-S6-06. Indeed, the serviceability approach, i.e., settlement and movement calculations, is the only approach that has a rational base.

Be it working stress or limit state design, the approach with regard to footings is straight-forward. Analytically, the triple N-formula prevails and for 'bearing capacity' little distinction is made between live loads and sustained (permanent, dead) loads (other than in choosing the safety factor or the resistance factor). However, for piled foundations the situation is more complex.

The pile design must distinguish between the design for **bearing capacity** (Eq. 7.3) and design for structural strength. The capacity is determined considering positive shaft resistance developed along the full length of the pile plus full toe resistance. The loads in reference to capacity consist of dead and live load, but no drag force (the drag force does not affect the bearing capacity of the pile; drag force is of structural concern, not geotechnical; see Section 7.17).

If design is based on only theoretical analysis, the usual factor of safety is about 3.0 in working stress design (WSD) and the usually applied resistance factor in limit states design (ULS) is about 0.4. If the analysis is supported by the results of a loading test, static or dynamic, the factor of safety is reduced (or the resistance factor is increased), depending on the level of reliance on and confidence in the capacity value, number of tests, and the particular importance and expected sensitivity of the structure to foundation deformations.

A static analysis is often considered uncertain enough to warrant a factor-of-safety of 3.0 in determining the safe embedment depth. This depth only too often becomes the installation depth for the design. Yet, the uncertainty can just as well hit the other way and not only hide that much shorter piles will do, the 'designed safe' installation depth may be totally unattainable. Blindly imposing a factor-of-safety is not a safe approach. See also Section 7.13.

---

<sup>1)</sup> This notwithstanding that in the special case of a footing in clay subjected to rapid loading, bearing capacity failure may occur. The latter is a situation where pore pressure dissipation is an issue and it may affect the short-term design of silos and storage tanks. However, simple bearing capacity analysis of such cases can then not be used to model the soil response because the foundation response to load is complex and a design based on 'simple' bearing capacity calculation is rarely satisfactory.

<sup>2)</sup> As prevailing in some codes, the serviceability consists of a capacity reasoning with "resistance" factors other than those applied in an ULS approach. This is a quasi and illogical approach that does not properly address the settlement issue.

Design of foundations should be with a "belt and braces" approach, where the "belt", say, represents the capacity analysis and the "braces", thus, the settlement analysis. Far too many piled foundation designs omit the settlement analysis. However, when fretting about accidentally dropping one's pants due to a fault in the belt, strengthening the "belt" buckle will not likely make the "braces" redundant.

#### 12.4 Factor of Safety and Resistance Factors for Piled Foundations

The principle behind applying a factor of safety is to guard against the always occurring variety of conditions and outcome. A theoretical analysis comprises more uncertainties than an actual test and requires a larger factor of safety,  $F_s$ , (partially also an "ignorance factor") in order to ensure that the actual "capacity" is still larger than the actual load demand on the pile. For example, if a piled foundation comprises piles loaded by a load equal to  $X_i$ , then, a theoretical analysis needs to show a "capacity" equal to  $3X_i$  for a  $F_s$  of 3.0. Figure 12.3 shows the deviation of "capacities" of actual piles in a piled foundation from that determined in a theoretical analysis and that determined in a static loading test. As an actual test (green curve) incorporates fewer variables than a theoretical analysis (blue curve)—its curve is steeper—, a smaller  $F_s$  is acceptable, usually a factor of 2.0 is applied. The red bar and the dashed blue curve shows the frequency (or number or ratio) of piles with a "capacity" smaller than the actual demand were the design to be based on a theoretical analysis with  $F_s$  of 2.0 instead of 3.0. A similar uncertainty effect applies to resistance factors applied to a Limit States Design.

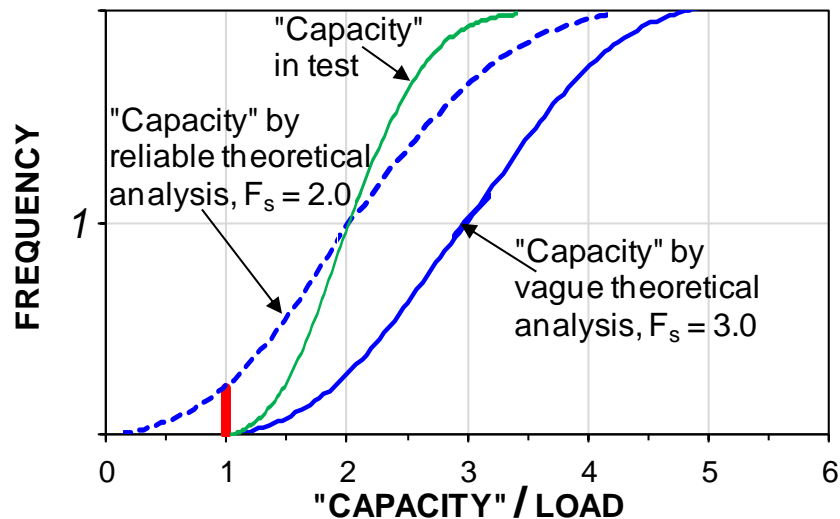


Fig. 12.3 "Capacity" determined by analysis or a loading test compared to that of an actual pile

Note because of a very large scatter of methods for determining "capacity", I strongly discourage basing a foundation design on a factor-of-safety approach, and disregarding settlement analysis. The problem is not removed by declaring that a certain method for determining "capacity" will be the one-and-only for everyone to use. The entire concept is flawed. Design of foundation should be based on deformation and settlement analysis.

#### 12.5 The Eurocode and the AASHTO Specs

The principles of the Unified Design as outlined in Section 7.17 is accepted in several standards and codes, e.g., the Canadian Highway Bridge Design Code, the Australian Piling Standard, the Hong Kong Geo Guidelines, the FHWA Pile Manual, the US Corps of Engineers Manual, to mention a few. However, two major codes, the Eurocode 7 and the AASHTO Specs, deviate considerably from those principles. The two will be discussed in the following.

### 12.5.1 The Eurocode

The Eurocode requirements for piled foundations are best demonstrated by review of two commentaries (guidelines) on the Eurocode 7 (Simpson and Driscoll 1998, Frank et al. 2004) presenting a design example comprised of a 300-mm diameter bored (circular) pile installed to 16.5 m depth through 5 m of soft clay above a thick layer of stiff clay (the two documents use the same example). The unfactored dead load assigned to the pile is 300 kN. Live load is not included.

The example information is summarized in Figure 12.4. The guidelines state that the pile shaft resistances are determined in an effective stress analysis that results in an average unit shaft resistance in the "soft clay" of 20 kPa and in the "stiff clay" of 50 kPa (50 kPa is right at the borderline between firm and stiff consistency). The toe resistance is assumed to be zero. The shaft resistances in the two layers are 94 kN and 543 kN, respectively, combining to a total capacity of 637 kN. A surcharge will be placed over the site, generating consolidation settlement. The specific surcharge stress is not mentioned. Nor is the location of the groundwater table indicated.

#### Eurocode Guide , Example 7.4 (Bored 0.3 m diameter pile)

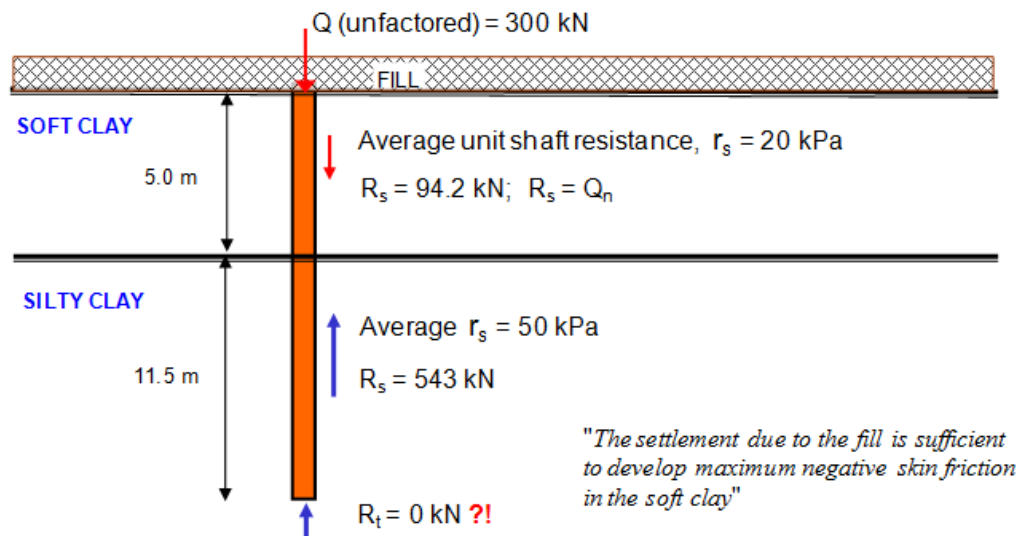


Fig. 12.4 Example 7.4 according to Simpson and Driscoll (1998) and Frank et al. (2004)

A back-calculation for the condition of the guidelines example (for long-term and when full consolidation has developed from the surcharge placed on the ground surface), applying the stated unit shaft resistance values, shows that the surcharge stress is 30 kPa, the groundwater table lies at the ground surface and the pore pressure is hydrostatically distributed with depth, the total density of the soft clay layer is  $1,800 \text{ kg/m}^3$  ( $w_n = 40 \%$ ;  $e_0 = 1.09$ ) and  $1,960 \text{ kg/m}^3$  ( $w_n = 28 \%$ ;  $e_0 = 0.74$ ) in the stiff clay layer, and the effective stress proportionality coefficient,  $\beta$ , is 0.40 in both clay layers. A beta-coefficient of 0.40 is very large for a soft clay and large for a stiff clay unless it would be a clay till or similar. However, as the stated purpose of the example is to demonstrate the Eurocode handling of negative skin friction, selecting realistic coefficients is not essential to the example.

It is likely that the piles are constructed before the surcharge is placed or before any appreciable consolidation from the surcharge has developed, which represents a short-term condition. Applying the same beta-coefficients, the effective stress calculation show the shaft resistance along the full length of the pile to be 450 kN for the short-term condition.



Checking the conditions for a conventional global factor of safety design, the factor of safety on the stated long-term capacity shows to be 2.1. Conventionally, a factor of safety of 3.0 applies to the design calculations based on theoretical static analysis. Thus, the "design" appears to be short on capacity. Had the 637-kN capacity been determined in a static loading test, the 2.1 factor of safety would have been acceptable in a conventional global factor of safety design. The factor of safety calculated for the short-term condition is 1.5, which by the conventional approach would be inadequate even if the capacity would have been determined in a static loading test!

Checking the conditions for a ULS design according to the Canadian Highway Code, the factored load is  $300 \times 1.25 = 375$  kN and the factored resistance is  $637 \times 0.4 = 255$  kN. Thus, the design is inadequate also in a ULS design.

According to Frank et al. (2004), the Eurocode considers the drag force to be a permanent load acting on the pile much the same way as the load applied to the pile head. Moreover, the assumption is made that the settlement due to the surcharge only causes negative skin friction in the soft clay (94 kN drag force) and no negative skin friction and no settlement develops in the lower layer, the stiff clay—but full positive shaft resistance does develop in that layer. Moreover, the Eurocode disregards the contribution from the shaft resistance in the soft clay layer allowing support only from the 543-kN shaft resistance in the stiff clay layer (as mentioned, the toe resistance is assumed to be zero).

Note that the original distribution of load and drag force combine to a total downward acting load of 394 kN and an upward acting force of 543 kN. That is, an unbalanced force of 147 kN. The pile should be shooting up from the ground!

The Eurocode applies the principles of ultimate limit states, ULS, for analysis of capacity (geotechnical strength), that is, factoring resistances and loads separately, requiring the sum of the factored resistances to be equal to or larger than the sum of the factored loads.

The guidelines apply two approaches to the design of the example pile. According to the Eurocode DA-1, Combination 2, ("normally considered first"), the load and resistance factors applicable to the design calculations for the dead load applied to the pile is 1.00 and the load factor for the drag force is 1.25. The resistance factor on the shaft resistance ("design resistance") is 0.77 (actually, this is the inverse of the partial factor safety, 1.30, that the Eurocode applies to shaft resistance). For the long-term condition, the sum of the factored loads is  $1 \times 300 + 1.25 \times 94 = 417$  kN and the factored resistance is  $0.77 \times 543 = 418$  kN. According to the Eurocode, therefore, the long-term condition is acceptable.

In the alternative approach, the Eurocode DA-1, Combination 1, the load factor for the dead load applied to the pile is 1.35 and the same load factor is applied to the drag force. The resistance factor on the shaft resistance is 1.00. Per the guidelines, the factored load is  $1.35 \times (300 + 94) = 532$  kN, and the factored resistance is  $1.00 \times 543 = 543$  kN. Thus, also for this approach, according to the guidelines, the long-term condition is acceptable.

For the short-term condition, it can be assumed that no drag force would have developed and, therefore, the guidelines would employ shaft resistance acting along the full length of the pile. With no surcharge effect on the effective stress distribution, short-term pile capacity is 450 kN and the short-term factor of safety is only 1.5. According to Eurocode DA-1, Combination 2, the factored load and the factored resistance are  $1.00 \times 300 = 300$  kN and  $0.77 \times 450 = 347$  kN, respectively. Thus, the Eurocode would find the pile design results acceptable also for the short-term condition. According to Combination 1, the factored load and the factored resistance are  $1.35 \times 300 = 405$  kN and  $1.00 \times 450 = 450$  kN, respectively, again showing the short-term conditions acceptable.

The foregoing is how the design approach is presented in the Simpson and Driscoll (1998) and Frank et al. (2004) commentaries (I have added the aspects of the short-term condition). In my opinion, the Eurocode approach, as presented in the two commentaries, is quite wrong—tending to be on the unsafe side. As mentioned, the guidelines state that negative skin friction only develops in the soft clay and imply that no settlement will develop in the stiff clay. This is hardly realistic. Why would negative skin friction not develop in the stiff clay? Numerous full-scale tests in different soils have shown that fully mobilized shaft shear—in the negative as well as in the positive direction—requires only a very small movement between the pile shaft and the soil. Possibly, the authors of the example had in mind that the settlement in the stiff clay is much smaller than in the soft clay and such small settlement might be of negligible concern for the structure supported on the pile(s), but that is an issue for the settlement of the foundation supported on the pile(s) and not for the development of negative skin friction and drag force. If positive direction shaft shear along the pile can be relied on during the development toward the long-term (ongoing consolidation), then, surely, the same "ability" must be assumed to be available also for the negative direction shaft shear.

In my opinion, typical and reasonable compressibility parameters for the two clay layers would be Janbu virgin modulus numbers,  $m$ , of 15 (optimistically) and 40, respectively, and re-loading modulus numbers,  $m_r$ , of 150 and 400, respectively. The virgin modulus numbers correlate to virgin compression indices,  $C_c$ , of 0.32 and 0.10, respectively (the corresponding void ratios are mentioned above). Moreover, it would be reasonable to assume that both layers are somewhat overconsolidated, and I have assumed preconsolidation margins of 5 kPa and 20 kPa, respectively. These values characterize the soft clay as compressible and the stiff clay as a soil of low compressibility. I also assume that the stiff clay layer is 15 m thick and deposited on a firm layer of minimal compressibility, e.g., a very dense glacial till.

Figure 12.5A shows the condition for the more realistic load distribution for the long-term condition when the consolidation process has developed an equilibrium between the downward acting forces and the upward acting resistances. The guidelines state that no the toe resistance is zero for the example.

The calculations of load distributions and settlement for the guidelines example and the modified example are performed using the UniPile program (Goudreau and Fellenius 2013). The analysis follows generally accepted principles of effective stress analysis as detailed in Fellenius (2012).

Figure 12.5B shows the calculated distribution of the long-term settlement of the soil and the pile. I have assumed that the pile is a single pile for which, then, the load applied to the pile will not cause any appreciable consolidation settlement below the pile toe.

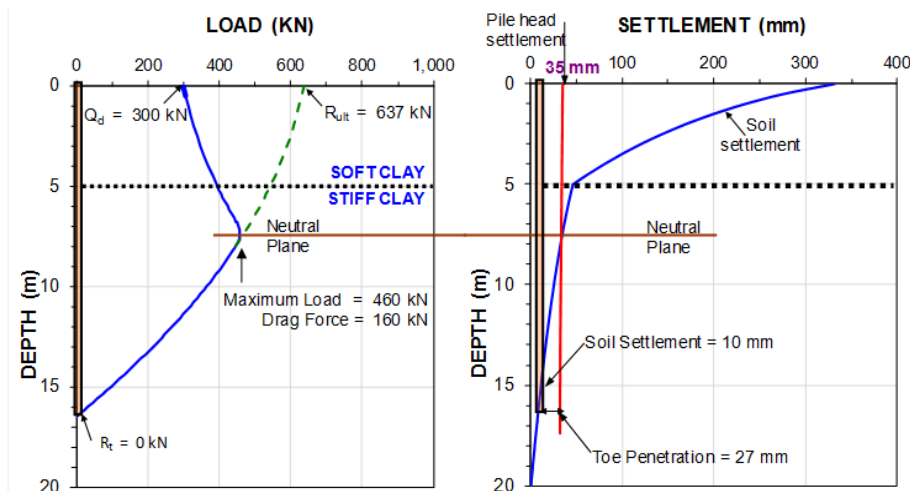


Fig. 12.5A Load distribution

Fig. 12.5B Settlement distribution

Some pile head movement (settlement) will develop due to load transfer of the 300 kN dead load to the soil during the construction of the structure. It will be limited to the compression of the pile for the imposed axial load and the small load-transfer movement of the pile element nearest the pile toe. It is not included in the 35-mm long-term settlement of the pile, which is due to downdrag, i.e., settlement due to imposed pile toe movement and a small amount from additional compression as the axial load in the pile increases.

The settlement distribution shown in the figure is that assumed developed at 90-% degree of consolidation, say, 30 years after placing the surcharge. Secondary compression would add about 10 to 20 mm of settlement to the 30-year value and then increase slightly with time. I would expect that the settlement after the first about 20 years after construction will be about 80 % of the values shown in the figure. In the long-term, the soil settlement will result in negative skin friction along the pile that will accumulate to a drag force. The drag force plus the dead load from the structure supported on the pile will always be in equilibrium with the positive direction forces. Eventually, a stationary force equilibrium will develop at a depth called "neutral plane" ("equilibrium plane" or "equipoise depth" might be better terms). For the guidelines example, as illustrated in Figure 12.4A, the neutral plane will be at a depth of 7.4 m. There is always a transition zone from negative to positive direction of shear along the pile and a small transition zone is indicated by the curved change from increasing load to decreasing. When the soil settlement relative to the pile is large, the height of the transition zone is small, when the settlement is small, the height is large. In the latter case, the drag force is smaller than in the former case. However, the location of the neutral plane for the example case is approximately the same, be the settlement small or large.

As indicated in Figure 12.4A, the drag force is 160 kN and the maximum load will be 460 kN. Below the neutral plane, in the what some call the "stable zone" (the soil is no less stable above, however), the accumulated positive shaft resistance is equal to the dead load plus the drag force, i.e., 460 kN—of course, this is what the force equilibrium means. However, the total ultimate shaft resistance is 637 kN, and after subtracting the 160-kN drag force, the remaining shaft resistance, the resistance below the neutral plane, is 477 kN, not 460 kN. The explanation to this discrepancy lies in the assumed transition zone. For example, if the transition zone is longer than the length indicated in Figure 12.4A, the drag force might reduce to, say, 100 kN, and the maximum load would become 400 kN. It would then seem as if the shaft resistance below the neutral plane, because of the equilibrium condition would be 400 kN, significantly smaller than 477 kN. The incongruity is due to comparing two mechanically conflicting conditions: when the pile responds to changing movement—is in flux—and when it is in a stationary condition.

The location of the force-equilibrium neutral plane is always the same as the location of the settlement equilibrium neutral plane, which is where there is no relative movement between the pile and the soil, i.e., where the soil and the pile(s) settle equally. (See Section 7.17 and Figure 7.31). This condition determines the settlement of the pile head after due consideration of the compression of the pile for the load between the pile head and the neutral plane. As mentioned, when the pile settlement is due to the soil dragging the pile down, it is termed "downdrag".

If one would argue that my assumed values of compressibility of the stiff clay are too conservative, and, quite optimistically, apply values resulting in much smaller consolidation settlement than shown in Figure 12.4B, then, the long-term soil settlement would still be sufficient to mobilize fully the negative skin friction and the positive shaft resistance. Indeed, were the piles to be constructed after the full consolidation had taken place, the distribution of load would still be the same as illustrated in Figure 12.4A, the final state would just take a longer time to develop. The long-term settlement would be small, of course. The transition height would therefore be longer.

Now, were the Eurocode principles applied with the correctly determined distribution of forces along the pile, the analysis would result in a factored load of  $1 \times 300 + 1.25 \times 160 = 500$  kN versus a factored resistance of  $0.77 \times 460 = 354$  kN, and the design would no longer be acceptable according to the Eurocode.

For a real case, it is likely that the stiff clay would provide some toe resistance. For example, if a 100-kN toe resistance would be included in the analysis, I think most would agree that the margin against failure of the pile would have improved. However, improvement would not be recognized in an analysis applying the Eurocode principles, because the location of the neutral plane would have moved down, the drag force would have increased by about 50 kN, and the positive shaft resistance, below the neutral plane would have decreased with the same amount. Despite the increase of capacity, the factored resistance would have become smaller by the amount of  $0.77 \times 50 = 38$  kN, and the increase of drag force would have added  $1.35 \times 50 = 68$  kN to the factored load. In effect, providing toe resistance to the pile would actually have made the Eurocode indicate that the adequacy of the pile design had gone down!

I strongly disagree with the Eurocode design principles. The magnitude of the maximum load in the pile (consisting of the dead load plus the drag force) is only of concern for the axial structural strength of the pile. In contrast, when assessing a design for bearing capacity (geotechnical strength), the drag force must not be lumped in with the load from the structure. The main requirement or premise of design for bearing capacity is the adequacy of the margin against the possibility of the loads applied to the pile could exceed total resistance of the pile, i.e., resistance acting along the entire length of the pile. The safety factors (resistance factors) are chosen to ensure a margin against that possibility. Drag force will develop only when the chosen factors are successful in providing that margin. If the factors are inadequate, the pile will start to fail, and, then, there is no negative skin friction and no drag force—nonetheless, the pile, most undesirably, fails. To avoid this misfortune, a proper design applies margins to the load and resistances. When considering the margin against failure—against the geotechnical response, i.e., capacity—the design must not add-in the drag force, which is a load that *à priori* assumes absence of failure. Indeed, the larger the drag force on a pile, the larger the margin against failure of the pile (provided the axial strength of the pile is not exceeded).

Consider a pile, similar to the guidelines example, installed in a uniform soft soil that is undergoing consolidation and has minimal toe resistance. (Such piles are often called floating piles). Assume further that the shaft resistance is about two to three times larger than the load to be applied to the pile—which would seem to be an adequate design. Eventually, a force equilibrium will develop between the downward direction loads (dead load plus drag force), and the upward direction shaft resistance with a neutral plane located somewhere below the mid-point of the pile. However, applying the Eurocode principles, the factored loads would be larger than the factored resistance. Actually, even if no dead load would be applied, the Eurocode would show that the pile would not even be adequate to support its own drag force. Indeed, when the geotechnical response is correctly analyzed, a mainly shaft bearing pile can never meet the requirements of the Eurocode.

Assume now that the pile would have a significant toe resistance, say, just about equal to the total shaft resistance and the capacity would be doubled to four to six times the applied load. Now, the neutral plane would lie deeper and the provision that all contribution to "bearing" above the neutral plane would be disregarded and instead be applied as load (drag force) would show this pile to be inadequate to support any load according to the Eurocode! In effect, the Eurocode lumping-in the drag force with the loads from the structure in assessing geotechnical pile response is absurd and leads to large unnecessary foundation costs.

I must point out that my criticism is for the Eurocode and not for the authors of the guidelines, who simply report how the code treats the design example, claiming it neither to be right nor wrong.

The guidelines example only includes a permanent load. The Eurocode, EC7 (2022) assumes that that live load and drag force act together—as if pile element would be able to have shaft shear simultaneously in negative and positive directions at the same time! They cannot. Only if the live load is about twice as large as the drag force will the maximum force in the pile (at the neutral plane) increase—by that live load, the drag force will have disappeared.

As mentioned, the objective of the guidelines example was to illustrate the principles of the Eurocode for analysis of a pile subjected to negative skin friction from settlements of the surrounding soil. It is, however, of interest to compare the settlement for the single pile to that of a group of piles. Let's assume that the example pile is one of a group of 64 piles in circular configuration at a center-to-center spacing of 4 pile diameters with a footprint of 130 m<sup>2</sup>. The load (64 x 300 kN) from the structure on the pile group will add stress (about 150 kPa, average) to the soil below the pile toe level, which will result in consolidation settlement between the pile toe level and the bearing, non-settling layer at 20 m depth. Calculations applying the method (See Chapter 7) and the soil parameters mentioned above show that the pile group will settle close to about 80 mm in the long term.

### 12.5.2 The AASHTO Specs

The AASHTO LRFD Specifications (AASHTO 2012) is very similar to Eurocode 7 in regard to principles, although the selection of factors is different. The "Specs" pertain to transportation projects, e.g., bridge foundations. It is the only Limits States geotechnical code in the USA although several guidelines, such as the FHWA Manual (2006), addressing LRFD exist that are by many taken as equal to codes. The AASHTO Code is therefore often also applied to foundations for buildings. For the most common load combination, called Strength Limit I, the AASHTO code applies a load factor of 1.25 to dead load. The load factor for drag force is 1.25. The AASHTO code specifies total stress analysis for piles in "clay", i.e., the  $\alpha$  method with a stress-independent unit shaft resistance often constant with depth, reserving effective-stress analysis, the  $\beta$  method, for piles in "sand". The stated resistance factors for ultimate shaft and toe resistance in "clay" are 0.45 and 0.40, and in "sand" 0.55 and 0.50, respectively, as recommended by O'Neill and Reese (1999). The AASHTO code applies the same approach to the drag force as the Eurocode, i.e., the drag force is considered a load similar to the dead load on the pile and no shaft resistance contribution is allowed from the soil above the neutral plane.

The AASHTO code is usually interpreted to require live load and drag force to act simultaneously. That is, the drag force is added to the applied dead load and live load on the pile in assessing the pile for bearing capacity (the Eurocode does not lump in the live load with the dead load). This notwithstanding that Article 3.11.8 of AASHTO states that *"If transient loads act to reduce the magnitude of downdrag forces and this reduction is considered in the design of the pile or shaft, the reduction shall not exceed that portion of transient load equal to the downdrag force"*. The commentary to this clause does not make the intent of the article more clear in stating that *"Transient loads can act to reduce the downdrag because they cause a downward movement of the pile resulting in a temporary reduction or elimination of the downdrag force. It is conservative to include the transient loads together with the downdrag"*. The latter is not "conservative", combining forces working in opposite directions is irrational and, therefore, including the drag force is simply "wrong".

The AASHTO Specs is now the only US Code that considers the drag force to be a load similar to that from the structure. The two other dominant piled foundation codes in the US, the FHWA (2016) and the Corps of Engineers (Greenfield and Filtz 2009), both recommend the unified method with the main "negative skin friction" issue being downdrag and the drag force being only of concern for the axial pile strength.

## 12.6 Serviceability Limit States

All designs must also consider the Serviceability Limit State, SLS; normally the state that develops in the long-term. It represents the stationary state for which the distance to the neutral plane and the load distribution stay essentially unchanged over time. (In contrast, design for ULS conditions considers the state where soil failure occurs and the pile is in flux—is moving fully mobilizing shaft resistance (along the entire length) and toe resistance).

Note, for the stationary condition—SLS—, the "assumed" values of toe resistance and toe penetration cannot be chosen independently of each other because they are interconnected by their q-z function. If the toe resistance would be assumed to be zero, this would only be possible if the q-z relation states that the toe resistance is zero regardless of toe penetration (such as for the guidelines example—a floating pile in soft clay might have next to no toe resistance). Most piles, however, will exhibit a toe resistance that is proportional to the imposed toe movement. The upper limit of toe resistance would be to assume that the neutral plane is at the pile toe level, which would result in a large toe resistance. However, in soils that would require a large toe penetration, as opposed to on bedrock, large toe resistance is not normally possible unless the downdrag is exceedingly large. In fact, for every distribution of settlement and every q-z relation, there is only one location of the neutral plane and only one value of mobilized toe resistance. That is, three interdependent parameters govern the condition and any two of them determine the third.

The objective of serviceability limit states design, SLS, for a piled foundation is to combine the geotechnical response to the dead load placed on the pile (load distribution) and the settlement distribution around the pile. This will determine the stationary conditions for the pile.

SLS is design for deformation—settlement—of the piled foundation, and it applies neither load factors nor resistance factors. The designer assesses the calculated settlement in relation to the settlement that can be tolerated by the structure. Of course, there has got to be a suitable margin between the calculated settlement and the maximum settlement the foundation can tolerate. This margin is not achieved by imposing a certain ratio between the two settlement values. Instead, in calculations using unfactored loads and resistances and applies realistically chosen values for resistances, a conservative q-z relation, and conservative values for compressibility parameters, etc., to determine the location of the neutral plane location and the downdrag. The so determined settlement must have a suitable margin to the maximum tolerable for the particular foundation and structure.

The depth to the neutral plane must be realistic. The upper boundary settlement will then represent sufficiently improbable outcome of the design; "improbable", yes, but still mechanically possible.

## 12.7 Concluding Remarks

The design for geotechnical strength, the ULS condition, addresses a non-stationary failure process—the pile is moving down relative to the soil; is in flux. By applying a factor of safety, or load and resistance factors to increase load and reduce the resistances, the designer ensures that the design has backed-off sufficiently from the possibility of the ULS condition. The premise is still that the pile would be failing! To include drag force in this scenario is a violation of principles because the pile approaches a failure condition, there is no longer any drag force present. To yet include it, perhaps defended by saying that "in a negative skin friction scenario, it is good to have some extra margin", is nothing other than design by ignorance. Why not instead boost the load factors and reduce the resistance factors? That would at least aim the ignorance toward the correct targets.

The fact is that the phenomenon of negative skin friction, NSF, resulting in drag force plus dead load in balance with positive direction forces occurs for every pile—eventually. In ultimate limit states, ULS design, whether the settlement is small or large, the NSF issue is limited to checking the adequacy of the pile axial strength, which could be a deciding factor for sites where the depth to the neutral plane is approaches about 100 times the pile diameter. Design of single piles and small pile groups must include assessing the expected settlement of the soil surrounding the pile and the downdrag of the pile(s), i.e., the settlement of the soil—and the pile—at the neutral plane in serviceability limit states, SLS. Indeed, for serviceability design, be the pile long or short, therefore, the issue is the downdrag, not the drag force. For pile groups, the settlement of the soil layers below the pile toe levels may show to be critical.

Addressing the ULS design for a NSF issue is not modeled by adding the drag force to the load from the structure. If a calculations model does not relate the depth to the neutral plane to a pertinent force equilibrium, the model would have little relevance to the actual conditions. Moreover, the tendency for many is to assume that the drag force only develops in soil that settles significantly in relation to the pile—a limit of 10 mm is often mentioned. Thus, the analysis returns a drag force conveniently small and of little bearing (pun intended) on the design calculations. In reality, long, mainly toe-bearing piles, even in soil exhibiting settlement much smaller than 10 mm, will be subjected to large drag force (which is only of concern for the axial strength of the pile). When the correct drag force and location of the neutral plane are applied, adding the drag force to the loads from the structure will result in a mechanically impossible design.

The serviceability, SLS, design must be based on a settlement analysis incorporating the pile (or piles or pile group) response to unfactored loads and unfactored responses of primarily the pile toe and the settlement of the soils as affected by the stress changes at the pile location. For a margin to represent uncertainty, the design can apply a pessimistic approach to compressibility of the soil used in the settlement analysis and the estimate of the stiffness response of the pile toe. Pessimistic, yes, but, yet, realistic.

There is a large lack of consistency in our practice for determining what really is the capacity of the pile. Yet, the practice seems to treat capacity as an assured number, proceeding to specify decimals for the various factors with no respect to how capacity was determined, the extent of the soils investigation, the number of static tests, the risks involved (i.e., the consequence of being wrong), the change with time, etc.

Most codes do either not address settlement of piled foundations or address them only very cursorily. The practice seems to assume that if the capacity has "plenty of FOS", or similar, the settlement issue is taken care of. This is far from the truth. I personally know of several projects where capacity was more than adequate with regard to geotechnical strength—the literature includes several additional cases—yet, the foundations suffered such severe distress that the structures had to be demolished.

A major weakness of most codes is that they refer to a "capacity" without properly defining what the capacity is, or not defining it by an acceptable method. See Section 8.10 and Figure 8.8.

The movements measured in a static test are from 'elastic' compression of the pile (shortening), from build-up of shaft resistance that may exhibit an ultimate—plastic—response, but more often a response that is either post-peak-softening or a strain-hardening, and from pile toe movement increasing as a function of the pile toe stiffness. There is no ultimate resistance for a pile toe! Indeed, the search for a pile capacity definition is charged with modeling the response to load by an elastic-plastic condition, when two of the three components definitely do not exhibit anything remotely like an elastic-plastic response and the third only rarely so.

As if the difficulty in choosing a suitable definition of capacity by itself would not cause enough uncertainty for applying the ULS code requirements, the practice employs a variety of definitions ranging from the Offset limit to the Chin-Kondner extrapolation (Sections 8.2 through 8.8). Basing a design on geotechnical strength—the capacity—be it by theoretical analysis or interpretation of results from a static loading test, is fraught with large uncertainty, hardly covered by the relatively small range of suggested factors of safety or resistance factors.

In answer to the requirement of the ULS condition, I prefer to recognize that what the structure supported on the piles is concerned with is the actual movement or settlement of the of the pile head, which is governed by the movement of the pile toe and soil settlement at the pile toe level, not by the shape of the load-movement curve or a value based on a pile diameter. The analyses leading up to assessing the SLS condition is the key to a successful design. Or more simply put: a large factor of safety does not ensure that the settlements will be small. However, an SLS analysis showing the settlements to be small does ensure that the capacity of the pile(s) is adequate. I am not suggesting we cease carrying out a ULS analysis, but we definitely need to improve how we do it and we need to pay more attention to the SLS.

If the Eurocode and AASHTO Specs would be combined with correct understanding of the short -term and long-term response of piled foundations, it would quickly be realized that the two codes are very wrong. Unfortunately, as they are usually applied without that understanding, they are the cause of large extra foundation costs and, yet, do not provide safe foundations. It is most urgent that the two codes be revised.

To repeat, the geotechnical designer could do well to recognize that, regardless of magnitude of safety factor and or load and resistance factors, a design based on capacity is a rather inadequate approach. Whether or not the foundation response is acceptable to a structure depends on deformation and settlement. The design should therefore foremost concentrate on establishing settlement. If settlement is not acceptable, capacity is not an issue. On the other hand, an acceptable safety against a calculated capacity does not guarantee that a foundation will not settle excessively.

Lately, people have been talking about "reliability-based design", RBD. The concept is yet not fully formulated. In broad terms, the RBD is the serviceability limit state, SLS, with reference to veracity of the data as well as to the models employed in the analyses. That is, a 'good old' settlement and deformation analysis with due consideration of how well we trust our analysis—procedures and results—and what is the risk for being wrong. Note, risk can be defined as probability of being wrong times the consequence of being wrong. Provided that the risk is small, that is, because, then, even if the probability of being wrong is recognized, but the consequence is just a matter of a small loss of money or time, we can take it on. However, when the consequence is large in terms of costs and, in particular, if it involves a consequence in terms of people getting physically hurt, then, even if the probability of it coming about is small, we may not, and should not, 'risk it'.



## CHAPTER 13

### SPECIFICATIONS AND DISPUTE AVOIDANCE

#### 13.1 Introduction and examples

Surprises costing money and causing delays occur frequently during the construction of foundation projects, and in particular for piling projects. The contract specifications often fail to spell out the responsibilities for such events and this omission invariably results in disputed claims that sometimes only can be resolved by litigation. Much of this can be avoided by careful wording of the specifications, expressing all quality requirements in quantifiable terms, and, in anticipating difficulties, setting out beforehand who is responsible.

When the unexpected occurs at a site and costs escalate and delays develop, the Contractor feels justified to submit a claim that the Owner may see little reason to accept. When the parties turn to the technical specifications for the rules of the contract, these often fuel the dispute instead of mitigating it, because the specifications are vague, unclear, unbalanced, and containing weasel clauses that help nobody in resolving the conflict. Rarely are specifications prepared for that deviations from the expected can occur.

Indeed, surprises occur frequently during the construction of foundation projects, and in particular in the case of piling projects. The surprises take many forms, but one aspect is shared between them: they invariably result in difficulties at the site and, more often than not, in disputes between the parties involved.

For example, the soil conditions sometimes turn out to differ substantially from what the contract documents indicate. For example, on a pile project, the piles do not go down as easily as anticipated by the Owner's design engineers and/or by the Contractor's estimator. Or, they may go down more easily and become much longer than anticipated. Or, a proof test shows that the pile capacity is inadequate. Or, the piles do not meet a distinct "refusal" and, consequently, the stringent termination criterion in the specifications results in a very prolonged driving causing delays and excessive wear on the Contractor's equipment.

Quite often, the Contractor's equipment appear to fail to do the job. Perhaps, the equipment required by the specifications is "misdirected". Perhaps, the Contractor is inexperienced and cannot perform well, or the equipment is poorly maintained and difficult to use. Whether or not the Contractor honestly believes that the subsequent delays, the inadequate capacity, the breakage, etc. are not his fault, he will submit a claim for compensation. Often, when the claim is disputed by the Owner, the Contractor nevertheless is awarded compensation by the court, because the contract specifications do not normally contain any specific or lucid requirement for the quality of the Contractor's equipment.

Or, the Contractor's leads are not straight and the helmet occasionally jams in the leads. However, are the leads out of the ordinary, after all, they are the same as used on the previous job—and, besides, although they are not straight can they really be called bent, or crooked?

Or, on looking down a pipe pile, the bottom of the pipe cannot be seen. Well, is then the pile bent and is it bent in excess?

Or, when the use of a water jet is required to aid the pile penetration, the pile does not advance or it advances too quickly and drifts to the side or a crater opens up in the soil next to the side of the pile. The

pump pressure and water flow are usually detailed in the specifications, but the size and length of the hose and the size of the nozzle are rarely indicated. Yet, these details are vital to the performance of the jetting system, indeed, they govern the pressure and flow (c.f., 7.20.6).

Frequently, judgments or satisfactions are to be assessed as "in the Engineer's opinion", but with no specific reference to what the opinion would be based on. Such general "come-into-my-parlor" clauses do not hold much water in court, but they are the root of much controversy.

Be careful of the meaning of the terms used. For example, 'allowable load capacity' is a totally confusing set of words. A few years ago, I worked on a litigation case where the Engineer used the words 'allowable load capacity' to indicate the required working load of the piles. Unfortunately, the Contractor interpreted the words to refer to the capacity (in the proper sense of the term as "ultimate resistance") to which he had to drive the piles with the result that the pile could not adequately carry the desired working load.

A similar confusion, but with an contrary consequence, appeared on a more recent project (nothing really changes in this regard), where the design engineer had deliberately reduced the pile lengths to about half the usual length in order to avoid driving into a boulder layer existing at depth at the site. He had, appropriately, also reduced the desired capacity and pile working load (50 tons), requiring a "capacity" of only 100 tons (on piles normally accepted and installed to a 200 ton "capacity"). The specs and drawings required piles at "100-ton capacity". However, someone—it was never determined who—thought that plain "100-ton capacity" sounded too casual and changed it to "100-ton load capacity". At the outset of the pile driving, the contractor asked what capacity he was to drive to and was told that the loads were "100 tons". So, naturally, he drove to a capacity of twice the load, which meant that the piles had to be longer and, as the designer had expected, the piles were driven into the boulder layers. The results was much breakage, problems, delays, and costs. The contractors claim for extra was \$300,000, and it was awarded.

Indeed, jargon terms can be very costly. Incidentally, of all terms, "capacity" is most often misused. It simply means "ultimate resistance" and it does not require an adjective (other than "axial" as opposed to "lateral", for example). I once saw a DOT specs text—spell-checked—requiring the Contractor to achieve an "intimate capacity". I'd say, that is a daring term in these politically correct times!

On the topic of using jargon: The word "set" is not a synonym for "blow-count" (the blows per a certain penetration length). "Set" is the penetration for one blow or, possibly for a series of blows. Its origin is an abbreviation of "settlement" meaning the penetration for one blow. I have one example of what "set" can cause: specifications stated that the Contractor was to drive the piles (concrete piles of limited strength concrete) "*to a very small set and the Contractor be cautioned not to overdrive the piles*". Of course, the Contractor took care not to damage the piles by driving them too hard, which is what "overdriving" means. In fact, the driving turned out to be very easy and several of the piles drove much deeper than the plans and drawings indicated. Unfortunately, in writing the sentence I just quoted, the spec-writer meant to warn the Contractor that the number of blows per unit of penetration (e.g., blows per foot) was expected to be very small and that the piles, therefore, could easily drive too deep. Talk about diametrically opposed interpretations. And predictable surprises. In this case, the Engineers insisted that their intended interpretation was the right one and a costly claim and litigation ensued (which the Contractor won). The word "set" is frequently misconstrued to be a synonym for "termination criterion", which, incidentally, is not the same as "blow count". As the industry has such a vague understanding of the proper meaning of the term "set", avoid using it in any context.

The jargon confusion does not get any better by shifting from "set" to "refusal". Although most people have a qualitative understanding of the meanings, one person's refusal can still be another person's promise. "Refusal" is an absolute term. It would imply that one just cannot drive the piles deeper having

exhausts all means to do so. A Contractor claiming this, is not believed. Then, specifications suggesting “a refusal of 6 blows/foot” sounds not only silly, but implies a spec writer with a poor command of language. “Termination criterion” is a neutral term that states exactly what is meant. Use it!

What about “battered”? It is a term that separates the men from the boys, or people experienced in—or at least exposed to—piling from people who are not. The latter group includes lawyers, judges, and people serving as jury members in jury trials. I once assisted a contractor who had to go to court to recover costs. This contractor had quite an uphill battle once the judge realized that the contractor had battered the piles, because the judge had experience of battered housewives and children, but he had no knowledge and little appreciation of that the term would have a discrete meaning for piling people. When the matter was made clear to him, he was quite annoyed by that a group of professionals would use a jargon term that had a perfectly suitable every-day English term available, i.e., “inclined”. I agreed then and I agree now. Please, stop using “batter”. My cry in the wilderness; it is getting worse instead of better. I recently read a journal paper where the term was used to characterize a leaning structure! "Battered Tower of Pisa" anyone?

In another court case, where the term "load test" was used, the judge wondered why it was needed to test the loads: "are they not known before the construction?" he asked. When educated that the term applies to testing a pile by placing a series of load increments on it, he requested the lawyers to use the term "loading test" to more correctly refer to what was dealt with. I have followed his admonition ever since, as you can see in Chapter 8.

Most specifications only identify a required pile driving hammer by the manufacturer's rated energy. However, the rated energy says very little of what performance to expect from the hammer. The performance of hammers varies widely and depend on pile size, choice of helmet and cushions, soil behavior, hammer age and past use, hammer fuel, etc. Whether or not a hammer is “performing to specs” is one of the most common causes of discord at a site. The reason is that most specifications are very poor in defining the hammer.

In bidding, a Contractor undertakes to construct a design according to drawings and documents. Amongst the latter are the Technical Specifications, which purport to describe the requirements for the project in regard to codes, stresses, loads, and materials. Usually, however, only little is stated about the construction. Yet, in the case of a piling project, the conditions during the construction are very different to those during the service of the foundation, and the latter conditions depend very much on the former. When the project is similar to previous projects and the Contractor is experienced and knowledgeable, the technical specifications can be short and essentially only spell out what the end product should be. Such specifications are Performance Specifications. However, these are very difficult to write and can easily become very unbalanced, detailing some aspects and only cursorily mentioning others of equal importance. A specs text, be it for Performance Specifications or for Compliance Specifications (another name is Detailed Specifications), must spell out what is optional to the Contractor and what the Contractor must comply with. Even if the intent is that the specifications be Performance Specifications, and even if they so state, most specifications are actually written as Compliance Specifications. Government specifications are almost always Compliance Specifications.

When surprises arise and the Contractor is, a consequence, slowed down, has to make changes to procedures and equipment, and loses time and money, disputes as to the interpretation of the specifications easily develop. Therefore, the writer of Specifications must strive to avoid loose statements when referring to quality and, instead, endeavor to quantify every aspect of importance. Do not just say that a pile must be straight, but define the limit for when it becomes bent! Do not just say that the pile shall have a certain capacity of such and such value, but indicate also how the capacity will be defined! Do not forget to give the maximum allowable driving stresses and how they will be measured, if measured! In short, take care not to include undefined or unquantified requirements. One of the most non-

constructive situation is when the Engineer says that a pile is damaged, or bent, or too short, etc. and the Contractor says “no, it ain’t”. The Engineer answers “it is, too!”, and before long whatever communication that existed is gone, the lawyers arrive, and everybody is a loser (well, perhaps not the lawyers).

You may enjoy the following direct quotes from contract specifications submitted by Government agencies, spelling mistakes and warts all.

1. Piles shall be driven to reach the design bearing pressures.
2. The minimum allowable pile penetration under any circumstance shall be 17 feet.
3. The Contracting Officer will determine the continued driving procedure to be followed if driving refusal occurs.
4. The hammer shall have a capacity equal to the weight of the pile and the character of the subsurface material to be encountered.
5. The hammer energy in foot-pounds shall be three times the weight of the pile in pounds.
6. Inefficient diesel, air, or steam hammers shall not be used.
7. Each pile shall be driven until the bearing power is equal to the design piles pressure.
8. All piles incorrectly driven as to be unsuitable as determined by the Contracting Officer shall be pulled and no payment will be made for furnishing, driving, or pulling such piles.
9. All piles determined to be unsuitable by the Contracting Officer shall be replaced by and at the expense of the Contractor.
10. The driving shall continue, using hammer falls of 150 mm to 200 mm in a series of 20 blows, until penetration of the pile has stopped. The height of the fall shall then be doubled and the pile again driven to refusal. This procedure shall be continued until the design load of the pile has been achieved.
11. The pile design load is defined as 1.5 times the working load. The design load will be deemed to have been achieved when the pile exhibits zero residual (= net?) set under 10 successive blows of the hammer, where each blow has a sufficient energy to cause elastic deformation of the pile at the ground level equal to the static shortening of the pile at design load, as calculated by Hooke’s Law.
12. The piles shall be driven using a single-acting diesel hammer with a minimum rated hammer energy of 63 kJ or an equivalent hammer. (*Should the "equivalent hammer" have no more than 63 kJ rated energy or not less than 63 kJ?*).

Or on having the following requirements imposed on you?

- A. The hammer shall have a capacity equal to the weight of the pile and the character of the subsurface material to be encountered.
- B. Cut off portions of pile which are battered, split, warped, buckled, damaged, or imperfect.
- C. Piles shall be driven with a single-acting, partial double-acting, or double acting diesel, air, or steam hammer developing a driving energy of not less than 32,530 newton meters per blow with a minimum ram weight of 3,175 kilograms for an air or steam hammer and 454 kilograms for a diesel hammer.
- D. Where unwatering is required, the Contractor shall effect a dewatering scheme.

- E. The founding elevation shall be established by driving to a set [sic!] determined in accordance with the dynamic formula specified or by the application of the wave equation analysis procedure that verifies the pile resistance. When new conditions such as change in hammer size, change in pile size or change in soil material may occur, new sets shall be determined.
- F. Hammer performance shall be verified to ensure that the actual potential energy is not less than 90 % of the stated potential energy.
- G. When the hammer performance is requested to be verified, all costs associated with this work will be included in the contract price when the energy delivered is less than 90 % of the stated potential energy specified in the submission. When the energy is greater than 90 % of the potential energy stated in the required submission, the costs will be paid as extra work.

I promise you that the above quotes are real and not made up by me for the occasion. I am sure that many of you have similar and worse examples to show. However, when you stop smiling, you should ponder what depths of ignorance and incompetence the nineteen quotes represent. And also ponder the consequence to Society for our industry having to function with such players in charge of the purse strings.

The following specs requirements I have not actually seen, but I would not be surprised if I were to find them or something similar to them one of these days:

- If the work is doed without no extra expense to the Contractor, then the work will be tookdown and doed over again until the Contractor's expense is satisfactory to the Engineers.
- If something is drawned wrong, it shall be discovered, corrected, and doed right with no extra expense to the Owner.
- The bid of any contractor walking around on the site with a smile on his face will be subjected to review.

### **13.2 A few special pointers**

Instead of specifying a pile driving hammer by its rated energy, specifications should specify a hammer by the energy transferred to the pile and the impact force delivered to the pile, which are well defined and measurable quantities. In the design phase, energy and force values should be obtained by means of a wave equation analysis. The wave equation analysis will "marry" the hammer to the pile and soil and to the particular drivability conditions and desired capacity. Naturally, the Contractor has the right to expect that the values specified are correct.

More often than not, the analysis will show that theoretical analysis alone is not able to sufficiently accurately determine the hammer requirements. This is then not an argument against performing the analysis or for not specifying the values. It is an argument addressing the inadequacy of omitting hammer details or just giving a rated energy, which puts the risk onto the Contractor. It is also an argument demonstrating the Owner's obligation to find out ahead of time, or at the outset of a project, what the correct hammer values are. For example, by means of taking dynamic measurements with the Pile Driving Analyzer (PDA). PDA measurements are since many years routinely used to finalize a pile design in connection with test driving or during the Contractor's installation of index piles.

When the potential use of the Pile Driving Analyzer (PDA) is included in the technical specifications, then, if during the course of the piling work, reasons arise to question the hammer performance, the PDA can quickly and with a minimum of fuss be brought to the site and the hammer can be accepted or rejected as based on the agreement of the measurements with the specified values. Opinion may differ with regard to the adequacy of the specified values, but such differences are technical in nature and easily resolved without involving the lawyers.

Dynamic measurements may interfere with the Contractor's work, therefore, the general section of the specifications should contain a clause that outlines how the measurements are performed and what the responsibilities are for the parties involved, as well as how the work is going to be paid.

Dynamic measurements are also commonly carried out to determine pile capacity and integrity. Notice, the PDA measurements need analysis to be useful. Also, the data must be combined with conventional records of the pile installation.

Further, what is bent by bending and doglegging of a pile must be defined by a specific bending radius defining straightness, and out-of-location need to be defined by means of specific tolerances. For example, before driving piles must not be bent more than a specific arc of curvature over a certain distance. After driving the bending radius must not be smaller than a certain value. For pipe piles, this is readily determined by means of an inspection probe designed to jam in the pipe at this radius (Detailed in the Canadian Foundation Engineering Manual 1985; 1992). A pipe pile for which the bottom cannot be seen, but into which the probe reaches the bottom, is then by definition straight and acceptable.

The need for well written and well thought-through specifications is illustrated by the following summary of four cases of project disputes that went to litigation.

1. Overdriving of a group of steel piles. Several steel piles were to be driven into a dense sand to a predetermined embedment depth of 85 feet. Already at a depth of about 30 ft, penetration resistance values began to exceed 200 blows/foot. The 'Engineer' insisted that the Contractor drive the piles to the specified depth despite that driving required an excess of 1,000 blows/foot! A "post mortem" review of the records makes it quite clear that although the heads of the about 90 feet long piles were beaten into the specified 5-ft stick-up above the ground surface, the pile toes probably never went past a depth of 60 feet. The Contractor had planned for a two-week project in early Fall. In reality, it took almost three months. As the project was located north of the 60th parallel, one can perhaps realize that the subsequent claim for \$6,000,000 was justified. Incidentally, the Contractor could not get out of his obligation to drive the piles. His bond saw to that. However, he won the full amount of his claim from the Owner. The Owner later sued the Engineer for negligence and won. The Engineer went bankrupt.
2. Complete breakdown of communications between Contractor and Engineer. A Contractor got permission to use a heavy diesel hammer at an energy setting lower than the maximum which, according to the hammer manufacturer's notes would be equal to the rated energy for a smaller hammer given in the specifications for the project. At the outset of the piling, it became obvious that the piles drove very slowly at that setting, requiring more than 1,000 blows before the specified termination criterion (minimum depth) was reached. Static testing showed that the capacity was insufficient. The specifications included provision for jetting and the Engineer required this for all piles. Yet, it was clear that the pile could be driven down to the depths and capacities quickly and without jetting if the hammer was set to work at the maximum energy setting. Of course, this meant that the hammer energy was to be set at a values higher than that given in the specifications. The Engineer was willing to accept this change. However, the Contractor required extra payment for the deviation from the contract to do this, which the Engineer did not want to grant. One thing led to another. The Contractor continued to drive at reduced hammer setting and diligently worked to adhere to the smallest detail of the specification wordings. The Engineer refused to budge and

required jetting and recorded everything the Contractor did to ensure that, as the Contractor now wanted to follow the specs to the letter, he was not to deviate from any of the details. Incidentally, the specifications called for outside jetting (rather than interior jetting) in silty soil, which resulted in drifting, bending, and breaking of piles. The final suit involved claims for compensation of more than \$10,000,000. The Contractor won about 40 % of the claim.

3. Specification for a near-shore piling project required piles to be driven flush with the sea bottom by means of a follower and stated that the follower should have ‘sufficient impedance’, but did not explain what this was and nobody checked the impedance of the follower. The Contractor drove the piles with a follower consisting of a steel pipe filled with wood chips. As the driving proceeded, the wood chips deteriorated and it became harder and harder to drive the piles. This was thought to be caused by densification of the sand at the site and the Contractor stated that the soil report failed to show that densifiable soils existed at the site and claimed compensation for changed soil conditions. The contract required that dynamic measurements be performed at the project, and they were. However, the results of the PDA measurements were not looked at by anyone! Eventually they were, of course, and it became obvious to all that the root of the problem was with the inadequate follower. Well, better late than never, but the delay certainly cost the parties a bundle of money.
4. Long prestressed piles were required to support a new dock for a port extension. The soil profile consisted of an about 35 m to 40 m very soft soil deposit with some dense sand layers of varying thickness and depth, followed by very dense gravel and sand with boulders. The depth to the bearing soil layer required piles of such length that they became heavier than the available equipment could handle. The piles problem was solved by building the piles as composite piles, the upper about 30 m long solid concrete section and a lower about 15 m long H pile section. The penetration into the dense soil was expected to vary because of the presence of the boulders. During driving through the soft soils, care was taken not to drive too hard as this would have induced damaging tension in the pile. However, when the pile toe reached the dense soil and the penetration resistance increased, the hammer was set to hit harder to build up capacity and to advance the H pile extension into the bearing layer. Several piles broke already at moderate blow-count and others a few feet further into the very dense bearing layer during hard termination driving. Expressed reasons for the breakage ranged from poor quality of the piles through sudden barge movements and inadequate equipment and/or use of wrong pile cushions. Not until the case was before the courts was it established that the H pile extension was so light that the impact wave on reaching the end of the concrete section, which was in the very soft soil, a large portion of the wave was reflected as a tension wave. Because the pile toe was in the dense soil, when the remainder of the wave reached the pile toe, a strong compression wave was reflected. The low blow-count and good toe response made the hammer ram rise high and provide the next blow as a stronger impact to the pile. The tension from the end of the concrete section being proportional to the impact force, therefore, reached damaging levels. A study compiling driving logs showed that the breakage correlated well with the presence of soft soil at the bottom end of the concrete section. Dynamic measurements had been conducted for determining capacity early in the project. The ‘post mortem’ study of the records established that when the bottom end of the concrete section was in soft soil, tension reflections occurred that exceeded safe levels.

It is not possible to give too many details on projects that went to dispute, because space limitation precludes giving an adequately impartial background to the cases. An account giving some of the details could easily appear slanted toward one or the other of the various players, who may then be justified in feeling slighted. Therefore, only the above cursorily information is presented in these notes.

Lucid, comprehensive, and equitable specifications are necessary for successful projects. However, even when the specs are good, if the communication lines break down, the project may still end up keeping our fellow professionals in the legal field living well. However, it is my experience that rarely are the initial ‘surprises’ and difficulties such that the parties really need to go the full way of the courts. Instead of

posturing and jockeying for legal position, if the parties show a bit of good intent and willingness to understand each other and make some effort toward finding out what really is happening and why so, litigation can often be avoided. When people keep talking to each other, an understanding can usually develop that the specs are unclear or special technical difficulties have indeed arisen, and that some common sense 'horse trading' may settle the money issues. Going to court should be a last resort.



## CHAPTER 14

### TERMINOLOGY AND STYLE

*Quote: English can be understood through tough thorough thought, though*

#### 14.1 Introduction and Basic Definitions

There is an abominable proliferation of terms, definitions, symbols, and units used in papers and engineering reports written by the geotechnical community. Not only do the terms vary between authors, many authors use several different words for the same thing, sometimes even in the same paper or report, which makes the documents difficult to read and conveys an impression of poor professional quality. More important, poor use of terminology in an engineering report could cause errors in the design and construction process and be the root of a construction dispute, which, ultimately, the report writer may have to defend in litigation. Throughout this book, I have strived to employ a consistent terminology as summarized in this chapter.

Figure 14.1 illustrates the main definitions and preferred piling terms, which subject area houses the greatest proliferation of muddled-up terms.

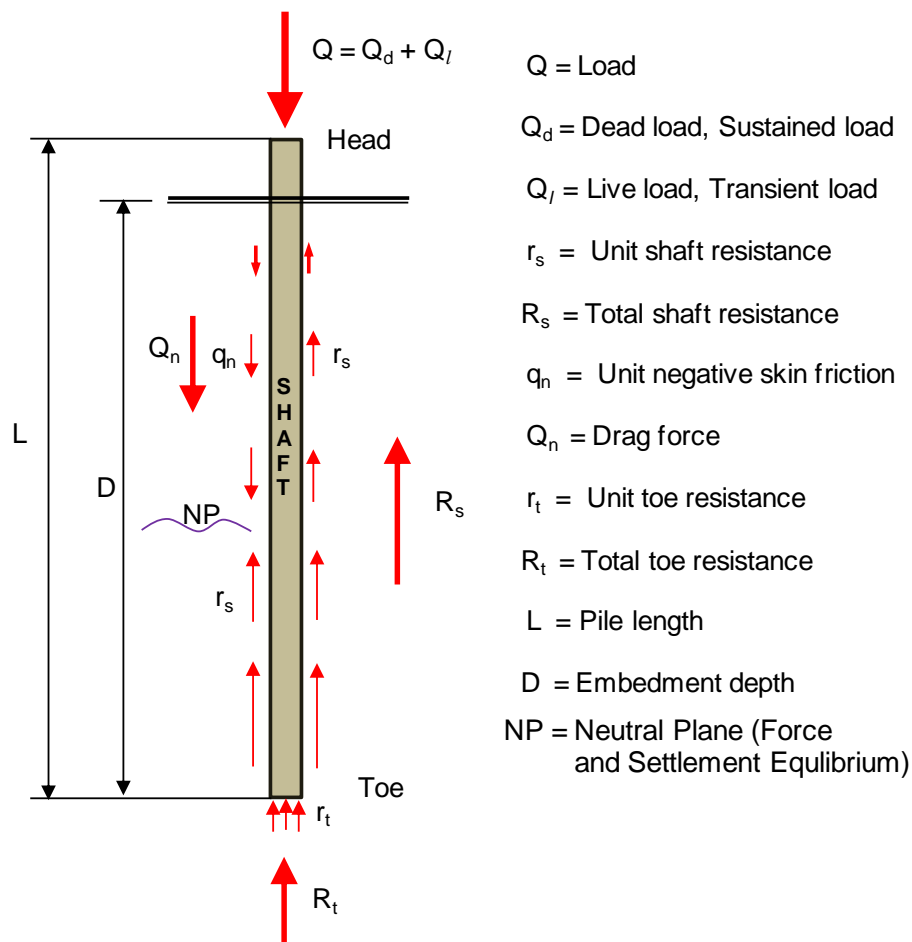


**Fig. 14.1. Definitions and Preferred Terms**

### Upper End of a Pile

One of the most abused terms is the name for the upper and lower ends of a pile. Terms in common use are, for the upper end, “top”, “butt”, and “head”, and for the lower end, “end”, “tip”, “base”, “point”, “bottom”, and “toe”.

The term “top” is not good, because, in case of wood piles, the top of the tree is not normally the 'top' of the pile, which can and has caused confusion. Also, what is meant by the word “top force”? Is it the force at the 'top of the pile' or the maximum (peak) force measured somewhere in the pile? “Butt” is essentially a wood-pile term. “**Head**” is the preferred term, as for example: “the forces were measured at the pile head”.

### Lower End of a Pile

With regard to the term for the lower end of a pile, the word “tip” is easily confused with “top”, should the latter term be used—the terms are but a typo apart. A case-in-point is provided by the 3rd edition (1992) of the Canadian Foundation Engineering Manual, Page 289, 2nd paragraph. More important, “tip” implies an uttermost end, usually a pointed end, which is not the way a pile is shaped.

The term “end” is not good for two reasons: the pile has two ends, not just one, and, more important, “end” has a connotation of time. Thus, “end resistance” implies a “final resistance”.

“Base” is not a bad term. However, it is used mainly for shallow footings, piers, and drilled-shafts. “Point” is often used for a separate rock-point, that is, a pile shoe with a hardened tip (see!) or point. Then, before driving, there is the point of the pile and on the ground next to the pile lies the separate rock-point, making a sum of two points. After driving, only one, the pile point, remains. Where did the other one go? And what is meant by “at a point in the pile”? Any point or just the one at the lower end?

The preferred term is “**toe**”, as it cannot be confused with any other term and it can, and is, easily be combined with other terms, such as “toe resistance”, “toe damping”, “toe quake”, etc.

Other than for its human connotation, the word “bottom” should be reserved for use as reference to the inside of a pile, for instance, when inspecting down a pipe pile, "the bottom of the hole", and such.

### The Pile Shaft

Commonly used for the part of the pile in between the head and toe of the pile are the terms “side”, “skin”, “surface”, and “shaft”. The terms “skin” and “shaft” are about as frequent. “Side” is mostly reserved for stubby piers. “Surface”, although is used, the term is not in frequent use. The preferred term is “**shaft**” because “skin” is restricted to indicate an outer surface and, therefore, if using “skin”, a second term would be necessary when referring to the actual shaft of the pile.

### Other Preferred Piling Terms

A word often causing confusion is “capacity”, especially when it is combined with other words. “Capacity” of a unit, as in “lateral capacity”, “axial capacity”, “bearing capacity”, “uplift capacity”, “shaft capacity” and “toe capacity”, is the **ultimate resistance** of the unit. The term “ultimate capacity” is a tautology, a mixed metaphor to avoid, although it cannot be misunderstood. However, the meaningless and utterly confusing combination terms, such as “load capacity”, “design capacity”, “allowable capacity”, “carrying capacity”, “load carrying capacity”, even “failure capacity”, which can be found in many papers, should not be used. (I have experienced a court case where the single cause of the \$300,000 dispute turned out to originate from the designer’s use of the term “load capacity” to mean

capacity, while the field people believed the designer's term to mean "allowable load". As a factor of safety of 2 was applied, the field people drove—attempted to drive—the piles to twice the capacity necessary with predictable results. Use "**capacity**" as a stand-alone term and as a synonym to "**ultimate resistance**".

Incidentally, the term "ultimate load" can be used as a substitute for "capacity" or "ultimate resistance". Its use could be acceptable is used to mean the capacity evaluated from the results of a static loading test, but it would just be confusing to have one term for a result of a test and another for result of an analysis.

As to the term "resistance", it can be modified to "ultimate resistance", "mobilized resistance", "shaft resistance", "toe resistance", "static resistance", "initial shaft resistance", "unit toe resistance", etc. If not referring to "ultimate resistance" as a force or stress, usually, it is better to use the term "response".

Obviously, combinations such as "skin friction and toe resistance" and "bearing of the pile toe" constitute poor language. They can be replaced with, for instance, "shaft and toe resistances", and "toe resistance" or "toe bearing", respectively. "Shaft bearing" is not commonly used.

Resistance develops when the pile forces the soil: "positive shaft resistance", when loading the pile in compression, and "negative shaft resistance", when loading in tension. The term "skin friction" by itself should not be used, but it may be combined with the 'directional' words "negative" and "positive": "Negative skin friction" is caused by settling soil and "positive skin friction" by swelling soil.

The terms "load test" and "loading test" are often thought to mean the same thing. However, the situation referred to is a test performed by loading a pile, not a test of a load, i.e., for finding out what load that is applied to a pile. Therefore, "**loading test**" is the semantically correct and the preferred term. Arguing for the term "loading test" as opposed to "load test" may suggest that I am a bit of a fusspot. I may call this favorite desserts of mine "iced cream", but most say "ice cream". In contrast, "iced tea" is the customary term for the thirst-quencher, and the semantically correct, and the normally used term for cream-deprived milk is "skimmed milk", not "skim milk". By any name, though, the calories are as many and a rose would smell as sweet. On the other hand, laymen, call them lawyers, judges, or first-year students, do subconsciously pick up on the true meaning of "load" as opposed to "loading" and are unnecessarily confused wondering why engineers desiring to determine the load that's going to be placed on a pile look down the soil instead of up the structure. So, why not use the term "loading test"?

While the terms "static loading test" "static testing" are good terms, do not use the term "dynamic load testing" or worse: "dynamic load test". Often a capacity determination is not even meant by these terms. Use "**dynamic test**" or "**dynamic testing**" and, when appropriate, "capacity determined by dynamic testing" (or "by a dynamic test").

When presenting the results of a loading test, many authors write "load-settlement curve" and "settlement" of the pile. The terms should be "**load-movement curve**" and "**movement**". The term "settlement" must be reserved to refer to what occurs over long time under a more or less constant load smaller than the ultimate resistance. The term "displacement" should not be used as synonym for "movement", but preferably be reserved for where soil actually has been displaced, e.g., moved aside. The term "deflection" instead of "movement" is normally used for lateral deflection, but "displacement" is also used for this situation. "Compression", of course, is not a term to use instead of "movement" as it means "shortening".

In fact, as mentioned in Chapter 3, not just in piling terminology, but as a general rule, the terms "movement", "settlement", and "creep" all mean deformation. However, they are not synonyms and it is important not to confuse them.

When there is a perfectly good common term understandable by a layman, one should not use professional jargon. For example, for an inclined pile, the terms “raker pile” and “batter pile” are often used. But “a raker” is not normally a pile, but an inclined support of a retaining wall. As to the term “batter”, I have experienced the difficulty of explaining a situation to a judge whose prior contact with the word “batter” was with regard to “battered wives” and “battered children” and who thought, no, was convinced, that “to batter a pile” was to drive it abusively! The preferred term is “**inclined**”.

The word “set” is a short form of “settlement”, but means penetration for one blow, often penetration for a series of blows. Sometimes, “set” is thought to mean “termination criterion” and applied as blows/inch! The term “set” is avoidable jargon and should not be used. (See my expanded comment in Chapter 12).

The word “refusal” is another example of confusing jargon. It is really an absolute word. It is often used in combinations, such as “practical refusal” meaning the penetration resistance for when the pile cannot reasonably be driven deeper. However, “refusal” used in a combination such as “refusal criterion” means “the criterion for (practical) refusal”, whereas the author might have meant “**termination criterion**”, that is, the criterion for when to terminate the driving of the pile. Avoid the term “refusal” and use “penetration resistance” and “termination criterion”, instead. (See my expanded comment in Chapter 12).

Terms such as “penetration resistance”, “blow-count”, and “driving resistance”, are usually taken to mean the same thing, but they do not. “**Penetration resistance**” is the preferred term for the effort required to advance a pile and, when quantified, it is either the number of blows required for the pile to penetrate a certain distance, or the distance penetrated for a certain number of blows.

“**Blow-count**” is a casual term and should be used only when an actual count of blows is considered. For instance, if blows are counted by the foot, one cannot state that “the blow-count is so and so many inches per blow”, not even say that it is in blows/inch, unless inserting words such as: “which corresponds to a penetration resistance of ...”. Obviously, the term “equivalent blow-count” is a no-good term. In contrast, when the actual blow-count is 0.6 inch for 9 blows, the “equivalent penetration resistance” is 15 blows/inch.

“Driving resistance” is an ambiguous term, as it can be used to also refer to the resistance in terms of force and, therefore, it should be avoided.

Often, the terms “allowable load”, “service load”, “working load” are taken to be equal. However, “allowable load” is the load obtained by dividing the capacity with a factor of safety. “Service load” or “working load” is the load actually applied to the pile. In most designs, it is smaller than the “allowable load”, and usually equal to “unfactored load”, a concept used in the LRFD approach. The term “design load” can be ambiguous—if using it, make sure to supply a clear definition.

The term for describing the effect of resistance increase with time after driving is “**set-up**” (soil set-up). Do not use the term “**freeze**” (soil freeze), as this term has a different meaning for persons working in cold regions of the world.

Soils can include water and be “moist”, “wet”, “damp”, and “saturated”. The measurement of the amount of water is the content of water in relation (percentage) of the weight of the solids, the dry weight. The term “moisture content” is sometimes used in the same sense as “**water content**”. However, the term “moisture content” is a spot-on example of an obfuscating jargon term to avoid. Most people, even geotechnical engineers, will consider that calling a soil “moist”, “damp”, or “wet” signifies three different conditions of the soils (though undefined). Moreover, a layman can understand what “water content”

means, as well as the terms “moisture” and “content”, when encountered separately, but understanding the meaning of the combination: “moisture content”, requires geotechnical training (read: “indoctrination”). It follows that laymen ( read: lawyers and judges) will believe and expect that “moisture content” is something different to “water content”, perhaps thinking that the former indicates a less than saturated soil. Yet, there is no difference. It is only that replacing the word “water” with “moisture” implies, or intends to imply, that the speaker possesses a greater degree of educational sophistication than conveyed by simply saying “water content” and, because the term is not immediately understood by the layman, it intends to send the message that the Speaker is in the “know”, a specialist of some stature. Don't fall into that trap. Use “water content”. Jargon that has no other purpose than to make the subject matter incomprehensible for the uninitiated is bad technical writing. We should strive to use simple terms that laymen can understand.

So, if “moisture content” is used because it is perceived to make the author appear refined and a true expert. Would someone writing “humidity content” then look even more refined? Or, could “wetness content” perhaps elevate that lofty goal? Then, why not use the even more ‘refinedly’ sounding term: “wetness quotient”? Please, the word to use to modify “content” is “water”!

In this context, note that the terms “moist density” and “wet density” do not mean “saturated density”.

Avoid the term “timber pile”, use “wood pile” in conformity with the terms “steel pile” and “concrete pile”.

Do not use the term “reliability” unless presenting an analysis based on probabilistic principles.

Unlike many other languages, English provides the means to express the important fact that soil forces have direction whereas forces in water do not. Expressed differently, stress is a tensor, while pressure is isotropic. Therefore, it is fundamentally wrong to state that a certain load on a footing results in a certain “pressure”. The term to use is “stress”—there is no pressure between soil particles—and it is important to recognize the distinction between soil and water in response to force. Logically, therefore, the old terms “earth pressure” and “earth pressure coefficient” should be “earth stress” and “earth stress coefficient”.

One of the silliest mistakes—unfortunately, also a very common one—is to use the word “predict” as a synonym to “calculate” or “compute”. Synonyms of “to predict” are “to forecast” or “to prophesy”. One does not “predict” the response of a pile from, say, pile test data. When a response is already known, one “calculates” or “computes”. “Prediction” is an absolute term, and it must only be used for a calculation that is truly a prediction of an expected behavior—indeed, a forecast. A design is based on prediction from available data and calculation results. That is, the latter are themselves not predictions, but the use of them in a design is.

The terms “specific weight” and “specific gravity” were canceled as technical terms long ago, but they are still found in many professional papers. “Specific weight” was used to signify the weight of material for a unit volume. However, the proper terms are “**solid density**” and “**unit weight**” (the units are mass/volume and force/volume, respectively). The dimensionless term “specific gravity” was used to mean the ratio of the density of the material over the density of water. The internationally assigned term for this ratio is “relative density”, which term, unfortunately, conflicts with the geotechnical meaning of the term “relative density” as a classification of soil density with respect to its maximum and minimum density. For the latter, however, the internationally assigned term is “**density index**”.

## 14.2 Brief Compilation of Some Definitions and Terms

**Bored pile** - A pile that is constructed by methods other than driving, commonly called **drilled shaft**.

**Buried pile** - See **Bored pile**

**Caisson** - A large, deep foundation unit other than a driven or bored pile. A caisson is sunk into the ground to carry a structural unit.

**Capacity** - The maximum or ultimate soil resistance mobilized by a foundation unit. A capacity must always be coupled to its associated movement. Note, modifiers such as "load capacity", "allowable capacity", "design capacity", "axial capacity", etc. are misleading and false terms that should never be used.

**Capacity, bearing** - The maximum or ultimate soil resistance mobilized by a foundation unit subjected to downward loading.

**Capacity, geotechnical** - See **capacity, bearing**.

**Capacity, lateral** - The maximum or ultimate soil resistance mobilized by a foundation unit subjected to horizontal loading.

**Capacity, structural** - The maximum or ultimate strength of the foundation unit (a poor term to use).

**Capacity, tension** - The maximum or ultimate soil resistance mobilized by a foundation unit subjected to tension (upward) loading.

**Consolidation** - The dissipation of excess pore pressure in the soil.

**Creep** - Deformation continuing under constant shear force.

**Cushion, hammer** - The material placed in a pile driving helmet to cushion the impact (formerly called "capblock").

**Cushion, pile** - The material placed on a **pile head** to cushion the impact.

**Dead load** - See **Load, dead**.

**Direction** - Direction of soil movement along a pile; negative if downward and positive if upward. See **skin friction** and **shaft resistance**.

**Downdrag** - The downward **settlement** of a deep foundation unit due to settlement at the **neutral plane** "dragging" the pile along; expressed in units of movement (mm or inch).

**Drag force** - The maximum **force** transferred to a deep foundation unit from accumulated **negative skin friction** and occurring at the **neutral plane (Equipoise)**

**Drag load** - See **Drag force**. "Drag load" implies that the drag force would be similar to a working load and this *faux pas* is avoided by the term "force".

**Drilled shaft** - See **Bored pile**.

**Dynamic method of analysis** - The determination of **capacity, impact force, transferred energy**, etc. of a driven **pile** using analysis of measured **stress-waves** induced by the driving of the pile.

**Dynamic monitoring** - The recording of strain and acceleration induced in a pile during driving and presentation of the data in terms of stress and **transferred energy** in the pile as well as of estimates of **capacity**.

**Equilibrium Plane** - A term for **neutral plane** that emphasizes that its depth is equal for the **Force Equilibrium** and **Settlement Equilibrium**, that is, the location where equilibrium exists between (1) the sum of downward acting permanent load applied to the pile together with **drag force** due to accumulated **negative skin friction** and (2) the sum of upward acting **positive shaft resistance** and mobilized **toe resistance** [Perhaps the best term for where the equilibrium of force and settlement are at equal depth should be called "the Equipoise"].

**Factor of safety** - The ratio of maximum available resistance or of the **capacity** to the allowable or to the working stress or load.

**Force** - A consequence of applying a **load** to a pile or soil or consequence of imposed settlement.

**Force Equilibrium** - The depth to maximum axial force in the pile, considering the force distribution. Can be at any depth, but is equal to the **Equilibrium Plane** if the depth is equal to the depth of the **Settlement Equilibrium**.

**Foundation unit, deep** - A unit that provides support for a structure by transferring load or stress to the soil at depth considerably larger than the width of the unit. A **pile** is the most common type of deep foundation unit.

**Foundations** - A system or arrangement of structural members through which the loads are transferred to supporting soil or rock.

**Full displacement pile, FDP** - A bored pile where the soil has been displaced rather than excavated.

**Groundwater table** - The upper surface (boundary) of the zone of saturation in the ground.

**Impact force** - The peak force delivered by a pile driving hammer to the **pile head** as measured by means of **dynamic monitoring** (the peak force must not be influenced by soil resistance reflections).

**Kentledge** - Term for loaded platform serving as reaction to the load applied to a pile in a static loading test. Originally the term for the ballast placed in a ship to ensure stability. Sometimes, and incorrectly, used for other reaction arrangements. The term is unnecessary jargon to avoid. Best is to use "loaded platform".

**Live load** - See **Load, live**.

**Load, allowable** - The maximum load that may be safely applied to a **foundation unit** under expected loading and soil conditions and determined as the **capacity** divided by the **factor of safety**. When "allowable" is used as a modifier with a second adjective, it refers to a maximum notwithstanding that the actual **working load** could be smaller.

**Load, applied, or load, service, or load, working** - The load actually applied to a foundation unit.

**Load, dead, or load, sustained, or load, permanent** – The "always there" load applied to a foundation unit.

**Load, design** - A term that easily confuses and best avoided.

**Load factor** - A reduction factor applied to a **working load** always considered together with a "resistance factor" applied to the **ultimate resistance** of a foundation unit.

**Load, factored** - A load increased by multiplication with the appropriate load factor.

**Load, live, or load, transient, or load, temporary** - The "there today, gone tomorrow" load actually applied to a foundation unit. "Sustained live load" is a misnomer to avoid. It tries to recognize that some loads called live or transient loads in structural design are really functioning as permanent or dead loads in geotechnical design.

**Load test** - a term loosely meaning **loading test**. However, the issue is not testing a load but performing a test by loading a pile or a footing.

**Loading test** - a test applying a series of load to a foundation unit (a pile or a footing) while monitoring the response of the unit.

**Neutral plane** - See Equilibrium Plane.

**Pile** - A slender **deep foundation unit**, made of wood, steel, or concrete, or combinations thereof, which is either premanufactured and placed by driving, jacking, jetting, or screwing, or cast-in-situ in a hole formed by driving, excavating, or boring. A pile can be a non-displacement, a low-displacement, or displacement type.

**Pile head** - The uppermost end of a **pile**.

**Pile impedance** -  $Z = EA/c$ , a material property of a pile cross section determined as the product of the Young's modulus (E) and area (A) of the cross section divided by the **wave speed** (c).

**Pile point** - A special type of **pile shoe**.

**Pile shaft** - The portion of the pile between the **pile head** and the **pile toe**.

**Pile shoe** - A separate reinforcement attached to the **pile toe** of a pile to facilitate driving, to protect the lower end of the pile, and/or to improve the toe resistance of the pile.

**Pile toe** - The lowermost end of a **pile**. (Use of terms such as pile tip, **pile point**, or pile end in the same sense as pile toe is discouraged).

**Pore pressure** - **Pressure** in the water and gas present in the voids between the soil grains minus the atmospheric pressure.

**Pore pressure, artesian** - **Pore pressure** in a confined body of water having a level of **hydrostatic pressure** (head) higher than the distance to the ground surface.

**Pore pressure, hydrostatic** - **Pore pressure** distribution as in a free-standing column of water (no gradient).

**Pore pressure elevation, phreatic** - The elevation of a **groundwater table** corresponding to a **hydrostatic pore pressure** equal to the actual **pore pressure**.

**Pore pressure gradient** - Non-hydrostatic pore pressure. The gradient can be upward or downward. At downward gradient, effective stress increases more than it would in a hydrostatic condition.

**Pressure** - Omnidirectional force per unit area. It must not be confused with the unidirectional force per unit area induced by, say, a loaded footing or the axial stress in a pile. (Compare **stress**).

**Resistance factor** - A reduction factor applied to a the **ultimate resistance** of a foundation unit and always considered together with a **load factor**.



**Resistance, factored** – A resistance reduced by multiplication with the appropriate **Resistance factor**.

**Resistance, ultimate** – Synonym to **capacity**.

**Secondary Compression - Settlement** occurring when there is no change of effective stress, but instigated at the start of consolidation, though, sometimes thought of as only occurring after end of primary consolidation. It should not be called "**creep**", as shear forces are not involved.

**Settlement** - The downward movement of a foundation unit or soil layer due to rapidly or slowly occurring compression of the soils located below the foundation unit or soil layer, usually requiring an increase of effective stress due to an applied load or lowering of pore pressure. When no change of effective stress occurs, the term is "**secondary compression**".

**Settlement Equilibrium** - The depth where there is no relative movement between a pile and soil. Can be at any depth, but is equal to the **Equilibrium Plane** if the same as the depth of the **Force Equilibrium**.

**Shaft resistance, negative** - Soil resistance acting downward along the pile because of an uplift load.

**Shaft resistance, positive** - Soil resistance acting upward along the pile shaft due to an applied load inducing compression in the pile.

**Shear velocity** - Particle velocity of a soil element

**Skin friction, negative** - Soil resistance acting downward along the pile shaft as a result of movement of the soil along the pile inducing compression in the pile.

**Skin friction, positive** - Soil resistance acting upward along the pile shaft caused by swelling of the soil inducing tension in the pile.

**Stress** - Unidirectional force per unit area. (Compare **pressure**).

**Stress, effective** - The total stress in a particular direction minus the **pore pressure**.

**Sustained load** - See **Load, dead**.

**Toe resistance** - Soil resistance acting against the **pile toe** (toe response).

**Transferred energy** - The energy transferred to the pile head and determined as the integral over time of the product of force, particle velocity, and **pile impedance**.

**Transient load** - See **Live load**.

**Velocity** – Term for particle velocity of a **pile** or **soil element**.

**Wave speed** - Term for speed of strain propagation in a **pile**.

**Wave trace** - A graphic representation against time of a force or velocity measurement.

**Working load** - See **Load, working**.

### 14.3 Units

In the SI-system, all parameters such as length, volume, mass, force, etc. are to be inserted in a formula with the value given in its base unit. If a parameter value is given in a unit using a multiple of the base unit, e.g., 50 MN—50 meganewton, the multiple is considered as an abbreviated number and inserted with the value, i.e., “mega” means million and the value is inserted into the formula as  $50 \cdot 10^6$ . Do not use a mongrel set of units, e.g., a certain stress as, say,  $34 \cdot 10^5$  kPa, must be written as 3.4 GPa. Moreover, while the kilogramme is written kg, it is really a single unit (base unit) although this is contradicted by the fact that its symbol, "kg", is composed of two letters. For true multiple units, such as kilonewton and kilometre, the “kilo” is a prefix meaning 1,000<sup>1</sup>.

Notice that the base units of hydraulic conductivity (permeability),  $k$ , and consolidation coefficient,  $c_v$ , are m/s and  $m^2/s$ , not cm/s or  $cm^2/s$ , and not  $m^2/year$  or  $m^2/hour$ , respectively. However, as indicated in Chapter 3, the " $m^2/year$ " is acceptable in practice.

When writing out SI-units, do not capitalize the unit. Write “67 newton, 15 pascal, 511 metre, 32° celcius, and 96 kilogramme. However, for these, it is better to simply write 67 N, 15 Pa, 511 m, 32 °C, and 96 kg.

If your text uses SI-units and the original work quoted from a paper used English, make sure to apply a soft conversion and avoid writing “30.48 metre”, when the original measure was “100 feet”, or maybe even “about 100 feet”. Similarly, “about one inch” is “about 20 mm” or “about 30 mm”, while a value of “2.27 inches” converts to “57.7 mm”.

When indicating length and distance in the SI-system, use the unit metre (m) and multiples millimetre (mm) or kilometre (km). Avoid using the unit centimetre (cm).

For area, square centimeter ( $cm^2$ ) can be used when it is alone. However, never in combined terms (for example, when indicating stress). The unit for stress is multiple of newton/square metre or pascal ( $N/m^2$  or Pa). Combination units, such as  $N/mm^2$  and  $MN/cm^2$  violate the principle of the international system (SI) and can be the cause of errors of calculation. That is, prefixes, such as “M” and “m”, must only be used in the numerator and never in the denominator. Notice also that the units “bar” and “atmosphere” (1 bar = 100 kPa; 1 at = 98.1 kPa, 1 atm = 98.7 kPa,) are aberrations to avoid.

Notice, the abbreviated unit for “second” is “s”, not “sec”! — a very common and unnecessary mistake.

The units “newton”, “pascal”, “joule”, etc. do not take plural ending. It is logical and acceptable, indeed preferable, to omit the plural ending for all units in the SI-system.

For the time of the day, use 24-hour convention, not the 12-hour “am” and “pm” convention. Thus, fifteen minutes before three o'clock in the afternoon is 14:45h and twenty minutes after five o'clock morning time is 05:20h. Note that the letter “h” is always included.

---

<sup>1</sup> It is a pity that in developing the SI-system from the old metric systems, the cgs- and MKSA-systems, the unit for mass, the kilogramme, was not given a single symbol letter, e.g., “R” for “ram or ramirez”. Surely there must have been a Herr Doctor Ram or Señor Ramirez somewhere who could have been so honored. Then, the old unit “kg” would be “R”, and a tonne would be superfluous as a term as it would be replaced by “kR (or, preferably “KR”. I very much would like to have the convention of capitalizing the multiplying prefix also applied to “kilo-prefix”. A capital “K” is thought to conflict with the term “kelvin”— the measure of temperature in degree celcius from the absolute lowest value of  $-273\text{ °C}$ —a weak point, I think, but, I have yielded to the convention).

Using the word "centigrade" to mean the unit for temperature is a far too common mistake. The correct term is "degree celsius" or just "celsius", abbreviated "°C", as in "a soil temperature of 14 °C". Incidentally, the "centigrade" is an obsolete unit for the 400° circle (as opposed to 360°).

#### 14.4 Spelling Rules and Special Aspects on Style

A design will invariably result in a written presentation of results and recommendations for a project. Even the best and most elaborate design resulting from a high standard engineering work can be totally shamed by poor report writing style. In the following, a few suggestions are made on how to avoid some of the more frequent gaffes in report writing, and, for that matter, in writing up the work in a manuscript for professional dissemination.

Use either English or U.S. spelling: for example, English spelling includes the letter "u" in words such as "behaviour", "colour", "favour", "harbour", "labour", "rumour", "neighbouring", "remould", "gauge" and doubles the consonant in words such as "modelling", "travelling", "controlled", "labelling", "omitted", "focussing", and "referring", "preferred", and "occurring", (but "offered" and "offering", because the stress is on the first syllable). American spelling omits the "u" and does not double the consonant in these words. ("Occurring" and "occurred", however, are written the same way by both conventions).

Write "z" instead of "s" such as "analyze", "analyzing", "analyzer", "emphasize", "organize", "capitalize", "idealize", "rationalize", "realize", "specialize", "summarize", "symbolize", and "horizontal".

Use the spelling "to advise" and "to practise" and "the advice" and "the practice" (verb versus noun), and omit "e" before "able" in "arguable", "drivability", "desirable", "lovable", etc. However, the "e" is retained in "serviceability" and "noticeable" (to separate the consonant "c" from the vowel "a" or the "c" would have been pronounced as "k").

A simple and useful distinction of meanings can be made by writing "metre" for distance and "meter" when referring to a measuring device. Similarly, the spelling "programme" as in "testing programme" keeps the meaning apart from "program" as in a "computer program".

When using the verbs "centre" (English) or "center" (U.S.), use the correct tense forms: "centred" and "centered", respectively.

Do not use loose contractions such as "don't" or "can't". Write "do not" and "cannot". Also, write "it is". Note, "its" is a possessive pronoun not to be written "it's".

Capitalize all months, days, and seasons.

Do not overuse nouns as adjectives. Four nouns in a row is an abomination. For instance, "the concrete pile toe capacity", which reads much better if changed to "the toe capacity of the concrete pile". In general, emphasizing adjectives "much", "very", etc. are redundant, and "extremely", "absolutely" have no place in a professional text. If something is larger than something else, better than to say "much larger", quantify it and let the reader judge from the numbers.

Avoid "there are " constructions; write "two critical points are shown. . . ", not "there are two critical points shown...".

Avoid "of the"-phrases. Thus, write "the page length should be 100 mm" rather than "the length of the page should be 100 mm".

The first time a noun, e.g., "test", "measurement", "borehole", etc., is mentioned, avoid using definite article (i.e., "the"). Often, the text flows better if an indefinite article is used, i.e., "a", or no article.

Use plain English and common words rather than fancy ones, and be concise (on account of the 'admonition that sesquipedality does not result in perspicacity'). Use short sentences and avoid lengthy or awkward constructions. If a sentence comes out to use more than three lines, it is usually better to split the sentence in two.

Think of the literal meaning of words and expressions and avoid 'ear-sores' such as "up to a depth of ...".

Take care (proof read) not to leave a number alone at line end with its units at the next line, e.g., "16 MPa". Use a non-break space command between numerals and units for getting the number and the unit, "16 MPa" to always be on the same line. Similarly, use the non break command to prevent a number from starting a line, i.e. the word immediately before the number should stay with the number.

When writing "Fig. 5", "Author B. C.", "i. e.", "e. g.", and other words using an abbreviation period, the automatic justification of the lines may result in too wide a space after the period, e.g., Fig. 5", "e. g., and Author B. C.". To avoid this, always follow such a period with a no-break-space command, or do not use a space.

Numerical values consisting of four or more digits can be difficult to read. Then, to improve clarity, separate each set of three digits with a comma, e.g., 7,312,940.42 (This is North American practice. European practice of separating the digits with a space for every three digits is less clear and can lead to mistakes).

Work on the interpunctuation and, in particular, the use of the comma. Commas are important for the understanding of the text and must not be neglected. Always place a comma before a conjunction introducing an independent clause. For example: "always remember, commas enhance the reader's understanding of the message". Also, ponder why the following two sentences have different meanings: "Also the professor may need assistance with regard to commas" and "Also, the professor may need assistance with regard to commas." (Either meaning may require a bit of diplomacy in rendering the assistance). Finally, consider the life and death importance of whether Caesar's order about your execution or liberation reads "Execute, not liberate" or "Execute not, liberate".

Use always the convention of the "serial comma". Thus, write "red, white, and blue" with a comma separating each item in the series (of three or more items). That is, place a comma before the "and", as well as before the "or" in a series of alternatives.

When the subject is the same for both sentence clauses and the connective is "but", a comma should be used after the word preceding "but". Note, when the subject is the same for both clauses and the connective is "and", the comma should be omitted.

Notice that there is often a difference between similar words. For example, "alternate" and "alternative", where "alternate" refers to every second in a series, and "alternative" is one of two possibilities. "Alternate", but not "alternative" can sometimes mean "substitute". The word "substitute" is then preferred. And, do not confuse the meaning of the words "objective" and "object"—a common mistake.

You may want to indicate that a particular observation or item is more important than others, starting the sentence making this point as "*More important, the measurements show that ...*". Do not write "importantly". The adverb of important, "importantly", is a synonym to "pompously". Similarly, when presenting items in order of importance, but you prefer not to use a bulleted or numbered list, do not write, "Firstly", "Secondly", "Thirdly", etc. Remove the "-ly" and write "First", "Second", "Third", etc.

Many times, the words "precision" and "accuracy" are improperly used. An example of "precision" is the reading precision of a gage, that is, the number of decimals given in the gage reading. "Accuracy" considers errors in the gage and in a combination of measurements and calculations. The following is a common error: "the accuracy of the prediction of settlement was 3 percent". The text actually means to refer to an "agreement" between values. Besides, accuracy in prediction of settlement can never be as good as 3 percent!

Notice that a verbal message can be spoken or written, heard, or read. If you want to say that the message is spoken as opposed to written, say "oral". A non-verbal message is not necessarily non-spoken, but one not conveyed by words, but instead, for example, by grunts and gestures.

The word "anybody" means "anyone". "Any body" means "any corpse". Similarly, "any one" means "any single person".

The word "data" is a plural word and takes plural verbs. So are and do the words "criteria", "formulae", "media", "memoranda", "phenomena", as well as "strata". Therefore, the appertained verb must be in plural form. The corresponding singular words are "datum", "criterion", "formula", "medium", "memorandum", "phenomenon", and "stratum".

Words such as "usage", "finalized", etc. may look refined, but are examples of convoluted style. Use the simple versions: "use", or "final or finished", etc. Note, "utilization" refers to the manner or "using", and "utilize" is not a refined synonym to the word "use".

The words "order of magnitude" imply a relation of ten! Usually, the intended meaning is better expressed by plain "magnitude" or "size".

Puristically, "in-situ" should be written in italics, but hyphenating it provides sufficient distinction. Do not write "insitu", or "in situ".

The word "less" is overused. Whenever possible, replace it by its various equivalents, such as "fewer", "smaller", "lighter", "lower", "poorer", etc.

Do not use the ampersand symbol, "&", write "and".

Prefixes such as "pre-" are often unnecessary. For example, the word "predominant" can often be written "dominant" (and preferably be replaced by words such as "governing", "principal", "leading", etc.).

Limit each paragraph to a single message. Short paragraphs focus the reader's attention and assist understanding.

## 14.5 References and Bibliography

All papers must include a section listing bibliographic information for works cited in the text called "References" (note the plural form). The format of the section varies between publications. For example, the Canadian Geotechnical Journal (CGJ) requires the author names to be capitalized, which is not how the ASCE Geotechnical and Environmental Journal (ASCE J.) wants it, for example. However, the latter puts the title of the paper inside quotation marks, which the CGJ does not. Both, as do most journals, require that a reference to a conference includes the dates and venue of the conference.

For publications cited in the text, use the author-date method. Note that the "al." in "et al." has an abbreviation period and that there is no comma between name and year. For example:

- "Terzaghi and Peck (1967) described ..."
- "Terzaghi et al. (1996) presented ..."
- "Major papers on stability analyses (e.g., Bishop and Bjerrum 1960) are ..."

The general format for listing references in alphabetical order in the References section is as follows.

- Last name and initials of all authors
- Year of publication (in parenthesis for the ASCE J., but no parenthesis for the CGJ)
- Title of paper, report or book chapter. (For a manuscript submitted to the ASCE, place the title inside quotation marks, but a manuscript intended for the CGJ has no quotation marks bracketing the title. The title should be in lower case letters but for the first letter of the first word)
- Title of journal, periodical, proceedings or book—often in italics
- Name and location of publisher (also for conference proceedings). Volume number followed without space by issue number in parenthesis and page numbers, or total number of pages (In 2014, the ASCE Journal ceased page numbering of issues, a senseless and regrettable change.)<sup>1</sup>
- For papers in conference proceedings indicate city (venue) and dates of conference

For author's first name initials, show only the first letter followed by a period. When more than one first name initial is used, the space after the period between a series of such letters should be omitted.

Use no line space between references, but employ a visual separation by an 8 mm (0.3 inch) hanging indent. Some journals may have different requirement in this regard.

#### 14.6 Examples of referenced works from published books, journals, and hard-copy documents

- Becker, D.E., Crooks, J.H.A., Been, K., and Jefferies, M.G., 1987. Work as a criterion for determining in-situ and yield stresses in clays. *Canadian Geotechnical J.* 24(4) 549-564.
- Begemann, H.K.S., 1965. The friction jacket cone as an aid in determining the soil profile. Proc. of the 6th ICSMFE, Montreal, September 8-15, Univ. of Toronto Press, Vol. 2, 17-20.
- Bjerrum L., Johannessen, I.J., and Eide, O., 1969. Reduction of negative skin friction on steel piles to rock. Proc. 7th ICSMFE, Mexico City, August 25-29, Mexico Geotechnical Society, Vol. 2, 27-34.
- Bruce, D.A., 2005. Glossary of grouting terminology. *ASCE J. Geotechnical and Geoenvironmental Engng.* 13(112) 1534-1542.
- Camp, W.M., 2004. Drilled and driven foundation behavior in a calcareous clay. *GeoSupport 2004, ASCE GSP124*, ASCE, Reston, VA, 1-18.
- Campanella, R.G. and Robertson, P.K., 1988. Current status of the piezocone test. *Penetration Testing 1988*, Vol. 1, Balkema, Rotterdam, 93-116.
- Crikey A.D., 2017. Exorbitant and extraneous finite extensions of alluvial fans in subservient geomorphology. *Journal of Quisquiliae Inutilia Geotechnica* 13(2) 1-8.
- Fellenius, B.H., 2023. Basics of foundation design, a text book. Revised Electronic Edition, [www.Fellenius.net], 548 p.
- Germaine, J.T., 1982. Development of the directional shear cell for measuring cross-anisotropic clay properties. ScD Thesis, Dept. of Civil Engineering, MIT, Cambridge, Mass, 569 p.
- Holtz, R.D. and Kovacs, W.D., 1981. An introduction to geotechnical engineering. Prentice-Hall Inc., New York, 780 p.
- Holtz, R.D., Jamiolkowski, M. B., Lancelotta, R., and Peroni, R., 1991. Prefabricated vertical drains. Design and Performance. Construction Industry Research and Information Association, CIRIA, London, 131 p.
- Hong Kong Geo, 2006. Foundation design and construction. Hong Kong Geotechnical Control Office, No. 1/2006, 376 p.
- Massarsch, K.R., 1994. Settlement analysis of compacted fill. Proceedings, 13th ICSMFE, New Delhi, January 5-10, Vol. 1, pp. 325-328.
- Rausche, F., Moses, F., and Goble, G. 1972. Soil resistance predictions from pile dynamics. *American Society of Civil Engineers, J. for Soil Mechanics and Foundation Engineering* 98(SM9) 917-937.
- Taylor, D.W., 1948. Fundamentals of soil mechanics. John Wiley & Sons, New York, 700 p.
- Westergaard, H.M., 1938. A problem of elasticity suggested by a problem in soil mechanics: A soft material reinforced by numerous strong horizontal sheets. In *Contributions to the Mechanics of Solids*, Stephen Timoshenko 60th Anniversary Volume, MacMillan, New York, 260-277 (as referenced by Holtz and Kovacs, 1981).

Data or facts taken from a company report should be listed in the reference section. For example:

Geotechnical Abundance Inc., 2010. Investigation for municipal works, East River, Project 09-10-7432, Report 2010-16, 64 p.

Reference to personal communication is usually included to give due credit to an individual, but such communication references are only placed in the body of the thesis or paper, not in the reference section. For example: (Zhining, B.C., 2010. Personal communication).

Below is the style for the referencing of a CD-type paper, which reference style is based on the Chicago Manual of Style format. No page numbers are needed, simply indicate that it is a CD-ROM (or find out if there would be a less dated storage medium, say an online linke).

Tamrakar, S. B., Mitachi, T., Toyosawa, Y., and Itoh, K., 2005. Development of a new soil tensile test apparatus. Proc., Geo-Frontiers 2005, Site Characterization and Modeling, ASCE Geotechnical Special Publication, GSP 138 (CD-ROM), ASCE, Reston, VA.

These days, the listing of a reference often includes a DOI reference ("Digital Object Identifier"). The DOI system is an international standard developed by the International Organization for Standardization. A DOI is a unique code that provides a link to an article online. The link connects to the reference and allows downloading or purchase, as the case may be. The below example places the DOI code at the end of the reference text.

Massarsch, K.R., and Fellenius, B.H., 2019. In situ tests for settlement design of compacted sand. Proc. of the Institution of Civil Engineers (ICE), Geotechnical Engineering, Ground Improvement Journal, Paper 180046, 172(3) 207–217. doi.org/10.1680/jgeen.18.00046.

Citations to papers in the body of a manuscript or paper are listed in References section. Occasionally, an author wants to list also relevant papers that were not specifically mentioned in the body. Those are then placed in a separate section called "Bibliography".

There is no convention with regard to spelling out the full name of a journal, e.g., writing "Canadian Geotechnical Journal", or writing it "Can. Geot. J.", but the "American Society of Civil Engineering" is usually abbreviated to "ASCE". The ASCE Journal of Geotechnical and Geoenvironmental Engineering" is sometimes abbreviated to J. of Geot. a. Geoenv. Engng." Mostly, the extent and manner of the abbreviation comes down to whether or not it is necessary for saving a line of text in the Reference section.

### **14.7 Re-use of Figures and Data**

The various journals and Editors are getting picky on the copyright issue. All re-used figures must have a copyright release submitted with the manuscript. This even if the "old" figure is from a paper by the author of the manuscript. To avoid this hassle, as it can be, the following is recommended: For your own previously used figures, replot them from your data with some appropriate adjustment to scale and symbols and then cite the original source, e.g., by writing "Data from ...". For figures from others, scan and digitize to extract the data, then, replot. Nobody will contest your use of the original figure, but, strictly, the copyright of the original figure is not fully removed. For that, you will have to add data points not included in the original. As to the citation, again, write: "*Data from ...*". Note while a Google map can be used freely, Google Earth does require a copyright release, which can be very time-consuming to obtain.



### 13.8 Some Useful Unit Conversions

1 millionth of a mouthwash = 1 microscope

The weight one evangelist carries with God = 1 billigram

Basic unit of laryngitis = 1 hoa

Half of a large intestine = 1 semicolon

1,000,000 aches = 1 megahurtz

365.25 days = 1 unicycle

1 million-million microphones = 1 megaphone

1 millionth of a fish = 1 microfiche

2 monograms = 1 diagram



## CHAPTER 15

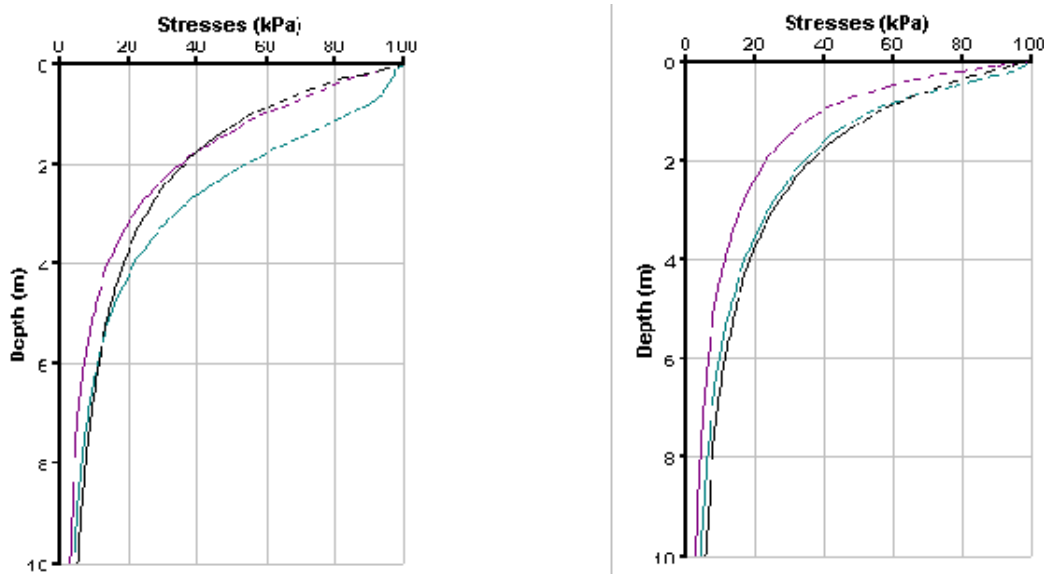
### EXAMPLES

#### 15.1 Introduction

This chapter offers a few examples to the analysis methods. They can all be solved by hand, although the computer and the UniSoft programs will make the effort easier.

#### 15.2 Stress Calculations

**Example 15.2-01.** Example 1 is intended for a comparison between stresses calculated using all three methods — Boussinesq, Westergaard, and 2:1 — for determining the stress distribution as applied to the center, the corner, and the characteristic point below a square 3.0 m footing loaded by a uniform stress of 40 kPa and placed on the surface of a soil of zero density. In the two diagrams below, the left diagram shows the stresses below the center of the footing and the right shows the stresses below the characteristic point (c.f., Section 1.9).



Below the center of the footing, the stresses computed by the 2:1-method and the Westergaard method are very similar and somewhat smaller than the stresses computed by the Boussinesq method. For the stresses below the characteristic point, the stresses computed by the 2:1-method and the Boussinesq method are similar. Of course, the 2:1-method makes no distinction between the points of computation.

The example implies that for single areas, the 2:1-method is as good as the more elaborate methods. The 2:1-method is simple to use in hand calculation, but only rarely does the problem relate to the stresses underneath the footprint of a single area. Therefore, stress calculations in soils will need to be by Boussinesq or Westergaard methods of stress distribution. These days, however, nobody has the time for establishing the detail distribution at a point from several loaded areas using the conventional influence diagram and Newmark's chart (see the next example). A detailed calculation necessitates access to the UniSettle program.

**Example 15.2-2.** The soil profile at a site consists of a 4.0 m thick upper layer of medium sand with a saturated total density of  $2,000 \text{ kg/m}^3$ , which is followed by 8.0 m of clay (density  $1,700 \text{ kg/m}^3$ ). Below the clay, an 8 m thick sand layer (density  $2,100 \text{ kg/m}^3$ ) has been found overlying glacial till (density  $2,300 \text{ kg/m}^3$ ) deposited on bedrock at depth of 23.0 m. The bedrock is pervious. Two piezometers installed at depths of 18.0 m and 23.0 m, respectively, indicate phreatic pressure heights of 11.0 m and 25.0 m, respectively. There is a perched groundwater table in the upper sand layer at a depth of 1.5 m. The water content of the non-saturated sand above the perched groundwater table is 12.6 percent.

Determine the distribution of effective overburden stress and the pore pressure in the soil. (Assume stationary conditions—no consolidation occurs). Compare the distribution of effective stress for the case to stress values calculated for a case with no piezometers and an assumption of hydrostatic distribution below the perched groundwater table at 1.5 m depth.

The first step in the solution is to arrange a soil profile that lists all pertinent values, that is, the thickness and soil density of each layer, as well as the depth to the groundwater table and the pore pressures determined from the piezometer readings. The density of the non-saturated sand above the perched groundwater table is not given directly. However, knowing that the total density is  $2,000 \text{ kg/m}^3$ , and assuming that the solid density is  $2,670 \text{ kg/m}^3$ , phase system calculation will quickly provide the dry density value:  $1,600 \text{ kg/m}^3$  and that the total density for a water content of 12.6 % is  $1,800 \text{ kg/m}^3$  (according to the formulae in Chapter 1.2).

Five soil layers will describe the profile. The key to determining the distribution of effective stress in the soil is realizing that the pore pressure distribution is affected by the existence of three aquifers. First, the perched water in the upper sand, second, the aquifer in the lower sand, and, third, the artesian aquifer in the bedrock below the till. The clay and glacial till layers are practically impervious in relation to the lower sand layer, which is actually draining both layers resulting in a downward gradient in the clay and an upward in the till. In the sand layers, because of the higher hydraulic conductivity (permeability), the pore pressure distribution is hydrostatic (a gradient of unity). Because of the stationary conditions, the pore pressure distribution, although not hydrostatic, is linear in the clay and the till. Therefore, the information given determines the pore pressures at all layer boundaries and a linear interpolation within each layer makes the pore pressure known throughout the profile. The total stress, of course, is equally well known. Finally, the effective stresses are simply determined by subtracting the pore pressure from the total stress.

A stress calculation done by means of UniSettle, UniPile, or any custom-made spreadsheet program, provides the total and effective stresses and pore pressures at top and bottom of each layer. The calculation results are shown in the following table as “Initial Conditions”. For comparison, the “Final Conditions show the stresses if a hydrostatic distribution of pore pressures is assumed throughout the soil profile. The existence of pore pressure gradients in the soil and more than one aquifer is a common occurrence. Considering the considerable influence pore pressure gradients can bring to bear, it is a conundrum hard to explain why so many in the industry rarely bother about measuring pore pressures other than as the height of water in the borehole, assuming, inanely, hydrostatic conditions throughout the site and profile!

**Example 15.2.1. Results**

Depth (m)	Initial Conditions			Final Conditions		
	Total Stress (kPa)	Pore Stress (kPa)	Eff. Stress (kPa)	Total Stress (kPa)	Pore Stress (kPa)	Eff. Stress (kPa)
Layer 1	Non-sat Sand			1,800 kg/m <sup>3</sup>		
0.00	0.0	0.0	<b>0.0</b>	0.0	0.0	<b>0.0</b>
1.50	27.0	0.0	<b>27.0</b>	27.0	0.0	<b>27.0</b>
Layer 2	Sand			2,000 kg/m <sup>3</sup>		
GWT 1.50	27.0	0.0	<b>27.0</b>	27.0	0.0	<b>27.0</b>
4.00	77.0	25.0	<b>52.0</b>	77.0	25.0	<b>52.0</b>
Layer 3	Clay			1,700 kg/m <sup>3</sup>		
4.00	77.0	25.0	<b>52.0</b>	77.0	25.0	<b>52.0</b>
12.00	213.0	50.0	<b>163.0</b>	213.0	105.0	<b>108.0</b>
Layer 4	Sand			2,100 kg/m <sup>3</sup>		
12.00	213.0	50.0	<b>163.0</b>	213.0	105.0	<b>108.0</b>
20.00	381.0	130.0	<b>251.0</b>	381.0	185.0	<b>196.0</b>
Layer 5	Till			2,300 kg/m <sup>3</sup>		
20.00	381.0	130.0	<b>251.0</b>	381.0	185.0	<b>196.0</b>
23.00	450.0	250.0	<b>200.0</b>	450.0	215.0	<b>235.0</b>

-----End of data-----

**Example 15.2-02.** A laboratory has carried out consolidation tests on a postglacial inorganic clay and reports the results as initial and final water contents ( $w_{\text{initial}}$  and  $w_{\text{final}}$ ) being 57.0 % and 50.0 %, respectively, an initial void ratio,  $e_0$ , of 1.44,  $S = 100$  %, and a total density,  $\rho_{\text{total}}$ , of 1,650 kg/m<sup>3</sup>. Do the values make sense?

Phase system calculations show that the values of  $w_{\text{initial}}$  of 57 % and the  $e_0$  of 1.44 combine only if the solid density of the material is 2,620 kg/m<sup>3</sup>, and the  $w_{\text{initial}}$  of 57 % and a void ratio of 1.44 combine only if the total density of 2,520 kg/m<sup>3</sup>. In reality, the solid density is more likely equal to 2,700 kg/m<sup>3</sup>. Then, a water content of 57 % corresponds to  $e_0 = 1.54$  and  $\rho_{\text{total}} = 1,670$  kg/m<sup>3</sup>.

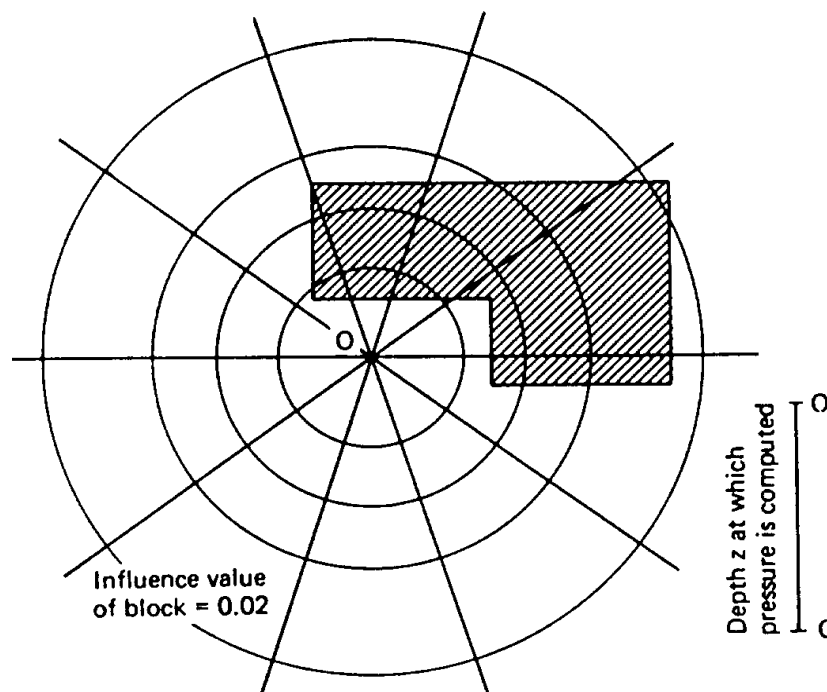
Are the errors significant? Well, the final water content of 50 % corresponds to a final void ratio of either 1.31 ( $\rho_s = 2,620$  kg/m<sup>3</sup>) or 1.35 ( $\rho_s = 2,700$  kg/m<sup>3</sup>). Adjusting the void ratio versus stress curve from the consolidation test, accordingly, changes the  $C_c$ -value from 0.80 to 1.25. This implies a significant error. However, the modulus number is equal to 7 (indicating a very compressible soil) whether based on the originally reported values or on the values adjusted to the proper value of solid density. In this case, the error in  $e_0$  compensates for the error in  $C_c$ .

The example is taken from a soil report produced by a reputable geotechnical engineering firm. Agreed, the errors are not significant. But they are nevertheless errors, and, while it never came about, it would have been a very uncomfortable experience for the responsible engineer under cross examination on the stand to try sound believable to the judge and jury in proclaiming that the errors "don't matter".

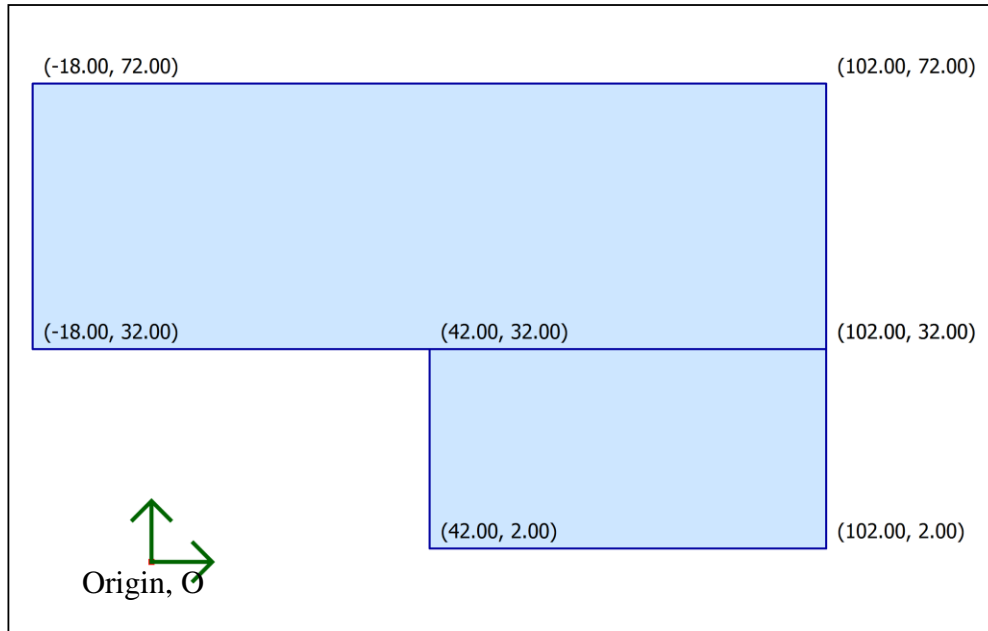
**Example 15.2.3.** Errors in the basic soil parameters are not unusual in geotechnical reports. For example, a laboratory report in my files produced by a professional company that deals with a sample of about the same type of clay as in Example 15.2.2(not same company) lists under the heading of “Determination of Density and Water Content” values of the weights of saturated and dry soil and dish etc., and, finally, the value of the water content as 50.8 % and also, although without showing calculations, the solid, total, and dry density values of  $2,600 \text{ kg/m}^3$ ,  $1,782 \text{ kg/m}^3$  and  $1,184 \text{ kg/m}^3$ , respectively. The two latter values match for calculations using an input of  $S = 100 \%$  and a solid density of  $2,960 \text{ kg/m}^3$ . With the reported and slightly more plausible value of solid density of  $2,600 \text{ kg/m}^3$ , the total, and dry density values are  $1,690 \text{ kg/m}^3$  and  $1,120 \text{ kg/m}^3$ , respectively. Notice that the ratio of the dry density over the total density is 0.66, the same value as the ratio 100% over (100% + 50.8%), implying accurate values. Yet, the value reported by the geotechnical laboratory for the total density is 5 % too large. Significant? Well, perhaps not very much, but it is a bad start of a foundation design.

**Example 15.2-03.** In illustrating Boussinesq stress distribution, Holtz and Kovacs (1981) borrowed (and converted to SI-units) an example by Newmark (1942): An L-shaped area is loaded by a uniform stress of 250 kPa. (The area is shown below with the dimensions indicated by x and y coordinates). The assignment is to calculate the stress induced at a point located 80 metre below Point O (coordinates  $x = 12 \text{ m}$ ;  $y = 2 \text{ m}$ ), a point well outside the loaded area. Back then, the effort involved using Newmark's nomograms and only one point could be calculated at a time. The plan view below shows the loaded area placed on the Newmark's influence diagram with Point O at the center of the diagram. A hand calculation documented by Holtz and Kovacs (1981), gives the results that the stress at Point O is 40 kPa.

The UniSettle4 manual contains the example in the file called “Example 1 - Newmark Diagram.Unisettle4”.



The following figure shows a plan view produced by UniSettle with the "O", at coordinates x=12; y=2.

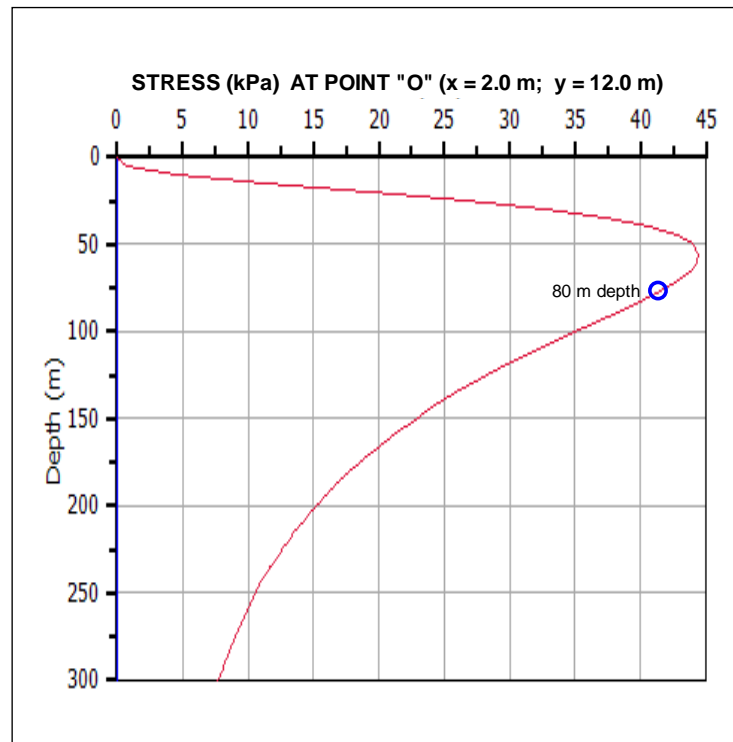


UniSettle shows that the hand calculation is correct; the calculated value of the stress is 40.6 kPa. The full results of the UniSettle calculations are presented in the table and diagram given below; in this case, the stresses at every 5 metre depth from 0 m to 200 m underneath Point O. (The table shows only the values for 75 m, 80 m, and 85 m).

**Stress Analysis - Boussinesq. ( 2 . , 12 . )**

Depth (m)	Initial Conditions			Final Conditions		
	Total Stress (kPa)	Pore Stress (kPa)	Eff. Stress (kPa)	Total Stress (kPa)	Pore Stress (kPa)	Eff. Stress (kPa)
75.00	0.0	0.0	0.0	41.8	0.0	41.8
80.00	0.0	0.0	0.0	40.6	0.0	40.6
85.00	0.0	0.0	0.0	39.2	0.0	39.2

The diagram presented below shows the vertical stress distribution underneath Point O according to Boussinesq as calculated by UniSettle.



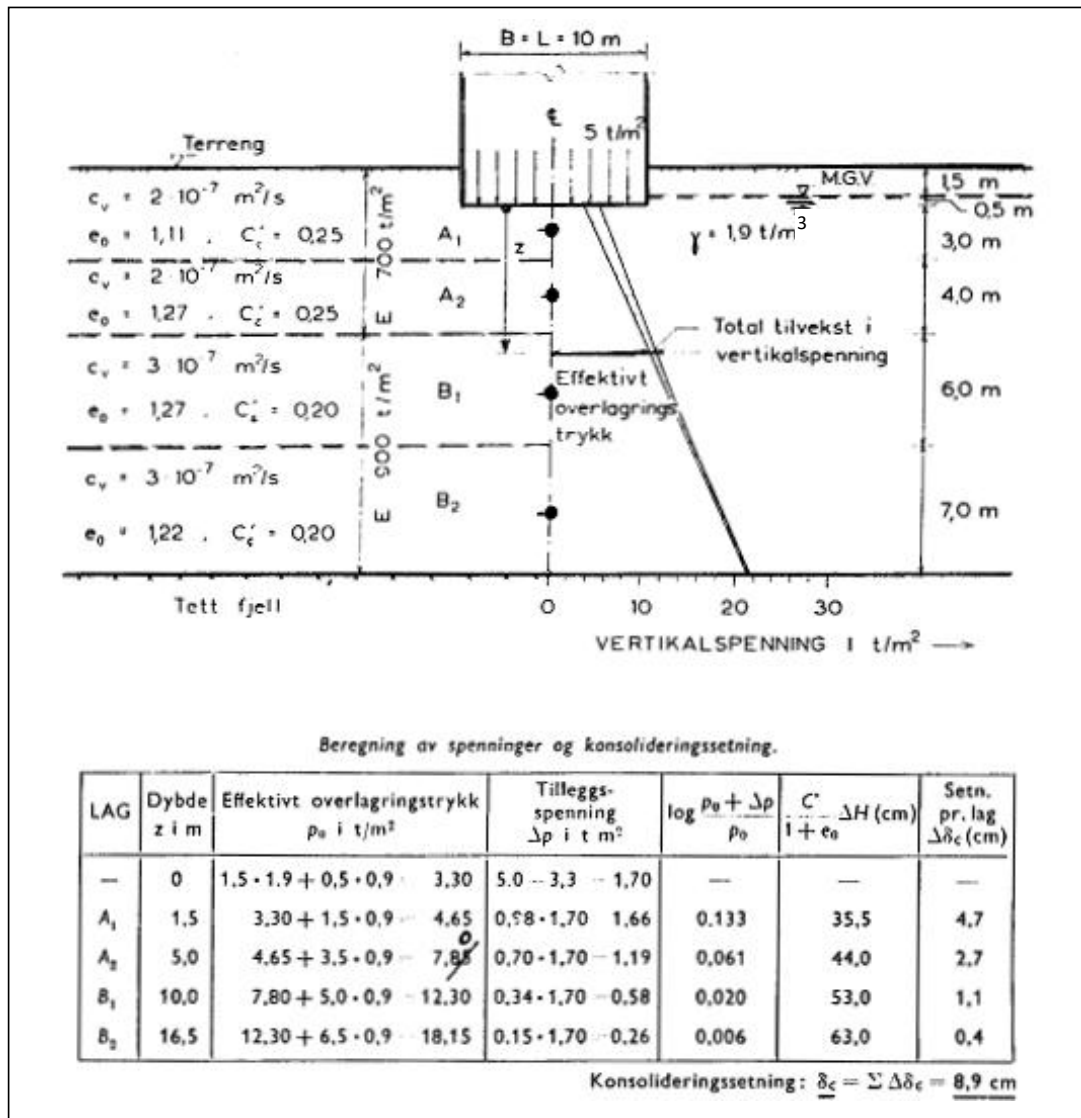
### 15.3 Settlement Calculations

**Example 15.3-01.** is taken from a classic geotechnical text: Norwegian Geotechnical Institute, Publication No. 16, Example 7, (Janbu et al., 1956): The example shows the results of calculations (pre-computer era, so the calculations were by hand) of settlement for a structure with a footprint of 10 m by 10 m founded at a depth of 2.0 m on 22 m of an inorganic, normally consolidated clay deposited on bedrock, as shown below (copy of the original NGI 16 figure). Boussinesq stress distribution is assigned and the settlement is to be determined below the center of the structure. The initial groundwater table lies at a depth of 1.5 m and the distribution of pore water pressure is hydrostatic. The clay is built up of four layers with the parameters indicated in the below figure. The upper and the lower pair of layers are identical. The split into two pairs is made in NGI 16 to indicate that of the two main layers are split for the calculation process.

As a somewhat cheeky comment, a calculation by means of the phase system equations in Chapter 1 of the Red Book shows that the void ratio values of about 1.22 indicated in the figure are not compatible with the  $1,900 \text{ kg/m}^3$  value indicated for the total saturated density unless the solid density of the clay particles is about  $3,000 \text{ kg/m}^3$ , about ten percent higher than the probable value. The void ratio values combined with the more realistic value of solid density of  $2,670 \text{ kg/m}^3$  require a saturated density of about  $1,750 \text{ kg/m}^3$ . The  $1,900 \text{ kg/m}^3$  value indicated in the figure has been retained in the following, however. (The Reader will have to excuse that also the Norwegian language has been retained; one does not tinker with the classics)!

The UniSettle4 manual contains the example in the file called “Example 2 - NGI 16.UniSettle4”.





The original units in "old metric" shown in the figure have been converted to "new metric", i.e. SI units, and the net input of 17 kPa for the stress imposed by the structure (final conditions) has been replaced by an input stress of 50 kPa plus input of final excavation to the 2.0 m depth (i.e., a reduction by 33 kPa). (N.B., because the excavation has the same footprint as the structure, no difference is caused by separating input of load from input of excavation, as opposed to first reducing the imposed stress by the excavation equivalent). The soil layers in the figure are indicated as normally consolidated with compressibility parameters in the format of conventional  $C_c$   $e_0$  parameters. The NGI 16 publication was published in 1956, seven years before the advent of the Janbu tangent modulus approach. The modulus numbers for layers A<sub>1</sub>, A<sub>2</sub>, B<sub>1</sub>, and B<sub>2</sub> are 19.4, 20.9, 26.1, and 25.5 (by soft conversion from the  $C_c$ - $e_0$  parameters; usually, modulus numbers are only used as whole numbers).

As given in the figure from NGI 16, settlement calculations result in 89 mm of consolidation settlement below the center of the foundation. The calculation using UniSettle results in 91 mm, which is practically the same. Assigning, say, 0.5 m thick sub layers and calculating using UniSettle reveals that no appreciable gain is achieved from using many sub layers: the settlement value is essentially the same, 93 mm.

The foundation for the structure is probably quite rigid. Therefore, the settlement calculated below the characteristic point ( $x = 3.7$  m;  $y = 3.7$  m) is more representative than below the center: In no time at all, UniSettle can calculate the consolidation settlement for the characteristic point, obtaining a value of 69 mm, about 25 % smaller than the value calculated for a point under the center of the structure (if assumed to be flexible).

Or, suppose that the structure would not be a rigid monolith, but a building with a basement. It is then very unlikely that the groundwater table stays at a depth of 1.5 m also inside the structure; most probably, the groundwater table is lowered at least to a depth of 2.0 m. After changing to a final groundwater table at 2.0 m and assuming hydrostatic distribution below this level, a re-calculation with UniSettle returns a settlement of 106 mm at the center and 91 mm at the characteristic point.

Well, perhaps the effect of lowering the groundwater table is not constant but changes linearly to the original value at bottom of the clay layer (22 m depth). UniSettle now calculates a settlement of 92 mm below the center of the structure and 77 mm at the characteristic point.

The NGI 16 text includes a separate calculation of the immediate settlement, a value of 22 mm is indicated to be added to the consolidation settlement of 89 mm for the example. Whether or not to include a calculation of immediate settlement in a case similar to the subject one can be argued. As can the method to use for its calculation: applying an elastic modulus, or adjusting the compressibility parameters; NGI 16 uses the elastic modulus approach with an E-value of 7,000 kPa for the two upper soil layers and 9,000 kPa for the two lower layers. UniSettle's calculation shows 20 mm for the original input values. (One might also question the magnitude of the immediate E-moduli, but is irrelevant to the example).

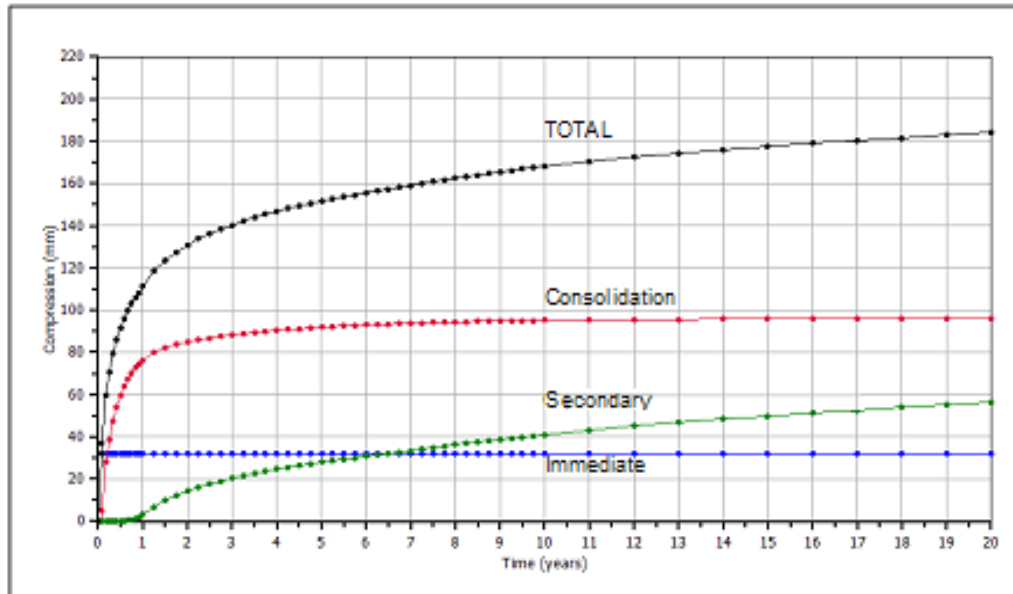
The NGI 16 figure also provides values of consolidation coefficient. With these values as input and indicating double-draining layers, then, about 90 % of the consolidation is completed after a year. However, a one-year duration of achieving a 90 % degree of consolidation is optimistic. Applying double drainage condition would mean that full drainage would occur at each clay layer boundary of the 4 to 7 m thick layers. That is, the layers would be assumed to drain into each other with no effect on the consolidation development! At best, the total 22-m soil thickness could be assumed double draining. This would mean that the consolidation time is not one year, but about  $(22/4)^2$  longer, i.e., 30 years. To calculate the development over time of the consolidation, because the upper and lower clay layer pairs are essentially equal, the two pairs can be turned into two layers, which now would be single-drained. The assigned coefficients of consolidation now show that 90-% degree of consolidation would require 12 and 15 years, respectively, for the two soil layers. UniSettle calculates the consolidation settlement over, at most, a hundred year duration. The maximum consolidation settlement is in most cases reached long before hundred years.

UniSettle calculates also the development over time of the secondary compression. The input required is the start of the consolidation, which is the time for when the first change (increase) occurred in the effective stress distribution, and the length of time for 90 % consolidation to develop. In contrast to the consolidation development, secondary compression continues indefinitely, albeit at a reducing rate. Therefore, UniSettle includes the option of choosing the relevant report period for the value of secondary compression to show in the results table.

The original example does not include values of secondary compression. The question is what coefficient of secondary compression,  $C_{\alpha}$ , to use as input. Some suggest that the coefficient should be in the range of 0.02, which here gives an  $\epsilon_{2nd}$  value of 0.005 (Section 3.0). However, in an inorganic clay, a secondary compression that is larger than the immediate compression will not likely occur within the first about 30 years after the end of the consolidation. The 0.005 value does not meet this empirical condition.

The largest point of contention is when the secondary compression should be assumed to start. Does it start at the start of the consolidation or at the end of the consolidation? The modern consensus is that it starts when the consolidation is initiated. However, calculation practice is to let it start at the end of the consolidation. UniSettle allows either alternative option.

The below figure shows the calculated immediate compression, consolidation settlement, secondary compression, and total settlement versus time for the original NGI 16 input calculated for the center of the excavation. The diagram is plotted after exporting the results to Excel and then plotting the data.



First 20 years of settlements for Example 2 at the center of the foundation

The above time-settlement diagram indicates the start of the secondary compression to be at the point of 90-consolidation. Because secondary compression is only of interest at a time long after the end of the consolidation, its initial portion is normally of little concern. However, a purist might find the initial horizontal portion of the secondary compression curve disturbing. UniSettle provides two ways of making the secondary compression start at the initiation of the consolidation. One "quick and dirty" approach is to input a very short time for the duration of the consolidation and adjust the coefficient so that, say, the 30-year compression is the same as the that for the actual duration. This approach, however, distorts initial portion of the curve. The second approach is to do the calculation for the consolidation considered and export the results to Excel and shift the secondary compression column to the end of consolidation.

**Example 15.3-02** is also taken from the classic textbook (Terzaghi and Peck 1948): Examples in Chapter V, Articles 35 and 36 (Problems 3 and 1, respectively). The following is the verbatim quote from the book: *A building of very great length has a width of 120 ft. Its weight constitutes a practically uniform surcharge of 5.0 ksf on the ground surface. Between the depths of 70 and 90 ft, there is a layer of soft clay. The rest of the subsoil is dense sand. The soft clay has a natural water content of 45 %. The unit weight of the solids is 168.5 pcf and the total unit weight of the dense sand is 130 pcf. The free water level (groundwater table) is at the ground surface. From the results of consolidation tests, it has been ascertained that the compression index,  $C_c$ , is equal to 0.50.*

Using the information given in the problem texts, phase system calculation provides the void ratio,  $e_0$ , and saturated total density of the clay is determined to 1.21 and 110 pcf, respectively. The void ratio and compression index combine to a Janbu modulus number of 10.

Calculations of the stress using UniSettle returns the following values at the four locations: 2.28, 2.95, 3.40, and 3.56 ksf, respectively, i.e., the same answers as given in Problem 3. Calculations of settlement using UniSettle returns settlements values of 8.59 and 12.32 in., again a full agreement with the text book for Problem 1.

Problem 3 in Art 35: *Compute the intensity of vertical stress (using Newmark influence chart) due to the weight of the building at the following points located in a horizontal plane at mid-height of the compressible layer: directly below the edge of the building, 20 ft from the edge toward the center line, 40 ft from the edge toward the center line, and directly below the center line.*

*Answer: 2.30, 2.96, 3.43, 3.57 ksf}.*

Problem 1 in Art 36: *Compute settlements at the edge and center of the building.*

*Answer: 8.5 and 12.3 in.*

In a real case, it would be of interest to input also the compressibility of the dense sand, say, a modulus number of 300 (30 MPa or 4,350 ksf) and calculate the settlement in the sand. With that compressibility, UniSettle indicates that the sand contributes about an additional 6 inches of settlement. However, the settlement in the sand would develop during the construction and rather soon after its completion, i.e., be "immediate". It is easy to input suitable consolidation coefficients and divide the stress imposed by the building into components constructed at different times to model development of settlement with time. For example, one can model the sand settlement as immediate settlement with an immediate compression modulus,  $E_i$ , of 3,000 ksf, which incorporates also the 'consolidation' settlement of the sand. For completeness, an  $E_i$  of for the clay of 500 ksf is input. To model the consolidation development of the clay, a consolidation coefficient,  $c_v$ , is input as  $6 \times 10^{-8} \text{ m}^2/\text{s}$  (1.90  $\text{m}^2/\text{year}$ ; 20.4  $\text{ft}^2/\text{year}$ ) for the clay. The building stress is modeled as four steps dividing the 5.0 ksf applied stress into four 1.25 ksf steps applied one month apart.

The UniSettle calculated development of settlement for the case is shown in Figure 15.3.2. Such compilations were rarely done in the 1940s. Indeed, they are rarely done today. While in the 1940s, the calculations would have taken a disproportionate amount of time, with UniSettle, all calculations results are now available immediately (after a minute or two of input). The UniSettle4 manual contains the example in the file called "Example 3 - Terzaghi-Peck.Unisettle4".

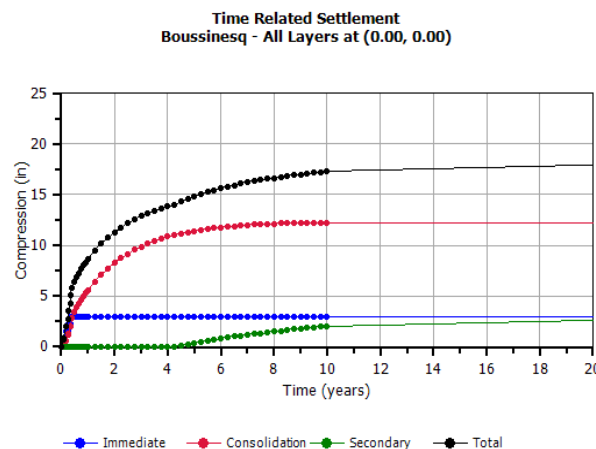
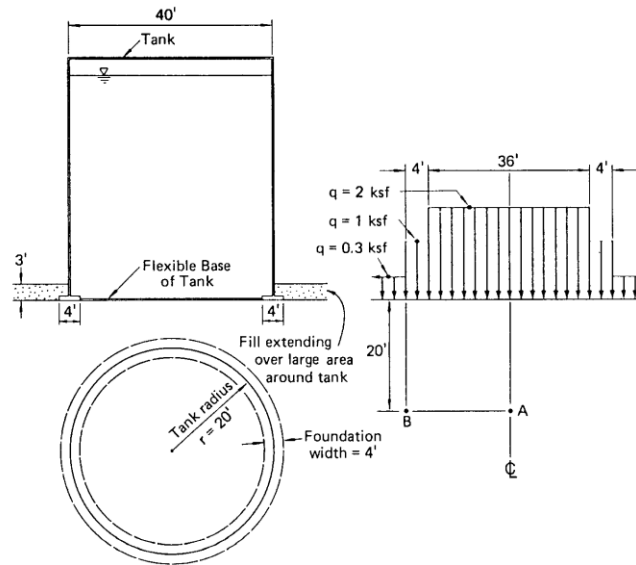
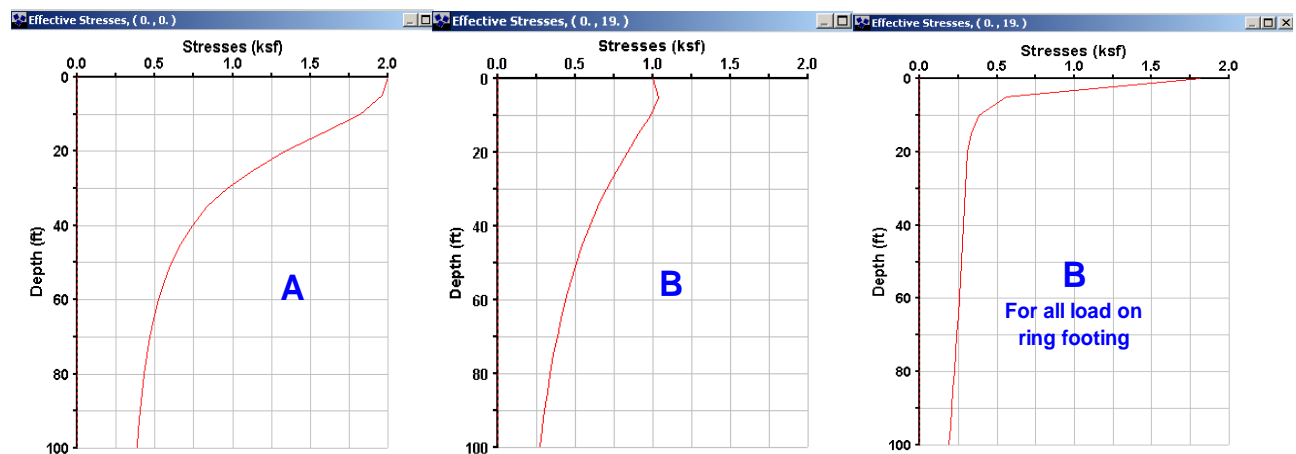


Fig. 15.3.2 Compilation of settlement development over time

**Example 15.3-03** is Example 4.4 in Chapter 4 of Perloff and Baron (1976) and presents a 40 feet wide circular water tank on a ring foundation, with fill placed outside the tank and with the tank bottom flexible and resting on the ground, as illustrated below. The assignment is to calculate Boussinesq stress at tank center (Point A) and at the ring at radius 20 ft (Point B) at a depth of 20 feet for both points. The input file shows the input of the stress from the surcharge and the tank as three overlapping areas. Area 1 is Surcharge of 0.3 ksf all over site, Area 2 is the 4 ft wide ring foundation for the tank structure with inside and outside radii of 18 ft and 22 ft with a uniform stress of 1.0 ksf. Area 3 is stress from the water inside the tank which has a radius of 18 ft and a uniform stress of 2.0 ksf. The stresses at the 20 ft depth calculated for A and B are 1.37 ksf and 0.84 ksf, respectively. The UniSettle4 manual contains the example in the file called “Example 4 - Ring Tank.Unisettle4”.



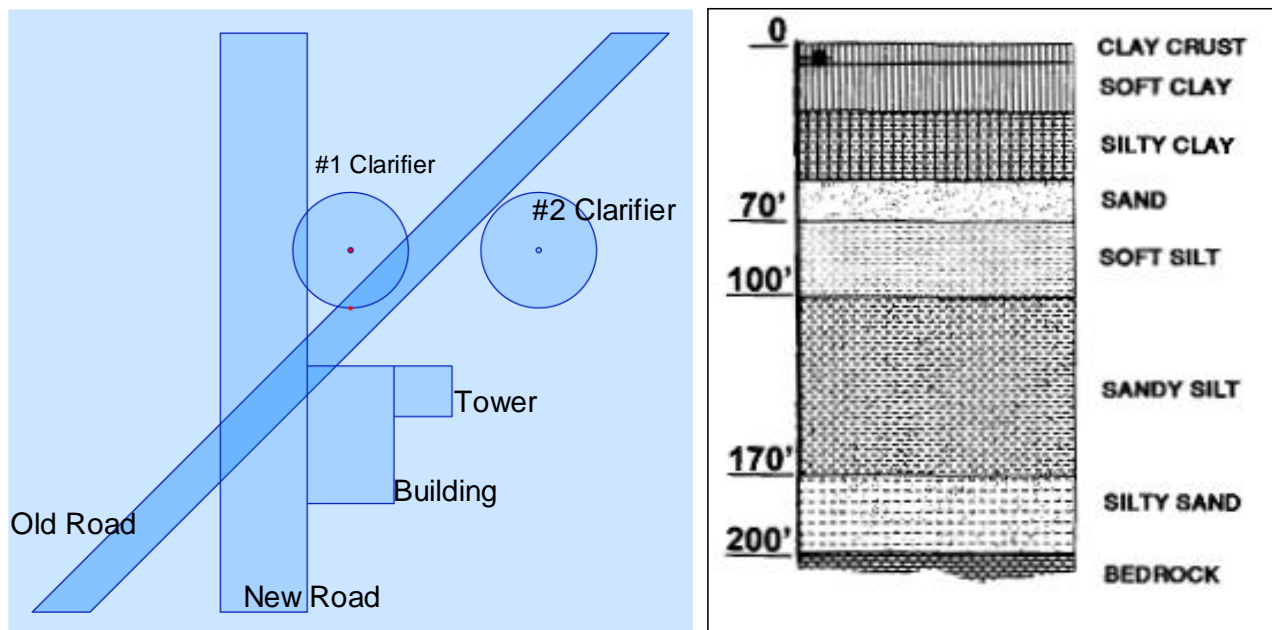
The example is interesting because it pertains to a realistic case and tempts to several what-if studies. So, what-if the base of the tank would not flexible, but rigid so that all the tank loads go to the ring foundation (no surcharge is placed under the tank)? What then about the stresses at A and B? And, what about settlements? Make up a soil profile with suitable values of density and modulus numbers, etc. and try it out.



Well, the calculated settlement may actually not change much, but will the ring footing be stable?

**Example 15.3.4-08.** This example is taken from the real world: A sewage treatment plant (or part of one) will be built in a low lying area, where the upper about 170 feet of soil is compressible. The clay soils are overconsolidated. The perched groundwater table will reduce following the construction, but the phreatic heads in the two aquifers will remain unchanged. One is slightly artesian, . An existing old road ( $q = 0.19$  ksf) crossing the area will be removed and replaced with a new road ( $q = 0.63$  ksf). The entire area will have to be raised about 1.5 ft by a general surcharge ( $q = 0.12$  ksf). The structures to build are two clarifiers ( $q = 1.8$  ksf), an administration building ( $q = 4.0$  ksf), and an office tower ( $q = 10.0$  ksf). The detailed soil profile is indicated on the borehole log. The UniSettle4 manual contains the example in the file called “Example 5 - Multi structures.Unisettle4”.

The task for the foundation design is to determine if the clarifiers can be placed on grade or not. The file is prepared for calculating the settlement in the center and edge of Clarifier No. 1. The calculation returns a total settlement of 4.8 in and a differential of 1.5 in. Depending on structural conditions and pipeline connections, etc., this much differential settlement can probably be accepted.



The building and the tower will require pile foundations. The question is how deep must the piles be installed to ensure that settlements will be no more than an inch? UniSettle can provide an immediate answer if the foundation depth of the building (and the tower, in turn) is changed from the 4 feet assigned in the file for a suitable depth for an equivalent footing. When details of the pile groups and loads have been decided (the UniPile program will be indispensable for this purpose), UniSettle can perform the necessary settlement calculations with full control of the contributory effects of the adjacent fill and structures.

Further calculation results are not presented here. The UniSettle file “Example 5 - Multi structures.Unisettle4” contains all the input and the User can phrase the relevant settlement questions and practice computing the answers. Notice that the general surcharge has been assigned a constant vertical stress distribution. Because its wide breadth and length, a Boussinesq distribution would have required a precision of about 1.0 ft to generate correct values, which would have required excessive computation time.

## 15.4 Earth Stress and Bearing Capacity of Retaining Walls

**Example 15.4-01** Taylor's unsurpassed textbook "Fundamentals of Soils" (Taylor, 1948) contains several illustrative examples on earth stress and bearing capacity of retaining walls. The first example quoted is a simple question of the difference in the earth stress coefficient when considering as opposed to disregarding that the ground surface behind a wall is sloping  $20^\circ$  (1(H):0.36(V)). The problem assumes Rankine earth stress (that is, wall friction angle is zero). Taylor writes: "*Determine the percentage error introduced by assuming a level fill when the slope angle actually equals 20 degrees. Assume a friction angle of 35 degrees and a vertical wall.*" A computation using UniBear<sup>1</sup> shows that the earth stress coefficient,  $K_a$ , is 0.27 for the level backfill and 0.34 for the sloping backfill. The error in disregarding the slope is a 20 % underestimation of the magnitude of the earth stress.

**Example 15.4-02** Taylor (1948) includes an example asking for the difference in earth stress coefficient between a wall leaning away from the soil as opposed to leaning toward the soil. The leaning (inclination) is 2 inches per foot, the soil density is 100 pcf, the friction angle is 35 degrees, the ground surface is level, and there is no wall friction. Computation shows that the  $K_a$ -coefficient is 0.33 for an inclination away from the backfill soil and 0.18 for leaning toward the backfill. The  $K_a$ -coefficient for a vertical wall is 0.25. Obviously, the inclination of the wall should not be disregarded in a design analysis.

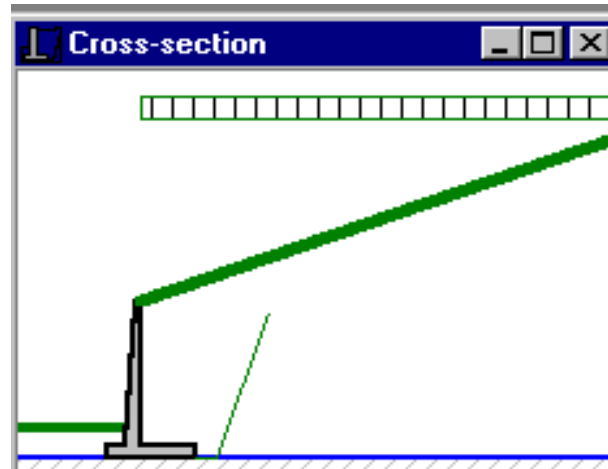
**Example 15.4-03** Taylor (1948) also deals with a 25 feet high concrete gravity wall (density 150 pcf) with a 4-foot width at the top. The inside face of the wall is vertical and the wall retains soil with a 35-degree friction angle and a density of 100 pcf. The wall friction angle is 30 degrees and the cohesion intercept is zero. Taylor asks for the required width of the wall if the resultant has to be located exactly in the third point of the base considering the case of (1) no wall friction and (2) wall friction included. He also asks for the base stresses and the safety against sliding. Taylor's text uses the Terzaghi original approach to the bearing capacity coefficients. A diagram in the book indicates that the  $N_q$ ,  $N_c$ , and  $N_\gamma$  coefficients are about 22, 37, and 21 for  $\phi = 30^\circ$ . According to the expressions by Meyerhof, the coefficients are 33, 36, and 44, respectively, and according to the expressions by Caquot and Kerisel, they are 33, 36, and 48, respectively. For the Caquot and Kerisel coefficients, for example, UniBear computes a necessary base width of 9.5 feet for the case of no wall friction on the condition that the resultant lies in the third point. The factor of safety on sliding is 2.09, which is adequate. However, the factor of safety for bearing is a mere 1.11, which is not adequate. Kind of a sly example, is it not?

The disregard of wall friction is not realistic, which perhaps is what Taylor intended to demonstrate. N.B., Taylor did not 'correct' for inclined load. When the wall friction is included, the numbers change considerably and even allow a reduction of the wall base width to 5 feet with adequate factors of safety for both sliding and bearing. As the wall has no footing, including wall friction is appropriate.

**Example 15.4-04** The following cantilever wall example is quoted from The Civil Engineering Handbook (Chen and McCarron, 1995): The wall is 7.6 m high and wall retains a sand soil with a  $\phi' = 35^\circ$  and a density of  $1,900 \text{ kg/m}^3$ . The wall friction is indicated as equal to the soil friction. The ground surface slopes upward and the slope is stated both as  $24^\circ$  and as 1 m over a distance of 2.8 m, that is, an angle of  $19.7^\circ$ . Both values are used in the calculations in the book. The applicable allowable bearing stress is stated to be 360 kPa. The location of the groundwater table is not mentioned in the book. It is therefore assumed to be well below the footing. A 0.6 m surcharge on the ground surface of soil with the same density as the backfill is included.

---

<sup>1</sup> Since 2009, the UniBear software, being inoperable under Windows 7 and later systems, is no longer marketed.



The calculations in the book estimate  $K_a$  from the 24-degree slope combined with a nomogram based on logarithmic spiral calculations to be 0.38, as opposed to 0.33 according to the usual Coulomb relation.

The calculations by Chen and McCarron (1995) are made with some effort-saving minor simplifications and the book gives the total gravity force as 614 kN/m and the horizontal and vertical (wall friction component) earth stress forces as 301 kN/m and 211 kN/m. Computations using UniBear<sup>2</sup> result in 669 kN/m, 315 kN/m, and 220 kN/m, respectively. A good agreement. The small difference lies in that UniBear allows including also the outside surcharge on the footing toe in the calculation of the gravity forces.

The book adds the gravity vertical force and the earth stress vertical forces to a total vertical force of 25 kN, and uses this value to calculate the sliding resistance to  $825 \text{ times } \tan 35^\circ = 578 \text{ kN/m}$ . UniBear calculates 890 kN/m and 670 kN/m, which are about the same values. The book gives an eccentricity of 0.25 m, UniBear 0.30 m. The book gives a sliding ratio of 1.9, UniBear 2.1. The differences are slight and the values would appear to indicate a safe situation.

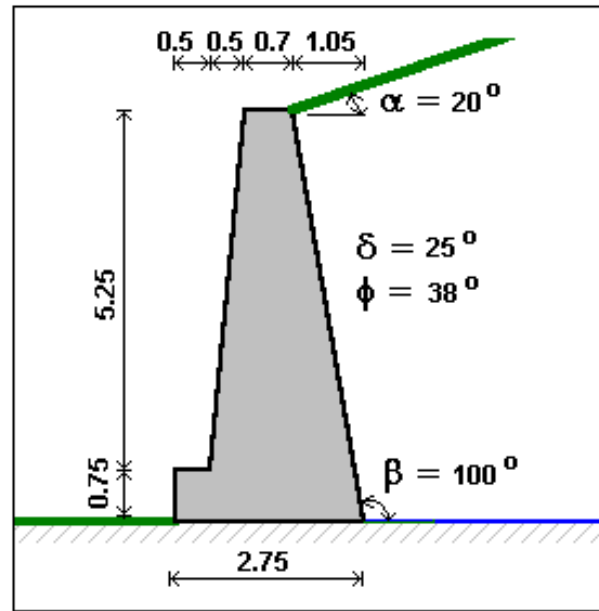
However, it is principally incorrect to calculate the earth stress using full wall friction on a cantilever wall. A UniBear calculation applying a zero wall friction results in an eccentricity of 1.4 m and a sliding ratio of 1.3. Neither is acceptably safe.

A further difference is that the textbook determines a maximum edge stress of 245 kPa for the full base width without considering the eccentricity and compares this to the allowable bearing, 360 kPa (the 360 kPa-value must be including a factor of safety). In contrast, UniBear determines the average stress over the equivalent footing and compares this to the allowable stress (WSD design). The particulars of the bearing soil were not given. With the assumption that the soil under the base is the same as the backfill, that the groundwater table lies at the base, and that the Meyerhof coefficients apply, the computations result in a bearing resistances of 580 kPa and a factor of safety of only 1.4.

**Example 15.4-05.** Example 15.4-05 is quoted from a soil mechanics textbook (Craig 1992). The example consists of a simple gravity wall as illustrated below and the text asks for the sliding resistance and the maximum and minimum stresses underneath the footing. The densities of the wall and of the backfill are  $2,350 \text{ kg/m}^3$  and  $1,800 \text{ kg/m}^3$ , respectively. The soil has friction only and  $\phi'$  and  $\delta'$  are equal to  $38^\circ$  and  $25^\circ$ , respectively. The wall slope angle,  $\beta$ , is  $100^\circ$  and the ground slope angle,  $\alpha$ , is  $20^\circ$ .

<sup>2</sup> Since 2009, the UniBear software, being inoperable under Windows 7 and later systems, is no longer marketed.





The textbook indicates that the earth stress coefficient is 0.39, which is calculated assuming that the earth stress acts on the wall with full wall friction present. The calculated horizontal and vertical components of the earth stress are 103 kN/m and 72 kN/m, respectively. The weight of the structure is 221 kN/m and the resultant is located 0.98 m from the toe. The eccentricity is 0.40 m or about 15 % of the footing width. That is, the resultant lies within the middle third. The calculated sliding ratio is 1.33, which is somewhat low.

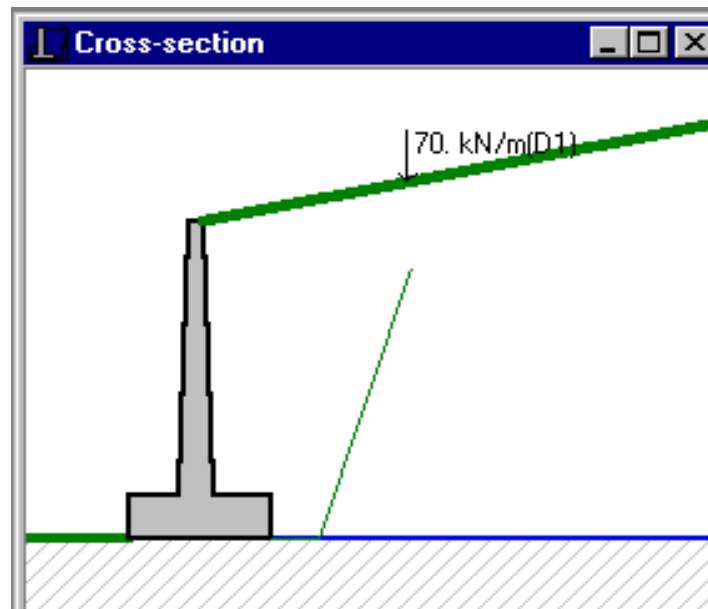
If the calculations are made for the earth stress acting against a normal rising from the heel of the footing and, therefore, with zero wall friction, an earth stress coefficient results of 0.29 and the horizontal component of the earth stress is 108 kN/m, which is close to the textbook's calculated value. The earth stress has no vertical component, but the weight of the backfill wedge on the wall (61 kN/m) is included in the analysis. It is about equal to the vertical component of the earth stress (72 kN/m) calculated by the textbook, so the new vertical force is essentially unchanged. The sliding ratio is 1.22, slightly smaller than before. A six-of-one-and-half-a-dozen-of-another case, is it? However, the resultant is not in the same location and the new eccentricity is 0.54 m or about 20 % of the footing width. That is, the resultant lies outside the middle third of the footing and this is not a safe situation. The UniBear approach is recommended for actual design situations.

The maximum and minimum stresses,  $q_{\max}$  and  $q_{\min}$  can be calculated from the following expression with input of the footing width,  $B$ , and eccentricity,  $e$ . For  $q_{\max}$  use the plus sign and for  $q_{\min}$  use the minus sign.

$$q_m = \frac{Q_v}{B} \left( 1 \pm \frac{6e}{B} \right)$$

Notice, the expression builds on that the stress distribution can be assumed to be linear. However, once the resultant lies outside the middle third, this is not a valid assumption.

**Example 15.4-06.** Example 15.4-06 demonstrates the influence of a line load. The case is taken from a text book by Bowles (1992) and presents a cantilever wall with a sloping ground surface and a 70-kN line load on the ground surface. The footing thickness and width are 1.0 m and 3.05 respectively (no information is given on the density of the wall, regular concrete density is assumed). The stem thickness is 0.73 m at the footing, 0.30 m at the top, and the stem height is 6.1 m. The ground surface slopes 5H:1V. The soil density is  $1,745 \text{ kg/m}^3$ , and the soil and wall friction angles are equal and  $35^\circ$ . The textbook requests the active earth stress and its point of application. The textbook gives the answer to the problem as "an earth stress of 164 kN/m acting  $58.6^\circ$  from the horizontal" (probably intending to say "vertical").



UniBear calculates a horizontal component of the backfill earth stress of 147 kN/m and the total horizontal stress from the line load of 31 kN/m, together 178 kN/m, not quite the value given in the textbook. However, these values are obtained using a wall friction of zero degrees, which as mentioned is recommended for cantilever walls. A calculation with the wall friction equal to the soil friction,  $35^\circ$ , results in horizontal and the vertical earth stress components of 112.5 kN/m and 78.75 kN/m, respectively. The sum of the horizontal components of the line load and earth stress is equal to 143.6 kN/m. The resultant to this load and the vertical earth stress is 164 kN, the same as given in the textbook. The angle between this load and the normal to the footing, the "vertical", is  $61^\circ$ , very similar to that given in the textbook.

Notice, that UniBear also calculated the vertical component of the line load that acts on the heel. For the subject example, it is 5 kN/m. Before UniBear, it was rather cumbersome to include this component and it was usually omitted. For reference to old analysis cases involving surface loads, some may desire to exclude the effect of this vertical component. This can be easily done by imposing a vertical line load on the footing that is equal on magnitude to the vertical component of the surface line load and which acts at the same distance from the toe but in the opposite direction.

## 15.5 Pile "Capacity" and Load-Transfer

**Example 15.5-01** Hunter and Davisson (1968) presented an important paper on analysis of load transfer of piles in sand. The paper was the first to show measurements of residual forces in full-scale tests, and that such forces will greatly affect the load transfer evaluated from load measurements in a static loading test (as was postulated by Nordlund 1963). The case history demonstrates that residual force is not restricted to piles in clay but will develop also for piles in sand. The findings were later confirmed by the case history reported by Gregersen et al. (1973). Indeed, the two cases show that a drag force will also develop for piles in sand.

The tests were performed in a homogeneous deposit of "medium dense medium to fine sand" with SPT N indices ranging from 20 through 40 (mean value of 27) and a bulk saturated density of the sand of 124 pcf. The groundwater table was at a depth of 3 ft (hydrostatic pore pressure distribution can be assumed). Laboratory tests indicated an internal friction angle in the range of 31 degrees through 35 degrees. The friction angle for a steel surface sliding on the sand was determined to 25 degrees.

Static loading tests in push (compression test) followed by pull (tension test) were performed on six piles instrumented with strain gages and/or telltales. The piles were all installed an embedment depth of 53 ft and had a 2-foot stick-up above ground. The detailed test data are not included in the paper, only the total load and the evaluated toe loads (in both push and pull).

Pile #	Type	Shaft area (ft <sup>2</sup> /ft)	Toe area (ft <sup>2</sup> )	Installation manner
1	Pipe 12.75"	3.96	0.98	Driven; Vulcan 140C

The shaft cross section area includes the areas of guide pipes and instrumentation channels. The shaft surface area of the H-pile is given as the area of a square with a side equal to the flange width.

The paper does not include the load-movement curves from the static loading tests, only the evaluated ultimate resistances. The following table summarizes the ultimate resistances (pile capacities) and the toe resistances evaluated from the tests.

Pile #	Push Test			Pull Test		Adjusted Push	
	R <sup>ult</sup> (kips)	R <sub>s</sub> (kips)	R <sub>t</sub> (kips)	R <sub>s</sub> (kips)	'R <sub>t</sub> ' (kips)	R <sub>s</sub> (kips)	R <sub>t</sub> (kips)
1	344	248	96	184	-74	174	170

The table data indicate that the piles were subjected to a negative (-74 kips) toe resistance during the pull test, which, of course, is not possible. (It would mean that there was someone down there holding on and pulling the other way). The negative toe resistance observed is due to residual force induced in the pile caused by the pile installation and the preceding push test. If the 184-kip resistance measured in the pull test is taken as the true shaft resistance, the true toe resistance would be 160 kips (344 - 184).

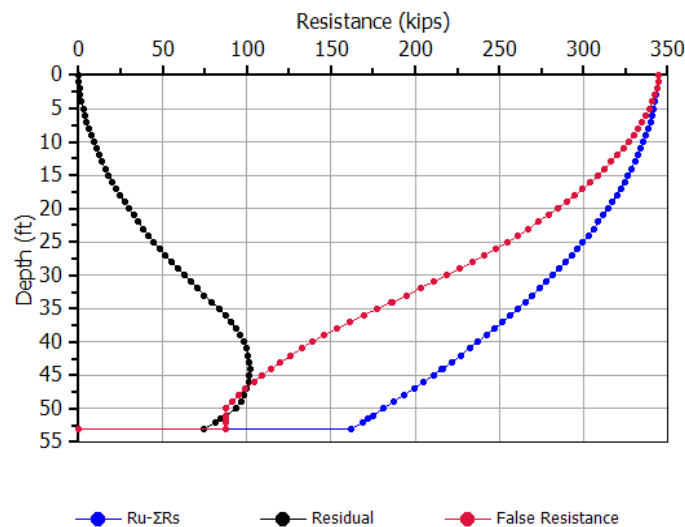
Hunter and Davisson (1969) adjusted the data for the push test by increasing the toe load by a value equal to the 74-kip apparent negative toe load of the pull test and decreasing the shaft resistance correspondingly—linearly to the pile head. The so-adjusted values are shown in the two rightmost columns above.

The paper reports the effective stress parameters in a beta-analysis matched to the data. These data have been compiled in the table below and used as input to the UniPile program<sup>3)</sup> together with the soil and pile data as given above. The results of the UniPile computations are included in the table.

Pile #	Input Values		UniPile Analysis		
	$N_t$ (--)	$\beta$ (--)	$R^{ult}$ (kips)	$R_t$ (kips)	$R_s$ (kips)
1	53	0.50	377	194	183

The paper concludes that there is a difference in shaft resistance in push and pull as indicated by the different beta-coefficients evaluated from the push and pull tests. However, a review of the data suggest that the beta-coefficient determining the shaft resistance lies in the range of 0.45 through 0.52 for the piles and that the shaft resistance is about the same in push and pull. A “perfect” match to the 344-kip total resistance and the shaft and toe resistances of 184 and 160 kips (165-ksf), respectively, is achieved using a  $\beta$ -coefficient of 0.47 and an  $N_t$ -coefficient of 47. However, the purpose of this account is not to discuss the merits of details given in the paper, but to use the data to demonstrate the load-transfer analysis. The significance of the paper is the clear demonstration that the influence of residual forces must be included in the evaluation of pile test data.

The amount and distribution of residual force in a pile can be calculated by the same effective stress approach as used for matching the test data. A computation of Pile 1 with a residual force portion of 46 % of the toe resistance results in a computed residual toe resistance of 74 kips, which would mean that the “negative toe resistance” is close to what the authors reported in the paper. The corresponding “false shaft and toe resistances” are 258 and 88 kips, respectively. The diagram presents the push-test load transfer curves for the True Resistance, the Residual Force, and the False Resistance distribution curves as determined using the UniPile program.



<sup>3)</sup> For information on the program, visit <https://www.unisoftGS.com>

**Example 15.5-0.2** Altaee et al. (1992) presented results and analysis of an instrumented 285 mm square precast concrete pile installed to an embedment of 11.0 m into a sand deposit. Three sequences of push (compression) testing were performed, each close to the ultimate resistance of the pile followed by a pull (tension) test. The instrumentation registered the loads in the pile during the static push testing, but did not provide accurate data during the pull test. During the push test, the groundwater table was at a depth of 6.2 m. During the pull test, it was at 5.0 m. The maximum load applied at the pile head was 1,000 kN, which value was very close the capacity of the pile. The pull test ultimate resistance was 580 kN.

The paper reports both the soil parameters and the magnitude of the residual force affecting the test data. The effective stress parameters are as follows.

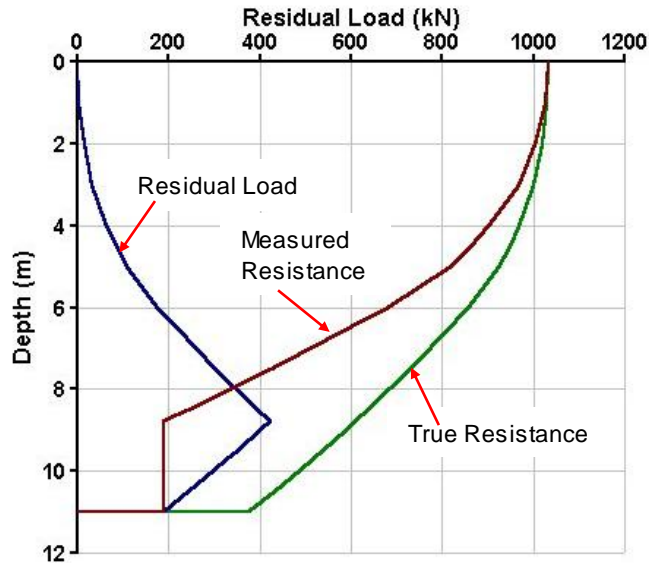
Layer	Depth (m)	Total Density (kg/m <sup>3</sup> )	$\beta$	$N_t$
Silt-Sand	0.0 - 3.0	1,600	0.40	--
Dry Sand	3.0 - 5.0	1,800	0.50	--
Moist Sand	5.0 - 6.5	1,900	0.65	--
Sat. Sand	6.5 - 11.0	2,000	0.65	30

The data have been used as input to a UniPile computation returning a capacity value of 1,034 kN, which is acceptably close to the measured load of 1,000 kN. The table below shows the computed results. The first column shows the computed resistance distribution (at ultimate resistance). The second column shows the results of a residual force computation with 50 % utilization of  $N_t$  (as matched to the data reported in the paper). The column headed “False Resistance” is obtained as the difference between the first two. A comparison with the recorded test data, shown in the far right column, indicates clearly that the data recorded during the test are affected by residual force. The small differences in agreement can easily be removed by inputting the soil parameters having the precision of an additional decimal.

DEPTH (m)	RES.DISTR. (kN)	RES.LOAD (kN)	FALSE RES. (kN)	TEST (kN)
0	1,034	0	1,034	1,000
4.5	948	85	863	848
6.0	856	177	679	646
7.5	732	302	430	431
9.0	591	(402)	~300	309
10.0	487	299		
10.5	433	245	188	191
11.0	376	188		

The computations assume that the change between increasing residual force (negative skin friction zone) to decreasing (positive shaft resistance zone) is abrupt (appearing as a ‘kink’ in the curve). In reality, however, the shift between the relative movement from negative and to positive directions occurs in a transition zone. For the tested pile, the analysis shows that this zone extends from about 1.0 m above the neutral plane (Depth 9.7 m) to about 1.0 m below the neutral plane. Therefore, the computed residual force at the Depth 9.0 m is overestimated, which is why it is given in parenthesis in the table. Instead, the residual force between 8.0 m and 12.5 m is approximately constant and about 300 kN. The about 2.0 m length of the transition zone corresponds to about 7 pile diameters in this case history.

The computed shaft resistance in the push test is 657 kN. Repeating the computation for “Final Conditions”, that is, with the groundwater at 5.0 m, the shaft resistance is 609 kN, again acceptably close the tested pull capacity (580 kN). Besides, the analysis of the test data indicates that a small degradation of the shaft resistance occurred during the push testing. Considering the degradation, the shaft resistances in push and pull are essentially of equal magnitude. The load-transfer curves are shown in the following diagram (the calculations do not include input of transition zone height).



**Example 15.5-03** Example 15.5-03 is a case history also obtained from the real world. However, in the dual interest of limiting the presentation and protecting the guilty, the case has been distorted beyond recognition. A small measure of poetic license has also been implemented. The example is from a foundation course that I used to give at University of Ottawa, where the students not only studied foundation analysis and design, but also practiced presenting the results in an engineering report. In this case, , the solution to the assignment was to be in the format of a consulting engineering letter report in reply to the assignment letter.

**Letter to Engineering Design and Perfection Inc. from Mr. So-So Trusting, P. Eng., of Municipal Waterworks in Anylittletown**

*Dear Sir: This letter will confirm our telephone conversation of this morning requesting your professional services for analysis of the subject piling project with regard to a review of integrity and proper installation procedure of the New Waterworks foundation piles.*

*The soil conditions at the site are described in the attached Summary of Borehole Records. These data were obtained before the site was excavated to a depth of 4.0 m. The piles are to support a uniformly loaded floor slab and consist of 305 mm (12 inch), square, prestressed concrete piles. The piles have been installed by driving to the predetermined depth below the original ground surface of 12.0 m (39 ft). The total number of piles is 700 and they have been placed at a spacing, center-to-center, of 2.0 m (6.5 ft) across the site.*

*An indicator pile-testing programme was carried out before the start of the construction. The testing programme included one static loading test of an instrumented test pile. Plunging failure of the test pile occurred at an applied load of 2,550 kN (287 tons) and the measured ultimate shaft resistance acting on the pile was 50 kN (6 tons) in the upper sand layer and 400 kN (45 tons) in the lower sand layer. The measured ultimate toe resistance was 2,100 kN (236 tons).*

*Relying on the results of the indicator test programme, our structural engineer, Mr. Just A. Textbookman, designed the piles for an allowable load of 1,000 kN incorporating a safety factor of 2.5 against the pile capacity taken as 2,500 kN (the 50-kN resistance in the upper sand layer was deducted because this layer was to be removed across the entire site after the pile driving).*

*The contractor installed the piles six weeks ago to the mentioned predetermined depth and before the site was excavated. The penetration resistance at termination of the driving was found to be about 130 blows/foot, the same value as found for the indicator piles.*

*After the completion of the pile driving and removal of the upper 4.0 m sand layer, our site inspector, Mr. Young But, requested the Contractor to restrike two piles. For both these piles, the blow count was a mere 4 blows for a penetration of 2 inches, i.e., equivalent to a penetration resistance of 24 blows/foot! A subsequent static loading test on one of the restruck piles reached failure in plunging when the load was being increased from 1,250 kN to 1,500 kN. We find it hard to believe that relaxation developed at the site reducing the pile capacity (and, therefore, also the penetration resistance) and we suspect that the piles have been broken by the contractor during the excavation work. As soon as we have completed the change-order negotiations with the contractor, we will restrike additional piles to verify the pile integrity. Meanwhile, we will appreciate your review of the records and your recommendations on how best to proceed.*

*Sincerely yours,*

*Mr. So-So Trusting, P. Eng.*

#### **SUMMARY OF BOREHOLE RECORDS**

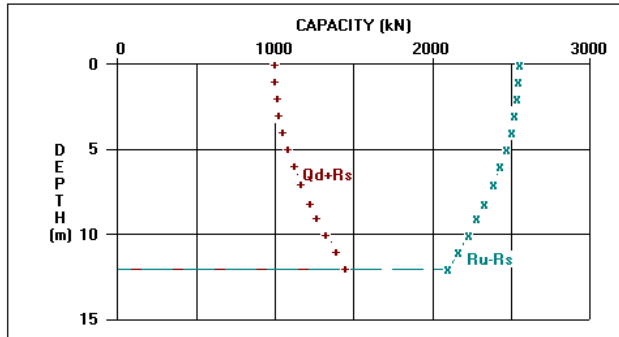
The soil consists of an upper layer of loose silty backfill of sand with a density of 1,700 kg/m<sup>3</sup> (112 pcf) to a depth of 4 m (13 ft) and placed over a wide area. The sand is followed by a thick deposit of compact to dense clean sand with a density of 2,000 kg/m<sup>3</sup> (125 pcf) changing to very dense sand at about 12.0 m (31 ft), probably ablation till. The groundwater table is encountered at a depth of 5.0 m (15 ft).

**Comments.** Hidden in Mr. Trusting's letter is an omission which cost the engineers in the ensuing litigation. The results of the two static tests were not analyzed! An effective stress analysis can easily be carried out on the records of the indicator pile test to show that the measured values of shaft resistance in the upper and lower sand layers correspond to beta ratios of 0.30 and 0.35, respectively and that the toe coefficient is 143 (the actual accuracy does not correspond to the precision of the numbers).

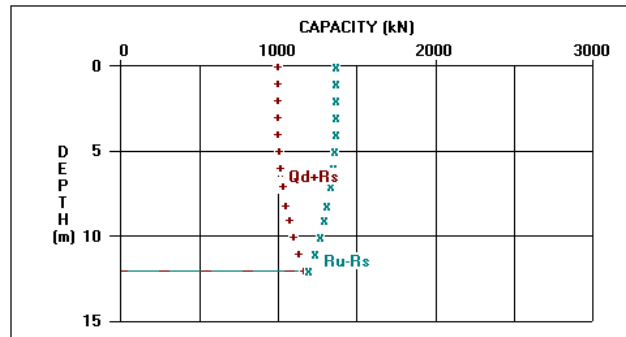
Had Mr. Trusting performed such an analysis, he would have realized that excavating the upper sand layer not only removed the small contribution to the shaft resistance in this layer, it also reduced the effective stress in the entire soil profile with a corresponding reduction of both shaft and toe resistance. In fact, applying the mentioned beta ratio and toe coefficient, the shaft and toe resistance values calculated after the excavation are 170 kN (19 tons) and 1200 kN (135 tons), respectively, to a total capacity of 1,366 kN (154 tons), a reduction to about half the original value. No wonder that the penetration resistance plummeted in restriking the piles! (Note that the reduction of toe resistance is not strictly proportional to the change of effective overburden stress. Had the load-movement curve from the static loading test been analyzed to provide settlement parameters, a load-movement curve could have been determined for the post-excavation conditions. This would have resulted in an evaluated toe resistance being slightly larger than the value mentioned above).

Obviously, there was no relaxation, no problem with the pile integrity, and the contractor had not damaged the piles when excavating the site. In the real case behind the story, the engineers came out of the litigation rather red-faced, but they had learnt—and paid for the lesson—the importance of not to exclude basic soil mechanics from their analyses and reports.

### BEFORE EXCAVATION



### AFTER EXCAVATION



**Example 15.5-04** deals with scour and it also originates in the real world. A couple of bridge piers are founded on groups of 18 inch (450 mm) pipe piles driven closed-toe through an upper 26 ft (8 m) thick layer of silty sand and 36 ft (11 m) into a thick deposit of compact sand. The dry-season groundwater table lies 6.5 ft (2 m) below the ground surface. During the construction work, a static loading test established that the pile "capacity" was 380 tons (3,400 kN), which corresponds to beta-coefficients of 0.35 and 0.50 in the silty sand and compact sand, respectively, and a toe bearing capacity coefficient of 60. The design load was 1,600 kN (180 tons), which indicates a factor of safety of 2.15—slightly more than adequate.

The static test had been performed during the dry season and a review was triggered when the question was raised whether the capacity would change during the wet season, when the groundwater table was expected to rise above the ground surface (bottom of the river). In the project review, it was discovered that the upper 3 m (10 ft) of the soil could be lost to scour. However, in the design of the bridge, this had been thought to be inconsequential to the pile capacity. So, what would the effect be of scour?

A static analysis will answer the question about the effect on the pile capacity after scour. The distribution of pore water pressure is hydrostatic at the site and, in the Spring, when the groundwater table will rise to the ground surface (and go above), the effective overburden stress reduces. As a consequence of the change of the groundwater table, both pile shaft resistance and toe resistance reduce correspondingly and the new total resistance is 670 kips (3,000 kN). That is, the factor of safety is no longer 2.11, but the somewhat smaller value of 1.86—not quite adequate.

When the effect of scour is considered, the situation worsens. The scour can be estimated to remove the soil over a wide area around the piers, which will further reduce the effective overburden stress. The capacity now becomes 275 tons (2,460 kN) and the factor of safety is only 1.51. The two diagrams below show the resistance distribution curves for the condition of the static loading tests and for when the full effect of scour has occurred. (The load distribution curve,  $Q_d + R_s$ , is not shown).

Missing the consequence of reduced effective stress is not that uncommon. The TRUSTING case history in the foregoing is an additional example. Fortunately, in the subject scour case, the consequence was not so traumatic. Of course, the review results created some excitement. And had the site conditions been different, for example, had there been an intermediate layer of settling soil, there would have been cause



for some real concern. As it were, the load reaching the toe of the piles was considered to be smaller than the original ultimate toe resistance, and therefore, the reduced toe resistance due to reduced effective overburden stress would result in only small and acceptable pile toe penetration, that is, the settlement concerns could be laid to rest. In this case, therefore, it was decided to not carry out any remedial measures, but to keep a watchful eye on the scour conditions during the wet seasons to come. Well, a happy ending, but perhaps the solution was more political than technical.



**Example 15.5-05** The unified method for design of piled foundations was developed in the early 1980s. It combines load transfer, drag force, settlement, and downdrag in an interactive—unified—approach and was first published by Fellenius (1984). Fellenius (1988) advanced the approach and included a design example which was the first example of how to pursue a numerical analysis per the method.

The example comprises a narrow pile group of 10 piles to be installed at the site, where the soil profile consisted of 10 m of slightly overconsolidated clay on a 4 m thick layer of sand. Below the sand lies a 20 m thick layer of overconsolidated silty clay deposited on dense ablation till. The groundwater table is at the original ground surface and the pore pressure is hydrostatically distributed. In conjunction with installing the piles and erecting the structure, a 2 m thick fill was placed across the site, imposing a stress of 36 kPa. The calculations assumed ultimate resistance conditions as indicated in the below table.

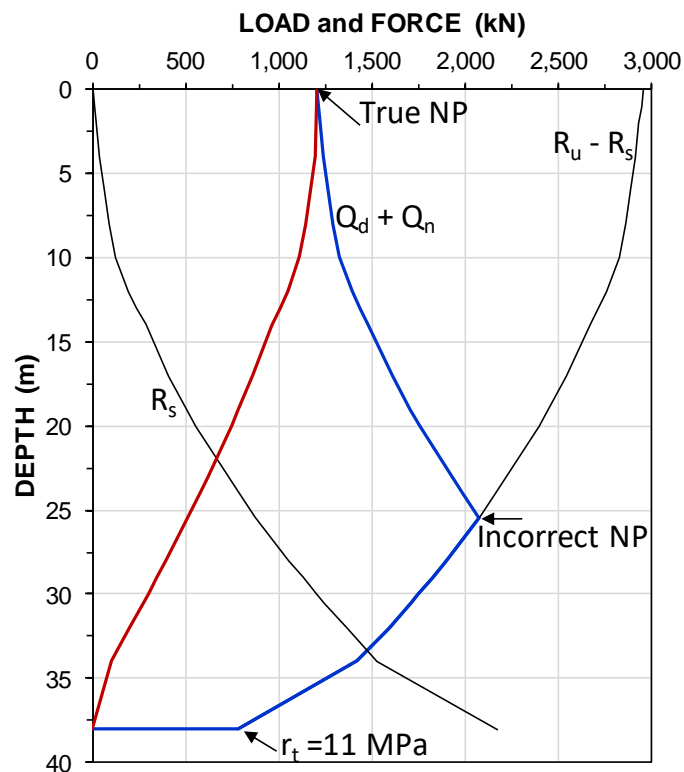
Depth Range (m)	Type (---)	Density kg/m <sup>3</sup>	$\beta$ (---)	$m$ (---)	$m_r$ (---)	$j$ (---)	$\Delta\sigma'$ (kPa)
0 - 2	Fill	1,800	0.50	--	--	--	--
2 - 10	Clay	1,550	0.25	<b>20</b>	200	0	<b>20</b>
10 - 14	Sand	2,000	0.45	250	---	0.5	--
14 - 34	Clay	1,740	0.35	<b>80</b>	350	0	120
34 - --	Till	2,100	0.60	400	---	0.5	--

Unit toe resistance was assumed to be 11 MPa

The values in the table were back-calculated from a static loading test on a 12.75-inch pipe pile in the indicated soil profile carried out before the fill was placed. The back-calculated values are at ultimate resistance conditions, that is, at relatively large pile movements—the paper indicates a toe movement of about 15 mm. The paper used the ultimate resistance values to calculate the long-term distribution of force and depth to the neutral plane for a single pile with the effect of the fill included.

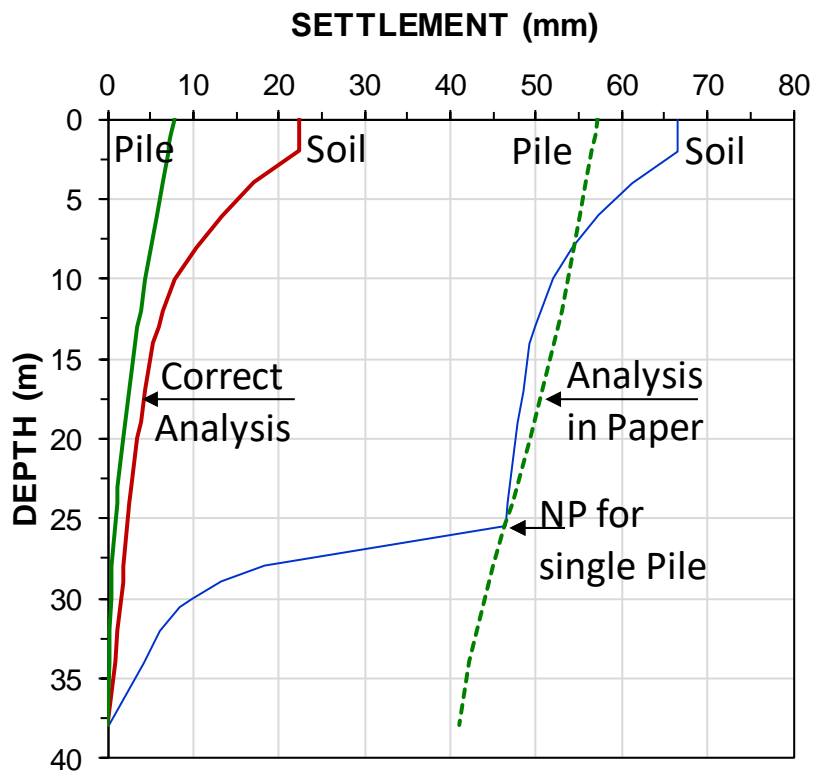
The 10 piles consisted of 300 mm diameter pipe piles driven closed-toe to 38 m depth below the fill surface. The piles were concrete-filled after driving and the intended allowable working load per pile was 1,400 kN of which 1,200 kN is dead load and 200 kN is live load. The maximum structurally allowable axial load at the neutral plane was set to 2,100 kN. The pile cap footprint is 3.5 m by 5.0 m, i.e., the area is 17.5 m<sup>2</sup> and, thus, the total 12,000 kN sustained load corresponds to a 686-kPa stress over the footprint.

The calculated values of capacity and resistance distribution are shown in the below figure. The original calculations were made before the advent of the personal computer which means that they included shortcuts and simplifications necessary for hand calculations. However, the main difference is that the original calculations applied ultimate resistances (i.e., large movements). When, which was not easily done before computers and software, the calculations are adjusted to the fact that the movements between the pile and the soil are small, essentially zero at the pile toe, the neutral plane (the force equilibrium) must be close to the pile head, as indicated ("true NP"). Note, as in the paper, no transition zone is indicated.



At the time of writing the paper, the fact that the pile toe load-movement relation is an essential part of the pile-soil response as well as of the location of the neutral plane was only partially understood—thus, the "ultimate" toe resistance was erroneously applied in determining the depth to the neutral plane, NP. Moreover, neither was the necessity of considering the stiffness effect of a group piles on the compressibility of the soil between the neutral plane and the pile toe level. The settlement distribution for the pile narrow group presented in the paper was therefore incorrect.

The below figure shows the distribution of the soil settlement and pile for the analysis presented in the paper and for a correct analysis. The latter includes less than ultimate shaft resistances and zero toe movement and, therefore, no toe resistance.

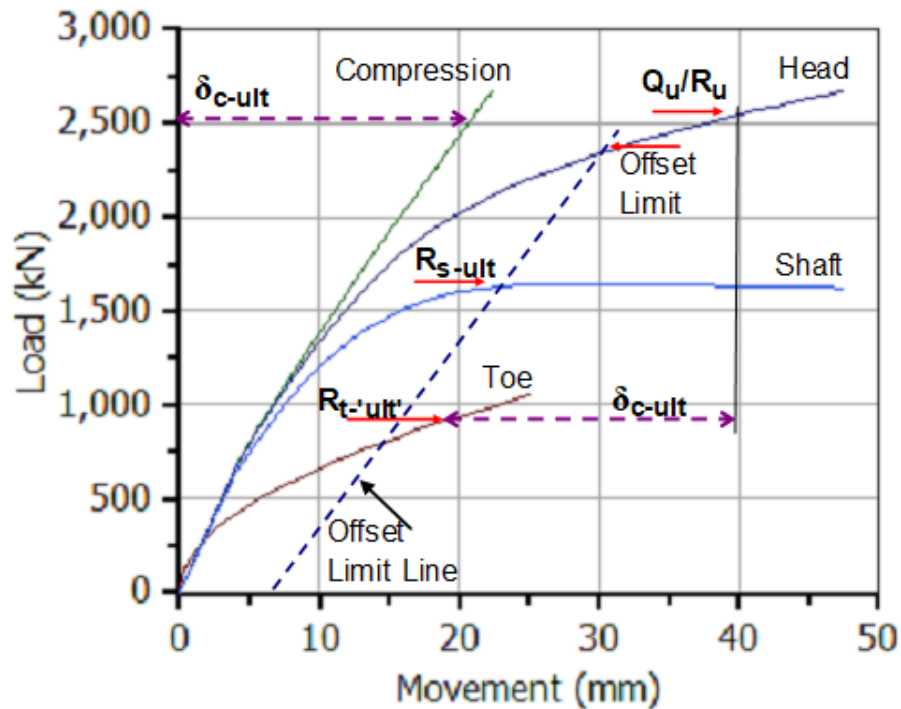


The "Analysis in Paper" refers to the analysis results in Fellenius (1988). It is marked incorrect because it assigned the equivalent raft to the depth of the N.P., as opposed to the depth of the pile toe. However, it did match the pile toe force to the pile toe movement.

Piles comprising a narrow pile group, as in the example, respond as single piles with regard to drag force and depth to the N.P. However, settlement should be calculated as from an equivalent raft at the pile toe level, with the raft breadth and width slightly expanded (the equivalent raft widened) to account for the spreading of stress from gradual increase of soil stress from the N.P. to the pile toe level (Section 7.17.2 and Fig. 7.26).

Back in the 1980s, there was no easy way to simulate the load-movement results of a static loading test. However, with UniPile it is very simple. By selecting suitable  $t-z$  and  $q-z$  functions, UniPile applies the soil parameters and pile properties and calculates the loading test results illustrated in the below figure. Each soil layer was assumed to be governed by a different  $t-z$  function. As no actual test data are available to fit to the results, the only effort made was to select the movement values, particularly for the  $q-z$  function in the till so that the capacity,  $Q_u/R_u$ , eye-balled from the test curve matches the ultimate shaft resistance,  $R_{S-ult}$ , and the calculated toe resistance,  $R_{t-ult}$ , mobilized in the test (before placing the fill).

The curves have been supplemented with the "Offset Limit Line", which indicates an Offset Limit slightly lower than the assumed capacity. It would neither be time-consuming nor difficult to re-select the  $t-z$  and  $q-z$  curves to establish a "perfect" agreement between the capacity calculation and a target load equal to the Offset Limit load. However, as there are no actual test data to fit to, such effort would only be for cosmetic reasons.



### 15.6 Back-analysis of Static Loading Test

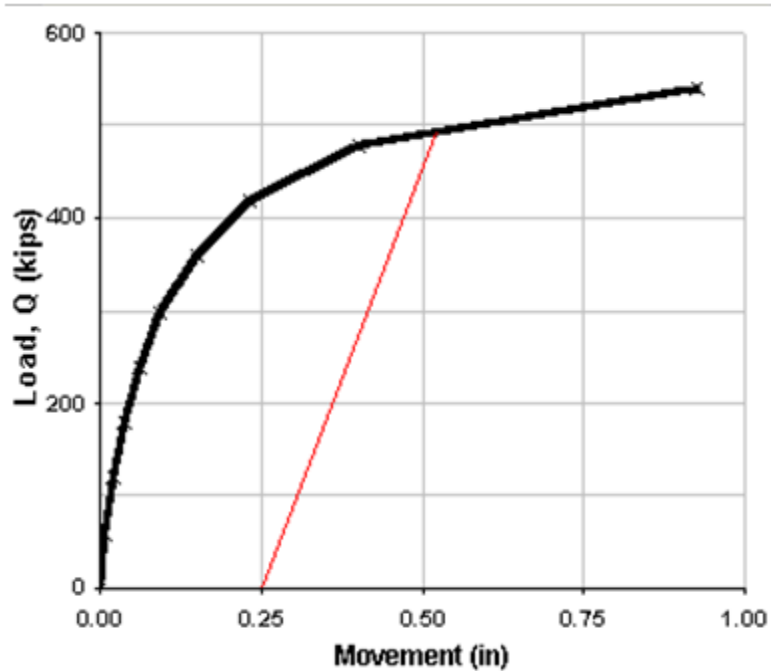
**Example 15.6-01** Example 15.6-01 is from the testing of a 40 ft long H-pile. The pile description and the load-movement test data are as follows:

Head diameter, $b$	= 12.0 inches	Length, $L$	= 40.0 ft
Shaft area, $A_s$	= 4 ft <sup>2</sup> /ft	Embedment, $D$	= 38.0 ft
Section area, $A_{sz}$	= 0.208 ft <sup>2</sup>	Stick-up	= 2.0 ft
Toe diameter, $b$	= 12.0 inches	Toe area, $A_t$	= 1.0 ft <sup>2</sup>
Modulus, $E$	= 29,000 ksi	$EA/L$	= 1,810 kips/inch

The test comprised ten load increments, as follows

Row No.	Jack Load (kips)	Movement Average (inches)
1	0	0.000
2	60	0.007
3	120	0.019
4	180	0.036
5	240	0.061
6	300	0.093
7	360	0.149
8	420	0.230
9	480	0.399
10	540	0.926

The pile capacity is determined by the offset limit construction indicated in the load-movement diagram. The Hansen, Chin-Kondner, and Decourt constructions are not shown, although these methods also work well for the case. However, neither the DeBeer nor the Curvature methods work very well here, and, of course, a capacity-value cannot be eyeballed from the load-movement diagram (change the scales of the abscissa and ordinate and the eyeballed value will change too).

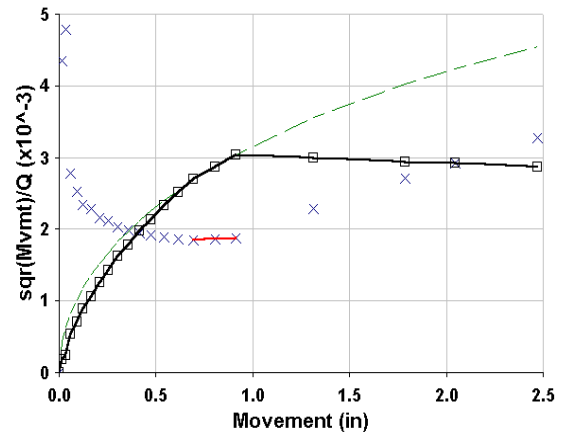
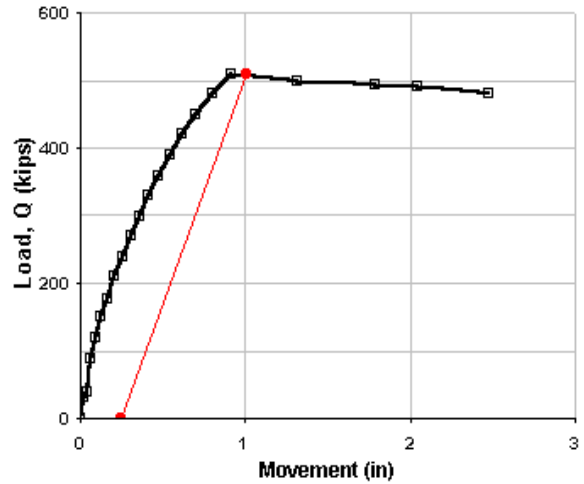


**Example 15.6-02** is from the testing of a hexagonal 12-inch diameter, 112 ft long precast concrete pile. As evidenced from the load-movement diagram shown below, the pile experienced a very sudden failure (soil failure was established) at the applied load of 480 kips. This loading test is an example of when the various interpretation methods are superfluous. Remember, the methods are intended for use when an obvious capacity value is not discernible in the test.

Head diameter, $b$	= 12.0 inches	Length, $L$	= 112 feet	Modulus, $E$	= 7,350 ksi
Shaft area, $A_s$	= 3.464 ft <sup>2</sup> /ft	Embedment, $D$	= 110 feet	$EA/L$	= 682 kips/inch
Section area, $A_{sz}$	= 0.866 ft <sup>2</sup>	Toe diameter, $b$	= 12.0 inches	Toe area, $A_t$	= 0.866 ft <sup>2</sup>
Stick-up	= 2 feet				

The test was aiming for a maximum load of 600 kips to prove out an allowable load of 260 kips with a factor of safety of 2.5. The 2nd diagram shows the Hansen construction and an extrapolation of the load-movement curve. Suppose the test had been halted at a maximum load at or slightly below the 480-kip maximum load. It would then have been easy to state from looking at the curve that the pile capacity is “clearly” much greater than 480 kip and show that “probably” the allowable load is safe as designed. This test demonstrates the importance of not extrapolating to a capacity higher than the maximum load applied to the pile in the test.

Row No.	Jack Load (kips)	Movement Average (inches)
1	0.0	0.000
2	30.0	0.017
3	39.6	0.036
4	88.8	0.061
5	119.2	0.091
6	149.8	0.124
7	177.8	0.166
8	211.0	0.209
9	238.0	0.253
10	271.0	0.305
11	298.2	0.355
12	330.4	0.414
13	357.6	0.473
14	390.2	0.540
15	420.8	0.630
16	450.4	0.694
17	481.0	0.804
18	509.0	0.912
19	500.0	1.314
20	492.4	1.787
21	489.8	2.046
22	480.4	2.472



Note, fitting the Hansen function to the pile head load-movement curve was just to show the trend of the test before the break. Proper use of t-z/q-z functions is to assign them to the individual pile elements and then calculate the pile-head load-movement as an accumulation of the pile element shortening and pile toe movement

**Example 15.6-03** presents analysis of a fictitious static loading test. The example intends to represent a procedure followed for a real test, although it is one "sans" reading errors and occasional data blurbs usually marring the world out there.

The soil profile comprises layers of silt and sand, clay, sandy silt, and sand to the bottom of a borehole drilled at the site. The groundwater level was at 1.0 m depth. Table I summarizes the soil profile and soil parameters at the site. The  $\Delta\sigma$  is the prestress margin of the soil,  $m$  and  $m_r$  are Janbu modulus numbers (compressibility for virgin and reloading conditions, respectively, c.f., Section 3.5). In order to make the settlement calculated in the 15 thick sand (starting at 25 m depth) more pronounced, the compressibility is indicated somewhat lower than realistic.

**TABLE 1 Soil Parameters**

Layer (name)	thickness (m)	density (kg/m <sup>3</sup> )	$\Delta\sigma$ (kPa)	j (--)	$m$ (--)	$m_r$ (--)
Sandy Silt	5	1,900	0	0.5	200	---
Clay	10	1,600	5	0	15	150
Sandy Silt and clay	10	2,000	10	0.5	80	800
Sand	15	2,100	30	1	400	1,000+

The test pile is a 355-mm, circular, 20 m long, precast concrete pile strain-gage instrumented with three gage levels, SG-1, SG-2, and SG-3, at depths of 6, 15, and 19 m, respectively. A toe telltale measured the pile compression. The test schedule comprised a series of twelve 200-kN load increments applied every 15 minute and no unloading/reloading events. Table 2 shows for the series of applied loads and last reading of each load level, the pile-head movement and pile compression and, also the measured strain-gage records. The pile-toe movement is obtained by subtracting the telltale-determined compression from the pile-head movement.

**TABLE 2 Records of Static Head-down Loading-test**

(#)	1	2	3	4	5	6	7	8	9	10	11	12
LOAD (kN)	200	400	600	800	1,000	1,200	1,400	1,600	1,800	2,000	2,200	2,400
HEAD (mm)	0.82	1.98	3.53	5.48	8.15	11.87	16.79	22.52	29.91	38.25	47.59	57.89
SG-1 ( $\mu\epsilon$ )	54	117	180	246	312	380	446	513	580	646	713	780
SG-3 ( $\mu\epsilon$ )	19	58	111	171	233	299	365	431	497	564	630	697
SG-3 ( $\mu\epsilon$ )	13	38	70	112	161	218	279	342	407	472	538	604
COMPR. (mm)	0.80	1.83	3.03	4.25	5.54	6.87	8.21	9.51	10.91	12.26	13.58	14.90

**Preparing Test Records for Back-Analysis.** The main test data comprise the measured pile-head load-movement and pile compression, as plotted in [Figure 1](#). The pile-head load-movement curve is by many used for determining a "capacity" of the test pile that is then related to the intended load; sustained (dead) plus transient (live), the ratio being called "safety factor" or "resistance factor". For many reasons, as listed below, this is a crude and ineffective approach originating in the early 1900s, now quite inadequate.

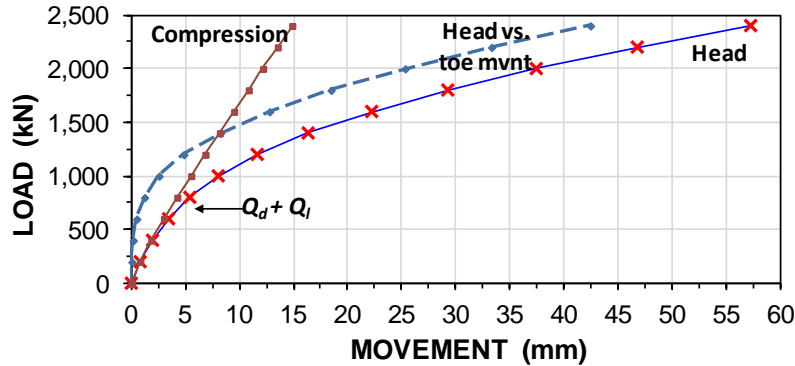


Fig. 1 Pile-head load-movement and pile compression

1. There are many diverging definitions of how to define "capacity" from pile-head load-movement—no generally accepted and applied method exists (c.f., Section 8.2).
2. "Capacity" addresses only one point on the curve.
3. The foundation cares about the settlement for the actual load supported, not about some almost randomly inflated value called "capacity".
4. The conditions of interest are not those of the test occasion, but those of the long-term, in this example case, after the effect of the fill.
5. The "capacity" of the specific test pile is of little use for determining the response of a shorter or longer, slender or wider project pile.
6. A "capacity" estimated from the pile-head load-movement curve cannot be directly coupled to axial force at depth and the "capacity" at the pile head does not represent the sum of "capacities" of the individual pile elements and, moreover, it is unsuitable for assessing changed conditions, in particular the conditions in the long-term in regard to resistance and settlement of the foundation supported on single piles and pile groups (c.f., Section 7.3 and Figure 7.10).

The purpose of instrumenting the test pile with strain gages is to obtain records of force and movement to enable an analysis to determine the parameters suitable for applying the response of different piles and conditions and to obtain the distribution of force in the pile by converting the strains to force. The conversion requires knowing the axial stiffness of the pile expressed as the  $EA$ -relation, where  $E$  is the Young's modulus of the pile materials and  $A$  is the pile cross sectional area. A first estimate of  $EA$  can be obtained from the slope of the measured load-strain as shown in Figure 2.

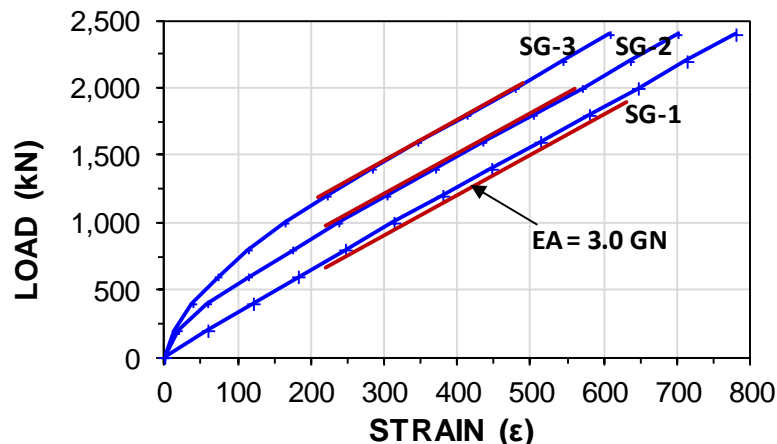


Fig. 2 The applied load versus measured strain



The first portion of each load-strain plot is curved due to the shaft resistance along the portion of the pile above the strain-gage level reducing the force reaching the gage level. The fact that the slopes are essentially constant after an initial portion and also quite parallel suggests that the soil shear response of the example case is essentially plastic.

Provided that the test data are accurate, a more precise estimate of the EA-parameter can be obtained by differentiating the EA-slopes to show change of load divided by change of stress plotted versus strain, i.e., the tangent EA-slopes, as shown in Figure 3. The curves plotted from the data start at large values reducing with increasing strain until the shaft resistance above the gage level has been engaged, whereupon the curves straighten out, here, to somewhat constant values. The slight increase with increasing strain suggests that the shaft resistance is slightly strain-hardening. Were they truly constant, this would indicate a plastic shaft resistance above the gage level. The curves confirm that the EA-parameter is about 3.0 GN, which corresponds to an E-modulus of 30 GPa for the 0.099 m<sup>2</sup>-pile cross section.

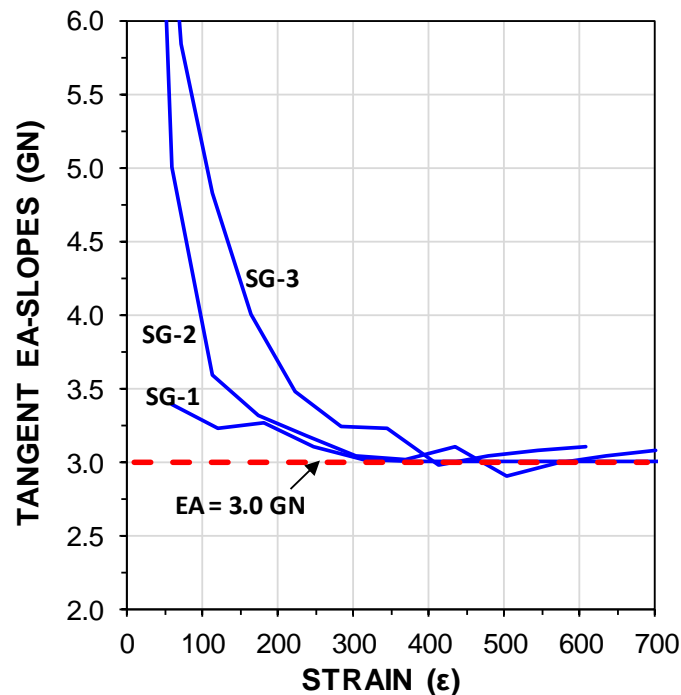


Fig. 3 EA-parameter by the tangent method

The next step is to convert all strain readings to force by multiplying them with the EA-parameter. The data are then plotted in a Load and Force Distribution graph as shown in Figure 4. The trend of force between SG-2 and SG-3 is extended to the pile toe. Curves showing the pile-head load-movement and the SG-3 versus the pile-toe movement are added.

The fact that the force distribution curves are almost parallel after about the 5th or 6th load level (after an about 5 mm toe movement) suggests that the soil response is essentially plastic. Indeed, the preparation of the "fake" example applied the t-z functions shown in Figure 5, which show an essentially plastic response in the upper 5 m (the silt and sand) and in the middle 5 through 15 m depths, and a somewhat strain hardening response below 15 m depth.

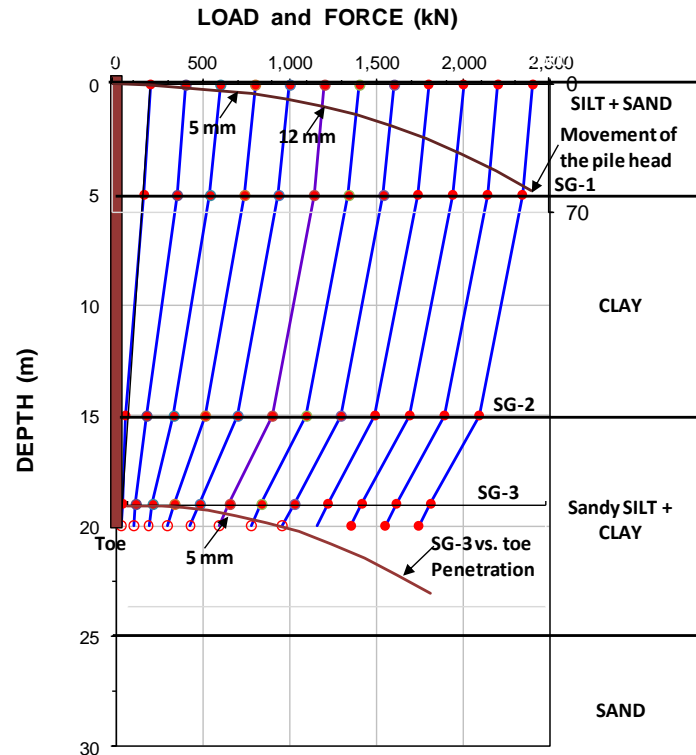


Fig. 4 Load and Force distributions after converting strain to force

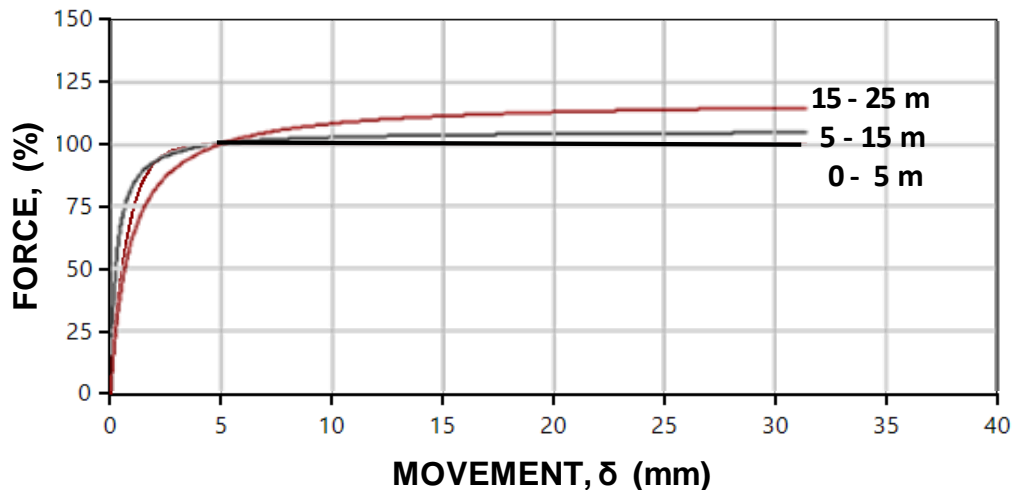


Fig. 5 t-z curves assigned to the preparation of the example

**Back-Analysis.** In an analysis of a real test, the first step after preparation of the data is to find the q-z and t-z functions behind the test data. Many will differentiate the force distributions. That is, try to simulate the response between gage levels as shown in Figure 6. Of course, a t-z function can be fitted to any of the curves shown. However, that t-z function will have little reference to simulating the pile-head load-movement curve or, for that matter, the force-movement curves of the strain gage levels. This because differentiation magnifies the error and imprecision of the measurements and fitting of the functions to the curves are in addition affected by the pile compression.

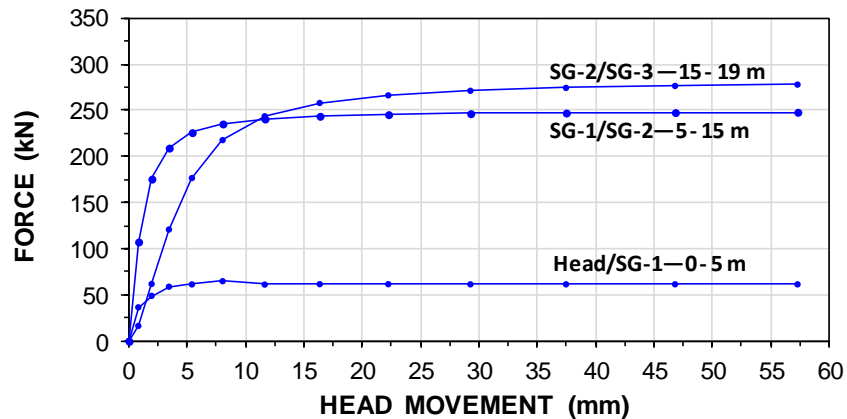


Fig. 6 Shaft resistance between gages levels

Fitting of  $q$ - $z$  and  $t$ - $z$  is best performed by first finding a suitable Target load for analysis, here chosen to be the forces and movements measured for the 6th applied load, 1,200 kN. A back-calculation of the force distribution produced by the Target applied load applying effective stress distribution shows that the  $\beta$ -coefficients in the three soil layers are 0.35, 0.25, 0.40 and the toe force and toe stress are 594 kN and 6 MPa, respectively. At the 1,200-kN Target load, the pile-toe movement is very close to 5 mm. The movement at the gage levels is up to 7 mm larger (soil shear entering plastic response).

The procedure is to first address the pile toe response and then one set of gage records up from the pile toe at the time. The pile toe movement is the easiest. Usually, the pile toe response follows a Gwizdala function (c.f., Clause 8.5.1) and it is a fast procedure to find out that for this example case, the Gwizdala function is:  $R_t = 594\sqrt{(\delta/5)}$  with force in units of kN and movement in mm. A hand calculation of the response of SG-3 is time-consuming, even when using a spreadsheet software like Excel. Using the UniPile software trying a couple of  $t$ - $z$  functions and letting the program calculate the gage response quickly establishes a hyperbolic  $t$ - $z$  function (Chin-Kondner, c.f., Section 8.5.2) coupled to a Target (or Reference) Force at a 5-mm Target (or Reference) Movement. The function that pivoted through the SG-3 value at 5-mm movement showed the SG-3 Reference Force to be equal to 90 % of the force for infinite movement (i.e.,  $C1 = 0.0090$ ). The function applied to the gage records is plotted in red in Figure 7. The simulation is referenced to the pile toe movement, which means that the simulation for SG-3 is only affected by the response of the one metre soil layer between SG-3 and the pile toe. Going next to simulate the response of SG-2, then to SG-1, and finally to that of the Pile-head shows that the same  $t$ - $z$  function acceptably satisfies all curves in the figure, i.e., it applied to all three soil layers, the full length of the pile.

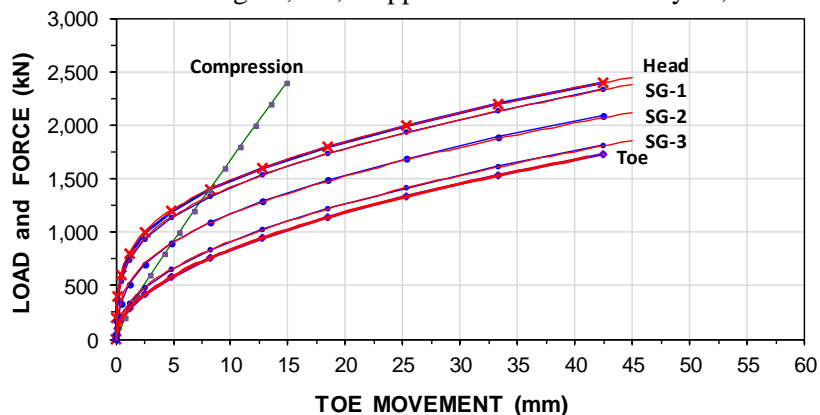


Fig. 7 "Measured" and fitted load and force-movement curves

Figure 8 is the same as Figure 5 but with the back-calculated t-z curve (dashed red curve) added to compare the latter curve to those used for (assigned to) the precise creation of the fictitious example. The comparison shows that there is some leeway in the simulation.

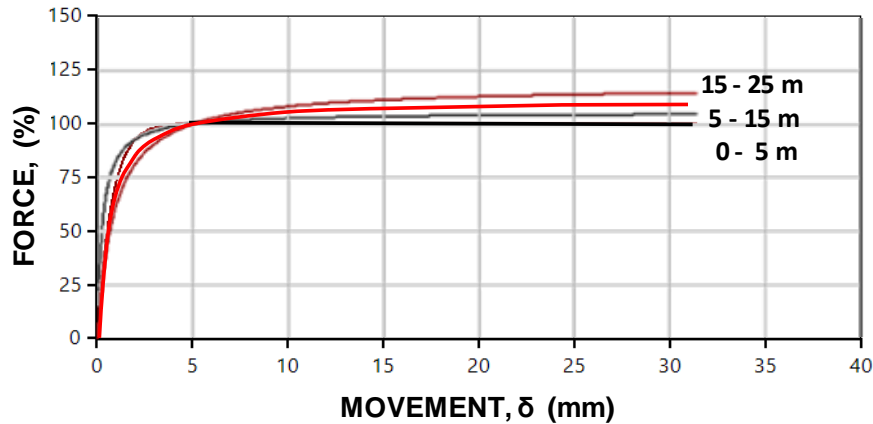


Fig. 8 The back-calculated t-z curve compared to the assigned t-z curves

This completes the back-analysis of the test on the 20 m long test pile and Figure 9 shows the simulated curves for the pile head, the pile shaft, and the pile toe as well as the pile compression along with the measured responses of the pile head, pile toe, and pile compression.

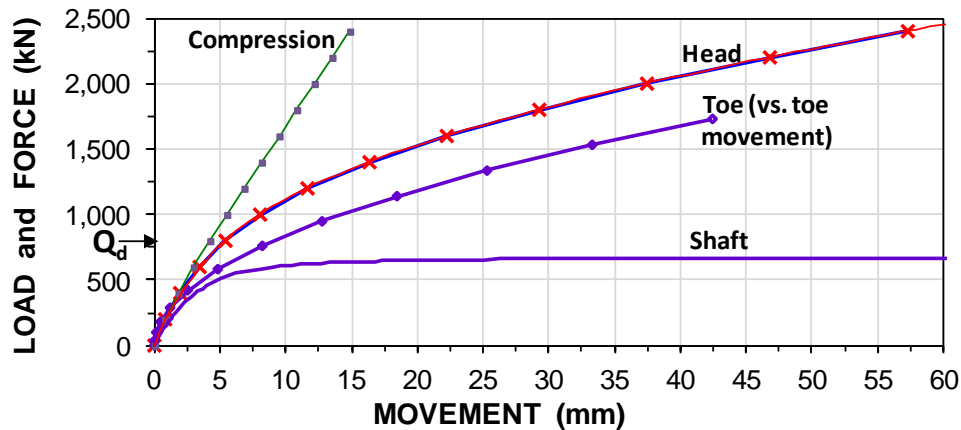


Fig. 9 Simulated load-movement curves of pile-head, pile-shaft, pile-toe, and pile-compression

Table 3 adds the back-analyzed parameters to Table 1. The results of the static loading test can now be used for the design of the piled foundations at the site.

**TABLE 3.** Parameters for the Design

Layer (name)	thickness (m)	density (kg/m <sup>3</sup> )	$\Delta\sigma$ (kPa)	$j$ (--)	$m$ (--)	$m_r$ (--)	$\beta_{ng}$ (--)	$\delta$ (mm)	$C_1$ (--)	$\theta$ (--)
Sandy Silt	5	1,900	0	0.5	200	---	0.35	5.0	0.90	---
Clay	10	1,600	5	0	15	150	0.25	5.0	0.90	---
Sandy Silt	10	2,000	10	0.5	80	800	0.40	5.0	0.90	0.50
Sand	15	2,100	30	1	400	1,000+	---	---	---	---

**Example 15.6-04** presents analysis of an actual bidirectional loading test performed in a very dense silt in Malaysia by Glostrex Inc., Singapore in 2021 (S.K. Lee, personal communication). The pile was a VW-instrumented, 900 mm diameter bored pile drilled to 15.1 m depth. The stick-up was 0.5 m. The bidirectional cell level was placed at 10.0 m depth. The test schedule comprised a series of equal load increments applied at equal (30 minutes) intervals. [Figure 1](#) shows a summary soil profile and the depths of the VW-gages. The example test pile contained six gage levels, SG1 through SG6.

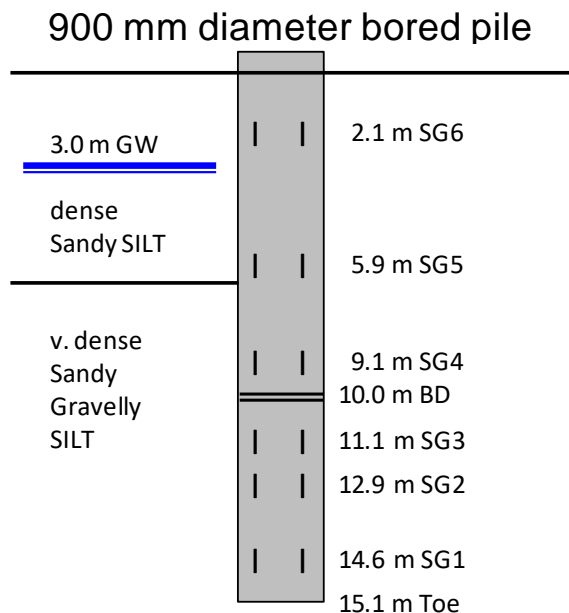


Fig. 1 Test pile and depth to strain-gage levels

The gages were placed in diametrically opposed pairs (denoted A+C, if only one pair and denoted A+C and B+D if two pairs were placed—as was the case for SG3 and SG4). In preparation for analysis, a primary records table was compiled that included all gage readings. This table was used in assessing the reliability of all gage records. For the EA-procedure, see Clause 8.6.3 and Figure 8.24. When this assessment is completed, a second table is prepared containing the average of each gage record. It may be reduced to show only the last reading for each load level. Table 1 shows the headings of such table prepared for the analysis of the test data. It contains the record headings typical of a bidirectional test, comprising Load Record Number, Time Stamp, Hold Time, Elapsed Time, Loads, Movements, and Average Strains

**Table 1.** Time, load, and movement records

RECORD (#)	TIME			LOAD		MOVEMENT				COMPRESSION		HEAD (mm)	STRAIN					
	(DD-MM:hh:mm)	(hour)	(min)	Downwrd (kN)	Upwrd (kN)	Upwrd (mm)	Downwrd (mm)	Opening (mm)	Toe (mm)	Downwrd (mm)	Upwrd (mm)		SG6 (µε)	SG5 (µε)	SG4 (µε)	SG3 (µε)	SG2 (µε)	SG1 (µε)
				Pile (kN): 105								DEPTH (m): 0.0	2.1	5.9	9.1	11.1	12.9	14.6

The downward load is the BD Load determined from the BD pressure (as measured at the ground surface) and the upward load is the BD load subtracted by the buoyant weight of the pile at the BD level (105 kN). In a conventional BD test, seven different movement values are recorded, as indicated in the table headings. Note that good practice includes monitoring the movement of the reference beam—the upward movement of the pile will lift the ground surface and the supports of the measuring beam, which will reduce the measured upward movement of the pile head (the pile-head movement records of the example were corrected for beam movements). All other movements are determined from measurements of compression correlated to the pile head movement.

Gage level SG5 at the boundary of the two soil layers is intended for use in separating the strain (force) between layer. It is good practice to include a gage level near the pile head in case it becomes desirable to carry out a follow-up head-down test (that gage level will then serve to calibrate the EA-parameter for the test pile). However, no gage should be placed closer than one pile diameter below any upper casing (a casing was here left in place from pile head to 1.5 m depth). Moreover, to ensure that the records are uninfluenced of uneven stress distribution over the pile cross sections, no gage level should be closer than one pile diameter away from pile boundaries, such as the BD and the pile head and toe; two pile diameters is a preferable distance.

Before commencing the test, the tack-welded connection between the upper and lower plates of the BD jacks must be broken buy cautiously raising the cell pressure until the tacks break, whereupon the pressure usually is reduced; sometimes the pressure is increased to the first load increment and the test starts. The records should be maintained and included in the test report. Figure 2 shows an example of tack-breaking records (not from the example case). The graph is from a case where the load to break the tack welds went well beyond the pile weight and to 2.5 times the scheduled load increments. The unloading after the break is unnecessary. The test could have proceeded from the tack-break as a first load increment.

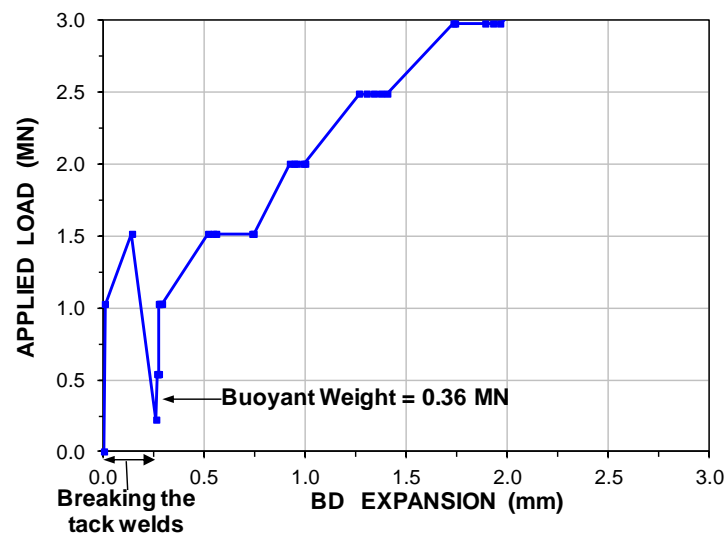


Fig. 2 Example of tack-weld breaking records

The measurements should include the records of the breaking of the tack-welded connection between the upper and lower plates of the BD jacks. It is also highly desirable to monitor the strain once the gages have been attached to the reinforcing cage, then to continue the monitoring as the cage is placed in the pile, frequently during the concrete hydration (36 h), and then intermittently until the start of the test. Tack-breaking records and records from start of construction are unfortunately rarely implemented and they were not obtained for the example.

Figure 3 shows the upward and downward load-movement curves and the load versus cell expansion recorded in the test and the load-time curve. The latter allows a verification that the assigned loading schedule was followed in the field. The maximum load was (8,700 kN). The test schedule included an unloading-reloading event at the fourth load increment. Such events are surprisingly, and regrettably, common, despite not providing any information useful for the assessment of the test pile. An unloading-reloading event only results in a disturbance of the test data, reducing test quality.

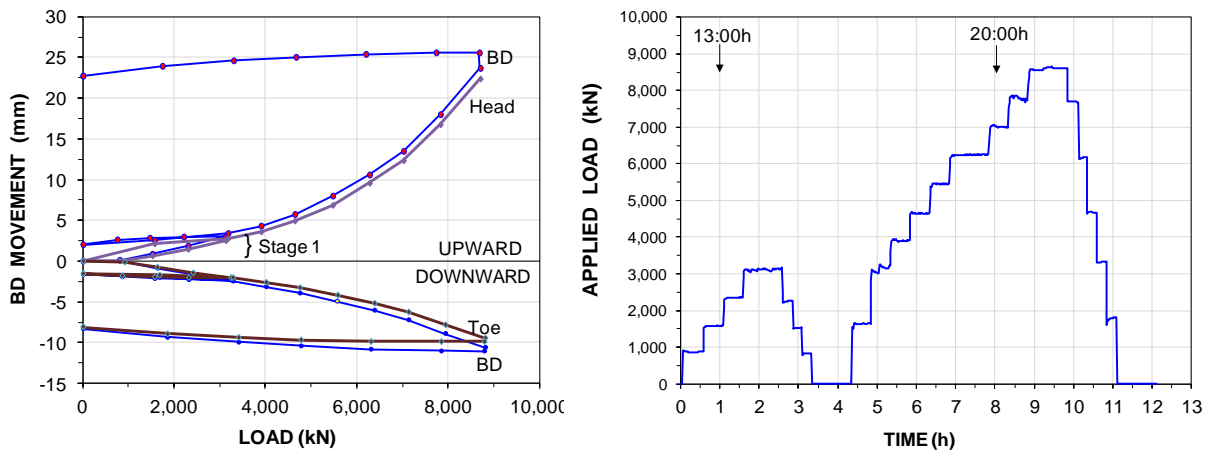


Fig. 3 Load-movement curves and

The records show that the test schedule included a few prolonged load-holding times, which, however, appear not to have impacted the analysis results. The load-movement curves show no unusual records. The maximum upward and downward movements were only 25 and 10 mm, respectively. However, the pile compression is small, which normally would indicate that the detailed analysis of the test records should be able to fully address the pile response.

The first step in assessing the test records is determining the EA-parameter from the strain-gage data. The left graph in Figure 4 shows the load-strain curves. The last 6 Stage 2 records of SG3 and 4 nearest below and above the BD level, respectively, form almost straight parallel lines with a slope (EA parameter) of 20.5 GN. The 20.5-GN value correlates to a 32-GPa E-modulus for the 900-mm nominal size pile. The slopes of the next distant gage level, SG2 and SG5 are steeper. This might be thought of as indicating a stiffer (wider) pile at these levels. However, the right graph, showing the calculated EA-parameter as the tangent modulus of the pile, plotted versus strain at the gage levels. The graph shows that the steeper slope for SG2 and SG5 is due to the fact that the shaft resistance at the gage levels has not yet been fully mobilized despite the movements exceeding 10 mm.

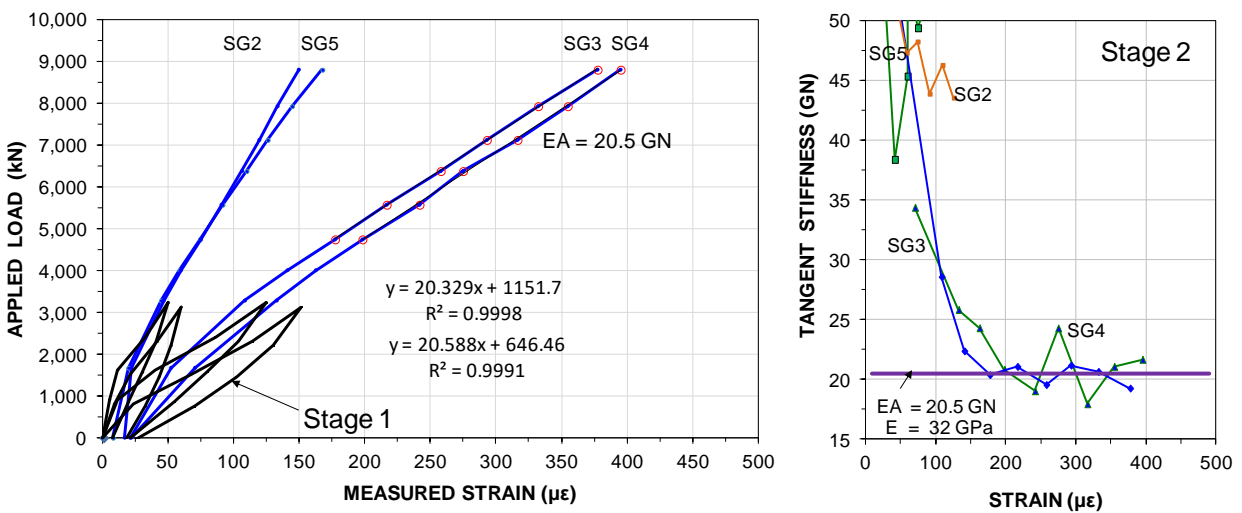


Fig. 4 Applied load and tangent EA-parameters versus strain

However, for the  $EA = 20.5$  GN slope to represent the true  $EA$ -parameter, requires that the soil shear response is plastic. Already a small strain-hardening will result in a larger than true  $EA$ . Applying the 20.5-value results in the unit shaft resistance force immediately above and below the BD level (Figure 5A) is smaller than further away. Figure 5B shows that applying an  $EA$ -parameter of 18.0 GN ( $E=28$  GPa) would appear to be more realistic, i.e., resulting in more consistent curves. An  $EA = 18.0$  GN would indicate that the shaft resistance is strain-hardening rather than plastic. The test data do not indicate a toe force, despite the fact that the pile toe moved about 10 mm. This lack of resistance, if real, could indicate that the pile toe was left with debris softening the pile toe response. Alternatively, it could imply the presence of a residual toe force.

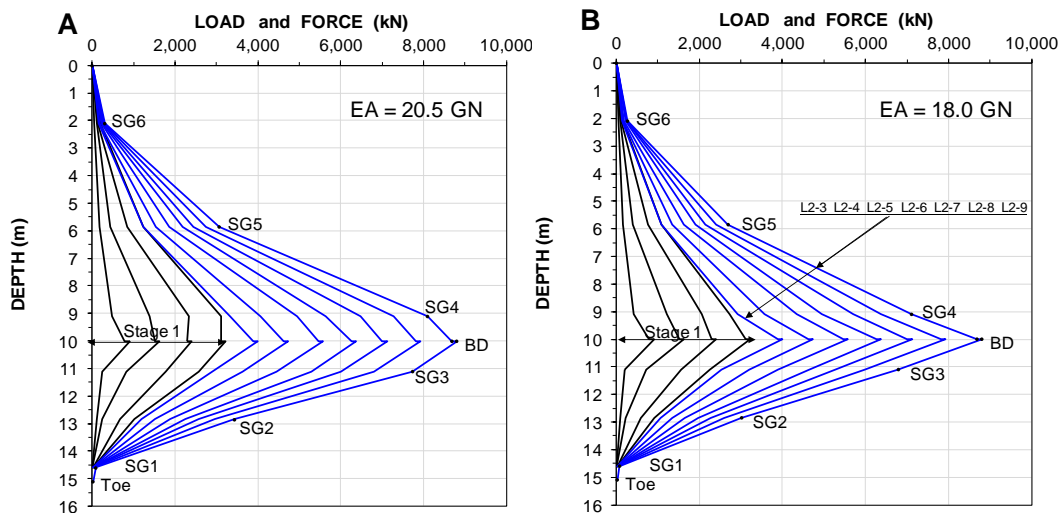


Fig. 5 Force distributions for  $EA = 20.5$  GN and 18.0 GN

The second step is to use the force distributions to establish the soil parameters that would describe the response, i.e., parameters to be used to simulate the load-movement results and allow for demonstrating the effect of changes to the pile, such as to width, length, etc., as well as analyzing the response of a pile group. The parameters are the unit shaft and toe resistances, and the  $t$ - $z$ / $q$ - $z$  functions of the pile-soil system. In most cases—the exception being in rock sockets—the unit shaft resistance should be expressed proportional to effective stress, i.e., by the  $\beta$ -coefficient. The unit toe resistance depends less on the overburden stress and is usually best expressed in unit resistance, units of kPa or MPa.

Figure 6A shows the distribution of the  $\beta$ -coefficient calculated as the average between gage levels for three of the load levels of Stage 2. The calculation determined the average unit shear force between the gage levels as the average pile force divided by the pile surface area (circumference and length between gage levels). The  $\beta$ -coefficient is the shear force divided by the average effective stress between the gage levels. The graph indicates that the  $\beta$ -coefficients differed between the gage levels and increased as the load increased. The only notable information is that the  $\beta$ -coefficients between SG1 and the pile toe, were much smaller than the coefficients further up the pile. Moreover, the  $\beta$ -coefficients are remarkably large, more representative for a pile in a rock socket than a pile in granular material.

Figure 6B associates the  $\beta$ -coefficients to movement. The movements at the BD were measured and the movements further up the and down the pile were obtained by reducing the BD movement by the calculated compression between the BD and the gage level. The graph confirms that the  $t$ - $z$  response of the soil is strain hardening. The method used for determining the beta is somewhat crude as it relies on differentiation between gage levels, which enlarges the error and uncertainty of the strain values used for determining force and movement. Moreover, it is difficult to use the results to simulate the response of the pile and to transfer the results to a pile with a modified geometry or soil profile.



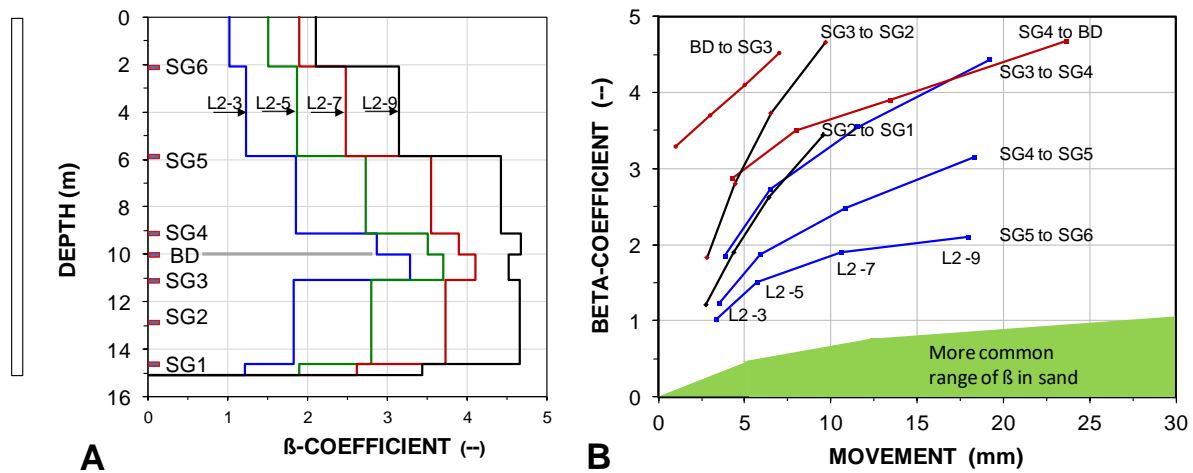


Fig. 6  $\beta$  distribution with depth and versus movement

The better method is to apply a trial-and-error procedure to fit a calculated force-movement response calculated by assuming (fitting) a t-z function to the actual force-movement records, starting with the lowest gage level (here SG2 because SG1 records are too diffuse). On reaching a reasonable fit between measured and calculated force-movement, the procedure is repeated for the gage level above, SG3, and then for the downward BD records and on to SG4, SG5, and SG6. As the procedure comprises extending the calculation in steps, it avoids differentiation. For the example case, and the rather uniform soil of the project, it turned out that one-and-the-same t-z Chin-Kondner (hyperbolic) curve gave the best fit. The variation was the actual  $\beta$ -coefficient for the so-called Target Movement, here chosen to be 10 mm as shown in Figure 7. The  $\beta$ -coefficient below the BD (BD to SG2) is about 50 % larger than above (SG5 to BD) despite the soils below and above the BD are quite similar.

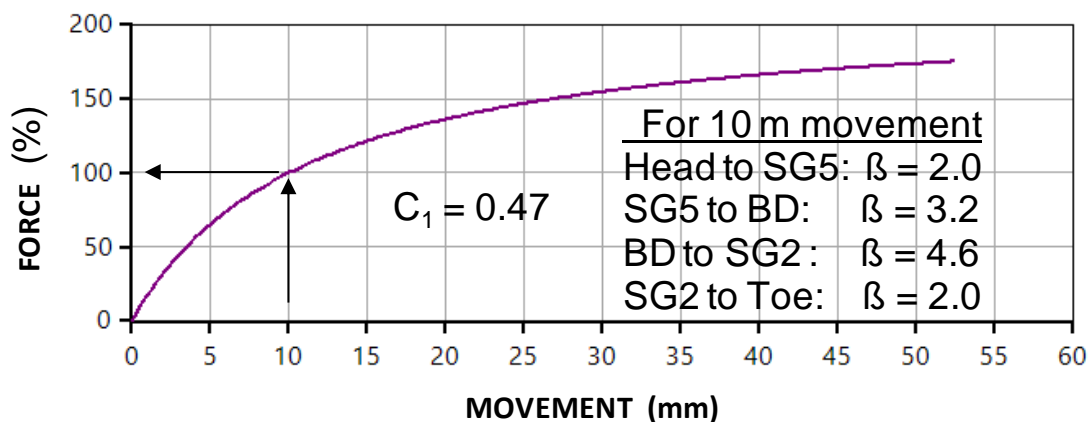


Fig. 7 Chin-Kondner t-z function fitted to the test records

Figure 8 shows the measured force-movement curves for the BD and gage levels. The movements for the latter were determined from combining compression and BD-movements the same way as used for the  $\beta$ -coefficients in Figure 6B. The fits between measured and calculated curves are good. Refinement is possible, but would mainly be cosmetic. It was achieved by interactively using the UniPile software.

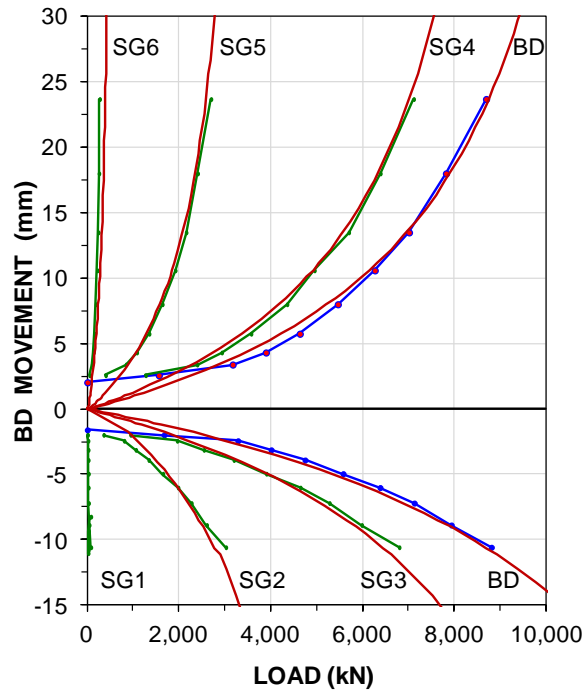


Fig. 8 Load-movement curves for BD and SGs

The fit simulations established the  $t$ - $z$  functions for the pile and soil enables the head-down static loading test results to be determined, as shown in Figure 9. There being no toe resistance, the "Head" curve also represents the pile shaft resistance.

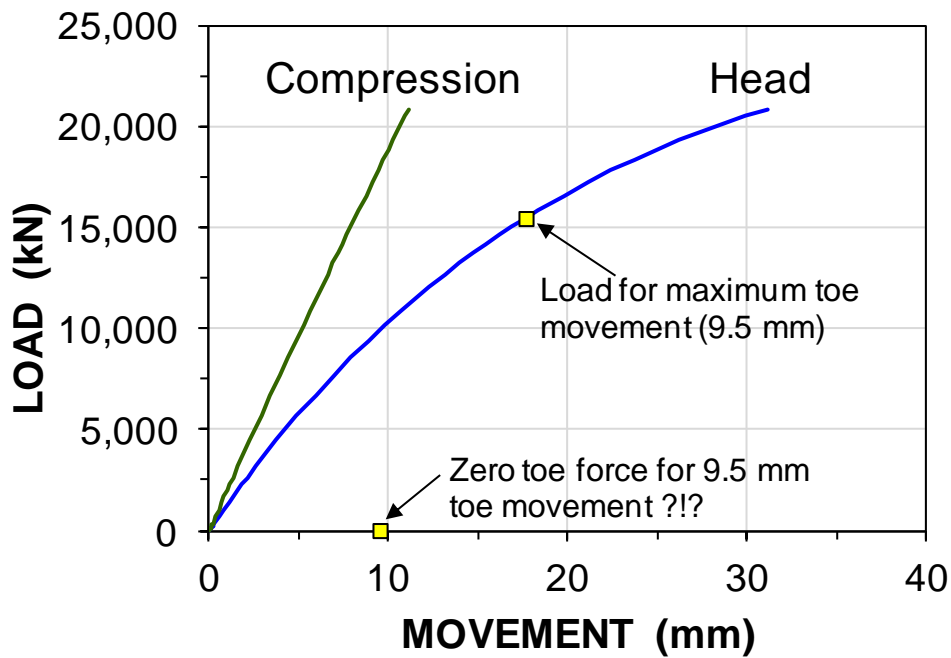


Fig. 9 Simulated head-down load-movement

As mentioned in connection with Figure 5, the fact that the records show no toe resistance for the pile despite the 10-mm toe movement could be the results of two effects: it could imply the presence of a residual toe-force or, alternatively, the pile construction could have concreted the pile with left debris in the drilled hole, thus, causing a soft pile toe response. Presence of residual toe force would reduce the evaluated toe resistance and could, indeed, even explain the appearance of no toe resistance—which would not be the first time (Fellenius et al. 2004). The force distributions above the BD do not leave much room for presence of residual force, however. The maximum residual force would be the force between a straight line from the pile head to the BD and the actual evaluated force curve. Therefore, residual force must, if present, be limited to the zone below the BD. If assuming that the unit shaft resistance below the BD is the same as above, then, the maximum residual toe force would be about 1,000 kN or less than 1.5 MPa stress at 10 mm movement, which is not very much considering the soil density and the large shaft shear. It is, therefore, quite clear that the pile construction left the pile with inadequate toe resistance and that the pile functions in shaft-bearing only. This would have been of no concern of the project, however, the stiff response of the pile to load indicates that the decision on what sustained load to assign to the pile lies not with the pile settlement or some "capacity" gleaned out from the equivalent head-down curve, but with the pile structural strength

## 15.7 Design of Piled Foundations for Settlement

**Example 15.7-01<sup>4</sup>** addresses using the back-analyzed test data of Example 15.6-03 in order to prepare for the piled foundation design of a fictitious project, comprising piled foundations supported on single piles and narrow and wide pile groups. Let's say that the test was carried out early in the project and the results are now used to assess the suitability of the originally considered 20-m pile length for supporting narrow and wide pile groups at the site and for analysis need and effect of potential lengthening to 25 m depth.

The 355-mm, circular, precast concrete piles are to be used as single piles, in narrow pile groups (3 by 3 piles) and in a wide pile group (7 by 7 piles). All pile groups have piles spaced at 3 pile diameters center-to-center. Thus, the narrow pile group has a 2.5 times 2.5 m pile cap. The wide pile group is connected to a square cap with a 6.8 m side and supports a uniformly distributed load. All piles are assumed to support an 800 kN/pile sustained load and a 100 kN/pile transient load. Immediately before installing the project piles, an about 1 m thick fill will be placed across the site generating 18-kPa stress and a general subsidence at the site. The fill will not be compacted around the piles.

**Single-Pile Load-Movement Response.** The evaluated parameters are first used to simulate the load-movement response of the test pile after placing the fill and the settlement of the single pile due to the loads from the structure. The project parameters (Table 3 of Example 15.6.3—back-calculated from the results of the static loading test, including the evaluated  $t$ - $z$ / $q$ - $z$  functions, as correlated to the pile response in regard to effective stress) were used to determine the long-term condition response of the same size (355 mm width and 20 m long) pile as single-pile foundations at the project. The results of a static loading test simulation show that, after placing the fill, applying the total load (800 + 100 kN) to the 20 m long pile will result in about 5 to 6 mm load-transfer movement due to pile compression and pile-toe penetration. The fill will also affect the load-movement and settlement response.

Figure 1 compares the pile-head load-movement response. As would be expected, the increase of effective stress has lifted the curve and a "capacity" determined by whatever definition preferred, would have increased. Not much else can be said about the load-movement curve.

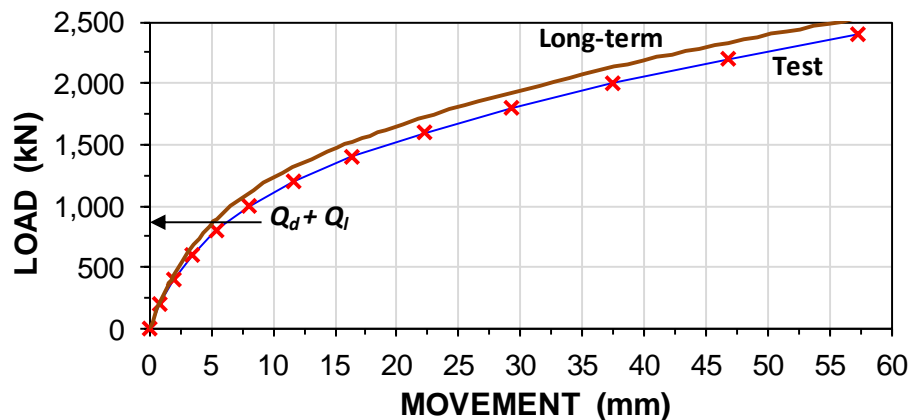


Fig. 1 Load-movement response of the static loading test and extrapolated to long-term

**Settlement of Single Piles and Perimeter piles.** The fill will cause the soils to compress and the site will subside. This will build up negative skin friction along the piles accumulating to a drag force. The drag force is inconsequential to the design of the piled foundation. More important, the piles will settle additionally due to downdrag. The drag force due to the soil settling around the single pile will also increase the pile compression, although only by a practically negligible amount.

<sup>4</sup> This example was edited April 2024

The pile settlement can be determined by combining distributions of pile force and pile and soil movements to obtain the depth to the Equilibrium Plane in a back-calculation of the results of the static loading test according to the **Unified Method**. The analysis is a manual or computer-aided trial-and-error fitting until the analysis shows the force and settlement equilibriums to be at equal depth. Calculations of the example were performed using the UniPile software and the results are shown in **Figures 2A - 2C**. Because the soil response is essentially plastic, each calculation step involves satisfying the  $q$ - $z$  function for the toe force,  $R_t$  (Fig. 2A), which controls the force distribution in the pile, and the toe movement,  $\delta_t$  (Fig. 2B), which controls the pile settlement distribution. The iteration is concluded when the force and settlement equilibriums are at equal depths, thus, establishing the Equilibrium Plane. For the example, the calculated long-term pile settlement of the single-pile foundation is calculated to be about 20 mm, including the about 5 mm load-transfer movement due to placing the 800-kN sustained load and the pile compression due to the transfer of load to the pile toe. If that value is acceptable to the supported structure (with a suitable margin to the maximum permissible settlement), the 20-m length can be accepted for the single-pile foundations. If not, the piles could be extended to 25 m depth. A repeated calculation shows that the net settlement of the single pile would then become about 5 mm smaller.

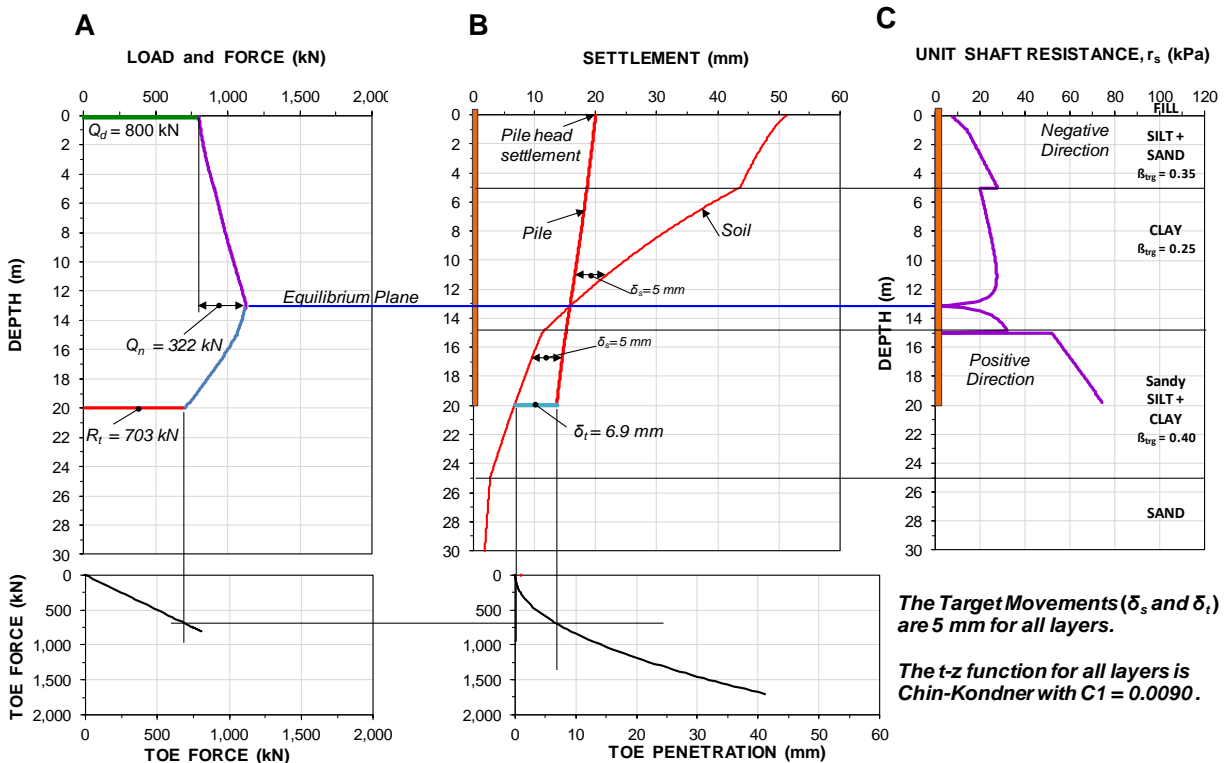


Fig. 2 Single pile after placing the fill. Unified Method results

**Pile Group Foundations. Equivalent Raft.** The loads supported by the pile are transferred to the soil layers below the pile toe level increasing, which causes settlement in addition to the axial compression of the piles and pile toe penetration due to the load-transfer ( $q$ - $z$ ) of the individual pile. For the single pile, the affected volume of soil is small and the compression can be assumed included in the  $q$ - $z$  response. The settlement of a group of piles supporting a uniformly (reasonably so) loaded raft will be larger than that of a single pile because of the affected volume of soil below the pile toe level being larger. The compression of the soil layers below the pile toe is calculated as that for a flexible *equivalent raft* (c.f. Clause 7.17.2) placed at the pile toe level (N.B., not at "the lower third point"), The equivalent raft is assumed loaded the same as the foundation raft. The distribution of the imposed stress in the soil below the equivalent raft can easily be calculated by means of Boussinesq or 2(V):1(H) stress distribution.

For wide groups, the equivalent raft can be assumed to have the same dimensions as the pile cap, disregarding the fact that shaft resistance below the equilibrium plane (estimated as that for a single pile) discharges portion of the applied load into the soil. (The drag force does not have this effect as it is a force unloaded from the soil and does not increase the force below the pile toe level). For narrow groups, i.e., groups with 4, or fewer, pile rows, this effect cannot be disregarded. It can be considered by widening the equivalent raft, assuming it to be larger than that of the actual raft (cap), with the sustained load distributed as average stress across the so-determined raft (c.f., Figure 7.26 in Section 7.12.2).

**Narrow Pile Group.** The nine-pile narrow group of 20 m long piles supports a total load of  $9 \times 800 = 7,200$  kN. The Equilibrium Plane being about 6.5 m above the pile toe, will result in a projected 1.3 m wide band around the 2.5 m pile group and, therefore, the side of the equivalent raft is 4.6 m (Section 7.12.2). The stress on the equivalent raft is  $7,200/4.6^2 = 340$  kPa. Figure 3 shows the calculated total settlement of the perimeter piles (eight of the nine piles), indicating a long-term settlement of about 100 mm at the side of the pile cap, which includes 5 mm of pile compression and 1 mm toe penetration. This settlement might be larger than permitted by the supported structure. If so, extending the pile into the underlying sand would reduce the settlement.

The blue curves show the pile and soil settlements as calculated a narrow group extended to 25 m depth, resulting in the perimeter pile settlement (pile cap level) reducing to about 50 mm. The narrow group comprising 25 m long piles would still settle about 30 mm more than a single 20 m long pile, which would be of concern for foundations that are close to each other.

It might be expected that the settlement in the sand below 25 m depth would occur quickly as the sand can be assumed free-draining. However, the settlement is due to the downdrag in the clay, consolidating due to the fill and increasing the pile force, causing the pile to move down, which, in contrast, occurs slowly over time.

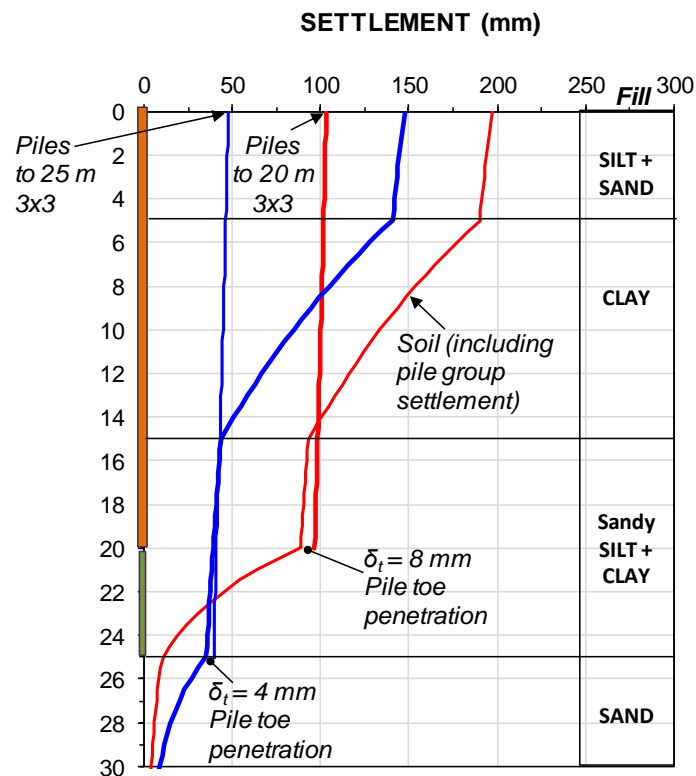


Fig. 3 Settlement of perimeter piles in a narrow pile group comprising 20 or 25 m piles

**Wide Pile Group Foundations. Interior piles.** The most common reason for using a piled foundation is because otherwise the settlement would be too large. Therefore, the settlement analysis is the most important part of the design of a piled foundation.

The simplest approach is to consider the pile and soil as a "block" and calculate the settlement as the sum of the compression of the block for the applied load (as an average stress) and the compression of the soil layers below the pile toe level (the bottom of the block). The compression of the block is then calculated as an E-modulus equal to the Footprint Ratio, FR, of the pile cap times the pile E-modulus. For the 7x7 pile example, the FR is about 10 % of 30 GPa = 3 GPa (c.f., Clause 7.18.2). Considering the average stress of 850 kPa and the 25-m pile length (height of the block), the calculated compression is 7 mm. Most of this will develop during the construction.

The compression of the soils below the pile toe level is the settlement of a 46-m<sup>2</sup> flexible raft placed at the pile toe level and stressed by 850 kPa. Applying Boussinesq stress distribution and including the fill placed on the ground, a conventional settlement analysis shows that the compression below the block will be 95 mm at the characteristic point, which can be considered to represent the settlement of a reasonably rigid pile raft (c.f., Section 1.9). The block analysis does not consider the differential settlement across the raft. To estimate this, would require recognizing the different response of interior piles to that of perimeter piles.

The responses of the individual piles in piled foundations supported on single piles and on narrow pile groups do not differ much. However, a **wide piled foundation**, i.e., a foundation supported on a pile group comprising 4 or more rows of piles, will show a different response in terms of settlement and distribution of loads on the piles between the interior piles and perimeter piles in the group, as summarized in the following points

1. The **perimeter piles** will respond similarly to single piles, that is, transfer the applied load engaging the shaft resistance from the pile head downward. In contrast, the **interior piles** will respond by engaging the pile toe and shaft resistance upward from the pile toe (c.f., Section 7.18 for the calculation by the Fellenius-Franke method, c.f., Clause 7.18.3).
2. In the absence of downdrag due to general subsidence, (**A**) because the perimeter piles engage shaft resistance from the pile head downward, they will appear stiffer than the interior piles and they will, therefore, unless the raft is flexible, attract larger portion of the applied load than the interior piles and (**B**) for equal pile-head load (flexible cap), the force reaching the pile toe is larger for interior than for perimeter piles and, therefore, the toe penetration will be larger.
3. General subsidence at the site, will affect the perimeter piles much like a single pile, whereas the interior piles will not be affected. This may reduce the effect of Point 2 and even invert it, as shown for the example case.
4. The settlement of the equivalent raft will develop similar to that of a flexible raft, unaffected by general subsidence and settlement at the toe level is larger at the center than at the perimeter.
5. A flexible pile cap supporting a uniformly distributed load will likely settle more in the center than along the perimeter due the effect of Point 2, potentially reduced by the effect of Point 3.
6. A rigid pile cap will settle equally across the cap, but the perimeter piles will receive a significantly larger portion of the applied load than the interior piles.
7. Piled foundation caps are neither fully flexible nor fully rigid and the distribution of load and settlement will be correspondingly affected by the degree of rigidity (c.f., Clause 17.18.6).

For interior piles, along a length from the pile head downward, there is no movement between the pile and the soil and the load at the pile head is undiminished transferred toward the pile toe, there causing a toe penetration. Because of the toe penetration, a movement between pile surface and soil will develop above the pile-toe level between pile shaft and soil that will mobilize shaft resistance, starting from the pile toe and progressing upward. The so-induced shaft resistance will reduce the force that reaches the pile toe and establish a movement equilibrium between the pile elements affected by the so-generated shaft resistance and the pile toe. The equal movement is when the shaft element movement (due to compression) is equal to the toe penetration for the shaft-resistance-reduced pile-toe force (Clause 7.18.3).

The scenario for the interior piles under a flexible pile cap is illustrated in Figure 4, showing how the sustained load (800 kN on average) at the pile head is reduced by the shaft resistance mobilized from the pile toe upward as the pile toe is pushed into the soil and the toe resistance increases with the increase of the toe penetration. The intersection of the two curves is the equilibrium of movement; the upward movement of the shaft is equal to the pile toe penetration. The toe penetration at the movement equilibrium (about 1 mm) plus the pile compression of the 800-kN load (about 5 mm), represents the settlement of the cap for the interior piles of the wide pile group. The difference in compression between interior and perimeter piles is about 2 mm, which is about the difference in toe penetration. However, the perimeter pile of the wide pile group is affected by the general subsidence at the site, which includes the difference of the soil settlement at the pile toe level between the center and perimeter of the piles supporting the wide group.

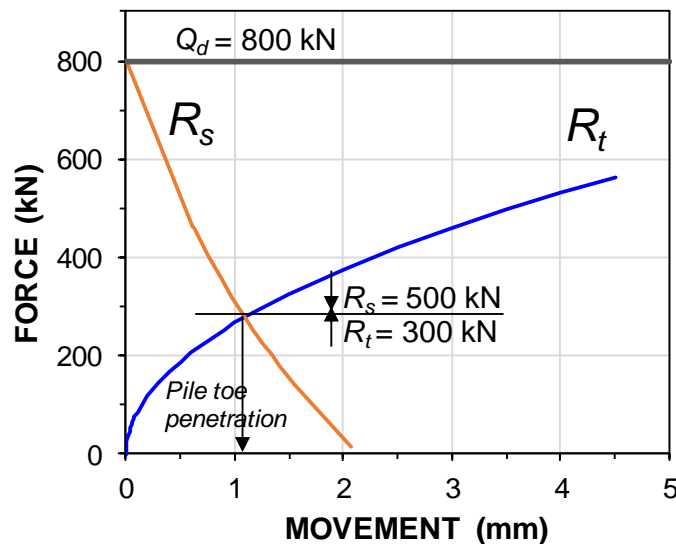


Fig. 4 Interaction between shaft and toe resistance at the pile toe level for a flexible-group interior pile

**Flexible-cap wide group.** The equivalent raft of a wide group can be assumed equal in size to that of the pile cap. For the example case, the calculated soil settlement at the pile toe level amounts to 16 mm at the side of the 6.8 m cap and 130 mm at the center. The calculated compression of the perimeter and interior piles are 8 mm and 5 mm, respectively. Thus, if the example group has a flexible cap, the calculated differential settlement amounts to a not inconsequential value of about 50 mm.

**Rigid-cap wide group.** An absolutely rigid cap would have no differential settlement, but considerable variation of actual pile loads. Theoretically, almost all load would be supported on the perimeter piles (i.e., 1,600 kN/pile) and almost no load on the interior piles. For a more probable and reasonably loaded wide group with a rigid cap, the 24 perimeter piles of the example would likely receive about 1,200 kN/pile, the 16 piles of the first interior row 600 kN/pile, the 8 piles of the next row, 200 kN/pile,



and the center pile 100 kN. Figure 5 shows these load areas as three bands with uniform stress: an outer band of 1.2 m width and 27 m<sup>2</sup> area containing the perimeter piles, a middle 1.1 m wide band and 14 m<sup>2</sup> area containing the next 16 piles, and a 2.2 m wide 9-pile 5 m<sup>2</sup> inner area. The areas would be stressed by about 1,100, 700, and 300 kPa, respectively. Or even more simplified: combining the two interior areas to a center area with 4.4 m side and each of the interior 25 piles carrying 400 kN and, therefore, the stress would be 500 kPa. Accepting these simplifications, the calculated settlement is simply pursued by conventional analysis.

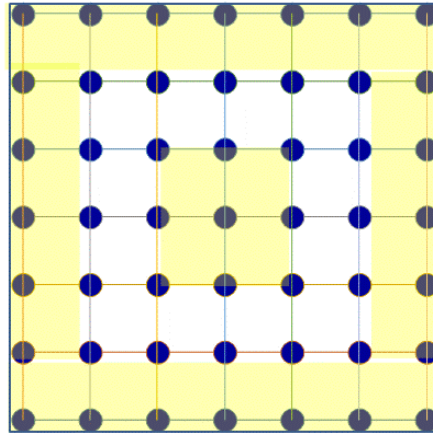


Fig. 5 Layout of the 6.8 m wide 49-pile pile groups showing the three bands with different stress

A calculation of the settlement distribution across an equivalent raft loaded by the three areas shows that the differential settlement has reduced to a more plausible and acceptable 10-mm value between the side and the center of the 6.8 m wide pile group. Thus, the design is now a matter for a structural engineering approach to determining the thickness and reinforcement necessary to achieve the needed raft rigidity considering the different pile loads. The assessment (per the Fellenius-Franke method analysis, c.f., Clause 7.18.3) would have to consider the fact that the toe penetration of the interior piles for the now half load will be smaller.

The example is fictitious and serves to illustrate the analysis procedure to apply to a wide pile group (c.f., Section 7.18). No case history exists that reports, specifically, simultaneous measurements over long time of load and settlement distributions on piles immediately under a pile raft. However, the several case histories addressed in Clause 7.18.1 indicate observations that support the analysis procedure.

### Comments

Were the case real, the piles in the wide pile group would likely be installed to a stiffer toe response, perhaps a metre or two into the sand, which would remove much of the transfer of load to the perimeter piles and lessen the demand for rigidity of the raft.

For a project similar to the example case, therefore, the compression of the soil below the pile toe level is the source of the main portion of the raft settlement. Unfortunately, in contrast to this example, real cases often lack adequate information on the compressibility of the soils below the pile toe level.

A project site normally includes a number of different, more or less closely spaced pile groups, narrow and wide, that interact, that is, affect the stress distributions underneath each other pile toe levels and, therefore, the differential settlements between the pile groups. The analysis of this example can easily be extended to incorporate the interaction of a practically unlimited number of different size pile groups with different applied load to determine the differential settlement between the pile groups.

The procedure applied to the analysis of the example assuming a flexible cap produces settlement values that would be larger than expected for an actual less flexible cap. Similarly, the non-differential settlement calculated for an absolutely rigid cap would be underestimated. However, the calculation results can be used to assess the differential settlement across a pile cap that affect the supported structure. They are less useful for estimating the bending stress of the pile cap. However, the latter is an issue for structural analysis of the cap, not for a geotechnical analysis of the foundation response.

The analysis of a wide pile group can also be carried out employing numerical methods to obtain a more detailed picture of the soil-pile response. Fellenius (2019) reported the results of numerical method calculations for uniformly distributed steps of movement applied to a rigid pile cap comprising 36 piles in uniform soil. However, advancing from this to a semi-rigid or semi flexible cap with a load distribution across the cap affected by the mutual cap-soil interaction of soil movement and stress makes for complex input of parameters. Moreover, the value of such analysis depends on satisfactory correlation to the results of full-scale monitoring of actual foundations. It is regrettable that the absence of such makes detailed theoretical calculations less supportive of actual design decisions.

## CHAPTER 16

### PROBLEMS

#### 16.1 Introduction

The following offers problems to solve and practice the principles presented in the preceding chapters. The common aspect of the problems is that they require a careful assessment of the soil profile and, in particular, the pore pressure distribution. They can all be solved by hand, although the computer and the UniSoft programs will make the effort easier.

#### 16.2 Stress Distribution

**Problem 16.2.1.** At a construction site with ground surface at Elev. +115.5 m, the soil consists of an upper 6 metre thick compact sand layer, which at elevation +109.5 m is deposited on layer of soft, overconsolidated clay. Below the clay, lies a 5 metre thick very dense, sandy coarse silt layer, which at elevation +97.5 m is underlain by very dense glacial till followed by bedrock at elevation +91.5 m.

Borehole observations have revealed a perched groundwater table at elevation +113.5 m, and measurements in standpipe piezometer show the existence of an artesian water pressure in the silt layer with a phreatic elevation of +119.5 m. The piezometric head measured at the interface between the pervious bedrock and the glacial till is 15.0 m.

Laboratory studies have shown index values and physical parameters of the soil to be as follows.

Parameter	Unit	Sand	Clay	Sandy Silt	Glacial till
$\rho_s$	kg/m <sup>3</sup>	2,670	2,670	2,670	2,670
$\rho$	kg/m <sup>3</sup>	2,050	1,600	2,100	2,300
$\varphi'$	°	33	22	38	43
$k$	m/s	$1 \cdot 10^{-3}$	$1 \cdot 10^{-9}$	$1 \cdot 10^{-4}$	$1 \cdot 10^{-8}$
$\tau_u$	kPa	--	24	--	--
$c'$	kPa	0	0	0	0
$w_L$	--	--	0.75	--	--
$w_n$	%	22	67	19	11
$e_0$	--	0.59	1.79	0.51	0.29
$c_v$	m <sup>2</sup> /s	-	$20 \cdot 10^{-8}$	--	--
$E_i$	MPa	100	10	120	>1,000
$m$	--	250	20	600	1,000
$m_r$	--	1,200	160	4,000	>10,000
$j$	--	1	0	0.5	1
$\Delta\sigma'$	kPa	--	50	100	1,000
OCR	--	3	--	--	--
$C_\alpha$					

- A. Calculate and tabulate the total stresses, the pore pressures, the effective stresses in the soil layers and **draw** (to scale) the corresponding pressure and stress diagrams.
- B. Verify that the values of water content,  $w_n$ , in the four soil layers agree with the values of density of the soil material assuming a solid density of  $2,670 \text{ kg/m}^3$  and a degree of saturation of 100 %
- C. Assume that the pore pressure in the lower sandy silt layer was let to rise. (Now, how would Mother Nature be able to do this)? How high (= to what elevation) could the phreatic elevation in the sand layer rise before an unstable situation would be at hand?

The table may seem to contain redundant information. This is true if considering only parameters useful to calculate stresses. However, the “redundant” parameters are helpful when considering which soil layers have hydrostatic pore pressure distribution and which have a pore pressure gradient. (Notice, as the conditions are stationary, all pore pressure distributions are linear).

**Problem 16.2.2.** A three metre deep excavation will be made in a homogeneous clay soil with a unit weight of  $16 \text{ kN/m}^3$ . Originally, the groundwater elevation is located at the ground surface and the pore pressure is hydrostatically distributed. As a consequence of the excavation, the groundwater table will be lowered to the bottom of the excavation and, in time, again be hydrostatically distributed over the general site area. There are three alternative ways of performing the excavation, as follows:

- A. First, excavate under water (add water to the hole as the excavation proceeds) and, then, pump out the water when the excavation is completed (1A and 1B).
- B. First, lower the water table to the bottom of the excavation (assume that it will become hydrostatically distributed in the soil below) and, then, excavate the soil (2A and 2B).

Calculate and tabulate the soil stresses for the original conditions and for the construction phases, Phases 1A and 1B, and 2A, and 2B at depths 0 m, 3 m, 5 m, and 7 m. Compare the calculated effective stresses of the construction phases with each other, in particular the end results Phases 1B and 2B. Comment on the difference.

**Problem 16.2.3.** The soil profile at a site consists of a 3 metre thick upper layer of medium sand (density  $1,800 \text{ kg/m}^3$ ) followed by 6 metre of clay (density  $1,600 \text{ kg/m}^3$ ) and 4 metre of sand (density  $2,000 \text{ kg/m}^3$ ) overlain dense glacial till (density  $2,250 \text{ kg/m}^3$ ). Pervious bedrock is encountered at a depth of 16 metre. A perched water table exists at a depth of 1.0 metre. Two piezometers are installed to depths of 7 metre and 16 metre, respectively, and the pore pressure readings indicate phreatic pressure heights of 10 metre and 11 metre, respectively. It can be assumed that the soil above the perched water table is saturated by capillary action. The area is surcharged by a widespread load of 10 kPa.

Draw-to scale and neatly-separate diagrams over effective overburden stress and pore pressures.

**Problem 16.2.4.** The soil profile at a site consists of a 4.0 m thick upper layer of medium sand (density  $1,800 \text{ kg/m}^3$ ), which is followed by 8.0 m of clay (density  $1,700 \text{ kg/m}^3$ ). Below the clay, a sand layer (density  $2,000 \text{ kg/m}^3$ ) has been found overlying glacial till (density  $2,100 \text{ kg/m}^3$ ) at a depth of 20.0 m deposited on bedrock at depth of 23.0 m. The bedrock is pervious. Two piezometers installed at depths of 18.0 m and 23.0 m, respectively, indicate phreatic pressure heights of 11.0 m and 19.0 m, respectively. There is a perched groundwater table in the upper sand layer at a depth of 1.5 m. The non-saturated but wet density of the sand above the perched groundwater table is  $1,600 \text{ kg/m}^3$ .

Draw-to scale and neatly-one diagram showing effective overburden stress and one separate diagram showing the pore pressure distribution in the soil.

**Problem 16.2.5.** The soil profile at a very level site consists of a 1 m thick upper layer of coarse sand (density  $1,900 \text{ kg/m}^3$ ) deposited on 5 m of soft clay (density  $1,600 \text{ kg/m}^3$ ). Below the clay, silty sand (density  $1,800 \text{ kg/m}^3$ ) is found. A piezometer installed to a depth of 8 m indicates a phreatic pressure height of 9 m. There is a seasonally occurring perched water table in the upper sand layer.

A very wide excavation will be carried out at the site to a depth of 4 m. Any water in the upper sand layer will be eliminated by means of pumping. The water pressure in the lower silty sand layer is difficult and costly to control. Therefore, it is decided not to try to lower it. Can the excavation be carried out to the planned depth? Your answer must be a "yes" or "no" and followed by a detailed rational supported by calculations.

**Problem 16.2.6.** The soil at a site consist of an upper 11 metre thick layer of soft, normally consolidated, compressible clay ( $c_v = 2 \cdot 10^{-8} \text{ m}^2/\text{s}$ , and unit weight =  $16 \text{ kN/m}^3$ ) deposited on a 4 metre thick layer of overconsolidated, silty clay ( $c_v = 10 \cdot 10^{-8} \text{ m}^2/\text{s}$ , unit weight =  $18 \text{ kN/m}^3$ , and a constant overconsolidation value of 20 kPa) which is followed by a thick layer of dense, pervious sand and gravel with a unit weight of  $20 \text{ kN/m}^3$ .

The groundwater table is located at a depth of 1.0 metre. The phreatic water elevation at the bottom of the soft clay layer is located 1.0 metre above the ground surface. At depth 16.0 metre, the pore water pressure is equal to 190 kPa.

In constructing an industrial building (area 20 by 30 metre) at the site, the area underneath the building is excavated to a depth of 1.0 metre. Thereafter, a 1.2 metre thick, compacted backfill (unit weight =  $20 \text{ kN/m}^3$ ) is placed over a vast area surrounding the building area. The building itself subjects the soil to a contact stress of 80 kPa.

As a preparation for a settlement analysis, calculate and **draw** the effective stress distribution in the soil below the midpoint of the building. Notice, a settlement analysis requires knowledge of both the original effective stress and the final effective stress. Also, there is no need to carry the calculation deeper into the soil than where the change of effective stress ceases to result in settlement. Settlement in "dense sand and gravel" is negligible compared to settlement in clay and silt.

**Problem 16.2.7.** In sequence, a lake bottom profile consists of a 6 m thick layer of clayey mud (density =  $1,700 \text{ kg/m}^3$ ), a 2 m thick layer of coarse sand (density =  $2,000 \text{ kg/m}^3$ ), and a 3 m thick layer of glacial clay till (density =  $2,200 \text{ kg/m}^3$ ) on pervious bedrock. The water depth in the lake is 3.0 m. Piezometer observations have discovered artesian pressure conditions in the sand layer: at a depth

of 7.0 m below the lake bottom the phreatic height is 12 m. Other piezometers have shown a phreatic height of 10 m in the interface between the till and the bedrock.

A circular embankment with a radius of 9 m and a height of 1.5 m (assume vertical sides) will be placed on the lake bottom. The fill material is coarse sand and it will be placed to a density of  $2,100 \text{ kg/m}^3$ .

Calculate and **draw** (in a combined diagram) the final effective stress and pore pressure profile from the embankment surface to the bedrock. Assume 2:1 distribution of the fill load.

**Problem 16.2.8.** A structure will be built in a lake where the water depth is 1.5 m and the lake bottom soils consist of an upper 1.5 m thick layer of pervious “muck” followed by 2.5 m layer of overconsolidated clayey silt deposited on a layer of overconsolidated coarse sand. Fractured bedrock is encountered at a depth of 16.0 m below the lake bottom. A soils investigation has established that the soil densities are  $1,500 \text{ kg/m}^3$ ,  $1,850 \text{ kg/m}^3$ , and  $2,100 \text{ kg/m}^3$ , respectively. Piezometers in the sand have shown an artesian head corresponding to a level of 2.0 m above the lake surface.

The structure will be placed on a series of widely spaced footings, each loaded by 1,500 kN dead load (which load includes the weight of the footing material; no live load exists). The footings are 3.0 m by 4.0 m in area and constructed immediately on the silt surface. Before constructing the footings, the muck is dredged out over an area of 6.0 m by 8.0 m, which area will not be back-filled.

Calculate the original and final (after full consolidation) effective stresses and the preconsolidation stresses in the soil underneath the mid-point of the footing.

### 16.3 Settlement Analysis

**Problem 16.3.1.** The soil at a site consists of an upper, 2 metre thick layer of sand having a density of  $1,900 \text{ kg/m}^3$  and a modulus number of 300. The sand layer is deposited on a very thick layer of clay having a density of  $1,600 \text{ kg/m}^3$  and a modulus number of 40. The groundwater table is located at the ground surface and is hydrostatically distributed.

A 3 metre wide, square footing supporting a permanent load of 900 kN is to be located at a depth of either 0.5 metre or 1.5 metre. Which foundation depth will result in the largest settlement? (During the construction, the groundwater table is temporarily lowered to prevent flooding. It is let to return afterward. Also, consider that backfill will be placed around the footing. You may assume that the footing itself is either very thin or that it is made of "concrete" having the density of soil).

**Problem 16.3.2.** The soil at a site consists of 2 metre thick layer of organic clay and silt with a density of  $1,900 \text{ kg/m}^3$  underlain by a layer of sand with a density of  $2,000 \text{ kg/m}^3$  deposited at the depth of 5 metre on a 4 metre thick layer of silty clay with a density of  $1,800 \text{ kg/m}^3$  followed by fractured bedrock. The groundwater table is located at a depth of 3.0 metre. The pressure head at the bedrock interface is 10 metre. The modulus number,  $m$ , of the clay and silt layer is 15. The sand layer can be considered overconsolidated by a constant value of 40 kPa and to have virgin modulus numbers,  $m$ , and reloading modulus numbers,  $m_r$ , of 120 and 250, respectively. Also the silty clay layer is overconsolidated, having an OCR-value of 2.0. Its virgin modulus and reloading modulus numbers are 30 and 140, respectively.

At the site, a building being 10 metre by 15 metre in plan area will be founded on a raft placed on top of the sand layer (after first excavating the soil). The load applied to the soil at the foundation level from the

building is 12 MN. Around the building, a fill having a density of  $1,600 \text{ kg/m}^3$ , will be placed to a height of 1.25 metre over an area of 50 by 50 metre and concentric with the building. Simultaneously with the construction of the building, the pore pressure at the bedrock interface will lowered to a phreatic height of 6 metre.

Determine the settlement of the sand and the silty clay layers assuming that all construction activities take place simultaneously and very quickly. You must calculate the settlement based on the stress change for each metre of depth. What would the settlement be if the fill had been placed well in advance of the construction of the building?

**Problem 16.3.3.** A 2.0 m deep lake with a surface elevation at +110.0 m will be used for an industrial development. The lake bottom consists of a 4 m thick layer of soft clayey silt mud followed by a 3-m layer of loose sand deposited on a 1 m thick layer of very dense glacial till. The pore pressures at the site are hydrostatically distributed. The soil densities are  $1,600 \text{ kg/m}^3$ ,  $1,900 \text{ kg/m}^3$ , and  $2,300 \text{ kg/m}^3$ , respectively. The clay is slightly overconsolidated with an OCR of 1.2 and has virgin and reloading modulus numbers of 20 and 80. The sand OCR is 3.0 and the modulus numbers are 200 and 500. For the till,  $m = 1,000$ . To reclaim the area, the pore pressure in the sand layer will be reduced temporarily to a phreatic elevation of +107.0 m and a sand and gravel fill (density =  $2,000 \text{ kg/m}^3$ ) will be dumped in the lake over a wide area and to a height of 2.5 m above Elevation +108.0. Although the lake, the fill rather, will be drained, it is expected that a perched groundwater table will always exist at Elevation +109.0.

Calculate the elevation of the surface of the fill when the soil layers have consolidated.

**Problem 16.3.4.** Is anyone or are any of the following four soil profile descriptions in error? If so, which and why? Comment on all four descriptions and include an effective stress diagram for each of A through D.

- A. A 10 m thick clay layer is deposited on a pervious sand layer, the groundwater table lies at the ground surface, the clay is overconsolidated, and the pore water pressure is hydrostatically distributed.
- B. A 10 m thick clay layer is deposited on a pervious sand layer, the groundwater table lies at the ground surface, the clay is normally consolidated, and the pore water pressure is artesian.
- C. A 10 m thick clay layer is deposited on a pervious sand layer, the groundwater table lies at the ground surface, the clay is undergoing consolidation, and the pore water pressure is linearly distributed.
- D. A 10 m thick clay layer is deposited on a pervious sand layer, the groundwater table lies at the ground surface, the clay is preconsolidated, and the pore water pressure has a downward gradient.

**Problem 16.3.5.** The silt and sand layers in Problem 15.2-08 have modulus numbers ( $m$  and  $m_r$ ) 35 and 80, and 120 and 280, respectively, and the stress exponents are 0 and 0.5, respectively. The OCR in the silt is 2.5 and the sand is preconsolidated to a 40 kPa preconsolidation stress margin. Calculate the settlement of the footing assuming that all construction takes place at the same instant.

## 16.4 Earth Stress and Bearing Capacity of Shallow Foundations

**Problem 16.4.1.** An anchor-wall (used as dead-man for a retaining wall) consists of a 4 m wide and 3 m high wall (with an insignificant thickness) and is founded at a depth of 4 m in a non-cohesive soil having an effective friction angle of  $32^\circ$  and no cohesion intercept. The soil density is  $1,900 \text{ kg/m}^3$  above the groundwater table and  $2,100 \text{ kg/m}^3$  below. At times, the groundwater table will rise as high as to a depth of 2.0 m.

Calculate the ultimate resistance of the anchor wall to a horizontal pull and determine the allowable pulling load using a factor of safety of 2.5.

**Problem 16.4.2.** A trench in a deep soil deposit is excavated between two sheetpile rows installed to adequate depth and with horizontal support going across the trench. As the Engineer responsible for the design of the wall, you have calculated the earth stress acting against the sheetpile walls considering fully developed wall resistance, effective cohesion, and internal effective friction angle of the soil. You have also considered the weight of a wide body, heavy crawler rig traveling parallel and close to the trench by incorporating two line-loads of appropriate magnitude and location in your calculation. Your calculated factor of safety is low, but as you will be in charge of the inspection of the work and physically present at the site at all times, you feel that a low factor of safety is acceptable.

When visiting the site one day during the construction work, you notice that one track of the crawling rig travels on top of one of the sheetpile walls instead of on the ground next to the wall, as you had thought it would be. The load of the crawler track causes a slight, but noticeable downward movement of the so loaded sheetpile row.

Quickly, what are your immediate two decisions, if any? Then, explain, using text and clear sketches including force polygons, the qualitative effect—as to advantage or disadvantage—that the location of the crawler track has on the earth stress acting against the sheetpile wall.

**Problem 16.4.3.** As a part of a renewal project, a municipality is about to shore up a lake front property and, at the same time, reclaim some land for recreational use. To this end, a 6.0 m high L-shaped retaining wall will be built directly on top of the lake bottom and some distance away from the shore. Inside the wall, hydraulic sand fill will be placed with a horizontal surface level with the top of the wall. The wall is very pervious. The water depth in the lake is kept to 2.0 m. The lake bottom and the hydraulic fill soil parameters are density  $1,900 \text{ kg/m}^3$  and  $1,000 \text{ kg/m}^3$ , and effective friction angle  $37^\circ$  and  $35^\circ$ , respectively, and zero effective cohesion intercept.

Calculate the earth stress against the retaining wall.

**Problem 16.4.4.** The soil at a site consists of a thick layer of sand with a unit weight of  $18 \text{ kN/m}^3$  above the groundwater table and  $20 \text{ kN/m}^3$  below the groundwater table. The effective friction angle of the sand is  $34^\circ$  above the groundwater table and  $36^\circ$  below. At this site, a column is founded on a footing having a 3 m by 4 m plan area and its base at a depth of 2.1 m, which is also the depth to the groundwater table. Acting at the ground surface and at the center of the column, the column is loaded by a vertical load of 2,100 kN and a 300 kN horizontal load parallel to the short side of the footing. There is no horizontal load parallel to the long side. Neither is there any surcharge on the ground surface.



Calculate the factor of safety against bearing failure. In the calculations, assume that the column and footing have zero thickness and that the natural soil has been used to backfill around the footing to a density equal to that of the undisturbed soil.

Considering that the bearing capacity formula is a rather dubious model of the soil response to a load, verify the appropriateness of the footing load by calculating the footing settlement using assumed soil parameters typical for the sand.

**Problem 16.4.5.** A 3.0 m wide strip footing ("strip" = infinitely long) is subjected to a vertical load of 360 kN/linear-metre. Earth stress and wind cause horizontal loads and a recent check on the foundation conditions has revealed that, while the factors of safety concerning bearing capacity and sliding modes are more than adequate, the magnitude of the edge stress is right at the allowable limit. How large is the edge stress?

**Problem 16.4.6** A footing for a continuous wall supports a load of 2,000 kN per metre at a site where the soil has a density of 1,900 kg/m<sup>3</sup>, an effective cohesion intercept of 25 kPa, and an effective friction angle of 33°. The footing is placed at a depth of 1.0 m which also is the depth to the groundwater table.

Determine the required width of the wall base (footing) to the nearest larger 0.5 m using a Global Factor of Safety of 3.0 and compare this width with the one required by the OHBDC in a ultimate limit states, ULS, design).

## 16.5 Deep Foundations

**Problem 16.5.1.** A bored pile with a diameter of 600 mm and E-modulus of 35 GPa, will be installed to 15.0 m depth at a site where the soil consists of a 10 m thick upper layer of overconsolidated clay deposited on a 18 m thick layer of normally consolidated sand deposited on bedrock. The groundwater table lies the ground surface and the distribution is hydrostatic.

The clay and sand densities are 1,750 kg/m<sup>3</sup> and 2,000 kg/m<sup>3</sup>, respectively, and the beta-coefficients are 0.25 and 0.40, respectively. The unit toe resistance at movement commensurate with the movement governing the  $\beta$ -coefficients is 4 MPa. The parameters can be assumed to have been back-calculated from the results of a static loading test (performed some time ago) and represent those at "capacity", as determined by one definition or other applied to the pile-head load-movement curve of the test. The telltale measured pile toe movement for the load representing the "capacity was 25 mm. At a 10-mm toe movement, the applied load was 500 kN smaller than the "capacity".

The test results serve as reference for a design of a group of 16 to be installed in a square configuration. The piles will be placed at a minimum center-to-center spacing of 2.5 times the pile diameter plus 2.0 % of the embedment length. The pile group will support a total sustained (dead) load of 9,600 kN, as determined by applying a factor of safety of 2.5 to the ultimate resistance determined from the test. It can be assumed that the piles carry the same load.

An 1.0 m thick backfill will be placed around the piles to a very large width just before the piles are installed. The fill consists of granular material with 1,800 kg/m<sup>3</sup> density. The Janbu modulus numbers,  $m$  and  $m_r$ , in the clay are 25 and 250, respectively, and the preconsolidation stress is 25 kPa above the existing effective stress (i.e., preconsolidation margin). The E-modulus of the sand is 20 MPa.

- A. What is the margin for allowable transient (live) load per pile when applying the same factor of safety as that is applied to the sustained load?
- B. Find the depth to the neutral plane (draw a diagram to scale and determine the long-term maximum force in the pile).
- C. Plot the pile-head, pile-shaft, and pile-toe load-movement curves of the referenced pre-design static loading test.
- D. Estimate the long-term settlement of the pile group.

**Problem 16.5.2.** An elevated road (a causeway) is to be built across a lake bay, where the water surface is at Elevation +10.0 and the water depth is 2.0 m. The lake bottom consists of a 12 m thick layer of compressible, normally consolidated silty clay deposited on a 40 m thick layer of sand on bedrock. The pore water pressure in the clay is hydrostatically distributed.

The causeway will be supported on a series of pile bents. Each bent will consist of a group of eight, 0.3 m square piles installed to Elevation -22.0 m in three equal rows at an equal spacing of 5 diameters (no pile in the center of the group). The beta-coefficients in the clay and the sand representing ultimate resistance are 0.33 and 0.45, respectively. The clay and the sand layers have unit weights of  $16 \text{ kN/m}^3$  and  $20 \text{ kN/m}^3$ , respectively. The commensurate unit toe resistance is 15 MPa. The effective cohesion intercept is zero for both layers. The modulus numbers and stress exponents are 50 and 280, and 0 and 0.5, respectively.

To provide lateral restraint for the piles, as well as establish a working platform above water, a sand fill is placed at the location of each bent. Thus, the sand fill will be permanent feature of each pile bent. The sand fill is 4.0 m thick and covers a 10 by 10 m square area. The saturated unit weight of the sand fill is  $20 \text{ kN/m}^3$ . Assume that the total unit weight of the sand fill is the same above as below the lake surface and that the shaft resistance in the fill can be neglected.

- A. Calculate and plot the distribution of the ultimate soil resistance along a single pile assuming that positive shaft resistance acts along the entire length of the pile and that all excess pore pressure induced by the pile driving and the placement of the sand fill have dissipated.
- B. Determine the allowable live load (for a single pile) acting simultaneously with a dead load of 900 kN and using a global factor of safety of 3.0.
- C. Calculate the consolidation settlement for the pile group. Then, draw the settlement distribution in the sand. (Assume that the fill has vertical sides).

**Problem 16.5.3.** A pile in a specific large (many piles) pile group is assigned a "capacity" of 200 tons and a toe resistance of 110 tons, and the allowable dead load is 80 tons. There is no live load acting on the pile group. The soil is homogeneous and large settlement is expected throughout the soil profile. The piles consist of pipes driven open-toe (open-end) into the soil and connected by means of a rigid pile cap. In driving, the inside of the pipe fills up with soil that afterward is drilled and cleaned out—of course, taking care not to disturb the soil at and below the pile toe. The pipe is then filled with concrete and the short column strength of the concreted pipe is 300 tons. By mistake, when cleaning one perimeter pile, the work was continued below the pile toe leaving a void right at the pile toe that was not discovered in time. The concreting did not close the void. The pile shaft was not affected, however, and the pile itself is

structurally good. As the geotechnical engineer for the project, you must now analyze the misshapen pile and recommend an adjusted allowable load for this pile. Give your recommendation and justify it with a sketch and succinct explanations.

**Problem 16.5.4.** The Bearing Graph representative for the system (hammer, helmet cushion) used for driving a particular pile into a very homogeneous non-cohesive soil of a certain density at a site is given by the following data points: [600 kN/1; 1,000/2; 1,400/4; 1,600/6; 1,700/8; and 1,900/20 blows/inch—that is, force resistance vs. penetration resistance, i.e., a Bearing Graph]. The groundwater table at the site lies at the ground surface and the pore pressure distribution is hydrostatic. The pile is driven open-toe and can be assumed to have no toe resistance (no plug is formed). At the end-of-initial-driving, the penetration resistance is 3 blows/inch and, in restriking the pile a few days after the initial driving, the penetration resistance is 12 blows/inch. This bearing difference is entirely due to pore pressures which were developed and present during initial driving, but which had dissipated at restriking. On assuming that the soil density is either 2,000 kg/m<sup>3</sup> or 1,800 kg/m<sup>3</sup> (i.e., two cases to analyze), determine the average excess pore pressure present during the initial driving in relation to (= in % of) the pore pressure acting during the restriking.

Notice, you will need to avail yourself of a carefully **drawn** bearing graph using adequately scaled axes.

**Problem 16.5.5.** Piles are being driven for a structure at a site where the soils consist of fine sand to 20 m depth. The density of the sand is 2,000 kg/m<sup>3</sup> and the groundwater table lies at a depth of 3.0 m. The piles are closed-toe pipe piles with a diameter (O.D.) of 12.75 inch and 0.316 inch wall. The beta-coefficient in the sand is assumed to increase linearly from 0.40 at the ground surface through 0.50 at the sand lower boundary and the values represent ultimate resistance. The commensurate unit pile-toe resistance near the lower sand boundary is 8 MPa. A test pile is installed to an embedment depth of 15.0 m.

- A. Determine the ultimate resistance to expect for the 15-m test pile.
- B. Determine the ultimate resistance for a new pile driven to an embedment depth of 18 m.

**Problem 16.5.6** A soil profile at a site consist of a 2.0 m thick layer of silt ( $\rho = 1,700 \text{ kg/m}^3$ ) followed by a thick deposit of sand ( $\rho = 2,050 \text{ kg/m}^3$ ). The groundwater table is located at a depth of 0.5 m and the pore pressures are hydrostatically distributed.

At the site, an industrial building is considered which will include a series of columns (widely apart), each transferring a permanent (dead) vertical load of 1,000 kN to the soil. The groundwater table will be lowered to a new stable level at a depth of 1.5 m below the ground surface.

A foundation option is to support the columns on 0.25 m diameter square piles installed to 10.0 m depth. The  $\beta$ -coefficients of the silt and sand are 0.35 and 0.55, respectively, and the toe bearing  $N_t$ -coefficient of the sand is 50.

Calculate using effective stress analysis how many piles that will be needed at each column if the Factor-of-Safety is to be at least 2.5.

**Problem 16.5.7** A pile group comprises 8 by 12 = 96 piles at a 3.0 c/c diameter spacing, square configuration. All piles are 350 mm diameter, 22 m long square precast concrete pile. The total sustained load on the pile raft is 90 MN. Assume that the pile material Young modulus is 30 GPa and calculate, approximately, the compression of the equivalent pier for the working load, assuming most of the load will reach the pile toe level.

**Problem 16.5.8** A static loading test has been carried out on a strain-gage instrumented, 400-mm diameter, 20 m long square, precast concrete, test pile installed in a uniform sand with a 2,000-kg/m<sup>3</sup> density. The groundwater table lies 6 m below the ground surface. The analysis of the strain-gage measurements showed that the beta-coefficient at a 12-m depth (gage location) was 0.40 for the specific Target Load considered in the analysis. The results of the test are applied to a design consisting of a series of essentially single piles of the same length after the site has been excavated to 5 m depth over a wide area. What is the ratio between the unit shaft resistance at the mentioned gage level for the two conditions for the pile in the middle of the excavation area at the same beta-coefficient? That is, first for the 12-m depth below ground surface and for the now 7 m below the excavation level.

**Problem 16.5.9** A static loading test has been carried out on a pile installed through a compressible soil into a competent bearing soil. In the test, a 270-kN pile-toe force was measured at a 12.5 mm pile-toe movement. Back-calculation of the pile-toe load-movement curve indicates that the toe response followed a Gwizdala (Ratio) function with a coefficient equal to 0.600. Immediately after construction of the pile-supported building, the loads from the building resulted in piled foundation settlement due to pile shortening plus an 4.2 mm load-transfer pile-toe movement. The piles are widely spaced and can be considered responding like single piles. Ongoing regional subsidence is expected to add a 200-kN force to the toe due to development of drag force and downdrag. How much additional pile toe movement will occur? Disregard additional pile shortening.

**Problem 16.5.10** After plotting measured strain-gage records from a static loading test on a 358-mm diameter circular pile per the incremental stiffness method (tangent stiffness method) and developing a linear regression line for the tangent stiffness,  $E_tA$  (GN), vs. strain ( $\mu\epsilon$ ), the following equation was obtained:  $E_t = 34 - 0.026 \mu\epsilon$ . At one gage level in the pile, the Target Load resulted in 330  $\mu\epsilon$ . What axial load does this value represent at the gage level?

-----

The correct answer to each of Problems 16.5.7 - 16.5.10 is one of the four alternatives (A through D):

- |                        |           |            |             |             |
|------------------------|-----------|------------|-------------|-------------|
| <b>Problem 16.5.7</b>  | A. 6 mm   | B. 9 mm    | C. 12 mm    | D. 20 mm    |
| <b>Problem 16.5.8</b>  | A. 0.8    | B. 1.2     | C. 1.6      | D. 2.2      |
| <b>Problem 16.5.9</b>  | A. 7.5 mm | B. 11.3 mm | C. 14.1 mm  | D. 22.7 mm  |
| <b>Problem 16.5.10</b> | A. 460 kN | B. 980 kN  | C. 1,140 kN | D. 1,820 kN |

## CHAPTER 17

### REFERENCES

- AASHTO Specifications, 1992. Standard specifications for highway bridges, 15th Edition. American Association of State Highway Officials, Washington.
- AASHTO Specifications 2010. LRFD Bridge Design Specification, 5th Edition. American Association of State Highway Officials, Washington.
- Abchir, Z., Burlon, S., Frank, R., and Reiffsteck, P., 2016. Prediction of pile behavior under static and bi-directional tests and comparison with field results. 3rd Bolivian International Conference on Deep Foundations, Santa Cruz de la Sierra, Bolivia, April 27-29, Vol. 3, pp. 53-60.
- AFNOR, 2012. Calcul des fondations profondes – NF P 94 282. Justification des ouvrages géotechniques, Normes d'application nationale de l'Eurocode 7, Afnor, Paris, July 2012).
- Altaee, A., Evgin, E., and Fellenius, B.H., 1992. Axial load transfer for piles in sand. I: Tests on an instrumented precast pile. Canadian Geotechnical Journal 29(1) 11-20.
- Altaee, A., Evgin, E., and Fellenius, B.H., 1993. Load transfer for piles in sand and the critical depth. Canadian Geotechnical Journal 30(2) 465-463.
- Altaee, A. and Fellenius, B.H., 1994. Physical modeling in sand. CGJ 31(3) 420-431.
- Aoki, N., 2000. Improving the reliability of pile bearing capacity prediction by the dynamic increasing energy test, DIET. Keynote Lecture. Proc. of the Sixth International Conference on the Application of Stress-Wave Theory to Piles. Sao Paulo, September 11-13, Balkema, pp. 635-650.
- API 2000. Recommended Practice for Planning, Designing, and Constructing Fixed Offshore Platforms-Working Stress Design, 21st Edition. American Petroleum Institute, 242 p.
- ASTM, 2007. D1143-07 Standard Test Method for Piles Under Static Axial Compressive Load. American Society for Testing and Materials, Annual Book of Standards, ASTM, Philadelphia, PA, Construction Vol. 4:08, 15 p.
- ASTM, 2007. D3689-07. Standard Test Method for Individual Piles Under Static Axial Tensile Load. American Society for Testing and Materials, Annual Book of Standards. ASTM, Philadelphia, PA, Construction Vol. 4:08.
- ASTM, 2010. D4945-10. Standard test method for high-strain dynamic testing of piles. American Society for Testing and Materials, Annual Book of Standards. ASTM, Philadelphia, PA, Construction Vol. 4:08.
- Amir, J.M., 1983. Interpretation of load tests on piles in rock. Proc. of the 7th Asian Regional Conference on Soil Mechanics and Foundation Engineering, Haifa, August 14-19, IV/4, pp. 235-238.
- Amir, J.M., Amir, E.J., and Lam, C., 2014. Modulus of elasticity in deep bored piles. Proc. of the DFI-EFFC International Conf. on Piling and Deep Foundations, Stockholm, May 21-23, pp. 397-402.
- Aoki, N., 2000. Improving the reliability of pile bearing capacity prediction by the dynamic increasing energy test, DIET. Keynote Lecture, Proc. of the Sixth Int. Conference on the Application of Stress-Wave Theory to Piles. Sao Paulo, September 11-13, Balkema, pp. 635-650.
- Asaoka, A., 1978. Observational procedure of settlement prediction. Soil and Foundations, Japan 18(4) 87-101.
- Axelsson, G., 2000. Long-term set-up of driven piles in sand. Department of Civil and Environmental Engineering, Royal Institute of Technology, Stockholm, 193 p.
- Authier, J. and Fellenius, B.H., 1980. Quake values determined from dynamic measurements. Proc. of the First International Seminar on Application of Stress-Wave Theory to Piles, Stockholm, September 10-13, H. Bredenberg Editor, A. A. Balkema, Rotterdam, pp., 197-216.
- Auxilia, G.B., Burke, P., Duranda, M., Ulini, F., Buffa, L., Terrioti, C., Dominijanni, A., and Manassero, M., 2009. Large storage capacity cement silos and clinker deposit on a near-shore sandy fill using piles for soil improvement and settlement reduction. 17th ICSMGE, Alexandria, October 5-9, 2009, Vol. 3, pp. 1181-1184.

- Baldi, G., Bellotti, R., Ghiona, R., Jamiolkowski, M., and Pasqualini, E., 1986. Interpretation of CPTs and CPTUs. 2nd Part: Drained penetration of sands. Proc. of the Fourth International Geotechnical Seminar on Field Instrumentation and In-situ Measurements, Singapore November 25-27, 1986, 143-156.
- Baligh, M., Vivatrat, V., Wissa, A., Martin R., and Morrison, M., 1981. The piezocone penetrometer. Proc. of Symposium on Cone Penetration Testing and Experience, ASCE National Convention, St. Louis, October 26-30, pp. 247-263.
- Barbie, D.L., Reece, B.D., and Eames, D.R., 2005. Water Resources Data--Texas, Water Year 2004, Volume 6, Groundwater Data. U.S. Geological Survey, Texas Water Science Center, Water-Data Report TX-04-6, 754 p.
- Barron, R.R., 1947. Consolidation of fine-grained soils by drain wells. Proc. of the ASCE 73(6) In Transactions of the ASCE 1948 (113) 718-742.
- Baquerizo, A. 2015. New cost effective, schedule drive solution for tall building foundations. DFI Superpile Conference, Kissimmee, Fl, May 6-7, 33 p.
- Basile, F., 2019. The role of cap flexibility in pile group design. Proc. of the 17th ECSMGE, Reykjavik, September 1-6, 11 p.
- Bean K., Jefferies M.G., and Hachey, J., 1991. The critical state of sand, *Geotechnique* 41(3) 365-381.
- Begemann, H.K.S., 1953. Improved method of determining resistance to adhesion by sounding through a loose sleeve placed behind the cone. Proc. of the 3rd ICSMFE, August 16-27, Zurich, Vol. 1, pp. 213-217.
- Begemann, H.K.S., 1963. The use of the static penetrometer in Holland. *New Zealand Engineering*, 18(2) 41.
- Begemann, H.K.S., 1965. The friction jacket cone as an aid in determining the soil profile. Proc. of the 6th ICSMFE, Montreal, September 8-15, Univ. of Toronto Press, Vol. 2, pp. 229-233.
- Bermingham, P., Ealy, C.D., and White J.K., 1993. A comparison of Statnamic and static field tests at seven FHWA sites. Bermingham Corporation Limited, Internal Report.
- Bishop, A.W., 1955. The use of the slip circle in stability analysis of slopes. *Geotechnique* 5(1) 7-17.
- Bjerrum, L., 1954. Norwegian experiences with steel piles to rock. *Geotechnique* 4(2) 73-96.
- Bjerrum L., Jönsson, W. and Ostenfeld, C 1957. The settlement of a bridge abutment on friction piles. Proc. 4th ICSMFE, London, August 12-24, Vol. 2, pp. 14-18.
- Bjerrum, L., Johannessen, I.J. and Eide O., 1969. Reduction of negative skin friction on steel piles to rock. Proc. 7th ICSMFE, Mexico City, August 25-29, Vol. 2 pp. 27-33.
- Bjerrum, L. and Flodin, N., 1960. The development of soil mechanics in Sweden 1900-1925. *Geotechnique* 10(1) 1-18.
- Boardman, T.B., 2007. Discussion on Assessment of the liquefaction susceptibility of fine-grained soils. *ASCE J. Geotechnical and Geoenvironmental Engineering* (134)7 1030-1031.
- Bohn, C., Lopes dos Santos, A., and Frank R., 2017. Development of axial pile load transfer curves based on instrumented load tests. *ASCE J. of Geotechnical and Geoenviron. Engng.*, 143(1) 15 p.
- Boulanger, R.W. and Idriss, I.M., 2007. Closure to Discussion on Liquefaction susceptibility criteria for silt and clays. *ASCE J. Geotechnical and Geoenvironmental Engineering* (134)7 1027-1028.
- Bray, J.D. and Sancio, R.B., 2006. Assessment of the liquefaction susceptibility of fine-grained soils. *ASCE J. Geotechnical and Geoenvironmental Engineering* (132)11 1165-1187.
- Bray, J.D. and Sancio, R.B., 2007. Closure to Discussion on Assessment of the liquefaction susceptibility of fine-grained soils. *ASCE, J. Geotechnical and Geoenvironmental Engineering* (134)7 1031-1034.
- Boussinesq, J., 1885. Application des potentiels a l'etude de l'equilibre et due mouvement des solids elastiques. Gauthiers-Villars, Paris, (as referenced by Holtz and Kovacs, 1981).
- Bowles, J.E., 1988. Foundation analysis and design, Fourth Edition. McGraw-Hill Book Company, New York, 1004 p.
- Bozozuk, M., 1977, 1981. Bearing capacity of pile preloaded by downdrag. Proc. of 10th ICSMFE, Stockholm. June 15-19, Vol. 2, pp. 631-636.

- Bozozuk, M. and Labrecque, A., 1968. Downdrag measurements on 270-ft composite piles. Proc. of Symposium of Deep Foundations, STP 444, Edited by R. Lundgren and E. D'Appolonia, ASTM 71st Annual Meeting, San Francisco June 23-28, pp. 15-40.
- Bozozuk, M., Fellenius, B.H. and Samson, L., 1978. Soil disturbance from pile driving in sensitive clay. Canadian Geotechnical Journal 15(3) 346-361.
- Bradshaw, A.S., Haffke, S., and Baxter, C.D.P., 2012. Load transfer curves from a large-diameter pipe pile in silty soil. In Full-scale testing and foundation design. ASCE Geotechnical Special Publication 227. Edited by M.H. Hussein, K.R. Massarsch, G.E. Likins, and R.D. Holtz. American Society of Civil Engineers, pp. 590–601.
- Briaud J.-L., 2013. Geotechnical Engineering, Wiley, 998 p.
- Briaud, J-L and Gibbens, R.M., 1994. Predicted and measured behavior of five spread footings on sand. Proc. of a Symposium sponsored by the Federal Highway Administration at the 1994 American Society of Civil Engineers, ASCE, Conference Settlement '94, College Station, Texas, June 16-18, pp., 192-128.
- Briaud, J.-L., and Gibbens, R.M., 1999. Behavior of five large spread footings in sand. ASCE J. Geotechnical and Geoenvironmental Engineering 125(9) 787-796.
- Briaud, J-L, Nicks J, Rhee, K., and Stieben, G., 2007. San Jacinto Monument case history. ASCE J. Geotechnical and Geoenvironmental Engineering (133)11 1337-1351.
- Broms, B.B., 1976. Pile foundations—pile groups. 6th ECSMF, Vienna, Vol. 2.1, pp. 103-132.
- Brown, M.J., Hyde, A.F.L., and Anderson, W.F. (2006). Analysis of a rapid load test on an instrumented bored pile in clay, Geotechnique, 56(9), 627-638.
- Brown, D.A., Reese, L.C., and O'Neill, M.W., 1987. Cyclic lateral loading of a large-scale pile group. ASCE J. 113(11).
- Brown, D.A., Morrison, C., and Reese, L.C., 1988. Lateral load behavior of pile group in sand. ASCE J. 114(GT11).
- Brown, D.A., 2012. Recent advances to the selection and use of drilled foundations. ASCE GeoInstitute Geo-Congress Oakland, March 25-29, 2012, Keynote Lectures, State of the Art and Practice in Geotechnical Engineering, ASCE, Reston, VA, Rollins, K. and Zekkos, D., eds., Geotechnical Special Publication 226, pp. 519-548.
- Brown, D.A., 2018. Drilled shafts: Construction procedures and design methods. US Fed. Highway Administration, FHWA,-GEC101, 756 p.
- Buisman, A.S.K., 1935. De weerstand van paalpunten in zand. De Ingenieur, No. 50, pp. 25-28 and 31-35. (As referenced by Vesic, 1973).
- Buisman, A.S.K., 1940. Grondmechanica. Walman, Delft, 281 p. (As referenced by Vesic, 1973, and Tschebotarioff, 1951).
- Bullock, P., Schmertmann, J., McVay, M.C., and Townsend, F.C., 2005. Side shear set-up. Test piles driven in Florida. ASCE Journal of Geotechnical and Geoenvironmental Engineering 131(3) 292-310.
- Bullock, P., 2012. Advantages of dynamic pile testing. ASCE GeoInstitute Geo-Congress Oakland, March 25-29, 2012, Full-scale Testing in Foundation Design, State of the Art and Practice in Geotechnical Engineering ASCE, Reston, VA, M.H. Hussein, K.R. Massarsch, G.E. Likins, and R.D. Holtz, eds., Geotechnical Special Publication 227, pp. 694-709.
- Burland, J.B., 1973. Shaft friction of piles in clay—A simple fundamental approach. Ground Engineering, Foundation Publications Ltd., London 6(3) 30-42.
- Burland, J.B., Broms, B.B., and deMello, V.F.B., 1981. Behavior of foundations and structures, Proc. 9th ICSMF, Tokyo, July 10-15, Vol. 2, pp. 495-546.
- Burlon, S., 2016. Design methods based on static pile load tests. ISSMGE-ETC 3 International Symposium on Design of Piles in Europe, General Report, Vol. 1, Brussels, April 28-29, pp. 87-96.
- Bustamante, M. and Gianeselli, L., 1982. Pile bearing capacity predictions by means of static penetrometer CPT. Proc. of the Second European Symposium on Penetration Testing, ESOPT II, Amsterdam, May 24-27, A.A. Balkema, Vol. 2, pp. 493-500.

- Campanella, R.G., Gillespie, D., and Robertson, P.K., 1982. Pore pressures during cone penetration testing, Proc. of the 2nd European Symposium on Penetration Testing, ESOPT-2, Amsterdam, May 24-27, Vol. 2, pp. 507-512.
- Campanella, R.G., and Robertson, P.K., 1988. Current status of the piezocone test. Proc. of First International Symposium on Penetration Testing, ISOPT-1, Orlando, March 22-24, Vol. 1, pp. 93-116.
- Canadian Standard Council, 2006. Canadian Highways Bridge Design Code, Section 6, Foundations. Canadian Standard Association, CSA-S6-06, Code and Commentary, 1,340 p.
- Canadian Foundation Engineering Manual, CFEM, 1985. Second Edition. Canadian Geotechnical Society, BiTech Publishers, Vancouver, 456 p.
- Canadian Foundation Engineering Manual, CFEM, 1992. Third Edition. Canadian Geotechnical Society, BiTech Publishers, Vancouver, 512 p.
- Canadian Foundation Engineering Manual, CFEM, 2006. Fourth Edition. Canadian Geotechnical Society, BiTech Publishers, Vancouver, 488 p.
- Caputo, V. and Viggiani, C., 1984. Pile foundation analysis: a simple approach to nonlinearity effects. *Rivista Italiana di Geotecnica*, 18(2) 32–51.
- Carrillo N. 1942. Simple two- and three-dimensional cases in the theory of consolidation of soils. *Journal of Mathematics and Physics*, 21(1) 1-5.
- Caquot, A. and Kerisel, J., 1953. Sur le terme de surface dans le calcul des fondations en milieu pulvérulent. Proc. of the 3rd ICSMFE, Zurich, August 16-27, Vol. 1, pp. 336-337.
- Casagrande, A., 1935. Characteristics of cohesionless soil affecting the stability of slopes and earth fills. *Journal of the Boston Society of Soil Mechanics*. Vol. 23, pp. 13-32.
- Casagrande, L. and Poulos, S., 1969. On the effectiveness of sand drains. *Canadian Geotechnical Journal* 6(3) 287-326.
- Chai, J.C., Carter, J.P., and Hayashi, S., 2005. Ground deformation induced by vacuum consolidation. *ASCE Journal for Geotechnical and Geoenvironmental Engineering* 131(12) 1552-1561.
- Chang, Y.C.E., 1981. Long-term consolidation beneath the test fills at Väsby, Sweden. Swedish Geotechnical Institute, Report 13, 192 p.
- Chai, J.C., Carter, J.P., and Hayashi, S., 2006. Vacuum consolidation and its combination with embankment loading. *Canadian Geotechnical Journal* 43(10) 985-996.
- Chellis, R.D., 1951. *Pile Foundations*. McGraw Hill Book Company, 704 p.
- Chin, F.K., 1970. Estimation of the ultimate load of piles not carried to failure. Proc. of the 2nd Southeast Asian Conference on Soil Engineering, pp. 81-90.
- Chin, F.K., 1971. Discussion on Pile test. Arkansas River project. *ASCE Journal for Soil Mechanics and Foundation Engineering* 97(SM6) 930-932.
- Chin, F.K., 1978. Diagnosis of pile condition. Sixth Southeast Asian Conference on Soil Engineering, Bangkok, July 1977, SEAGS Geotechnical Engineering 9(2) 85-104.
- Clausen, C.J.F., Aas, P.M., and Karlsrud, K., 2005. Bearing capacity of driven piles in sand, the NGI approach. Proc. International Symposium. on Frontiers in Offshore Geotechnics, Perth, September 2005, A.A. Balkema Publishers, pp. 574-580.
- Clemente, F.M., 1981. Downdrag on bitumen-coated piles in a warm climate. Proc. of 10th ICSMFE, Stockholm. June 15-19, Vol. 2, pp. 673-676.
- Coffman, R.A., Blanchard, J.D., Stuedlein, A.W., Jana, A., and Budge, A.S., 2024. Design of piles for downdrag. NCHRP 1112, The Unified Method, TRB, Wa, 353 p.
- Cooke, R. W. (1986). Pile raft foundations on stiff clays—a contribution to design philosophy. *Geotechnique* 36(2) 169-203.
- Cooke, R. W., Price, G. and Tarr, K. (1979). Jacked piles in London Clay: a study of load transfer and settlement under working conditions. *Geotechnique* 29(2) 113-147.
- Cooke, R.W., Price, G., and Tarr, K. (1980). Jacked piles in London Clay: interaction and group behaviour under working conditions. *Geotechnique* 30(2), 97-136.



- Cooke, R.W., Bryden-Smith, D.W., Gooch, M.N., and Sillett, D.F. (1981). Some observations of the foundation loading and settlement of a multi-storey building on a piled raft foundation in London Clay. *Proc. Inst. Civ. Engrs, Part I-70*, pp. 433-460".
- Cortlever, N.G., Visser, G.T., and deZwart, T.P., 2006. Geotechnical History of the development of the Suvarnabhumi International Airport. Special Issue of the *Journal of South-East Asian Geotechnical Society*, December 2006, 37(3) 189-194.
- Coyle, H.M. and Sulaiman, I.H. (1967). Skin Friction for Steel Piles in Sand. *Journal of the Soil Mechanics and Foundations Division*, 93(6) 261-278.
- Coyle, H.M. and Sulaiman, I.H., 1970. Bearing capacity of foundation piles. State of the Art. Proc. of 49th Annual Meeting of the Highway Research Board, pp. 87- 103.
- Crawford, C.B., 1968. Instrumentation and downdrag. Proc. of Symposium of Deep Foundations, STP 444, Edited by R. Lundgren and E. D'Appolonia, ASTM 71st Annual Meeting, San Francisco June 23-28, pp. 223-226.
- Dahlberg, R., 1975. Settlement Characteristics of Preconsolidated Natural Sands. Swedish Council for Building Research, Document D1:1975, 315 p.
- Davisson, M.T., 1972. High capacity piles. Proc. of Lecture Series on Innovations in Foundation Construction, ASCE Illinois Section, Chicago, March 22, pp. 81-112.
- DeBeer, E.E., 1968. Proefondervindlijke bijdrage tot de studie van het grensdrag vermogen van zand onder funderingen op staal. *Tijdschrift der Openbar Verken van België*, No. 6, 1967 and No. 4, 5, and 6, 1968.
- DeBeer, E.E. and Walays, M., 1972. Franki piles with overexpanded bases. *La Technique des Travaux*, Liege, Belgium, No. 333.
- Decourt, L., 1982. Prediction of bearing capacity of piles based exclusively on N-values of the SPT. Proc. ESOPT II, Amsterdam, May 24-27, pp. 19-34.
- Decourt, L., 1989. The Standard Penetration Test. State-of-the-Art report. A.A. Balkema, Proc. of 12th International Conference on Soil Mechanics and Foundation Engineering, Rio de Janeiro, Brazil, August 13-18, Vol. 4, pp. 2405-2416.
- Decourt, L., 1995. Prediction of load-settlement relationships for foundations on the basis of the SPT. Proc. of the Conf. in honor of Leonardo Zeevaert, Mexico City, Oct. 28-Nov. 6, pp. 87-103.
- Decourt, L., 1999. Behavior of foundations under working load conditions. Proc. of 11th Pan-American Conference on Soil Mechanics and Geotechnical Engineering, Foz DoIguassu, Brazil, August 1999, Vol. 4, pp. 453-488.
- Decourt, L., 2008. Loading tests: interpretation and prediction of their results. ASCE GeoInstitute Geo-Congress New Orleans, March 9-12, Honoring John Schmertmann—From Research to Practice in Geotechnical Engineering, Geotechnical Special Publication, GSP 180, Edited by J.E. Laier, D.K. Crapps, and M.H. Hussein, pp. 452-488.
- Deep Foundations Institute, DFI, 1979. A pile inspector's guide to hammers, Sparta, New Jersey, 41 p.
- DeRuiter, J. and Beringen, F.L., 1979. Pile foundations for large North Sea structures. *Marine Geotechnology*, 3(3) 267-314.
- Doan, L.V., and Lehane, B.M., 2019. Axial capacity of bored piles in very stiff intermediate soils. *Can. Geotech. J.* 57(9), 1417–1426. <https://doi.org/10.1139/cgj-2019-0324>.
- Doan, L.V., and Lehane, B.M., 2020. Relating shaft friction of buried piles and CPT resistance in clayey sands. *Geotechnique* 70(9) 791–802. <https://doi.org/10.1680/jgeot.18.P.290>.
- Doan, L.V. and Lehane, B.M., 2021. CPT-Based Design Method for Axial Capacities of Drilled Shafts and Auger Cast-in-Place Piles. *ASCE Geotechnical and Geoenvironmental Engineering*, 147(8) 15 p.
- Doan, L.V., and Lehane, B.M., 2022. New CPT methods for evaluation of the axial capacity of driven piles. Proceedings of 5th International Symposium on Cone Penetration Testing (CPT'22), Edited by Gottardi, G. and Tonni, L, June 8-10, 2022, Bologna, Italy. pp. 3 - 15.
- Dobry R., Peck, R.B., and Pecker, A., 2007 Rion-Antirion Bridge. An Olympian effort to overcome extreme geohazards. *Deep Foundations Institute Magazine*, Fall issue, pp. 5- 8.
- Duncan, J.M., Evans, L.T., and Ool, P.S.K., 1992. Lateral load analysis of single piles and drilled shafts. *ASCE Journal of Geotechnical Engineering Division*, 120(5) 1018-1033.

- Douglas, B.J., and Olsen, R.S., 1981. Soil classification using electric cone penetrometer. ASCE Proc. of Conference on Cone Penetration Testing and Experience, St. Louis, October 26-30, pp. 209-227.
- Dunnicliff, J., 1988. Geotechnical Instrumentation for monitoring field performance. John Wiley & Sons, New York, 577 p.
- Elisio, P.C.A.F., 1983. Celula expansiva hidrodinamica – Uma nova maneira de executar provas de carga (Hydrodynamic expansive cell. A new way to perform loading tests). Independent publisher, Belo Horizonte, Minas Gerais State, Brazil, 106 p.
- Elisio, P.C.A.F., 1986. Celula expansiva hidrodinamica; uma nova maneira de executar provas de carga (Hydrodynamic expansion cell; a new way of performing loading tests). Proc. of VIII Congresso Brasileiro de Mecânica dos Solos e Engenharia de Fundações, VIII COBRAMSEF, Porto Alegre, Brazil, October 12-16, 1986, Vol. 6, pp. 223-241.
- Endley, S.N., Yeung, A.T., and Vennalaganti, K.M., 1996. A study of consolidation characteristics of Gulf Coast clays. Proc. of Texas Section of ASCE, Fall Meeting, San Antonio, Texas, September 18-21, 152-160.
- Endo M., Minou, A., Kawasaki T, and Shibata, T, 1969. Negative skin friction acting on steel piles in clay. Proc. 7th ICSMFE, Mexico City, August 25-29, Vol. 2, pp. 85- 92.
- Erwig, H., 1988. The Fugro guide for estimating soil type from CPT data. Proc. of Seminar on Penetration Testing in the UK, Thomas Telford, London, pp. 261-263.
- Eslami, A., 1996. Bearing capacity of piles from cone penetrometer test data. Ph. D. Thesis, University of Ottawa, Department of Civil Engineering, 516 p.
- Eslami, A., and Fellenius, B.H., 1995. Toe bearing capacity of piles from cone penetration test (CPT) data. Proc. of the International Symposium on Cone Penetration Testing, CPT 95, Linköping, Sweden, October 4-5, Swedish Geotechnical Institute, SGI, Report 3:95, Vol. 2, pp. 453-460.
- Eslami, A., and Fellenius, B.H., 1996. Pile shaft capacity determined by piezocone (CPTU) data. Proc. of 49th Canadian Geotechnical Conference, September 21-25, St. John's, Newfoundland, Vol. 2, pp. 859-867.
- Eslami, A. and Fellenius, B.H., 1997. Pile capacity by direct CPT and CPTu methods applied to 102 case histories. Canadian Geotechnical Journal 34(6) 886–904.
- Eslami, A., Moshfeghi, S., Molaabasi, H., and Eslami, M., 2020. Piezocone and cone penetration test (CPTU and CPT) applications in foundation engineering. Elsevier, 393 p.
- Eurocode, 1990. Eurocode, Chapter 7, Pile Foundations, 25 p.
- Federal Highway Administration, FHWA, 2016. Geotechnical Engineering Circular No. 12, Design and Construction of Driven Pile Foundations, Report No. FHWA-NH-16-009, Volumes 1 and 2., 539 p.
- Fellenius, W. 1918. Kaj- och jordrasen i Göteborg (The quay and earth slides in Gothenburg). Teknisk Tidskrift 48 17-19.
- Fellenius W., 1926. Erdstatische Berechnungen mit Reibung und Kohäsion (Adhäsion) und unter Annahme kreiszylindrischer Gleitflächen. Verlag von Ernst und Sohn, Berlin.47 p.
- Fellenius, W. 1926. Jordstatiska beräkningar med friktion och kohesion för cirkulär-cylindriska glidytor (Earth stability calculations with friction and cohesion for circular-cylindrical slip surfaces). Kungl. Väg- och Vattenbyggarkårens 75-årsskrift, pp. 79-127.
- Fellenius, W. 1929. Jordstatiska beräkningar för vertikalbelastning på horisontal markyta under antagande av cirkulär-cylindriska glidytor (Stability calculations for vertical loads on horizontal ground surface assuming cylindrical failure surfaces). Teknisk Tidskrift 29 57-63.
- Fellenius, W. 1936. Calculation of the stability of earth dams. Proc. of the Second Congress on Large Dams, Washington, DC, p. 445-462.
- Fellenius, B.H., 1970. Undersökning av deformationer i betongpålar under ett bostadshus i Kv. Stagnelius, Uppsala (Monitoring deformations and settlement at a housing complex in Uppsala). National Swedish Council for Building Research, Report Grant C212:b, 50 p. (In Swedish).
- Fellenius, B.H., 1972a. Bending of piles determined by inclinometer measurements. Canadian Geotechnical Journal 9(1) 25-32.
- Fellenius, B.H., 1972b. Downdrag on piles in clay due to negative skin friction. Canadian Geotechnical Journal 9(4) 323-337.

- Fellenius B.H., 1975a. Reduction of negative skin friction with bitumen slip layers. Discussion. ASCE Journal of Geotechnical Engineering Division, 101(GT4) 412-414.
- Fellenius B.H., 1975b. Test loading of piles. Methods, interpretation, and new proof testing procedure. ASCE Journal of Geotechnical Engineering Division, 101(GT9) 855-869.
- Fellenius B.H., 1979. Downdrag on bitumen coated piles. Discussion. ASCE Journal of Geotechnical Engng., 105(GT10) 1262-1265.
- Fellenius, B.H., 1980. The analysis of results from routine pile loading tests. Ground Engineering, London, 13(6) 19-31.
- Fellenius, B.H., 1981. Consolidation of clay by band-shaped premanufactured drains. Discussion. Ground Engineering, London, 14(8) 39-40.
- Fellenius, B.H., 1984a. Negative skin friction and settlement of piles. Proc. of the Second International Seminar, Pile Foundations, Nanyang Technological Institute, Singapore, 18 p.
- Fellenius, B.H., 1984b. Ignorance is bliss—and that is why we sleep so well. Geotechnical News, 2(4) 14-15.
- Fellenius, B.H., 1984c. Wave equation analysis and dynamic monitoring. Deep Foundations Journal, Deep Foundations Institute, Springfield, New Jersey 1(1) 49-55.
- Fellenius, B.H., 1988. Unified design of piles and pile groups. Transportation Research Board, Washington, TRB Record 1169, pp. 75-82.
- Fellenius, B.H., 1989. Tangent modulus of piles determined from strain data. The ASCE, Geotechnical Engineering Division, the 1989 Foundation Congress, Foundation Engineering: Current Principles and Practice, F.H. Kulhawy, Editor, GSP 22, Vol. 1, pp. 500-510.
- Fellenius, B.H., 1994. Limit states design for deep foundations. FHWA International Conference on Design and Construction of Deep Foundations, Orlando, December 1994, Vol. II, pp. 415-426.
- Fellenius, B.H., 1995. Foundations. Chapter 22 in Civil Engineering Handbook, Edited by W. F. Chen. CRC Press, New York, pp. 817-853.
- Fellenius, B.H., 1996. Reflections on pile dynamics. Proc. of the 5th International Conference on the Application of Stress-Wave Theory to Piles, September 10 through 13, Orlando, Florida, Edited by M.C. McVay, F. Townsend, and M. Hussein, Keynote Paper, pp. 1-15.
- Fellenius, B.H., 1998. Recent advances in the design of piles for axial loads, drag load, downdrag, and settlement. Proc. of a Seminar by ASCE and Port of New York and New Jersey, April 1998, 19 p.
- Fellenius, B.H., 1999. Bearing capacity of footings and piles—A delusion? Proc. of the Deep Foundation Institute Annual Meeting, October 14 though 16, Dearborn 17 p.
- Fellenius, B.H., 2002a. Side resistance in piles and drilled-shafts. Discussion. ASCE Journal of Geotechnical Engineering 127(5), pp. 446-448.
- Fellenius, B.H., 2002b. Determining the resistance distribution in piles. Part 1: Notes on shift of no-load reading and residual load. Part 2: Method for Determining the Residual Load. Geotechnical News Magazine. Geotechnical News Magazine, 20(2 35-38), and 20(3 25-29).
- Fellenius, B.H., 2002c. Pile Dynamics in Geotechnical Practice—Six Case Histories. ASCE International Deep Foundation Congress, An International Perspective on Theory, Design, Construction, and Performance, Geotechnical Special Publication No. 116, Edited by M.W. O'Neill, and F.C. Townsend, Orlando Florida February 14-16, 2002, Vol. 1, pp. 619-631.
- Fellenius, B.H., 2004. Unified design of piled foundations with emphasis on settlement analysis. Current Practice and Future Trends in Deep Foundations GeoInstitute Geo-TRANS Conference, Los Angeles, July 27-30, 2004, Edited by J.A. DiMaggio and M.H. Hussein. ASCE Geotechnical Special Publication, GSP 125, pp. 253-275.
- Fellenius, B.H., 2006. Results from long-term measurement in piles of drag load and downdrag. Canadian Geotechnical Journal 43(4) 409-430.
- Fellenius, B.H., 2008. Effective stress analysis and set-up for shaft capacity of piles in clay. ASCE GeoInstitute Geo-Congress New Orleans, March 9-12, Honoring John Schmertmann—From Research to practice in Geotechnical Engineering, ASCE Geotechnical Special Publication, Edited by J.E. Laier, D.K. Crapps, and M.H. Hussein, GSP180, pp. 384-406.

- Fellenius, B.H., 2011. Capacity versus deformation analysis for design of footings and piled foundations. Southeast Asian Geotechnical Society, Bangkok, *Geotechnical Engineering Journal* 41(2) 70-77.
- Fellenius, B.H., 2012. Critical assessment of pile modulus determination methods—Discussion. *Canadian Geotechnical Journal* 49(5) 614-621.
- Fellenius, B.H., 2013. Capacity and load-movement of a CFA pile: A prediction event. GeoInstitute Geo Congress San Diego, March 3-6, 2013, Honoring Fred H. Kulhawy—Foundation Engineering in the Face of Uncertainty, ASCE, Reston, VA, James L. Withiam, Kwok-Kwang Phoon, and Mohamad H. Hussein, eds., *Geotechnical Special Publication, GSP 229*, pp. 707-719.
- Fellenius, B.H., 2014a. Analysis of results from routine static loading tests with emphasis on the bidirectional test. Proceedings of the 17th Congress of the Brasileiro de Mecanica dos Solos e Engenharia, Comramseg, Goiania, Brazil, September 10-13, 22 p.
- Fellenius, B.H., 2014b. Pile aging in cohesive soils, Discussion. *ASCE J of Geotechnical and Environmental Engineering* 141 (4), pp. 07014039-1 and 07014039-2.
- Fellenius, B.H., 2014c. Piled foundation design as reflected in codes and standards. Proc. of the DFI-EFFC International Conference on Piling and Deep Foundations, Stockholm, May 21-23, pp. 1013-1030.
- Fellenius, B.H., 2015a. The response of a "plug" in an open-toe pipe pile. *Geotechnical Engineering Journal of the SEAGS & AGSSEA* 46(2) 82-86.
- Fellenius, B.H., 2015b. Static tests on instrumented piles affected by residual load. *Journal of the Deep Foundation Institute*, 9(1) 11-20.
- Fellenius, B.H., 2016a. The unified design of piled foundations. The Sven Hansbo Lecture. *Geotechnics for Sustainable Infrastructure Development – Geotec Hanoi 2016*, edited by Phung Duc Long, Hanoi, November 23-25, pp. 3-28.
- Fellenius, B.H., 2016b. Fallacies in piled foundation design. *Geotechnics for Sustainable Infrastructure Development– Geotec Hanoi 2016*, edited by Phung Duc Long, Hanoi, November 23-25, pp. 41-46.
- Fellenius, B.H., 2016. An Excel template cribsheet for use with UniPile and UniSettle. [www.Fellenius.net](http://www.Fellenius.net).
- Fellenius, B.H., 2017. Report on the results of the prediction survey of the 3rd CBFP event. 3rd Bolivian International Conference on Deep Foundations, Santa Cruz de la Sierra, Bolivia, April 27-29, Vol. 3, 19p.
- Fellenius, B.H., 2019. Observations and analysis of wide piled foundations. *Canadian Geotechnical Journal*, 56(3), 378-397. [doi.org/10.1139/cgj-2018-0031](https://doi.org/10.1139/cgj-2018-0031).
- Fellenius, B.H., 2022. Basics of foundation design. Electronic Edition, [www.Fellenius.net](http://www.Fellenius.net), 538 p.
- Fellenius B.H., Samson, L., Thompson, D. E., and Trow, W., 1978. Dynamic Behavior of foundation piles and driving equipment. Terratech Ltd. and the Trow Group Ltd., Final Report, Department of Supply and Services, Canada, Contract No. 1ST77.00045, Vol. I and II, 580 p.
- Fellenius, B.H. and Wager, O., 1977. The equivalent cylinder diameter of the bandshaped drain. Proceedings of the 9th ICSMF, Tokyo, July 11-15, Vol. 3, p. 395-396.
- Fellenius, B.H., Riker, R. E., O'Brien, A. J. and Tracy, G. R., 1989. Dynamic and static testing in a soil exhibiting setup. *ASCE Journal of Geotechnical Engineering* 115(7) 984-1001.
- Fellenius, B.H., Samson, L., and Tavenas, F.A., 1989. Pile design. Chapter 5, *Standards and Guidelines*, Public Works Canada, Marine Engineering Branch, 68 p.
- Fellenius, B.H. and Altaee, A., 1994. The critical depth—How it came into being and why it does not exist. Proc. of the Institution of Civil Engineers, *Geotechnical Engineering Journal*, London, 113(2) 107-111.
- Fellenius, B.H. and Goudreault, P.A., 1996. Shallow foundations and retaining walls, earth stress, bearing capacity, and stability. UniBear Version 1.0 for Windows. Users Manual. UniSoft Ltd., Ottawa, 45 p.
- Fellenius, B.H. and Altaee, A., 1996. The critical depth – How it came into being and why it does not exist. Reply to Discussion. Proc. of the Institution of Civil Engineers, *Geotechnical Engineering Journal*, London, 119(4) 244-245.

- Fellenius, B.H., Altaee, A., Kulesza, R, and Hayes, J, 1999. O-cell Testing and FE analysis of a 28 m Deep Barrette in Manila, Philippines. *ASCE Journal of Geotechnical and Environmental Engineering* 125(7) 566-575.
- Fellenius, B.H., Brusey, W. G., and Pepe, F., 2000. Soil set-up, variable concrete modulus, and residual load for tapered instrumented piles in sand. *ASCE Specialty Conference on Performance Confirmation of Constructed Geotechnical Facilities*, University of Massachusetts, Amherst, April 9-12, 2000, Special Geotechnical Publications, GSP94, pp. 98-114.
- Fellenius, B.H. and Eslami, A., 2000. Soil profile interpreted from CPTu data. *Proc. of Year 2000 Geotechnics Conference*, Southeast Asian Geotechnical Society, Asian Institute of Technology, Bangkok, Thailand, November 27-30, 2000, Editors Balasubramaniam, A.S., Bergado, D.T., Der Gye, L., Seah, T.H., Miura, K., Phien wej, N., and Nutalaya, P., Vol. 1, pp. 163-171.
- Fellenius, B.H., Harris, D., and Anderson, D.G., 2004. Static loading test on a 45 m long pipe pile in Sandpoint, Idaho. *Canadian Geotechnical Journal* 41(4) 613-628.
- Fellenius, B.H. and Massarsch, K.M., 2008. Comments on the current and future use of pile dynamic testing. Keynote Lecture, The 8th International Conference on the Application of Stress Wave Theory to Piles. Edited by L.A. Santos, Lisbon September 8 10, 2008, pp. 7-17.
- Fellenius, B.H. and Siegel, T.C, 2008. Pile design consideration in a liquefaction event. *ASCE Journal of Geotechnical and Environmental Engineering* 132(9) 1312-1416.
- Fellenius, B.H., Kim, S.R., and Chung, S.G., 2009. Long-term monitoring of strain in instrumented piles. *ASCE Journal of Geotechnical and Geoenvironmental Engineering* 135(11) 1583-1595.
- Fellenius, B.H. and Ochoa, M., 2009a. San Jacinto Monument Case History. Discussion. *ASCE Journal of Geotechnical Engineering* 133(1) 162-167.
- Fellenius, B.H., and Ochoa, M., 2009b. Testing and design of a piled foundation project. A case history. *Southeast Asian Geot. Society, Bangkok, Geotechnical Engineering. Journal* 40(3) 129-137.
- Fellenius, B.H. and Tan, S.A., 2010. Combination of O-cell test and conventional head-down test. *Honoring Clyde Baker—the Art of Foundation Engineering Practice*, eds., ASCE Geotechnical Special Publication, GSP198, pp. 240 259.
- Fellenius, B.H. and Tan, S.A., 2012. Analysis of bidirectional-cell tests for Icon Condominiums, Singapore. *Proc. of the 9th International Conference on Testing and Design Methods for Deep Foundations*, Kanazawa, Japan, September 18-20, 2012. 10 p.
- Fellenius, B.H., and Nguyen, M.H., 2013. Large diameter long bored piles in the Mekong delta. *International Journal of Case Histories* 2(3) 196-207.
- Fellenius, B.H., and Nguyen, M.H., 2014. Bidirectional-cell tests on two 70 m long bored piles in Vietnam. *GeoInstitute Geo Congress*, Atlanta, February 23-26, ASCE, Reston, VA, Honoring Roy Olson—From Soil Behavior Fundamentals to Innovations in Geotechnical Engineering, Magued Iskander, John E. Garlanger, and Mohamad H. Hussein, editors, *Geotechnical Special Publication*, GSP 233, pp. 482-496.
- Fellenius, B.H. and Ochoa, M., 2016. Wide storage tanks on piled foundations. *Geotechnical Engineering Journal of the SEAGS & AGSSEA* 47(1) 50-62.
- Fellenius, B.H. and Nguyen M.H., 2018. Wick Drains and Piling for Cai Mep Container Port, Vietnam. *GeoMEast 2018 International Congress on Innovative Infrastructure Solutions*, Cairo, Egypt, November 24-28, Springer, 14 p.
- Fellenius, B.H., Terceros, H.M., Terceros, A.M., Massarsch, K.R., and Mandolini, A., 2019. Static response of a group of 13 piles tested simultaneously. *Fourth Bolivian International Conference on Deep Foundations*, Santa Cruz de la Sierra, Bolivia, May 23-24, 13 p.
- Finno, R. J., 1989. Subsurface conditions and pile installation data. *American Society of Civil Engineers, Proc. of Symposium on Predicted and Observed Behavior of Piles*, Evanston, June 30, ASCE Geotechnical Special Publication, GSP23, pp. 1-74.
- Flodin, N. and Broms, B.B., 1981 History of civil engineering in soft clay. In "Soft Clay Engineering" Edited by. E.W. Brand and R.P. Brenner., Elsevier Scientific Publishing Co., Chapter 1, pp.27-156.

- Frank, R., Baudin, C., Driscoll, M., Kavvada, M., Krebs Ovesen, N., Orr, T., and Schuppener, B., 2004. Designers' Guide to EN 1997-1. Eurocode 7: Geotechnical Design, General Rules. Thomas Telford, 216 p.
- Frank, R., 2017. Some aspects of research and practice for pile design in France. *Innovative Infrastruct. Solutions* 2 (1): 32. <https://doi.org/10.1007/s41062-017-0085-4>
- Franke E., 1991. Measurements beneath piled rafts. International Conference on Deep Foundations, Ecole National des Ponts et Chaussees, Paris, March 19-21, pp. 599-626.
- Gibson, G.L. and Devenny, D.W., 1973. Concrete to bedrock testing by jacking from bottom of a borehole, *Canadian Geotechnical Journal* 10(2) 304-306.
- Gilboy, G., 1928. The compressibility of sand-mica mixtures. *Proc. of American Society of Civil Engineers*, 54(6) 555-568.
- Goossens, D. and Van Impe, W.F., 1991. Long-term settlement of a pile group foundation in sand, overlying a clayey layer. *Proc. 10th European Conference on Soil Mechanics and Foundation Engineering*, Firenze, May 26-30, Vol. I, pp. 425-428.
- Goble, G. G., Rausche, F., and Likins, G.E., 1980. The analysis of pile driving—a state-of-the-art. *Proc. of the 1st International Seminar of the Application of Stress-wave Theory to Piles*, Stockholm, Edited by H. Bredenberg, A. A. Balkema Publishers Rotterdam, pp. 131-161.
- Goudreault, P.A. and Fellenius, B.H., 2011. UniSettle Version 4 tutorial with background and analysis examples. UniSoft Geotechnical Solutions Ltd. [[www.UniSoftLtd.com](http://www.UniSoftLtd.com)]. 85 p.
- Goudreault, P.A. and Fellenius, B.H., 2014. UniPile Version 5, User and Examples Manual. UniSoft Geotechnical Solutions Ltd. [[www.UniSoftLtd.com](http://www.UniSoftLtd.com)]. 120 p.
- Gregersen, O.S., Aas, G., and DiBiagio, E., 1973. Load tests on friction piles in loose sand. *Proc. of 8th ICSMFE*, Moscow, August 12-19, Vol. 2.1, Paper 3/17, pp. 109–117.
- Greenfield, M. and Filtz, G. 2009. Downdrag and drag loads on piles. Virginia Tech Center for Geotechnical Practice and Research, Blacksburg, CGPR #56, 108 p.
- GRL, 2002. Background and Manual on GRLWEAP Wave equation analysis of pile driving. GRL Engineers Inc., Cleveland.
- Grozic, J.L.H., Lunne, T., and Pande, S, 2003. An oedometer test study of the preconsolidation stress of glaciomarine clays. *Canadian Geotechnical Journal* 40(5) 857-872.
- Gwizdala, K., 1996. The analysis of pile settlement employing load-transfer functions (in Polish). *Zeszyty Naukowe No. 532, Budownictwo Wodne No.41*, Technical University of Gdansk, Poland, 192 p.
- Gwizdala, K. and Kesik, P., 2015. Pile group settlement, methods, examples of calculations referred to measurement results carried out in field tests. 16th ICSMGE, Edinburgh, September 13-17, pp. 1091-1096.
- Hanifah, A.A. and Lee S.K., 2006. Application of global strain extensometer (Glostrext) method for instrumented bored piles in Malaysia. *Proc. of the DFI-EFFC 10th Int. Conference on Piling and Deep Foundations*, May 31-June 2, Amsterdam, 8 p.
- Hannigan, P.J., 1990. Dynamic monitoring and analysis of pile foundation installations. *Deep Foundation Institute*, Sparta, New Jersey, 69 p.
- Hannigan, P.J., Goble, G.G, Likins, G.E., and Rausche, F. 2006 Design and Construction of Driven Pile Foundations, Federal Highway Administration, FHWA, Reference Manual – Volume I and II, National Highway Institute, NHI-05-042, Courses Nos. 132021 and 132022, 1,454 p.
- Hansbo, S., 1960. Consolidation of clay with special reference to influence of vertical sand drains. *Swedish Geotechnical Institute*, Stockholm, Proceedings No. 18, 160 p.
- Hansbo, S., 1979. Consolidation of clay by band-shaped prefabricated drains. *Ground Engineering*, London, 12(5) 16-25.
- Hansbo, S., 1981. Consolidation of fine-grained soil by prefabricated drains. 10th ICSMFE, Stockholm June 15-19, pp. 677-682.
- Hansbo, S. 1984. Foundations on creep piles in soft clays. *First International Conference on Case Histories in Geotechnical Engineering*, St. Louis, May 6-11, 1984, pp. 259-264.

- Hansbo, S., 1993. Interaction problems related to the installation of pile groups. Proceedings of the 2nd International Geotechnical Seminar on Deep Foundations on Bored and Auger Piles, Ghent, 1–4 June, 1993, pp. 119–130.
- Hansbo, S., 1994. Foundation Engineering. Elsevier Science B. V., Amsterdam, Developments in Geotechnical Engineering No. 75, 519 p.
- Hansbo, S. and Jendebly, L., 1998. A follow-up of two different foundation principles. Foundations on friction creep piles in soft clays. International Conference on Case Histories in Geotechnical Engineering. St. Louis, March 9-12, 259-264.
- Hansen, J.B., 1961. A general formula for bearing capacity. Ingeniøren International Edition, Copenhagen, Vol. 5, pp. 38-46. Also in Bulletin No. 11, Danish Geotechnical Institute Copenhagen, 9 p.
- Hansen, J.B., 1963. Discussion on hyperbolic stress-strain response. Cohesive soils. ASCE Journal for Soil Mechanics and Foundation Engineering 89(SM4) 241-242.
- Heckman, W.S. and Hagerty, D.J., 1978. Vibrations associated with pile driving. American Society of Civil Engineering, Journal of the Construction Division 104 (CO4) 385-394.
- Harris, D., Anderson, D.G., Fellenius, B.H., Butler, J.J., and Fischer, G.S., 2003. Design of Pile Foundations for the Sand Creek Byway, Sandpoint, Idaho. Proc. of Deep Foundation Institute Annual Meeting, Miami, October 23-26, 2003.
- Horikoshi, K., and Randolph, M.F. 1997. On the definition of raft-soil stiffness ratio. Geotechnique 47(5) 1055–1061.
- Holloway, D.M., Clough, G.W., and Vesic A.S., 1978. The effects of residual driving stresses on pile performance under axial load. Proc. of the 10th Offshore Technology Conference, Houston, TX., Vol. 4, pp. 2225-2236.
- Holtz, R.D. and Wager, O., 1975. Preloading by Vacuum—Current Prospects. Transportation Research Record 548, pp. 26-29.
- Holtz, R.D. and Kovacs, W.D., 1981. An introduction to geotechnical engineering. Prentice-Hall Inc., New York, 780 p.
- Holtz, R.D., 1990. Stress distribution and settlement of shallow foundations. Chapter 5, Foundation Engineering Handbook, 2nd Edition, H-Y Fang, Editor, Van Nostrand Reinhold Book Co., pp. 166-216.
- Holtz, R.D., Jamiolkowski, M. B., Lancelotta, R., and Peroni, R., 1991. Prefabricated vertical drains. Design and Performance. Construction Industry Research and Information Association, CIRIA, London, 131 p.
- Holtz, R.D., Kovacs, W.D., and Sheahan, T., 2011. An introduction to geotechnical engineering, 2nd Edition. Pearson, New York, 853 p.
- Hong Kong Geo, 2006. Foundation design and construction. Hong Kong Geotechnical Engineering Office, No. 1/2006, 376 p.
- Horvath, R.G., Kenney, T.C., and Kozicki, P., 1983. Methods of improving the performance of drilled piers in weak rock. Canadian Geotechnical Journal 20(3) 758-772.
- Housel, W.S., 1956. Field and laboratory correlation of the bearing capacity of hardpan for the design of deep foundation. Proc. of American Society for Materials and Testing, ASTM, Vol. 56, pp. 1,320-1,346.
- Huang, A.B., Huai, H.H., and Chang, J.W., 1999. The behavior of a compressible silty fine sand, Canadian Geotechnical Journal 36(1) 88–101.
- Hunter, A.H. and Davisson, M.T., 1969. Measurements of pile load transfer. Proc. of Symposium on Performance of Deep Foundations, San Francisco, June 23-28, 1968, American Society for Testing and Materials, ASTM, Special Technical Publication, STP 444, pp. 106-117.
- Indraratna, B., Balusubramaniam, A.S., Phamvan P., and Wong, Y. K., 1992. Development of negative skin friction on driven piles in soft Bangkok clay. Canadian Geotechnical Journal (29)3, 393-404.
- Inoue, Y., Tamaoki, K., Ogai, T., 1977. Settlement of building due to pile downdrag. Proc. 9th ICSMFE, Tokyo, Vol. 1, pp. 561–564.

- Ismael, N.F., 1985. Allowable bearing pressure from loading tests on Kuwaiti soils. *Canadian Geotechnical Journal* 22(2) 151-157.
- Iwanowski, T. and Bodare, A., 1988. On soil damping factor used in wave analysis of pile driving. Third International Conference on Application of Stress-wave Theory to Piles, Ottawa, May 25-27, 1988, Edited by B.H. Fellenius, pp. 343-352.
- Jaky, J., 1948. Earth pressure in silos. *Proc. 2nd ICSMFE*, Rotterdam, June 21–30, Vol. 1, pp. 103-107.
- Jamiolkowski, M., Ghionna, V. N, Lancelotta R. and Pasqualini, E., 1988. New correlations of penetration tests for design practice. *Proc. Penetration Testing, ISOPT-1*, DeRuiter (ed.), Balkema, Rotterdam, ISBN 90 6191 801 4, pp 263-296.
- Janbu, N., 1963. Soil compressibility as determined by oedometer and triaxial tests. *European Conference on Soil Mechanics and Foundation Engineering*, Wiesbaden, October 15 -18, Vol. 1, pp., 19-25, and Discussion contribution, Vol. 2, pp. 17-21.
- Janbu, N., 1965. Consolidation of clay layers based on non-linear stress-strain. *Proc. 6th ICSMFE*, Montreal, Vol. 2, pp. 83-87.
- Janbu, N., 1967. Settlement calculations based on the tangent modulus concept. University of Trondheim, Norwegian Institute of Technology, Geotechnical Institution, Bulletin 2, 57 p.
- Janbu, N., 1998. Sediment deformations. University of Trondheim, Norwegian University of Science and Technology, Geotechnical Institution, Bulletin 35, 86 p.
- Janbu, N., Bjerrum, L., and Kjaernsli B, 1956. *Veiledning ved losning av fundamenteringsoppgaver*. Norwegian Geotechnical Institute, Publication No. 16, 93 p. (in Norwegian).
- Jardine, J., Chow, F., Overy, R., and Standing, J., 2005. *ICP design method for driven piles in sands and clays*. Thomas Telford Publishing Ltd., London, 105 p.
- Jefferies, M.G., and Davies, M.P., 1991. Soil classification using the cone penetration test. Discussion. *Canadian Geotechnical Journal* 28(1) 173-176.
- Johannessen, I.J. and Bjerrum, L. 1965. Measurements of the compression of a steel pile to rock due to settlement of the surrounding clay. *Proc. 6th ICSMFE*, Montreal, September 8-15, Vol. 6, pp. 261-264.
- Jones G.A., and Rust, E., 1982. Piezometer penetration testing, CUPT. *Proc. of the 2nd European Symposium on Penetration Testing, ESOPT-2*, Amsterdam, May 24-27, Vol. 2, pp. 607-614.
- Justason, M. and Fellenius, B.H., 2001. Static capacity by dynamic methods for three bored piles. Discussion. *ASCE Journal of Geotechnical Engineering* Vol. 127, No. 12, pp. 1081-1084.
- Kakurai, M., Yamashita, K., and Tomono, M., 1987. Settlement behavior of piled raft foundations on soft ground. *Proceedings of the 8th Asian Regional Conf. on SMFE ARCSMFE*, Kyoto, 20 -24 July 1987, Vol. 1. pp. 373 -376.
- Justason, M., Mullins, A.G., Robertson, D., and Knight, W., 1998. A comparison of static and Statnamic load tests in sand: a case study of the Bayou Chico bridge in Pensacola, Florida. *Proc. of the 7th Int. Conf. and Exhibition on Piling and Deep Foundations*, Deep Foundations Institute, Vienna, Austria, 5.22.2-5.22.7.
- Kany M., 1959. *Beitrag zur berechnung von flachengrundungen*. Wilhelm Ernst und Zohn, Berlin, 201 p. (as referenced by the *Canadian Foundation Engineering Manual*, 1985).
- Karlsrud, K., Clausen, C.J.F., and Aas, P.M., 2005. Bearing capacity of driven piles in clay, the NGI approach. *Proc. of Int. Symp. on Frontiers in Offshore Geotechnics*, Perth, September 2005, A.A. Balkema, Publishers, pp. 775-782.
- Katzenbach, R., Ramm, H., and Choudhury, D., 2012. Combined pile-raft foundations—a sustainable foundation concept, *Ninth Int. Conf. on Testing and Design Methods for Deep Foundations*, Kanazawa Sept. 18-20, 10 p.
- Kerisel, J., 1961. *Fondations profondes en milieusableux*. *Proc. 5th ICSMFE*, Paris, July 17-21, Vol. 2, pp. 73-83.
- Kezdi, A. 1965. *Deep Foundations—Discussion*, ICSMFE, Montreal, Sep. 8-15, Vol.3, pp. 473-476.
- Kim, S.R., Chung, S.G., and Fellenius, B.H., 2011. Distribution of residual load and true shaft resistance for a driven instrumented test pile. *Canadian Geotechnical Journal* 48(4) 384-398.



- Kjellman, W., 1947. Consolidation of fine-grained soils by drain wells. Discussion. Proc. of the ASCE 73(6) In Transactions of the ASCE 1948 (113) 748-751.
- Kjellman, W., 1948a. Accelerating consolidation of fine-grained soils by means of cardboard wicks. Proc. 2nd ICSMF, Rotterdam, June 21–30, Vol. 2, pp. 302-305.
- Kjellman, W., 1948b. Consolidation of fine-grained soils by drain wells. Discussion. ASCE Transactions, Vol. 113, pp. 748-751.
- Ko, J. and Jeong, S., 2015. Plugging effect of open-end piles in sandy soil. Canadian Geotechnical Journal 52(1) 1-13.
- Kondner, R.L., 1963. Hyperbolic stress-strain response. Cohesive soils. ASCE Journal for Soil Mechanics and Foundation Engineering 89(SM1) 115-143.
- Konrad J-M and Roy, M., 1981. Bearing capacity of friction piles in marine clay. Geotechnique 31(2) 163-175.
- Krogh, P., Lindgren, A., 1997. Dynamic field measurements during deep compaction at Changi Airport, Singapore, Examensarbete 97/9. Royal Institute of Technology (KTH), Stockholm, 88p.
- Kulhawy, F.H. and Mayne, P.W., 1990. Manual on estimating soil properties for foundation design. Electric Power Research Institute, EPRI, 250 p.
- Kusakabe, O., Maeda, Y., and Ohuchi, M., 1992. Large-scale loading tests of shallow footings in pneumatic caisson. ASCE Journal of Geotechnical Engineering, 118(11) 1681-1695.
- Ladd, C.C., 1991. Stability evaluation during staged construction. The Twenty-Second Terzaghi Lecture, ASCE Journal of Geotechnical Engineering 117(4) 540-615.
- Larsson, R., and Mulabdic, M., 1991. Piezocone tests in clay. Swedish Geotechnical Institute, SGI, Report No. 42, 240 p.
- Lechowicz, Z., Rabarijoely, S., Tetiana, K., 2017. Determination of undrained shear strength and constrained modulus from DMT for stiff overconsolidated clays. Annals of Warsaw University of Life Sciences – SGGW49(2) 107–116.
- Lee, K.M., 2001 Influence of placement method on the cone penetration resistance of hydraulically placed sand fills. Canadian Geotechnical Journal 38(3) 592–607.
- Lee, K.M. and Xiao, Z.R., 2001. A simplified nonlinear approach for pile group settlement analysis in multilayered soils. Canadian Geotechnical Journal 38(10) 1063-1080.
- Lehane, B.M., Bittar, E., Lacasse, S., Liu, Z., and Nadim, F., 2022. New CPT methods for evaluation of the axial capacity of driven piles. Proceedings of the 5th International Symposium on Cone Penetration Testing (CPT'22), June 8 - 10, Bologna, Italy, Edited by Gottardi B. and Tonni, L. 15 p.
- Leung, C.F., Radhakrishnan, R., and Tan, S.A., 1991. Performance of precast driven piles in marine clay. ASCE Journal of Geotechnical Engineering 117(4) 637-657.
- Lin, P.S. and Lovell and C.W, 1981. Compressibility of field-compacted clay. Purdue University, FHWA Joint Highway Research Project No. C-36-5M, 169 p.
- Liew, S.S., Gue, S.S, and Tan, Y.C., 2002. Design and instrumentation results of a reinforced concrete piled raft supporting 2500-tonne oil storage tank on very soft alluvium deposits. 9th Int. Conf. on Piling and Deep Foundations, Nice, June 3-5, pp. 263-269.
- Likins, G.E., Fellenius, B.H., and Holtz, R.D., 2012. Pile Driving Formulas—Past and Present. Full-scale Testing in Foundation Design, M.H. Hussein, R.D. Holtz, K.R. Massarsch, and G.E. Likins, eds. ASCE GeoInstitute Geo-Congress Oakland March 25-29, 2012, State of the Art and Practice in Geotechnical Engineering ASCE, Reston, VA., Geotechnical Special Publication 227, 737-753.
- Lu Ning and Likos, W.J., 2023. The inadequacy of conventional pore water pressure theory. Geostrata, October/November, pp. 18-19.
- Lutenegger, A.J. and Miller, G.A., 1995. Uplift capacity of small diameter drilled shafts from in situ tests. ASCE Journal of Geotechnical Engineering 120(8) 1362-1380.
- Lunne, T., Eidsmoen, D., and Howland, J. D., 1986. Laboratory and field evaluation of cone penetrometer. American Society of Civil Engineers, Proc. of In-Situ 86, ASCE SPT 6, Blacksburg, June 23-25, pp. 714-729.
- Lunne, T. Robertson, P.K., and Powell, J.J.M., 1997. Cone penetration testing in geotechnical practice. Spon Press, London, 312p.

- Mandolini A., 2023. 1943-2023: 80 years of research and practice for piled foundations. Proc. of Geotechnics for Sustainable Infrastructure Development, Geotec Hanoi 2023, Phung (Ed.), December 14 - 15, Hanoi, 28 p.
- Mandolini, A., Russo, G., and Viggiani, C. (2005). Pile foundations: experimental investigations, analysis, and design. Proc. 16th ICSMGE, September 12 -16, Osaka, Japan, pp. 177-213.
- Mansur C.L. and Kaufman, R.I., 1956. Pile tests, low sill structure, Old River, Louisiana. Pile tests, low sill structure, Old River, Louisiana, Transactions, ASCE J. 82(10) 715-744
- Mansur C.I. and Hunter, A.H., 1970. Pile tests–Arkansas River project. ASCE J. 96(SM5) 1545-1582.
- Massarsch, K.R., 1990. Deep soil compaction using vibratory probes. Proc. of Symposium on Design, Construction, and Testing of Deep Foundations: Stone Columns and Related Techniques, Las Vegas January 25, ASTM Special Technical Publication, STP 1089, pp. 297–319.
- Massarsch, K.R. 1991. Deep Vibratory Compaction of Land Fill using Soil Resonance. Proceedings, Infrastructure '91, Int. Workshop on Technology for Hong Kong's Infrastructure Development, December 16, pp. 677-697.
- Massarsch, K.R., 1992. Static and dynamic soil displacements caused by pile driving. Keynote Lecture, Fourth International Conference on the Application of Stress Wave Theory to Piles, the Hague, the Netherlands, September 21-24, 1992, pp. 15-24.
- Massarsch K.R., 1994a. Design aspects of deep soil compaction. In Proceedings of Seminar on Ground Improvement Methods. Geotech. Div., Hong Kong Institution of Engineers, Hong Kong, pp. 61 74.
- Massarsch, K.R., 1994b. Settlement analysis of compacted fill. Proc. of 13th ICSMFE, New Delhi, January 5-10, Vol. 1, pp. 325-328.
- Massarsch, K.R. 1999a. Deep compaction of granular soils. State-of-the art report, Lecture Series: A Look Back for the Future, Lecture Series, University of Zhejiang, China, pp. 181-223.
- Massarsch, K.R., 1999b. Soil compaction for improvement of reclaimed land. International Conference on Offshore and Near-Shore Geotechnical Engineering, Proceedings GEOShore, Panvel, Navi, Mumbai, India, December pp. 399–409.
- Massarsch, K.R. 2000. Settlement and damage caused by construction-induced vibrations. Proc., Int. Workshop, Wave 2000, Bochum, Germany, December 13-15, 2000, pp. 299–315.
- Massarsch, K.R. 2002. Effects of vibratory compaction. TransVib 2002 – International Conference on Vibratory Pile Driving and Deep Soil Compaction. Louvain-la-Neuve. Keynote Lecture, pp. 33–42.
- Massarsch, K.R., 2004a. Deformation properties of fine-grained soils from seismic tests. Keynote Lecture, International Conf. on Site Characterization, ISC'2 Sept. 19-22, 2004, Porto, pp. 133-146.
- Massarsch, K.R., 2004b. Vibrations caused by pile driving. Deep Foundations Institute, DFI Magazine, Part 1: Summer Edition, pp. 41–44, Part 2: Fall Edition, pp. 39–42.
- Massarsch, K.R., 2005. Ground vibrations caused by impact pile driving. Keynote Lecture, Second International Conference on Prediction Monitoring, Mitigation, and Evaluation, September 20-22, Okayama University, Okayama, Taylor and Francis Group, London, pp. 369-379.
- Massarsch, K.R., 2023. Application of deep vertical vibratory compaction using resonance amplification. Geotechnical Engineering Journal of the SEAGS & AGSSEA 54 (1) 1-7.
- Massarsch, K.R. and Westerberg, E., 1995. The active design concept applied to soil compaction. Proc. of Bengt B. Broms Symposium in Geotechnical Engineering, Singapore, December 13 15, pp. 262-276.
- Massarsch, K.R., Westerberg, E., and Broms, B.B., 1997. Footings supported on settlement-reducing vibrated soil nails. Proc. 14th ICSMGE Hamburg, September, 5-12, Vol. 3, pp. 1533-1539.
- Massarsch, K.R. and Fellenius, B.H., 2001. Vibratory compaction of granular soils. Canadian Geotechnical Journal 39(3) 695-709.
- Massarsch, K.R. and Fellenius, B.H., 2002. Dynamic compaction of granular soils. Canadian Geotechnical Journal 39(3) 695-709.
- Massarsch, K.R. and Fellenius, B.H. 2005. Deep vibratory compaction of granular soils. In Ground Improvement Case Histories, Geo-Engineering Series Vol. 3, Chapter 19, Elsevier Publishers (UK), Edited by Buddhima Indraratna and Jian Chu, pp. 633-658.
- Massarsch, K.M., and Fellenius, B.H., 2008. Ground vibrations induced by impact pile driving. Proceedings of the Sixth International Conference on Case Histories in Geotechnical Engineering,

- Edited by S. Prakash, Missouri University of Science and Technology, August 12-16, 2008, Arlington, Virginia, 38 p.
- Massarsch, K.R. and Fellenius, B.H., 2012. Early Swedish Contributions to Geotechnical Engineering. ASCE GeoInstitute Geo-Congress Oakland, March 25-29, 2012, Full-scale Testing in Foundation Design, State of the Art and Practice in Geotechnical Engineering, ASCE, Reston, VA, M.H. Hussein, K.R. Massarsch, G.E. Likins, and R.D. Holtz, eds., Geotechnical Special Publication, GSP 227, pp. 239-256.
- Massarsch, K.R. and Fellenius, B.H., 2014a. Ground vibrations from pile and sheet pile driving. Part 1 Building Damage. Proc. of the DFI-EFFC International Conference on Piling and Deep Foundations, Stockholm, May 21-23, pp. 487-502.
- Massarsch, K.R. and Fellenius, B.H., 2014b. Ground vibrations from pile and sheet pile driving. Part 2. Review of Vibration Standards. Proc. of the DFI-EFFC International Conference on Piling and Deep Foundations, Stockholm, May 21-23, pp. 487-501.
- Massarsch, K.R. and Fellenius, B.H., 2014c. Use of CPT for design, monitoring, and performance verification of compaction projects. 3rd Int. Symp. on Cone Penetration Testing, Las Vegas, May 12-14, pp. 1187-1200.
- Massarsch, K.R. and Fellenius, B.H., 2015a. Engineering assessment of ground vibrations caused by impact pile driving. Geotechnical Engineering Journal of the SEAGS & AGSSEA 46(2) 54-63.
- Massarsch, K.R. and Fellenius, B.H., 2015b. Deep vibratory compaction of granular soils. Ch. 4 in Ground Improvement Case Histories, Compaction, Grouting, and Geosynthetics, Edited by Buddhima Indraratna, Jian Chu, and Cholachat Rujikiatkamjorn, Elsevier Ltd., pp. 111-135.
- Massarsch, K.R. and Fellenius, B.H., 2017a. Evaluation of resonance compaction of sand fills based on cone penetration tests. Ground Improvement. Proceedings of the Institution of Civil Engineers. Paper 1700004, ICE Publishing, pp. 1-10.
- Massarsch, K.R. and Fellenius, B.H., 2017b. Liquefaction assessment by full-scale vibratory testing. Proceedings of the 70th Annual Canadian Geot. Conf., Paper 147, Ottawa, October 1-3, p. 7.
- Massarsch, K.R., Fellenius, B.H., and Bodare, A., 2017a. Fundamentals of the vibratory driving of piles and sheet piles. Geotechnik. Ernst & Sohn Verlag für Architektur und technische Wissenschaften GmbH & Co. KG, Berlin • Geotechnik (2017), pp. 1-16.
- Massarsch, K.R., Zackrisson, P., and Fellenius, B.H., 2017b. Underwater resonance compaction of sand fill. Proceedings of the 19th ICSMGE, Seoul, Korea, September 17-22, pp. 2587-2590.
- Massarsch, K.R., Wersäll, C., and Fellenius, B.H., 2019. Horizontal stress increase induced by deep vibratory compaction. Proceedings of the Institution of Civil Engineers, ICE, ICE Publishing, pp. 1-26. doi.org/10.1680/jgeen.19.00040.
- Massarsch, K.R., Wersäll, C., and Fellenius, B.H., 2019. Liquefaction induced by deep vertical vibratory compaction. Proceedings of the Institution of Civil Engineers (ICE), Geotechnical Engineering, Ground Improvement Journal, pp. 1-12. doi.org/10.1680/jgrim.19.00018.
- Massarsch, K.R., Wersäll, C., and Fellenius, B.H., 2019. Horizontal stress increase induced by deep vibratory compaction. Ground Improvement. Proceedings of the Institution of Civil Engineers, ICE Publishing. doi.org/10.1680/jgeen.19.00040, pp. 1-26.
- Massarsch, K.R., Wersäll, C., and Fellenius, B.H., 2021. Vibratory driving of piles and sheet piles—State of practice. Proceedings of the Institution of Civil Engineers, ICE—Geotechnical Engineering, 174(1) 22 p. https://doi.org/10.1680/jgeen.20.00127.
- Massarsch, K.R., Wersäll, C., and Fellenius, B.H., 2021. Dynamic ground response during vibratory sheet pile driving. ASCE Journal of Geotechnical and Geoenvironmental Engineering. 148(GT7) doi. 10.1061/(ASCE)GT.1943-5606.0002520.
- Mayne, P.W., 2007. Cone penetration testing, a synthesis of highway practice. NCHRP Synthesis 368, Transportation Research Board, Washington, DC, 120 p.
- Mayne, P.W., 2011. Engineering design using the cone penetration test. Geotechnical Applications Guide, ConeTec Inc., Third printing, 165 p.
- Mayne, P.W. and Kulhawy, F.H., 1982.  $K_0$ -OCR relationship in soil. ASCE Journal of Geotechnical Engineering 108(6) 851-870.

- Mayne, P.W., Kulhawy, F, and Kay, J.N., 1990. Observations on the development of pore water pressure during piezocone penetration in clays. *Canadian Geotechnical Journal* 27(4) 418-428.
- Mayne, P.W., Christopher, B.R., and DeJong, J. 2001. *Geotechnical Site Characterization. Manual on Subsurface Investigations*, National Highway Institute Publication No. FHWA NHI-01-031, FHWA, Washington, DC. 305 p.
- Mayne, P.W, Christopher, B.R. and DeJong, J. 2002. *Manual on Subsurface Investigations, Geotechnical Site Characterization*. National Highway Institute Publication No. FHWA NHI-01-031, Federal Highway Administration, U.S. Department of Transportation, Washington, DC. 332 p.
- Mazurkiewics, B.K., 1972. Test loading of piles according to Polish Regulations. Preliminary Report No. 15, Commission on Pile Research, Royal Swedish Academy of Engineering Sciences, Stockholm, Sweden.
- McKenna G., Mann V., Fisseha B., Beier N., and Olmedo, N., 2017. The geotechnical vane strength of soft tailings compared to soft food. *Geotechnical News March*, pp. 28-32.
- McVay, M.C., Schmertmann, J., Townsend, F, and Bullock, P., 1999. Pile freeze, a field and laboratory study. Final Report, Florida Department of Transportation, Research Center, Contract No. B-7967, 1,314 p.
- Meyerhof, G.G., 1951. The bearing capacity of foundations. *Geotechnique* 2(4) 301-332.
- Meyerhof, G.G., 1963. Some recent research on bearing capacity of foundations. *Canadian Geotechnical Journal* 1(1) 16-26.
- Meyerhof, G.G., 1976. Bearing capacity and settlement of pile foundations. The Eleventh Terzaghi Lecture, November 5, 1975. *ASCE Journal of Geotechnical Engineering* 102(GT3) 195-228.
- Meyerhof, G.G., Brown, J.D, and Moulard, G.D., 1981. Prediction of friction pile capacity in a till. *Proceedings of 10th International Conference on Soil Mechanics and Foundation Engineering, ICSMFE, Stockholm, June 15-19, pp. 777-780.*
- Middendorp, P., Bermingham, P., and Kuiper, B., 1992. Statnamic loading test of foundation piles. *Proc. 4th Int. Conf. on the Application of Stress Wave Theory to Piles*, edited by B.J. Barends, Balkema, Rotterdam, The Netherlands, 581-588.
- Middendorp, P., Beck, C., and Lambo, A., 2008. Verification of Statnamic load testing with static testing in a cohesive soil type in Germany. *Proc. of the 8th International Conference on the Application of Stress-wave Theory to Piles*, pp. 531-536.
- Mitchell, J.K., 1982. Soil improvement-state-of-the-art. *Proceedings of 10th International Conference on Soil Mechanics and Foundation Engineering, ICSMFE, Stockholm, June 15-19, pp. 509-565.*
- Moh, Z.C. and Lin, P.C., 2006. Geotechnical History of the development of the Suvarnabhumi International Airport. *Special Issue of the Journal of South-East Asian Geotechnical Society, Geotechnical Engineering, December 2006, 37(3) 143-155.*
- Moh, Z.C. and Woo, S.M., 1987. Preconsolidation of soft Bangkok clay by non-displacement sand drains and surcharge. *Proc. of 9th Southeast Asian Geotechnical Conference, Vol. 2, pp. 171-184.*
- Mokwa, R.L., and Duncan, J.M., 2001. Experimental evaluation of lateral load resistance of pile caps. *ASCE, Journal of Geotechnical and Geoenvironmental Engineering* 127(2) 185-192.
- Mosher R.L., 1987 Comparison of axial capacity of vibration-driven piles to impact-driven piles. Final Report. US Corp of Engineers, Waterways Experiment Station, Technical Report ITL-87-7, 57 p.
- Moss, R.E.S., Seed, R.B., Kayen, R.E., Stewart, J.P., DerKiureghian, A., and Cetin, K.O., 2006, CPT-based probabilistic and deterministic assessment of in situ seismic soil liquefaction potential. *ASCE, Journal of Geotechnical and Geoenvironmental Engineering* 132(8) 1032-1051.
- NAVFAC DM7, 1982. *Design Manual for Soil Mechanics, Foundations, and Earth Structures*. US Department of the Navy, Washington, DC.
- Newmark, N.M., 1935. Simplified computation of vertical stress below foundations. Univ. of Illinois Engineering Experiment Station, Circular 24, Urbana, Illinois, 19 p. (as referenced by Holtz and Kovacs 1985).
- Nelissen, H.A.M., 1983. Under water compaction of sand-gravel layers by vibration plates. *Proc. 8th ECSMFE. Helsinki, May 23-26, Vol. 2, pp. 861 – 863.*

- Newmark, N.M., 1942. Influence chart for computation of stresses in elastic foundations. University of Illinois Engineering Experiment Station, Bulletin Series 338, Vol. 61, No. 92, Urbana, Illinois, 28 p. (as referenced by Holtz and Kovacs 1981, Holtz et al 1999).
- Nilsson, G., 1989. Markvibrationer vid påslagning (Ground vibrations during pile driving). Examensarbete Nr. 3:89. Dept. of Soil and Rock Mechanics, Royal Institute of Technology (KTH). Stockholm, Sweden, 43 p. and Appendix (In Swedish).
- Nishimura, S., Matsumoto, T., Kusakabe, O., Nishiumi, K., and Yoshizawa, Y., 2000. Case studies of Statnamic loading test in Japan. Proc. 6th Int. Conf. on the Application of Stress Wave Theory to Piles, Edited by S. Niyama and J. Beim, Balkema, Rotterdam, The Netherlands, 591-598.
- Nordlund, R.L., 1963. Bearing capacity of piles in cohesionless soils. ASCE Journal of Soil Mechanics and Foundation Engineering 89(SM3) 1-35.
- Nottingham, L.C., 1975. Use of quasi-static friction cone penetrometer data to predict capacity of displacement piles. Ph.D. thesis, Dept of Civil Engineering, Univ. of Florida, 553 p.
- Ochoa, M. and O'Neill, M.W., 1988. Lateral pile-group interaction factors for free-headed pile groups in sand from full-scale experiments. Final Report. FHWA, USAED, MMS, GL-88-12. 214 p.
- Ochoa, M. and O'Neill, M.W., 1989. Lateral pile interaction factors in submerged sand. ASCE J. 115(GT3) 359-378.
- OHBD, 1991. Ontario Highway Bridge Design Code, 3rd. Edition, Code and Commentary, Min. of Transp., Quality and Standards Division, Toronto.
- Okabe, T., 1977. Large negative friction and friction-free piles methods. 9th ICSMFE, Tokyo, July 11-15, Vol. 1, pp. 679-682.
- Olson R.E., 1998. Settlement of Embankments on Soft Clays. ASCE Journal of Geotechnical Engineering 124(4) 278-288.
- Oliveira, M.A., Falconi, F.F., and Perez, W., 2008. Estaca hélice contínua – ensaio dinâmico e prova de carga estática. 6th Seminário de Engenharia de Fundações Especiais e Geotecnia, SEFE VI, Sao Paulo, Brazil, November 3-5, Vol. 1 pp. 423-431.
- Olsen, R.S., and Farr, V., 1986. Site characterization using the cone penetration test. American Society of Civil Engineers, Proc. of In-Situ 86, ASCE SPT 6, Blacksburg, June 23-25, pp. 854-868.
- Olsen, R.S., and Malone, P.G., 1988. Soil classification and site characterization using the cone penetrometer test. Proc. of First International Symposium on Cone Penetration Testing, ISOPT-1, Orlando, March 22-24, Vol. 2, pp. 887-893.
- Olsen, R.S., and Mitchell, J.K., 1995. CPT stress normalization and prediction of soil classification. Proc. of International Symposium on Cone Penetration Testing, CPT95, Linköping, Sweden, SGI Report 3:95, Vol. 2, pp. 257-262.
- O'Neill, M.W., 2001. Side resistance in piles and drilled shafts. ASCE Journal of Geotechnical and Environmental Engineering 126(1) 3-16.
- O'Neill, M.W., Hawkins, R.A., and Audibert, J.M.E., 1982. Installation of pile group in overconsolidated clay. ASCE Journal of Geotechnical Engineering Div., Vol. 108(11) 1369-1386.
- O'Neill, M.W., Hawkins, R.A., and Mahar, L.J., 1982. Load transfer mechanisms in piles and pile groups. ASCE Journal of Geotechnical Engineering Div., Vol. 108(12) 1605-1623.
- O'Neill, M.W. and Raines, R.D., 1991 Load transfer for pipe piles in highly pressured dense sand. ASCE Journal of Geotechnical Engineering 117(8) 1208-1226.
- O'Neill, M.W. and Reese, L.C., 1999. Drilled shafts. Construction procedures and design methods, Federal Highway Administration, Transportation Research Board, Washington, FHWA-IF99-025.
- Osterberg, J., 1989. New device for load testing driven piles and bored piles separates friction and end-bearing. Deep Foundations Institute, Proc. of the Int. Conference on Piling and Deep Foundations, London, London June 2-4, Eds. J.B. Burland and J.M. Mitchell, A.A. Balkema, Vol. 1, pp. 421-427.
- Osterberg, J.O., 1998. The Osterberg load test method for drilled shaft and driven piles. The first ten years. Deep Foundation Institute, Seventh International Conference and Exhibition on Piling and Deep Foundations, Vienna, Austria, June 15-17, 1998, 17 p.
- Paik, K.H., Salgado, R., Lee, J.H., Kim B.J., 2003. Behavior of open- and closed-end piles driven into sands. ASCE Journal of Geotechnical and Geoenvironmental Engineering 129(4) 296-306.

- Paniagua, W., Ibarra, E., and Valle, J.A., 2007. Rigid inclusions for soil improvement in a 76 building complex. *Deep Foundations Institute Magazine*, Fall issue. 7p.
- Peck, R.B., Hanson, W.E., and Thornburn, T. H., 1974. *Foundation Engineering*, Second Edition. John Wiley and Sons Inc., New York, 514 p.
- Pecker, A., 2004. Design and Construction of the Rion Antirion Bridge. *Proc. of the Conference on Geotechnical Engineering for Transportation Projects*, , *Geo-Trans*, ASCE GeoInstitute, Los Angeles July 27-31, 2004, Eds. M.K. Yegian and E. Kavazanjian, Vol. 1 pp. 216-240.
- Perloff W.H. and Baron W., 1976. *Soil mechanics principles and applications*. John Wiley and Sons, New York, 745 p.
- Poulos, H.G., 2013. Pile design for ground movement. *Proc. of the Int. Conf. on State-of-the-Art of Pile Foundations and Case Histories*, Bandung, Indonesia, June 2-4, pp. A2-1-A2-18.
- Randolph, M., 1985. Shaft capacity of driven piles in clay. *Proc. 17th Annual OTC Conference*, Houston, May 6-9, 8p.
- Rausche, F., Moses, F., and Goble, G.G., 1972. Soil resistance predictions from pile dynamics. *ASCE Journal of Soil Mechanics and Foundation Engineering* 8(SM9) 17-937.
- Rausche F. and Goble G. G., 1979. Determination of pile damage by top measurements. *American Society for Testing and Materials, ASTM, Proceeding of Symposium on Behavior of Deep Foundations*, R. Lundgren Editor, ASTM STP 670, pp. 500-506.
- Rausche, F., Goble, G.G., and Likins, G.E., 1985. Dynamic determination of pile capacity. *ASCE Journal of the Geotechnical Engineering Division* 111(GT3) 367-383.
- Reese, L.C. 1979. Design and construction of drilled shaft. 12th Terzaghi Lecture. *ASCE J.* 104(GT1) 91-116.
- Robertson, P.K., 1986. In-Situ testing and its application to foundation engineering. 1985 Canadian Geotechnical Colloquium, *Canadian Geotechnical Journal* 23(4) 573-594.
- Robertson, P.K., 1990. Soil classification using the cone penetration test. *Canadian Geotechnical Journal* 27(1) 151-158.
- Robertson, P.K., 2007a. Cone penetration testing. *Geotechnical applications guide*. Cone Tech Inc., Fifth Edition, 600 p.
- Robertson, P.K., 2007b. Cone penetration test (CPT)-based soil behaviour type (SBT) classification system— an update. *Canadian Geotechnical Journal* 53(11) 1-18.
- Robertson, P.K., 2016. Cone penetration test (CPT)-based soil behaviour type (SBT) classification system--an update. *Canadian Geotechnical Journal* 53(12) 1910-1927.
- Robertson, P.K., Campanella, R.G., and Wightman, A., 1983. SPT-CPT correlations. *ASCE Journal of the Geotechnical Engineering Division* 109(GT11) 1449–1459.
- Robertson, P.K. and Campanella, R.G., 1983. Interpretation of cone penetrometer tests, Part I sand and Part II clay. *Canadian Geotechnical Journal* (20)4 718-733 and 734-745.
- Robertson, P.K., and Campanella, R.G., 1985. Liquefaction potential of sands using the cone penetration test. *ASCE Journal of Geotechnical Engineering* 22(GT3) 298–307
- Robertson, P.K., Campanella, R. G., Gillespie, D., and Grieg, J., 1986. Use of piezometer cone data. *Proc. of ASCE In-Situ 86 Specialty Conference*, Edited by S. Clemence, Blacksburg, June 23-25, *Geotechnical Special Publication GSP No. 6*, pp. 1263-1280.
- Robertson, P.K. and Campanella, R.G., 1986. Guidelines for use, interpretation, and application of the CPT and CPTU. *Manual*, Hogentogler & Company, Inc., 196 p.
- Robertson, P.R., Campanella, M., Davies, M. and Sy, A., 1988. Axial capacity of driven piles in deltaic soils using CPT. *Proc. 1st Int. Symp. on Penetration Testing, ISOPT-1*, Orlando, March 20-24, Vol. 2, 919–928. A.A. Balkema.
- Robertson, P.K. and Wride, C.E., 1998. Evaluating cyclic liquefaction potential using the cone penetration test. *Canadian Geotechnical Journal* 35(3) 442-459.
- Rollins, K.M., Peterson, K.T., and Weaver, T.J., 1998. Lateral load behavior of full-scale pile group in clay. *ASCE Journal of Geotechnical and Geoenvironmental Engineering*, 124(6) 468-476.
- Rollins, K.M., Clayton, R.J., Mikesell, R.C., and Blaise, B.C., 2005. Drilled shaft side friction in gravelly soils. *ASCE Journal of Geotechnical and Geoenvironmental Engineering* 131(8) 987-1003.

- Roscoe, K.H., Schofield, A.N., and Wroth, C.P., 1958. On the yielding of soils. *Geotechnique* 8(1) 22-53.
- Russo, G. and Viggiani C. 1995. Long-term monitoring of a piled foundation. Fourth International Symposium on Field Measurements in Geomechanics, Bergamo, April 10-12, pp. 283–290.
- Sampaco, K., Pham, H., and Anderson, D. 2008. The Golden Ears Bridge design-build project: foundation design for segment 4 approach structures. Proc. of the FHWA, and SCDOT Sixth National Seismic Conference on Bridges and Highways, Charleston, South Carolina, July 27-30, Paper 2B1-2, 12 p.
- Salem, H., Agharazi, F. and Fellenius, B.H., 1995. Detection of toe damage in steel piles driven to bedrock. 1995 PDA User's Days, Cleveland, 14 p.
- Sanglerat, G., Nhim, T.V., Sejourne, M., and Andina, R., 1974. Direct soil classification by static penetrometer with special friction sleeve. Proc. of the First European Symposium on Penetration Testing, ESOPT-1, June 5-7, Stockholm, Vol. 2.2, pp. 337-344.
- Savvaiddis, P., 2003. Long-term geodetic monitoring of the deformation of a liquid storage tank founded on piles. Proc. 11th FIG Symposium on deformation measurements, Santorini, Greece, May 25-28, 2003, 8p.
- Schlösser, F., 1997. Amelioration et reinforcement des sols (improvement and reinforcement of soils). Proc. 14th ICSMGE Hamburg, September, 5-12, pp. 2445–2466.
- Schmertmann, J.H., 1970. Static cone to compute settlement over sand. *ASCE Journal Soil Mechanics and Foundation Engineering* 96(SM3) 1011-1043.
- Schmertmann, J.H., 1975. Measurement of In-situ Shear Strength. Proc. of ASCE Geotechnical Division, Specialty Conference on In-Situ Measurement of Soil Properties, June 1-4, 1974, Raleigh, NC, Vol. 2. pp. 57-138.
- Schmertmann, J.H., 1978. Guidelines for cone penetration test, performance, and design. U.S. Federal Highway Administration, Washington, Report FHWA-TS-78-209, 145 p.
- Schmertmann, J.H., 1983. A simple question about consolidation. *ASCE J. of Geotechnical. Engineering* 109(1) 119-123.
- Schmertmann, J.H. 1985. Measure and use of the in-situ lateral stress. In *The practice of foundation engineering, a volume honoring Jorj O. Osterberg*. Edited by R.J. Krizek, C.H. Dowding, and F. Somogyi. Department of Civil Engineering, The Technological Institute, Northwestern University, Evanston, IL. pp. 189–213.
- Schmertmann, J.H., 1991. The mechanical aging of soil. The 25th Terzaghi Lecture, *ASCE J. of the Geot. Engng. Div.*, 115(7) 1003-1018.
- Schmertmann, J.H. and Schmertmann, C.P., 2009. "Test every non redundant foundation bored pile to reduce uncertainty and cost". Lecture to Hong Kong Institution of Engineers, Polytech University, Hong Kong, July 11, 2009, 41 p.
- Schmertmann, J.H. and Schmertmann, C.P., 2012. "Testing and Remediation Observational Method for the Design and Construction of Pile Foundations." *The Role of Full-Scale Testing in Foundation Design*, ASCE Geotechnical Special Publication, Ed. by M.H. Hussein, R.D. Holtz, K.R. Massarsch, and G.E. Likins, GSP 227, pp. 349 -361.
- Searle, I.E., 1979. The interpretation of Begemann friction jacket cone results to give soil types and design parameters. Proc. of 7th European Conference on Soil Mechanics and Foundation Engineering, ECSMFE, Brighton, Vol. 2, pp. 265-270.
- Seed, H.B., and Idriss, I.M. 1971. Simplified procedure for evaluating soil liquefaction potential. *ASCE J. Geotech. Engng. Div.* 97(9) 1249–1273.
- Sharp, B.N., Settlement of quay walls, quay aprons, and crane rails involving rockfill, Proc. Inst. of Civil Engineers, Maritime and Energy, 118(9) 177-188.
- Sheah, T.H., 2006. Design and Construction of ground improvement works at Suvarnabhumi Airport. Special Issue of the Journal of South-East Asian Geotechnical Society, *Geotechnical Engineering*, December 2006, 37(3) 171-188.
- Shen Bao-Han and Niu Dong-Sheng, 1991. A new method for determining the yield load of piles. Proc. of the Fourth International Conference on Piling and Deep Foundations, Deep Foundation Institute, Stresa April 7-12, Balkema Publishers, Vol. 1, pp. 531-534.

- Simpson, B. and Driscoll, R., 1998. Eurocode 7A Commentary. Construction Research Communications, Watford.
- Sinnreich, J., 2012. Strain gage analysis for nonlinear pile stiffness. *Geotechnical Testing Journal*. American Society for Testing Materials, ASTM 35(2) 1-8.
- Skempton, A.W., and Bjerrum, L., 1957. A contribution to the settlement analysis of foundations on clay. *Geotechnique* 7(4) 168-178.
- Smith, E.A.L., 1960. Pile driving analysis by the wave equation. *Journal of the Soil Mechanics and Foundation Engineering Division, Proc. ASCE* 86(SM4) 35-61.
- Sridharan, A., Abraham, B.M., and Jose, B.T., 1991. Improved technique for estimation of preconsolidation pressure. *Geotechnique* 41(2) 263-268.
- Stark, T.D., and Olsen, S.M., 1995. Liquefaction resistance using CPT and field case histories. *ASCE Journal of Geotechnical Engineering* 121(GT12) 856–869.
- Steinbrenner, W., 1934. Tafeln sur Setzungberechnung. *Die Strasse* 1:221.
- Steinbrenner, W., 1936. A rational method for the determination of the vertical normal stresses under foundations. 1st ICSMFE, Vol. 2, pp. 142-143.
- Stoll, M.U.W., 1961. Discussion on New approach to pile testing by T. Whitaker and R. W. Cooke, Proc. 5th ICSMFE, Paris, July 17-21, Vol. 3, pp. 279-281.
- Swedish State Railways Geotechnical Commission, 1922. Statens Järnvägars Geotekniska Kommission – Slutbetänkande. Swedish State Railways, Bulletin 2 (in Swedish with English summary), 228 p.
- Tan, S.A. and Fellenius, B.H., 2016. Negative skin friction pile concepts with soil-structure interaction. *ICE Geotechnical Research Journal*, UK. Paper 16.00006. pp 1-11.
- Tanaka, H., Ritoh, F., and Omukai, N., 2002. Quality of samples retrieved from great depth and its influence on consolidation properties. *Canadian Geotechnical Journal* (39)6 1288-1301.
- Tavenas, F. and LaRochelle, P., 1972. Accuracy of relative density measurements. *Geotechnique* 22(4) 549-562.
- Taylor, D.W., 1948. *Fundamentals of soil mechanics*. John Wiley & Sons, New York, 700 p.
- Teparaksa, W. 2015. Deep barrette pile capacity with aging effect. *Geotechnical Engineering Journal of the SEAGS & AGSSEA* 46(2) 68-76.
- Tschebotarioff, G.P., 1951. *Soil mechanics, foundations, and earth structures*. McGraw-Hill Book Company Inc., New York, 655 p.
- Tschebotarioff, G.P., and Palmer, L.A., 1948. Some experiences with tests on model piles. Proc. of 2nd ICSMFE, Rotterdam, June 21–30, Vol. 2, p. 196.
- Tschebotarioff, G.P., 1951. *Soil Mechanics, Foundations, and Earth Structures*. McGraw Hill Book Co. Inc., New York, p. 440 (p. 230 in 2nd Ed., 1979).
- Terzaghi, K., 1942. Discussion of the Progress Report of the Committee on the Bearing Capacity of Pile Foundations. *ASCE Proc.* 68(2) 311-323.
- Terzaghi, K., 1943. *Theoretical Soil Mechanics*. John Wiley and Sons, New York, 511 p.
- Terzaghi, K., 1954. Anchored bulkheads. *ASCE Transactions*, 119 1243-1324.
- Terzaghi, K. and Peck, R.B., 1948. *Soil Mechanics in Engineering Practice*. John Wiley and Sons, New York, 566 p.
- Terzaghi, K., 1955. Evaluation of coefficients of subgrade reaction. *Geotechnique* 5(4) 297-326.
- Terzaghi, K., Peck, R.B., and Mesri G., 1996. *Soil Mechanics in Engineering Practice, Third Edition*. John Wiley and Sons, New York, 549 p.
- Tomlinson, M.J., 1957. The adhesion of piles driven into clay soils. Proc. 4th ICSMFE, London August 12-24, Vol. 2, pp. 66-71.
- Tomlinson, M.J., 1980. *Foundation design and construction, Fourth Edition*. Pitman Publishing Inc., London, 793 p.
- Torstensson, B\_A., 1975. Pore pressure sounding instrument. Proc. ASCE Specialty Conference on In-Situ Measurements of Soil Properties., Raleigh, NC, June 1-4, Vol. 2, pp. 48-54. \
- Tumay, M. T., and Fakhroo, M., 1981. Pile capacity in soft clays using electric QCPT data. *ASCE Cone Penetration Testing and Experience*, St. Louis, October 26-30, pp. 434-455.



- Umar, M. and Sadrekarimi, A. (2017). Accuracy of determining preconsolidation stress from laboratory tests. *Canadian Geotechnical Journal* 54(2) 441-450.
- US Corps of Engineers (USCOE), 2012. Hurricane and storm damage risk reduction systems design guidelines (HSDRRSDG), Chapter 3, Geotechnical, 67 p.
- Vander Veen, C., 1953. The bearing capacity of a pile. Proc. 3rd ICSMFE, Zurich, Switzerland, August 16-27, Vol. 2, pp. 84-90.
- Verstraelen, J., Maekelberg, W., and Medaets, M., 2016 Recent experiences with static pile load testing on real job sites. Symposium on Design of Piles in Europe, Vol. 1, Brussels, April 28- 29, pp. 63-85.
- Vesic, A.S., 1964. Investigations of bearing capacity of piles in sand. Proc. of North American Conference on Deep Foundations, Mexico City, December 1964. pp. 197-224.
- Vesic, A.S., 1970. Test on instrumented piles, Ogeechee River site. *ASCE J.* 96(SM2) 561-584.
- Vesic, A.S., 1973. Analysis of ultimate loads of shallow foundations. *ASCE J.* 99(SM1) 45-73.
- Vesic, A.S., 1975. Bearing capacity of shallow foundations. In *Foundation Engineering Handbook*, edited by H.F. Winterkorn and H-Y Fang, VanNostrand Reinhold Co., New York, pp. 121-147.
- Vijayvergiya, V.N. and Focht, J.A. Jr., 1972. A new way to predict the capacity of piles in clay. Fourth Annual Offshore Technology Conference, Houston, Vol. 2, pp. 865-874.
- Vijayvergiya, V.N., 1977. Load-movement characteristics of piles. Proc. of Port '77 Conference, ASCE, Long beach, Ca, March 9-11, Vol. 2, pp. 269-284.
- Vos, J.D., 1982. The practical use of CPT in soil profiling, Proc. of the Second European Symposium on Penetration Testing, ESOPT-2, Amsterdam, May 24-27, Vol. 2, pp. 933-939.
- van Weele, A.F., 1988. Cast-in-situ piles—installation methods, soil disturbance, and resulting pile behavior. Proc. of First International Geotechnical Seminar on Deep Foundations on Bored and Augered Piles, Ed. van Impe W., Ghent, October 19-21, pp. 219-226.
- Wendel, E., 1900. Om profbelastning med tillämpning deraf på grundläggningförhållandena i Göteborg. *Tekniska Samfundets Handlingar*, No. 7, pp. 3-62.
- Wellington, A.M., 1988. Formulae for safe loads of bearing piles. *Engineering News Records*, pp 500-512.
- Westerberg, E., Massarsch, K.R., and Eriksson, K., 1995. Soil resistance during vibratory pile driving. International symposium on cone penetration testing, CPT'95, Linköping, Oct. 1995. Proceedings, Vol. 3. Swedish Geotechnical Society. SGF Report 3:95, pp. 241-250.
- Westergaard, H.M., 1938. A problem of elasticity suggested by a problem in soil mechanics: A soft material reinforced by numerous strong horizontal sheets. In *Contributions to the Mechanics of Solids*, Stephen Timoshenko 60th Anniversary Volume, MacMillan, New York, pp. 260-277 (as referenced by Holtz and Kovacs 1981).
- Whitaker, T. and Cooke, R.W., 1961. A new approach to pile testing. Proc. 5th ICSMFE, Paris, July 17-21, Vol. 2, pp. 171-176.
- Wissa A.E.Z., Martin, R.T., and Garlanger, J.E., 1975. The piezometer probe. Proc. ASCE Specialty Conference on In-Situ Measurements of Soil Properties., Raleigh, NC, June 1-4, Vol. 2, pp. 536-545.
- Youd, T.L., Idriss, I.M, Andrus, R.D., Arango, I., Castro, G., Christian, J.T., Dobry, R., Finn, W.D.L., Harder, L.F., Hynes, M.E., Ishihara, K., Koester, J.P., Liao, S.S.C., Marcuson, W.F., Martin, G.R., Mitchell, J.K., Moriwaki, Y., Power, M.S., Robertson, P.K., Seed, R.B., Stokoe, K.H. 2001. Liquefaction resistance of soils: Summary report from the 1996 NCEER and 1998 NCEER/NSF Workshops on evaluation of liquefaction resistance of soils, *ASCE Journal of Geotechnical and Geoenvironmental Engineering* 127(4) 297–313.
- Zhang Q.Q. and Zhang, Z.M., 2012. Simplified non-linear approach for single pile settlement analysis. *Canadian Geotechnical Journal* 49(11) 1256-1266.
- Yamashita, K. Hamada, J., Takeshi, Y., 2011a. Field measurements on piled rafts with grid-form deep mixing walls on soft ground. *Geotechnical Engineering Journal of the SEAG & AGSSEA*, 42(2) 1-10.
- Yamashita, K. Hamada, J., Takeshi, Y., 2011b. Investigation of settlement and load sharing on piled rafts by monitoring full-scale structures. *Soil and Foundations* 51(3) 513-532.

- Yamashita, K. Hamada, J., Onimaru, S., Higashino, M., 2012. Seismic behavior of a piled raft with ground improvement supporting a base-isolated building on soft ground in Tokyo. *Soil and Foundations* 52(5) 1000-1015.
- Yamashita, K., Wakai, S., and Hamada, J. 2013. Large-scale piled raft with grid-form deep mixing walls on soft ground. *Proc. 18th ICSMGE, September 2-6, Paris, France, Vol. 3, pp. 2637-2640.*
- Yamashita, K. and Hamada, J. 2013. Field monitoring of piled rafts in soft ground–Japanese experience. *Proc. of Fourth Bolivian International Conference on Deep Foundations, Santa Cruz de la Sierra, Bolivia, May 23-24, 16 p.*
- Yang, Y., Them, E.G., Lee, P.K.K., and Yu, F., 2006. Observed performance of long steel H-piles jacked into sandy soils. *ASCE Journal of Geotechnical and Environmental Engineering* 132(1) 24-35.

## CHAPTER 18

### INDEX

Reference is to "#.#.#; "Chapter.Section.Clause"

Aquifer	1.4	Davisson Offset limit	8.2
Average degree of consolidation	4.3	DeBeer method	8.6
		Decourt method	8.5
Bearing capacity factors	6.1	Deformation	1.1, 3.1
Bearing capacity formula	6.1	Degree of consolidation	3.14
Bending	7.20.10	Degree of saturation	1.2
Beta coefficient	7.2.1	Density	1.2
Bidirectional test	8.13	Density, bulk	1.2
Bitumen coating	7.20.7	Density, dry	1.2
Block analysis	3.19	Density, saturated	1.2
Blow rate	9.9	Density, solid	1.2
Boussinesq	1.6	Density, total	1.2
Buckling	7.20.8	DIET	9.11
		Dilatometer, DMT, Method	7.10, 10.7
CAPWAP	9.33	Discharge capacity	4.14
Case method estimate of capacity	9.30	Downdrag	7.5, 7.34
Characteristic Point	1.9	Drag force	7.15, 7.34
Chin-Kondner method	8.4	Drainage blanket	4.4
Coefficient of consolidation	3.14	Drains	4.1
Coefficient of horizontal consolidation	4.3	Dutch CPT method	7.9.2
Coefficient of restitution	9.16		
Coefficient of secondary compression	3.15	Earth pressure	5.1
Coefficient, earth pressure	5.2	Earth stress	5.1
Coefficient, shaft correlation	7.9.7	Earth stress coefficient	5.2
Compactability	2.3, 10.5	Effective stress	1.4
Compression index	3.3	Eccentric load	5.2
Compression ratio	3.3, 3.4	Energy ratio	9.4
Compaction	9.16	Equivalent cylinder diameter	4.3
Compression wave	9.12	Equilibrium plane	7.2.4, 7.14
Cone penetrometer, electric	2.1	Equivalent footing width	6.4
Cone penetrometer, mechanical	2.1	Equivalent head -down test	8.13.2
Cone penetrometer, piezocone	2.1, 7.9	Equivalent load distribution	8.13.1
Cone resistance	2.2		
Cone resistance, "effective"	2.13	Equivalent raft	7.2.4, 7.17.2
Cone resistance, corrected	2.7	Eslami-Fellenius CPTU method	7.9.7
Cone resistance, normalized	2.9	Exponential function	8.11.3
Contact stress	6.2, 7.17.3, 7.18.1, 7.18.5		
Continuous sampling	2.20	Factor of safety	6.2, 7.9, 8.9
CPTU method for piles	7.9	Factor, inclination	6.3
Creep	3.1, 3.15, 8.3	Factor, shape	6.4
Crimping	4.13	Filter jacket	4.11
Critical depth	7.4	Follower	9.14
		Force equilibrium	7.2.4, 7.15.1
Damping	9.18	Force, pile head	9.15
Damping factor	9.19, 9.20, 9.31	Force, pile toe	9.17

Friction angle, internal	5.2	Maximum stress	9.17
Friction angle, wall	5.2	Meyerhof CPT method	7.9.4
Friction ratio	3.2, 3.3, 3.5	Microfolding	4.14
Friction ratio, normalized	2.10	Mineral density	1.2
Fundex test	9.37	Modulus number, m	3.4, 3.7
Gradient	1.7, 4.4, 4.7	Modulus of elasticity	8.16
Grain size classifications	1.3	Modulus, constrained	3.2
Gwizdala function	8.11.1	Modulus, elastic	3.2
Hammer efficiency	9.4	Modulus, from CPTU	3.21
Hammer function	9.2	Modulus number, Janbu	3.4
Hammer selection	9.22	Modulus, Young's	3.2
Hammer types	9.5	Movement	3.1
Hansen method	8.3	Negative skin friction	7.4
Hansen function	8.11.4	Newmark Influence Chart	1.7
Heave	7.20.11	Overconsolidation ratio, OCR	3.6
High strain testing	9.24	Overturning	6.6
Hooke's Law	3.3	PDA diagram	9.35
Horizontal loading	7.20	Permeability, filter jacket	4.12
Hydraulic conductivity	4.1, 4.10	Phase parameters	1.2
Hyperbolic method	8.4, 8.5	Phreatic height	1.4
Hyperbolic function	8.11.2	Pile Driving Analyzer, PDA	9.24
ICP CPT method	7.9.6	Pile group effect	7.17.2, 7.18
Impact duration	9.3	Pile integrity	9.29
Impedance, Z	9.25	Piled pad	7.19
Inclination factor	6.4	Piled raft	7.2.4, 7.17.2
Inclined load	6.3	Plugged toe	7.20.9. 9.15
Inclinometer	7.20.10	Poisson's Ratio	3.2
Instrumented test	8.13	Pore pressure at shoulder, U2	2.3, 2.10
Jetting	7.20.6	Pore pressure gradient	4.7
Kjellman-Barron method	4.2	Pore pressure ratio	2.10
Lambda method	7.2.1	Pore pressure ratio, "effective"	2.10
Lateral movement	4.8	Porosity	1.2
LCPC CPT method	7.9.3	Preconsolidation	3.6
Limit States Design	6.13	Preconsolidation margin	3.7
Liquefaction susceptibility	10.7	Pressuremeter, PMT, Method	7.10.
Load and Resistance Factor Design	6.13	Proctor test	3.5.7
Load, eccentric	6.3	Quake	9.15
Load, inclined	6.4	q-z curve	8.11
Load, line	5.6	Racking	9.9
Load, residual	7.6	Rahman function	8.11.7
Load, strip	5.8	Ratio function	8.11.1
Load, surcharge	5.8	RAU	9.32
Low strain testing	9.29	Recompression index	3.3
Maximum curvature method	8.8	Recompression modulus number	3.7
		Residual force	7.6, 8.12, 8.15, 8.22, 8.29
		Resistance, shaft	8.1

Resistance, toe	8.2	Sweeping of pile	7.20.10
Resistance, ultimate	8.3		
Resonance compaction	10.4, 10.7	Tangent Modulus Method	8.16
RSP	9.31	Tapered pile	7.7
RSU	9.31	Telltale	8.13
		Ternary diagram	1.3
Scour	7.22	Time coefficient	3.14
Salt content	1.2	Time effect	7.21
Sand drains	4.10	Time dependent settlement	3.14
Sand drains	4.3, 4.8	Toe coefficient	7.4
Schmertmann CPT method	7.9.1	Transferred energy	9.21
Secant stiffness	8.16.2	Transition zone, length	7.14.2
Secondary compression	3.9, 3.14, 4.4	Tumay-Fakhroo CPT method	7.9.5
Seismic design	7.20.4		
Settlement	3.1	Unified pile design method	7.15
Settlement, acceptable	3.15	Unit weight, buoyant	1.2
Settlement of piled foundations	7.17.2, 7.24	Unit weight, total	1.2
Settlement below pile toe level	7.17.2	Unloading Point Method, UPM	9.39
Shape factor	6.4		
Shoulder area ratio, a	2.7	Vacuum loading	4.9
Sleeve resistance	2.4	vander Veen function	8.11.3
Sliding	6.7	Vibrations	2.12.8
Smear zone	4.15	Vibratory hammer	9.3
Spacing of drains	4.12	Vibratory compaction	10.3
Spacing of piles	7.18.2, 7.20.1	Vibratory driving	9.14
Stage construction	4.8	Vibration damage	9.15
Stage construction	4.6	Vijayvergiya function	8.11.6
Standard penetration test, SPT	7.8	Void ratio	1.2
Statnamic test	9.37		
Stiffness	9.15	Water content	1.2
Strain wave	9.10	Water ponding	4.4
Strain wave length	9.13	Wave equation analysis	9.21
Stress distribution	1.5	Wave traces	9.25
Stress exponent, j	3.4	Westergaard distribution	1.14
Stress wave	9.10	Wick drains	4.6
Stress, effective	1.5	Wide pile groups	7.18
Stress, effective	1.5	Winter conditions	4.5
Stress, impact	9.17		
Stress, overburden	1.5	Zhang function	8.11.5
Surcharge	4.6, 5.5		
Swelling soil	7.16		
Tangent stiffness	8.16.3		
Transition zone	7.14.2, 7.15		
t-z curve	8.11		

